

EXPERIMENTAL AND THEORETICAL ANALYSIS
OF OXIDATION AND GROWTH CHEMISTRY
IN A FUEL-RICH ACETYLENE FLAME

Vol. 1

by

PHILLIP RAY WESTMORELAND

B. S. Chemical Engineering, North Carolina State University
(1973)

M. S. Chemical Engineering, Louisiana State University
(1975)

SUBMITTED TO THE
DEPARTMENT OF CHEMICAL ENGINEERING
IN PARTIAL FULFILMENT
OF THE REQUIREMENTS FOR THE DEGREE OF

DOCTOR OF PHILOSOPHY

at the

MASSACHUSETTS INSTITUTE OF TECHNOLOGY

May 1986

© Massachusetts Institute of Technology 1986

Signature of author _____
Department of Chemical Engineering
May 21, 1986

Certified by _____
Jack B. Howard
Thesis Supervisor

John P. Longwell
Thesis Supervisor

Accepted by _____
William C. Deen, Chair
Departmental Committee for Graduate Students

MASSACHUSETTS INSTITUTE
OF TECHNOLOGY

JUN 03 1986

LIBRARIES

ARCHIVES

Vol. 1

EXPERIMENTAL AND THEORETICAL ANALYSIS OF OXIDATION AND GROWTH
CHEMISTRY IN A FUEL-RICH ACETYLENE FLAME

by

PHILLIP RAY WESTMORELAND

Submitted to the Department of Chemical Engineering on May 21, 1986,
in partial fulfillment of the requirements for the Degree of Doctor
of Philosophy in Chemical Engineering

ABSTRACT

A low-pressure, fuel-rich flat flame of acetylene and oxygen was characterized experimentally by mapping temperature and the profiles of mole fractions for 38 stable species and free radicals. Flame pressure was 2.67 kPa (20 torr), and the feed mixture of 46.5 mol % C₂H₂, 48.5% O₂, and 5.0 % Ar ($\phi=2.40$) was introduced through the water-cooled burner at 0.5 m·s⁻¹ (298 K). In addition, 174 stable species with molecular weights 68 to 180 were quantified by GC/MS.

Predictions of mole-fraction profiles using the temperature profile and mechanisms from the literature provide an unprecedented test of mechanisms against such a detailed set of data. While many general features were well-predicted, reaction-path analysis identified causes for serious discrepancies that occurred for some species with all mechanisms.

Bimolecular QRRK theory, a means of predicting rate constants of chemically activated addition reactions, has been refined and tested against measured rate constants in order to resolve some of these problems. By quantitatively explaining reaction kinetics for applications from H + O₂ chemistry to the formation process of benzene, bimolecular QRRK proves to be a powerful supplement to the more accurate but more parameter-rich RRKM theory.

It is proposed that all chemical reactions in combustion may be classified as one of three types: (I) H-atom metathesis, (II) chemically activated association, or (III) thermal isomerization. This insight comes from the modeling and theoretical studies, particularly from the general result, derived at the outset from bimolecular QRRK theory, that chemically activated addition/decomposition is pressure-independent in its low-pressure limit, not its high-pressure limit. Classifying literature mechanisms in this way shows that the majority of flame reactions are chemically activated associations.

Thesis Supervisors and Titles:

Dr. Jack B. Howard, Professor of Chemical Engineering
Dr. John P. Longwell, E. R. Gilliland Professor of Chemical
Engineering

ACKNOWLEDGMENTS

Kathleen Beach, my wife, has made my research and happiness possible more than anyone else, and to her I dedicate this dissertation. We have worked hard to keep a balance among the different aspects of our lives, and now that our son Nate has thrown any sense of balance out the window, we're happy together about that, too. I also thank my parents, Ray and Judy Westmoreland, for their love and help.

I am deeply grateful to Professors Jack B. Howard and John P. Longwell, my advisors, not only for their professional guidance but also for their support and personal kindnesses. The confidence in me and the good advice from Professor Adel Sarofim also have meant much. Each of these individuals has dealt with me as a colleague, which has made my time at MIT satisfying and productive. They have set remarkably good examples for the development of my own career and of others.

I am glad to have known two generations of co-workers among graduate students in the Fuels Research Laboratory and hope that I have passed on help to the current group, just as my predecessors did for me. Achieving the quality and breadth of the thesis projects of Jim Bittner and Barry Taylor would be worthy goals for anyone to aim for, but I value their friendships even more than their trail-blazing and their ample consulting to me. Cathryn Sundback, Sam Amponsah, and I have developed enormous affection for and faith in each other, which have been great sources of comfort and strength. Tom McKinnon, Craig Vaughn, Fred Lam, Bob Barat, Carl Wikstrom, and John Pope have helped me one-to-one and by taking part in our common project of lunches and self-instruction via 10.731. Thanks also go to Larry Monroe, (who knows the importance of good okra), Peter Walsh, Sue Faist, and Jerry Cole.

Sue Phillips, John Robinson, Mark Manton, Kate Sawallisch, Cathy Taylor, and Ellen Bolick have all been special friends to me.

I am pleased to have worked with some exceptional students through the UROP program and on B.S. theses. I very much appreciate

the contributions of Jim Oliver, Kathy Anderson, Ken Koehlert, and Ray Henry.

Gilles Prado and Annie Garo of CNRS/France have made valuable contributions to my work during their stays at MIT, Gilles to the 1-atm toluene flame work of my first year here and Annie to the modeling studies and final thesis preparation in my last year.

Kin Chiu, Art Lafleur, and Professor Klaus Biemann provided time on the GC/MS equipment and special output formats for me to use in interpreting the GC/MS results.

My work also has benefited directly from software shared with me by Bob Kee of Sandia National Laboratories, by Mitch Smooke of Yale University, and by Miguel Bibbo of this department. I thank still other generous members of the combustion community who have shared their ideas and their unpublished work with me, including Med Colket, Jean-Louis Delfau, Christian Vovelle, John Kiefer, Thomas Just, Fred Temps, Charlie Westbrook, Jacques Vandooren, and Wing Tsang.

Tony Dean of Exxon Research and Engineering generously shared his work on bimolecular QRRK at an early stage. I believe that our collaboration is producing significant insights into gas-phase chemistry, helping create a sound basis for the still-new area of mechanistic modeling of combustion.

Finally, I am particularly grateful to Exxon Research and Engineering Company, which has supported this work financially through the Exxon-MIT Combustion Research program.

TABLE OF CONTENTS

	<u>Page</u>
Abstract	2
Acknowledgments	3
Table of contents	5
List of figures	8
List of tables	10
 SUMMARY	
S.1 Introduction	20
S.2 Experimental measurements of fuel-rich flame structure	21
S.3 Critical evaluation of predictions by literature mechanisms	29
.1 Flame model and mechanisms	29
.2 General comparisons	31
.3 Analysis of reaction paths	33
S.4 Bimolecular QRRK and its application to combustion chemistry	42
.1 Principles, equations, and necessary input data	42
.2 Applications, including H+O ₂ and benzene formation	46
S.5 Conclusions	60
S.6 Recommendations	63
 CHAPTERS	
I. Introduction	65
.1 Overview	65
.2 Combustion as science and technology	65
.3 Recent progress in combustion chemistry	67
.4 Goals of this research	68
.5 Summary of the experimental approach	69
II. Literature on study of flat flames by MBMS	71
.1 Flat flames	71
.2 Molecular-beam mass spectrometry (MBMS)	74
III. Equipment and procedure	80
.1 Introduction	80
.2 Low-pressure flat-flame burner system	81
.3 Molecular-beam sampling, mass spectrometer, and calibration	84
.4 Temperature measurement	85
.5 Analysis of data	89
IV. Mole-fraction data and identification of species	92
.1 Introductory overview of data	92
.2 Comparisons with other data	97
.3 Discussion of MBMS data	99
.4 Analysis of heavy species by GC/MS	151
V. Tests of literature combustion mechanisms	156
.1 Introduction	156
.2 Flame model and mechanisms	156
.3 General comparisons	159
.4 Analysis of critical reaction paths	159
.5 Remarks on the other predictions	194
.6 Summary and conclusions	197

VI.	Equations for unimolecular and bimolecular QRRK	199
.1	General background	199
.2	Unimolecular reaction theory	201
.3	Unimolecular QRRK	206
.4	Bimolecular QRRK - Chemically activated decomposition ...	211
.5	Bimolecular QRRK with chemically activated isomerization	214
.6	Secondary decompositions of excited products	216
.7	Implications for reaction analysis	217
VII.	Tests and applications of Bimolecular QRRK	219
.1	Introduction	219
.2	Necessary input data	220
.3	Reactions of $H+O_2$, HO_2 , and $O+OH$	221
.4	Reactions of $H+C_2H_2$ and of $CH+^3CH_2$ via $C_2H_3^*$	230
.5	Reactions of $H+C_2H_3$, $H_2+C_2H_2$, and $^3CH_2+^3CH_2$	240
.6	Reactions of $H+C_2H_4$, $^3CH_2+CH_3$ and $^1CH_2+CH_3$	255
.7	Reaction of $O+CO \rightarrow CO_2$	262
.8	Conclusions	268
VIII.	Benzene formation in acetylene flames	272
.1	Introduction	272
.2	Literature mechanisms	273
.3	Preliminary screening	277
.4	Detailed calculation of rate constants and rates	281
.5	Re-interpretation of literature tests	292
.6	Rate constants for phenyl pyrolysis	294
.7	Summary	298
IX.	The three types of combustion reactions	299
X.	Conclusions and recommendations	312
.1	Conclusions	312
.2	Recommendations	315
APPENDICES		
Appendix A.	Directly measured and extrapolated temperatures	317
Appendix B.	List of files by species in acetylene flame ($\phi=2.4$)	318
Appendix C.	Mole-fraction data points	329
Appendix D.	Smoothed curves of mole fraction data	344
Appendix E.	Species fluxes and flux balances from flame data	359
E.1.	Molar fluxes of species	360
E.2.	Element and overall mass flux balances	374
Appendix F.	Net molar reaction rates of species from flame data	378
Appendix G.	Estimates of ionization potentials	393
Appendix H.	Summary of data from GC/MS analysis of sample V3650, tabulated by elution time (spectrum number)	397
Appendix I.	Summary of data from GC/MS analysis of sample V3650, tabulated by molecular weight	401
Appendix J.	Reaction mechanisms tested in Chapter V	405
J.1.	Reaction mechanism tested as MMSK	406
J.2.	Reaction mechanism tested as WB	409
J.3.	Reaction mechanism tested as WD	414
J.4.	Reaction mechanism tested as WZ	418

J.5.	Reaction mechanism tested as WZ' (reversible)	421
J.6.	Solution for MMSK	424
J.7.	Solution for WB	426
J.8.	Solution for WD	428
J.9.	Solution for WZ	432
J.10.	Solution for WZ'	434
Appendix K.	Summary of thermochemical properties	436
Appendix L.	QRRK computer programs and sample inputs	442
L.1.	BASIC program for bimolecular QRRK	443
L.2.	Example of input form for bimolecular QRRK	461
L.3.	BASIC program for unimolecular QRRK	463
L.4.	Example of input form for unimolecular QRRK	480
Appendix M.	Selection of $\langle \Delta E_{coll} \rangle$ from compiled data	482
Appendix N.	Estimation of rate constants for recombination of radicals	483
N.1.	Benson's formulation	483
N.2.	Estimation of β_1 for the present calculations	484
N.3.	Estimates of rate constants for Ch. VII	495
Appendix O.	Estimation of rate constants by thermochemical kinetics	499
O.1.	Rate constant for $C_2H_3 \rightarrow (\cdot HC=CH\text{---}H)^\ddagger$ [$\rightarrow C_2H_2+H$]	499
O.2.	Rate constant for $C_2H_4 \rightarrow (4\text{-centered})^\ddagger$ [$\rightarrow C_2H_2+H_2$]	499
O.3.	Rate constants for cyclization	501
	List of nomenclature	503
	Literature cited	505
	Biographical note	516

LIST OF FIGURES

	<u>Page</u>
Fig. S.1. Cross-section of the MBMS apparatus.	27
Fig. S.2. Concentration profiles of acetylene in flat flame. Points: data of present study (O) and of Bonne et al. (Δ). Curves: predictions using mechanisms of Miller, Mitchell, Smooke, and Kee (MMSK); Westbrook (WB); Westbrook and Dryer (WD); Warnatz (WZ); and reversible Warnatz (WZ').	32
Fig. S.3. H ₂ O predictions compared to data. Data points and curve labels defined in Fig. S.2.	34
Fig. S.4. CO ₂ predictions compared to data. Data points and curve labels defined in Fig. S.2.	35
Fig. S.5. Predictions of C ₂ H ₂ , C ₃ H ₃ , and C ₃ H ₄ compared to data. Data points and curve labels defined in Fig. S.2.	36
Fig. S.6. C ₄ H ₂ predictions compared to data. Data points and curve labels defined in Fig. S.2.	37
Fig. S.7. OH compared to data. Data points and curve labels defined in Fig. S.2.	38
Fig. S.8. C ₂ H ₃ predictions compared to data. Data points and curve labels defined in Fig. S.2.	39
Fig. S.9. Energy diagram for addition with a chemically activated decomposition channel.	44
Fig. S.10. Energy diagram for reactions of activated HO ₂	49
Fig. S.11. Rate constants for H+O ₂ → HO ₂ : (a) predicted fall-off curve (—) of the bimolecular rate constant with pressure at 298 K (M=Ar) compared to measurements (●) and to correlation by Troe's formalism (---) (Cobos et al., 1985a); (b) Arrhenius plot of the predicted low-pressure limit (—) for M=H ₂ compared with literature data (- - -, ···, O, and ●) and recom- mendation (— — —) from Warnatz (1984).	51
Fig. S.12. Predicted rate constant (—) for the chemically activated addition/decomposition reaction H+O ₂ → (HO ₂) [*] → O+OH compared with literature data (- - - - -, ···, X, and +) and recommendation (— — —) from Warnatz (1984) and with the predicted addition/stabilization rate constant for H+O ₂ → (HO ₂) [*] → HO ₂	52
Fig. S.13. Predicted rate constant (—) for O+OH → (HO ₂) [*] → H+O ₂ compared to literature data (- - - - -, X, O, and ●) and recommendation (— — —) from Warnatz (1984).	53
Fig. S.14. Energy diagram for the addition of 1-C ₄ H ₅ to C ₂ H ₂ . ..	55

Fig. S.15. Predicted rate constants for $1\text{-C}_4\text{H}_5 + \text{C}_2\text{H}_2$	58
Fig. S.16. Predicted rate constants for $1\text{-C}_4\text{H}_3 + \text{C}_2\text{H}_2$	59
Fig. S.17. Test of predicted rate of benzene formation against measured net rate of benzene formation.	61
Fig. III.1. Cross-section of the burner system.	83
Fig. III.2. Temperature data for laminar, premixed flame of $\text{C}_2\text{H}_2/\text{O}_2/5\% \text{ Ar}$, $\phi=2.40$, 2.67 kPa (20 torr), and $0.5 \text{ m}\cdot\text{s}^{-1}$ velocity of unburned gas (298 K).	88
Fig. IV.1. Profiles of temperature and of mole fractions for major stable species in the first 1.0 cm of a laminar, premixed flame of $\text{C}_2\text{H}_2/\text{O}_2/5\% \text{ Ar}$, $\phi=2.40$, 2.67 kPa (20 torr), and 0.5 $\text{m}\cdot\text{s}^{-1}$ velocity of unburned gas (298 K).	95
Fig. IV.2. Profiles of temperature and of mole fractions for major stable species in a laminar, premixed flame of $\text{C}_2\text{H}_2/\text{O}_2/5\%$ Ar , $\phi=2.40$, 2.67 kPa (20 torr), and $0.5 \text{ m}\cdot\text{s}^{-1}$ velocity of unburned gas (298 K).	96
Fig. IV.3. Mass flux balances on carbon, hydrogen, oxygen, and total mass flux.	98
Fig. IV.4. Data (\circ) and smoothed curve for H-atom in a laminar, premixed flame of $\text{C}_2\text{H}_2/\text{O}_2/5\% \text{ Ar}$, $\phi=2.40$, 2.67 kPa (20 torr), and $0.5 \text{ m}\cdot\text{s}^{-1}$ velocity of unburned gas (298 K).	101
Fig. IV.5. Data profile for H_2 (\circ) in a laminar, premixed flame of $\text{C}_2\text{H}_2/\text{O}_2/5\% \text{ Ar}$, $\phi=2.40$, 2.67 kPa (20 torr), and $0.5 \text{ m}\cdot\text{s}^{-1}$ velocity of unburned gas (298 K), compared to data of Bonne et al. (1965; Δ) in a $\text{C}_2\text{H}_2/\text{O}_2$, $\phi=2.38$ flame.	101
Fig. IV.6. Data profiles for CH_3 (\circ) and CH_4 (\diamond) in a laminar, premixed flame of $\text{C}_2\text{H}_2/\text{O}_2/5\% \text{ Ar}$, $\phi=2.40$, 2.67 kPa (20 torr), and $0.5 \text{ m}\cdot\text{s}^{-1}$ velocity of unburned gas (298 K). Also shown are CH_4 data of Bonne et al. (1965; \blacktriangle) in a $\text{C}_2\text{H}_2/\text{O}_2$, $\phi=2.38$ flame.	104
Fig. IV.7. Data (\circ) and smoothed curve for OH in a laminar, premixed flame of $\text{C}_2\text{H}_2/\text{O}_2/5\% \text{ Ar}$, $\phi=2.40$, 2.67 kPa (20 torr), and $0.5 \text{ m}\cdot\text{s}^{-1}$ velocity of unburned gas (298 K).	106
Fig. IV.8. Data profile for H_2O (\diamond) in a laminar, premixed flame of $\text{C}_2\text{H}_2/\text{O}_2/5\% \text{ Ar}$, $\phi=2.40$, 2.67 kPa (20 torr), and $0.5 \text{ m}\cdot\text{s}^{-1}$ velocity of unburned gas (298 K), compared to data of Bonne et al. (1965; Δ) in a $\text{C}_2\text{H}_2/\text{O}_2$, $\phi=2.38$ flame.	106

Fig. IV.9. Data profile for C_2H_2 (○) in a laminar, premixed flame of $C_2H_2/O_2/5\%$ Ar, $\phi=2.40$, 2.67 kPa (20 torr), and 0.5 $m \cdot s^{-1}$ velocity of unburned gas (298 K), compared to data of Bonne et al. (1965; Δ) in a C_2H_2/O_2 , $\phi=2.38$ flame.	109
Fig. IV.10. Data and smoothed curve for C_2H_3 (◇) in a laminar, premixed flame of $C_2H_2/O_2/5\%$ Ar, $\phi=2.40$, 2.67 kPa (20 torr), and 0.5 $m \cdot s^{-1}$ velocity of unburned gas (298 K).	109
Fig. IV.11. Data and smoothed curve for C_2H_4 (○) in a laminar, premixed flame of $C_2H_2/O_2/5\%$ Ar, $\phi=2.40$, 2.67 kPa (20 torr), and 0.5 $m \cdot s^{-1}$ velocity of unburned gas (298 K).	111
Fig. IV.12. Data profile for CO (○) in a laminar, premixed flame of $C_2H_2/O_2/5\%$ Ar, $\phi=2.40$, 2.67 kPa (20 torr), and 0.5 $m \cdot s^{-1}$ velocity of unburned gas (298 K), compared to data of Bonne et al. (1965; Δ) in a C_2H_2/O_2 , $\phi=2.38$ flame.	111
Fig. IV.13. Data and smoothed curve for mass 29 (○; apparently HCO) in a laminar, premixed flame of $C_2H_2/O_2/5\%$ Ar, $\phi=2.40$, 2.67 kPa (20 torr), and 0.5 $m \cdot s^{-1}$ velocity of unburned gas (298 K). .	113
Fig. IV.14. Data profile for mass 30 (○) in a laminar, premixed flame of $C_2H_2/O_2/5\%$ Ar, $\phi=2.40$, 2.67 kPa (20 torr), and 0.5 $m \cdot s^{-1}$ velocity of unburned gas (298 K), compared to data of Bonne et al. (1965; Δ) in a C_2H_2/O_2 , $\phi=2.38$ flame. Calibration assumes H_2CO , but H_2CO and C_2H_6 are apparently both present. ...	115
Fig. IV.15. Data profile for O_2 (○) in a laminar, premixed flame of $C_2H_2/O_2/5\%$ Ar, $\phi=2.40$, 2.67 kPa (20 torr), and 0.5 $m \cdot s^{-1}$ velocity of unburned gas (298 K), compared to data of Bonne et al. (1965; Δ) in a C_2H_2/O_2 , $\phi=2.38$ flame.	116
Fig. IV.16. Data (○) and smoothed curve for HO_2 in a laminar, premixed flame of $C_2H_2/O_2/5\%$ Ar, $\phi=2.40$, 2.67 kPa (20 torr), and 0.5 $m \cdot s^{-1}$ velocity of unburned gas (298 K).	116
Fig. IV.17. Data profiles for C_3H_2 (○), C_3H_3 (◇), and C_3H_4 (□) in a laminar, premixed flame of $C_2H_2/O_2/5\%$ Ar, $\phi=2.40$, 2.67 kPa (20 torr), and 0.5 $m \cdot s^{-1}$ velocity of unburned gas (298 K). Also shown are C_3H_4 data of Bonne et al. (1965; \blacktriangle) in a C_2H_2/O_2 , $\phi=2.38$ flame.	119
Fig. IV.18. Data curve for Ar in a laminar, premixed flame of $C_2H_2/O_2/5\%$ Ar, $\phi=2.40$, 2.67 kPa (20 torr), and 0.5 $m \cdot s^{-1}$ velocity of unburned gas (298 K).	122
Fig. IV.19. Data (○) and smoothed curve for HCCO in a laminar, premixed flame of $C_2H_2/O_2/5\%$ Ar, $\phi=2.40$, 2.67 kPa (20 torr), and 0.5 $m \cdot s^{-1}$ velocity of unburned gas (298 K).	122

Fig. IV.20. Data profile for mass 42 (○) in a laminar, premixed flame of C ₂ H ₂ /O ₂ /5% Ar, ϕ=2.40, 2.67 kPa (20 torr), and 0.5 m·s ⁻¹ velocity of unburned gas (298 K), compared to data of Bonne et al. (1965; Δ) in a C ₂ H ₂ /O ₂ , ϕ=2.38 flame. Calibration assumes CH ₂ CO.	124
Fig. IV.21. Data profile for CO ₂ (○) in a laminar, premixed flame of C ₂ H ₂ /O ₂ /5% Ar, ϕ=2.40, 2.67 kPa (20 torr), and 0.5 m·s ⁻¹ velocity of unburned gas (298 K), compared to data of Bonne et al. (1965; Δ) in a C ₂ H ₂ /O ₂ , ϕ=2.38 flame.	124
Fig. IV.22. Data profile for C ₄ H ₂ (○) in a laminar, premixed flame of C ₂ H ₂ /O ₂ /5% Ar, ϕ=2.40, 2.67 kPa (20 torr), and 0.5 m·s ⁻¹ velocity of unburned gas (298 K), compared to data of Bonne et al. (1965; Δ) in a C ₂ H ₂ /O ₂ , ϕ=2.38 flame.	126
Fig. IV.23. Data (○) and smoothed curve for C ₄ H ₃ in a laminar, premixed flame of C ₂ H ₂ /O ₂ /5% Ar, ϕ=2.40, 2.67 kPa (20 torr), and 0.5 m·s ⁻¹ velocity of unburned gas (298 K).	126
Fig. IV.24. Data profile for C ₄ H ₄ (○) in a laminar, premixed flame of C ₂ H ₂ /O ₂ /5% Ar, ϕ=2.40, 2.67 kPa (20 torr), and 0.5 m·s ⁻¹ velocity of unburned gas (298 K), compared to data of Bonne et al. (1965; Δ) in a C ₂ H ₂ /O ₂ , ϕ=2.38 flame.	129
Fig. IV.25. Data (○) and smoothed curve for C ₄ H ₅ in a laminar, premixed flame of C ₂ H ₂ /O ₂ /5% Ar, ϕ=2.40, 2.67 kPa (20 torr), and 0.5 m·s ⁻¹ velocity of unburned gas (298 K).	129
Fig. IV.26. Data (○) and smoothed curve for C ₄ H ₆ in a laminar, premixed flame of C ₂ H ₂ /O ₂ /5% Ar, ϕ=2.40, 2.67 kPa (20 torr), and 0.5 m·s ⁻¹ velocity of unburned gas (298 K).	131
Fig. IV.27. Data (○) and smoothed curve for C ₅ H ₂ in a laminar, premixed flame of C ₂ H ₂ /O ₂ /5% Ar, ϕ=2.40, 2.67 kPa (20 torr), and 0.5 m·s ⁻¹ velocity of unburned gas (298 K).	132
Fig. IV.28. Data (◇) and smoothed curve for C ₅ H ₃ in a laminar, premixed flame of C ₂ H ₂ /O ₂ /5% Ar, ϕ=2.40, 2.67 kPa (20 torr), and 0.5 m·s ⁻¹ velocity of unburned gas (298 K).	134
Fig. IV.29. Data (◇) and smoothed curve for C ₅ H ₄ in a laminar, premixed flame of C ₂ H ₂ /O ₂ /5% Ar, ϕ=2.40, 2.67 kPa (20 torr), and 0.5 m·s ⁻¹ velocity of unburned gas (298 K).	135
Fig. IV.30. Data (○) and smoothed curve for C ₅ H ₅ in a laminar, premixed flame of C ₂ H ₂ /O ₂ /5% Ar, ϕ=2.40, 2.67 kPa (20 torr), and 0.5 m·s ⁻¹ velocity of unburned gas (298 K).	137
Fig. IV.31. Data (○) and smoothed curve for C ₅ H ₆ in a laminar, premixed flame of C ₂ H ₂ /O ₂ /5% Ar, ϕ=2.40, 2.67 kPa (20 torr), and 0.5 m·s ⁻¹ velocity of unburned gas (298 K).	138

Fig. IV.32. Data profile for C_6H_2 (\circ) in a laminar, premixed flame of $C_2H_2/O_2/5\%$ Ar, $\phi=2.40$, 2.67 kPa (20 torr), and $0.5\text{ m}\cdot\text{s}^{-1}$ velocity of unburned gas (298 K), compared to data of Bonne et al. (1965; Δ) in a C_2H_2/O_2 , $\phi=2.38$ flame.	140
Fig. IV.33. Data (\circ) and smoothed curve for C_6H_4 in a laminar, premixed flame of $C_2H_2/O_2/5\%$ Ar, $\phi=2.40$, 2.67 kPa (20 torr), and $0.5\text{ m}\cdot\text{s}^{-1}$ velocity of unburned gas (298 K).	141
Fig. IV.34. Data (\circ) and smoothed curve for C_6H_5 in a laminar, premixed flame of $C_2H_2/O_2/5\%$ Ar, $\phi=2.40$, 2.67 kPa (20 torr), and $0.5\text{ m}\cdot\text{s}^{-1}$ velocity of unburned gas (298 K).	143
Fig. IV.35. Data (\circ) and smoothed curve for C_6H_6 in a laminar, premixed flame of $C_2H_2/O_2/5\%$ Ar, $\phi=2.40$, 2.67 kPa (20 torr), and $0.5\text{ m}\cdot\text{s}^{-1}$ velocity of unburned gas (298 K).	145
Fig. IV.36. Data (\circ) and smoothed curve for C_8H_2 in a laminar, premixed flame of $C_2H_2/O_2/5\%$ Ar, $\phi=2.40$, 2.67 kPa (20 torr), and $0.5\text{ m}\cdot\text{s}^{-1}$ velocity of unburned gas (298 K).	147
Fig. IV.37. Data (\circ) and smoothed curve for C_8H_6 in a laminar, premixed flame of $C_2H_2/O_2/5\%$ Ar, $\phi=2.40$, 2.67 kPa (20 torr), and $0.5\text{ m}\cdot\text{s}^{-1}$ velocity of unburned gas (298 K).	149
Fig. IV.38. Data (\circ) and smoothed curve for $C_{10}H_2$ in a laminar, premixed flame of $C_2H_2/O_2/5\%$ Ar, $\phi=2.40$, 2.67 kPa (20 torr), and $0.5\text{ m}\cdot\text{s}^{-1}$ velocity of unburned gas (298 K).	150
Fig. V.1. Concentration profiles of acetylene in flat flame. Data (\circ) and predicted curves using predictions using mechanisms of Miller, Mitchell, Smooke, and Kee (MMSK, - - - -); Westbrook (WB, - - - - -); Westbrook and Dryer (WD, — — —); Warnatz (WZ, ———); and reversible Warnatz (WZ', - - -).	160
Fig. V.2. H predictions compared to data. Data points and curve labels defined in Fig. V.1.	161
Fig. V.3. H_2 predictions compared to data. Data points and curve labels defined in Fig. V.1.	162
Fig. V.4. CH predictions compared to upper limits of data (∇). Curve labels defined in Fig. V.1.	163
Fig. V.5. CH_2 predictions compared to upper limit of data (∇) and data point (\circ). Curve labels defined in Fig. V.1.	164
Fig. V.6. CH_3 predictions compared to data. Data points and curve labels defined in Fig. V.1.	165
Fig. V.7. CH_4 predictions compared to data. Data points and curve labels defined in Fig. V.1.	166

Fig. V.8. Predictions of O-atom. Curve labels defined in Fig. V.1.	167
Fig. V.9. OH predictions compared to data. Data points and curve labels defined in Fig. V.1.	168
Fig. V.10. H ₂ O predictions compared to data (O). Curve labels defined in Fig. V.1.	169
Fig. V.11. C ₂ H predictions compared to data points from this study (O) and from Bonne, Homann, and Wagner (1965; Δ). Curve labels defined in Fig. V.1.	170
Fig. V.12. C ₂ H ₃ predictions compared to data: (top) linear scale for mole fraction, (bottom) logarithmic scale. Data points and curve labels defined in Fig. V.1.	171
Fig. V.13. C ₂ H ₄ predictions compared to data. Data points and curve labels defined in Fig. V.1.	172
Fig. V.14. CO predictions compared to data. Data points and curve labels defined in Fig. V.1.	173
Fig. V.15. Prediction of profiles for mass 29, treating data as HCO and combining predictions of HCO and C ₂ H ₅ to HCO equivalents using MBMS calibration factors.	174
Fig. V.16. Predictions of profiles for mass 29 species: (top) predictions of HCO and data treated as being exclusively HCO and (bottom) predictions of C ₂ H ₅ and data treated as being exclusively C ₂ H ₅	175
Fig. V.17. Prediction of profiles for mass 30, treating data as H ₂ CO and combining predictions of H ₂ CO and C ₂ H ₆ to H ₂ CO equivalents using MBMS calibration factors. Data points and curve labels defined in Fig. V.1.	176
Fig. V.18. Predictions of profiles for mass 30 species: (top) predictions of H ₂ CO and data treated as being exclusively H ₂ CO and (bottom) predictions of C ₂ H ₆ and data treated as being exclusively C ₂ H ₆	177
Fig. V.19. Predictions of CH ₃ O and CH ₂ OH profiles. Curve labels defined in Fig. V.1; curve types for CH ₃ O are - · - · - (WB), — — — (WD), - - - (MMSK) and for CH ₂ OH are — — — (WD) and - - - (WB).	178
Fig. V.20. O ₂ predictions compared to data (O). Curve labels defined in Fig. V.1.	179
Fig. V.21. HO ₂ predictions compared to data (O). Curve labels defined in Fig. V.1.	180

Fig. V.22. Predictions of H_2O_2 . Curve labels defined in Fig. V.1.	181
Fig. V.23. Predictions of C_3H_2 , C_3H_3 , and C_3H_4 compared to data. Data points and curve labels defined in Fig. V.1.	182
Fig. V.24. Ar predictions compared to data from mass balance (heavy solid line). Curve labels defined in Fig. V.1.	183
Fig. V.25. Predictions of mass 41 compared to data (\circ), which are treated as HCCO: (top) scale emphasizing HCCO predictions and (bottom) expanded scale emphasizing C_3H_5 predictions. Curve labels defined in Fig. V.1.	184
Fig. V.26. Predictions of CH_2CO and C_3H_6 compared to data for mass 42 (\circ), treated as CH_2CO . Curve labels defined in Fig. V.1.	185
Fig. V.27. CO_2 predictions compared to data (\circ). Curve labels defined in Fig. V.1.	186
Fig. V.28. C_4H_2 predictions compared to data (\circ). Curve labels defined in Fig. V.1.	187
Fig. V.29. C_4H_2 predictions compared to data (\circ). Curve labels defined in Fig. V.1.	188
Fig. V.30. C_4H_6 predictions compared to data (\circ and —). Curve labels defined in Fig. V.1.	189
Fig. V.31. C_6H_2 predictions compared to data (\circ). Curve labels defined in Fig. V.1.	190
Fig. VI.1. Energy diagram for unimolecular decomposition.	205
Fig. VI.2. Energy diagram for addition with a chemically activated decomposition channel.	212
Fig. VII.1. Energy diagram for $H+O_2 / HO_2 / O(^3P)+OH$. Units are mol, cm, s, kJ.	223
Fig. VII.2. Predicted low-pressure limit k_0 (—) for $H+O_2+M \rightarrow HO_2+M$, $M=H_2$, compared with literature data (---, ..., \circ , and \bullet) and recommendation (— — —) from Warnatz (1984).	225
Fig. VII.3. Predicted fall-off curve (—) for $H+O_2 \rightarrow HO_2$ in Ar at 298 K compared to measurements (\bullet) and to correlation by Troe's formalism (---) (Cobos et al., 1985a).	226

- Fig. VII.4. Predicted rate constant (—) for the chemically activated addition/decomposition reaction $\text{H} + \text{O}_2 \rightarrow (\text{HO}_2)^* \rightarrow \text{O} + \text{OH}$ compared with literature data (---, ···, χ , and \times) and recommendation (— — —) from Warnatz (1984) and with the predicted addition/stabilization rate constant for $\text{H} + \text{O}_2 \rightarrow (\text{HO}_2)^* \rightarrow \text{HO}_2$ 227
- Fig. VII.5. Predicted rate constant (—) for $\text{O} + \text{OH} \rightarrow (\text{HO}_2)^* \rightarrow \text{H} + \text{O}_2$ compared to literature data (---, χ , \circ , and \bullet) and recommendation (— — —) from Warnatz (1984). Prediction uses estimated $k_{\infty}(\text{O} + \text{OH} \rightarrow \text{HO}_2) = 2.0 \cdot 10^{13} \text{ cm}^3 \text{ mol}^{-1} \text{ s}^{-1}$ 228
- Fig. VII.6. Fall-off curves for $\text{H} + \text{C}_2\text{H}_2$ addition at 298 K in He, including data (χ , \square) with error bars, RRKM prediction (—), and QRRK prediction (— — —). 235
- Fig. VII.7. Low-pressure-limit rate constants k_0 for thermal decomposition of C_2H_2 ($\text{M} = \text{Ar}$). Predictions by unimolecular QRRK using $k_{\infty, 298}$ (····) and a more appropriate $k_{\infty, 1660}$ (—), compared to data (— — —, \square) from Warnatz (1984). 236
- Fig. VII.8. Predictions of the bimolecular rate constant for $\text{H} + \text{C}_2\text{H}_2 \rightarrow \text{C}_2\text{H}_3$ at 2.67 and 100 kPa (20 torr and 1 atm) compared with k_{∞} and the rate constant for pressure-independent abstraction. 237
- Fig. VII.9. Predictions of the rate constants and branching for the reactions of $\text{CH} + ^3\text{CH}_2 \rightarrow \text{C}_2\text{H}_2 + \text{H}$ and $\text{C}_2\text{H} + \text{H}_2$ at 2.67 kPa, $\text{M} = \text{CO}$. Dotted line is fit of $\text{AT}^b \exp(-\text{C}/\text{T})$ to the $\text{C}_2\text{H}_2 + \text{H}$ channel. 239
- Fig. VII.10. Energy diagram for $\text{H} + \text{C}_2\text{H}_3$ combination and chemically activated decomposition to $\text{C}_2\text{H}_2 + \text{H}_2$ 241
- Fig. VII.11. Predictions of rate constants for thermal decomposition $\text{C}_2\text{H}_4 + \text{M} \rightarrow \text{products} + \text{M}$ compared to the data of Just, Roth, and Damm (1977) [JRD ·····] and of Tanzawa and Gardiner (1980) [TG — — —]. Pressure 2.8 atm, $\text{M} = \text{Ar}$. Predictions differ by the use of different estimates for $k_{\infty}(\text{C}_2\text{H}_4 \rightarrow \text{C}_2\text{H}_2 + \text{H}_2)$: — by Tsang and Hampson (1985) and — — — from Appendix O using the method of Benson and Haugen (1967). 245
- Fig. VII.12. Predictions of fall-off curves at 2000 K, $\text{M} = \text{Ar}$, for thermal decomposition $\text{C}_2\text{H}_4 \rightarrow \text{C}_2\text{H}_2 + \text{H}_2$ and $\text{C}_2\text{H}_3 + \text{H}$ compared to the data of Just, Roth, and Damm (1977) [JRD: \times and \square] and of Tanzawa and Gardiner (1980) [TG: \times and \blacksquare]. Predictions differ by the use of different estimates for $k_{\infty}(\text{C}_2\text{H}_4 \rightarrow \text{C}_2\text{H}_2 + \text{H}_2)$: — by Tsang and Hampson (1985) and — — — from Appendix O using the method of Benson and Haugen (1967). Pressure dependence of $\text{C}_2\text{H}_4 \rightarrow \text{C}_2\text{H}_2 + 2\text{H}$ also shown. 246

Fig. VII.13. Predictions at 0.01 to 10 atm compared to data for $\text{H}+\text{C}_2\text{H}_3 \rightarrow \text{C}_2\text{H}_2+\text{H}_2$. Data: Skinner et al. (1971) [SSD - -]; Tanzawa and Gardiner (1980) [TG - -]; Benson and Haugen (1967) [BH est. - -]; Volpi and Zocci (1966) [VZ \square]; Keil et al. (1976) [KLCM \square]; and Hoyermann (1981) [H \square]. M=Ar.	248
Fig. VII.14. Predictions at 0.01 to 10 atm for $\text{H}+\text{C}_2\text{H}_3 \rightarrow \text{C}_2\text{H}_4$, M=Ar.	249
Fig. VII.15. Comparison of predicted rate constants for $\text{H}+\text{C}_2\text{H}_3 \rightarrow \text{C}_2\text{H}_4$, $\text{C}_2\text{H}_2+\text{H}_2$, and overall at conditions of the present flame: 400 to 1900 K, M=CO, and 2.67 kPa (20 torr).	252
Fig. VII.16. Predicted branching of rate constants for $^3\text{CH}_2+^3\text{CH}_2$ to $\text{C}_2\text{H}_2+\text{H}_2$ and $\text{C}_2\text{H}_2+2\text{H}$ product channels; 400 to 1900 K, M=CO, and 2.67 kPa (20 torr).	254
Fig. VII.17. Energy diagram for $\text{H}+\text{C}_2\text{H}_4$ addition and abstraction (energies in kJ/mol except where stated otherwise).	256
Fig. VII.18. QRRK prediction (solid line) of the low-pressure limit k_0 for $\text{C}_2\text{H}_5 \rightarrow \text{H}+\text{C}_2\text{H}_4$ compared to data (- - -): Lin and Back (1966) [LB], Loucks and Laidler (1967) [LL], and Glänzer and Troe (1973) [GT]. Recommendation of Warnatz (1984) also shown (— — —).	258
Fig. VII.19. Predictions of rate constants for $\text{H}+\text{C}_2\text{H}_4$ addition at 2.67 kPa in CO; metathesis reaction to $\text{H}_2+\text{C}_2\text{H}_3$ and resulting overall rate constant for $\text{H}+\text{C}_2\text{H}_4$ also shown for reference. .	260
Fig. VII.20. Predictions and data for $^3\text{CH}_2+\text{CH}_3 \rightarrow \text{H}+\text{C}_2\text{H}_4$: Laufer and Bass (1975) [LB \square], Pilling and Robertson (1975) [PR \blacksquare], Laufer (1981) [LB(L) \square and PR(L) \square], and Olson and Gardiner [OG - -]. Dashed line is QRRK prediction using $k_{\infty}(^3\text{CH}_2+\text{CH}_3 \rightarrow \text{C}_2\text{H}_5)$ estimated from steric factors; solid line uses the mean of LB(L) and LB(PR) as an improved estimate of k_{∞}	261
Fig. VII.21. Predictions for $^1\text{CH}_2+\text{CH}_3 \rightarrow \text{H}+\text{C}_2\text{H}_4$, $\rightarrow ^3\text{CH}_2+\text{CH}_3$, and overall.	263
Fig. VII.22. Energy diagram for $\text{O}(^3\text{P})+\text{CO} \rightarrow \text{CO}_2$ (energies in kJ/mol except where stated otherwise).	265
Fig. VII.23. Comparison of QRRK predictions (solid lines) to data (- - -, \cdots , +, X; Warnatz, 1984) for rate constants of $\text{O}(^3\text{P})+\text{CO} \rightarrow \text{CO}_2$	267
Fig. VIII.1. Energy diagram for addition of $1-\text{C}_4\text{H}_5 + \text{C}_2\text{H}_2$	285
Fig. VIII.2. Predictions at 2.67 kPa (20 torr) of bimolecular rate constants for product channels of $1-\text{C}_4\text{H}_5 + \text{C}_2\text{H}_2$	287
Fig. VIII.3. Predictions at 101 kPa (1 atm) of bimolecular rate constants for product channels of $1-\text{C}_4\text{H}_5 + \text{C}_2\text{H}_2$	288

Fig. VIII.4. Predictions at 2.67 kPa (20 torr) of bimolecular rate constants for product channels of $1\text{-C}_4\text{H}_3 + \text{C}_2\text{H}_2$	290
Fig. VIII.5. Predictions at 101 kPa (1 atm) of bimolecular rate constants for product channels of $1\text{-C}_4\text{H}_3 + \text{C}_2\text{H}_2$	291
Fig. VIII.6. Comparison of the predicted rates for $1\text{-C}_4\text{H}_5 + \text{C}_2\text{H}_2 \rightarrow \text{H} + \text{benzene}$ and for $1\text{-C}_4\text{H}_3 + \text{C}_2\text{H}_2 \rightarrow \text{phenyl}$ to the net rate of benzene formation measured at 2.67 kPa in a $\phi=2.40 \text{ C}_2\text{H}_2/\text{O}_2/5\% \text{ Ar}$ flame, temperatures increasing from 900 to 1600 K in this region.	293
Fig. VIII.7. Predictions of rate constants for product channels of phenyl pyrolysis at 101 kPa (1 atm).	296
Fig. VIII.8. Comparison of predicted rate constants for phenyl pyrolysis to literature values of Colket (1986) [— — — — —], Fujii and Asaba (1973) [— — — FA], Kiefer et al. [— — — KMPW] (1985), and Rao and Skinner (1984) [— — — RS].	297

LIST OF TABLES

	<u>Page</u>
Table S.1. Summary of species in the low-pressure C ₂ H ₂ /O ₂ /Ar flame (ϕ=2.40, 5% Ar, 2.67 kPa, 0.5 m/s burner velocity at 298 K).	22
Table S.2. Rate constants calculated by QRRK methods for 400-1900 K, M=CO, and 2.67 kPa (20 torr).	48
Table S.3. Parameters needed for bimolecular QRRK calculations for 1-C ₄ H ₅ + C ₂ H ₂ reactions via the chemically activated intermediates <i>l</i> -C ₆ H ₇ * and <i>c</i> -C ₆ H ₇ *.	56
Table S.4. Parameters needed for bimolecular QRRK calculations for 1-C ₄ H ₃ + C ₂ H ₂ reactions via the chemically activated intermediates <i>l</i> -C ₆ H ₅ * and <i>c</i> -C ₆ H ₅ *.	57
Table II.1. Flat-flame/MBMS studies of C/H/O flames.	76
Table III.1. Mass-discrimination factors α(i,Ar).	90
Table IV.1. Summary of species measured by molecular-beam mass spectrometry in ϕ=2.40 C ₂ H ₂ /O ₂ /5% Ar flame, 50 cm·s ⁻¹ at 298 K.	93
Table IV.2. Summary of species detected by GC/MS.	152
Table VII.1. Parameters needed for bimolecular QRRK calculation in the system of reactions involving H+O ₂ , HO ₂ , and O+OH.	224
Table VII.2. Parameters needed for QRRK calculations in the reactions involving C ₂ H ₃ * as a chemically activated intermediate: H+C ₂ H ₂ → C ₂ H ₃ and ² CH+ ³ CH ₂ → products.	231
Table VII.3. Data and estimates for k _∞ of H+C ₂ H ₂ → C ₂ H ₃	232
Table VII.4. Parameters needed for QRRK calculations for the potential-energy surface of C ₂ H ₄ involving H+C ₂ H ₃ , H ₂ +C ₂ H ₂ , and ³ CH ₂ + ³ CH ₂	242
Table VII.5. Parameters needed for QRRK calculations for the potential-energy surface of C ₂ H ₅ involving H+C ₂ H ₄ , ³ CH ₂ +CH ₃ , and ¹ CH ₂ +CH ₃	257
Table VII.6. Parameters needed for QRRK calculations for the potential-energy surface of CO ₂ involving CO+O(³ P).	266
Table VII.7. Components of the rate constant for O(³ P)+CO → CO ₂ in its low-pressure limit k ₀ , which is the sum over energy of (Numerator/Denominator)·f(E,T). Units: cm, mol, s.	269
Table VII.8. Rate constants calculated by QRRK methods for 400-1900 K, M=CO, and 2.67 kPa (20 torr).	271

Table VIII.1. Literature mechanisms for forming aromatics. Single carbon-carbon bonds illustrated by —, double bonds by =, triple bonds by ≡; H implied in structures and reactions but not shown.	274
Table VIII.2. Testing literature mechanisms for benzene formation using k_{∞} for the initial addition/combination step. ..	280
Table VIII.3. Parameters needed for bimolecular QRRK calcula- tions for $l\text{-C}_4\text{H}_5 + \text{C}_2\text{H}_2$ reactions via the chemically activated intermediates $l\text{-C}_6\text{H}_7^*$ and $c\text{-C}_6\text{H}_7^*$ (mol, cm, s, kcal units).	283
Table VIII.4. Parameters needed for bimolecular QRRK calcula- tions for $l\text{-C}_4\text{H}_3 + \text{C}_2\text{H}_2$ reactions via the chemically activated intermediates $l\text{-C}_6\text{H}_5^*$ and $c\text{-C}_6\text{H}_5^*$ (mol, cm, s, kcal units).	284
Table IX.1. Types of reactions in the Warnatz mechanism (Warnatz, 1983).	301
Table O.1. Calculation of Arrhenius constants for the reaction $\text{C}_2\text{H}_2 \rightarrow (\cdot\text{CH}=\text{CH}---\text{H})\ddagger \rightarrow \text{HC}\equiv\text{CH}+\text{H}$	500

SUMMARY

S.1. Introduction

Chemistry in flames is complicated (1) by the critical role of free radicals, which are difficult to measure; (2) by the large number of species and reactions, which may have highly nonlinear interactions; and (3) by the elementary reactions themselves, for which rate constants may be unknown or poorly known. Knowledge about fuel-rich combustion is especially limited, yet this condition is unavoidable in diffusion flames, the type of flame that is used most commonly. The consequences of fuel-rich combustion are very important in practice because they can be desirable (e.g., generating heat-radiating soot in furnaces) or undesirable (e.g., generating chemicals that are health hazards).

The ability to model flame structure of laminar, premixed hydrocarbon flames was demonstrated by Warnatz (1981). Since then, computer programs that take a chemical mechanism and predict concentration profiles have become widely available. Consequently, the main needs are for better sets of kinetics of the elementary reactions and for detailed data to test these mechanisms.

Several mechanisms for fuel-rich combustion have been proposed, most notably by Levy et al. (1983), by Miller et al. (1983), by Warnatz (1983; Warnatz et al. 1983), by Westbrook et al. (1983 and Westbrook, 1983), and by Westbrook and Dryer (1984). These mechanisms generally have been tested against measured profiles of concentration but, at fuel-rich conditions, only for a few stable species (Miller et al., 1983; Warnatz, 1983) and for H-atom in the post-flame region (Levy et al., 1983). Many features of the profiles were well-predicted, and quantitative agreement was a factor of two or better. To improve and verify their performance, more complete testing and examination of the mechanisms is necessary.

The present research addresses many of the needs described above. Specifically:

- (1) Detailed concentration and temperature data were measured in a lightly sooting, low-pressure flat flame of acetylene, the principal hydrocarbon in fuel-rich combustion.

(2) With these data, detailed comparisons have been made for the first time between the predictions of reaction networks and a complete set of mole fraction data, identifying how the predictions succeed or break down by using reaction-path analysis, a novel but simple type of sensitivity analysis.

(3) Rate constants for addition reactions and their non-Arrhenius temperature and pressure dependences are predicted by bimolecular quantum-RRK theory (bimolecular QRRK), a newly developed extension of unimolecular reaction theory. Examples include oxidation reactions of small species, such as $H + O_2 \rightarrow HO_2$ or $O + OH$, and molecular weight growth, such as the formation of benzene by chemically activated addition/isomerization/decomposition starting from $C_2H_2 + 1-C_4H_3$ and C_4H_5 , which are tested with the flame data.

(4) Finally, the chemical reactions of combustion can be categorized broadly for the first time as abstraction, chemically activated addition/recombination, or thermal isomerization/decomposition reactions.

S.2. Experimental measurements of fuel-rich flame structure

Concentration profiles of 38 stable and free-radical species were measured using molecular-beam mass spectrometry (MBMS) in a low-pressure, premixed acetylene-oxygen flame ($\phi=2.40$). The conditions were chosen to be similar to one of the flames ($\phi=2.38$) in the pioneering MBMS study of Bonne, Homann, and Wagner (1965). In addition, point concentrations or upper limits were measured for 20 more species, and 174 stable species of molecular weights 68 to 180 were measured by microprobe sampling and GC/MS (Table S.1).

The flat-flame burner, molecular-beam sampling system, in-line quadrupole mass spectrometer (Fig. S.1), and techniques of species identification and measurement have been described previously (Bittner, 1981; Cole, 1982) and were used with minor modifications. Flame conditions were 2.67 kPa (20 mm Hg), burner velocity of $0.5 \text{ m}\cdot\text{s}^{-1}$ at 298 K, and a feed gas ($\phi=2.40$) of 46.5 mol % C_2H_2 , 48.5 % O_2 , and 5.0 % Ar. The area expansion ratio at a distance Z (cm) from the burner was taken from previous measurements (Bittner, 1981) to be

Table S.1. Summary of species measured in $\phi=2.40$ $C_2H_2/O_2/5\%$ Ar flame, $50\text{ cm}\cdot\text{s}^{-1}$ at 298 K.

<u>Mass Species</u>	<u>Profile or point by MBMS; or GC/MS</u>	<u>Maximum mole fraction [or point value]</u>	<u>Calibration uncertainty</u>
1 H atom	Profile	0.018, 0.41 cm	Factor of 2
2 H ₂	Profile	Asymptote of 0.183	$\pm 16\%$
13 CH	Point	[$\leq(0.6\pm 2.1)10^{-6}, 0.141\text{ cm};$ $\leq(0\pm 1.5)10^{-5}, 0.276\text{ cm};$ $\leq(0\pm 9)10^{-6}, 0.363\text{ cm}]$	
14 CH ₂	Point	[$\leq(1.1\pm 4.8)10^{-6}, 0.141\text{ cm};$ $3.2\cdot 10^{-4}, 0.363\text{ cm}]$	
15 CH ₃	Profile	$4.7\cdot 10^{-3}, 0.36\text{ cm}$	$\pm 50\%$
16 CH ₄	Profile	$3.7\cdot 10^{-3}, 0.18\text{ cm}^*$	$\pm 3\%$
17 OH	Profile	$9.7\cdot 10^{-4}, 0.41\text{ cm}$	$\pm 50\%$
18 H ₂ O	Profile	0.14, 0.61 cm	$\pm 25\%$
25 C ₂ H	Point	[$(6.6\pm 3.7)10^{-6}, 0.103\text{ cm};$ $4\cdot 10^{-6}, 0.161\text{ cm}]$	
26 C ₂ H ₂	Profile	Minimum of 0.06 at 3.35 cm*	$\pm 3\%$
27 C ₂ H ₃	Profile	$1.9\cdot 10^{-4}, 0.46\text{ cm}^*$	$\pm 50\%$
28 C ₂ H ₄	Profile	$7.8\cdot 10^{-4}, 0.27\text{ cm}^*$	$\pm 50\%$
28 CO	Profile	Asymptote of 0.537	$\pm 3\%$
29 HCO (and C ₂ H ₅ ?)	Profile	$6.0\cdot 10^{-5}, 0.38\text{ cm}$	$\pm 50\%$
30 H ₂ CO, some C ₂ H ₆	Profile	$1.0\cdot 10^{-3}, <0.01\text{ cm}$	$\pm 50\%$
32 O ₂	Profile	Asymptotic minimum of $3\cdot 10^{-4}$	$\pm 3\%$
33 HO ₂	Profile	$3.2\cdot 10^{-4}, 0.04\text{ cm}$	$\pm 50\%$
34 H ₂ O ₂	Point	[$5\cdot 10^{-5}, 0.176\text{ cm}]$	
36 C ₃	Point	[$\leq(5\pm 9)\cdot 10^{-6}, 0.294\text{ cm}]$	
37 C ₃ H	Point	[$\ll 3\cdot 10^{-5}, 0.294\text{ cm}]$	

<u>Mass Species</u>	<u>Type of data</u>	<u>Maximum mole fraction [or point value]</u>	<u>Calibration uncertainty</u>
38 C ₃ H ₂	Profile	1.94 · 10 ⁻⁴ , 0.56 cm	±50%
39 C ₃ H ₃ (propargyl)	Profile	1.02 · 10 ⁻³ , 0.37 cm	±50%
40 C ₃ H ₄ (propyne and propadiene)	Profile	9.8 · 10 ⁻⁴ , 0.21 cm*	±50%
40 Ar	Profile	Monotonic decrease from 0.050 to 0.040	±10%
41 HCCO, some C ₃ H ₅	Profile	4 · 10 ⁻⁵ , 0.35 cm	±50%
42 CH ₂ CO (and C ₃ H ₆ ?)	Profile	7.2 · 10 ⁻⁴ , 0.14 cm	±50%
43 CH ₃ CO and/or C ₃ H ₇	Point	[≤(0.1±1.2) · 10 ⁻⁵ , 0.294 cm]	
44 CH ₃ CHO and/or C ₃ H ₈	Point	[≤(6±4) · 10 ⁻⁵ , 0.039 cm; ≤(0.9±2) · 10 ⁻⁵ , 0.294 cm]	
44 CO ₂	Profile	0.086, 0.70 cm	± 3%
49 C ₄ H	Point	[≤(2±3) · 10 ⁻⁶ , 0.32 cm]	
50 C ₄ H ₂ (butadiyne)	Profile	9.7 · 10 ⁻³ , 0.65 cm	±50%
51 C ₄ H ₃	Profile	2 · 10 ⁻⁵ , 0.43 cm	Factor of 2
52 C ₄ H ₄ (3-butenyne)	Profile	1.8 · 10 ⁻⁴ , 0.31 cm*	±50%
53 C ₄ H ₅	Profile	9.7 · 10 ⁻⁶ , 0.22 cm	±50%
54 C ₄ H ₆ (1,3-butadiene)	Profile	5.0 · 10 ⁻⁵ , 0.17 cm*	±50%
56 C ₄ H ₈ (one or more dimethylenes)	Point	[1.5 · 10 ⁻⁶ , 0.318 cm]	
62 C ₅ H ₂	Profile	1.8 · 10 ⁻⁵ , 0.65 cm	±50%
63 C ₅ H ₃	Profile	5.5 · 10 ⁻⁵ , 0.46 cm	±50%
64 C ₅ H ₄	Profile	6 · 10 ⁻⁵ , 0.36 cm	±50%
65 C ₅ H ₅ (and C ₄ HO?)	Profile	1.8 · 10 ⁻⁵ , 0.39 cm	±50%
66 C ₅ H ₆ (3-pentenyne) and/or C ₄ H ₂ O	Profile	4.6 · 10 ⁻⁵ , 0.23 cm*	±50%
68 C ₅ H ₈ or C ₄ H ₄ O	GC/MS	[8 · 10 ⁻⁶ , 0.45 cm]	
73 C ₆ H	Point	[≤(0.8±3) · 10 ⁻⁶ , 0.544 cm]	

<u>Mass Species</u>	<u>Type of data</u>	<u>Maximum mole fraction [or point value]</u>	<u>Calibration uncertainty</u>
74 C ₆ H ₂ (hexatriyne)	Profile GC/MS	1.3·10 ⁻³ , 0.70 cm [7·10 ⁻⁴ , 0.45 cm]	±50%
76 C ₆ H ₄	Profile GC/MS	5.2·10 ⁻⁵ , 0.45 cm* [4·10 ⁻⁵ , 0.45 cm]	±50%
77 C ₆ H ₅	Profile	1·10 ⁻⁶ , 0.2 cm	Factor of 3
78 C ₆ H ₆ Benzene 3 other C ₆ H ₆ 's	Profile GC/MS GC/MS	4.0·10 ⁻⁵ , 0.28 cm* [2·10 ⁻⁵ , 0.45 cm] [8·10 ⁻⁶ , 0.45 cm]	±50%
79 C ₆ H ₇ and/or C ₅ H ₃ O	Point	[≤1·10 ⁻⁶ , 0.544 cm]	
80 C ₆ H ₈ and/or C ₅ H ₄ O	Point	[≤5·10 ⁻⁷ , 0.544 cm]	
81 C ₆ H ₉ and/or C ₅ H ₅ O	Point	[≤5·10 ⁻⁸ , 0.544 cm]	
88 C ₇ H ₄ (5 species)	GC/MS	[5·10 ⁻⁷ , 0.45 cm]	
90 C ₇ H ₆ (12 species)	GC/MS	[4·10 ⁻⁷ , 0.45 cm]	
91 C ₇ H ₇	Point	[≤1.3·10 ⁻⁶ , 0.395 cm]	
92 C ₇ H ₈ Toluene 9 other species	Point GC/MS GC/MS	[4·10 ⁻⁷ , 0.45 cm] [3·10 ⁻⁷ , 0.45 cm] [5·10 ⁻⁸ , 0.45 cm]	
94 Phenol (C ₆ H ₅ OH) C ₇ H ₁₀ or other C ₆ H ₆ O	GC/MS GC/MS	[7·10 ⁻⁷ , 0.45 cm] [9·10 ⁻⁹ , 0.45 cm]	
96 C ₇ H ₁₂ or C ₆ H ₈ O	GC/MS	[1·10 ⁻⁸ , 0.45 cm]	
98 C ₈ H ₂ Octatetrayne	Profile GC/MS	7.4·10 ⁻⁵ , 0.68 cm [2·10 ⁻⁵ , 0.45 cm]	±50%
100 C ₈ H ₄	GC/MS	[7·10 ⁻⁷ , 0.45 cm]	
102 C ₈ H ₆ Phenylacetylene 13 other mass 102 (C ₈ H ₆ , C ₇ H ₄ O)	Profile GC/MS GC/MS	3.3·10 ⁻⁶ , 0.35 cm [2·10 ⁻⁶ , 0.45 cm] [7·10 ⁻⁷ , 0.45 cm]	±50%
104 C ₈ H ₈ Styrene 16 other mass 104 (C ₈ H ₈ , C ₇ H ₆ O)	Point GC/MS GC/MS	[<2·10 ⁻⁷ , 0.395 cm] [4·10 ⁻⁷ , 0.45 cm] [3·10 ⁻⁷ , 0.45 cm]	

Mass	Species	Type of data	Maximum mole fraction [or point value]	Calibration uncertainty
106	Ethylbenzene	GC/MS	[$3 \cdot 10^{-7}$, 0.45 cm]	
	m- and/or p-Xylene	GC/MS	[$4 \cdot 10^{-8}$, 0.45 cm]	
	o-Xylene	GC/MS	[$2 \cdot 10^{-8}$, 0.45 cm]	
	Benzaldehyde	GC/MS	[$4 \cdot 10^{-8}$, 0.45 cm]	
	4 more C_8H_{10} , C_7H_8O	GC/MS	[$7 \cdot 10^{-8}$, 0.45 cm]	
108	Benzyl alcohol	GC/MS	[$8 \cdot 10^{-8}$, 0.45 cm]	
	o-Cresol	GC/MS	[$4 \cdot 10^{-8}$, 0.45 cm]	
	Other C_7H_8O	GC/MS	[$2 \cdot 10^{-8}$, 0.45 cm]	
112	C_9H_4	GC/MS	[$5 \cdot 10^{-8}$, 0.45 cm]	
114	C_9H_8 (4 species)	GC/MS	[$2 \cdot 10^{-7}$, 0.45 cm]	
116	Indene	GC/MS	[$1 \cdot 10^{-6}$, 0.45 cm]	
	8 more C_9H_8 , C_8H_4O	GC/MS	[$2 \cdot 10^{-7}$, 0.45 cm]	
118	C_9H_{10} or C_8H_6O (5)	GC/MS	[$3 \cdot 10^{-8}$, 0.45 cm]	
120	C_9H_{12} or C_8H_8O (3)	GC/MS	[$2 \cdot 10^{-8}$, 0.45 cm]	
122	$C_{10}H_2$	Profile	$7.3 \cdot 10^{-6}$, 0.78 cm	$\pm 50\%$
126	$C_{10}H_8$	Point	[$\leq (1 \pm 1) \cdot 10^{-6}$, 0.395 cm]	
	Butadiynylbenzene	GC/MS	[$2 \cdot 10^{-7}$, 0.45 cm]	
	3 diethynylbenzenes	GC/MS	[$2 \cdot 10^{-7}$, 0.45 cm]	
	Other $C_{10}H_8$	GC/MS	[$9 \cdot 10^{-9}$, 0.45 cm]	
128	$C_{10}H_8$	Point	[$4.7 \cdot 10^{-7}$, 0.395 cm]	
	Naphthalene	GC/MS	[$7 \cdot 10^{-7}$, 0.45 cm]	
	$C_{10}H_8$ or C_9H_4O (8)	GC/MS	[$2 \cdot 10^{-7}$, 0.45 cm]	
130	$C_{10}H_{10}$ or C_9H_6O (15)	GC/MS	[$6 \cdot 10^{-7}$, 0.45 cm]	
132	$C_{10}H_{12}$ or C_9H_8O (3)	GC/MS	[$4 \cdot 10^{-8}$, 0.45 cm]	
134	$C_{10}H_{10}$ or C_9H_6O (1)	GC/MS	[$1 \cdot 10^{-8}$, 0.45 cm]	
136	$C_{10}H_{12}$ or C_9H_8O (1)	GC/MS	[$1 \cdot 10^{-7}$, 0.45 cm]	
140	$C_{11}H_8$ (4 species)	GC/MS	[$1 \cdot 10^{-7}$, 0.45 cm]	
142	2-methylnaphthalene	GC/MS	[$8 \cdot 10^{-8}$, 0.45 cm]	
	1-methylnaphthalene	GC/MS	[$7 \cdot 10^{-8}$, 0.45 cm]	
	Other $C_{11}H_{10}$	GC/MS	[$7 \cdot 10^{-8}$, 0.45 cm]	
144	$C_{11}H_{12}$ or $C_{10}H_{10}O$ (4)	GC/MS	[$7 \cdot 10^{-7}$, 0.45 cm]	
150	$C_{12}H_8$ (2 species)	GC/MS	[$2 \cdot 10^{-8}$, 0.45 cm]	

<u>Mass Species</u>	<u>Type of data</u>	<u>Maximum mole fraction [or point value]</u>	<u>Calibration uncertainty</u>
152 C ₁₂ H ₈	Point	[$(5 \pm 5) \cdot 10^{-7}$, 0.395 cm]	
Acenaphthylene	GC/MS	[$4 \cdot 10^{-7}$, 0.45 cm]	
C ₁₂ H ₈ (2)	GC/MS	[$8 \cdot 10^{-8}$, 0.45 cm]	
154 C ₁₂ H ₁₀ or C ₁₁ H ₈ O (6)	GC/MS	[$9 \cdot 10^{-8}$, 0.45 cm]	
156 C ₁₂ H ₁₂ or C ₁₁ H ₈ O (7)	GC/MS	[$5 \cdot 10^{-8}$, 0.45 cm]	
166 C ₁₃ H ₁₀ or C ₁₂ H ₈ O (3)	GC/MS	[$6 \cdot 10^{-8}$, 0.45 cm]	
178 C ₁₄ H ₁₀ or C ₁₃ H ₈ O (1)	GC/MS	[$1 \cdot 10^{-7}$, 0.45 cm]	
180 C ₁₄ H ₁₂ or C ₁₃ H ₈ O (4)	GC/MS	[$2 \cdot 10^{-8}$, 0.45 cm]	

* Species that had a maximum but also, at a greater distance from the burner, had a minimum followed by a steady rise to the end of the measurement region (4.0 cm).

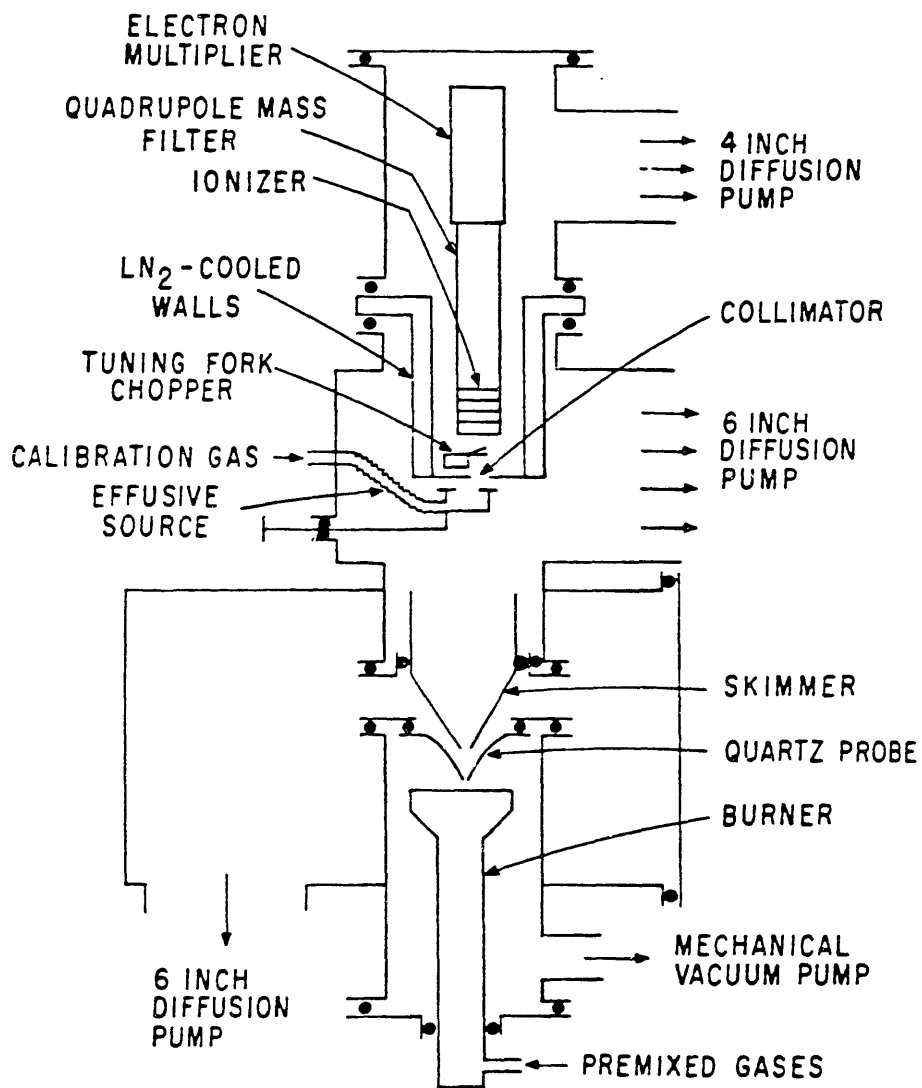


Fig. S.1. Cross-section of the MBMS apparatus.

$A(Z)=(1 - 0.116 \cdot Z)^{-1}$. The flame was sampled with a conical quartz nozzle of 0.55-mm orifice diameter, 40° tip, and 90° body.

Calibration was direct for H₂, CH₄, C₂H₂, CO, O₂, Ar, and CO₂; indirect for H₂O using an O-atom balance in the post-flame gas; and indirect for minor stable species and free radicals by the method of relative ionization cross-sections (Lazzara et al., 1973). Experimental uncertainties were nominally ±3%, ±10%, and ±50% for the three methods, respectively.

The temperature profile was measured using Pt/Pt-13%Rh thermocouples coated with BeO-Y₂O₃ (after Kent, 1970). The junction between the 0.076-mm-diam. wires was butt-welded with no detectable change in diameter. Temperatures close to and far from the burner were low enough that the resistive-heating method could be used. At intermediate positions, temperatures of the unheated thermocouple were corrected for radiation losses using an emissivity $\epsilon=0.38$ determined from the resistive-heating measurements.

Selected profiles are shown in Section 3.2 where mechanism predictions are evaluated. The full set of data extends the work of Bonne et al. (1965) by being sufficiently complete as to allow calculation of fluxes and reaction rates. In comparison, profiles for the nine stable species shown by Bonne et al. agree well both in shape and magnitude with the previous measurements even though the previous flame was Ar-free and presumably higher in temperature. (No temperatures were reported by Bonne et al., but recent temperature profiles by Delfau and Vovelle (1984a) suggest a maximum of 2100 K for Bonne et al., vs. 1900 K here.)

Only three profiles of radical mole fractions were reported in the previous study (CH₃, HCO, and C₂H), and all three apparently were erroneous. Mole fractions in the present study were much lower. The difference is apparently the result of fragmentation of stable species in the mass-spectrometer ionizer in the earlier work, based on a series of experiments with varied ionizing energies and on the comments of Homann (1984).

Biordi et al. (1974) and Stepowski et al. (1981) measured the perturbation of MBMS profiles from true profiles. Except very near the burner, the perturbation was effectively a shift of approximately

two nozzle diameters from the burner surface. Accordingly, the data presented here are translated 1.1 mm toward the burner relative to the height of probe tip above the burner.

S.3. Critical evaluation of predictions by literature mechanisms

S.3.1. Flame model and mechanisms

The flame code used here is a boundary-value method (Smooke, 1982) which uses the chemical-kinetics subroutine package CHEMKIN (Kee et al., 1980) and a related transport-properties package (Kee et al., 1983) which includes both molecular and thermal diffusion. Experimental profiles of area expansion ratio and temperature were used in the calculations, leaving reaction kinetics as the focus of this analysis.

Mechanisms of Miller et al. (1983), Warnatz (1983), Westbrook (1983), and Westbrook and Dryer (1984) were tested in addition to a modification of the Warnatz mechanism to make all the reactions reversible. These will be designated in the discussion and figures as MMSK, WZ, WB, WD, and WZ', respectively. The mechanism of Levy et al. (1983) was not tested because of its limitation to 1 atm pressure and to temperatures of 1992 to 2126 K.

For all but WZ, the mechanisms have not been tested before for an acetylene flame at such fuel-rich conditions. Our intent is to test each mechanism as faithfully as possible to the original authors' descriptions. Previous ranges of testing, restrictions, and the types of adaptations should be noted accordingly:

(1) Mechanism MMSK has been tested for C_2H_2 oxidation in low-pressure flames ($\phi=0.09$ to 1.56) and in shock tubes (Miller et al., 1983). In developing their mechanism, Miller et al. carefully examined CH_2 , C_2H , and HCCO reactions. Reactions of alkenes, alkyl radicals, and alkanes were not included except for CH_3 and C_3H_4 , based on the assumption that these species were unimportant to the overall results at the tested conditions. They expressed fall-off in a Lindemann form for three reactions, which is fitted here to the semi-Arrhenius form $[AT^b \exp(-E/RT)]$ at 2.67 kPa. Rate constants for reactions in the reverse direction are calculated from thermodynamics using reversibility.

(2) The mechanism of Warnatz (WZ) was based on a review of rate constants for elementary reactions (Warnatz, 1984). It has been tested against data for fuel-lean and fuel-rich flames and for shock-tube experiments (Warnatz et al., 1983). Here, WZ is the form of the mechanism specified by Warnatz (1983), with reverse reactions included only for some reactions and their rate constants stated explicitly. Fall-off curves (Warnatz, 1984) for seven of the reactions are used here to fit semi-Arrhenius rate constants. Finally, the rate constant of $3 \cdot 10^{13} \text{ cm}^3 \text{ mol}^{-1} \text{ s}^{-1}$ used by Warnatz for $\text{OH} + \text{C}_4\text{H}_2$ (and $\text{OH} + \text{C}_6\text{H}_2$) was interpreted consistently with his description for C_2H_2 as forming H and a ketene-like species, the latter being destroyed by "fast reaction" with OH to form H, 2CO, and C_2H_2 (or C_4H_2). An extreme value of $10^{14} \text{ cm}^3 \text{ mol}^{-1} \text{ s}^{-1}$ was used for the second OH reaction.

(3) The WZ mechanism was modified here as WZ' to include reverse rate constants from thermodynamics for any two-product reactions that were not reversible in WZ.

(4) Westbrook, Dryer, and Schug (1983) tested a mechanism for ethylene oxidation ($\phi=0.125$) and pyrolysis at 1-12 atm. All reactions are stated as the high- or low-pressure limit for addition or pyrolysis, and rate constants are reported explicitly for forward and reverse directions. An updated tabulation by Westbrook (1983) is used here as mechanism WB.

(5) Westbrook and Dryer (1984) compiled 335 rate constants from the above mechanisms and other data in their recent survey of combustion chemistry. No tests of this reaction set were presented. Fall-off is acknowledged but not included in the tabulated values, and reactions are stated as reversible. Mechanism WD is selected from this compilation.

Differences in thermodynamic data could make the mechanisms used here different from the versions of the original authors because rate constants for the implicitly reversible reactions are calculated using microscopic reversibility. Where this calculation was made, thermodynamics were taken from the Sandia compilation (Kee et al., 1984) with the modifications of $\Delta H_f^\circ, 298 = 135 \text{ kcal/mol}$ for C_2H , 70.4

kcal/mol for C_2H_3 (McMillen and Golden, 1982), and 4.2 kcal/mol for HO_2 (Howard, 1980).

Some species could be predicted but not measured, while others were measured but are not listed in the mechanisms. As examples, CH , CH_2 , and O-atom (obscured at mass 16 by CH_4) were too low in concentration to be detected, and profiles for mass 29 and 30 were measured but HCO/C_2H_5 and H_2CO/C_2H_6 were not resolvable. However, no mechanisms included C_4H_4 , C_4H_5 , C_5 species, C_6H_4 , C_6H_5 , C_6H_6 , and C_7 or heavier species, which were detected in the flame by MBMS and/or GC/MS.

Methylene chemistry is especially misunderstood, as no existing mechanism takes the fundamental distinctions between triplet methylene (3CH_2) and singlet methylene (1CH_2) into account. Ground-state 3CH_2 is quite reactive, but electronically excited 1CH_2 is even more reactive to many species and can be an appreciable fraction of the total CH_2 . Furthermore, 3CH_2 reacts by abstraction and by radical addition, while 1CH_2 inserts into σ and π bonds.

S.3.2. General comparisons

Twenty-five of the measured profiles were used as tests for the above mechanisms. As observed at other conditions, profile shapes and magnitudes for major stable species are usually in approximate agreement with the data (within a factor of two in mole fraction). The predictions from WZ' are good or satisfactory for more species than from MMSK, WB, WD, or WZ, and all of the mechanisms give poor predictions for some species.

The profile for C_2H_2 (Fig. S.2) illustrates the differences among predictions. The mole fraction of C_2H_2 at 4 cm was 4.5% experimentally, while the predictions vary from 2.5 to 9.7%. (For reference, the data of Bonne et al. (1965) are included.) The predictions vary from the data by more than this factor of two for other species, notably for the C_3 's. MMSK and WD make predictions for C_3H_2 , C_3H_3 , and C_3H_4 that are one to two orders of magnitude higher than the data.

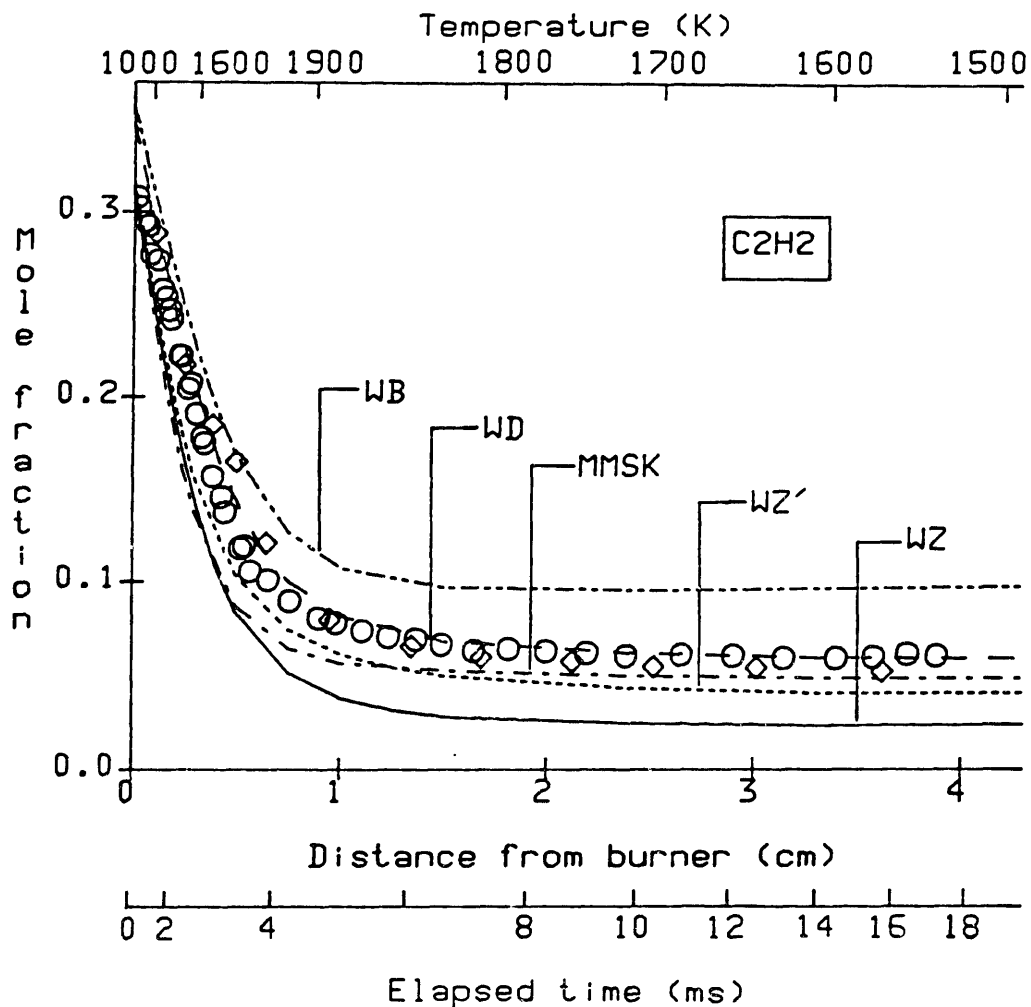


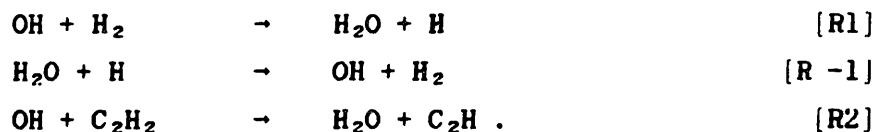
Fig. S.2. Concentration profiles of acetylene in flat flame. Points: data of present study (\circ) and of Bonne et al. (\diamond). Curves: predictions using mechanisms of Miller, Mitchell, Smooke, and Kee (MMSK); Westbrook (WB); Westbrook and Dryer (WD); Warnatz (WZ); and reversible Warnatz (WZ').

S.3.3. Analysis of reaction paths

Certain deficiencies in the mechanisms that are especially important can be identified by analyzing the profiles of H₂O, CO₂, C₃'s, C₄H₂, OH, and C₂H₃ (Figs. S.3 to S.8), which vary in shape and in magnitude from the data.

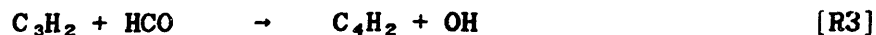
The technique of sensitivity analysis that gave the most insight will be called reaction-path analysis. In it, reaction rates for the predicted profiles are compared in order to identify sources and sinks for a species of interest. These calculations included (1) the net rate of species formation for each reaction, (2) the actual rate of formation or destruction by each forward or reverse step, expressed both absolutely and as a fraction of the sum of formation (or destruction) rates at a position, and (3) the cumulative amount of formation or destruction, obtained by integrating the product of reaction rate and A(Z) over distance.

H₂O. - The WZ mechanism gave the best predictions of shape and magnitude for H₂O (Fig. S.3). Reactions involving H₂O in this mechanisms are dominated by



H₂O is formed primarily by Rxn. 1. with a small contribution from Rxn. 2. The maximum occurs when destruction by Rxn. -1 balances formation. Throughout the flame, Rxn. 1/-1 is never predicted to reach partial equilibrium (net rate less than 5% of the forward or reverse rate).

Among the other mechanisms, H₂O in WZ' is slightly less than in WZ beyond 0.4 cm because the reverse of Rxn. 2 is included, which then causes 48% of the destruction. MMSK overpredicts H₂O by overpredicting OH, thus producing H₂O too rapidly to be destroyed. Overproduction of OH was caused by



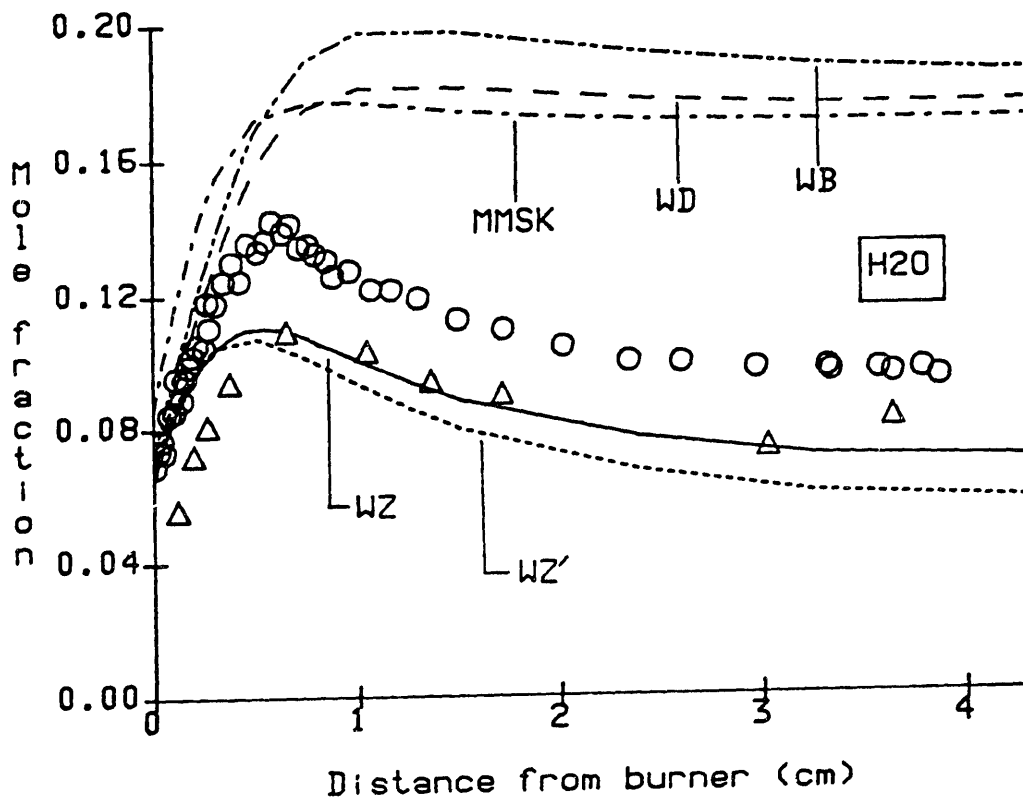


Fig. S.3. H₂O predictions compared to data. Data points and curve labels defined in Fig. S.2.

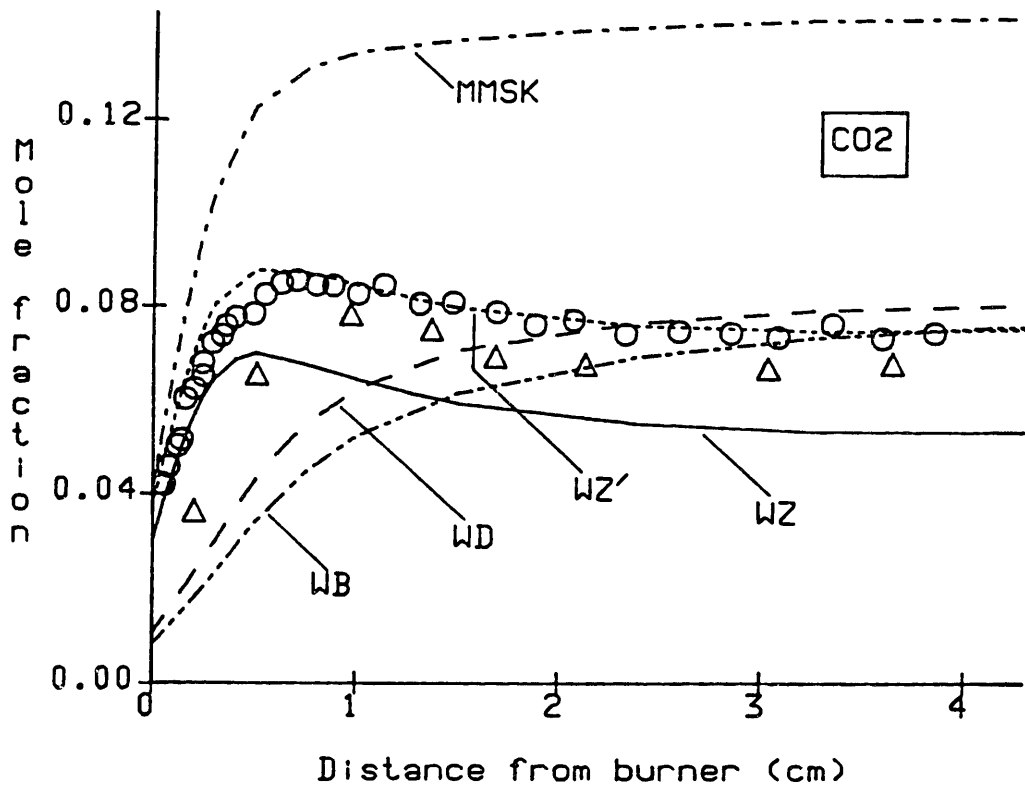


Fig. S.4. CO₂ predictions compared to data. Data points and curve labels defined in Fig. S.2.

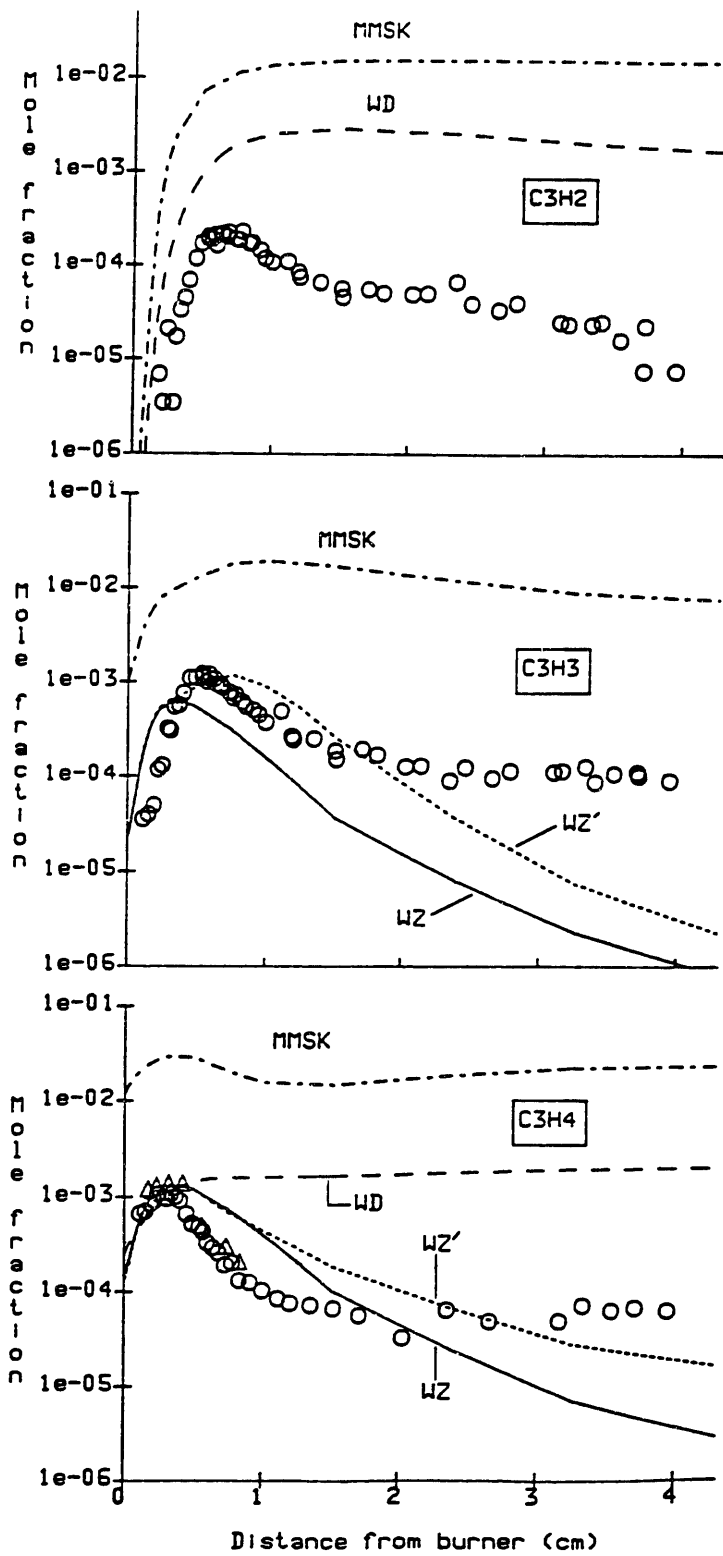


Fig. S.5. Predictions of C_3H_2 , C_3H_3 , and C_3H_4 compared to data. Data points and curve labels defined in Fig. S.2.

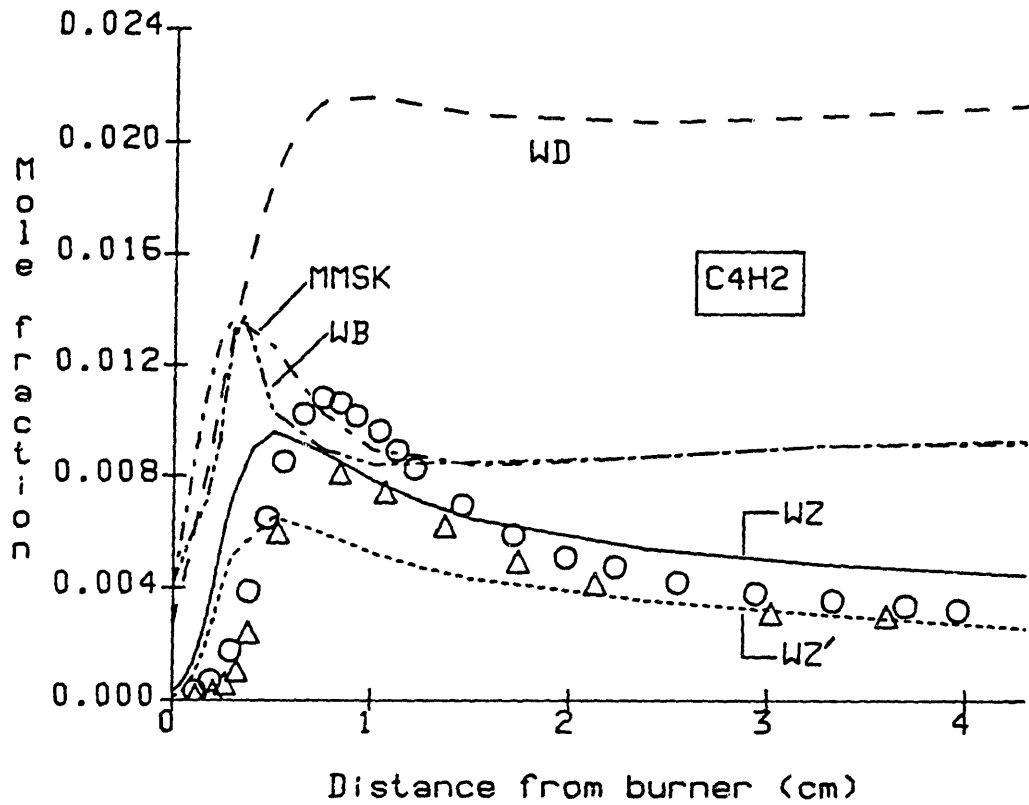


Fig. S.6. C_4H_2 predictions compared to data. Data points and curve labels defined in Fig. S.2.

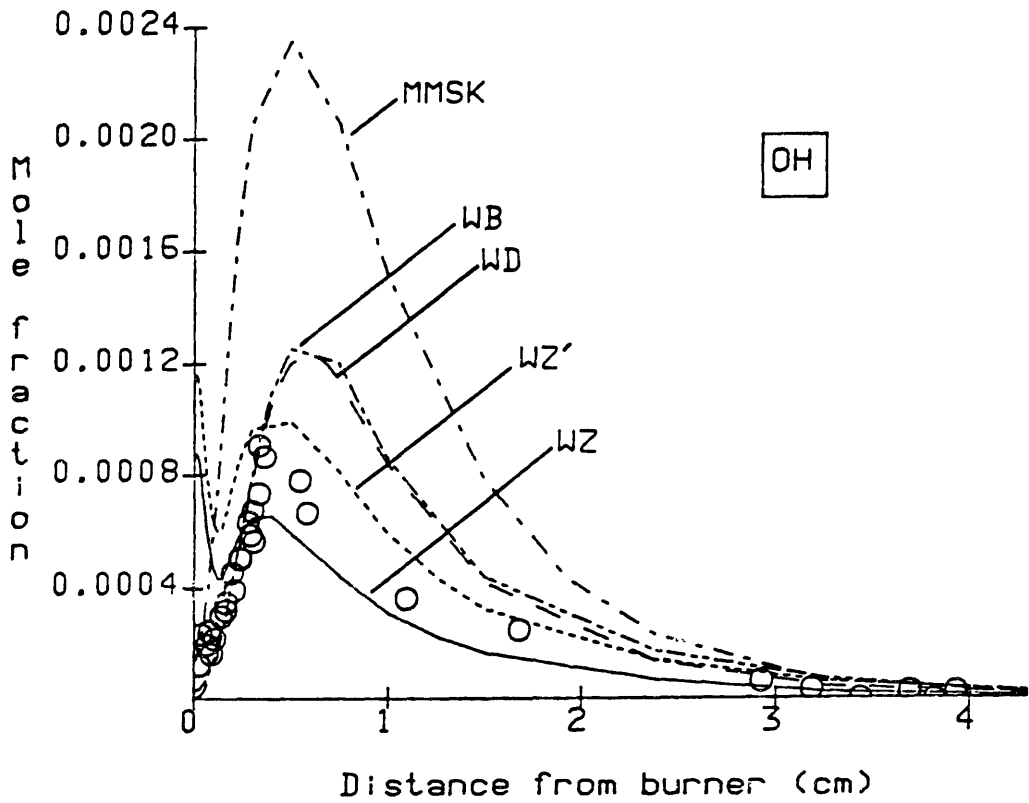


Fig. S.7. OH compared to data. Data points and curve labels defined in Fig. S.2.

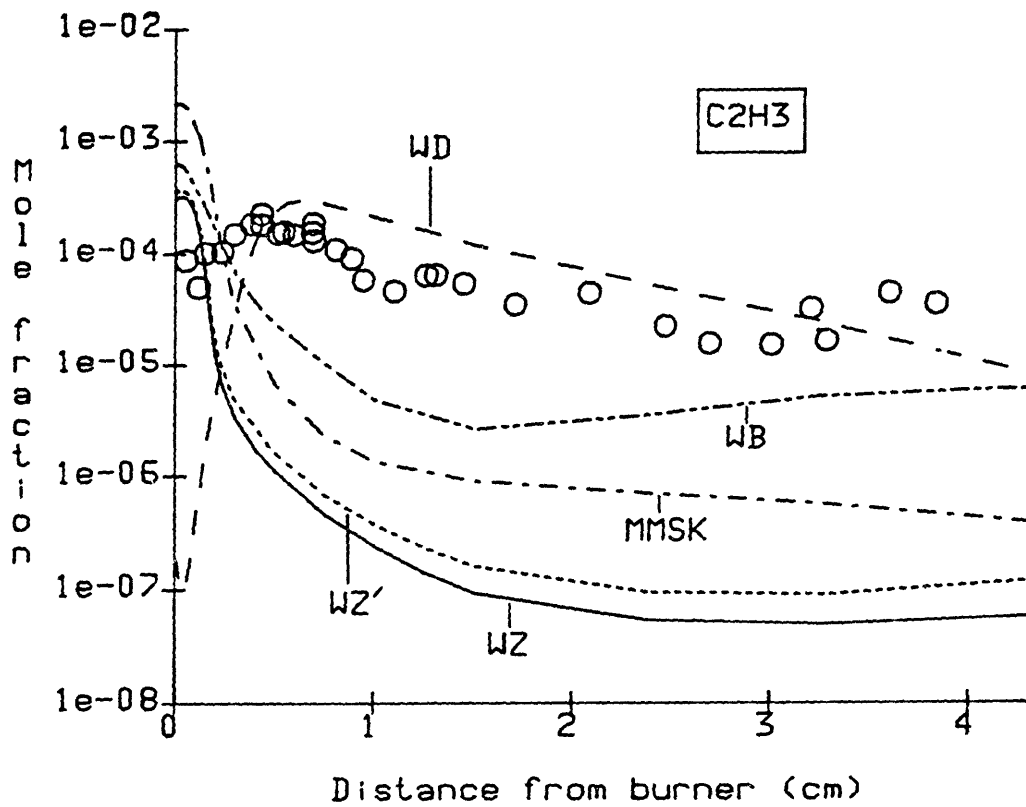


Fig. S.8. C₂H₃ predictions compared to data. Data points and curve labels defined in Fig. S.2.

which is discussed below in more detail.

WB and WD also overpredict H_2O . WB underpredicts H because there is no H-producing $CH_2 + O_2$ channel, so H_2O is formed but Rxn. -1 is too slow to destroy it. WD has such a CH_2 channel, but H is still underpredicted.

CO₂. - The only important destruction reaction for CO_2 (Fig. S.4) in the mechanisms is



but formation by the reverse reaction is supplemented in all but WB by one or both of the $CH_2 + O_2$ reactions:



The peak in the CO_2 predictions of WZ and WZ' is caused by destruction (Rxn. 4) overtaking formation by a combination of Rxns. -4 and 6. WZ' predicts higher CO_2 concentration because CH_2 is slightly higher than in the WZ case.

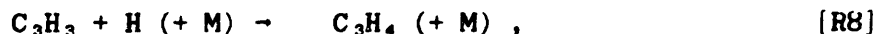
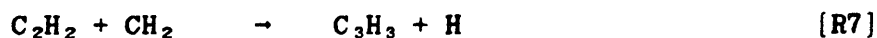
Destruction of CO_2 never exceeds formation in MMSK, WD, or WB, so no maximum occurs. MMSK and WD use both Rxns. 5 and 6 with somewhat different rate constants than in WZ and WZ'. The reactions cause an overproduction of CO_2 in MMSK but make little CO_2 in WD because CH_2 is higher than in WZ or WZ' by a factor of ten in MMSK, while it is lower by the same factor in WD. WB can only produce CO_2 by Rxn. 4, causing it to gradually accumulate.

C_3H_2 , C_3H_3 , C_3H_4 , and C_4H_2 . - The large overprediction of C_3 species (Fig. S.5) by the MMSK and WD mechanisms affects many other species, in part by tying up so much carbon. This effect on other species is not observed in the other mechanisms because WB did not include any C_3 's, while the predictions of WZ and WZ' for C_3H_3 and C_3H_4 are much lower and closer to the magnitude of the data (C_3H_2 was not included).

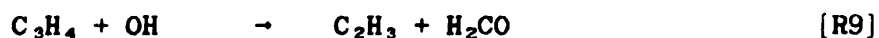
C_3H_2 is produced from C_4H_2 by OH attack (Rxn. -3) in MMSK and by an O-atom attack in WD. Because no C_3H_2 destruction reactions are

included except for the reverse of its formation paths, C_3H_2 builds up to excessive levels. This blocks the destruction of C_4H_2 in WD (Fig. S.6) and causes the overproduction of H_2O in MMSK.

Similarly, C_3H_3 and C_3H_4 are produced in MMSK predominantly by the sequence:



but C_3H_4 is not destroyed effectively, causing a build-up of those species. WD does not include C_3H_3 , but C_3H_4 reaches 0.2% at 0.4 cm (a reasonable value) and then changes little, in contrast to decaying by 95% as seen in the data. The dominant C_3H_4 destruction reactions in WD are:

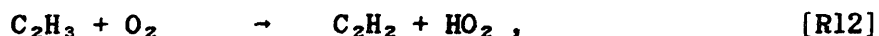


each with a rate constant of $1.0 \cdot 10^{12} \text{ cm}^3\text{mol}^{-1}\text{s}^{-1}$, but neither reaction is predicted to destroy C_3H_4 effectively.

OH. - An interesting anomaly in the OH predictions (Fig. S.7) is a secondary maximum predicted by WZ and WZ' near the burner. Formation of OH in WZ and WZ' is dominated near the burner by:



but the rate constant for this reaction is not the source of error; it is approximately the same for all the mechanisms examined. Instead, it is the C_2H_3 destruction reaction:



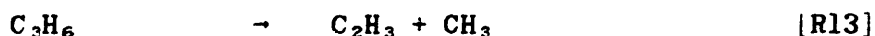
which is used in all the mechanisms, that generates HO_2 too rapidly at low temperatures in WZ and WZ'. Warnatz assumed a barrierless rate constant, while MMSK, WB, and WD include an activation energy of

10 kcal/mol. As a consequence, Rxn. 12 is about 3 orders of magnitude faster near the burner in WZ and WZ'.

The absence of this anomaly in MMSK, WB, and WD does not mean that their rate constant or even the reaction $C_2H_3 + O_2$ is correct. On the contrary, Slagle et al. (1984) found no HO_2 in a study of the elementary reaction at 297-602 K, but the products instead were $HCO + H_2CO$ with a different rate constant than that used above.

C_2H_3 . - The impact of Rxn. 12 on the predictions is also apparent in the C_2H_3 profiles (Fig. S.8) from MMSK, WB, WZ, and WZ'. C_2H_3 is produced rapidly at the burner by pressure-dependent addition of H to C_2H_2 , increasing to the high-pressure limit as H diffuses back to the burner (low temperatures). As distance from the burner increases, C_2H_3 is predicted to be destroyed rapidly by O_2 attack, while the experimental mole fraction is more nearly constant.

The prediction by WD corresponds much better to the experimental results. WD includes a pyrolysis reaction:



that maintains a higher mole fraction of C_2H_3 beyond 0.57 cm. (The reverse of this reaction accounts for the low mole fraction of C_2H_3 near the burner, consuming C_2H_3 more rapidly than it can be produced by $H + C_2H_2$.) The other mechanisms either do not include C_3 's heavier than C_3H_4 (MMSK and WB) or do not link the lighter and heavier C_3 's (WZ and WZ').

The WD rate constant for Rxn. 13 is written as a high-pressure limit, while QRRK analysis (Sec. S.4) indicates that $CH_3 + C_2H_3$ gives C_3H_5 at these temperatures. Nevertheless, growth chemistry involving C_3 species may be important in determining the concentration of light hydrocarbon radicals.

S.4. Bimolecular QRRK and its application to combustion chemistry

S.4.1. Principles, equations, and necessary input data

Bimolecular quantum-RRK or QRRK analysis uses a small, readily available set of input data to predict rate constants for gas-phase addition and recombination reactions with good accuracy (Dean, 1985;

Westmoreland et al., in press). It is useful for many important reactions that may not appear to be additions at all, but that proceed via chemically activated complexes.

The origin of the method is unimolecular rate theory, in particular the modification of RRK theory by Kassel (1928) which recognizes that energy storage in thermal decomposition is quantized and may be expressed in terms of quanta of size $h\langle\nu\rangle$, where $\langle\nu\rangle$ is a mean frequency for the molecule. By adding modern understanding of chemical activation (Robinson and Holbrook, 1972) and of inefficiencies in collisional energy transfer (Troe, 1977), the method becomes quantitatively useful.

Consider the case in which reactants $R+R'$ form an excited adduct A^* , illustrated in Fig. S.9. This process will occur with a rate constant equal to the high-pressure limit k_{∞} for the addition to form A . However, A^* is excited relative to its ground state (A) by an amount of energy equal to the energy barrier E_{-1} for redissociation back to the reactants; that is, the dissociation is chemically activated rather than thermally activated. If no other unimolecular reactions of A^* are possible, the competition between redissociation and stabilization, due to energy-removing collisions, determines the fate of A^* and the rate constant for $R+R' \rightarrow A$.

However, any unimolecular reaction i of the adduct can occur for which the amount of chemical-activation energy E exceeds the energy barrier E_i for the reaction. If the energy remaining in the products of this chemically activated decomposition is sufficient, they can also fragment in similar fashion. Thus, bimolecular reactions of the form $R+R' \rightarrow A$, $P+P'$, or even $P+P'+P''$ can result from addition.

In QRRK, the energy variable E and the barriers E_i are expressed in vibrational quanta as $n=E/h\langle\nu\rangle$ and $m=E_i/h\langle\nu\rangle$, where $\langle\nu\rangle$ is the geometric mean of the s frequencies of A . The bimolecular rate constant for forming the addition/stabilization product A from $R+R'$ then is written in terms of the variables in Fig. S.9:

$$k_{a/s} = \sum_{\substack{E=E_{-1} \\ (n=m-1)}}^{\infty} \frac{k_{1,\infty} \cdot \beta Z[M]}{\beta Z[M] + k_{-1}(E) + k_2(E)} \cdot f(E,T) \quad [S.1]$$

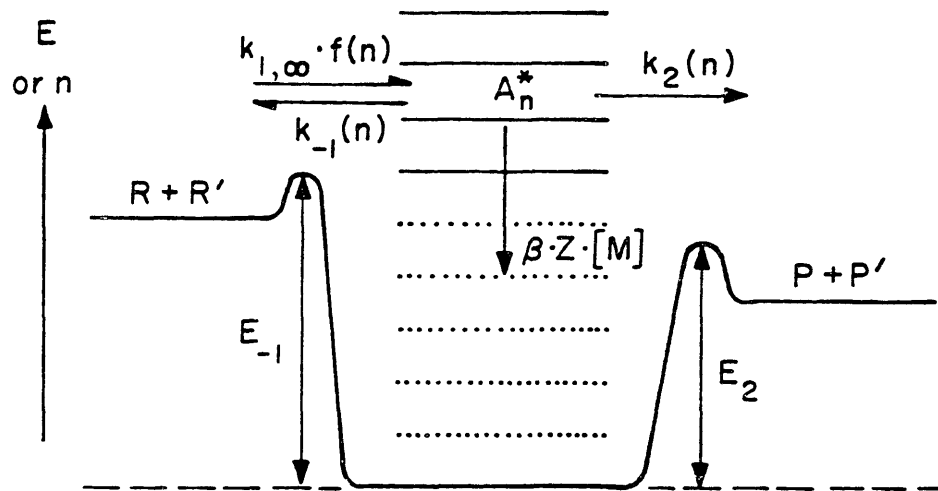


Fig. S.9. Energy diagram for addition with a chemically activated decomposition channel.

and, for forming the addition/decomposition products P and P', the observable rate constant is:

$$k_{a/d} = \sum_{\substack{E=E_{-1} \\ (n=m-1)}}^{\infty} \frac{k_{1,\infty} \cdot k_2(E)}{\beta Z[M] + k_{-1}(E) + k_2(E)} \cdot f(E,T) . \quad [S.2]$$

Here, Z is a collision-frequency rate constant, and β is a collision efficiency calculated from the expression of Troe (1977):

$$\frac{\beta}{1 - (\beta)^{1/2}} = \frac{-\langle \Delta E_{coll} \rangle}{F(E) \cdot \kappa T} \quad [S.3]$$

where $\langle \Delta E_{coll} \rangle$ is the average amount of energy transferred per collision (a function of the third-body species M), and $F(E) \approx 1.15$.

The rate constants $k_i(E)$ are calculated from:

$$k_i(E) = A_{\infty,i} \cdot \frac{n!(n-m+s-1)!}{(n-m)!(n+s-1)!} \quad [S.4]$$

and the quantized chemical-activation and thermal-activation distributions $f(E,T)$ and $K(E,T)$ are:

$$f(E,T) = \frac{k_{-1}(E) \cdot K(E,T)}{\sum_{\substack{E=E_{-1} \\ (n=m-1)}}^{\infty} k_{-1}(E) \cdot K(E,T)} \quad [S.5]$$

$$K(E,T) = (e^{-h\nu/\kappa T})^n \cdot (1 - e^{-h\nu/\kappa T})^s \cdot \frac{(n+s-1)!}{n!(s-1)!} . \quad [S.6]$$

Explicit expressions for the low-pressure limits can be easily derived from Eqs. S.1 and S.2 as $[M] \rightarrow 0$. An especially interesting insight, which extends to RRKM and other analysis methods, is that fall-off behavior for chemically activated decompositions has the inverse of the usual concept of fall-off trends. Instead, for these channels, the rate constant in the low-pressure limit is pressure-

independent and the high-pressure limit is inversely proportional to pressure.

Seen in this light, many radical-radical and radical-molecule reactions which have been measured as having pressure-independent rate constants can be recognized as chemically activated, addition-initiated reactions. Furthermore, all the reactions in combustion chemistry then can be categorized as metathetical H-atom transfer (abstraction or disproportionation), as chemically activated bimolecular reactions, or as thermal, unimolecular isomerizations. A dramatic transition becomes possible from current mechanisms - which are collections of reaction and rate-constant data, categorized by key reactants - to new mechanisms that make use of the fundamental differences and similarities among molecular events.

S.4.2. Applications, including H + O₂ reactions and benzene formation

The mechanism analysis indicates that all the bimolecular reactions in combustion can be categorized either as pressure-independent H-atom transfers (abstraction or disproportionation) or as chemically activated association reactions. Because the latter class of reactions is so widespread, application of bimolecular QRRK promises to make mechanisms more realistic.

Such rate constants can be estimated with good accuracy from a small set of readily available data. Specifically, bimolecular QRRK requires as input only (1) k_{∞} data or estimates for the various steps, (2) s , the number of vibrational degrees of freedom, (3) $\langle \nu \rangle$, the geometric-mean frequency of the adduct, and (4) collision properties of the adduct and the third-body species.

In contrast, RRKM theory is even more accurate but requires complete sets of frequencies, moments of inertia, and barrier heights for each transition state. While RRKM is potentially more accurate, the number, availability, and uncertainty of these input data can restrict its predictive powers, particularly for chemically activated reactions, which can involve numerous transition states for the decompositions and isomerizations of the adduct. Not only does bimolecular QRRK require fewer input data, but effects of uncertainties are readily apparent.

QRRK calculations were tested successfully against data and used to extrapolate and predict rate constants. Rate constants predicted here for reactions of aliphatic species are listed in Table S.2 for conditions of the present flame. Three-constant, modified Arrhenius expressions were generally required to fit the data because of non-Arrhenius behavior.

Particularly noteworthy are the predictions for $^3\text{CH}_2$ and $^1\text{CH}_2$ reactions, which compare well with the very limited data for kinetics of these species. Ground-state $^3\text{CH}_2$ undergoes free-radical addition and combination reactions, while the low-lying $^1\text{CH}_2$ inserts into σ and π bonds. Both of these types of reactions are chemically activated and thus well-suited to analysis by bimolecular QRRK analysis.

H + O₂ reactions and benzene formation are good examples of the method and its usefulness.

Prediction of H + O₂ ⇌ HO₂ ⇌ O + OH rate constants. - The reaction H + O₂ → O + OH is the principal chain-branching reaction in combustion, and it causes most of the destruction of O₂. The reverse reaction of O+OH → H+O₂ is also important. At low temperatures H+O₂ forms HO₂, in effect a chain-terminating step because it scavenges H atom and replaces it by less reactive HO₂. Experimentally, the first two reactions have pressure-independent rate constants, while formation of HO₂ is pressure-dependent.

In fact, rate constants can be predicted for all these reactions by recognizing that they are all based on chemically activated HO₂*. Figure S.10 illustrates this concept and shows the major input parameters needed for the calculation.

The first type of input data are kinetic parameters. For O + OH → HO₂, k_{∞} was estimated as $2.0 \cdot 10^{13} \text{ cm}^3 \text{ mol}^{-1} \text{ s}^{-1}$ by modifying an estimation method (Benson, 1983) for recombination of alkyl radicals and using geometrically estimated steric factors β . The k_{∞} for H + O₂ → HO₂ was taken from Cobos et al. (1985a), and Arrhenius parameters for the reverse reactions were calculated using equilibrium constants at 298 K. All thermodynamic data were taken from the JANAF tables (Stull et al., 1971) except for $\Delta H_f^{\circ}, 298(\text{HO}_2) = 10.5 \text{ kJ/mol}$ (2.5 kcal/mol) (Howard, 1980).

Table S.2. Rate constants ($\text{cm}^3\text{mol}^{-1}\text{s}^{-1}$) for reactions of aliphatic species, CO, and CO_2 calculated by QRRK methods for 400–1900 K, $M=\text{CO}$, and 2.67 kPa (20 torr).

Reaction	Predicted rate constant	Max. devn	$\log_{10} k(1500)$
$\text{H}+\text{C}_2\text{H}_2 \rightarrow \text{C}_2\text{H}_3$	$3.89 \cdot 10^{21} T^{-3.66} \exp(+0.20/RT)$	9%	10.00
$\text{CH}+^3\text{CH}_2 \rightarrow \text{C}_2\text{H}_3$	$3.09 \cdot 10^{14} T^{-1.98} \exp(-0.62/RT)$	1.5%	8.11
$\rightarrow \text{H}+\text{C}_2\text{H}_2$	$2.50 \cdot 10^{12} T^{-3.68} \exp(-4.19/RT)$	15%	13.11
$\rightarrow 2\text{H}+\text{C}_2\text{H}$	$5.49 \cdot 10^{22} T^{-2.41} \exp(-11.52/RT)$	4%	13.41
$\text{H}+\text{C}_2\text{H}_3 \rightarrow \text{C}_2\text{H}_4$	$5.62 \cdot 10^{29} T^{-5.54} \exp(-4.35/RT)$	9%	11.54
$\rightarrow \text{C}_2\text{H}_2+\text{H}_2$	$3.70 \cdot 10^{12} T^{-0.55} \exp(+0.04/RT)$	3%	13.69
$\text{H}_2+\text{C}_2\text{H}_2 \rightarrow \text{C}_2\text{H}_4$	$2.86 \cdot 10^{29} T^{-5.24} \exp(-52.6/RT)$	21%	5.18
$\rightarrow \text{C}_2\text{H}_3+\text{H}$	$4.02 \cdot 10^{15} T^{-0.56} \exp(-65.8/RT)$	3%	4.26
$^3\text{CH}_2+^3\text{CH}_2 \rightarrow \text{C}_2\text{H}_4$	$1.11 \cdot 10^{20} T^{-3.43} \exp(-2.07/RT)$	5%	8.86
$\rightarrow \text{C}_2\text{H}_2+\text{H}_2$	$4.02 \cdot 10^{14} T^{-0.47} \exp(-0.48/RT)$	1.5%	13.06
$\rightarrow \text{C}_2\text{H}_3+\text{H}$	$7.12 \cdot 10^{21} T^{-3.90} \exp(-2.46/RT)$	5%	9.11
$\rightarrow \text{C}_2\text{H}_2+2\text{H}$	$4.97 \cdot 10^{12} T^{+0.19} \exp(+0.15/RT)$	0.5%	13.30
$\text{H}+\text{C}_2\text{H}_4 \rightarrow \text{C}_2\text{H}_5$	$1.99 \cdot 10^{41} T^{-8.76} \exp(-11.70/RT)$	15%	11.78
$^3\text{CH}_2+\text{CH}_3 \rightarrow \text{C}_2\text{H}_5$	$2.53 \cdot 10^{20} T^{-3.49} \exp(-2.03/RT)$	4%	9.02
$\rightarrow \text{C}_2\text{H}_4+\text{H}$	$4.2 \cdot 10^{13}$	2%	13.62
$^1\text{CH}_2+\text{CH}_3 \rightarrow \text{C}_2\text{H}_4$	$1.11 \cdot 10^{19} T^{-3.20} \exp(-1.78/RT)$	4%	8.63
$\rightarrow \text{C}_2\text{H}_4+\text{H}$	$4.94 \cdot 10^{13} T^{-0.076} \exp(-0.094/RT)$	1%	13.60
$\rightarrow ^3\text{CH}_2+\text{CH}_3$	$6.82 \cdot 10^{-8} T^{+5.71} \exp(+4.20/RT)$	7%	11.60
$\text{O}+\text{CO} \rightarrow \text{CO}_2$	$1.31 \cdot 10^{21} T^{-3.85} \exp(-4.95/RT)$	3%	8.18

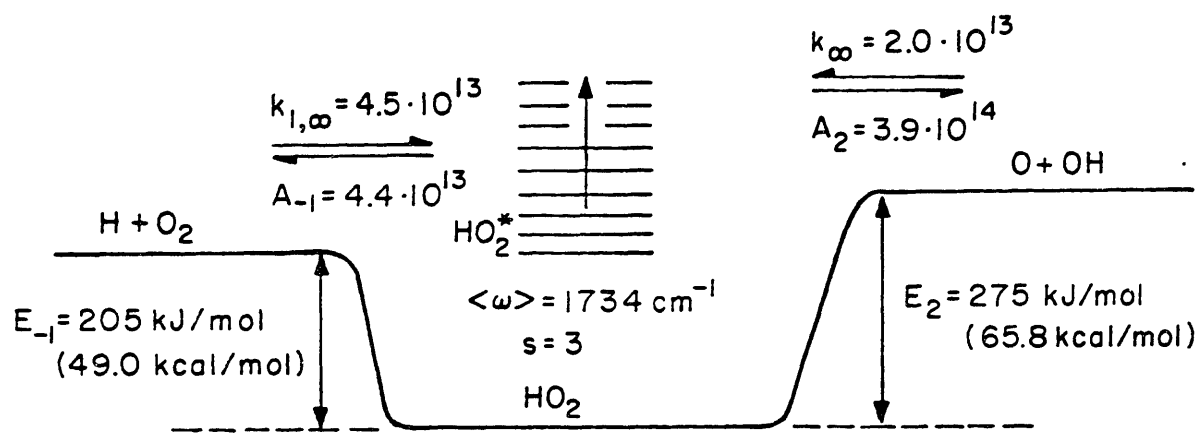


Fig. S.10. Energy diagram for reactions of activated HO_2 .

Certain properties of the adduct and the third-body gas are also required. The geometric mean frequency $\langle \omega \rangle$ for HO_2 is calculated as 1734 cm^{-1} (frequencies from Stull et al., 1971) with $s=3$ oscillators. Collision properties for HO_2 and the third-body gases were taken from Kee et al. (1983). Finally, $\langle \Delta E_{\text{coll}} \rangle$ of $\text{M}=\text{H}_2$ and Ar were taken from a review of the literature to be 2.1 and 3.6 kJ/mol (610 and 740 cal/mol), respectively.

For the fall-off curve for $\text{H} + \text{O}_2 \rightarrow \text{HO}_2$ and for k_0 of $\text{H} + \text{O}_2 + \text{M} \rightarrow \text{HO}_2 + \text{M}$, $\text{M}=\text{H}_2$ (Figs. S.11a and b), agreement with the data is excellent. Agreement with the pronounced non-Arrhenius behavior in Fig. S.11b is particularly remarkable. For comparison, prediction of the fall-off curve is also shown for Troe's formalism, a more parameter-rich predictive method.

Rate constants for the chain-branching reaction $\text{H} + \text{O}_2 \rightarrow \text{O} + \text{OH}$ (Fig. S.12) are slightly higher than the data, but their temperature dependence is correct. At elevated pressures, this reaction would also be pressure-dependent, but at 100 kPa (1 atm), it is in a pressure-independent low-pressure limit. The predicted curve of bimolecular rate constants is also shown for $\text{H} + \text{O}_2 \rightarrow \text{HO}_2$ at 1 atm. The dominant product channel changes from HO_2 to $\text{O} + \text{OH}$ at about 1000 K, accounting for the shift in importance of the two channels in combustion chemistry.

Finally, predictions for the chemically activated addition/decomposition reaction $\text{O} + \text{OH} \rightarrow \text{H} + \text{O}_2$ are shown in Fig. S.13. Agreement with the data is quite good. A slight decrease with increasing temperature is shown in one of the data sets and also in the prediction. This was the only rate constant that was sensitive to the estimated $k_{\infty}(\text{O} + \text{OH} \rightarrow \text{HO}_2)$, and the values of the two rate constants are directly proportional.

Benzene formation. - Benzene can be formed from smaller, nonaromatic hydrocarbons in flames and in cracking processes, but the chemical mechanism for its formation has remained elusive. This issue is significant for combustion because polycyclic aromatic hydrocarbons and soot, both undesirable pollutants, probably grow from single aromatic rings. In contrast, ethylene production can

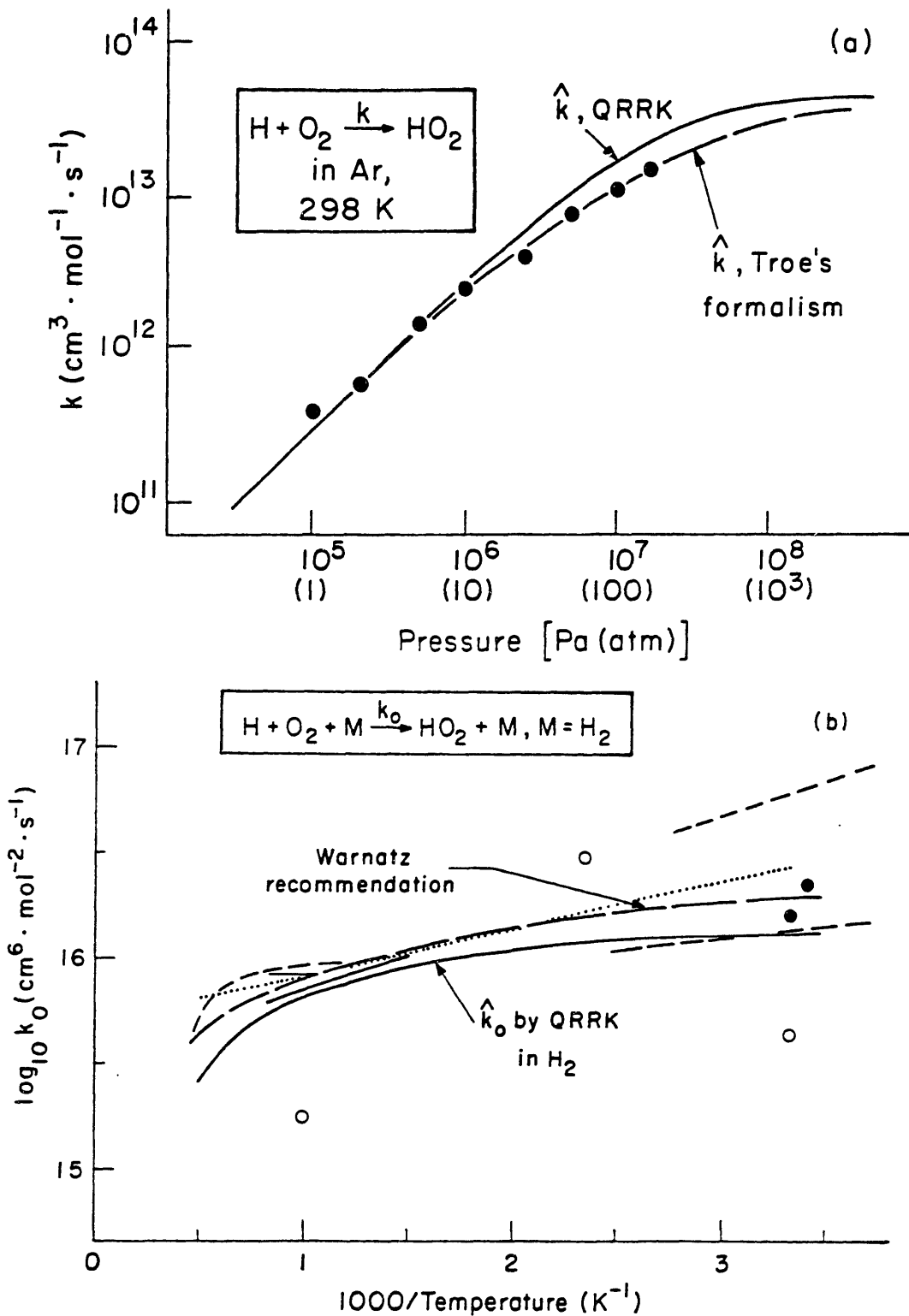


Fig. S.11. Rate constants for $H+O_2 \rightarrow HO_2$: (a) predicted fall-off curve (—) of the bimolecular rate constant with pressure at 298 K ($M=Ar$) compared to measurements (\bullet) and to correlation by Troe's formalism (---) (Cobos et al., 1985a); (b) Arrhenius plot of the predicted low-pressure limit (—) for $M=H_2$ compared with literature data (---, \cdots , \circ , and \bullet) and recommendation (— — —) from Warnatz (1984).

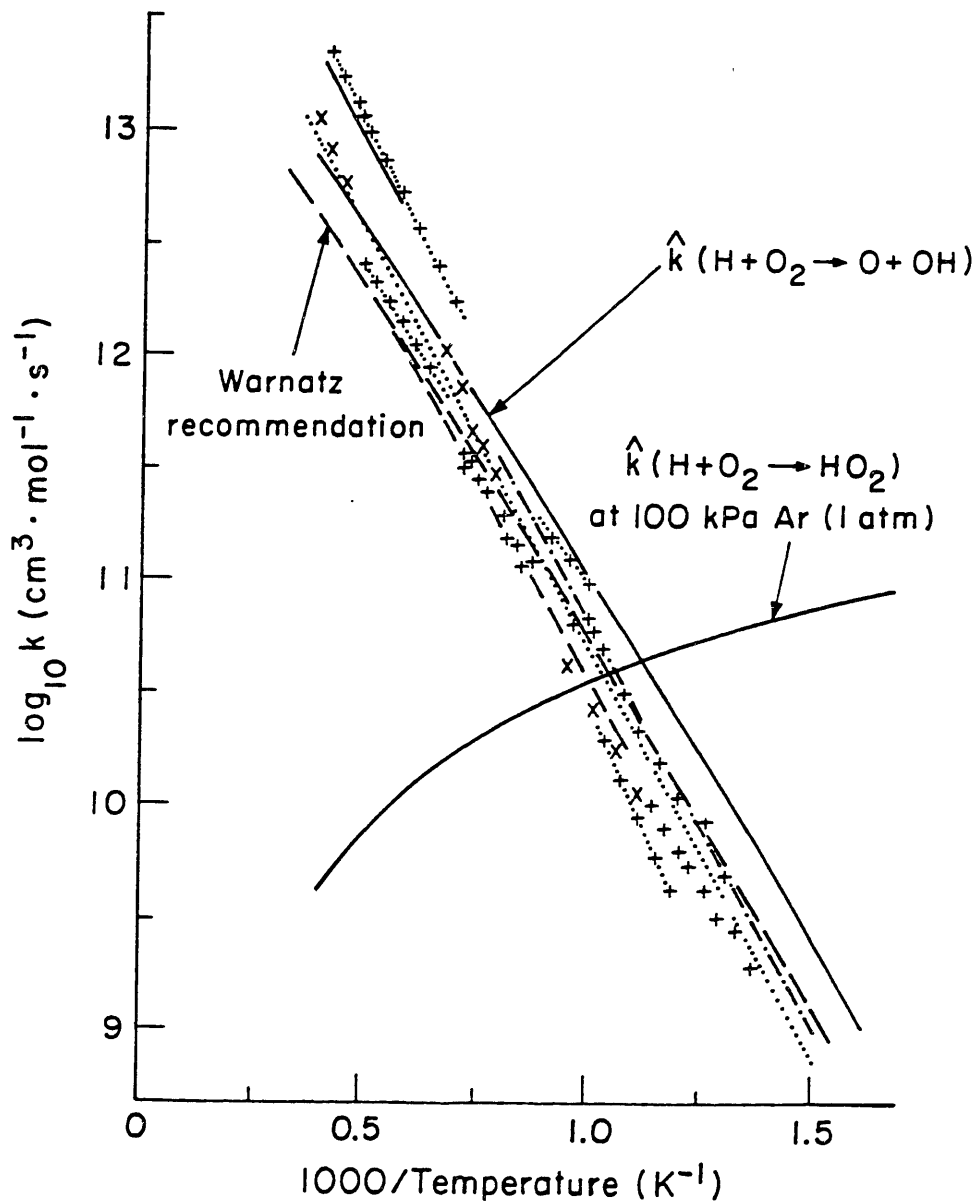


Fig. S.12. Predicted rate constant (—) for the chemically activated addition/decomposition reaction $\text{H} + \text{O}_2 \rightarrow (\text{HO}_2)^* \rightarrow \text{O} + \text{OH}$ compared with literature data (---, ···, x, and +) and recommendation (— — —) from Warnatz (1984) and with the predicted addition/stabilization rate constant for $\text{H} + \text{O}_2 \rightarrow (\text{HO}_2)^* \rightarrow \text{HO}_2$.

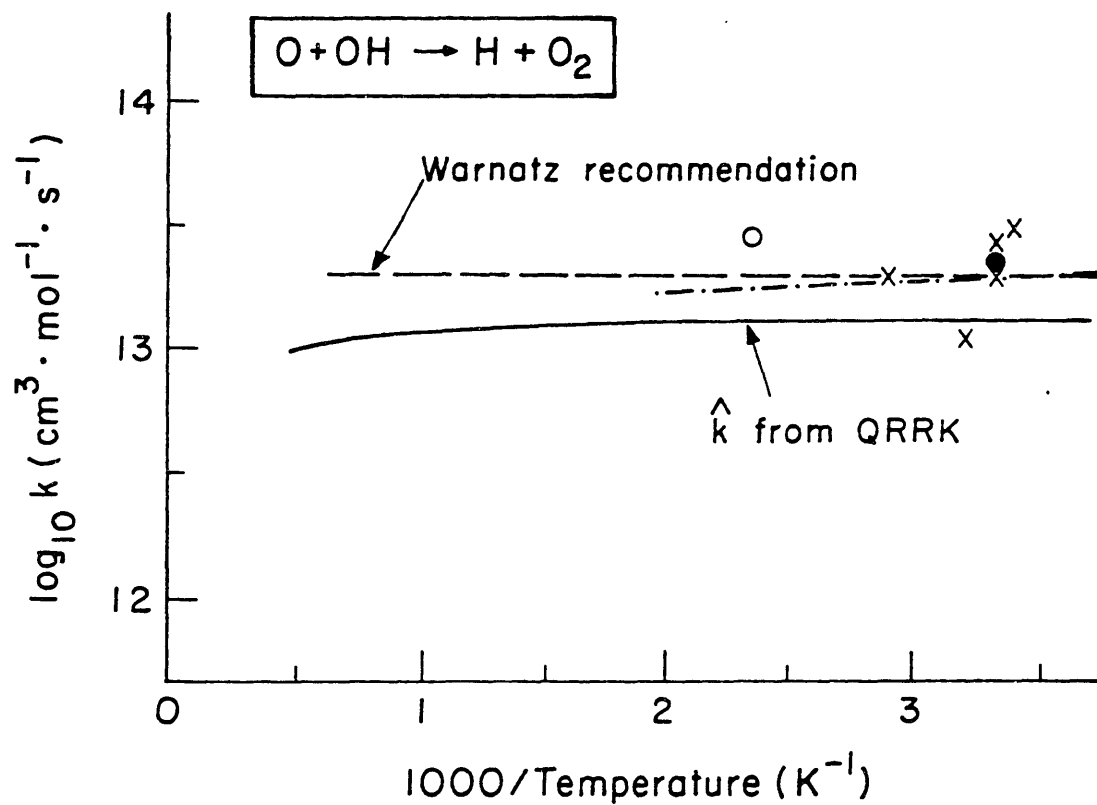


Fig. S.13. Predicted rate constant (—) for $\text{O} + \text{OH} \rightarrow (\text{HO}_2)^* \rightarrow \text{H} + \text{O}_2$ compared to literature data (---, χ , \circ , and \bullet) and recommendation (— — —) from Warnatz (1984).

make benzene and other aromatics as valuable by-products, particularly from C₄ and heavier feedstocks.

The present study provides a powerful means of testing chemical mechanisms of benzene formation. Measured mole fractions and temperatures from the C₂H₂ flame are combined with estimated rate constants, giving rates of benzene formation. These predictions are then compared to formation rates deduced from the data, an approach that has been used previously (Cole et al., 1984). However, when fall-off effects on the addition reactions are properly taken into account using bimolecular QRRK, all previous mechanisms fail because the initial, thermalized adduct is formed too slowly.

The results are explained instead by chemically activated reactions that form the aromatic ring directly. Reactants l-C₄H₅, l-C₄H₃, and C₂H₂, which have been proposed before (Cole et al., 1984; Frenklach et al., 1985), account for the rate of benzene formation, but reaction proceeds through excited intermediates rather than through a sequence of thermalized intermediates. This is a fundamental change in our understanding of benzene formation because thermalized species can be attacked and destroyed by bimolecular reactions, while the chemically activated species forms the aromatic ring too fast for bimolecular collisions to take place.

The reactions are initiated by additions of l-C₄H₅ and l-C₄H₃ to C₂H₂. Rather than forming linear, aliphatic adducts t-C₆H₇ and t-C₆H₅ in their ground vibrational states, the aliphatic adducts are excited species t-C₆H₇* and t-C₆H₅* that rapidly isomerize to excited ring compounds c-C₆H₇* and c-C₆H₅*. These intermediates undergo chemically activated decomposition or collision stabilization to benzene and phenyl, respectively. An energy diagram for l-C₄H₅ + C₂H₂ is shown in Fig. S.14, illustrating this description, and the QRRK input parameters for l-C₄H₅ + C₂H₂ and l-C₄H₃ + C₂H₂ are shown in Tables S.3 and S.4.

The QRRK calculation at 2.67 kPa (M=Ar) leads to rate constants for each of the product channels resulting from l-C₄H₅ + C₂H₂ (Fig. S.15) and from l-C₄H₃ + C₂H₂ (Fig. S.16). At the temperatures of 1100 to 1600 K, where the net rate of benzene formation is greatest, the rate constants for direct formation of benzene + H and

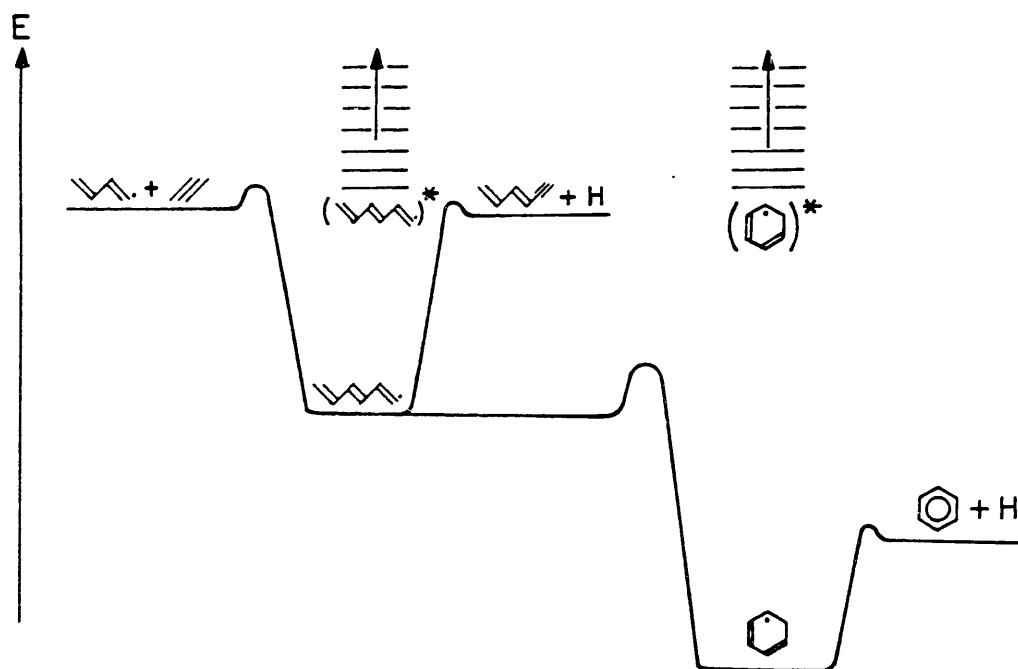


Fig. S.14. Energy diagram for the addition of 1-C₄H₅ to C₂H₂.

Table S.3. Parameters needed for bimolecular QRRK calculations for $l\text{-C}_4\text{H}_5 + \text{C}_2\text{H}_2$ reactions via the chemically activated intermediates $l\text{-C}_6\text{H}_7^*$ and $c\text{-C}_6\text{H}_7^*$ (mol, cm, s, kcal units).

Parameter description	Parameter value	Source
- Kinetic parameters -		
$l\text{-C}_4\text{H}_5 + \text{C}_2\text{H}_2 \rightarrow l\text{-C}_6\text{H}_7$ ($\cdot\text{---c---c}$)	$k_{\infty}(300\text{--}1500\text{ K}) = 2.8 \cdot 10^2 T^{2.9} \exp(-1.4/RT)$ $\text{cm}^3 \text{mol}^{-1} \text{s}^{-1}$ $= 7.2 \cdot 10^{12} \exp(-10.0/RT)$ at 1500 K	$k(400\text{ K}) = 10^{11.2} \exp(-3.5/RT)$ by Cole et al. (1984) and $\langle \Delta C_V^\ddagger \rangle = 3.75$ cal/mol·K from Benson and Weissman (1984)
$l\text{-C}_6\text{H}_7 \rightarrow l\text{-C}_4\text{H}_5 + \text{C}_2\text{H}_2$	$A_{\infty} = 3.6 \cdot 10^{14} \text{ s}^{-1}$ $E_{\infty} = 46.1 \text{ kcal/mol}$	Microscopic reversibility
$l\text{-C}_6\text{H}_6 + \text{H} \rightarrow l\text{-C}_6\text{H}_7$ ($\blacksquare\text{---c---c}$) ($\cdot\text{---c---c}$)	$A_{\infty} = 1.6 \cdot 10^{12} \text{ cm}^3 \text{mol}^{-1} \text{s}^{-1}$ $E_{\infty} = 1.0 \text{ kcal/mol}$	$A_{\infty}/4$ for $\text{H} + \blacksquare\text{---}\blacksquare$ E_{∞} for $\text{H} + \blacksquare\text{---}\blacksquare$
$l\text{-C}_6\text{H}_7 \rightarrow l\text{-C}_6\text{H}_6 + \text{H}$	$A_{\infty} = 4 \cdot 10^{12} \text{ s}^{-1}$ $E_{\infty} = 36.7 \text{ kcal/mol}$	Microscopic reversibility
$l\text{-C}_6\text{H}_7 \rightarrow c\text{-C}_6\text{H}_7$	$A_{\infty} = 1.7 \cdot 10^{11} \text{ s}^{-1}$ (1500K) $E_{\infty} = 7 \text{ kcal/mol}$	Estimate by thermochemical kinetics Estimate as E_{act} for radical addition ^a
$c\text{-C}_6\text{H}_7 \rightarrow l\text{-C}_6\text{H}_7$	$A_{\infty} = 1.0 \cdot 10^{14} \text{ s}^{-1}$ $E_{\infty} = 53.2 \text{ kcal/mol}$ ^b	Microscopic reversibility
$\text{H} + \text{Benzene} \rightarrow c\text{-C}_6\text{H}_7$	$A_{\infty} = 4 \cdot 10^{13} \text{ cm}^3 \text{mol}^{-1} \text{s}^{-1}$ $E_{\infty} = 4.3 \text{ kcal/mol}$	Nicovich and Ravishankara (1984)
$c\text{-C}_6\text{H}_7 \rightarrow \text{H} + \text{Benzene}$	$A_{\infty} = 2 \cdot 10^{13} \text{ s}^{-1}$ (550 K) $E_{\infty} = 26.0 \text{ kcal/mol}$	Tsang (1986)
- Properties of $l\text{-C}_6\text{H}_7$ and $c\text{-C}_6\text{H}_7$ -		
Number of vibrational degrees of freedom (s):	33	$3 \cdot (13 \text{ atoms}) - 6$
Geometric-mean frequencies $\langle \nu \rangle$:		
$l\text{-C}_6\text{H}_7$	1050 cm^{-1}	From estimated frequencies
$c\text{-C}_6\text{H}_7$	1070 cm^{-1}	From estimated frequencies
Molecular weight	79.11 g/g-mol	-
Lennard-Jones well depth ϵ/k and diameter σ	412.3 K, 5.349 Å	Same as benzene (Reid et al., 1977)

^a Based on Kerr and Moss (1981).

^b Using $\Delta H_f^\circ, 298 = 50.0 \text{ kcal/mol}$ (Tsang, 1986).

Table S.4. Parameters needed for bimolecular QRRK calculations for $l\text{-C}_4\text{H}_3 + \text{C}_2\text{H}_2$ reactions via the chemically activated intermediates $l\text{-C}_6\text{H}_5^*$ and $c\text{-C}_6\text{H}_5^*$ (mol, cm, s, kcal units).

Parameter description	Parameter value	Source
- Kinetic parameters -		
$l\text{-C}_4\text{H}_3 + \text{C}_2\text{H}_2 \rightarrow l\text{-C}_6\text{H}_5$ ($\cdot\text{C}_4\text{H}_3 + \text{C}_2\text{H}_2$)	$k_{\infty}(300\text{-}1500\text{ K}) =$ $2.8 \cdot 10^{22} T^{2.9} \exp(-1.4/RT)$ $\text{cm}^3 \text{mol}^{-1} \text{s}^{-1}$ $= 7.2 \cdot 10^{12} \exp(-10.0/RT)$ at 1500 K	Estimate for $l\text{-C}_4\text{H}_3 + \text{C}_2\text{H}_2$ $\rightarrow \text{C}_6\text{H}_7$
$l\text{-C}_6\text{H}_5 \rightarrow l\text{-C}_4\text{H}_3 + \text{C}_2\text{H}_2$	$A_{\infty} = 5.5 \cdot 10^{14} \text{ s}^{-1}$ $E_{\infty} = 45.8 \text{ kcal/mol}$ at 1500 K	Microscopic reversibility
$l\text{-C}_6\text{H}_4 + \text{H} \rightarrow l\text{-C}_6\text{H}_5$ ($\text{C}_6\text{H}_4 + \text{H}$) ($\cdot\text{C}_6\text{H}_4$)	$A_{\infty} = 3.2 \cdot 10^{12} \text{ cm}^3 \text{mol}^{-1} \text{s}^{-1}$ $E_{\infty} = 1.0 \text{ kcal/mol}$	$0.5 \cdot A_{\infty}$ for $\text{H} + \text{C}_6\text{H}_4$ E_{∞} for $\text{H} + \text{C}_6\text{H}_4$
$l\text{-C}_6\text{H}_5 \rightarrow l\text{-C}_6\text{H}_4 + \text{H}$	$A_{\infty} = 8 \cdot 10^{12} \text{ s}^{-1}$ $E_{\infty} = 36.7 \text{ kcal/mol}$	Microscopic reversibility
$l\text{-C}_6\text{H}_5 \rightarrow \text{Phenyl}$	$A_{\infty} = 4 \cdot 10^{10} \text{ s}^{-1}$ (1500 K) $E_{\infty} = 7 \text{ kcal/mol}$	Estimate, thermo- chemical kinetics Estimate as E_{act} for radical addition
Phenyl $\rightarrow l\text{-C}_6\text{H}_5$	$A_{\infty} = 1.2 \cdot 10^{14} \text{ s}^{-1}$ $E_{\infty} = 70.9 \text{ kcal/mol}$	Microscopic reversibility
H+Benzyne \rightarrow Phenyl	$A_{\infty} = 6.5 \cdot 10^{12} \text{ cm}^3 \text{mol}^{-1} \text{s}^{-1}$ $E_{\infty} = 2.0 \text{ kcal/mol}$	Estimate from k of $\text{H} + \text{C}_6\text{H}_4 \rightarrow \text{C}_6\text{H}_5$
Phenyl \rightarrow H+Benzyne	$A_{\infty} = 4.9 \cdot 10^{13} \text{ s}^{-1}$ $E_{\infty} = 87.5 \text{ kcal/mol}$	Microscopic reversibility
-Properties of $l\text{-C}_6\text{H}_5$ and phenyl -		
Number of vibrational degrees of freedom (s):	27	$3 \cdot (11 \text{ atoms}) - 6$
Geometric-mean frequencies $\langle \nu \rangle$:		
$l\text{-C}_6\text{H}_5$	990 cm^{-1}	From estimated frequencies
Phenyl	1180 cm^{-1}	From Burcat (1984)
Molecular weight	77.11 g/g-mol	-
Lennard-Jones well depth ϵ/k and diameter σ	412.3 K, 5.349 Å	Same as benzene (Reid et al., 1977)

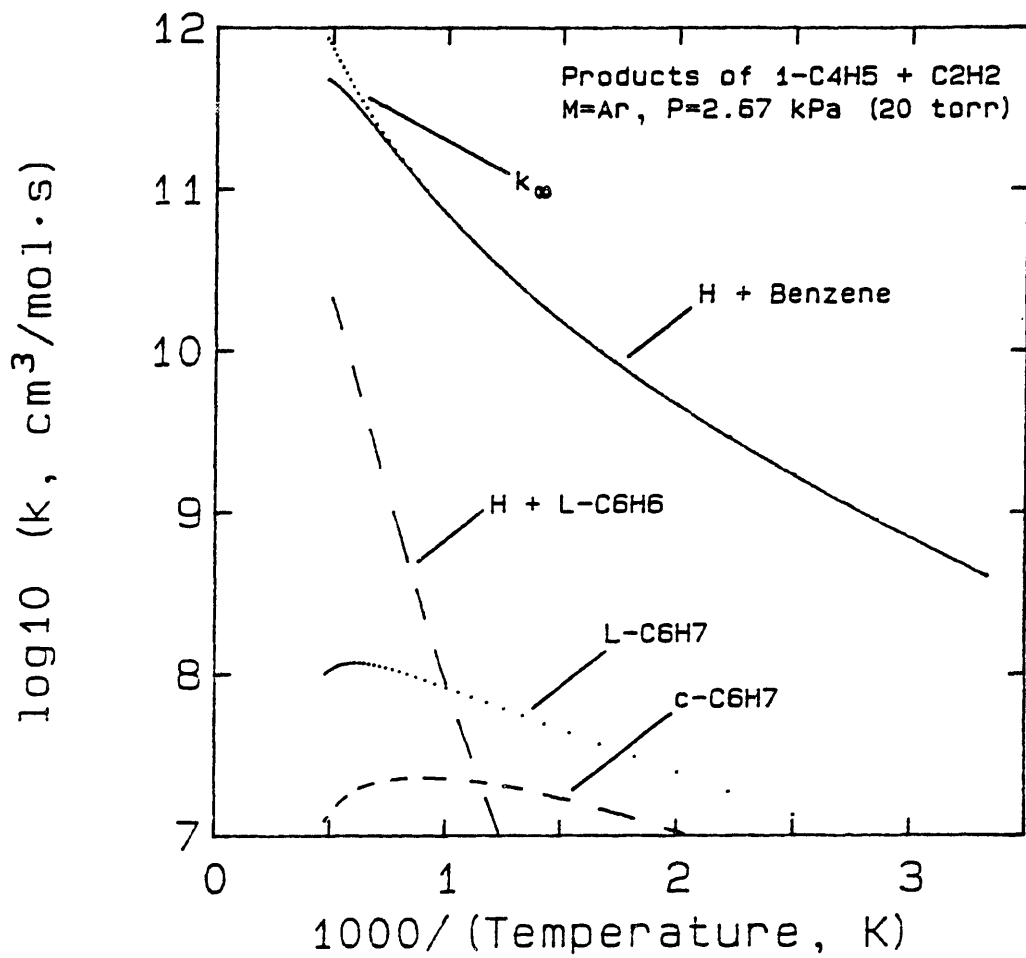


Fig. S.15. Predicted rate constants for 1-C₄H₅ + C₂H₂.

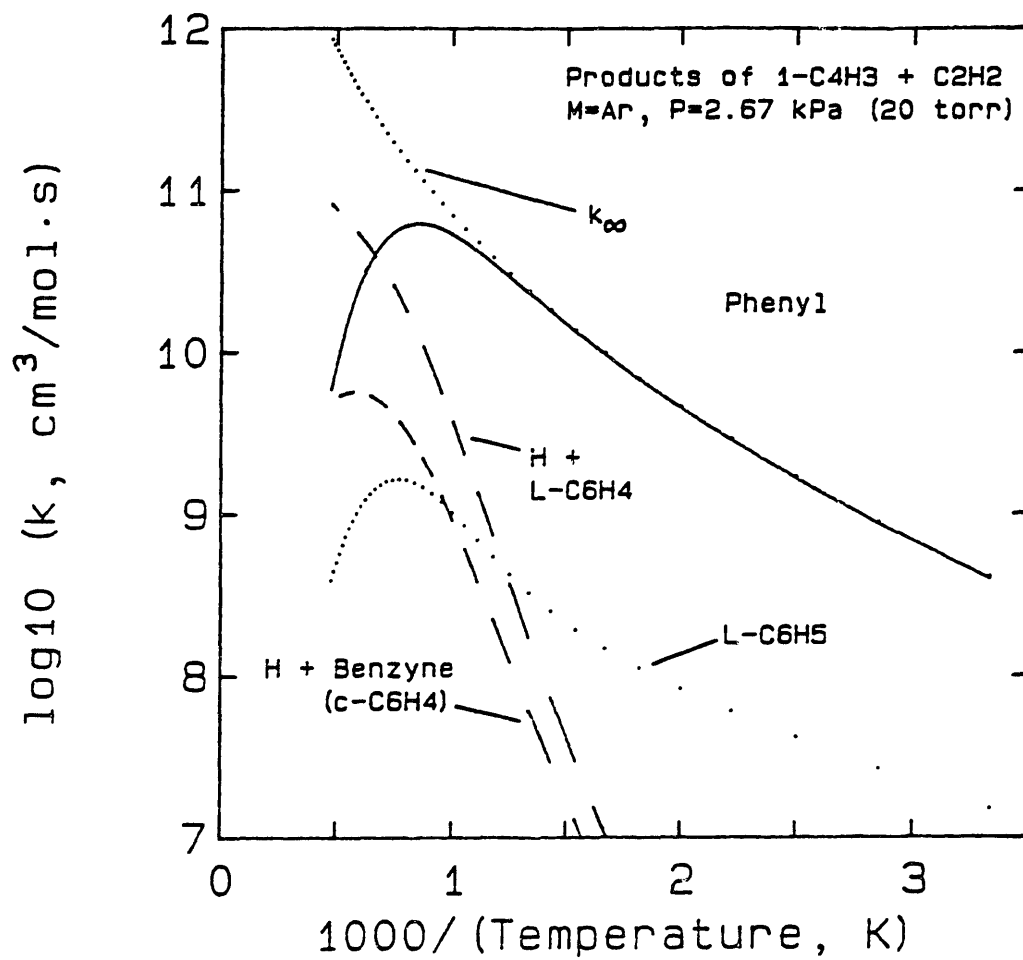


Fig. S.16. Predicted rate constants for 1-C₄H₃ + C₂H₂.

of phenyl are highest. For $1-C_4H_3 + C_2H_2$, chemically activated decompositions to $1-C_6H_4$ and benzyne begin to dominate at higher temperatures. The rate constants to aromatics are very similar at 100 kPa (1 atm) except that the transitions to $1-C_6H_4$ and benzyne begin at slightly higher temperatures.

Finally, the predictions for formation of the single-ring aromatic products are compared to the net rate of benzene formation in Fig. S.17. Within the uncertainty of the data, both channels may be considered to be involved in benzene formation in this flame. All of the other chemically activated or thermal pathways proved to be too slow.

S.5. Conclusions

Based on the data and modeling, it can be concluded that:

- (1) Literature mechanisms for less fuel-rich conditions predicted mole fractions fairly well (a factor of two) for major species at sooting conditions, but for hydrocarbon radicals, they show serious deficiencies. These failures prevent the predictions of important features like formation of aromatics.
- (2) The key cause is a lack of rate and product data for reactions that are crucial to such predictions.
- (3) Bimolecular QRRK is a practical, accurate tool for estimating rate constants and branching for many of these reactions.
- (4) Analyses of rate constants by QRRK leads to the insight that all the reactions in combustion chemistry can be categorized as metathetical H-atom transfer (abstraction or disproportionation), as chemically activated bimolecular reactions, or as thermal, unimolecular isomerizations.

Critical evaluation of mechanisms. - Specific conclusions from testing the mechanisms are:

- (1) Elementary reactions that are reversible should be included with rate constants for both forward and reverse directions if the mechanism is to be used generally, even if the predictions at a given condition are insensitive to a particular direction.
- (2) CH_2 chemistry is very important to the predictions, but there is no distinction made between singlet and triplet CH_2 in

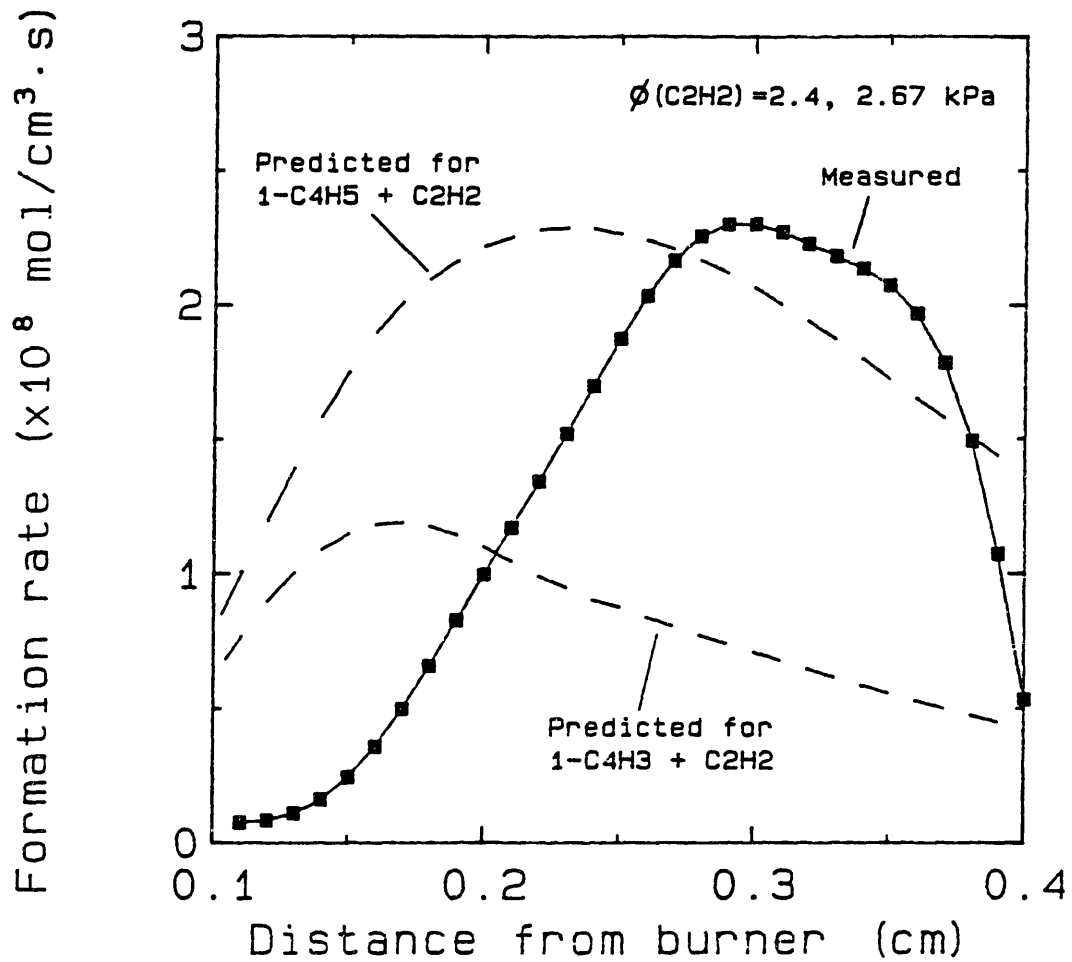


Fig. S.17. Test of predicted rate of benzene formation against measured net rate of benzene formation.

the mechanisms, despite the presence of each and their greatly differing reactivities.

(3) H_2O and CO_2 predictions are strongly affected by the product branching and rates of $\text{CH}_2 + \text{O}_2$ and of $\text{C}_4\text{H}_2 + \text{OH}$, but only two mechanisms (WZ and WZ') predict shape and magnitude well for both species.

(4) The absence of destruction kinetics for C_3 species in two mechanisms (MMSK and WD) leads to a misprediction that these species would be formed in quantities much greater than is observed, which makes them unrealistically large sinks for carbon and impairs predictions for other species in the affected mechanisms.

(5) Peculiarities in the OH prediction are caused by differences in $\text{C}_2\text{H}_3 + \text{O}_2$ activation energies, but recent measurements indicate that the rate constant and even the products of the reaction are drastically different ($\rightarrow \text{HCO} + \text{H}_2\text{CO}$) from those used in existing mechanisms ($\rightarrow \text{C}_2\text{H}_2 + \text{HO}_2$).

(6) C_2H_3 is largely determined by its reaction with O_2 and, in one mechanism (WD), by the inclusion of a $\text{C}_3\text{H}_6 = \text{C}_2\text{H}_3 + \text{CH}_3$ reaction which is assumed to be in the high-pressure limit.

Prediction of rate constants by bimolecular QRRK. - This method is a practical tool for the modeler and a valuable supplement to RRRKM theory. The reason is that the key input data are high-pressure-limit Arrhenius parameters A_∞ and $E_{\text{act},\infty}$ for each bimolecular and unimolecular step involved, which are generally available from experimental data or which can be estimated by thermochemical kinetics. Specific results and conclusions are:

(1) Bimolecular QRRK accurately predicts rate constants for chemically activated reactions including pressure dependence, low-pressure limits for addition/stabilization reactions, and non-Arrhenius temperature dependences.

(2) Chemically activated decomposition is shown as outgrowth of the QRRK equations to have the inverse of classical fall-off behavior. Its bimolecular rate constants are pressure-independent at low pressure rather than high pressure, a prediction that is supported by the products and rate constants of many

radical-radical reactions. Also, at high pressure, these rate constants are predicted to be *inversely* proportional to pressure.

(4) The reactions of " CH_2 ", which were shown by testing mechanisms to be of great importance, can be analyzed by using bimolecular QRRK for the distinctly different reactions of the electronic ground-state $^3\text{CH}_2$ and for the low-lying electronic state $^1\text{CH}_2$.

(5) The reactions of $\text{H} + \text{O}_2$ are shown to be classical cases of chemical activation, leading to HO_2 by addition/stabilization and to $\text{O} + \text{OH}$ by addition/decomposition, and rate constants for these reactions and for $\text{O} + \text{OH} \rightarrow \text{H} + \text{O}_2$ are predicted well.

Benzene formation. - Calculations of rate constants for $1\text{-C}_4\text{H}_3$ and $1\text{-C}_4\text{H}_5 + \text{C}_2\text{H}_2$ show that simple addition to make linear adducts is too slow to account for the rate of benzene formation. Instead, benzene formation is described well by chemically activated addition/isomerization of these reactants, which leads directly to aromatic products without forming thermalized intermediates that could be destroyed before leading to aromatics.

Types of combustion reactions. - From the above conclusions, it follows that all reactions in combustion chemistry can be categorized as metathetical H-atom transfer, as chemically activated, addition-initiated reactions, or as thermal isomerizations. The widespread occurrence of chemically activated reactions has not been recognized, probably because the inverse pressure dependence of chemically activated decompositions has not been recognized.

By examining the Warnatz mechanism, it was shown that all of the oxidation and molecular-weight-growth reactions are of this type. This breakdown is more than just a descriptive tool, then, but a means of insight to the fundamental differences and similarities among chemical reactions in combustion.

S.6. Recommendations for continued research

Further data are necessary to understand fuel-rich combustion, and bimolecular QRRK should be applied to estimate rate constants where no data are available or where extrapolation from low tempera-

tures or different pressures is required. Sensitivity analyses must identify whether these reactions are important. Specifically:

- (1) The destruction kinetics of C_3H_4 , C_4H_2 , and of the radicals " CH_2 " (3CH_2 and 1CH_2), C_2H_3 , C_3H_2 , and C_3H_3 should be estimated by using bimolecular QRRK, rationalizing data that exist for these reactions and anticipating better experimental data.
- (2) Combustion kinetics for hydrocarbons heavier than C_2 's, including formation and destruction of polycyclic aromatics, are largely unexplored but should be addressed using these data and predictive methods.
- (3) In particular, sources of C_4 species that lead to benzene formation are not understood, but unimolecular and bimolecular QRRK again should be used to investigate such reactions.
- (4) QRRK methods also should be applied to other systems as diverse as NO_x chemistry, nitrogen fixation, chemi-ionization, ion-molecule reactions, and plasma chemistry.
- (5) Data on pure fuels C_2H_4 , C_2H_6 , C_3H_6 , C_3H_8 , toluene, and on mixtures will yield data that are sensitive to different reactions, allowing improvement of mechanisms.

CHAPTER I. INTRODUCTION

I.1. Overview

It has become possible to pick apart the detailed chemistry of combustion for some gaseous fuels under certain conditions. That is, many of the molecular events can be described mathematically - molecular collisions that result in reaction, transfer of thermal and mechanical energy, and different rates of movement among different molecules. These descriptions of reaction rates and of heat, mass, and momentum transfer can be combined in detailed and increasingly accurate models.

Using these models, histories can be predicted for the destruction and formation of fuel, oxygen, reaction intermediates, and ultimate products of the combustion. The successes of these models - and at some level, the origins of the models - must be determined by tests against experimental data.

This study of acetylene combustion includes both the detailed experimental measurements of concentrations and temperature in a laboratory flame and the use of those data as exacting tests for models of chemical kinetics. Before presenting the research and its results, context and potential usefulness of the work should be described.

I.2. Combustion as science and as technology

To be able to understand and to predict such complex natural behavior is a significant scientific goal, but combustion is, first of all, one of the oldest of industrial technologies. Its complexity is not a subtle thing, but rather it was obvious to the earliest "technologists." Starting a fire, keeping it burning, and keeping it under control have been problems since before history began.

Some of the problems are linked to the physical phenomena of mixing fuel and air, retaining enough heat to maintain the fire and releasing (and capturing) enough heat or light to make it useful. Nevertheless, the burning itself is a chemical phenomenon, and the interplay between chemistry and physics make the field interesting to the scientist and the engineer.

For the scientist, the details of the burning process are of interest in themselves and because of their relationships to other systems. As an example, ignition and extinction are classic demonstrations of transitions between multiple steady states. Also, a broad variety of free radicals is produced, taking part in intricate networks of chain reactions. The relative importance of different parts of these mechanisms changes dramatically as the proportions of fuel and air change, as temperature changes, and, in some cases, as pressure changes.

Fire is much easier to use than to understand. In particular, it is not necessary to understand the chemistry of combustion to be able to put combustion to work. Throughout the history of industrial civilization, it has been the principal method of generating energy for work and for heat. The familiarity of the candle, the fireplace, the automobile, the jumbo jet, the home furnace, and the electricity-generation plant leave the details of the energy-conversion process to be taken for granted.

In many cases, the chemistry has been assumed to be instantaneous or irrelevant. Sometimes that assumption has been forced because the details of the chemistry were unknown or because the complexity of the modeling make it intractable. Frequently, though, the high speed of combustion kinetics can make chemistry a minor aspect relative to the technical issues of mixing fuel and air effectively or recovering energy efficiently by gas expansion or by heat transfer. As a result, to a large extent combustion technology has been perceived as a mechanical-engineering problem in the past.

However, understanding chemistry may be important for efficient uses of the technology. Combustion may involve a fuel that must be destroyed, as in incineration of hazardous wastes. Even from innocuous fuels, pollutant byproducts may be produced. Also, mechanical aspects of the process may be affected by chemical complications, such as engine knock or soot formation. Soot is undesirable as an emission, but it is a necessity if heat is to be recovered by radiative heat transfer. (It even may be the reason for the process, as in the production of carbon black.)

I.3. Recent progress in combustion chemistry

Identification of the key reactions, reactants, and reaction rates in combustion would make it possible to control or avert undesirable aspects, as well as to bring about desirable features. During recent years, combustion chemistry has become a research area of vigorous activity, in part because of new tools for the researcher. Improved data on kinetics of elementary reactions have appeared because of advances in theoretical interpretation and in experimental methods. Many of the new experiments depend on laser chemistry and on computerized data acquisition. New mathematical methods and more powerful computers have also become available to attack the problem.

As a result, mechanistic modeling of the combustion of some simple hydrocarbons has been attempted in the last five years. The tested fuels have included H_2 , CO , CH_4 , C_2H_4 , and C_2H_6 at fuel-lean, stoichiometric, and slightly fuel-rich conditions. The models have been applied to shock-tube conditions and to laminar premixed flames, either freely propagating flames or burner-stabilized flat flames.

For flat-flame data, several computer programs are now available that accept a given mechanism and predicted concentration profiles. Different mathematical methods are used, but for an accurate mechanism, a method's accuracy is affected most by its level of sophistication in accounting for realistic heat losses and transport properties. Previous studies demonstrated that satisfactory predictions can be obtained by using measured temperature profiles and transport properties calculated from kinetic theory.

Detailed mechanisms from several different groups of researchers have been successful in modeling various conditions; see, for example, the Nineteenth Symposium (International) on Combustion, 1981. Hydrocarbon mechanisms have included 123-200 reactions to predict either single properties of these flames, such as burning velocity, or concentration profiles of a few species.

Modeling very fuel-rich flames generally has been avoided, largely because the formation and destruction of high-molecular-weight species is so poorly understood. As a consequence, only two species of molecular weight greater than C_4H_3 (C_4H_6 and C_6H_2) are included in any of the flame mechanisms in the literature.

No mechanisms have been tested against a complete set of mole fractions for radical and stable species. Admittedly, few flames have been analyzed experimentally in such great detail, but comparisons with such data would permit better assessment of the components of the mechanisms. Combined with sensitivity analysis of the mechanisms' predictions, detailed tests against experimental data would improve the use of the mechanisms in modeling more complex systems.

I.4. Goals of this research

In this dissertation, the driving force is a desire to understand how the formation, growth, and destruction reactions of flame intermediates occur in fuel-rich combustion. Ideally, those reactions ultimately might be understood which lead to soot and to polynuclear aromatics.

An appropriate place to begin is the study of acetylene. Whether aliphatic or aromatic fuels are burned, acetylene is formed as the predominant hydrocarbon when a sooting condition is approached and achieved. By making measurements in a flat flame of acetylene and oxygen that is just sooting and by comparing these data to mechanistic predictions, the insights obtained are basic to the understanding of fuel-rich combustion.

Concentrations of stable species and free radicals are obtained from the flame in this study by molecular-beam mass spectrometry. With temperature measurements and sufficiently detailed data, net reaction rates can be calculated for each species as demonstrated by Bittner (1981).

Reaction kinetics can be quantitatively tested using these mole fractions and rates. One way is shown by Cole (1982), who compared the rate data to rates predicted from measured concentrations and rate constants.

The data also can be applied as a powerful test of the reaction networks. Only one mechanism has been tested at such fuel-rich conditions, and none has been tested against such detailed data. The questions that are addressed are not only how well the mechanisms worked, but also which reactions or rate constants cause poor

predictions. This research then has been the first attempt to critically evaluate the four major mechanisms which have been proposed.

Because important uncertainties were found, it was necessary to estimate rate constants. Chemically activated reactions proved to be the key problem area, but the rate constants and branching of these reactions, which are inherently pressure-dependent, can be analyzed by a newly revived technique, Bimolecular QRRK. Both pyrolysis (C/H) and oxidation (C/H/O) reactions were tested. The mechanism of benzene formation had been unresolved, but it too could be analyzed by this method.

1.5. Summary of the experimental approach

The experimental data are central to the analysis and modeling segment of this research, so it is necessary to describe briefly the nature of the data and the chosen flame conditions.

The flat flame is especially suitable for laboratory study because concentrations and temperatures vary only with the distance from the burner surface; radial gradients are negligible in the core of the flame, and the flame properties do not vary with time if the pressure and flows of gases are steady. By operating the flame in a vacuum chamber, the thickness of the flame is expanded to give good spatial resolution.

The principal technique for measuring concentrations in the flame is molecular-beam sampling from the premixed, laminar flame into a mass spectrometer. Using molecular-beam mass spectrometry, concentrations of both stable species and free radicals were measured. A supersonic expansion of the sampled gases cools the molecules, and near-collisionless flow permits them to pass unreacted into the mass spectrometer. Pulse-counting techniques improved the lower limits of detection to 0.1 ppm for some species.

These data are supplemented by thermocouple data and by probe sampling for gas chromatography/mass spectrometry (GC/MS). The probe samples were collected by adsorption onto polymeric beads (XAD-2), extracted with methylene chloride, and analyzed for C₆ and heavier

species by gas chromatography with a flame ionization detector or mass-spectrometric detection.

Net reaction rates can be determined for each species at each position in the flame if a sufficiently large number of precise concentration data were measured. From velocity and concentration, the convective flux is calculated. From temperature and concentration, mixture diffusion coefficients are calculated and used with the concentration gradients to calculate the diffusive flux. Flux due to thermal diffusion can contribute, and it also can be calculated from the data. The net reaction rate then is calculated from the slope of the total flux curve.

Bonne, Homann, and Wagner (1965) made limited measurements in a lightly sooting acetylene flame. A mixture of 49% C_2H_2 and 51% O_2 (fuel equivalence ratio 2.38) introduced at 50 cm/s was burned at 2.67 kPa (20 torr). Over a range of 0 to 5.5 cm from the burner surface, five to 15 data points of mole fraction were reported for each of 13 stable species and two free radicals, and 16 other species were also detected.

In the present research, a similar flame containing 5% argon was selected. The same C_2H_2/O_2 ratio, burner velocity, and pressure were used. Although flame temperature is lowered slightly relative to Bonne et al. by the addition of Ar, the shapes and magnitudes of the concentration profiles are similar, allowing limited comparison between the sets of data.

CHAPTER II. LITERATURE ON STUDY OF FLAT FLAMES BY MBMS

II.1. Flat flames

The flat flame is a one-dimensional, laminar premixed flame that is well-suited for laboratory study of combustion chemistry. Scientific literature on the utility, development, and mathematical description of flat flames is discussed briefly in this section (Ch. II.1). In Ch. II.2, application of molecular-beam mass spectrometry (MBMS) to flat flames is discussed.

Measurements of temperature and concentration in a flat flame are useful for understanding the physical and chemical processes of combustion, qualitatively and quantitatively. More importantly, only laminar flow phenomena and reaction are present, so the flame can be modeled using simple equations of motion. This feature has made it possible in recent years to begin testing entire mechanisms of reactions with flat-flame data.

Experimental description. - Fuel and oxidant are mixed and then flow through channels or pores in a cooled flameholder. The combustible mixture is ignited, and the resulting flame initially propagates toward the source of the fuel-air mix. A steady-state is quickly established, however, because the large conductive heat loss to the cooled burner arrests the propagation through space while the incoming gases continue to feed the flame. By maintaining stable flows and uniform cooling of the burner face, a flame is created that is quite reproducible and time-invariant in the continuum. The thickness of the flame is inversely proportional to pressure, so low-pressure conditions are often chosen to improve spatial resolution of samples and optical measurements.

Stability is key among the favorable properties of this flame. Because the flame is time-stable and spatially one-dimensional, changes in its properties can be followed as a function of that one coordinate. Its laminar flow allows classical one-dimensional flow equations to describe it well by using only convection, diffusion, and reaction terms. Being premixed and strongly burner-stabilized, the flame can tolerate the physical intrusion of probes much better than can diffusion flames.

Origins. - The experimental method dates from 1949 when the Powling-Egerton burner was developed to measure flame velocities and flammability limits (Powling, 1949; Egerton and Thabat, 1952). This burner was constructed by winding a corrugated metal strip into a 6-cm-diam cylinder, forming 4000 channels with cross-sections of 0.65 mm². Open flow channels are useful when seeding of the flame is required, as for Na d-line temperature measurements (Taylor, 1984), and in sooting flames that form burner deposits (Bittner, 1981; this work).

Botha and Spalding (1952) developed an alternative design using sintered-bronze disks, soldered to a water jacket. Kaskan (1957) refined the cooling by imbedding a cooling coil in the burner, originally using copper pellets covered with a fine brass filter. Present designs combine these designs, fabricating the flameholder by sintering bronze with an imbedded cooling coil and cooling the periphery of this cylinder as well.

Flame equations of Fristrom and Westenberg. - The flow equation for the flame that results from such an experiment can be described by the equations for one-dimensional cylindrical flow (Bird et al., 1960). The flow cross-sectional area expands slightly, though not enough to interfere with the effective one-dimensionality. Taking this area expansion into account, Fristrom and Westenberg (1965) express the flame equations as an equation of motion for species *i*:

$$K_i A = \frac{d}{dz} [F_i A] \quad [II.1]$$

and a flux equation

$$F_i = x_i \rho_m (v + V_i) A \quad [II.2]$$

where

K_i is the net molar rate of formation of species *i*;

A is the area-expansion ratio, a function of z ;

z is the distance from the burner;

F_i is the net molar flux of *i*;

x_i is the mole fraction of i ;
 ρ_m is the molar density (total concentration);
 v is the mass-average convection velocity; and
 V_i is the diffusion velocity of i .

The area expansion ratio is measured either from the observed flow cross-sections S or from non-flame experiments using

$$A(z) = \frac{S_z}{S_0} = \frac{(\rho v)_0}{(\rho v)_z} \quad [\text{II.3}]$$

where ρ is mass density and the subscript 0 refers to the burner surface. Diffusion velocity V_i was defined, in the absence of thermal diffusion, as

$$V_i = - \frac{D_{i,mix}}{x_i} \frac{dx_i}{dz} \quad [\text{II.4}]$$

where $D_{i,mix}$ is the molecular diffusivity of species i in the mixture.

Analysis of fluxes and reaction rates by these equations then requires data on mole fractions $x_i(z)$, temperature $T(z)$, and area expansion ratio $A(z)$. An energy equation corresponding to the equations of motion may also be written and used, but normally a measured temperature profile is used because of ill-defined heat losses to the burner and surroundings.

First, the diffusion velocity V_i is calculated from the diffusivity, the mole fractions, and the slopes of the mole fraction curves by using Eq. II.4. Mixture diffusivity $D_{i,mix}$ is calculated from binary diffusivities $D_{i,j}$ by some mixing rule, and $D_{i,j}$'s are calculated from molecular theory. [In analyzing the present data, $D_{i,j}$ is calculated from temperature and Lennard-Jones parameters (Kee et al, 1983) using the expression of Fristrom and Westenberg (1965), and $D_{i,mix}$ is calculated by the Wilke rule (Fairbanks and Wilke, 1950).]

Next, the molar fluxes F_i are calculated from Eq. II.2 using V_i

and v . Convective velocity v is calculated by rewriting Eq. II.3, assuming ideal gas behavior, as

$$v = \frac{(\rho v)_0}{A \cdot \left(\frac{P}{RT}\right) \sum_i (x_i M_i)} \quad [\text{II.5}]$$

Reaction rates K_i follow directly from the fluxes by using Eq. II.1.

Fristrom and Westenberg (1965) recommend checking the data and this analysis by calculating mass flux balances for the elements and the total mass flux. The reasoning is that frequently some mole fraction in the flame is calculated by difference, so mass balances are not useful.

II.2. Molecular-beam mass spectrometry (MBMS)

MBMS is one of several methods for measuring concentrations in flat flames, but it is unique in its potential to measure a wide diversity of species, notably including free radicals. Microprobe sampling (Fristrom and Westenberg, 1965), followed by gas chromatography, can be used to measure profiles of many species, but it is restricted to stable species. In contrast, spectroscopic methods based on emission or absorption can detect stable species and free radicals, but fewer species can be analyzed in a given flame because different species require different methods.

Components. - In MBMS, molecular-beam sampling is used to obtain a sample from the flame and to introduce it into the ionizer of a mass spectrometer, maintaining collisionless flow. An orifice of 0.1 to 1 mm diameter is the source of the beam, and it is located in a probe tip protruding into the flame so that the convective, diffusive, and temperature fields will be perturbed as little as possible. Biordi et al. (1974) showed that with proper design of the shape of the quartz sampling probe, concentrations of CH_4 and OH could be measured with only slight perturbation, and the temperature profile was characterized simply.

The initial, supersonic expansion into a vacuum chamber reduces pressure by orders of magnitude, cooling the gases to translational

temperatures on the order of 20 K. By cooling the gas and eliminating collisions, free radicals ideally are prevented from being destroyed by unimolecular and bimolecular reactions.

The core of the molecular flow from the sampling nozzle is sampled through a skimmer nozzle and reduced further in pressure. This second nozzle eliminates molecules at the outside of the flow which might have contacted the nozzle wall.

The mass spectrometer may be located in the second stage of the sampling system or a third, higher-vacuum stage may be necessary, depending on pressure requirements. Magnetic-sector, time-of-flight and quadrupole mass spectrometers have each been used, and the quadrupole may be collinear with the molecular beam or normal to it. Electron-impact ionization is used most commonly, and the beam is normally chopped so that background contributions in the mass-spectrometer chamber can be subtracted.

Significant studies. - Eltenton (1942, 1947) and Foner and Hudson (1953) reported the ability to detect free radicals by molecular-beam sampling into magnetic-sector mass spectrometers. Neither spatial resolution nor calibration of the signals was attempted. Eltenton sampled pyrolysis of $\text{Pb}(\text{CH}_3)_4$ and diffusion-flame jets for CH_4 , C_3H_8 , and CO , detecting signals assigned to the radicals CH_3 , OH , HCO , CH_3O , and HO_2 . Foner and Hudson sampled the exhaust of a tubular flow reactor containing O_2 into which fuel was injected at different distances from the exhaust. H_2 and CH_4 flames were examined, and H , O , and OH were detected in the H_2/O_2 flame.

The work of Homann, Wagner, and co-workers in the 1960's made this approach quantitative. Beginning with that work, MBMS analyses of C/H/O flames that have been reported in the literature are summarized in Table II.1.

In the pioneering paper by Homann, Mochizuki, and Wagner (1963), low-pressure, fuel-rich flat flames of C_2H_2 ($\phi=2.1$ ¹), C_2H_4 ($\phi=3$), C_3H_8 ($\phi=2.7$), and benzene ($\phi=1.92$) were studied in a time-of-flight

¹Fuel-equivalence ratio ϕ is the fuel/oxygen ratio of the actual feed gas divided by the fuel/oxygen ratio for stoichiometric complete combustion; thus, $\phi=1$ for a stoichiometric fuel/oxygen mixture, $\phi<1$ for a fuel-lean mixture, and $\phi>1$ for a fuel-rich mixture.

Table II.1. Flat-flame/MBMS studies of C/H/O flames.

<u>Fuel; ϕ, P</u>	<u>Reference</u>	<u>Nature of mole-fraction data</u>
<u>CO/H₂</u>		
$\phi = 0.131$, 5.34 kPa (40 torr)	Vandooren, Peeters, and Van Tiggelen (1975)	T, H, H ₂ , O, OH, H ₂ O, CO, O ₂ , HO ₂ , and CO ₂ profiles (fed 9.4% CO, 11.4% H ₂ , 79.2% O ₂)
1.00, 6.68 (50 torr)	Safieh, Vandooren, and Van Tiggelen (1982)	T, H, H ₂ , O, OH, H ₂ O, CO, O ₂ , HO ₂ , and CO ₂ (fed 39.6% CO, 2.1% H ₂ , 20.8% O ₂ , 37.5% Ar)
<u>CH₄</u>		
0.21, 5.34 (40 torr)	Peeters and Mahnen (1973a)	T, H, H ₂ , CH ₃ , CH ₄ , O, OH, H ₂ O, CO, H ₂ CO, CH ₃ OH, O ₂ , CO ₂ , CH ₃ OO
0.56, 2.20 (16.5 torr)	Peeters and Vinckier (1975)	H, CH, CH ₂ , CH ₃ , O, OH, O ₂ ; Estimated T _{max} (fed 29.9% Ar)
0.83, 101 (1 atm)	Milne and Greene (1965)	T, H ₂ , H ₂ O, CO, O ₂ , Ar, CO ₂ (fed 70.2% Ar; metal nozzle)
0.95, 4.27 (32 torr)	Biordi, Lazzara, and Papp (1975a)	T, H, H ₂ , CH ₃ , CH ₄ , O, OH, H ₂ O, CO, O ₂ , CO ₂ (fed 68% Ar)
0.98, 2.20 (16.5 torr)	Peeters and Vinckier (1975)	H, CH, CH ₂ , CH ₃ , O, OH, O ₂ (fed 54.5% Ar)
1.00, 2.67 (20 torr)	Harvey and Maccoll (1979)	T, CH ₃ , C ₂ H ₂ , C ₂ H ₄ , H ₂ CO
1.00, 101 (1 atm)	Milne and Greene (1965)	T, H ₂ , H ₂ O, CO, O ₂ , Ar, CO ₂ (fed 72.7% Ar; metal nozzle)
1.00, 101 (1 atm)	Cattolica, Yoon, and Knuth (1982)	OH by MBMS and laser absorption and T by thermocouple and mol- ecular-beam time of flight
<u>C₂H₂</u>		
0.13, 5.34 (40 torr)	Vandooren and Van Tiggelen (1977)	T, H, H ₂ , CH ₂ , CH ₃ , O, OH, H ₂ O, C ₂ H ₂ , CO, H ₂ CO, O ₂ , C ₂ H ₂ O, CO ₂
1.0, 5.34 (40 torr)	Vandooren (1976)	T, H, H ₂ , CH ₂ , CH ₃ , O, OH, H ₂ O, C ₂ H ₂ , CO, H ₂ CO, O ₂ , C ₂ H ₂ O, CO ₂ (fed 83.46% Ar)
2.1, 2.67 (20 torr)	Homann et al. (1963)	H ₂ , CH ₄ , H ₂ O, C ₂ H ₂ , CO, H ₂ CO, O ₂ , C ₃ H ₄ , CO ₂ , C ₄ H ₂ , C ₄ H ₄ , C ₄ H ₆ , C ₆ H ₂ , C ₆ H ₆ , C ₈ H ₂
2.38, 2.67 (20 torr)	Bonne, Homann, and Wagner (1965)	H ₂ , CH ₄ , H ₂ O, C ₂ H ₂ , CO, H ₂ CO, O ₂ , C ₃ H ₄ , CO ₂ , C ₄ H ₂ , C ₄ H ₄ , C ₆ H ₂ , C ₆ H ₆ , C ₈ H ₂ ; C ₂ H and HCO profiles reported (see text)
2.40, 2.67 (20 torr)	This work	T, mole-fraction profiles of 38 species (fed 5.0% Ar)
2.6, 2.67 (20 torr)	Delfau and Vovelle (1985)	T, mole-fraction profiles of 37 species
3.0, 2.67 (20 torr)	Cole (1982)	C ₂ H ₂ , O ₂ , C ₄ H ₂ , C ₄ H ₄ , C ₆ H ₆ , C ₁₀ H ₈ , C ₁₂ H ₈ , C ₁₄ H ₈ (fed 3.0% Ar)
3.0, 2.67 (20 torr)	Delfau and Vovelle (1984a)	T, mole-fraction profiles of 23 species

<u>C₂H₄</u>		
0.21, 5.34 (40 torr)	Peeters and Mahnen (1973b) Mahnen (1973)	T, H, H ₂ , CH ₂ , CH ₃ , O, OH, H ₂ O, C ₂ H ₂ , C ₂ H ₃ , C ₂ H ₄ , CO, H ₂ CO, O ₂ , CO ₂
0.59, 2.20 (16.5 torr)	Peeters and Vinckier (1975)	H, CH, CH ₂ , CH ₃ , O, OH, O ₂ (fed 31.3% Ar)
0.80, 2.20 (16.5 torr)	Peeters and Vinckier (1975)	H, CH, CH ₂ , CH ₃ , O, OH, O ₂ (fed 45.6% Ar)
1.06, 2.20 (16.5 torr)	Peeters and Vinckier (1975)	H, C, CH, CH ₂ , CH ₃ , O, OH, O ₂ (fed 54.5% Ar)
3.0, 4.54 (34 torr)	Homann et al. (1963)	H ₂ , H ₂ O, C ₂ H ₂ , C ₂ H ₄ , CO, H ₂ CO, O ₂ , C ₃ H ₄ , Mass 42, CO ₂ , C ₄ H ₂ , C ₄ H ₄ , C ₄ H ₆ , C ₆ H ₂ , C ₆ H ₆
<u>C₃H₆</u>		
2.7, 8.01 (60 torr)	Homann et al. (1963)	H ₂ , CH ₄ , H ₂ O, C ₂ H ₂ , C ₂ H ₄ , CO, H ₂ CO, O ₂ , C ₃ H ₄ , Mass 42, CO ₂ , C ₄ H ₂ , C ₆ H ₂ , C ₆ H ₆
<u>1,3-C₄H₆</u>		
1.0, 2.67 (20 torr)	Cole (1982)	Mole fraction profiles of 19 species (fed 60.0% Ar)
2.4, 2.67 (20 torr)	Cole, Bittner, Howard, and Longwell (1984)	Mole fraction profiles of 37 species (fed 3.0% Ar)
<u>Benzene</u>		
1.00, 2.67 (20 torr)	Bittner (1981)	T, mole-fraction profiles of 25 species (fed 30% Ar)
1.80, 2.67 (20 torr)	Bittner and Howard, (1981)	T, mole-fraction profiles of 51 species (fed 30% Ar)
1.92, 5.34 (40 torr)	Homann et al. (1963)	H ₂ , CH ₄ , H ₂ O, C ₂ H ₂ , C ₂ H ₄ , CO, O ₂ , C ₃ H ₄ , CO ₂ , C ₄ H ₂ , C ₆ H ₂ , C ₆ H ₆ , C ₆ H ₆ O, C ₈ H ₆ , C ₉ H ₆ , C ₁₀ H ₆ , C ₁₂ H ₆ , C ₁₂ H ₁₀
<u>H₂CO</u>		
0.22, 3.00 (22.5 torr)	Vandooren et al. (1986)	T, H, H ₂ , O, OH, H ₂ O, CO, HCO, H ₂ CO, O ₂ , HO ₂ , CO ₂
<u>CH₃OH</u>		
0.36, 5.34 (40 torr)	Vandooren and Van Tiggelen (1981)	T, H, H ₂ , O, OH, H ₂ O, CO, H ₂ CO, CH ₃ O, CH ₃ OH, O ₂ , CO ₂
0.89, 5.34 (40 torr)	Vandooren and Van Tiggelen (1981)	T, H, H ₂ , CH ₃ , O, OH, H ₂ O, CO, H ₂ CO, CH ₃ O, CH ₃ OH, O ₂ , Ar, CO ₂ (fed 46.1% Ar)
1.0, 13.4 (100 torr)	Olsson et al. (1986)	Intensity profiles only (no mole fractions; also with added H ₂ O)
<u>CH₃OH/H₂</u>		
0.21, 5.34 (40 torr)	Vandooren and Van Tiggelen (1981)	T, H, H ₂ , OH, H ₂ O, CO, H ₂ CO, CH ₃ O, CH ₃ OH, O ₂ , CO ₂ (10.9% CH ₃ OH, 3.2% H ₂ , 85.9% O ₂ fed)

MBMS system. Profiles of mole fraction vs. distance were shown for 15 to 16 stable species in each flame. More extensive work on C_2H_2/O_2 flames (Bonne, Homann, and Wagner, 1965; Homann and Wagner, 1965) included mole-fraction profiles by MBMS for a flame at $\phi=2.38$, 2.67 kPa (20 torr) and $0.5 \text{ m}\cdot\text{s}^{-1}$ burner velocity (at 298 K). Profiles for 12 stable species, C_2H , and HCO were presented, although the radical profiles have since been recognized to be incorrectly high (Ch. IV, this work; Homann, 1984).

The work of Van Tiggelen, Peeters, and Vandooren (see table) covers the longest period of study, from 1973 to the present, and the greatest range of fuels. Early in that time, analysis and calibration procedures for flame radicals were worked out (Peeters and Mahnen, 1973). This body of work is fairly complete as far as including temperature profiles and most or all of the detectable species. Flames of CO/H_2 , CH_4 , C_2H_2 , C_2H_4 , H_2CO , and CH_3OH have been studied for fuel-lean and stoichiometric mixtures at pressures of 2.20 to 6.68 kPa (16.5 to 50 torr).

Data by Biordi and co-workers, Milne and Greene (1965), Harvey and Maccoll (1979), the UCLA group (Yoon, Knuth, and Smith), Delfau and Vovelle, Olsson and co-workers, and the MIT group are also important parts of the literature for MBMS sampling of C/H/O flames.

Other important studies, not shown in Table II.1, include flames containing halogen additives (Biordi et al., 1973, 1975a, 1975b), nitrogen and/or sulfur compounds (Blauwens et al., 1977; Seery and Zabielski, 1981; Smith et al., 1983; Tseregounis and Smith, 1985), and MBMS study of ions (Michaud et al., 1981; Olson and Calcote, 1981).

Application and limitations of these data. - In this decade, it has become possible to predict mole-fraction profiles for flat flames using mechanisms of elementary reactions. Table II.1 then is not only an overview of many of the MBMS flame studies that have been conducted, but it is also a review of C/H/O flames that could be used for testing chemical mechanisms.

Note that many of the studies do not include temperature profiles. Mechanistic modeling of such data is then difficult or

impossible, even using an energy equation, because there is no way to quantify heat losses to the burner.

Furthermore, many of the studies report profiles only for stable species or for a very limited set of species. These data are still useful for testing mechanisms, but obtaining as complete a characterization of the flame as possible permits the most extensive testing.

These studies then represent a valuable data base for testing mechanistic models, but in many cases the absence of profiles for temperature, radicals, and other key species limits their utility. The present data are intended to confirm and extend the data of Bonne, Homann, and Wagner (1965) by including temperatures, radical profiles, and more detailed profiles for the stable species they reported as well as for other detectable species. Microprobe sampling and GC/MS analysis also extend the earlier work by identifying high-molecular-weight species ($MW = 68$ to 180) in the flame and establishing their relative amounts.

CHAPTER III. APPARATUS AND EXPERIMENTAL PROCEDURES

III.1. Introduction

The experimental goal of the thesis was to map concentrations in a fuel-rich premixed, laminar flame of acetylene and oxygen using molecular-beam mass spectrometry (MBMS). In the unburned feed gas, the mole fractions were 0.465 C₂H₂, 0.485 O₂, and 0.050 Ar, giving a fuel equivalence ratio $\phi=2.40$.

These conditions were chosen to approximate the acetylene flame ($\phi=2.30$, no Ar) of Bonne, Homann and Wagner (1965), which was mapped in one of the first MBMS flame studies. They reported mole-fraction profiles for 13 stable species, C₂H, and HCO. Unfortunately, the radical profiles were incorrect (Ch. IV, this work; Homann, 1984) and no temperatures were reported. The purpose of that work was to follow quantitatively the evolution of species in the flame, so only 4 to 13 points per species were measured. In this study, by comparison, more detailed data on more species permit improved testing of detailed flame models.

Experiments were conducted in a low-pressure burner system which was assembled originally by Wersborg (1972) and later modified extensively by Bittner (1981). The key modification of Bittner was to install a quadrupole mass spectrometer collinearly with an improved molecular-beam sampling system, which permitted analysis of concentrations for stable species and free radicals. In the present work, ion-counting detection was added in collaboration with Cole (1982), and computerized data acquisition and processing was developed. Also, an approximate technique for estimating mass-spectrometer calibration was developed.

Bittner (1981) has described design, hardware, and operating procedures for the apparatus in some detail. Certain significant changes have been made during the present research, some of which have been described by Cole (1982) in a thesis that was completed earlier:

- The flameholder was redesigned and modified so that it could be disassembled for cleaning or repair (see Cole, 1982);

- The 0.7-mm-diam. sampling nozzle of Bittner was replaced with a 0.55-mm-diam. nozzle;
- A liquid-nitrogen-cooled cryotrap was installed above the third-stage diffusion pump;
- Pulse-counting detection was added to the mass spectrometer in order to improve sensitivity to sub-ppm levels (see Cole, 1982);
- A digital mass programmer was added to the mass spectrometer that allows up to 15 positions in the mass spectrum to be addressed, permitting better corrections for isotopic interferences;
- Computerized data acquisition and computer-aided preparation of smoothed curves; and
- A calibration method that requires only the electron energy (MS ionizing energy) used to measure Ar and the species of interest.

Components of the system, general procedures, and these changes are described briefly here. The reader is referred to Bittner (1981) for further detail on the overall apparatus and procedure and to Cole (1982) for further details on the pulse-counting feature. Measurements of temperature and of mass-discrimination factors are also described here.

III.2. Low-pressure flat-flame burner system

The flat flame was stabilized at 2.67 kPa (20.0 torr) on a circular, water-cooled, copper burner. By making heat loss to a burner uniform across its face and by setting flow to be laminar, flame conditions can be chosen to give nearly one-dimensional flow; that is, radial gradients in the core of the flame will be negligible.

The flameholder was machined from copper and drilled with 1-mm-diam. holes spaced 2.5 mm apart on a triangular pitch. These holes covered an approximately circular area of 3970 mm². To insure a uniform surface temperature, the burner surface was thick (12.7 mm) with respect to the supporting walls (2.7 mm) that connected it to

the cooling-water chamber. Also, a drilled flow straightener and mixing region helped insure a uniform flow of feed gas through the flameholder. Finally, to facilitate cleaning, the flameholder assembly was modified from the unit used by Bittner (1981) so that it could be taken apart using threaded surfaces and O-ring seals.

The flameholder was mounted vertically inside the burner chamber on a brass pipe. This pipe was sealed by a double O-ring seal in a mounting flange. To adjust the axial distance from the flameholder to the sampling nozzle, the brass pipe was fastened to an external, manually operated lathe positioner.

The surrounding burner chamber was a 150-mm-diam., water-jacketed cylinder of stainless steel (see Fig. III.1). A 70-mm-diam. window normal to the burner axis provided optical access for measuring the relative positions of the flameholder and the sampling nozzle. In addition, two compression fittings in the burner mounting flange provided access for the ignitor and for a thermocouple or microprobe.

Low pressure was maintained by pumping flame gases from the burner chamber with a Stokes/Pennwalt Microvac vacuum pump (Model 149-11, capacity 0.038 m³/s), which was protected from soot by a high-surface-area filter. The desired pressure was set approximately by adjusting a gate valve at the vacuum pump and more precisely by a ballast-air valve. [By maintaining critical flow through the gate valve, the burner-chamber pressure was also protected from fluctuations due to the vacuum pump.] Pressure in the exhaust line was monitored by a capacitance manometer (MKS Baratron Model 270A with Model 370A-00100 sensor head).

Oxygen, argon, and calibration gases were metered directly from cylinder regulators using critical orifices (0.038- and 0.032-mm-diam. for O₂ and Ar, respectively). Upstream pressures of the oxygen and argon feed gases were monitored using 1600-mm mercury manometers, while the pressures of calibration gases (H₂, CH₄, CO, O₂, CO₂) were measured with pressure gauges.

Acetylene was purified of acetone (in which it is supplied) by passing the gas through a saturated solution of NaHSO₃(aq), 10 wt% NaOH(aq), and silica gel in a series of three traps. From the

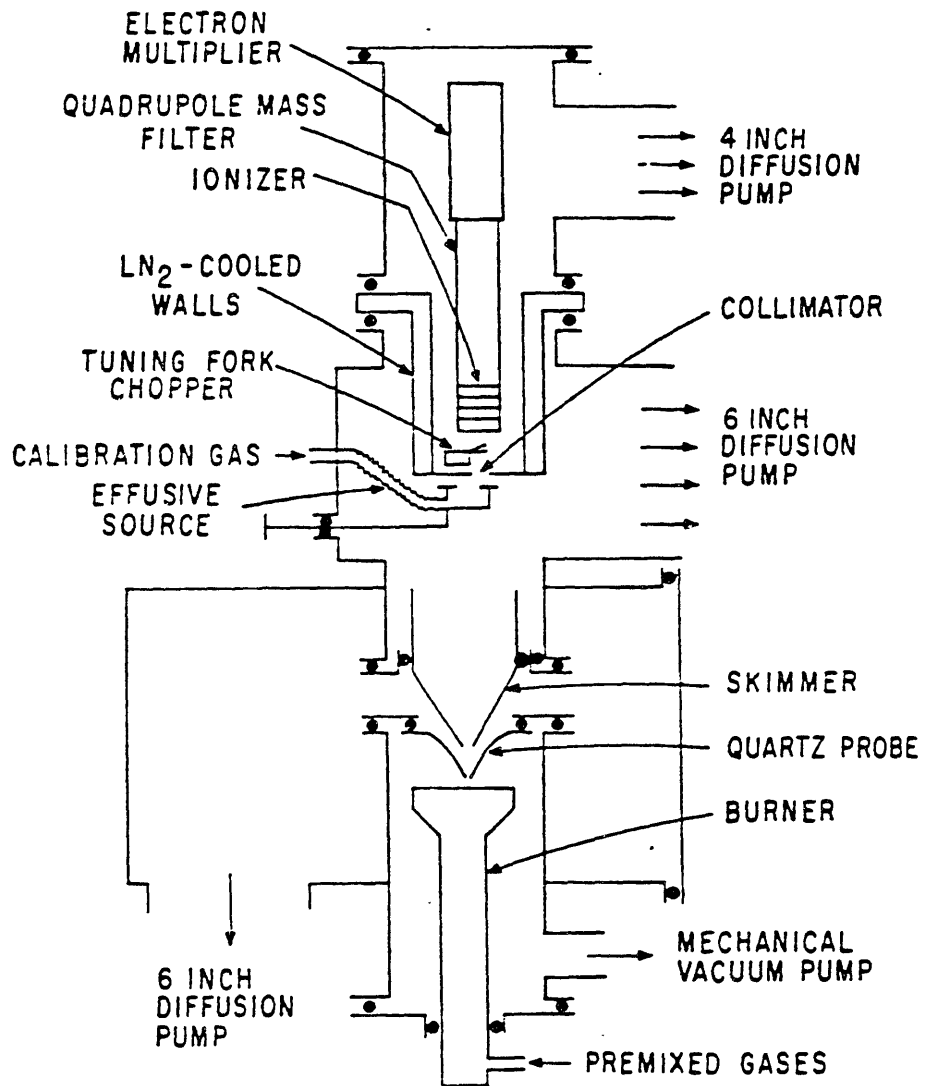


Fig. III.1. Cross-section of the MBMS apparatus.

purification traps, a steady delivery pressure was maintained using a pancake-type line regulator. Flow of C_2H_2 was adjusted with a needle valve and measured with a 0.032-mm-diam. critical-flow orifice and a diaphragm-style pressure transducer (Validyne model DP-7-50).

III.3 Molecular-beam sampling, mass spectrometer, and calibration

A cross-section of the burner chamber and the three-stage MBMS system is shown in Fig. III.1. Gases are sampled from the flame through a 0.55-mm-diam. quartz nozzle, are rapidly quenched by a supersonic expansion into the first stage, with a nominal pressure of 10^{-2} Pa (10^{-4} torr) maintained by a 6-in. diffusion pump (polyphenyl-silicone oil). A molecular beam is formed by a 0.90-mm-diam. skimmer located 18 mm behind the sampling nozzle, and it travels 340 mm through background gas in the second stage at 10^{-4} Pa (10^{-6} torr), maintained by another 6-inch diffusion pump. Finally, the beam is collimated by a 3.0-mm-diam orifice, chopped at 220 Hz with a tuning-fork chopper, and ionized in a collinearly mounted quadrupole mass spectrometer approximately 410 mm from the sampling nozzle. Pressure was maintained at 3 μ Pa ($2 \cdot 10^{-8}$ torr) by a liquid-nitrogen-cooled partition surrounding the quadrupole, and by a liquid-nitrogen-cooled cryotrap on a 4-inch diffusion pump.

The mass spectrometer is an Extranuclear Laboratories (Extrel) Model 54-162-8 quadrupole unit with electron-impact ionization. Mass number is set by the quadrupole power supply or by a digital mass programmer (both by Extranuclear). Signal is collected with a channeltron-type electron multiplier (Galileo Electro-optics 4816), which can be operated to give analog or pulse (single-ion) electron multiplication. For the analog signal, background is subtracted from the beam using a lock-in amplifier (Princeton Applied Research Model HR-8) tuned to the resonant circuit of the chopper. For high-sensitivity pulse counting, photon-counting electronics (Princeton Applied Research Model 1112) are used. Foreground and background counting windows are set by mapping them directly, using narrow time intervals and a strong signal.

An IBM PC $\text{\textcircled{C}}$ computer and a Tecmar Labmaster $\text{\textcircled{C}}$ data acquisition board were used to collect, plot, and store the analog data from the

lock-in amplifier (-10 to +10 V with 12-bit accuracy) and from the pulse counting output (BCD integer counts on a parallel port). Programs were also written to draw smoothed curves through the data points using analog graphics input (Koalapad graphics tablet) or cursor keys, refining these curves with the smoothing algorithms of Savitsky and Golay (1964; and Steinier et al., 1972).

The general procedure for data collection begins by igniting the flame and allowing 45 min for the temperatures in the burner chamber to stabilize. Then the burner is moved vertically to various burner-to-nozzle distances, which are measured with a cathetometer. An Ar signal is read as a reference, then the species of interest, then the Ar again. For species whose signals are affected by isotopic contributions from lower-mass species (which may be affected by still lower-mass species), Ar is read first, then the sequence from lowest-mass through highest-mass species of interest, the sequence in reverse, and Ar again; for example, Ar, CH₃, CH₄, OH, and OH, CH₄, CH₃, Ar. The intent is to minimize any effects of long-term drift in the mass-spectrometer electronics (caused primarily by ambient temperature changes).

Because the flame was so fuel-rich, a deposit formed on the sampling nozzle beyond approximately 5 mm, causing it to glow red and causing some scavenging of radicals. No drift was observed in most of the species measurements, but H and OH were strongly affected. To counter this effect, the nozzle was burned off periodically for all species by switching temporarily to a fuel-lean flame. For H and OH, the signal was followed in time after switching back to the $\phi=2.40$ condition and later was extrapolated to zero time. This problem affects H and OH in the post-flame zone and may account for the difficulty in measuring CH₂ and C₂H in that region.

III.4. Temperature measurement

Temperatures were measured using a combination of unheated and electrically compensated thermocouple techniques. A Pt/Pt-13%Rh thermocouple was used, coated with BeO-Y₂O₃ as described by Kent (1970) to minimize catalytic activity of the metal. The junction between the 0.076-mm-diam. wires was butt-welded so that there was no

detectable change in diameter, permitting the thermocouple to be modeled as a cylinder in a transverse flow field. This 40-mm-long thermocouple wire was welded to 0.38-mm support wires.

Temperatures close to and far from the burner were low enough that the electrical-compensation method could be used (Bittner, 1981; Neoh, 1980). In this technique, the thermocouple is resistively heated by an AC, variable-current circuit (3 kHz, 0-1 A), capacitively isolated from the DC thermocouple voltage. The thermocouple voltage then is measured as a function of the AC heating current, first in vacuum, then in the flame at different positions, and finally in vacuum again.

The vacuum measurement is in effect a calibration for the flame measurements. Thermal processes in the general case are convective heating (or cooling), radiative cooling, and resistive heating. In vacuum, there is no convection. Likewise, there is no convection in the flame if flame and thermocouple temperatures are equal. Thus, the flame temperature can be determined when the same heating current gives matching temperatures in the flame and in vacuum.

This technique is limited to temperatures below the softening and melting points of the thermocouple. An alternative method was used at higher temperatures. The lower temperatures were measured using the resistive heating technique, and the thermocouple emissivity (as an emissivity-diameter product ϵd) was calculated from a heat balance. Temperatures of the unheated thermocouple were measured for the higher temperatures, and the temperature correction was calculated from the heat balance and ϵd .

Heat-transfer analysis. - The governing heat-transfer equation is:

$$\begin{array}{rcccl} \text{Conductive} & & \text{Radiative} & & \text{Resistive} & & \\ \text{heating} & - & \text{cooling} & + & \text{heating} & = & 0 \\ \\ h \cdot L \pi d (T_{\text{flame}} - T_{\text{TC}}) & - & L \pi d \cdot \epsilon \sigma (T_{\text{TC}}^4 - T_{\text{wall}}^4) & + & L \cdot \frac{\rho_e I^2}{\pi d^2 / 4} & = & 0 \quad \text{[III.1]} \end{array}$$

where h is the heat transfer coefficient; L is the basis length; d is the thermocouple diameter; T_{flame} , T_{TC} , and T_{wall} are the absolute

temperatures of the flame, thermocouple, and wall; ϵ is the thermocouple surface emissivity; σ is the Stefan-Boltzmann constant; ρ_e is the electrical resistivity per unit length; and I is the (variable) heating current.

This equation can be re-expressed in more useful form. T_{wall} (298 K) is much less than T_{TC} , the thermocouple temperature, so T_{wall} drops out of the radiation term. The heat transfer coefficient can be obtained from the expression for transverse laminar flow across a cylinder (Kramers, 1946; Bittner, 1981):

$$Nu = 0.42 \cdot Pr^{0.2} + 0.57 \cdot Pr^{1/3} Re^{1/2} \quad [III.2]$$

where the Nusselt number Nu is hd/k , the Prandtl number Pr is $C_p \mu/k$, the Reynolds number Re is $\rho v d/\mu$, and C_p , μ , k , and ρ are the specific heat, viscosity, thermal conductivity, and density of the gas at a film temperature $T_{film} = (T_{TC} + T_{flame})/2$. Equation III.1 then reduces to the general form:

$$hd(T_{flame} - T_{TC}) - (\epsilon d)\sigma T_{TC}^4 + \frac{4\rho_e I^2}{\pi^2 d^3} = 0 \quad [III.3]$$

At relatively low temperatures, both T_{flame} and the unheated T_{TC} are measured, and Eq. III.2 and III.3 are solved for ϵd . For the unheated thermocouple in the higher-temperature measurements, ϵ is assumed not to change. The resistive heating term drops out, and T_{flame} is determined by ϵd , Eq. III.2, and Eq. III.3.

Measurements. - The temperatures of the flame and the unheated thermocouple are shown in Fig. III.2. In the previous attempt, the calibration curve had changed between the time it had been measured with a clean (ceramic-coated) thermocouple and after the measurements in the sooting flame, which left the thermocouple charcoal-grey. Both the thermocouple and the calibration were left unchanged by the experiment of Fig. III.2, so thermocouple emissivity was considered to have remained constant.

The most reliable measurement of ϵd was taken to be the measurement at the highest temperature, where the temperature correction

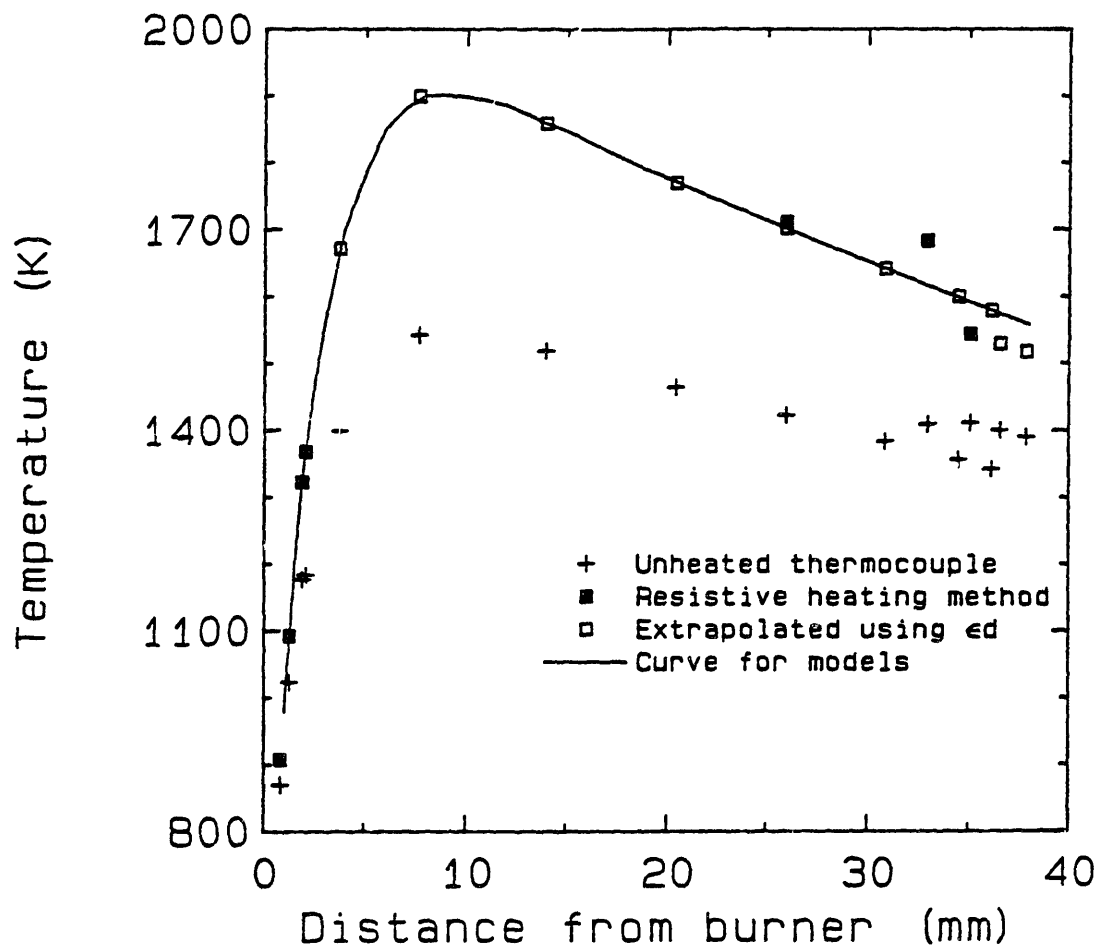


Fig. III.2. Temperature data for laminar, premixed flame of $C_2H_2/O_2/5\% Ar$, $\phi=2.40$, 2.67 kPa (20 torr), and $0.5 \text{ m}\cdot\text{s}^{-1}$ velocity of unburned gas (298 K).

should be greatest. This measurement gave $\epsilon d = 3.63 \cdot 10^{-3}$ cm, or $\epsilon \approx 0.38$, at 35.09 mm, $T_{\text{flame}} = 1543$ K, and $T_{\text{TC}}(\text{unheated}) = 1411$ K. At high temperatures, this ϵd leads to correction factors as large as 357 K [7.67 mm, $T_{\text{TC}}(\text{unheated}) = 1542$ K, so $T_{\text{flame}} = 1899$ K]. For comparison, Peterson and Laurendeau (1985) report $\epsilon = 0.60$ for clean, Y_2O_3 -BeO-coated thermocouples but cite a range in the literature of 0.25 to 0.75.

Measurements of ϵd at lower temperatures, which were considered less reliable, were $7.85 \cdot 10^{-3}$ or $\epsilon \approx 0.74$ at 1.89 mm [$T_{\text{TC}}(\text{unheated}) = 1177$ K, $T_{\text{flame}} = 1322$ K] and $8.79 \cdot 10^{-3}$ or $\epsilon \approx 0.83$ at 2.06 mm [$T_{\text{TC}}(\text{unheated}) = 1183$ K, $T_{\text{flame}} = 1672$ K]. If these were more accurate, the maximum measured T_{flame} would be as high as 2320 K. A mean of the three emissivities is 0.65, which would lead to a maximum of 2150 K. This variation is an important uncertainty, but $\epsilon = 0.38$ was used in calculating the temperatures shown in Fig. III.2 and Appendix A for the reasons noted in the previous paragraph.

III.5. Analysis of data

Mole fractions were calculated from a mass balance on Ar. Calibration factors for major stable species (except H_2O), which make up nearly all the mass, were determined directly, as discussed in Ch. IV, and the calibration factor for H_2O was determined from an O-atom balance at 35 mm. Mass-discrimination factors for changes in the beam concentrations were calculated from cold-gas experiments, with the results listed in Table III.1. The area expansion ratio was measured previously for this burner flux and system (Bittner, 1981) to be $A(z) = (1 - 0.116z)^{-1}$, where z is the distance from the burner in cm. Fluxes and reaction rates were calculated using the flame equations and analysis methods described in Ch. II.1.

The use of Ar as a reference for the mass balance is compromised by interference with C_3H_4 . Ar was introduced in the unburned gas at 5.00 mol%. C_3H_4 is lower in concentration, but it has a much lower ionization potential and can affect the Ar signal in this flame by as much as 10%. Profile of mass 40 were measured at electron-energy settings of 12, 12.5, 13, 13.5, 14, and 19 eV, and the correction factor for Ar was determined as a function of distance from the

Table III.1. Mass discrimination factors $\alpha(i,Ar)$.

<u>Species</u>	<u>Mass discrimination factor at 298 K and:</u>		<u>$\alpha(i,Ar)$ for flame calibration</u>
	<u>2 torr</u>	<u>12 torr</u>	
H ₂	0.1773	0.1302	0.154 ± 16%
CH ₄	0.444	0.422	0.435 ± 3%
C ₂ H ₂	0.86	0.76	0.81 ± 6%
CO	0.822	0.773	0.798 ± 3%
O ₂	0.847	0.833	0.841 ± 1%
Ar	-	-	[1]
CO ₂	0.991	0.994	1.017 ^a
Toluene	1.029	1.193	1.111 ± 7%

^a Mean of measurements at 2, 4.5, 7, 9.5, 12 torr.

burner. Because the measured signal ratio of species to Ar is needed for calibration, each of these ratios was corrected for the hydrocarbon contribution to the mass 40 signal.

The measured temperatures were taken to be accurately positioned in space, but the mole fraction data are reported here to be 1.10 mm less than their measured burner-to-nozzle distances. Biordi et al. (1974) and Stepowski et al. (1981) showed that MBMS profiles are perturbed from the true profiles (measured by optical means) and that, except very near the burner, the perturbation was approximately a translation in distance of two nozzle diameters from the burner surface. This perturbation is caused by a combination of cooling by the probe (approximately 100 K) and disturbance of flow fields. The nozzle diameter in this study was 0.55 mm, so the shift was 1.10 mm. Temperatures were used as measured for model calculation, but for the flux calculations, the temperatures were decreased 100 K from their measured values.

CHAPTER IV. MOLE-FRACTION DATA AND IDENTIFICATION OF SPECIES

IV.1. Introductory overview of data

Profiles of mole fraction, flux, and net reaction rate for 38 species were measured by molecular-beam mass spectrometry (MBMS) in a lightly sooting, $\phi=2.40$ $C_2H_2/O_2/5\%$ Ar flame. The same technique was used to determine mole fractions (or upper limits) at specific points in the flame for an additional 20 species. In addition, microprobe sampling and GC/MS were used to resolve isomers and to measure the relative proportions of 174 stable species having molecular weights from 68 to 180.

Mole-fraction data and estimates of uncertainty for species are summarized in Table IV.1. Data files for the MBMS data are indexed in Appendix B, data points are listed in Appendix C, smoothed data curves are tabulated in Appendix D, and the calculated fluxes (with balances) and reaction rates are included as Appendix E and F.

Seven stable species - C_2H_2 , O_2 , H_2 , CO , H_2O , CO_2 , and Ar - make up at least 0.97 of the mole fraction throughout the flame. Maximum mole fractions of these species range upward from 0.050 for Ar. In contrast, the species with the next highest mole fractions are H-atom (0.018 maximum at 0.041 cm), C_4H_2 (0.0097 at 0.65 cm), CH_3 (0.0047 at 0.037 cm), and CH_4 (0.0037 at 0.17 cm). All other species had mole fractions no greater than 0.001.

Mole fractions of the major species and the temperatures are shown for the first 1.0 cm in Fig. IV.1 and for the whole flame in Fig. IV.2. A conventional description of alkane/ O_2 combustion (Warnatz, 1981) is that CO and H_2 are initially formed as intermediates and converted to products CO_2 and H_2O by reactions with OH :



To oversimplify somewhat, H rather than OH is the dominant radical in this flame because the conditions are so fuel-rich. As a result, the

Table IV.1. Summary of species measured by molecular-beam mass spectrometry in $\phi=2.40$ C₂H₂/O₂/5% Ar flame, 50 cm·s⁻¹ at 298 K.

<u>Mass Species</u>	<u>Mole fraction profile?</u>	<u>Maximum mole fraction [or point value]</u>	<u>Calibration uncertainty</u>
1 H atom	Yes	0.018, 0.41 cm	Factor of 2 ±16%
2 H ₂	Yes	Asymptote of 0.183	
13 CH	-No-	[≤(0.6±2.1)·10 ⁻⁶ , 0.141 cm; ≤(0±1.5)·10 ⁻⁵ , 0.276 cm; ≤(0±9)·10 ⁻⁶ , 0.363 cm]	
14 CH ₂	-No-	[≤(1.1±4.8)10 ⁻⁶ , 0.141 cm; 3.2·10 ⁻⁴ , 0.363 cm]	
15 CH ₃	Yes	4.7·10 ⁻³ , 0.36 cm	±50%
16 CH ₄	Yes	3.7·10 ⁻³ , 0.18 cm*	± 3%
17 OH	Yes	9.7·10 ⁻⁴ , 0.41 cm	±50%
18 H ₂ O	Yes	0.14, 0.61 cm	±25%
25 C ₂ H	-No-	[(6.6±3.7)10 ⁻⁶ , 0.103 cm; 4·10 ⁻⁶ , 0.161 cm]	
26 C ₂ H ₂	Yes	Minimum of 0.06 at 3.35 cm*	± 3%
27 C ₂ H ₃	Yes	1.9·10 ⁻⁴ , 0.46 cm*	±50%
28 C ₂ H ₄	Yes	7.8·10 ⁻⁴ , 0.27 cm*	±50%
28 CO	Yes	Asymptote of 0.537	± 3%
29 HCO (and C ₂ H ₅ ?)	Yes	6.0·10 ⁻⁵ , 0.38 cm	±50%
30 H ₂ CO, some C ₂ H ₆	Yes	1.0·10 ⁻³ , <0.01 cm	±50%
32 O ₂	Yes	Asymptotic minimum of 3·10 ⁻⁴	± 3%
33 HO ₂	Yes	3.2·10 ⁻⁴ , 0.04 cm	±50%
34 H ₂ O ₂	-No-	[5·10 ⁻⁵ , 0.176 cm]	
36 C ₃	-No-	[≤(5±9)·10 ⁻⁶ , 0.294 cm]	
37 C ₃ H	-No-	[<<3·10 ⁻⁵ , 0.294 cm]	
38 C ₃ H ₂	Yes	1.94·10 ⁻⁴ , 0.56 cm	±50%
39 C ₃ H ₃ (propargyl)	Yes	1.02·10 ⁻³ , 0.37 cm	±50%
40 C ₃ H ₄ (propyne and propadiene)	Yes	9.8·10 ⁻⁴ , 0.21 cm*	±50%
40 Ar	Yes	Monotonic decrease from 0.050 to 0.040	±10%
41 HCCO, some C ₃ H ₅	Yes	4·10 ⁻⁵ , 0.35 cm	±50%
42 CH ₂ CO (and C ₃ H ₆ ?)	Yes	7.2·10 ⁻⁴ , 0.14 cm	±50%
43 CH ₃ CO and/or C ₃ H ₇	-No-	[≤(0.1±1.2)·10 ⁻⁵ , 0.294 cm]	
44 CH ₃ CHO and/or C ₃ H ₈	-No-	[≤(6±4)·10 ⁻⁵ , 0.039 cm; ≤(0.9±2)·10 ⁻⁵ , 0.294 cm]	
44 CO ₂	Yes	0.086, 0.70 cm	± 3%

<u>Mass Species</u>	<u>Mole fraction profile?</u>	<u>Maximum mole fraction [or point value]</u>	<u>Calibration uncertainty</u>
49 C ₄ H	-No-	[$\leq(2\pm 3) \cdot 10^{-6}$, 0.32 cm]	
50 C ₄ H ₂ (butadiyne)	Yes	9.7 · 10 ⁻³ , 0.65 cm	±50%
51 C ₄ H ₃	Yes	2 · 10 ⁻⁵ , 0.43 cm	Factor of 2
52 C ₄ H ₄ (3-butenyne)	Yes	1.8 · 10 ⁻⁴ , 0.31 cm*	±50%
53 C ₄ H ₅	Yes	9.7 · 10 ⁻⁶ , 0.22 cm	±50%
54 C ₄ H ₆ (1,3-butadiene)	Yes	5.0 · 10 ⁻⁵ , 0.17 cm*	±50%
56 C ₄ H ₈ (one or more dimethylethenes)	-No-	[1.5 · 10 ⁻⁶ , 0.318 cm]	
62 C ₅ H ₂	Yes	1.8 · 10 ⁻⁵ , 0.65 cm	±50%
63 C ₅ H ₃	Yes	5.5 · 10 ⁻⁵ , 0.46 cm	±50%
64 C ₅ H ₄	Yes	6 · 10 ⁻⁵ , 0.36 cm	±50%
65 C ₅ H ₅ (and C ₄ HO?)	Yes	1.8 · 10 ⁻⁵ , 0.39 cm	±50%
66 C ₅ H ₆ (3-pentenyne) and/or C ₄ H ₂ O	Yes	4.6 · 10 ⁻⁵ , 0.23 cm*	±50%
73 C ₆ H	-No-	[$\leq(0.8\pm 3) \cdot 10^{-6}$, 0.544 cm]	
74 C ₆ H ₂ (hexatriyne)	Yes	1.3 · 10 ⁻³ , 0.70 cm	±50%
76 C ₆ H ₄	Yes	5.2 · 10 ⁻⁵ , 0.45 cm*	±50%
77 C ₆ H ₅	Yes	1 · 10 ⁻⁶ , 0.2 cm	Factor of 3
78 C ₆ H ₆ * (mostly benzene, some aliphatics)	Yes	4.0 · 10 ⁻⁵ , 0.28 cm*	±50%
79 C ₆ H ₇ and/or C ₅ H ₃ O	-No-	[$\leq 1 \cdot 10^{-6}$, 0.544 cm]	
80 C ₆ H ₈ and/or C ₅ H ₄ O	-No-	[$\leq 5 \cdot 10^{-7}$, 0.544 cm]	
81 C ₆ H ₉ and/or C ₅ H ₅ O	-No-	[$\leq 5 \cdot 10^{-8}$, 0.544 cm]	
91 C ₇ H ₇	-No-	[$\leq 1.3 \cdot 10^{-6}$, 0.395 cm]	
92 C ₇ H ₈ (mostly toluene, some aliphatics)	-No-	[4 · 10 ⁻⁷ , 0.45 cm]	
98 C ₈ H ₂	Yes	7.4 · 10 ⁻⁵ , 0.68 cm	±50%
102 C ₈ H ₆ (mostly phenylacetylene)	Yes	3.3 · 10 ⁻⁶ , 0.35 cm	±50%
104 C ₈ H ₈ (styrene)	-No-	[$< 2 \cdot 10^{-7}$, 0.395 cm]	
122 C ₁₀ H ₂	Yes	7.3 · 10 ⁻⁶ , 0.78 cm	±50%
126 C ₁₀ H ₆	-No-	[$\leq(1\pm 1) \cdot 10^{-6}$; 0.395 cm]	
128 C ₁₀ H ₈ (naphthalene)	-No-	[4.7 · 10 ⁻⁷ , 0.395 cm]	
152 C ₁₂ H ₈ (acenaphthylene)	-No-	[$\leq(5\pm 5) \cdot 10^{-7}$; 0.395 cm]	

* Species that had a maximum but also, at a greater distance from the burner, had a minimum followed by a steady rise to the end of the measurement region (4.0 cm).

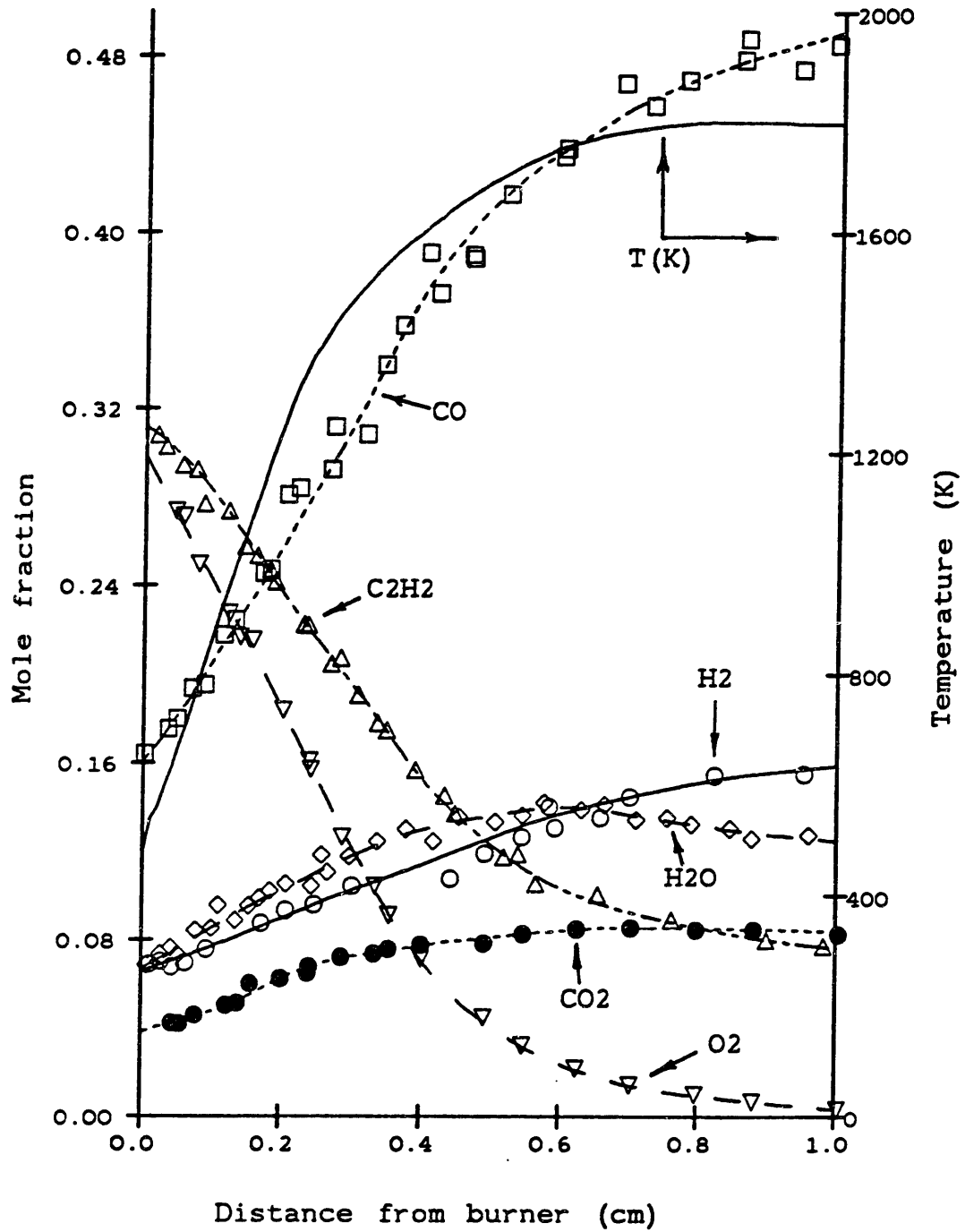


Fig. IV.1. Profiles of temperature and of mole fractions for major stable species in the first 1.0 cm of a laminar, premixed flame of $C_2H_2/O_2/5\% Ar$, $\phi=2.40$, 2.67 kPa (20 torr), and 0.5 $m \cdot s^{-1}$ velocity of unburned gas (298 K).

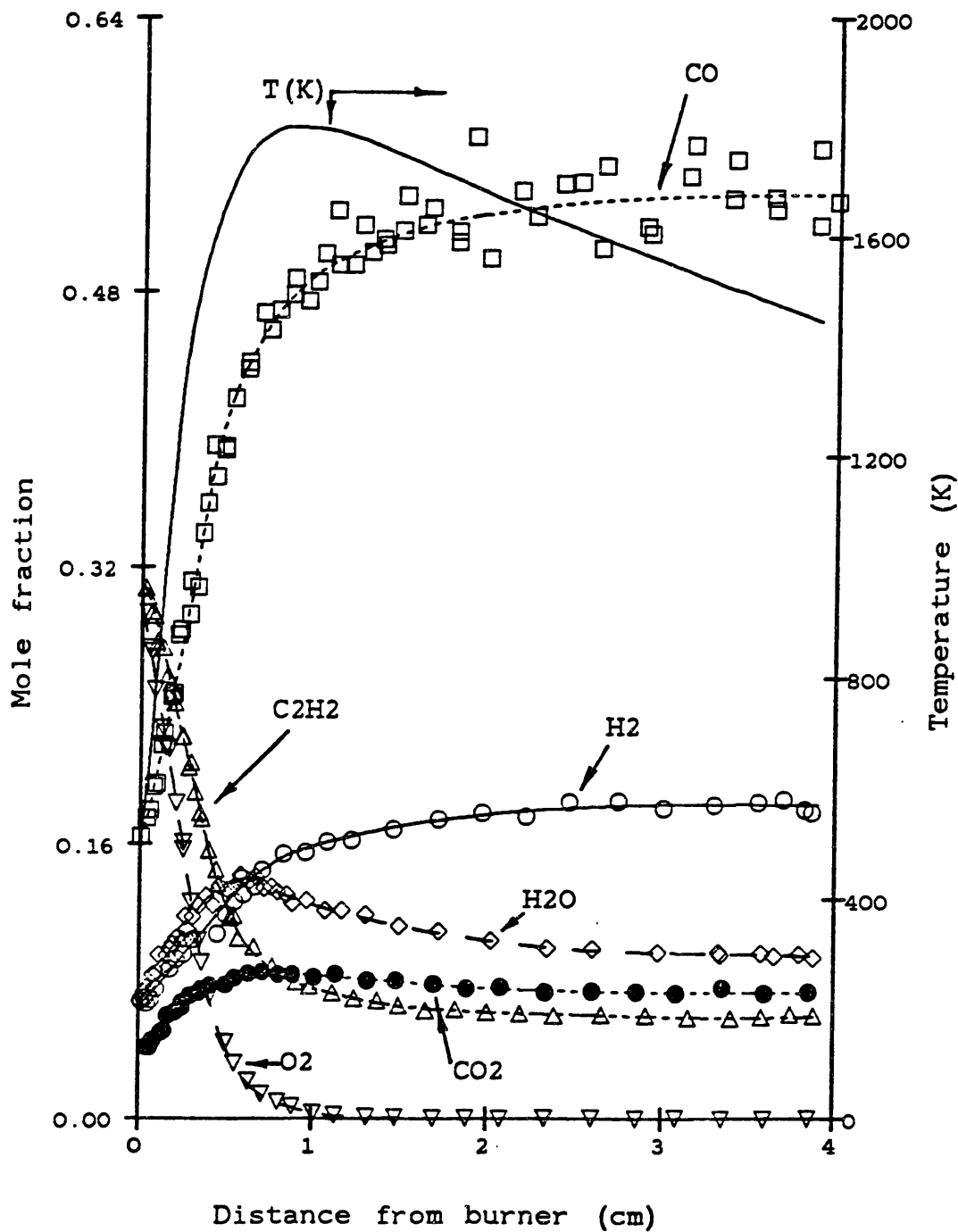


Fig. IV.2. Profiles of temperature and of mole fractions for major stable species in a laminar, premixed flame of $C_2H_2/O_2/5\%$ Ar, $\phi=2.40$, 2.67 kPa (20 torr), and $0.5 \text{ m}\cdot\text{s}^{-1}$ velocity of unburned gas (298 K).

reverse reactions become important and the "intermediates" CO and H₂ are the dominant products.

The principal radicals involved in hydrocarbon destruction are H, O, OH, and HO₂. Profiles of mole fraction were measured for all these species except O-atom, which was obscured by the signal for CH₄.

Mass flux balances for carbon, hydrogen, oxygen, and total mass are strong internal checks on the data because they depend not only on the magnitudes of the mole fractions, but also on the shapes because of diffusion fluxes. As shown in Fig. IV.3, the closure of these balances is excellent except for the hydrogen balance near the burner. By comparison, the closure is generally as good or better than the closure in previous work (Bittner, 1981).

The deviation near the burner is largely caused by uncertainties in the diffusive fluxes. The net mass flux of hydrogen near the burner (0.0197 g H/cm²·s at 0.26 cm vs. 0.03166 in the feed gas) is largely determined by the mass fluxes of C₂H₂ (+0.0273 g H/cm²·s), H-atom (-0.0062), H₂ (-0.0056), and H₂O (+0.0028). For these species, the ratio of diffusive flux to convective flux is 0.66, -16.1, -1.75, and -0.67, respectively, so the net flux is especially sensitive to the concentration gradients of these species. In particular, the location of the maximum deviation corresponds to the maximum negative flux of H-atom.

IV.2. Comparisons with other data

No detailed MBMS data have been reported before in C₂H₂ flames at the specific conditions of this study, but the conditions of Bonne, Homann, and Wagner (1965) are sufficiently close to allow useful comparison. In addition, there are limited data by Bittner (1981) in this flame, and Delfau and Vovelle (1984a, 1984b, 1985) have measured detailed profiles for C₂H₂ flames at conditions near those of this study.

The flame of Bonne et al. is the same as studied here except that 5% Ar was added to the feed gas of the present flame. The same burner velocity of 50 cm·s⁻¹ (at 298 K) and virtually the same equivalence ratio of $\phi=2.40$ (vs. 2.38) were used here, but the

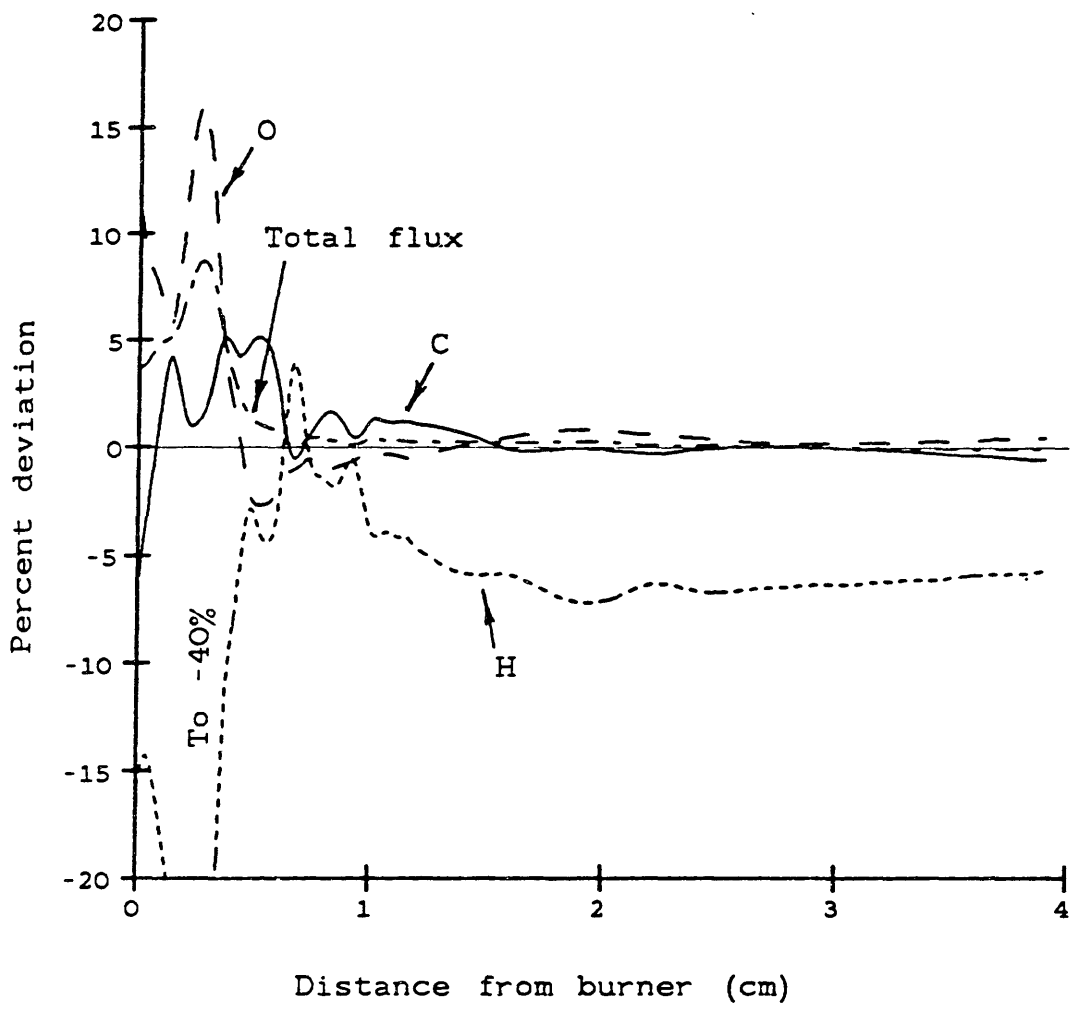


Fig. IV.3. Mass flux balances on carbon, hydrogen, oxygen, and total mass flux.

earlier flame was Ar-free. The added Ar dilutes the flame gases, changing mole fractions by the dilution itself and by lowering the temperature, changing reaction rates. Differences in cooling of the burner can also change the temperature profile at nominally identical flame conditions (Calcote, 1984).

Bittner (1981) briefly searched for C_2H at the conditions of the present flame and in the same burner/MBMS system used here. By inference, the same burner cooling and would cause the same temperature profile as measured in the present flame. He reported approximate concentrations at 3.5 cm for 6 stable species, intensity-ratio (raw data) profiles for 12 species, and the absence of C_2H from 0.2 to 1.2 cm above the burner.

MBMS data of Delfau and Vovelle (1984a, 1984b, 1985) can also be compared to the present data, at least to a limited extent. They measured profiles for selected profiles in Ar-free C_2H_2/O_2 flames at $50 \text{ cm}\cdot\text{s}^{-1}$ (298 K) and equivalence ratios of $\phi=1.8, 2.1, 2.2, 2.6,$ and 3.0 . Interpolation of the $\phi=2.2$ data (Delfau and Vovelle, 1984b) and the $\phi=2.6$ data (Delfau and Vovelle, 1985) should give mole fractions that are similar to the present data, although temperatures were reported to be approximately 200 K higher than measured here.

IV.3. Discussion of MBMS data

The profiles of mole fraction and the identities of species are examined here in some detail, with an eye toward using the data to explain the flame chemistry. Plots of the profiles include data points, smoothed curves drawn for flux calculations, and, where possible, the data points of Bonne et al. The species will be discussed in order of increasing molecular weight and compared to literature data from similar flames.

H-atom. - H-atom at 0.337 cm had an ionization potential of 13.89 ± 0.27 referenced to Ar, compared to the literature value of 13.60 eV (Rosenstock et al., 1977). No appearance potential was observed up to 19.75 eV, and the profile was measured at 15.85 eV (corrected from the metered setting based on the shift between metered and literature ionization potential for H_2 ; 15.50 eV was the actual setting used). For the calibration factor $(\alpha S)_{H, Ar}$, the

mass-spectrometer sensitivity $S_{H,Ar}$ was determined from the ionization efficiency at 0.337 cm, and the beam mass-discrimination factor α_H was estimated from α_{H_2} by scaling with molecular weight:

$$\frac{\alpha_i(,Ar)}{\alpha_j(,Ar)} = \left(\frac{MW_i}{MW_j} \right)^{0.5} \quad [IV.3]$$

Measurement of H-atom was complicated by uncertainties in α_H (particularly near the burner), by scatter of data at the peak mole fraction, and by consumption of H by deposits on the probe at larger distances.

As described above, α_H was taken as a fixed value based on α_{H_2} . The uncertainty in α_{H_2} was $\pm 16\%$; however, α_{H_2} is affected more by the density of the sampled gas (see Ch. III.3) than are the mass-discrimination factors of heavier gases. As a result, α_H should be affected most by this uncertainty near the burner where the variation of gas density is greatest. Thus, a fixed value of α_H may be inappropriate.

H-atom data are shown in Fig. IV.4. At the peak mole fraction of 0.018 (0.41 cm), there is considerable scatter in H-atom data, possibly due to effects there of scavenging (discussed below and in Ch. III.3). The higher data points were taken to be more credible, as shown by the smoothed curve. However, if the lower data points were taken as true, the positive convective flux would be a factor of two lower, but the larger, negative diffusion flux of H-atom also would be reduced. The net flux (negative) then would decrease, reducing the maximum deviation of the H mass flux balance (Fig IV.3) from -40% to -25% .

At some positions H measurements were affected by losses to the probe. Beyond 0.5 cm, the probe tip glowed red from the formation of a visible deposit by the sooting flame. Hydrocarbon radicals did not appear to be seriously affected, but H and OH apparently were scavenged. To obtain signals free from this effect, the deposit was burned away with a lean flame, the rich flame was restored, and signal was measured as a function of time. The signal used to calculate mole fraction was extrapolated to zero time, although the

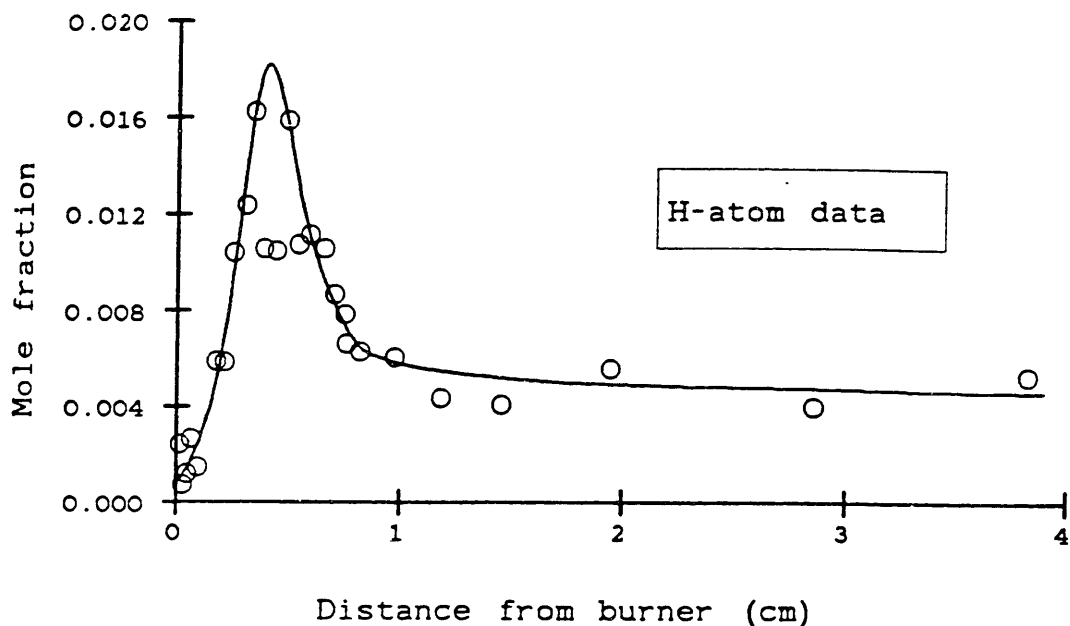


Fig. IV.4. Data (O) and smoothed curve for H-atom in a laminar, premixed flame of $C_2H_2/O_2/5\% Ar$, $\phi=2.40$, 2.67 kPa (20 torr), and $0.5\text{ m}\cdot\text{s}^{-1}$ velocity of unburned gas (298 K).

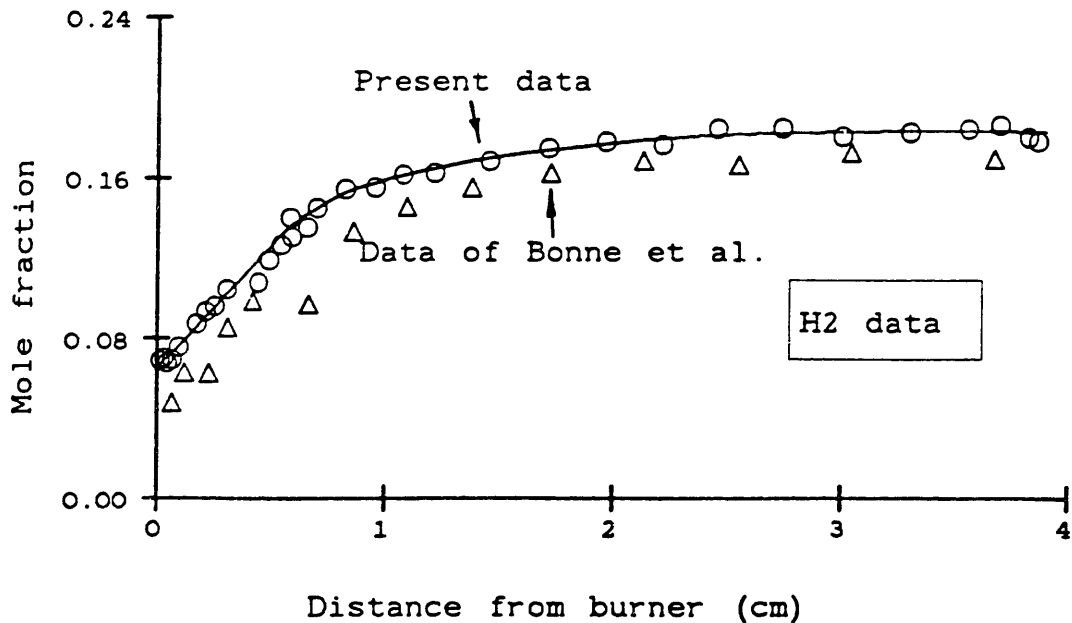


Fig. IV.5. Data profile for H_2 (O) in a laminar, premixed flame of $C_2H_2/O_2/5\% Ar$, $\phi=2.40$, 2.67 kPa (20 torr), and $0.5\text{ m}\cdot\text{s}^{-1}$ velocity of unburned gas (298 K), compared to data of Bonne et al. (1965; Δ) in a C_2H_2/O_2 , $\phi=2.38$ flame.

switch in flame conditions and stabilization of pressure occurs over about 30 s.

For these reasons, the uncertainty in the mole fraction of H is considered to be a factor of two.

The only comparison with other data is by interpolation from data of Delfau and Vovelle, although their flame was hotter by 200 K. Interpolating to $\phi=2.4$, the maximum mole fraction would be 0.0044 at 1 cm (mean of $6.5 \cdot 10^{-3}$ at 1.1 and $2.3 \cdot 10^{-3}$ at 0.85 cm), compared to 0.018 at 0.41 cm in the present data. To decide whether this disagreement is consistent with the flame differences requires examination of flame mechanisms.

H₂. - The calibration factor for H₂ was obtained by direct measurement using pure gases and mixtures. The ionization potential was 14.83 ± 0.10 eV referenced to Ar, and the profile was measured at 18.75 eV (referenced to Ar; setting 19.00 eV). The profile is shown relative to other major species in Figs. IV.1 and IV.2. As noted above, the calibration uncertainty of $\pm 16\%$ is due primarily to ω_{H_2} .

Comparison with other data shows reasonable agreement considering the differences among the flames. Shape, alignment, and magnitude are all in good agreement between this measurement and that of Bonne et al. (Fig. IV.5), with the present measurements leveling off at 0.183 and the Bonne measurement slightly lower, leveling off at a mole fraction of 0.165 at 4 cm. As a further comparison, Bittner (1981) estimated a mole fraction of 0.21 for H₂ at 4 cm. Also, interpolation of the Delfau and Vovelle $\phi=2.2$ and 2.6 flames gave an ultimate yield of 0.215 (mean of 0.22 and 0.21).

CH. - No signal was detected, but using the literature ionization potential and an estimated ionization cross-section, it is possible to set an upper limit on the mole fraction at positions where ionization efficiency curves were measured. Such measurements were made at 0.141, 0.276, and 0.363 cm. Each measurement of mole fraction gave zero within experimental error with the largest possible value being $(0 \pm 1.5) \cdot 10^{-5}$ at 0.276 cm.

CH₂. - No CH₂ profile was measured successfully, but an ionization efficiency at 0.363 cm gave a mole fraction of $3.2 \cdot 10^{-4}$. The ionization potential was measured to be 10.41 ± 0.36 eV vs.

10.396±0.003 eV from the literature for CH₂. Closer to the burner at 0.141 cm, the upper limit was measured to be a mole fraction of (1.1±4.8)10⁻⁶. If CH₂ is present in detectable concentrations at greater distances from the burner, it may have been obscured by the radical scavenging that made H-atom measurements difficult. Its low ionization cross-section also makes for a weaker signal. An intercept at 13.71±0.09 eV (0.141 cm) is the appearance potential for CH₂⁺ from CH₂CO, which is reported as 13.8±0.2 eV (Rosenstock et al., 1977).

Delfau and Vovelle report mole fraction profiles for CH₂ that would maximize at 1.7·10⁻⁴ at 0.4 cm (mean of 1.8·10⁻⁴ at 0.3 cm and 1.5·10⁻⁴ at 0.45 cm). This value is similar to the value of 3.2·10⁻⁴ cited above.

Methylene can be present in flames at significant concentrations in two electronic states: the ground, triplet state (\tilde{X}^3B_1) and an excited, singlet state (\tilde{a}^1A_1) that lies 9.0 kcal/mol above the ground state (Goddard, 1985). Although equilibrium favors the ground state, the equilibrium at 2000 K can be calculated to be 95:5:triplet:singlet. These states cannot be resolved by MBMS because the resolution would have to be made by difference in ionization potential. If this difference were the same as the difference in enthalpies, it would be 0.4 eV, too small to be observed.

CH₃. - Methyl was formed in appreciable amounts, reaching a maximum mole fraction of 0.005. The measured ionization potential was 9.6±0.4 eV vs. the literature value of 9.84 eV. For the calibration factor, S_{CH₃,Ar} was determined from three ionization efficiency measurements and α_{CH₃} was estimated by molecular-weight scaling from the directly measured α_{CH₄}. The profile was measured at 11.7 eV (ref. Ar; setting 12.00 eV).

The profile of mole fraction is shown in Fig. IV.6. For comparison, interpolating the measurements of Delfau and Vovelle gives a maximum of 1·10⁻³ at 0.6 cm (from 0.0010 at 0.5 cm and 0.0009 at 0.65 cm), similar to 4.7·10⁻³ at 0.36 cm measured here.

Mass 16 (CH₄). - Measurements of the ionization potential as 12.63±0.58 eV supported the assumption that in this fuel-rich flame,

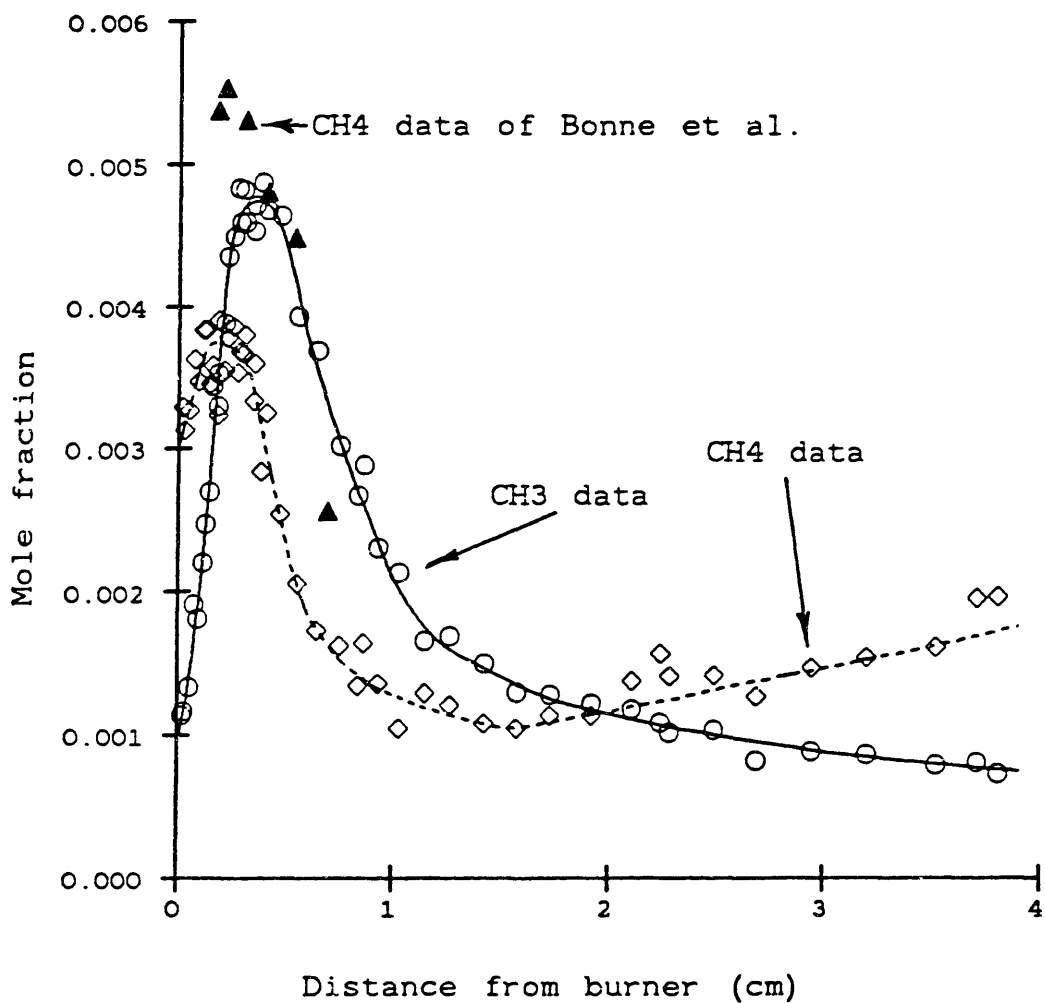


Fig. IV.6. Data profiles for CH₃ (○) and CH₄ (◇) in a laminar, premixed flame of C₂H₂/O₂/5% Ar, $\phi=2.40$, 2.67 kPa (20 torr), and 0.5 m·s⁻¹ velocity of unburned gas (298 K). Also shown are CH₄ data of Bonne et al. (1965; ▲) in a C₂H₂/O₂, $\phi=2.38$ flame.

mass 16 was CH_4 (IP=12.70 eV) rather than O-atom (IP=13.62 eV). Both α_{CH_4} and $S_{\text{CH}_4, \text{Ar}}$ were measured directly, but the mean of three estimates of $S_{\text{CH}_4, \text{Ar}}$ by ionization efficiency was within 3% of the direct calibration. The profile was measured at 13.2 eV (ref. Ar; 13.50 eV setting).

The mole-fraction profile for CH_4 (Fig. IV.6) has an early maximum of $3.7 \cdot 10^{-3}$ at 0.17 cm, declines to $1.05 \cdot 10^{-3}$ at 1.55 cm, and then rises again. Note that such a minimum is not observed in the CH_3 data. The data of Bonne et al. are very similar to the present data but stop at 0.7 cm. Their maximum was $5.6 \cdot 10^{-3}$ at 0.35 cm, but the data did not extend to the region of the minimum. No minimum was observed in the hotter $\phi=2.2$ and 2.6 flames of Delfau and Vovelle, but interpolation gives a maximum of $1.3 \cdot 10^{-3}$ at 0.5 cm (from $1.2 \cdot 10^{-3}$ at 0.4 cm and $1.4 \cdot 10^{-3}$ at 0.6 cm), which is slightly lower than the present measurements.

OH. - The maximum in this profile (Fig IV.7) was $9.7 \cdot 10^{-4}$ at 0.41 cm. Data were noisy at the greater distances from the burner because of scavenging by probe deposits, requiring burn-off, establishment of the new condition, following the changing signal, and extrapolating back to initial measurement with the clean nozzle (as for H-atom). The only intrinsic interferences were fragmentation of H_2O at 18.05 eV and isotopic contributions from CH_4 . For the latter, mass 16 was assumed to be exclusively CH_4 , as discussed above.

OH was measured at 15.66 eV (ref. Ar; 16.00 eV setting), 2.5 eV above the ionization potential. The mass discrimination factor was obtained by molecular-weight scaling of the direct CH_4 measurement, and $S_{\text{OH}, \text{Ar}}$ was determined from the mean of three ionization efficiencies with 50% uncertainty.

By comparison, Bonne et al. showed an uncalibrated OH emission signal with a maximum at about 0.4 cm, the same position as for the maximum mole fraction in this study. Interpolation of the Delfau and Vovelle data predicted a maximum mole fraction of $3.4 \cdot 10^{-4}$ at 0.75 (from $4.7 \cdot 10^{-4}$ at 0.8 cm and $2.1 \cdot 10^{-4}$ at 0.7 cm), somewhat lower in magnitude and further from the burner than observed here.

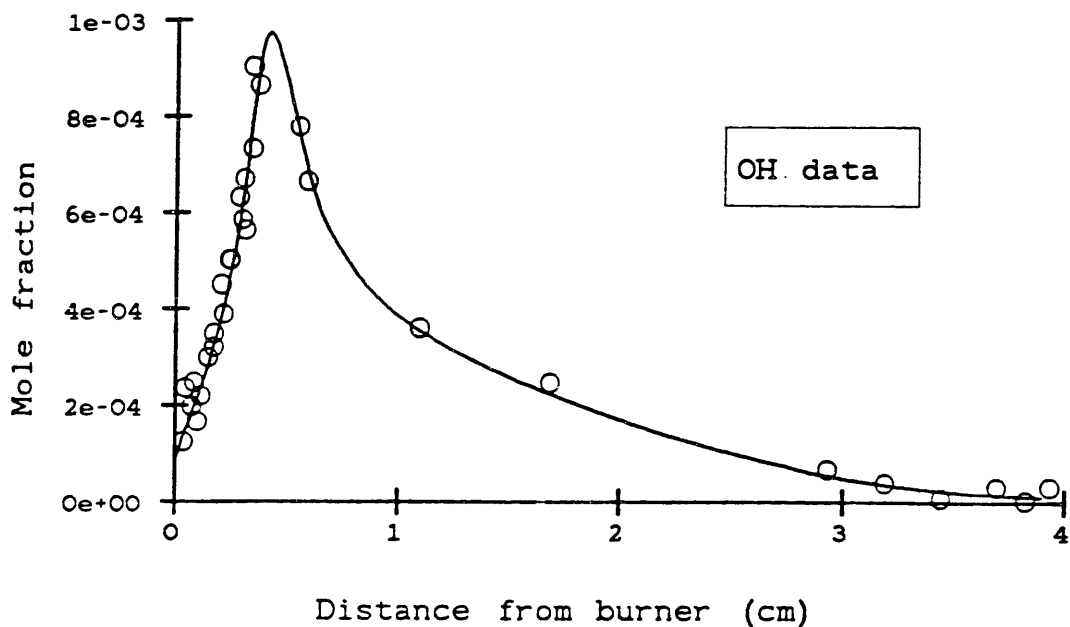


Fig. IV.7. Data (○) and smoothed curve for OH in a laminar, premixed flame of $C_2H_2/O_2/5\% Ar$, $\phi=2.40$, 2.67 kPa (20 torr), and $0.5 \text{ m}\cdot\text{s}^{-1}$ velocity of unburned gas (298 K).

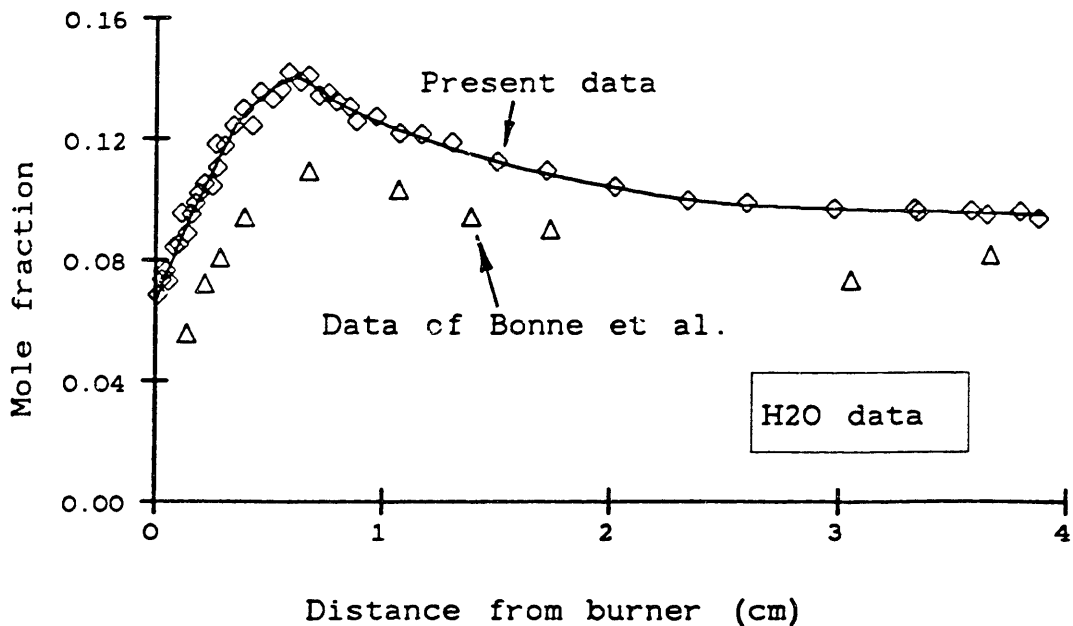


Fig. IV.8. Data profile for H_2O (◇) in a laminar, premixed flame of $C_2H_2/O_2/5\% Ar$, $\phi=2.40$, 2.67 kPa (20 torr), and $0.5 \text{ m}\cdot\text{s}^{-1}$ velocity of unburned gas (298 K), compared to data of Bonne et al. (1965; △) in a C_2H_2/O_2 , $\phi=2.38$ flame.

H₂O. - The H₂O profile (Fig. IV.1 and IV.2) was measured at 17.1 eV (ref. H₂O ionization potential; setting 17.00 eV). It shows a maximum mole fraction of 0.14 at 0.61 cm, followed by decline to a nearly constant value of 0.095. H₂O is usually considered to be an end product of combustion, but the peaked shape is caused by net formation of H₂O being followed by net destruction.

No direct calibration of H₂O was made, in contrast to the other major stable species. Rather, α_{H_2O} was estimated by molecular-weight scaling from α_{CH_4} , and $S_{H_2O, Ar}$ was determined from a mass balance on oxygen at 3.5 cm. The oxygen balance is primarily determined by CO, which has a mole fraction of 0.54 at that point, so the 3% uncertainty in the CO calibration causes 15% uncertainty for H₂O. With the uncertainty of α_{H_2O} , the uncertainty for the H₂O calibration becomes 25%.

The data may be compared to other H₂O data at similar conditions. First, Bittner (1981) estimated a mole fraction of 0.075 at 4 cm in an identical flame vs. 0.095 here. Second, comparison with the data of Bonne et al. is shown in Fig. IV.7. The Bonne data are lower by approximately 20% but have the same shape as the present data. Third, the interpolated Delfau and Vovelle data maximize as 0.132 at 0.81 cm (mean of 0.140 at 0.68 cm and 0.124 at 0.94 cm) and decline to 0.087 by 2.5 cm (mean of 0.096 and 0.078), rather similarly to the present measurements. Quantitative difference may result from calibration uncertainties or from the absence of Ar-dilution and the higher temperatures of the latter two studies.

C₂H. - Little or no ethynyl was detected despite several attempts. Ionization efficiencies were difficult because of the weak signal. In the most reliable measurement, an ionization potential of 10.7±0.25 eV (ref. Ar) was measured at 0.161 cm, corresponding to a mole fraction of 4·10⁻⁶. The ionization potential compares poorly with the value of 11.51±0.05 eV that was recently recommended (Wodtke and Lee, 1985). No other species should be interfering, and the lowest appearance potential for C₂H⁺ is 17.22 eV from C₂H₂ (Rosenstock et al., 1977).

Nevertheless, attempts were made to measure the profiles. In one attempt, the range of positions from 0.1 to 0.9 cm was sampled,

giving only noise corresponding to a mole fraction of $(0 \pm 1.5) \cdot 10^{-6}$. Because of concerns about radical scavenging above 0.4 cm (as for H and OH), careful measurements were made from 0.024 to 0.27 cm, but the mole fractions were again in the noise of the measurement. The largest apparent mole fraction was $(6.6 \pm 3.7) 10^{-6}$ at 0.103 cm, and the values from 0.2 to 0.3 cm were 0 to $2 \cdot 10^{-6} \pm 3 \cdot 10^{-6}$.

The only "measurement" of C_2H in a flame is that of Bonne et al. (1965). They reported a mole-fraction profile for C_2H from 0.1 to 0.7 cm that had a maximum of $3.3 \cdot 10^{-3}$ at 0.22 cm, while Bittner (1981) and Delfau and Vovelle (1984c) could not detect C_2H . In fact, the profile of Bonne et al. is incorrect, the result of C_2H^+ formed below its nominal appearance potential from C_2H_2 . Because the electron-impact ionizer used in the mass spectrometer generates a distribution of electron energies, ionizing (or fragmenting) electrons can be generated even though the median electron energy is lower. To confirm this explanation, the shape of the Bonne profile was experimentally reproduced by measuring mass 25 at 16.7 eV, 0.5 eV below the appearance potential of C_2H from C_2H_2 . Homann (1984) has expressed agreement with this explanation.

C_2H_2 . - The C_2H_2 profile was measured at 12.8 eV (ref. Ar; setting 13.00 eV). Direct measurements of $Sc_{2H_2,Ar}$ and α_{2H_2} were used, giving an estimated calibration uncertainty of $\pm 3\%$.

Acetylene is consumed rapidly as it leaves the burner (Fig. IV.1) and reaches a near-constant mole fraction of 0.06 beyond 2 cm (Fig. IV.2). A slight (1.5%) increase between 3.35 and 3.9 cm seems to be present.

Data of Bonne et al. are very close to the present data, going to an ultimate mole fraction of 0.053 (Fig. IV.9). Bittner estimated his mole fraction at 3.5 cm to be 0.055, and interpolation of data from Delfau and Vovelle gives 0.062 at 2.5 cm (mean of 0.042 and 0.082), all in reasonable agreement with the present data.

C_2H_3 . - No data have been reported before for vinyl in acetylene flames, despite its mechanistic importance (Chap. V). A reason is that isotopic contribution of C_2H_2 to mass 27 is 2.2% of the mass 26 signal, obscuring the C_2H_3 signal even below the ionization potential of C_2H_2 (11.41 eV). The profile was measured at 9.8

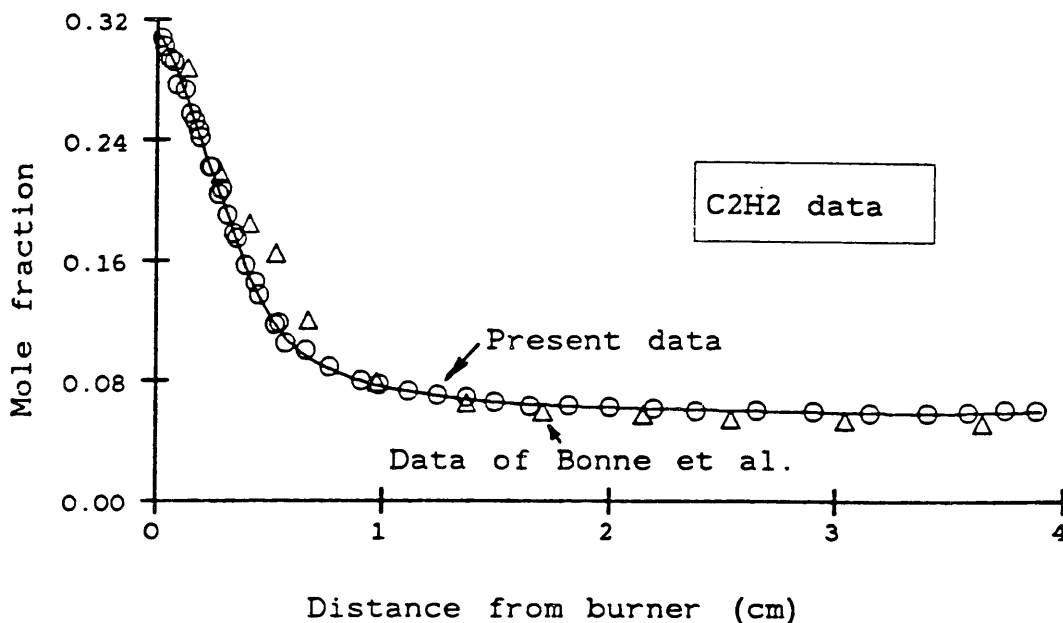


Fig. IV.9. Data profile for C_2H_2 (\circ) in a laminar, premixed flame of $C_2H_2/O_2/5\% Ar$, $\phi=2.40$, 2.67 kPa (20 torr), and $0.5\text{ m}\cdot\text{s}^{-1}$ velocity of unburned gas (298 K), compared to data of Bonne et al. (1965; Δ) in a C_2H_2/O_2 , $\phi=2.38$ flame.

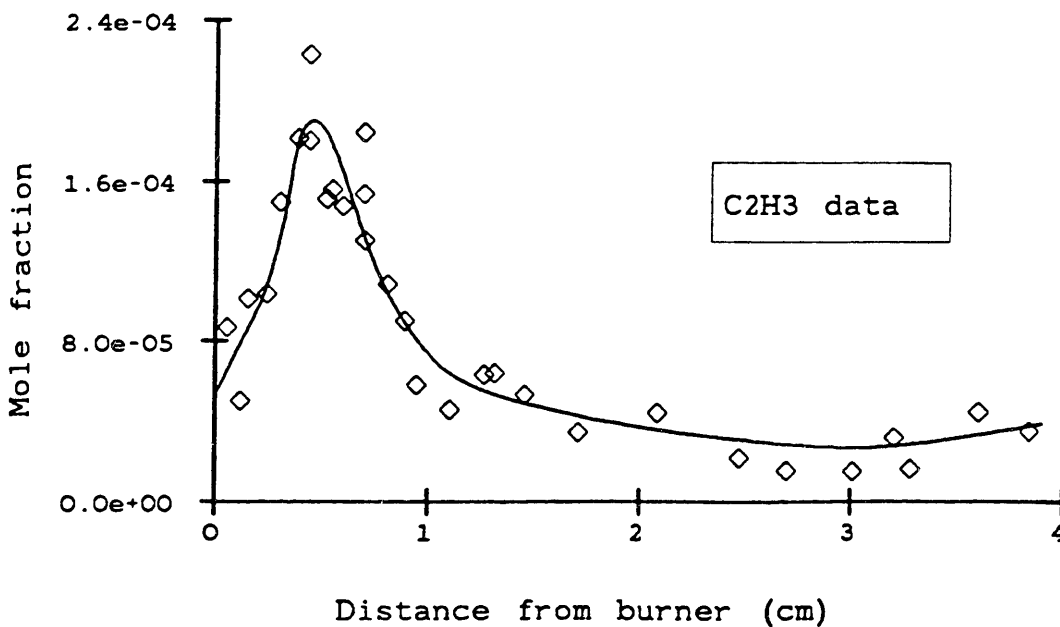


Fig. IV.10. Data and smoothed curve for C_2H_3 (\diamond) in a laminar, premixed flame of $C_2H_2/O_2/5\% Ar$, $\phi=2.40$, 2.67 kPa (20 torr), and $0.5\text{ m}\cdot\text{s}^{-1}$ velocity of unburned gas (298 K).

eV (ref. Ar; setting 10.00 eV), 1.6 eV below the ionization potential of C_2H_2 and 0.8 eV above the ionization potential of C_2H_3 (8.95 eV). Even at this electron energy, the contribution from C_2H_2 (also measured at 9.8 eV) was typically 50%. To obtain sufficient signal, each measurement of mass 27 was made by pulse-counting detection for 20 min.

Calibration was by ionization efficiency for $Sc_{2H_3,Ar}$ and by interpolation between C_2H_2 and CO for α_{2H_3} . Because of the noise in the low-level C_2H_3 signal and the isotopic correction, the ionization potential measurements were 9.47 ± 0.46 , 8.91 ± 0.5 , and 9.70 ± 0.54 eV.

Measurements of this key hydrocarbon radical (Fig. IV.10) are important for testing flame mechanisms. The mole fraction reaches a maximum of $1.9 \cdot 10^{-4}$ at 0.46 cm, declines to a minimum of $2.7 \cdot 10^{-5}$ at 3.0 cm, and has climbed to $3.9 \cdot 10^{-5}$ at 3.9 cm. Again, no previous data are available for comparison.

Mass 28 - C_2H_4 . - The profile for C_2H_4 can be measured separately from CO, the other mass 28 species in this system, because their ionization potentials are so different - 10.51 for C_2H_4 vs. 14.013 eV for CO. (N_2 , also a mass 28 species, is present only in the background because of inleakage). C_2H_4 was measured at 10.8 eV (ref. Ar; setting 11.00 eV). The sensitivity $Sc_{2H_4,Ar}$ was determined by ionization efficiency, and α_{2H_4} was assumed equal to α_{CO} .

As shown in Fig. IV.11, the mole-fraction profile of C_2H_4 reached a maximum of $7.8 \cdot 10^{-4}$ at 0.27 cm and then declined to $1.3 \cdot 10^{-5}$ at 3.9 cm. No C_2H_4 data were reported by Bonne et al., Bittner, or Delfau and Vovelle.

Mass 28 - CO. - Carbon monoxide is very much the dominant species through the latter part of the flame (Fig. IV.1 and IV.2). The mole fractions of all species are particularly sensitive to its accurate calibration (1) because the mole fraction of Ar, to which all mole fractions are ratioed, is determined by mass balance and (2) because the calibration factor for H_2O is calculated from an oxygen balance at 3.5 cm, which is mostly CO. Calibration factors were measured directly, and the profile was measured at 18.7 eV (ref. Ar; setting 19.00 eV). Interference with background N_2 causes most of the scatter in the data.

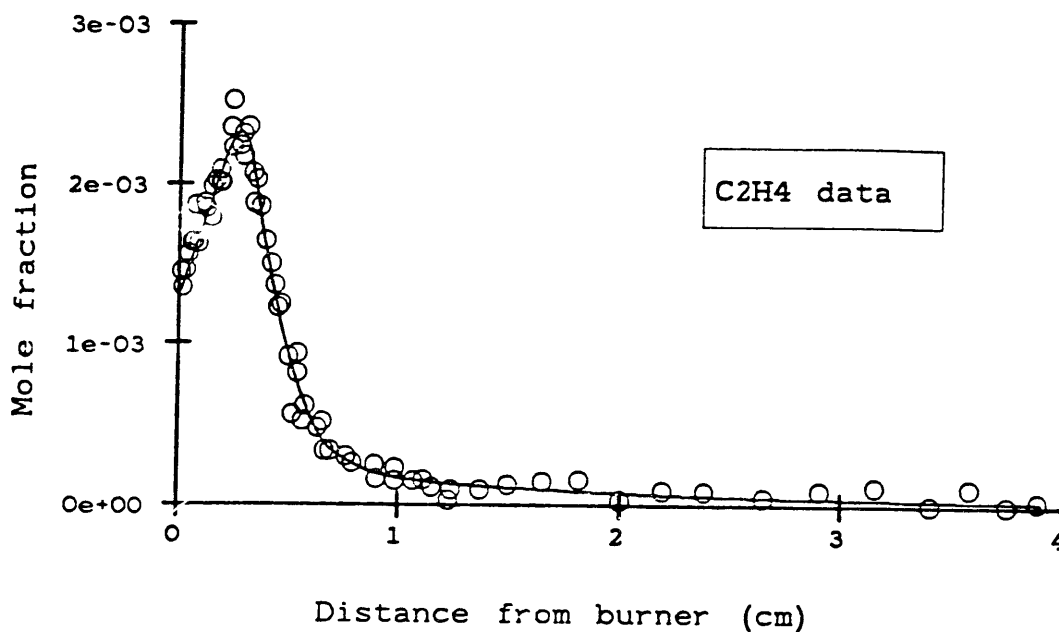


Fig. IV.11. Data and smoothed curve for C_2H_4 (\circ) in a laminar, premixed flame of $C_2H_2/O_2/5\%$ Ar, $\phi=2.40$, 2.67 kPa (20 torr), and $0.5\text{ m}\cdot\text{s}^{-1}$ velocity of unburned gas (298 K).

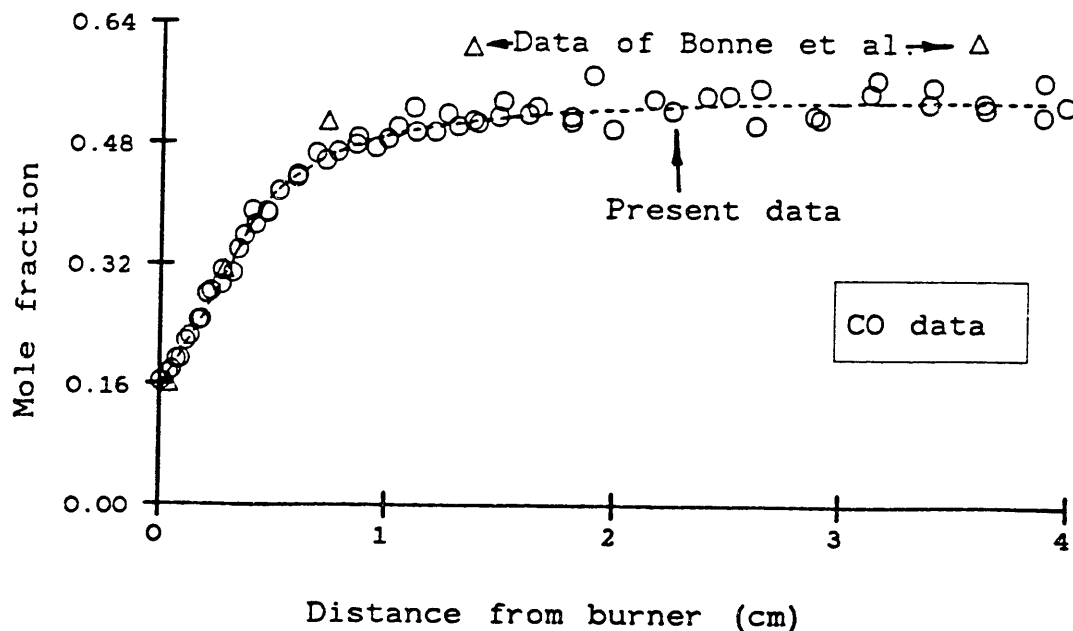


Fig. IV.12. Data profile for CO (\circ) in a laminar, premixed flame of $C_2H_2/O_2/5\%$ Ar, $\phi=2.40$, 2.67 kPa (20 torr), and $0.5\text{ m}\cdot\text{s}^{-1}$ velocity of unburned gas (298 K), compared to data of Bonne et al. (1965; Δ) in a C_2H_2/O_2 , $\phi=2.38$ flame.

The measured profile is a monotonic rise to a mole fraction of 0.54 at 3.9 cm. By comparison, the data of Bonne et al. reach 0.62 (Fig. IV.12) which, if diluted by 5% Ar, would become 0.59. Bittner estimated 0.56 at 3.5 cm in a flame which includes 5% Ar. Finally, interpolation of the data of Delfau and Vovelle gives 0.585 at 2.5 cm (mean of 0.58 and 0.59), which would become 0.56 with Ar dilution. Ignoring the likely effects of temperature on CO formation, these values (corrected for Ar dilution) are in good agreement.

Mass 29 (HCO and/or C₂H₅). - A profile was measured for mass 29, which seems to be predominantly HCO based on ionization potentials. The literature ionization potentials are 9.83 ± 0.18 eV for HCO and 8.38 ± 0.05 eV for C₂H₅ (Rosenstock, 1977). At 0.161 cm, well-defined ionization potentials were measured in repeated ionization efficiency tests to be 10.36 ± 0.23 (ref. Ar or 10.17 ± 1.1 eV, ref. CO) and 9.85 ± 0.23 eV (ref. Ar), matching well with HCO. A tailing signal from HCO or a weak contribution from C₂H₅ gives 7.7 ± 1.1 eV (ref. Ar). If this is C₂H₅, the signals would imply a mole fraction ratio HCO/C₂H₅ of 200. At 0.201 cm, only the ionization potential of 9.8 ± 0.6 (ref. C₂H₄) for HCO was detected.

The HCO profile shown in Fig. IV.13 was measured at 11.8 eV (ref. C₂H₄; setting 11.50 eV). If the identity were completely mistaken and the data corresponded only to C₂H₅, the mole fractions would be higher by a factor of 2.3, based on estimated ionization cross-sections. A profile for mass 29 was simultaneously measured at 9.8 eV (ref. C₂H₄; setting 9.50 eV) on the chance of detecting a C₂H₅ profile, but the signals were not significantly different from zero.

The present data, all measured at less than 0.74 cm, show a broad, flat maximum of $6.0 \cdot 10^{-5}$ centered at about 0.38 cm. Bonne et al. report the only other HCO measurements in a similar flame, but they report a maximum of approximately 10^{-3} at 0.16 cm. This marked difference may have been caused by use of too high an electron energy by Bonne et al., as had been the case for C₂H.

Mass 30 (H₂CO and/or C₂H₆). - Both H₂CO and C₂H₆ appear to be present in the flame. Ionization potentials for the species are 10.88 ± 0.01 eV for H₂CO and 11.521 ± 0.007 eV for C₂H₆. However, curvature in the ionization efficiency data caused measurements of

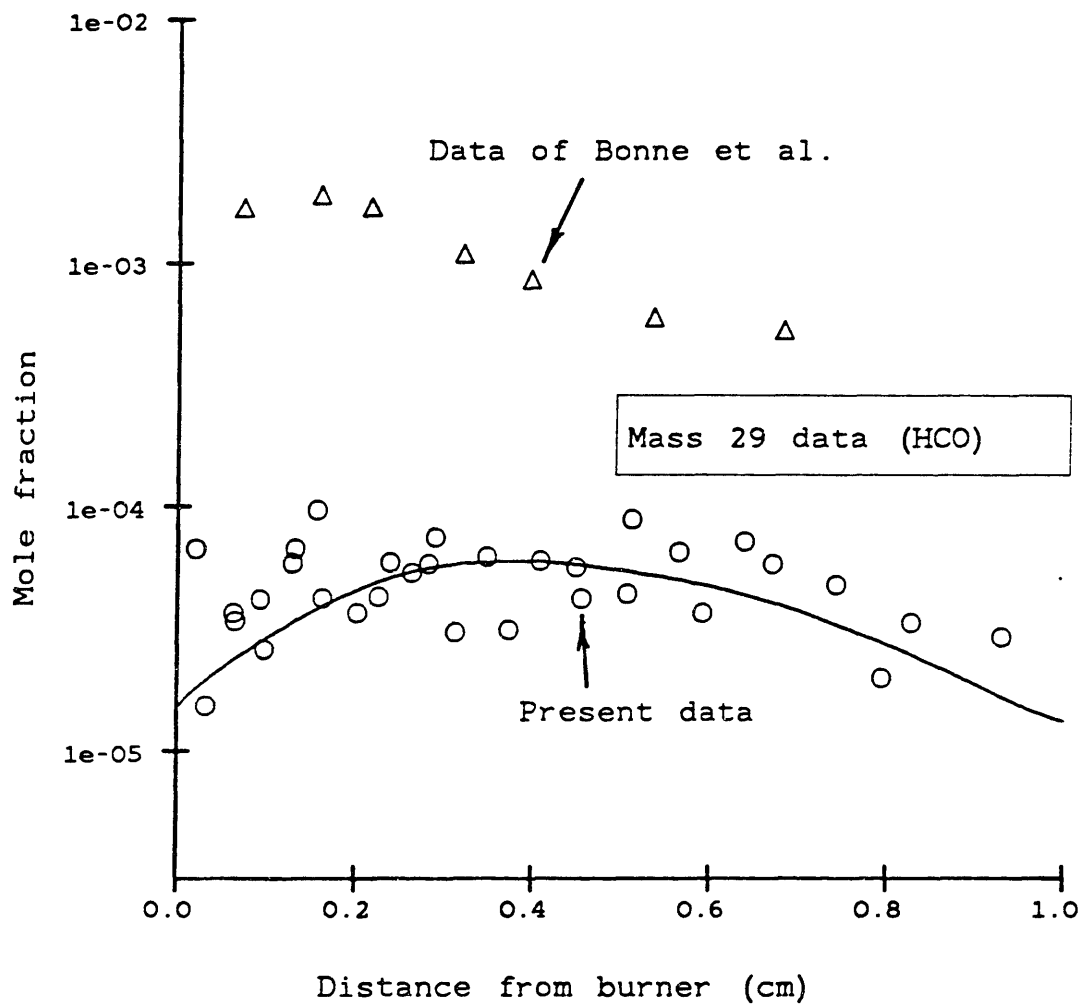


Fig. IV.13. Data and smoothed curve for mass 29 (\circ ; apparently HCO) in a laminar, premixed flame of $C_2H_2/O_2/5\%$ Ar, $\phi=2.40$, 2.67 kPa (20 torr), and $0.5 \text{ m}\cdot\text{s}^{-1}$ velocity of unburned gas (298 K).

10.18 to 11.24 eV at 0.161 cm and 10.80 to 11.86 eV at 0.201 cm. Both species are apparently present at similar concentrations at these positions, a situation that would give the curvature observed. To measure the profile for mass 30, an electron energy of 11.8 eV (ref. C₂H₄; setting 11.50 eV) was used. The calibration factor was based on the signal being all H₂CO because of the excess of HCO over C₂H₅, but if the signal were all C₂H₆, the mole fraction would be higher by a factor of 2.1.

The present data may be compared with those of Bonne et al. (Fig. IV.14) and of Delfau and Vovelle. For the combined H₂CO/C₂H₂ profile, a maximum of $1.0 \cdot 10^{-3}$ occurred very close to the burner. By comparison, Bonne et al. attribute mass 30 solely to H₂CO and report a maximum of $2.3 \cdot 10^{-3}$ at 0.25 cm. Delfau and Vovelle also cited only H₂CO for mass 30. The mean of their $\phi=2.2$ and $\phi=2.6$ maxima was $1.9 \cdot 10^{-3}$ at 0.22 cm (from $1.6 \cdot 10^{-3}$ at 0.23 and $2.1 \cdot 10^{-3}$ at 0.2). Lower temperatures in the present flame could explain a greater importance of C₂H₆ by limiting the chemically activated addition/decomposition channels of CH₃ recombination (Ch. VI).

O₂. - The profile for O₂ was measured at 15.7 eV (ref. Ar; setting 16.00 eV), 3.6 eV above the ionization potential (12.07 eV). Components of calibration factor were measured directly. No CH₃OH was detected (IP=10.85 eV), but any that was present might have been obscured by O₂ signal in the tail of the electron energy distribution. O₂ is relatively noisy for a major species because of background O₂ from air leakage.

Comparison with data of Bonne et al. is shown in Fig. IV.15 using linear axes. Agreement appears good with some what faster disappearance in the present data. However, from the present data it is found that the mole fraction does not go to zero as suggested by the linear plots but rather goes to $3 \cdot 10^{-4}$.

HO₂. - Hydroperoxyl was corrected for isotopic contribution from O₂ (¹⁷O¹⁶O vs. ¹⁶O₂), which was measured to be 0.0851% of mass 32 (0.074% theoretical). At the burner, the point of the largest contribution, O₂ was 44% of the signal for mass 33. The profile was measured at 14.7 eV (ref. Ar; setting 15.00 eV), 3.2 eV above the ionization potential (11.53±0.02 eV). Experimental ionization

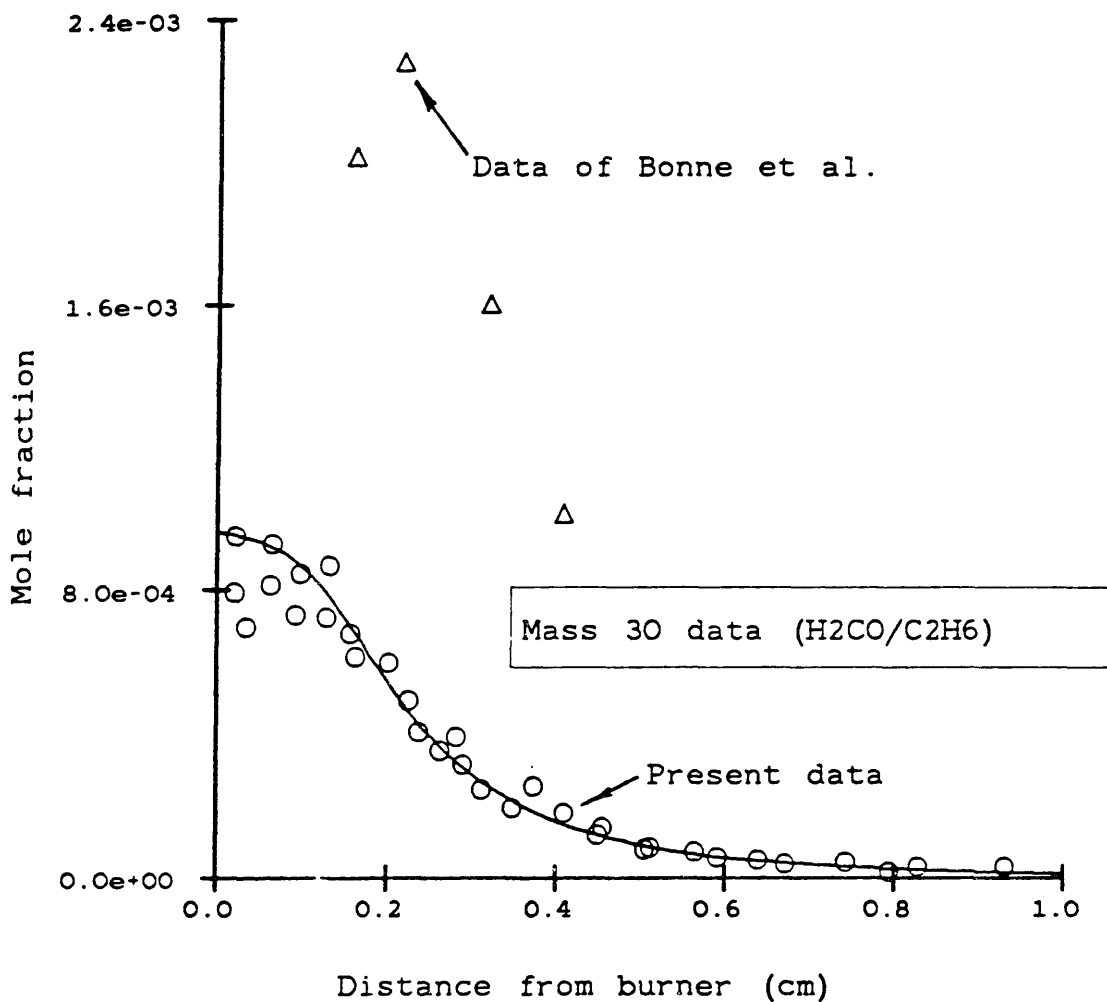


Fig. IV.14. Data profile for mass 30 (O) in a laminar, premixed flame of $C_2H_2/O_2/5\% Ar$, $\phi=2.40$, 2.67 kPa (20 torr), and $0.5 \text{ m}\cdot\text{s}^{-1}$ velocity of unburned gas (298 K), compared to data of Bonne et al. (1965; Δ) in a C_2H_2/O_2 , $\phi=2.38$ flame. Calibration assumes H_2CO , but H_2CO and C_2H_6 are apparently both present.

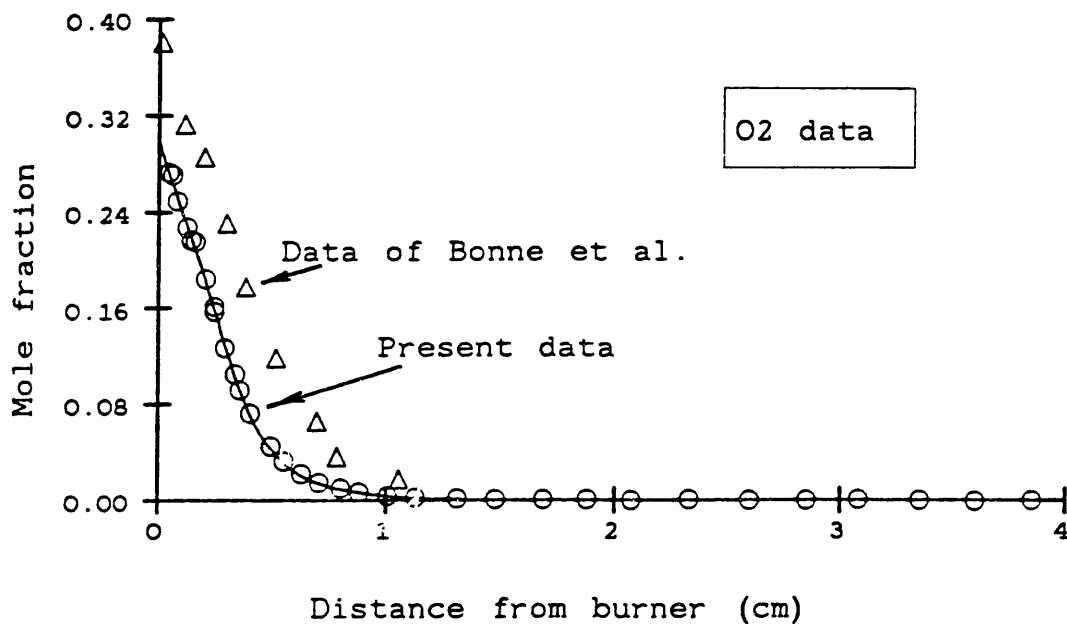


Fig. IV.15. Data profile for O₂ (○) in a laminar, premixed flame of C₂H₂/O₂/5% Ar, $\phi=2.40$, 2.67 kPa (20 torr), and 0.5 m·s⁻¹ velocity of unburned gas (298 K), compared to data of Bonne et al. (1965; Δ) in a C₂H₂/O₂, $\phi=2.38$ flame.

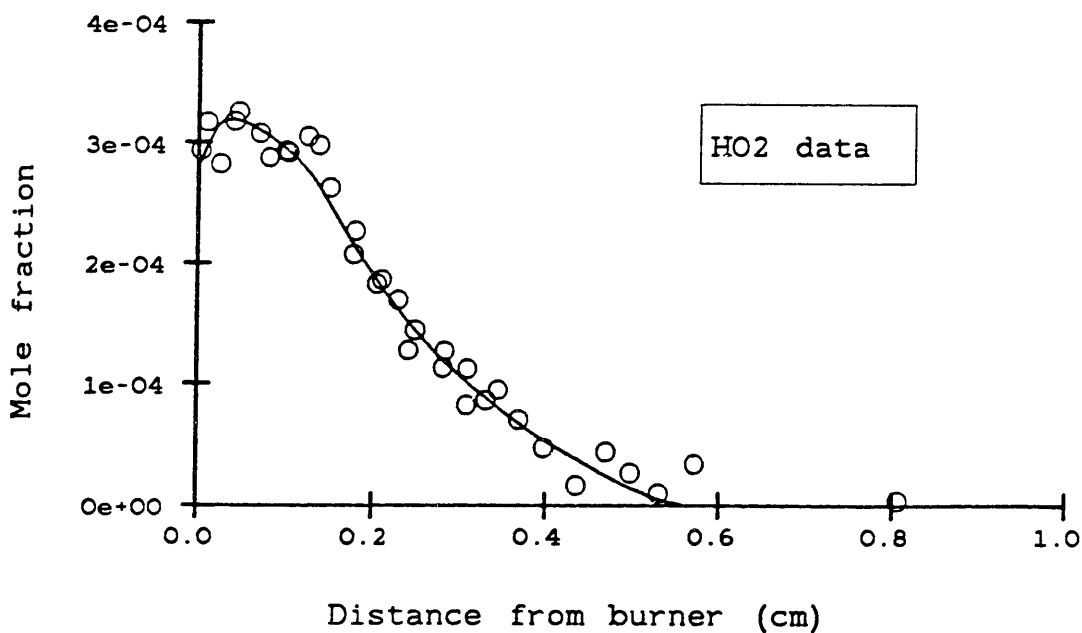


Fig. IV.16. Data (○) and smoothed curve for HO₂ in a laminar, premixed flame of C₂H₂/O₂/5% Ar, $\phi=2.40$, 2.67 kPa (20 torr), and 0.5 m·s⁻¹ velocity of unburned gas (298 K).

potentials were 12.1 ± 0.5 eV (ref. Ar) at 0.102 cm and 11.65 ± 0.33 eV (ref. Ar) at 0.276 cm.

A maximum mole fraction of $3.2 \cdot 10^{-4}$ occurred very near the burner at approximately 0.04 cm (Fig. IV.16). The only data that can be compared are those of Delfau and Vovelle, which indicate a maximum of $1.6 \cdot 10^{-4}$ at 0.2 cm (mean of $1.3 \cdot 10^{-4}$ and $1.8 \cdot 10^{-4}$, both at 0.2 cm), similar in magnitude to the present data.

H₂O₂. - Mass 34 was examined for H₂O₂ but none could be detected. One reason is that the isotopic contribution from O₂ is higher at mass 34 than at mass 33 - experimentally 0.469% vs. 0.0851%. At the burner, an H₂O₂ signal at the size of this correction would correspond to a mole fraction for H₂O₂ of 0.009.

A profile of mass 34 was measured at 14.7 eV (ref. Ar; setting 15.00 eV) but the data after isotopic correction were not statistically distinguishable from zero. An ionization efficiency measurement at 0.176 cm indicated the presence of H₂O₂ at a mole fraction of $5 \cdot 10^{-5}$ based on an ionization potential of 10.4 ± 0.8 eV (ref. Ar) vs. 10.92 ± 0.05 eV (Rosenstock et al., 1977). No data on H₂O₂ was reported from the comparable flames.

C₃ and C₃H. - Ionization efficiency measurements at 0.294 cm did not show the presence of either species. ³⁶Ar (ionization potential 15.76 eV) can be mistaken for C₃, but no literature value is available for the ionization potential of C₃. If the latter is less than 10 eV, then the attempted measurement at 11.7 eV (ref. Ar; setting 12.00 eV) gives a mole fraction of less than $(5 \pm 9) \cdot 10^{-6}$.

The ionization potential for C₃H can be estimated to be 6.5 ± 1.7 eV (Appendix G), but no signal at 0.294 cm was detected below an appearance potential that was measured to be 10.4 ± 0.5 (ref. Ar). If this intercept were taken to be the ionization potential, then the mole fraction would be estimated (incorrectly) as $2.9 \cdot 10^{-5}$.

Delfau and Vovelle report profiles for these species in their slightly hotter flames. C₃ is reported at $\phi=2.2$ but not at $\phi=2.6$, having a maximum of $4.3 \cdot 10^{-5}$ at 0.82 cm. Profiles for C₃H are reported at $\phi=2.2$ and 2.6, giving an interpolated maximum of $5.1 \cdot 10^{-5}$ at 0.87 cm (from $5.5 \cdot 10^{-5}$ at 0.82 cm and $4.7 \cdot 10^{-5}$ at 0.91 cm). At 0.294 cm, where a comparison might be made more fairly, they show a

zero mole fraction (less than $0.5 \cdot 10^{-6}$) for C_3 and $2 \cdot 10^{-6}$ for C_3H (mean of $0.8 \cdot 10^{-6}$ and $3 \cdot 10^{-6}$). Thus, there appear to be no serious discrepancies between the profiles of Delfau and Vovelle for C_3 and C_3H vs. the ionization efficiency data in this study.

C_3H_2 . - Measurements of the ionization potential for C_3H_2 gave well-defined straight-line ionization efficiency plots leading to 8.8 ± 0.1 eV (ref. Ar). These values may be compared to an estimate of 10.3 eV (Appendix G) and to 9.8 eV observed by Bittner (1981). The C_3H_2 profile was measured at 10.2 eV (ref. Ar; setting 10.50 eV).

The shape of the profile (Fig. IV.17) was characterized by little C_3H_2 at the burner, increasing rapidly to a maximum of $1.94 \cdot 10^{-4}$ at 0.56 cm and slowly decreasing to $1.0 \cdot 10^{-5}$ at 3.9 cm. For comparison, the profile shapes were similar in the flames of Delfau and Vovelle with the maximum at $\phi=2.4$ estimated to be $1.8 \cdot 10^{-4}$ at 0.7 cm (mean of $1.7 \cdot 10^{-4}$ at 0.6 cm and $1.9 \cdot 10^{-4}$ at 0.8 cm), very close to the maximum value in the present study.

C_3H_3 . - Measurements of the ionization potential for C_3H_3 were 8.81 ± 0.10 eV at 0.294 cm and 9.17 ± 0.05 eV at 0.430 cm (ref. Ar), indicating that the species was propargyl ($HC \equiv C-CH_2 \cdot$ or $\cdot HC=C-CH_2$) rather than cyclopropenyl. For propynyl, Rosenstock et al. (1977) cite an ionization potential of 8.68 eV, while Field and Franklin (1970) cite 5.8 eV for cyclopropenyl. The profile was measured at 10.2 eV (ref. Ar; setting 10.50 eV).

The C_3H_3 profile (Fig. IV.17) is shaped similarly to that of C_3H_2 but it peaks closer to the burner. It reaches a maximum of $1.02 \cdot 10^{-3}$ at 0.37 cm and declines to $8.7 \cdot 10^{-5}$ at 3.9 cm. Interpolation of data by Delfau and Vovelle predicts a maximum of $4.0 \cdot 10^{-4}$ at 0.59 cm (mean of $3.6 \cdot 10^{-4}$ at 0.55 cm and $4.3 \cdot 10^{-4}$ at 0.63 cm), somewhat lower than in the present study.

Mass 40 - C_3H_4 . - Although Ar has virtually the same mass as C_3H_4 , the ionization potential for Ar is sufficiently higher that C_3H_4 can be measured without interference from Ar. The complication for C_3H_4 is that it can represent three isomers - propadiene (allene), cyclopropane, and propyne (methylacetylene) - having ionization potentials of 9.53, 9.95, and 10.36 eV, respectively (Rosenstock et al., 1977). [The ionization potential of Ar is 15.76 eV.]

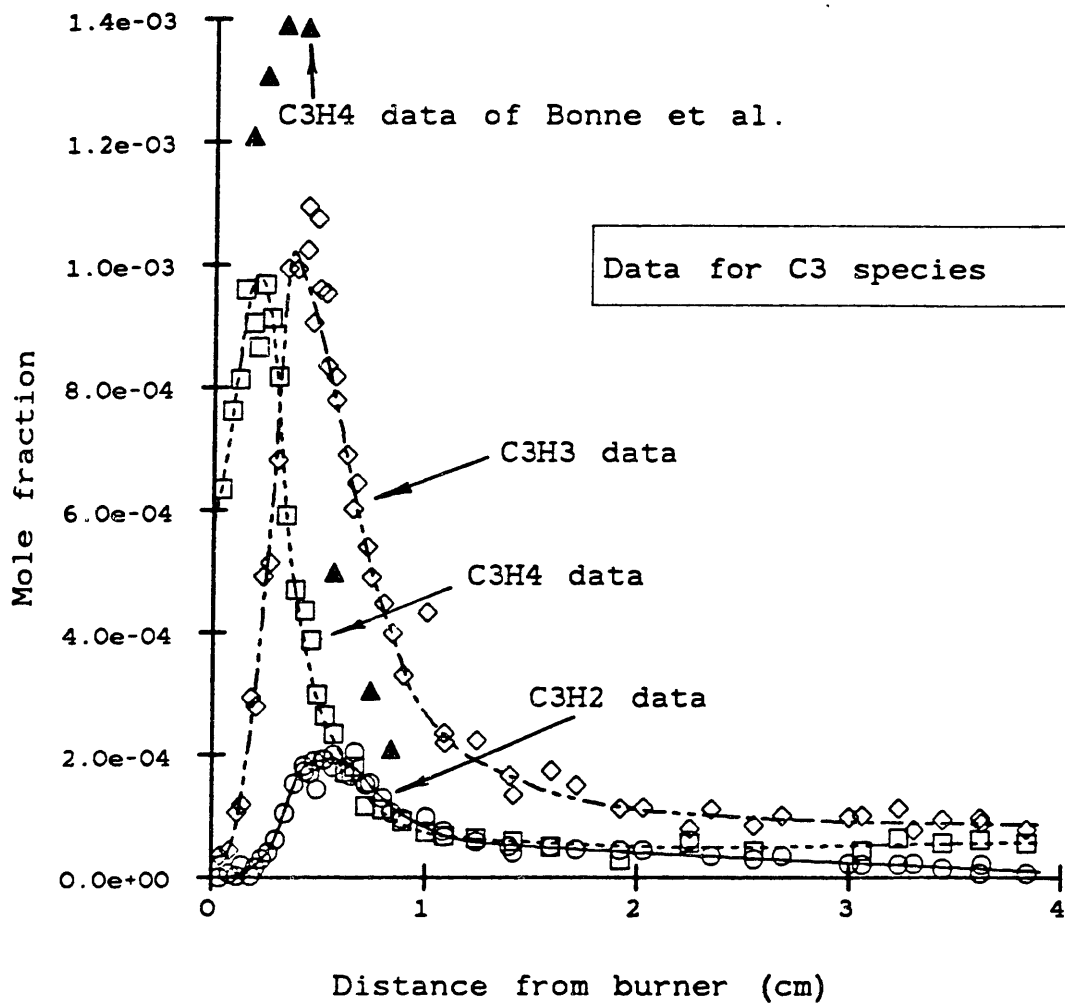


Fig. IV.17. Data profiles for C_3H_2 (\circ), C_3H_3 (\diamond), and C_3H_4 (\square) in a laminar, premixed flame of $C_2H_2/O_2/5\%$ Ar, $\phi=2.40$, 2.67 kPa (20 torr), and $0.5\text{ m}\cdot\text{s}^{-1}$ velocity of unburned gas (298 K). Also shown are C_3H_4 data of Bonne et al. (1965; \blacktriangle) in a C_2H_2/O_2 , $\phi=2.38$ flame.

The three isomers could not be resolved satisfactorily by MBMS methods. In twelve measurements of ionization efficiency curves (signal vs. electron energy), the characteristics were a linear segment from 11.5-13.5 eV, yielding an "ionization potential" of 10.2 to 10.5 eV, and an unusually linear tailing off as electron energy was reduced further. If this tail was extrapolated to zero signal, the apparent ionization potential was 9.0 to 9.7 eV. This behavior suggests that propyne is the dominant C_3H_4 , that propadiene is also present at significant levels, and that cyclopropene is in the lowest concentration if it is present at all. Analyzing the slopes of the linear segments, the propyne/propadiene ratio is 1.15/1 or greater.

An overall C_3H_4 profile was measured at 12.7 eV (ref. Ar; setting 13.00 eV). The mass-discrimination factor $\alpha_{C_3H_4}$ was assumed to be unity (" α_{Ar} "), and $S_{C_3H_4,Ar}$ was estimated using a mean of the estimated ionization cross-sections for propadiene and propyne (6.3 and $6.7 \cdot 10^{-16} \text{ cm}^2$).

This profile (Fig. IV.17) has a maximum mole fraction at 0.21 cm, closer to the burner than for C_3H_2 (0.37 cm) or C_3H_4 (0.56 cm). The data reach a shallow minimum at about 2.35 cm and rise about 15% by 3.9 cm. By comparison, Bonne et al. show a profile for C_3H_4 that agrees well in shape and magnitude so far as they measured (0.84 cm). Their maximum of $1.4 \cdot 10^{-3}$ occurred near 0.3 cm. As for other species, the C_3H_4 profiles of Delfau and Vovelle are shifted further from the burner. Interpolating their maxima to $\phi=2.4$ gives $3.5 \cdot 10^{-4}$ at 0.48 cm (mean of $3.2 \cdot 10^{-4}$ at 0.43 cm and $3.8 \cdot 10^{-4}$ at 0.53 cm), somewhat lower than the other measurements. However, because of the calibration difficulties caused by the isomers, the spread of values is probably within the uncertainty of the calibration.

Mass 40 - Ar. - In the measurement of each data point for each species, two measurements for Ar were made as internal reference, one before the species data point and one after. Argon was measured with a setting of 19.00 eV, at least 2.5 eV higher than its ionization potential.

However, with an Ar mole fraction of 5%, the contribution to mass 40 from C_3H_4 is extrapolated to be as high as 9.7% (at 0.27 cm). To measure this correction accurately, profiles for mass 40

were measured at 11.7, 12.2, 12.7, 13.2, 13.7, and 18.7 eV (ref. Ar; settings 12.00, 12.50, 13.00, 13.50, 14.00, 19.00 eV). The five low-eV points were fitted at each position by linear regression and extrapolated to 18.7 eV to determine the correction. Profiles of data points and smoothed curves were then corrected by this factor.

The profile of Ar is shown in Fig. IV.18. Its mole fraction decreases with increasing distance from the burner because the number of moles in the system increases, but the mass fraction and mass flux must remain constant.

No comparisons are possible. Only Bittner added any Ar to the C_2H_2/O_2 mixture, and to obtain his mole fractions, he assumed that the mole fraction always was 0.05, the feed mole fraction.

Mass 41 (HCCO and/or C_3H_5). - After isotopic correction, a low-mass 41 signal with contributions from C_3H_5 and HCCO could be detected. Ionization potential measurements gave 9.3 ± 0.7 eV at 0.276 cm from a segment that was reasonably linear over 9.7 to 12.2 eV (ref. Ar) and 9.3 ± 0.2 eV at 0.294 cm over 9.7 to 11.7 eV (ref. Ar). The latter curve could also be treated as having two ionization potentials at 8.3 and 10.0 eV.

No ionization potential has been reported for HCCO, but it can be calculated to be 10.3 ± 0.3 eV (Appendix G). The ionization potential for C_3H_5 (allyl radical) is 8.07 ± 0.03 eV (Rosenstock et al., 1977). Thus the ionization potentials that were measured are consistent with comparable concentrations of C_3H_5 and HCCO. The relative slopes indicate that HCCO dominates, possibly by an order of magnitude.

The profile for mass 41 (Fig. IV.19) was measured at 10.3 eV (ref. Ar; setting 10.50 eV) and the calibration factor was calculated assuming that only HCCO was present. If all the signal were C_3H_5 , the mole fractions would be lower by a factor of 1.9. A maximum mole fraction of $3.7 \cdot 10^{-5}$ was observed at about 0.35 cm.

Delfau and Voveile report profiles for mass 41 as C_3H_5 . Interpolating their maxima would give a maximum of $5.7 \cdot 10^{-5}$ at 0.38 cm (mean of $5.9 \cdot 10^{-5}$ at 0.33 cm and $5.4 \cdot 10^{-5}$ at 0.43 cm), which would be $3.0 \cdot 10^{-5}$ if the signal were interpreted as HCCO. The two profiles

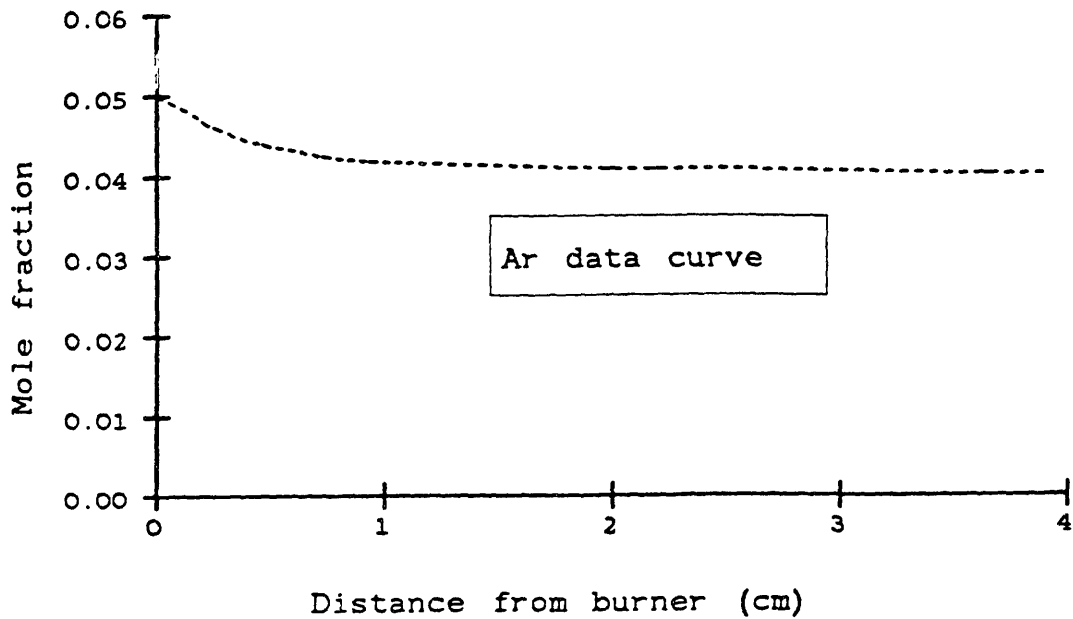


Fig. IV.18. Data curve for Ar in a laminar, premixed flame of $C_2H_2/O_2/5\%$ Ar, $\phi=2.40$, 2.67 kPa (20 torr), and $0.5\text{ m}\cdot\text{s}^{-1}$ velocity of unburned gas (298 K).

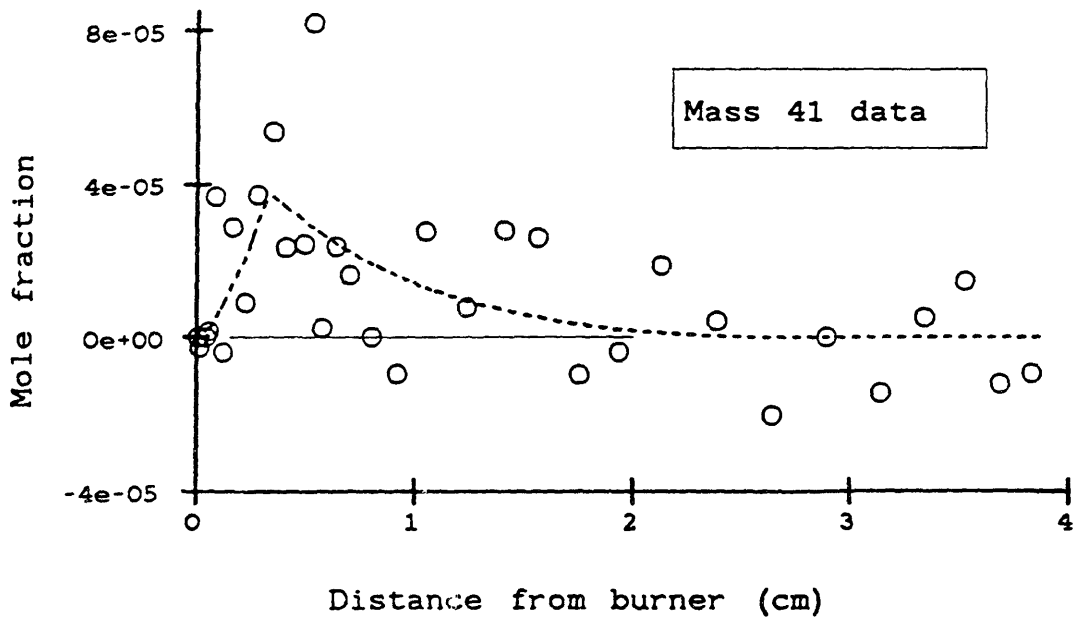


Fig. IV.19. Data (O) and smoothed curve for HCCO in a laminar, premixed flame of $C_2H_2/O_2/5\%$ Ar, $\phi=2.40$, 2.67 kPa (20 torr), and $0.5\text{ m}\cdot\text{s}^{-1}$ velocity of unburned gas (298 K).

are thus similar in magnitude, but the uncertainty remains about the relative proportions of C_3H_5 and HCCO.

Mass 42 (CH_2CO and/or C_3H_5). - Ketene ($CH_2=C=O$) has been proposed as a key intermediate in acetylene oxidation. Mass 42 cannot be identified specifically as CH_2CO by ionization potential, but the presence of CH_2CO is confirmed by mass 14. At that mass, an appearance potential of 13.71 ± 0.09 eV for a strong fragmentation was measured, corresponding to CH_2^+ from CH_2CO (13.8 ± 0.8 eV).

CH_2CO and C_3H_6 have ionization potentials of 9.61 and 9.74 eV, respectively (Rosenstock et al., 1977). This difference is too small to be resolved here, as shown by the measured ionization potentials of 9.1 ± 0.3 , 9.6 ± 0.1 , and 9.4 ± 0.1 eV (ref. Ar). Because of the likelihood and evidence of CH_2CO , the calibration factor was calculated assuming an ionization cross-section for CH_2CO . If all the signal were due instead to C_3H_6 , the mole fractions would be lower by a factor of 1.9. The species profile was measured at 10.3 eV (ref. Ar; setting 10.50 eV).

The profile for mass 42 (Fig. IV.20) had a maximum of $7.2 \cdot 10^{-4}$ at 0.14 cm and declined to $3.2 \cdot 10^{-4}$ at 3.9 cm. Delfau and Vovelle report profiles for mass 42, attributed to CH_2CO at $\phi=2.2$ but to " CH_2CO/C_3H_6 " at $\phi=2.6$. Interpolation of the maxima gives $6.3 \cdot 10^{-4}$ at 0.32 cm (mean of $6.6 \cdot 10^{-4}$ at 0.26 cm and $6.0 \cdot 10^{-4}$ at 0.38 cm), quite similarly to the present data.

Mass 43 (CH_3CO and/or C_3H_7). - No signal due to these species was detected at 0.294 cm. Isotopic correction reduced the possible mole fraction to $(0.1 \pm 1.2) \cdot 10^{-5}$ if mass 42 was assumed to be CH_2CO . The "mole fraction" would become significantly negative if the isotopic correction were due instead to C_3H_6 , indirectly supporting the assignment of mass 42 to CH_2CO .

Mass 44 (CH_3CHO and/or C_3H_8). - These are species of mass 44 with ionization potentials 10.23 and 11.0 eV, respectively, compared to CO_2 at 13.77 eV. At 0.039 cm, ionization potentials of 9.9 ± 0.7 eV and 13.6 ± 0.15 eV were measured for mass 44, but at 0.294 cm, only the ionization potential of CO_2 was detected. The level of CH_3CHO at 0.039 cm was estimated to be less than $(8 \pm 5) \cdot 10^{-5}$. No data are available for comparison.

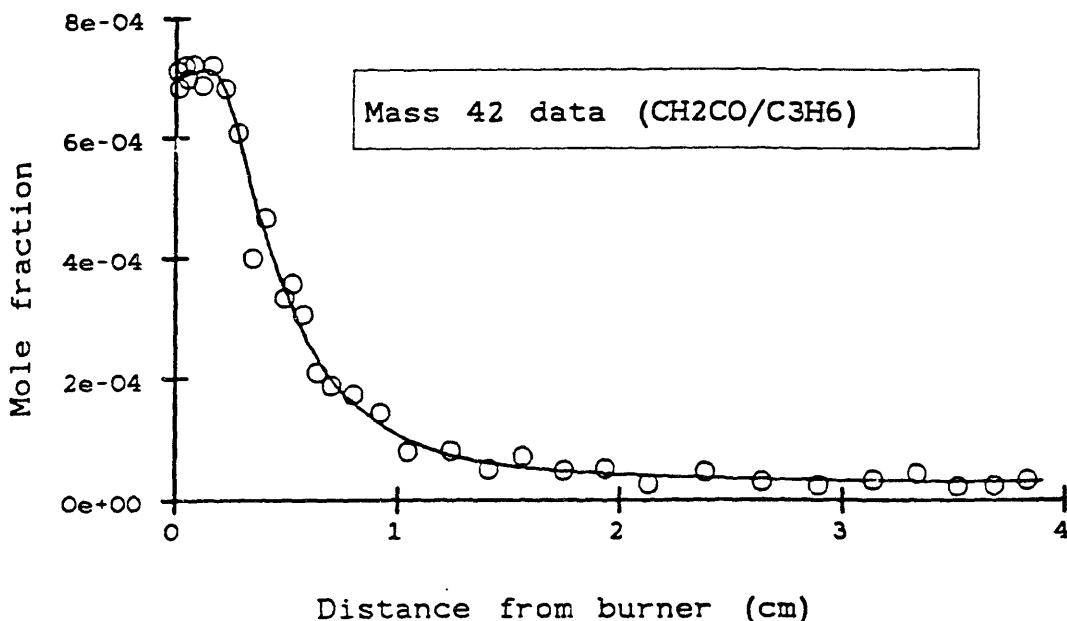


Fig. IV.20. Data profile for mass 42 (○) in a laminar, premixed flame of C₂H₂/O₂/5% Ar, $\phi=2.40$, 2.67 kPa (20 torr), and 0.5 m·s⁻¹ velocity of unburned gas (298 K), compared to data of Bonne et al. (1965; Δ) in a C₂H₂/O₂, $\phi=2.38$ flame. Calibration assumes CH₂CO.

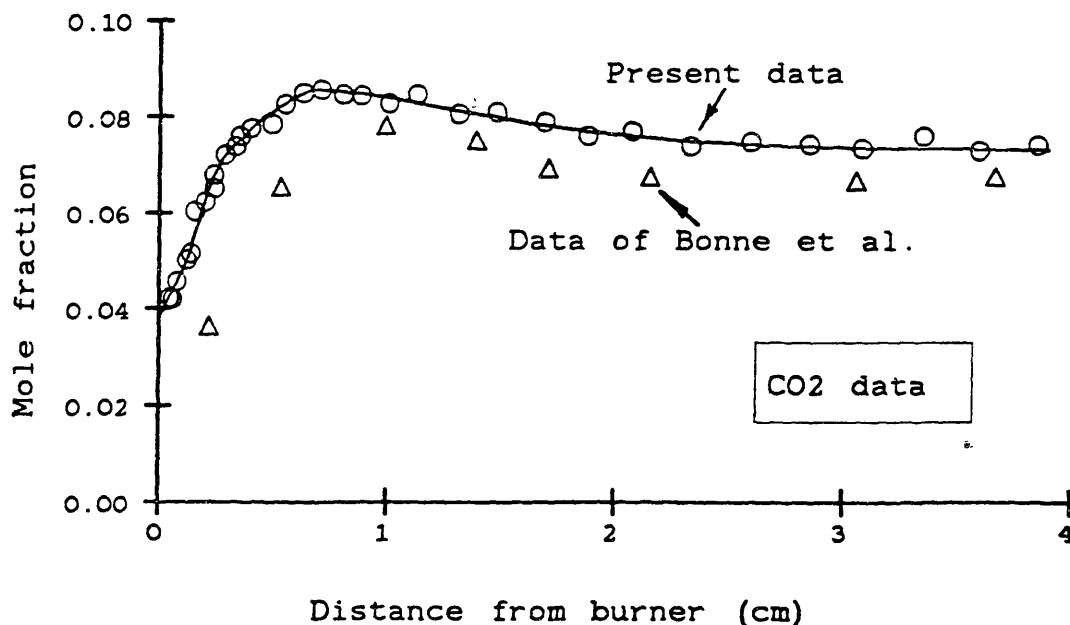


Fig. IV.21. Data profile for CO₂ (○) in a laminar, premixed flame of C₂H₂/O₂/5% Ar, $\phi=2.40$, 2.67 kPa (20 torr), and 0.5 m·s⁻¹ velocity of unburned gas (298 K), compared to data of Bonne et al. (1965; Δ) in a C₂H₂/O₂, $\phi=2.38$ flame.

Mass 44 (CO₂). - Carbon dioxide is normally expected to be an end product of combustion, but the profile of Figs. IV.1 and IV.2 shows that the mole fraction of CO₂ rises rapidly and then declines due to destruction reaction(s). The signal was measured at 18.7 eV (ref. Ar; setting 19.00 eV), and the terms in the calibration factor were measured directly.

The maximum mole fraction of CO₂ is 0.086 and occurs at 0.70 cm. At 3.9 cm, the mole fraction has declined by 15% to 0.073, compared to Bittner's estimate of 0.061 at that point. In Fig. IV.21 the data of Bonne et al. are shown for comparison. Their data have very much the same shape as observed here. The highest data point was 0.078 at 0.98 cm, and the data within the range of positions 2 to 5 cm are all approximately 0.068. Finally the profiles of Delfau and Vovelle may be interpolated to give a maximum of 0.069 at 0.85 cm (mean of 0.074 at 0.9 cm and 0.063 at 0.8 cm) and a value of 0.055 (from 0.062 and 0.048) at 2.5 cm. Considering the differences among the experiments, all the data are in reasonable agreement.

C₄H. - Estimation of the ionization potential gives 5.1 ± 0.1 eV (Appendix G). Appearance potentials from C₄H₂ and C₄H₄ occur at 12.1 eV (Rosenstock et al., 1977), but no signal at mass 49 could be detected at 0.32 cm for electron energies as high as 13.35 eV (ref. Ar; setting 13.50 eV). An appearance potential at 15.1 eV was observed, possibly due to C₄H₆ (15.75 eV). The upper limit to the mole fraction at this point is $(2 \pm 3) \cdot 10^{-6}$.

C₄H₂. - The ionization potential of diacetylene was measured as 10.7 ± 0.1 or 10.2 ± 0.1 eV (ref. Ar) compared to a literature value of 10.18 eV (Rosenstock et al., 1977). Its profile was measured at 12.85 eV (ref. Ar; setting 13.00 eV).

C₄H₂ persists in the post-flame zone as the hydrocarbon with the second highest mole fraction after C₂H₂. As shown in Fig. IV.22, it rises abruptly to nearly 1% (mole fraction $9.7 \cdot 10^{-3}$) at 0.65 cm and then gradually declines to $3.0 \cdot 10^{-3}$ at 3.9 cm. Shape and magnitude agree well with the data of Bonne et al., which have a maximum of 0.008 near 0.7 cm. For further comparison, interpolating the maxima of Delfau and Vovelle gives $5.8 \cdot 10^{-3}$ at 0.9 cm (mean of $4.7 \cdot 10^{-3}$ at 0.82 cm and $6.8 \cdot 10^{-3}$ at 1.0 cm).

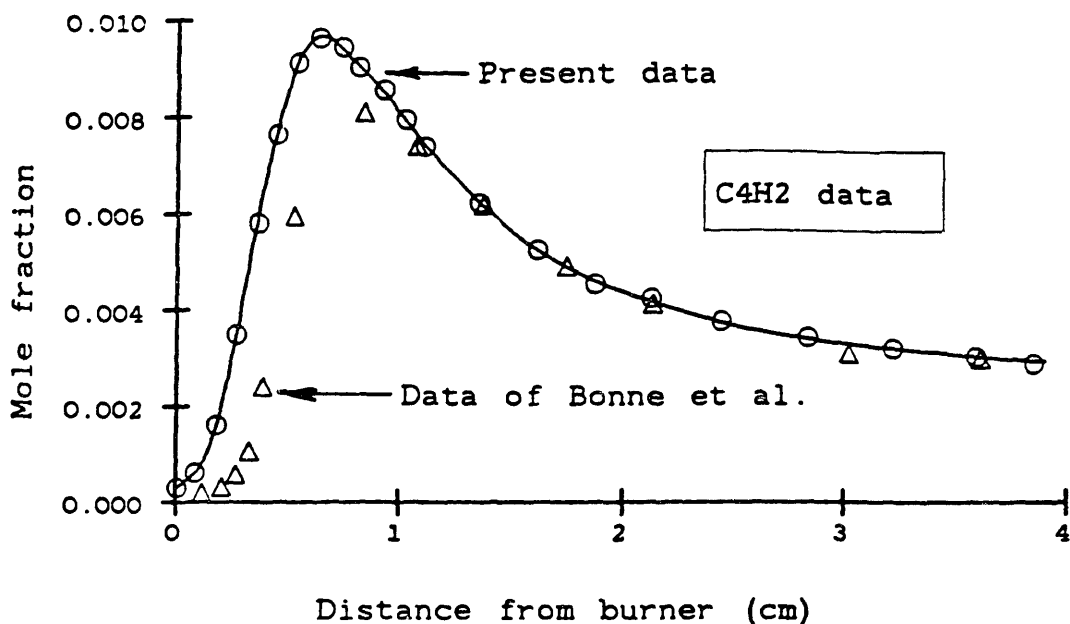


Fig. IV.22. Data profile for C₄H₂ (○) in a laminar, premixed flame of C₂H₂/O₂/5% Ar, $\phi=2.40$, 2.67 kPa (20 torr), and 0.5 m·s⁻¹ velocity of unburned gas (298 K), compared to data of Bonne et al. (1965; Δ) in a C₂H₂/O₂, $\phi=2.38$ flame.

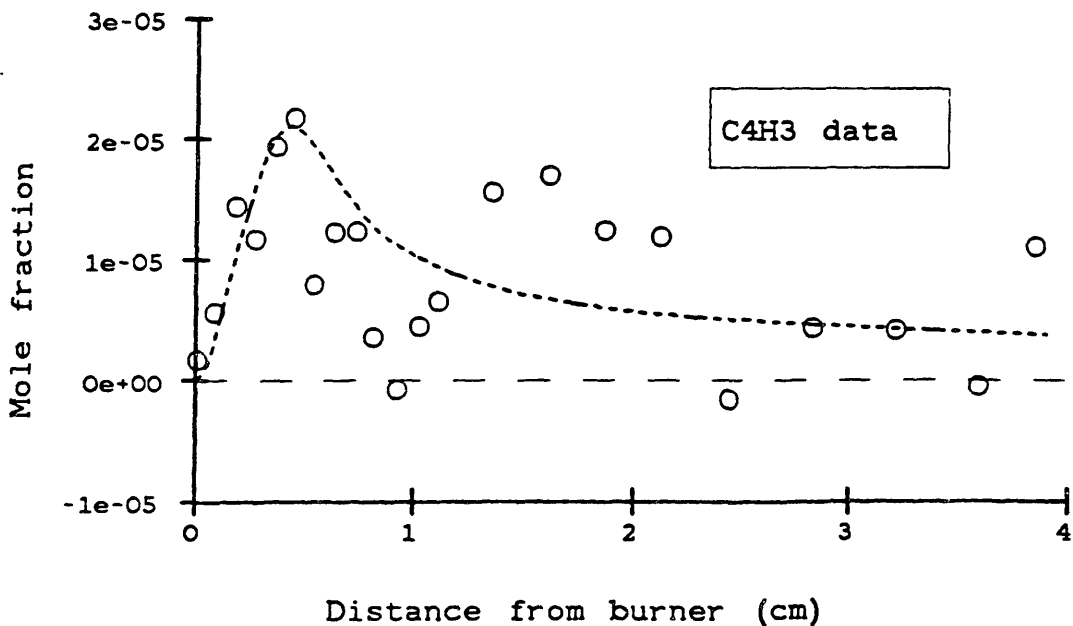


Fig. IV.23. Data (○) and smoothed curve for C₄H₃ in a laminar, premixed flame of C₂H₂/O₂/5% Ar, $\phi=2.40$, 2.67 kPa (20 torr), and 0.5 m·s⁻¹ velocity of unburned gas (298 K).

C₄H₃. - The two most likely isomers of C₄H₃ in the flame are 1-C₄H₃ (HC≡C-CH=CH·) and 2-C₄H₃ (HC≡C-C·=CH₂). The closeness of their ionization potentials and the noise resulting from the large isotope correction from C₄H₂ prevent resolution of the isomers. Estimation of the ionization potentials (Appendix G) gives 8.4 eV for 2-C₄H₃ and 8.9 eV for 1-C₄H₃, while measurement gives 8.6±0.65 eV (ref. Ar).

The more stable isomer by 12 kcal/mol is 2-C₄H₃ (Appendix G). If the two isomers are in partial equilibrium, then 2-C₄H₃ would dominate the signal by 20/1 at 2000 K. Partial equilibrium could be established late in the flame by H-abstraction reactions from C₄H₄ or H addition to C₄H₂, but early in the flame 1-C₄H₃ may be formed by direct addition of C₂H to C₂H₂, a route that is not available to form 2-C₄H₃. In this region, 1-C₄H₃ could exceed an equilibrium level or even could exceed 2-C₄H₃.

Mole fraction data for C₄H₃ were measured at 10.85 eV (ref. Ar; setting 11.00 eV). The profile for C₄H₃ was measured at 10.85 eV (ref. Ar; setting 11.00 eV). Fig. IV.23 defines the level of C₄H₃ in the region below 0.5 cm, where deposits on the probe are not a problem. [At 10.85 eV, the isotopic contribution from C₄H₂ was greater than 80% of the signal for mass 51 beyond 0.5 cm, so slight noise in mass 50 causes very noisy data there. Nevertheless, a nonzero signal with an upper limit 2·10⁻⁵ in the post-flame region can still be identified within the scatter.]

At less than 0.5 cm, the shape and magnitude of the profile are well-defined. The isotopic contribution of C₄H₂ falls to 60 to 80%, but mass 50 and 51 signals each contain less noise. This increased proportion of C₄H₃ relative to the C₄H₂ effect is quantitatively consistent with its formation by addition reactions such as C₂H + C₂H₂. In the lower temperatures near the burner, this exothermic addition reaction is faster than at higher temperatures because of fall-off (Chapter VI).

No other data on C₄H₃ have been reported.

C₄H₄. - The identification of mass 52 as vinylacetylene (3-butenyne or HC≡C-CH=CH₂) was established by measurement of the ionization potential as 9.95±0.2 eV at 0.138 cm (ref. Ar).

In comparison, ionization potentials from Rosenstock et al. (1977) are 9.25 eV for butatriene ($\text{CH}_2=\text{C}=\text{C}=\text{CH}_2$) and 9.87 eV for vinylacetylene. The profile was measured at 12.85 eV (ref. Ar; setting 13.00 eV).

This profile (Fig. IV.24) early in the flame is characterized by rapid increase to a maximum mole fraction of $1.8 \cdot 10^{-4}$ at 0.31 cm, followed by rapid decline. This general behavior was also detected by Bonne et al., whose maximum was approximately $5 \cdot 10^{-4}$ at 0.6 cm. (The difference in position and magnitude may be due to different temperatures or to calibration uncertainties in one or both experiments).

However, the present data extend beyond this peak in the data, showing that C_4H_4 mole fraction goes through a minimum of $7 \cdot 10^{-6}$ at about 2.5 cm and then rises through the rest of the flame by 40% (at 3.9 cm). Beyond 1.0 cm, Bonne et al. reported no data for C_4H_4 .

Delfau and Vovelle show only the maximum in their flames of $\phi=2.2$ (to 2.8 cm) and $\phi=2.6$ (to 3.0 cm). Interpolation predicts a maximum of $1.6 \cdot 10^{-4}$ at 0.55 cm (mean of $9.5 \cdot 10^{-5}$ at 0.5 cm and $2.2 \cdot 10^{-4}$ at 0.6 cm). The absence of the subsequent minimum and rise may be due to the narrower range of positions examined, but the hotter temperature profile is most likely the cause.

C_4H_5 . - Just as for C_4H_3 , two isomers of C_4H_5 are likely: 1- C_4H_5 ($\text{CH}_2=\text{CH}-\text{CH}=\text{CH}\cdot$) and 2- C_4H_5 ($\text{H}_2\text{C}=\text{CH}-\text{C}\cdot=\text{CH}_2$). From appearance potentials in the literature, the ionization potentials of these species can be estimated to be 7.7 and 7.2 eV, respectively (Appendix G). This distinction is too small to be resolved by measuring ionization potentials in this apparatus (resolution 0.5-1 eV). At 0.318 cm, the ionization potential was measured to be 8.9 ± 0.25 eV (ref. Ar).

Again, equilibrium would favor 2- C_4H_5 , but kinetics could cause 1- C_4H_5 to dominate early in the flame. Heats of formation for 1- and 2- C_4H_5 are 84 and 73 kcal/mol (Appendix G), so the equilibrium ratio at 2000 K would be 16/1 in favor of 2- C_4H_5 . However, formation of C_4H_5 by addition of C_2H_3 to C_2H_2 could only lead to 1- C_4H_5 . Also, Cole (1982) showed quantitatively that formation of C_4H_5 by H-abstraction from 1,3-butadiene would favor 1- C_4H_5 kinetically.

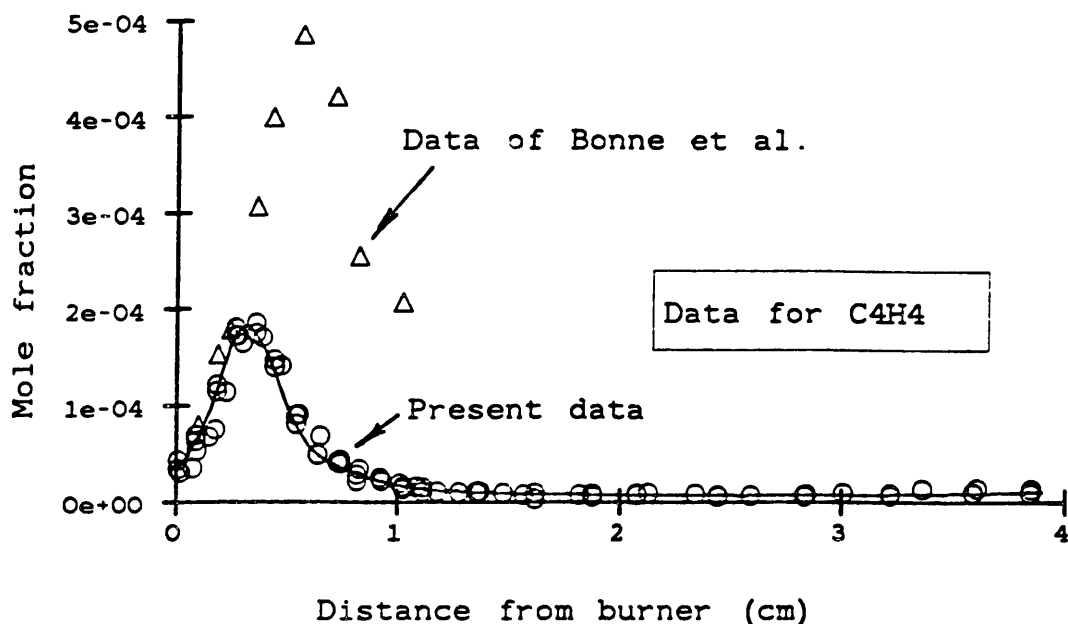


Fig. IV.24. Data profile for C_4H_4 (O) in a laminar, premixed flame of $C_2H_2/O_2/5\%$ Ar, $\phi=2.40$, 2.67 kPa (20 torr), and $0.5 \text{ m}\cdot\text{s}^{-1}$ velocity of unburned gas (298 K), compared to data of Bonne et al. (1965; Δ) in a C_2H_2/O_2 , $\phi=2.38$ flame.

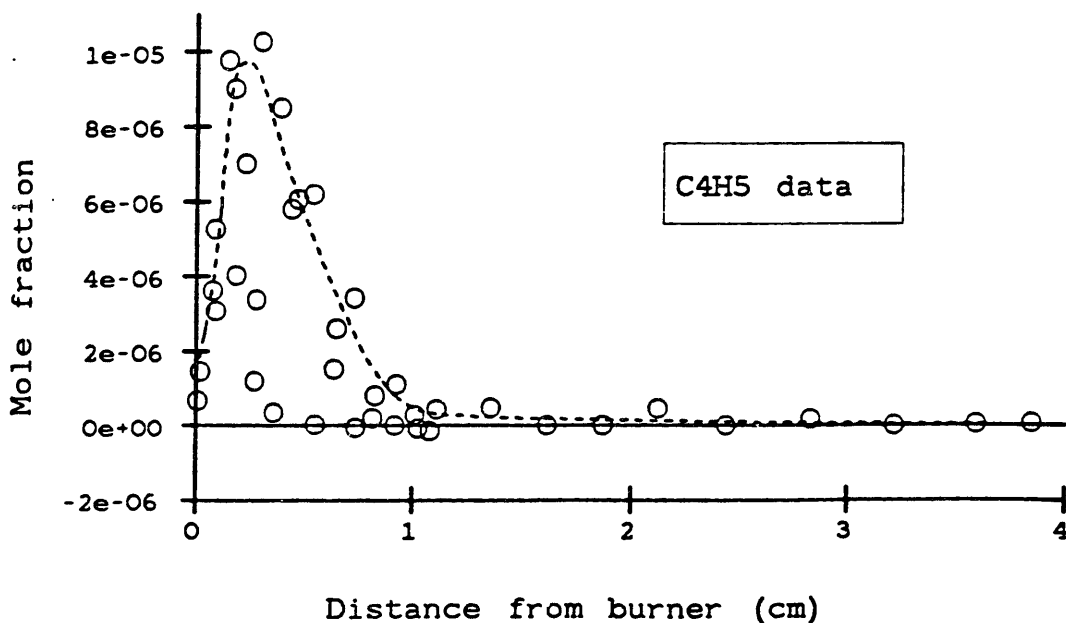


Fig. IV.25. Data (O) and smoothed curve for C_4H_5 in a laminar, premixed flame of $C_2H_2/O_2/5\%$ Ar, $\phi=2.40$, 2.67 kPa (20 torr), and $0.5 \text{ m}\cdot\text{s}^{-1}$ velocity of unburned gas (298 K).

The profile for C_4H_5 (Fig. IV.25) was measured at 10.85 eV (ref. Ar; setting 11.00 eV). The data are less scattered than for C_4H_3 , but signal noise and isotopic correction again lead to significant scatter. Nevertheless, the data points outline the profile quite well. The maximum mole fraction is approximately $9.7 \cdot 10^{-6}$ at 0.22 cm. No other data have been reported that might be compared.

C_4H_6 . - Mass 54 is probably 1,3-butadiene. Measurement of its ionization potential gave 9.1 ± 0.1 eV (ref. Ar), compared to 9.06 and 9.2 eV for trans- and cis-1,3-butadiene, 9.23 for the 1,2-butadiene, 9.56 for 2-butyne (1,2-dimethylacetylene), and 10.13 for 1-butyne. Other possibilities for which no ionization potentials have been reported, are ethynylaldehyde ($HC=C-CH=O$) and $CH_2=C=C=O$, structures isoelectronic with C_4H_4 species. The absence of acrolein at mass 56 suggests these oxygenates are also absent.

The C_4H_6 profile was measured at 10.85 eV (ref. Ar; setting 11.00 eV) and is shown in Fig. IV.26. It displays a rapid rise to $5.0 \cdot 10^{-5}$ at 0.17 cm, then gradually declines to a minimum of $5 \cdot 10^{-8}$ at 1.9 cm and rises again to $7 \cdot 10^{-7}$ at 3.9 cm.

No C_4H_6 data are reported elsewhere for comparison.

C_4H_8 . - Measurement of the ionization efficiency at 0.318 cm indicates that C_4H_8 is present with a mole fraction of $1.5 \cdot 10^{-6}$ and occurs as dimethylethene structures. Identification is based on the ionization potential of 9.1 ± 0.6 (ref. Ar), which was compared to 2-butene at 9.13 eV, isobutene (2-methylpropene) at 9.23 eV, 1-butene at 9.58 eV, and acrolein ($CH_2=CH-CH=O$) at 10.10 eV).

C_5H_2 . - Mass 62 can only be C_5H_2 , a species analogous in structure to C_3H_2 . Its most stable structure would be a resonantly stabilized diradical with terminal hydrogens on a chain of sp carbons. The measured ionization potential was 8.0 ± 0.1 eV at 0.395 cm, linear over 8.3 to 10.8 eV (ref. Ar). No literature value is reported.

The profile for C_5H_2 (Fig. IV.27) was measured at 10.5 eV (ref. Ar; setting 10.25 eV). Profiles for C_5H_3 - C_5H_6 were measured during the same experiment and were corrected for isotopic contributions. The profile for C_5H_2 rises quickly to a maximum of $1.8 \cdot 10^{-5}$ at 0.65 cm and then declines steadily.

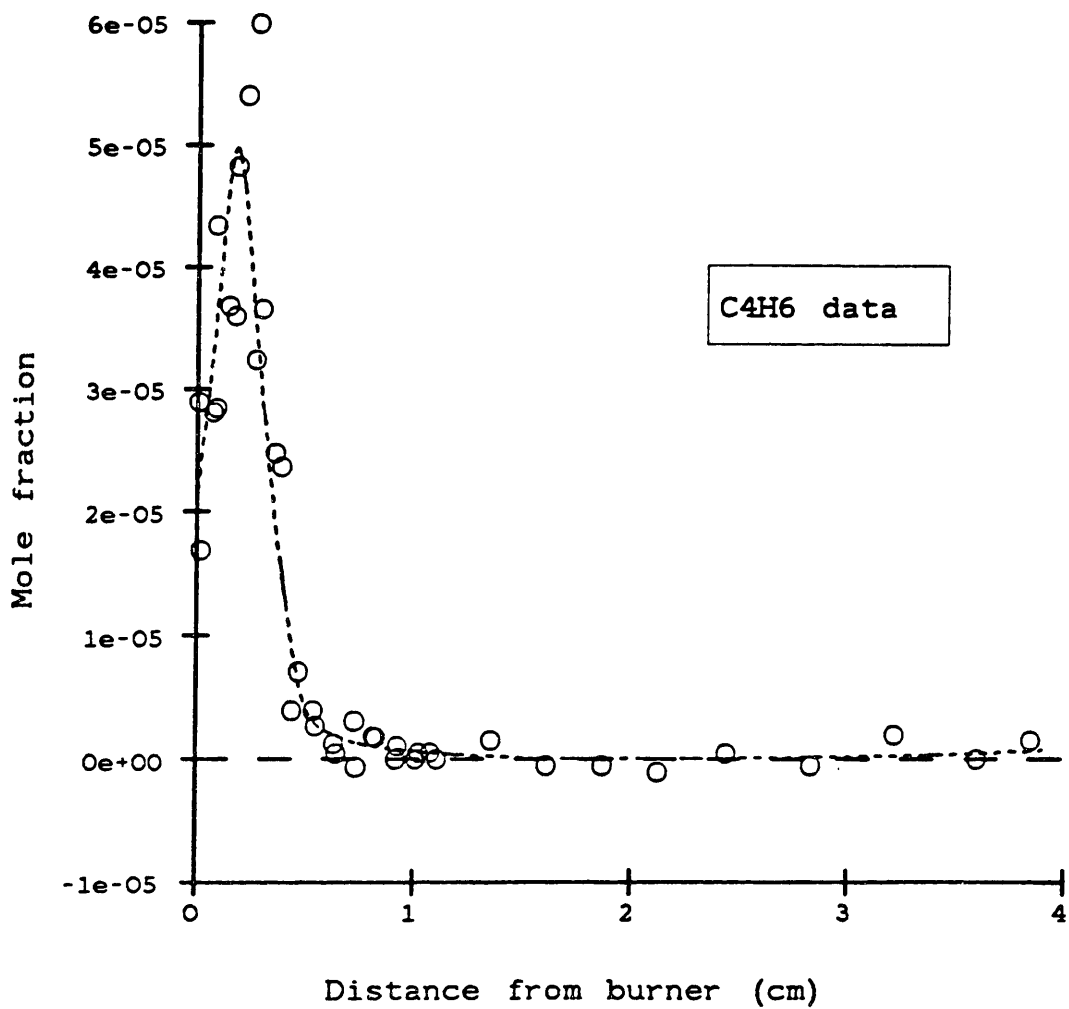


Fig. IV.26. Data (O) and smoothed curve for C_4H_6 in a laminar, premixed flame of $C_2H_2/O_2/5\%$ Ar, $\phi=2.40$, 2.67 kPa (20 torr), and $0.5\text{ m}\cdot\text{s}^{-1}$ velocity of unburned gas (298 K).

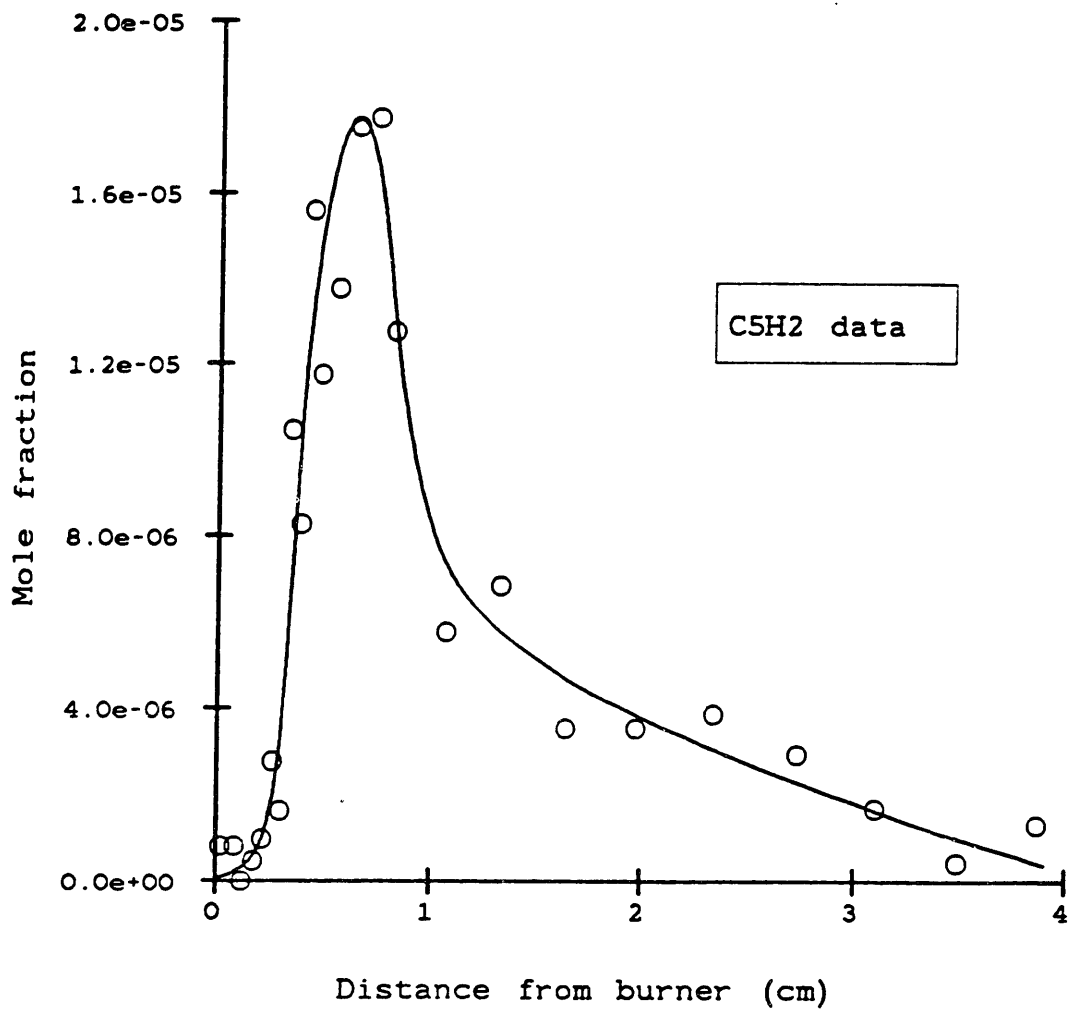


Fig. IV.27. Data (○) and smoothed curve for C_5H_2 in a laminar, premixed flame of $C_2H_2/O_2/5\% Ar$, $\phi=2.40$, 2.67 kPa (20 torr), and $0.5\text{ m}\cdot\text{s}^{-1}$ velocity of unburned gas (298 K).

Delfau and Vovelle emphasized C_3 and C_5 species in their studies. They observed C_5H_2 at similar levels to those shown in Fig. IV.27. Interpolating between the positions and magnitudes of their maximum mole fractions at $\phi=2.2$ and 2.6 , an maximum of $2 \cdot 10^{-5}$ at 0.79 cm can be estimated if they had sampled at $\phi=2.40$ (mean of $3.8 \cdot 10^{-6}$ at 0.73 cm and $3.8 \cdot 10^{-5}$ at 0.85 cm). This result is in excellent agreement with the present data.

C_5H_3 . - The species at mass 63 with an ionization potential of 8.4 ± 0.25 eV (ref. Ar, 0.395 cm) must be C_5H_3 . Usual references for ionization potentials report only appearance potentials for $C_5H_3^+$. Bittner (1981) reported a species of mass 63 with an ionization potential of 9.1 eV (ref. benzene). He proposed that it might be $HC \equiv C - C \equiv C - CH_2 \cdot$, similar in structure to C_3H_3 , and having three resonance structures.

A profile for C_5H_3 was measured (Fig. IV.28) using an electron energy of 10.5 eV (ref. Ar; setting 10.25 eV). As for C_5H_2 , only a maximum was observed, $5.5 \cdot 10^{-5}$ at 0.46 cm. By comparison, interpolation of maxima from Delfau and Vovelle gives $3.3 \cdot 10^{-5}$ at 0.82 cm (mean of $1.3 \cdot 10^{-5}$ and $5.2 \cdot 10^{-5}$ at 0.82 cm). This is slightly lower than in Fig. IV.28 but well within calibration uncertainty, and the position of the maximum is further from the burner.

C_5H_4 . - This species is probably an ethynyl-substituted C_3H_4 , either $HC \equiv C - C \equiv C - CH_3$, or $HC \equiv C - C = C = CH_2$. Its ionization efficiency was not measured successfully at 0.395 cm, so an ionization potential of 9.5 eV was estimated based on propyne and allene.

The profile shown in Fig. IV.29 was determined from measurements at 10.5 eV (ref. Ar; setting 10.25 eV). Again, a simple maximum was observed with mole fraction $6.3 \cdot 10^{-5}$ at 0.36 cm. Interpolation from the work of Delfau and Vovelle leads to a value of $2.8 \cdot 10^{-5}$ at 0.7 cm (mean of $2.2 \cdot 10^{-5}$ and $3.4 \cdot 10^{-5}$ at 0.7 cm). These values are in good agreement considering calibration uncertainties and differences in the temperature profiles.

C_5H_5 . - At mass 65, a cyclic, resonantly stabilized species becomes a possibility. C_5H_5 could be cyclopentadienyl (8.56 eV) or a noncyclic radical, quite likely an ethynyl-substituted allyl (8.1 eV estimated from allyl). An approximate ionization potential of

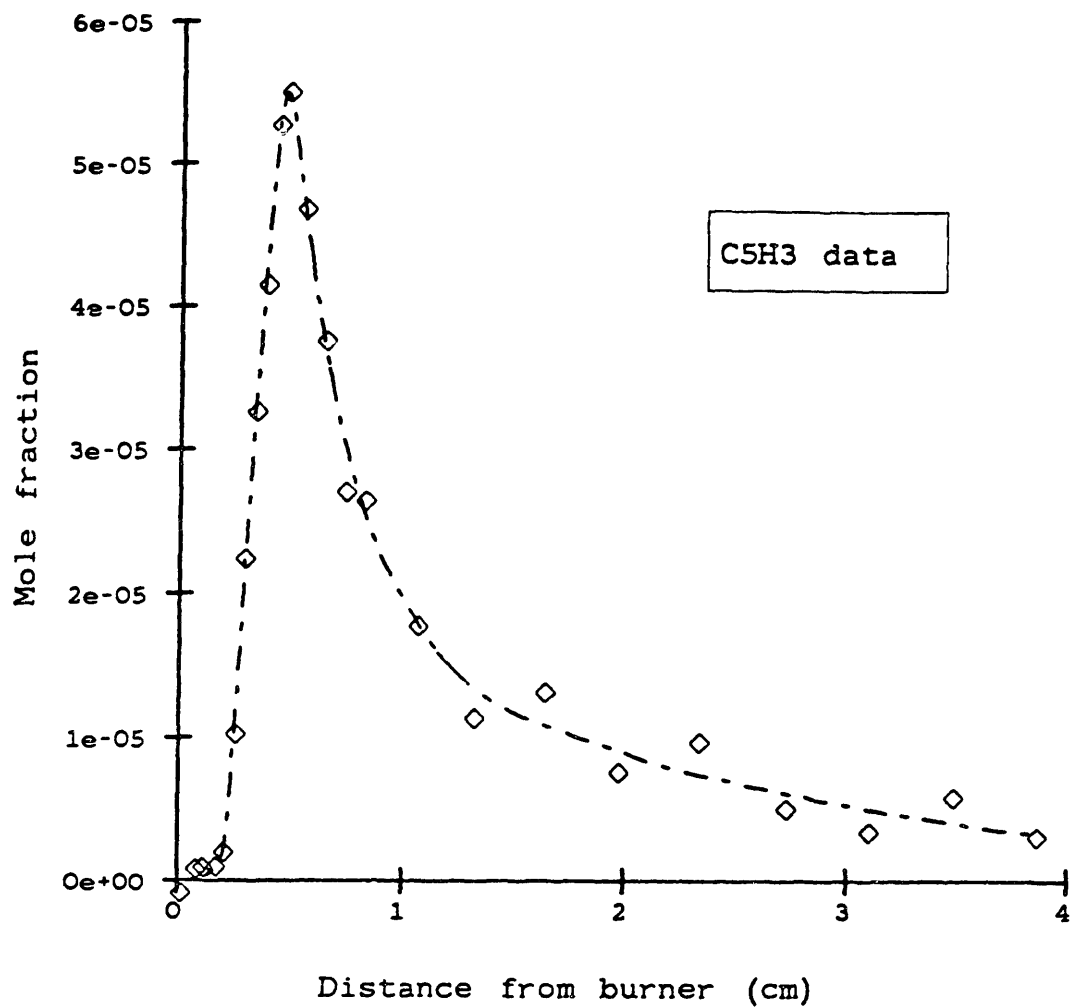


Fig. IV.28. Data (\diamond) and smoothed curve for C_5H_3 in a laminar, premixed flame of $C_2H_2/O_2/5\%$ Ar, $\phi=2.40$, 2.67 kPa (20 torr), and $0.5\text{ m}\cdot\text{s}^{-1}$ velocity of unburned gas (298 K).

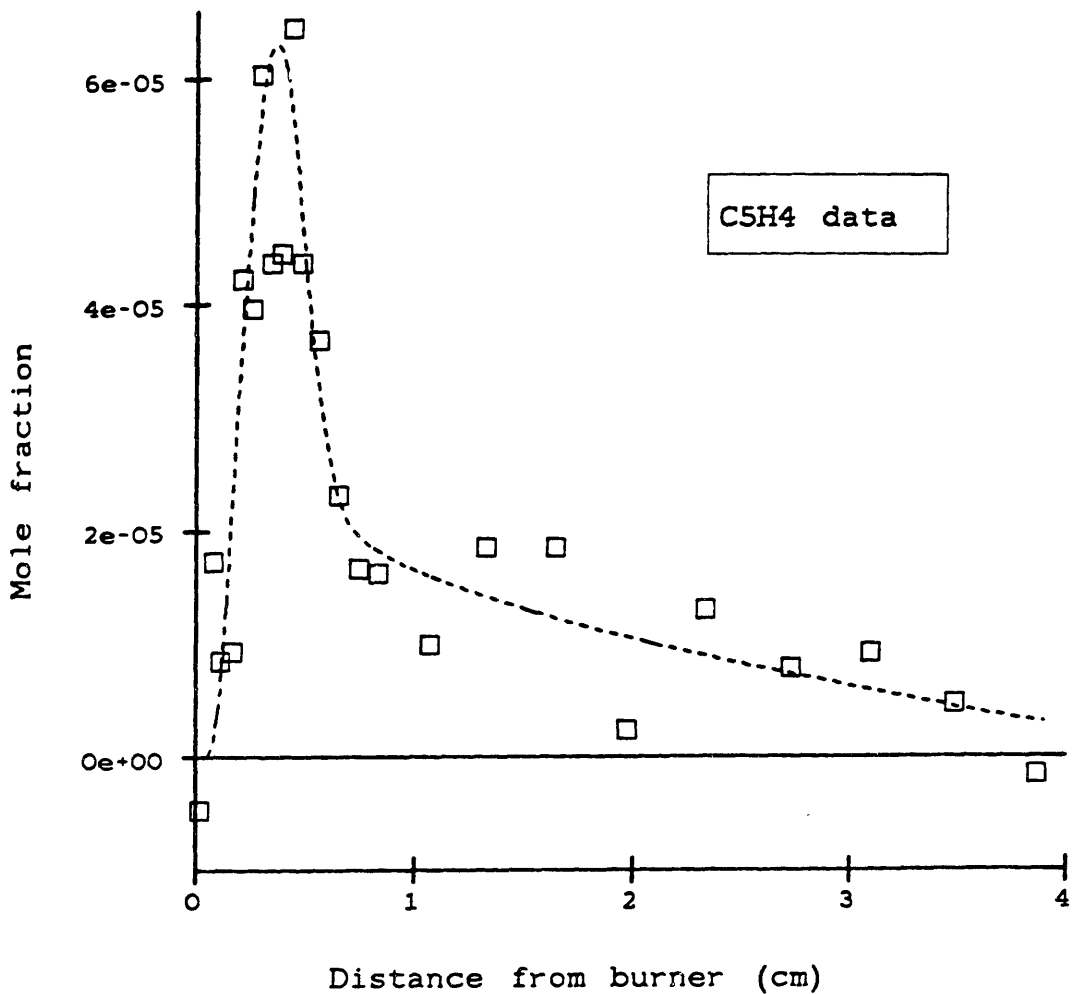


Fig. IV.29. Data (□) and smoothed curve for C₅H₄ in a laminar, premixed flame of C₂H₂/O₂/5% Ar, $\phi=2.40$, 2.67 kPa (20 torr), and 0.5 m·s⁻¹ velocity of unburned gas (298 K).

9.6±0.6 eV was determined at 0.395 cm after isotopic corrections, but the apparent absence of cyclopentadiene at mass 66 would make cyclopentadienyl unlikely. Still another possibility is ethynylketyl ($\text{HC}\equiv\text{C}\cdot\text{C}=\text{C}=\text{CO}$ or $\text{HC}\cdot\text{C}=\text{C}=\text{C}=\text{O}$), which would have an ionization potential of about 10.3±0.3 eV by analogy to HCCO (Appendix G).

A noisy signal was extracted after measurements at 11.3 eV (ref. Ar; setting 11.00 eV). The maximum for the profile (Fig. IV.30) is approximately $1.8 \cdot 10^{-5}$ at 0.39 cm with the calibration based on the identity as C_5H_5 . If mass 65 were ethynylketyl, then the mole fractions would be higher by a factor or two.

Interpolation of maxima from Delfau and Vovelle gives $1.8 \cdot 10^{-5}$ at 0.6 cm (mean of $1.6 \cdot 10^{-5}$ at 0.6 cm and $1.9 \cdot 10^{-5}$ at 0.55 cm). Despite experimental difficulties, those measurements are in good agreement with the present data.

Mass 66 - C_5H_6 and/or $\text{C}_4\text{H}_2\text{O}$. - An ionization potential of 9.6±0.6 was measured for mass 66. Cyclopentadiene (8.57 eV) and 1-penten-3-yne ($\text{CH}_2=\text{CH}-\text{C}\equiv\text{C}-\text{CH}_3$, 8.1 eV) then would be unlikely, while better possibilities are 3-pentenyne ($\text{HC}\equiv\text{C}-\text{CH}=\text{CH}-\text{CH}_3$, 9.14 eV) and an ethynyl-substituted ketene ($\text{HC}\equiv\text{C}-\text{CH}=\text{C}=\text{O}$, approximately 9.6 eV by analogy to ketene).

The profile for mass 66 (Fig. IV.31) was measured at an electron energy of 11.3 eV (ref. Ar; setting 11.00 eV) and its calibration factor was based on the species being C_5H_6 . Mole fractions would be higher by a factor of two if mass 66 were $\text{C}_4\text{H}_2\text{O}$. These measurements reveal an early maximum of $4.6 \cdot 10^{-5}$ at 0.23 cm, followed by a later minimum of $8.2 \cdot 10^{-7}$ at 2.25 cm and subsequent rise to $2.8 \cdot 10^{-6}$ at 3.9 cm.

Delfau and Vovelle observed the maximum but did not report any data beyond 1.4 cm, into the region of the minimum. They identified the species as C_5H_6 . From their data at $\phi=2.2$ and $\phi=2.6$, the maximum for $\phi=2.4$ in their hotter flames would be $2.5 \cdot 10^{-5}$ at 0.48 cm (mean of $0.79 \cdot 10^{-5}$ at 0.47 cm and $4.1 \cdot 10^{-5}$ at 0.48 cm). This maximum is in fair agreement with the present data.

Delfau and Vovelle also report a C_5H_7 species, which was not examined here. Interpolation of their maxima for C_5H_7 gives $2.1 \cdot 10^{-5}$ at 0.35 cm.

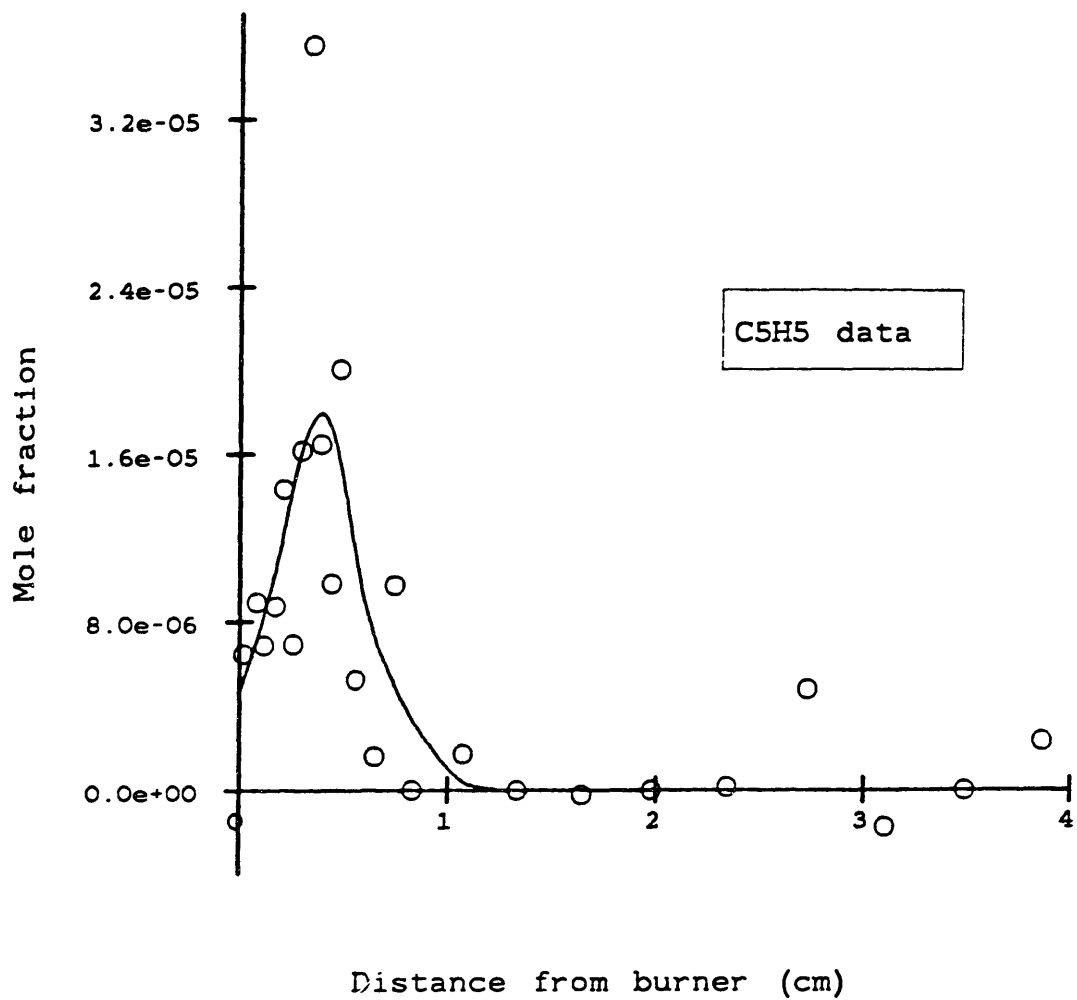


Fig. IV.30. Data (O) and smoothed curve for C_5H_5 in a laminar, premixed flame of $C_2H_2/O_2/5\%$ Ar, $\phi=2.40$, 2.67 kPa (20 torr), and $0.5\text{ m}\cdot\text{s}^{-1}$ velocity of unburned gas (298 K).

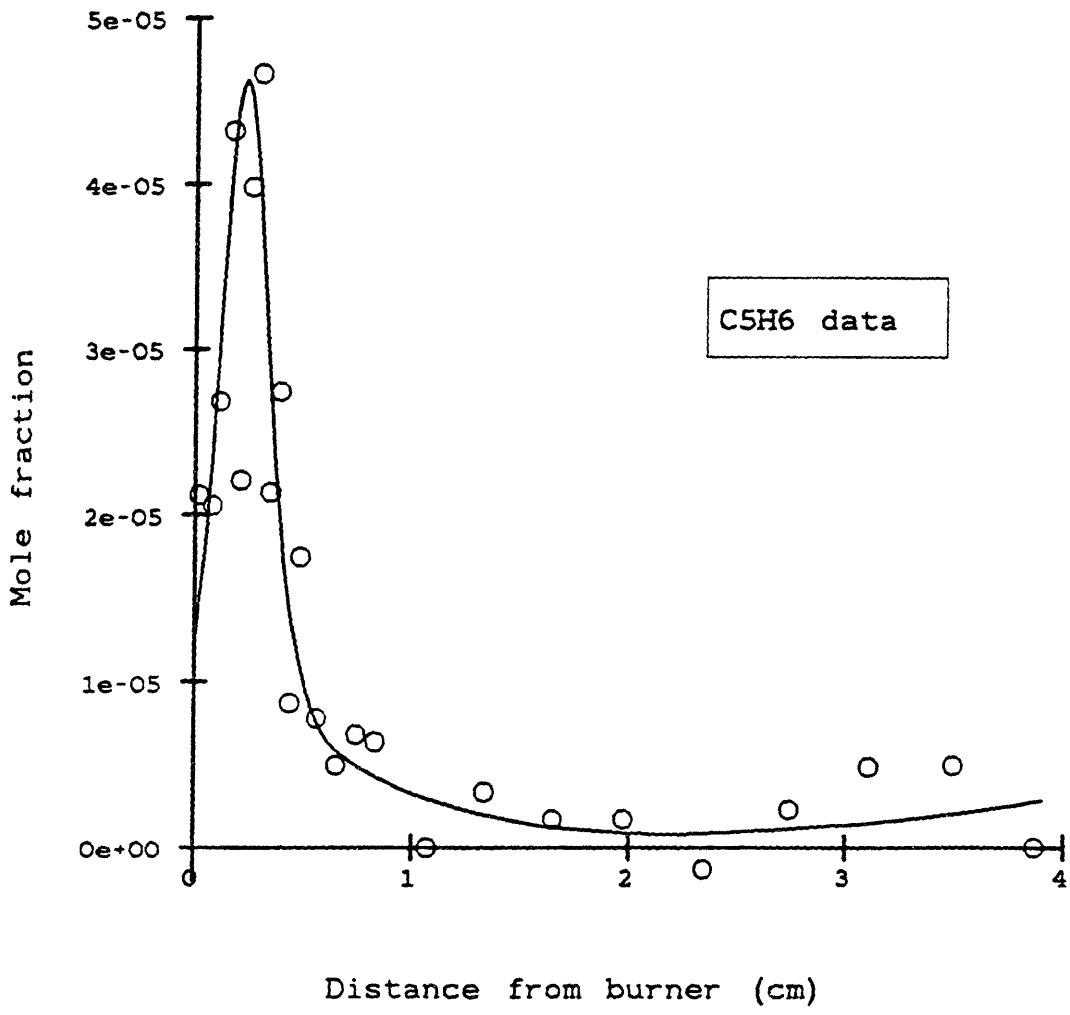


Fig. IV.31. Data (○) and smoothed curve for C₅H₆ in a laminar, premixed flame of C₂H₂/O₂/5% Ar, $\phi=2.40$, 2.67 kPa (20 torr), and 0.5 m·s⁻¹ velocity of unburned gas (298 K).

C₆H. - No C₆H could be detected in measurements at 0.544 cm. If the ionization potential is 12 eV, as for C₂H, the signal at 13.8 eV (ref. Ar) leads to an upper limit on the mole fraction of $(0.8 \pm 3) \cdot 10^{-6}$. At 14.6 eV and above, fragmentation of C₆H₂ was apparent.

C₆H₂. - Mass 74 must be triacetylene HC≡C-C≡C-CH (9.8±0.1 eV, Rosenstock et al., 1977). This identification is confirmed by measurements of the ionization potential as 9.76±0.19 and 9.84±0.1 eV (ref. Ar) at 0.483 and 0.544 cm, respectively. Triacetylene was also detected in the GC/MS analysis.

The profile shown in Fig. IV.32 was measured at 12.8 eV (ref. Ar; setting 13.00 eV). It rises rapidly to a maximum of $1.3 \cdot 10^{-3}$ at 0.70 cm and then declines steadily.

Measurements of Bonne et al. and of Delfau and Vovelle may be compared to these data. The data points of Bonne et al. are shown on the figure to have the same shape as observed here. Their highest value was $1.7 \cdot 10^{-3}$ at 1.0 cm, similar in magnitude but further from the burner than the present maximum. Delfau and Vovelle also found the same shape. Interpolating their maxima yields an estimated maximum for $\phi=2.4$ of $4.8 \cdot 10^{-4}$ at 0.9 cm (mean of $2.1 \cdot 10^{-4}$ at 0.81 cm and $7.4 \cdot 10^{-4}$ at 1 cm). This is a factor of three lower than the present maximum or that of Bonne et al., although with a similar position. Calibration uncertainty is probably the source of difference.

C₆H₃. - Measurement of this species was not attempted because of the large isotopic contribution at mass 75 from C₆H₂, 6.6% of mass 74.

C₆H₄. - The experimental profile (Fig. IV.33) shows an appreciable amount of this species, reaching $5.2 \cdot 10^{-5}$ at 0.45 cm, but its identity or identities remain uncertain. Three isomers seem likely: benzyne, a highly strained aromatic ring containing a triple bond (9.45±0.2 eV); 3-hexen-1,5-diyne (HC≡C-CH=CH-C≡CH, 9.60±0.2 eV); or 5-hexen-1,3-diyne (HC≡C-C≡C-CH=CH₂, unknown ionization potential). Measurements of the ionization potential were 9.5±0.2 eV at 0.483 cm and 9.7±0.2 eV at 0.544 cm, consistent with each of the above values.

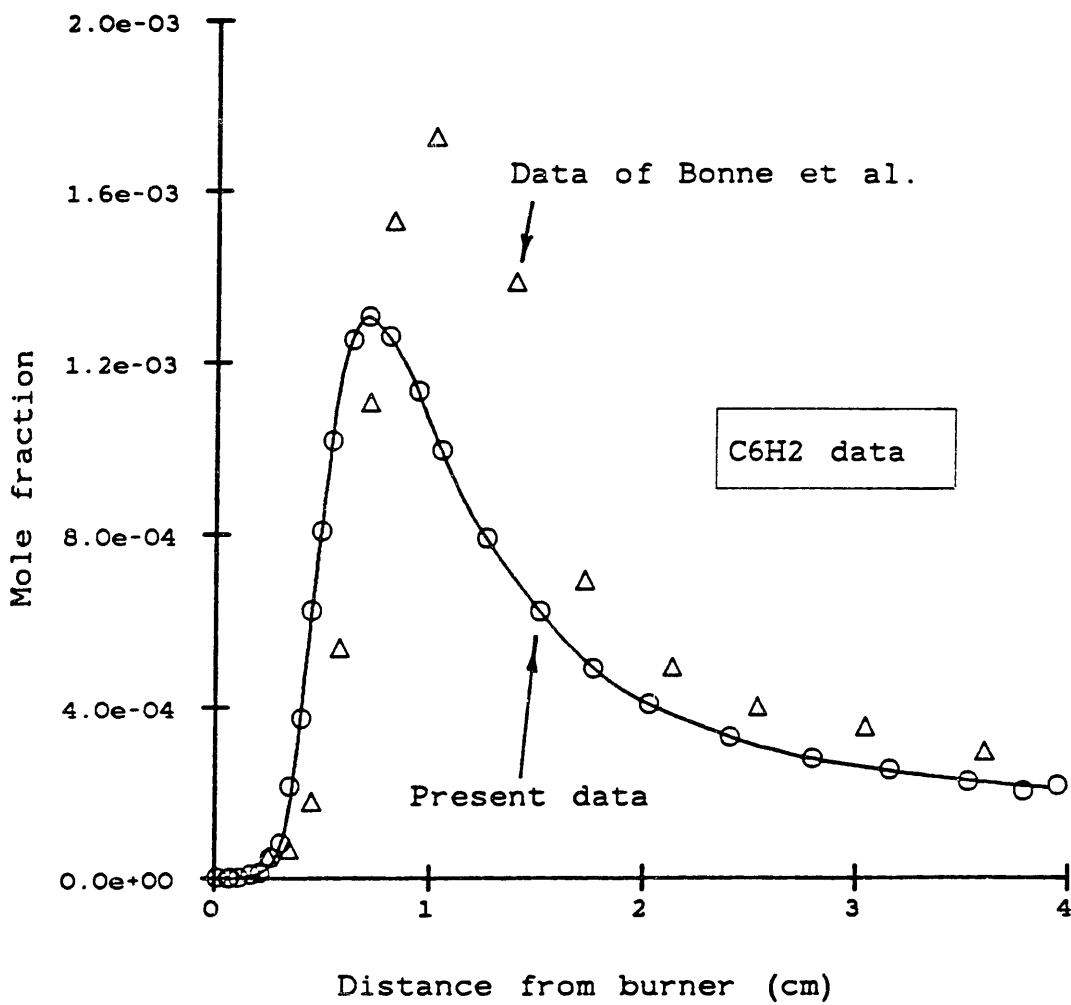


Fig. IV.32. Data profile for C_6H_2 (○) in a laminar, premixed flame of $C_2H_2/O_2/5\% Ar$, $\phi=2.40$, 2.67 kPa (20 torr), and $0.5 \text{ m}\cdot\text{s}^{-1}$ velocity of unburned gas (298 K), compared to data of Bonne et al. (1965; △) in a C_2H_2/O_2 , $\phi=2.38$ flame.

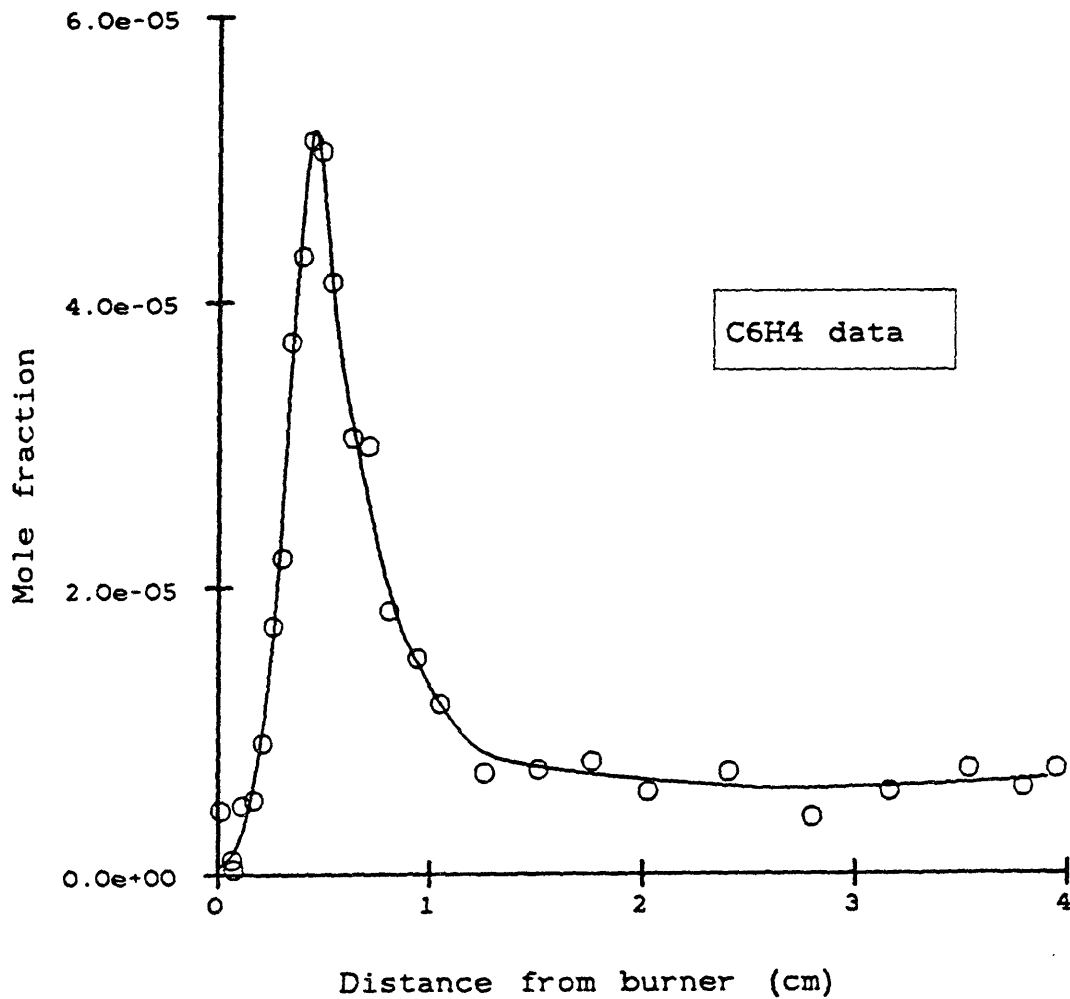


Fig. IV.33. Data (○) and smoothed curve for C₆H₄ in a laminar, premixed flame of C₂H₂/O₂/5% Ar, $\phi=2.40$, 2.67 kPa (20 torr), and 0.5 m·s⁻¹ velocity of unburned gas (298 K).

GC/MS analysis of the microprobe sample showed only one peak with a molecular ion of mass 76. [Other mass 76 species could have been eluted earlier but would have been discarded with the solvent peak.] The sample was collected at a probe-to-burner distance of 0.450 cm, where (ignoring any flame perturbation by the microprobe), the total-ion count (GC/MS output) for the single mass-76 species was 8.2% of that for C_6H_2 . By comparison, C_6H_4 was 8.4% of C_6H_2 as measured by MBMS.

The profile for C_6H_4 was measured at 12.8 eV (ref. Ar; setting 13.00 eV). In addition to the maximum described above, a minimum of $5.9 \cdot 10^{-6}$ at 2.65 cm also occurred (Fig. IV.33).

Delfau and Vovelle report a profile for C_6H_4 at $\phi=2.6$ but not at $\phi=2.2$. That profile had a maximum mole fraction of $2.2 \cdot 10^{-5}$ at 0.8 cm, lower and further from the burner than the maximum in Fig. IV.33, but the differences of equivalence ratios and temperatures makes this a rough comparison at best. Bonne et al. noted the presence of C_6H_4 but reported no profile.

C_6H_5 . - This signal could result from phenyl radical (8.1±0.1 eV) and/or from noncyclic radicals such as $HC \equiv C-CH=CH-CH \cdot$ (approximately 8.95 eV by analogy with C_2H_3). At 0.544 cm, no ionization efficiency curve could be detected after the isotopic correction due to C_6H_4 was made.

Nevertheless, a profile was attempted (Fig. IV.34) at 10.3 eV (ref. Ar; setting 10.5 eV). The isotopic contribution from C_6H_4 was assumed to be 1.56% of the 12.8 eV, isotope-corrected signal for mass 76, based on the ionization efficiency data. The calibration factor was estimated by the voltage method (Ch. III), probably with an uncertainty of a factor of three. A maximum of 10^{-6} may be occurring at about 0.2 cm, but the value of the data are really limited to describing the magnitude of the signal.

No other data are available for comparison.

C_6H_6 . - Mass 78 is predominately benzene (IP=9.25 eV), as inferred from ionization potentials and GC/MS analysis. The principal alternatives would be the noncyclic hydrocarbons 3,5-hexadienyne ($HC \equiv C-CH=CH-CH=CH_2$, 9.5 eV) and 1,5-hexadien-

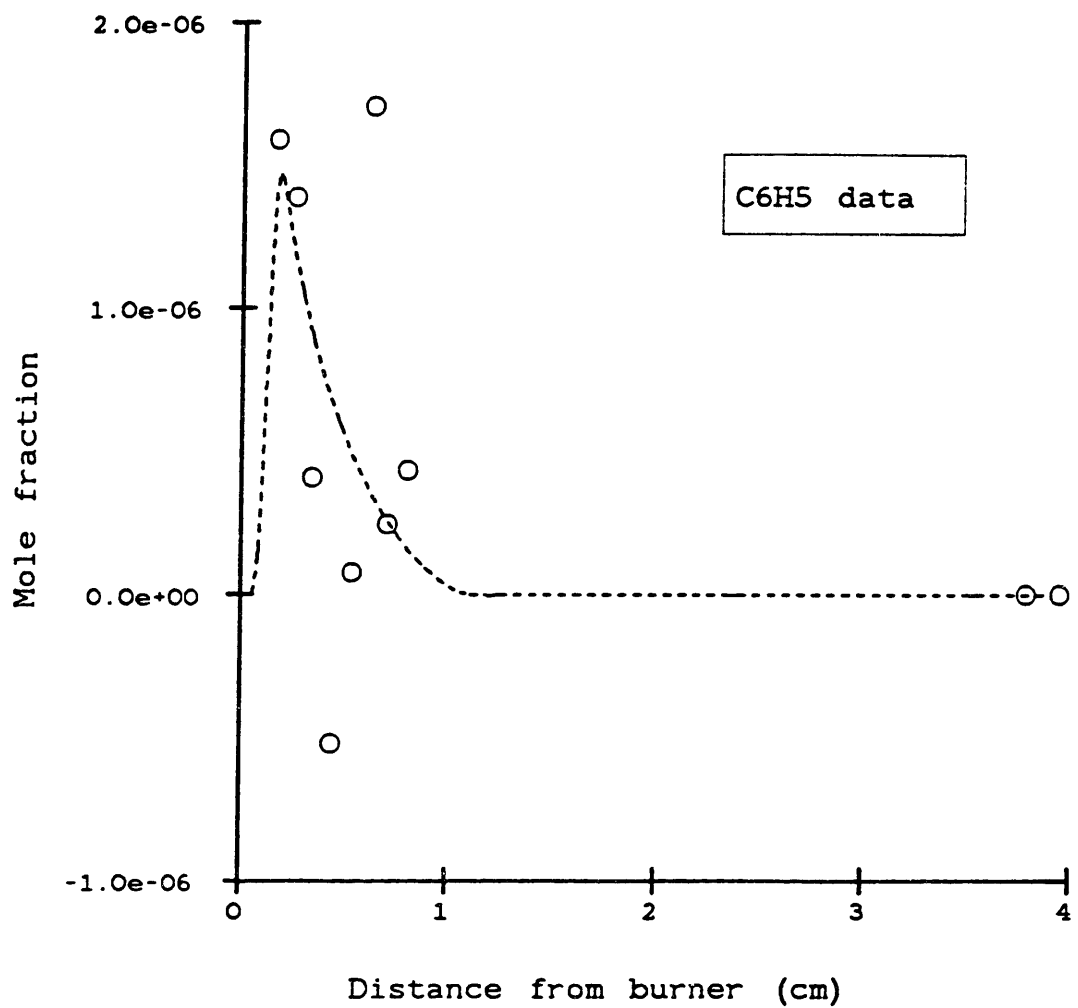


Fig. IV.34. Data (○) and smoothed curve for C_6H_5 in a laminar, premixed flame of $C_2H_2/O_2/5\%$ Ar, $\phi=2.40$, 2.67 kPa (20 torr), and $0.5\text{ m}\cdot\text{s}^{-1}$ velocity of unburned gas (298 K).

3-yne ($\text{H}_2\text{C}=\text{CH}-\text{C}\equiv\text{C}-\text{CH}=\text{CH}_2$, 10.5 eV). Measurement of the ionization potential at 0.395 and 0.483 cm gave 9.4 ± 0.4 and 9.15 ± 0.4 (ref. Ar), respectively, eliminating the second linear species.

GC/MS of the microprobe sample from 0.45 cm showed two GC peaks having molecular ions of mass 78. The earlier peak, eluting before C_6H_2 , was an aliphatic molecule (or molecules) with 1.4% of the total-ion count relative to C_6H_2 . The second peak was benzene. It followed C_6H_2 and was 4.9% of the total-ion count of C_6H_2 . These measurements imply that at this position, 77% of C_6H_6 was benzene. For further comparison, the total-ion counts suggest that C_6H_6 is 6.3% relative to C_6H_2 , while MBMS gives 3.1% at 0.45 cm and 7.2% at 0.40 cm. Again, the two methods show excellent agreement within the position uncertainty due to microprobe perturbation of the flame.

C_6H_6 reaches a maximum mole fraction of $4.0 \cdot 10^{-5}$ at 0.28 cm, as shown in Fig. IV.35. This profile was measured at 12.8 eV (ref. Ar; setting 13.00 eV). Interestingly, the profile also has a minimum of $1.7 \cdot 10^{-6}$ at 1.8 cm, and it rises by a factor of three in the next 2 cm.

Delfau and Vovelle showed profiles for C_6H_6 both at $\phi=2.2$ and $\phi=2.6$. In the former flame, data were collected only at 1.2 cm or less, so the region of the minimum was not reached. At $\phi=2.6$, a minimum may have been detected if the highest point (3 cm) is too low. To estimate the maximum at $\phi=2.4$, the mean for the two flames was $2.6 \cdot 10^{-5}$ at 0.5 cm (from $3.2 \cdot 10^{-5}$ at 0.45 cm and $1.9 \cdot 10^{-5}$ at 0.55 cm), virtually the same mole fraction as measured here within calibration uncertainty. Again Bonne et al. observed C_6H_6 but reported no profile.

Masses 79-81. - None of these species were detected despite attempts to measure ionization potentials at 0.544 cm.

Mass 79 has several isomers, including cyclohexadienyl, methylcyclopentadienyl, aliphatic C_6H_7 species, and $\text{C}_5\text{H}_3\text{O}$ species. Based on an estimated ionization potential of 8.0 eV and ionization cross-section, the signal (isotope-corrected) gave a "mole fraction" of $(-0.1\pm 1.1) \cdot 10^{-6}$, corresponding to an upper limit of 10^{-6} at 0.544 cm.

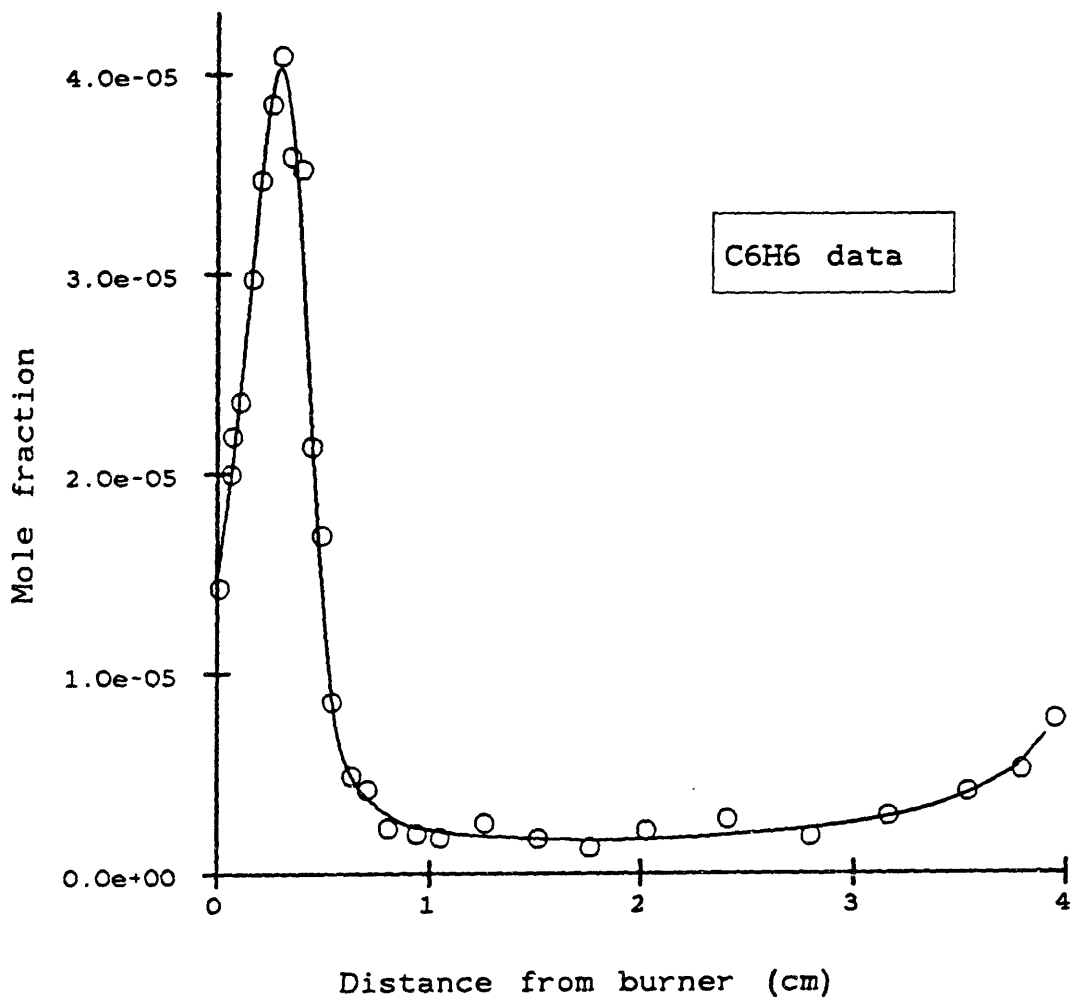


Fig. IV.35. Data (O) and smoothed curve for C_6H_6 in a laminar, premixed flame of $C_2H_2/O_2/5\%$ Ar, $\phi=2.40$, 2.67 kPa (20 torr), and $0.5\text{ m}\cdot\text{s}^{-1}$ velocity of unburned gas (298 K).

Mass 80 could be 1,3-or 1,4-cyclohexadiene, aliphatic C_6H_8 , such as hexatriene, and/or C_5H_4O species such as cyclopentadienone. Again, an upper limit of 10^{-6} was determined at 0.544 cm, derived from the "mole fraction" of $(-0.2 \pm 0.7) \cdot 10^{-6}$.

Mass 81 could be C_6H_9 or C_5H_5O . Assuming it is cyclohexenyl (7.54 eV), the upper limit at 0.544 cm is $5 \cdot 10^{-8}$, based on a "mole fraction" of $(-0.5 \pm 5) \cdot 10^{-8}$.

Benzyl radical - C_7H_7 . - If mass 91 is benzyl, its upper limit at 0.395 cm is 10^{-6} , based on $(0 \pm 1.3) \cdot 10^{-6}$.

Toluene. - GC/MS analysis at 0.45 cm shows three peaks for species of mass 92, but 95% of the total is toluene. By reference to the mole fraction of C_8H_6 (phenylacetylene), the mole fraction of toluene at that point is $4 \cdot 10^{-7}$. This value is consistent with attempts to detect C_7H_8 at 0.395 cm, which indicated that its mole fraction was less than $(5 \pm 6) \cdot 10^{-6}$.

C_8H_2 . - The polyacetylene C_8H_2 (9.09 ± 0.02 eV, Levin and Lias, 1982) had measured ionization potentials of 9.8 ± 0.3 eV at 0.395 cm and 8.95 ± 0.35 eV at 0.900 cm (ref. Ar). It also appeared in the GC/MS analysis, eluting between the C_8 and C_9 aromatic hydrocarbons, just prior to phenol.

The profile for C_8H_2 (Fig. IV.36) was measured at 13.8 eV (ref. Ar; setting 13.50 eV). It began to appear (less than 10^{-7}) at about 0.25 cm and reached a maximum of $7.4 \cdot 10^{-5}$ at 0.68 cm.

These results can be compared with those of Bonne et al. and of Delfau and Vovelle. Bonne et al. show a curve without data points for C_8H_2 . Their maximum mole fraction was $3.6 \cdot 10^{-4}$ at 1.1 cm. Interpolation of the Delfau and Vovelle results to $\phi=2.4$ predicts a maximum of $5 \cdot 10^{-5}$ at 1.0 cm (mean of $3.0 \cdot 10^{-5}$ at 0.9 cm and $7 \cdot 10^{-5}$ at 1.1 cm). This interpolation from Delfau and Vovelle is very similar to the present results, while the reported maximum of Bonne et al. is higher by a factor of five to seven than the other two studies.

C_8H_6 . - Phenylacetylene (ethynylbenzene) makes up 92% of mass 102 at 0.45 cm, according to analysis of GC/MS data. Four additional species of mass 102 were detected eluting after phenylacetylene, probably aliphatic C_8H_6 species containing two double and two triple bonds. The measured ionization potential was 9.8 ± 0.5 eV (ref. Ar) at

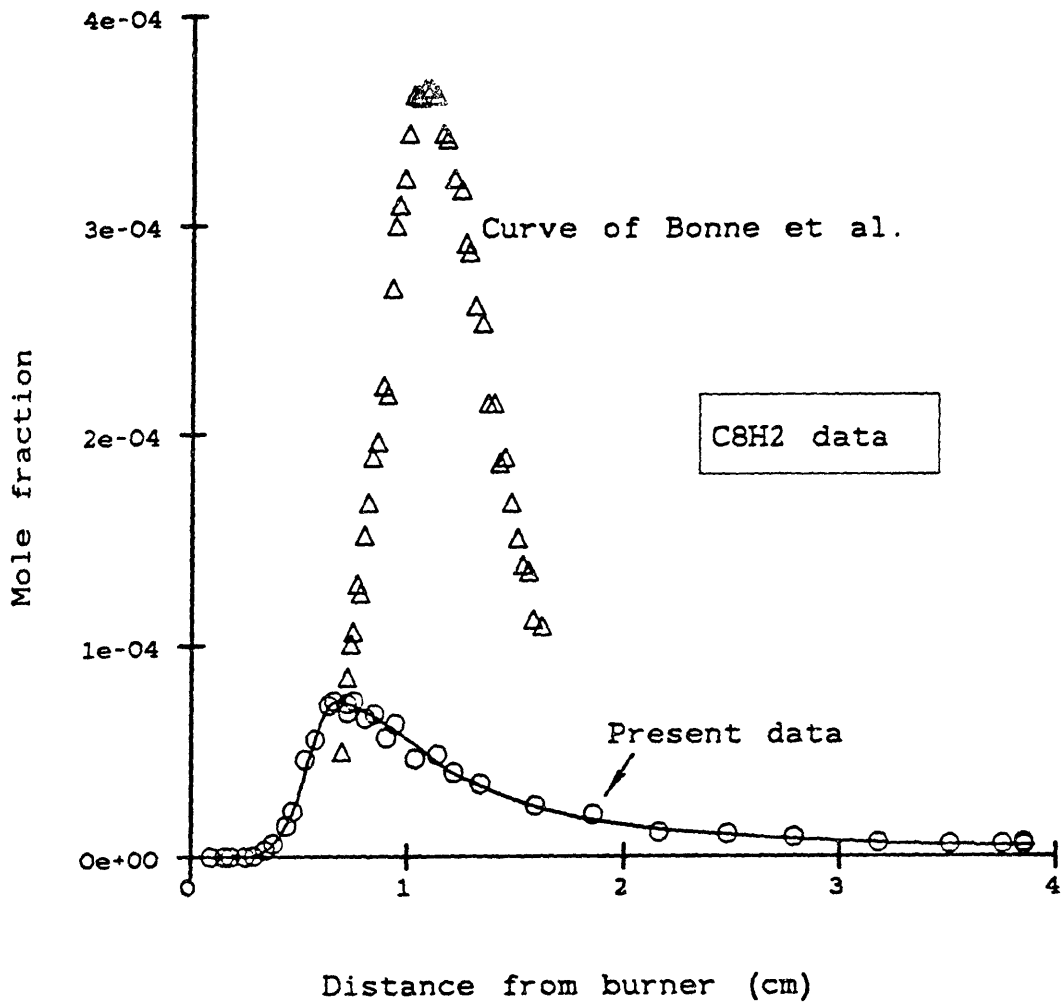


Fig. IV.36. Data (O) and smoothed curve for C_8H_2 in a laminar, premixed flame of $C_2H_2/O_2/5\% Ar$, $\phi=2.40$, 2.67 kPa (20 torr), and $0.5 \text{ m}\cdot\text{s}^{-1}$ velocity of unburned gas (298 K).

0.395 cm. This is somewhat high relative to the literature value (8.75 eV, Levin and Lias, 1982), but in the same way that C_8H_2 had been in the same series of ionization efficiency measurements (same mass-spectrometer tuning, same position).

Figure IV.37 shows the profile for C_8H_6 , which was measured at 13.8 eV (ref. Ar; setting 13.50 eV). The species becomes detectable at 0.04 cm, reaches a maximum of $3.3 \cdot 10^{-6}$ at 0.35 cm, falls to a minimum of $1.6 \cdot 10^{-7}$ at 1.8 cm, and rises again by a factor of two in the next 2 cm.

Delfau and Vovelle report slightly higher numbers. Their maximum for $\phi=2.2$ was $4.7 \cdot 10^{-6}$ at 0.55 cm, and for $\phi=2.6$ it was $8 \cdot 10^{-6}$ at 0.65 cm. Interpolating, at $\phi=2.4$ they would have observed a maximum of $6 \cdot 10^{-6}$ at 0.6 cm. They do not show a minimum at $\phi=2.6$, and their data at $\phi=2.2$ end at 1.4 cm.

C_8H_8 . - Analysis of the sample by GC/MS indicated that this mass was principally styrene (ethenylbenzene). No signal was detected at 0.395 cm, so its mole fraction is less than $2 \cdot 10^{-7}$.

$C_{10}H_2$. - The species at mass 122 is most likely the polyacetylene $C_{10}H_2$. Benzoic acid (9.73 eV), hydroxybenzaldehydes (about 9.3 eV), propylbenzenes (8.7 eV), and trimethylbenzenes (8.3 to 8.6 eV) also have molecular weights of 122, but the absence of smaller, similar compounds makes these unlikely. At 0.900 cm, an ionization potential of 10.4 ± 0.7 eV (ref. Ar) was measured. This is very similar to literature values for the other polyacetylenes: 10.2 eV for C_4H_2 , 9.8 eV for C_6H_2 , and 9.1 eV for C_8H_2 . To measure the profile, an electron energy of 13.8 eV (ref. Ar; setting 13.50 eV) was used.

The profile shape is consistent with those of the other polyacetylenes, further supporting the identification. The profile (Fig. IV.38) begins slightly further from the burner than for C_8H_2 , then rises to $7.3 \cdot 10^{-6}$ at 0.78 cm, and slowly declines to a minimum of $1.4 \cdot 10^{-7}$ at 3.10 cm. Bonne et al. did not show a profile for $C_{10}H_2$, and the data of Delfau and Vovelle suggest a maximum of $5 \cdot 10^{-6}$ at 1.1 cm (mean of $4.3 \cdot 10^{-6}$ at 0.95 cm and $5 \cdot 10^{-6}$ at 1.2 cm).

$C_{10}H_6$. - The mole fraction of $C_{10}H_6$ at 0.395 cm was less than $(1 \pm 1) \cdot 10^{-6}$ by MBMS.

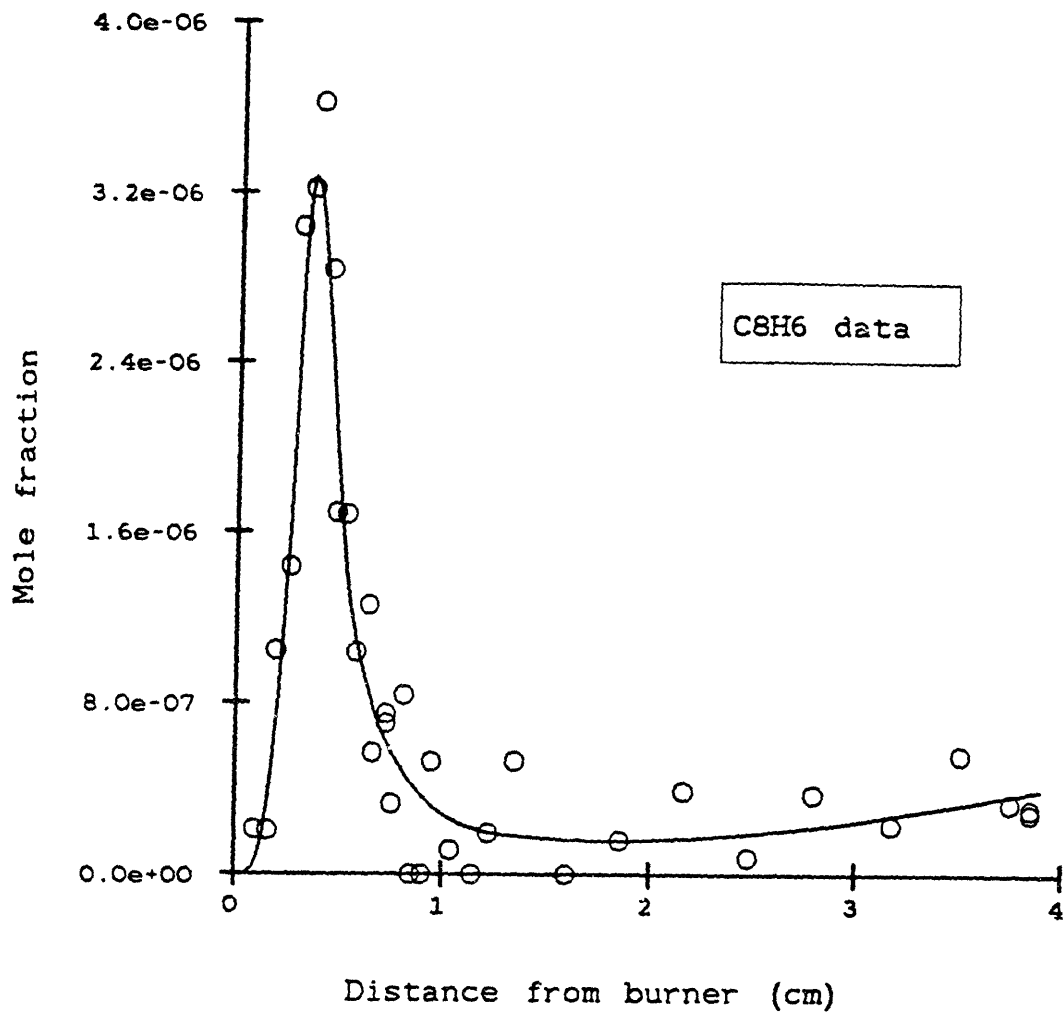


Fig. IV.37. Data (O) and smoothed curve for C_8H_6 in a laminar, premixed flame of $C_2H_2/O_2/5\%$ Ar, $\phi=2.40$, 2.67 kPa (20 torr), and $0.5 \text{ m}\cdot\text{s}^{-1}$ velocity of unburned gas (298 K).

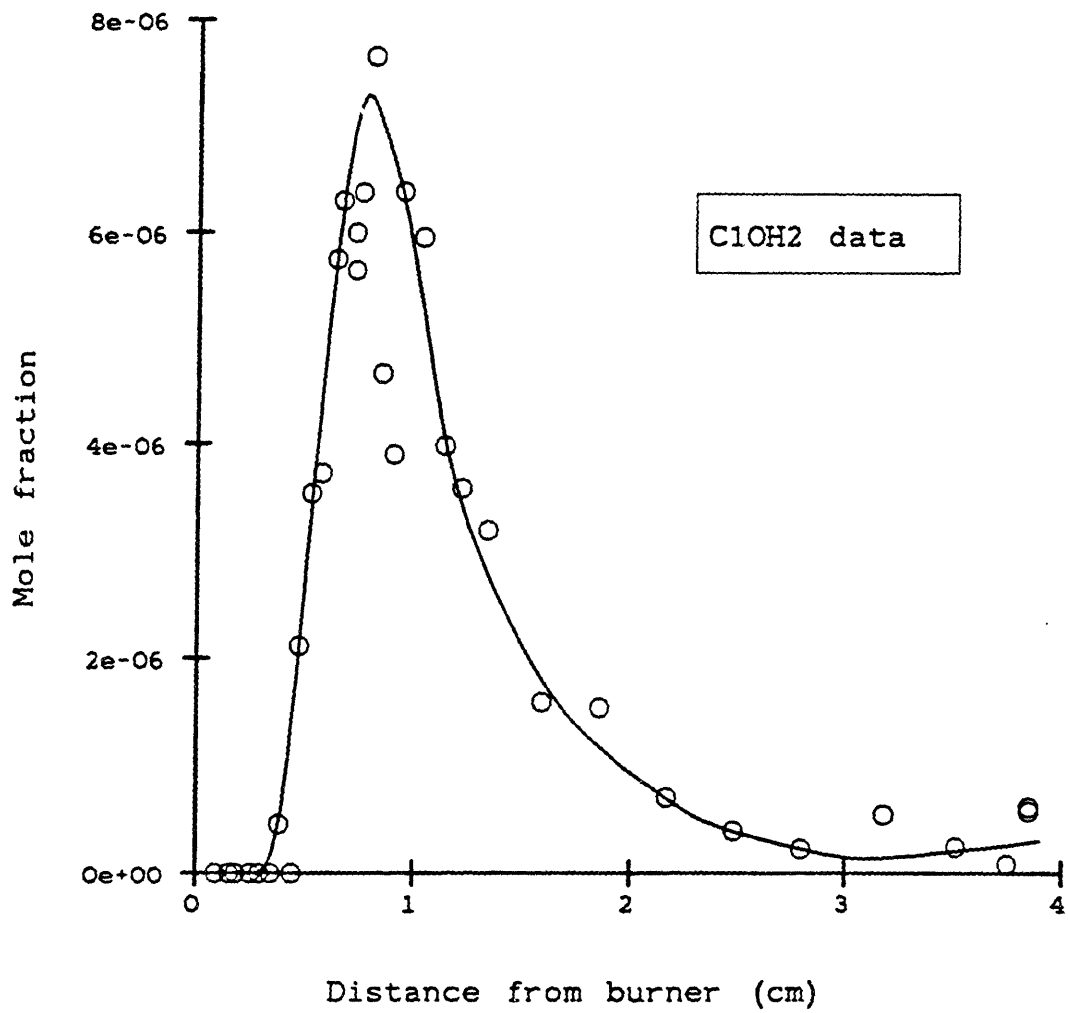


Fig. IV.38. Data (○) and smoothed curve for $C_{10}H_2$ in a laminar, premixed flame of $C_2H_2/O_2/5\% Ar$, $\phi=2.40$, 2.67 kPa (20 torr), and $0.5 \text{ m}\cdot\text{s}^{-1}$ velocity of unburned gas (298 K).

C₁₀H₈ - Naphthalene. - At 0.395 cm, the ionization potential was measured to be 9.8±0.7 eV (ref. Ar), which compares poorly to the literature value of 8.14 eV.

Calculating the calibration factor based on the measured ionization potential, the mole fraction of C₁₀H₈ was 4.7·10⁻⁷ at 0.395 cm.

IV.4. Analysis of heavy species by GC/MS

From a microprobe sample collected at 0.45 cm, 174 peaks were identified by their structures or molecular weights, which ranged from 68 to 180. Some of this information was used above to resolve isomers of C₆H₆, C₇H₈, and C₈H₆. A summary of all the identified GC/MS peaks is presented in Table IV.2 along with estimates of their mole fractions, and the data set is presented in more complete form in Appendices H and I.

Determination of identities and mole fractions. - The probe of Faist (1979) was used, but the molecules of interest were trapped from the gas stream in a small filter basket filled with 4 g of XAD-2 resin, a styrene/divinylbenzene copolymer. Sample was collected for 4:00:00 hr. To extract the sample from the XAD-2, dichloromethane was used in a 50-ml Soxhlet apparatus. The liquid was evaporated to 0.2 ml using a stream of N₂, maintaining the liquid near room temperature using a water bath.

The resulting sample was analyzed by GC/MS in a Varian 3700 gas chromatograph and Finnigan MAT 212 mass spectrometer in the Department of Chemistry. GC separation was effected with 1.5 ml/min of helium carrier gas in a 30 m DB-5 fused-silica capillary column, ramped in temperature from 45 to 180°C. Electron energy was 70 eV, and a spectrum was scanned from 45 to 500 amu every 3 s.

Species were identified both by mass spectrum and by elution time where possible. Correlated or predicted relative elution times (retention indices) were used in some cases. The reader should keep in mind that presence of a species does not necessarily mean that the species is present (at least at this concentration) in the flame because radical recombination can occur in the microprobe.

Table 4.2. Summary of species detected by GC/MS.

Molecular weight	Species	Multiple Peaks?	Mole fraction $\times 10^6$ (ppm)
68	C_6H_8 or C_4H_4O	-	8
74	C_6H_2 - hexatriyne	-	700
76	C_6H_4	-	40
78	Benzene	-	20
	Other C_6H_8	3	8
88	C_8H_4	5	0.5
90	C_8H_6	12	0.4
92	Toluene	-	0.3
	Other C_7H_8	9	0.05
94	Phenol (C_6H_5OH)	-	0.7
	C_7H_{10} ; other C_6H_8O	-	0.009
96	C_7H_{12} or C_6H_8O	-	0.01
98	C_8H_2 - octatetrayne	-	20
100	C_8H_4	-	0.7
102	Phenylacetylene	-	2
	Other C_8H_6 ; C_7H_4O	13	0.7
104	Styrene	-	0.4
	Other C_8H_8 ; C_7H_6O	16	0.3
106	Ethylbenzene	-	0.3
	m- and/or p-Xylene	-	0.04
	o-Xylene	-	0.02
	Benzaldehyde	-	0.04
	Other C_8H_{10} ; C_7H_8O	4	0.07
108	Benzyl alcohol	-	0.08
	o-Cresol	-	0.04
	Other C_7H_8O	-	0.02
112	C_9H_4	-	0.05
114	C_9H_6	4	0.2
116	Indene	-	1
	Other C_9H_8 ; C_8H_4O	8	0.2
118	C_9H_{10} or C_8H_6O	5	0.03
120	C_9H_{12} or C_8H_8O	3	0.02
122	Not detected		
126	Butadiynylbenzene	-	0.2
	Diethynylbenzenes	3	0.2
	Other $C_{10}H_8$	-	0.009
128	Naphthalene	-	0.7
	Other $C_{10}H_8$; C_9H_4O	8	0.2
130	$C_{10}H_{10}$ or C_9H_6O	15	0.6
132	$C_{10}H_{12}$ or C_9H_8O	3	0.04
134	$C_9H_{10}O$ or $C_8H_6O_2$	-	0.01
136	$C_9H_{12}O$ or $C_8H_8O_2$	-	0.1

<u>Molecular weight</u>	<u>Species</u>	<u>Multiple Peaks?</u>	<u>Mole fraction x10⁶ (ppm)</u>
140	C ₁₁ H ₈	4	0.1
142	2-methylnaphthalene	-	0.08
	1-methylnaphthalene	-	0.07
	Other C ₁₁ H ₁₀	-	0.07
144	C ₁₁ H ₁₂ or C ₁₀ H ₁₀ O	4	0.7
150	C ₁₂ H ₈	2	0.02
152	Acenaphthylene	-	0.4
	Other C ₁₂ H ₈	2	0.08
154	C ₁₂ H ₁₀ or C ₁₁ H ₈ O	6	0.09
156	C ₁₂ H ₁₂ or C ₁₁ H ₈ O	7	0.05
166	C ₁₃ H ₁₀ or C ₁₂ H ₈ O	3	0.06
178	C ₁₄ H ₁₀ or C ₁₃ H ₈ O	-	0.1
180	C ₁₄ H ₁₂ or C ₁₃ H ₈ O	4	0.02

The mole fractions were based on total-ionization signals from the GC/MS mass spectra. These signals were sums of the counted ion signals from given mass spectra, representing ionization and fragmentation at 70 eV.

The signal is corrected for baseline drift and converted to mole fraction by reference to MBMS data. For C₆'s, the mole fraction of C₆H₂ was used as the reference. These lightest species could be reduced in concentration from the flame relative to heavier species because they are more likely to be lost by evaporation during sample preparation. For C₇'s, the reference was to C₇H₈, for the reasons above, but the conversion factor was quite close to that calculated for C₈H₆. C₈H₆ was the reference for C₈ species, and for heavier species, the C₈H₆ conversion factor was adjusted slightly downward assuming that the signals were proportional to carbon number, as for GC flame-ionization detectors.

Comments on species. - First, aromatic and polyaromatic species are observed as expected, but significant amounts of nonaromatic species are also observed. These species are generally less abundant than the aromatics, but this difference does not necessarily mean that the aromatic species are more important to molecular-weight growth. Relative abundance of any species may indicate a higher-concentration reaction partner, but it could also indicate an unreactive, "dead-end" species.

As an example of the presence of nonaromatics, consider mass 102. While most of that mass number is phenylacetylene, the only possible aromatic species at mass 102, 13 nonaromatic peaks were observed. If these are C₈H₆ species, they most likely would contain two triple bonds and two double bonds in a linear or branched structure. Examples of the structures would be cis- and trans-isomers of HC≡C-CH=CH-C≡C-CH=CH₂.

Likewise, no aromatics other than benzene and toluene occur from mass 78 to 92, so in that range 29 peaks were observed that must be nonaromatic. Similar contributions by nonaromatics can be inferred up through mass 152.

Second, oxygenated aromatics are observed in appreciable concentrations. Phenol, a likely oxidation product of benzene

(Bittner and Howard, 1980; Bittner, 1981), is present in higher concentrations than any other species in the mass 88-96 range. By using standards and the mass spectra, benzaldehyde, benzyl alcohol, and cresol were identified, which are possible oxidation products of benzyl radical or toluene. Identification of oxygenates at higher masses is more difficult, but they are surely present.

Third, C_2H - and C_4H -substituted aromatics are observed. Phenylacetylene (ethynylbenzene) has long been reported as a flame species in fuel-rich combustion, but only recently have similar, larger species been identified (Bockhorn et al., 1983; Wenz, 1983) by GC/MS. Some of the mass 116 species are probably ethynyltoluenes, and some mass 130 species are probably ethynylindenes. Furthermore, all three diethynylbenzenes were detected at mass 126 (for o-, m-, and p- $C_6H_5C_2H$).

Butadiynylbenzene ($C_6H_5C_4H$) is present at a mole fraction as large as those of the three diethynylbenzenes combined. This species could be produced by successive additions of C_2 's to benzene and to ethynyl- or ethenylbenzene, by addition of C_4H to benzene, or by H-elimination from $C_6H_5-C\equiv C-CH=CH\cdot$ or $C_6H_5-C\equiv C-C\cdot=CH_2$. The identification of a C_4 -benzene suggests that formation of the second ring (naphthalene vs. benzene) could occur by self-addition of a C_4 terminal radical to the ring, such as $C_6H_5-C\equiv C-CH=CH\cdot$, or the analogous self-addition of an ortho phenylic radical to the end of a C_4 side chain.

C_4H_3 - and C_4H_5 -benzenes are better indicators of the radicals that would cause such processes. These species are surely present at masses 128 and 130 but are not specifically identified here. Also at masses 128, 130, and 132 would be the ortho- $(C_2)_2$ benzenes that could represent another growth mechanism for the second ring.

CHAPTER V. TESTS OF LITERATURE COMBUSTION MECHANISMS

V.1. Introduction

The ability to model flame structure of hydrocarbon flames was demonstrated by Warnatz (1980). Since then, mechanisms of elementary reactions for combustion have been proposed by Levy et al. (1983), Miller et al. (1983), Warnatz (1983), Westbrook et al. (1983a,b), and Westbrook and Dryer (1984) to model fuel-rich combustion. The mechanisms have been tested against measured profiles of concentration but, at fuel-rich conditions, only for a few stable species (Miller et al., 1983; Warnatz, 1983) and for H-atom in the post-flame region (Levy et al., 1983). Features of the profiles were generally well-predicted, and quantitative agreement was a factor of two or better. However, to model such processes as molecular-weight growth and nitrogen-fixation reactions of fuel-rich hydrocarbon flames, accurate profiles of free radicals are required.

Published mechanisms are tested here for lightly sooting combustion. Concentration profiles of 38 stable and free-radical species were measured using molecular-beam mass spectrometry (MBMS) in a low-pressure, premixed acetylene-oxygen flame ($\phi=2.40$) similar to one of the flames ($\phi=2.38$) in the pioneering MBMS study of Bonne, Homann, and Wagner (1965). Five mechanisms were tested using the one-dimensional flame model of Smooke (1982). Important reactions in the mechanisms were identified using reaction-path analysis, a simple type of sensitivity analysis.

V.2. Flame model and mechanisms

The flame code used here (Smooke, 1982) is a boundary-value method which solves the flame equations of Ch. II.1. It uses the CHEMKIN reaction-kinetics computer codes (Kee et al., 1980) and the transport-properties codes of Kee et al. (1983), which includes both molecular and thermal diffusion. Experimental profiles of area expansion ratio and temperature were used in the calculations, leaving reaction kinetics as the focus of this analysis.

Mechanisms that were tested were from Miller et al. (1983), Warnatz (1983), Westbrook (1983b), Westbrook and Dryer (1984), and a

modification from this work of the Warnatz mechanism. These are referred to in the following discussion as MMSK, WZ, WB, WD, and WZ', respectively. The mechanism of Levy et al. (1983), mentioned in Ch. V.1 as having been tested in fuel-rich flames, was not tested in this work because of its limitation to 1 atm pressure and to temperatures of 1992 to 2126 K.

For all but WZ, the present test is outside the range of conditions that the other authors have given for their mechanisms. Specifically, the mechanisms have not been tested before for an acetylene flame that is so fuel-rich. Our intent is to test each mechanism as faithfully as possible to the original authors' descriptions. Previous ranges of testing and the types of adaptation should be noted:

(1) Mechanism MMSK has been tested for C_2H_2 oxidation in low-pressure flames ($\phi=0.09$ to 1.56) and in shock tubes (Miller et al., 1983). Miller et al. carefully examined CH_2 , C_2H , and HCCO reactions, but reactions of alkenes, alkyl radicals, and alkanes were not included except for CH_3 and possibly allene (a general C_3H_4 was used). They expressed fall-off in a Lindemann form for three reactions, which is fitted here to the semiArrhenius form $[AT^B \exp(-E/RT)]$ at 2.67 kPa. Rate constants for reactions in the reverse direction are calculated from thermodynamics using reversibility.

(2) The mechanism of Warnatz (WZ) was based on a review of rate constants for elementary reactions (Warnatz, 1984) and previously has been tested against data for fuel-lean and fuel-rich flames and for shock-tube experiments (Warnatz et al., 1983). WZ is the form of the mechanism specified by Warnatz (1983), with reverse reactions included only for some reactions and their rate constants stated explicitly. Fall-off curves (Warnatz, 1984) for seven of the reactions are used here to fit semi-Arrhenius rate constants. Finally, the rate constant of $3 \cdot 10^{13} \text{ cm}^3 \text{ mol}^{-1} \text{ s}^{-1}$ which Warnatz used for $OH + C_4H_2$ (and $OH + C_6H_2$) was interpreted consistently with his description as forming H and a ketene-like species, the latter being destroyed by "fast reaction" with OH to form H, 2CO, and C_2H_2 (or

C₄H₂). An extreme value of 10¹⁴ cm³mol⁻¹s⁻¹ was used for the second OH reaction.

(3) The WZ mechanism was modified here as WZ' to include reverse rate constants from thermodynamics for any two-product reactions that were not reversible in WZ.

(4) Westbrook, Dryer, and Schug (1983a) tested a mechanism for ethylene oxidation ($\phi=0.125$) and pyrolysis at 1-12 atm. All reactions are stated as the high- or low-pressure limit for addition or pyrolysis, and rate constants are reported explicitly for forward and reverse directions. An updated tabulation by Westbrook (1983b) is used here as WB.

(5) Westbrook and Dryer (1984) compiled 335 rate constants from the above mechanisms and other data in their recent survey of combustion chemistry. No tests of this reaction set were presented. Fall-off is acknowledged but not included in the tabulated values, and reactions are stated as reversible. Mechanism WD is selected from this compilation.

Differences in thermodynamic data could make the mechanisms used here different from the original authors because rate constants for the implicitly reversible reactions are calculated using microscopic reversibility. Where this calculation was made, thermodynamics from the Sandia compilation (Kee et al., 1984) generally were used, with the modifications of $\Delta H_f^\circ,_{298}=135$ kcal/mol for C₂H, 70.4 kcal/mol for C₂H₃ (McMillen and Golden, 1982), and 4.2 kcal/mol for HO₂ (Howard, 1980).

Some species could be predicted but not measured, while others were measured but are not listed in the mechanisms. As examples, CH, CH₂, and O-atom (obscured at mass 16 by CH₄) were too low in concentration to be detected, and profiles for mass 29 and 30 were measured but HCO/C₂H₅ and H₂CO/C₂H₆ were not resolvable. However, no mechanisms included C₄H₄, C₄H₅, C₅ species, C₆H₄, C₆H₅, C₆H₆, and C₇ or heavier species, which were detected in the flame by MBMS and/or GC/MS (Ch. IV).

The mechanisms as tested are tabulated in Appendices J.1 to J.5, and solutions at the present flame conditions are included as Appendices J.6 to J.10. Computer time required for each solution,

including thermal diffusion and having the same convergence criterion, ranged from 25 to 35 CPU-hours on a VAX 11/780 computer.

V.3. General comparisons

Data points and measured profiles from Ch. IV were used as tests for the above mechanisms. For some purposes, the predictions are quite satisfactory. There is deviation from the data, but profile shapes and magnitudes for major stable species are usually in approximate agreement with the data - within a factor of two in mole fraction.

The profile for C_2H_2 (Fig. V.1) illustrates the differences among predictions in a case where all mechanisms agreed approximately with the data. The mole fraction of C_2H_2 at 4 cm was 4.5% experimentally, while the predictions vary from 2.5 to 9.7%. Temperatures and elapsed time for flow through the flame are also shown, which also emphasizes that the flame is a steady-state phenomenon, but that it is not isothermal or static.

The predictions vary from the data by more than this factor of two for other species, notably for the C_3 's; MMSK and WD make predictions for C_3H_2 , C_3H_3 , and C_3H_4 that are one to two orders of magnitude higher than the data. Each mechanism predicts some profiles well and predicts some profiles poorly, as shown in Figs. V.2 to V.31 for the rest of the species examined. As a rough indication of predictive power, the predictions from WZ' are good or satisfactory for more species than from MMSK, WB, WD, or WZ.

V.4. Analysis of critical reaction paths

We can identify certain deficiencies in the mechanisms that are especially important by analyzing the profiles of H_2O , CO_2 , C_3 's, C_4H_2 , OH, and C_2H_3 , which vary in shape and in magnitude from the data.

The technique of sensitivity analysis that gave the most insight was reaction-path analysis, in which reaction rates for the predicted profiles are compared in order to identify sources and sinks for a species of interest. These calculations included (1) the net rate of species formation for each reaction, (2) the actual rate of formation

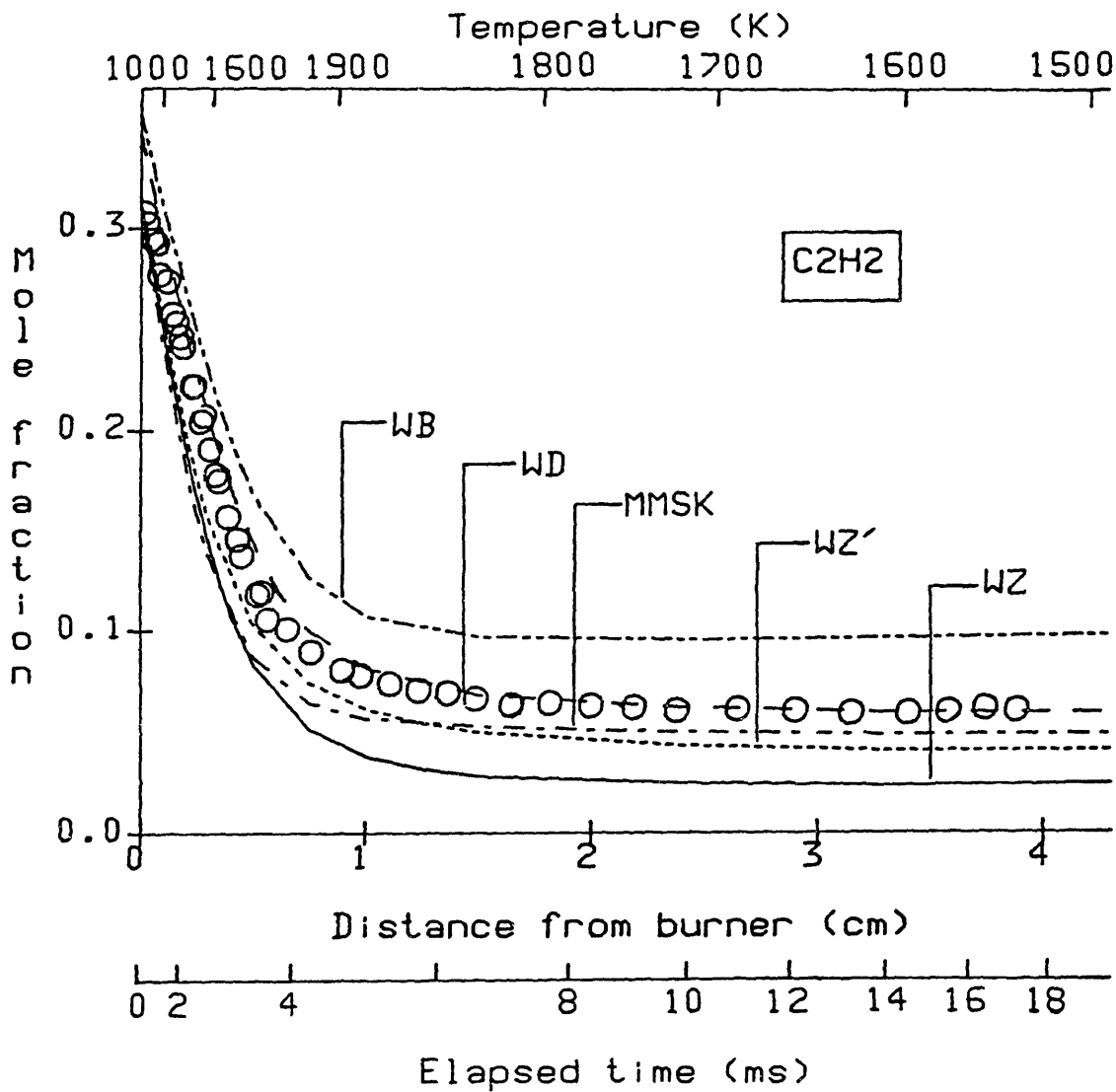


Fig. V.1. Concentration profiles of acetylene in flat flame. Data (O) and predicted curves using predictions using mechanisms of Miller, Mitchell, Smooke, and Kee (MMSK, - · - · - ·); Westbrook (WB, · · · · ·); Westbrook and Dryer (WD, - - -); Warnatz (WZ, —); and reversible Warnatz (WZ', - - -).

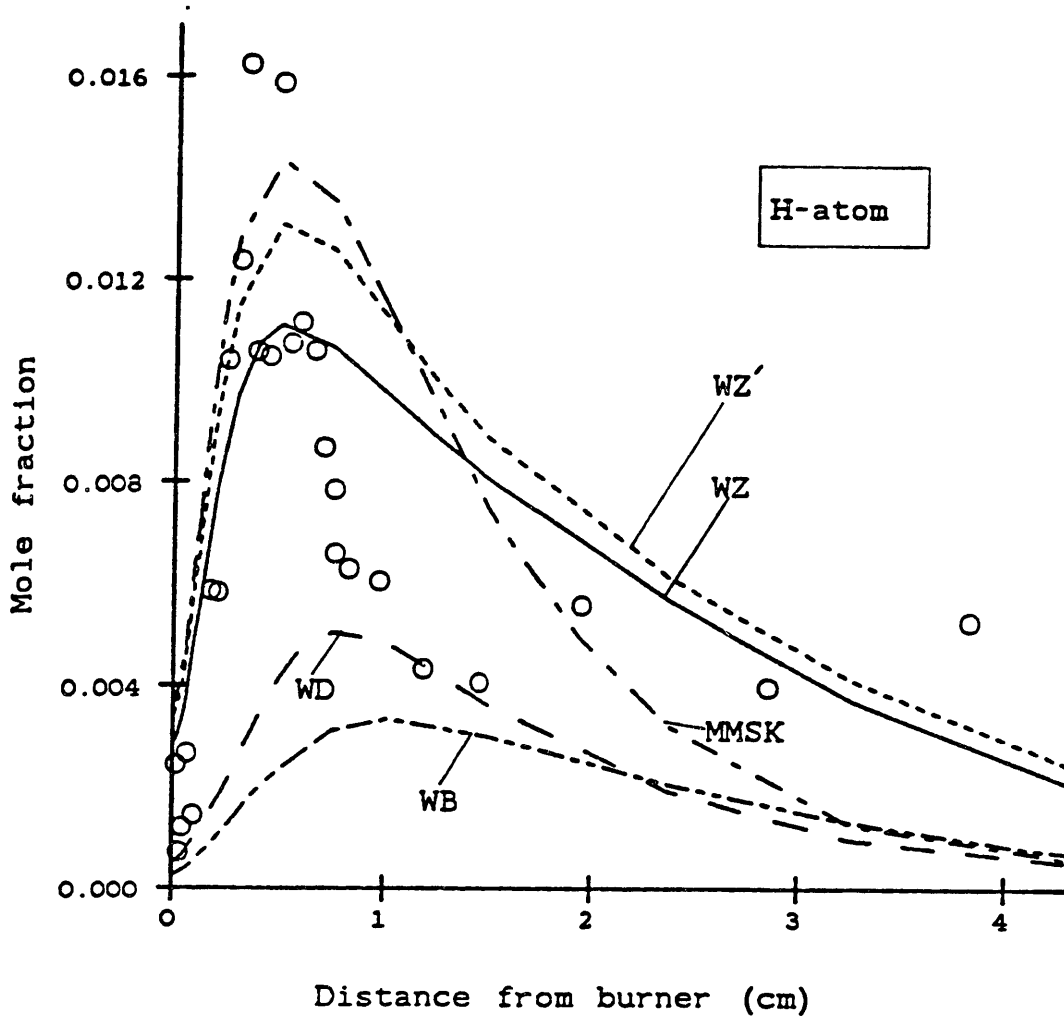


Fig. V.2. H predictions compared to data. Data points and curve labels defined in Fig. V.1.

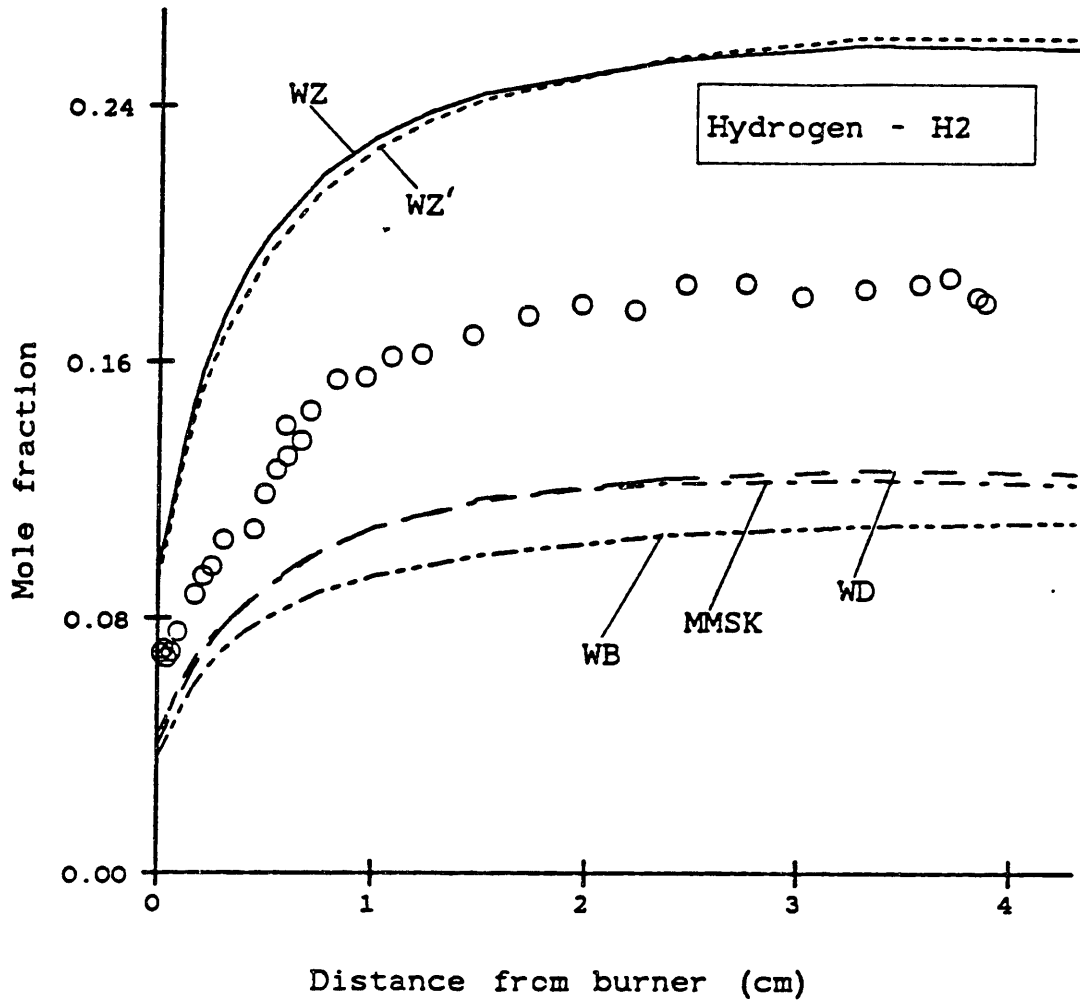


Fig. V.3. H_2 predictions compared to data. Data points and curve labels defined in Fig. V.1.

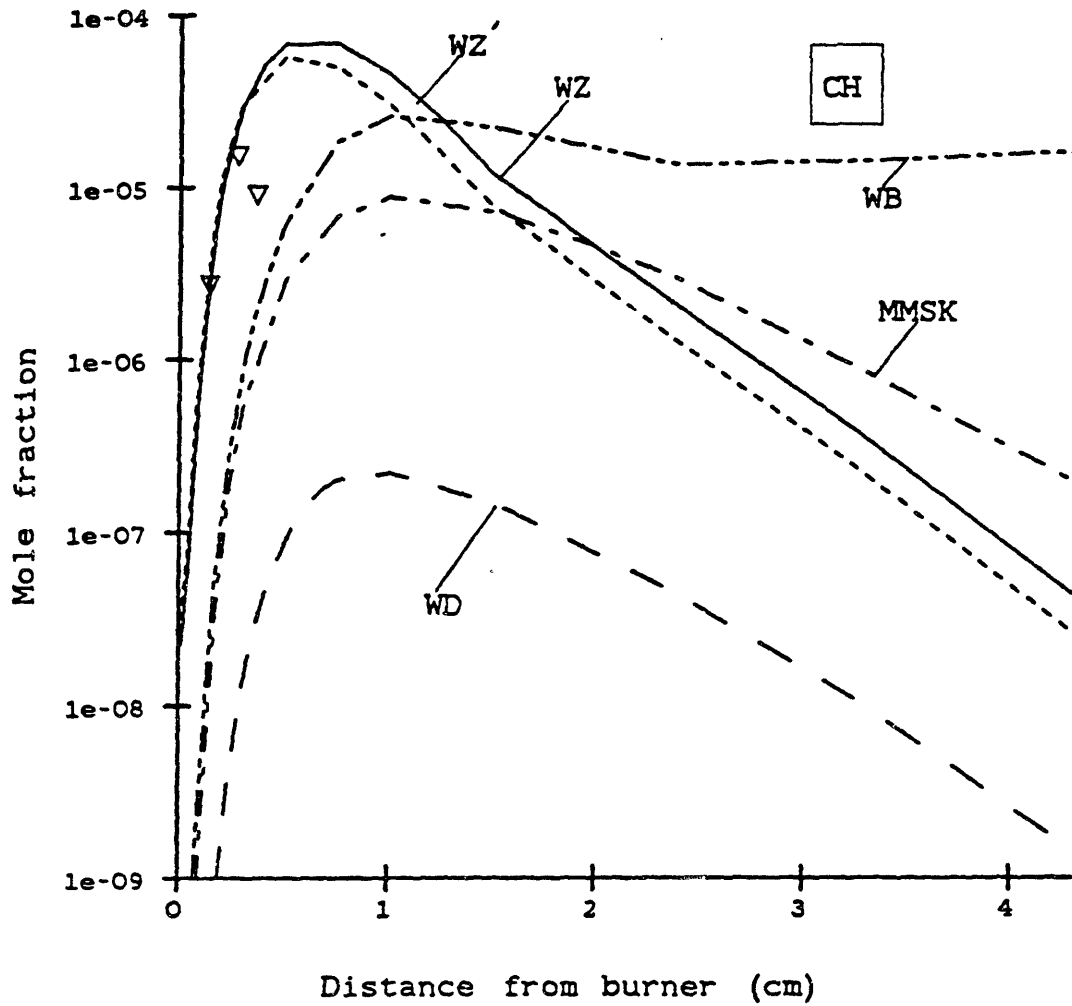


Fig. V.4. CH predictions compared to upper limits of data (∇).
 Curve labels defined in Fig. V.1.

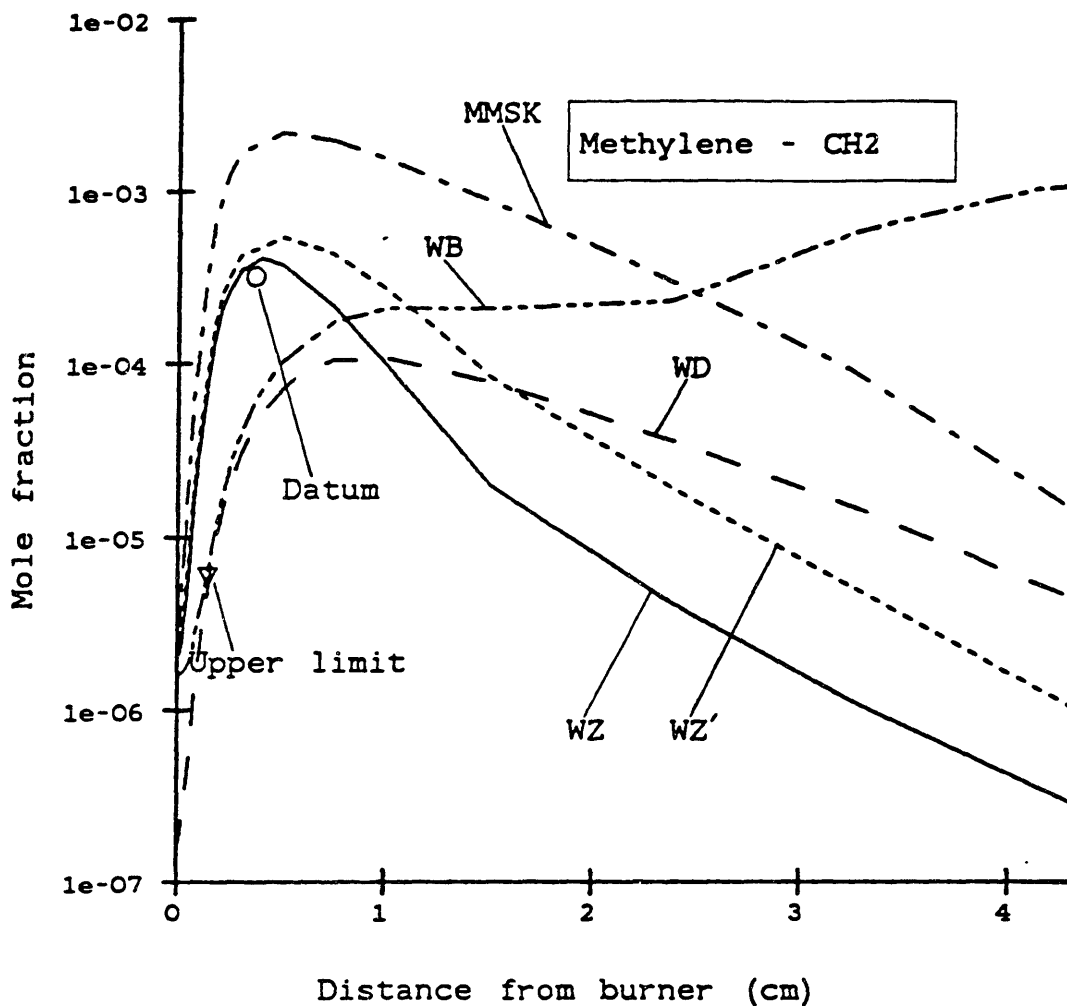


Fig. V.5. CH_2 predictions compared to upper limit of data (∇) and data point (O). Curve labels defined in Fig. V.1.

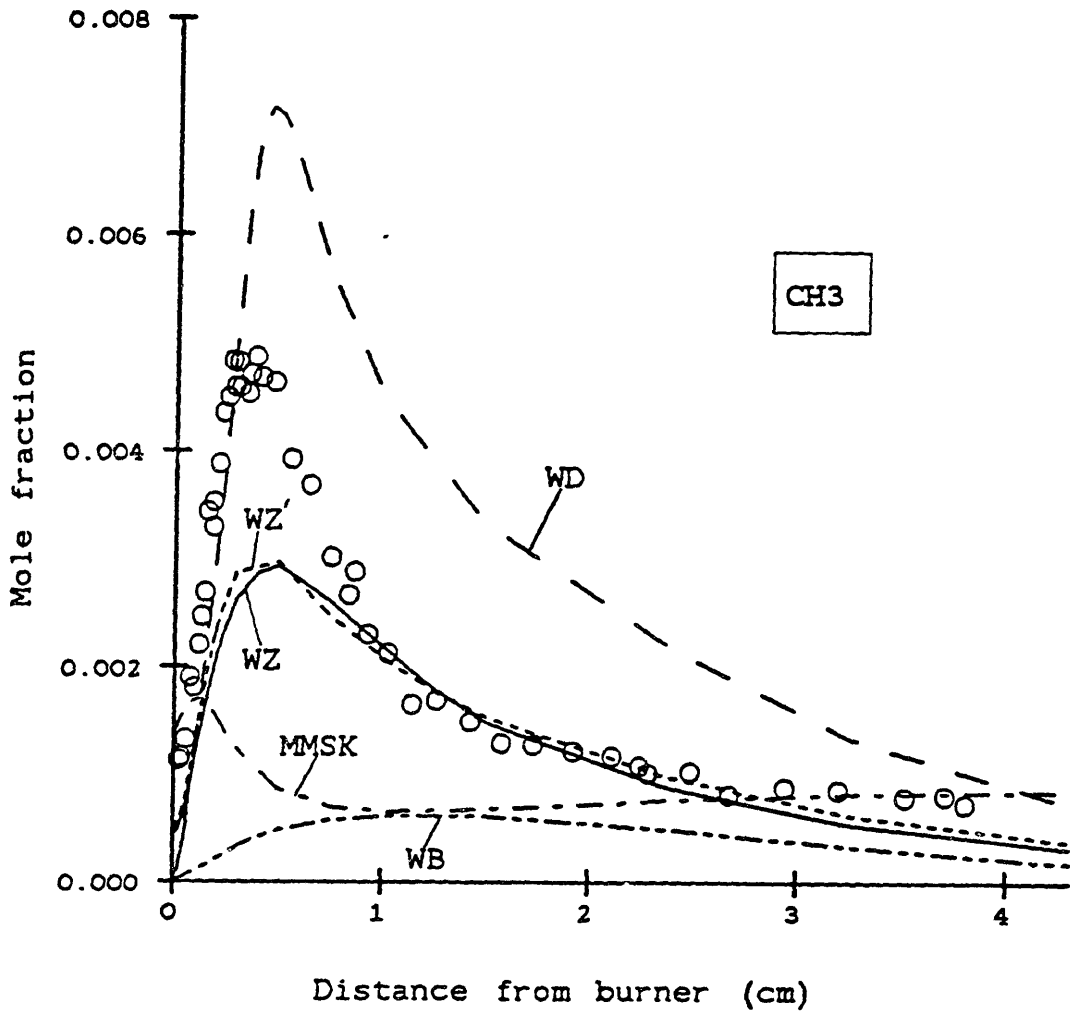


Fig. V.6. CH₃ predictions compared to data. Data points and curve labels defined in Fig. V.1.

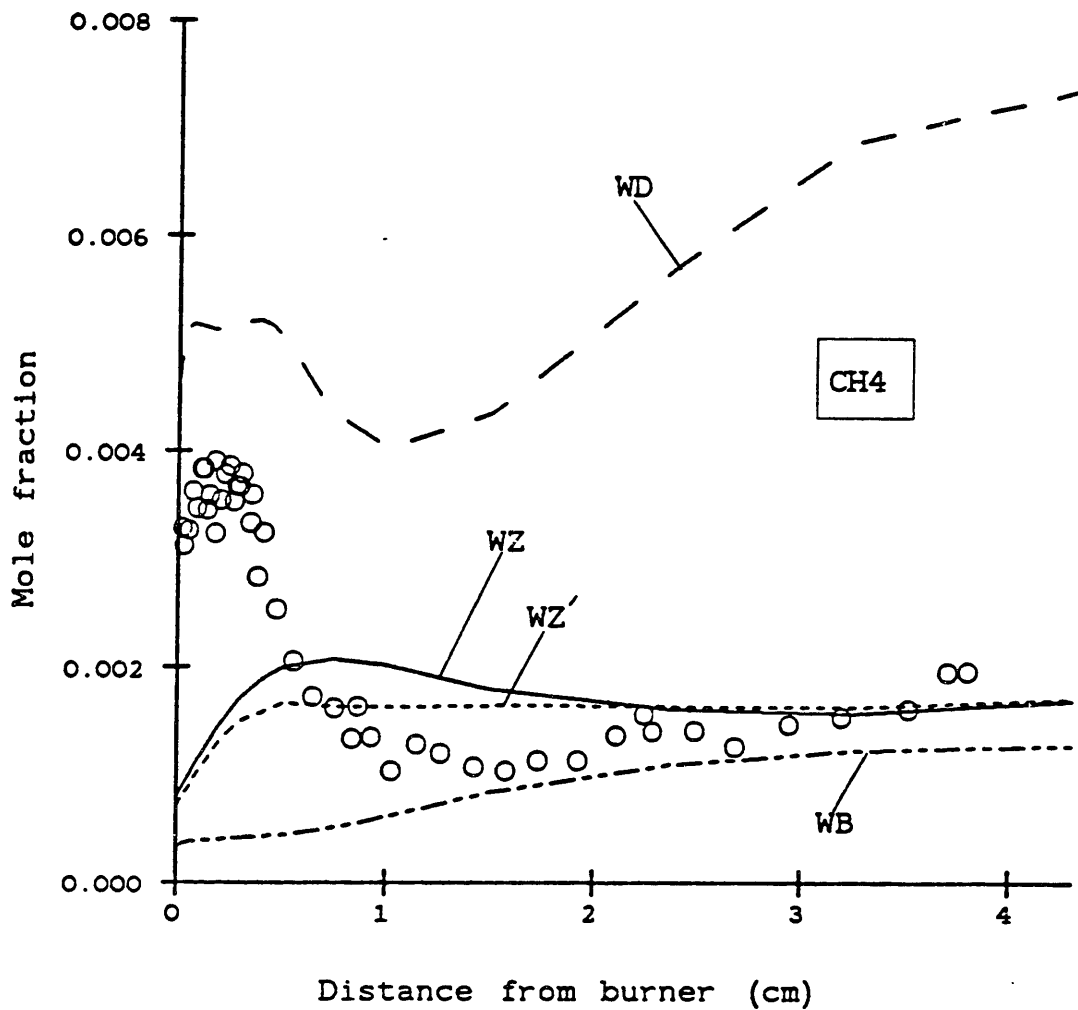


Fig. V.7. CH₄ predictions compared to data. Data points and curve labels defined in Fig. V.1.

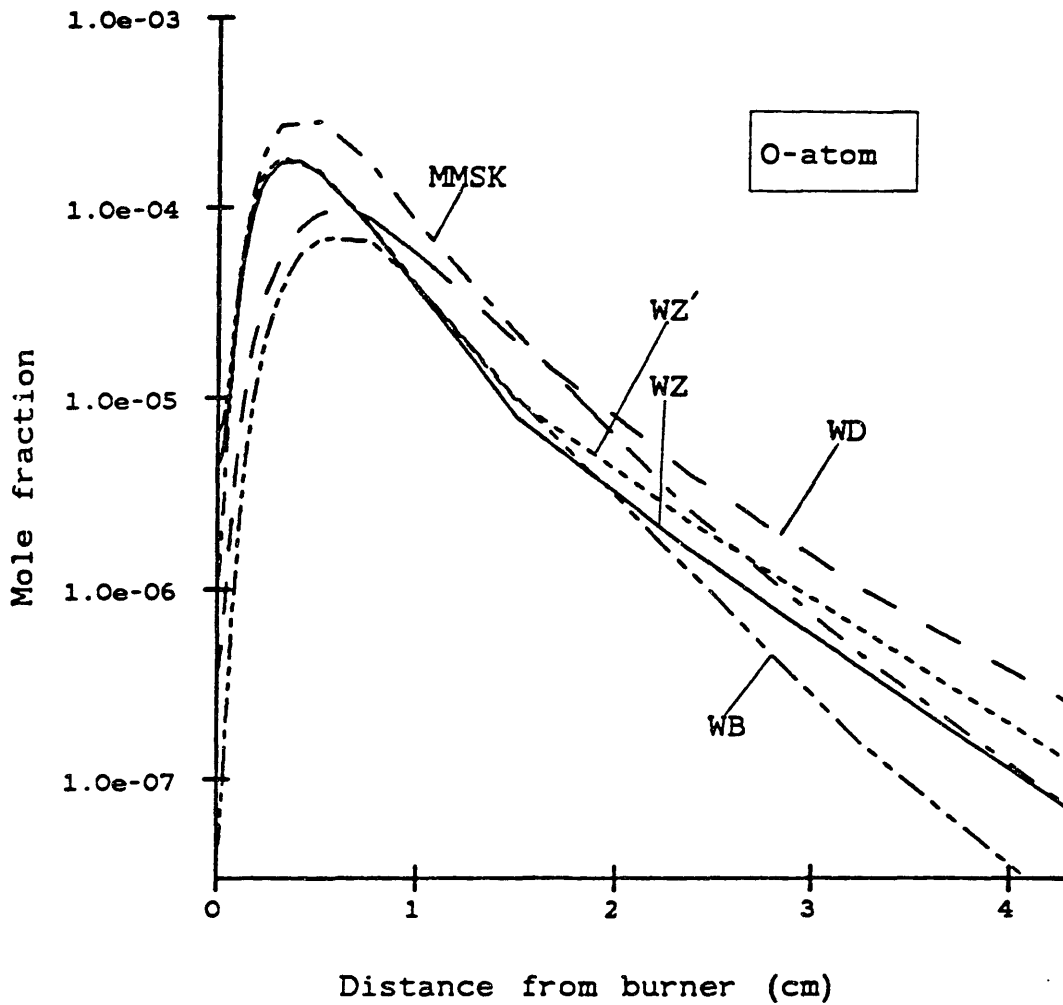


Fig. V.8. Predictions of O-atom. Curve labels defined in Fig. V.1.

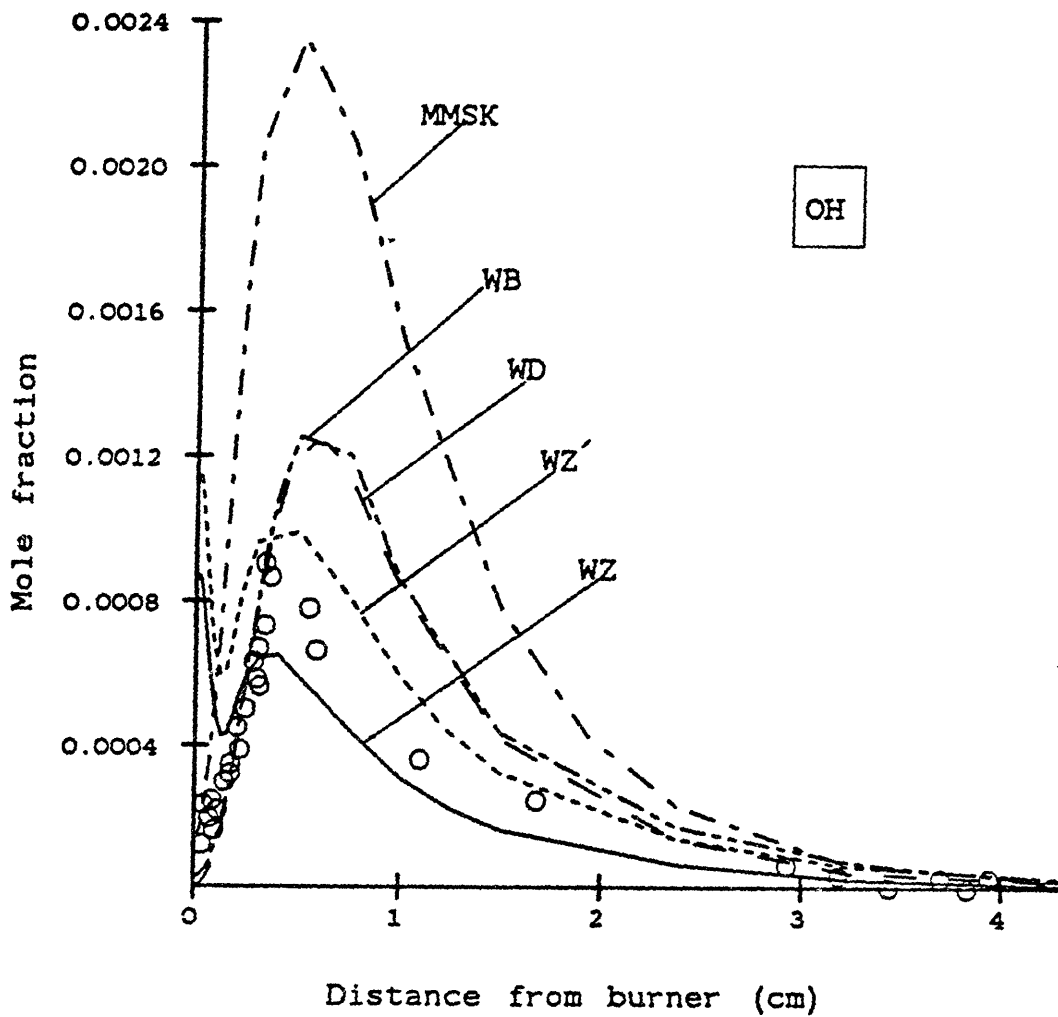


Fig. V.9. OH predictions compared to data. Data points and curve labels defined in Fig. V.1.

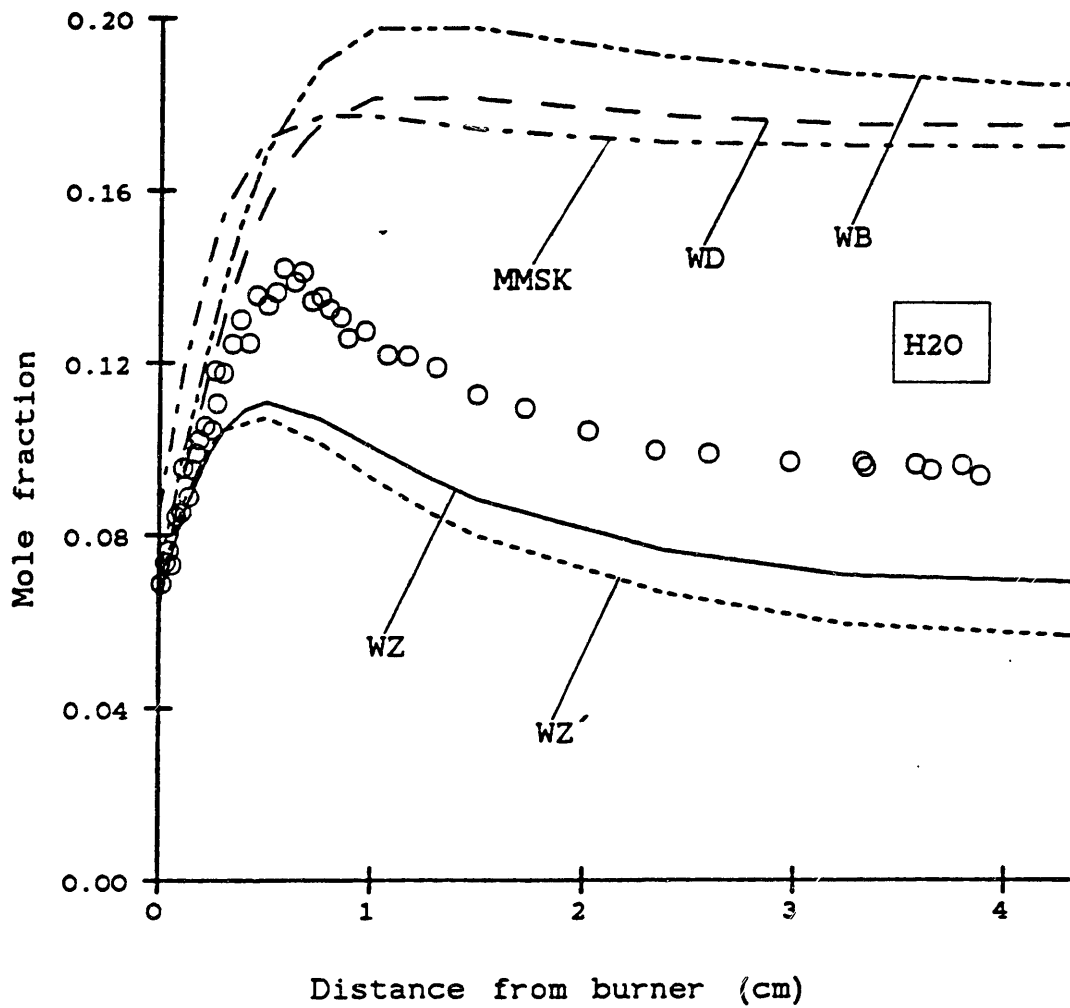


Fig. V.10. H₂O predictions compared to data (O). Curve labels defined in Fig. V.1.

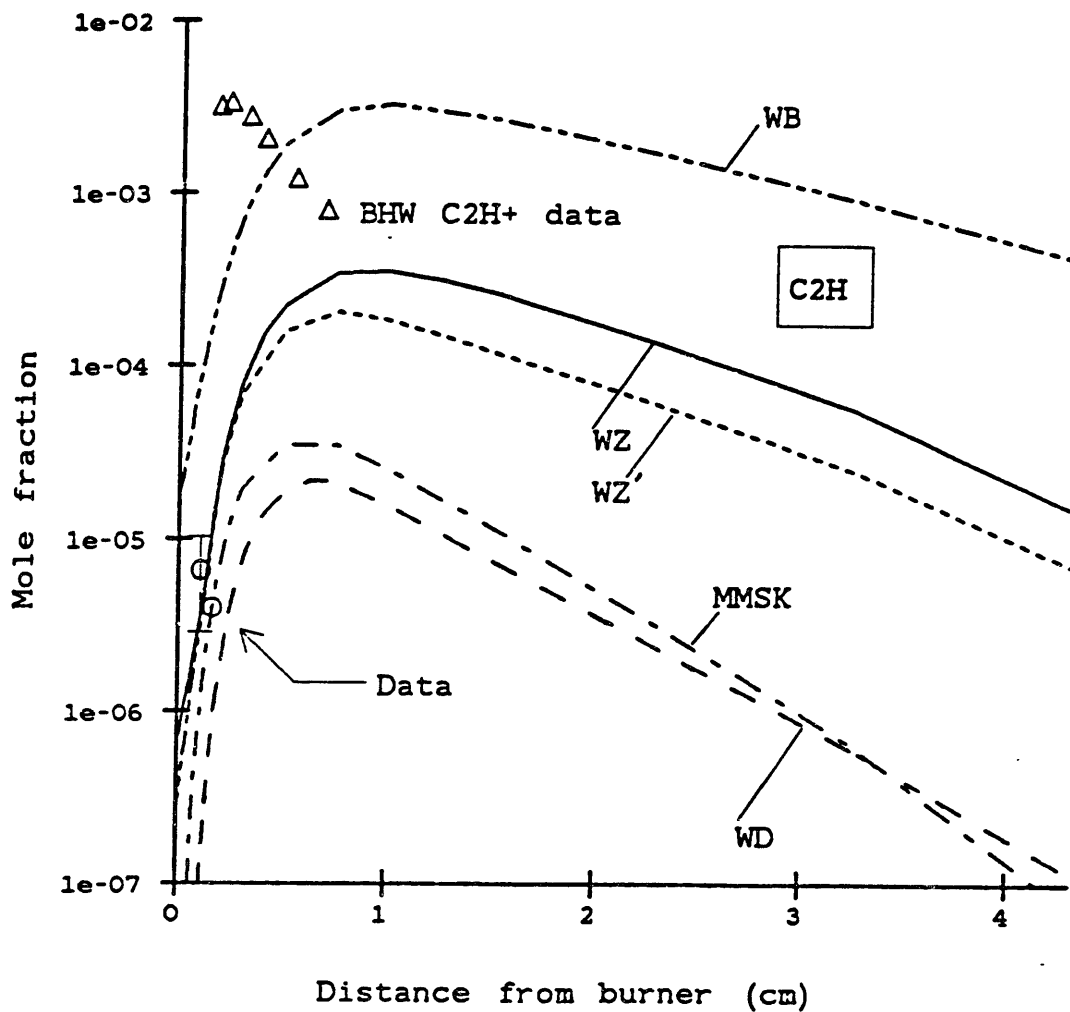


Fig. V.11. C_2H predictions compared to data points from this study (O) and from Bonne, Homann, and Wagner (1965; Δ). Curve labels defined in Fig. V.1.

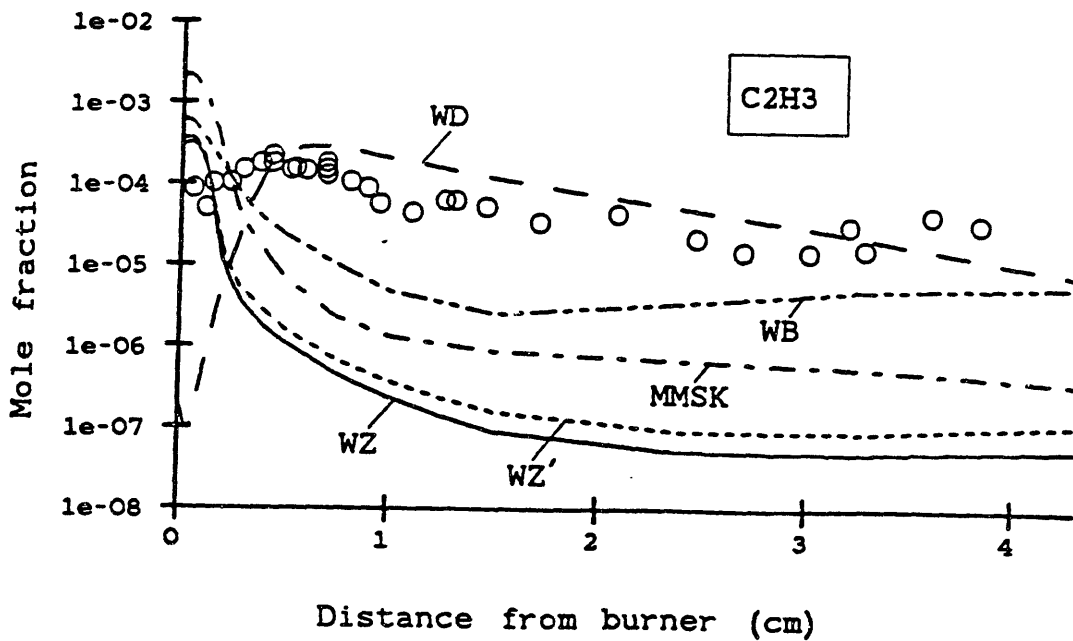
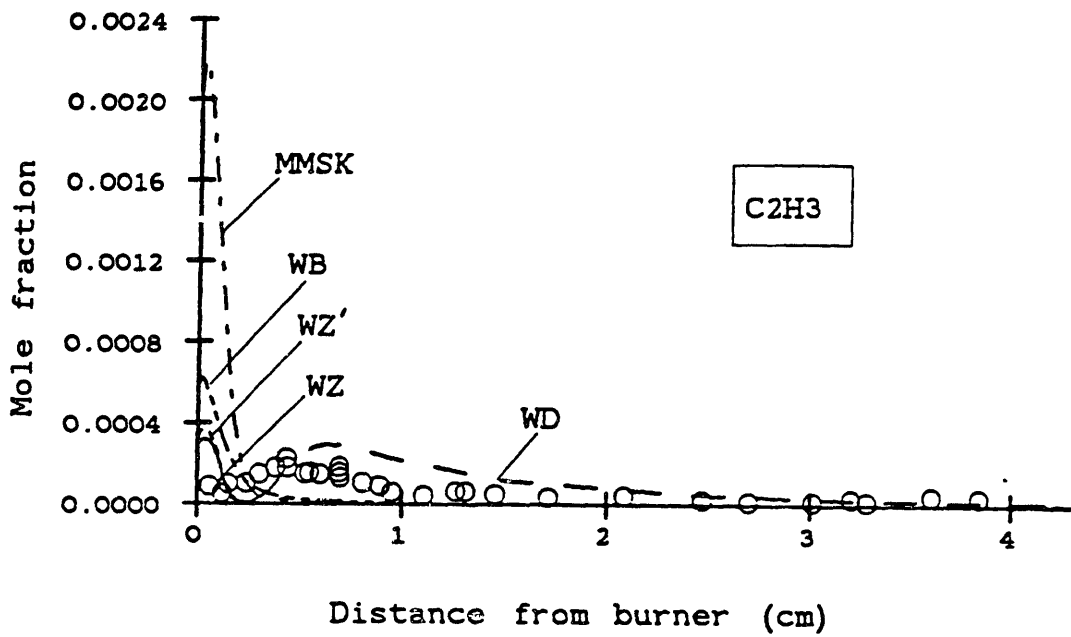


Fig. V.12. C_2H_3 predictions compared to data: (top) linear scale for mole fraction, (bottom) logarithmic scale. Data points and curve labels defined in Fig. V.1.

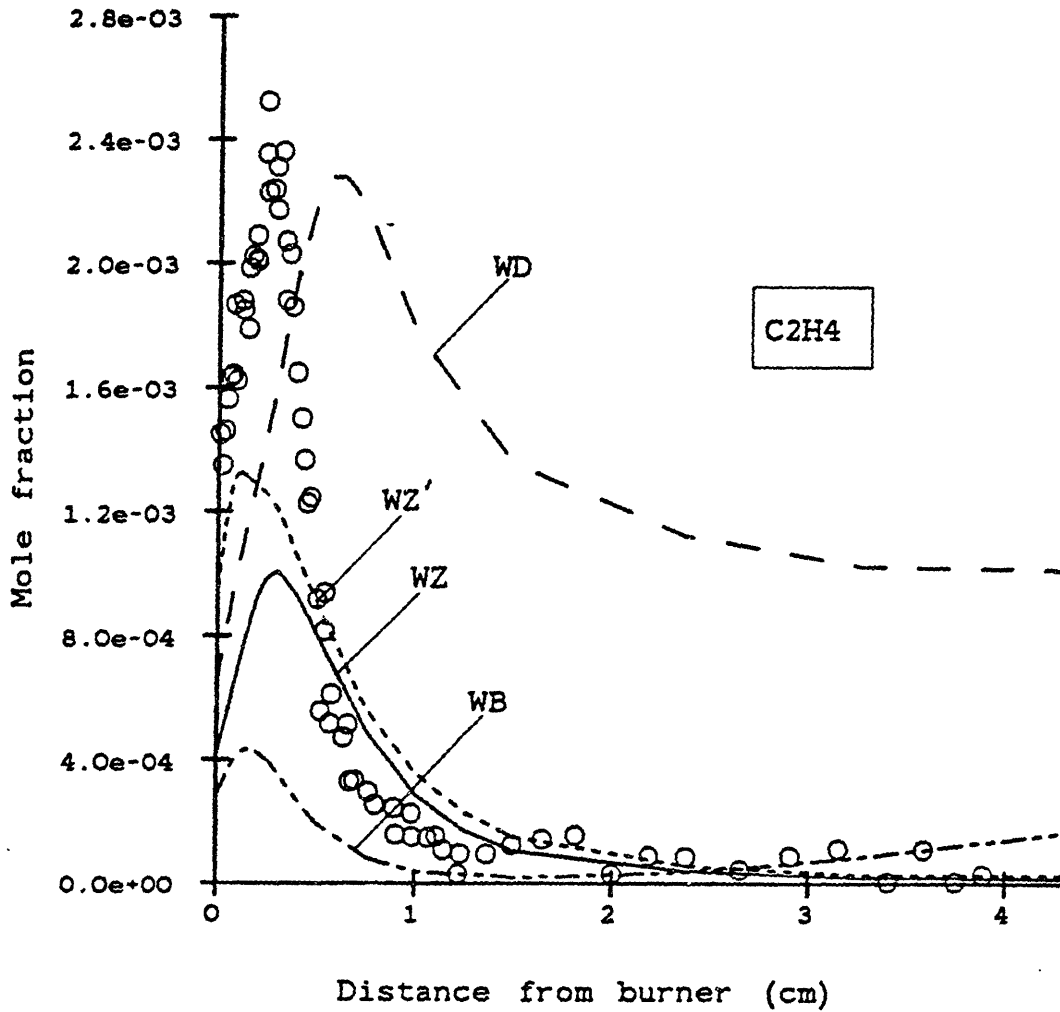


Fig. V.13. C_2H_4 predictions compared to data. Data points and curve labels defined in Fig. V.1.

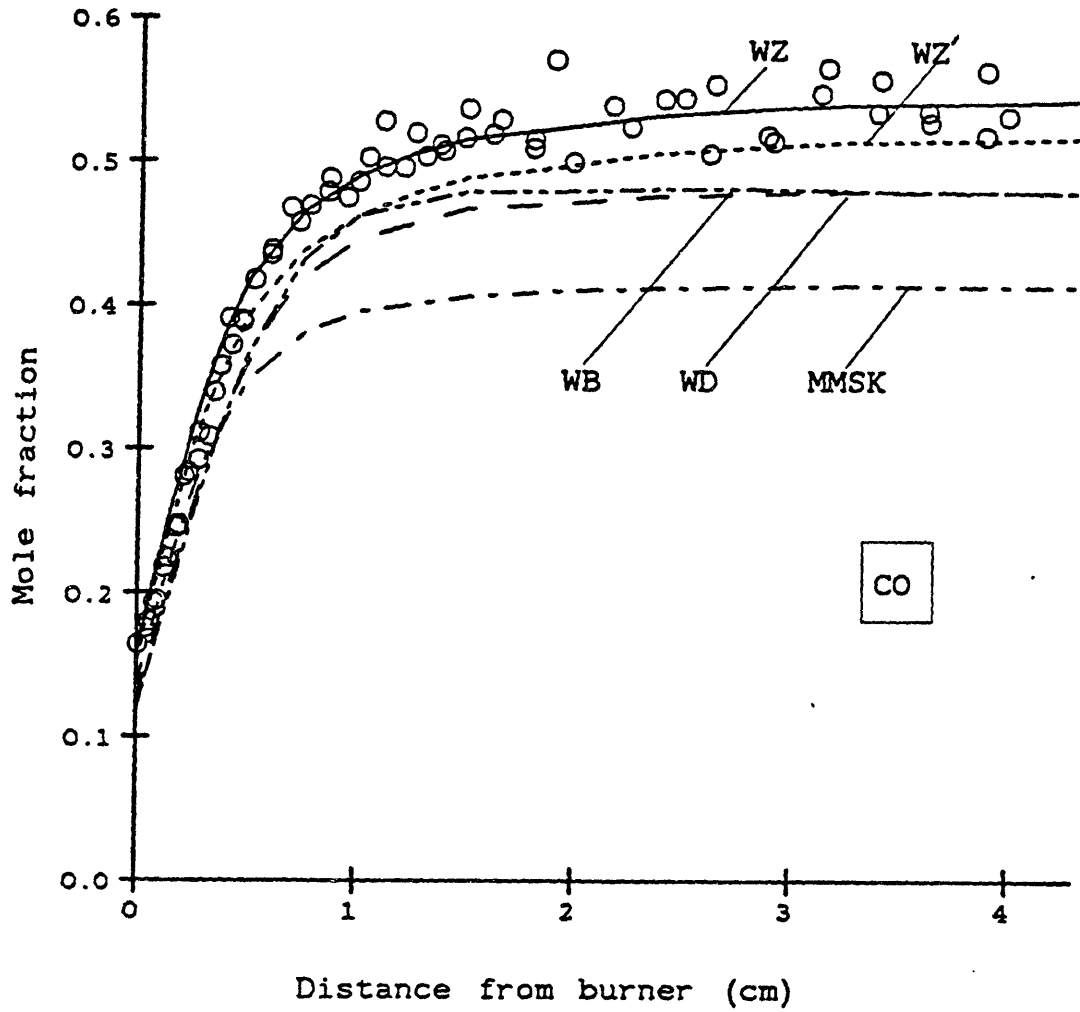


Fig. V.14. CO predictions compared to data. Data points and curve labels defined in Fig. V.1.

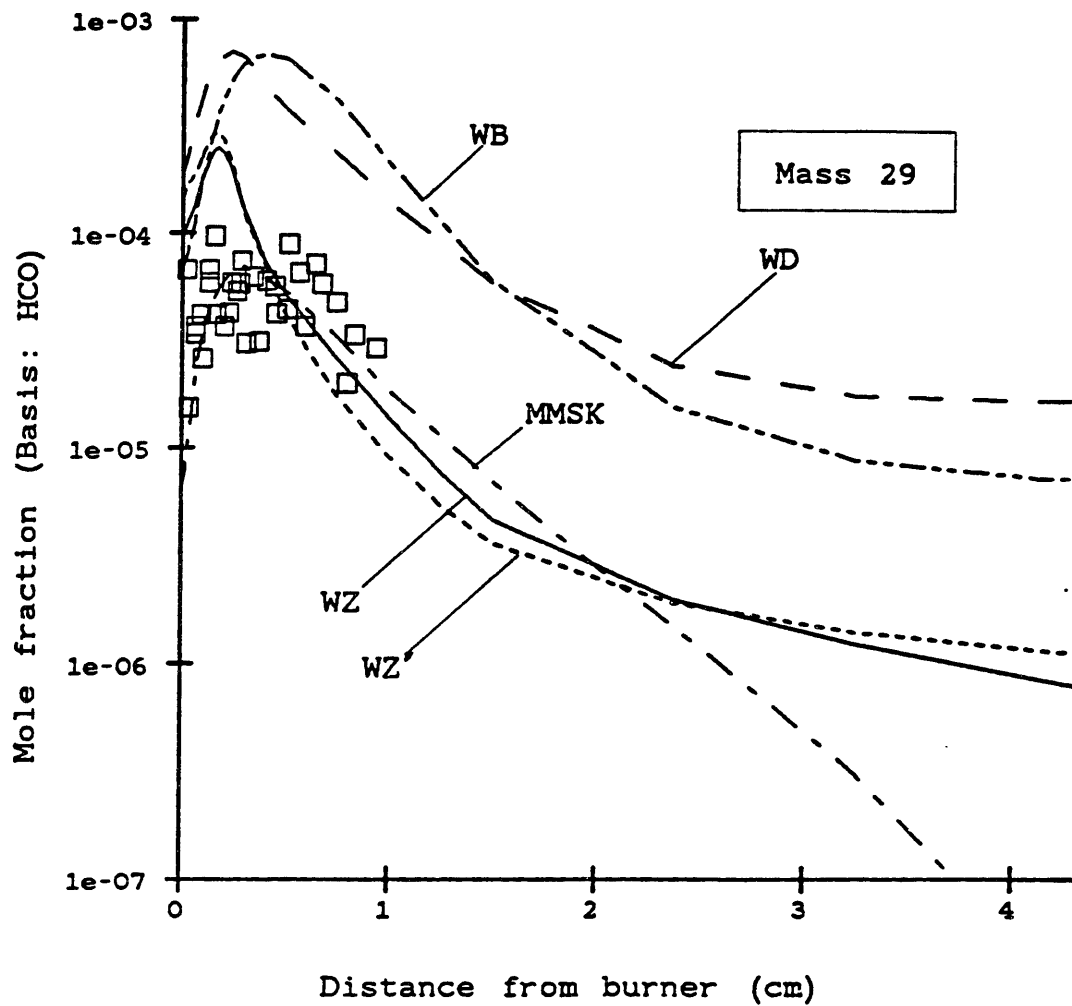


Fig. V.15. Prediction of profiles for mass 29, treating data as HCO and combining predictions of HCO and C_2H_5 to HCO equivalents using MBMS calibration factors.

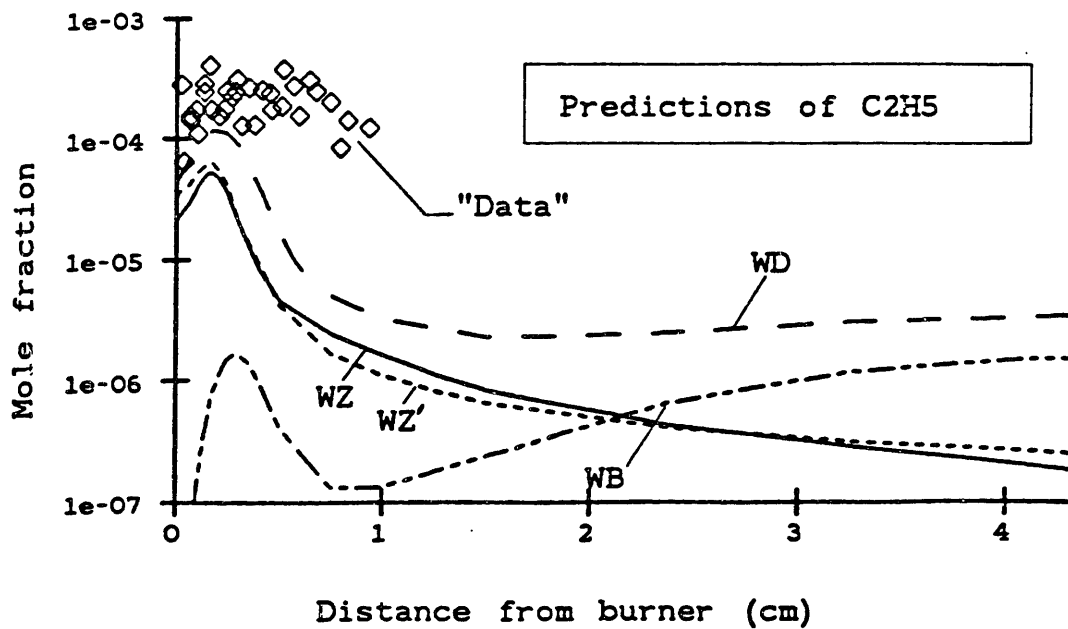
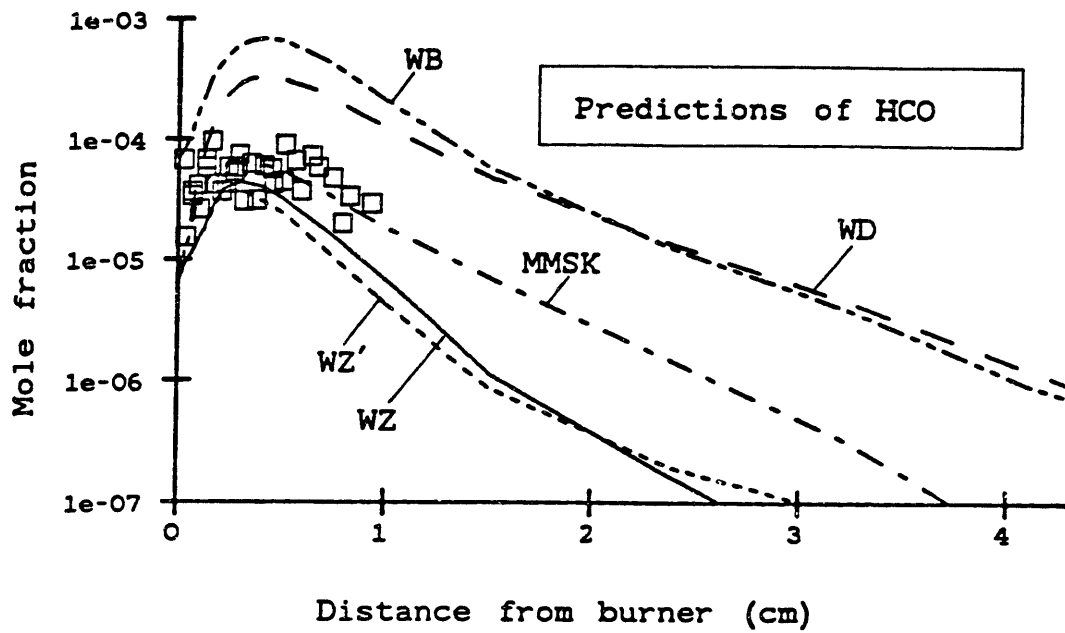


Fig. V.16. Predictions of profiles for mass 29 species: (top) predictions of HCO and data treated as being exclusively HCO and (bottom) predictions of C₂H₅ and data treated as being exclusively C₂H₅.

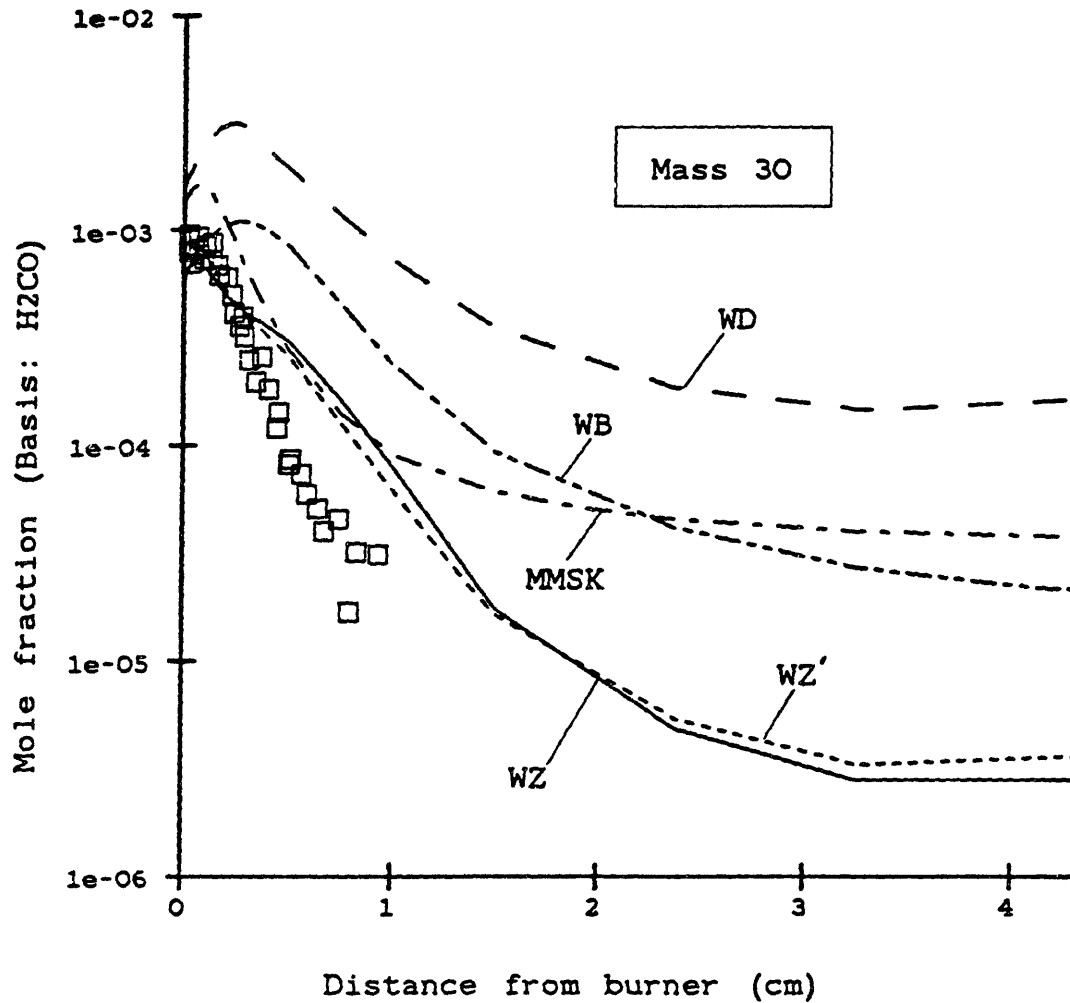


Fig. V.17. Prediction of profiles for mass 30, treating data as H₂CO and combining predictions of H₂CO and C₂H₆ to H₂CO equivalents using MBMS calibration factors.

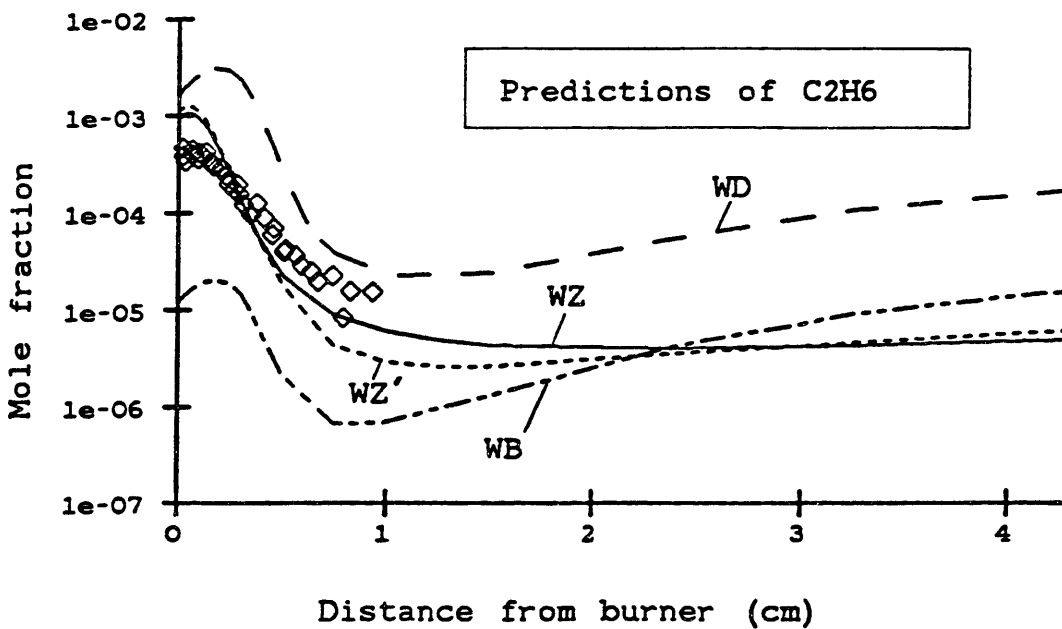
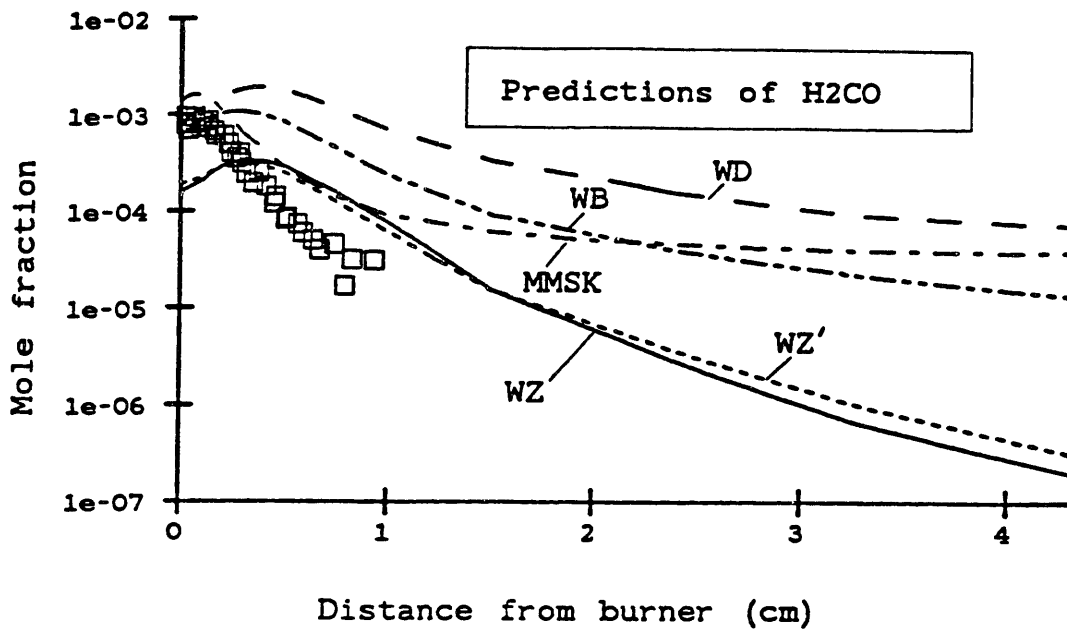


Fig. V.18. Predictions of profiles for mass 30 species: (top) predictions of H₂CO and data treated as being exclusively H₂CO and (bottom) predictions of C₂H₆ and data treated as being exclusively C₂H₆.

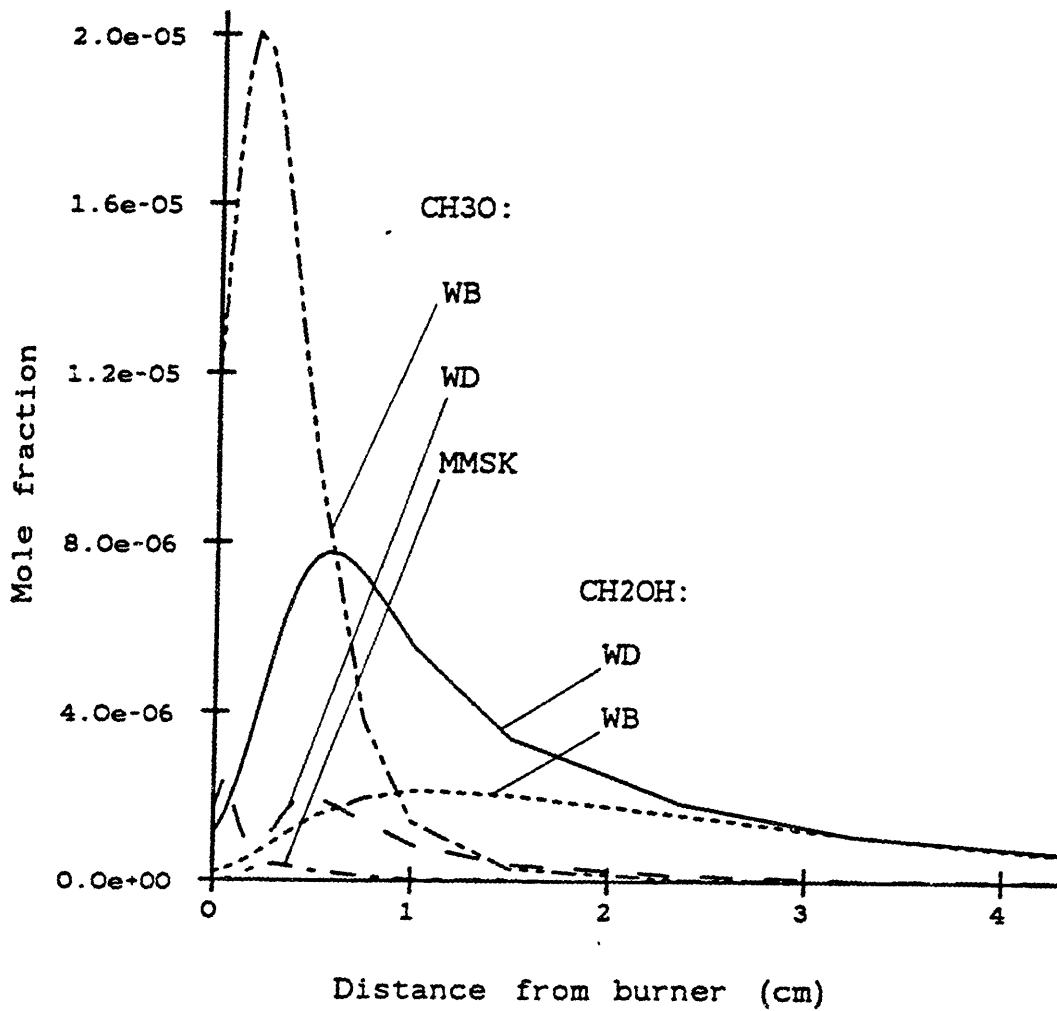


Fig. V.19. Predictions of CH_3O and CH_2OH profiles. Curve labels defined in Fig. V.1; curve types for CH_3O are - - - - (WB), ——— (WD), - - - (MMSK) and for CH_2OH are ——— (WD) and - - - (WB).

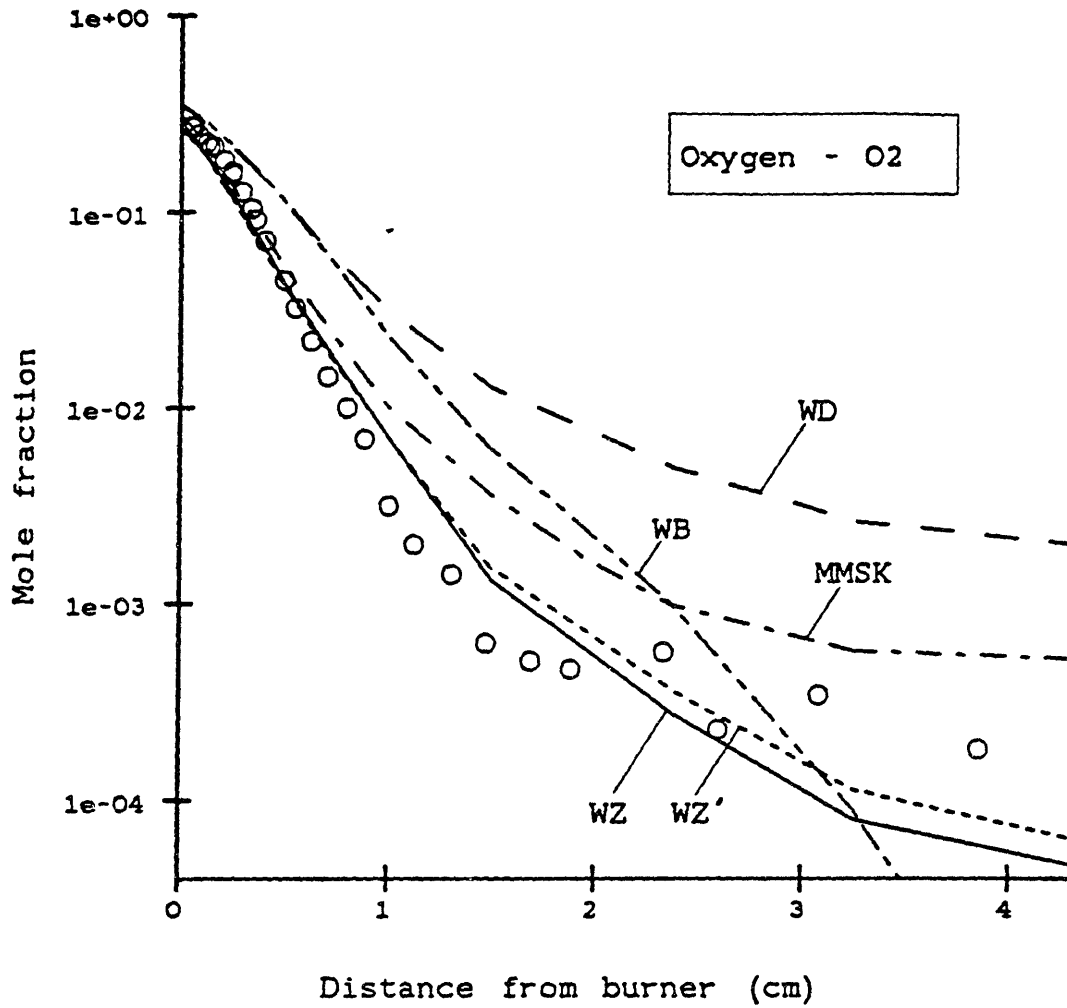


Fig. V.20. O₂ predictions compared to data (O). Curve labels defined in Fig. V.1.

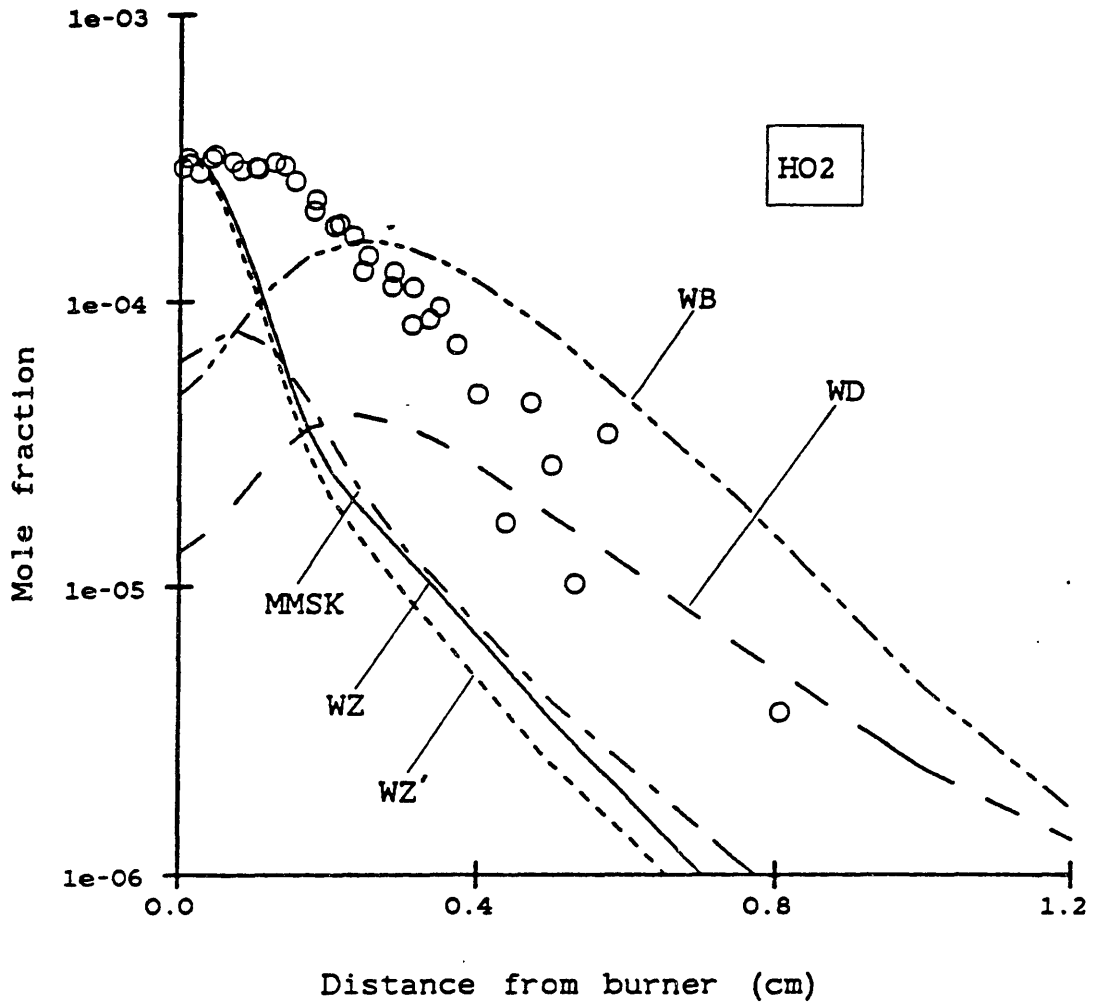


Fig. V.21. HO₂ predictions compared to data (O). Curve labels defined in Fig. V.1.

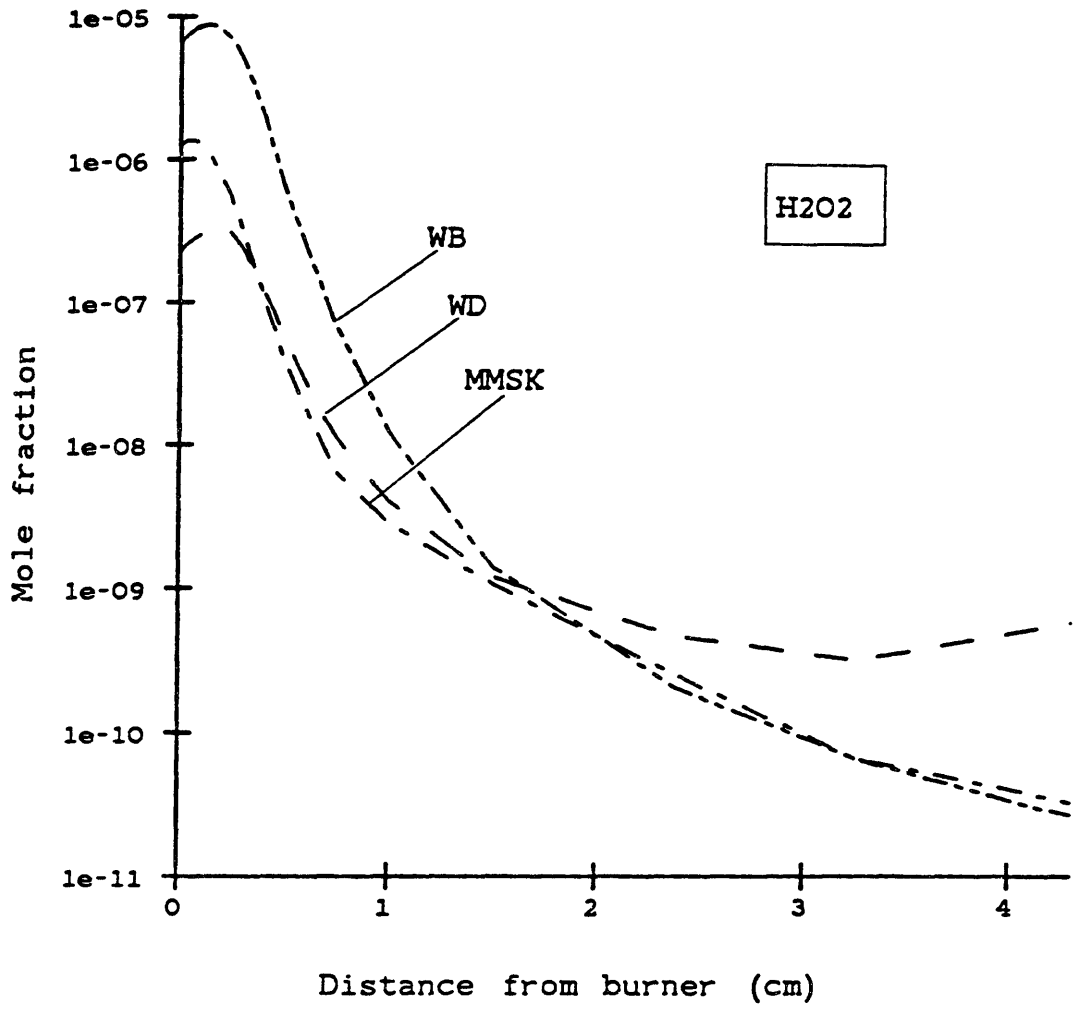


Fig. V.22. Predictions of H₂O₂. Curve labels defined in Fig. V.1.

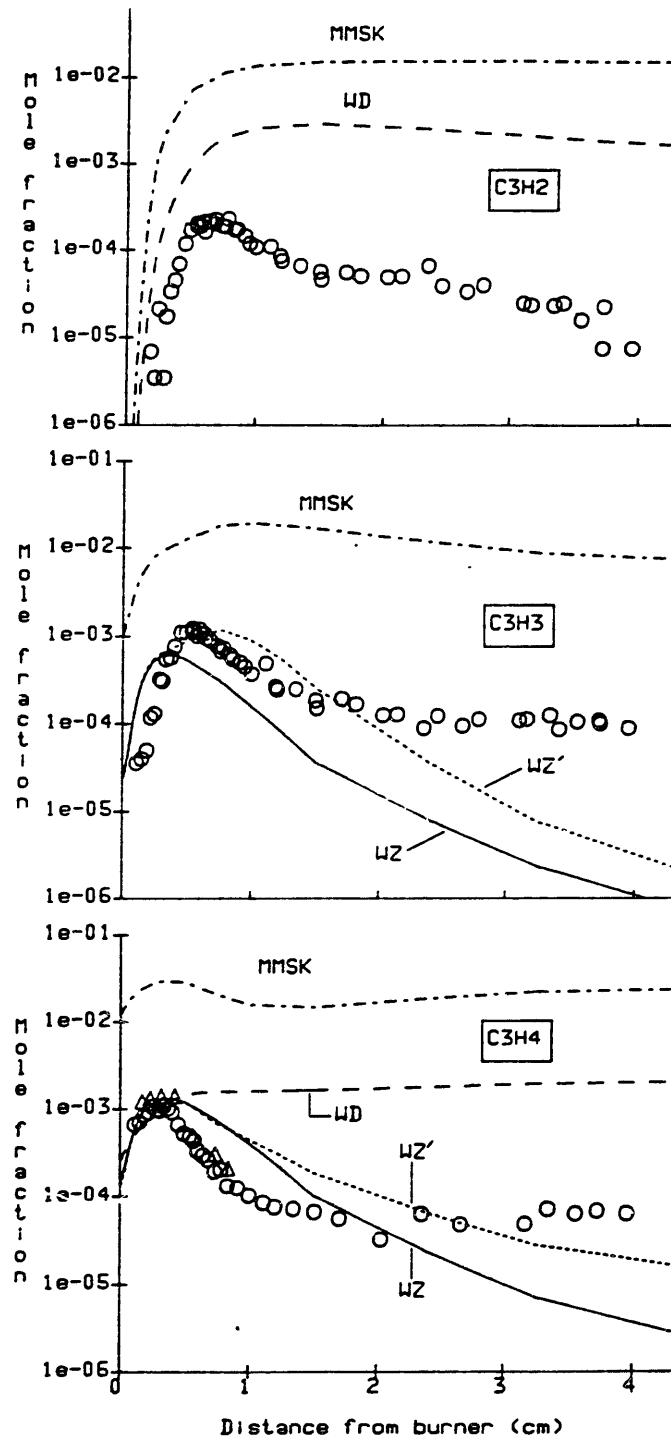


Fig. V.23. Predictions of C_3H_2 , C_3H_3 , and C_3H_4 compared to data. Data points and curve labels defined in Fig. V.1.

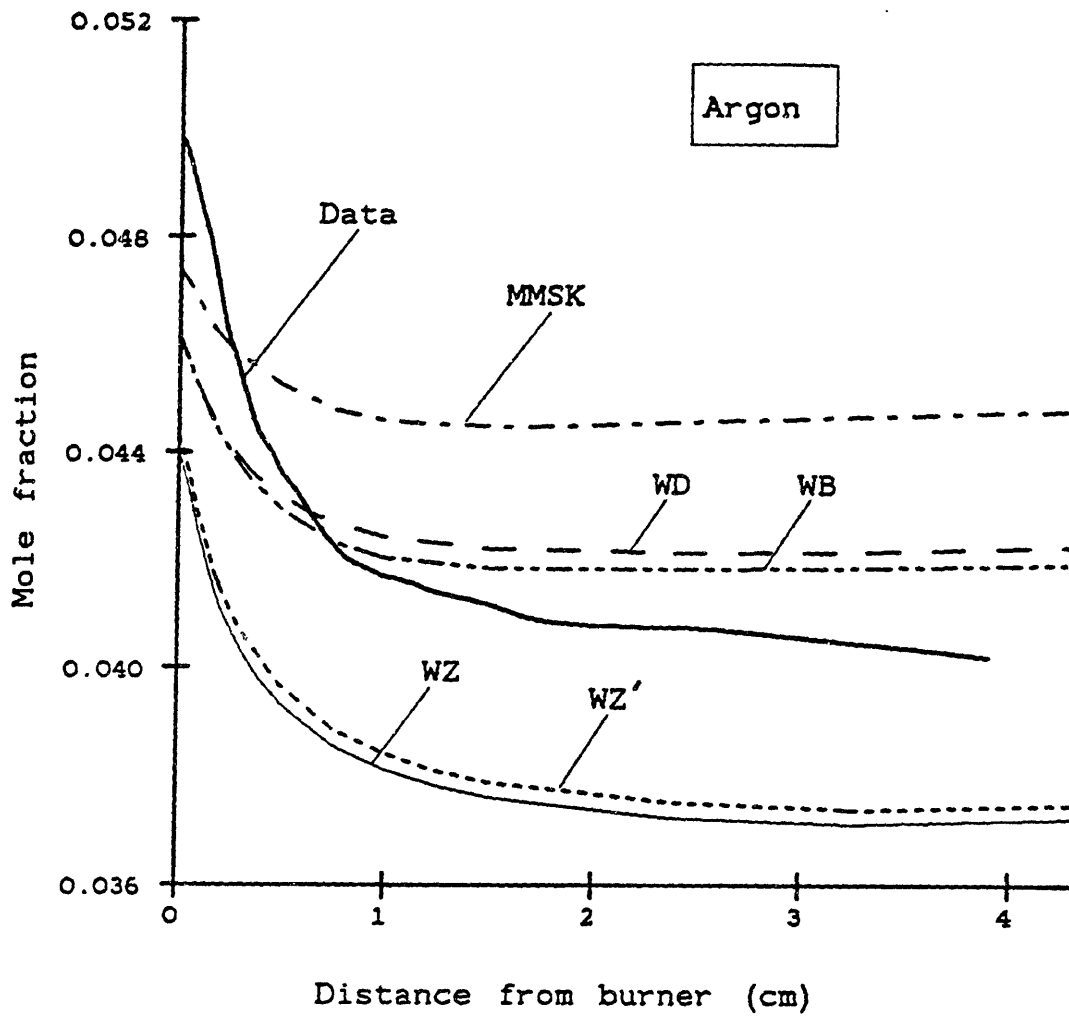


Fig. V.24. Ar predictions compared to data from mass balance (heavy solid line). Curve labels defined in Fig. V.1.

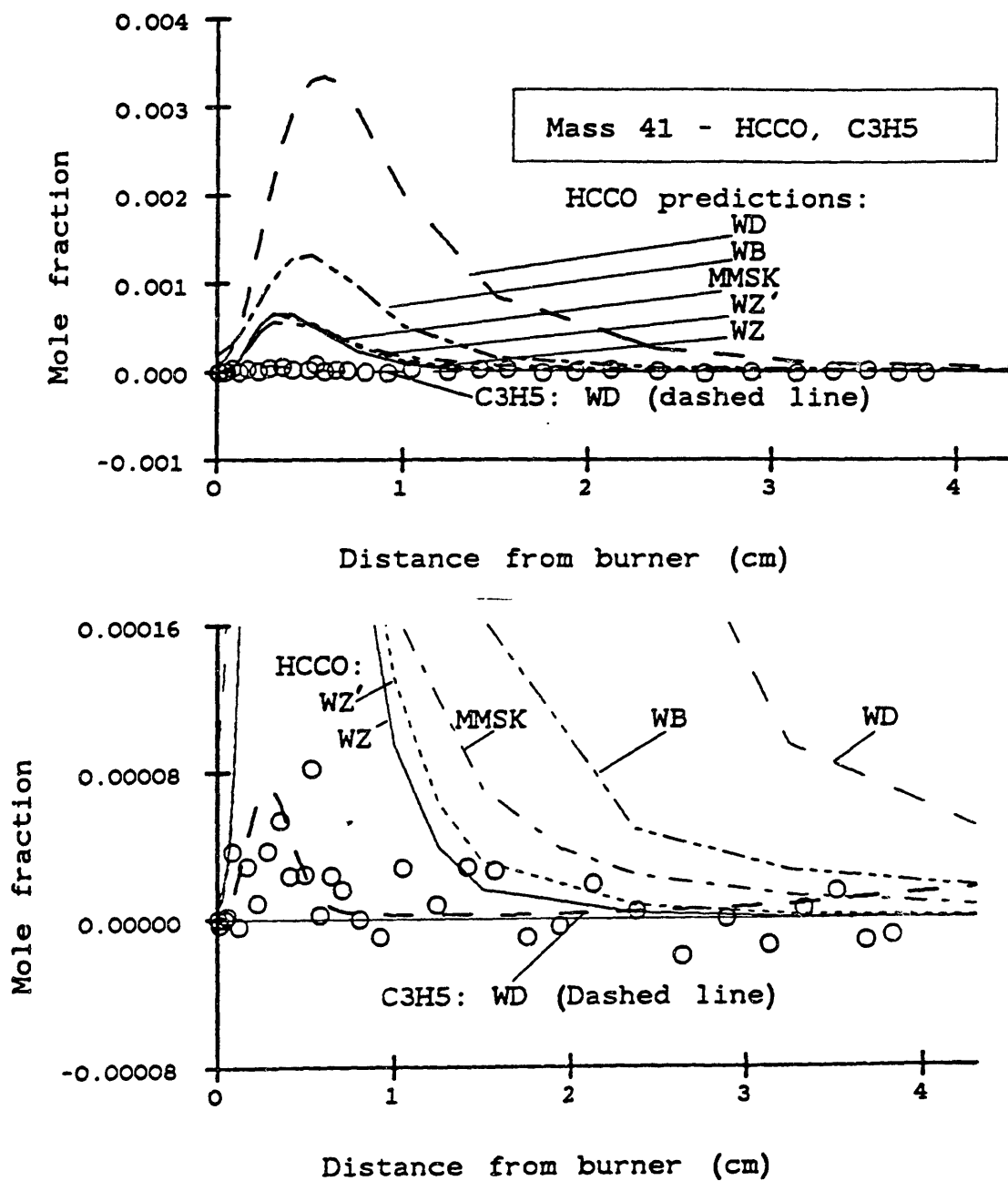


Fig. V.25. Predictions of mass 41 compared to data (O), which are treated as HCCO: (top) scale emphasizing HCCO predictions and (bottom) expanded scale emphasizing C₃H₅ predictions. Curve labels defined in Fig. V.1.

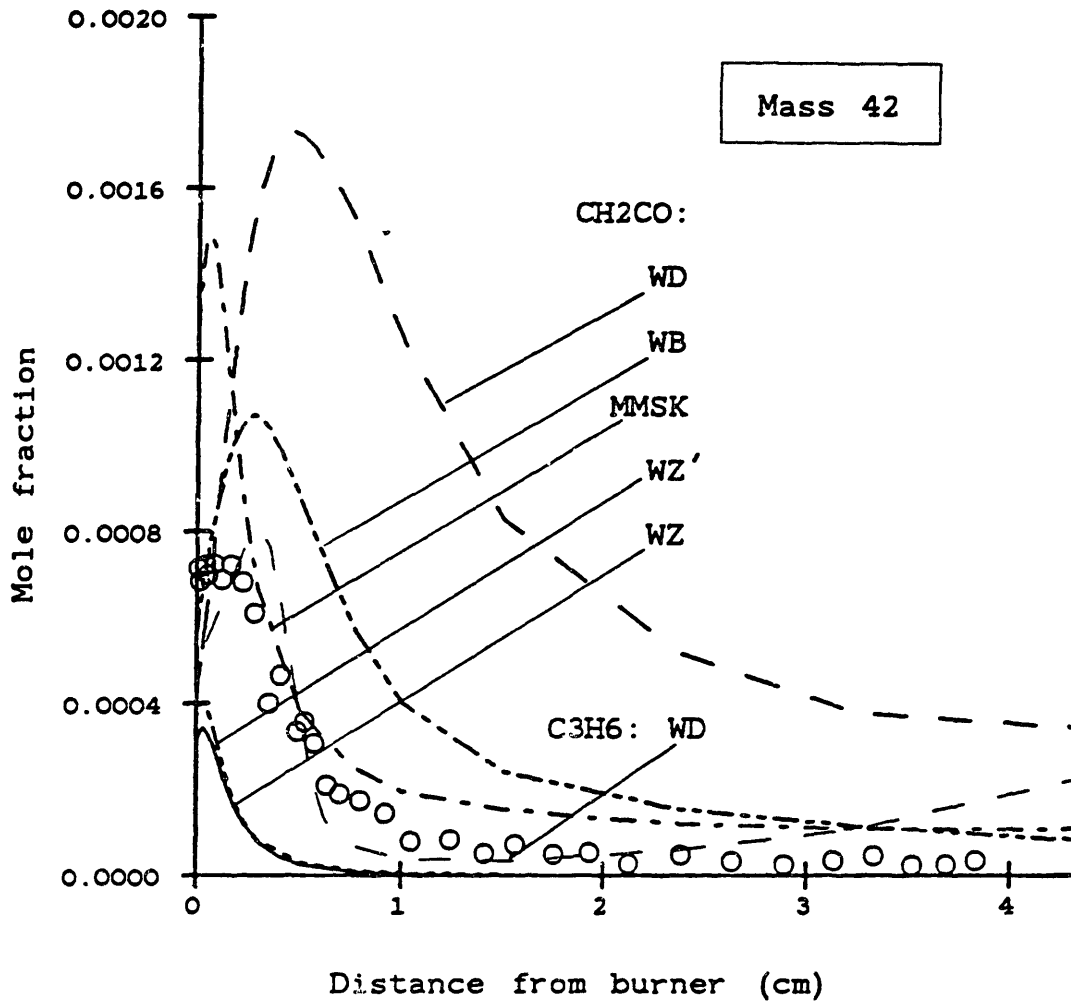


Fig. V.26. Predictions of CH₂CO and C₃H₆ compared to data for mass 42 (O), treated as CH₂CO. Curve labels defined in Fig.V.1.

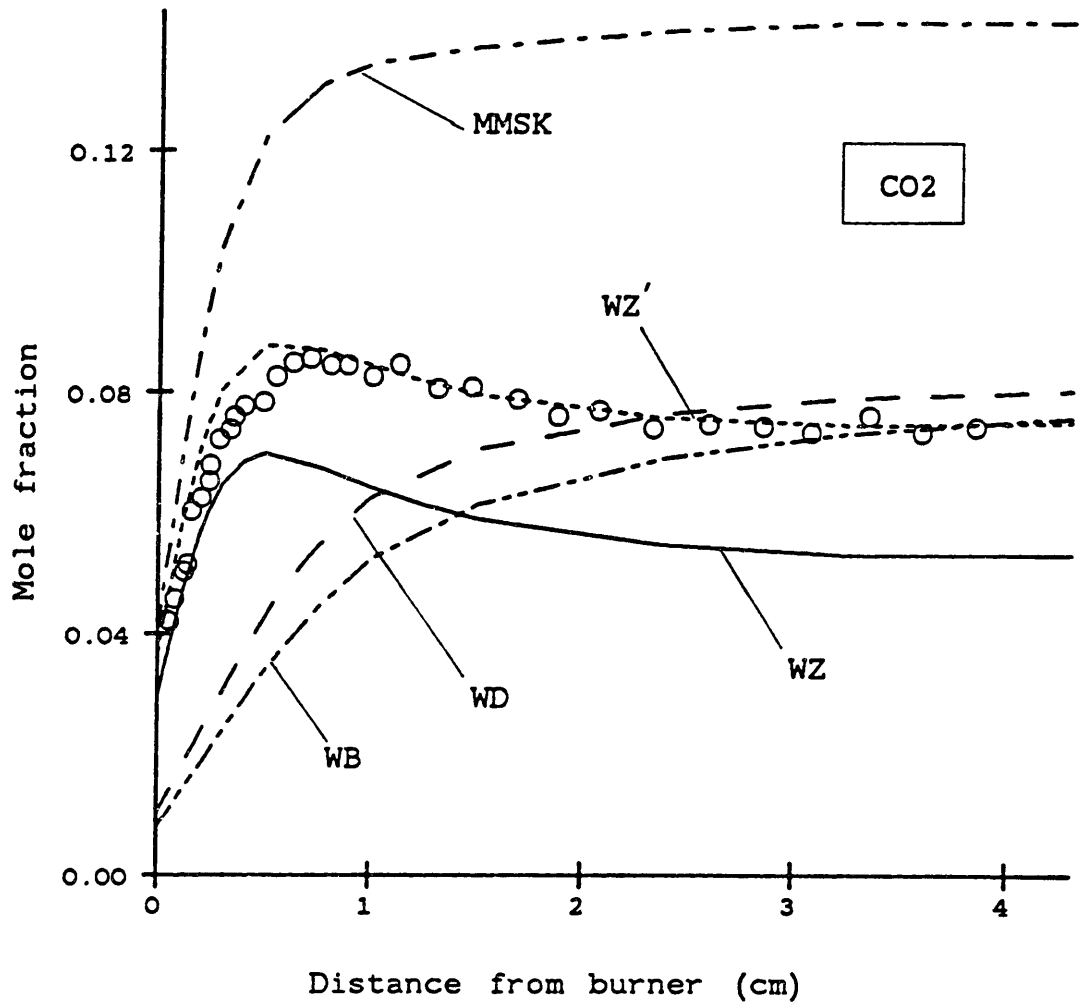


Fig. V.27. CO₂ predictions compared to data (O). Curve labels defined in Fig. V.1.

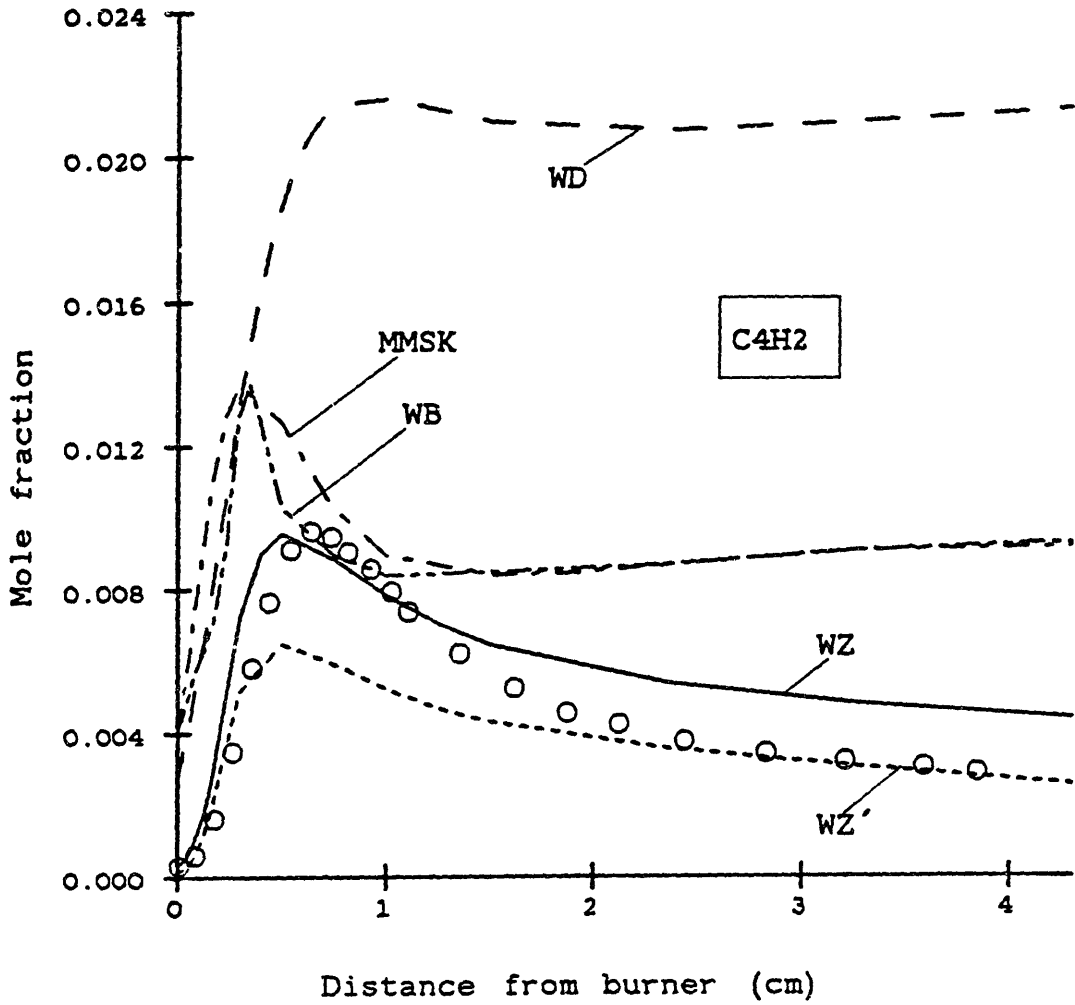


Fig. V.28. C_4H_2 predictions compared to data (O). Curve labels defined in Fig. V.1.

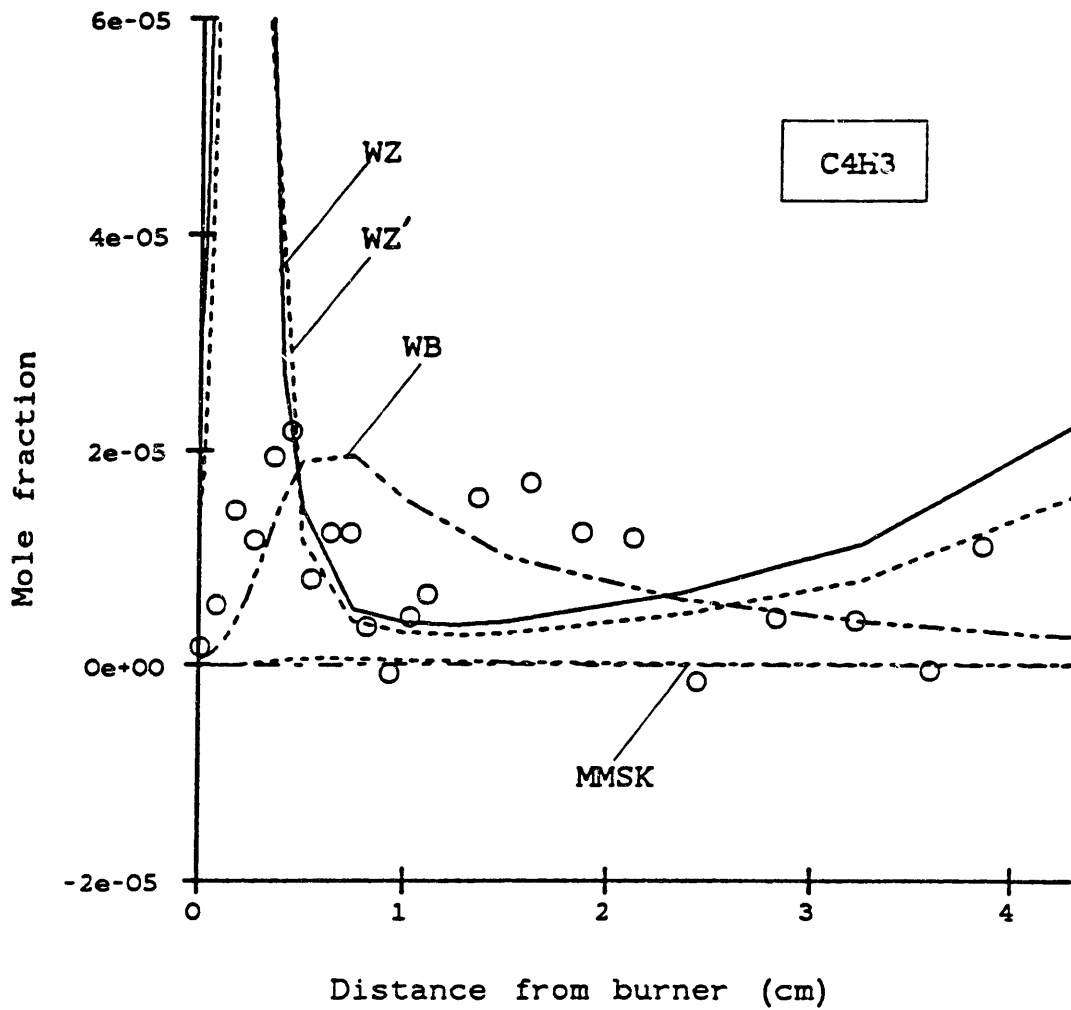


Fig. V.29. C_4H_3 predictions compared to data (O). Curve labels defined in Fig. V.1.

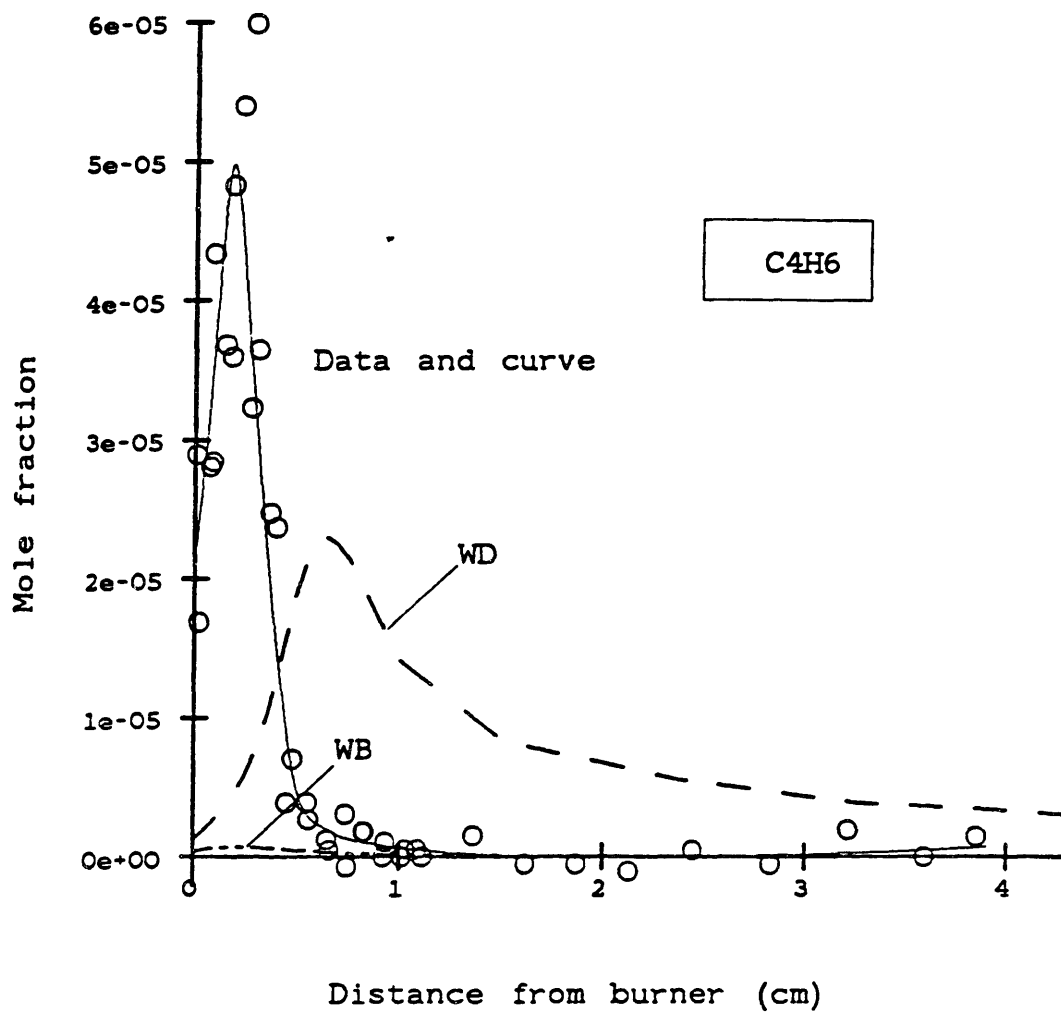


Fig. V.30. C_4H_6 predictions compared to data (\circ and —).
Curve labels defined in Fig. V.1.

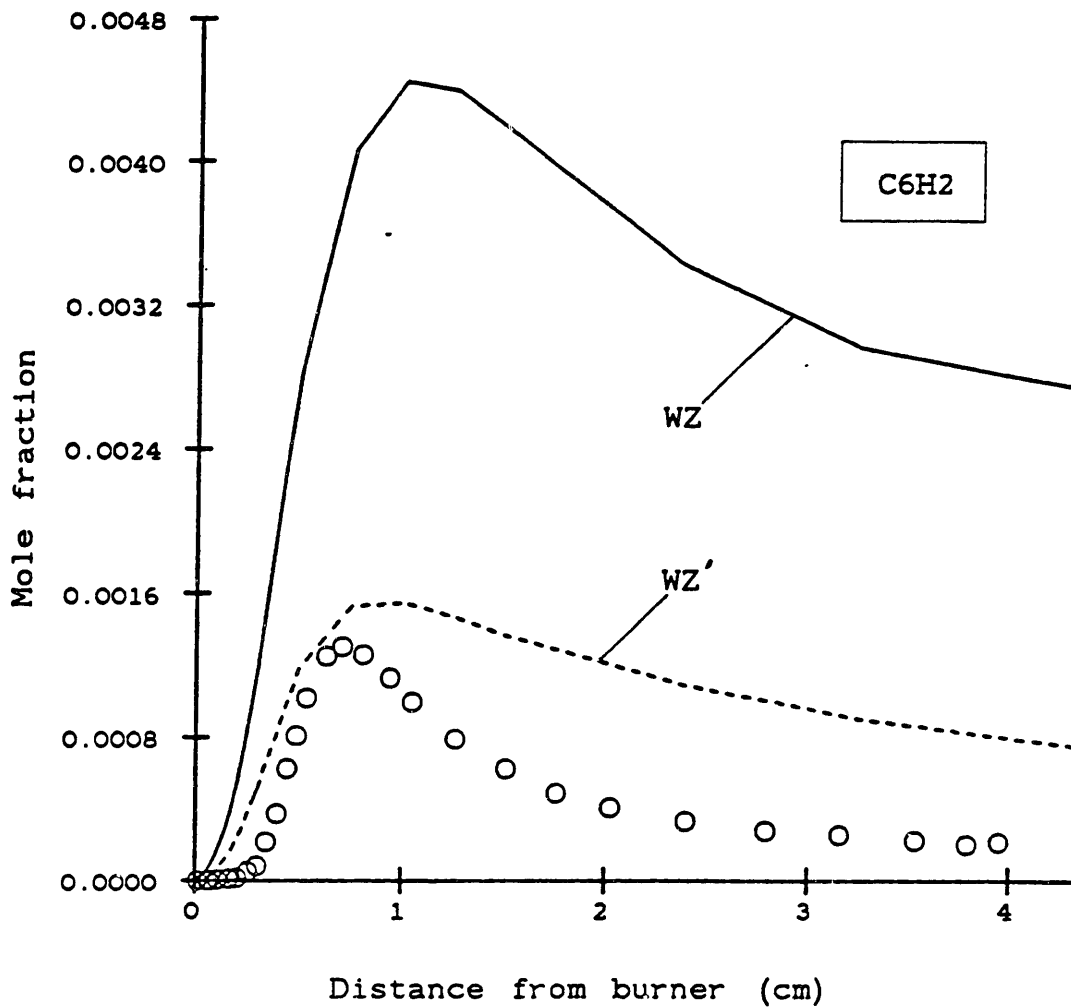
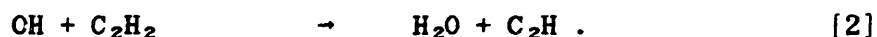


Fig. V.31. C_6H_2 predictions compared to data (O). Curve labels defined in Fig. V.1.

or destruction by each forward or reverse step, expressed both absolutely and as a fraction of the sum of formation (or destruction) rates at a position, and (3) the cumulative amount of formation or destruction, obtained by integrating the product of reaction rate and $A(Z)$ over distance.

First-order linear sensitivity coefficients (e.g., Kramer et al., 1984) were calculated for the rate constants, using small perturbations in a brute-force analysis. This information was less useful, primarily because the system is not yet well-modeled by the reactions chosen or by the rate constants used. In such a nonlinear system, this classic type of sensitivity analysis is less useful. An example of this limitation is the OH analysis below, which was relatively insensitive to the rate constant in question. However, the difference from other mechanisms was absence of a 10 kcal/mol activation, which no linear sensitivity analysis could be expected to examine.

H₂O. - Reactions involving H₂O (Fig. V.10) in the WZ mechanism, which gave the best predictions of shape and magnitude, are dominated by



H₂O is formed primarily by Rxn. 1 with a small contribution from Rxn. 2. The maximum occurs when destruction by Rxn. -1 balances formation. Throughout the flame, Rxn. 1/-1 is never predicted to reach partial equilibrium (net rate less than 5% of the forward or reverse rate).

Among the other mechanisms, H₂O in WZ' is slightly less than in WZ beyond 0.4 cm because the reverse of Rxn. 2 is included, which then causes 48% of the destruction. MMSK overpredicts H₂O by overpredicting OH, thus producing H₂O too rapidly to be destroyed. Overproduction of OH was caused by



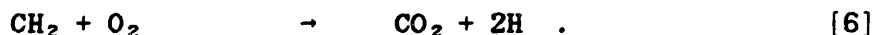
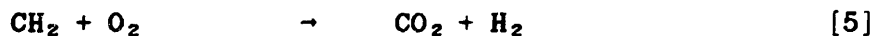
(discussed below).

WB and WD also overpredict H₂O. WB underpredicts H because there is no H-producing CH₂+O₂ channel, so H₂O is formed but Rxn. -1 is too slow to destroy it. WD has such a CH₂ channel, but H is still underpredicted.

CO₂. - The only important destruction reaction for CO₂ (Fig. V.27) in the mechanisms is



but formation by the reverse reaction is supplemented in all but WB by one or both of the CH₂+O₂ reactions:



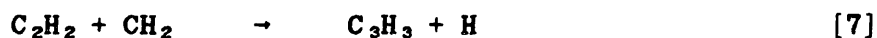
The peak in the CO₂ predictions of WZ and WZ' is caused by destruction (Rxn. 4) overtaking formation by a combination of Rxns. -4 and 6. WZ' predicts higher CO₂ concentration because CH₂ is slightly higher than in the WZ case.

Destruction of CO₂ never exceeds formation in MMSK, WD, or WB, so no maximum occurs. MMSK and WD use both Rxns. 5 and 6 with somewhat different rate constants than in WZ and WZ'. The reactions cause an overproduction of CO₂ in MMSK but make little CO₂ in WD because CH₂ is higher than in WZ or WZ' by a factor of ten in MMSK, while it is lower by the same factor in WD. WB can only produce CO₂ by Rxn. 4, causing it to gradually accumulate.

C₃H₂, C₃H₃, C₃H₄ and C₄H₂. - The large overprediction of C₃ species (Fig. V.23) by the MMSK and WD mechanisms affects many other species, in part by tying up so much carbon. This effect on other species is not observed in the other mechanisms because WB did not include any C₃'s, while the predictions of WZ and WZ' for C₃H₃ and C₃H₄ are much lower and closer to the magnitude of the data (C₃H₂ was not included).

C_3H_2 is produced from C_4H_2 by OH attack (Rxn. -3) in MMSK and by an O-atom attack in WD. Because no C_3H_2 destruction reactions are included except for the reverse of its formation paths, C_3H_2 builds up to excessive levels. This blocks the destruction of C_4H_2 in WD (Fig. V.28) and causes the overproduction of H_2O in MMSK.

Similarly, C_3H_3 and C_3H_4 are produced in MMSK predominantly by the sequence:

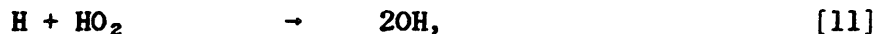


but C_3H_4 is not destroyed effectively, causing a build-up of those species. WD does not include C_3H_3 , but C_3H_4 reaches 0.2% at 0.4 cm (a reasonable value) and then changes little, in contrast to decaying by 95% as seen in the data. The dominant C_3H_4 destruction reactions in WD are:



each with a rate constant of $1.0 \cdot 10^{12} \text{ cm}^3\text{mol}^{-1}\text{s}^{-1}$, but neither reaction is predicted to destroy C_3H_4 effectively.

OH. - An interesting anomaly in the OH predictions (Fig. V.9) is a secondary maximum predicted by WZ and WZ' near the burner. Formation of OH in WZ and WZ' is dominated near the burner by:



but the rate constant for this reaction is not the source of error; it is approximately the same for all the mechanisms examined. Instead, it is the C_2H_3 destruction reaction:



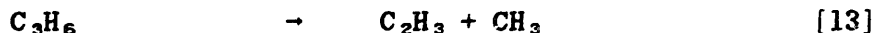
which is used in all the mechanisms, that generates HO_2 too rapidly at low temperatures in WZ and WZ'. Warnatz assumed a barrierless

rate constant, while MMSK, WB, and WD include an activation energy of 10 kcal/mol. As a consequence, Rxn. 12 is about 3 orders of magnitude faster near the burner in WZ and WZ'.

The absence of this anomaly in MMSK, WB, and WD does not mean that their rate constant or even the reaction $C_2H_3+O_2$ is correct. In fact, Slagle et al. (1984) found no HO_2 in a study of this elementary reaction at 297-602 K, but the products were instead $HCO+H_2CO$ with a different rate constant than used above.

C_2H_3 . - The impact of Rxn. 12 on the predictions is also seen in the C_2H_3 profiles (Fig. V.12) from MMSK, WB, WZ, and WZ'. C_2H_3 is produced rapidly at the burner by pressure-dependent addition of H to C_2H_2 , approaching the high-pressure limit at low temperatures. As distance from the burner increases, C_2H_3 is predicted to be destroyed rapidly by O_2 attack, while the experimental mole fraction is more nearly constant.

The prediction by WD corresponds much better to the experimental results. WD includes a pyrolysis reaction:



that maintains a higher mole fraction of C_2H_3 beyond 0.57 cm. (The reverse of this reaction accounts for the low mole fraction of C_2H_3 near the burner, consuming C_2H_3 more rapidly than it can be produced by $H+C_2H_2$.) The other mechanisms either do not include C_3 's heavier than C_3H_4 (MMSK and WB) or do not link the lighter and heavier C_3 's (WZ and WZ'). If the WD rate constant for Rxn. 13 is correct, then growth chemistry like this reaction is important in determining the concentration of light hydrocarbon radicals.

V.5. Remarks on the other predictions

It was noted in Ch. V.3 that WZ' gave satisfactory predictions for more species than any of the other mechanisms. Nevertheless, inspection of the predictions in Figs. V.1 to V.31 shows how varied these predictions can be:

H (Fig. V.2): None of the mechanisms shows the sharpness of the

peak that appears in the data, but each predicts the peak and is within an order of magnitude of the data.

H₂ (Fig. V.3): The present data and those of Bonne et al. (1965) had been in good agreement, but the predictions are significantly high (WZ and WZ') or low (MMSK, WB, WD), in each case by about 8 mol%.

CH (Fig. V.4): Predictions vary by two or more orders of magnitude for this species. Upper limits determined in the flame imply that WZ and WZ' overpredict CH, but the need for more data is apparent.

CH₂ (Fig. V.5): Data appear to support the predictions of WZ and WZ' in the early part of the flame below 1700 K. Methylene chemistry is especially neglected, as no existing mechanism takes the fundamental distinctions between triplet methylene (³CH₂) and singlet methylene (¹CH₂) into account. Ground-state ³CH₂ is quite reactive, but electronically excited ¹CH₂ is even more reactive to many species and can be an appreciable fraction of the total CH₂. Furthermore, ³CH₂ reacts by abstraction and by radical addition, while ¹CH₂ inserts into σ and π bonds. The problems due to this ambiguity between ¹CH₂ and ³CH₂ should be worst at higher temperatures, where the equilibrium population of ¹CH₂ is highest.

CH₃ (Fig. V.6): WZ and WZ' predictions agree quite well beyond 1 cm, which is caused by partial equilibration of metathesis reactions with CH₄. WD agrees reasonably well in magnitude and best reproduces the shape of the curve.

CH₄ (Fig. V.7): None of the predictions is especially good, and MMSK did not include this species. All predicted the increase at the greater distances from the burner, which is a consequence of the decreasing temperature and the temperature dependence of the equilibrium constant.

O-atom (Fig. V.8): The shapes are similar for all five mechanisms although magnitudes vary.

C₂H (Fig. V.11): The limited data support WZ and WZ', but measurements in the predicted high-concentration region were not successful. WB is too high, but more data are required for this growth species.

C_2H_4 (Fig. V.13): WZ and WZ' gave the best predictions, but the sharpness and magnitude of the initial peak was not predicted.

Mass 29, HCO and/or C_2H_5 (Figs. V.15, V.16): MMSK, WZ, and WZ' predict the data well as being HCO, while WB and WD significantly overpredict HCO (Fig. V.16).

Mass 30, H_2CO and/or C_2H_6 (Figs. V.17, V.18): Mass 30 is overpredicted by all the mechanisms (Fig. V.17). The shapes of the predictions suggest that the data are C_2H_6 and that H_2CO is the problem species (Fig. V.18).

CH_3O and CH_2OH (Fig. V.19): Although no data are available for comparison, the variation among predictions is notable.

O_2 (Fig. V.20): The data and all the mechanisms except WB show that destruction of O_2 slows dramatically as the concentration decreases to tens of ppm. WZ and WZ' fit the data best.

HO_2 (Fig. V.21): Data were restricted to 0.8 cm or less, but the predictions were all poor.

H_2O_2 (Fig. V.22): Predictions of H_2O_2 by WB compare favorably to a measured mole fraction of $5 \cdot 10^{-5}$ at 0.176 cm. WD and MMSK were still lower, and WZ and WZ' did not include the species.

Ar (Fig. V.24): These predictions show that all mechanisms were within 0.01 of the measured Ar mole fraction, which changed from 0.05 to 0.04 through the flame.

Mass 41, HCCO and/or C_3H_6 (Fig. V.25): Only WD included C_3H_5 , but its prediction agrees rather well within the noise of the data for mass 41. In contrast, HCCO is clearly overpredicted by each of the mechanisms.

Mass 42, CH_2CO and/or C_3H_6 (Fig. V.26): Mass 42 is not predicted well by any of the mechanisms, although C_3H_6 predictions by WD are similar to the mass 42 data. CH_2CO predictions are all higher than the data except for WZ and WZ', which are low. This low prediction is caused by the assignment of classical fall-off kinetics by Warnatz to the reaction $C_2H_2+OH \rightarrow H+CH_2CO$. In fact, addition/stabilization to form C_2H_2OH would have the classical behavior that Warnatz assumed, in which the rate constant decreases markedly as temperature increases (Smith et al., 1984). The product channel $H+CH_2CO$ would be a chemically activated addition/decomposition, which

has inverse fall-off behavior (Ch. VI, IX) and a rate constant that rapidly increases as temperature (and fall-off of the adduct channel) increases.

C_4H_3 (Fig. V.29): Despite the noise in the data, comparison to predictions unquestionably rules out the excessive production of C_4H_3 by WZ and WZ' and the insufficient production by MMSK. WB gives a reasonably good prediction. Note that the isomers 1- C_4H_3 and 2- C_4H_3 are not distinguished in the mechanisms.

C_4H_6 (Fig. V.30): Neither C_4H_4 nor C_4H_5 is included in any of the mechanisms, but WB and WD include C_4H_6 . Unfortunately, these predictions are unsatisfactory.

C_6H_2 (Fig. V.31): Only the Warnatz mechanism includes a C_6 species, and the reversible modification WZ' predicts the data reasonably well. The WZ mechanism as described by Warnatz gives too high a prediction by a factor of three.

V.6. Summary and conclusions

Although published mechanisms adequately describe some features of acetylene combustion chemistry, testing against detailed species profiles reveals deficiencies that can be important in modeling fuel-rich and sooting acetylene flames. H_2O and CO_2 are strongly affected by the product branching and rates of CH_2+O_2 and, for MMSK, of C_4H_2+OH ; only WZ and WZ' predict shape and magnitude well for both species. The absence of destruction kinetics for C_3 species in MMSK and WD leads to a misprediction that they would be formed in excessive quantities, acting as a significant sink for carbon and hurting predictions for many other species. Peculiarities in the OH prediction are caused by differences in $C_2H_3+O_2$ kinetics, and C_2H_3 is affected both by uncertainties in that reaction and, in WD, by the inclusion of a C_3H_6 pyrolysis to C_2H_3 .

These limitations point out ways in which the mechanisms can be improved. The destruction kinetics of C_3H_4 , C_4H_2 , and the radicals CH_2 , C_2H_3 , C_3H_2 , and C_3H_3 are shown to need attention. For these and other "minor" species, particularly CH and C_2H , the chemistry is not well-understood despite the importance of these radicals to

hydrocarbon flame chemistry and to flame processes like nitrogen fixation.

The comparison of WZ and WZ' emphasizes that mechanisms of elementary reactions should include microscopic reversibility even though the calculation is limited by the availability of accurate thermodynamics. The reverse reaction might have been unimportant at earlier test conditions, but it can become important at new conditions.

Finally, the accurate treatment of chemically activated reactions is another important area for improvement, as are the kinetics for growth and destruction of C₄ and heavier hydrocarbons, including aromatics.

CHAPTER VI. EQUATIONS FOR UNIMOLECULAR AND BIMOLECULAR QRRK

Bimolecular QRRK is a powerful tool for predicting and extrapolating rate constants of addition-initiated reactions. Bond making is exothermic, so the freshly formed adduct is "chemically activated" with respect to its ground state. There is a kinetic competition for the excited states of this adduct between collisions (leading to stabilization) and unimolecular reactions that can re-form the reactants or form new products. Among the possible consequences of this competition are pressure-dependent and non-Arrhenius rate constants for addition, chemically activated decompositions, chemically activated isomerizations, and low- and high-pressure limits for the rate constant of each product channel.

Unimolecular reaction theory is the basis for analyzing these problems. It is reviewed briefly in Sec. VI.2, followed in Sec. VI.3 by a description of the classical (unimolecular) QRRK method (Kassel, 1928b). Unimolecular QRRK equations are developed for isomerizations and multiple product channels.

Equations for bimolecular QRRK are developed in Sec. VI.4 for simultaneous addition/stabilization and addition/decomposition channels after Dean (1985). Low- and high-pressure limits are analyzed and found to have opposite meanings for the two types of channels. Again returning to the description of Dean (1985), equations that include addition/isomerization are developed in Sec. VI.5. Finally, in Sec. VI.6, multiple decompositions of the chemically activated adduct are analyzed, rationalizing two-reactant, three-product reactions that have been inferred from data.

VI.1. General background

Accurate modeling of pyrolysis and combustion chemistry demands accurate rate expressions for radical-radical and radical-molecule reactions. Generally, the rate for the elementary reaction of reactants $R+R'$ is expressed as the product of a bimolecular rate constant k_{bi} and the molar concentrations $[R]$ and $[R']$.

The rate constant k_{bi} frequently is a function only of temperature, having the form of an Arrhenius equation:

$$k_{bi} = A \cdot \exp(-E_{act}/RT) \quad [VI.1]$$

Certain small deviations from Eq. VI.1 may be fitted rationally (Cohen, 1982) by using the alternative function:

$$k_{bi} = A' \cdot T^D \cdot \exp(-E'/RT) \quad [VI.2]$$

which again is a function only of temperature. These equations are generally sufficient for metathesis reactions involving transfer of H atoms (such as $O+CH_4 \rightarrow OH+CH_3$). A key reason is that k_{bi} for such reactions is inherently independent of pressure at ideal-gas conditions.

Classical fall-off behavior for addition. - For simple addition or recombination reactions that form a stable adduct, the rate constant is independent of pressure only at "high" pressures, where it is commonly termed k_{∞} , the high-pressure limit.

At sufficiently low pressures, rate constants for addition will be directly proportional to pressure. More precisely, the bimolecular rate constant k_{bi} can be proportional to $[M]$, the overall concentration of species (P/RT for ideal gases). For example, in atom-atom recombination, the rate at atmospheric pressure is proportional to $[Atom]^2 \cdot [M]$. The bimolecular rate constant then can be divided into a pressure-independent rate constant k_0 (the "low-pressure limit") and the pressure-dependent concentration $[M]$. The rate constant k_0 is pressure-independent, but it is a function of T and of the specific species M .

At intermediate pressures, k_{bi} for addition may be in transition from the high-pressure limit of pressure-independence ($k_{bi}=k_{\infty}$) to a decreasing k_{bi} as it approaches the low-pressure limit of pressure-dependence ($k_{bi}=k_0 \cdot [M]$). This transition region is called the fall-off region.

The transition also will cause non-Arrhenius behavior at fixed pressure. At low temperatures, k_{bi} is independent of $[M]$ and would have a positive or zero E_{act} . As temperature is increased, k_{bi}

becomes pressure-dependent, decreases as $k_0 \cdot P/RT$ in the limit, and thus can have a negative E_{act} .

Qualitative explanation. - The reason for this behavior is that addition (or recombination) initially forms an excited or energized state of the adduct that contains a large amount of energy relative to its unexcited state. For recombinations, the excess is the bond dissociation energy, while for additions, the energy barrier to addition is a part of the excess. This energy must be dissipated by collisions with M if the excited adduct is to be stabilized before it can decompose to re-form the reactants. Examples are $O+CO \rightarrow CO_2$ and $H+C_2H_4 \rightarrow C_2H_5$.

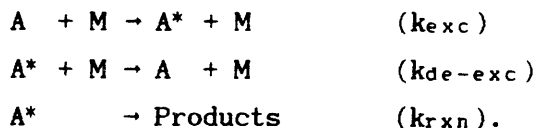
Effects of chemical activation. - Another possible consequence is that new pathways may become accessible because of chemical activation. The energized adduct may react unimolecularly to form products other than the original reactants. Because the high energy content of the adduct is caused by the reaction, this new reaction is said to be chemically activated. For example, combination of H-atom and O_2 produces excited HO_2^* , which can be collisionally stabilized to HO_2 or which can decompose, either to $H+O_2$ (the reactants) or, by a chemically activated pathway, to $O+OH$.

Based on the qualitative discussion above, it seems reasonable that chemically activated pathways could have pressure-dependent rate constants. Analysis of the issue by bimolecular QRRK will show that they display fall-off, but inversely to the classic form; that is, these rate constants will be pressure-independent in their low-pressure limits and pressure-dependent in their high-pressure limits.

VI.2. Unimolecular reaction theory

The basis of our understanding of the bimolecular rate constant is the occurrence of gas-phase reactions that have first-order, or unimolecular, kinetics. Unimolecular reaction theory (Robinson and Holbrook, 1972; Forst, 1973) has been quite successful in qualitatively and quantitatively describing high-pressure limits, low-pressure limits, and fall-off for simple pyrolyses, which are the reverse of simple additions.

In 1922, Lindemann rationalized the unimolecular reaction of a species A as occurring by a competition among collisional excitation to A*, collisional de-excitation of A*, and true unimolecular reaction of A* (Laidler, 1965):



Here, A* is an excited or energized state of the species A; an energy diagram for the system is shown in Fig. VI.1. The apparent unimolecular rate constant, assuming at this point in the development only a single excited state, is:

$$k_{\text{uni}} = \frac{1}{[\text{A}]} \cdot \frac{d[\text{Products}]}{dt} = \frac{1}{[\text{A}]} \cdot k_{\text{rxn}} \cdot [\text{A}^*] \quad [\text{VI.3}]$$

or, by a pseudo-steady-state assumption for the concentration of A*,

$$k_{\text{uni}} = k_{\text{rxn}} \cdot \frac{1}{1 + \frac{k_{\text{rxn}}}{k_{\text{de-exc}} \cdot [\text{M}]}} \cdot \left(\frac{k_{\text{exc}}}{k_{\text{de-exc}}} \right) \cdot \quad [\text{VI.4}]$$

(This could be reduced to a simpler form still, but, as will be shown, the ratio $k_{\text{exc}}/k_{\text{de-exc}}$ is usefully kept separate.) Eq. VI.4 also may be restated in terms of its high-pressure limit k_{∞} and its low-pressure limit $k_0 \cdot [\text{M}]$ as:

$$\frac{k_{\text{uni}}}{k_{\infty}} = \frac{1}{1 + \frac{k_{\infty}}{k_0 \cdot [\text{M}]}} \quad , \quad [\text{VI.5}]$$

the general Lindemann form. For $k_{\text{de-exc}}$, Lindemann used Z, the collision-theory rate constant. This is the strong-collision assumption that essentially all collisions are de-activating. The ratio $k_{\text{exc}}/k_{\text{de-exc}}$ in this formulation is an equilibrium constant for excitation from A to A*, which Lindemann described as a Boltzmann

distribution $\exp(-E_0/RT)$, where E_0 is the energy barrier to reaction (see Fig. VI.1) and, for Lindemann, the energy content of A^* relative to A .

The importance of Lindemann's equation was to rationalize qualitatively the first-order, unimolecular rate constant as k_∞ . The occurrence of a low-pressure limit and the general shape of the fall-off curve, $\log(k_{uni})$ vs. $\log(P)$ at a given T , were also correct. Quantitatively, the equation was not successful. The experimental transition occurred over a broader range of pressures than predicted, and the choice of species for M had a greater effect on k_0 than would have been predicted from the effect of M on Z .

More sophisticated methods were developed later to analyze the components of the Lindemann model. Several useful methods retained the structure of Eq. VI.4, but the new equations referred instead to the rate constant for reaction via A^* at each energy level E . Equation VI.4 then gives an energy-specific $k_{uni}(E)$, and $k_{uni}(E)$ is summed or integrated over the range of energy. To describe this energy-dependent $k_{uni}(E)$, the terms k_{exc}/k_{de-exc} , k_{rxn} , and k_{de-exc} were treated more realistically.

First, the ratio k_{exc}/k_{de-exc} was treated more accurately. Hinshelwood recognized that it is the internal modes of energy storage - primarily vibrations - that should be excited (Robinson and Holbrook, 1972). Excitation to a given energy then would be faster for more complex molecules because they have more vibrational degrees of freedom that can be excited. Furthermore, excitation will produce a distribution of energies $E \geq E_0$. By assuming that the excess energy in A^* was stored in s classical harmonic oscillators, he derived k_{exc}/k_{de-exc} as a continuous function of energy.

Rice and Ramsperger (1927) and Kassel (1928a) assumed that k_{rxn} was also a function of the energy of A^* . Following Kassel's development, if the excess energy in A^* were stored in s classical harmonic oscillators, then accumulation of sufficient energy in a given (classical) oscillator could cause reaction to occur. An appropriate form of $k_{rxn}(E)$ was then derived, and the energy-dependent Lindemann equation was integrated using $k_{de-exc} = Z$ and the Hinshelwood

k_{exc}/k_{de-exc} . Application of this classical RRK theory is complicated by the need to determine an effective number of oscillators s_{eff} , which is roughly one-half (Robinson and Holbrook, 1972) to two-thirds (Benson, 1976) of s , the total number of vibrational degrees of freedom.

RRKM theory, a modification of RRK theory by Rice and Marcus, provides a much more accurate way of calculating k_{uni} (Robinson and Holbrook, 1972). In RRKM theory, $k_{rxn}(E)$ is evaluated using the number of vibrationally excited states of A^* at a given energy. Strong-collision deactivation is assumed, but k_{exc}/k_{de-exc} is determined as a function of the energy content of A^* by counting states at each energy E using statistical mechanics. While more accurate, the application of RRKM theory is complicated by the detailed input data that are required.

Troe has developed a useful, simpler procedure for calculating k_{∞} (Troe, 1981), k_0 (Troe, 1977), and the interpolation of k_{uni} through the fall-off region (Troe, 1979). The Troe formalism has been applied successfully to a variety of unimolecular bond fissions, and it is less complex computationally than is RRKM. Nevertheless, the method seems suited best to unimolecular reactions having a single dissociation pathway.

A weakness in the methods above (except for Troe's) was the use of a strong-collision assumption for k_{de-exc} ; that is, a single collision between A^* and M would have to remove all the excess energy from A^* . Note that each species included as M would have to accommodate this energy content, regardless of its capacity for accepting the energy.

In practice, a collisional efficiency β can be applied to the strong-collision de-excitation term $Z \cdot [M]$. Analyzing collisional energy transfer by master-equation methods, Troe (1977) fit most of the temperature dependence of β with the equation:

$$\frac{\beta}{1 - (\beta)^{1/2}} = \frac{-\langle \Delta E_{coll} \rangle}{F(E) \cdot kT} \quad [VI.6]$$

where $\langle \Delta E_{coll} \rangle$ is the average amount of energy transferred per collision and $F(E)$ is a factor, weakly dependent on energy, that is

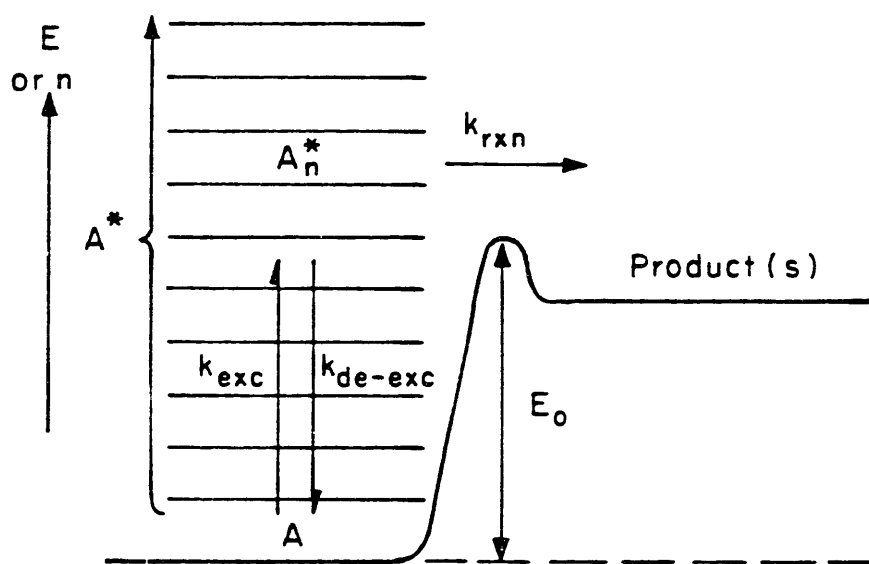


Fig. VI.1. Energy diagram for unimolecular decomposition.

related to the number of excited states. Over the temperature range of 300–2500 K for a series of reactions (Troe, 1977), $F(E)=1.15$ was a median value. The value of β also depends on the specific third-body molecule M through the value of $\langle \Delta E_{coll} \rangle$.

VI.3. Unimolecular QRRK

Kassel's development. - The unimolecular quantum-RRK (QRRK) method (Kassel, 1928b) complements the above methods by being reasonably accurate but simpler to use. Shortly after RRK theory was proposed, Kassel described this alternative method, treating the storage of vibrational energy as being quantized. Although RRK theory has been used more extensively for simple calculations, QRRK has been recognized to be more realistic than RRK (Robinson and Holbrook, 1972). Also, QRRK does not require an adjustable parameter to achieve good accuracy. For the present purposes, QRRK also is well-suited to simple analysis of pressure effects in bimolecular reactions, where an excited adduct A^* can undergo unimolecular bond fissions or reversible isomerizations.

In QRRK theory, a molecule is treated as if its s vibrations can be represented by a single frequency ν . A geometric mean $\langle \nu \rangle$ of the molecule's frequencies is normally used (Robinson and Holbrook, 1972). Instead of treating the distribution of energy as continuous, as in RRK theory, each energy term is divided into $E/h\langle \nu \rangle$ vibrational quanta, where h is Planck's constant. For the QRRK energy variable, the symbol n is used, and for the energy barrier to reaction E_0 , the quantized energy is m quanta; quantum levels are illustrated in Fig. VI.1. The apparent k_{uni} then is a sum of Eq. VI.4 evaluated at each energy level n from 0 ($E=E_0$) to ∞ . Noting that $k_{rxn}(E)=0$ for $n < m$, then

$$k_{uni} = \sum_{\substack{E=E_0 \\ (n=m)}}^{\infty} k_{rxn}(E) \cdot \frac{k_{de-exc}^{[M]}}{k_{de-exc}^{[M]} + k_{rxn}(E)} \cdot K(E,T) \quad [VI.7]$$

where $K(E,T)$ is the thermal-activation distribution function

k_{exc}/k_{de-exc} in Eq. VI.4; $k_{exc}[M]=k_{de-exc}[M] \cdot K(E,T)$ is the rate constant for formation of A^* as a first-order process in $[A]$.

Kassel assumed, as in the classical RRK theory, that if a molecule were excited to an energy E , then $k_{rxn}(E)$ would be proportional to the the probability that one of the s oscillators could have energy E_0 or greater (sufficient energy to cause reaction). In a real molecule, vibrational energy is quantized, but in classical RRK theory, the energy distribution was treated as continuous. Then, in terms of vibrational quanta, $k_{rxn}(E)$ would be proportional to the probability that one of the s oscillators could contain m or more of the n total quanta. The proportionality constant subsequently was shown to be the Arrhenius pre-exponential factor A_∞ (high-pressure limit) for dissociation of A , so:

$$k_{rxn}(E) = A_\infty \cdot \frac{n!(n-m+s-1)!}{(n-m)!(n+s-1)!} \quad [VI.8]$$

Likewise, he derived the quantized thermal energy distribution $K(E,T)$ to be:

$$K(E,T) = (e^{-h\nu/\kappa T})^n \cdot (1 - e^{-h\nu/\kappa T})^s \cdot \frac{(n+s-1)!}{n!(s-1)!}, \quad [VI.9]$$

where κ is the Boltzmann constant.

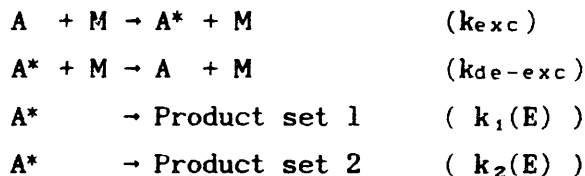
Low-pressure limit. - An explicit expression for the rate constant in the limit of low pressure ($[M]=P/RT \rightarrow 0$) can then be derived from Eq. VI.7 to be:

$$\lim_{[M] \rightarrow 0} k_{uni} = \sum_{\substack{E=E_0 \\ (n \neq m)}}^{\infty} k_{de-exc}[M] \cdot K(E,T) \quad [VI.10]$$

As it must, k_{uni} reduces to $k_{rxn,\infty}$ in the high-pressure limit.

Multiple decomposition channels. - A key step in the previous analysis was derivation of the concentration $[A^*]$ from a pseudo-steady-state assumption. This $[A^*]$ was substituted in Eq. VI.5 to obtain Eq. VI.4 or, as $[A^*]$ in the QRRK form, Eq. VI.7.

If multiple channels exist, forming different sets of decomposition products, the same sort of analysis can be made with a result similar to Eq. VI.7. Let the channels be designated as $i=1,2,\dots$ so that the fate of A^* is determined by the reactions



and so on. Each channel has Arrhenius parameters A_i, ∞ and E_i, ∞ , and the energy barrier E_i, ∞ is quantized to \hbar by $h\langle\nu_A\rangle$ as before. Each $k_i(E)$ is calculated with Kassel's equation (Eq. VI.8) using the corresponding \hbar .

As a consequence, the multiple decomposition rate constants occur as a sum in the denominator of $[A^*]_{ss}$ and of $k_{uni,i}$:

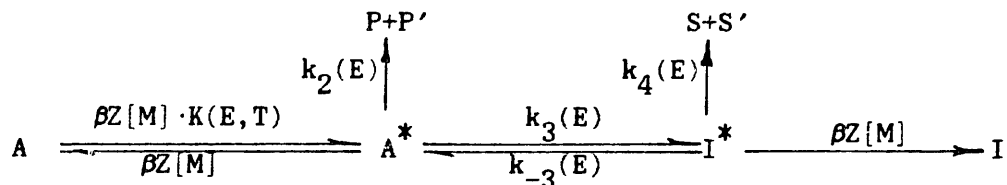
$$\begin{aligned} k_{uni,i} &= \sum_{\substack{E=0 \\ (n \neq 0)}}^{\infty} k_i(E) \cdot \frac{k_{de-exc}[M]}{k_{de-exc}[M] + \sum_i (k_i(E))} \cdot K(E,T) \\ &= \sum_{\substack{E=0 \\ (n \neq 0)}}^{\infty} k_i(E) \cdot \frac{\beta Z[M]}{\beta Z[M] + \sum_i (k_i(E))} \cdot K(E,T) \end{aligned} \quad [VI.11]$$

This is virtually the same equation as Eq. VI.7. The lower limit on E or n is written here explicitly as zero (unexcited A), and the summation effectively would begin at the lowest energy barrier \hbar .

It is worth noting the two implicit assumptions that β is still the appropriate collision efficiency and that $K(E,T)$ is still the appropriate energy distribution. Practically, β is determined for single-channel unimolecular reactions and correlated with $\langle\Delta E_{coll}\rangle$. Just and Troe (1983) have proposed that a second collision efficiency may be better for the second, higher energy barrier. Also, $K(E,T)$ may overpredict the distribution at high energy levels if the population of these levels is depleted by the reaction channels. The

second question is also relevant to single-channel reactions and is best addressed by master-equation methods (Pritchard, 1985) that explicitly calculate state-to-state energy transfer.

Unimolecular reaction with isomerization. - Unimolecular QRRK equations can be derived for isomerization reactions, which introduce the additional complexity that the excited isomer I* can itself decompose (channel 2) or it can re-isomerize to A*:



Note that this scheme allows for decompositions of A* and of I*.

Equations are derived as before, except that [A_n*] and [I_n*] are both evaluated using the pseudo-steady-state assumption. The observable rate constant for forming I then is a sum over energy of βZ[M] · [I_n*], and for forming S+S' is a sum of k₄(E) · [I_n*]. The equations that result are, for unimolecular decomposition of A to P+P':

$$k_d = \sum_{\substack{E=0 \\ (J=0)}}^{\infty} \frac{k_2(E) \cdot \beta Z[M] \cdot K(E,T) \cdot (\beta Z[M] + k_{-3}(E) + k_4(E))}{(\beta Z[M] + k_2(E) + k_3(E)) \times (\beta Z[M] + k_{-3}(E) + k_4(E)) - k_{-3}(E)k_3(E)}, \quad \text{[VI.12]}$$

for unimolecular isomerization/stabilization or A → I:

$$k_I = \sum_{\substack{E=0 \\ (J=0)}}^{\infty} \frac{k_3(E) \cdot (\beta Z[M])^2 \cdot K(E,T)}{(\beta Z[M] + k_2(E) + k_3(E)) \times (\beta Z[M] + k_{-3}(E) + k_4(E)) - k_{-3}(E)k_3(E)}, \quad \text{[VI.13]}$$

and for unimolecular isomerization/decomposition or A → S+S':

$$k_{I/d} = \sum_{\substack{E=0 \\ (I \neq 0)}}^{\infty} \frac{k_4(E) \cdot k_3(E) \cdot \beta Z[M] \cdot K(E, T)}{(\beta Z[M] + k_2(E) + k_3(E)) \times (\beta Z[M] + k_{-3}(E) + k_4(E)) - k_3(E)k_{-3}(E)} \quad [\text{VI.14}]$$

These equations all have the same denominator, all are summations from $I=0$ to ∞ , and all contain the same excitation term $k_{exc}[M] = \beta Z[M] \cdot K(E, T)$. If isomerization and multiple decomposition channels were to occur, $k_2(E)$ would be replaced in the numerator by the other decomposition rate constant(s) $k_i(E)$, and it would be replaced in the denominator by a sum of the decomposition rate constants.

Low-pressure limit for isomerization reactions. - It is instructive to note the form of the low-pressure limit for simple, reversible isomerization, neglecting any decomposition channels ($k_2(E) = k_4(E) = 0$). The full equation for the rate constant of $A \rightarrow I$ in this case is a simplified Eq. VI.13:

$$k_I = \sum_{\substack{E=0 \\ (I \neq 0)}}^{\infty} \frac{k_3(E) \cdot (\beta Z[M])^2 \cdot K(E, T)}{(\beta Z[M] + k_3(E)) \times (\beta Z[M] + k_{-3}(E)) - k_3(E)k_{-3}(E)} \quad [\text{VI.15}]$$

Evaluating the limit as $[M] \rightarrow 0$ requires the use of l'Hôpital's rule, yielding an expression like Eq. VI.10 (low-pressure limit for simple unimolecular decomposition) but with a term involving K_{eq} , the equilibrium constant for isomerization:

$$\lim_{[M] \rightarrow 0} k_I = \sum_{\substack{E=E_0 \\ (I \neq 0)}}^{\infty} 2 \left(\frac{K_{eq}}{K_{eq} + 1} \right) \beta Z[M] \cdot K(E, T) \quad [\text{VI.16}]$$

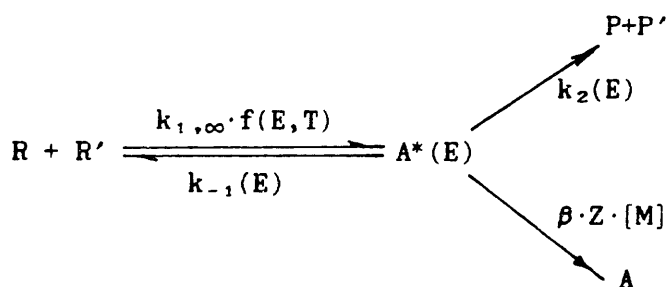
This expression will equal Eq. VI.10 only if $K_{eq} = 1$. If the isomerization is irreversible ($K_{eq} \gg 1$), the asymptotic value of the low-pressure limit is twice the result of Eq. VI.10. If the isomerization is thermodynamically unfavorable ($K_{eq} \ll 1$), then:

$$\lim_{\substack{[M] \rightarrow 0; \\ K_{eq} \ll 1}} k_I = \sum_{\substack{E=E_0 \\ (I=m)}}^{\infty} 2K_{eq} \cdot \beta Z[M] \cdot K(E,T) \quad , \quad [VI.17]$$

a low-pressure limit much lower than that predicted by Eq. VI.10, in which there were no decomposition channels included.

VI.4. Bimolecular QRRK - Chemically activated decomposition

Dean (1985) has developed the QRRK equations which apply to bimolecular reactions. A similar formulation and extensions of those equations are derived here. Consider the general case of addition to form an excited adduct A^* , followed by stabilization, redissociation to reactants, or chemically activated decomposition:



Here, $k_{1,\infty}$ is the rate constant in the high-pressure-limit for forming adduct and $f(E,T)$ is the energy distribution for chemical activation:

$$f(E,T) = \frac{k_{-1}(E) \cdot K(E,T)}{\sum_{\substack{E=E_{-1} \\ (I=m_{-1})}}^{\infty} k_{-1}(E) \cdot K(E,T)} \quad , \quad [VI.18]$$

derived (Dean, 1985) by analogy from the RRKM formulation (Robinson and Holbrook, 1972); $K(E,T)$ is the QRRK thermal distribution from Eq. VI.9. Rate constants $k_{-1}(E)$ and $k_2(E)$ are calculated from the QRRK equation for $k_{rxn}(E)$ (Eq. VI.8) using m_{-1} ($E_{-1}/h\langle\nu\rangle$) and m_2 ($E_2/h\langle\nu\rangle$), respectively. A typical energy diagram for these reactions is shown in Fig. VI.2.

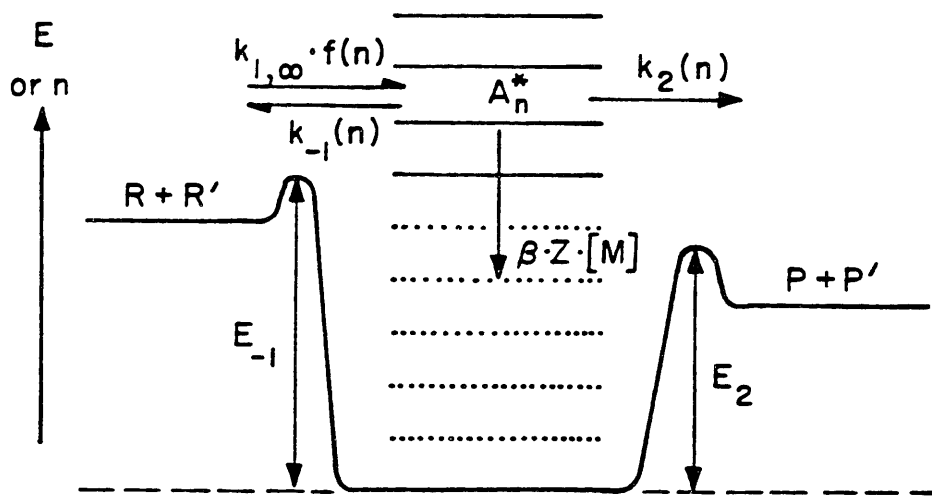


Fig. VI.2. Energy diagram for addition with a chemically activated decomposition channel.

For a given quantum level n , a pseudo-steady-state analysis can be made with a result analogous to Eq. VI.4. Then, analogously to the QRRK k_{uni} (Eq. VI.7), the experimentally observable rate constant for forming the addition/stabilization product A from R+R' is:

$$k_{a/s} = \sum_{\substack{E=E_{-1} \\ (J=J_{-1})}}^{\infty} \frac{k_{1,\infty} \cdot \beta Z[M]}{\beta Z[M] + k_{-1}(E) + k_2(E)} \cdot f(E,T) \quad [VI.19]$$

and, for forming the addition/decomposition products P and P', the observable rate constant is:

$$k_{a/d} = \sum_{\substack{E=E_{-1} \\ (J=J_{-1})}}^{\infty} \frac{k_{1,\infty} \cdot k_2(E)}{\beta Z[M] + k_{-1}(E) + k_2(E)} \cdot f(E,T) \quad [VI.20]$$

If more than one dissociation channel is available, the $k_{rxn}(E)$ for each channel is added in the denominator of Eq. VI.19 and VI.20, and an equation in the form of Eq. VI.20 is written for each new channel, substituting the respective $k_{rxn}(E)$ for $k_2(E)$ in the numerator.

Low- and high-pressure limits. - The structure of these equations effectively shows the dynamics among its components because each term has a readily understood physical significance. For example, as pressure changes, the observable rate constants change because of the relative magnitudes of terms in the denominator - $\beta \cdot Z \cdot [M]$ for deactivation, $k_{-1}(E)$ for dissociation to reactants, and $k_2(E)$ for dissociation to new products. It is especially useful to consider the low-pressure and high-pressure limits of the stabilization and the chemically activated reactions.

The low-pressure limit for recombination (or addition) is derived from Eq. VI.19:

$$\lim_{[M] \rightarrow 0} k_{a/s} = \sum_{\substack{E=E_{-1} \\ (J=J_{-1})}}^{\infty} \frac{k_{1,\infty} \cdot \beta Z[M]}{k_{-1}(E) + k_2(E)} \cdot f(E,T) \quad [VI.21]$$

which is directly proportional to pressure through [M]. In the high-pressure limit, Eq. VI.19 reduces properly to $k_{1,\infty}$. At a given temperature, a fall-off curve for stabilization joins these asymptotes, plotted as $\log(k_{a/s})$ vs $\log(P)$.

Ignoring the chemically activated pathway could give incorrect recombination rate constants. If chemically activated conversion of A^* is more rapid than decomposition to reactants ($k_2(E) \gg k_{-1}(E)$), then Eq. VI.21 shows that the recombination $k_{a/s,0}$ will be determined by $k_2(E)$ rather than by $k_{-1}(E)$.

Chemically activated pathways will have an inverse fall-off behavior, having rate constants that are pressure-independent at low pressure but inversely proportional to pressure at high pressure. From Eq. VI.20, the rate constant for the chemically activated pathway to P and P' will have a low-pressure asymptote:

$$\lim_{[M] \rightarrow 0} k_{a/d} = \sum_{i=1}^{\infty} \frac{k_{1,\infty} \cdot k_2(E)}{k_{-1}(E) + k_2(E)} \cdot f(E,T) \quad [\text{VI.22}]$$

that contains no [M] term to cause pressure dependence. At high pressures, the same pathway would have an asymptote:

$$\lim_{[M] \rightarrow \infty} k_{a/d} = \frac{1}{[M]} \cdot \sum_{i=1}^{\infty} \frac{k_{1,\infty} \cdot k_2(E)}{\beta Z} \cdot f(E,T) \quad [\text{VI.23}]$$

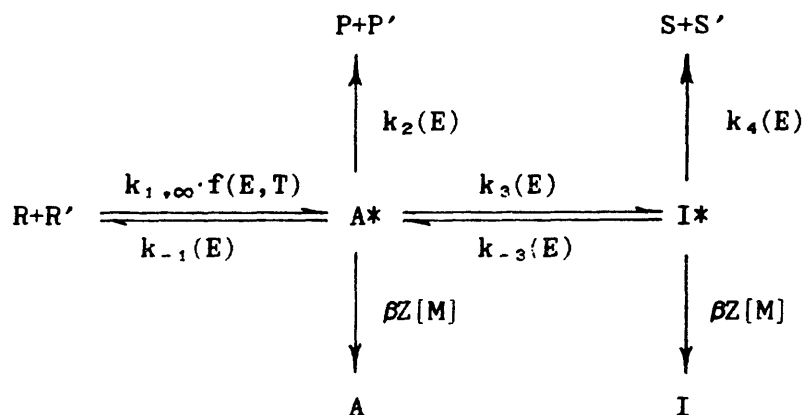
which is *inversely* proportional to pressure. Thus, the fall-off curve for a simple chemically activated decomposition would have a mirror-image shape of the classical addition fall-off curve, falling off from pressure-independence as pressure *increases*.

VI.5. Bimolecular QRRK with chemically activated isomerization

Chemically activated isomerization is a plausible extension of the above phenomena. Any unimolecular reaction that is open to the ground-state adduct also can occur for the excited adduct, and isomerization clearly fits this requirement. The one complication is that an excited isomer is formed, so chemically activated pathways of

the isomer must be considered, including re-isomerization back to the adduct.

The general form of this reaction network, including chemically activated decomposition and isomerization, may be described schematically in terms of the variables described previously:



For each set of stabilized products, the rate of formation can be described by an apparent bimolecular rate constant with respect to reactants R and R'. For products A (addition/stabilization), P and P' (addition/decomposition), I (isomerization/stabilization), and S and S' (isomerization/decomposition), respectively, the rate constants are:

$$k_{a/s} = \sum_{\substack{E=E_{-1} \\ (I=m_{-1})}}^{\infty} \frac{\beta Z[M]}{\beta Z[M] + k_{-1}(E) + k_2(E) + k_3(E) - Q} \cdot k_{1,\infty} \cdot f(E,T) \quad [\text{VI.24}]$$

$$k_{a/d} = \sum_{\substack{E=E_{-1} \\ (m_{-1})}}^{\infty} \frac{k_2(E)}{\beta Z[M] + k_{-1}(E) + k_2(E) + k_3(E) - Q} \cdot k_{1,\infty} \cdot f(E,T) \quad [\text{VI.25}]$$

$$k_{I/s} = \sum_{\substack{E=E_{-1} \\ (m_{-1})}}^{\infty} \frac{\beta Z[M] \cdot k_3(E) \cdot \{k_{-3}(E) + \beta \cdot Z \cdot [M] + k_4(E)\}}{\beta Z[M] + k_{-1}(E) + k_2(E) + k_3(E) - Q} \cdot k_{1,\infty} \cdot f(E,T) \quad [\text{VI.26}]$$

$$k_{I/d} = \sum_{\substack{E_{-1} \\ (I=m-1)}}^{\infty} \frac{k_4(E) \cdot k_3(E) \cdot \{k_{-2}(E) + \beta Z[M] + k_4(E)\}}{\beta Z[M] + k_{-1}(E) + k_2(E) + k_3(E) - Q} \cdot k_{1,\infty} \cdot f(E, T) \quad [\text{VI.27}]$$

where:

$$Q = \frac{k_{-2}(E) \cdot k_3(E)}{\beta Z[M] + k_{-3}(E) + k_4(E)} \quad [\text{VI.28}]$$

Additional addition/decomposition channel(s) j may be included by calculating $k_j(E)$, replacing $k_2(E)$ by a sum of $k_j(E)$ in the denominators of Eq. VI.24 through VI.27, and writing a rate constant $(k_{a/d})_j$ in the new form of Equation VI.25, substituting $k_j(E)$ in the numerator for $k_2(E)$.

VI.6. Secondary decompositions of excited products

Secondary decomposition can occur in a chemically activated reaction if all the excess energy of the chemically activated adduct is not dissipated by the initial decomposition. Thus, a bimolecular reaction could lead to three products by the processes $R+R' \rightarrow A^* \rightarrow P^*+P'^*$, $P^* \rightarrow P$, and $P'^* \rightarrow S+S'$. Branching studies might indicate A , $P+P'$, or $P+S+S'$ as product channels.

Such branched three-product channels have been inferred from data in the past, for example $\text{CH}_3+\text{CH}_3 \rightarrow \text{C}_2\text{H}_6$, $\text{C}_2\text{H}_5+\text{H}$, and $\text{C}_2\text{H}_4+2\text{H}$. In such cases, either the observation has not been explained or it has been attributed to a sequence of thermal reactions $R+R' \rightarrow P+P'$ and $P' \rightarrow S+S'$. However, unlike a thermal sequence, chemically activated secondary decomposition is not microscopically reversible because the reverse reaction would require excited P'^* (from $S+S'$) as a reactant.

Properly apportioning the undissipated energy between P^* and P'^* is the difficulty in calculating the apparent rate constant. If P^* is an atom and P'^* is polyatomic, then all the undissipated energy may be assigned to the species P'^* as a first approximation. The rationale is that the excess in A^* is treated as stored in vibrational energy modes. The polyatomic P'^* contains vibrational degrees of freedom, while the atom P^* has neither vibrational or rotational

modes (i.e., it can only be translationally hot). Decomposition or stabilization of P'^* then is calculated by unimolecular reaction theory.

By similar reasoning, if both P^* and P'^* are polyatomic, then the undissipated chemical-activation energy should be apportioned by the vibrational energy storage capacity of each.

Analysis by QRRK first requires calculation of the rate constant for chemically activated decomposition $k_{a/d}(n)$ at energy level n (term within the summation of Eq. VI.20 or VI.25). The difference between the energy $E=n \cdot h \langle \nu \rangle$ and the ground-state energies of $P+P'$ then is the undissipated energy. If only P' is polyatomic, then this energy is quantized as n' , unimolecular QRRK is used to calculate the proportions of stabilization or decomposition channels for $P'(n)$, and $k_{a/d}(n)$ is divided up accordingly.

If both P^* and P'^* are polyatomic, QRRK methods would treat their energy storage as being within s and s' harmonic oscillators. The undissipated energy would be divided between the two species. The amount of energy that each could contain would be proportional to $s \cdot \exp(h\nu/kT)$ and $s' \cdot \exp(h\nu'/kT)$, and a reasonable assumption is that the excess energy could be assigned proportionally to energy storage capacity.

Note that this analysis requires only that some of the energy of A^* be undissipated by the decomposition to P^* and P'^* . Thus, the same phenomenon of secondary decomposition can result from unimolecular decomposition (Eq. VI.7 and VI.11) and from isomerization/decomposition (Eq. VI.14 and VI.27).

Rate constants for the multiple-decomposition reaction of ${}^3\text{CH}_2+{}^3\text{CH}_2 \rightarrow \text{C}_2\text{H}_2+2\text{H}$ are estimated in Ch. VII. These calculations illustrate the quantitative analysis by bimolecular QRRK, but RRKM and other sophisticated unimolecular-reaction theories also may be applied in analogous fashion.

VI.7. Implications for reaction analysis

A bimolecular adaptation of unimolecular QRRK, proposed in its original form by Dean (1985), predicts pressure and temperature dependences of many reactions important to combustion and pyrolysis.

These reactions are recombinations, additions, and insertions that form an excited intermediate. Such an excited species then may be stabilized by collisions with surrounding molecules or it may undergo energy-dependent unimolecular reactions such as decomposition and isomerization.

Using bimolecular QRRK methods, pressure-dependent rate constants may be quickly evaluated with reasonable accuracy, but the method also provides a way of clearly describing the physical significance of the different mechanistic steps. As a result, some general aspects of pressure-dependence and chemical activation, such as the low- and high-pressure limits for chemical activation, may be more obvious than they would be from more complex RRKM analysis.

Most researchers recognize that to model high-temperature gas-phase processes like pyrolysis and combustion, the pressure dependence must be taken into account for thermal decompositions and their bimolecular reverse reactions. However, pressure effects on bimolecular reactions of the form $R+R' \rightarrow P+P'$ often are omitted.

It should be emphasized that the intermediate is not the thermalized or ground-state adduct, but it is rather a distribution of excited adduct states having a distribution of energies from E_{-1} (m_{-1}) above the ground state to ∞ . Thus, the products of chemically activated decomposition are formed directly and at a different rate than if they had been formed by a sequence of thermalized reactions of recombination (to adduct) and decomposition (of adduct).

Temperature dependence of the rate constants is strongly affected by the energy distribution $f(E,T)$, which spreads toward higher energy levels as temperature increases. Also, because A^* has energies of E_{-1} and above, new channels may become accessible, even though they might be unimportant steps for thermal unimolecular reaction of A .

CHAPTER VII. TESTS AND APPLICATIONS OF BIMOLECULAR QRRK

VII.1. Introduction

Analysis of the mechanisms in Ch. V shows that many reactions important to combustion are addition or recombination reactions. In this chapter, predictions of rate constants are made using bimolecular QRRK, comparing the predictions against literature where possible. There are at least three good reasons for doing this: (1) to establish the accuracy of this simplified method; (2) to illustrate how input parameters are selected; and (3) to generate (or extrapolate) accurate rate constants for improving combustion mechanisms.

The method is a potent supplement to RRKM analysis despite being less rigorous. The key modification from the original unimolecular QRRK method is calculation of the chemical-activation distribution functions, as described in Ch. VI. Bimolecular QRRK requires only (1) k_{∞} data or estimates for the various steps and (2) a geometric-mean frequency of the adduct. In contrast, RRKM requires complete sets of frequencies, moments of inertia, and barrier heights for each transition state. While RRKM is potentially more accurate, the number, availability, and uncertainty of these input data can restrict its predictive powers, particularly for chemically activated reactions, which can involve numerous transition states for the decompositions and isomerizations of the adduct. Not only does bimolecular QRRK require fewer input data, but effects of uncertainties are readily apparent, as will be shown here.

Examples are presented here to demonstrate the method and to calculate rate constants needed for improving the realism and accuracy of flame mechanisms. First, the reactions of $H+O_2$ and $O+OH$ are shown to be classical chemical activation reactions, proceeding through excited HO_2 . Second, the series of H-atom additions to C_2H_2 , C_2H_3 , and C_2H_4 (which proceed through $C_2H_3^*$, $C_2H_4^*$, and $C_2H_5^*$) are examined, along with the C_1 reactions that share the same excited intermediates. Finally, rate constants for addition of the triplet species O to CO are calculated. Where possible, these predictions are tested against data.

VII.2. Necessary input data and limitations

Reasonably accurate predictions can be made quickly using bimolecular QRRK, in part because of the input data are few and relatively easy to obtain:

- Pre-exponential factors and activation energies in the high-pressure limit, A_{∞} and $E_{act, \infty}$;
- The number of vibrational degrees of freedom for the adduct, s ($3 \cdot n_{atoms} - 5$ for linear molecules, $3 \cdot n_{atoms} - 6$ for nonlinear);
- The geometric mean of the adduct's vibrational frequencies, $\langle \nu \rangle$;
- Molecular weight and the Lennard-Jones transport properties, σ and ϵ/k , for the adduct and for the third-body gas; and
- The average energy transferred per collision with the third-body gas, $\langle \Delta E_{coll} \rangle$, which has been experimentally evaluated for a variety of gases.

Obtaining A_{∞} and $E_{act, \infty}$ may be the most difficult. These parameters can come from literature data, from estimates by Benson's methods (Benson, 1976; Benson, 1983), from Dean's generic rate constants (Dean, 1985), or from the reverse rate constant (high-pressure-limit) and the equilibrium constant. This last approach is generally necessary at some point in the selection of input parameters, and it demands that the thermodynamics of the species be well-known.

Lennard-Jones collisional properties (Reid, Prausnitz and Sherwood, 1977; Kee et al., 1983) for the stabilized species A and the third-body gas M are used to calculate a collision number Z_{LJ} . Establishing the $\langle \Delta E_{coll} \rangle$ needed to calculate collisional efficiency β (from Eq. VI.4) is an active area of research. In Appendix M, compilations (Troe, 1979; Gardiner and Troe, 1984) are reviewed and values of $\langle \Delta E_{coll} \rangle$ are selected.

Ambiguities in these parameters cause uncertainty in the predictions. For example, the QRRK $k_{rxn}(E)$ equation (Eq. VI.8) contains the assumption that A_{∞} and $E_{act, \infty}$ are independent of temperature (purely Arrhenius behavior), but they may not be.

Second, the vibrational degrees of freedom include internal rotations, which are not approximated well as harmonic oscillators. The equivalent frequency for an internal rotation can be rather low, so uncertainty in this value can affect a geometric-mean $\langle \nu \rangle$ dramatically. Third, the assignment of all excess energy to vibrational energy can be inexact when there are significant changes in angular momentum. Finally, using a single $\langle \nu \rangle$ to represent all the ν 's in a molecule may be too great an approximation.

Nevertheless, bimolecular QRRK is remarkably effective in predicting the pressure-dependent rate constants of many combustion and pyrolysis reactions. The detailed applications here demonstrate how parameters are selected and show the nature of the results that can be obtained.

VII.3. Reactions of H+O₂, HO₂, and O+OH

Destruction of O₂ by H-atom, which is one of the most important reactions in combustion, leads to two different sets of products. A common misconception is that there are two mechanistically unrelated reactions - one dependent on pressure and forming HO₂, the other independent of pressure and forming O+OH. In fact, there are two product channels that both begin with addition to form HO₂^{*}, which can be stabilized or which can decompose.

These two pathways are important for opposite reasons. When HO₂ is formed, H, which is much more reactive, is scavenged from the system. The second, chain-branching pathway forms two highly reactive radicals, O and OH, which themselves have important roles in combustion, including the regeneration of H from reactions with H₂, H₂O, and CO. Modeling of combustion is also sensitive to the reverse reaction of O+OH to form H+O₂, and thermal decomposition of HO₂ can be significant in ignition (Warnatz, 1984).

Consequently, these rate constants have been studied extensively in experiment and theory. Most recently, Frank and Just (1985) have clarified the rate constant for H+O₂ → O+OH using shock-tube measurements at 1700 to 2500 K. Cobos et al. (1985a) studied the fall-off behavior of H+O₂ → HO₂ at 298 K. By theoretical analysis in the

latter study, k_{∞} for that reaction and k for $O+OH \rightarrow H+O_2$ were determined.

Selection of input parameters. - The broad data base of rate constants for these reactions make them good test cases for the bimolecular QRRK method. Parameters are shown on the energy diagram of Fig. VII.1 and in Table VII.1.

The first type of input data are kinetic parameters. For $O+OH \rightarrow HO_2$, k_{∞} was estimated as $2.0 \cdot 10^{13} \text{ cm}^3 \text{ mol}^{-1} \text{ s}^{-1}$ by modifying an estimation method (Benson, 1983) for recombination of alkyl radicals (Appendix N) and using geometrically estimated steric factors β . The k_{∞} for $H+O_2 \rightarrow HO_2$ was taken from Cobos et al. (1985a), and Arrhenius parameters for the reverse reactions were calculated using equilibrium constants at 298 K. All thermodynamic data were taken from the JANAF tables (Stull et al., 1971) except for $\Delta H_{f,298}^{\circ}(HO_2) = 10.5 \text{ kJ/mol}$ (2.5 kcal/mol) (Howard, 1980).

Next are the adduct properties and the collision properties of the third-body gas. The geometric mean frequency $\langle \omega \rangle$ for HO_2 is calculated to be 1734 cm^{-1} (frequencies from Stull et al., 1971) with ≈ 3 oscillators. Collision properties for HO_2 and the third-body gases were taken from Kee et al. (1983). Finally, $\langle \Delta E_{coll} \rangle$ of the third-body gases were taken from a review of the literature (Appendix M).

Tests against data. - Predictions of the rate constants are remarkably good, as shown in Figs. VII.2 through VII.5.

For k_0 of $H+O_2+M \rightarrow HO_2+M$, $M=H_2$ (Fig. VII.2), and the fall-off curve for $H+O_2 \rightarrow HO_2$ (Fig. VII.3), agreement with the data is excellent. Agreement with the pronounced non-Arrhenius behavior in Fig. VII.2 is particularly remarkable. For comparison, correlation of the fall-off curve is also shown for Troe's formalism, a method of correlation and prediction that is more parameter-rich.

Rate constants for the chain-branching reaction $H+O_2 \rightarrow O+OH$ (Fig. VII.4) are slightly higher than the data, but their temperature dependence is correct. At elevated pressures, this reaction would also be pressure-dependent, but at 100 kPa (1 atm), it is in a pressure-independent low-pressure limit (Eq. VI.22). The predicted curve of bimolecular rate constants is also shown for $H+O_2 \rightarrow HO_2$ at 1

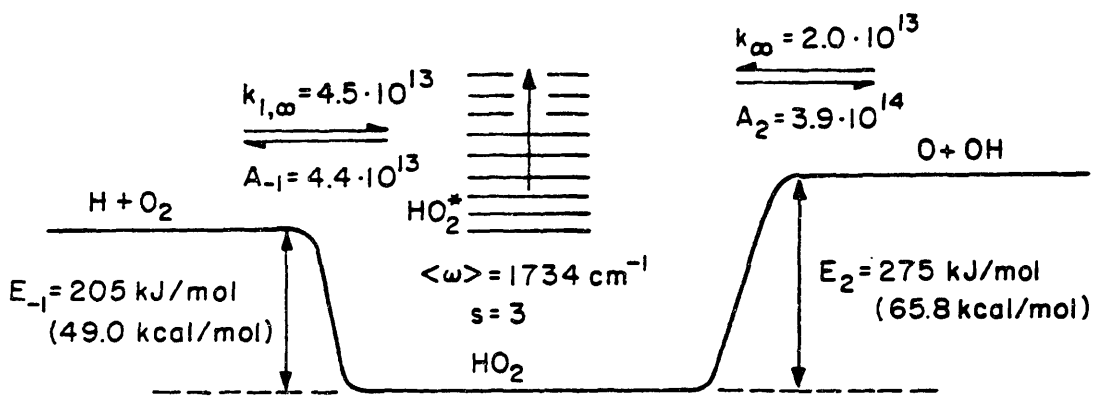


Fig. VII.1. Energy diagram for $\text{H} + \text{O}_2 / \text{HO}_2 / \text{O}(^3\text{P}) + \text{OH}$. Units are mol, cm, s, kJ.

Table VII.1. Parameters needed for bimolecular QRRK calculation in the system of reactions involving H+O₂, HO₂, and O+OH.

<u>Parameter description</u>	<u>Parameter value</u>	<u>Source</u>
High-pressure limit pre-exponential factors and activation energies:		
H+O ₂ → HO ₂	A ₀₀ =4.5·10 ¹³ cm ³ mol ⁻¹ s ⁻¹ E ₀₀ =0	Cobos et al., 1985
HO ₂ → H+O ₂	A ₀₀ =4.4·10 ¹³ s ⁻¹ E ₀₀ =49.0 kcal/mol	Microscopic reversibility
O(³ P)+OH→ HO ₂	A ₀₀ =2.0·10 ¹³ cm ³ mol ⁻¹ s ⁻¹ E ₀₀ =0	Estimate; results imply that this rate constant is k(O+OH → H+O ₂)= 3·10 ¹³ (see text)
HO ₂ → O(³ P)+OH	A ₀₀ =3.9·10 ¹⁴ s ⁻¹ E ₀₀ =65.8 kcal/mol	Microscopic reversibility
-Properties of HO₂-		
Number of vibrational degrees of freedom (<i>s</i>):	3	3·(3 atoms)-6
Geometric-mean frequency <ν _{HO₂} >:	1734 cm ⁻¹	³ √1389·1101·3414 (Stull et al., 1972)
Molecular weight	33.0 g/g-mol	-
Lennard-Jones well depth ε/ <i>K</i> and diameter σ	107.4 K, 3.458 Å	Kee et al., 1983
-Properties of M-		
M=H ₂ : Molecular weight	2.016 g/g-mol	-
ε/ <i>K</i>	38.0 K	Kee et al., 1983
σ	2.92 Å	1983
<ΔE _{coll} >	0.61 kcal/mol	Appendix M
M=He: Molecular weight	4.00 g/g-mol	-
ε/ <i>K</i>	10.2 K	Kee et al., 1983
σ	2.576 Å	1983
<ΔE _{coll} >	0.47 kcal/mol	Appendix M
M=CO: Molecular weight	28.01 g/g-mol	-
ε/ <i>K</i>	98.1 K	Kee et al., 1983
σ	3.650 Å	1983
<ΔE _{coll} >	1.2 kcal/mol	Appendix M
M=Ar: Molecular weight	39.96 g/g-mol	-
ε/ <i>K</i>	135.5 K	Kee et al., 1983
σ	3.33 Å	1983
<ΔE _{coll} >	0.74 kcal/mol	Appendix M

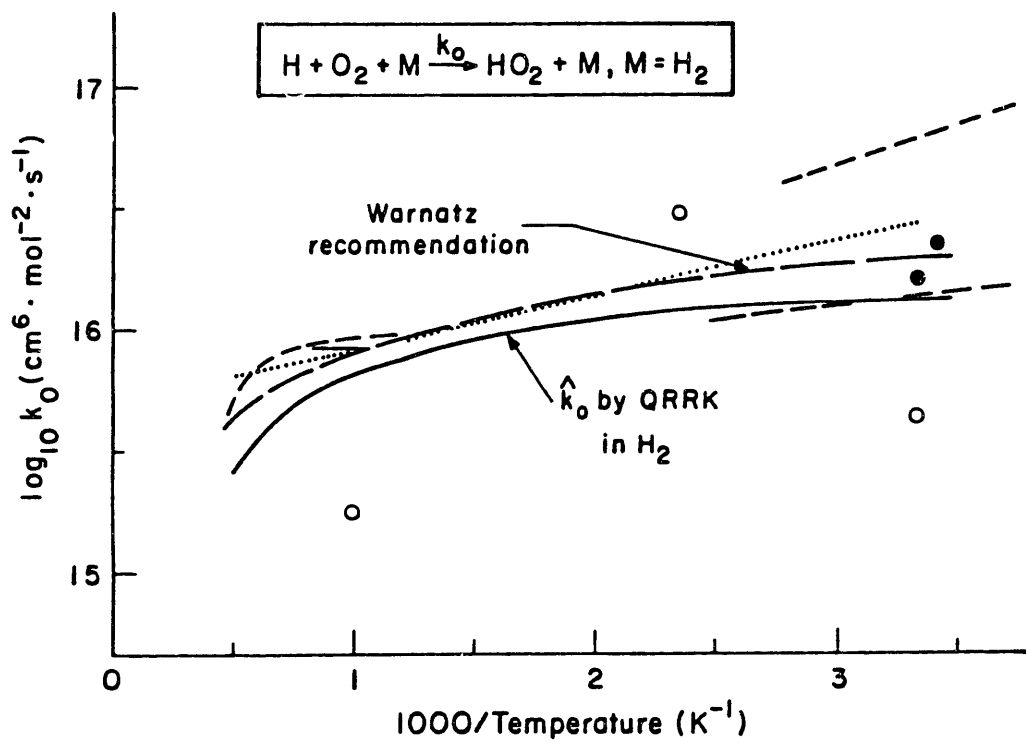


Fig. VII.2. Predicted low-pressure limit k_0 (—) for $\text{H} + \text{O}_2 + \text{M} \rightarrow \text{HO}_2 + \text{M}$, $\text{M} = \text{H}_2$, compared with literature data (---, ····, ○, and ●) and recommendation (— — —) from Warnatz (1984).

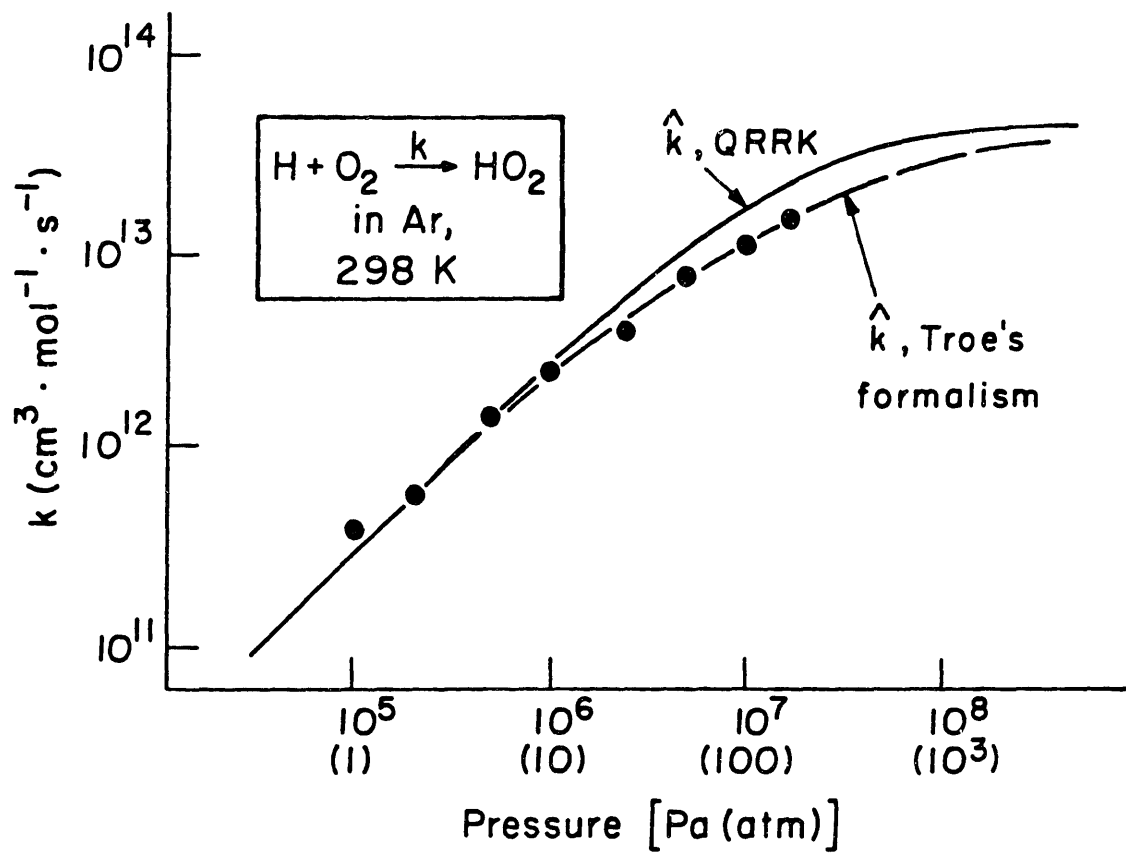


Fig. VII.3. Predicted fall-off curve (—) for $\text{H} + \text{O}_2 \rightarrow \text{HO}_2$ in Ar at 298 K compared to measurements (●) and to correlation by Troe's formalism (---) (Cobos et al., 1985a).

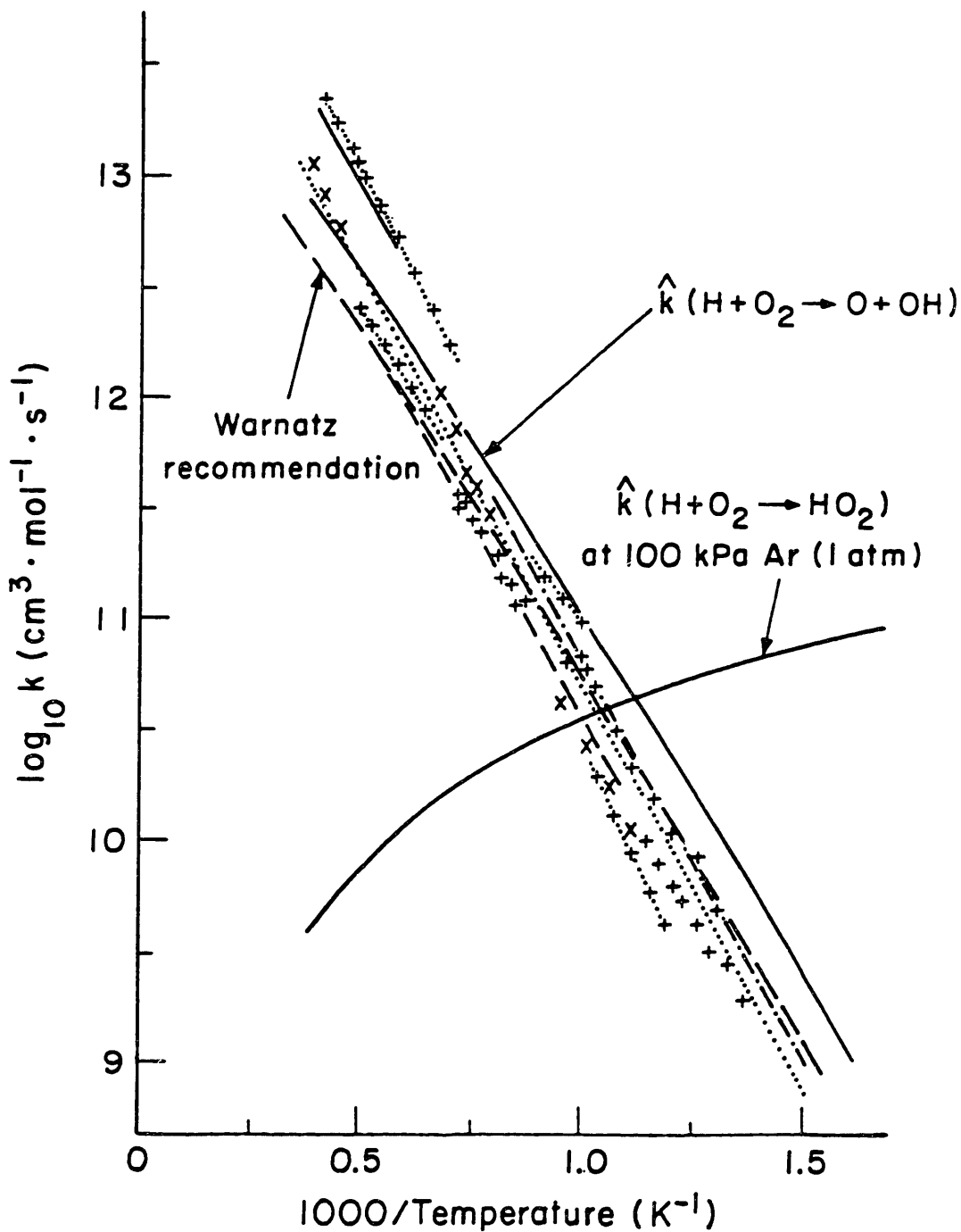


Fig. VII.4. Predicted rate constant (—) for the chemically activated addition/decomposition reaction $\text{H+O}_2 \rightarrow (\text{HO}_2)^* \rightarrow \text{O+OH}$ compared with literature data (---, ···, x, and +) and recommendation (— — —) from Warnatz (1984) and with the predicted addition/stabilization rate constant for $\text{H+O}_2 \rightarrow (\text{HO}_2)^* \rightarrow \text{HO}_2$.

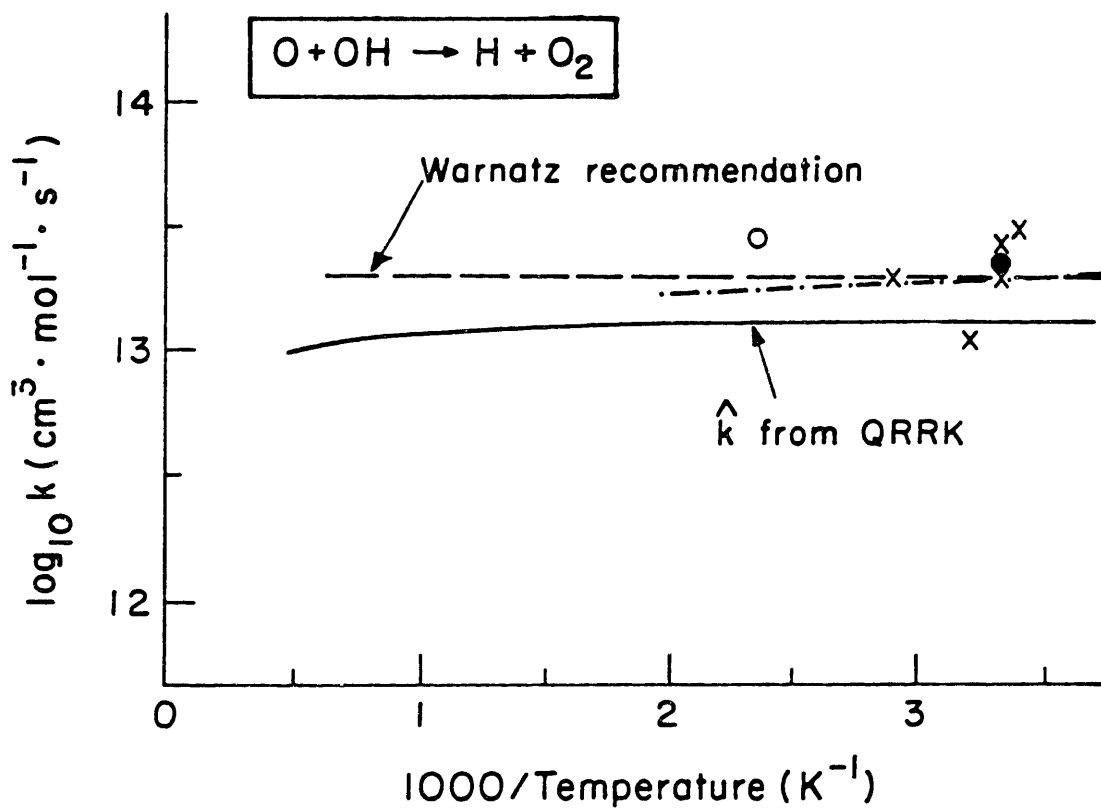


Fig. VII.5. Predicted rate constant (—) for $O+OH \rightarrow (HO_2)^* \rightarrow H+O_2$ compared to literature data (---, x, o, and •) and recommendation (— — —) from Warnatz (1984). Prediction uses estimated $k_{\infty}(O+OH \rightarrow HO_2) = 2.0 \cdot 10^{13} \text{ cm}^3 \text{ mol}^{-1} \text{ s}^{-1}$.

atm. The dominant product channel changes from HO₂ to O+OH at about 1000 K, accounting for the shift in importance of the two channels in combustion chemistry.

Finally, predictions for the chemically activated addition/decomposition reaction O+OH → H+O₂ are shown in Fig. VII.5. Agreement with the data is quite good in magnitude. A slight decrease with increasing temperature is shown in one of the data sets (Lewis and Watson, 1980) and also in the prediction.

This reaction is in a pressure-independent low-pressure limit:

$$\lim_{[M] \rightarrow 0} k_{a/d} = \sum_{\substack{E=E_{-1} \\ (J=J_{-1})}}^{\infty} \frac{k_{1,\infty} \cdot k_2(E)}{k_{-1}(E) + k_2(E)} \cdot f(E,T) \quad [\text{VI.22}]$$

in which $k_{-1}(E)$ and $k_2(E)$ are both approximately $10^{12.6}$ in the lowest energy level of the chemically activated HO₂ ($J=0$). At 300 K, only this ground state is important, as the distribution function $f(E,T)$ is 1.00 for the $J=0$ state but $7.3 \cdot 10^{-4}$ for the $J=1$ state. As a result, $k_{a/d}$ at 300 K is 53% of $k_{\infty}(O+OH \rightarrow HO_2)$. In part because the barrier to H+O₂ is so much lower than the barrier to reform O+OH, the rate constant remains near this value. It decreases as temperature goes up because $f(E,T)$ gives more weight to higher energy levels, and $k_{-1}(E)$ increases faster than $k_2(E)$ as energy level increases.

This rate constant was the only estimated parameter in the calculation, so the measurements of Fig. VII.5, although for products H+O₂, indicate what $k_{\infty}(O+OH \rightarrow HO_2)$ should be. Because $n > 0$ terms in Eq. VI.22 may be neglected, the expression may be solved directly for $k_{1,\infty}$ using $k_{\text{meas}}(O+OH \rightarrow H+O_2) = 1.8 \cdot 10^{13}$, $k_{\text{pred}} = 1.06 \cdot 10^{13}$, $k_2(E) = 10^{12.6}$ and $k_{-1}(E)$ proportional to $k_{1,\infty}$ (predicted $10^{12.6}$ using $k_{1,\infty} = 2 \cdot 10^{13}$). A rate constant $k_{1,\infty} = 3.0 \cdot 10^{13}$ instead of $2.0 \cdot 10^{13}$ would make agreement with the data nearly exact.

Furthermore, the analysis shows that none of the other predicted rate constants in this system were sensitive to the one estimated parameter. Thus, in such cases where the rate constant for chemically activated addition/decomposition is proportional or equal to k_{∞} for addition, the steric factors β for the reactants can be estimated from measured rate constants for this channel, as in Appendix N.

VII.4. Reactions of $H+C_2H_2$ and of $CH+^3CH_2$ via $C_2H_3^*$

In fuel-rich combustion, the reactions of $H+C_2H_2$ are important because of the abundance of C_2H_2 and H-atom. There are two channels: an addition reaction that forms C_2H_3 , and an abstraction channel that forms C_2H+H_2 . The first reaction displays fall-off, while the second is inherently pressure-independent.

The addition channel then provides a basic test of the predictive power of bimolecular QRRK. The forward reaction, $H+C_2H_2 \rightarrow C_2H_3$, is simple H-atom addition to a triple bond, which initially forms chemically activated $(C_2H_3)^*$. Its reverse reaction is a case of elimination of H from a radical by beta-scission. [Beta-scission describes the breaking of a bond on an atom adjacent to the radical site (i.e., β to the radical), leaving a π bond between the original radical site and the adjacent atom.]

Selection of input parameters. - The input data for QRRK are presented in Table VII.2 and can be broken into two categories: high-pressure-limit Arrhenius parameters and the properties of the adduct. This adduct is C_2H_3 , so frequencies may be obtained easily from literature sources (JANAF tables or Harding et al., 1982) as can collisional properties (Kee et al., 1983). Collisional properties of the third body M are the same as in Table VII.1.

Kinetic parameters for addition of H to C_2H_2 are more controversial, as suggested by Table VII.3. The measurements all have been taken at relatively low temperatures, and among them, the first three sets of data group together fairly well. In contrast, the fourth, most recent set has higher rate constants by more than a factor of two. Those authors (Sugawara et al., 1981) were aware of the difference but could not rationalize it.

Theoretical analyses have not resolved this difference. Rather, calculations in Table VII.3 show that absolute rate theory and thermochemical kinetics predict A-factors that are 4 to 30 times higher than the measurements. Keil et al. (1976), whose rate constants were much lower than such predictions, suggested that either energy was not randomly distributed in the chemically activated C_2H_3 , or that the potential energy surface was not well-behaved.

Table VII.2. Parameters needed for QRRK calculations in the reactions involving $C_2H_3^*$ as a chemically activated intermediate: $H+C_2H_2 \rightarrow C_2H_3$ and ${}^2CH+{}^3CH_2 \rightarrow$ products.

Parameter description	Parameter value	Source
- Kinetic parameters for $H+C_2H_2$ -		
$H+C_2H_2 \rightarrow C_2H_3$	$k_{\infty}(400-1900 \text{ K}) = 1.06 \cdot 10^6 T^{1.9} \exp(+4.4/RT)$ $\text{cm}^3 \text{mol}^{-1} \text{s}^{-1}$ or $A_{\infty}(660 \text{ K}) = 1.6 \cdot 10^{12}$, $E_{\infty}(660 \text{ K}) = -1.9 \text{ kcal/mol}$	See text
$C_2H_3 \rightarrow H+C_2H_2$	$A_{\infty}(660 \text{ K}) = 4.7 \cdot 10^{13} \text{ s}^{-1}$ $E_{\infty}(660 \text{ K}) = 40.0 \text{ kcal/mol}^a$	Microscopic reversibility
- Properties of C_2H_3 -		
Number of vibrational degrees of freedom (s):	9	$3 \cdot (5 \text{ atoms}) - 6$
Geometric-mean frequency $\langle \nu \rangle_{C_2H_3}$:	1604 cm^{-1}	From 3311, 3295, 3178, 1774, 1357, 1176, 1174, 791, 773 (Harding et al., 1982)
Molecular weight	27.01 g/g-mol	-
Lennard-Jones well depth ϵ/k and diameter σ	209 K, 4.100 Å	Kee et al., 1983
- Additional kinetic parameters needed for ${}^2CH+{}^3CH_2$ -		
${}^2CH+{}^3CH_2 \rightarrow C_2H_3$	$A_{\infty} = 4 \cdot 10^{13} \text{ cm}^3 \text{mol}^{-1} \text{s}^{-1}$ $E_{\infty} = 0$	Appendix N
$C_2H_3 \rightarrow {}^2CH+{}^3CH_2$	$A_{\infty} = 3.6 \cdot 10^{16} \text{ s}^{-1}$ $E_{\infty} = 162 \text{ kcal/mol}^a$	Microscopic reversibility
$H+C_2H \rightarrow C_2H_2$	$A_{\infty} = 9 \cdot 10^{13} \text{ cm}^3 \text{mol}^{-1} \text{s}^{-1}$ $E_{\infty} = 0$	Estimate, methods of App. N
$C_2H_2 \rightarrow H+C_2H$	$A_{\infty} = 3 \cdot 10^{15} \text{ s}^{-1}$ $E_{\infty} = 132 \text{ kcal/mol}$	Microscopic reversibility

^a Based on $\Delta H_f^{\circ}, 298(C_2H_3) = 70.4 \text{ kcal/mol}$ (McMillen and Golden, 1982).

Table VII.3. Data and estimates for k_{∞} of $\text{H}+\text{C}_2\text{H}_2 \rightarrow \text{C}_2\text{H}_3$.

Source	$A_{\infty} \cdot 10^{-12}$, $\text{cm}^3 \text{mol}^{-1} \text{s}^{-1}$	E_{∞} , kcal/mol	T, K	$k_{298} \cdot 10^{10}$, $\text{cm}^3 \text{mol}^{-1} \text{s}^{-1}$
Measurements				
Keil et al. (1976)	-	-	298 ^a	9.5±1.5
Payne and Stief (1976)	5.5±1.6	2.41±0.14	193-400 ^b	9.4±1.7
Ellul et al. (1981)	8.4±1.8	2.71±0.16	298-473	8.7
Sugawara et al. (1981)	22.9±1.2	2.73±0.04	207-451 ^c	22.8±2.2
Calculation				
Absolute rate theory (Keil et al.)	100 to 160	-	298	-
Thermochemical kinetics (Appendix O)	100 ^d	-	300	-

-
- ^a From fall-off curve with measurements to 0.987 kPa (742 torr).
^b Average of measurements at 0.53, 0.67 and 0.93 kPa (400, 500, and 700 torr).
^c From fall-off curve with measurements to 1.7 kPa (1300 torr).
^d From equilibrium constant $K_{c,dec}(298 \text{ K})=0.565\exp(-35.3/RT)$ and calculated $A_{\infty,dec}(298 \text{ K})=5.4 \cdot 10^{13}$.

They chose to use a transmission coefficient of $\kappa=0.0422$ as a correction factor. Harding et al. (1982) adopted this approach and used κ as a fitting parameter in their RRKM calculations to match the data of Keil et al. and Payne and Stief (1976). Their result was $\kappa=0.039$.

Using the reverse reaction and its equilibrium constant is not helpful in resolving this difference, either. In the first place, there is considerable controversy as to $\Delta H_{f,298}^{\circ}(C_2H_3)$; 70.4 kcal/mol (McMillen and Golden, 1982) has been used here. Decomposition rate constants for C_2H_3 have been measured at temperatures of 1200 to 2365 K, but all but one are low-pressure limits. In that study, Skinner et al. (1971) inferred $k_{\infty}(C_2H_3 \rightarrow H+C_2H_2)=1.6 \cdot 10^{14} \exp(-38.0/RT) \text{ s}^{-1}$ at 1100-1500 K. Using $k_{c,dec}=1.87 \exp(-36.6/RT)$ at 1270 K, the mean $1/T$ for those experiments, $k_{\infty}(C_2H_2+H \rightarrow C_2H_3)=9 \cdot 10^{13} \exp(-1.4/RT)$ can be inferred. Superficially, this result would seem to be more in accord with the theoretical estimates at 298 K than with addition data.

However, some of the variations in addition data and over ranges of temperature are due to a non-Arrhenius k_{∞} . From analyzing the A-factor for $C_2H_3 \rightarrow C_2H_2+H$ by thermochemical kinetics (Appendix O), $\langle \Delta C_p^{\ddagger} \rangle$ is found to vary from 0.91 to 4.23, giving a weighted average of 2.50 over 400 to 1900 K, the experimental range of interest in the flame being modeled. This $\langle \Delta C_p^{\ddagger} \rangle$ introduces a $T^{2.26}$ dependence in k_{∞} for decomposition over 400-1400 K, causing some slight curvature, but the dominating influence on temperature dependence is $E_{\infty,dec}$.

The power-law dependence for addition would be $T^{1.8}$ at room temperature, which brings the results of Payne and Stief and of Ellul et al. even closer to $k_{298}=4.0 \cdot 10^{12} \exp(-37.8/RT)$ and $3.3 \cdot 10^{12} \exp(-37.8/RT)$. The same adjustment to the results of Sugawara et al. changes it only to $k_{298}=14.1 \cdot 10^{12} \exp(-38.1/RT)$, leaving an unexplained difference from the other addition rate constants.

Because of the agreement among the first three measurements, the rate constant of Payne and Stief (1976) was used to establish k_{∞} for decomposition and addition. The non-Arrhenius temperature dependence in $k_{\infty,dec}$ is a problem for QRRK because the method requires Arrhenius parameters for calculating $C_2H_3^* \rightarrow C_2H_2+H$. The compromise that was made in these addition calculations was to use $k_{\infty,add}$ in the full,

three-parameter non-Arrhenius form for the temperature range of interest and $k_{\infty,dec}$ at the $1/T$ mean, expressed in Arrhenius form (derivable from the non-Arrhenius form). These parameters for the range 400 to 1900 K are reported in Ch. VII.8.

Tests against data and RRKM prediction. - To test the QRRK predictions, fall-off data at 298 K and low-pressure-limit, high-temperature data on the decomposition were used.

The fall-off calculation is shown in Fig. VII.6, compared to the data of Keil et al. (1976) and of Payne and Stief (1976) and to RRKM correlation by Harding et al. (1982). Agreement with the RRKM curve is excellent and, with the data, agreement is quite good except at the lowest pressures. Keil et al. noted that there were experimental problems at these lowest pressures, but there do not seem to be grounds for ruling out those data without more information.

Understanding the natures of the RRKM calculation as prediction and correlation is revealing. As noted above, Harding et al. forced their prediction to match $k_{\infty,add}$ of Payne and Stief by using a transmission coefficient much less than 1. In addition, both the transmission coefficient κ and the collision efficiency β were adjustable parameters. The value of β that resulted was 0.33, compared with 0.31 from Troe's equation (Eq. VI.6) in the present calculation.

The second comparison with data is prediction of the low-pressure limit for decomposition of C_2H_3 (Fig. VII.7), where Ar was the third-body gas. The rate constant $k_{\infty}(C_2H_3 \rightarrow C_2H_2+H)$ is calculated at 1660 K (the $1/T$ midpoint of the range of data), properly taking into account the power-law dependence. This calculation gives excellent agreement with the data. For comparison, calculations based improperly on $k_{\infty}(298)$ are shown for comparison as a dotted line, which lies an order of magnitude above the data curves.

Figure VII.8 summarizes these calculations by showing the abstraction, addition, and overall rate constants for $H+C_2H_2$. At the flame condition of 2.67 kPa (20 torr, 0.0263 atm) and $M=CO$, addition dominates up to 1400 K, where abstraction begins to have a higher rate constant. This crossover occurs near 2000 K at 1 atm because of the higher rate constants for addition. The non-Arrhenius shape of

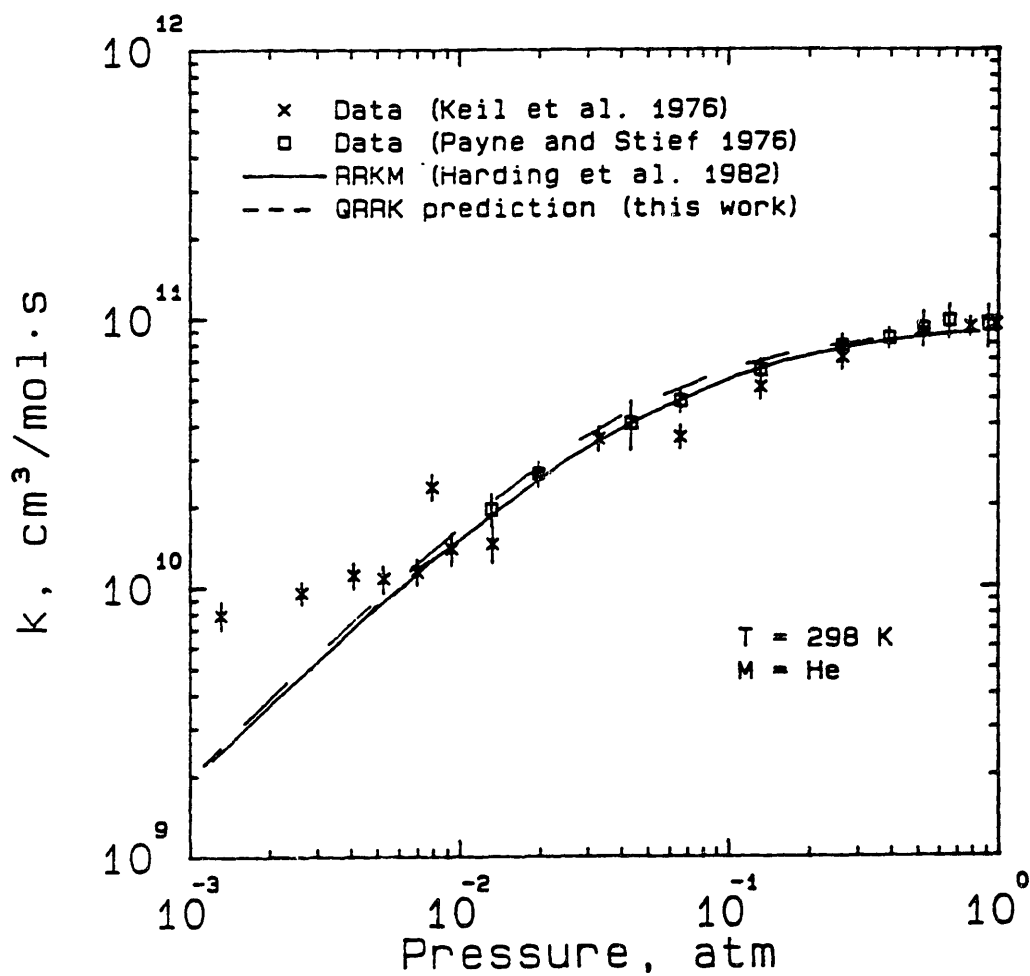


Fig. VII.6. Fall-off curves for $\text{H}+\text{C}_2\text{H}_2$ addition at 298 K in He, including data (\times , \square) with error bars, RRKM prediction (—), and QRRK prediction (— — —).

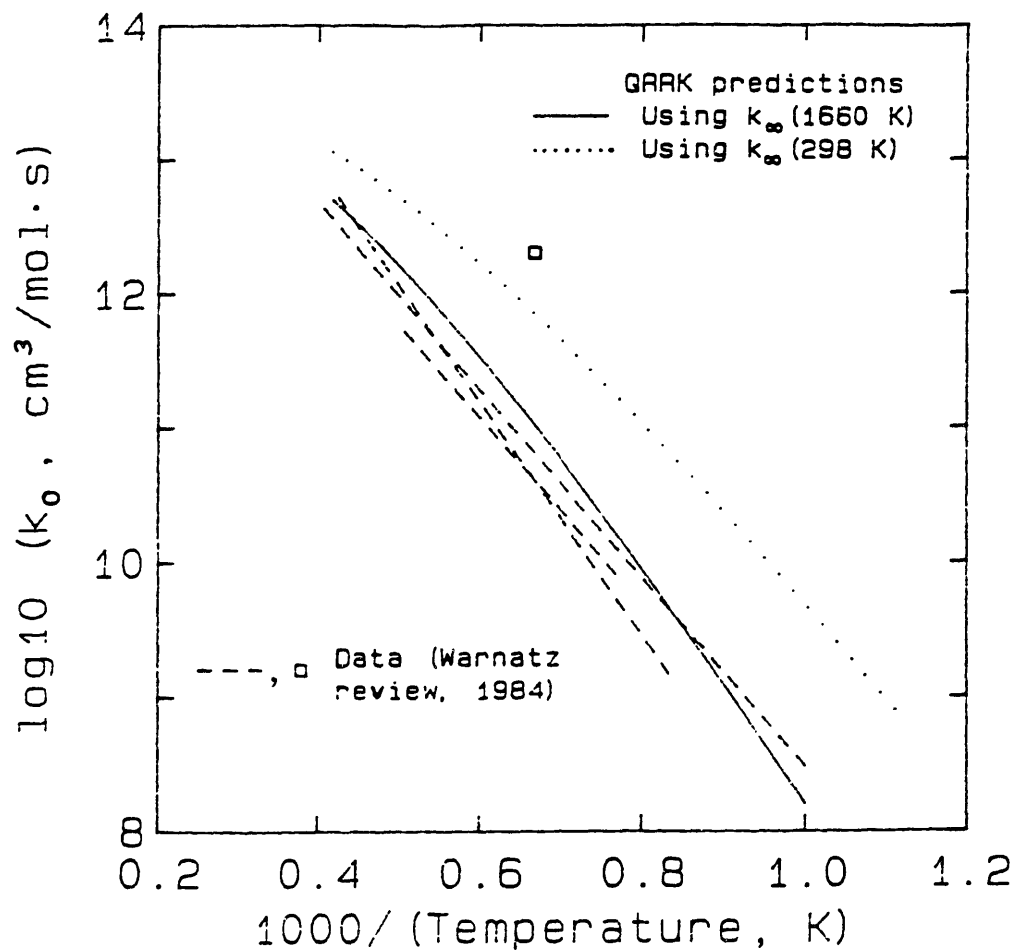


Fig. VII.7. Low-pressure-limit rate constants k_0 for thermal decomposition of C_2H_2 ($M=\text{Ar}$). Predictions by unimolecular QRRK using $k_{\infty,298}$ (\cdots) and a more appropriate $k_{\infty,1660}$ (---), compared to data (--- , \square) from Warnatz (1984).

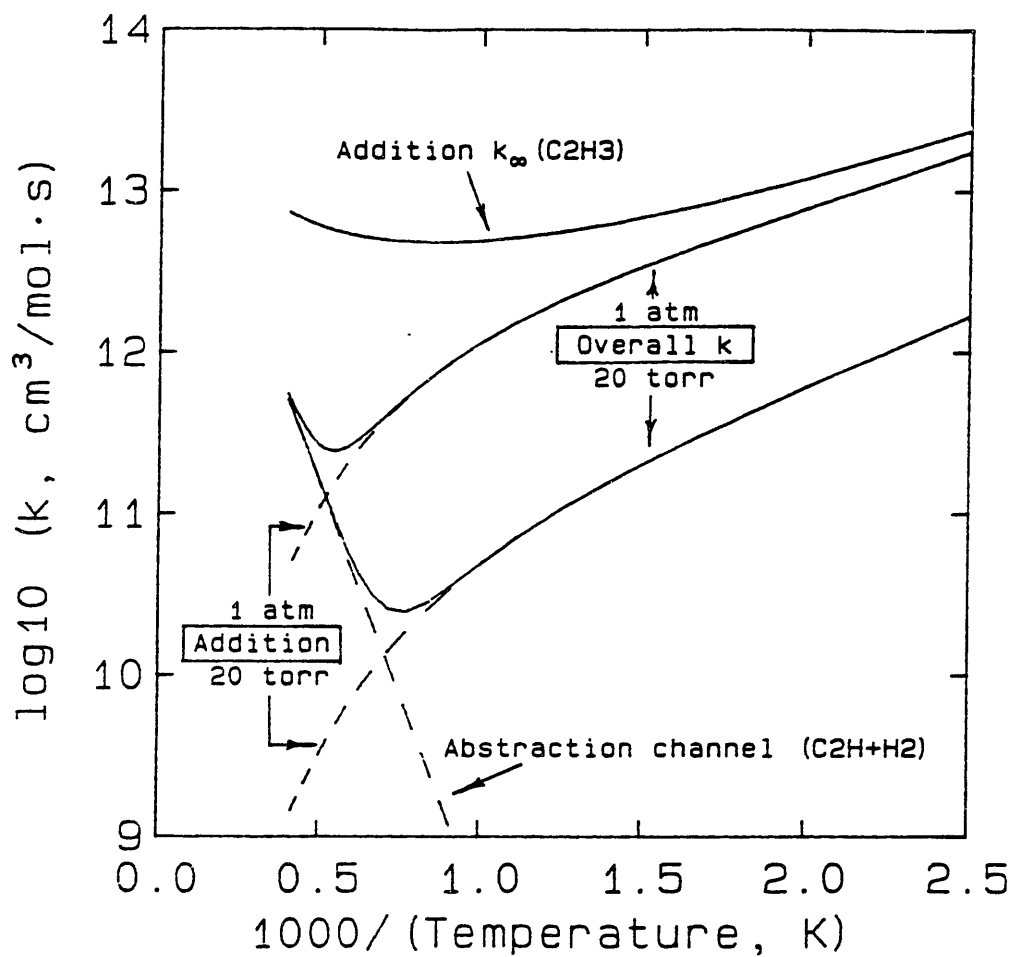


Fig. VII.8. Predictions of the bimolecular rate constant for $\text{H} + \text{C}_2\text{H}_2 \rightarrow \text{C}_2\text{H}_3$ at 2.67 and 100 kPa (20 torr and 1 atm) compared with k_{∞} and the rate constant for pressure-independent abstraction.

k_{∞} is also apparent from this plot. The fit of the predicted rate constant for addition at 2.67 kPa, M=CO, and 400-1900 K is $3.89 \cdot 10^{21} T^{-3.66} \exp(+0.195/RT)$, having a maximum deviation of 8.5% from the calculated rate constants. Its falloff from $k_{\infty,add}$ varies from 0.07 at 400 K to $7 \cdot 10^{-4}$ at 1900 K.

Reaction of $CH+^3CH_2$ via $C_2H_3^*$. - Simple combination of these two radicals leads to a doublet species $:CH-(CH_2\cdot)$, which should proceed rapidly to vibrationally excited, electronic ground-state vinyl ($\cdot CH=CH_2$). The assumptions made for these calculations are that (1) the reaction results from radical combination rather than by insertion of CH and that, in effect, (2) the reaction proceeds on the potential energy surface of vinyl radical; that is, via vibrationally excited C_2H_3 .

The necessary kinetic parameters are shown at the bottom of Table VII.2. Any C_2H_2 that is produced by decomposition of $C_2H_3^*$ will have a significant amount of excess energy because the reactants combine with 162 kcal/mol energy above ground-state C_2H_3 . Accordingly, parameters are also listed for the secondary decomposition reaction (Ch. VI.6) of $C_2H_2^* \rightarrow C_2H+H$, where the reverse, recombination rate constant is estimated to be $9 \cdot 10^{13}$. C_2H_2 has 7 oscillators with a mean frequency of 1604 cm^{-1} (Stull et al., 1971), and its Leonard-Jones parameters are $\sigma=4.10$ Å and $\epsilon/\kappa=209$ K. Chemi-ionization to form $C_2H_3^+ + e^-$ is possible (barrier=208 kcal/mol), but secondary decomposition of $C_2H_2^*$ to form $C_2H_2^+ + e^- (+H)$ is unlikely because the ionization potential of C_2H_2 and the barrier for $C_2H_3 \rightarrow C_2H_2+H$ combine to imply an effective barrier of 360 kcal/mol. Molecular elimination of H_2 from $C_2H_2^*$ to form C_2 might be another possibility, but it is not included here.

Formation of $C_2H_2^*+H$ is predicted to occur with $k(\text{overall})=k_{\infty}(:CH=CH_2\cdot)$, as shown in Fig. VII.9. For 2.67 kPa and M=CO, collisional stabilization of $C_2H_2^*$ to C_2H_2 dominates below 1300 K, but above that temperature, secondary decomposition dominates, forming $C_2H+H(+H)$. The curve fitted to predictions for the C_2H_2+H channel is shown as a dotted line to emphasize the approximation caused by fitting.

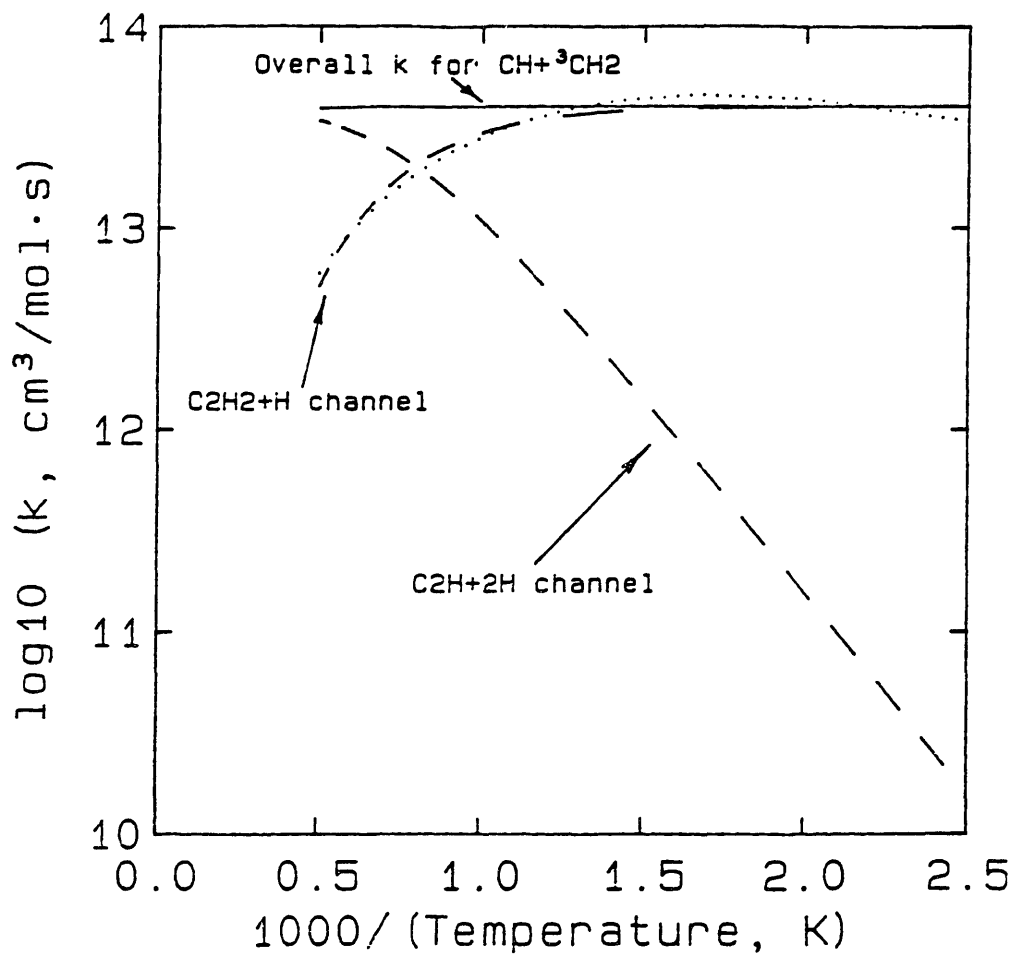


Fig. VII.9. Predictions of the rate constants and branching for the reactions of $\text{CH} + {}^3\text{CH}_2 \rightarrow \text{C}_2\text{H}_2 + \text{H}$ and $\text{C}_2\text{H} + \text{H}_2$ at 2.67 kPa, $\text{M}=\text{CO}$. Dotted line is fit of $\text{AT}^b \exp(-\text{C}/\text{T})$ to the $\text{C}_2\text{H}_2 + \text{H}$ channel.

VII.5. Reactions of H+C₂H₃, H₂+C₂H₂, and ³CH₂+³CH₂

Next, the reaction of H-atom and vinyl radical is considered. Both of these species are important in pyrolysis and fuel-rich combustion, and this is especially important in the present C₂H₂ flame.

The reaction of H+C₂H₃ is reported to form H₂+C₂H₂ with a large rate constant ($2.0 \cdot 10^{13}$) and no activation energy. The data are rather scattered and pressure-independence has been assumed (Warnatz, 1984). From this information, the mechanism of this reaction has been generally attributed to H-transfer by disproportionation (for example, Keil et al., 1976).

A problem with this description is apparent if Benson's work on disproportionation is considered (Benson, 1983). He found that this class of reactions is explained best by invoking long-range forces of polarization. This presents a problem in the case of H+C₂H₃, because H cannot be polarized.

Instead, analysis of the rate constant by bimolecular QRRK showed that the data were described well by combination of H and C₂H₃ to excited C₂H₄^{*}, which could decompose to H₂+C₂H₂ by a 4-center molecular elimination. From the same analysis, rate constants were determined for the pyrolysis of C₂H₄ to H+C₂H₃, 2H+C₂H₂, or to H₂+C₂H₂; for the reaction H₂+C₂H₂ → C₂H₄, H+C₂H₃, and to ³CH₂+³CH₂; and for the various product channels of ³CH₂+³CH₂.

Selection of input parameters. - Input parameters are shown in Fig. VII.10 and Table VII.4. The k_{∞} for H+C₂H₃ was estimated as $5.7 \cdot 10^{13} \text{ cm}^3 \text{ mol}^{-1} \text{ s}^{-1}$ by the recombination method of Appendix N. It relies on a steric factor $\beta(\text{C}_2\text{H}_3)$ estimated as 0.33 (50% uncertainty). The other aspect of uncertainty in this estimate is using 295 kJ/mol (70.4 kcal/mol) as the heat of formation of C₂H₃, as recommended by McMillen and Golden (1982). This recommendation for $\Delta H_f^{\circ},_{298}$ seems well-founded (Sharma et al., 1985; Lee, 1985), but if the lower numbers such as 264 kJ/mol (63 kcal/mol) were correct, the rate constant would be lowered only by 2%. The uncertainty in the steric factor $\beta(\text{C}_2\text{H}_3)$ is much greater than this. Of course, E_{act} for the reverse rate constant, calculated by microscopic reversibility, would be directly affected by $\Delta H_f^{\circ},_{298}(\text{C}_2\text{H}_3)$.

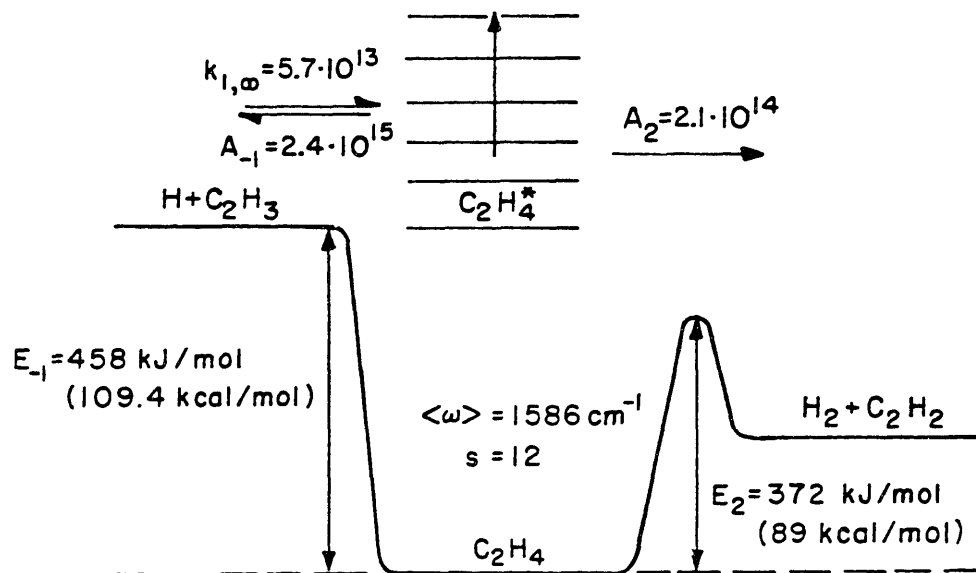


Fig. VII.10. Energy diagram for $\text{H} + \text{C}_2\text{H}_3$ combination and chemically activated decomposition to $\text{C}_2\text{H}_2 + \text{H}_2$.

Table VII.4. Parameters needed for QRRK calculations for the potential-energy surface of C_2H_4 involving $H+C_2H_3$, $H_2+C_2H_2$, and $^3CH_2+^3CH_2$.

<u>Parameter description</u>	<u>Parameter value</u>	<u>Source</u>
<u>-Kinetic parameters-</u>		
$H+C_2H_3 \rightarrow C_2H_4$	$A_{00}=5.7 \cdot 10^{13} \text{ cm}^3\text{mol}^{-1}\text{s}^{-1}$ $E_{00}=0$	Appendix N
$C_2H_4 \rightarrow H+C_2H_3$	$A_{00}=2.4 \cdot 10^{15} \text{ s}^{-1}$ $E_{00}=109.4 \text{ kcal/mol}^a$	Microscopic reversibility
$H_2+C_2H_2 \rightarrow C_2H_4$	$A_{00}=5.3 \cdot 10^{12} \text{ cm}^3\text{mol}^{-1}\text{s}^{-1}$ $E_{00}=47.1 \text{ kcal/mol}$	See text
$C_2H_4 \rightarrow H_2+C_2H_2$	$A_{00}=2.1 \cdot 10^{14} \text{ s}^{-1}$ $E_{00}=88.8 \text{ kcal/mol}^a$	See text
$^3CH_2+^3CH_2 \rightarrow C_2H_4$	$A_{00}=3.2 \cdot 10^{13} \text{ cm}^3\text{mol}^{-1}\text{s}^{-1}$ $E_{00}=0$	Braun, Bass, and Pilling (1970) [see text]
$C_2H_4 \rightarrow ^3CH_2+^3CH_2$	$A_{00}=3.0 \cdot 10^{17} \text{ s}^{-1}$ $E_{00}=169 \text{ kcal/mol}$	Microscopic reversibility
<u>-Properties of C_2H_4-</u>		
Number of vibrational degrees of freedom (s):	12	$3 \cdot (6 \text{ atoms}) - 6$
Geometric-mean frequency $\langle \nu \rangle_{C_2H_4}$:	1586 cm^{-1}	From frequencies in JANAF tables (Stull et al., 1971)
Molecular weight	28.05 g/g-mol	-
Lennard-Jones well depth ϵ/k and diameter σ	280.8 K, 3.971 Å	Kee et al., 1983

^a Based on $\Delta H_f^{\circ},_{298}(C_2H_3)=70.4 \text{ kcal/mol}$ (McMillen and Golden, 1982).

Obtaining k_{∞} for the molecular elimination of H_2 from C_2H_4 is more approximate. $E_{\infty,add}$ has been estimated by Benson and Haugen (1966) for the reaction as a four-center, concerted, 1,2-H elimination, giving 167 kJ/mol (40 kcal/mol) at 298 K and (by implication) $E_{\infty,dec}=81.1$ kcal/mol.

A_{∞} for the elimination is calculated in Appendix O from their transition-state geometry and from frequencies estimated here. The resulting value of $k_{\infty,298}(C_2H_4 \rightarrow H_2+C_2H_2)=1.1 \cdot 10^{14} s^{-1}$ can be compared with the recent estimate of $10^{12.9T^{0.44}} \exp(-44670/T)$ by Tsang and Hampson (1985), which becomes $1.5 \cdot 10^{14} \exp(-88.8/RT)$ at 298 K. The estimated energy barrier to elimination is the principal difference.

A 1,1-H elimination (three-center transition state) is an interesting alternative because of the molecular elimination of H_2 from $H_2C=O$, a species which is isoelectronic with $H_2C=CH_2$. Bauer (1967) investigated the addition of molecular deuterium to C_2H_2 by examining deuterium exchange in a single-pulse shock tube at 1300 to 1660 K ($M=Ar$). He interpreted the results as 1,1- D_2 addition, forming triplet $(\cdot CH \cdot)-CHD_2$, which would rearrange to excited $CHD=CHD$ by 1,2-D shift, rearrange to triplet $\cdot CD \cdot -CH_2D$, and finally eliminate HD . He correlated his rate data using the expression $8 \cdot 10^7 \exp(-33.8/RT)[D_2][C_2H_2]^{0.24}[Ar]^0$ for formation of $HC=CD$. Unfortunately, the fractional order of $[C_2H_2]$ makes it difficult to assess these activation energies in terms of barriers.

Tests against pyrolysis data. - The value of $k_{\infty}(C_2H_4 \rightarrow C_2H_2+H_2)$ and the transition state may be uncertain, but this product channel is now recognized to be the dominant channel in ethylene pyrolysis. Testing against data for the thermal decomposition of C_2H_4 is a way of verifying the k_{∞} used here.

Separate rate constants for C_2H_4 decomposition to $C_2H_2+H_2$ and to C_2H_3+H have been measured by Just, Roth, and Damm (1977) and by Tanzawa and Gardiner (1980). The rate constants were determined by modeling a signal-time curve from shock-tube pyrolysis of ethylene using a proposed chemical mechanism. In the first case, the modeled parameter was H-atom concentration measured by atomic resonance

absorption, and in the second, density gradients (time-dependent heat of reaction) from laser-schlieren methods were used.

Predictions by unimolecular QRRK are compared to these rate constants in the Arrhenius plot of Fig. VII.11, expressing the predictions as $k_{uni}/[M]$. Both the Tsang value of $k_{\infty}(C_2H_4 \rightarrow C_2H_2+H_2)$, expressed in Arrhenius form at 1920 K, and the estimate by methods of Benson and Haugen (1967) (Appendix O) are used. Use of the Tsang rate constant gives good agreement for both the $C_2H_2+H_2$ and the C_2H_3+H channel, while k_{∞} from Appendix O gives a rate constant for the $C_2H_2+H_2$ channel that is a factor of five too high. The higher barrier (91 vs. 81) of the Tsang estimate is the principal cause of this difference.

Some thermal production of C_2H_2+2H is also predicted (Fig. VII.11), although with a lower rate constant than for the other reactions. This channel comes from the highest energy levels of thermally excited $C_2H_4^*$ which decompose to H and $C_2H_3^*$, which in turn can either decompose or be stabilized by collisions.

One conflict with the rate constants of Just et al. and of Tanzawa and Gardiner is that those workers expressed the decompositions as being in the low-pressure limit ($C_2H_4+M \rightarrow Products+M$). The fall-off curves of Fig. VII.12 show the effect of pressure on the apparent k_{uni} at 2000 K. Again, predictions using the Tsang k_{∞} are quite good, while the estimate of Appendix O is much poorer and would predict a transition to C_2H_3+H dominance with increasing pressure.

However, the predictions also show that the low-pressure limit is not a good assumption for the dominant $C_2H_2+H_2$ channel. QRRK calculations indicate that the C_2H_3+H channel is close to the low-pressure limit, but the $C_2H_2+H_2$ channel is predicted to be intermediate between the low- and high-pressure limits. For 2.8 atm, the median pressure of Just et al., the fractional order dependence is predicted to be $[Ar]^{0.37}$. Similarly, at 0.66 atm for Tanzawa and Gardiner, the fractional order is predicted to be 0.46.

Other data in the literature support this aspect of the predictions. Gay et al. (1966) reported from their shock-tube studies that the apparent k_{uni} for C_2H_4 decomposition was proportional to $[Ne]^{0.5}$ at 1712-2170 K and neon pressures of 0.26-1.9 atm. (As noted above,

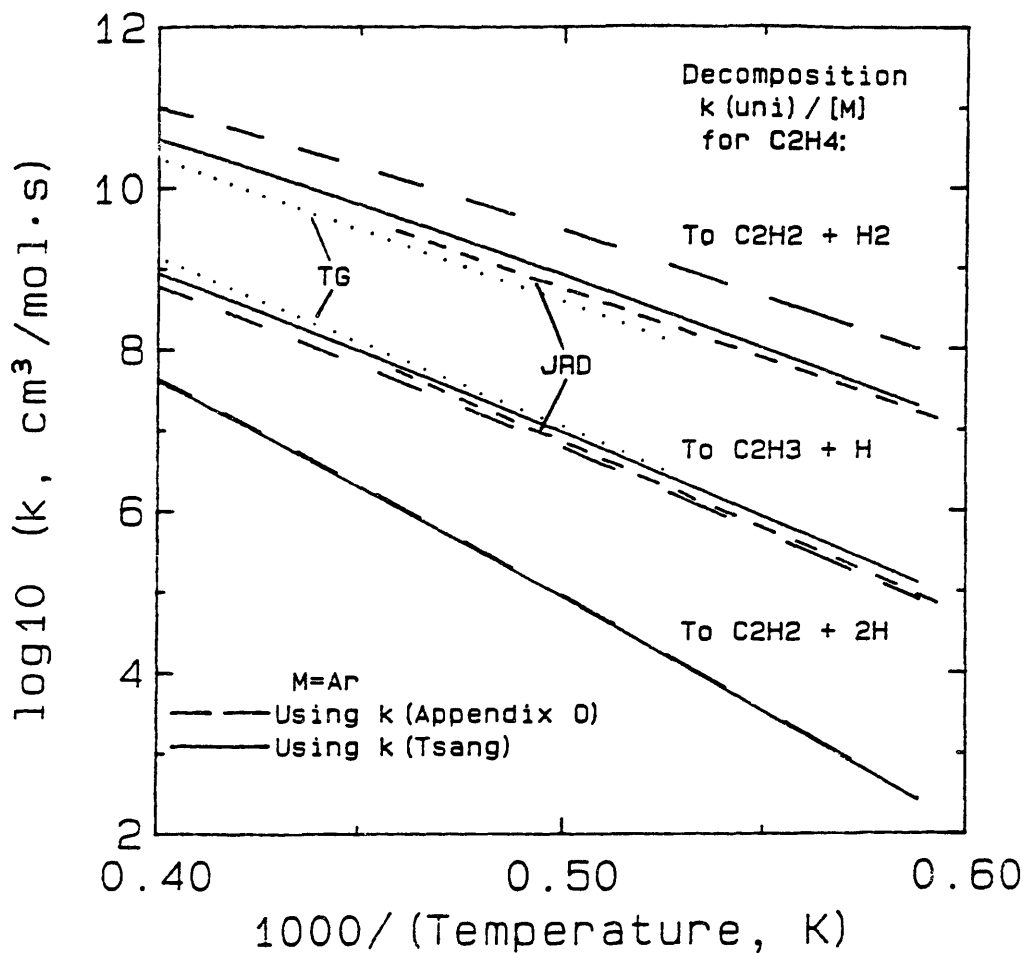


Fig. VII.11. Predictions of rate constants for thermal decomposition $C_2H_4 + M \rightarrow \text{products} + M$ compared to the data of Just, Roth, and Damm (1977) [JRD] and of Tanzawa and Gardiner (1980) [TG - - - -]. Pressure 2.8 atm, M=Ar. Predictions differ by the use of different estimates for $k_{\infty}(C_2H_4 \rightarrow C_2H_2 + H_2)$: ——— by Tsang and Hampson (1985) and — — — from Appendix 0 using the method of Benson and Haugen (1967).

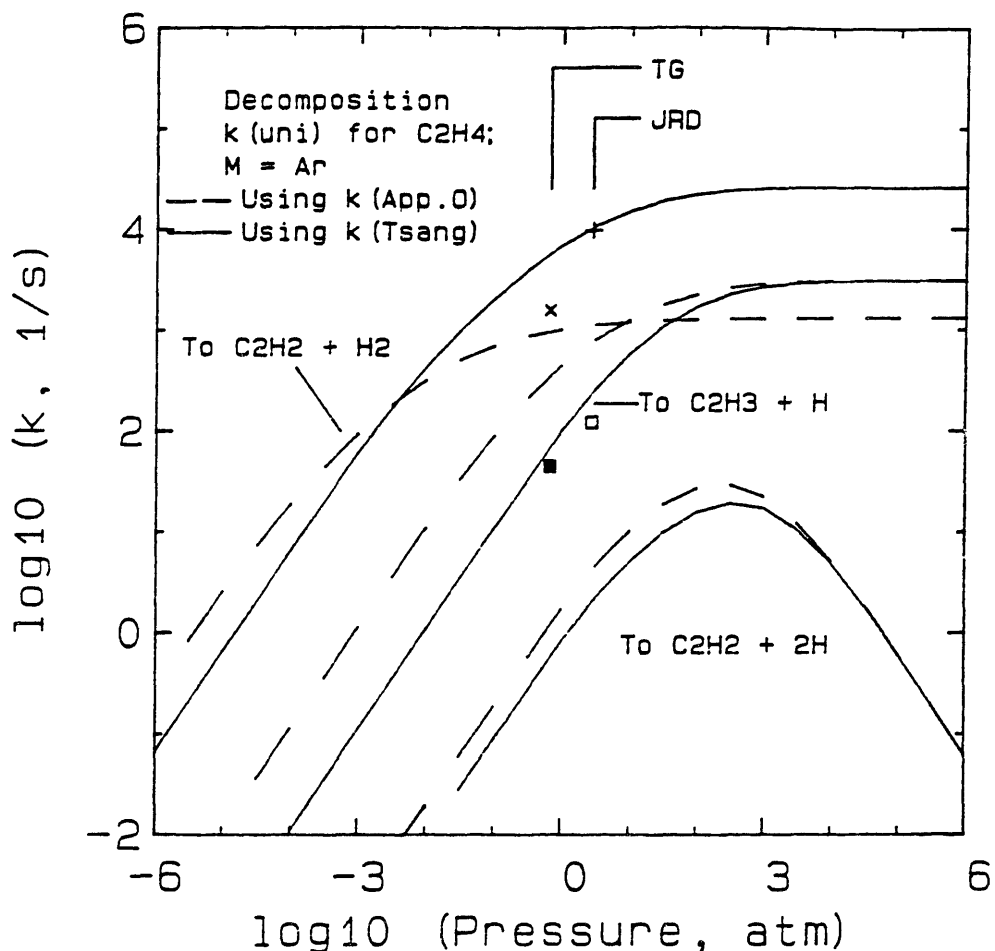


Fig. VII.12. Predictions of fall-off curves at 2000 K, $M=Ar$, for thermal decomposition $C_2H_4 \rightarrow C_2H_2+H_2$ and C_2H_3+H compared to the data of Just, Roth, and Damm (1977) [JRD: + and \square] and of Tanzawa and Gardiner (1980) [TG: x and \blacksquare]. Predictions differ by the use of different estimates for $k_{\infty}(C_2H_4 \rightarrow C_2H_2+H_2)$: — by Tsang and Hampson (1985) and - - - from Appendix 0 using the method of Benson and Haugen (1967). Pressure dependence of $C_2H_4 \rightarrow C_2H_2+2H$ also shown.

$C_2H_2+H_2$ is now recognized to be the dominant product channel, so the overall rate constant describes the pressure dependence of this channel in particular. More directly, Bauer (1967) found that the apparent k_{uni} for C_2H_2 formation by shock-tube pyrolysis of C_2H_4 was actually of order 0.6 ± 0.1 with respect to Ar at 1120-1560 K and pressures on the order of 0.05 atm. Predictions by unimolecular QRRK for these conditions give fractional orders of 0.42 and 0.40 for the two studies, respectively, in good agreement with the data.

The pressure dependence of $C_2H_4 \rightarrow C_2H_2+2H$ (Fig. VII.12) does not follow classical fall-off behavior, but instead it has a maximum at 2.5 atm (250 kPa). At low pressures, this channel is dominated by collisional excitation and de-excitation of C_2H_4 and has a classical low-pressure limit, $C_2H_4+M \rightarrow C_2H_2+2H+M$. As pressure increases beyond the high-pressure limit for $C_2H_4 \rightarrow C_2H_3+H$, $C_2H_3^*$ is still formed from the highest energy levels of $C_2H_3^*$, but it is stabilized rapidly by collisions and cannot lead to C_2H_2+H . As a consequence, the rate constant for the secondary-decomposition channel becomes proportional to $[M]^{-1}$.

In summary, unimolecular QRRK is quantitatively successful in predicting rate constants for ethylene pyrolysis. The estimate of k_{∞} for 1,2- H_2 molecular elimination by the method of Benson and Haugen (1967) was qualitatively correct. However, Tsang's k_{∞} is chosen for further calculations. It gave much better predictions of thermal decomposition data because of its higher A_{∞} and E_{∞} .

Reactions of $H+C_2H_3$. - The data for this reaction are rather scattered (Fig. VII.13), but bimolecular QRRK analysis predicts the rate constant well. The overall rate constant is not pressure-dependent, but it is the sum of $C_2H_2+H_2$ formation and C_2H_4 formation (Fig. VII.14). Each of these reactions has a pressure-dependence, but addition/decomposition decreases with increasing pressure, while addition/stabilization increases with increasing pressure.

Disproportionation cannot account for the reaction mechanistically, as noted above. However, a high, pressure-independent rate constant, such as is observed for disproportionation, has been observed or assumed in the past. By comparing the details of the

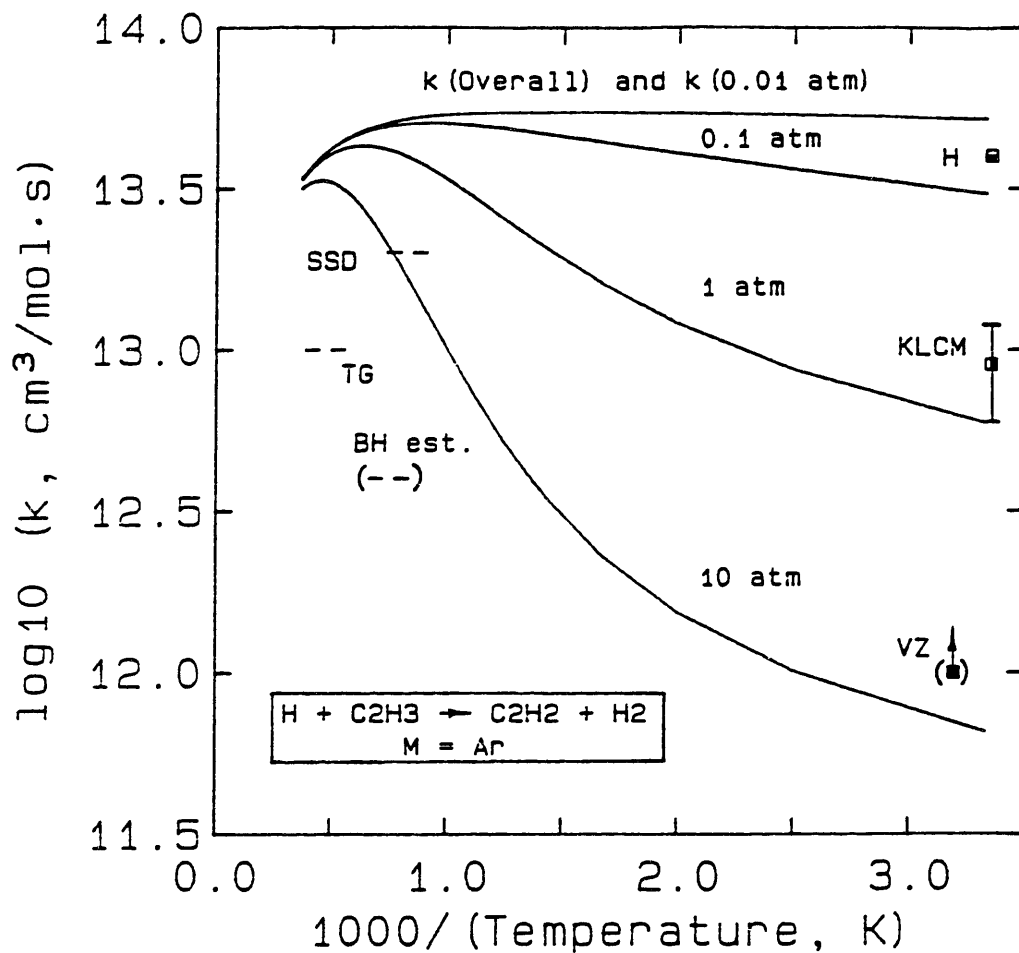


Fig. VII.13. Predictions at 0.01 to 10 atm compared to data for $\text{H} + \text{C}_2\text{H}_3 \rightarrow \text{C}_2\text{H}_2 + \text{H}_2$. Data: Skinner et al. (1971) [SSD - -]; Tanzawa and Gardiner (1980) [TG - -]; Benson and Haugen (1967) [BH est. - -]; Volpi and Zocci (1966) [VZ ■]; Keil et al. (1976) [KLCM □]; and Hoyer mann (1981) [H □]. M=Ar.

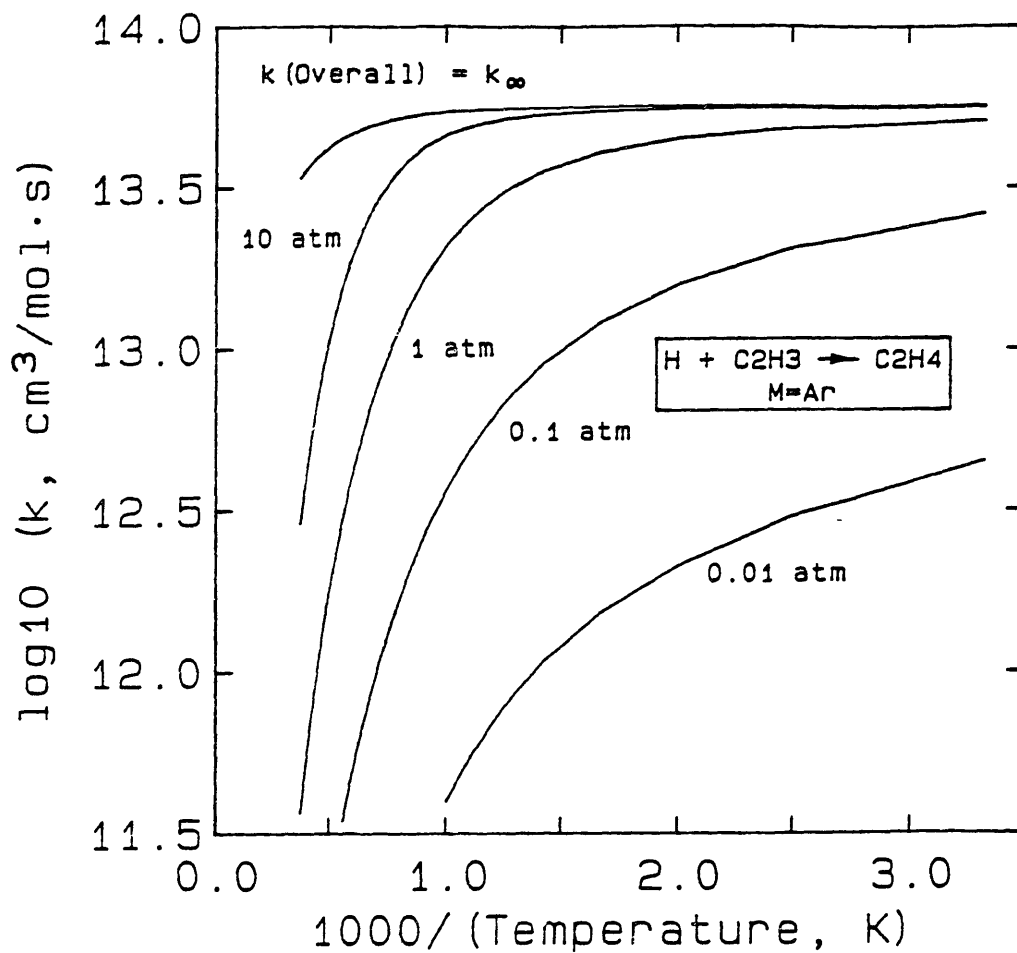


Fig. VII.14. Predictions at 0.01 to 10 atm for $\text{H} + \text{C}_2\text{H}_3 \rightarrow \text{C}_2\text{H}_4$, $\text{M} = \text{Ar}$.

data, it seems clear that they are in fact consistent with these predictions.

As shown in Fig. VII.13, the rate constant is predicted to be only a weak function of pressure at high temperatures. Shock-tube measurements by Skinner et al. (1971) gave k (overall) for $H+C_2H_3$ as pressure-independent. Tanzawa and Gardiner (1980) estimated k for the specific reaction $H+C_2H_3 \rightarrow C_2H_2+H_2$, also from shock-tube measurements, and found no apparent pressure effect. Benson and Haugen (1967) report an estimate for the reaction but do not base it on specific measurements.

Three low-temperature measurements may be compared. First, Volpi and Zocci (1966) observed that the reaction must have been equilibrated in their system (313 K, 1.35-2.00 torr) and thus inferred a lower limit of 10^{12} for the rate constant. Second, Keil et al. (1976) estimated $k=0.6$ to $1.2 \cdot 10^{13}$ (assuming pressure-independence and the identities of the products) because a higher value would introduce discrepancies in $k(H+C_2H_2 \rightarrow C_2H_3)$ at pressures approaching 1 atm. Finally, Warnatz (1984) cites a rate constant measured directly by Hoyermann (private communication, 1981) in a flow reactor with mass spectrometric analysis. No conditions are given, but the flow reactor of Hoyermann et al. (1981) typically operates at 0.5 to 2 torr (0.7 to $3 \cdot 10^{-4}$ atm).

Again, the predictions are consistent with the data. The lower limit of 10^{12} from Volpi and Zocchi presents no difficulties, as the prediction for their conditions is $5.7 \cdot 10^{13}$, a low-pressure limit (pressure-independent) for chemically activated decomposition. For the rate constant of Keil et al., the range of the rate constant is as would be expected for conditions at which the estimate is based (pressures approaching 1 atm), although Keil's study extended to much lower pressures. The value of Hoyermann is the only direct measurement, and it is in excellent agreement with the prediction.

Abstraction of H from the non-radical end of $H_2C=CH\cdot$ may be possible, but even at high temperatures, it does not appear to contribute. If it were occurring, it would have a positive E_{act} and would cause the rate constant to increase with increasing temperature. Instead, the progression among the reliable rate constants of

Hoyermann (298 K), Skinner et al. (1100-1500 K), and Tanzawa and Gardiner (2000-2540) show only a steady decline in the rate constant.

Based on the agreement of QRRK predictions with data, rate constants may be calculated and used for the present flame conditions of 400 to 1900 K, 2.67 kPa (20 torr), and M=CO (Fig. VII.15). Because of the non-Arrhenius shapes of the curves, the fits to the rate constants are $6.2 \cdot 10^{14} T^{-0.32} \exp(+0.085/RT)$ within 3% for $H_2 + C_2H_2$ and $3.3 \cdot 10^{26} T^{-4.7} \exp(-3.4/RT)$ within 7% for C_2H_4 formation. The product channel $^3CH_2 + ^3CH_2$ (see below) was also considered, but even at 1900 K, this rate constant was four orders of magnitude lower than the overall rate constant.

Reactions of $^3CH_2 + ^3CH_2$ via $C_2H_4^*$. - The combination reaction of methylene with itself must proceed via excited C_2H_4 , so it can be analyzed with the information above. Laufer (1981) has concluded that the products of combination of triplet methylene are both $C_2H_2(\tilde{a}^3B_2) + H_2$ and $C_2H_2(\tilde{X}^1\Sigma_g^+) + 2H$.

Rate constants are limited to a room-temperature measurement and a high-temperature measurement. At 298 K, Braun, Bass, and Pilling (1970) observed the formation of C_2H_2 and, at the same time, a disappearance of 3CH_2 that was second-order in 3CH_2 . Their rate constant of $3.2 \cdot 10^{13} \text{ cm}^3 \text{ mol}^{-1} \text{ s}^{-1}$ was pressure-independent at 0.01 to 93 kPa He, and the assumed co-product was H_2 .

Russell and Rowland (1979) posed a convincing challenge that H+H were the co-products at 298 K. In photolysis of ketene and tritiated ketene (CT_2CO) at 298 K and 0.61 kPa (3.5 torr), singlet methylenes 1CH_2 and 1CT_2 were generated and were assumed to be quenched to triplet species 3CH_2 and 3CT_2 , which could react with each other. They also assumed that molecular elimination would give $HC \equiv CT$ and HT in roughly equal amounts, while loss of H or T atoms would lead to $HC \equiv CT$ and $HC \equiv CH$ but not HT , as T atoms would be scavenged by CH_2CO to form $CH_2T + CO$. Experimentally, they observed an $HC \equiv CT/HT$ ratio of 12/1, which led to an estimate that the $C_2H_2 + H_2$ channel accounted for no more than 15% of the products of methylene combination. They postulated that $^3CH_2 + ^3CH_2$ formed $C_2H_4^*$ which in turn formed $C_2H_3^* + H$, and that $C_2H_3^*$ could decompose further to $C_2H_2 + H$.

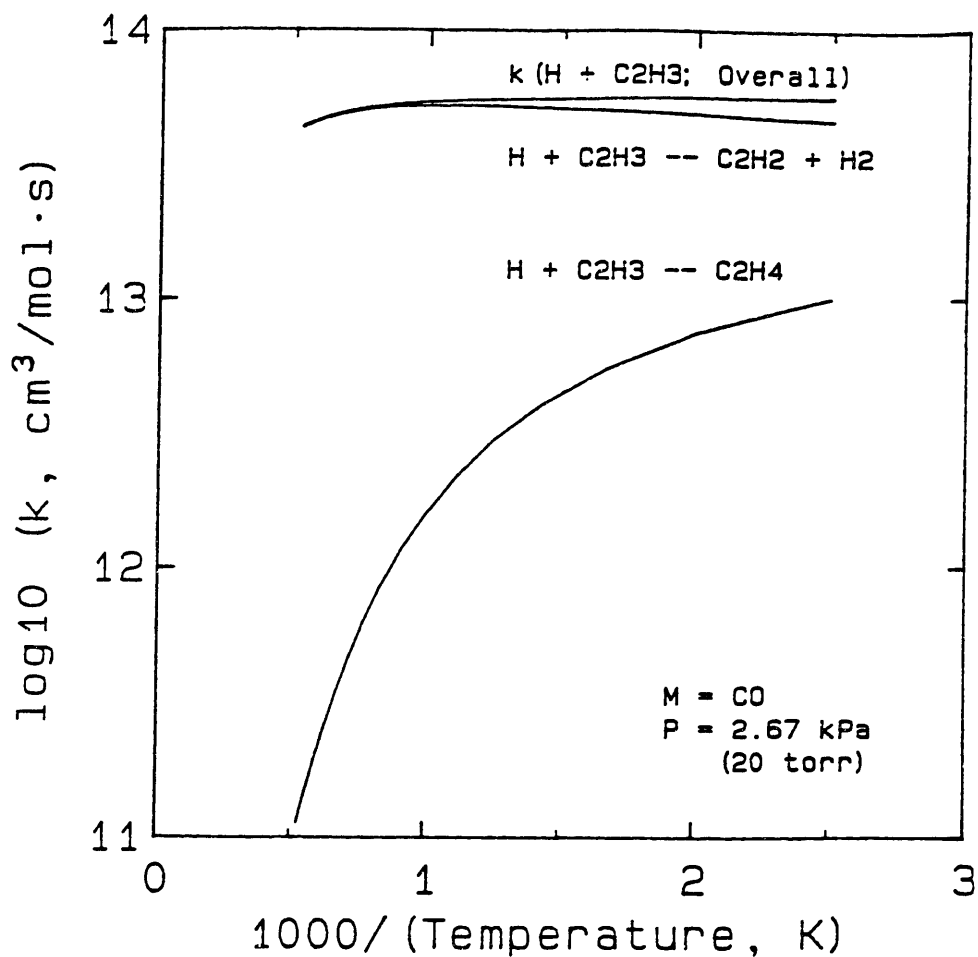


Fig. VII.15. Comparison of predicted rate constants for $\text{H} + \text{C}_2\text{H}_3 \rightarrow \text{C}_2\text{H}_4$, $\text{C}_2\text{H}_2 + \text{H}_2$, and overall at conditions of the present flame: 400 to 1900 K, $M = \text{CO}$, and 2.67 kPa (20 torr).

Frank, Bhaskaran, and Just (in press) deduced $k=(1\pm 0.2)\cdot 10^{14}$ $\text{cm}^3\text{mol}^{-1}\text{s}^{-1}$ for $\text{CH}_2+\text{CH}_2 \rightarrow \text{C}_2\text{H}_2+2\text{H}$ by modeling H-atom measurements from shock-tube pyrolysis of ketene at 2000–2800 K and Ar pressures of approximately 0.16 MPa (1.6 atm). CH_2 was recognized in that study to be present as a mixture of singlet and triplet states. Branching between product channels was concluded to favor $\text{C}_2\text{H}_2+2\text{H}$ over $\text{C}_2\text{H}_2+\text{H}_2$.

Rate constants from ${}^3\text{CH}_2+{}^3\text{CH}_2$ to thermal (collisionally stabilized) products C_2H_4 , $\text{C}_2\text{H}_3+\text{H}$, $\text{C}_2\text{H}_2+2\text{H}$, and $\text{C}_2\text{H}_2+\text{H}_2$ can be calculated by bimolecular QRRK using the input parameters of Table VII.4. In Fig. VII.16, the calculations for 400–1900 K, $M=\text{CO}$, and 2.67 kPa (20 torr) are shown to favor only the C_2H_2 channels, with $\text{C}_2\text{H}_2+2\text{H}$ dominating by 0.57/0.43 at low temperatures and 2/1 at 1900 K. For both these reactions, the rate constants are at their low-pressure limits for chemically activated decomposition. C_2H_4 and $\text{C}_2\text{H}_3+\text{H}$ channels were 3 to 5 orders of magnitude slower than the dominant channels at these conditions, and the overall rate constant was virtually the same throughout the temperature range.

The qualitative dominance of $\text{C}_2\text{H}_2+2\text{H}$ is as Russell and Rowland had observed, but successive decompositions of $\text{H}_2\text{C}=\text{CH}_2^*$ and C_2H_3^* are predicted to dominate molecular elimination by less than their 7/1 ratio. A possible reason for this difference is that the initial adduct $\cdot\text{CH}_2-\text{CH}_2\cdot^*$ could have a long enough lifetime to decompose to $\text{C}_2\text{H}_3^*+\text{H}$ before forming C_2H_4^* . However, this seems unlikely, as formation of C_2H_4^* should be very rapid.

The rate constant of Frank et al. for CH_2+CH_2 , $(1.0\pm 0.2)\cdot 10^{14}$ at 2000 to 2800 K, is 3 to 5 times greater than the room-temperature measurement of Braun et al., probably because of the high reactivity of ${}^1\text{CH}_2$. Applying the recombination method of Benson and Haugen (1967) in Appendix N and assuming the steric factor $\beta({}^3\text{CH}_2)$ to be constant, the combination rate constant for ${}^3\text{CH}_2+{}^3\text{CH}_2$ would be proportional to $T^{1/6}$ and would increase only to $4.5\cdot 10^{13}$ at high temperatures, still less than measured. However, singlet ${}^1\text{CH}_2$ can insert rapidly into C-H bonds, and it should make up 5% or more of the CH_2 . The rate constant then probably corresponds to ${}^1\text{CH}_2+\text{CH}_2 \rightarrow (\cdot\text{CH}\cdot\text{CH}_2)^* \rightarrow (\cdot\text{CH}=\text{CH}_2)^*+\text{H} \rightarrow \text{C}_2\text{H}_2+2\text{H}$.

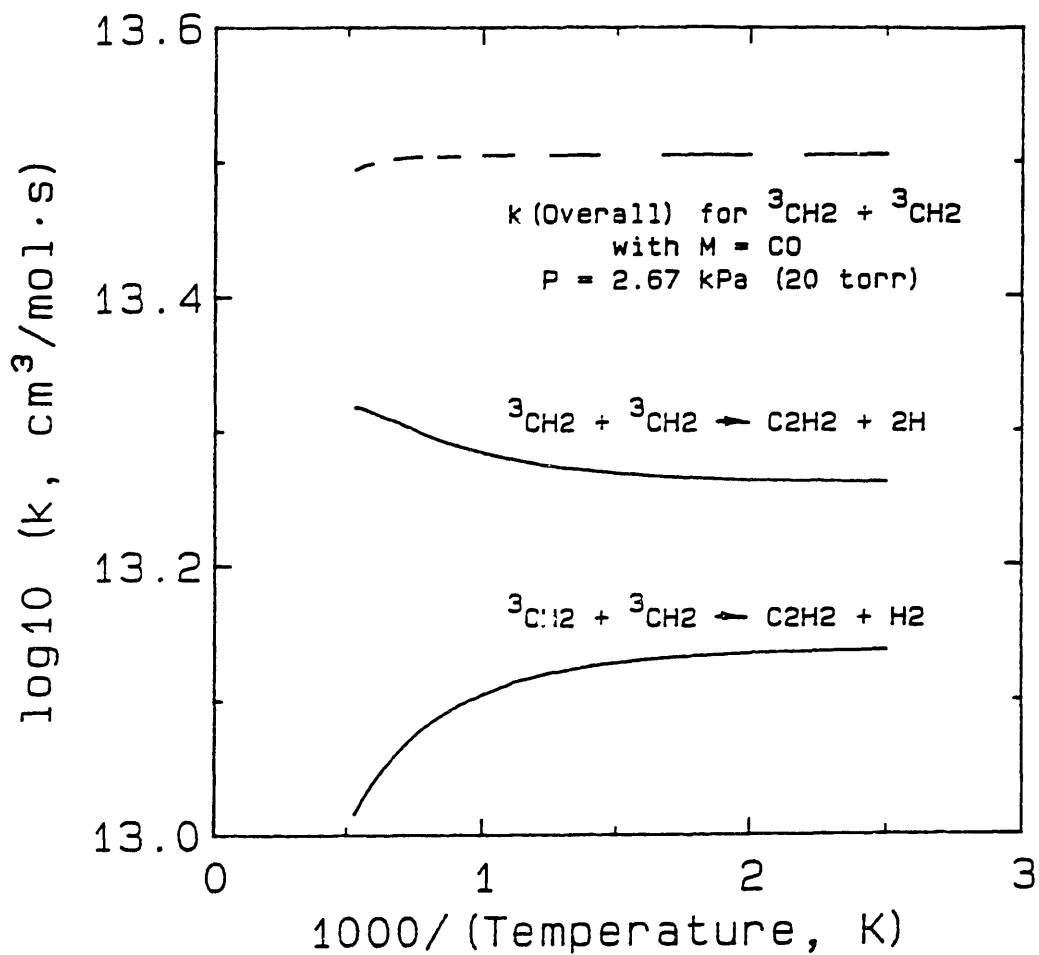


Fig. VII.16. Predicted branching of rate constants for ${}^3\text{CH}_2+{}^3\text{CH}_2$ to $\text{C}_2\text{H}_2+\text{H}_2$ and $\text{C}_2\text{H}_2+2\text{H}$ product channels; 400 to 1900 K, $M=\text{CO}$, and 2.67 kPa (20 torr).

In summary, the bimolecular QRRK calculations show rapidly and easily the effects of the different input parameters. Observations of $\text{H}+\text{C}_2\text{H}_3$ and CH_2+CH_2 rate constants are shown to be consistent with predicted pressure dependences or independence, and physically, chemically realistic rate constants are predicted for testing in mechanistic models. Finally, the importance of discriminating between $^3\text{CH}_2$ and $^1\text{CH}_2$ in models is re-emphasized by the comparisons between data and QRRK predictions.

VII.6. Reactions of $\text{H}+\text{C}_2\text{H}_4$, $^3\text{CH}_2+\text{CH}_3$ and $^1\text{CH}_2+\text{CH}_3$

C_2H_5 is produced as an intermediate by hydrogen abstraction or beta-scission of larger radicals during cracking processes to make ethylene. The radical then can decompose to $\text{H}+\text{C}_2\text{H}_4$ with a pressure-dependent rate constant. The reverse reaction, addition, is likewise important, and it competes with a pressure-independent abstraction reaction $\text{H}+\text{C}_2\text{H}_4 \rightarrow \text{H}_2+\text{C}_2\text{H}_3$. As noted before, fall-off curves for decomposition and addition will be the same if there is no other decomposition channel involved.

Selection of input parameters. - To make predictions of the rate constant by bimolecular QRRK, A_∞ and E_∞ for addition and decomposition are the key parameters. Hase and Schlegel (1982) identified non-Arrhenius curvature in $k_{\infty, \text{dec}}$ that is like that of C_2H_3 decomposition, discussed above and in App. O. Just as for C_2H_3 and $\text{H}+\text{C}_2\text{H}_2$, measurements of the forward and reverse rates are also brought into agreement by this understanding. A_∞ and E_∞ for decomposition were taken from Hase and Schlegel at 660 K, the mean of T^{-1} for the present temperature range of 400-1900 K. The addition rate constant was calculated by microscopic reversibility.

These and other necessary parameters are summarized on the energy diagram of Fig. VII.17 and in Table VII.5.

Tests against data. - Calculation of the low-pressure limit for decomposition of C_2H_5 , shown in Fig. VII.18, shows the success of the unimolecular QRRK method, modified by Troe's collision efficiency β . The prediction is in excellent agreement with data. Calculations of fall-off are also in good agreement with data.

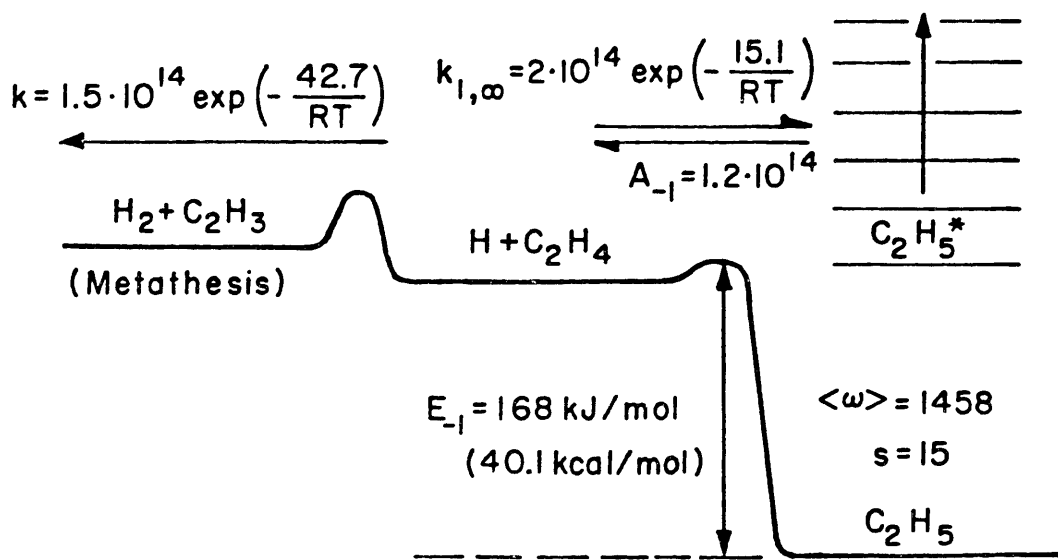


Fig. VII.17. Energy diagram for H+C₂H₄ addition and abstraction (energies in kJ/mol except where stated otherwise).

Table VII.5. Parameters needed for QRRK calculations for the potential-energy surface of C_2H_5 involving $H+C_2H_4$, $^3CH_2+CH_3$, and $^1CH_2+CH_3$.

<u>Parameter description</u>	<u>Parameter value</u>	<u>Source</u>
-Kinetic parameters-		
$H+C_2H_4 \rightleftharpoons C_2H_5$	$A_{00}=2.0 \cdot 10^{14} \text{ cm}^3 \text{ mol}^{-1} \text{ s}^{-1}$ $E_{00}=3.6 \text{ kcal/mol}$	Microscopic reversibility
$C_2H_5 \rightarrow H+C_2H_4$	$A_{00}=1.22 \cdot 10^{14} \text{ s}^{-1}$ $E_{00}=40.1 \text{ kcal/mol}$	Hase and Schlegel (1982), 660 K
$^3CH_2+CH_3 \rightleftharpoons C_2H_5$	$A_{00}=4.2 \cdot 10^{13} \text{ cm}^3 \text{ mol}^{-1} \text{ s}^{-1}$ $E_{00}=0 \text{ kcal/mol}$	See text
$C_2H_5 \rightleftharpoons ^3CH_2+CH_3$	$A_{00}=8.3 \cdot 10^{15} \text{ s}^{-1}$ $E_{00}=97.4 \text{ kcal/mol}$	Microscopic reversibility
$^1CH_2+CH_3 \rightleftharpoons C_2H_5$	$A_{00}=2.8 \cdot 10^{13} \text{ cm}^3 \text{ mol}^{-1} \text{ s}^{-1}$ $E_{00}=0$	Estimated from $^1CH_2+CH_4$ (see text)
$C_2H_5 \rightleftharpoons ^1CH_2+CH_3$	$A_{00}=3.1 \cdot 10^{15} \text{ s}^{-1}$ $E_{00}=106.4 \text{ kcal/mol}$	Microscopic reversibility
-Properties of C_2H_5-		
Number of vibrational degrees of freedom (s):	15	$3 \cdot (7 \text{ atoms}) - 6$
Geometric-mean frequency $\langle \nu \rangle_{C_2H_5}$:	1458 cm^{-1}	From 2925, 3000, 2950, 21050, 1400, 1400, 31450, 800, 1250, 1300, 200 (Appendix N)
Molecular weight	29.01 g/g-mol	-
Lennard-Jones well depth ϵ/k and diameter σ	252.3 K, 4.302 Å	Kee et al., 1983

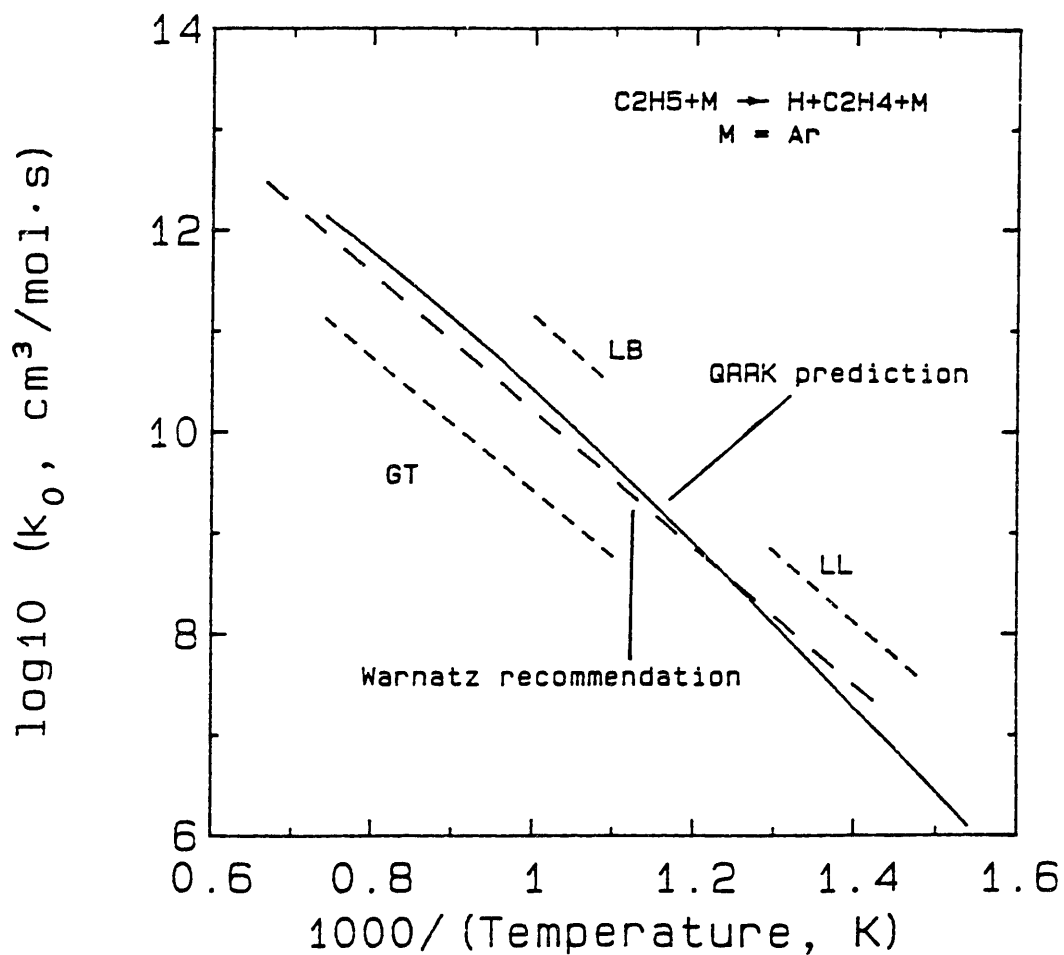


Fig. VII.18. QRRK prediction (solid line) of the low-pressure limit k_0 for $\text{C}_2\text{H}_5 \rightarrow \text{H} + \text{C}_2\text{H}_4$ compared to data (---): Lin and Back (1966) [LB], Loucks and Laidler (1967) [LL], and Glänzer and Troe (1973) [GT]. Recommendation of Warnatz (1984) also shown (— — —).

In Fig. VII.19, prediction of the rate constant for addition is compared to the rate constant for the metathesis reaction to $C_2H_3+H_2$ that was selected by Warnatz (1984). The present flame conditions of $M=CO$, 2.67 kPa, and 400 to 1900 K were used.

Addition dominates the branching between products at low temperature, and H-atom abstraction dominates at high temperatures. However, pressure determines the temperature at which abstraction becomes more important than addition. At 2.67 kPa, k_{add} is near k_{∞} below 500 K, but fall-off with increasing temperature causes a minimum in the overall rate constant at 1200 K when k_{add} crosses over k_{abs} . Increasing the pressure to 100 kPa (1 atm) increases this crossover point by about 200 K.

Reactions of $^3CH_2+CH_3$ and $^1CH_2+CH_3$ via $C_2H_5^*$. - 3CH_2 reaction with CH_3 is known experimentally to produce $H+C_2H_4$ (Warnatz, 1984). These products result from a radical-combination reaction (Laufer, 1981), but not all researchers have recognized that chemically activated $C_2H_5^*$ rather than thermal C_2H_5 is involved. In the closely related reaction of $^1CH_2+CH_3$, $H+C_2H_4$ are also thought to result from 1CH_2 insertion into a C-H bond, followed by chemically activated decomposition (Tsang and Hampson, 1985). No data are available.

These rate constants can be easily evaluated by bimolecular QRRK. For $^3CH_2+CH_3 \rightarrow C_2H_5$, k_{∞} is estimated in Appendix N to be $6.9 \cdot 10^{13} \text{ cm}^3 \text{ mol}^{-1} \text{ s}^{-1}$. For $^1CH_2+CH_3 \rightarrow C_2H_5$, k_{∞} is estimated to be $2.8 \cdot 10^{13} \text{ cm}^3 \text{ mol}^{-1} \text{ s}^{-1}$, based on the rate constants for the $^1CH_2+CH_4$ insertion reaction by Ashford et al. (1981) and by Langford et al. (1983) corrected for reaction-path degeneracy. These and other necessary parameters are shown in Table VII.5.

As shown in Fig. VII.20, $^3CH_2+CH_3$ goes to $H+C_2H_4$ with a rate constant (shown as a dashed line) that is within 10% of k_{∞} for $^3CH_2+CH_3 \rightarrow C_2H_5$ at as high a temperature as 1700 K. Even at 2700 K, the prediction is 60% of $k_{\infty,add}$. Formation of thermalized C_2H_5 was 2 to 4 orders of magnitude slower.

These calculations were made at 2.67 kPa for $M=CO$, but the rate constant is at a pressure-independent, low-pressure limit for chemically activated addition/decomposition. For Ar at 1 atm, the result is virtually the same.

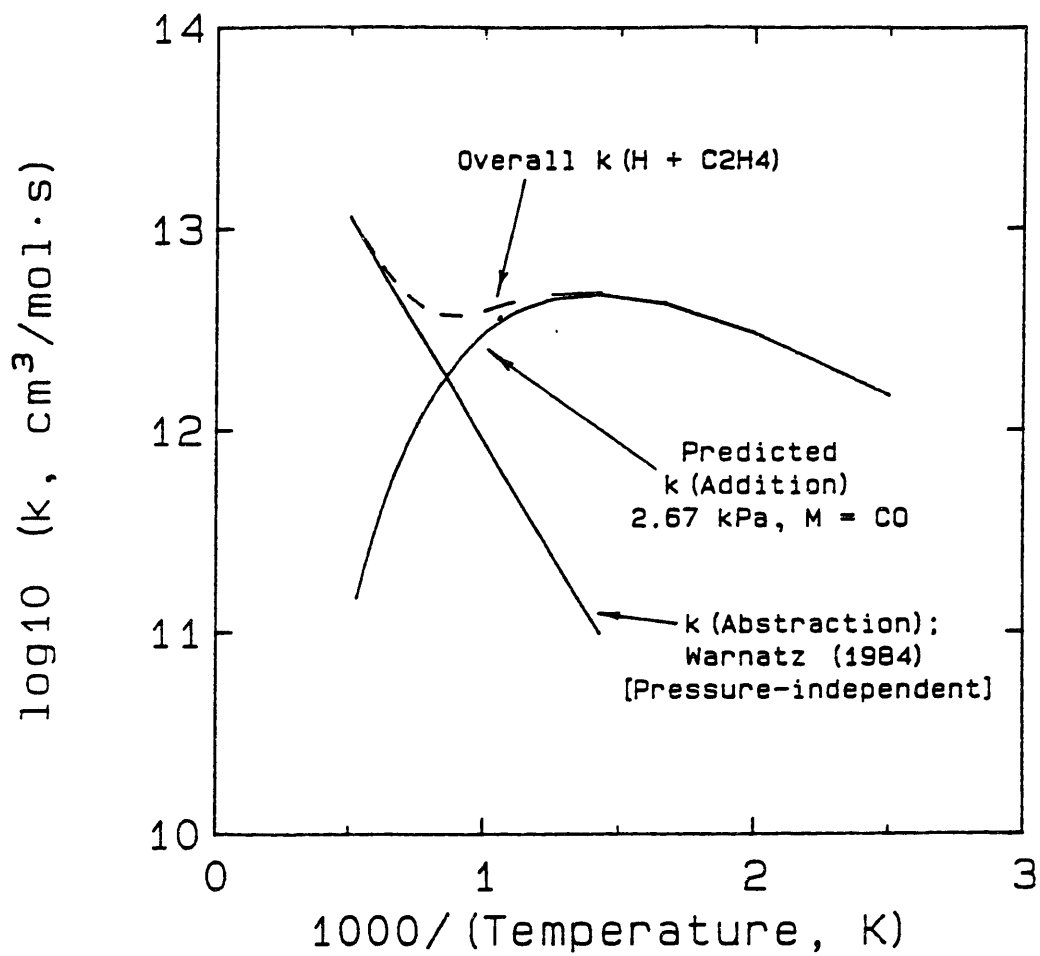


Fig. VII.19. Predictions of rate constants for $\text{H}+\text{C}_2\text{H}_4$ addition at 2.67 kPa in CO; metathesis reaction to $\text{H}_2+\text{C}_2\text{H}_3$, and resulting overall rate constant for $\text{H}+\text{C}_2\text{H}_4$ also shown for reference.

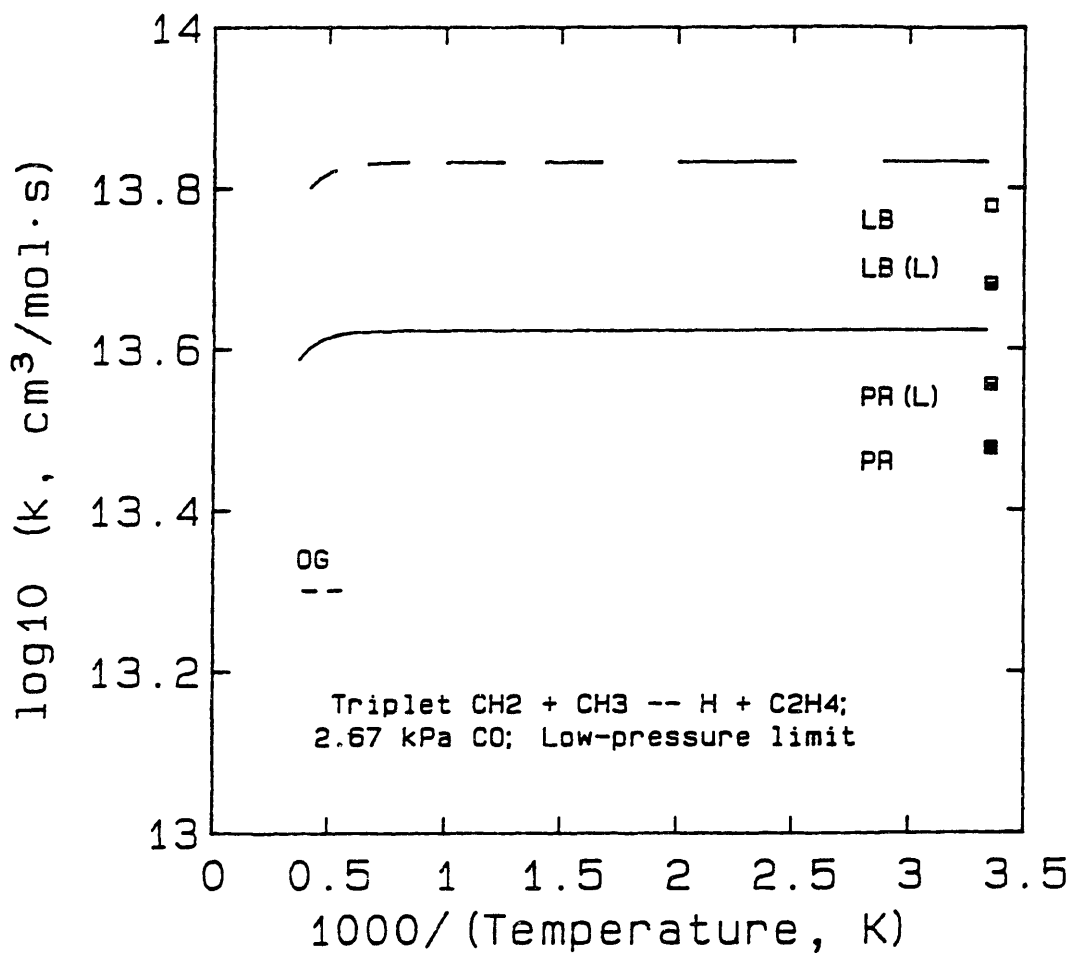


Fig. VII.20. Predictions and data for $^3\text{CH}_2 + \text{CH}_3 \rightarrow \text{H} + \text{C}_2\text{H}_4$: Laufer and Bass (1975) [LB \square], Pilling and Robertson (1975) [PR \blacksquare], Laufer (1981) [LB(L) \blacksquare and PR(L) \square], and Olson and Gardiner [OG $--$]. Dashed line is QRRK prediction using $k_\infty(^3\text{CH}_2 + \text{CH}_3 \rightarrow \text{C}_2\text{H}_5)$ estimated from steric factors; solid line uses the mean of LB(L) and LB(PR) as an improved estimate of k_∞ .

The predictions (dashed line in Fig. VII.20) are slightly higher than the data. QRRK analysis shows that the source of the difference is solely the choice of $k_{\infty}({}^3\text{CH}_2+\text{CH}_3 \rightarrow \text{C}_2\text{H}_5)$ as $6.9 \cdot 10^{13}$. Laufer (1981) has re-evaluated the room-temperature measurements of Laufer and Bass (1975; $6 \cdot 10^{13}$) and of Pilling and Robertson (1975; $3 \cdot 10^{13}$) based on new data on the rate constant for CH_3 recombination. This had been a competing reaction that strongly affected the original data analyses, and differing values had been used. The new values move closer to each other, becoming $4.8 \cdot 10^{13}$ and $3.6 \cdot 10^{13}$ respectively. Based on these rate constants and the QRRK analysis, a better value of k_{∞} is $4.2 \cdot 10^{13}$. Predictions using this k_{∞} are shown in Fig. VII.20 as a solid line.

Predictions for ${}^1\text{CH}_2+\text{CH}_3$ (Fig. VII.21) show that $\text{H}+\text{CH}_4$ is the dominant product channel over most of the temperature range, but also that reactive quenching to ${}^3\text{CH}_2$ is important. [The improved estimate of $k_{\infty}({}^3\text{CH}_2+\text{CH}_3 \rightarrow \text{C}_2\text{H}_5)$ is used.] The overall rate constant stays approximately at $k_{\infty}({}^1\text{CH}_2+\text{CH}_3 \rightarrow \text{C}_2\text{H}_5)$, so the magnitudes of the individual rate constants are again shown to depend directly on the rate constant for forming C_2H_5^* . Formation of thermalized C_2H_5 is again negligible, occurring 3 to 5 orders of magnitude more slowly than the overall reaction. The branching into ${}^3\text{CH}_2+\text{CH}_3$ formation is also a reasonable consequence of the reaction, but it is another way that the reactivities of the two species differ.

VII.7. Reaction of $\text{O}+\text{CO} \rightarrow \text{CO}_2$

Destruction of CO by $\text{O}({}^3\text{P})$, the ground electronic state of O-atom, is important in the dry combustion of CO and because of the puzzling non-Arrhenius behavior of its rate constant. It is unimportant for hydrocarbon combustion, where OH is formed, because destruction of CO by OH is much faster. As an example, at 2000 K and 1 atm, k_{OH} is $5 \cdot 10^{11} \text{ s}^{-1}$, while $k_{\text{O-atom}}$ is $1 \cdot 10^9 \text{ s}^{-1}$ (Warnatz, 1984). In fact, a major problem in accurately measuring the rate constant for $\text{O}+\text{CO}$ has been that any H_2O impurity leads to OH, which accelerates CO destruction significantly (Baulch et al., 1976).

Available data on the reaction (Baulch et al., 1976; Warnatz, 1984) are treated as third-order ($\text{O}+\text{CO}+\text{M} \rightarrow \text{CO}_2+\text{M}$ with rate constant

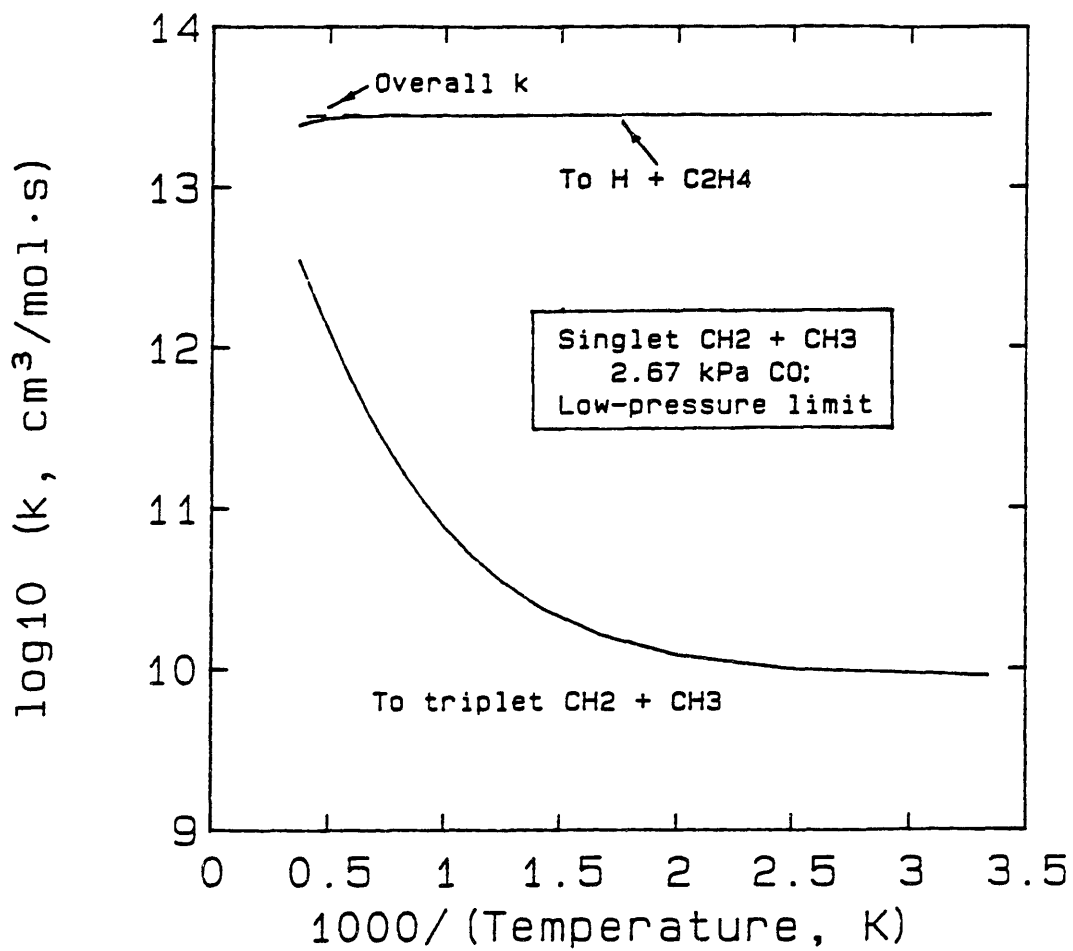


Fig. VII.21. Predictions for $^1\text{CH}_2+\text{CH}_3 \rightarrow \text{H}+\text{C}_2\text{H}_4$, $\rightarrow ^3\text{CH}_2+\text{CH}_3$, and overall.

k_0). The puzzle is that the data, despite scatter, seem to show a positive E_{act} at low temperatures but negative E_{act} at high temperatures. This switch seems to occur at about 1000 K. As a consequence, Baulch et al. (1976) recommended k_0 only for the range 250–500 K, while Warnatz (1984) recommended k_0 only for 1000–3000 K.

Selection of input parameters. - The input parameters for this bimolecular QRRK analysis are shown on the energy diagram of Fig. VII.22 and in Table VII.6. Experimental Arrhenius parameters A_{∞} and $E_{act,\infty}$ for addition are given by Troe (1974). For the dissociation, $A_{-1,\infty}$ and E_{-1} are calculated by detailed balancing using the equilibrium constant at 298 K.

The analysis showed good agreement with the data, including the maximum in the rate constant. In Fig. VII.23, recent measurements made in Ar are taken from a recent review (Warnatz, 1984). In comparison to these data, predictions are shown for the low-pressure limit k_0 for addition/stabilization and for $k_{bi}/[M]$ at 100 kPa (1 atm). Agreement is quite good. It is notable that (1) no parameters were adjusted and (2) not all the measurements were experimentally confirmed to be in the low-pressure limit. Most notably, the prediction resolves the apparent inconsistency between the low- and high-temperature data by showing a maximum near 1000 K.

The reasons for the maximum also can be established from QRRK components of k_0 . Equation VI.21 for $k_{0,a/s}$ may be rewritten in this case ($k_2(E)=0$) as

$$\begin{aligned}
 k_{a/s,0} &= \sum_{\substack{E=E_{-1} \\ (I=M_{-1})}}^{\infty} \frac{k_{1,\infty} \cdot \beta \cdot Z}{k_{-1}(E)} \cdot f(E,T) \\
 &= \sum_{\substack{E=E_{-1} \\ (I=M_{-1})}}^{\infty} \frac{\text{Numerator}(T)}{\text{Denominator}(E)} \cdot f(E,T) \quad [\text{VII.2}]
 \end{aligned}$$

Values of these parameters are shown in Table VII.7. There, the energy distribution function $f(E,T)$ is shown to be a weighting function for a ratio that has a temperature-dependent numerator and an energy-dependent denominator.

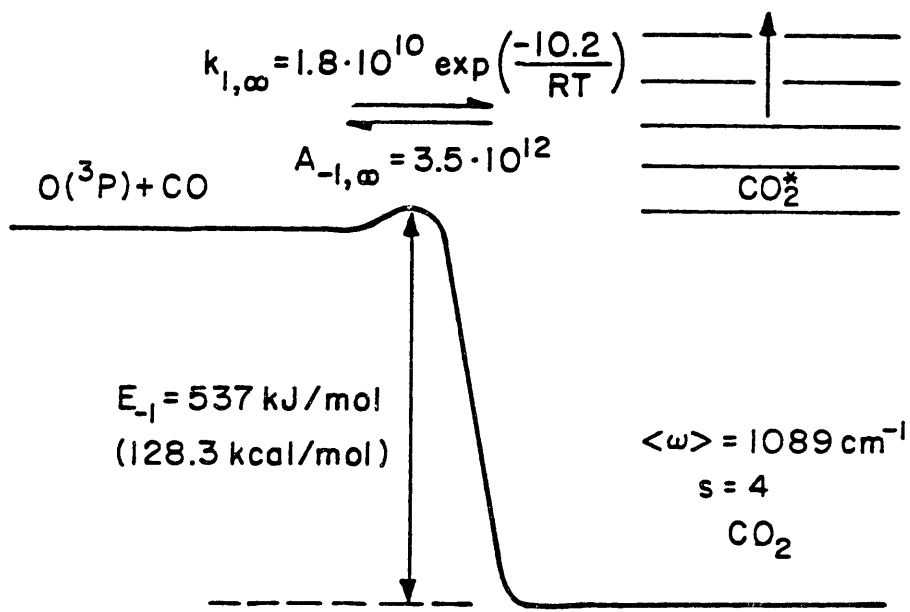


Fig. VII.22. Energy diagram for $O(^3P) + CO \rightarrow CO_2$ (energies in kJ/mol except where stated otherwise).

Table VII.6. Parameters needed for QRRK calculations for $O(^3P)+CO \rightarrow CO_2$.

<u>Parameter description</u>	<u>Parameter value</u>	<u>Source</u>
<u>-Kinetic parameters-</u>		
$O+CO \rightarrow CO_2$	$A_{co} = 1.8 \cdot 10^{10} \text{ cm}^3 \text{ mol}^{-1} \text{ s}^{-1}$ $E_{co} = 10.2 \text{ kcal/mol}$	Troe (1974)
$CO_2 \rightarrow O+CO$	$A_{co} = 3.5 \cdot 10^{12} \text{ s}^{-1}$ $E_{co} = 128.3 \text{ kcal/mol}$	Microscopic reversibility
<u>-Properties of CO_2-</u>		
Number of vibrational degrees of freedom (s):	4	$3 \cdot (3 \text{ atoms}) - 5$
Geometric-mean frequency $\langle \nu \rangle_{CO_2}$:	1089 cm^{-1}	From Stull et al. (1971)
Molecular weight	44.01 g/g-mol	-
Lennard-Jones well depth ϵ/k and diameter σ	244 K, 3.763 Å	Kee et al., 1983

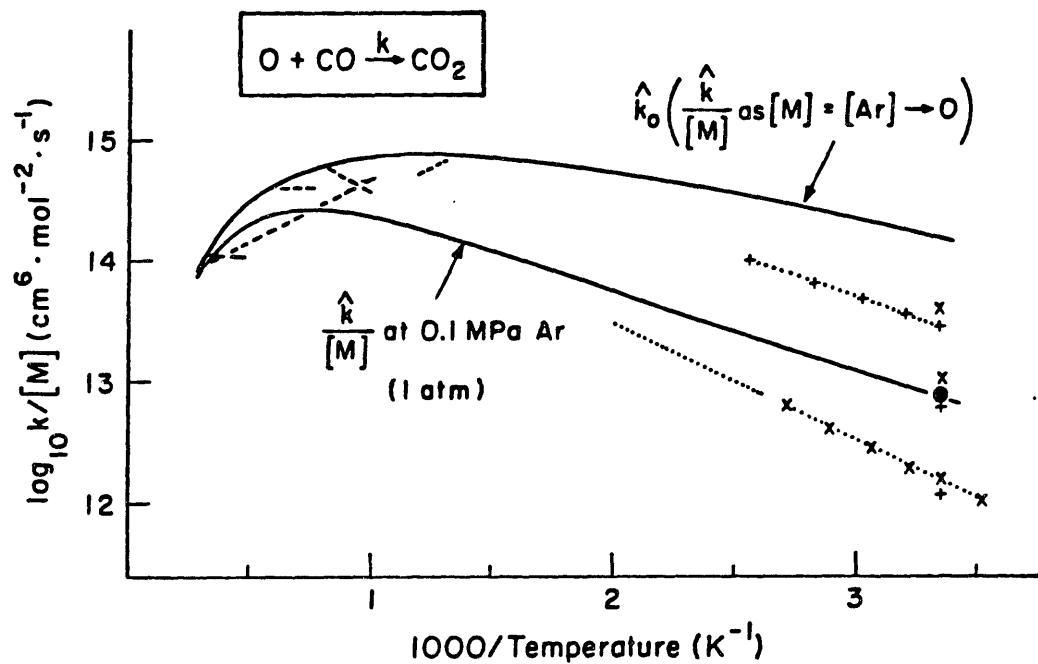


Fig. VII.23. Comparison of QRRK predictions (solid lines) to data (---, ····, +, X; Warnatz, 1984) for rate constants of $O(^3P)+CO \rightarrow CO_2$.

The predicted maximum in k_0 can be understood from the elements of Table VII.7 by inspecting the interplay between energy- and temperature-dependence. At a given energy level, the ratio increases with temperature (because of the numerator) by an order of magnitude from 300 to 1000 K, but it increases only slightly from 1000 to 2000 K. At a given temperature, the ratio increases sharply with increasing energy (because of the denominator) in the lower quantum levels. There would be no maximum if only a single energy of CO_2^* were involved, but the weighting function $f(E,T)$ shifts to higher energy levels as temperature increases. Thus, at low temperatures, the lowest energy state dominates, causing k_0 to increase with increasing temperature as if there were only one energy; while at higher temperatures, the shift in $f(E,T)$ toward the higher energy levels and the weak temperature-dependence of the numerator causes k_0 to fall with increasing temperature.

VII.8. Conclusions

The bimolecular adaptations of unimolecular QRRK (Kassel, 1928b) by Dean (1985), and in the present work correctly predict pressure and temperature dependences of many reactions important to combustion and pyrolysis. These reactions are recombinations and additions that form an excited intermediate, which then may be stabilized by collisions with surrounding molecules or may undergo energy-dependent unimolecular reactions such as decomposition or isomerization. In contrast, H-atom transfer reactions (abstraction and disproportionation) pass through a single transition state to stable products, so they have pressure-independent rate constants.

The simple input parameters of this method makes the reaction steps and the results easier to understand, particularly when chemically activated pathways are involved. Some accuracy is sacrificed relative to the more complex methods, but direct comparisons here with RRKM and Troe's formalism show that the differences can be quite small. Furthermore, the necessary data for QRRK are all properties of the radical or molecule that is the stabilized adduct: collision properties, vibrational frequencies, and high-pressure-

Table VII.7. Components of the rate constant for $O(^3P)+CO-CO_2$ in its low-pressure limit k_0 , which is the sum over energy of (Numerator/Denominator)·f(E,T). Units: cm, mol, s.

	Temperature (K)	300	500	1000	1500	2000
$\text{Log}_{10}(\text{Numerator},$		22.59	23.20	23.58	23.65	23.67
$k_{1,\infty} \cdot \beta \cdot Z_{L,j})$						
Quantum level	Log₁₀	Log₁₀	Log₁₀	Log₁₀	Log₁₀	Log₁₀
vs. $m_{-1}=41$	[(Denom,	(Numer/	(Numer/	(Numer/	(Numer/	(Numer/
	$k_{-1}(E)]$	Denom)	Denom)	Denom)	Denom)	Denom)
		f(K)	f(E)	f(E)	f(E)	f(E)
0 (at E_{-1})	8.42	0.98	0.84	0.39	0.18	0.087
1	8.99	0.021	0.15	0.33	0.25	0.16
2	9.36		0.016	0.17	0.22	0.18
3	9.64			0.071	0.15	0.17
4	9.85			0.026	0.095	0.13
5	10.03				0.053	0.097
6	10.18				0.028	0.066
7	10.30					0.043
8	10.42					0.027
Log₁₀(k_0)		14.15	14.72	14.86	14.69	14.48

limit rate constants for its unimolecular reactions. Such parameters often are available in the literature or can be estimated with good accuracy.

For modeling combustion or pyrolysis, use of this method gives useful predictions of the effects of pressure on rate constants. Three-parameter fits of rate constants are shown in Table VII.8 for the reactions studied in this chapter, using the experimental flame conditions of $M=CO$, 2.67 kPa, and 400–1900 K.

The method's success with applications in this chapter illustrate how it can be used to correlate data and to help the researcher understand what chemical mechanisms may be involved. By applying this technique, we can make reasonable estimates of rate constants of reactions for which we have few or no measurements.

Table VII.8. Rate constants ($\text{cm}^3\text{mol}^{-1}\text{s}^{-1}$) for reactions of aliphatic species, CO, and CO_2 calculated by QRRK methods for 400–1900 K, $M=\text{CO}$, and 2.67 kPa (20 torr).

<u>Reaction</u>	<u>Predicted rate constant</u>	<u>Max. log₁₀ devn</u>	<u>k(1500)</u>
$\text{H}+\text{C}_2\text{H}_2 \rightarrow \text{C}_2\text{H}_3$	$3.89 \cdot 10^{21} T^{-3.66} \exp(+0.20/RT)$	9%	10.00
$\text{CH}+^3\text{CH}_2 \rightarrow \text{C}_2\text{H}_3$	$3.09 \cdot 10^{14} T^{-1.98} \exp(-0.62/RT)$	1.5%	8.11
$\rightarrow \text{H}+\text{C}_2\text{H}_2$	$2.50 \cdot 10^{12} T^{-3.68} \exp(-4.19/RT)$	15%	13.11
$\rightarrow 2\text{H}+\text{C}_2\text{H}$	$5.49 \cdot 10^{22} T^{-2.41} \exp(-11.52/RT)$	4%	13.41
$\text{H}+\text{C}_2\text{H}_3 \rightarrow \text{C}_2\text{H}_4$	$5.62 \cdot 10^{29} T^{-5.54} \exp(-4.35/RT)$	9%	11.54
$\rightarrow \text{C}_2\text{H}_2+\text{H}_2$	$3.70 \cdot 10^{12} T^{-0.55} \exp(+0.04/RT)$	3%	13.69
$\text{H}_2+\text{C}_2\text{H}_2 \rightarrow \text{C}_2\text{H}_4$	$2.86 \cdot 10^{29} T^{-5.24} \exp(-52.6/RT)$	21%	5.18
$\rightarrow \text{C}_2\text{H}_3+\text{H}$	$4.02 \cdot 10^{15} T^{-0.56} \exp(-65.8/RT)$	3%	4.26
$^3\text{CH}_2+^3\text{CH}_2 \rightarrow \text{C}_2\text{H}_4$	$1.11 \cdot 10^{20} T^{-3.43} \exp(-2.07/RT)$	5%	8.86
$\rightarrow \text{C}_2\text{H}_2+\text{H}_2$	$4.02 \cdot 10^{14} T^{-0.47} \exp(-0.48/RT)$	1.5%	13.06
$\rightarrow \text{C}_2\text{H}_3+\text{H}$	$7.12 \cdot 10^{21} T^{-3.90} \exp(-2.46/RT)$	5%	9.11
$\rightarrow \text{C}_2\text{H}_2+2\text{H}$	$4.97 \cdot 10^{12} T^{+0.19} \exp(+0.15/RT)$	0.5%	13.30
$\text{H}+\text{C}_2\text{H}_4 \rightarrow \text{C}_2\text{H}_5$	$1.99 \cdot 10^{41} T^{-8.76} \exp(-11.70/RT)$	15%	11.78
$^3\text{CH}_2+\text{CH}_3 \rightarrow \text{C}_2\text{H}_5$	$2.53 \cdot 10^{20} T^{-3.49} \exp(-2.03/RT)$	4%	9.02
$\rightarrow \text{C}_2\text{H}_4+\text{H}$	$4.2 \cdot 10^{13}$	2%	13.62
$^1\text{CH}_2+\text{CH}_3 \rightarrow \text{C}_2\text{H}_4$	$1.11 \cdot 10^{19} T^{-3.20} \exp(-1.78/RT)$	4%	8.63
$\rightarrow \text{C}_2\text{H}_4+\text{H}$	$4.94 \cdot 10^{13} T^{-0.076} \exp(-0.094/RT)$	1%	13.60
$\rightarrow ^3\text{CH}_2+\text{CH}_3$	$6.82 \cdot 10^{-8} T^{+5.71} \exp(+4.20/RT)$	7%	11.60
$\text{O}+\text{CO} \rightarrow \text{CO}_2$	$1.31 \cdot 10^{21} T^{-3.85} \exp(-4.95/RT)$	3%	8.18

CHAPTER VIII. MECHANISMS OF BENZENE FORMATION FROM SMALLER HYDROCARBONS

VIII.1. Introduction

Benzene can be formed from smaller, nonaromatic hydrocarbons in flames and in cracking processes, but the mechanism for its formation has remained elusive. This question is significant for combustion because polycyclic aromatic hydrocarbons and soot, both undesirable pollutants, probably grow from single aromatic rings. In contrast, ethylene production can make benzene and other aromatics as valuable by-products, particularly from C_4 and heavier feedstocks.

The present study provides the means and opportunity for testing chemical mechanisms of benzene formation. Measured mole fractions and temperatures from the C_2H_2 flame are combined with estimated rate constants, giving rates of benzene formation. These predictions are then compared to formation rates deduced from the data, an approach that has been used previously (Cole et al., 1984). However, when fall-off effects on the addition reactions are properly taken into account using bimolecular QRRK, all previous mechanisms fail because the initial, thermalized adduct is formed too slowly.

The results are explained instead by chemically activated reactions that form the aromatic ring directly. The species $l-C_4H_5$, $l-C_4H_3$, and C_2H_2 , which have been proposed before (Cole et al., 1984; Frenklach et al., 1985), react fast enough to account for benzene formation, but the reactions proceed through excited intermediates rather than through a sequence of thermalized intermediates. This is a fundamental change in our understanding of benzene formation because thermalized species can be attacked and destroyed by bimolecular reactions, while the chemically activated species forms the aromatic ring too fast for bimolecular collisions to take place.

The chemically activated reactions are initiated by additions of $l-C_4H_5$ and $l-C_4H_3$ to C_2H_2 . Rather than forming linear, aliphatic adducts $l-C_6H_7$ and $l-C_6H_5$ in their ground vibrational states, the aliphatic adducts are excited species $l-C_6H_7^*$ and $l-C_6H_5^*$ that rapidly isomerize to excited ring compounds $c-C_6H_7^*$ and $c-C_6H_5^*$.

These intermediates undergo chemically activated decomposition or collision stabilization to benzene and phenyl, respectively.

Rate constants for phenyl pyrolysis are predicted as an out-growth of the 1-C₄H₃ + C₂H₂ case. The same species and potential surface are appropriate as for phenyl formation. Rate constants and products for this thermal decomposition are controversial, but unimolecular QRRK analysis shows that four product channels are involved. Predicted rate constants agree well with the literature.

The mechanisms that have proposed previously will be reviewed briefly, followed by a screening test using high-pressure-limit rate constants. Rate constants for the product channels of the remaining possibilities are then calculated by bimolecular QRRK and discussed. Completing the analysis of benzene formation, these pathways are tested against the flame data. Finally, rate constants for phenyl pyrolysis will be presented and discussed.

VIII.2. Literature mechanisms

Many mechanisms have been proposed, but few have been tested quantitatively. Some of these proposed routes (Table VIII.1) suggest reaction paths from the two initial reactants, but only Cole et al. (1984), Frenklach et al. (1985), and Colket (1985a, 1985b) have proposed detailed mechanisms and showed quantitative tests. The issue of chemical activation has not been addressed in any of the literature mechanisms.

Overview; Types of reactions involved. - To form an aromatic ring from smaller aliphatic species, there must be molecular-weight growth, cyclization, and aromatization reactions. It is useful to examine the mechanisms that have been proposed in the literature by examining the types of reactions that are involved in order to decide how to test them and also to consider alternatives.

Literature mechanisms are shown in Table VIII.1 and are categorized by the three types of growth reactions that have been suggested: radical addition, radical combination, and Diels-Alder reaction.

(1) Radical addition to π bonds has been proposed for various vinylic radicals, for example C₂H₃ (Kinney and Crowley, 1954; Weissman and Benson, 1984; Colket, 1985a, 1985b); 1-buten-3-ynyl or

Table VIII.1. Literature mechanisms for forming aromatics. Single carbon-carbon bonds illustrated by —, double bonds by =, triple bonds by ≡; H implied in structures and reactions but not shown.

Mechanism	Reference
<p>Radical addition:</p> $\text{CH}_3 + \text{CH}_2=\text{CH} \cdot \rightarrow \text{CH}_3\text{CH}_2\text{CH}_2 \cdot \rightarrow \text{CH}_3\text{CH}=\text{CH} \cdot \rightarrow \text{CH}_3\text{C} \equiv \text{CH} \cdot$ $\text{C}_6\text{H}_5 \cdot \rightarrow \text{C}_6\text{H}_6 \rightarrow \text{C}_6\text{H}_7 \cdot \rightarrow \text{C}_6\text{H}_8 \rightarrow \text{C}_6\text{H}_9 \cdot \rightarrow \text{C}_6\text{H}_{10}$	Weissman and Benson, 1985
$\text{C}_6\text{H}_5 + \text{C} \equiv \text{C} \cdot \rightarrow \text{C}_6\text{H}_7 (\text{C} \equiv \text{C} \cdot) \rightarrow \text{C} - \text{C}_6\text{H}_7 \rightarrow \text{C}_6\text{H}_6$	Colket, 1985
$\text{C}_6\text{H}_5 + \text{CH}_2=\text{CH} \cdot \rightarrow \text{C}_6\text{H}_5\text{CH}_2\text{CH}_2 \cdot \rightarrow \text{C}_6\text{H}_5\text{CH}=\text{CH} \cdot \rightarrow \text{C}_6\text{H}_5\text{C} \equiv \text{CH} \cdot$ $\text{C}_6\text{H}_5 + \text{C}_6\text{H}_5 \cdot \rightarrow \text{C}_{12}\text{H}_{10} \cdot \rightarrow \text{C}_6\text{H}_6 + \text{C}_6\text{H}_5 \cdot$	Kinney and Crowley, 1954; Weissman and Benson, 1984
$\text{C}_6\text{H}_5 + \text{C} \equiv \text{C} \cdot \rightarrow \text{C}_6\text{H}_5\text{C} \equiv \text{C} \cdot \rightarrow \text{C}_6\text{H}_6$	Stehling et al., 1956; Frenklach et al., 1985
$\text{C}_6\text{H}_5 + \text{C} \equiv \text{C} \cdot \rightarrow \text{C}_6\text{H}_5\text{C} \equiv \text{C} \cdot \rightarrow \text{C}_6\text{H}_6$	Cole et al., 1984
$\text{C}_6\text{H}_5 + \text{C}_6\text{H}_5 \cdot \rightarrow \text{C}_{12}\text{H}_{10} \cdot \rightarrow \text{C}_6\text{H}_6 + \text{C}_6\text{H}_5 \cdot$	Kinney and Crowley, 1954
$\text{C}_6\text{H}_5 + \text{C} \equiv \text{C} \cdot \rightarrow \text{C}_6\text{H}_5\text{C} \equiv \text{C} \cdot \rightarrow \text{C}_6\text{H}_6$	Bockhorn et al., 1983
<p>Radical recombination:</p> $\text{C}_6\text{H}_5 \cdot + \text{C}_6\text{H}_5 \cdot \rightarrow \text{C}_{12}\text{H}_{10} \cdot \rightarrow \text{C}_6\text{H}_6 + \text{C}_6\text{H}_5 \cdot$	Kinney and Crowley, 1954; similarly, Sakai et al., 1976
<p>Diels-Alder addition of butadiene</p> $\text{CH}_2=\text{CH} + \text{C} \equiv \text{C} \rightarrow \text{C}_6\text{H}_6$	Glassman, 1976
$\text{CH}_2=\text{CH} + \text{C}_6\text{H}_5 \cdot \rightarrow \text{C}_6\text{H}_5\text{CH}_2\text{CH}_2 \cdot \rightarrow \text{C}_6\text{H}_5\text{CH}=\text{CH} \cdot \rightarrow \text{C}_6\text{H}_5\text{C} \equiv \text{CH} \cdot$	Hague and Wheeler, 1929; Wheeler and Wood, 1930
$\text{CH}_2=\text{CH} + \text{CH}_2=\text{CH} \rightarrow \text{C}_6\text{H}_6$	Badger, 1951

1-C₄H₂ (Stehling et al., 1956; Frenklach et al., 1985); and 1,3-butadienyl or 1-C₄H₅ (Cole et al., 1984; Weissman and Benson, 1984). Weissman and Benson have also suggested CH₃ reaction in a sequence of additions, abstractions and combinations. Addition of a vinylic radical to acetylene is especially advantageous for several reasons. For one, the radical site is an end carbon, permitting subsequent cyclization by internal radical addition. Also, the adduct radical would have conjugated π bonds, adding to its thermal stability. Last, the vinylic carbon and the two acetylenic carbons carry one H each, as do aromatic carbons, so they would not need to add or lose hydrogen.

Radical combination in the high-pressure limit forms a molecular adduct. This adduct would not have the stability associated with conjugated π bonds unless each radical site had been a doubly or triply bonded carbon. For example, allyl recombination (Kinney and Crowley, 1954; Sakai et al., 1976) forms 1,5-hexadiene with two internal carbons that are saturated, while a reaction like C₂H₃ + 1-C₄H₅ would form 1,3,5-hexatriene.

Diels-Alder addition is both a growth and a cyclization reaction. Historically, it was the first mechanism described for forming cyclic hydrocarbons. In forming aromatics, a 1,3-butadiene structure would add across a double bond (Hague and Wheeler, 1929; Wheeler and Wood, 1930; Badger, 1951) or a triple bond (Glassman, 1976) to form a cyclohexene or a 1,4-cyclohexadiene structure, respectively. These are concerted reactions, proceeding via six-electron pericyclic pathways.

Cyclization reactions then include Diels-Alder addition and two types of isomerization, radical self-addition (e.g., $\text{C}_6\text{H}_5\text{C}\equiv\text{C}\cdot \rightarrow \text{phenyl}$) and molecular cyclization. To be viable, a molecular cyclization must involve a pericyclic pathway, for example the isomerization of 1,3,5-hexatriene to 1,3-cyclohexadiene (Benson and O'Neal, 1970).

Aromatization generally requires dehydrogenation of the cyclic intermediate or redistribution of hydrogen. [An exception is the radical self-addition noted in the previous paragraph, which forms phenyl in the cyclization step.] Possible mechanisms for hydrogen removal are unimolecular elimination of H from cyclic radicals,

unimolecular elimination of H₂, notably from 1,4-cyclohexadiene, and bimolecular abstraction of H, which would produce a radical that could eliminate H unimolecularly. Redistribution could result from internal H-shifts. Alternatively, abstraction of an allylic hydrogen could be followed by H-acquisition at a different site in the resonance structure, effectively shifting the location of the π bond.

Having too much hydrogen or having hydrogen in the wrong place will slow the formation of aromatics through a given pathway. For example, addition of C₂H or addition to the end of a substituted acetylene [such as the 1- position of 3-butenyne (vinylacetylene)] would create a hydrogen-deficient position. Similarly, addition of CH₃ or allyl to a π bond would leave a saturated carbon, from which H would have to be removed.

Quantitative tests. - Only three studies have compared quantitative predictions of mechanisms with data.

Cole, Bittner, Howard, and Longwell (1984) described full details of a mechanism and a quantitative, apparently successful test against data. Mole fractions of stable and free-radical species were measured in a 1,3-butadiene (C₄H₆) flame using molecular-beam mass spectrometry. Pressure was 2.67 kPa (20 torr), and temperatures in the region of benzene formation were 500 to 1500 K. For various pathways to benzene, rate constants were estimated by correlation or transition-state theory, and rates were predicted using these rate constants, mole fractions, and pseudo-steady-state assumptions. When predicted and measured rates of benzene formation were compared, the only satisfactory pathway had addition of 1,3-butadienyl (1-C₄H₅) to acetylene (C₂H₂) as its rate-limiting step. The rate constant estimated for this step was $10^{11.2} \exp(-3.7/RT)$ cm³mol⁻¹s⁻¹, which would be a high-pressure-limit value.

Frenklach, Clary, Gardiner and Stein (1985) presented an alternative mechanism, also apparently successful. For their shock-tube pyrolyses of acetylene [1700-2300 K, 500-700 kPa (5-7 atm)], they concluded that addition of 1-C₄H₃ to C₂H₂ was the major pathway in forming the first aromatic ring. This pathway was inferred from a 600-reaction, 180-species model, comparing several pathways within the model using ultimate production of soot (measured by light

absorption) as an experimental test. Predicted yield of soot was low by a factor of four, but the temperature dependence of the prediction was very good. Compared to other pathways in the analysis, the $1\text{-C}_4\text{H}_3$ route was faster by orders of magnitude, assuming a rate constant of $10^{13} \text{ cm}^3\text{mol}^{-1}\text{s}^{-1}$ for the addition to form $1\text{-C}_6\text{H}_5$.

Finally, Colket measured concentrations of stable species from pyrolysis of C_2H_2 and vinylacetylene in a single-pulse shock tube. In the first study (Colket, 1985a), he assumed that $1\text{-C}_4\text{H}_5 + \text{C}_2\text{H}_2$ addition was the rate-limiting step in forming benzene, as Cole et al. (1984) had found, and that the rate constant for $1\text{-C}_4\text{H}_5 + \text{C}_2\text{H}_2 \rightarrow 1\text{-C}_6\text{H}_7$ was $10^{12.6} \exp(-9/RT) \text{ cm}^3\text{mol}^{-1}\text{s}^{-1}$. Predictions for 1100–1500 K were low by a factor of four but followed the experimental trends. In the second study (Colket, 1985b), $\text{C}_2\text{H}_3 + \text{vinylacetylene}$ was proposed to lead to benzene (Table VIII.1). A barrierless rate constant of $10^{11.3} \text{ cm}^3\text{mol}^{-1}\text{s}^{-1}$ was required for the overall reaction $\text{C}_2\text{H}_3 + \text{C}_4\text{H}_4 \rightarrow \text{H} + \text{benzene}$ in order to fit the data for 1200–1800 K.

VIII.3. Preliminary screening

To screen the above mechanisms before making more detailed calculations, rates for the addition steps are calculated from high-pressure-limit rate constants k_∞ and the measured concentrations of possible reactants. Note that neither a thermal reaction sequence nor a chemically activated pathway can be faster than the rate predicted in this way.

If the ratio of this predicted rate to the measured rate of benzene formation is much less than unity, then this step, and thus the mechanism, is too slow to lead to benzene in this flame. The ratio can be greater than unity because benzene destruction is also occurring, particularly beyond 0.35 cm.

Uncertainties other than kinetics. - The uncertainties in the prediction and the measurement determine how near unity their ratio must be. There are four areas of uncertainty in the measurements which must be recognized: the temperature uncertainty, calibration uncertainties, the identification of mass 78 as benzene, and the identities of reactants which may have isomers.

Temperature measurements and uncertainty were discussed in Ch. III.4. For the present problem, temperature affects the predicted rate explicitly through the rate constant, but it affects the measured net rate implicitly, mainly through the diffusion term. Thus, temperature uncertainties will affect the two rates differently. Also, the temperature profile and the mole-fraction profiles are aligned by shifting the mole-fraction profiles toward the burner by two orifice diameters or 1.10 mm, an approximate correction that is most subject to error near the burner.

Calibration uncertainties were discussed in Ch. IV. For acetylene, this uncertainty is 3%, and for minor stable species and free radicals, it is estimated to be 50%. The benzene formation rate is proportionately affected by this uncertainty.

It is reasonable to question whether the 78-amu species detected in the flame is in fact benzene. A usual test, measurement of the ionization potential, is not conclusive (Ch. IV). The ionization potential measured for mass 78 at 4.0 mm (distance from burner) was 9.3 ± 0.5 eV. In comparison, the ionization potential is 9.25 eV for benzene, 9.50 for 3,5-hexadienyne, and 10.5 for 1,5-hexadien-3-yne (Rosenstock et al., 1977). Other isomers containing CH_3 groups have ionization potentials varying from 9.20 to 10.35, and it is 8.36 eV for 5-methylenecyclopentadiene.

Analysis of a microprobe sample by GC/MS (Sec. IV.4) identified benzene as the principal species measured by molecular-beam mass spectrometry at mass 78. Four species were detected at this mass, benzene and three aliphatic C_6H_6 species. From gas chromatography, the benzene represented 72% of the mass at 0.45 cm.

There is similar uncertainty about the isomeric identity of certain reactants and thermalized intermediates. Here, GC/MS is of little help because (1) radicals are destroyed in the microprobe sampling, (2) species lighter than C_6H_2 were too volatile to be retained in the sample, and (3) no C_6 species heavier than 78 amu (i.e., C_6H_8 , C_6H_{10} , C_6H_{12}) were detected with sensitivity for C_6 's at 1 ppm or less. Ionization potentials are too close to be helpful in distinguishing among these isomers.

These limitations do not preclude using the screening for examining feasibility. For example, the rate calculated for $1\text{-C}_4\text{H}_3 + \text{C}_2\text{H}_2$ may overpredict the rate of benzene formation if mass 51 is a mixture of C_4H_3 isomers or if the thermalized intermediates undergo other reactions not leading to benzene. However, if the true rate by a pathway was lower than predicted and the rate was already much slower than the net rate of benzene formation, then the mechanism would be even less plausible.

In summary, the uncertainties discussed here imply that if the predicted rate is within an order of magnitude of the measured rate, it could be important as a path to benzene in this flame.










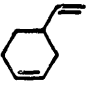
Screening using k_{∞} . - Only the additions of $1\text{-C}_4\text{H}_3$ and $1\text{-C}_4\text{H}_5$ to C_2H_2 prove to be fast enough in the high-pressure limit. The possible reactants from Table VIII.1 that have been proposed to lead to benzene are tested in Table VIII.2 using the ratio of the predicted rate to the measured net rate. The maximum and minimum values of the ratio are listed for the range 0.11 to 0.39 cm, as is the value at 0.30 cm, where the benzene formation rate is greatest. Sources of k_{∞} values are also included.

The reaction $1\text{-C}_4\text{H}_5 + \text{C}_2\text{H}_2$ is always faster than 1.9 times the measured rate, and the minimum ratio for $1\text{-C}_4\text{H}_3 + \text{C}_2\text{H}_2$ is 0.95. The largest ratio for the other reactions is 0.37 for C_3H_5 combination at 0.12 cm, where the rate of benzene formation is low. However, at the peak measured rate of formation, the ratio for this reaction is only 0.07.

With one exception, all the reactions that proved unfeasible involve pairings of minor species. This is in pointed contrast to the feasible reactions above, which involve C_2H_2 and a minor C_4 species. The exception is Diels-Alder addition of C_4H_6 to C_2H_2 , which has a high activation energy and, even at these temperatures, a low rate constant. Thus it is a combination of the low concentration product and/or the rate constant that prevents these other paths from being important in this flame.

Three additional radical-combination reactions that were tested were $\text{C}_2\text{H}_3 + 1\text{-C}_4\text{H}_3$, $\text{C}_2\text{H}_3 + 1\text{-C}_4\text{H}_5$, and $\text{C}_3\text{H}_3 + \text{C}_3\text{H}_3$. Using $k_{\infty}=8.5 \cdot 10^{12}$ as for C_3H_5 , the two C_2H_3 reactions were too slow with

Table VIII.2. Testing literature mechanisms for benzene formation using k_{∞} for the initial addition/combination step.

Addition reaction	k_{∞} in mol, cm ³ , s, cal units	Ref.	Ratio of predicted to measured rate of benzene formation		
			Max	Min	At 0.3 cm
CH ₃ + C ₄ H ₆ → 	$8.1 \cdot 10^{10} \exp(-4.1/RT)$	a	0.12	0.004	0.006
C ₂ H ₃ + C ₄ H ₄ → 	$3 \cdot 10^{11} \exp(-3/RT)$	b	0.013	0.051	0.011
C ₂ H ₃ + C ₄ H ₆ → 	$3 \cdot 10^{11} \exp(-3/RT)$	b	0.029	8E-4	9E-4
1-C ₄ H ₃ + C ₂ H ₂ → 	$280T^{2.9} \exp(-1.4/RT)$	c	12.	1.9	1.9
1-C ₄ H ₅ + C ₂ H ₂ → 	$280T^{2.9} \exp(-1.4/RT)$	c	13.	0.95	1.0
1-C ₄ H ₅ + C ₂ H ₄ → 	$3 \cdot 10^{11} \exp(-3/RT)$	b	0.1	0.004	0.005
C ₃ H ₅ + C ₃ H ₅ → 	$8.5 \cdot 10^{12}$	d	0.4	0.05	0.07
C ₄ H ₆ + C ₂ H ₂ → 	$2.3 \cdot 10^{12} \exp(-35/RT)$	e	3E-4	2E-5	2E-4
C ₄ H ₆ + C ₂ H ₄ → 	$2.3 \cdot 10^{10} \exp(-27/RT)$	f	4E-7	1E-7	3E-7
C ₄ H ₆ + C ₄ H ₆ → 	$5 \cdot 10^{10} \exp(-27/RT)$	g	2E-8	6E-9	1E-8

^a Evaluation of Kerr and Parsonage (1972).

^b Estimate of Weissman and Benson (1984) for C₂H₃ + C₄H₆; compare to estimate of $2.4 \cdot 10^{11} \exp(-4/RT)$ by Cole (1982).

^c Estimate of Cole et al. (1984) of $k_{\infty}(400 \text{ K}) = 10^{11.2} \exp(-3.7/RT)$, written for 300-2000 K using $\langle \Delta C_p^\ddagger \rangle = 3.75 \text{ cal/mol} \cdot \text{K}$ from Benson and Weissman (1984).

^d Measurement by Van den Bergh and Callear at 298 K (1970); Throssell (1972) estimated $4 \cdot 10^{12} \text{ cm}^3 \text{ mol}^{-1} \text{ s}^{-1}$; Golden et al. (1969) measured $7.4 \cdot 10^{12}$ at 913 K and $5.0 \cdot 10^{12}$ at 1063 K, recognizing that some fall-off was a possibility.

^e Estimate of Cole et al. (1984).

^f Uchiyama et al. (1964).

^g Tsang (1965).

ratios at 0.30 cm of 0.04 and 0.02, respectively. The third reaction was more promising, with a high-pressure-limit prediction that was more than an order of magnitude higher than the measured rate of benzene production. However, hydrogen redistribution in the products is a serious problem. C_3H_3 has two resonance structures, 2-propynyl ($\cdot CH_2-C\equiv CH$) and propadienyl ($\cdot CH=C=CH_2$), so the products of simple combination are $HC\equiv C-CH_2-CH_2-C\equiv CH$, $HC\equiv C-CH_2-CH=C=CH_2$, and $CH_2=C=CHCH=C=CH_2$ in the proportions 1:2:1. Ring closure via triplet (biradical) states is conceivable, but two 1,2-H-shifts would be necessary to lead to benzene. This problem was considered to be a sufficient liability that the reactants were not considered further.

VIII.4. Detailed calculation of rate constants and rates

Bimolecular QRRK rate constants were calculated for $1-C_4H_5$ and $1-C_4H_3$ based on the results of preliminary screening. Simple addition had a rate constant much less than the high-pressure limit, but chemically activated isomerization was predicted to proceed fast enough to account for the rate of benzene formation.

Implications of relaxing the high-pressure-limit assumption. -

The assumption that an addition or combination reaction is in a high-pressure limit generally should be checked. There are rules of thumb that molecules with more than eight atoms are typically in the high-pressure limit (Benson, 1976), but such generalizations break down as temperature increases above room temperature.

When the adduct is freshly formed, its excess energy relative to the thermalized, ground state must be dissipated by energy-removing collisions if the adduct is to be stabilized. In the simplest case, if stabilization is too slow, the energized adduct will decompose to the reactants, making the effective rate of addition/stabilization slower than the high-pressure limit.

Significantly for benzene formation, the energized adduct also may decompose or isomerize unimolecularly to new products. Such pathways are described as chemically activated because they are driven by the excess chemical energy released in the addition. The energy distribution in the energized adduct is higher than that of the thermalized adduct, so the unimolecular reaction rate of the

energized adduct proceeds at a faster rate than the unimolecular rate of the ground state. Chemical activation has been studied experimentally and analyzed successfully by applying unimolecular reaction-rate theory (see Chapters VI and VII and references within).

The bimolecular rate constant measured for each set of products is a weighted average of the rate constants for available energy states, just as for the measured unimolecular rate constant. For modeling chemistry in complex mixtures, it is convenient to determine the apparent bimolecular rate constants for simple addition and chemically activated reactions as functions of temperature for a given pressure and third-body gas.

Bimolecular QRRK analysis (Ch. VI) is used here to estimate the pressure-dependent rate constants. Although RRKM or other more precise methods could be used, bimolecular QRRK has been shown to predict well the pressure- and temperature-dependence of many combustion and pyrolysis reactions (Ch. VII). The present application also demonstrates that relatively few parameters and a simple computation scheme are needed to evaluate these complex reaction sequences.

Input parameters for calculation of rate constants. - Rate constants were calculated at 2.67 kPa (20 torr) and at 101 kPa (1 atm) for the product channels of $1\text{-C}_4\text{H}_3 + \text{C}_2\text{H}_2$ and $1\text{-C}_4\text{H}_5 + \text{C}_2\text{H}_2$.

Kinetic input parameters and how they were determined are shown in Tables VIII.3 and VIII.4 for the two reactions.

The other inputs that are needed are collisional properties of the adduct, the isomer, and the third-body gas. The reasonable assumption was made that for all C_6 adduct and isomer species, the Lennard-Jones parameters for benzene could be used, $\sigma=5.349 \text{ \AA}$ and $\epsilon/k=412.3 \text{ K}$ (Reid et al., 1977). Ar was the third-body gas M in these calculations, but using CO did not change the result. For Ar as the collision partner, $-\langle\Delta E_{\text{co11}}\rangle$ was chosen to be 740 cal/mol (Appendix M), $\sigma=3.33 \text{ \AA}$, and $\epsilon/k=136.5 \text{ K}$ (Kee et al., 1983).

Formation of benzene from $1\text{-C}_4\text{H}_5 + \text{C}_2\text{H}_2$. - Radical addition of $1\text{-C}_4\text{H}_5$ to C_2H_2 forms little of the thermalized adduct, but rather it forms H + benzene by isomerization and decomposition of the chemically activated adduct. An energy diagram for this reaction

Table VIII.3. Parameters needed for bimolecular QRRK calculations for $l\text{-C}_4\text{H}_5 + \text{C}_2\text{H}_2$ reactions via the chemically activated intermediates $l\text{-C}_6\text{H}_7^*$ and $c\text{-C}_6\text{H}_7^*$ (mol, cm, s, kcal units).

<u>Parameter description</u>	<u>Parameter value</u>	<u>Source</u>
- Kinetic parameters -		
$l\text{-C}_4\text{H}_5 + \text{C}_2\text{H}_2 \rightarrow l\text{-C}_6\text{H}_7$ ($\cdot\text{---}\text{---}\text{---}$)	$k_{\infty}(300\text{--}1500\text{ K}) = 2.8 \cdot 10^2 T^{2.9} \exp(-1.4/RT)$ $\text{cm}^3 \text{mol}^{-1} \text{s}^{-1}$ $= 7.2 \cdot 10^{12} \exp(-10.0/RT)$ at 1500 K	$k(400\text{ K}) = 10^{11.2} \exp(-3.5/RT)$ by Cole et al. (1984) and $\langle \Delta C_p^\ddagger \rangle = 3.75$ cal/mol·K from Benson and Weissman (1984)
$l\text{-C}_6\text{H}_7 \rightarrow l\text{-C}_4\text{H}_5 + \text{C}_2\text{H}_2$	$A_{\infty} = 3.6 \cdot 10^{14} \text{ s}^{-1}$ $E_{\infty} = 46.1 \text{ kcal/mol}$	Microscopic reversibility
$l\text{-C}_6\text{H}_6 + \text{H} \rightarrow l\text{-C}_6\text{H}_7$ ($\text{---}\text{---}\text{---}$) ($\cdot\text{---}\text{---}\text{---}$)	$A_{\infty} = 1.6 \cdot 10^{12} \text{ cm}^3 \text{mol}^{-1} \text{s}^{-1}$ $E_{\infty} = 1.0 \text{ kcal/mol}$	$A_{\infty}/4$ for $\text{H} + \text{---}\text{---}\text{---}$ E_{∞} for $\text{H} + \text{---}\text{---}\text{---}$
$l\text{-C}_6\text{H}_7 \rightarrow l\text{-C}_6\text{H}_6 + \text{H}$	$A_{\infty} = 4 \cdot 10^{12} \text{ s}^{-1}$ $E_{\infty} = 36.7 \text{ kcal/mol}$	Microscopic reversibility
$l\text{-C}_6\text{H}_7 \rightarrow c\text{-C}_6\text{H}_7$	$A_{\infty} = 1.7 \cdot 10^{11} \text{ s}^{-1}$ (1500K) $E_{\infty} = 7 \text{ kcal/mol}$	Estimate by thermochemical kinetics (Appendix O) Estimate as E_{act} for radical addition ^a
$c\text{-C}_6\text{H}_7 \rightarrow l\text{-C}_6\text{H}_7$	$A_{\infty} = 1.0 \cdot 10^{14} \text{ s}^{-1}$ $E_{\infty} = 53.2 \text{ kcal/mol}^b$	Microscopic reversibility
$\text{H} + \text{Benzene} \rightarrow c\text{-C}_6\text{H}_7$	$A_{\infty} = 4 \cdot 10^{13} \text{ cm}^3 \text{mol}^{-1} \text{s}^{-1}$ $E_{\infty} = 4.3 \text{ kcal/mol}$	Nicovich and Ravishankara (1984)
$c\text{-C}_6\text{H}_7 \rightarrow \text{H} + \text{Benzene}$	$A_{\infty} = 2 \cdot 10^{13} \text{ s}^{-1}$ (550 K) $E_{\infty} = 26.0 \text{ kcal/mol}$	Tsang (1986)
- Properties of $l\text{-C}_6\text{H}_7$ and $c\text{-C}_6\text{H}_7$ -		
Number of vibrational degrees of freedom (s):	33	$3 \cdot (13 \text{ atoms}) - 6$
Geometric-mean frequencies $\langle \nu \rangle$:		
$l\text{-C}_6\text{H}_7$	1050 cm^{-1}	From estimated frequencies
$c\text{-C}_6\text{H}_7$	1070 cm^{-1}	From estimated frequencies
Molecular weight	79.11 g/g-mol	-
Lennard-Jones well depth ϵ/k and diameter σ	412.3 K, 5.349 Å	Same as benzene (Reid et al., 1977)

^a Based on Kerr and Moss (1981).

^b Using $\Delta H_f^\circ, 298 = 50.0 \text{ kcal/mol}$ (Tsang, 1986).

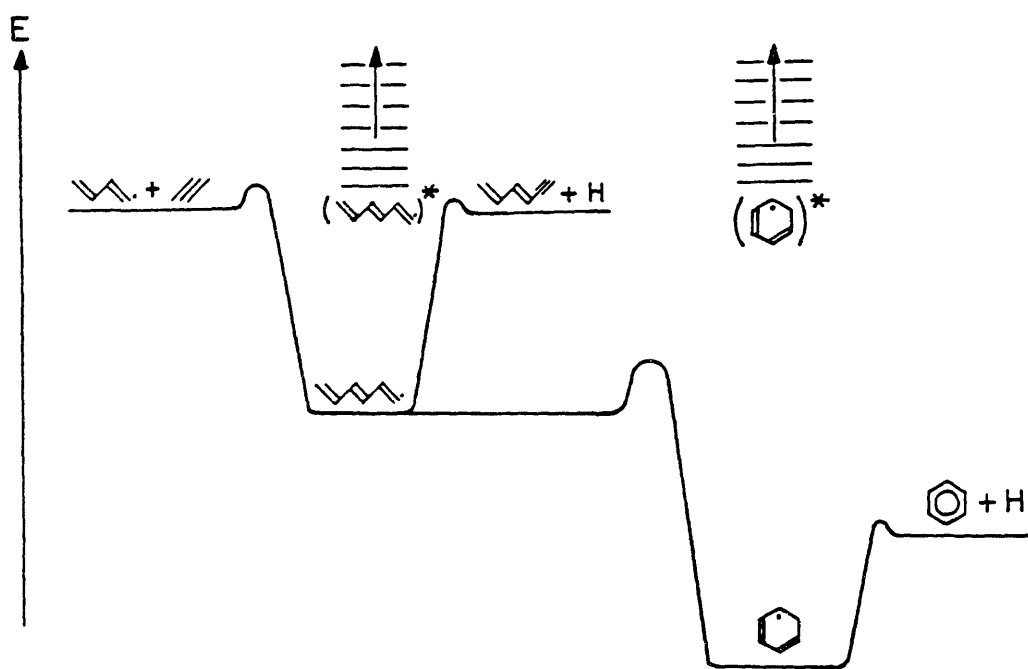


Fig. VIII.1. Energy diagram for addition of $1\text{-C}_4\text{H}_5 + \text{C}_2\text{H}_2$

(Fig. VIII.1) shows the amount of excess energy to be the driving force. Addition forms excited $\text{l-C}_6\text{H}_7^*$, which goes preferably to $\text{c-C}_6\text{H}_7^*$ because of the excess of energy in $\text{l-C}_6\text{H}_7^*$ relative to the low barrier to conversion and the difficulty of collisional stabilization. Likewise, the preferred fate of $\text{c-C}_6\text{H}_7^*$ is β -scission to eliminate H and form benzene rather than re-isomerization or collisional stabilization.

Calculation of the rate constants for each channel (Fig. VIII.2 for 2.67 kPa and Fig. VIII.3 for 101 kPa) shows not only that $\text{H} + \text{C}_6\text{H}_6$ dominates at all temperatures, but also that its rate constant is generally quite near k_∞ for addition. Thus, although Cole et al. (1982) and Colket (1985a) used k_∞ values for addition that were somewhat different from the k_∞ expression derived here, their decisions to use that reaction as the rate-limiting step would give them approximately the right rate constant. *Despite the fact that the high-pressure-limit thermal mechanism that they used was incorrect*, their tests then would give "correct" predictions.

At 2.67 kPa (20 torr; Fig. VIII.2), k for the channel $\text{H} + \text{C}_6\text{H}_6$ slightly diverges from $k_{\infty, a/d}$ only at about 1400 K. The reason for this dropoff is not diversion into other product channels but the growing importance of the decomposition back to reactants, $\text{l-C}_6\text{H}_7^* \rightarrow \text{l-C}_4\text{H}_5 + \text{C}_2\text{H}_2$. Decomposition of $\text{l-C}_6\text{H}_7^*$ to $\text{H} + \text{l-C}_6\text{H}_6$ is the other important product channel, but it is an order of magnitude slower than $\text{H} + \text{benzene}$ even at 2000 K. Both stabilization channels (to $\text{l-C}_6\text{H}_7$ and $\text{c-C}_6\text{H}_7$) are two or more orders slower at all temperatures than formation of $\text{H} + \text{benzene}$.

At 101 kPa (1 atm; Fig. VIII.3), the rate constants for the chemically activated decomposition channels $\text{H} + \text{benzene}$ and $\text{H} + \text{l-C}_6\text{H}_6$ are changed very little from their values at 2.67 kPa. The stabilization channels are more important because of the higher pressure, but they are still slower than $\text{H} + \text{benzene}$ at all temperatures examined.

Formation of phenyl from $\text{l-C}_4\text{H}_3 + \text{C}_2\text{H}_2$. - Chemically activated $\text{l-C}_6\text{H}_5^*$ is formed by addition of $\text{l-C}_4\text{H}_3$ and C_2H_2 and, just as for $\text{l-C}_6\text{H}_7^*$, it isomerizes rapidly to a chemically activated cyclic structure. Unlike $\text{c-C}_6\text{H}_7^*$, though, $\text{c-C}_6\text{H}_5^*$ (phenyl*) has a high exit

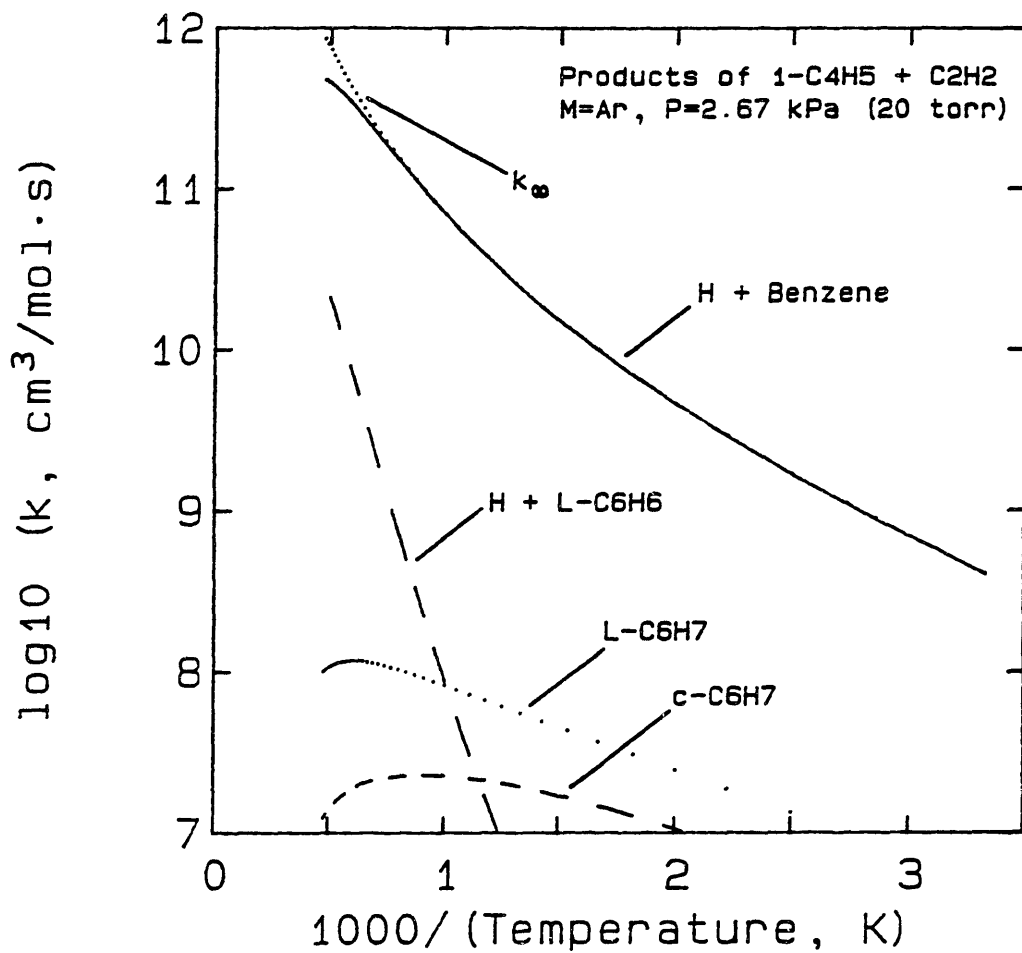


Fig. VIII.2. Predictions at 2.67 kPa (20 torr) of bimolecular rate constants for product channels of 1-C₄H₅ + C₂H₂.

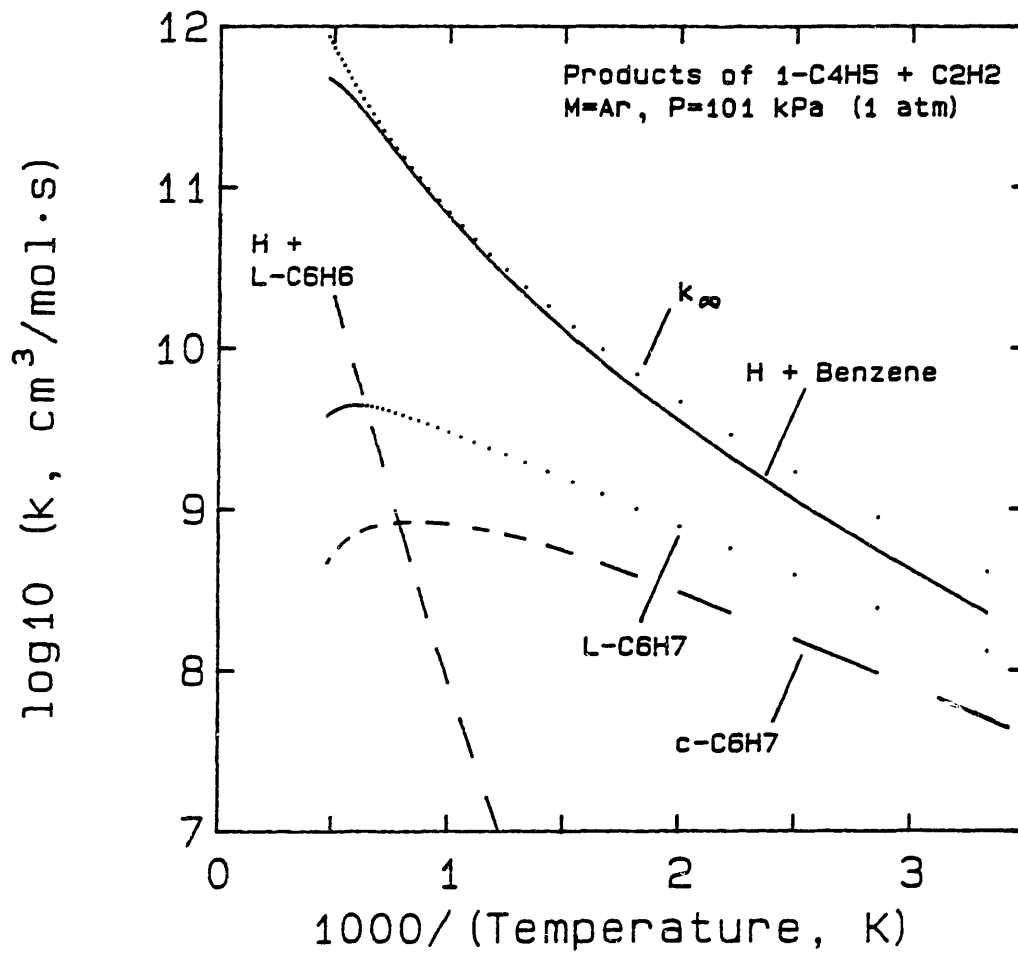


Fig. VIII.3. Predictions at 101 kPa (1 atm) of bimolecular rate constants for product channels of 1-C₄H₅ + C₂H₂.

barrier for decomposition because benzyne ($c\text{-C}_6\text{H}_4$) is a highly strained, high-energy species. Thus, collisional stabilization of the cyclic intermediate to phenyl is feasible.

Calculations at 2.67 kPa (Fig. VIII.4) and 101 kPa (Fig. VIII.5) confirm the importance of the phenyl channel, but they also show that this isomerization/stabilization channel is affected more by pressure and alternative channels than was $l\text{-C}_4\text{H}_5 + \text{C}_2\text{H}_2 \rightarrow \text{H} + \text{benzene}$. At both pressures, the rate constant to phenyl has a maximum that is caused by collisional stabilization becoming more difficult as temperature increases; i.e., as $[M]=P/RT$ decreases. High temperatures also extend the energy distribution of excited $l\text{-C}_6\text{H}_5^*$ and $c\text{-C}_6\text{H}_5^*$ states to higher energy levels, where chemically activated decomposition is more likely.

Thus at 2.67 kPa (20 torr; Fig. VIII.4), phenyl is still the dominant product to 1500 K, but the rate constant has a maximum at 1150 K. Above 1500 K, chemically activated decomposition to $\text{H} + l\text{-C}_6\text{H}_4$ predominates, and above 2100 K, $\text{H} + \text{benzyne}$ also becomes faster than phenyl formation. The rate constant for the high-pressure adduct $l\text{-C}_6\text{H}_5$ is about 5% of k_∞ and the rate constant for phenyl formation through much of the temperature range.

Formation of $l\text{-C}_6\text{H}_5$ is more important at 101 kPa (1 atm; Fig. VIII.5) than at 2.67 kPa. However, the phenyl rate constant both remains near $k_{\infty, \text{add}}$ and predominates over the other channels for a greater range of temperatures. The $l\text{-C}_6\text{H}_5$ is slightly favored below 370 K, and $\text{H} + l\text{-C}_6\text{H}_4$ dominates above 2000 K. Benzyne formation is unimportant at all temperature. All of these differences at the higher pressure reflect greater collisional stabilization.

Test of predicted rates against measurements. - With rate constants that correctly allow for pressure and chemically activated channels, rates for the different channels can be predicted and compared to the measured net rates of benzene formation. The rate of benzene formation is predicted directly for $l\text{-C}_4\text{H}_5 + \text{C}_2\text{H}_2$. For $l\text{-C}_4\text{H}_3 + \text{C}_2\text{H}_2 \rightarrow \text{phenyl}$, applying this test assumes that benzene formation via phenyl can be no faster than the rate of phenyl formation.

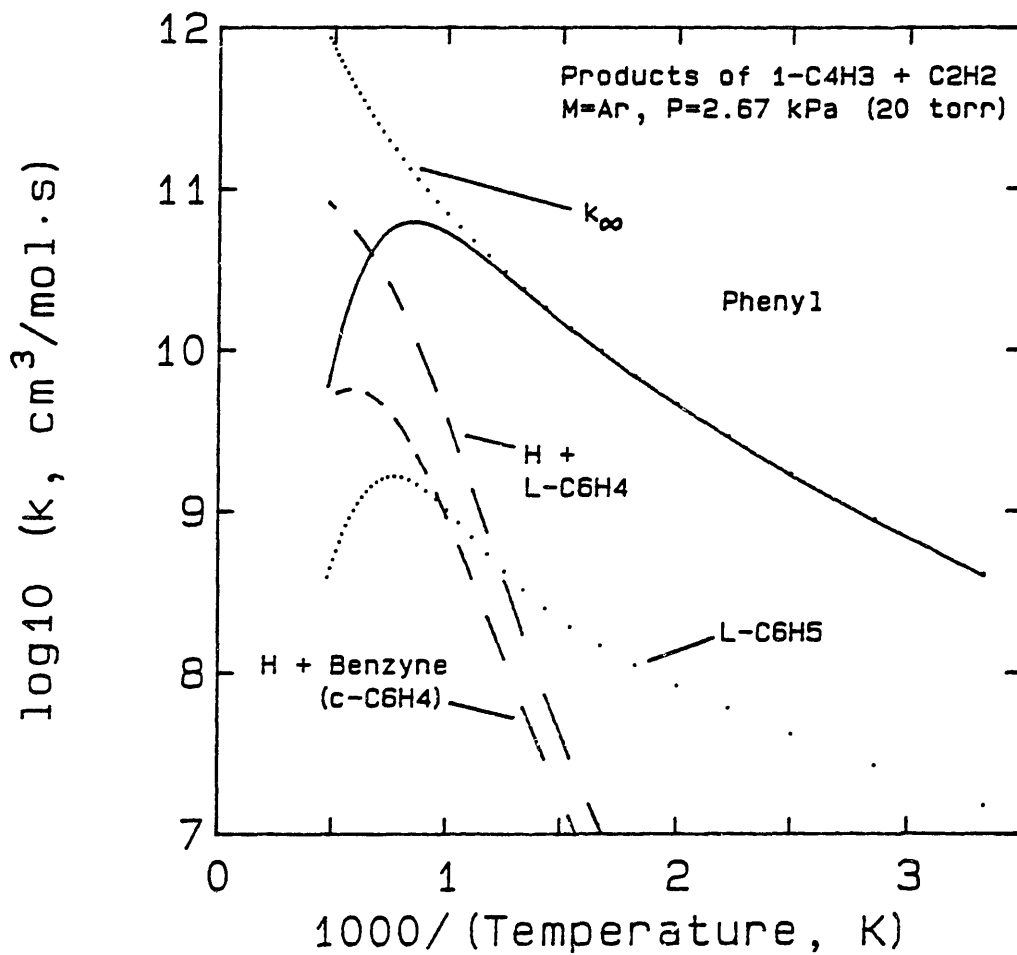


Fig. VIII.4. Predictions at 2.67 kPa (20 torr) of bimolecular rate constants for product channels of 1-C₄H₃ + C₂H₂.

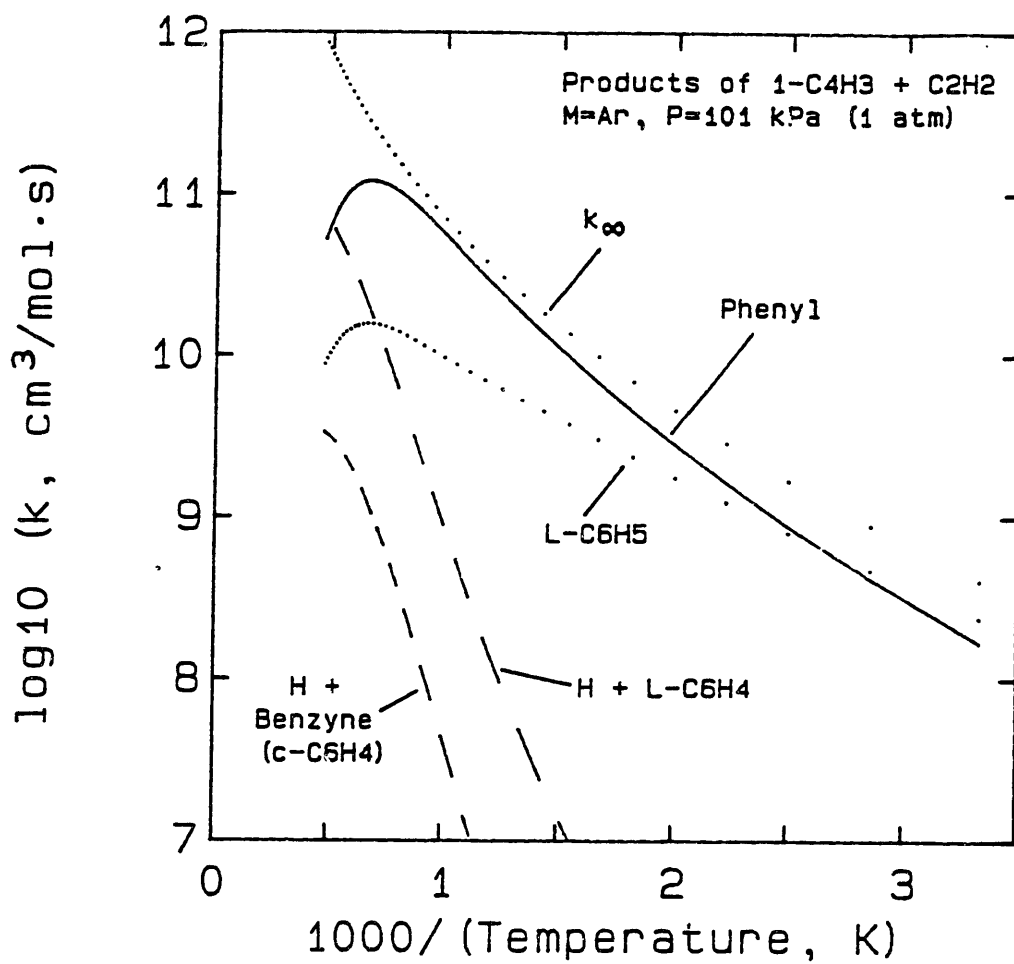


Fig. VIII.5. Predictions at 101 kPa (1 atm) of bimolecular rate constants for product channels of 1-C₄H₃ + C₂H₂.

The results are shown in Fig. VIII.6. The $l\text{-C}_4\text{H}_5$ route is always near to or faster than the measured net rate, while the $l\text{-C}_4\text{H}_3$ route is somewhat slower. Nevertheless, both channels are within the uncertainty of the measurements and of the predicted rate constants. It seems likely, then, that (1) both channels contribute to benzene formation and (2) the predicted rate constants are well-suited for use in a flame mechanism to predict benzene formation from an entire network of reactions.

Even the shape of the predicted curve would seem to match that of the measured rate except for an apparent shift toward the burner. This is entirely possible, as the alignment of the temperature profile affects the two rates differently (discussed in Ch. VIII.3).

VIII.5. Re-interpretation of literature tests

The test of Cole et al. (1984) is still valid in light of these rate constants, even though their mechanism via thermal, collisionally stabilized intermediates is mistaken. The present study shows that direct, chemically activated formation of benzene from $l\text{-C}_4\text{H}_5 + \text{C}_2\text{H}_2$ would proceed at approximately k_∞ for simple addition. Cole et al. assumed a thermal mechanism but inferred that in their mechanism, the addition $l\text{-C}_4\text{H}_5 + \text{C}_2\text{H}_2 \rightarrow l\text{-C}_6\text{H}_7$ would be the rate-limiting step. Except for the slightly different k_∞ estimated here, their test results would be unchanged.

Frenklach et al. (1985) identified cyclization of $l\text{-C}_6\text{H}_5$ to phenyl as the fastest route to single-ring aromatics by three orders of magnitude. However, the rate constant for producing $l\text{-C}_6\text{H}_5$ from $l\text{-C}_4\text{H}_3 + \text{C}_2\text{H}_2$ was $10^{13} \text{ cm}^3\text{mol}^{-1}\text{s}^{-1}$, three orders of magnitude too high for $l\text{-C}_6\text{H}_5$ by the present calculations and two orders of magnitude higher than the rate constant predicted here for direct phenyl production. Their sensitivity analysis varied rate constants by a factor of five, much less than the difference indicated here, so the effects of the present rate constants on relative pathways from their mechanism is unclear. Also, their quantitative test was more indirect, predicting total soot yield that was a factor of 20 lower than they measured.

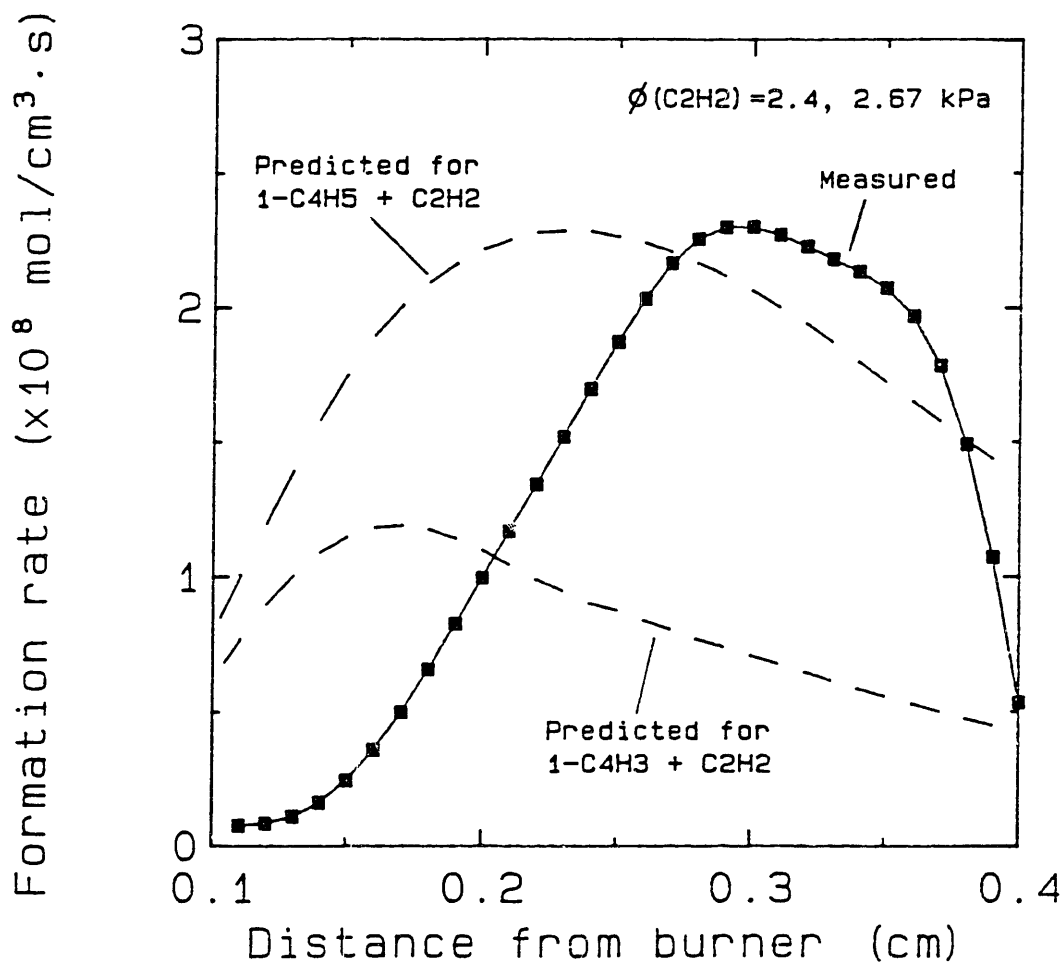


Fig. VIII.6. Comparison of the predicted rates for $1\text{-C}_4\text{H}_5 + \text{C}_2\text{H}_2 \rightarrow \text{H} + \text{benzene}$ and for $1\text{-C}_4\text{H}_3 + \text{C}_2\text{H}_2 \rightarrow \text{phenyl}$ to the net rate of benzene formation measured at 2.67 kPa in a $\phi=2.40 \text{ C}_2\text{H}_2/\text{O}_2/5\% \text{ Ar}$ flame, temperatures increasing from 900 to 1600 K in this region.

These authors found that their predicted rate of cyclization for $\text{l-C}_6\text{H}_7 \rightarrow \text{c-C}_6\text{H}_7$ was five orders of magnitude slower than the predicted rate for $\text{l-C}_6\text{H}_5 \rightarrow \text{phenyl}$. Note that the present analysis, taking fall-off and chemical activation into account, indicates that neither thermal cyclization is likely to be important. For the same reasons, susceptibility of the thermal intermediates to bimolecular or unimolecular destruction reactions would be unimportant.

Colket's study of acetylene pyrolysis (1985a) was in Ar at approximately 100 kPa. He used the same assumption as Cole et al. that $\text{l-C}_4\text{H}_5 + \text{C}_2\text{H}_2$ was the rate-limiting step, so his success can be explained by the same reasons as above. A significant difference is that Colket tested an entire pyrolysis mechanism against his profiles of stable species, while Cole et al. tested only the steps from $\text{l-C}_4\text{H}_5$ to benzene.

Study of vinylacetylene pyrolysis in the same laboratory (Colket, 1985b) suggested instead that $\text{C}_2\text{H}_3 + \text{C}_4\text{H}_4$ might lead to benzene. While this reaction was unimportant in the present system, one reason was the low mole fractions of both these species. In C_4H_4 pyrolysis, much more C_4H_4 would be available, so this alternative route might be more important. An unresolved problem in Colket's pathway is the isomerization of the adduct $\text{H}_2\text{C}=\text{C}-\text{CH}=\text{C}-\text{CH}=\text{CH}_2$ to cyclohexadienyl.

VIII.6. Rate constants for phenyl pyrolysis

The same input data for bimolecular QRRK calculation of phenyl formation (Table VIII.4) can be used for unimolecular QRRK calculation of phenyl pyrolysis. Good agreement is obtained with the literature, and the products can be better understood.

Phenyl pyrolyzes as thermally activated phenyl ($\text{c-C}_6\text{H}_5^*$) undergoes unimolecular reactions. Breaking one bond would lead to benzyne (by β -scission) or to $\text{l-C}_6\text{H}_5$ (ring rupture), but the latter channel must actually produce $\text{l-C}_6\text{H}_5^*$. This excited species can re-isomerize to $\text{c-C}_6\text{H}_5^*$, be collisionally stabilized as $\text{l-C}_6\text{H}_5$, or undergo decomposition to $\text{H} + \text{l-C}_6\text{H}_4$ or to $\text{l-C}_4\text{H}_3 + \text{C}_2\text{H}_2$. To make this clearer, compare this situation to the energy diagram of Fig.

VIII.1 for $l\text{-C}_4\text{H}_5 + \text{C}_2\text{H}_2$. The major difference is that phenyl \rightarrow benzyne+H has a much higher energy barrier than $c\text{-C}_6\text{H}_7 \rightarrow$ benzene+H.

Rate constants for the four product channels are shown in Fig. VIII.7 along with the sum of the rate constants, $k(\text{Overall})$. Temperatures were 1250 to 2500 K and the pressure was chosen as 1 atm Ar for comparison to shock-tube data below. Two Arrhenius segments of different slope are predicted for $k(\text{Overall})$. One segment below 1600 K corresponds to the dominance of the channel that forms thermalized $l\text{-C}_6\text{H}_5$, while above 1900 K, the segment largely results from the $\text{C}_4\text{H}_3 + \text{C}_2\text{H}_2$ channel. Formation of $\text{H} + l\text{-C}_6\text{H}_4$ is an order of magnitude slower than the latter channel, and benzyne formation is less than 2% of $k(\text{overall})$.

These predictions are compared to literature rate constants in Fig. VIII.8. All the literature rate constants come from testing assumed models against shock-tube data, and all but Colket (1986) assume that $\text{C}_4\text{H}_3 + \text{C}_2\text{H}_2$ is produced directly. [Rao and Skinner (1984) assumed that C_4H_3 decomposes rapidly to $\text{C}_4\text{H}_2 + \text{H}$.] The agreement with three of the sets of data - Rao and Skinner, Kiefer et al. (1985), and Fujii and Asaba (1973) - is quite good and resolves the differences among their apparent activation energies. Note that Fujii and Asaba had assumed that the products were $\text{C}_4\text{H}_3 + \text{C}_2\text{H}_2$, but the present analysis would predict $l\text{-C}_6\text{H}_5$.

The difference from the rate constant of Colket (1986) comes from the different treatment of $l\text{-C}_6\text{H}_5$. Colket assumed that $l\text{-C}_6\text{H}_5$ would be formed as a thermalized intermediate, which could re-isomerize to phenyl or decompose to $\text{C}_4\text{H}_3 + \text{C}_2\text{H}_2$. Assuming that thermalized $l\text{-C}_6\text{H}_5$ was at a steady-state concentration, he estimated an effective rate constant for $\text{C}_6\text{H}_5 \rightarrow \text{C}_4\text{H}_3 + \text{C}_2\text{H}_2$. The present calculations allow formation of thermalized C_6H_5 only by collisional stabilization of $l\text{-C}_6\text{H}_5^*$ and recognize that $l\text{-C}_4\text{H}_3$ can be formed directly from $l\text{-C}_6\text{H}_5^*$. The present approach seems more physically realistic and is more consistent with the other literature rate constants.

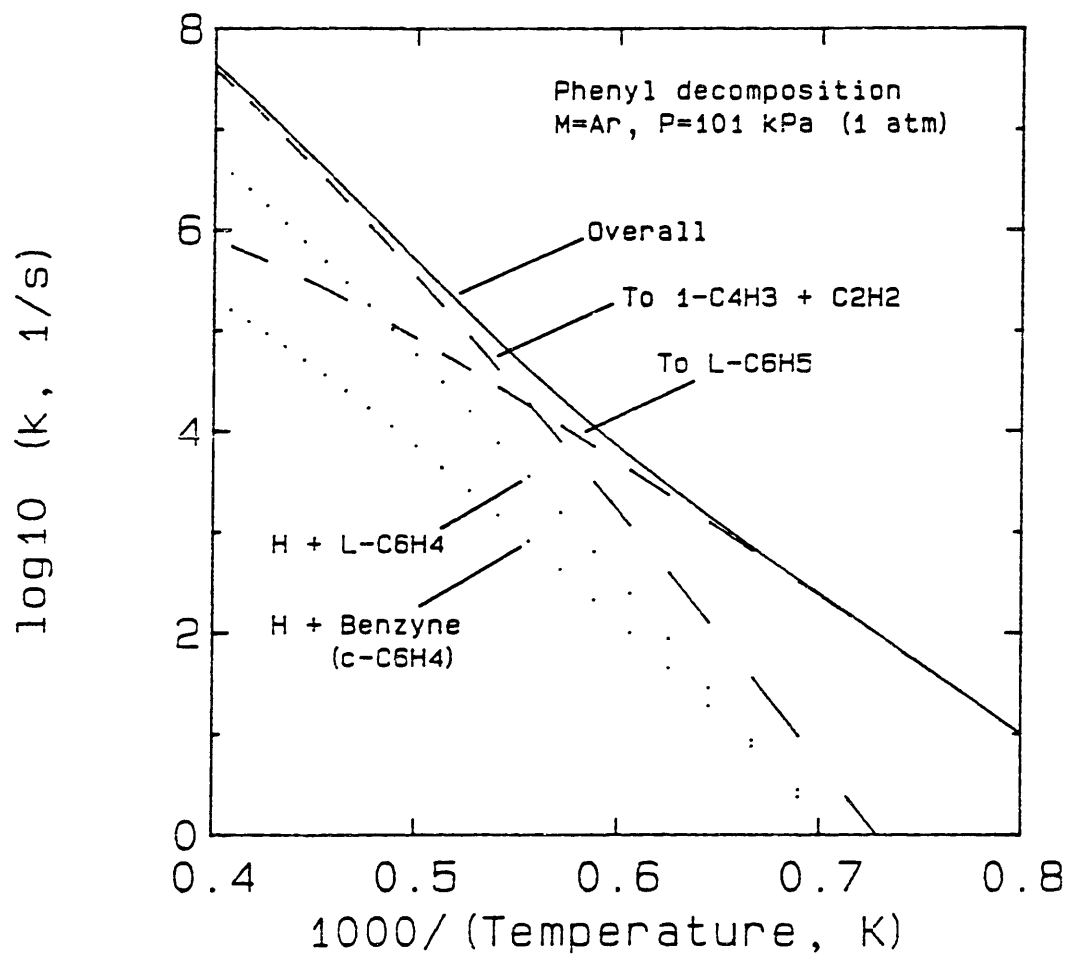


Fig. VIII.7. Predictions of rate constants for product channels of phenyl pyrolysis at 101 kPa (1 atm).

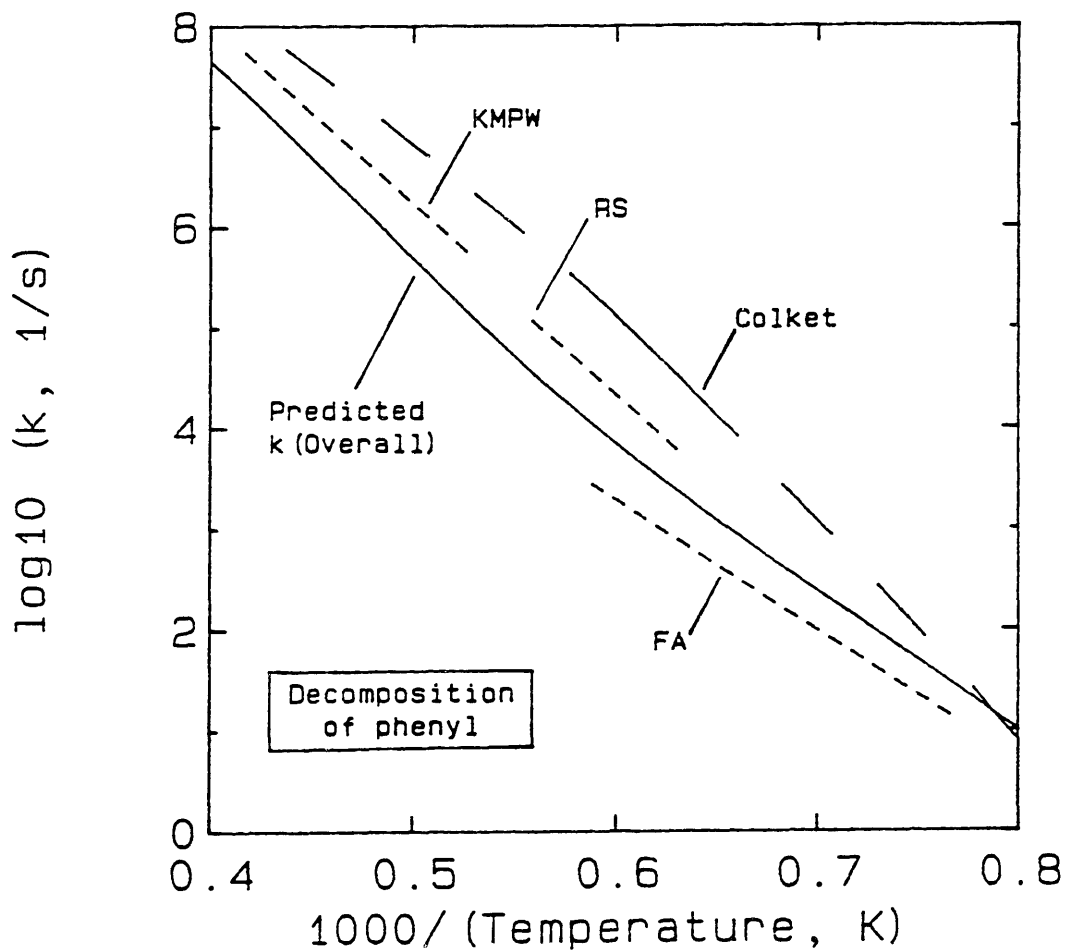


Fig. VIII.8. Comparison of predicted rate constants for phenyl pyrolysis to literature values of Colket (1986) [---], Fujii and Asaba (1973) [--- FA], Kiefer et al. [--- KMPW] (1985), and Rao and Skinner (1984) [--- RS].

VIII.7. Summary

Benzene formation was shown to be reasonably accounted for by radical additions of $1\text{-C}_4\text{H}_5$ and $1\text{-C}_4\text{H}_3$ to C_2H_2 , but production of the aromatic ring is direct rather than through thermal intermediates. The cause is chemical activation of the initial adduct, which has not been recognized before. Because no thermal intermediates are involved, they cannot be destroyed en route to benzene, which would have reduced the yield of benzene. A C_3H_3 (propargyl) combination seems to be another possibility based on screening with a k_{∞} , but it appeared less likely because it would involve molecular 1,2-H shifts.

The same input parameters that are used to evaluate phenyl production from $1\text{-C}_4\text{H}_3 + \text{C}_2\text{H}_2$ were used to estimate rate constants for phenyl pyrolysis. Product channels to $1\text{-C}_6\text{H}_5$ and to $1\text{-C}_4\text{H}_3 + \text{C}_2\text{H}_2$ were predicted, giving good agreement with three of the literature rate constants and rationalizing their differences.

CHAPTER IX. THE THREE TYPES OF COMBUSTION REACTIONS

The insights from testing literature mechanisms (Ch. V) and the insights into reaction structures (Ch. VI and VII) make it possible to propose improved mechanisms. Even more significantly, a pattern among the reactions in such mechanisms becomes clear.

It is proposed here that there are only three types of reactions among the homogeneous, gas-phase reactions that occur in hydrocarbon combustion:

(I) H-atom metathesis - a class of bimolecular reactions which includes abstraction reactions and disproportionation and which has inherently pressure-independent rate constants;

(II) Association reactions - addition- and recombination-initiated bimolecular reactions which proceed through addition complexes and thus have *inherently pressure-dependent rate constants* at some pressure; these include additions with stabilization, decomposition, or isomerization of the chemically activated adduct; and

(III) Unimolecular reactions which are not the reverse of association reactions - specifically thermal isomerizations like phenyl \rightarrow ℓ -C₆H₅; these rate constants are inherently pressure-dependent.

Furthermore, any reaction that cannot fit into one of these classifications is unlikely to proceed - at least not in the way it has been described.

Class II reactions have been particularly misunderstood. The key to the present insight is to recognize that two-reactant, two- (or more) product reactions can be association reactions because of chemically activated decomposition. Likewise, a pressure-dependent rate constant for bimolecular reaction does not necessarily imply a simple addition to form an adduct, nor does pressure-independence necessarily imply that an association reaction is in a high-pressure limit for a simple addition product.

These points can be illustrated best by examining the reactions in the mechanisms. The mechanism of Warnatz (1983), which is WZ in Ch. V, predicted more profiles well than did the other three

literature mechanisms. Its reactions, which were categorized by Warnatz according to key species, are re-categorized as class I and class II reactions in Table IX.1. This mechanism has no class III reactions.

As a general comment, it should be noted again that the reversibility of reactions should be included in a mechanism, as shown by the improved predictions of a "fully reversible" Warnatz mechanism WZ' in Ch. V. The only elementary reactions identified in this work as nonreversible are reactions that proceed via secondary decomposition, e.g., ${}^3\text{CH}_2 + \text{O}({}^3\text{P}) \rightarrow \text{CH}_2\text{O}^* \rightarrow \text{H} + \text{HCO}^*$, $\text{HCO}^* \rightarrow \text{H} + \text{CO}$, which is effectively ${}^3\text{CH}_2 + \text{O}({}^3\text{P}) \rightarrow \text{CO} + 2\text{H}$. Here, $2\text{H} + \text{CO}$ cannot lead to ${}^3\text{CH}_2 + \text{O}({}^3\text{P})$ by a rate constant calculated from the forward reaction and thermodynamics. The reason is that, while $\text{H} + \text{CO}$ does form HCO^* , addition of H to that HCO^* (which would have to have the proper energy distribution) would be necessary to form CH_2O^* with sufficient energy to make ${}^3\text{CH}_2 + \text{O}({}^3\text{P})$, a concerted addition of two H atoms that is quite unlikely.

Also, radical-radical reactions that result in H -transfer can proceed in principle either by direct abstraction (pressure-independent) or by addition/decomposition (pressure-dependent at some pressures). The reaction $\text{H} + \text{C}_2\text{H}_3 \rightarrow \text{C}_2\text{H}_2 + \text{H}_2$ is an example, as discussed in Ch. VII.5. In reality, one route may dominate over the other.

With these comments in mind, the reactions in Table IX.1 and their classification can be understood.

Reactions of $\text{H}_2/\text{O}_2/\text{H}_2\text{O}/\text{HO}_2$. - Branching of $\text{H}+\text{O}_2$ to HO_2 or $\text{O}+\text{OH}$ is a competition for HO_2^* that proceeds through a chemically activated addition complex, as was shown in Ch. VII.3 and elsewhere (Zellner, 1984). Likewise, it is well-recognized that abstraction transition states describe well the reactions of $\text{O}+\text{H}_2$, $\text{OH}+\text{H}_2$, $\text{H}+\text{H}_2\text{O}$, and $\text{O}+\text{H}_2\text{O}$ (for example, see Zellner, 1984) and that the third-order reactions of $\text{H}+\text{H}$ and $\text{H}+\text{OH}$ are simple combinations. Note that $\text{H}+\text{OH}$ reaction may proceed either by metathesis ($\rightarrow \text{O}+\text{H}_2$) or by addition ($\rightarrow \text{H}_2\text{O}$).

Formation of $\text{OH}+\text{OH}$ from $\text{H}+\text{HO}_2$ must proceed through H_2O_2^* ($\text{HO}-\text{OH}^*$), which can undergo simple bond fission to $\text{OH}+\text{OH}$. It is not

Table IX.1. Types of reactions in the Warnatz mechanism (Warnatz, 1983).

Class I: H-transfer (Abstraction, Disproportionation)	Class II: Association reactions		
	Addition/ stabilization	Addition/ Decomposition	Addition/ Isomerization
H ₂ /O ₂ /H ₂ O/HO ₂ :			
O+H ₂ = H+OH	H+O ₂ +M → HO ₂ +M	H+O ₂ = OH+O	
OH+H ₂ = H ₂ O+H	H+OH+M → H ₂ O+M		
O+H ₂ O = OH+OH	H+H+M → H ₂ +M		
H+HO ₂ → H ₂ +O ₂ ^a		H+HO ₂ → OH+OH	
O+HO ₂ → OH+O ₂ ^a			
OH+HO ₂ → H ₂ O+O ₂			
CO/CO ₂ :		CO+OH = CO ₂ +H	
CH ₄ :			
CH ₄ +H = CH ₃ +H ₂			
CH ₄ +O = CH ₃ +OH			
CH ₄ +OH = CH ₃ +H ₂ O			
CH ₃ :	CH ₃ +H = CH ₄		
	CH ₃ +CH ₃ → C ₂ H ₆	CH ₃ +O → H ₂ CO+H	
		CH ₃ +CH ₃ = C ₂ H ₅ +H	
		CH ₃ +CH ₃ → C ₂ H ₄ +H ₂	
CH ₂ :		CH ₂ +H → CH+H ₂	
		CH ₂ +O → CO+H+H	
			CH ₂ +O ₂ → CO ₂ +H+H
		CH ₂ +CH ₃ → C ₂ H ₄ +H	
CH:		CH+O → CO+H	
		CH+O ₂ → CO+OH	
H ₂ CO:			
H ₂ CO+H → HCO+H ₂			
H ₂ CO+O → HCO+OH			
H ₂ CO+OH → HCO+H ₂ O			
HCO:			
HCO+H → CO+H ₂ ^a			
HCO+O → CO+OH ^a		HCO+O → CO ₂ +H	
HCO+OH → CO+H ₂ O			
[HCO+O ₂ → CO+HO ₂ ^b]	H+CO+M → HCO+M		
C ₂ H ₆ :			
C ₂ H ₆ +H → C ₂ H ₅ +H ₂			
C ₂ H ₆ +O → C ₂ H ₅ +OH			
C ₂ H ₆ +OH → C ₂ H ₅ +H ₂ O			
C ₂ H ₅ :		C ₂ H ₅ +O → CH ₃ CHO+H	
[C ₂ H ₅ +O ₂ → C ₂ H ₄ +HO ₂]			
C ₂ H ₄ :			
C ₂ H ₄ +H → C ₂ H ₃ +H ₂	C ₂ H ₄ +H = C ₂ H ₅		
C ₂ H ₄ +OH → C ₂ H ₃ +H ₂ O			C ₂ H ₄ +O → HCO+CH ₃

<u>Abstraction, Disproportionation</u>	<u>Addition/ stabilization</u>	<u>Addition/ Decomposition</u>	<u>Addition/ Isomerization</u>
$C_2H_3:$		$C_2H_3+H \rightarrow C_2H_2+H_2$	
$[C_2H_3+O_2 \rightarrow C_2H_2+HO_2^b]$			
$C_2H_2:$	$C_2H_2+H = C_2H_3$	$C_2H_2+O \rightarrow HCCO+H$	$C_2H_2+O \rightarrow CH_2+CO$
$C_2H_2+H = C_2H+H_2$			$C_2H_2+OH \rightarrow CH_2CO+H$
$C_2H_2+OH \rightarrow C_2H+H_2O$			
$C_2H:$		$C_2H+O \rightarrow CO+CH$	$C_2H+O_2 \rightarrow HCO+CO$
$CH_3CHO:$			
$CH_3CHO+H \rightarrow (CH_3+CO)+H^c$			
$CH_3CHO+O \rightarrow (CH_3+CO)+OH$			
$CH_3CHO+OH \rightarrow (CH_3+CO)+H_2O$			
$CH_2CO:$	$CH_2+CO+M \rightarrow CH_2CO+M$	$CH_2CO+H \rightarrow CH_3+CO$	$CH_2CO+O \rightarrow HCO+HCO$
			$CH_2CO+OH \rightarrow H_2CO+HCO$
$HCCO:$		$HCCO+H \rightarrow CH_2+CO$	
		$HCCO+O \rightarrow CO+CO+H$	
$C_3H_n:$			$CH_3+C_2H_2 \rightarrow C_3H_4+H$
	$C_3H_3+H \rightarrow C_3H_4$	$CH_2+C_2H_2 \rightarrow C_3H_3+H$	$C_3H_4+OH \rightarrow HCO+C_2H_4$
	$CH+C_2H_2 \rightarrow C_3H_3$		
			$C_3H_3+O \rightarrow C_2H_3+CO$
$C_4H_n:$			
$C_4H_2+H = C_4H+H_2$	$C_4H_2+H = C_4H_3$	$C_4H_2+H = C_2H+C_2H_2$ $[C_4H_3+H=C_2H_2+C_2H_2^d]$	$C_4H_2+OH \rightarrow$ Products [Warnatz suggests: $C_4H_2+OH \rightarrow X+H$ $X+OH \rightarrow C_2H_2+2CO+H]$
$C_6H_n:$	$C_6H_2+H \rightarrow$ Product [Apparently C_6H_3]	$C_6H_2+H = C_2H+C_4H_2$ $C_6H_2+H = C_4H+C_2H_2$	$C_6H_2+OH \rightarrow$ Products [Same rate as for C_4H_2+OH , so (?) $C_6H_2+OH \rightarrow X'+H$; $X'+OH \rightarrow C_4H_2+2CO+H]$

^a Same reactants and products could come from abstraction or addition/decomposition.

^b Reaction probably proceeds by addition, with different rate constant and possibly with different products.

^c Warnatz assumed CH_3CO is produced and rapidly decomposes to CH_3+CO .

^d Reaction probably does not proceed as shown (see text).

so clear whether the product channel H_2+O_2 proceeds by abstraction or by combination of $H+O_2$ and concerted elimination of H_2 . Just as for $H+OH$, note that $OH+OH$ has both metathesis ($\rightarrow O+H_2O$) and addition ($\rightarrow H+HO_2$) channels.

Similarly, $O+HO_2 \rightarrow OH+O_2$ has not been identified as to whether it is abstraction or addition, but $OH+HO_2$ is surely abstraction because concerted elimination of H_2O from HO_2OH^* is unlikely.

$CO+OH = H+CO_2$. - This reaction is the primary destruction path for CO in hydrocarbon flames, but its rate constant is quite peculiar. At temperatures below 1000 K, the rate constant seems to be temperature-independent, and at higher temperatures, it curves upward into a positive E_{act} (Warnatz, 1984). Pressure-dependence has been reported recently in the mid-range of temperatures (Zellner, 1984).

Not surprisingly, this behavior has been interpreted as chemically activated decomposition of $HO-C=O^*$ radical (e.g., Golden, 1979; Zellner, 1984; Mozurkewich et al., 1985). Variations among the predictions are due primarily to uncertainties about barrier heights for $HO-C=O \rightarrow H + CO_2$.

CH_4 reactions. - Methane has only C-H bonds, so free radicals can only abstract H and cannot add to it. Thus, the only reactions shown by Warnatz (1983) for CH_4 are metatheses by H, O, and OH, and the reverse metatheses involving CH_3 .

CH_3 reactions. - The other CH_3 reactions can be recognized as association reactions with H, O, and itself. [Warnatz (1984) considered the data on rate constants and products for CH_3+OH to be in too great a state of disarray for any recommendation to be made.]

The review of Warnatz (1984) includes low-pressure-limit ($M=Ar$) and high-pressure-limit rate constants for $H+CH_3 \rightarrow CH_4$ as well as fall-off curves from 298 to 2200 K. The fall-off curves were estimated by fitting fall-off data at 308 and 2200 K with unimolecular QRRK, using collision efficiency β as a fitting parameter.

The reaction CH_3+O can be recognized as combination to make chemically activated CH_3O^* , which can undergo β -scission to give $H_2C=O + H$.

Methyl recombination forms chemically activated $C_2H_6^*$

($\text{CH}_3\text{-CH}_3^*$), which can be collisionally stabilized as C_2H_6 or can break a C-H bond to give C_2H_5 . The reported product channel of $\text{C}_2\text{H}_4+\text{H}_2$ would have to result from concerted elimination of H_2 .

Methylene chemistry. - Neither the mechanism of Warnatz (1983) nor any of the other flame mechanisms examined in Ch. V distinguish ground-state triplet $^3\text{CH}_2$ from the low-lying singlet $^1\text{CH}_2$ ($\Delta E_{S-T} = 9$ kcal/mol). This lumping represents a serious limitation on predictive power in acetylene flames and, thus, at fuel-rich conditions where acetylene is the dominant hydrocarbon.

The types of reactions of the two electronic states are very different, as $^3\text{CH}_2$ undergoes the typical radical reactions of abstraction and association while $^1\text{CH}_2$ inserts into σ and π bonds. Thus $^3\text{CH}_2$ +radical reactions are very fast recombination events, while $^1\text{CH}_2$ is not a radical and cannot undergo recombination. On the other hand, $^1\text{CH}_2$ insertion reactions may be orders of magnitude faster than $^3\text{CH}_2$ addition reactions to the same species. $^1\text{CH}_2$ also can be present at appreciable levels, reaching an equilibrium fraction of 0.05 of the total CH_2 at 2000 K.

Warnatz (1983) did not show any abstraction reactions, which would have been the results of $^3\text{CH}_2$. Recent papers from the research group of Wagner (Dóbé et al., 1985; Böhland et al., in press) report experimental data on abstraction of H from alkanes and aldehydes by $^3\text{CH}_2$, which permits inclusion of these reactions and, by inference and analogy, abstraction from other species.

CH_2 reactions with H and O are probably reactions of $^3\text{CH}_2$ because these are atoms with no bonds where $^1\text{CH}_2$ can insert. Abstraction by H is a possibility. More likely, radical combination of $^3\text{CH}_2$ with H forms chemically activated CH_3^* , which can eliminate molecular H_2 to form CH. Combination of $^3\text{CH}_2$ with $\text{O}(^3\text{P})$ is highly exothermic and would lead to $\text{CO} + 2\text{H}$ by the decompositions $\text{H}_2\text{CO}^* \rightarrow \text{HCO}^* \rightarrow \text{CO}$. New data on these reactions have been reported recently (Böhland and Temps, 1984; Böhland et al., 1984b).

Warnatz did not list any reactions of CH_2 with OH. Combination of $^3\text{CH}_2$ with OH would form CH_2OH^* , which would decompose to $\text{H}_2\text{CO}+\text{H}$, while insertion of $^1\text{CH}_2$ would form CH_3O^* , which would also yield $\text{H}_2\text{CO}+\text{H}$. These reactions are analogous to the reactions of $^3\text{CH}_2$ and

$^1\text{CH}_2$ with CH_3 to form $\text{C}_2\text{H}_4+\text{H}$, for which rate constants were calculated in Ch. VII.6 by bimolecular QRRK.

Finally, CH_2+O_2 was shown in Ch. V to be of great importance in this flame, but the state of CH_2 is not specified and the product distribution is the subject of considerable controversy. Warnatz chose the rate constant from a low-temperature study so CH_2 was probably $^3\text{CH}_2$, but he chose the products CO_2+2H in order to fit flame data on flame speeds and CO_2 profiles. Miller et al. (1983) described a mechanism treating CH_2 as $^3\text{CH}_2$ to account for the CO , CO_2 , H_2 , H_2 , and OH which have been attributed to this reaction. Böhland et al. (1984a) prefer the products $\text{HCO}+\text{OH}$ and $\text{H}+\text{CO}+\text{OH}$ from their experimental study of $^3\text{CH}_2+\text{O}_2$. For $^1\text{CH}_2+\text{O}_2$, the product mix and rate constant may be quite different.

CH reactions. - The ground state is $\text{CH}(^2\Delta)$. This species has both an unpaired electron, allowing free-radical reactions, and an empty orbital, allowing insertion reactions. Warnatz shows only CH reactions with H_2 (discussed above and by Berman and Lin, 1984), O , O_2 , and C_2H_2 (under C_3 reactions). Except for $\text{CH}+\text{O}$, which is a radical combination reaction, these reactions all seem to be insertions with chemically activated decompositions.

As for CH_3 and CH_2 , no reaction with OH was listed by Warnatz.

A rate constant for the radical combination (addition/decomposition) reaction $\text{CH}+^3\text{CH}_2 \rightarrow \text{H}+\text{C}_2\text{H}_2$ was estimated by bimolecular QRRK in Ch. VII.4.

H_2CO and HCO reactions. - Warnatz (1983) includes only abstraction reactions for H_2CO , but radical additions to its π bond are also possible.

$\text{HCO}+\text{H}$ may proceed by abstraction and/or association, but the only difference in products would be formation of H_2CO at low temperatures and high pressures from the combination reaction.

For $\text{HCO}+\text{O}$, either abstraction or association would lead to $\text{CO}+\text{OH}$, but only the association reaction could lead to CO_2+H .

The reaction $\text{HCO}+\text{OH} \rightarrow \text{CO}+\text{H}_2\text{O}$ is an abstraction, and $\text{H}+\text{CO}+\text{M} \rightleftharpoons \text{HCO}+\text{M}$ is a simple addition.

Warnatz (1983) includes a reaction $\text{HCO}+\text{O}_2 \rightarrow \text{CO}+\text{HO}_2$, assigning a temperature-independent, disproportionation-type of rate constant.

However, in his review (Warnatz, 1984), he shows good agreement among room-temperature measurements, a slightly negative E_{act} (-0.1 kcal/mol) from a single set of measurements at intermediate temperatures, and extreme variation - over three orders of magnitude - in the rate constant at high temperatures. In light of this behavior, $HCO+O_2$ is probably a chemically activated addition reaction, and the products and rate constant cited by Warnatz would not be valid.

C_2H_6 and C_2H_5 reactions. - Radical reactions with C_2H_6 are exclusively abstractions, as there are no π bonds for radical addition and no unpaired electrons for radical-radical combinations. The non-radical addition reaction of 1CH_2 insertion can occur.

The reaction C_2H_5+O is expected to be analogous to CH_3+O , a radical combination followed by chemically activated decomposition to H and the aldehyde CH_2CHO .

Gutman and co-workers (Slagle et al., 1984) have studied $C_2H_5+O_2$ and find that, contrary to the recommendation of Warnatz (1984), this reaction has a downward-curving Arrhenius plot as temperatures increase from 298 to 1003 K. Also, the pressure-dependence of the rate constant decreased with increasing temperature. Such behavior indicates addition/stabilization rather than the abstraction implied by Warnatz.

C_2H_4 reactions. - The reactants $H+C_2H_4$ form the adduct C_2H_5 at low temperatures and the abstraction products $C_2H_3+H_2$ at high temperatures, as was shown in Ch. VII.6.

To form $HCO+CH_3$ from $O+C_2H_4$, the addition complex ($\cdot CH_2-CH_2-O\cdot$)* must undergo chemically activated isomerization by a 1,2-H-shift before decomposing.

Warnatz (1983) used only an abstraction channel for $OH+C_2H_4$ although low-temperature rate constants show the effects of an addition channel (Warnatz, 1984).

C_2H_3 reactions. - Two bimolecular C_2H_3 destruction reactions were given by Warnatz (1983). The first, $H+C_2H_3 \rightarrow H_2+C_2H_2$, was shown in Ch. VII.5 to be consistent with chemically activated addition/decomposition.

The second is reaction of C_2H_3 with O_2 , which assumed by Warnatz (1983, 1984) to be a barrierless abstraction to $HO_2+C_2H_2$. The

absence of an activation energy was shown in Ch. V to cause erroneous OH profiles at low temperatures because of excessive formation rates predicted for HO₂ by this reaction.

However, the products as well as the rate constant are incorrect for C₂H₃+O₂ in the Warnatz mechanism, as shown by Gutman and co-workers. In those studies, the products were shown instead to be HCO+H₂CO with pressure-independent rate constants at 296 K over 0.4 to 4 torr (Park et al., 1984) and pressure-dependent rate constants at 600 K over 0.8 to 3.6 torr (Slagle et al., 1984). These products and pressure-dependences are consistent with chemically activated isomerization and decomposition steps.

C₂H₂ reactions. - As for H+C₂H₄, H+C₂H₂ forms the adduct C₂H₃ at low temperatures and abstraction products at high temperatures. Rate constants for the addition/stabilization channel were calculated in Ch. VII.4.

Reaction of C₂H₂ with O is important even in fuel-rich flames, and there is good agreement that O adds to C₂H₂. The branching between products H+HCCO and CH₂+CO is quite uncertain, though, and recent experimental studies (Löhr and Roth, 1981; Vinckier et al., 1985; Frank et al., 1986) and theoretical calculations (Harding, 1981) have focused on the problem. The identity of the CH₂ electronic state has not been examined.

The products and rate constants of C₂H₂+OH are even more controversial. Warnatz (1983) treated the reaction as having low-temperature and high-temperature pathways. At high temperatures, he used C₂H+H₂O as products corresponding to the measured rate constants. He uses classical fall-off curves estimated for addition/stabilization, but this is in conflict with his choice of products as CH₂CO+H, which would not have the same kind of fall-off as for simple addition (Ch. VI). These products could be rationalized as coming from chemically activated isomerization/decomposition, which would follow an inverse fall-off behavior. Smith, Fairchild, and Crosley (1984) interpret their OH+C₂H₂ data as simple addition at lower temperatures, based on their measured rate constant for disappearance of OH.

C₂H reactions. - Warnatz (1983) shows reactions with O and O₂ for oxidation of C₂H. The first can be explained as radical combination to form chemically activated ·HC=C=O*, which decomposes to CH+CO.

The reaction of C₂H+O₂ was listed as giving HCO+CO, which can be explained by a chemically activated isomerization reaction like that proposed for C₂H₃+O₂ (above). Warnatz (1983, 1984) estimated a rate constant for this reaction such that C₄H₂ formation rates could be matched by his mechanism. Laufer and Lechleider (1984) also report HCCO+O as a second channel, which would be consistent with simple bond fission in the chemically activated adduct HC≡C-O-O*.

No OH reaction was shown.

CH₃CHO reactions. - Warnatz (1983) shows abstraction reactions by H, O, and OH. He assumes that unimolecular decomposition of the product CH₃CO (the reverse of the addition step CH₃+CO → CH₃CO) is very rapid, and no explicit kinetics for this step are included.

CH₂CO reactions. - Ketene was assumed to be formed by OH+C₂H₂. Four CH₂CO destruction reactions were shown, each of which can be explained best as an association type of reaction.

Ketene pyrolysis is included as giving CH₂+CO, but again the electronic state of CH₂ is not specified. In fact, ¹CH₂ is formed (Laufer, 1981). Most of the ¹CH₂ would be rapidly quenched to ³CH₂, particularly at lower temperatures where the equilibrium level of ¹CH₂ is very low. Warnatz (1984) recommends the rate constant only for 1000-2000 K and includes it in his mechanism (Warnatz, 1983) only as decomposition. As a result, making the reaction CH₂CO → CH₂+CO reversible and applying it at low temperatures would falsely give a high addition rate constant for "CH₂" + CO, while the CH₂ actually would be ³CH₂, which should add even more slowly than the very slow reaction O+CO.

The destruction reactions of CH₂CO by H, O, and OH can be recognized as addition to the CH₂ group on the end of the molecule, followed by chemically activated steps.

HCCO reactions. - Ketyl (HCCO) is formed in the Warnatz mechanism by O+C₂H₂. Similarly to ketene, the listed destruction reactions by H and O can be interpreted as radical combinations with

$\cdot\text{CH}=\text{C}=\text{O}$ followed by chemically activated steps. The H-atom reaction should give ${}^1\text{CH}_2$, as the adduct is chemically activated CH_2CO .

C_3H_n reactions. - Warnatz (1983) included the C_3 species C_3H_3 and C_3H_4 , and all of the reactions he used can be explained as association reactions with chemically activated adducts.

One problem in speculating about the mechanisms of C_3H_4 reactions is that two isomers of comparable stability exist: propadiene (allene, $\text{CH}_2=\text{C}=\text{CH}_2$) and propyne (methylacetylene, $\text{HC}\equiv\text{C}-\text{CH}_3$). Warnatz did not distinguish between the reactions of these species. Similarly, both propargyl ($\text{t}-\text{C}_3\text{H}_3$) and cyclopropenyl ($\text{c}-\text{C}_3\text{H}_3^*$) exist as isomers of C_3H_3 .

Methyl addition to C_2H_2 forms $\text{CH}_3-\text{CH}=\text{CH}\cdot^*$, which can be stabilized or eliminate H by β -scission to form propyne. As another alternative, this adduct also can isomerize to $\cdot\text{CH}_2-\text{CH}=\text{CH}_2^*$ (allyl), which can eliminate H by β -scission to form propadiene (Dean, 1985).

Destruction of C_3H_4 by OH to $\text{HCO}+\text{C}_2\text{H}_4$ was listed with a rate constant that had been chosen from room-temperature measurements of OH + propyne (Warnatz, 1984). A chemically activated sequence can be postulated, but several H-shifts must occur. At flame conditions, abstraction seems more likely.

Warnatz (1983) assumes that $\text{H}+\text{C}_3\text{H}_3 \rightarrow \text{"C}_3\text{H}_4\text{"}$ occurs with a high-pressure-limit combination rate constant for $\text{t}-\text{C}_3\text{H}_3$.

Both " CH_2 " and CH are shown as leading to C_3H_3 by addition to C_2H_2 , based on room-temperature measurements. The cited rate constant for CH_2 then would refer to ${}^3\text{CH}_2$ addition, forming $\cdot\text{CH}_2-\text{CH}=\text{CH}\cdot^*$ that would eliminate H from the central carbon by β -scission to form $\text{t}-\text{C}_3\text{H}_3$. Radical addition of CH to C_2H_2 would require H-shifts to form $\text{t}-\text{C}_3\text{H}_3$. Insertion into the C-H bond give $\text{t}-\text{C}_3\text{H}_3^*$ directly, while insertion into the π bond would form $\text{c}-\text{C}_3\text{H}_3^*$. The chemically activated C_3H_3^* species would probably reach equilibrium between each other before being collisionally stabilized, although with sufficient activation, $\text{c}-\text{C}_3\text{H}_3^*$ could eliminate an electron to form C_3H_3^+ .

The reaction $\text{C}_3\text{H}_3+\text{O} \rightarrow \text{C}_2\text{H}_3+\text{CO}$ can be explained as isomerization/decomposition if C_3H_3 is $\text{t}-\text{C}_3\text{H}_3$. Combination of $\text{CH}_2=\text{C}=\text{CH}\cdot$ with O

would give $\text{HC}\equiv\text{C}-\text{CH}_2-\text{O}\cdot^*$ or $\text{H}_2\text{C}=\text{C}=\text{CH}-\text{O}\cdot^*$ (equivalently, $\text{H}_2\text{C}=\text{C}-\text{CH}=\text{O}^*$), which could decompose to the cited products after one H-shift.

C₄H_n reactions. - These are principally the reactions involving C₄H₂, which bring C₄H and C₄H₃ (isomer unspecified) into the mechanism.

Abstraction and addition channels are open to $\text{H}+\text{C}_4\text{H}_2$. Abstraction forms C₄H+H₂, while addition will form either isomer of C₄H₃*. If 1-C₄H₃* is formed with sufficient energy, it can decompose to C₂H + C₂H₂, the reverse of which has been shown to be a fast, chemically activated addition/decomposition reaction (Dean, 1985).

The reaction $\text{C}_2\text{H}_2+\text{C}_2\text{H}_2 \rightleftharpoons \text{H}+\text{C}_4\text{H}_3$ is rather controversial and is based on observation of rates for C₂H₂ pyrolysis that are second-order in C₂H₂. Frenklach et al. (in press) have recently proposed that the reaction is the reverse of simple disproportionation between C₂H and C₂H₃.

Warnatz proposes that destruction of C₄H₂ by OH proceeds analogously to his reaction $\text{C}_2\text{H}_2+\text{OH} \rightarrow \text{CH}_2\text{CO}+\text{H}$, followed by OH attack on the product [ethynylketene?] to give C₂H₂, 2CO, and H with a high rate. If C₄H₂ +OH proceeds this way, it would have to proceed by chemically activated reactions. Obviously, this sequence of reactions for C₄H₂+OH needs further examination.

The reaction $\text{C}_4\text{H}_2+\text{O} \rightarrow \text{C}_3\text{H}_2+\text{CO}$ (Warnatz, 1984) is not present in this mechanism, but it could be explained by chemically activated addition of O.

C₆H_n reactions. - These reactions are completely analogous to the reaction set for C₄H_n. The only variation is that C₆H₃* can be formed by $\text{H}+\text{C}_6\text{H}_2$, by $\text{C}_4\text{H}+\text{C}_2\text{H}_2$, or by $\text{C}_2\text{H}+\text{C}_4\text{H}_2$.

In summary, this analysis illustrates that only three types of reactions occur in combustion. Class I reactions - H-atom transfers - are important ways of converting saturated hydrocarbons and C/H/O species into more-reactive free radicals. Class II reactions - associations - account for all the oxidation and molecular-weight-

growth steps. Although the Warnatz mechanism did not include any class III reactions - thermal isomerizations, this type of reaction is well-recognized.

This analysis also emphasizes the importance of chemically activated association reactions and the uncertainties associated with their products and rate constants. It is this type of reaction that can be analyzed by bimolecular QRRK, showing the great potential of this method for improving the chemical mechanisms and placing them on a physically and chemically sound basis.

CHAPTER X. CONCLUSIONS AND RECOMMENDATIONS

X.1. Conclusions

Data have been collected that give a thorough description of a lightly sooting acetylene flame. Thirty-eight profiles of mole fraction were measured for stable species and for free radicals by MBMS, and mole fraction data were collected for 20 other species using MBMS and for 174 stable species from C_6H_2 to $C_{14}H_{12}$ using microprobe sampling and GC/MS. These data significantly extend the pioneering results of Bonne, Homann, and Wagner (1965) and provide an extensive data base for detailed testing of chemical mechanisms.

Based on the data and modeling, general conclusions are:

- (1) Literature mechanisms for less fuel-rich conditions predicted mole fractions fairly well (a factor of two) for major species at sooting conditions, but for hydrocarbon radicals, they show serious deficiencies. These failures prevent the predictions of important features like formation of aromatics.
- (2) The key cause is a lack of rate and product data for reactions that are crucial to such predictions.
- (3) Bimolecular QRRK is a practical, accurate tool for estimating rate constants and branching for many of these reactions.
- (4) Analyses of rate constants by QRRK leads to the insight that all the reactions in combustion chemistry can be categorized as metathetical H-atom transfer (abstraction or disproportionation), as chemically activated bimolecular reactions, or as thermal, unimolecular isomerizations.

Critical evaluation of mechanisms. - Specific conclusions from testing the mechanisms are:

- (1) Elementary reactions that are reversible should be included with rate constants for both forward and reverse directions if the mechanism is to be used generally, even if the predictions at a given condition are insensitive to a particular direction.
- (2) CH_2 chemistry is very important to the predictions, but there is no distinction made between singlet and triplet CH_2 in

the mechanisms, despite the presence of each and their greatly differing reactivities.

(3) H_2O and CO_2 predictions are strongly affected by the product branching and rates of $\text{CH}_2 + \text{O}_2$ and of $\text{C}_4\text{H}_2 + \text{OH}$, but only two mechanisms (WZ and WZ') predict shape and magnitude well for both species.

(4) The absence of destruction kinetics for C_3 species in two mechanisms (MMSK and WD) leads to a misprediction that these species would be formed in quantities much greater than is observed, which makes them unrealistically large sinks for carbon and impairs predictions for other species in the affected mechanisms.

(5) Peculiarities in the OH prediction are caused by differences in $\text{C}_2\text{H}_3 + \text{O}_2$ activation energies, but recent measurements indicate that the rate constant and even the products of the reaction are drastically different ($\rightarrow \text{HCO} + \text{H}_2\text{CO}$) from those used in existing mechanisms ($\rightarrow \text{C}_2\text{H}_2 + \text{HO}_2$).

(6) C_2H_3 is largely determined by its reaction with O_2 and, in one mechanism (WD), by the inclusion of a $\text{C}_3\text{H}_6 = \text{C}_2\text{H}_3 + \text{CH}_3$ reaction which is assumed to be in the high-pressure limit.

Prediction of rate constants by bimolecular QRRK. - This method is a practical tool for the modeler and a valuable supplement to RRKM theory. The reason is that the key input data are high-pressure-limit Arrhenius parameters A_∞ and $E_{\text{act},\infty}$ for each bimolecular and unimolecular step involved, which are generally available from experimental data or which can be estimated by thermochemical kinetics. Specific results and conclusions are:

(1) Bimolecular QRRK accurately predicts rate constants for chemically activated reactions including pressure dependence, low-pressure limits for addition/stabilization reactions, and non-Arrhenius temperature dependences.

(2) Chemically activated decomposition is shown as outgrowth of the QRRK equations to have the inverse of classical fall-off behavior. Its bimolecular rate constants are pressure-independent at *low* pressure rather than high pressure, a prediction

that is supported by the products and rate constants of many radical-radical reactions. Also, at high pressure, these rate constants are predicted to be *inversely* proportional to pressure.

(3) The reactions of " CH_2 ", which were shown by testing mechanisms to be of great importance, can be analyzed by using bimolecular QRRK for the distinctly different reactions of the electronic ground-state $^3\text{CH}_2$ and for the low-lying electronic state $^1\text{CH}_2$.

(4) The reactions of $\text{H} + \text{O}_2$ are shown to be classical cases of chemical activation, leading to HO_2 by addition/stabilization and to $\text{O} + \text{OH}$ by addition/decomposition, and rate constants for these reactions and for $\text{O} + \text{OH} \rightarrow \text{H} + \text{O}_2$ are predicted well.

Benzene formation. - Calculations of rate constants for $1\text{-C}_4\text{H}_3$ and $1\text{-C}_4\text{H}_5 + \text{C}_2\text{H}_2$ show that simple addition to make linear adducts is too slow to account for the rate of benzene formation. Instead, benzene formation is described well by chemically activated addition/isomerization of these reactants, which leads directly to aromatic products without forming thermalized intermediates that could be destroyed before leading to aromatics.

Types of combustion reactions. - From the above conclusions, it follows that all reactions in combustion chemistry can be categorized as metathetical H-atom transfer, as chemically activated, addition-initiated reactions, or as thermal isomerizations. The widespread occurrence of chemically activated reactions has not been recognized, probably because the inverse pressure dependence of chemically activated decompositions has not been recognized.

By examining the Warnatz mechanism, it was shown that all of the oxidation and molecular-weight-growth reactions are of this type. This breakdown is more than just a descriptive tool, then, but a means of insight to the fundamental differences and similarities among chemical reactions in combustion.

X.2. Recommendations for continued research

Further data are necessary to understand fuel-rich combustion, and bimolecular QRRK should be applied to estimate rate constants where no data are available or where extrapolation from low temperatures or different pressures is required. Sensitivity analyses must identify whether these reactions are important. Specifically:

- (1) The destruction kinetics of C_3H_4 , C_4H_2 , and of the radicals " CH_2 " (3CH_2 and 1CH_2), C_2H_3 , C_3H_2 , and C_3H_3 should be estimated by using bimolecular QRRK, rationalizing data that exist for these reactions and anticipating better experimental data.
- (2) Combustion kinetics for hydrocarbons heavier than C_2 's, including formation and destruction of polycyclic aromatics, are largely unexplored but should be addressed using these data and predictive methods.
- (3) In particular, sources of C_4 species that lead to benzene formation are not understood, but unimolecular and bimolecular QRRK again should be used to investigate such reactions.
- (4) QRRK methods also should be applied to other systems as diverse as NO_x chemistry, nitrogen fixation, chemi-ionization, ion-molecule reactions, and plasma chemistry.
- (5) Data on pure fuels C_2H_4 , C_2H_6 , C_3H_6 , C_3H_8 , toluene, and on mixtures will yield data that are sensitive to different reactions, allowing improvement of mechanisms.

APPENDICES

APPENDIX A.

Directly measured and extrapolated temperatures

Distance from burner (mm)	T (K)	Distance from burner (mm)	T (K)	Distance from burner (mm)	T (K)
Unheated thermocouple:		Resistive heating method:		Curve used in modeling:	
0.82	870	0.82	907	0.0	570
1.28	1023	1.28	1092	0.5	770
1.89	1177	1.89	1322	1.0	979
3.75	1399	25.97	1710	1.5	1185
7.67	1542	32.96	1682	2.0	1358
14.01	1518	35.09	1543	2.5	1469
20.43	1464	2.06	1367	3.0	1560
25.97	1422			4.0	1701
30.88	1383	Extrapolated using emissivity-diameter product:		5.0	1781
34.50	1356			6.0	1850
36.14	1342			7.0	1882
32.96	1409			8.0	1900
35.09	1411	3.75	1671	9.0	1901
37.86	1390	7.67	1899	10.0	1898
36.54	1400	14.01	1858	11.0	1893
2.06	1183	20.43	1769	12.0	1885
		25.97	1701	13.0	1872
		30.88	1640	14.0	1858
		34.50	1599	15.0	1846
		36.14	1578	16.0	1831
		37.86	1517	17.0	1816
		36.54	1529	18.0	1802
				19.0	1788
				20.0	1776
				22.0	1750
				24.0	1725
				26.0	1700
				28.0	1675
				30.0	1651
				34.0	1603
				38.0	1557
				42.0	1510
				46.0	1462
				50.0	1414

APPENDIX B.

List of files by species in acetylene flame ($\phi=2.4$)

APPENDIX B. List of files by species in acetylene flame ($\phi=2.4$)

MW Species	Ionization Efficiency (mm)	At (mm)	Range of beam, eV	Profile source	Measured at (eV)	Remarks
1 H-atom	111183.DAT	6.37	13.5-22	111383.DAT	16.5	16 pts, 40.40-0.68 mm IEff in lean flame
1 H-atom	111984.IEF	Lean	12.5-22	112084.DAT	15	57 pts, 41.65-.96-36.5; 7.92-6.90
1 H-atom	112184.DAT	4.47	13-20	112184.SCI	15.5	27 pts, 1.72-.79-39.75-6.93
*** 2 H ₂	101683.IEF	Pure	15-21	111383.DAT	19	16 pts, 40.40-0.68 mm IEff in lean flame
*** 2 H ₂	101983.MSC	Pure	14-22	112384.DAT	16.5, 19	Calibrate with 16.5 eV 63 pts, 1.72-.79-39.75-6.93 57 pts, 40.49-1.41-37.94 Ratio of H ₂ (16.5)/H ₂ (19) in 112384
*** 13 CH	011684.IES	2.51	14.25-15.75	112184.DAT	19	63 pts, 1.72-.79-39.75-6.93
*** 13 CH	112584.IES	3.86	13.5-18.5	112384.DAT	16.5, 19	57 pts, 40.49-1.41-37.94 Ratio of H ₂ (16.5)/H ₂ (19) in 112384
*** 14 CH ₂	112884.IES	4.73	14-18	H2RATIO.DAT	16.5, 19	Ratio of H ₂ (16.5)/H ₂ (19) in 112384
*** 14 CH ₂	011684.IES	2.51	11.75-15.75	112184.DAT	19	63 pts, 1.72-.79-39.75-6.93
*** 14 CH ₂	112584.IES	3.86	11.5-16.75	112384.DAT	16.5, 19	57 pts, 40.49-1.41-37.94 Ratio of H ₂ (16.5)/H ₂ (19) in 112384
*** 14 CH ₂	112884.IES	4.73	9-18	112384.DAT	16.5, 19	57 pts, 40.49-1.41-37.94 Ratio of H ₂ (16.5)/H ₂ (19) in 112384
*** 14 CH ₂	112984.IES	3.58	10-15	112984.DAT	13.5	48 pts, 39.14-.83-23.54
*** 14 CH ₂	112984.IES	3.58	10-15	112984.DAT	13.5	48 pts, 39.14-.83-23.54

15 CH₃

010984.IES 2.82 8-21, 11-20
 011684.IES 2.51 9-16,
 11.75-15.75
 011784.IES (+) 12-16
 050984.DAT (+) 13-16
 112584.IES 3.86 8.5-20
 112884.IES 4.73 8-18
 112984.IES 3.58 8.5-15
 011784.ISO 13.5 CH₃⁺ fragment from pure CH₄
 22 pts, 4.39-1.23-6.98
 CH₃⁺ fragment from pure CH₄
 112884.DAT 16 [For isotopic correction]

*** *****

16 CH₄

101683.IEF Pure 13-20
 102083.IEF Pure 12-20
 010984.IES 2.82 17-20
 011684.IES 2.51 11.5-16,
 11.75-15.75
 011784.IES Pure 11-16
 050984.DAT Pure 11-16
 112584.IES 3.86 10.5-20
 112884.IES 4.73 9.5-18
 112984.IES 3.58 11.5-15
 011784.ISO 13.5 CH₄ from effusive source
 22 pts, 4.39-1.23-6.98
 CH₄ from effusive source
 112884.ISO 16 40 pts, 4.44-.85-9.31;40.43-12.04
 112984.ISO 13.5 48 pts, 39.14-.83-23.54

*** *****

17 CH

010984.IES 2.82 11-20
 011684.IES 2.51 11.5-16,
 12.25-15.75,
 12.5-16
 112584.IES 3.86 13-20
 112884.IES 4.73 11.5-18
 011784.ISO 13.5 22 pts, 4.39-1.23-6.98
 112884.ISO 16 40 pts, 4.44-.85-9.31;40.43-12.04

*** *****

121384. IES 4.17	9.25-20	121384. DAT	13,11	43 pts, 39.91-1.26-6.74 mm
*** *****				
27 C ₂ H ₃	9.5-22, 9.5-14			
112883. IES 2.71				
120483. IES 4.77	9-13	113083. IS1	13	10-min count; 20 pts, 19.09-1.28 1-min counts
		120483. ISO	11	1-min cnt; 24 pts, 13.34-1.16-4.77
		120583. ISO	10	5-min cnt; 10 pts, 4.17-9.18 mm
		120783. ISO	10	2-min; 20 pts, 5.92-1.44-25.92, 5.02
		120883. ISO	10	20-min; 2 pts
		121283. ISO	10	20-min; 17 pts, 0.91-9.21; 8.00-14.21
		121483. ISO	10	20-min; 14 pts, 39.48-6.54 mm
		VINYL. ISO	-	Composite: 121283 w/ 121383*factor
121384. IES 4.17	9.5-20	121384. ISO	11	
*** *****				
28 C ₂ H ₄	9-15, 10-22			
112883. IES 2.71				
120483. IES 4.77	9-13	120483. ISO	11	24 pts, 13.34-1.16-4.77
122983. IES 3.11	9.5-13	122983. ISO	11.5	34 pts, 1.29-10.40-1.06
121284. IES 1.49	9.5-20			
121384. IES 4.17	9.5-20	121384. ISO	11	43 pts, 39.91-1.26-6.74 mm
*** *****		C2H4. ISO	-	Composite: 121384 w/ 120483*factor
CO (and above for Ieff)	14-22 12.5-22, 13-22			
101683. IEF Pure				
102083. IEF Pure				
*** *****				
		120183. DAT	19	63 pts, 40.92-1.11-39.92
		121384. DAT	18.5	43 pts, 39.91-1.26-6.74 mm
		CO. ISO	-	Composite: 121384 w/ 120183*factor

29 HCO/C ₂ H ₅	112883. IES 2.71	8-15				
	122983. IES 3.11	9.5-13				
*** *****					122983. ISO 9.5, 11.5	15 pts, 1.29-6.74, 8.52
30 H ₂ CO/C ₂ H ₆	112883. IES 2.71	9.5-15				
	122983. IES 3.11	9.5-13				
*** *****					122983. ISO	11.5 34 pts, 1.29-10.40-1.06
32 O ₂	101683. IEF Pure	12-22				
	102083. IEF Pure	11.5-22				
	122083. IES 4.04	10-21				
	112584. IES 3.86	11-20			122783. DAT	16 34 pts, 39.62-1.08-4.43
	121184. IES 2.12	10-18, 12-18			121184. DAT	15 62 pts, 4.41-1.00-26.03
*** *****						
33 HO ₂	112584. IES 3.86	11.5-20				
	121184. IES 2.12	10-18				
*** *****						
34 H ₂ O ₂	112584. IES 3.86	10.5-20				
	121184. IES 2.12	12-18				
*** *****						
36 "C ₃ "/Ar	122083. IEF 4.04	12				
*** *****						At 12eV, 2(+/- 4) counts in 60 sec
37 C ₃ H	122083. IES 4.04	11-12				
*** *****						11: 2±3; 12: 9±6
38 C ₃ H ₂	122083. IES 4.04	9-12				
	122383. IES 5.40	8.75-14.5				
*** *****						
39 C ₃ H ₃	122083. IES 4.04	8.5-12				
					122383. DAT	10.5 51 pts, 1.09-39.48-5.4
					121284. DAT	10.5 33 pts, 39.4-1.12-1.49
					C3H2. ISO	- Composite: 121284 w/ 122383*factor

122383. IES 5.40 8-14.5,
7.75-10

122383. ISO 10.5 51 pts, 1.09-39.48-5.4
121284. ISO 10.5 33 pts, 39.4-1.12-1.49

*** *****
40 C₃H₄

111783. IES 6.54 9-22
112083. IES 5.93 10-20
112183. IES 4.28 9.5-22
112883. IES 2.71 9.5-20.5
120483. IES 4.77 10-20
122083. IES 4.04 9-21, 8.5-12
122383. IES 5.40 8.75-14.5

122383. ISO 10.5, 13 51 pts, 1.09-39.48-5.4

010484. IES 5.05 9-21
010784. IES 10.10 9-21
112084. IES 4.01 9-20
112584. IES 3.86 9-22
112984. IES 3.58 9-22
121284. IES 1.49 8.5-20

121384. IES 4.17 10.5-20

121284. ISO 10.5 33 pts, 39.4-1.12-1.49

Ar

101683. IEF Pure 15-22
101983. MSC Pure 14-22
102083. IEF Pure 13.5-22
111183. IES 6.37 11-22
112583. IES 4.46 11-20
122383. IES 5.40 16-21

122883. DAT 12, 12.5, 39 pts, 39.22-1.14-7.08
13, 13.5,
14, 19

010784. DAT 10.10 12.5-20
011684. IEF 2.51 16.5-20
050984. IEF Pure 15-21
111984. DAT Lean 13-22
112984. DAT 3.58 12.5-19.5

*** *****									
41 HCCO/C ₃ H ₅	122083. IES	4.04	8.5-12						
	112584. IES	3.86	8.5-18						
	121284. ISO	10.5	33 pts, 39.4-1.12-1.49						
*** *****									
42 CH ₂ CO/C ₃ H ₆	122083. IES	4.04	9-12						
	112584. IES	3.86	9-17.5						
	121284. IES	1.49	8.5-14						
	121284. ISO	10.5	33 pts, 39.4-1.12-1.49						
*** *****									
43 C ₂ H ₃ O/C ₃ H ₇	122083. IES	4.04	10-12						
*** *****									
44 C ₂ H ₄ O/C ₃ H ₈	122083. IES	4.04	11.5-21						
	121284. IES	1.49	9-20						
*** *****									
CO ₂ (and	101683. IEF	Pure	13.5-22						
IEff's	102083. IEF	Pure	14-22						
above)									
*** *****									
49 C ₄ H	112183. IES	4.28	13.5-16.5						
*** *****									
50 C ₄ H ₂	112183. IES	4.28	9-19						
	112583. IES	4.46	10-13						
*** *****									
51 C ₄ H ₃	112183. IES	4.28	9-16						
	112583. IES	4.46	9.5-13						
*** *****									
52 C ₄ H ₄	112183. IES	4.28	9-16						
	112283. ISO	13,11	22 pts, 39.56-1.12						
	112583. ISO	11	18 pts, 11.90-1.00-3.83						
*** *****									
	112283. DAT	13,11	22 pts, 39.56-1.12						
	112583. DAT	11	* Losing C ₂ H ₂ fuel during IEff [For isotopic correction]						
*** *****									
	112283. ISO	11	22 pts, 39.56-1.12						
	112583. ISO	11	* Losing C ₂ H ₂ fuel during IEff						
*** *****									
	112283. ISO	13,11	22 pts, 39.56-1.12						
	112583. ISO	11	34 pts, 42.26-1.00-3.83						

53 C ₄ H ₆	112183. IES 4.28	8.5-16						
*** *****				112283. ISO	11	22 pts, 39.56-1.12		
54 C ₄ H ₆	112183. IES 4.28	8-16		112583. ISO	11	18 pts, 11.90-1.00-3.83		
*** *****								
56 C ₄ H ₆ /C ₃ H ₄ O	112183. IES 4.28	9-16.5		112283. ISO	11	22 pts, 39.56-1.12		
*** *****				112583. ISO	11	18 pts, 11.90-1.00-3.83		
62 C ₅ H ₂	010484. IES 5.05	7.5-14						
*** *****				010584. DAT	10.25	24 pts, 39.74-1.24 mm		
63 C ₅ H ₃	010484. IES 5.05	7.5-14						
*** *****				010584. ISO	10.25	24 pts, 39.74-1.24 mm		
64 C ₅ H ₄	010484. IES 5.05	14						
*** *****				010584. ISO	10.25	-1(+/- 5) counts/60 sec 24 pts, 39.74-1.24 mm		
65 C ₅ H ₅	010484. IES 5.05	9-14						
*** *****				010584. ISO	11	24 pts, 39.74-1.24 mm		
66 C ₅ H ₆	010484. IES 5.05	9-14						
*** *****				010584. ISO	11	24 pts, 39.74-1.24 mm		
73 C ₆ H	111783. IES 6.54	13.5-17						
*** *****								
74 C ₆ H ₂	111783. IES 6.54	8.5-14						
*** *****				112083. IES 5.93	10-13.5			
*** *****				112083. DAT	13	24 pts, 40.58-0.79-5.93 mm		
75 C ₆ H ₃								
*** *****								
76 C ₆ H ₄	111783. IES 6.54	8.5-14						
*** *****				112083. IES 5.93	10-13.5			
*** *****				112083. ISO	13	24 pts, 40.58-0.79-5.93 mm		


```

*** *****
122 C10H2 010784.DAT 10.10 10.5-15 010784.DAT 13.5 1-min counts for ion'n effcy.
*** ***** 2-min cnt;32 pts, 39.59-1.99-10.10
126 C10H6 010484.IES 5.05 14 4(+/- 4) at 14eV
*** *****
128 C10H8 010484.IES 5.05 16,10-16 1- and 10-min counts
*** *****
152 C12H8 010484.IES 5.05 14,19 8(+/-6) at 19, 3(+/-3) at 14
*** *****

```

APPENDIX C.

Mole-fraction data points

Points were measured by molecular-beam mass-spectrometry as signal intensities for mass 40, the species of interest, any other species that might make isotopic contributions, and mass 40 again. The signal ratio was corrected for isotopic contributions to the species of interest and for non-Ar contributions to mass 40. A mole-fraction ratio to Ar was calculated by dividing the signal ratio by a calibration factor, the product of the calibration sensitivity $S_{i,Ar}$ and the beam mass-discrimination factor α_i . Finally, the mole fraction of Ar was computed by difference and the mole-fraction ratios were converted to absolute mole fractions.

Distances from the burner to the nozzle, Z (cm), were adjusted for probe perturbation by subtracting 0.11 cm (two orifice diameters) from the measured distances (see Ch. III).

The calibration factors determine the appropriate number of significant digits that should be attributed to the mole fractions of each species.

Mass 1 - H atom.	0.972 +6.0502E-03
Calibration factor 0.0151	1.184 +4.3429E-03
Source: 112184.SC1	1.454 +4.0717E-03
	1.944 +5.5787E-03
<u>Z(cm) Mole fraction</u>	2.857 +3.9776E-03
0.062 +2.6667E-03	3.824 +5.2663E-03
0.042 +1.2116E-03	0.821 +6.2905E-03
0.010 +2.4412E-03	
0.027 +7.1631E-04	
0.092 +1.4454E-03	Mass 2 - H ₂ .
0.171 +5.8694E-03	Calibration factor 0.283
0.207 +5.8362E-03	Source: 112184.ALT
0.247 +1.0389E-02	<u>Z(cm) Mole fraction</u>
0.301 +1.2367E-02	0.062 +6.9448E-02
0.337 +1.6240E-02	0.042 +6.7588E-02
0.383 +1.0560E-02	0.010 +6.9047E-02
0.441 +1.0476E-02	0.027 +7.0315E-02
0.491 +1.5869E-02	0.092 +7.5602E-02
0.543 +1.0718E-02	0.171 +8.7333E-02
0.591 +1.1144E-02	0.207 +9.3159E-02
0.657 +1.0578E-02	0.247 +9.6065E-02
0.703 +8.6766E-03	0.301 +1.0450E-01
0.752 +7.8465E-03	0.441 +1.0773E-01
0.757 +6.6003E-03	0.491 +1.1890E-01

(H₂ continued)
 0.543 +1.2632E-01
 0.591 +1.3056E-01
 0.657 +1.3519E-01
 3.697 +1.8612E-01
 3.865 +1.7835E-01
 3.824 +1.8020E-01
 3.555 +1.8416E-01
 3.298 +1.8267E-01
 3.002 +1.8054E-01
 2.740 +1.8456E-01
 2.457 +1.8419E-01
 2.214 +1.7622E-01
 1.964 +1.7799E-01
 1.710 +1.7445E-01
 1.455 +1.6838E-01
 1.213 +1.6217E-01
 1.073 +1.6157E-01
 0.951 +1.5516E-01
 0.821 +1.5435E-01
 0.699 +1.4468E-01
 0.583 +1.4011E-01

Mass 15 - CH₃.
 Calibration factor 0.286
 Source: 112984.ISO (12 eV)

<u>Z(cm)</u>	<u>Mole fraction</u>
3.804	+7.3048E-04
3.705	+8.0858E-04
3.517	+7.8915E-04
3.197	+8.6172E-04
2.942	+8.8418E-04
2.683	+8.1857E-04
2.490	+1.0318E-03
2.287	+1.0168E-03
2.109	+1.1761E-03
1.920	+1.2169E-03
1.730	+1.2802E-03
1.575	+1.2937E-03
1.425	+1.4971E-03
1.263	+1.6897E-03
1.143	+1.6542E-03
1.024	+2.1317E-03
0.927	+2.3036E-03
0.834	+2.6667E-03
0.748	+3.0187E-03
0.646	+3.6855E-03
0.553	+3.9243E-03
0.468	+4.6379E-03
0.407	+4.6780E-03
0.380	+4.8707E-03
0.352	+4.7127E-03
0.305	+4.5906E-03

0.268	+4.8318E-03
0.224	+4.3495E-03
0.179	+3.2945E-03
0.141	+2.6946E-03
0.113	+2.2027E-03
0.071	+1.9098E-03
0.018	+1.1376E-03
0.027	+1.1646E-03
0.050	+1.3328E-03
0.091	+1.8127E-03
0.124	+2.4706E-03
0.153	+3.4365E-03
0.179	+3.5275E-03
0.207	+3.8803E-03
0.248	+4.4904E-03
0.278	+4.5935E-03
0.295	+4.8199E-03
0.347	+4.5290E-03
0.861	+2.8825E-03
2.244	+1.0818E-03

Mass 16 - CH₄.
 Calibration factor 0.1219
 Source: 112984.ISO (13.5eV)

<u>Z(cm)</u>	<u>Mole fraction</u>
3.804	+1.9696E-03
3.705	+1.9570E-03
3.517	+1.6155E-03
3.197	+1.5423E-03
2.942	+1.4701E-03
2.683	+1.2665E-03
2.490	+1.4133E-03
2.287	+1.4090E-03
2.109	+1.3715E-03
1.920	+1.1342E-03
1.730	+1.1347E-03
1.575	+1.0414E-03
1.425	+1.0791E-03
1.263	+1.2053E-03
1.143	+1.2873E-03
1.024	+1.0419E-03
0.927	+1.3547E-03
0.834	+1.3390E-03
0.748	+1.6196E-03
0.646	+1.7279E-03
0.553	+2.0548E-03
0.468	+2.5380E-03
0.407	+3.2476E-03
0.380	+2.8353E-03
0.352	+3.5960E-03
0.305	+3.7940E-03
0.268	+3.5323E-03
0.224	+3.7810E-03

(CH₄ continued)
 0.179 +3.2338E-03
 0.141 +3.4555E-03
 0.113 +3.8351E-03
 0.071 +3.6279E-03
 0.018 +3.2891E-03
 0.027 +3.1267E-03
 0.050 +3.2670E-03
 0.091 +3.4694E-03
 0.124 +3.8343E-03
 0.153 +3.5855E-03
 0.179 +3.9021E-03
 0.207 +3.5473E-03
 0.248 +3.8587E-03
 0.278 +3.6769E-03
 0.295 +3.6699E-03
 0.347 +3.3325E-03
 0.861 +1.6354E-03
 2.244 +1.5617E-03

Mass 17 - OH.
 Calibration factor 0.311
 Source: 112884.ISO

<u>Z(cm)</u>	<u>Mole fraction</u>
0.334	+9.0445E-04
0.306	+5.6386E-04
0.293	+5.8520E-04
0.240	+5.0123E-04
0.235	+5.0249E-04
0.197	+4.5021E-04
0.166	+3.4803E-04
0.140	+2.9904E-04
0.093	+1.6535E-04
0.067	+1.9840E-04
0.031	+1.2474E-04
0.038	+2.3668E-04
0.080	+2.4753E-04
0.108	+2.1952E-04
0.167	+3.2026E-04
0.209	+3.8901E-04
0.279	+6.3196E-04
0.301	+6.6920E-04
0.335	+7.3245E-04
0.363	+8.6532E-04
0.396	+5.7483E-04
0.546	+7.7860E-04
0.584	+6.6398E-04
3.933	+3.1606E-05
3.824	+3.6535E-06
3.691	+3.2293E-05
3.438	+9.0335E-06
3.184	+3.9481E-05
2.927	+6.8212E-05

1.677 +2.4811E-04
 1.094 +3.6031E-04
 1.094 +3.6031E-04

Mass 18 - H₂O.
 Calibration factor 0.647
 Source: 011084.DAT

<u>Z(cm)</u>	<u>Mole fraction</u>
0.257	+1.1820E-01
0.184	+1.0203E-01
0.153	+9.5210E-02
0.108	+9.5532E-02
0.076	+8.4254E-02
0.041	+7.6458E-02
0.006	+6.8697E-02
0.026	+7.3572E-02
0.052	+7.3054E-02
0.099	+8.5216E-02
0.133	+8.8754E-02
0.168	+9.8876E-02
0.207	+1.0519E-01
0.243	+1.0436E-01
0.265	+1.1051E-01
0.297	+1.1761E-01
0.336	+1.2435E-01
0.377	+1.2996E-01
0.416	+1.2451E-01
0.453	+1.3550E-01
0.505	+1.3319E-01
0.544	+1.3622E-01
0.575	+1.4196E-01
0.629	+1.3867E-01
0.663	+1.4096E-01
0.709	+1.3426E-01
0.753	+1.3510E-01
0.788	+1.3241E-01
0.844	+1.3049E-01
0.876	+1.2566E-01
0.959	+1.2732E-01
1.065	+1.2170E-01
1.162	+1.2147E-01
1.297	+1.1892E-01
1.493	+1.1246E-01
1.714	+1.0937E-01
2.016	+1.0419E-01
2.338	+9.9539E-02
2.596	+9.8902E-02
2.973	+9.6938E-02
3.339	+9.5876E-02
3.576	+9.6367E-02
3.794	+9.6290E-02
3.877	+9.3915E-02
3.647	+9.5070E-02
3.325	+9.6946E-02

Mass 26 - C₂H₂.
Calibration factor 1.075
Source: 121384.SCL

<u>Z(cm)</u>	<u>Mole fraction</u>
3.881	+6.0347E-02
3.744	+6.1064E-02
3.579	+5.9496E-02
3.400	+5.8811E-02
3.150	+5.8931E-02
2.903	+6.0150E-02
2.649	+6.0860E-02
2.379	+6.0178E-02
2.188	+6.1632E-02
1.997	+6.2613E-02
1.813	+6.4046E-02
1.646	+6.3186E-02
1.490	+6.6103E-02
1.366	+6.8954E-02
1.234	+7.0435E-02
1.110	+7.3531E-02
0.981	+7.7421E-02
0.899	+8.0063E-02
0.760	+8.9174E-02
0.654	+1.0041E-01
0.538	+1.1878E-01
0.432	+1.4543E-01
0.348	+1.7466E-01
0.282	+2.0713E-01
0.236	+2.2201E-01
0.181	+2.4665E-01
0.144	+2.5756E-01
0.084	+2.7675E-01
0.053	+2.9434E-01
0.016	+3.0792E-01
0.028	+3.0252E-01
0.072	+2.9226E-01
0.119	+2.7349E-01
0.161	+2.5310E-01
0.188	+2.4164E-01
0.229	+2.2221E-01
0.269	+2.0438E-01
0.307	+1.9035E-01
0.335	+1.7792E-01
0.389	+1.5667E-01
0.447	+1.3704E-01
0.518	+1.1744E-01
0.564	+1.0528E-01

Mass 27 - C₂H₃.
Calibration factor 0.35
Source: VINYL.ISO

<u>Z(cm)</u>	<u>Mole fraction</u>
0.054	+8.7067E-05
0.118	+5.0157E-05
0.151	+1.0128E-04
0.237	+1.0352E-04
0.300	+1.4933E-04
0.382	+1.8132E-04
0.434	+2.2282E-04
0.435	+1.8022E-04
0.519	+1.5094E-04
0.595	+1.4750E-04
0.691	+1.8434E-04
0.806	+1.0862E-04
0.690	+1.5364E-04
0.888	+8.9998E-05
1.104	+4.5782E-05
1.311	+6.4192E-05
3.838	+3.4993E-05
3.600	+4.4481E-05
3.282	+1.6474E-05
3.206	+3.1926E-05
3.008	+1.5028E-05
2.695	+1.5506E-05
2.468	+2.2089E-05
2.085	+4.4346E-05
1.710	+3.4771E-05
1.454	+5.3463E-05
1.263	+6.3509E-05
0.947	+5.8017E-05
0.695	+1.3051E-04
0.544	+1.5591E-04

Mass 28(a) - C₂H₄.
Calibration factor 0.41
Source: C2H4.ISO

<u>Z(cm)</u>	<u>Mole fraction</u>
3.881	+2.8592E-05
3.744	+4.7064E-06
3.579	+1.1043E-04
3.400	+5.9467E-06
3.150	+1.1360E-04
2.903	+8.8963E-05
2.649	+4.4029E-05
2.379	+8.5693E-05
2.188	+8.9036E-05
1.997	+3.0332E-05
1.813	+1.5679E-04
1.646	+1.4418E-04
1.490	+1.2625E-04

(C₂H₄ continued)

1.366E+9.5599E+05.5
 1.234E+9.5774E+05.5
 1.110E+1.5479E+04.4
 0.981E+2.2853E+04.4
 0.899E+1.5969E+04.4
 0.760E+2.9827E+04.4
 0.654E+5.1449E+04.4
 0.538E+9.3903E+04.4
 0.432E+1.3669E+03.3
 0.348E+2.0269E+03.3
 0.282E+2.3106E+03.3
 0.236E+2.2285E+03.3
 0.181E+2.0886E+03.3
 0.144E+1.7878E+03.3
 0.084E+1.6232E+03.3
 0.053E+1.6335E+03.3
 0.016E+1.3504E+03.3
 0.028E+1.4608E+03.3
 0.072E+1.8652E+03.3
 0.119E+1.8472E+03.3
 0.161E+2.0238E+03.3
 0.188E+2.0082E+03.3
 0.229E+2.3527E+03.3
 0.269E+2.2370E+03.3
 0.307E+2.3595E+03.3
 0.335E+1.8777E+03.3
 0.389E+1.6466E+03.3
 0.447E+1.2261E+03.3
 0.518E+5.5714E+04.4
 0.564E+5.1934E+04.4
 1.224E+3.0373E+05.5
 1.148E+1.0925E+04.4
 1.064E+1.4847E+04.4
 0.982E+1.5121E+04.4
 0.890E+2.4674E+04.4
 0.792E+2.5698E+04.4
 0.691E+3.3546E+04.4
 0.666E+3.3337E+04.4
 0.632E+4.7366E+04.4
 0.574E+6.1159E+04.4
 0.537E+8.1587E+04.4
 0.498E+9.1927E+04.4
 0.463E+1.2482E+03.3
 0.416E+1.5007E+03.3
 0.366E+1.8585E+03.3
 0.330E+2.0687E+03.3
 0.285E+2.1724E+03.3
 0.233E+2.5235E+03.3
 0.181E+2.0128E+03.3
 0.145E+1.9827E+03.3
 0.112E+1.8800E+03.3
 0.066E+1.6397E+03.3
 0.039E+1.5617E+03.3
 0.006E+1.4509E+03.3

Mass: 28(b) - C₂H₄
 Calibration factor: 1.0938
 Source: 120183.DAT

Z (cm) Mole fraction

3.982E+5.3244E+01.1
 3.881E+5.1888E+01.1
 3.625E+5.2793E+01.1
 3.378E+5.3426E+01.1
 3.120E+5.64718E+01.1
 2.875E+5.1774E+01.1
 2.616E+5.0520E+01.1
 2.497E+5.4405E+01.1
 2.242E+5.2380E+01.1
 1.981E+4.9937E+01.1
 1.799E+5.1518E+01.1
 1.799E+5.0893E+01.1
 1.609E+5.1894E+01.1
 1.480E+5.1562E+01.1
 1.386E+5.0709E+01.1
 1.300E+5.0321E+01.1
 1.199E+4.9540E+01.1
 1.115E+4.9578E+01.1
 1.035E+5.0220E+01.1
 0.939E+4.7419E+01.1
 0.860E+4.8771E+01.1
 0.774E+4.6893E+01.1
 0.683E+4.6719E+01.1
 0.599E+4.3802E+01.1
 0.519E+4.1720E+01.1
 0.468E+3.8786E+01.1
 0.403E+3.9040E+01.1
 0.342E+3.3935E+01.1
 0.271E+3.3147E+01.1
 0.205E+2.8094E+01.1
 0.170E+2.4555E+01.1
 0.114E+2.1754E+01.1
 0.068E+1.9337E+01.1
 0.035E+1.7539E+01.1
 0.001E+1.6423E+01.1
 0.048E+1.7977E+01.1
 0.087E+1.9504E+01.1
 0.130E+2.2433E+01.1
 0.181E+2.4704E+01.1
 0.221E+2.8366E+01.1
 0.267E+2.9235E+01.1
 0.316E+3.0817E+01.1
 0.367E+3.5714E+01.1
 0.418E+3.7197E+01.1
 0.466E+3.8932E+01.1
 0.595E+4.3430E+01.1
 0.724E+4.5718E+01.1
 0.854E+4.7833E+01.1
 0.991E+4.8551E+01.1

(CO continued)

1.105 +5.2779E-01
1.252 +5.1908E-01
1.366 +5.1075E-01
1.498 +5.3611E-01
1.645 +5.2889E-01
1.893 +5.7058E-01
2.159 +5.3907E-01
2.397 +5.4322E-01
2.635 +5.5336E-01
2.900 +5.1337E-01
3.148 +5.6536E-01
3.393 +5.5736E-01
3.617 +5.3533E-01
3.882 +5.6400E-01

Mass 29 - HCO; some C₂H₅
Calibration factor 0.42
Source: 122983.ISO

Z(cm) Mole fraction

0.019 +6.7334E-05
0.032 +1.5367E-05
0.061 +3.6571E-05
0.091 +4.1619E-05
0.127 +5.8675E-05
0.155 +9.6980E-05
0.225 +4.2493E-05
0.262 +5.3413E-05
0.288 +7.4448E-05
0.347 +6.2466E-05
0.408 +5.9919E-05
0.448 +5.6209E-05
0.505 +4.4065E-05
0.564 +6.5309E-05
0.639 +7.1680E-05
0.742 +4.7646E-05
0.827 +3.3350E-05
0.930 +2.9190E-05
0.793 +1.9883E-05
0.671 +5.8075E-05
0.591 +3.6619E-05
0.511 +8.8942E-05
0.454 +4.1921E-05
0.372 +3.1173E-05
0.311 +3.0487E-05
0.281 +5.8239E-05
0.237 +5.8913E-05
0.201 +3.6652E-05
0.162 +4.1908E-05
0.130 +6.7389E-05
0.096 +2.6107E-05
0.063 +3.4044E-05
0.020 +6.7321E-05

Mass 30 - H₂CO and/or C₂H₆;
probably mostly H₂CO.
Calibration factor 0.45
Source: 122983.ISO

Z(cm) Mole fraction

0.019 +7.9347E-04
0.032 +6.9692E-04
0.061 +8.1471E-04
0.091 +7.3164E-04
0.127 +7.2475E-04
0.155 +6.7933E-04
0.225 +4.9383E-04
0.262 +3.5526E-04
0.288 +3.1575E-04
0.347 +1.9600E-04
0.408 +1.8146E-04
0.448 +1.2008E-04
0.505 +8.1680E-05
0.564 +7.3558E-05
0.639 +5.0519E-05
0.742 +4.5320E-05
0.827 +3.1789E-05
0.930 +3.1090E-05
0.793 +1.6829E-05
0.671 +3.9646E-05
0.591 +5.8998E-05
0.511 +8.5360E-05
0.454 +1.4168E-04
0.372 +2.5579E-04
0.311 +2.4682E-04
0.281 +3.9333E-04
0.237 +4.0535E-04
0.201 +5.9792E-04
0.162 +6.1569E-04
0.130 +8.6733E-04
0.096 +8.4591E-04
0.063 +9.2781E-04
0.020 +9.4999E-04

Mass 32 - O₂.
Calibration factor 0.365
Source: 122783.DAT

Z(cm) Mole fraction

3.852 +1.8225E-04
3.596 -4.4176E-04
3.350 -2.3153E-04
3.079 +3.4155E-04
2.850 -1.7929E-04
2.595 +2.2785E-04
2.331 +5.6582E-04
2.073 -1.2114E-04
1.879 +4.6520E-04

(O₂ continued)

1.689 +5.0880E-04
1.474 +6.2895E-04
1.309 +1.4047E-03
1.127 +1.9840E-03
1.003 +3.1271E-03
0.880 +6.8747E-03
0.797 +9.9749E-03
0.702 +1.4439E-02
0.624 +2.1901E-02
0.547 +3.2278E-02
0.491 +4.4703E-02
0.400 +7.1624E-02
0.353 +9.1051E-02
0.286 +1.2656E-01
0.241 +1.5704E-01
0.200 +1.8374E-01
0.156 +2.1519E-01
0.121 +2.2711E-01
0.076 +2.4922E-01
0.043 +2.7336E-01
0.055 +2.7121E-01
0.137 +2.1651E-01
0.239 +1.6098E-01
0.333 +1.0422E-01

Mass 33 - HO₂.

Calibration factor 0.68

Source: 121184.ISO

Z(cm) Mole fraction

0.331 +8.6402E-05
0.308 +8.2541E-05
0.281 +1.1317E-04
0.241 +1.2773E-04
0.210 +1.8569E-04
0.179 +2.2678E-04
0.137 +2.9762E-04
0.102 +2.9177E-04
0.079 +2.8775E-04
0.040 +3.1759E-04
0.009 +3.1665E-04
0.002 +2.9363E-04
0.024 +2.8215E-04
0.044 +3.2545E-04
0.068 +3.0779E-04
0.099 +2.9300E-04
0.124 +3.0512E-04
0.150 +2.6220E-04
0.177 +2.0719E-04
0.204 +1.8257E-04
0.229 +1.6951E-04
0.248 +1.4423E-04
0.283 +1.2663E-04

0.309 +1.1238E-04
0.344 +9.5212E-05
0.368 +7.0461E-05
0.397 +4.7254E-05
0.435 +1.6649E-05
0.469 +4.4017E-05
0.497 +2.6623E-05
0.529 +1.0191E-05
0.571 +3.4060E-05
0.805 +3.6498E-06
1.473 +1.3003E-05

Mass 38 - C₃H₂.

Calibration factor 0.51

Source: 122383.DAT

Z(cm) Mole fraction

0.035 +0.0000E+00
0.081 +6.1180E-06
0.113 +3.1025E-06
0.135 +1.9121E-05
0.177 +3.1652E-06
0.200 +1.5563E-05
0.231 +3.0354E-05
0.262 +4.0298E-05
0.294 +6.1980E-05
0.337 +1.0504E-04
0.383 +1.5270E-04
0.427 +1.8221E-04
0.456 +1.7028E-04
0.488 +1.4454E-04
0.527 +1.9196E-04
0.568 +2.0049E-04
0.619 +1.7050E-04
0.666 +2.0365E-04
0.720 +1.5225E-04
0.799 +1.2988E-04
0.891 +9.5289E-05
1.000 +9.8092E-05
1.087 +6.6992E-05
1.236 +5.8762E-05
1.414 +4.0969E-05
1.596 +4.9739E-05
1.920 +4.3997E-05
2.244 +5.9816E-05
2.552 +2.9954E-05
3.060 +2.1227E-05
3.233 +2.1005E-05
3.439 +1.4259E-05
3.613 +6.7980E-06
3.838 +6.7684E-06
3.621 +2.0349E-05
3.304 +2.2339E-05
2.998 +2.2179E-05

(C₃H₂ continued)
 2.684 +3.5809E-05
 2.347 +3.4808E-05
 2.026 +4.5128E-05
 1.713 +4.5445E-05
 1.396 +5.0583E-05
 1.084 +7.6365E-05
 0.838 +1.0614E-04
 0.738 +1.5495E-04
 0.650 +1.6589E-04
 0.563 +1.8038E-04
 0.517 +1.9231E-04
 0.476 +1.8921E-04
 0.430 +1.7221E-04

Mass 39 - C₃H₃ (propargyl).
 Calibration factor 0.49
 Source: 122383.ISO

<u>Z(cm)</u>	<u>Mole fraction</u>
0.035	+3.5509E-05
0.081	+4.4362E-05
0.113	+1.0645E-04
0.135	+1.1874E-04
0.177	+2.9308E-04
0.200	+2.7808E-04
0.231	+4.9180E-04
0.262	+5.1483E-04
0.294	+6.8165E-04
0.337	+9.9274E-04
0.383	+9.9197E-04
0.427	+1.0231E-03
0.456	+9.0430E-04
0.488	+9.5842E-04
0.527	+8.3386E-04
0.568	+7.7904E-04
0.619	+6.9000E-04
0.666	+6.4343E-04
0.720	+5.4077E-04
0.799	+4.4737E-04
0.891	+3.2994E-04
1.000	+4.3356E-04
1.087	+2.1916E-04
1.236	+2.2349E-04
1.414	+1.3426E-04
1.596	+1.7349E-04
1.920	+1.1295E-04
2.244	+7.9639E-05
2.552	+8.4696E-05
3.060	+1.0053E-04
3.233	+1.1223E-04
3.439	+9.4121E-05
3.613	+9.7055E-05
3.838	+7.9018E-05

3.621 +8.9308E-05
 3.304 +7.7281E-05
 2.998 +9.8164E-05
 2.684 +1.0041E-04
 2.347 +1.1078E-04
 2.026 +1.1418E-04
 1.713 +1.5046E-04
 1.396 +1.6606E-04
 1.084 +2.3580E-04
 0.838 +3.9900E-04
 0.738 +4.9073E-04
 0.650 +6.0224E-04
 0.563 +8.1632E-04
 0.517 +9.5199E-04
 0.476 +1.0740E-03
 0.430 +1.0933E-03

Mass 40(a) - C₃H₄ - propyne and propadiene.
 Calibration factor 1.28
 Source: 122383.ISO

<u>Z(cm)</u>	<u>Mole fraction</u>
0.035	+6.3394E-04
0.081	+7.6178E-04
0.113	+8.1214E-04
0.135	+9.5865E-04
0.177	+9.0419E-04
0.200	+8.6443E-04
0.231	+9.6632E-04
0.262	+9.1152E-04
0.294	+8.1617E-04
0.337	+5.9188E-04
0.383	+4.7004E-04
0.427	+4.3556E-04
0.456	+3.8755E-04
0.488	+2.9775E-04
0.527	+2.6374E-04
0.568	+2.3365E-04
0.619	+1.7183E-04
0.666	+1.8047E-04
0.720	+1.1694E-04
0.799	+1.1088E-04
0.891	+9.1121E-05
1.000	+7.5038E-05
1.087	+6.7517E-05
1.236	+6.4385E-05
1.414	+5.9360E-05
1.596	+5.0307E-05
1.920	+2.9217E-05
2.244	+5.6602E-05
2.552	+4.3264E-05
3.060	+4.3697E-05
3.233	+6.4161E-05

(C₃H₄ continued)
3.439 +5.6814E-05
3.613 +6.0944E-05
3.838 +5.6631E-05

Mass 41 - HCCO and/or C₃H₅
Calibration factor 0.4
Source: 121284.ISO

Z(cm) Mole fraction

3.830 -9.5033E-06
3.684 -1.2188E-05
3.516 +1.4639E-05
3.332 +5.1533E-06
3.134 -1.4400E-05
2.889 +0.0000E+00
2.638 -2.0265E-05
2.381 +4.2946E-06
2.126 +1.8828E-05
1.930 -3.9041E-06
1.749 -9.6939E-06
1.560 +2.6003E-05
1.408 +2.7868E-05
1.238 +7.7311E-06
1.044 +2.7631E-05
0.917 -9.4473E-06
0.796 +0.0000E+00
0.696 +1.6201E-05
0.631 +2.3726E-05
0.570 +2.4314E-06
0.524 +8.1799E-05
0.487 +2.4277E-05
0.405 +2.3540E-05
0.348 +5.3741E-05
0.278 +3.7320E-05
0.222 +9.0639E-06
0.163 +2.8693E-05
0.118 -3.9143E-06
0.081 +3.6771E-05
0.052 +1.6052E-06
0.010 -2.6080E-06
0.002 +0.0000E+00
0.039 +0.0000E+00

Mass 42 - CH₂CO and/or C₃H₆
Calibration factor 0.44
Source: 121284.ISO

Z(cm) Mole fraction

3.830 +3.2830E-05
3.684 +2.4107E-05
3.516 +2.2598E-05
3.332 +4.4501E-05
3.134 +3.3512E-05
2.889 +2.3957E-05

2.638 +3.0868E-05
2.381 +4.6045E-05
2.126 +2.6410E-05
1.930 +5.1635E-05
1.749 +4.8888E-05
1.560 +7.1227E-05
1.408 +5.0911E-05
1.238 +8.1594E-05
1.044 +7.9118E-05
0.917 +1.4370E-04
0.796 +1.7386E-04
0.696 +1.8864E-04
0.631 +2.0978E-04
0.570 +3.0610E-04
0.524 +3.5792E-04
0.487 +3.3379E-04
0.405 +4.6619E-04
0.348 +4.0056E-04
0.278 +6.0876E-04
0.222 +6.8258E-04
0.163 +7.2181E-04
0.118 +6.8842E-04
0.081 +7.2314E-04
0.052 +6.9938E-04
0.010 +6.8408E-04
0.002 +7.1423E-04
0.039 +7.2154E-04

Mass 44 - CO₂.
Calibration factor 1.180
Source: 122783.DAT

Z(cm) Mole fraction

3.852 +7.4227E-02
3.596 +7.3172E-02
3.350 +7.6094E-02
3.079 +7.3383E-02
2.850 +7.4259E-02
2.595 +7.4680E-02
2.331 +7.3986E-02
2.073 +7.7004E-02
1.879 +7.6003E-02
1.689 +7.8822E-02
1.474 +8.0822E-02
1.309 +8.0559E-02
1.127 +8.4544E-02
1.003 +8.2644E-02
0.880 +8.4418E-02
0.797 +8.4474E-02
0.702 +8.5556E-02
0.624 +8.4899E-02
0.547 +8.2580E-02
0.491 +7.8343E-02
0.400 +7.7632E-02
0.353 +7.5854E-02

(CO₂ continued)
 0.286 +7.2169E-02
 0.241 +6.7862E-02
 0.200 +6.2367E-02
 0.156 +6.0252E-02
 0.121 +5.0235E-02
 0.076 +4.5683E-02
 0.043 +4.2218E-02
 0.055 +4.2004E-02
 0.137 +5.1470E-02
 0.239 +6.5155E-02
 0.333 +7.3721E-02

Mass 50 - C₄H₂.
 Calibration factor 1.52
 Source: 112283.DAT

<u>Z(cm)</u>	<u>Mole fraction</u>
3.846	+2.8941E-03
3.590	+3.0395E-03
3.215	+3.2043E-03
2.830	+3.4316E-03
2.442	+3.7649E-03
2.123	+4.2493E-03
1.869	+4.5487E-03
1.613	+5.2572E-03
1.355	+6.2160E-03
1.107	+7.3874E-03
1.023	+7.9491E-03
0.925	+8.5677E-03
0.813	+9.0355E-03
0.735	+9.4559E-03
0.635	+9.6281E-03
0.538	+9.1154E-03
0.440	+7.6463E-03
0.357	+5.8007E-03
0.265	+3.4805E-03
0.176	+1.6172E-03
0.083	+6.1450E-04
0.002	+3.0305E-04

Mass 51 - C₄H₃.
 Calibration factor 1.45
 Source: 112283.ISO

<u>Z(cm)</u>	<u>Mole fraction</u>
3.846	+1.1089E-05
3.590	-4.7249E-07
3.215	+4.1539E-06
2.830	+4.3848E-06
2.442	-1.5552E-06
2.123	+1.1841E-05
1.869	+1.2395E-05
1.613	+1.7001E-05
1.355	+1.5559E-05

1.107	+6.5336E-06
1.023	+4.4602E-06
0.925	-7.6888E-07
0.813	+3.5443E-06
0.735	+1.2332E-05
0.635	+1.2287E-05
0.538	+7.9543E-06
0.440	+2.1763E-05
0.357	+1.9365E-05
0.265	+1.1646E-05
0.176	+1.4361E-05
0.083	+5.6049E-06
0.002	+1.6767E-06

Mass 52 - C₄H₄ (vinylacetylene)
 Calibration factor 3.9
 Source: C4H4.ISO

<u>Z(cm)</u>	<u>Mole fraction</u>
3.846	+1.0300E-05
3.590	+9.8840E-06
3.215	+7.0421E-06
2.830	+6.4332E-06
2.442	+6.3862E-06
2.123	+8.9713E-06
1.869	+8.4524E-06
1.613	+8.8676E-06
1.355	+1.0628E-05
1.107	+1.5125E-05
1.023	+1.5747E-05
0.925	+2.2674E-05
0.813	+2.8399E-05
0.735	+3.9988E-05
0.635	+4.9350E-05
0.538	+8.0677E-05
0.440	+1.3952E-04
0.357	+1.7470E-04
0.265	+1.7233E-04
0.176	+1.1459E-04
0.083	+6.3316E-05
0.002	+3.4020E-05
3.846	+8.8144E-06
3.590	+9.2286E-06
3.215	+8.4425E-06
2.830	+5.9647E-06
2.442	+5.6686E-06
2.123	+9.1645E-06
1.869	+5.8056E-06
1.613	+3.7334E-06
1.355	+1.0193E-05
1.107	+1.0885E-05
1.023	+1.3632E-05
0.925	+2.1216E-05
0.813	+2.1414E-05
0.735	+4.2861E-05

(C₄H₄ continued)

0.635	+4.9365E-05
0.538	+8.9787E-05
0.440	+1.4720E-04
0.357	+1.8488E-04
0.265	+1.7984E-04
0.176	+1.2152E-04
0.083	+6.9078E-05
0.002	+4.3039E-05
4.116	+1.3336E-05
3.850	+1.2995E-05
3.608	+1.4043E-05
3.360	+1.3524E-05
3.002	+9.1808E-06
2.839	+7.4935E-06
2.589	+6.2368E-06
2.341	+8.2750E-06
2.071	+8.7197E-06
2.072	+7.1738E-06
1.813	+7.4282E-06
1.564	+7.6435E-06
1.470	+8.7894E-06
1.365	+1.0646E-05
1.271	+9.9979E-06
1.175	+1.0966E-05
1.080	+1.5787E-05
1.009	+1.8980E-05
0.917	+2.5100E-05
0.823	+3.3889E-05
0.726	+4.1314E-05
0.646	+6.8056E-05
0.549	+9.0933E-05
0.470	+1.4157E-04
0.388	+1.7037E-04
0.296	+1.6408E-04
0.220	+1.1376E-04
0.141	+6.7615E-05
0.070	+3.5058E-05
0.014	+3.0520E-05
0.085	+5.3466E-05
0.171	+7.4838E-05
0.273	+1.7187E-04

Mass 53 - C₄H₅.
 Calibration factor 1.25
 Source: C4H5.ISO

<u>Z(cm)</u>	<u>Mole fraction</u>
3.846	+7.5410E-08
3.590	+5.3647E-08
3.215	+0.0000E+00
2.830	+1.7557E-07
2.442	+0.0000E+00
2.123	+4.6377E-07
1.869	+0.0000E+00

1.613	+0.0000E+00
1.355	+4.7816E-07
1.107	+4.4930E-07
1.023	-7.2929E-08
0.925	+1.1185E-06
0.813	+2.0474E-07
0.735	-5.0819E-08
0.635	+1.5186E-06
0.538	+6.1948E-06
0.440	+5.8010E-06
0.357	+3.4855E-07
0.265	+1.2047E-06
0.176	+4.0201E-06
0.083	+5.2488E-06
0.002	+6.8730E-07
1.080	-1.4995E-07
1.009	+2.7958E-07
0.917	+0.0000E+00
0.823	+8.0275E-07
0.726	+3.4108E-06
0.646	+2.5946E-06
0.549	+2.5882E-08
0.470	+6.0606E-06
0.388	+8.4915E-06
0.296	+1.0262E-05
0.220	+7.0079E-06
0.141	+9.7720E-06
0.070	+3.6084E-06
0.014	+1.4512E-06
0.085	+3.0835E-06
0.171	+9.0239E-06
0.273	+3.3850E-06

Mass 54 - C₄H₆
 (1,3-butadiene).
 Calibration factor 1.21
 Source: C4H6.ISO

<u>Z(cm)</u>	<u>Mole fraction</u>
3.846	+1.4936E-06
3.590	+0.0000E+00
3.215	+1.9656E-06
2.830	-5.0130E-07
2.442	+4.8124E-07
2.123	-1.0112E-06
1.869	-4.9915E-07
1.613	-5.1283E-07
1.355	+1.5337E-06
1.107	+0.0000E+00
1.023	+5.4361E-07
0.925	+1.0847E-06
0.813	+1.8385E-06
0.735	-6.7738E-07
0.635	+1.2520E-06
0.538	+3.9366E-06

(C₄H₆ continued)

0.440 +3.9286E-06
0.357 +2.4733E-05
0.265 +3.2327E-05
0.176 +4.8241E-05
0.083 +4.3362E-05
0.002 +2.8915E-05
1.080 +5.3350E-07
1.009 +0.0000E+00
0.917 +0.0000E+00
0.823 +1.7999E-06
0.726 +3.0809E-06
0.646 +4.9692E-07
0.549 +2.6994E-06
0.470 +7.0644E-06
0.388 +2.3653E-05
0.296 +3.6501E-05
0.220 +5.3967E-05
0.141 +3.6802E-05
0.070 +2.8087E-05
0.014 +1.6894E-05
0.085 +2.8415E-05
0.171 +3.5940E-05
0.273 +5.9890E-05

Mass 62 - C₅H₂.

Calibration factor 1.79
Source: 010584.DAT

Z(cm) Mole fraction

3.864 +1.3015E-06
3.486 +4.3220E-07
3.100 +1.6805E-06
2.733 +2.9296E-06
2.338 +3.8740E-06
1.973 +3.5263E-06
1.642 +3.5293E-06
1.327 +6.8487E-06
1.069 +5.7735E-06
0.826 +1.2752E-05
0.740 +1.7747E-05
0.647 +1.7535E-05
0.554 +1.3765E-05
0.477 +1.1735E-05
0.432 +1.5587E-05
0.383 +8.2586E-06
0.338 +1.0457E-05
0.292 +1.6182E-06
0.252 +2.7645E-06
0.207 +9.7730E-07
0.168 +4.6126E-07
0.112 +0.0000E+00
0.079 +7.9902E-07
0.014 +7.9680E-07

Mass 63 - C₅H₃.

Calibration factor 1.72
Source: 010584.ISO

Z(cm) Mole fraction

3.864 +3.0855E-06
3.486 +5.8223E-06
3.100 +3.4011E-06
2.733 +5.0577E-06
2.338 +9.6325E-06
1.973 +7.5952E-06
1.642 +1.3111E-05
1.327 +1.1315E-05
1.069 +1.7693E-05
0.826 +2.6385E-05
0.740 +2.7000E-05
0.647 +3.7516E-05
0.554 +4.6742E-05
0.477 +5.4956E-05
0.432 +5.2634E-05
0.383 +4.1424E-05
0.338 +3.2589E-05
0.292 +2.2360E-05
0.252 +1.0198E-05
0.207 +1.9779E-06
0.168 +9.3352E-07
0.112 +8.7357E-07
0.079 +7.8555E-07
0.014 -8.7509E-07

Mass 64 - C₅H₄.

Calibration factor 0.7
Source: 010584.ISO

Z(cm) Mole fraction

3.864 -1.5338E-06
3.486 +4.7312E-06
3.100 +9.2001E-06
2.733 +7.8629E-06
2.338 +1.2985E-05
1.973 +2.3356E-06
1.642 +1.8509E-05
1.327 +1.8452E-05
1.069 +9.8746E-06
0.826 +1.6215E-05
0.740 +1.6610E-05
0.647 +2.3067E-05
0.554 +3.6789E-05
0.477 +4.3598E-05
0.432 +6.4527E-05
0.383 +4.4487E-05
0.338 +4.3658E-05
0.292 +6.0396E-05
0.252 +3.9604E-05
0.207 +4.2212E-05

(C₅H₄ continued)
0.168 +9.3074E-06
0.112 +8.4674E-06
0.079 +1.7257E-05
0.014 -4.6374E-06

Mass 65 - C₅H₅.
Calibration factor 0.7
Source: 010584.ISO

Z(cm) Mole fraction
3.864 +2.3338E-06
3.486 +0.0000E+00
3.100 -1.7643E-06
2.733 +4.7610E-06
2.338 +1.2685E-07
1.973 +0.0000E+00
1.642 -2.6004E-07
1.327 +0.0000E+00
1.069 +1.7200E-06
0.826 +0.0000E+00
0.740 +9.7082E-06
0.647 +1.5914E-06
0.554 +5.2408E-06
0.477 +2.0069E-05
0.432 +9.7757E-06
0.383 +1.6462E-05
0.338 +3.5498E-05
0.292 +1.6159E-05
0.252 +6.9267E-06
0.207 +1.4328E-05
0.168 +8.7383E-06
0.112 +6.8778E-06
0.079 +8.9218E-06
0.014 +6.4604E-06

Mass 66 - C₅H₆.
Calibration factor 1.56
Source: 010584.ISO

Z(cm) Mole fraction
3.864 +0.0000E+00
3.486 +4.9592E-06
3.100 +4.8648E-06
2.733 +2.2819E-06
2.338 -1.3203E-06
1.973 +1.6859E-06
1.642 +1.6939E-06
1.327 +3.3680E-06
1.069 +0.0000E+00
0.826 +6.3618E-06
0.740 +6.7791E-06
0.647 +4.9281E-06
0.554 +7.7664E-06
0.477 +1.7451E-05

(C₅H₆ continued)
0.432 +8.6982E-06
0.383 +2.7425E-05
0.338 +2.1309E-05
0.292 +4.6633E-05
0.252 +3.9797E-05
0.207 +2.2069E-05
0.168 +4.3182E-05
0.112 +2.6797E-05
0.079 +2.0558E-05
0.014 +2.1171E-05

Mass 74 - C₆H₂.
Calibration factor 2.5
Source: 112083.ISO

Z(cm) Mole fraction
3.948 +2.1670E-04
3.787 +2.0386E-04
3.533 +2.2609E-04
3.159 +2.5379E-04
2.794 +2.7975E-04
2.404 +3.3121E-04
2.024 +4.0703E-04
1.763 +4.9052E-04
1.513 +6.2334E-04
1.259 +7.9004E-04
1.048 +9.9457E-04
0.939 +1.1326E-03
0.801 +1.2597E-03
0.703 +1.3074E-03
0.628 +1.2531E-03
0.533 +1.0172E-03
0.439 +6.2429E-04
0.342 +2.1441E-04
0.255 +4.8009E-05
0.164 +8.5845E-06
0.068 +1.3136E-06
0.009 +1.9350E-06
0.059 +6.4560E-07
0.107 +2.2526E-06
0.203 +1.2470E-05
0.298 +8.1977E-05
0.394 +3.7330E-04
0.483 +8.0730E-04

Mass 76 - C₆H₄.
Calibration factor 2.35
Source: 112083.ISO

Z(cm) Mole fraction
3.948 +7.3143E-06
3.787 +5.9927E-06
3.533 +7.2729E-06
3.159 +5.7154E-06

(C₆H₄ continued)

2.794	+3.9382E-06
2.404	+7.0896E-06
2.024	+5.7146E-06
1.763	+7.7720E-06
1.513	+7.2138E-06
1.259	+6.9968E-06
1.048	+1.1834E-05
0.939	+1.5020E-05
0.801	+1.8342E-05
0.703	+2.9837E-05
0.628	+3.0463E-05
0.533	+4.1316E-05
0.439	+5.1256E-05
0.342	+3.7149E-05
0.255	+1.7294E-05
0.164	+5.1764E-06
0.068	+3.4683E-07
0.009	+4.4563E-06
0.059	+1.0290E-06
0.107	+4.7886E-06
0.203	+9.1599E-06
0.298	+2.2027E-05
0.394	+4.3161E-05
0.483	+5.0516E-05

1.763	+1.2916E-06
1.513	+1.7216E-06
1.259	+2.4771E-06
1.048	+1.7630E-06
0.939	+1.9872E-06
0.801	+2.2677E-06
0.703	+4.1648E-06
0.628	+4.8622E-06
0.533	+8.5786E-06
0.439	+2.1324E-05
0.342	+3.5851E-05
0.255	+3.8470E-05
0.164	+2.9727E-05
0.068	+2.1867E-05
0.009	+1.4264E-05
0.059	+1.9981E-05
0.107	+2.3595E-05
0.203	+3.4665E-05
0.298	+4.0878E-05
0.394	+3.5215E-05
0.483	+1.6884E-05

Mass 98 - C₆H₂.
 Calibration factor 6.7
 Source: 010784.DAT

Mass 77 - C₆H₅.
 Calibration factor 2
 Source: 112083.ISO

<u>Z(cm)</u>	<u>Mole fraction</u>
3.948	+0.0000E+00
3.787	+0.0000E+00
0.801	+4.3285E-07
0.703	+2.4544E-07
0.628	+1.7027E-06
0.533	+7.6457E-08
0.439	-5.2110E-07
0.342	+4.0800E-07
0.255	+1.3855E-06
0.164	+1.5883E-06

Mass 78 - C₆H₆ (primarily
 benzene).
 Calibration factor 5.2
 Source: 112083.ISO

<u>Z(cm)</u>	<u>Mole fraction</u>
3.948	+7.6624E-06
3.787	+5.1467E-06
3.533	+4.0654E-06
3.159	+2.8494E-06
2.794	+1.8446E-06
2.404	+2.6875E-06
2.024	+2.1373E-06

<u>Z(cm)</u>	<u>Mole fraction</u>
3.849	+6.6665E-06
3.849	+5.2851E-06
3.750	+5.5189E-06
3.505	+5.6599E-06
3.173	+6.3072E-06
2.794	+9.2229E-06
2.480	+1.0504E-05
2.163	+1.1330E-05
1.854	+1.9771E-05
1.591	+2.4068E-05
1.338	+3.4337E-05
1.216	+3.9795E-05
1.137	+4.8178E-05
1.035	+4.6208E-05
0.941	+6.2905E-05
0.845	+6.7451E-05
0.750	+7.3628E-05
0.656	+7.3694E-05
0.570	+5.5631E-05
0.467	+2.1234E-05
0.378	+6.2422E-06
0.288	+4.2729E-07
0.181	+0.0000E+00
0.089	+0.0000E+00
0.150	+0.0000E+00
0.249	+0.0000E+00
0.341	+2.8485E-06
0.435	+1.4659E-05

(C₈H₂ continued)
 0.520 +4.6041E-05
 0.631 +7.1708E-05
 0.720 +6.8227E-05
 0.720 +7.2536E-05
 0.805 +6.5566E-05
 0.900 +5.6145E-05

3.750 +8.3620E-08
 3.505 +2.3940E-07
 3.173 +5.3999E-07
 2.794 +2.2470E-07
 2.480 +3.9493E-07
 2.163 +7.0417E-07
 1.854 +1.5315E-06
 1.591 +1.5844E-06
 1.338 +3.1850E-06
 1.216 +3.5759E-06
 1.137 +3.9780E-06
 1.035 +5.9493E-06
 0.941 +6.3814E-06
 0.845 +4.6618E-06
 0.750 +6.3729E-06
 0.656 +6.2970E-06
 0.570 +3.7236E-06
 0.467 +2.1132E-06
 0.378 +4.5263E-07
 0.288 +0.0000E+00
 0.181 +0.0000E+00
 0.089 +0.0000E+00
 0.150 +0.0000E+00
 0.249 +0.0000E+00
 0.341 +0.0000E+00
 0.435 +0.0000E+00
 0.520 +3.5306E-06
 0.631 +5.7446E-06
 0.720 +5.6393E-06
 0.720 +5.9958E-06
 0.805 +7.6501E-06
 0.900 +3.8937E-06

Mass 104 - C₈H₆.
 Calibration factor 6.6
 Source: 010784.DAT

Z(cm) Mole fraction

3.849 +3.0761E-07
 3.849 +2.8742E-07
 3.750 +3.3448E-07
 3.505 +5.5860E-07
 3.173 +2.3142E-07
 2.794 +3.7450E-07
 2.480 +7.8989E-08
 2.163 +3.9120E-07
 1.854 +1.6121E-07
 1.591 +0.0000E+00
 1.338 +5.3083E-07
 1.216 +1.9329E-07
 1.137 +0.0000E+00
 1.035 +1.1441E-07
 0.941 +5.2450E-07
 0.845 +0.0000E+00
 0.750 +3.2963E-07
 0.656 +5.6673E-07
 0.570 +1.0343E-06
 0.467 +1.6906E-06
 0.378 +3.6210E-06
 0.288 +3.0364E-06
 0.181 +1.0429E-06
 0.089 +2.0769E-07
 0.150 +2.0609E-07
 0.249 +1.4355E-06
 0.341 +3.2130E-06
 0.435 +2.8345E-06
 0.520 +1.6813E-06
 0.631 +1.2566E-06
 0.720 +7.0493E-07
 0.720 +7.4946E-07
 0.805 +8.3457E-07
 0.900 +0.0000E+00

Mass 122 - C₁₀H₂.
 Calibration factor 6.6
 Source: 010784.DAT

Z(cm) Mole fraction

3.849 +6.1519E-07
 3.849 +5.7484E-07

APPENDIX D.

Smoothed curves of mole fraction data

Curves were drawn through the data points of App. C using direct graphics input (Koalapad graphics tablet) or cursor input, observed on the graphics display screen of a computer monitor. These were smoothed using the algorithms of Savitsky and Golay (1964; and Steinier et al., 1972), and the whole process was repeated until the curve was represented satisfactorily, expanding the displayed scale as necessary.

APPENDIX D.

Smoothed curves of mole fraction data

Z	AR	H	H2	CH3	CH4	OH	H2O	C2H3	C2H4	CO
0.00	4.963E-02	8.532E-05	6.583E-02	9.561E-04	3.022E-03	9.140E-05	6.699E-02	3.114E-01	1.310E-03	1.609E-01
0.01	4.979E-02	9.659E-05	6.703E-02	1.025E-03	3.073E-03	1.046E-04	6.879E-02	3.094E-01	1.349E-03	1.649E-01
0.02	4.972E-02	1.082E-04	6.807E-02	1.093E-03	3.124E-03	1.180E-04	7.058E-02	3.072E-01	1.387E-03	1.688E-01
0.03	4.962E-02	1.222E-04	6.925E-02	1.179E-03	3.179E-03	1.321E-04	7.237E-02	3.047E-01	1.429E-03	1.730E-01
0.04	4.949E-02	1.374E-04	7.035E-02	1.271E-03	3.234E-03	1.416E-04	7.416E-02	3.021E-01	1.470E-03	1.773E-01
0.05	4.936E-02	1.533E-04	7.143E-02	1.371E-03	3.291E-03	1.585E-04	7.597E-02	2.992E-01	1.511E-03	1.817E-01
0.06	4.921E-02	1.722E-04	7.252E-02	1.485E-03	3.351E-03	1.719E-04	7.782E-02	2.960E-01	1.552E-03	1.865E-01
0.07	4.907E-02	1.938E-04	7.365E-02	1.610E-03	3.415E-03	1.843E-04	7.972E-02	2.927E-01	1.592E-03	1.914E-01
0.08	4.893E-02	2.160E-04	7.475E-02	1.746E-03	3.477E-03	1.973E-04	8.164E-02	2.892E-01	1.632E-03	1.965E-01
0.09	4.879E-02	2.407E-04	7.586E-02	1.888E-03	3.537E-03	2.100E-04	8.358E-02	2.855E-01	1.673E-03	2.016E-01
0.10	4.866E-02	2.674E-04	7.711E-02	2.039E-03	3.592E-03	2.230E-04	8.549E-02	2.815E-01	1.713E-03	2.068E-01
0.11	4.854E-02	2.946E-04	7.832E-02	2.203E-03	3.641E-03	2.368E-04	8.740E-02	2.775E-01	1.755E-03	2.119E-01
0.12	4.842E-02	3.240E-04	7.959E-02	2.370E-03	3.681E-03	2.503E-04	8.926E-02	2.732E-01	1.799E-03	2.170E-01
0.13	4.830E-02	3.574E-04	8.092E-02	2.548E-03	3.712E-03	2.652E-04	9.110E-02	2.688E-01	1.843E-03	2.220E-01
0.14	4.817E-02	3.943E-04	8.218E-02	2.738E-03	3.734E-03	2.806E-04	9.287E-02	2.643E-01	1.888E-03	2.270E-01
0.15	4.803E-02	4.350E-04	8.350E-02	2.933E-03	3.749E-03	2.967E-04	9.463E-02	2.598E-01	1.934E-03	2.318E-01
0.16	4.787E-02	4.810E-04	8.485E-02	3.137E-03	3.758E-03	3.136E-04	9.633E-02	2.552E-01	1.980E-03	2.368E-01
0.17	4.770E-02	5.310E-04	8.615E-02	3.347E-03	3.764E-03	3.300E-04	9.801E-02	2.506E-01	2.025E-03	2.421E-01
0.18	4.752E-02	5.834E-04	8.743E-02	3.557E-03	3.764E-03	3.475E-04	9.965E-02	2.462E-01	2.069E-03	2.475E-01
0.19	4.733E-02	6.400E-04	8.875E-02	3.761E-03	3.761E-03	3.649E-04	1.013E-01	2.417E-01	2.112E-03	2.529E-01
0.20	4.713E-02	6.983E-04	8.975E-02	3.952E-03	3.756E-03	3.829E-04	1.028E-01	2.373E-01	2.154E-03	2.587E-01
0.21	4.695E-02	7.581E-04	9.130E-02	4.126E-03	3.750E-03	4.025E-04	1.045E-01	2.330E-01	2.193E-03	2.645E-01
0.22	4.678E-02	8.191E-04	9.270E-02	4.272E-03	3.745E-03	4.227E-04	1.061E-01	2.288E-01	2.230E-03	2.702E-01
0.23	4.663E-02	8.805E-04	9.404E-02	4.395E-03	3.741E-03	4.462E-04	1.077E-01	2.247E-01	2.263E-03	2.759E-01
0.24	4.651E-02	9.404E-04	9.539E-02	4.496E-03	3.736E-03	4.708E-04	1.094E-01	2.207E-01	2.292E-03	2.816E-01
0.25	4.640E-02	9.966E-04	9.685E-02	4.563E-03	3.730E-03	4.960E-04	1.110E-01	2.167E-01	2.316E-03	2.870E-01
0.26	4.631E-02	1.048E-03	9.825E-02	4.625E-03	3.724E-03	5.231E-04	1.127E-01	2.128E-01	2.336E-03	2.927E-01
0.27	4.624E-02	1.094E-03	9.962E-02	4.670E-03	3.717E-03	5.510E-04	1.144E-01	2.089E-01	2.348E-03	2.984E-01
0.28	4.616E-02	1.133E-03	1.010E-01	4.703E-03	3.706E-03	5.803E-04	1.160E-01	2.051E-01	2.350E-03	3.043E-01
0.29	4.608E-02	1.166E-03	1.023E-01	4.733E-03	3.691E-03	6.112E-04	1.176E-01	2.011E-01	2.339E-03	3.103E-01
0.30	4.599E-02	1.193E-03	1.035E-01	4.755E-03	3.670E-03	6.447E-04	1.191E-01	1.972E-01	2.316E-03	3.166E-01
0.31	4.589E-02	1.214E-03	1.049E-01	4.772E-03	3.643E-03	6.816E-04	1.207E-01	1.932E-01	2.278E-03	3.228E-01
0.32	4.579E-02	1.232E-03	1.061E-01	4.785E-03	3.607E-03	7.220E-04	1.222E-01	1.891E-01	2.222E-03	3.292E-01
0.33	4.569E-02	1.246E-03	1.074E-01	4.797E-03	3.563E-03	7.663E-04	1.237E-01	1.850E-01	2.153E-03	3.356E-01
0.34	4.559E-02	1.256E-03	1.086E-01	4.805E-03	3.507E-03	8.107E-04	1.252E-01	1.808E-01	2.074E-03	3.421E-01
0.35	4.548E-02	1.264E-03	1.098E-01	4.811E-03	3.443E-03	8.536E-04	1.267E-01	1.764E-01	1.988E-03	3.486E-01
0.36	4.538E-02	1.271E-03	1.110E-01	4.816E-03	3.375E-03	8.938E-04	1.280E-01	1.720E-01	1.901E-03	3.551E-01
0.37	4.528E-02	1.276E-03	1.122E-01	4.818E-03	3.303E-03	9.281E-04	1.292E-01	1.676E-01	1.814E-03	3.616E-01
0.38	4.518E-02	1.280E-03	1.133E-01	4.816E-03	3.228E-03	9.550E-04	1.303E-01	1.633E-01	1.730E-03	3.679E-01
0.39	4.510E-02	1.284E-03	1.145E-01	4.812E-03	3.152E-03	9.741E-04	1.312E-01	1.591E-01	1.650E-03	3.738E-01
0.40	4.503E-02	1.287E-03	1.158E-01	4.805E-03	3.077E-03	9.856E-04	1.319E-01	1.551E-01	1.575E-03	3.793E-01
0.41	4.496E-02	1.289E-03	1.170E-01	4.792E-03	3.002E-03	9.901E-04	1.327E-01	1.515E-01	1.504E-03	3.843E-01
0.42	4.490E-02	1.290E-03	1.183E-01	4.776E-03	2.929E-03	9.891E-04	1.334E-01	1.480E-01	1.433E-03	3.890E-01
0.43	4.485E-02	1.289E-03	1.196E-01	4.755E-03	2.857E-03	9.833E-04	1.342E-01	1.448E-01	1.364E-03	3.933E-01
0.44	4.477E-02	1.286E-03	1.209E-01	4.728E-03	2.786E-03	9.736E-04	1.348E-01	1.417E-01	1.296E-03	3.976E-01
0.45	4.470E-02	1.281E-03	1.221E-01	4.698E-03	2.716E-03	9.614E-04	1.355E-01	1.387E-01	1.230E-03	4.015E-01
0.46	4.461E-02	1.274E-03	1.232E-01	4.662E-03	2.648E-03	9.469E-04	1.361E-01	1.357E-01	1.166E-03	4.053E-01
0.47	4.452E-02	1.265E-03	1.244E-01	4.622E-03	2.580E-03	9.306E-04	1.366E-01	1.328E-01	1.105E-03	4.090E-01
0.48	4.442E-02	1.256E-03	1.255E-01	4.578E-03	2.512E-03	9.108E-04	1.371E-01	1.300E-01	1.048E-03	4.126E-01
0.49	4.432E-02	1.246E-03	1.266E-01	4.531E-03	2.445E-03	8.935E-04	1.376E-01	1.273E-01	9.937E-04	4.159E-01
0.50	4.424E-02	1.236E-03	1.278E-01	4.481E-03	2.378E-03	8.736E-04	1.381E-01	1.247E-01	9.438E-04	4.190E-01
0.51	4.416E-02	1.225E-03	1.290E-01	4.426E-03	2.312E-03	8.529E-04	1.386E-01	1.222E-01	8.973E-04	4.219E-01

(Appendix D . Continued)

0.52	4.409E-02	1.213E-03	1.302E-01	4.367E-03	2.249E-03	8.321E-04	1.391E-01	1.198E-01	1.859E-04	8.534E-04	4.246E-01
0.53	4.401E-02	1.200E-03	1.314E-01	4.301E-03	2.191E-03	8.110E-04	1.395E-01	1.175E-01	1.838E-04	8.113E-04	4.273E-01
0.54	4.394E-02	1.186E-03	1.326E-01	4.230E-03	2.138E-03	7.899E-04	1.399E-01	1.153E-01	1.815E-04	7.703E-04	4.298E-01
0.55	4.388E-02	1.171E-03	1.337E-01	4.158E-03	2.084E-03	7.693E-04	1.403E-01	1.131E-01	1.791E-04	7.303E-04	4.321E-01
0.56	4.382E-02	1.156E-03	1.347E-01	4.085E-03	2.035E-03	7.492E-04	1.406E-01	1.111E-01	1.765E-04	6.912E-04	4.344E-01
0.57	4.375E-02	1.139E-03	1.357E-01	4.016E-03	1.988E-03	7.297E-04	1.409E-01	1.093E-01	1.737E-04	6.527E-04	4.365E-01
0.58	4.368E-02	1.121E-03	1.366E-01	3.948E-03	1.948E-03	7.107E-04	1.412E-01	1.075E-01	1.708E-04	6.150E-04	4.385E-01
0.59	4.360E-02	1.100E-03	1.375E-01	3.886E-03	1.910E-03	6.925E-04	1.414E-01	1.059E-01	1.677E-04	5.790E-04	4.404E-01
0.60	4.352E-02	1.079E-03	1.384E-01	3.828E-03	1.877E-03	6.752E-04	1.415E-01	1.044E-01	1.645E-04	5.455E-04	4.421E-01
0.61	4.344E-02	1.056E-03	1.393E-01	3.774E-03	1.847E-03	6.588E-04	1.415E-01	1.030E-01	1.612E-04	5.152E-04	4.438E-01
0.62	4.337E-02	1.032E-03	1.402E-01	3.722E-03	1.820E-03	6.434E-04	1.414E-01	1.017E-01	1.579E-04	4.876E-04	4.455E-01
0.63	4.329E-02	1.008E-03	1.410E-01	3.669E-03	1.798E-03	6.288E-04	1.412E-01	1.005E-01	1.545E-04	4.625E-04	4.473E-01
0.64	4.322E-02	9.835E-04	1.418E-01	3.616E-03	1.778E-03	6.152E-04	1.408E-01	9.926E-02	1.512E-04	4.396E-04	4.492E-01
0.65	4.315E-02	9.592E-04	1.425E-01	3.565E-03	1.753E-03	6.027E-04	1.404E-01	9.813E-02	1.479E-04	4.189E-04	4.511E-01
0.66	4.308E-02	9.357E-04	1.432E-01	3.511E-03	1.732E-03	5.914E-04	1.399E-01	9.704E-02	1.445E-04	3.999E-04	4.531E-01
0.67	4.301E-02	9.131E-04	1.439E-01	3.460E-03	1.707E-03	5.815E-04	1.393E-01	9.601E-02	1.413E-04	3.828E-04	4.550E-01
0.68	4.294E-02	8.902E-04	1.446E-01	3.408E-03	1.685E-03	5.724E-04	1.387E-01	9.502E-02	1.380E-04	3.675E-04	4.569E-01
0.69	4.287E-02	8.681E-04	1.452E-01	3.357E-03	1.662E-03	5.639E-04	1.382E-01	9.410E-02	1.348E-04	3.538E-04	4.587E-01
0.70	4.281E-02	8.466E-04	1.459E-01	3.308E-03	1.639E-03	5.560E-04	1.377E-01	9.324E-02	1.318E-04	3.417E-04	4.604E-01
0.71	4.275E-02	8.250E-04	1.466E-01	3.258E-03	1.618E-03	5.483E-04	1.371E-01	9.242E-02	1.289E-04	3.312E-04	4.620E-01
0.72	4.270E-02	8.045E-04	1.472E-01	3.212E-03	1.596E-03	5.409E-04	1.365E-01	9.166E-02	1.260E-04	3.213E-04	4.634E-01
0.73	4.264E-02	7.845E-04	1.479E-01	3.165E-03	1.577E-03	5.335E-04	1.361E-01	9.092E-02	1.233E-04	3.118E-04	4.650E-01
0.74	4.259E-02	7.655E-04	1.485E-01	3.119E-03	1.558E-03	5.262E-04	1.356E-01	9.019E-02	1.206E-04	3.026E-04	4.664E-01
0.75	4.254E-02	7.475E-04	1.492E-01	3.072E-03	1.540E-03	5.190E-04	1.350E-01	8.949E-02	1.180E-04	2.936E-04	4.678E-01
0.76	4.249E-02	7.304E-04	1.498E-01	3.026E-03	1.525E-03	5.118E-04	1.345E-01	8.880E-02	1.154E-04	2.850E-04	4.692E-01
0.77	4.244E-02	7.155E-04	1.505E-01	2.982E-03	1.508E-03	5.046E-04	1.340E-01	8.813E-02	1.130E-04	2.767E-04	4.705E-01
0.78	4.239E-02	7.008E-04	1.511E-01	2.936E-03	1.495E-03	4.974E-04	1.335E-01	8.746E-02	1.106E-04	2.689E-04	4.718E-01
0.79	4.235E-02	6.865E-04	1.516E-01	2.893E-03	1.482E-03	4.903E-04	1.330E-01	8.680E-02	1.084E-04	2.613E-04	4.730E-01
0.80	4.231E-02	6.735E-04	1.522E-01	2.850E-03	1.470E-03	4.834E-04	1.326E-01	8.614E-02	1.064E-04	2.539E-04	4.742E-01
0.81	4.227E-02	6.616E-04	1.527E-01	2.807E-03	1.459E-03	4.767E-04	1.321E-01	8.550E-02	1.043E-04	2.468E-04	4.754E-01
0.82	4.224E-02	6.518E-04	1.532E-01	2.767E-03	1.446E-03	4.702E-04	1.317E-01	8.487E-02	1.023E-04	2.400E-04	4.765E-01
0.83	4.222E-02	6.431E-04	1.537E-01	2.728E-03	1.436E-03	4.641E-04	1.312E-01	8.426E-02	1.004E-04	2.335E-04	4.776E-01
0.84	4.219E-02	6.358E-04	1.542E-01	2.692E-03	1.424E-03	4.584E-04	1.308E-01	8.366E-02	9.854E-05	2.274E-04	4.787E-01
0.85	4.217E-02	6.300E-04	1.547E-01	2.658E-03	1.413E-03	4.530E-04	1.304E-01	8.308E-02	9.675E-05	2.217E-04	4.797E-01
0.86	4.215E-02	6.255E-04	1.551E-01	2.624E-03	1.402E-03	4.477E-04	1.300E-01	8.252E-02	9.508E-05	2.165E-04	4.808E-01
0.87	4.213E-02	6.220E-04	1.555E-01	2.591E-03	1.390E-03	4.426E-04	1.297E-01	8.200E-02	9.341E-05	2.118E-04	4.817E-01
0.88	4.212E-02	6.180E-04	1.559E-01	2.554E-03	1.380E-03	4.376E-04	1.293E-01	8.148E-02	9.178E-05	2.074E-04	4.827E-01
0.89	4.210E-02	6.137E-04	1.563E-01	2.517E-03	1.369E-03	4.327E-04	1.290E-01	8.098E-02	9.022E-05	2.033E-04	4.837E-01
0.90	4.208E-02	6.099E-04	1.567E-01	2.478E-03	1.359E-03	4.280E-04	1.286E-01	8.051E-02	8.861E-05	1.995E-04	4.848E-01
0.91	4.206E-02	6.063E-04	1.570E-01	2.438E-03	1.351E-03	4.234E-04	1.283E-01	8.005E-02	8.698E-05	1.959E-04	4.858E-01
0.92	4.204E-02	6.032E-04	1.573E-01	2.398E-03	1.341E-03	4.189E-04	1.280E-01	7.962E-02	8.538E-05	1.925E-04	4.867E-01
0.93	4.202E-02	6.002E-04	1.576E-01	2.357E-03	1.334E-03	4.144E-04	1.276E-01	7.921E-02	8.381E-05	1.893E-04	4.877E-01
0.94	4.200E-02	5.972E-04	1.579E-01	2.318E-03	1.327E-03	4.101E-04	1.273E-01	7.881E-02	8.227E-05	1.862E-04	4.887E-01
0.95	4.197E-02	5.945E-04	1.582E-01	2.280E-03	1.319E-03	4.059E-04	1.270E-01	7.844E-02	8.081E-05	1.832E-04	4.897E-01
0.96	4.195E-02	5.919E-04	1.585E-01	2.241E-03	1.313E-03	4.018E-04	1.266E-01	7.809E-02	7.942E-05	1.804E-04	4.906E-01
0.97	4.194E-02	5.894E-04	1.588E-01	2.203E-03	1.305E-03	3.979E-04	1.263E-01	7.774E-02	7.794E-05	1.776E-04	4.914E-01
0.98	4.192E-02	5.869E-04	1.592E-01	2.166E-03	1.299E-03	3.940E-04	1.260E-01	7.739E-02	7.673E-05	1.749E-04	4.923E-01
0.99	4.191E-02	5.846E-04	1.595E-01	2.131E-03	1.293E-03	3.903E-04	1.257E-01	7.704E-02	7.555E-05	1.724E-04	4.930E-01
1.00	4.189E-02	5.822E-04	1.598E-01	2.099E-03	1.286E-03	3.868E-04	1.254E-01	7.671E-02	7.439E-05	1.700E-04	4.938E-01
1.01	4.189E-02	5.800E-04	1.601E-01	2.069E-03	1.280E-03	3.836E-04	1.251E-01	7.637E-02	7.326E-05	1.677E-04	4.945E-01
1.02	4.188E-02	5.778E-04	1.605E-01	2.041E-03	1.273E-03	3.805E-04	1.248E-01	7.606E-02	7.215E-05	1.655E-04	4.951E-01
1.03	4.187E-02	5.757E-04	1.608E-01	2.014E-03	1.267E-03	3.773E-04	1.245E-01	7.576E-02	7.105E-05	1.635E-04	4.958E-01

(Appendix D. Continued)

1.04	4.186E+02	5.737E-04	1.611E-01	1.989E-03	1.261E-03	3.742E-04	1.243E-01	7.547E-02	7.004E-05	1.616E-04	4.964E-01
1.05	4.195E-02	5.718E-04	1.614E-01	1.965E-03	1.255E-03	3.710E-04	1.240E-01	7.521E-02	6.907E-05	1.598E-04	4.971E-01
1.06	4.194E-02	5.699E-04	1.616E-01	1.941E-03	1.249E-03	3.678E-04	1.237E-01	7.495E-02	6.815E-05	1.582E-04	4.977E-01
1.07	4.193E-02	5.682E-04	1.619E-01	1.919E-03	1.242E-03	3.647E-04	1.234E-01	7.472E-02	6.724E-05	1.566E-04	4.983E-01
1.08	4.192E-02	5.666E-04	1.622E-01	1.897E-03	1.237E-03	3.617E-04	1.231E-01	7.448E-02	6.641E-05	1.550E-04	4.989E-01
1.09	4.191E-02	5.650E-04	1.624E-01	1.876E-03	1.231E-03	3.588E-04	1.229E-01	7.426E-02	6.569E-05	1.534E-04	4.994E-01
1.10	4.190E-02	5.634E-04	1.627E-01	1.856E-03	1.225E-03	3.561E-04	1.226E-01	7.403E-02	6.498E-05	1.519E-04	4.999E-01
1.11	4.179E-02	5.619E-04	1.629E-01	1.835E-03	1.220E-03	3.535E-04	1.224E-01	7.380E-02	6.423E-05	1.502E-04	5.005E-01
1.12	4.178E-02	5.604E-04	1.632E-01	1.816E-03	1.214E-03	3.508E-04	1.221E-01	7.357E-02	6.351E-05	1.486E-04	5.010E-01
1.13	4.176E-02	5.590E-04	1.634E-01	1.796E-03	1.208E-03	3.481E-04	1.218E-01	7.333E-02	6.283E-05	1.470E-04	5.015E-01
1.14	4.175E-02	5.576E-04	1.637E-01	1.776E-03	1.203E-03	3.454E-04	1.216E-01	7.309E-02	6.223E-05	1.454E-04	5.020E-01
1.15	4.173E-02	5.561E-04	1.639E-01	1.757E-03	1.197E-03	3.425E-04	1.213E-01	7.285E-02	6.164E-05	1.438E-04	5.026E-01
1.16	4.171E-02	5.547E-04	1.642E-01	1.739E-03	1.191E-03	3.396E-04	1.210E-01	7.261E-02	6.102E-05	1.423E-04	5.031E-01
1.17	4.166E-02	5.534E-04	1.645E-01	1.722E-03	1.185E-03	3.368E-04	1.207E-01	7.237E-02	6.040E-05	1.407E-04	5.036E-01
1.18	4.165E-02	5.521E-04	1.648E-01	1.705E-03	1.179E-03	3.340E-04	1.204E-01	7.213E-02	5.978E-05	1.391E-04	5.041E-01
1.19	4.164E-02	5.508E-04	1.651E-01	1.688E-03	1.173E-03	3.312E-04	1.201E-01	7.189E-02	5.916E-05	1.375E-04	5.046E-01
1.20	4.163E-02	5.495E-04	1.654E-01	1.671E-03	1.167E-03	3.284E-04	1.198E-01	7.165E-02	5.854E-05	1.359E-04	5.051E-01
1.21	4.162E-02	5.482E-04	1.657E-01	1.654E-03	1.161E-03	3.256E-04	1.195E-01	7.141E-02	5.792E-05	1.343E-04	5.056E-01
1.22	4.161E-02	5.469E-04	1.660E-01	1.637E-03	1.155E-03	3.228E-04	1.192E-01	7.117E-02	5.730E-05	1.327E-04	5.061E-01
1.23	4.160E-02	5.456E-04	1.663E-01	1.620E-03	1.149E-03	3.200E-04	1.189E-01	7.093E-02	5.668E-05	1.311E-04	5.066E-01
1.24	4.159E-02	5.443E-04	1.666E-01	1.603E-03	1.143E-03	3.172E-04	1.186E-01	7.069E-02	5.606E-05	1.295E-04	5.071E-01
1.25	4.158E-02	5.430E-04	1.669E-01	1.586E-03	1.137E-03	3.144E-04	1.183E-01	7.045E-02	5.544E-05	1.279E-04	5.076E-01
1.26	4.157E-02	5.417E-04	1.672E-01	1.569E-03	1.131E-03	3.116E-04	1.180E-01	7.021E-02	5.482E-05	1.263E-04	5.081E-01
1.27	4.156E-02	5.404E-04	1.675E-01	1.552E-03	1.125E-03	3.088E-04	1.177E-01	6.997E-02	5.420E-05	1.247E-04	5.086E-01
1.28	4.155E-02	5.391E-04	1.678E-01	1.535E-03	1.119E-03	3.060E-04	1.174E-01	6.973E-02	5.358E-05	1.231E-04	5.091E-01
1.29	4.154E-02	5.378E-04	1.681E-01	1.518E-03	1.113E-03	3.032E-04	1.171E-01	6.949E-02	5.296E-05	1.215E-04	5.096E-01
1.30	4.153E-02	5.365E-04	1.684E-01	1.501E-03	1.107E-03	3.004E-04	1.168E-01	6.925E-02	5.234E-05	1.199E-04	5.101E-01
1.31	4.152E-02	5.352E-04	1.687E-01	1.484E-03	1.101E-03	2.976E-04	1.165E-01	6.901E-02	5.172E-05	1.183E-04	5.106E-01
1.32	4.151E-02	5.339E-04	1.690E-01	1.467E-03	1.095E-03	2.948E-04	1.162E-01	6.877E-02	5.110E-05	1.167E-04	5.111E-01
1.33	4.150E-02	5.326E-04	1.693E-01	1.450E-03	1.089E-03	2.920E-04	1.159E-01	6.853E-02	5.048E-05	1.151E-04	5.116E-01
1.34	4.149E-02	5.313E-04	1.696E-01	1.433E-03	1.083E-03	2.892E-04	1.156E-01	6.829E-02	4.986E-05	1.135E-04	5.121E-01
1.35	4.148E-02	5.300E-04	1.699E-01	1.416E-03	1.077E-03	2.864E-04	1.153E-01	6.805E-02	4.924E-05	1.119E-04	5.126E-01
1.36	4.147E-02	5.287E-04	1.702E-01	1.399E-03	1.071E-03	2.836E-04	1.150E-01	6.781E-02	4.862E-05	1.103E-04	5.131E-01
1.37	4.146E-02	5.274E-04	1.705E-01	1.382E-03	1.065E-03	2.808E-04	1.147E-01	6.757E-02	4.800E-05	1.087E-04	5.136E-01
1.38	4.145E-02	5.261E-04	1.708E-01	1.365E-03	1.059E-03	2.780E-04	1.144E-01	6.733E-02	4.738E-05	1.071E-04	5.141E-01
1.39	4.144E-02	5.248E-04	1.711E-01	1.348E-03	1.053E-03	2.752E-04	1.141E-01	6.709E-02	4.676E-05	1.055E-04	5.146E-01
1.40	4.143E-02	5.235E-04	1.714E-01	1.331E-03	1.047E-03	2.724E-04	1.138E-01	6.685E-02	4.614E-05	1.039E-04	5.151E-01
1.41	4.142E-02	5.222E-04	1.717E-01	1.314E-03	1.041E-03	2.696E-04	1.135E-01	6.661E-02	4.552E-05	1.023E-04	5.156E-01
1.42	4.141E-02	5.209E-04	1.720E-01	1.297E-03	1.035E-03	2.668E-04	1.132E-01	6.637E-02	4.490E-05	1.007E-04	5.161E-01
1.43	4.140E-02	5.196E-04	1.723E-01	1.280E-03	1.029E-03	2.640E-04	1.129E-01	6.613E-02	4.428E-05	9.91E-05	5.166E-01
1.44	4.139E-02	5.183E-04	1.726E-01	1.263E-03	1.023E-03	2.612E-04	1.126E-01	6.589E-02	4.366E-05	9.75E-05	5.171E-01
1.45	4.138E-02	5.170E-04	1.729E-01	1.246E-03	1.017E-03	2.584E-04	1.123E-01	6.565E-02	4.304E-05	9.59E-05	5.176E-01
1.46	4.137E-02	5.157E-04	1.732E-01	1.229E-03	1.011E-03	2.556E-04	1.120E-01	6.541E-02	4.242E-05	9.43E-05	5.181E-01
1.47	4.136E-02	5.144E-04	1.735E-01	1.212E-03	1.005E-03	2.528E-04	1.117E-01	6.517E-02	4.180E-05	9.27E-05	5.186E-01
1.48	4.135E-02	5.131E-04	1.738E-01	1.195E-03	1.000E-03	2.500E-04	1.114E-01	6.493E-02	4.118E-05	9.11E-05	5.191E-01
1.49	4.134E-02	5.118E-04	1.741E-01	1.178E-03	9.94E-04	2.472E-04	1.111E-01	6.469E-02	4.056E-05	8.95E-05	5.196E-01
1.50	4.133E-02	5.105E-04	1.744E-01	1.161E-03	9.88E-04	2.444E-04	1.108E-01	6.445E-02	3.994E-05	8.79E-05	5.201E-01
1.51	4.132E-02	5.092E-04	1.747E-01	1.144E-03	9.82E-04	2.416E-04	1.105E-01	6.421E-02	3.932E-05	8.63E-05	5.206E-01
1.52	4.131E-02	5.079E-04	1.750E-01	1.127E-03	9.76E-04	2.388E-04	1.102E-01	6.397E-02	3.870E-05	8.47E-05	5.211E-01
1.53	4.130E-02	5.066E-04	1.753E-01	1.110E-03	9.70E-04	2.360E-04	1.099E-01	6.373E-02	3.808E-05	8.31E-05	5.216E-01
1.54	4.129E-02	5.053E-04	1.756E-01	1.093E-03	9.64E-04	2.332E-04	1.096E-01	6.349E-02	3.746E-05	8.15E-05	5.221E-01
1.55	4.128E-02	5.040E-04	1.759E-01	1.076E-03	9.58E-04	2.304E-04	1.093E-01	6.325E-02	3.684E-05	8.00E-05	5.226E-01
1.56	4.127E-02	5.027E-04	1.762E-01	1.059E-03	9.52E-04	2.276E-04	1.090E-01	6.301E-02	3.622E-05	7.84E-05	5.231E-01
1.57	4.126E-02	5.014E-04	1.765E-01	1.042E-03	9.46E-04	2.248E-04	1.087E-01	6.277E-02	3.560E-05	7.68E-05	5.236E-01
1.58	4.125E-02	5.001E-04	1.768E-01	1.025E-03	9.40E-04	2.220E-04	1.084E-01	6.253E-02	3.498E-05	7.52E-05	5.241E-01
1.59	4.124E-02	4.988E-04	1.771E-01	1.008E-03	9.34E-04	2.192E-04	1.081E-01	6.229E-02	3.436E-05	7.36E-05	5.246E-01
1.60	4.123E-02	4.975E-04	1.774E-01	9.91E-04	9.28E-04	2.164E-04	1.078E-01	6.205E-02	3.374E-05	7.20E-05	5.251E-01
1.61	4.122E-02	4.962E-04	1.777E-01	9.74E-04	9.22E-04	2.136E-04	1.075E-01	6.181E-02	3.312E-05	7.04E-05	5.256E-01
1.62	4.121E-02	4.949E-04	1.780E-01	9.57E-04	9.16E-04	2.108E-04	1.072E-01	6.157E-02	3.250E-05	6.88E-05	5.261E-01
1.63	4.120E-02	4.936E-04	1.783E-01	9.40E-04	9.10E-04	2.080E-04	1.069E-01	6.133E-02	3.188E-05	6.72E-05	5.266E-01
1.64	4.119E-02	4.923E-04	1.786E-01	9.23E-04	9.04E-04	2.052E-04	1.066E-01	6.109E-02	3.126E-05	6.56E-05	5.271E-01
1.65	4.118E-02	4.910E-04	1.789E-01	9.06E-04	8.98E-04	2.024E-04	1.063E-01	6.085E-02	3.064E-05	6.40E-05	5.276E-01
1.66	4.117E-02	4.897E-04	1.792E-01	8.89E-04	8.92E-04	1.996E-04	1.060E-01	6.061E-02	3.002E-05	6.24E-05	5.281E-01
1.67	4.116E-02	4.884E-04	1.795E-01	8.72E-04	8.86E-04	1.968E-04	1.057E-01	6.037E-02	2.940E-05	6.08E-05	5.286E-01
1.68	4.115E-02	4.871E-04	1.798E-01	8.55E-04	8.80E-04	1.940E-04	1.054E-01	6.013E-02	2.878E-05	5.92E-05	5.291E-01
1.69	4.114E-02	4.858E-04	1.801E-01	8.38E-04	8.74E-04	1.912E-04	1.051E-01	5.989E-02	2.816E-05	5.76E-05	5.296E-01
1.70	4.113E-02	4.845E-04	1.804E-01	8.21E-04	8.68E-04	1.884E-04	1.048E-01	5.965E-02	2.754E-05	5.60E-05	5.301E-01
1.71	4.112E-02	4.832E-04	1.807E-01	8.04E-04	8.62E-04	1.856E-04	1.045E-01	5.941E-02	2.692E-05	5.44E-05	5.306E-01
1.72	4.111E-02	4.819E-04	1.810E-01	7.87E-04	8.56E-04	1.828E-04	1.042E-01	5.917E-02	2.630E-05	5.28E-05	5.311E-01
1.73	4.110E-02	4.806E-04	1.813E-01	7.70E-04	8.50E-04	1.800E-04	1.039E-01	5.893E-02	2.568E-05	5.12E-05	5.316E-01
1.74	4.109E-02	4.793E-04	1.816E-01	7.53E-04	8.44E-04	1.772E-04	1.036E-01	5.869E-02	2.506E-05	4.96E-05	5.321E-01
1.75	4.108E-02	4.780E-04	1.819E-01	7.36E-04	8.38E-04	1.744E-04	1.033E-01	5.845E-02	2.444E-05	4.80E-05	5.326E-01
1.76	4.107E-02	4.767E-04	1.822E-01	7.19E-04	8.32E-04	1.716E-04	1.030E-01	5.821E-02	2.382E-05	4.64E-05	5.331E-01
1.77	4.106E-02	4.754E-04	1.825E-01	7.02E-04	8.26E-04	1.688E-04	1.027E-01	5.797E-02	2.320E-05	4.48E-05	5.336E-01
1.78	4.105E-02	4.741E									

(Appendix D. Continued)

3.10	4.070E-02	4.747E-04	1.839E-01	8.720E-04	1.505E-03	4.338E-05	9.712E-02	5.971E-02	2.739E-05	3.943E-05	5.379E-01
3.15	4.068E-02	4.738E-04	1.839E-01	8.625E-04	1.521E-03	4.010E-05	9.702E-02	5.963E-02	2.769E-05	3.851E-05	5.381E-01
3.20	4.066E-02	4.730E-04	1.840E-01	8.535E-04	1.537E-03	3.695E-05	9.692E-02	5.956E-02	2.810E-05	3.765E-05	5.382E-01
3.25	4.064E-02	4.722E-04	1.840E-01	8.449E-04	1.553E-03	3.392E-05	9.683E-02	5.950E-02	2.858E-05	3.679E-05	5.384E-01
3.30	4.063E-02	4.715E-04	1.841E-01	8.367E-04	1.569E-03	3.109E-05	9.674E-02	5.945E-02	2.914E-05	3.591E-05	5.386E-01
3.35	4.061E-02	4.708E-04	1.841E-01	8.289E-04	1.585E-03	2.858E-05	9.666E-02	5.941E-02	2.974E-05	3.505E-05	5.387E-01
3.40	4.059E-02	4.701E-04	1.841E-01	8.213E-04	1.601E-03	2.631E-05	9.658E-02	5.939E-02	3.038E-05	3.421E-05	5.388E-01
3.45	4.057E-02	4.695E-04	1.841E-01	8.138E-04	1.617E-03	2.416E-05	9.649E-02	5.940E-02	3.107E-05	3.337E-05	5.390E-01
3.50	4.055E-02	4.688E-04	1.841E-01	8.065E-04	1.635E-03	2.225E-05	9.640E-02	5.942E-02	3.187E-05	3.257E-05	5.391E-01
3.55	4.053E-02	4.681E-04	1.841E-01	7.994E-04	1.652E-03	2.050E-05	9.632E-02	5.946E-02	3.271E-05	3.181E-05	5.392E-01
3.60	4.051E-02	4.675E-04	1.841E-01	7.924E-04	1.669E-03	1.893E-05	9.624E-02	5.951E-02	3.360E-05	3.109E-05	5.393E-01
3.65	4.049E-02	4.668E-04	1.841E-01	7.856E-04	1.686E-03	1.754E-05	9.624E-02	5.951E-02	3.452E-05	3.041E-05	5.394E-01
3.70	4.047E-02	4.661E-04	1.840E-01	7.792E-04	1.702E-03	1.629E-05	9.615E-02	5.957E-02	3.543E-05	2.974E-05	5.395E-01
3.75	4.045E-02	4.655E-04	1.840E-01	7.730E-04	1.718E-03	1.512E-05	9.599E-02	5.978E-02	3.636E-05	2.907E-05	5.396E-01
3.80	4.043E-02	4.648E-04	1.839E-01	7.672E-04	1.735E-03	1.407E-05	9.590E-02	5.993E-02	3.730E-05	2.840E-05	5.396E-01
3.85	4.040E-02	4.641E-04	1.838E-01	7.616E-04	1.754E-03	1.306E-05	9.581E-02	6.011E-02	3.826E-05	2.774E-05	5.396E-01
3.90	4.037E-02	4.634E-04	1.838E-01	7.559E-04	1.775E-03	1.203E-05	9.571E-02	6.028E-02	3.921E-05	2.708E-05	5.397E-01
Z	HCO	H2CO	HO2	O2	C3H2	C3H3	C3H4	HCCO	CH2CO	CO2	C4H2
0.00	1.523E-05	9.627E-04	2.980E-01	2.820E-04	5.862E-09	3.136E-05	5.808E-04	4.983E-08	6.967E-04	3.852E-02	2.927E-04
0.01	1.657E-05	9.596E-04	2.919E-01	2.992E-04	1.399E-08	3.224E-05	5.961E-04	1.162E-07	6.999E-04	3.940E-02	3.311E-04
0.02	1.793E-05	9.556E-04	2.864E-01	3.135E-04	2.345E-08	3.312E-05	6.114E-04	1.977E-07	7.025E-04	4.028E-02	3.689E-04
0.03	1.930E-05	9.497E-04	2.805E-01	3.187E-04	4.387E-08	3.426E-05	6.286E-04	4.929E-07	7.045E-04	4.126E-02	4.062E-04
0.04	2.059E-05	9.426E-04	2.750E-01	3.195E-04	7.462E-08	3.553E-05	6.477E-04	1.029E-06	7.061E-04	4.214E-02	4.435E-04
0.05	2.195E-05	9.349E-04	2.695E-01	3.181E-04	1.712E-07	3.558E-05	6.686E-04	1.747E-06	7.074E-04	4.304E-02	4.804E-04
0.06	2.333E-05	9.254E-04	2.638E-01	3.144E-04	3.609E-07	3.694E-05	6.915E-04	2.593E-06	7.086E-04	4.399E-02	5.182E-04
0.07	2.480E-05	9.146E-04	2.581E-01	3.101E-04	6.575E-07	3.979E-05	7.160E-04	3.576E-06	7.098E-04	4.489E-02	5.571E-04
0.08	2.622E-05	9.014E-04	2.523E-01	3.056E-04	1.139E-06	4.586E-05	7.415E-04	4.590E-06	7.108E-04	4.584E-02	5.994E-04
0.09	2.769E-05	8.852E-04	2.468E-01	3.008E-04	1.778E-06	5.502E-05	7.688E-04	5.652E-06	7.120E-04	4.677E-02	6.484E-04
0.10	2.926E-05	8.656E-04	2.410E-01	2.954E-04	2.579E-06	6.726E-05	7.969E-04	6.721E-06	7.131E-04	4.783E-02	7.074E-04
0.11	3.079E-05	8.422E-04	2.354E-01	2.890E-04	3.582E-06	8.313E-05	8.253E-04	7.791E-06	7.143E-04	4.895E-02	7.776E-04
0.12	3.235E-05	8.153E-04	2.300E-01	2.812E-04	4.742E-06	1.013E-04	8.541E-04	8.868E-06	7.155E-04	5.014E-02	8.584E-04
0.13	3.402E-05	7.859E-04	2.246E-01	2.720E-04	6.030E-06	1.223E-04	8.825E-04	9.993E-06	7.166E-04	5.148E-02	9.522E-04
0.14	3.562E-05	7.545E-04	2.193E-01	2.613E-04	7.478E-06	1.446E-04	9.083E-04	1.108E-05	7.171E-04	5.290E-02	1.064E-03
0.15	3.721E-05	7.218E-04	2.140E-01	2.495E-04	9.063E-06	1.671E-04	9.315E-04	1.218E-05	7.168E-04	5.453E-02	1.194E-03
0.16	3.887E-05	6.880E-04	2.085E-01	2.372E-04	1.082E-05	1.926E-04	9.512E-04	1.336E-05	7.157E-04	5.622E-02	1.336E-03
0.17	4.047E-05	6.539E-04	2.028E-01	2.250E-04	1.285E-05	2.195E-04	9.670E-04	1.450E-05	7.135E-04	5.787E-02	1.493E-03
0.18	4.212E-05	6.193E-04	1.970E-01	2.132E-04	1.506E-05	2.503E-04	9.785E-04	1.565E-05	7.103E-04	5.956E-02	1.667E-03
0.19	4.389E-05	5.848E-04	1.911E-01	2.021E-04	1.742E-05	2.828E-04	9.857E-04	1.685E-05	7.059E-04	6.119E-02	1.855E-03
0.20	4.560E-05	5.509E-04	1.849E-01	1.915E-04	2.003E-05	3.157E-04	9.870E-04	1.801E-05	7.002E-04	6.275E-02	2.054E-03
0.21	4.725E-05	5.172E-04	1.787E-01	1.815E-04	2.277E-05	3.518E-04	9.885E-04	1.924E-05	6.934E-04	6.424E-02	2.260E-03
0.22	4.899E-05	4.846E-04	1.725E-01	1.718E-04	2.578E-05	3.881E-04	9.819E-04	2.060E-05	6.855E-04	6.566E-02	2.473E-03
0.23	5.039E-05	4.540E-04	1.663E-01	1.624E-04	2.922E-05	4.276E-04	9.726E-04	2.197E-05	6.765E-04	6.695E-02	2.693E-03
0.24	5.174E-05	4.256E-04	1.601E-01	1.532E-04	3.308E-05	4.687E-04	9.601E-04	2.346E-05	6.660E-04	6.815E-02	2.925E-03
0.25	5.306E-05	3.991E-04	1.541E-01	1.443E-04	3.750E-05	5.085E-04	9.438E-04	2.510E-05	6.542E-04	6.932E-02	3.167E-03
0.26	5.429E-05	3.746E-04	1.479E-01	1.361E-04	4.260E-05	5.517E-04	9.226E-04	2.682E-05	6.417E-04	7.035E-02	3.416E-03
0.27	5.541E-05	3.517E-04	1.417E-01	1.284E-04	4.853E-05	5.948E-04	8.979E-04	2.852E-05	6.284E-04	7.126E-02	3.675E-03
0.28	5.651E-05	3.303E-04	1.357E-01	1.213E-04	5.514E-05	6.436E-04	8.682E-04	3.028E-05	6.146E-04	7.211E-02	3.942E-03
0.29	5.750E-05	3.106E-04	1.296E-01	1.148E-04	6.237E-05	6.975E-04	8.325E-04	3.195E-05	6.004E-04	7.285E-02	4.216E-03
0.30	5.822E-05	2.925E-04	1.236E-01	1.085E-04	7.057E-05	7.577E-04	7.907E-04	3.346E-05	5.858E-04	7.349E-02	4.494E-03
0.31	5.902E-05	2.754E-04	1.177E-01	1.024E-04	7.975E-05	8.231E-04	7.438E-04	3.485E-05	5.709E-04	7.409E-02	4.770E-03
0.32	5.956E-05	2.593E-04	1.119E-01	9.642E-05	8.977E-05	8.864E-04	6.947E-04	3.597E-05	5.559E-04	7.464E-02	5.042E-03

(Appendix D, Continued)

0.33	5.995E-05	2.445E-04	1.061E-01	9.051E-05	9.998E-05	9.444E-04	6.465E-04	3.672E-05	5.410E-04	7.517E-02	5.306E-03
0.34	6.027E-05	2.308E-04	1.006E-01	8.461E-05	1.107E-04	9.904E-04	6.021E-04	3.717E-05	5.262E-04	7.566E-02	5.564E-03
0.35	6.057E-05	2.179E-04	9.521E-02	7.898E-05	1.216E-04	1.036E-03	5.628E-04	3.728E-05	5.118E-04	7.615E-02	5.817E-03
0.36	6.082E-05	2.056E-04	9.002E-02	7.335E-05	1.325E-04	1.036E-03	5.291E-04	3.711E-05	4.983E-04	7.662E-02	6.065E-03
0.37	6.099E-05	1.937E-04	8.515E-02	6.805E-05	1.430E-04	1.037E-03	5.021E-04	3.671E-05	4.853E-04	7.710E-02	6.307E-03
0.38	6.108E-05	1.824E-04	8.032E-02	6.301E-05	1.526E-04	1.031E-03	4.803E-04	3.619E-05	4.738E-04	7.758E-02	6.543E-03
0.39	6.107E-05	1.716E-04	7.618E-02	5.826E-05	1.611E-04	1.020E-03	4.607E-04	3.563E-05	4.618E-04	7.806E-02	6.772E-03
0.40	6.097E-05	1.617E-04	7.208E-02	5.369E-05	1.686E-04	1.011E-03	4.423E-04	3.510E-05	4.505E-04	7.859E-02	6.995E-03
0.41	6.076E-05	1.525E-04	6.816E-02	4.933E-05	1.749E-04	1.002E-03	4.243E-04	3.460E-05	4.392E-04	7.911E-02	7.209E-03
0.42	6.046E-05	1.442E-04	6.438E-02	4.508E-05	1.798E-04	9.926E-04	4.064E-04	3.414E-05	4.279E-04	7.962E-02	7.409E-03
0.43	6.007E-05	1.367E-04	6.080E-02	4.094E-05	1.831E-04	9.826E-04	3.888E-04	3.369E-05	4.167E-04	8.012E-02	7.600E-03
0.44	5.958E-05	1.298E-04	5.742E-02	3.688E-05	1.858E-04	9.712E-04	3.714E-04	3.324E-05	4.055E-04	8.054E-02	7.786E-03
0.45	5.907E-05	1.233E-04	5.435E-02	3.286E-05	1.878E-04	9.599E-04	3.545E-04	3.280E-05	3.945E-04	8.094E-02	7.966E-03
0.46	5.850E-05	1.173E-04	5.151E-02	2.888E-05	1.894E-04	9.479E-04	3.382E-04	3.235E-05	3.836E-04	8.127E-02	8.141E-03
0.47	5.787E-05	1.115E-04	4.866E-02	2.502E-05	1.906E-04	9.356E-04	3.230E-04	3.190E-05	3.730E-04	8.156E-02	8.314E-03
0.48	5.718E-05	1.061E-04	4.641E-02	2.129E-05	1.917E-04	9.219E-04	3.090E-04	3.143E-05	3.627E-04	8.182E-02	8.482E-03
0.49	5.646E-05	1.007E-04	4.406E-02	1.775E-05	1.926E-04	9.075E-04	2.961E-04	3.097E-05	3.529E-04	8.208E-02	8.639E-03
0.50	5.574E-05	9.566E-05	4.178E-02	1.432E-05	1.935E-04	8.937E-04	2.845E-04	3.051E-05	3.434E-04	8.236E-02	8.791E-03
0.51	5.499E-05	9.082E-05	3.957E-02	1.104E-05	1.942E-04	8.789E-04	2.742E-04	3.005E-05	3.340E-04	8.262E-02	8.929E-03
0.52	5.425E-05	8.630E-05	3.743E-02	8.011E-06	1.948E-04	8.642E-04	2.652E-04	2.960E-05	3.251E-04	8.290E-02	9.054E-03
0.53	5.350E-05	8.199E-05	3.535E-02	5.365E-06	1.953E-04	8.482E-04	2.569E-04	2.915E-05	3.164E-04	8.317E-02	9.168E-03
0.54	5.274E-05	7.791E-05	3.340E-02	3.244E-06	1.958E-04	8.322E-04	2.492E-04	2.871E-05	3.079E-04	8.345E-02	9.273E-03
0.55	5.197E-05	7.412E-05	3.162E-02	1.606E-06	1.958E-04	8.175E-04	2.416E-04	2.828E-05	2.996E-04	8.373E-02	9.366E-03
0.56	5.117E-05	7.062E-05	2.992E-02	5.317E-07	1.957E-04	8.019E-04	2.341E-04	2.786E-05	2.914E-04	8.400E-02	9.448E-03
0.57	5.035E-05	6.744E-05	2.832E-02	-4.149E-08	1.948E-04	7.861E-04	2.268E-04	2.744E-05	2.832E-04	8.428E-02	9.523E-03
0.58	4.950E-05	6.452E-05	2.682E-02	-2.217E-07	1.948E-04	7.705E-04	2.194E-04	2.701E-05	2.751E-04	8.454E-02	9.587E-03
0.59	4.863E-05	6.185E-05	2.541E-02	-1.587E-07	1.941E-04	7.502E-04	2.122E-04	2.659E-05	2.672E-04	8.478E-02	9.637E-03
0.60	4.774E-05	5.943E-05	2.411E-02	-7.517E-08	1.932E-04	7.326E-04	2.051E-04	2.618E-05	2.596E-04	8.503E-02	9.678E-03
0.61	4.683E-05	5.717E-05	2.286E-02	-1.921E-08	1.922E-04	7.141E-04	1.982E-04	2.577E-05	2.522E-04	8.526E-02	9.707E-03
0.62	4.591E-05	5.501E-05	2.174E-02	-4.683E-09	1.910E-04	6.965E-04	1.916E-04	2.537E-05	2.452E-04	8.550E-02	9.731E-03
0.63	4.499E-05	5.285E-05	2.064E-02	-2.671E-09	1.896E-04	6.783E-04	1.853E-04	2.497E-05	2.385E-04	8.571E-02	9.749E-03
0.64	4.404E-05	5.074E-05	1.958E-02	0.000E+00	1.879E-04	6.604E-04	1.792E-04	2.459E-05	2.320E-04	8.590E-02	9.760E-03
0.65	4.308E-05	4.874E-05	1.856E-02	0.000E+00	1.858E-04	6.438E-04	1.731E-04	2.421E-05	2.260E-04	8.606E-02	9.764E-03
0.66	4.209E-05	4.684E-05	1.760E-02	0.000E+00	1.833E-04	6.265E-04	1.671E-04	2.385E-05	2.201E-04	8.617E-02	9.760E-03
0.67	4.109E-05	4.506E-05	1.672E-02	0.000E+00	1.804E-04	6.101E-04	1.614E-04	2.350E-05	2.146E-04	8.625E-02	9.746E-03
0.68	4.008E-05	4.338E-05	1.592E-02	0.000E+00	1.772E-04	5.933E-04	1.558E-04	2.315E-05	2.093E-04	8.627E-02	9.722E-03
0.69	3.901E-05	4.181E-05	1.519E-02	0.000E+00	1.737E-04	5.771E-04	1.506E-04	2.282E-05	2.042E-04	8.627E-02	9.690E-03
0.70	3.791E-05	4.032E-05	1.452E-02	0.000E+00	1.698E-04	5.623E-04	1.456E-04	2.249E-05	1.994E-04	8.625E-02	9.654E-03
0.71	3.679E-05	3.888E-05	1.391E-02	0.000E+00	1.656E-04	5.477E-04	1.410E-04	2.217E-05	1.946E-04	8.621E-02	9.610E-03
0.72	3.567E-05	3.746E-05	1.332E-02	0.000E+00	1.615E-04	5.346E-04	1.365E-04	2.184E-05	1.901E-04	8.618E-02	9.566E-03
0.73	3.455E-05	3.603E-05	1.272E-02	0.000E+00	1.573E-04	5.210E-04	1.321E-04	2.151E-05	1.858E-04	8.613E-02	9.522E-03
0.74	3.345E-05	3.462E-05	1.215E-02	0.000E+00	1.533E-04	5.075E-04	1.277E-04	2.118E-05	1.817E-04	8.608E-02	9.476E-03
0.75	3.238E-05	3.322E-05	1.160E-02	0.000E+00	1.492E-04	4.949E-04	1.236E-04	2.086E-05	1.779E-04	8.604E-02	9.429E-03
0.76	3.135E-05	3.183E-05	1.111E-02	0.000E+00	1.451E-04	4.821E-04	1.196E-04	2.054E-05	1.741E-04	8.597E-02	9.381E-03
0.77	3.035E-05	3.050E-05	1.066E-02	0.000E+00	1.414E-04	4.704E-04	1.160E-04	2.023E-05	1.705E-04	8.591E-02	9.333E-03
0.78	2.941E-05	2.925E-05	1.024E-02	0.000E+00	1.374E-04	4.585E-04	1.127E-04	1.993E-05	1.671E-04	8.583E-02	9.282E-03
0.79	2.841E-05	2.808E-05	9.852E-03	0.000E+00	1.342E-04	4.473E-04	1.098E-04	1.963E-05	1.637E-04	8.577E-02	9.235E-03
0.80	2.746E-05	2.699E-05	9.488E-03	0.000E+00	1.304E-04	4.371E-04	1.071E-04	1.935E-05	1.605E-04	8.571E-02	9.188E-03
0.81	2.651E-05	2.597E-05	9.132E-03	0.000E+00	1.268E-04	4.269E-04	1.047E-04	1.907E-05	1.573E-04	8.566E-02	9.138E-03
0.82	2.557E-05	2.501E-05	8.788E-03	0.000E+00	1.234E-04	4.175E-04	1.023E-04	1.879E-05	1.542E-04	8.562E-02	9.090E-03
0.83	2.465E-05	2.410E-05	8.441E-03	0.000E+00	1.201E-04	4.074E-04	1.001E-04	1.851E-05	1.512E-04	8.557E-02	9.043E-03
0.84	2.375E-05	2.322E-05	8.105E-03	0.000E+00	1.171E-04	3.978E-04	9.801E-05	1.824E-05	1.483E-04	8.553E-02	8.994E-03

(Appendix D. Continued)

0.85	2.286E-05	2.239E-05	7.774E-03	0.000E+00	1.141E-04	3.899E-04	9.596E-05	1.797E-05	1.454E-04	8.549E-02	8.947E-03
0.86	2.201E-05	2.160E-05	7.448E-03	0.000E+00	1.114E-04	3.807E-04	9.398E-05	1.771E-05	1.425E-04	8.545E-02	8.900E-03
0.87	2.118E-05	2.085E-05	7.137E-03	0.000E+00	1.090E-04	3.703E-04	9.211E-05	1.745E-05	1.397E-04	8.541E-02	8.851E-03
0.88	2.039E-05	2.015E-05	6.815E-03	0.000E+00	1.067E-04	3.591E-04	9.033E-05	1.719E-05	1.370E-04	8.535E-02	8.803E-03
0.89	1.962E-05	1.943E-05	6.494E-03	0.000E+00	1.046E-04	3.477E-04	8.864E-05	1.693E-05	1.344E-04	8.530E-02	8.755E-03
0.90	1.888E-05	1.874E-05	6.175E-03	0.000E+00	1.024E-04	3.366E-04	8.704E-05	1.667E-05	1.318E-04	8.524E-02	8.704E-03
0.91	1.813E-05	1.805E-05	5.855E-03	0.000E+00	1.003E-04	3.261E-04	8.548E-05	1.642E-05	1.292E-04	8.517E-02	8.654E-03
0.92	1.741E-05	1.737E-05	5.535E-03	0.000E+00	9.836E-05	3.162E-04	8.399E-05	1.617E-05	1.267E-04	8.511E-02	8.604E-03
0.93	1.673E-05	1.671E-05	5.244E-03	0.000E+00	9.637E-05	3.074E-04	8.258E-05	1.591E-05	1.242E-04	8.503E-02	8.549E-03
0.94	1.609E-05	1.608E-05	4.948E-03	0.000E+00	9.450E-05	3.002E-04	8.124E-05	1.566E-05	1.217E-04	8.495E-02	8.492E-03
0.95	1.550E-05	1.548E-05	4.659E-03	0.000E+00	9.257E-05	2.954E-04	7.998E-05	1.540E-05	1.193E-04	8.487E-02	8.437E-03
0.96	1.496E-05	1.492E-05	4.375E-03	0.000E+00	9.071E-05	2.896E-04	7.877E-05	1.515E-05	1.170E-04	8.479E-02	8.376E-03
0.97	1.448E-05	1.440E-05	4.117E-03	0.000E+00	8.897E-05	2.841E-04	7.759E-05	1.490E-05	1.147E-04	8.471E-02	8.312E-03
0.98	1.405E-05	1.391E-05	3.860E-03	0.000E+00	8.721E-05	2.791E-04	7.647E-05	1.465E-05	1.125E-04	8.463E-02	8.251E-03
0.99	1.366E-05	1.342E-05	3.626E-03	0.000E+00	8.556E-05	2.740E-04	7.543E-05	1.441E-05	1.104E-04	8.455E-02	8.187E-03
1.00	1.330E-05	1.296E-05	3.416E-03	0.000E+00	8.384E-05	2.694E-04	7.443E-05	1.417E-05	1.084E-04	8.447E-02	8.122E-03
1.01	1.297E-05	1.273E-05	3.223E-03	0.000E+00	8.214E-05	2.648E-04	7.350E-05	1.394E-05	1.064E-04	8.440E-02	8.062E-03
1.02	1.267E-05	1.243E-05	3.058E-03	0.000E+00	8.058E-05	2.604E-04	7.266E-05	1.372E-05	1.045E-04	8.432E-02	7.999E-03
1.03	1.239E-05	1.214E-05	2.897E-03	0.000E+00	7.891E-05	2.560E-04	7.189E-05	1.350E-05	1.027E-04	8.424E-02	7.936E-03
1.04	1.213E-05	1.188E-05	2.753E-03	0.000E+00	7.733E-05	2.518E-04	7.119E-05	1.328E-05	1.010E-04	8.415E-02	7.876E-03
1.05	1.189E-05	1.162E-05	2.619E-03	0.000E+00	7.570E-05	2.479E-04	7.054E-05	1.307E-05	9.936E-05	8.406E-02	7.815E-03
1.06	1.166E-05	1.137E-05	2.494E-03	0.000E+00	7.414E-05	2.439E-04	6.994E-05	1.286E-05	9.772E-05	8.397E-02	7.751E-03
1.07	1.144E-05	1.114E-05	2.386E-03	0.000E+00	7.271E-05	2.403E-04	6.938E-05	1.266E-05	9.613E-05	8.388E-02	7.690E-03
1.08	1.124E-05	9.978E-06	2.281E-03	0.000E+00	7.131E-05	2.365E-04	6.887E-05	1.246E-05	9.460E-05	8.378E-02	7.631E-03
1.09	1.105E-05	9.638E-06	2.185E-03	0.000E+00	7.004E-05	2.328E-04	6.842E-05	1.226E-05	9.311E-05	8.369E-02	7.572E-03
1.10	1.087E-05	9.301E-06	2.095E-03	0.000E+00	6.878E-05	2.291E-04	6.799E-05	1.207E-05	9.165E-05	8.359E-02	7.516E-03
1.11	1.069E-05	8.973E-06	2.004E-03	0.000E+00	6.760E-05	2.253E-04	6.760E-05	1.187E-05	9.022E-05	8.349E-02	7.462E-03
1.12	1.053E-05	8.654E-06	1.924E-03	0.000E+00	6.661E-05	2.215E-04	6.724E-05	1.168E-05	8.883E-05	8.340E-02	7.407E-03
1.13	1.038E-05	8.350E-06	1.846E-03	0.000E+00	6.565E-05	2.178E-04	6.689E-05	1.150E-05	8.750E-05	8.330E-02	7.356E-03
1.14	1.024E-05	8.065E-06	1.777E-03	0.000E+00	6.478E-05	2.144E-04	6.656E-05	1.131E-05	8.622E-05	8.320E-02	7.306E-03
1.15	1.010E-05	7.800E-06	1.714E-03	0.000E+00	6.396E-05	2.112E-04	6.623E-05	1.112E-05	8.497E-05	8.310E-02	7.254E-03
1.16	9.967E-06	7.552E-06	1.658E-03	0.000E+00	6.325E-05	2.081E-04	6.590E-05	1.093E-05	8.373E-05	8.300E-02	7.204E-03
1.20	9.464E-06	6.727E-06	1.461E-03	0.000E+00	6.000E+00	1.989E-04	6.470E-05	1.072E-05	8.263E-02	8.263E-02	6.996E-03
1.25	8.612E-06	5.093E-06	1.264E-03	0.000E+00	5.837E-05	1.891E-04	6.342E-05	9.402E-06	7.350E-05	8.218E-02	6.754E-03
1.35	8.311E-06	4.429E-06	9.632E-04	0.000E+00	5.654E-05	1.814E-04	6.218E-05	8.646E-06	6.909E-05	8.18E-02	6.519E-03
1.40	8.044E-06	3.856E-06	8.470E-04	0.000E+00	5.500E-05	1.741E-04	6.100E-05	7.940E-06	6.542E-05	8.136E-02	6.287E-03
1.45	7.795E-06	3.374E-06	7.492E-04	0.000E+00	5.252E-05	1.668E-04	5.989E-05	7.254E-06	6.242E-05	8.097E-02	6.070E-03
1.50	7.544E-06	2.968E-06	6.624E-04	0.000E+00	5.144E-05	1.592E-04	5.889E-05	6.590E-06	5.972E-05	8.058E-02	5.861E-03
1.55	7.310E-06	2.638E-06	5.876E-04	0.000E+00	5.031E-05	1.518E-04	5.795E-05	5.972E-06	5.733E-05	8.017E-02	5.661E-03
1.60	7.100E-06	2.360E-06	5.270E-04	0.000E+00	4.920E-05	1.450E-04	5.708E-05	5.397E-06	5.525E-05	7.975E-02	5.480E-03
1.65	6.907E-06	2.126E-06	4.814E-04	0.000E+00	4.812E-05	1.391E-04	5.626E-05	4.861E-06	5.334E-05	7.933E-02	5.315E-03
1.70	6.729E-06	1.921E-06	4.461E-04	0.000E+00	4.707E-05	1.341E-04	5.548E-05	4.351E-06	5.160E-05	7.893E-02	5.165E-03
1.75	6.562E-06	1.739E-06	4.188E-04	0.000E+00	4.603E-05	1.300E-04	5.476E-05	3.847E-06	5.004E-05	7.855E-02	5.031E-03
1.80	6.394E-06	1.565E-06	3.944E-04	0.000E+00	4.503E-05	1.264E-04	5.411E-05	3.365E-06	4.862E-05	7.820E-02	4.904E-03
1.85	6.229E-06	1.400E-06	3.717E-04	0.000E+00	4.403E-05	1.230E-04	5.349E-05	2.925E-06	4.731E-05	7.787E-02	4.789E-03
1.90	6.066E-06	1.250E-06	3.488E-04	0.000E+00	4.307E-05	1.198E-04	5.290E-05	2.535E-06	4.609E-05	7.757E-02	4.684E-03
1.95	5.906E-06	1.120E-06	3.274E-04	0.000E+00	4.211E-05	1.167E-04	5.234E-05	2.197E-06	4.497E-05	7.728E-02	4.586E-03
2.00	5.749E-06	1.009E-06	3.073E-04	0.000E+00	4.117E-05	1.135E-04	5.180E-05	1.912E-06	4.396E-05	7.701E-02	4.496E-03
2.05	5.598E-06	9.167E-07	2.896E-04	0.000E+00	4.024E-05	1.115E-04	5.131E-05	1.664E-06	4.304E-05	7.675E-02	4.411E-03
2.10	5.449E-06	8.395E-07	2.713E-04	0.000E+00	3.934E-05	1.097E-04	5.048E-05	1.445E-06	4.218E-05	7.651E-02	4.326E-03
2.15	5.302E-06	7.699E-07	2.547E-04	0.000E+00	3.844E-05	1.069E-04	5.016E-05	1.253E-06	4.137E-05	7.627E-02	4.246E-03
											4.170E-03

(Appendix D, Continued)

2.30	5.162E-06	7.061E-07	2.389E-04	0.000E+00	3.757E-05	1.055E-04	4.990E-05	8.958E-07	3.987E-05	7.584E-02	4.095E-03
2.25	5.030E-06	6.485E-07	2.237E-04	0.000E+00	3.669E-05	1.043E-04	4.972E-05	7.325E-07	3.920E-05	7.566E-02	4.024E-03
2.30	4.903E-06	5.984E-07	2.090E-04	0.000E+00	3.583E-05	1.031E-04	4.962E-05	5.813E-07	3.858E-05	7.548E-02	3.955E-03
2.35	4.786E-06	5.511E-07	1.949E-04	0.000E+00	3.497E-05	1.020E-04	4.959E-05	4.409E-07	3.804E-05	7.532E-02	3.885E-03
2.40	4.676E-06	5.172E-07	1.814E-04	0.000E+00	3.410E-05	1.008E-04	4.965E-05	3.190E-07	3.755E-05	7.515E-02	3.820E-03
2.45	4.569E-06	4.828E-07	1.688E-04	0.000E+00	3.324E-05	9.965E-05	4.977E-05	2.145E-07	3.711E-05	7.499E-02	3.759E-03
2.50	4.464E-06	4.506E-07	1.565E-04	0.000E+00	3.237E-05	9.861E-05	4.991E-05	1.243E-07	3.669E-05	7.484E-02	3.704E-03
2.55	4.361E-06	4.211E-07	1.443E-04	0.000E+00	3.152E-05	9.766E-05	5.007E-05	5.933E-08	3.629E-05	7.470E-02	3.656E-03
2.60	4.257E-06	3.932E-07	1.318E-04	0.000E+00	3.067E-05	9.687E-05	5.026E-05	1.847E-08	3.592E-05	7.458E-02	3.612E-03
2.65	4.152E-06	3.667E-07	1.187E-04	0.000E+00	2.982E-05	9.612E-05	5.047E-05	1.096E-09	3.557E-05	7.447E-02	3.569E-03
2.70	4.049E-06	3.414E-07	1.058E-04	0.000E+00	2.897E-05	9.534E-05	5.072E-05	4.067E-09	3.524E-05	7.438E-02	3.528E-03
2.75	3.947E-06	3.173E-07	9.263E-05	0.000E+00	2.816E-05	9.469E-05	5.101E-05	-5.200E-10	3.492E-05	7.429E-02	3.488E-03
2.80	3.848E-06	2.954E-07	7.967E-05	0.000E+00	2.735E-05	9.398E-05	5.132E-05	-1.522E-10	3.462E-05	7.422E-02	3.451E-03
2.85	3.756E-06	2.766E-07	6.761E-05	0.000E+00	2.659E-05	9.335E-05	5.164E-05	0.000E+00	3.434E-05	7.415E-02	3.416E-03
2.90	3.669E-06	2.606E-07	5.540E-05	0.000E+00	2.581E-05	9.290E-05	5.197E-05	0.000E+00	3.409E-05	7.410E-02	3.384E-03
2.95	3.582E-06	2.465E-07	4.443E-05	0.000E+00	2.504E-05	9.240E-05	5.231E-05	0.000E+00	3.387E-05	7.406E-02	3.356E-03
3.00	3.497E-06	2.338E-07	3.481E-05	0.000E+00	2.426E-05	9.199E-05	5.265E-05	0.000E+00	3.366E-05	7.402E-02	3.329E-03
3.05	3.415E-06	2.220E-07	2.646E-05	0.000E+00	2.348E-05	9.167E-05	5.301E-05	0.000E+00	3.346E-05	7.399E-02	3.307E-03
3.10	3.337E-06	2.109E-07	2.004E-05	0.000E+00	2.270E-05	9.116E-05	5.338E-05	0.000E+00	3.328E-05	7.397E-02	3.283E-03
3.15	3.263E-06	2.005E-07	1.541E-05	0.000E+00	2.193E-05	9.074E-05	5.373E-05	0.000E+00	3.312E-05	7.395E-02	3.261E-03
3.20	3.192E-06	1.909E-07	1.157E-05	0.000E+00	2.117E-05	9.054E-05	5.409E-05	0.000E+00	3.298E-05	7.393E-02	3.238E-03
3.25	3.123E-06	1.815E-07	8.941E-06	0.000E+00	2.042E-05	9.018E-05	5.445E-05	0.000E+00	3.285E-05	7.392E-02	3.216E-03
3.30	3.057E-06	1.744E-07	6.785E-06	0.000E+00	1.968E-05	8.987E-05	5.480E-05	0.000E+00	3.273E-05	7.390E-02	3.194E-03
3.35	2.992E-06	1.643E-07	4.971E-06	0.000E+00	1.816E-05	8.922E-05	5.515E-05	0.000E+00	3.261E-05	7.389E-02	3.173E-03
3.40	2.927E-06	1.569E-07	3.645E-06	0.000E+00	1.892E-05	8.956E-05	5.550E-05	0.000E+00	3.251E-05	7.387E-02	3.151E-03
3.45	2.865E-06	1.499E-07	2.686E-06	0.000E+00	1.741E-05	8.901E-05	5.584E-05	0.000E+00	3.240E-05	7.386E-02	3.128E-03
3.50	2.804E-06	1.435E-07	1.955E-06	0.000E+00	1.666E-05	8.910E-05	5.616E-05	0.000E+00	3.230E-05	7.384E-02	3.106E-03
3.55	2.746E-06	1.374E-07	1.444E-06	0.000E+00	1.592E-05	8.900E-05	5.647E-05	0.000E+00	3.221E-05	7.382E-02	3.083E-03
3.60	2.691E-06	1.316E-07	1.069E-06	0.000E+00	1.521E-05	8.870E-05	5.721E-05	0.000E+00	3.211E-05	7.381E-02	3.061E-03
3.65	2.638E-06	1.262E-07	7.819E-07	0.000E+00	1.445E-05	8.833E-05	5.699E-05	0.000E+00	3.195E-05	7.377E-02	3.043E-03
3.70	2.587E-06	1.211E-07	5.807E-07	0.000E+00	1.373E-05	8.799E-05	5.742E-05	0.000E+00	3.187E-05	7.376E-02	3.024E-03
3.75	2.541E-06	1.161E-07	4.288E-07	0.000E+00	1.301E-05	8.776E-05	5.742E-05	0.000E+00	3.195E-05	7.377E-02	3.024E-03
3.80	2.496E-06	1.114E-07	3.211E-07	0.000E+00	1.229E-05	8.779E-05	5.759E-05	0.000E+00	3.179E-05	7.376E-02	3.001E-03
3.85	2.448E-06	1.070E-07	2.422E-07	0.000E+00	1.159E-05	8.773E-05	5.771E-05	0.000E+00	3.172E-05	7.375E-02	2.984E-03
3.90	2.398E-06	1.027E-07	1.664E-07	0.000E+00	1.088E-05	8.767E-05	5.779E-05	0.000E+00	3.164E-05	7.371E-02	2.963E-03
Z	C4H3	C4H4	C4H5	C4H6	C5H2	C5H3	C5H4	C5H5	C5H6	C6H2	C6H4
0.00	1.454E-07	3.353E-05	1.411E-06	2.168E-05	7.700E-08	1.151E-08	2.020E-08	4.779E-06	1.277E-05	3.161E-07	5.024E-07
0.01	2.617E-07	3.658E-05	1.716E-06	2.309E-05	8.851E-08	1.696E-08	3.556E-08	5.094E-06	1.389E-05	3.773E-07	6.026E-07
0.02	3.936E-07	3.959E-05	1.986E-06	2.454E-05	1.005E-07	2.375E-08	5.329E-08	5.368E-06	1.504E-05	4.420E-07	7.077E-07
0.03	6.013E-07	4.272E-05	2.308E-06	2.611E-05	1.146E-07	3.177E-08	8.173E-08	5.656E-06	1.625E-05	5.133E-07	8.387E-07
0.04	8.763E-07	4.618E-05	2.625E-06	2.769E-05	1.305E-07	3.938E-08	8.410E-08	5.934E-06	1.751E-05	6.036E-07	9.933E-07
0.05	1.277E-06	4.991E-05	2.947E-06	2.925E-05	1.491E-07	5.018E-08	1.108E-07	6.222E-06	1.892E-05	7.173E-07	1.175E-06
0.06	1.760E-06	5.376E-05	3.287E-06	3.088E-05	1.705E-07	6.679E-08	3.986E-07	6.517E-06	2.047E-05	8.504E-07	1.389E-06
0.07	2.300E-06	5.780E-05	3.672E-06	3.259E-05	1.956E-07	8.907E-08	8.925E-07	6.839E-06	2.215E-05	1.008E-06	1.645E-06
0.08	2.972E-06	6.201E-05	4.086E-06	3.441E-05	2.242E-07	1.170E-07	1.563E-06	7.159E-06	2.396E-05	1.201E-06	1.944E-06
0.09	3.661E-06	6.641E-05	4.602E-06	3.633E-05	2.552E-07	1.518E-07	2.592E-06	7.497E-06	2.588E-05	1.436E-06	2.288E-06
0.10	4.384E-06	7.096E-05	5.234E-06	3.837E-05	2.882E-07	1.910E-07	4.048E-06	7.861E-06	2.788E-05	1.723E-06	2.669E-06
0.11	5.123E-06	7.573E-05	5.930E-06	4.051E-05	3.225E-07	2.387E-07	5.923E-06	8.221E-06	2.993E-05	2.074E-06	3.058E-06
0.12	5.863E-06	8.071E-05	6.666E-06	4.278E-05	3.588E-07	2.987E-07	8.185E-06	8.595E-06	3.198E-05	2.502E-06	3.569E-06
0.13	6.609E-06	8.602E-05	7.405E-06	4.467E-05	3.984E-07	3.775E-07	1.082E-05	8.994E-06	3.401E-05	3.015E-06	4.120E-06
0.14	7.354E-06	9.165E-05	8.070E-06	4.667E-05	4.426E-07	4.803E-07	1.375E-05	9.374E-06	3.601E-05	3.673E-06	4.717E-06

(Appendix D. Continued)

0.15	8.108E-06	9.773E-05	8.617E-06	4.822E-05	4.920E-07	6.074E-07	1.693E-05	9.760E-06	3.796E-05	4.503E-06	5.379E-06
0.16	8.872E-06	1.043E-04	9.046E-06	4.931E-05	5.479E-07	7.424E-07	2.033E-05	1.017E-05	3.983E-05	5.487E-06	6.083E-06
0.17	9.636E-06	1.113E-04	9.336E-06	4.989E-05	6.145E-07	8.988E-07	2.376E-05	1.057E-05	4.159E-05	6.641E-06	6.872E-06
0.18	1.038E-05	1.186E-04	9.504E-06	4.990E-05	6.941E-07	1.029E-07	2.709E-05	1.100E-05	4.314E-05	7.985E-06	7.762E-06
0.19	1.110E-05	1.261E-04	9.636E-06	4.934E-05	7.864E-07	1.218E-06	3.039E-05	1.147E-05	4.445E-05	9.584E-06	8.700E-06
0.20	1.180E-05	1.336E-04	9.722E-06	4.830E-05	9.020E-07	1.664E-06	3.358E-05	1.194E-05	4.545E-05	1.150E-05	9.679E-06
0.21	1.249E-05	1.410E-04	9.768E-06	4.689E-05	1.038E-06	2.504E-06	3.664E-05	1.243E-05	4.613E-05	1.382E-05	1.072E-05
0.22	1.315E-05	1.481E-04	9.802E-06	4.519E-05	1.205E-06	3.811E-06	3.957E-05	1.296E-05	4.648E-05	1.671E-05	1.184E-05
0.23	1.381E-05	1.547E-04	9.813E-06	4.331E-05	1.379E-06	5.606E-06	4.239E-05	1.347E-05	4.653E-05	2.020E-05	1.302E-05
0.24	1.446E-05	1.609E-04	9.796E-06	4.132E-05	1.582E-06	7.845E-06	4.507E-05	1.398E-05	4.622E-05	2.458E-05	1.426E-05
0.25	1.512E-05	1.664E-04	9.764E-06	3.928E-05	1.819E-06	1.046E-05	4.767E-05	1.448E-05	4.577E-05	2.998E-05	1.563E-05
0.26	1.578E-05	1.714E-04	9.716E-06	3.725E-05	2.083E-06	1.328E-05	5.022E-05	1.495E-05	4.461E-05	3.649E-05	1.720E-05
0.27	1.642E-05	1.755E-04	9.639E-06	3.527E-05	2.439E-06	1.616E-05	5.268E-05	1.540E-05	4.333E-05	4.413E-05	1.898E-05
0.28	1.703E-05	1.789E-04	9.538E-06	3.334E-05	2.883E-06	1.896E-05	5.499E-05	1.583E-05	4.172E-05	5.319E-05	2.100E-05
0.29	1.760E-05	1.815E-04	9.422E-06	3.150E-05	3.382E-06	2.168E-05	5.710E-05	1.621E-05	3.983E-05	6.423E-05	2.328E-05
0.30	1.813E-05	1.832E-04	9.286E-06	2.974E-05	3.973E-06	2.437E-05	5.895E-05	1.656E-05	3.766E-05	7.786E-05	2.574E-05
0.31	1.862E-05	1.841E-04	9.132E-06	2.803E-05	4.654E-06	2.699E-05	6.050E-05	1.690E-05	3.531E-05	9.469E-05	2.830E-05
0.32	1.907E-05	1.841E-04	8.970E-06	2.637E-05	5.377E-06	2.954E-05	6.176E-05	1.719E-05	3.294E-05	1.146E-04	3.085E-05
0.33	1.949E-05	1.833E-04	8.795E-06	2.467E-05	6.158E-06	3.202E-05	6.276E-05	1.745E-05	3.062E-05	1.397E-04	3.336E-05
0.34	1.987E-05	1.817E-04	8.602E-06	2.300E-05	6.990E-06	3.442E-05	6.344E-05	1.769E-05	2.834E-05	1.701E-04	3.574E-05
0.35	2.020E-05	1.793E-04	8.409E-06	2.135E-05	7.814E-06	3.676E-05	6.386E-05	1.788E-05	2.615E-05	2.035E-04	3.799E-05
0.36	2.050E-05	1.763E-04	8.213E-06	1.975E-05	8.648E-06	3.904E-05	6.406E-05	1.804E-05	2.413E-05	2.446E-04	4.011E-05
0.37	2.074E-05	1.727E-04	8.009E-06	1.822E-05	9.499E-06	4.126E-05	6.402E-05	1.816E-05	2.266E-05	2.863E-04	4.204E-05
0.38	2.094E-05	1.688E-04	7.814E-06	1.677E-05	1.029E-05	4.347E-05	6.376E-05	1.824E-05	2.056E-05	3.306E-04	4.386E-05
0.39	2.111E-05	1.645E-04	7.623E-06	1.540E-05	1.101E-05	4.566E-05	6.324E-05	1.824E-05	1.903E-05	3.771E-04	4.565E-05
0.40	2.125E-05	1.602E-04	7.433E-06	1.410E-05	1.169E-05	4.782E-05	6.249E-05	1.819E-05	1.765E-05	4.250E-04	4.735E-05
0.41	2.136E-05	1.558E-04	7.257E-06	1.285E-05	1.228E-05	4.986E-05	6.148E-05	1.809E-05	1.642E-05	4.732E-04	4.894E-05
0.42	2.143E-05	1.510E-04	7.089E-06	1.165E-05	1.280E-05	5.173E-05	6.022E-05	1.791E-05	1.536E-05	5.216E-04	5.036E-05
0.43	2.147E-05	1.456E-04	6.915E-06	1.049E-05	1.331E-05	5.337E-05	5.869E-05	1.767E-05	1.443E-05	5.709E-04	5.151E-05
0.44	2.145E-05	1.398E-04	6.747E-06	9.345E-06	1.375E-05	5.465E-05	5.685E-05	1.737E-05	1.362E-05	6.205E-04	5.236E-05
0.45	2.138E-05	1.334E-04	6.581E-06	8.266E-06	1.415E-05	5.548E-05	5.477E-05	1.701E-05	1.288E-05	6.695E-04	5.278E-05
0.46	2.126E-05	1.265E-04	6.407E-06	7.275E-06	1.456E-05	5.584E-05	5.253E-05	1.659E-05	1.220E-05	7.168E-04	5.271E-05
0.47	2.110E-05	1.196E-04	6.241E-06	6.390E-06	1.494E-05	5.572E-05	5.021E-05	1.614E-05	1.157E-05	7.622E-04	5.213E-05
0.48	2.090E-05	1.125E-04	6.075E-06	5.634E-06	1.528E-05	5.519E-05	4.785E-05	1.563E-05	1.096E-05	8.064E-04	5.107E-05
0.49	2.069E-05	1.056E-04	5.904E-06	4.995E-06	1.562E-05	5.433E-05	4.551E-05	1.508E-05	1.039E-05	8.494E-04	4.966E-05
0.50	2.048E-05	9.955E-05	5.746E-06	4.468E-06	1.591E-05	5.328E-05	4.330E-05	1.454E-05	9.859E-06	8.915E-04	4.803E-05
0.51	2.028E-05	9.406E-05	5.587E-06	4.042E-06	1.618E-05	5.209E-05	4.119E-05	1.398E-05	9.356E-06	9.325E-04	4.627E-05
0.52	2.007E-05	8.876E-05	5.423E-06	3.699E-06	1.644E-05	5.090E-05	3.922E-05	1.339E-05	8.906E-06	9.738E-04	4.450E-05
0.53	1.987E-05	8.402E-05	5.267E-06	3.417E-06	1.666E-05	4.967E-05	3.736E-05	1.281E-05	8.502E-06	1.015E-03	4.276E-05
0.54	1.964E-05	7.971E-05	5.113E-06	3.170E-06	1.686E-05	4.844E-05	3.564E-05	1.223E-05	8.148E-06	1.056E-03	4.118E-05
0.55	1.942E-05	7.544E-05	4.953E-06	2.969E-06	1.705E-05	4.724E-05	3.406E-05	1.164E-05	7.822E-06	1.094E-03	3.975E-05
0.56	1.918E-05	7.152E-05	4.798E-06	2.803E-06	1.723E-05	4.609E-05	3.260E-05	1.108E-05	7.526E-06	1.129E-03	3.845E-05
0.57	1.893E-05	6.783E-05	4.648E-06	2.666E-06	1.737E-05	4.495E-05	3.123E-05	1.054E-05	7.267E-06	1.160E-03	3.728E-05
0.58	1.866E-05	6.418E-05	4.489E-06	2.554E-06	1.750E-05	4.381E-05	2.995E-05	1.001E-05	7.029E-06	1.186E-03	3.621E-05
0.59	1.837E-05	6.090E-05	4.336E-06	2.453E-06	1.760E-05	4.273E-05	2.874E-05	9.529E-06	6.815E-06	1.208E-03	3.523E-05
0.60	1.809E-05	5.812E-05	4.196E-06	2.356E-06	1.768E-05	4.166E-05	2.762E-05	9.092E-06	6.618E-06	1.226E-03	3.432E-05
0.61	1.781E-05	5.554E-05	4.050E-06	2.264E-06	1.775E-05	4.061E-05	2.653E-05	8.659E-06	6.436E-06	1.242E-03	3.345E-05
0.62	1.753E-05	5.327E-05	3.908E-06	2.177E-06	1.781E-05	3.965E-05	2.552E-05	8.260E-06	6.281E-06	1.257E-03	3.261E-05
0.63	1.724E-05	5.130E-05	3.777E-06	2.095E-06	1.785E-05	3.864E-05	2.458E-05	7.911E-06	6.139E-06	1.271E-03	3.179E-05
0.64	1.697E-05	4.939E-05	3.640E-06	2.011E-06	1.787E-05	3.767E-05	2.374E-05	7.570E-06	6.015E-06	1.283E-03	3.098E-05
0.65	1.670E-05	4.769E-05	3.505E-06	1.930E-06	1.787E-05	3.679E-05	2.300E-05	7.259E-06	5.889E-06	1.293E-03	3.019E-05
0.66	1.643E-05	4.610E-05	3.375E-06	1.850E-06	1.784E-05	3.597E-05	2.235E-05	6.989E-06	5.769E-06	1.301E-03	2.942E-05
0.67	1.616E-05	4.452E-05	3.242E-06	1.771E-06	1.780E-05	3.516E-05	2.179E-05	6.722E-06	5.662E-06	1.308E-03	2.867E-05

(Appendix D. Continued)

0.68	1.590E-05	4.306E-05	3.106E-06	1.695E-06	1.773E-05	3.441E-05	2.133E-05	6.473E-06	5.555E-06	1.313E-03	2.793E-05
0.69	1.564E-05	4.172E-05	2.978E-06	1.624E-06	1.762E-05	3.370E-05	2.096E-05	6.250E-06	5.458E-06	1.315E-03	2.720E-05
0.70	1.539E-05	4.050E-05	2.852E-06	1.557E-06	1.749E-05	3.299E-05	2.065E-05	6.009E-06	5.359E-06	1.316E-03	2.648E-05
0.71	1.514E-05	3.937E-05	2.722E-06	1.498E-06	1.735E-05	3.233E-05	2.038E-05	5.766E-06	5.263E-06	1.315E-03	2.577E-05
0.72	1.489E-05	3.830E-05	2.599E-06	1.447E-06	1.718E-05	3.169E-05	2.013E-05	5.533E-06	5.177E-06	1.312E-03	2.507E-05
0.73	1.464E-05	3.725E-05	2.477E-06	1.404E-06	1.697E-05	3.103E-05	1.990E-05	5.305E-06	5.092E-06	1.308E-03	2.438E-05
0.74	1.440E-05	3.623E-05	2.350E-06	1.363E-06	1.671E-05	3.038E-05	1.969E-05	5.071E-06	5.014E-06	1.302E-03	2.370E-05
0.75	1.417E-05	3.522E-05	2.231E-06	1.325E-06	1.642E-05	2.978E-05	1.949E-05	4.851E-06	4.933E-06	1.296E-03	2.303E-05
0.76	1.393E-05	3.418E-05	2.114E-06	1.288E-06	1.607E-05	2.916E-05	1.931E-05	4.636E-06	4.853E-06	1.290E-03	2.239E-05
0.77	1.370E-05	3.320E-05	1.998E-06	1.253E-06	1.569E-05	2.857E-05	1.914E-05	4.421E-06	4.777E-06	1.285E-03	2.177E-05
0.78	1.348E-05	3.228E-05	1.890E-06	1.220E-06	1.528E-05	2.803E-05	1.898E-05	4.219E-06	4.699E-06	1.279E-03	2.118E-05
0.79	1.326E-05	3.140E-05	1.790E-06	1.188E-06	1.483E-05	2.749E-05	1.884E-05	4.024E-06	4.625E-06	1.266E-03	2.061E-05
0.80	1.305E-05	3.056E-05	1.691E-06	1.158E-06	1.434E-05	2.697E-05	1.870E-05	3.828E-06	4.548E-06	1.266E-03	2.007E-05
0.81	1.286E-05	2.977E-05	1.602E-06	1.129E-06	1.387E-05	2.649E-05	1.857E-05	3.648E-06	4.473E-06	1.259E-03	1.955E-05
0.82	1.268E-05	2.901E-05	1.519E-06	1.101E-06	1.338E-05	2.600E-05	1.845E-05	3.478E-06	4.404E-06	1.251E-03	1.904E-05
0.83	1.251E-05	2.825E-05	1.434E-06	1.073E-06	1.290E-05	2.552E-05	1.833E-05	3.310E-06	4.333E-06	1.244E-03	1.855E-05
0.84	1.234E-05	2.750E-05	1.355E-06	1.046E-06	1.246E-05	2.507E-05	1.822E-05	3.156E-06	4.266E-06	1.236E-03	1.808E-05
0.85	1.219E-05	2.676E-05	1.280E-06	1.018E-06	1.206E-05	2.463E-05	1.810E-05	3.009E-06	4.196E-06	1.228E-03	1.764E-05
0.86	1.205E-05	2.603E-05	1.203E-06	1.203E-06	1.168E-05	2.419E-05	1.798E-05	2.858E-06	4.127E-06	1.219E-03	1.723E-05
0.87	1.191E-05	2.532E-05	1.128E-06	9.901E-07	1.168E-05	2.379E-05	1.787E-05	2.717E-06	4.062E-06	1.211E-03	1.687E-05
0.88	1.178E-05	2.462E-05	1.060E-06	9.733E-07	1.105E-05	2.341E-05	1.775E-05	2.579E-06	3.995E-06	1.201E-03	1.653E-05
0.89	1.164E-05	2.392E-05	9.927E-07	9.125E-07	1.074E-05	2.304E-05	1.764E-05	2.436E-06	3.931E-06	1.192E-03	1.623E-05
0.90	1.152E-05	2.325E-05	9.304E-07	8.888E-07	1.044E-05	2.270E-05	1.753E-05	2.301E-06	3.864E-06	1.182E-03	1.595E-05
0.91	1.140E-05	2.260E-05	8.765E-07	8.657E-07	1.016E-05	2.238E-05	1.742E-05	2.168E-06	3.799E-06	1.171E-03	1.567E-05
0.92	1.129E-05	2.196E-05	8.235E-07	8.429E-07	9.885E-06	2.205E-05	1.733E-05	2.029E-06	3.737E-06	1.159E-03	1.539E-05
0.93	1.118E-05	2.134E-05	7.749E-07	8.209E-07	9.631E-06	2.176E-05	1.723E-05	1.897E-06	3.674E-06	1.146E-03	1.511E-05
0.94	1.107E-05	2.074E-05	7.329E-07	7.985E-07	9.398E-06	2.147E-05	1.713E-05	1.766E-06	3.615E-06	1.133E-03	1.482E-05
0.95	1.096E-05	2.017E-05	6.902E-07	7.763E-07	9.183E-06	2.117E-05	1.704E-05	1.629E-06	3.555E-06	1.120E-03	1.454E-05
0.96	1.086E-05	1.961E-05	6.486E-07	7.547E-07	8.985E-06	2.088E-05	1.695E-05	1.498E-06	3.498E-06	1.107E-03	1.425E-05
0.97	1.076E-05	1.908E-05	6.082E-07	7.340E-07	8.798E-06	2.060E-05	1.678E-05	1.376E-06	3.445E-06	1.093E-03	1.396E-05
0.98	1.066E-05	1.856E-05	5.711E-07	7.142E-07	8.618E-06	2.031E-05	1.678E-05	1.255E-06	3.393E-06	1.080E-03	1.367E-05
0.99	1.057E-05	1.806E-05	5.350E-07	6.953E-07	8.444E-06	2.004E-05	1.670E-05	1.138E-06	3.345E-06	1.068E-03	1.340E-05
1.00	1.048E-05	1.758E-05	5.020E-07	6.777E-07	8.275E-06	1.977E-05	1.661E-05	1.026E-06	3.296E-06	1.056E-03	1.314E-05
1.01	1.038E-05	1.712E-05	4.739E-07	6.606E-07	8.117E-06	1.949E-05	1.653E-05	9.140E-07	3.249E-06	1.044E-03	1.289E-05
1.02	1.030E-05	1.668E-05	4.481E-07	6.444E-07	7.972E-06	1.924E-05	1.645E-05	8.070E-07	3.205E-06	1.032E-03	1.265E-05
1.03	1.020E-05	1.626E-05	4.258E-07	6.284E-07	7.841E-06	1.899E-05	1.637E-05	7.078E-07	3.159E-06	1.020E-03	1.240E-05
1.04	1.011E-05	1.587E-05	4.076E-07	6.129E-07	7.719E-06	1.872E-05	1.629E-05	6.126E-07	3.116E-06	1.008E-03	1.217E-05
1.05	1.002E-05	1.550E-05	3.911E-07	5.979E-07	7.606E-06	1.848E-05	1.621E-05	5.282E-07	3.071E-06	9.956E-04	1.193E-05
1.06	9.926E-06	1.515E-05	3.773E-07	5.833E-07	7.500E-06	1.823E-05	1.613E-05	4.569E-07	3.027E-06	9.835E-04	1.170E-05
1.07	9.835E-06	1.484E-05	3.654E-07	5.692E-07	7.400E-06	1.798E-05	1.605E-05	3.976E-07	2.985E-06	9.715E-04	1.148E-05
1.08	9.745E-06	1.455E-05	3.544E-07	5.555E-07	7.304E-06	1.775E-05	1.598E-05	3.485E-07	2.942E-06	9.597E-04	1.126E-05
1.09	9.658E-06	1.429E-05	3.450E-07	5.422E-07	7.212E-06	1.752E-05	1.590E-05	3.067E-07	2.903E-06	9.483E-04	1.105E-05
1.10	9.572E-06	1.403E-05	3.373E-07	5.291E-07	7.123E-06	1.728E-05	1.582E-05	2.720E-07	2.861E-06	9.369E-04	1.084E-05
1.11	9.488E-06	1.377E-05	3.297E-07	5.162E-07	7.038E-06	1.705E-05	1.575E-05	2.432E-07	2.819E-06	9.258E-04	1.064E-05
1.12	9.407E-06	1.353E-05	3.226E-07	5.035E-07	6.958E-06	1.684E-05	1.567E-05	2.171E-07	2.779E-06	9.151E-04	1.045E-05
1.13	9.318E-06	1.329E-05	3.159E-07	4.908E-07	6.883E-06	1.662E-05	1.560E-05	1.940E-07	2.738E-06	9.047E-04	1.025E-05
1.14	9.234E-06	1.306E-05	3.099E-07	4.786E-07	6.811E-06	1.641E-05	1.552E-05	1.743E-07	2.699E-06	8.946E-04	1.006E-05
1.15	9.153E-06	1.284E-05	3.044E-07	4.658E-07	6.741E-06	1.622E-05	1.544E-05	1.562E-07	2.658E-06	8.849E-04	9.880E-06
1.16	9.072E-06	1.263E-05	2.995E-07	4.531E-07	6.676E-06	1.602E-05	1.537E-05	1.395E-07	2.617E-06	8.755E-04	9.702E-06
1.20	8.784E-06	1.198E-05	2.811E-07	4.036E-07	6.439E-06	1.533E-05	1.508E-05	7.042E-08	2.458E-06	8.399E-04	9.106E-06
1.25	8.457E-06	1.128E-05	2.655E-07	3.461E-07	6.176E-06	1.453E-05	1.472E-05	3.218E-08	2.270E-06	7.994E-04	8.581E-06
1.30	8.162E-06	1.071E-05	2.527E-07	2.939E-06	5.939E-06	1.380E-05	1.438E-05	7.598E-09	2.093E-06	7.628E-04	8.242E-06

(Appendix D, Continued)

1.35	7.889E-06	1.020E-05	2.414E-07	2.460E-07	5.724E-06	1.317E-05	1.405E-05	-1.667E-09	1.930E-06	7.289E-04	8.023E-06
1.40	7.334E-06	9.734E-06	2.133E-07	2.000E-07	5.332E-06	1.264E-05	1.373E-05	-2.220E-09	1.785E-06	6.964E-04	7.834E-06
1.45	7.998E-06	9.327E-06	2.220E-07	1.609E-07	5.357E-06	1.219E-05	1.343E-05	5.222E-10	1.653E-06	6.647E-04	7.672E-06
1.50	7.185E-06	8.982E-06	2.138E-07	1.282E-07	5.187E-06	1.183E-05	1.313E-05	0.000E+00	1.534E-06	6.333E-04	7.537E-06
1.55	6.995E-06	8.707E-06	2.065E-07	1.027E-07	5.021E-06	1.149E-05	1.284E-05	0.000E+00	1.425E-06	6.034E-04	7.423E-06
1.60	6.822E-06	8.497E-06	1.996E-07	8.500E-08	4.856E-06	1.117E-05	1.255E-05	0.000E+00	1.326E-06	5.744E-04	7.316E-06
1.65	6.664E-06	8.331E-06	1.928E-07	7.344E-08	4.698E-06	1.087E-05	1.227E-05	0.000E+00	1.239E-06	5.477E-04	7.213E-06
1.70	6.516E-06	8.186E-06	1.860E-07	6.612E-08	4.551E-06	1.059E-05	1.199E-05	0.000E+00	1.166E-06	5.225E-04	7.115E-06
1.75	6.375E-06	8.055E-06	1.792E-07	6.202E-08	4.414E-06	1.032E-05	1.173E-05	0.000E+00	1.105E-06	4.994E-04	7.025E-06
1.80	6.234E-06	7.937E-06	1.728E-07	5.807E-08	4.285E-06	1.005E-05	1.147E-05	0.000E+00	1.053E-06	4.782E-04	6.940E-06
1.85	6.099E-06	7.834E-06	1.670E-07	5.516E-08	4.164E-06	9.778E-06	1.121E-05	0.000E+00	1.005E-06	4.592E-04	6.858E-06
1.90	5.972E-06	7.744E-06	1.616E-07	5.428E-08	4.047E-06	9.520E-06	1.097E-05	0.000E+00	9.636E-07	4.421E-04	6.778E-06
1.95	5.856E-06	7.664E-06	1.562E-07	5.566E-08	3.929E-06	9.259E-06	1.073E-05	0.000E+00	9.268E-07	4.273E-04	6.701E-06
2.00	5.752E-06	7.593E-06	1.511E-07	5.850E-08	3.816E-06	8.990E-06	1.049E-05	0.000E+00	8.945E-07	4.145E-04	6.628E-06
2.05	5.658E-06	7.525E-06	1.461E-07	6.220E-08	3.703E-06	8.726E-06	1.026E-05	0.000E+00	8.653E-07	4.032E-04	6.556E-06
2.10	5.570E-06	7.460E-06	1.415E-07	6.558E-08	3.591E-06	8.466E-06	1.003E-05	0.000E+00	8.415E-07	3.923E-04	6.488E-06
2.15	5.485E-06	7.398E-06	1.371E-07	6.916E-08	3.481E-06	8.216E-06	9.801E-06	0.000E+00	8.267E-07	3.819E-04	6.422E-06
2.20	5.406E-06	7.340E-06	1.329E-07	7.304E-08	3.371E-06	7.995E-06	9.576E-06	0.000E+00	8.235E-07	3.717E-04	6.358E-06
2.25	5.332E-06	7.286E-06	1.287E-07	7.733E-08	3.260E-06	7.791E-06	9.355E-06	0.000E+00	8.320E-07	3.616E-04	6.296E-06
2.30	5.265E-06	7.238E-06	1.247E-07	8.247E-08	3.155E-06	7.603E-06	9.138E-06	0.000E+00	8.512E-07	3.520E-04	6.236E-06
2.35	5.200E-06	7.194E-06	1.208E-07	8.868E-08	3.054E-06	7.426E-06	8.925E-06	0.000E+00	8.763E-07	3.429E-04	6.177E-06
2.40	5.136E-06	7.155E-06	1.169E-07	9.603E-08	2.955E-06	7.251E-06	8.716E-06	0.000E+00	9.057E-07	3.340E-04	6.119E-06
2.45	5.069E-06	7.119E-06	1.130E-07	1.043E-07	2.860E-06	7.077E-06	8.508E-06	0.000E+00	9.382E-07	3.256E-04	6.067E-06
2.50	5.006E-06	7.095E-06	1.091E-07	1.134E-07	2.766E-06	6.907E-06	8.305E-06	0.000E+00	9.724E-07	3.179E-04	6.016E-06
2.55	4.947E-06	7.087E-06	1.051E-07	1.229E-07	2.670E-06	6.740E-06	8.103E-06	0.000E+00	1.008E-06	3.105E-04	5.970E-06
2.60	4.892E-06	7.097E-06	1.013E-07	1.329E-07	2.575E-06	6.577E-06	7.903E-06	0.000E+00	1.045E-06	3.038E-04	5.947E-06
2.65	4.839E-06	7.123E-06	9.756E-08	1.433E-07	2.479E-06	6.416E-06	7.703E-06	0.000E+00	1.083E-06	2.975E-04	5.946E-06
2.70	4.787E-06	7.160E-06	9.392E-08	1.539E-07	2.383E-06	6.256E-06	7.503E-06	0.000E+00	1.122E-06	2.917E-04	5.953E-06
2.75	4.734E-06	7.203E-06	9.043E-08	1.648E-07	2.289E-06	6.098E-06	7.301E-06	0.000E+00	1.162E-06	2.861E-04	5.972E-06
2.80	4.684E-06	7.254E-06	8.711E-08	1.757E-07	2.198E-06	5.944E-06	7.102E-06	0.000E+00	1.203E-06	2.810E-04	5.988E-06
2.85	4.636E-06	7.310E-06	8.384E-08	1.873E-07	2.108E-06	5.790E-06	6.902E-06	0.000E+00	1.245E-06	2.763E-04	5.997E-06
2.90	4.588E-06	7.368E-06	8.071E-08	2.004E-07	2.018E-06	5.637E-06	6.700E-06	0.000E+00	1.289E-06	2.719E-04	6.018E-06
2.95	4.540E-06	7.429E-06	7.755E-08	2.150E-07	1.927E-06	5.489E-06	6.502E-06	0.000E+00	1.334E-06	2.678E-04	6.040E-06
3.00	4.492E-06	7.498E-06	7.446E-08	2.308E-07	1.837E-06	5.346E-06	6.305E-06	0.000E+00	1.380E-06	2.640E-04	6.060E-06
3.05	4.443E-06	7.579E-06	7.134E-08	2.471E-07	1.748E-06	5.208E-06	6.104E-06	0.000E+00	1.428E-06	2.603E-04	6.084E-06
3.10	4.398E-06	7.675E-06	6.832E-08	2.634E-07	1.659E-06	5.076E-06	5.911E-06	0.000E+00	1.479E-06	2.567E-04	6.109E-06
3.15	4.354E-06	7.786E-06	6.531E-08	2.803E-07	1.571E-06	4.944E-06	5.721E-06	0.000E+00	1.533E-06	2.532E-04	6.135E-06
3.20	4.311E-06	7.906E-06	6.229E-08	2.986E-07	1.484E-06	4.814E-06	5.521E-06	0.000E+00	1.592E-06	2.498E-04	6.163E-06
3.25	4.268E-06	8.033E-06	5.934E-08	3.180E-07	1.397E-06	4.689E-06	5.330E-06	0.000E+00	1.655E-06	2.466E-04	6.189E-06
3.30	4.226E-06	8.169E-06	5.656E-08	3.394E-07	1.314E-06	4.567E-06	5.140E-06	0.000E+00	1.725E-06	2.435E-04	6.219E-06
3.35	4.184E-06	8.318E-06	5.385E-08	3.624E-07	1.232E-06	4.442E-06	4.948E-06	0.000E+00	1.802E-06	2.404E-04	6.246E-06
3.40	4.145E-06	8.478E-06	5.123E-08	3.904E-07	1.150E-06	4.320E-06	4.762E-06	0.000E+00	1.885E-06	2.375E-04	6.275E-06
3.45	4.109E-06	8.646E-06	4.866E-08	4.211E-07	1.070E-06	4.199E-06	4.576E-06	0.000E+00	1.972E-06	2.347E-04	6.309E-06
3.50	4.075E-06	8.820E-06	4.616E-08	4.548E-07	9.902E-07	4.078E-06	4.389E-06	0.000E+00	2.060E-06	2.320E-04	6.344E-06
3.55	4.040E-06	8.993E-06	4.387E-08	4.899E-07	9.127E-07	3.962E-06	4.209E-06	0.000E+00	2.149E-06	2.294E-04	6.382E-06
3.60	4.005E-06	9.174E-06	4.173E-08	5.257E-07	8.368E-07	3.850E-06	4.036E-06	0.000E+00	2.242E-06	2.269E-04	6.421E-06
3.65	3.971E-06	9.371E-06	3.966E-08	5.622E-07	7.616E-07	3.738E-06	3.865E-06	0.000E+00	2.339E-06	2.245E-04	6.459E-06
3.70	3.939E-06	9.596E-06	3.768E-08	6.004E-07	6.867E-07	3.631E-06	3.701E-06	0.000E+00	2.439E-06	2.222E-04	6.499E-06
3.75	3.909E-06	9.856E-06	3.570E-08	6.399E-07	6.132E-07	3.528E-06	3.538E-06	0.000E+00	2.542E-06	2.199E-04	6.543E-06
3.80	3.880E-06	1.015E-05	3.373E-08	6.818E-07	5.411E-07	3.429E-06	3.376E-06	0.000E+00	2.649E-06	2.177E-04	6.591E-06
3.85	3.853E-06	1.046E-05	3.183E-08	7.279E-07	4.704E-07	3.339E-06	3.223E-06	0.000E+00	2.764E-06	2.155E-04	6.642E-06
3.90	3.826E-06	1.078E-05	2.993E-08	7.755E-07	3.999E-07	3.250E-06	3.071E-06	0.000E+00	2.882E-06	2.133E-04	6.695E-06

(Appendix D. Continued)

0.52	5.229E-07	1.011E-05	3.892E-05	1.447E-06	3.384E-06
0.53	5.053E-07	9.105E-06	4.264E-05	1.360E-06	3.613E-06
0.54	4.884E-07	8.260E-06	4.632E-05	1.285E-06	3.837E-06
0.55	4.711E-07	7.570E-06	4.984E-05	1.219E-06	4.056E-06
0.56	4.550E-07	7.013E-06	5.313E-05	1.161E-06	4.275E-06
0.57	4.389E-07	6.555E-06	5.626E-05	1.108E-06	4.493E-06
0.58	4.231E-07	6.171E-06	5.920E-05	1.060E-06	4.707E-06
0.59	4.083E-07	5.844E-06	6.198E-05	1.018E-06	4.918E-06
0.60	3.938E-07	5.560E-06	6.463E-05	9.797E-07	5.127E-06
0.61	3.803E-07	5.311E-06	6.703E-05	9.441E-07	5.333E-06
0.62	3.664E-07	5.076E-06	6.915E-05	9.091E-07	5.533E-06
0.63	3.537E-07	4.860E-06	7.092E-05	8.748E-07	5.726E-06
0.64	3.404E-07	4.667E-06	7.228E-05	8.413E-07	5.913E-06
0.65	3.272E-07	4.496E-06	7.323E-05	8.090E-07	6.092E-06
0.66	3.140E-07	4.342E-06	7.381E-05	7.782E-07	6.266E-06
0.67	3.008E-07	4.200E-06	7.409E-05	7.490E-07	6.435E-06
0.68	2.888E-07	4.075E-06	7.415E-05	7.217E-07	6.588E-06
0.69	2.765E-07	3.963E-06	7.409E-05	6.965E-07	6.727E-06
0.70	2.653E-07	3.856E-06	7.394E-05	6.733E-07	6.853E-06
0.71	2.537E-07	3.752E-06	7.371E-05	6.517E-07	6.965E-06
0.72	2.424E-07	3.654E-06	7.341E-05	6.313E-07	7.059E-06
0.73	2.316E-07	3.558E-06	7.303E-05	6.122E-07	7.137E-06
0.74	2.213E-07	3.465E-06	7.259E-05	5.942E-07	7.205E-06
0.75	2.116E-07	3.376E-06	7.213E-05	5.768E-07	7.263E-06
0.76	2.013E-07	3.289E-06	7.160E-05	5.602E-07	7.305E-06
0.77	1.916E-07	3.205E-06	7.104E-05	5.435E-07	7.332E-06
0.78	1.819E-07	3.126E-06	7.045E-05	5.264E-07	7.336E-06
0.79	1.724E-07	3.049E-06	6.987E-05	5.091E-07	7.323E-06
0.80	1.633E-07	2.973E-06	6.930E-05	4.919E-07	7.293E-06
0.81	1.543E-07	2.899E-06	6.875E-05	4.755E-07	7.249E-06
0.82	1.459E-07	2.827E-06	6.820E-05	4.601E-07	7.195E-06
0.83	1.377E-07	2.759E-06	6.762E-05	4.460E-07	7.135E-06
0.84	1.304E-07	2.696E-06	6.703E-05	4.330E-07	7.077E-06
0.85	1.231E-07	2.638E-06	6.641E-05	4.212E-07	7.018E-06
0.86	1.158E-07	2.587E-06	6.578E-05	4.103E-07	6.956E-06
0.87	1.087E-07	2.544E-06	6.516E-05	3.994E-07	6.894E-06
0.88	1.016E-07	2.507E-06	6.452E-05	3.886E-07	6.829E-06
0.89	9.488E-08	2.474E-06	6.385E-05	3.778E-07	6.762E-06
0.90	8.817E-08	2.443E-06	6.321E-05	3.671E-07	6.692E-06
0.91	8.193E-08	2.414E-06	6.255E-05	3.570E-07	6.619E-06
0.92	7.567E-08	2.388E-06	6.187E-05	3.473E-07	6.543E-06
0.93	6.943E-08	2.362E-06	6.120E-05	3.380E-07	6.461E-06
0.94	6.346E-08	2.338E-06	6.049E-05	3.292E-07	6.373E-06
0.95	5.767E-08	2.315E-06	5.975E-05	3.209E-07	6.286E-06
0.96	5.199E-08	2.293E-06	5.905E-05	3.128E-07	6.192E-06
0.97	4.628E-08	2.271E-06	5.833E-05	3.050E-07	6.091E-06
0.98	4.082E-08	2.251E-06	5.757E-05	2.976E-07	5.988E-06
0.99	3.557E-08	2.231E-06	5.684E-05	2.904E-07	5.876E-06
1.00	3.067E-08	2.212E-06	5.610E-05	2.836E-07	5.757E-06
1.01	2.634E-08	2.194E-06	5.534E-05	2.771E-07	5.639E-06
1.02	2.239E-08	2.176E-06	5.461E-05	2.710E-07	5.514E-06
1.03	1.882E-08	2.159E-06	5.388E-05	2.653E-07	5.385E-06

(Appendix D. Continued)

1.04	1.572E-08	2.142E-06	5.311E-05	2.600E-07	5.260E-06
1.05	1.287E-08	2.126E-06	5.237E-05	2.549E-07	5.136E-06
1.06	1.023E-08	2.111E-06	5.161E-05	2.502E-07	5.006E-06
1.07	7.906E-09	2.094E-06	5.080E-05	2.458E-07	4.881E-06
1.08	5.935E-09	2.079E-06	4.998E-05	2.416E-07	4.756E-06
1.09	4.285E-09	2.064E-06	4.916E-05	2.376E-07	4.626E-06
1.10	3.016E-09	2.049E-06	4.832E-05	2.337E-07	4.503E-06
1.11	2.055E-09	2.035E-06	4.747E-05	2.300E-07	4.384E-06
1.12	1.312E-09	2.022E-06	4.666E-05	2.264E-07	4.263E-06
1.13	8.105E-10	2.010E-06	4.583E-05	2.230E-07	4.152E-06
1.14	4.457E-10	1.998E-06	4.502E-05	2.198E-07	4.050E-06
1.15	1.626E-10	1.989E-06	4.425E-05	2.168E-07	3.950E-06
1.16	-3.574E-11	1.979E-06	4.347E-05	2.140E-07	3.860E-06
1.20	-8.090E-10	1.940E-06	4.094E-05	2.041E-07	3.557E-06
1.25	-2.710E-10	1.901E-06	3.807E-05	1.949E-07	3.238E-06
1.30	-5.449E-12	1.868E-06	3.562E-05	1.884E-07	2.978E-06
1.35	0.000E+00	1.840E-06	3.338E-05	1.835E-07	2.736E-06
1.40	0.000E+00	1.815E-06	3.120E-05	1.794E-07	2.517E-06
1.45	0.000E+00	1.792E-06	2.912E-05	1.755E-07	2.316E-06
1.50	0.000E+00	1.770E-06	2.716E-05	1.719E-07	2.126E-06
1.55	0.000E+00	1.751E-06	2.536E-05	1.686E-07	1.949E-06
1.60	0.000E+00	1.733E-06	2.374E-05	1.657E-07	1.784E-06
1.65	0.000E+00	1.718E-06	2.229E-05	1.633E-07	1.630E-06
1.70	0.000E+00	1.705E-06	2.098E-05	1.614E-07	1.499E-06
1.75	0.000E+00	1.697E-06	1.975E-05	1.604E-07	1.385E-06
1.80	0.000E+00	1.694E-06	1.862E-05	1.603E-07	1.284E-06
1.85	0.000E+00	1.696E-06	1.760E-05	1.611E-07	1.190E-06
1.90	0.000E+00	1.704E-06	1.671E-05	1.624E-07	1.105E-06
1.95	0.000E+00	1.715E-06	1.594E-05	1.639E-07	1.021E-06
2.00	0.000E+00	1.728E-06	1.525E-05	1.655E-07	9.424E-07
2.05	0.000E+00	1.743E-06	1.459E-05	1.673E-07	8.674E-07
2.10	0.000E+00	1.760E-06	1.397E-05	1.694E-07	7.947E-07
2.15	0.000E+00	1.781E-06	1.337E-05	1.716E-07	7.214E-07
2.20	0.000E+00	1.805E-06	1.282E-05	1.740E-07	6.529E-07
2.25	0.000E+00	1.832E-06	1.231E-05	1.765E-07	5.894E-07
2.30	0.000E+00	1.862E-06	1.185E-05	1.794E-07	5.322E-07
2.35	0.000E+00	1.894E-06	1.142E-05	1.826E-07	4.850E-07
2.40	0.000E+00	1.928E-06	1.101E-05	1.864E-07	4.459E-07
2.45	0.000E+00	1.962E-06	1.062E-05	1.907E-07	4.111E-07
2.50	0.000E+00	2.000E-06	1.026E-05	1.952E-07	3.806E-07
2.55	0.000E+00	2.040E-06	9.916E-06	2.000E-07	3.524E-07
2.60	0.000E+00	2.083E-06	9.594E-06	2.049E-07	3.247E-07
2.65	0.000E+00	2.132E-06	9.276E-06	2.099E-07	2.988E-07
2.70	0.000E+00	2.181E-06	8.965E-06	2.150E-07	2.738E-07
2.75	0.000E+00	2.233E-06	8.666E-06	2.202E-07	2.488E-07
2.80	0.000E+00	2.287E-06	8.377E-06	2.256E-07	2.248E-07
2.85	0.000E+00	2.344E-06	8.109E-06	2.317E-07	2.015E-07
2.90	0.000E+00	2.404E-06	7.854E-06	2.383E-07	1.798E-07
2.95	0.000E+00	2.468E-06	7.609E-06	2.456E-07	1.621E-07
3.00	0.000E+00	2.540E-06	7.373E-06	2.533E-07	1.491E-07
3.05	0.000E+00	2.622E-06	7.143E-06	2.610E-07	1.421E-07
3.10	0.000E+00	2.714E-06	6.919E-06	2.688E-07	1.413E-07

(Appendix D. Continued)

3.15	0.000E+00	2.813E-06	6.707E-06	2.765E-07	1.451E-07
3.20	0.000E+00	2.920E-06	6.497E-06	2.842E-07	1.516E-07
3.25	0.000E+00	3.036E-06	6.304E-06	2.920E-07	1.596E-07
3.30	0.000E+00	3.164E-06	6.136E-06	2.999E-07	1.678E-07
3.35	0.000E+00	3.313E-06	5.994E-06	3.079E-07	1.766E-07
3.40	0.000E+00	3.477E-06	5.880E-06	3.159E-07	1.859E-07
3.45	0.000E+00	3.661E-06	5.785E-06	3.239E-07	1.957E-07
3.50	0.000E+00	3.863E-06	5.696E-06	3.320E-07	2.058E-07
3.55	0.000E+00	4.088E-06	5.619E-06	3.402E-07	2.159E-07
3.60	0.000E+00	4.330E-06	5.557E-06	3.484E-07	2.261E-07
3.65	0.000E+00	4.592E-06	5.507E-06	3.566E-07	2.365E-07
3.70	0.000E+00	4.874E-06	5.470E-06	3.649E-07	2.473E-07
3.75	0.000E+00	5.223E-06	5.443E-06	3.733E-07	2.588E-07
3.80	0.000E+00	5.659E-06	5.421E-06	3.819E-07	2.713E-07
3.85	0.000E+00	6.284E-06	5.404E-06	3.905E-07	2.856E-07
3.90	0.000E+00	6.957E-06	5.387E-06	3.992E-07	3.005E-07

APPENDIX E.

Species fluxes and flux balances from flame data

Molar fluxes (App. E.1) were calculated from the smoothed mole-fraction curves of App. D using the equations of Fristrom and Westenberg (1966) described in Ch. II. Mass flux balances (App. E.2) then were calculated for carbon flux, hydrogen flux, oxygen flux, and total mass flux, also as described in Ch. II; percent deviation from the mass flux in the feed is also shown.

Appendix E.1. Molar fluxes of species

Z	AR	H	H2	CH3	CH4	OH	H2O	C2H2	C2H3	C2H4	CO
0.00	3.209E-06	-7.306E-07	9.335E-07	-3.446E-08	1.264E-07	-1.807E-08	2.003E-06	2.186E-05	1.765E-09	4.766E-08	5.537E-06
0.01	3.249E-06	-8.368E-07	9.399E-07	-4.244E-08	1.250E-07	-1.921E-08	1.955E-06	2.213E-05	1.723E-09	4.686E-08	5.493E-06
0.02	3.289E-06	-9.497E-07	9.541E-07	-5.141E-08	1.234E-07	-2.022E-08	1.910E-06	2.241E-05	1.675E-09	4.615E-08	5.427E-06
0.03	3.329E-06	-1.106E-06	1.018E-06	-6.550E-08	1.202E-07	-2.059E-08	1.860E-06	2.271E-05	1.618E-09	4.606E-08	5.245E-06
0.04	3.353E-06	-1.294E-06	1.132E-06	-8.254E-08	1.165E-07	-2.064E-08	1.798E-06	2.303E-05	1.567E-09	4.635E-08	5.001E-06
0.05	3.373E-06	-1.506E-06	1.303E-06	-1.015E-07	1.135E-07	-2.062E-08	1.726E-06	2.336E-05	1.527E-09	4.683E-08	4.742E-06
0.06	3.388E-06	-1.736E-06	1.523E-06	-1.219E-07	1.121E-07	-2.065E-08	1.658E-06	2.370E-05	1.501E-09	4.732E-08	4.499E-06
0.07	3.396E-06	-1.981E-06	1.796E-06	-1.435E-07	1.129E-07	-2.085E-08	1.594E-06	2.405E-05	1.492E-09	4.775E-08	4.292E-06
0.08	3.400E-06	-2.236E-06	2.111E-06	-1.635E-07	1.168E-07	-2.139E-08	1.542E-06	2.440E-05	1.504E-09	4.795E-08	4.154E-06
0.09	3.402E-06	-2.498E-06	2.455E-06	-1.892E-07	1.242E-07	-2.229E-08	1.511E-06	2.473E-05	1.533E-09	4.786E-08	4.092E-06
0.10	3.405E-06	-2.773E-06	2.809E-06	-2.116E-07	1.349E-07	-2.353E-08	1.506E-06	2.505E-05	1.577E-09	4.751E-08	4.097E-06
0.11	3.411E-06	-3.067E-06	3.153E-06	-2.355E-07	1.486E-07	-2.505E-08	1.530E-06	2.533E-05	1.632E-09	4.699E-08	4.148E-06
0.12	3.423E-06	-3.389E-06	3.468E-06	-2.596E-07	1.646E-07	-2.675E-08	1.581E-06	2.557E-05	1.692E-09	4.644E-08	4.215E-06
0.13	3.441E-06	-3.753E-06	3.739E-06	-2.827E-07	1.818E-07	-2.854E-08	1.656E-06	2.576E-05	1.750E-09	4.605E-08	4.262E-06
0.14	3.465E-06	-4.168E-06	4.168E-06	-3.032E-07	1.990E-07	-3.037E-08	1.747E-06	2.588E-05	1.798E-09	4.602E-08	4.262E-06
0.15	3.494E-06	-4.642E-06	4.136E-06	-3.186E-07	2.154E-07	-3.226E-08	1.845E-06	2.594E-05	1.827E-09	4.655E-08	4.203E-06
0.16	3.523E-06	-5.178E-06	4.410E-06	-3.260E-07	2.299E-07	-3.426E-08	1.940E-06	2.593E-05	1.828E-09	4.777E-08	4.090E-06
0.17	3.549E-06	-5.773E-06	4.544E-06	-3.453E-07	2.515E-07	-3.611E-08	2.093E-06	2.573E-05	1.708E-09	4.978E-08	3.944E-06
0.18	3.568E-06	-6.419E-06	4.410E-06	-3.653E-07	2.721E-07	-3.813E-08	2.244E-06	2.534E-05	1.791E-09	5.264E-08	3.801E-06
0.19	3.575E-06	-7.104E-06	4.695E-06	-3.905E-07	2.987E-07	-4.018E-08	2.412E-06	2.556E-05	1.574E-09	5.640E-08	3.695E-06
0.20	3.573E-06	-7.813E-06	4.865E-06	-4.165E-07	3.262E-07	-4.218E-08	2.582E-06	2.534E-05	1.388E-09	6.115E-08	3.656E-06
0.21	3.557E-06	-8.530E-06	5.045E-06	-4.455E-07	3.652E-07	-4.588E-08	2.765E-06	2.510E-05	1.156E-09	6.706E-08	3.693E-06
0.22	3.531E-06	-9.237E-06	5.218E-06	-4.781E-07	4.055E-07	-4.945E-08	2.992E-06	2.483E-05	8.841E-10	7.446E-08	3.799E-06
0.23	3.500E-06	-9.916E-06	5.361E-06	-5.141E-07	4.420E-07	-5.383E-08	3.244E-06	2.457E-05	5.782E-10	8.385E-08	3.949E-06
0.24	3.467E-06	-1.055E-05	5.453E-06	-5.535E-07	4.790E-07	-5.841E-08	3.499E-06	2.432E-05	2.391E-10	9.581E-08	4.110E-06
0.25	3.438E-06	-1.110E-05	5.478E-06	-5.978E-07	5.144E-07	-6.343E-08	3.729E-06	2.409E-05	-1.412E-10	1.110E-07	4.246E-06
0.26	3.416E-06	-1.155E-05	5.432E-06	-6.478E-07	5.476E-07	-6.914E-08	3.949E-06	2.389E-05	-1.788E-10	1.298E-07	4.331E-06
0.27	3.404E-06	-1.188E-05	5.318E-06	-6.978E-07	5.776E-07	-7.584E-08	4.131E-06	2.373E-05	-1.092E-09	1.525E-07	4.351E-06
0.28	3.401E-06	-1.204E-05	5.148E-06	-7.587E-07	6.037E-07	-8.378E-08	4.263E-06	2.363E-05	-1.691E-09	1.787E-07	4.307E-06
0.29	3.407E-06	-1.202E-05	4.940E-06	-8.240E-07	6.287E-07	-9.298E-08	4.353E-06	2.357E-05	-2.365E-09	2.074E-07	4.215E-06
0.30	3.417E-06	-1.179E-05	4.713E-06	-9.093E-07	6.541E-07	-1.031E-07	4.403E-06	2.355E-05	-3.068E-09	2.372E-07	4.102E-06
0.31	3.429E-06	-1.133E-05	4.487E-06	-1.000E-07	6.787E-07	-1.131E-07	4.417E-06	2.356E-05	-3.720E-09	2.662E-07	4.002E-06
0.32	3.438E-06	-1.065E-05	4.281E-06	-1.083E-07	7.037E-07	-1.219E-07	4.344E-06	2.358E-05	-4.401E-09	2.922E-07	3.954E-06
0.33	3.442E-06	-9.735E-06	4.117E-06	-1.176E-07	7.287E-07	-1.276E-07	4.217E-06	2.358E-05	-5.082E-09	3.134E-07	4.001E-06
0.34	3.438E-06	-8.613E-06	4.013E-06	-1.274E-07	7.542E-07	-1.366E-07	4.063E-06	2.352E-05	-4.187E-09	3.285E-07	4.184E-06
0.35	3.425E-06	-7.305E-06	3.985E-06	-1.375E-07	7.791E-07	-1.418E-07	3.929E-06	2.336E-05	-3.488E-09	3.367E-07	4.538E-06
0.36	3.404E-06	-5.844E-06	4.038E-06	-1.480E-07	8.037E-07	-1.488E-07	3.803E-06	2.309E-05	-2.291E-09	3.383E-07	5.086E-06
0.37	3.377E-06	-4.269E-06	4.166E-06	-1.583E-07	8.282E-07	-1.576E-07	3.682E-06	2.269E-05	-6.509E-10	3.342E-07	5.834E-06
0.38	3.347E-06	-2.629E-06	4.349E-06	-1.684E-07	8.521E-07	-1.682E-07	3.566E-06	2.215E-05	1.314E-09	3.259E-07	6.763E-06
0.39	3.317E-06	-9.706E-07	4.551E-06	-1.787E-07	8.754E-07	-1.791E-07	3.446E-06	2.152E-05	3.446E-09	3.149E-07	7.833E-06
0.40	3.291E-06	6.558E-07	4.735E-06	-1.890E-07	9.000E-07	-1.913E-07	3.329E-06	2.082E-05	5.581E-09	3.029E-07	8.988E-06
0.41	3.272E-06	2.207E-06	4.864E-06	-2.000E-07	9.257E-07	-2.040E-07	3.212E-06	2.010E-05	7.577E-09	2.910E-07	1.017E-05
0.42	3.260E-06	3.646E-06	4.917E-06	-2.111E-07	9.521E-07	-2.181E-07	3.103E-06	1.940E-05	9.339E-09	2.796E-07	1.131E-05
0.43	3.256E-06	4.952E-06	4.892E-06	-2.222E-07	9.791E-07	-2.332E-07	3.000E-06	1.875E-05	1.083E-08	2.691E-07	1.237E-05
0.44	3.259E-06	6.114E-06	4.808E-06	-2.333E-07	1.006E-07	-2.488E-07	2.903E-06	1.817E-05	1.206E-08	2.590E-07	1.334E-05
0.45	3.269E-06	7.133E-06	4.698E-06	-2.444E-07	1.037E-07	-2.648E-07	2.800E-06	1.721E-05	1.308E-08	2.491E-07	1.421E-05
0.46	3.269E-06	8.018E-06	4.598E-06	-2.555E-07	1.068E-07	-2.816E-07	2.700E-06	1.680E-05	1.394E-08	2.390E-07	1.500E-05
0.47	3.272E-06	8.780E-06	4.532E-06	-2.666E-07	1.099E-07	-2.994E-07	2.593E-06	1.642E-05	1.471E-08	2.284E-07	1.573E-05
0.48	3.269E-06	9.424E-06	4.508E-06	-2.777E-07	1.130E-07	-3.176E-07	2.487E-06	1.604E-05	1.542E-08	2.176E-07	1.644E-05
0.49	3.260E-06	9.950E-06	4.507E-06	-2.888E-07	1.161E-07	-3.364E-07	2.382E-06	1.604E-05	1.610E-08	2.067E-07	1.713E-05
0.50	3.248E-06	1.035E-05	4.496E-06	-2.999E-07	1.192E-07	-3.554E-07	2.277E-06	1.565E-05	1.675E-08	1.962E-07	1.782E-05
0.51	3.233E-06	1.060E-05	4.431E-06	-3.110E-07	1.223E-07	-3.746E-07	2.172E-06	1.526E-05	1.736E-08	1.866E-07	1.851E-05

(Appendix E.1. Continued)

0.52	3.1219E-06	F.1.069E-05	1.4728E-06	5.347E-07	3.659E-07	1.594E-07	7.561E-06	1.485E-05	1.792E-08	1.781E-07	1.920E-05
0.53	3.208E-06	1.061E-05	-4.016E-06	5.488E-07	3.531E-07	1.585E-07	7.675E-06	1.444E-05	1.843E-08	1.708E-07	1.989E-05
0.54	3.202E-06	1.038E-05	-8.649E-06	5.488E-07	3.390E-07	1.568E-07	7.810E-06	1.401E-05	1.833E-08	1.708E-07	2.056E-05
0.55	3.202E-06	1.000E-05	-3.199E-06	5.491E-07	3.238E-07	1.543E-07	7.977E-06	1.358E-05	1.927E-08	1.588E-07	2.122E-05
0.56	3.206E-06	9.524E-06	-2.1700E-06	5.444E-07	3.078E-07	1.510E-07	8.185E-06	1.315E-05	1.961E-08	1.533E-07	2.185E-05
0.57	3.213E-06	8.981E-06	-2.189E-06	5.355E-07	2.913E-07	1.472E-07	8.445E-06	1.271E-05	1.990E-08	1.476E-07	2.243E-05
0.58	3.222E-06	8.419E-06	-1.691E-06	5.231E-07	2.749E-07	1.428E-07	8.760E-06	1.229E-05	2.013E-08	1.414E-07	2.294E-05
0.59	3.230E-06	7.874E-06	-1.218E-06	5.092E-07	2.593E-07	1.379E-07	9.129E-06	1.188E-05	2.039E-08	1.344E-07	2.336E-05
0.60	3.240E-06	6.925E-06	-7.718E-07	4.953E-07	2.449E-07	1.327E-07	9.543E-06	1.150E-05	2.069E-08	1.268E-07	2.368E-05
0.61	3.241E-06	6.539E-06	-3.425E-06	4.827E-07	2.323E-07	1.271E-07	9.984E-06	1.116E-05	2.042E-08	1.186E-07	2.389E-05
0.62	3.239E-06	6.207E-06	4.920E-07	4.641E-07	2.221E-07	1.211E-07	1.043E-05	1.084E-05	2.028E-08	1.102E-07	2.401E-05
0.63	3.234E-06	5.922E-06	8.939E-07	4.580E-07	2.143E-07	1.150E-07	1.085E-05	1.056E-05	2.025E-08	1.018E-07	2.408E-05
0.64	3.227E-06	5.677E-06	1.265E-06	4.534E-07	2.088E-07	1.088E-07	1.122E-05	1.030E-05	2.006E-08	9.369E-08	2.412E-05
0.65	3.219E-06	5.464E-06	1.601E-06	4.494E-07	2.054E-07	1.027E-07	1.152E-05	1.007E-05	1.950E-08	8.605E-08	2.432E-05
0.66	3.209E-06	5.279E-06	1.874E-06	4.458E-07	2.020E-07	9.690E-08	1.174E-05	9.848E-06	1.900E-08	7.900E-08	2.452E-05
0.67	3.200E-06	5.118E-06	2.082E-06	4.409E-07	2.007E-07	9.163E-08	1.188E-05	9.635E-06	1.876E-08	7.263E-08	2.480E-05
0.68	3.190E-06	4.976E-06	2.226E-06	4.358E-07	1.990E-07	8.704E-08	1.195E-05	9.428E-06	1.834E-08	6.697E-08	2.515E-05
0.69	3.180E-06	4.847E-06	2.322E-06	4.308E-07	1.965E-07	8.228E-08	1.192E-05	9.240E-06	1.792E-08	6.202E-08	2.553E-05
0.70	3.171E-06	4.722E-06	2.388E-06	4.246E-07	1.930E-07	7.811E-08	1.187E-05	9.040E-06	1.748E-08	5.778E-08	2.593E-05
0.71	3.163E-06	4.594E-06	2.449E-06	4.191E-07	1.886E-07	7.461E-08	1.176E-05	8.866E-06	1.705E-08	5.424E-08	2.631E-05
0.72	3.156E-06	4.456E-06	2.526E-06	4.138E-07	1.835E-07	7.163E-08	1.165E-05	8.711E-06	1.662E-08	5.124E-08	2.667E-05
0.73	3.150E-06	4.303E-06	2.635E-06	4.089E-07	1.780E-07	7.499E-08	1.171E-05	8.546E-06	1.620E-08	4.712E-08	2.699E-05
0.74	3.143E-06	4.130E-06	2.786E-06	4.042E-07	1.723E-07	7.451E-08	1.159E-05	8.371E-06	1.577E-08	4.358E-08	2.729E-05
0.75	3.136E-06	3.937E-06	2.981E-06	3.994E-07	1.668E-07	7.400E-08	1.153E-05	8.224E-06	1.534E-08	4.033E-08	2.756E-05
0.76	3.128E-06	3.721E-06	3.217E-06	3.942E-07	1.617E-07	7.342E-08	1.148E-05	8.098E-06	1.492E-08	3.733E-08	2.782E-05
0.77	3.118E-06	3.484E-06	3.483E-06	3.883E-07	1.572E-07	7.260E-08	1.146E-05	7.998E-06	1.450E-08	3.461E-08	2.808E-05
0.78	3.108E-06	3.221E-06	3.771E-06	3.815E-07	1.534E-07	7.151E-08	1.139E-05	7.933E-06	1.410E-08	3.193E-08	2.833E-05
0.79	3.095E-06	2.955E-06	4.072E-06	3.734E-07	1.481E-07	7.017E-08	1.131E-05	7.839E-06	1.371E-08	2.931E-08	2.857E-05
0.80	3.082E-06	2.673E-06	4.372E-06	3.654E-07	1.431E-07	6.852E-08	1.122E-05	7.763E-06	1.330E-08	2.679E-08	2.881E-05
0.81	3.070E-06	2.389E-06	4.672E-06	3.570E-07	1.381E-07	6.691E-08	1.114E-05	7.686E-06	1.298E-08	2.436E-08	2.904E-05
0.82	3.060E-06	2.117E-06	4.968E-06	3.492E-07	1.341E-07	6.541E-08	1.106E-05	7.633E-06	1.255E-08	2.216E-08	2.925E-05
0.83	3.044E-06	1.853E-06	5.253E-06	3.427E-07	1.301E-07	6.393E-08	1.098E-05	7.595E-06	1.235E-08	2.046E-08	2.944E-05
0.84	3.037E-06	1.646E-06	5.546E-06	3.365E-07	1.261E-07	6.265E-08	1.091E-05	7.528E-06	1.183E-08	1.842E-08	2.961E-05
0.85	3.040E-06	1.428E-06	5.846E-06	3.305E-07	1.221E-07	6.149E-08	1.077E-05	7.431E-06	1.162E-08	1.699E-08	2.989E-05
0.86	3.039E-06	1.281E-06	6.142E-06	3.251E-07	1.183E-07	6.039E-08	1.071E-05	7.366E-06	1.143E-08	1.566E-08	3.000E-05
0.87	3.043E-06	1.084E-06	6.443E-06	3.202E-07	1.146E-07	5.939E-08	1.061E-05	7.296E-06	1.126E-08	1.447E-08	3.009E-05
0.88	3.043E-06	1.112E-06	6.743E-06	3.159E-07	1.110E-07	5.842E-08	1.055E-05	7.240E-06	1.111E-08	1.347E-08	3.019E-05
0.89	3.045E-06	1.058E-06	7.047E-06	3.117E-07	1.075E-07	5.749E-08	1.052E-05	7.187E-06	1.095E-08	1.247E-08	3.029E-05
0.90	3.044E-06	1.033E-06	7.347E-06	3.071E-07	1.040E-07	5.659E-08	1.048E-05	7.136E-06	1.058E-08	1.143E-08	3.040E-05
0.91	3.044E-06	1.003E-06	7.647E-06	3.024E-07	1.004E-07	5.572E-08	1.045E-05	7.086E-06	1.036E-08	1.043E-08	3.054E-05
0.92	3.044E-06	9.747E-06	7.947E-06	2.977E-07	9.68E-08	5.492E-08	1.043E-05	7.036E-06	1.012E-08	9.388E-08	3.070E-05
0.93	3.044E-06	9.544E-06	8.247E-06	2.930E-07	9.29E-08	5.406E-08	1.041E-05	6.986E-06	9.862E-09	8.338E-08	3.089E-05
0.94	3.043E-06	9.341E-06	8.547E-06	2.883E-07	8.90E-08	5.320E-08	1.039E-05	6.936E-06	9.602E-09	7.282E-08	3.110E-05
0.95	3.043E-06	9.138E-06	8.847E-06	2.836E-07	8.51E-08	5.234E-08	1.038E-05	6.886E-06	9.346E-09	6.232E-08	3.132E-05
0.96	3.043E-06	8.935E-06	9.147E-06	2.789E-07	8.12E-08	5.148E-08	1.038E-05	6.836E-06	9.086E-09	5.182E-08	3.155E-05
0.97	3.043E-06	8.732E-06	9.447E-06	2.742E-07	7.73E-08	5.062E-08	1.038E-05	6.786E-06	8.826E-09	4.132E-08	3.177E-05
0.98	3.043E-06	8.529E-06	9.747E-06	2.695E-07	7.34E-08	4.976E-08	1.038E-05	6.736E-06	8.566E-09	3.082E-08	3.199E-05
0.99	3.043E-06	8.326E-06	1.0047E-06	2.648E-07	6.95E-08	4.890E-08	1.038E-05	6.686E-06	8.306E-09	2.027E-08	3.221E-05
0.99	3.016E-06	9.170E-07	7.392E-07	2.949E-07	1.176E-07	4.758E-08	1.079E-05	6.527E-06	9.101E-09	9.979E-08	3.177E-05

(Appendix E.1. Continued)

1.00	3.010E-06	9.008E-07	7.424E-06	1.170E-07	4.669E-08	1.025E-05	6.477E-06	8.870E-09	1.925E-08	3.198E-05
1.01	3.006E-06	8.848E-07	7.494E-06	1.164E-07	4.591E-08	1.022E-05	6.423E-06	8.651E-09	1.870E-08	3.216E-05
1.02	3.004E-06	8.682E-07	7.597E-06	1.157E-07	4.525E-08	1.019E-05	6.366E-06	8.442E-09	1.816E-08	3.234E-05
1.03	3.003E-06	8.505E-07	7.725E-06	1.150E-07	4.468E-08	1.016E-05	6.306E-06	8.238E-09	1.765E-08	3.249E-05
1.04	3.004E-06	8.319E-07	7.864E-06	1.143E-07	4.416E-08	1.013E-05	6.246E-06	8.036E-09	1.718E-08	3.263E-05
1.05	3.006E-06	8.130E-07	8.001E-06	1.137E-07	4.367E-08	1.010E-05	6.188E-06	7.835E-09	1.678E-08	3.276E-05
1.06	3.008E-06	7.945E-07	8.127E-06	1.130E-07	4.317E-08	1.006E-05	6.136E-06	7.636E-09	1.645E-08	3.288E-05
1.07	3.010E-06	7.772E-07	8.233E-06	1.124E-07	4.265E-08	1.003E-05	6.091E-06	7.441E-09	1.619E-08	3.299E-05
1.08	3.013E-06	7.618E-07	8.318E-06	1.118E-07	4.213E-08	9.990E-06	6.056E-06	7.253E-09	1.601E-08	3.309E-05
1.09	3.016E-06	7.487E-07	8.383E-06	1.113E-07	4.164E-08	9.959E-06	6.030E-06	7.075E-09	1.577E-08	3.326E-05
1.10	3.019E-06	7.382E-07	8.432E-06	1.108E-07	4.122E-08	9.934E-06	6.013E-06	6.905E-09	1.554E-08	3.333E-05
1.11	3.022E-06	7.300E-07	8.469E-06	1.103E-07	4.088E-08	9.916E-06	6.001E-06	6.745E-09	1.566E-08	3.333E-05
1.12	3.025E-06	7.236E-07	8.501E-06	1.103E-07	4.088E-08	9.916E-06	6.001E-06	6.593E-09	1.554E-08	3.339E-05
1.13	3.028E-06	7.184E-07	8.532E-06	1.097E-07	4.064E-08	9.904E-06	5.992E-06	6.450E-09	1.539E-08	3.345E-05
1.14	3.030E-06	7.133E-07	8.563E-06	1.091E-07	4.048E-08	9.896E-06	5.984E-06	6.318E-09	1.519E-08	3.352E-05
1.15	3.031E-06	7.070E-07	8.603E-06	1.083E-07	4.032E-08	9.887E-06	5.975E-06	6.18E-09	1.496E-08	3.359E-05
1.16	3.031E-06	6.997E-07	8.654E-06	1.074E-07	4.013E-08	9.876E-06	5.962E-06	6.131E-09	1.471E-08	3.366E-05
1.20	3.019E-06	6.717E-07	8.779E-06	1.064E-07	3.990E-08	9.863E-06	5.946E-06	6.212E-09	1.496E-08	3.359E-05
1.25	3.015E-06	6.401E-07	8.969E-06	1.031E-07	3.845E-08	9.788E-06	5.833E-06	5.758E-09	1.370E-08	3.399E-05
1.30	3.010E-06	6.095E-07	9.167E-06	1.003E-07	3.709E-08	9.679E-06	5.739E-06	5.343E-09	1.295E-08	3.432E-05
1.35	3.007E-06	5.831E-07	9.384E-06	9.851E-08	3.563E-08	9.557E-06	5.637E-06	5.041E-09	1.229E-08	3.464E-05
1.40	3.008E-06	5.622E-07	9.623E-06	9.645E-08	3.412E-08	9.428E-06	5.525E-06	4.813E-09	1.173E-08	3.493E-05
1.45	3.011E-06	5.482E-07	9.877E-06	9.350E-08	3.268E-08	9.306E-06	5.409E-06	4.628E-09	1.126E-08	3.521E-05
1.50	3.016E-06	5.409E-07	1.013E-05	8.998E-08	3.143E-08	9.199E-06	5.294E-06	4.471E-09	1.084E-08	3.545E-05
1.55	3.018E-06	5.373E-07	1.037E-05	8.296E-08	3.040E-08	9.106E-06	5.186E-06	4.377E-09	1.044E-08	3.567E-05
1.60	3.017E-06	5.324E-07	1.058E-05	7.640E-08	2.952E-08	9.016E-06	5.088E-06	4.222E-09	1.002E-08	3.589E-05
1.65	3.011E-06	5.221E-07	1.075E-05	7.068E-08	2.867E-08	8.919E-06	5.002E-06	4.120E-09	9.591E-09	3.612E-05
1.70	3.002E-06	5.052E-07	1.088E-05	6.690E-08	2.776E-08	8.813E-06	4.930E-06	4.023E-09	9.186E-09	3.636E-05
1.75	2.993E-06	4.844E-07	1.098E-05	6.542E-08	2.682E-08	8.706E-06	4.874E-06	3.922E-09	8.827E-09	3.661E-05
1.80	2.985E-06	4.642E-07	1.106E-05	6.723E-08	2.592E-08	8.608E-06	4.831E-06	3.813E-09	8.522E-09	3.683E-05
1.85	2.980E-06	4.481E-07	1.113E-05	6.891E-08	2.516E-08	8.525E-06	4.797E-06	3.696E-09	8.260E-09	3.702E-05
1.90	2.977E-06	4.373E-07	1.121E-05	7.037E-08	2.456E-08	8.455E-06	4.769E-06	3.579E-09	8.018E-09	3.718E-05
1.95	2.976E-06	4.306E-07	1.130E-05	7.148E-08	2.406E-08	8.394E-06	4.745E-06	3.472E-09	7.775E-09	3.731E-05
2.00	2.975E-06	4.260E-07	1.141E-05	7.238E-08	2.355E-08	8.337E-06	4.723E-06	3.381E-09	7.522E-09	3.742E-05
2.05	2.974E-06	4.223E-07	1.154E-05	7.320E-08	2.292E-08	8.283E-06	4.703E-06	3.306E-09	7.261E-09	3.752E-05
2.10	2.974E-06	4.189E-07	1.166E-05	7.403E-08	2.211E-08	8.233E-06	4.685E-06	3.239E-09	7.001E-09	3.759E-05
2.15	2.974E-06	4.157E-07	1.182E-05	7.489E-08	2.115E-08	8.186E-06	4.666E-06	3.171E-09	6.754E-09	3.766E-05
2.20	2.974E-06	4.126E-07	1.195E-05	7.565E-08	2.012E-08	8.135E-06	4.647E-06	3.096E-09	6.526E-09	3.773E-05
2.25	2.974E-06	4.096E-07	1.196E-05	7.633E-08	1.915E-08	8.073E-06	4.626E-06	3.013E-09	6.315E-09	3.781E-05
2.30	2.975E-06	4.066E-07	1.207E-05	7.633E-08	1.834E-08	7.995E-06	4.606E-06	2.929E-09	6.112E-09	3.790E-05
2.35	2.976E-06	4.037E-07	1.225E-05	7.706E-08	1.713E-08	7.904E-06	4.589E-06	2.853E-09	5.911E-09	3.802E-05
2.40	2.978E-06	4.010E-07	1.232E-05	7.766E-08	1.661E-08	7.864E-06	4.576E-06	2.791E-09	5.708E-09	3.813E-05
2.45	2.981E-06	3.988E-07	1.241E-05	7.864E-08	1.661E-08	7.717E-06	4.566E-06	2.746E-09	5.511E-09	3.823E-05
2.50	2.983E-06	3.972E-07	1.250E-05	8.065E-08	1.606E-08	7.637E-06	4.557E-06	2.712E-09	5.326E-09	3.832E-05
2.55	2.985E-06	3.964E-07	1.260E-05	8.149E-08	1.549E-08	7.501E-06	4.547E-06	2.680E-09	5.158E-09	3.840E-05
2.60	2.987E-06	3.964E-07	1.269E-05	8.498E-08	1.495E-08	7.501E-06	4.537E-06	2.642E-09	5.004E-09	3.847E-05
2.65	2.988E-06	3.967E-07	1.278E-05	8.288E-08	1.446E-08	7.438E-06	4.525E-06	2.591E-09	4.857E-09	3.855E-05
2.70	2.989E-06	3.968E-07	1.286E-05	8.418E-08	1.399E-08	7.378E-06	4.513E-06	2.526E-09	4.709E-09	3.862E-05
2.75	2.989E-06	3.962E-07	1.292E-05	8.560E-08	1.349E-08	7.327E-06	4.502E-06	2.452E-09	4.557E-09	3.868E-05
2.80	2.989E-06	3.951E-07	1.297E-05	8.709E-08	1.291E-08	7.289E-06	4.491E-06	2.378E-09	4.405E-09	3.874E-05
2.85	2.989E-06	3.939E-07	1.301E-05	8.858E-08	1.223E-08	7.265E-06	4.482E-06	2.307E-09	4.262E-09	3.878E-05
2.90	2.988E-06	3.930E-07	1.304E-05	9.127E-08	1.148E-08	7.251E-06	4.472E-06	2.238E-09	4.135E-09	3.882E-05
					1.069E-08	7.241E-06	4.463E-06	2.166E-09	4.024E-09	3.885E-05

(Appendix E.1, Continued)

2.95	2.988E-06	3.927E-07	1.307E-05	7.637E-08	9.227E-08	9.908E-09	7.232E-06	4.452E-06	2.086E-09	3.924E-09	3.889E-05
3.00	2.987E-06	3.928E-07	1.309E-05	7.544E-08	9.299E-08	9.176E-09	7.221E-06	4.441E-06	1.966E-09	3.826E-09	3.892E-05
3.05	2.986E-06	3.927E-07	1.312E-05	7.459E-08	9.350E-08	8.534E-09	7.209E-06	4.429E-06	1.902E-09	3.725E-09	3.896E-05
3.10	2.985E-06	3.920E-07	1.316E-05	7.378E-08	9.399E-08	7.994E-09	7.197E-06	4.417E-06	1.815E-09	3.621E-09	3.899E-05
3.15	2.983E-06	3.905E-07	1.320E-05	7.292E-08	9.463E-08	7.532E-09	7.184E-06	4.406E-06	1.744E-09	3.525E-09	3.901E-05
3.20	2.981E-06	3.883E-07	1.324E-05	7.202E-08	9.548E-08	7.100E-09	7.173E-06	4.395E-06	1.695E-09	3.441E-09	3.903E-05
3.25	2.980E-06	3.859E-07	1.328E-05	7.105E-08	9.649E-08	6.654E-09	7.163E-06	4.383E-06	1.669E-09	3.371E-09	3.905E-05
3.30	2.978E-06	3.838E-07	1.331E-05	7.011E-08	9.747E-08	6.179E-09	7.154E-06	4.371E-06	1.658E-09	3.309E-09	3.907E-05
3.35	2.977E-06	3.822E-07	1.334E-05	6.926E-08	9.834E-08	5.691E-09	7.147E-06	4.352E-06	1.655E-09	3.247E-09	3.910E-05
3.40	2.976E-06	3.813E-07	1.337E-05	6.850E-08	9.908E-08	5.219E-09	7.142E-06	4.344E-06	1.652E-09	3.179E-09	3.912E-05
3.45	2.976E-06	3.807E-07	1.340E-05	6.782E-08	9.980E-08	4.781E-09	7.136E-06	4.334E-06	1.652E-09	3.102E-09	3.914E-05
3.50	2.975E-06	3.803E-07	1.344E-05	6.717E-08	1.007E-07	4.375E-09	7.131E-06	4.306E-06	1.651E-09	3.019E-09	3.916E-05
3.55	2.974E-06	3.798E-07	1.347E-05	6.652E-08	1.019E-07	3.997E-09	7.125E-06	4.297E-06	1.664E-09	2.936E-09	3.917E-05
3.60	2.973E-06	3.792E-07	1.350E-05	6.583E-08	1.033E-07	3.644E-09	7.118E-06	4.286E-06	1.693E-09	2.860E-09	3.919E-05
3.65	2.972E-06	3.788E-07	1.353E-05	6.509E-08	1.047E-07	3.323E-09	7.112E-06	4.273E-06	1.736E-09	2.793E-09	3.921E-05
3.70	2.971E-06	3.787E-07	1.356E-05	6.431E-08	1.056E-07	3.046E-09	7.107E-06	4.255E-06	1.842E-09	2.738E-09	3.923E-05
3.75	2.971E-06	3.790E-07	1.359E-05	6.359E-08	1.061E-07	2.829E-09	7.105E-06	4.238E-06	1.842E-09	2.690E-09	3.926E-05
3.80	2.971E-06	3.797E-07	1.361E-05	6.294E-08	1.061E-07	2.670E-09	7.105E-06	4.225E-06	1.898E-09	2.645E-09	3.928E-05
3.85	2.971E-06	3.808E-07	1.363E-05	6.246E-08	1.060E-07	2.587E-09	7.107E-06	4.227E-06	1.955E-09	2.600E-09	3.928E-05
3.90	2.971E-06	3.819E-07	1.364E-05	6.203E-08	1.059E-07	2.517E-09	7.109E-06	4.232E-06	2.014E-09	2.554E-09	3.927E-05
Z	HCO	H2CO	O2	HO2	C3H2	C3H3	C3H4	HCCO	CH2CO	CO2	CAH2
0.00	-3.626E-10	6.403E-08	2.619E-05	-2.929E-09	3.721E-13	1.355E-09	2.587E-08	-9.048E-11	4.179E-08	1.645E-06	-4.118E-09
0.01	-3.109E-10	6.508E-08	2.603E-05	1.830E-09	-4.778E-12	1.376E-09	2.572E-08	-2.064E-10	4.286E-08	1.633E-06	-3.017E-09
0.02	-2.639E-10	6.613E-08	2.588E-05	6.952E-09	-1.022E-11	1.457E-09	2.547E-08	-3.514E-10	4.275E-08	1.625E-06	-1.799E-09
0.03	-2.473E-10	6.733E-08	2.582E-05	1.253E-08	-3.861E-11	1.465E-09	2.472E-08	-6.057E-10	4.323E-08	1.638E-06	-2.444E-10
0.04	-2.388E-10	6.889E-08	2.584E-05	1.743E-08	-9.965E-11	1.046E-09	2.367E-08	-8.892E-10	4.364E-08	1.659E-06	-1.058E-09
0.05	-2.278E-10	7.101E-08	2.590E-05	2.140E-08	-1.955E-10	6.228E-11	2.242E-08	-1.165E-09	4.395E-08	1.677E-06	1.627E-09
0.06	-3.115E-10	7.363E-08	2.596E-05	2.486E-08	-3.180E-10	2.115E-08	2.115E-08	-1.425E-09	4.419E-08	1.684E-06	1.128E-09
0.07	-3.538E-10	7.686E-08	2.602E-05	2.754E-08	-4.721E-10	3.275E-09	1.996E-08	-1.650E-09	4.435E-08	1.674E-06	-7.784E-10
0.08	-3.969E-10	8.065E-08	2.606E-05	2.958E-08	-6.520E-10	5.655E-09	1.903E-08	-1.820E-09	4.447E-08	1.637E-06	-4.446E-09
0.09	-4.370E-10	8.487E-08	2.603E-05	3.136E-08	-8.516E-10	8.313E-09	1.854E-08	-1.943E-09	4.458E-08	1.571E-06	-1.004E-08
0.10	-4.719E-10	8.934E-08	2.603E-05	3.308E-08	-1.065E-09	1.109E-08	1.865E-08	-2.025E-09	4.475E-08	1.475E-06	-1.762E-08
0.11	-5.010E-10	9.381E-08	2.599E-05	3.483E-08	-1.289E-09	1.386E-08	1.953E-08	-2.074E-09	4.503E-08	1.356E-06	-2.708E-08
0.12	-5.250E-10	9.804E-08	2.596E-05	3.666E-08	-1.517E-09	1.651E-08	2.132E-08	-2.101E-09	4.550E-08	1.223E-06	-5.046E-08
0.13	-5.453E-10	1.018E-07	2.596E-05	3.848E-08	-1.748E-09	1.900E-08	2.408E-08	-2.118E-09	4.620E-08	1.090E-06	-8.817E-08
0.14	-5.628E-10	1.049E-07	2.603E-05	4.009E-08	-1.978E-09	2.131E-08	2.783E-08	-2.130E-09	4.715E-08	9.717E-07	-6.341E-08
0.15	-5.761E-10	1.072E-07	2.618E-05	4.132E-08	-2.209E-09	2.349E-08	3.249E-08	-2.146E-09	4.837E-08	8.845E-07	-7.640E-08
0.16	-5.812E-10	1.086E-07	2.638E-05	4.204E-08	-2.443E-09	2.554E-08	3.794E-08	-2.172E-09	4.985E-08	8.407E-07	-8.883E-08
0.17	-5.718E-10	1.092E-07	2.664E-05	4.218E-08	-2.688E-09	2.744E-08	4.395E-08	-2.217E-09	5.155E-08	8.486E-07	-1.002E-07
0.18	-5.397E-10	1.089E-07	2.690E-05	4.178E-08	-2.956E-09	2.913E-08	5.032E-08	-2.291E-09	5.345E-08	9.113E-07	-1.100E-07
0.19	-4.773E-10	1.077E-07	2.715E-05	4.094E-08	-3.266E-09	3.057E-08	5.683E-08	-2.402E-09	5.548E-08	1.027E-06	-1.182E-07
0.20	-3.787E-10	1.056E-07	2.734E-05	3.978E-08	-3.640E-09	3.174E-08	6.365E-08	-2.558E-09	5.759E-08	1.190E-06	-1.249E-07
0.21	-2.412E-10	1.027E-07	2.745E-05	3.844E-08	-4.106E-09	3.277E-08	7.685E-08	-2.757E-09	5.973E-08	1.391E-06	-1.300E-07
0.22	-6.549E-11	9.905E-08	2.748E-05	3.699E-08	-4.691E-09	3.388E-08	8.985E-08	-2.994E-09	6.181E-08	1.622E-06	-1.340E-07
0.23	1.451E-10	9.482E-08	2.742E-05	3.551E-08	-5.420E-09	3.541E-08	8.307E-08	-3.246E-09	6.378E-08	1.874E-06	-1.369E-07
0.24	3.859E-10	9.016E-08	2.729E-05	3.400E-08	-6.308E-09	3.770E-08	9.005E-08	-3.485E-09	6.557E-08	2.138E-06	-1.387E-07
0.25	6.520E-10	8.523E-08	2.710E-05	3.249E-08	-7.360E-09	4.091E-08	9.741E-08	-3.657E-09	6.714E-08	2.407E-06	-1.393E-07
0.26	9.388E-10	8.023E-08	2.686E-05	3.100E-08	-8.564E-09	4.490E-08	1.050E-07	-3.756E-09	6.843E-08	2.675E-06	-1.381E-07
0.27	1.242E-09	7.532E-08	2.659E-05	2.955E-08	-9.891E-09	4.909E-08	1.050E-07	-3.756E-09	6.941E-08	2.933E-06	-1.346E-07
0.28	1.557E-09	7.062E-08	2.627E-05	2.819E-08	-1.129E-08	5.248E-08	1.197E-07	-3.460E-09	7.005E-08	3.176E-06	-1.283E-07
0.29	1.878E-09	6.622E-08	2.591E-05	2.696E-08	-1.270E-08	5.377E-08	1.254E-07	-3.019E-09	7.034E-08	3.397E-06	-1.186E-07
0.30	2.197E-09	6.217E-08	2.548E-05	2.588E-08	-1.402E-08	5.165E-08	1.292E-07	-2.375E-09	7.025E-08	3.591E-06	-1.055E-07

(Appendix E.1. Continued)

0.31	2.505E-09	5.847E-08	7.498E-05	2.495E-08	-1.515E-08	-4.510E-08	1.302E-07	-1.551E-09	6.978E-08	3.754E-06	-8.924E-08
0.32	2.795E-09	5.512E-08	4.43E-05	2.415E-08	-1.599E-08	-3.373E-08	1.283E-07	-5.944E-10	6.893E-08	3.883E-06	-7.014E-08
0.33	3.061E-09	5.210E-08	2.371E-05	2.343E-08	-1.641E-08	-1.793E-08	1.235E-07	4.286E-10	6.772E-08	3.980E-06	-4.886E-08
0.34	3.304E-09	4.934E-08	2.294E-05	2.272E-08	-1.633E-08	-1.100E-09	1.161E-07	1.442E-09	6.622E-08	4.045E-06	-2.602E-08
0.35	3.527E-09	4.680E-08	2.209E-05	2.200E-08	-1.566E-08	1.161E-09	1.069E-07	2.372E-09	6.450E-08	4.082E-06	-2.159E-08
0.36	3.737E-09	4.442E-08	2.119E-05	2.122E-08	-1.439E-08	4.160E-08	9.709E-08	3.157E-09	6.267E-08	4.099E-06	2.234E-08
0.37	3.941E-09	4.211E-08	2.025E-05	2.039E-08	-1.253E-08	5.926E-08	8.750E-08	3.756E-09	6.083E-08	4.103E-06	4.724E-08
0.38	4.147E-09	3.984E-08	1.930E-05	1.954E-08	-1.016E-08	7.333E-08	7.897E-08	4.156E-09	5.910E-08	4.103E-06	7.235E-08
0.39	4.357E-09	3.757E-08	1.836E-05	1.869E-08	-7.324E-08	8.324E-08	7.204E-08	4.371E-09	5.755E-08	4.110E-06	9.749E-08
0.40	4.572E-09	3.530E-08	1.743E-05	1.789E-08	-4.416E-09	8.181E-08	6.684E-08	4.434E-09	5.621E-07	4.131E-06	1.224E-07
0.41	4.786E-09	3.306E-08	1.651E-05	1.716E-08	-1.401E-09	9.187E-08	6.322E-08	4.391E-09	5.508E-08	4.172E-06	1.469E-07
0.42	4.994E-09	3.090E-08	1.562E-05	1.652E-08	-1.469E-09	9.236E-08	6.077E-08	4.290E-09	5.411E-08	4.237E-06	1.705E-07
0.43	5.186E-09	2.887E-08	1.476E-05	1.598E-08	-4.044E-09	8.169E-08	5.900E-08	4.172E-09	5.322E-06	4.322E-06	1.932E-07
0.44	5.357E-09	2.702E-08	1.392E-05	1.550E-08	-9.071E-08	5.742E-08	5.742E-08	4.065E-09	5.235E-08	4.423E-06	2.150E-07
0.45	5.502E-09	2.540E-08	1.313E-05	1.507E-08	-7.943E-09	8.995E-08	5.567E-08	3.985E-09	5.142E-08	4.528E-06	2.361E-07
0.46	5.617E-09	2.399E-08	1.239E-05	1.464E-08	-9.227E-09	8.961E-08	5.355E-08	3.933E-09	5.040E-08	4.630E-06	2.570E-07
0.47	5.703E-09	2.278E-08	1.172E-05	1.416E-08	-1.013E-08	8.966E-08	5.102E-08	3.903E-09	4.928E-08	4.719E-06	2.783E-07
0.48	5.795E-09	2.174E-08	1.112E-05	1.358E-08	-1.073E-08	8.992E-08	4.817E-08	3.886E-09	4.807E-08	4.790E-06	3.005E-07
0.49	5.811E-09	1.990E-08	1.059E-05	1.285E-08	-1.114E-08	8.922E-08	4.516E-08	3.872E-09	4.683E-08	4.841E-06	3.239E-07
0.50	5.815E-09	1.902E-08	1.012E-05	1.191E-08	-1.145E-08	9.042E-08	4.220E-08	3.854E-09	4.560E-08	4.875E-06	3.487E-07
0.51	5.815E-09	1.902E-08	1.012E-05	1.191E-08	-1.145E-08	9.042E-08	4.220E-08	3.854E-09	4.560E-08	4.875E-06	3.487E-07
0.52	5.815E-09	1.902E-08	1.012E-05	1.191E-08	-1.145E-08	9.042E-08	4.220E-08	3.854E-09	4.560E-08	4.875E-06	3.487E-07
0.53	5.815E-09	1.902E-08	1.012E-05	1.191E-08	-1.145E-08	9.042E-08	4.220E-08	3.854E-09	4.560E-08	4.875E-06	3.487E-07
0.54	5.815E-09	1.902E-08	1.012E-05	1.191E-08	-1.145E-08	9.042E-08	4.220E-08	3.854E-09	4.560E-08	4.875E-06	3.487E-07
0.55	5.815E-09	1.902E-08	1.012E-05	1.191E-08	-1.145E-08	9.042E-08	4.220E-08	3.854E-09	4.560E-08	4.875E-06	3.487E-07
0.56	5.837E-09	1.429E-08	7.605E-06	3.087E-09	1.377E-08	9.003E-08	3.153E-08	3.648E-09	3.983E-08	4.963E-06	4.824E-07
0.57	5.855E-09	1.338E-08	7.182E-06	1.820E-09	1.426E-08	9.001E-08	3.082E-08	3.613E-09	3.903E-08	5.028E-06	5.329E-07
0.58	5.872E-09	1.254E-08	6.776E-06	8.448E-10	1.475E-08	8.992E-08	3.020E-08	3.579E-09	3.819E-08	5.069E-06	5.562E-07
0.59	5.887E-09	1.179E-08	6.394E-06	1.812E-10	1.524E-08	8.968E-08	2.960E-08	3.544E-09	3.728E-08	5.117E-06	5.780E-07
0.60	5.896E-09	1.114E-08	6.041E-06	1.956E-10	1.574E-08	8.921E-08	2.896E-08	3.505E-09	3.629E-08	5.171E-06	5.984E-07
0.61	5.900E-09	1.058E-08	5.718E-06	-3.437E-10	1.629E-08	8.848E-08	2.827E-08	3.460E-09	3.524E-08	5.235E-06	6.175E-07
0.62	5.901E-09	1.010E-08	5.420E-06	-3.380E-10	1.689E-08	8.745E-08	2.753E-08	3.411E-09	3.413E-08	5.310E-06	6.354E-07
0.63	5.901E-09	9.680E-09	5.138E-06	-2.524E-10	1.756E-08	8.614E-08	2.674E-08	3.356E-09	3.300E-08	5.397E-06	6.524E-07
0.64	5.905E-09	9.295E-09	4.866E-06	-1.468E-10	1.830E-08	8.458E-08	2.593E-08	3.297E-09	3.187E-08	5.494E-06	6.687E-07
0.65	5.913E-09	8.929E-09	4.598E-06	-5.891E-11	1.909E-08	8.282E-08	2.511E-08	3.237E-09	3.077E-08	5.599E-06	6.844E-07
0.66	5.926E-09	8.573E-09	4.334E-06	-4.201E-11	1.989E-08	8.090E-08	2.429E-08	3.177E-09	2.972E-08	5.706E-06	6.993E-07
0.67	5.941E-09	8.228E-09	4.075E-06	1.932E-11	2.065E-08	7.886E-08	2.347E-08	3.121E-09	2.872E-08	5.809E-06	7.130E-07
0.68	5.954E-09	7.900E-09	3.827E-06	2.235E-11	2.133E-08	7.674E-08	2.267E-08	3.071E-09	2.778E-08	5.903E-06	7.253E-07
0.69	5.956E-09	7.601E-09	3.594E-06	1.540E-11	2.186E-08	7.461E-08	2.189E-08	3.028E-09	2.690E-08	5.984E-06	7.357E-07
0.70	5.941E-09	7.338E-09	3.382E-06	6.675E-12	2.223E-08	7.249E-08	2.113E-08	2.991E-09	2.605E-08	6.049E-06	7.438E-07
0.71	5.902E-09	7.113E-09	3.193E-06	6.264E-13	2.240E-08	7.044E-08	2.039E-08	2.959E-09	2.524E-08	6.099E-06	7.495E-07
0.72	5.837E-09	6.921E-09	3.023E-06	-1.743E-13	2.238E-08	6.847E-08	1.967E-08	2.930E-09	2.446E-08	6.134E-06	7.529E-07
0.73	5.745E-09	6.750E-09	2.869E-06	-1.565E-12	2.219E-08	6.659E-08	1.894E-08	2.901E-09	2.372E-08	6.158E-06	7.543E-07
0.74	5.632E-09	6.583E-09	2.726E-06	-5.642E-13	2.187E-08	6.478E-08	1.821E-08	2.870E-09	2.300E-08	6.174E-06	7.541E-07
0.75	5.504E-09	6.406E-09	2.589E-06	8.396E-14	2.145E-08	6.302E-08	1.745E-08	2.836E-09	2.233E-08	6.184E-06	7.528E-07
0.76	5.370E-09	6.207E-09	2.455E-06	1.438E-13	2.099E-08	6.127E-08	1.666E-08	2.797E-09	2.170E-08	6.189E-06	7.507E-07
0.77	5.237E-09	5.981E-09	2.327E-06	3.243E-15	2.050E-08	5.950E-08	1.586E-08	2.755E-09	2.112E-08	6.190E-06	7.482E-07
0.78	5.110E-09	5.731E-09	2.205E-06	7.34E-16	2.000E-08	5.771E-08	1.507E-08	2.711E-09	2.058E-08	6.187E-06	7.454E-07
0.79	4.992E-09	5.465E-09	2.095E-06	3.608E-17	1.949E-08	5.595E-08	1.432E-08	2.666E-09	2.010E-08	6.181E-06	7.425E-07
0.80	4.880E-09	5.193E-09	1.999E-06	-8.251E-17	1.896E-08	5.430E-08	1.362E-08	2.624E-09	1.965E-08	6.174E-06	7.395E-07
0.81	4.774E-09	4.927E-09	1.919E-06	-8.465E-18	1.840E-08	5.285E-08	1.300E-08	2.583E-09	1.923E-08	6.165E-06	7.364E-07

(Appendix E.1. Continued)

0.82	4.667E-09	4.676E-09	1.856E-06	-6.953E-18	1.780E-08	5.169E-08	1.246E-08	2.546E-09	1.885E-08	6.157E-05	7.333E-07
0.83	4.557E-09	4.447E-09	1.805E-06	-9.245E-18	1.717E-08	5.089E-08	1.201E-08	2.512E-09	1.848E-08	6.151E-06	7.303E-07
0.84	4.443E-09	4.244E-09	1.765E-06	0.000E+00	1.650E-08	5.044E-08	1.162E-08	2.491E-09	1.813E-08	6.148E-06	7.273E-07
0.85	4.324E-09	4.068E-09	1.733E-06	0.000E+00	1.582E-08	5.028E-08	1.128E-08	2.452E-09	1.779E-08	6.150E-06	7.244E-07
0.86	4.201E-09	3.916E-09	1.704E-06	0.000E+00	1.516E-08	5.024E-08	1.098E-08	2.435E-09	1.746E-08	6.156E-06	7.217E-07
0.87	4.076E-09	3.785E-09	1.678E-06	0.000E+00	1.453E-08	5.012E-08	1.068E-08	2.399E-09	1.714E-08	6.166E-06	7.194E-07
0.88	3.950E-09	3.671E-09	1.652E-06	0.000E+00	1.399E-08	4.973E-08	1.040E-08	2.375E-09	1.683E-08	6.178E-06	7.175E-07
0.89	3.822E-09	3.568E-09	1.624E-06	0.000E+00	1.352E-08	4.888E-08	1.011E-08	2.353E-09	1.653E-08	6.192E-06	7.159E-07
0.90	3.690E-09	3.470E-09	1.595E-06	0.000E+00	1.311E-08	4.749E-08	9.836E-09	2.333E-09	1.624E-08	6.206E-06	7.150E-07
0.91	3.550E-09	3.372E-09	1.563E-06	0.000E+00	1.277E-08	4.598E-08	9.566E-09	2.314E-09	1.596E-08	6.218E-06	7.145E-07
0.92	3.400E-09	3.270E-09	1.525E-06	0.000E+00	1.248E-08	4.327E-08	9.306E-09	2.295E-09	1.567E-08	6.237E-06	7.144E-07
0.93	3.239E-09	3.161E-09	1.482E-06	0.000E+00	1.223E-08	4.076E-08	9.059E-09	2.276E-09	1.539E-08	6.243E-06	7.145E-07
0.94	3.066E-09	3.043E-09	1.433E-06	0.000E+00	1.199E-08	3.826E-08	8.823E-09	2.257E-09	1.510E-08	6.245E-06	7.143E-07
0.95	2.886E-09	2.919E-09	1.375E-06	0.000E+00	1.176E-08	3.598E-08	8.596E-09	2.235E-09	1.479E-08	6.245E-06	7.143E-07
0.96	2.702E-09	2.791E-09	1.310E-06	0.000E+00	1.154E-08	3.404E-08	8.377E-09	2.210E-09	1.447E-08	6.244E-06	7.135E-07
0.97	2.522E-09	2.663E-09	1.238E-06	0.000E+00	1.133E-08	3.249E-08	8.160E-09	2.182E-09	1.413E-08	6.242E-06	7.121E-07
0.98	2.352E-09	2.538E-09	1.161E-06	0.000E+00	1.113E-08	3.132E-08	7.945E-09	2.150E-09	1.379E-08	6.238E-06	7.098E-07
0.99	2.195E-09	2.419E-09	1.081E-06	0.000E+00	1.093E-08	3.045E-08	7.729E-09	2.115E-09	1.343E-08	6.235E-06	7.068E-07
1.00	2.057E-09	2.310E-09	1.000E-06	0.000E+00	1.075E-08	2.977E-08	7.512E-09	2.078E-09	1.308E-08	6.232E-06	7.032E-07
1.01	1.936E-09	2.211E-09	9.217E-07	0.000E+00	1.058E-08	2.920E-08	7.297E-09	2.040E-09	1.274E-08	6.232E-06	6.991E-07
1.02	1.833E-09	2.123E-09	8.473E-07	0.000E+00	1.041E-08	2.857E-08	7.085E-09	2.002E-09	1.241E-08	6.233E-06	6.946E-07
1.03	1.746E-09	2.047E-09	7.792E-07	0.000E+00	1.023E-08	2.815E-08	6.881E-09	1.964E-09	1.211E-08	6.236E-06	6.899E-07
1.04	1.670E-09	1.982E-09	7.183E-07	0.000E+00	1.003E-08	2.763E-08	6.686E-09	1.928E-09	1.183E-08	6.239E-06	6.849E-07
1.05	1.603E-09	1.928E-09	6.650E-07	0.000E+00	9.806E-09	2.714E-08	6.503E-09	1.894E-09	1.157E-08	6.243E-06	6.796E-07
1.06	1.544E-09	1.882E-09	6.190E-07	0.000E+00	9.555E-09	2.670E-08	6.335E-09	1.862E-09	1.132E-08	6.247E-06	6.739E-07
1.07	1.489E-09	1.841E-09	5.794E-07	0.000E+00	9.276E-09	2.630E-08	6.184E-09	1.833E-09	1.109E-08	6.249E-06	6.679E-07
1.08	1.438E-09	1.802E-09	5.447E-07	0.000E+00	8.974E-09	2.595E-08	6.048E-09	1.806E-09	1.087E-08	6.250E-06	6.617E-07
1.09	1.390E-09	1.762E-09	5.136E-07	0.000E+00	8.653E-09	2.560E-08	5.925E-09	1.781E-09	1.066E-08	6.250E-06	6.553E-07
1.10	1.344E-09	1.715E-09	4.842E-07	0.000E+00	8.323E-09	2.524E-08	5.825E-09	1.758E-09	1.045E-08	6.248E-06	6.489E-07
1.11	1.301E-09	1.661E-09	4.553E-07	0.000E+00	7.991E-09	2.482E-08	5.734E-09	1.738E-09	1.024E-08	6.245E-06	6.429E-07
1.12	1.260E-09	1.598E-09	4.262E-07	0.000E+00	7.664E-09	2.433E-08	5.656E-09	1.721E-09	1.004E-08	6.241E-06	6.374E-07
1.13	1.222E-09	1.526E-09	3.963E-07	0.000E+00	7.351E-09	2.375E-08	5.587E-09	1.704E-09	9.851E-09	6.236E-06	6.323E-07
1.14	1.188E-09	1.447E-09	3.659E-07	0.000E+00	7.053E-09	2.310E-08	5.524E-09	1.689E-09	9.672E-09	6.229E-06	6.278E-07
1.15	1.159E-09	1.367E-09	3.373E-07	0.000E+00	6.779E-09	2.243E-08	5.468E-09	1.673E-09	9.513E-09	6.221E-06	6.233E-07
1.16	1.135E-09	1.289E-09	3.112E-07	0.000E+00	6.528E-09	2.176E-08	5.419E-09	1.656E-09	9.370E-09	6.214E-06	6.187E-07
1.20	9.934E-10	1.142E-09	2.677E-07	0.000E+00	6.159E-09	1.959E-08	5.258E-09	1.526E-09	8.686E-09	6.184E-06	6.041E-07
1.25	9.046E-10	9.639E-10	2.132E-07	0.000E+00	5.465E-09	1.801E-08	5.103E-09	1.417E-09	7.905E-09	6.147E-06	5.825E-07
1.30	8.398E-10	8.238E-10	1.838E-07	0.000E+00	5.001E-09	1.685E-08	5.002E-09	1.322E-09	7.212E-09	6.111E-06	5.628E-07
1.35	7.896E-10	7.124E-10	1.636E-07	0.000E+00	4.723E-09	1.606E-08	4.914E-09	1.238E-09	6.613E-09	6.081E-06	5.442E-07
1.40	7.519E-10	6.190E-10	1.452E-07	0.000E+00	4.560E-09	1.552E-08	4.819E-09	1.151E-09	6.115E-09	6.059E-06	5.257E-07
1.45	7.237E-10	5.362E-10	1.272E-07	0.000E+00	4.454E-09	1.501E-08	4.720E-09	1.095E-09	5.715E-09	6.041E-06	5.068E-07
1.50	6.998E-10	4.618E-10	1.101E-07	0.000E+00	4.369E-09	1.440E-08	4.623E-09	1.010E-09	5.393E-09	6.024E-06	4.877E-07
1.55	6.762E-10	3.941E-10	9.443E-08	0.000E+00	4.289E-09	1.365E-08	4.533E-09	9.393E-10	5.124E-09	6.004E-06	4.689E-07
1.60	6.516E-10	3.440E-10	8.023E-08	0.000E+00	4.209E-09	1.283E-08	4.451E-09	8.750E-10	4.889E-09	5.977E-06	4.509E-07
1.65	6.281E-10	3.029E-10	6.798E-08	0.000E+00	4.126E-09	1.207E-08	4.374E-09	8.164E-10	4.678E-09	5.944E-06	4.344E-07
1.70	6.077E-10	2.722E-10	5.834E-08	0.000E+00	4.041E-09	1.143E-08	4.303E-09	7.587E-10	4.489E-09	5.907E-06	4.196E-07
1.75	5.912E-10	2.484E-10	5.163E-08	0.000E+00	3.959E-09	1.095E-08	4.237E-09	6.963E-10	4.318E-09	5.870E-06	4.063E-07
1.80	5.776E-10	2.281E-10	4.742E-08	0.000E+00	3.879E-09	1.059E-08	4.177E-09	6.265E-10	4.163E-09	5.835E-06	3.942E-07
1.85	5.653E-10	2.082E-10	4.477E-08	0.000E+00	3.802E-09	1.026E-08	4.123E-09	5.522E-10	4.021E-09	5.804E-06	3.833E-07
1.90	5.531E-10	1.875E-10	4.272E-08	0.000E+00	3.727E-09	9.928E-09	4.070E-09	4.791E-10	3.889E-09	5.777E-06	3.736E-07
1.95	5.406E-10	1.663E-10	4.066E-08	0.000E+00	3.652E-09	9.568E-09	4.017E-09	4.136E-10	3.768E-09	5.752E-06	3.649E-07
2.00	5.278E-10	1.461E-10	3.845E-08	0.000E+00	3.578E-09	9.208E-09	3.963E-09	3.596E-10	3.661E-09	5.729E-06	3.571E-07

(Appendix E.1. Continued)

2.05	5.151E-10	1.285E-10	3.623E-08	0.000E+00	3.505E-09	8.888E-09	3.907E-09	3.177E-10	3.566E-09	5.707E-06	3.500E-07
2.10	5.021E-10	1.144E-10	3.417E-08	0.000E+00	3.434E-09	8.635E-09	3.851E-09	2.862E-10	3.481E-09	5.684E-06	3.433E-07
2.15	4.887E-10	1.031E-10	3.231E-08	0.000E+00	3.365E-09	8.453E-09	3.795E-09	2.616E-10	3.402E-09	5.661E-06	3.369E-07
2.20	4.747E-10	9.385E-11	3.063E-08	0.000E+00	3.298E-09	8.324E-09	3.739E-09	2.401E-10	3.323E-09	5.639E-06	3.308E-07
2.25	4.603E-10	8.552E-11	2.904E-08	0.000E+00	3.234E-09	8.226E-09	3.685E-09	2.189E-10	3.243E-09	5.619E-06	3.249E-07
2.30	4.463E-10	7.776E-11	2.750E-08	0.000E+00	3.173E-09	8.139E-09	3.635E-09	1.965E-10	3.165E-09	5.602E-06	3.191E-07
2.35	4.333E-10	7.072E-11	2.599E-08	0.000E+00	3.114E-09	8.051E-09	3.594E-09	1.752E-10	3.092E-09	5.588E-06	3.132E-07
2.40	4.218E-10	6.465E-11	2.457E-08	0.000E+00	3.055E-09	7.954E-09	3.565E-09	1.468E-10	3.028E-09	5.574E-06	3.069E-07
2.50	4.038E-10	5.564E-11	2.333E-08	0.000E+00	2.996E-09	7.844E-09	3.541E-09	1.191E-10	2.973E-09	5.560E-06	3.004E-07
2.55	3.965E-10	5.228E-11	2.155E-08	0.000E+00	2.936E-09	7.726E-09	3.518E-09	8.966E-11	2.926E-09	5.545E-06	2.942E-07
2.60	3.896E-10	4.931E-11	2.091E-08	0.000E+00	2.876E-09	7.610E-09	3.539E-09	5.971E-11	2.926E-09	5.545E-06	2.942E-07
2.65	3.823E-10	4.648E-11	2.027E-08	0.000E+00	2.814E-09	7.507E-09	3.539E-09	3.278E-11	2.884E-09	5.528E-06	2.898E-07
2.70	3.741E-10	4.357E-11	1.951E-08	0.000E+00	2.750E-09	7.423E-09	3.539E-09	1.256E-11	2.847E-09	5.510E-06	2.838E-07
2.75	3.650E-10	4.047E-11	1.858E-08	0.000E+00	2.682E-09	7.350E-09	3.540E-09	8.731E-13	2.812E-09	5.493E-06	2.797E-07
2.80	3.554E-10	3.720E-11	1.747E-08	0.000E+00	2.613E-09	7.280E-09	3.545E-09	2.778E-12	2.744E-09	5.479E-06	2.761E-07
2.85	3.461E-10	3.398E-11	1.616E-08	0.000E+00	2.547E-09	7.206E-09	3.555E-09	3.181E-12	2.710E-09	5.465E-06	2.725E-07
2.90	3.373E-10	3.106E-11	1.463E-08	0.000E+00	2.485E-09	7.129E-09	3.570E-09	1.051E-12	2.677E-09	5.443E-06	2.689E-07
2.95	3.293E-10	2.864E-11	1.286E-08	0.000E+00	2.429E-09	7.057E-09	3.587E-09	2.973E-15	2.645E-09	5.434E-06	2.615E-07
3.00	3.214E-10	2.672E-11	1.089E-08	0.000E+00	2.378E-09	6.997E-09	3.606E-09	2.376E-13	2.616E-09	5.425E-06	2.581E-07
3.05	3.136E-10	2.520E-11	8.852E-09	0.000E+00	2.327E-09	6.950E-09	3.626E-09	8.046E-14	2.589E-09	5.418E-06	2.552E-07
3.10	3.056E-10	2.393E-11	6.922E-09	0.000E+00	2.274E-09	6.910E-09	3.648E-09	2.913E-14	2.565E-09	5.412E-06	2.527E-07
3.15	2.978E-10	2.279E-11	5.264E-09	0.000E+00	2.217E-09	6.871E-09	3.672E-09	1.030E-15	2.542E-09	5.406E-06	2.507E-07
3.20	2.905E-10	2.171E-11	3.965E-09	0.000E+00	2.159E-09	6.834E-09	3.698E-09	8.705E-17	2.520E-09	5.402E-06	2.490E-07
3.25	2.839E-10	2.064E-11	3.013E-09	0.000E+00	2.101E-09	6.803E-09	3.724E-09	1.037E-17	2.500E-09	5.399E-06	2.474E-07
3.30	2.780E-10	1.958E-11	2.327E-09	0.000E+00	2.047E-09	6.774E-09	3.750E-09	9.572E-18	2.500E-09	5.399E-06	2.474E-07
3.35	2.725E-10	1.853E-11	1.809E-09	0.000E+00	1.996E-09	6.738E-09	3.776E-09	0.000E+00	2.468E-09	5.398E-06	2.458E-07
3.40	2.671E-10	1.752E-11	1.390E-09	0.000E+00	1.946E-09	6.688E-09	3.802E-09	0.000E+00	2.456E-09	5.397E-06	2.443E-07
3.45	2.615E-10	1.660E-11	1.043E-09	0.000E+00	1.896E-09	6.630E-09	3.830E-09	0.000E+00	2.456E-09	5.397E-06	2.429E-07
3.50	2.557E-10	1.578E-11	7.637E-10	0.000E+00	1.843E-09	6.588E-09	3.861E-09	0.000E+00	2.435E-09	5.397E-06	2.415E-07
3.55	2.495E-10	1.506E-11	5.529E-10	0.000E+00	1.789E-09	6.580E-09	3.894E-09	0.000E+00	2.425E-09	5.396E-06	2.400E-07
3.60	2.432E-10	1.440E-11	4.015E-10	0.000E+00	1.734E-09	6.604E-09	3.929E-09	0.000E+00	2.416E-09	5.395E-06	2.365E-07
3.65	2.371E-10	1.379E-11	2.940E-10	0.000E+00	1.679E-09	6.628E-09	3.964E-09	0.000E+00	2.406E-09	5.393E-06	2.348E-07
3.70	2.316E-10	1.321E-11	2.160E-10	0.000E+00	1.626E-09	6.623E-09	3.999E-09	0.000E+00	2.397E-09	5.392E-06	2.330E-07
3.75	2.272E-10	1.267E-11	1.612E-10	0.000E+00	1.572E-09	6.573E-09	4.034E-09	0.000E+00	2.388E-09	5.390E-06	2.313E-07
3.80	2.241E-10	1.218E-11	1.238E-10	0.000E+00	1.520E-09	6.504E-09	4.068E-09	0.000E+00	2.381E-09	5.389E-06	2.291E-07
3.85	2.223E-10	1.176E-11	1.068E-10	0.000E+00	1.468E-09	6.438E-09	4.101E-09	0.000E+00	2.375E-09	5.389E-06	2.264E-07
3.90	2.207E-10	1.135E-11	9.300E-11	0.000E+00	1.417E-09	6.427E-09	4.128E-09	0.000E+00	2.371E-09	5.389E-06	2.229E-07
Z	C4H3	C4H4	C4H5	C4H6	C5H2	C5H3	C5H4	C5H5	C5H6	C6H2	C6H4
0.00	5.922E-11	3.466E-10	8.858E-11	5.554E-10	1.844E-12	2.454E-12	7.667E-12	1.333E-10	2.423E-10	1.337E-11	2.090E-11
0.01	7.553E-11	3.892E-10	7.950E-11	5.599E-10	2.095E-12	2.825E-12	4.732E-12	1.505E-10	2.551E-10	1.436E-11	2.369E-11
0.02	9.620E-11	4.216E-10	7.002E-11	5.682E-10	2.439E-12	3.278E-12	5.841E-13	1.670E-10	2.659E-10	1.592E-11	2.731E-11
0.03	1.384E-10	4.102E-10	6.511E-11	5.834E-10	3.361E-12	3.900E-12	1.434E-11	1.783E-10	2.578E-10	2.033E-11	3.577E-11
0.04	1.903E-10	3.821E-10	7.189E-11	5.876E-10	4.639E-12	4.897E-12	6.578E-11	1.853E-10	2.346E-10	2.681E-11	4.791E-11
0.05	2.447E-10	3.497E-10	9.362E-11	5.720E-10	6.086E-12	7.586E-12	1.675E-10	1.889E-10	2.016E-10	3.607E-11	6.328E-11
0.06	2.970E-10	3.096E-10	1.236E-10	5.477E-10	7.542E-12	1.190E-11	3.135E-10	1.907E-10	1.677E-10	5.015E-11	8.153E-11
0.07	3.440E-10	2.645E-10	1.627E-10	5.125E-10	8.942E-12	1.791E-11	5.133E-10	1.909E-10	1.345E-10	7.008E-11	1.028E-10
0.08	3.800E-10	2.150E-10	2.052E-10	4.756E-10	1.015E-11	2.472E-11	7.625E-10	1.910E-10	1.098E-10	9.725E-11	1.268E-10
0.09	4.040E-10	1.504E-10	2.427E-10	4.553E-10	1.118E-11	3.044E-11	1.049E-09	1.919E-10	1.098E-10	1.333E-10	1.533E-10
0.10	4.158E-10	5.964E-10	2.658E-10	4.738E-10	1.219E-11	3.233E-11	1.358E-09	1.943E-10	1.086E-10	1.794E-10	1.827E-10
0.11	4.161E-10	6.600E-11	2.664E-10	5.542E-10	1.347E-11	2.786E-11	1.667E-09	1.981E-10	1.411E-10	2.361E-10	2.151E-10

(Appendix E.1. Continued)

0.12	4.061E-10	-2.315E-10	-2.381E-10	7.192E-10	-1.541E-11	-1.656E-11	-1.954E-09	2.032E-10	2.016E-10	-3.041E-10	-2.503E-10
0.13	3.879E-10	-4.332E-10	-1.788E-10	9.844E-10	-1.847E-11	-1.900E-12	-2.195E-09	2.087E-10	2.939E-10	3.844E-10	-2.877E-10
0.14	3.627E-10	-6.556E-10	-9.127E-11	1.355E-09	-2.305E-11	7.015E-12	-2.371E-09	2.135E-10	4.218E-10	-4.799E-10	-3.262E-10
0.15	3.317E-10	-8.724E-10	1.751E-11	1.823E-09	-2.942E-11	-4.917E-12	-2.467E-09	2.167E-10	5.888E-10	-5.963E-10	-3.639E-10
0.16	-2.960E-10	-1.048E-09	1.376E-10	2.368E-09	-3.764E-11	-5.729E-11	-2.478E-09	2.178E-10	7.979E-10	-7.423E-10	-3.992E-10
0.17	-2.564E-10	-1.143E-09	2.582E-10	2.958E-09	-4.765E-11	-1.705E-10	-2.407E-09	2.170E-10	1.050E-09	-9.294E-10	-4.306E-10
0.18	-2.140E-10	-1.118E-09	3.697E-10	3.554E-09	-5.943E-11	-3.608E-10	-2.263E-09	2.152E-10	1.345E-09	-1.169E-09	-4.585E-10
0.19	-1.701E-10	-9.392E-10	4.655E-10	4.117E-09	-7.321E-11	-6.343E-10	-2.062E-09	2.144E-10	1.679E-09	-1.472E-09	-4.851E-10
0.20	-1.256E-10	-5.839E-10	5.426E-10	4.611E-09	-8.970E-11	-9.836E-10	-1.821E-09	2.168E-10	2.046E-09	-1.846E-09	-5.154E-10
0.21	-8.128E-11	-4.204E-11	6.016E-10	5.009E-09	-1.103E-10	-1.387E-09	-1.557E-09	2.250E-10	2.441E-09	-2.299E-09	-5.566E-10
0.22	-3.715E-11	6.837E-10	6.455E-10	5.294E-09	-1.368E-10	-1.808E-09	-1.281E-09	2.411E-10	2.853E-09	-2.841E-09	-6.166E-10
0.23	7.597E-12	1.580E-09	6.789E-10	5.462E-09	-1.714E-10	-2.207E-09	-9.994E-10	2.667E-10	3.274E-09	-3.495E-09	-7.020E-10
0.24	5.448E-11	2.625E-09	7.062E-10	5.522E-09	-2.162E-10	-2.542E-09	-7.122E-10	3.022E-10	3.693E-09	-4.307E-09	-8.154E-10
0.25	1.054E-10	3.793E-09	7.308E-10	5.489E-09	-2.722E-10	-2.779E-09	-4.129E-10	3.470E-10	4.096E-09	-5.350E-09	-9.534E-10
0.26	1.621E-10	5.059E-09	7.308E-10	5.386E-09	-3.393E-10	-2.901E-09	-9.277E-11	3.996E-10	4.472E-09	-6.724E-09	-1.106E-09
0.27	2.258E-10	6.395E-09	7.787E-10	5.236E-09	-4.157E-10	-2.904E-09	-2.571E-10	4.580E-10	4.804E-09	-8.544E-09	-1.255E-09
0.28	2.968E-10	7.777E-09	8.024E-10	5.061E-09	-4.977E-10	-2.801E-09	-6.424E-10	5.201E-10	5.077E-09	-1.092E-08	-1.381E-09
0.29	3.747E-10	9.178E-09	8.246E-10	4.879E-09	-5.802E-10	-2.615E-09	-1.063E-09	5.838E-10	5.277E-09	-1.391E-08	-1.460E-09
0.30	4.581E-10	1.057E-08	8.443E-10	4.701E-09	-6.571E-10	-2.373E-09	-1.515E-09	6.476E-10	5.393E-09	-1.752E-08	-1.477E-09
0.31	5.450E-10	1.192E-08	8.605E-10	4.532E-09	-7.219E-10	-2.106E-09	-1.986E-09	7.110E-10	5.420E-09	-2.166E-08	-1.421E-09
0.32	6.334E-10	1.319E-08	8.722E-10	4.373E-09	-7.682E-10	-1.837E-09	-2.464E-09	7.738E-10	5.208E-09	-3.075E-08	-1.100E-09
0.33	7.213E-10	1.436E-08	8.791E-10	4.219E-09	-7.908E-10	-1.584E-09	-2.935E-09	8.369E-10	5.356E-09	-2.616E-08	-1.292E-09
0.34	8.070E-10	1.537E-08	8.807E-10	4.067E-09	-7.859E-10	-1.355E-09	-3.390E-09	9.011E-10	4.989E-09	-3.514E-08	-8.614E-10
0.35	8.894E-10	1.622E-08	8.772E-10	3.911E-09	-7.519E-10	-1.152E-09	-3.823E-09	9.679E-10	4.713E-09	-3.905E-08	-5.962E-10
0.36	9.680E-10	1.691E-08	8.689E-10	3.749E-09	-6.895E-10	-9.663E-10	-4.235E-09	1.038E-09	4.398E-09	-4.222E-08	-3.204E-10
0.37	1.043E-09	1.744E-08	8.566E-10	3.583E-09	-6.018E-10	-7.822E-10	-4.630E-09	1.113E-09	4.062E-09	-4.448E-08	-4.253E-11
0.38	1.115E-09	1.785E-08	8.410E-10	3.413E-09	-4.942E-10	-5.786E-10	-5.013E-09	1.192E-09	3.721E-09	-4.573E-08	-2.391E-11
0.39	1.185E-09	1.820E-08	8.235E-10	3.243E-09	-3.733E-10	-3.306E-10	-5.391E-09	1.275E-09	3.387E-09	-4.596E-08	5.361E-10
0.40	1.256E-09	1.852E-08	8.051E-10	3.076E-09	-2.467E-10	-1.436E-11	-5.764E-09	1.361E-09	3.072E-09	-4.519E-08	8.673E-10
0.41	1.327E-09	1.884E-08	7.871E-10	2.912E-09	-1.214E-10	3.885E-10	-6.126E-09	1.447E-09	2.782E-09	-4.352E-08	1.253E-09
0.42	1.399E-09	1.916E-08	7.701E-10	2.748E-09	-3.302E-12	8.862E-10	-6.467E-09	1.532E-09	2.524E-09	-4.104E-08	1.707E-09
0.43	1.471E-09	1.946E-08	7.547E-10	2.579E-09	-1.039E-10	1.473E-09	-6.770E-09	1.612E-09	2.300E-09	-3.787E-08	2.234E-09
0.44	1.541E-09	1.970E-08	7.408E-10	2.402E-09	1.987E-10	2.128E-09	-7.016E-09	1.686E-09	2.108E-09	-3.416E-08	2.824E-09
0.45	1.604E-09	1.981E-08	7.282E-10	2.212E-09	2.815E-10	2.818E-09	-7.185E-09	1.750E-09	1.948E-09	-3.009E-08	3.450E-09
0.46	1.659E-09	1.972E-08	7.164E-10	2.010E-09	3.542E-10	3.500E-09	-7.265E-09	1.803E-09	1.814E-09	-2.584E-08	4.074E-09
0.47	1.702E-09	1.941E-08	7.050E-10	1.798E-09	4.195E-10	4.130E-09	-7.249E-09	1.843E-09	1.702E-09	-2.159E-08	4.652E-09
0.48	1.733E-09	1.886E-08	6.937E-10	1.581E-09	4.800E-10	4.671E-09	-7.139E-09	1.871E-09	1.603E-09	-1.744E-08	5.141E-09
0.49	1.750E-09	1.810E-08	6.822E-10	1.369E-09	5.377E-10	5.095E-09	-6.945E-09	1.885E-09	1.514E-09	-1.344E-08	5.506E-09
0.50	1.758E-09	1.718E-08	6.708E-10	1.168E-09	5.939E-10	5.391E-09	-6.684E-09	1.887E-09	1.429E-09	-9.477E-09	5.728E-09
0.51	1.759E-09	1.618E-08	6.593E-10	9.876E-10	6.491E-10	5.562E-09	-6.376E-09	1.876E-09	1.345E-09	-5.389E-09	5.802E-09
0.52	1.757E-09	1.515E-08	6.480E-10	8.311E-10	7.033E-10	5.624E-09	-6.043E-09	1.854E-09	1.263E-09	-9.331E-10	5.743E-09
0.53	1.755E-09	1.417E-08	6.369E-10	7.008E-10	7.564E-10	5.602E-09	-5.704E-09	1.821E-09	1.181E-09	-4.117E-09	5.574E-09
0.54	1.754E-09	1.326E-08	6.259E-10	5.959E-10	8.081E-10	5.521E-09	-5.375E-09	1.777E-09	1.103E-09	-9.905E-09	5.331E-09
0.55	1.757E-09	1.242E-08	6.147E-10	4.515E-10	9.060E-10	5.406E-09	-5.066E-09	1.724E-09	1.028E-09	-9.600E-10	5.047E-09
0.56	1.760E-09	1.166E-08	6.032E-10	4.046E-10	9.519E-10	5.275E-09	-4.784E-09	1.662E-09	9.600E-10	-2.358E-08	4.755E-09
0.57	1.764E-09	1.094E-08	5.912E-10	4.046E-10	9.519E-10	5.143E-09	-4.529E-09	1.594E-09	8.981E-10	-3.104E-08	4.478E-09
0.58	1.766E-09	1.026E-08	5.784E-10	3.697E-10	1.0357E-10	5.014E-09	-4.297E-09	1.519E-09	8.429E-10	-3.847E-08	4.233E-09
0.59	1.764E-09	9.590E-09	5.652E-10	3.441E-10	1.037E-09	4.891E-09	-4.083E-09	1.441E-09	7.939E-10	-4.555E-08	4.027E-09
0.60	1.758E-09	8.946E-09	5.515E-10	3.255E-10	1.077E-09	4.770E-09	-3.879E-09	1.362E-09	7.508E-10	-5.201E-08	3.859E-09
0.61	1.746E-09	8.331E-09	5.379E-10	3.120E-10	1.116E-09	4.650E-09	-3.680E-09	1.282E-09	7.086E-10	-6.772E-08	3.725E-09
0.62	1.730E-09	7.759E-09	5.246E-10	3.019E-10	1.153E-09	4.527E-09	-3.479E-09	1.206E-09	6.795E-10	-5.772E-08	3.618E-09
0.63	1.710E-09	7.243E-09	5.119E-10	2.939E-10	1.190E-09	4.401E-09	-3.274E-09	1.133E-09	6.504E-10	-6.704E-08	3.529E-09
0.64	1.688E-09	6.787E-09	4.999E-10	2.868E-10	1.227E-09	4.271E-09	-3.066E-09	1.066E-09	6.252E-10	-7.097E-08	3.452E-09

(Appendix E.1. Continued)

0.65	1.664E-09	6.393E-09	4.887E-10	2.793E-10	1.265E-09	4.140E-09	2.857E-09	1.007E-09	6.035E-10	7.466E-08	3.382E-09
0.66	1.640E-09	6.054E-09	4.780E-10	2.708E-10	1.303E-09	4.012E-09	2.654E-09	9.546E-10	5.847E-10	7.827E-08	3.316E-09
0.67	1.615E-09	5.760E-09	4.678E-10	2.608E-10	1.343E-09	3.889E-09	2.463E-09	9.108E-10	5.683E-10	8.186E-08	3.251E-09
0.68	1.592E-09	5.503E-09	4.577E-10	2.492E-10	1.384E-09	3.775E-09	2.291E-09	8.747E-10	5.536E-10	8.543E-08	3.188E-09
0.69	1.569E-09	5.273E-09	4.477E-10	2.363E-10	1.428E-09	3.672E-09	2.141E-09	8.452E-10	5.403E-10	8.887E-08	3.125E-09
0.70	1.547E-09	5.069E-09	4.376E-10	2.266E-10	1.475E-09	3.580E-09	2.017E-09	8.210E-10	5.280E-10	9.207E-08	3.062E-09
0.71	1.525E-09	4.886E-09	4.272E-10	2.088E-10	1.525E-09	3.498E-09	1.918E-09	8.002E-10	5.164E-10	9.488E-08	2.999E-09
0.72	1.504E-09	4.724E-09	4.163E-10	1.955E-10	1.580E-09	3.424E-09	1.841E-09	7.811E-10	5.056E-10	9.722E-08	2.934E-09
0.73	1.483E-09	4.579E-09	4.046E-10	1.833E-10	1.637E-09	3.354E-09	1.783E-09	7.623E-10	4.956E-10	9.900E-08	2.867E-09
0.74	1.462E-09	4.449E-09	3.921E-10	1.727E-10	1.697E-09	3.287E-09	1.738E-09	7.426E-10	4.855E-10	1.003E-07	2.797E-09
0.75	1.439E-09	4.328E-09	3.784E-10	1.637E-10	1.756E-09	3.219E-09	1.701E-09	7.213E-10	4.782E-10	1.010E-07	2.725E-09
0.76	1.415E-09	4.210E-09	3.637E-10	1.563E-10	1.810E-09	3.149E-09	1.670E-09	6.983E-10	4.707E-10	1.014E-07	2.650E-09
0.77	1.389E-09	4.093E-09	3.480E-10	1.502E-10	1.856E-09	3.079E-09	1.641E-09	6.737E-10	4.637E-10	1.015E-07	2.575E-09
0.78	1.361E-09	3.975E-09	3.318E-10	1.453E-10	1.899E-09	3.008E-09	1.615E-09	6.480E-10	4.570E-10	1.015E-07	2.499E-09
0.79	1.332E-09	3.857E-09	3.155E-10	1.412E-10	1.904E-09	2.938E-09	1.590E-09	6.215E-10	4.505E-10	1.015E-07	2.424E-09
0.80	1.300E-09	3.742E-09	2.997E-10	1.377E-10	1.899E-09	2.870E-09	1.568E-09	5.949E-10	4.440E-10	1.015E-07	2.350E-09
0.81	1.268E-09	3.633E-09	2.848E-10	1.346E-10	1.873E-09	2.805E-09	1.548E-09	5.687E-10	4.376E-10	1.014E-07	2.275E-09
0.82	1.237E-09	3.533E-09	2.711E-10	1.318E-10	1.828E-09	2.743E-09	1.532E-09	5.435E-10	4.311E-10	1.015E-07	2.200E-09
0.83	1.206E-09	3.444E-09	2.586E-10	1.290E-10	1.768E-09	2.682E-09	1.518E-09	5.198E-10	4.247E-10	1.015E-07	2.124E-09
0.84	1.177E-09	3.363E-09	2.471E-10	1.264E-10	1.696E-09	2.621E-09	1.507E-09	4.978E-10	4.185E-10	1.016E-07	2.046E-09
0.85	1.151E-09	3.290E-09	2.362E-10	1.237E-10	1.619E-09	2.560E-09	1.497E-09	4.780E-10	4.125E-10	1.017E-07	1.967E-09
0.86	1.127E-09	3.221E-09	2.255E-10	1.209E-10	1.541E-09	2.499E-09	1.488E-09	4.604E-10	4.068E-10	1.019E-07	1.890E-09
0.87	1.106E-09	3.153E-09	2.146E-10	1.180E-10	1.468E-09	2.437E-09	1.478E-09	4.448E-10	4.012E-10	1.022E-07	1.817E-09
0.88	1.086E-09	3.084E-09	2.034E-10	1.151E-10	1.400E-09	2.375E-09	1.468E-09	4.310E-10	3.957E-10	1.025E-07	1.751E-09
0.89	1.068E-09	3.013E-09	1.919E-10	1.122E-10	1.340E-09	2.316E-09	1.457E-09	4.187E-10	3.902E-10	1.030E-07	1.694E-09
0.90	1.051E-09	2.938E-09	1.803E-10	1.093E-10	1.287E-09	2.261E-09	1.445E-09	4.073E-10	3.845E-10	1.035E-07	1.648E-09
0.91	1.035E-09	2.861E-09	1.689E-10	1.066E-10	1.238E-09	2.210E-09	1.433E-09	3.963E-10	3.785E-10	1.039E-07	1.612E-09
0.92	1.020E-09	2.782E-09	1.582E-10	1.040E-10	1.192E-09	2.166E-09	1.420E-09	3.853E-10	3.722E-10	1.042E-07	1.585E-09
0.93	1.006E-09	2.702E-09	1.483E-10	1.015E-10	1.149E-09	2.126E-09	1.407E-09	3.740E-10	3.655E-10	1.043E-07	1.565E-09
0.94	9.923E-10	2.623E-09	1.395E-10	9.909E-11	1.107E-09	2.092E-09	1.395E-09	3.621E-10	3.584E-10	1.041E-07	1.547E-09
0.95	9.795E-10	2.545E-09	1.315E-10	9.659E-11	1.067E-09	2.062E-09	1.384E-09	3.496E-10	3.511E-10	1.036E-07	1.529E-09
0.96	9.676E-10	2.468E-09	1.241E-10	9.400E-11	1.028E-09	2.034E-09	1.374E-09	3.366E-10	3.438E-10	1.028E-07	1.510E-09
0.97	9.565E-10	2.393E-09	1.171E-10	9.130E-11	9.923E-10	2.008E-09	1.364E-09	3.229E-10	3.366E-10	1.018E-07	1.487E-09
0.98	9.463E-10	2.320E-09	1.100E-10	8.852E-11	9.584E-10	1.983E-09	1.356E-09	3.087E-10	3.297E-10	1.007E-07	1.461E-09
1.00	9.286E-10	2.176E-09	9.512E-11	8.297E-11	8.962E-10	1.932E-09	1.340E-09	2.778E-10	3.233E-10	9.945E-08	1.432E-09
1.01	9.210E-10	2.103E-09	8.729E-11	8.034E-11	8.702E-10	1.906E-09	1.333E-09	2.607E-10	3.174E-10	9.826E-08	1.402E-09
1.02	9.139E-10	2.029E-09	7.946E-11	7.788E-11	8.390E-10	1.880E-09	1.326E-09	2.420E-10	3.120E-10	9.715E-08	1.372E-09
1.03	9.071E-10	1.954E-09	7.190E-11	7.561E-11	8.121E-10	1.855E-09	1.319E-09	2.218E-10	3.071E-10	9.613E-08	1.343E-09
1.04	9.004E-10	1.880E-09	6.487E-11	7.352E-11	7.867E-10	1.831E-09	1.313E-09	2.003E-10	3.026E-10	9.519E-08	1.316E-09
1.05	8.936E-10	1.806E-09	5.861E-11	7.159E-11	7.631E-10	1.806E-09	1.306E-09	1.780E-10	2.985E-10	9.430E-08	1.290E-09
1.06	8.865E-10	1.737E-09	5.322E-11	6.978E-11	7.418E-10	1.783E-09	1.300E-09	1.555E-10	2.945E-10	9.342E-08	1.265E-09
1.07	8.792E-10	1.672E-09	4.874E-11	6.807E-11	7.217E-10	1.759E-09	1.294E-09	1.339E-10	2.907E-10	9.249E-08	1.240E-09
1.08	8.716E-10	1.614E-09	4.510E-11	6.646E-11	7.058E-10	1.735E-09	1.289E-09	1.139E-10	2.870E-10	9.150E-08	1.216E-09
1.09	8.639E-10	1.563E-09	4.217E-11	6.494E-11	6.908E-10	1.710E-09	1.284E-09	1.030E-10	2.834E-10	9.043E-08	1.193E-09
1.10	8.561E-10	1.519E-09	3.980E-11	6.352E-11	6.702E-10	1.684E-09	1.278E-09	9.625E-11	2.799E-10	8.926E-08	1.169E-09
1.11	8.482E-10	1.478E-09	3.784E-11	6.225E-11	6.647E-10	1.657E-09	1.274E-09	9.135E-11	2.766E-10	8.801E-08	1.145E-09
1.12	8.400E-10	1.441E-09	3.615E-11	6.115E-11	6.528E-10	1.629E-09	1.269E-09	8.982E-11	2.734E-10	8.669E-08	1.122E-09
1.13	8.315E-10	1.404E-09	3.469E-11	6.033E-11	6.413E-10	1.601E-09	1.264E-09	8.726E-11	2.703E-10	8.533E-08	1.099E-09
1.14	8.224E-10	1.365E-09	3.336E-11	5.953E-11	6.300E-10	1.601E-09	1.264E-09	8.526E-11	2.674E-10	8.395E-08	1.077E-09
1.15	8.130E-10	1.325E-09	3.217E-11	5.902E-11	6.185E-10	1.545E-09	1.254E-09	8.271E-11	2.645E-10	8.257E-08	1.057E-09
1.16	8.036E-10	1.286E-09	3.110E-11	5.862E-11	6.068E-10	1.519E-09	1.248E-09	8.065E-11	2.588E-10	8.126E-08	1.037E-09
											1.018E-09

(Appendix E.1. Continued)

1.20	7.713E-10	1.172E-09	2.569E-11	5.196E-11	5.683E-10	1.444E-09	1.220E-09	2.495E-11	2.434E-10	7.690E-08	8.892E-10
1.25	7.354E-10	1.060E-09	2.310E-11	4.667E-11	5.388E-10	1.348E-09	1.193E-09	7.271E-12	2.274E-10	7.227E-08	7.847E-10
1.30	7.028E-10	9.825E-10	2.206E-11	4.170E-11	5.142E-10	1.260E-09	1.166E-09	1.261E-13	2.113E-10	6.843E-08	7.048E-10
1.35	6.741E-10	9.236E-10	2.135E-11	3.675E-11	4.927E-10	1.180E-09	1.140E-09	-1.639E-12	1.952E-10	6.527E-08	6.516E-10
1.40	6.483E-10	8.722E-10	2.052E-11	3.166E-11	4.738E-10	1.109E-09	1.114E-09	-1.406E-12	1.798E-10	6.257E-08	6.198E-10
1.45	6.243E-10	8.229E-10	1.957E-11	2.646E-11	4.574E-10	1.049E-09	1.090E-09	-7.449E-13	1.657E-10	6.010E-08	6.010E-10
1.50	6.017E-10	7.751E-10	1.868E-11	2.133E-11	4.431E-10	1.000E-09	1.067E-09	-2.652E-13	1.528E-10	5.766E-08	5.879E-10
1.55	5.808E-10	7.317E-10	1.792E-11	1.658E-11	4.298E-10	9.615E-10	1.045E-09	-5.561E-15	1.409E-10	5.518E-08	5.769E-10
1.60	5.622E-10	6.955E-10	1.730E-11	1.255E-11	4.167E-10	9.311E-10	1.023E-09	6.803E-14	1.298E-10	5.262E-08	5.668E-10
1.65	5.464E-10	6.679E-10	1.676E-11	9.498E-12	4.032E-10	9.056E-10	1.002E-09	3.283E-14	1.194E-10	5.006E-08	5.577E-10
1.70	5.329E-10	6.478E-10	1.624E-11	7.425E-12	3.895E-10	8.826E-10	9.807E-10	-5.476E-15	1.100E-10	4.755E-08	5.494E-10
1.75	5.209E-10	6.326E-10	1.570E-11	5.113E-12	3.762E-10	8.610E-10	9.595E-10	-8.186E-16	1.019E-10	4.513E-08	5.417E-10
1.80	5.093E-10	6.198E-10	1.515E-11	3.230E-12	3.640E-10	8.407E-10	9.386E-10	-5.889E-16	9.513E-11	4.282E-08	5.345E-10
1.85	4.974E-10	6.083E-10	1.459E-11	4.502E-12	3.532E-10	8.216E-10	9.184E-10	-8.174E-18	8.959E-11	4.062E-08	5.277E-10
1.90	4.851E-10	5.978E-10	1.407E-11	3.831E-12	3.436E-10	8.036E-10	8.990E-10	3.239E-17	8.495E-11	3.858E-08	5.213E-10
1.95	4.729E-10	5.886E-10	1.359E-11	3.284E-12	3.348E-10	7.861E-10	8.806E-10	0.000E+00	8.083E-11	3.675E-08	5.151E-10
2.00	4.615E-10	5.810E-10	1.314E-11	2.970E-12	3.264E-10	7.678E-10	8.630E-10	0.000E+00	7.685E-11	3.521E-08	5.092E-10
2.05	4.514E-10	5.746E-10	1.271E-11	2.927E-12	3.183E-10	7.478E-10	8.459E-10	0.000E+00	7.267E-11	3.394E-08	5.033E-10
2.10	4.424E-10	5.688E-10	1.229E-11	3.075E-12	3.102E-10	7.254E-10	8.291E-10	0.000E+00	6.813E-11	3.293E-08	4.977E-10
2.15	4.342E-10	5.633E-10	1.189E-11	3.274E-12	3.021E-10	7.015E-10	8.123E-10	0.000E+00	6.339E-11	3.206E-08	4.924E-10
2.20	4.266E-10	5.578E-10	1.153E-11	3.408E-12	2.938E-10	6.776E-10	7.953E-10	0.000E+00	5.894E-11	3.125E-08	4.873E-10
2.25	4.196E-10	5.525E-10	1.119E-11	3.437E-12	2.852E-10	6.555E-10	7.782E-10	0.000E+00	5.538E-11	3.047E-08	4.824E-10
2.30	4.134E-10	5.474E-10	1.087E-11	3.399E-12	2.765E-10	6.363E-10	7.614E-10	0.000E+00	5.318E-11	2.965E-08	4.778E-10
2.35	4.080E-10	5.423E-10	1.058E-11	3.368E-12	2.679E-10	6.202E-10	7.449E-10	0.000E+00	5.243E-11	2.885E-08	4.733E-10
2.40	4.029E-10	5.367E-10	1.030E-11	3.416E-12	2.597E-10	6.062E-10	7.289E-10	0.000E+00	5.293E-11	2.804E-08	4.685E-10
2.45	3.979E-10	5.302E-10	1.003E-11	3.588E-12	2.522E-10	5.932E-10	7.134E-10	0.000E+00	5.427E-11	2.725E-08	4.628E-10
2.50	3.926E-10	5.229E-10	9.758E-12	3.896E-12	2.453E-10	5.805E-10	6.982E-10	0.000E+00	5.606E-11	2.648E-08	4.557E-10
2.55	3.873E-10	5.153E-10	9.472E-12	4.332E-12	2.389E-10	5.678E-10	6.835E-10	0.000E+00	5.809E-11	2.574E-08	4.476E-10
2.60	3.821E-10	5.087E-10	9.169E-12	4.874E-12	2.324E-10	5.553E-10	6.692E-10	0.000E+00	6.023E-11	2.504E-08	4.395E-10
2.65	3.774E-10	5.040E-10	8.855E-12	5.493E-12	2.257E-10	5.430E-10	6.552E-10	0.000E+00	6.248E-11	2.440E-08	4.329E-10
2.70	3.732E-10	5.016E-10	8.540E-12	6.129E-12	2.186E-10	5.310E-10	6.414E-10	0.000E+00	6.482E-11	2.380E-08	4.290E-10
2.75	3.691E-10	5.013E-10	8.233E-12	6.709E-12	2.114E-10	5.192E-10	6.276E-10	0.000E+00	6.722E-11	2.325E-08	4.276E-10
2.80	3.652E-10	5.026E-10	7.943E-12	7.176E-12	2.043E-10	5.075E-10	6.137E-10	0.000E+00	6.966E-11	2.272E-08	4.280E-10
2.85	3.615E-10	5.047E-10	7.674E-12	7.541E-12	1.976E-10	4.957E-10	5.997E-10	0.000E+00	7.213E-11	2.223E-08	4.290E-10
2.90	3.580E-10	5.066E-10	7.424E-12	7.893E-12	1.911E-10	4.837E-10	5.856E-10	0.000E+00	7.465E-11	2.178E-08	4.298E-10
2.95	3.545E-10	5.078E-10	7.188E-12	8.357E-12	1.848E-10	4.715E-10	5.713E-10	0.000E+00	7.720E-11	2.138E-08	4.305E-10
3.00	3.510E-10	5.081E-10	6.960E-12	9.010E-12	1.784E-10	4.593E-10	5.570E-10	0.000E+00	7.973E-11	2.102E-08	4.312E-10
3.05	3.473E-10	5.080E-10	6.736E-12	9.832E-12	1.720E-10	4.475E-10	5.427E-10	0.000E+00	8.215E-11	2.070E-08	4.322E-10
3.10	3.435E-10	5.084E-10	6.510E-12	1.072E-11	1.654E-10	4.363E-10	5.285E-10	0.000E+00	8.438E-11	2.039E-08	4.334E-10
3.15	3.398E-10	5.099E-10	6.279E-12	1.156E-11	1.588E-10	4.256E-10	5.143E-10	0.000E+00	8.638E-11	2.010E-08	4.348E-10
3.20	3.363E-10	5.126E-10	6.042E-12	1.223E-11	1.522E-10	4.155E-10	5.003E-10	0.000E+00	8.819E-11	1.981E-08	4.365E-10
3.25	3.329E-10	5.163E-10	5.800E-12	1.268E-11	1.455E-10	4.058E-10	4.863E-10	0.000E+00	9.001E-11	1.953E-08	4.382E-10
3.30	3.294E-10	5.207E-10	5.559E-12	1.294E-11	1.389E-10	3.966E-10	4.725E-10	0.000E+00	9.213E-11	1.926E-08	4.398E-10
3.35	3.258E-10	5.261E-10	5.324E-12	1.311E-11	1.324E-10	3.875E-10	4.587E-10	0.000E+00	9.489E-11	1.900E-08	4.413E-10
3.40	3.221E-10	5.331E-10	5.092E-12	1.339E-11	1.261E-10	3.785E-10	4.448E-10	0.000E+00	9.848E-11	1.874E-08	4.424E-10
3.45	3.187E-10	5.416E-10	4.860E-12	1.403E-11	1.199E-10	3.693E-10	4.306E-10	0.000E+00	1.029E-10	1.849E-08	4.436E-10
3.50	3.130E-10	5.508E-10	4.627E-12	1.518E-11	1.138E-10	3.599E-10	4.161E-10	0.000E+00	1.078E-10	1.825E-08	4.450E-10
3.55	3.130E-10	5.590E-10	4.400E-12	1.681E-11	1.078E-10	3.504E-10	4.014E-10	0.000E+00	1.130E-10	1.801E-08	4.469E-10
3.60	3.074E-10	5.641E-10	4.188E-12	1.872E-11	1.019E-10	3.409E-10	3.868E-10	0.000E+00	1.182E-10	1.779E-08	4.489E-10
3.65	3.074E-10	5.659E-10	4.062E-12	2.062E-11	9.608E-11	3.313E-10	3.726E-10	0.000E+00	1.233E-10	1.758E-08	4.509E-10
3.70	3.043E-10	5.653E-10	3.828E-12	2.231E-11	9.034E-11	3.215E-10	3.588E-10	0.000E+00	1.282E-10	1.739E-08	4.524E-10
3.75	3.013E-10	5.669E-10	3.675E-12	2.388E-11	8.470E-11	3.118E-10	3.456E-10	0.000E+00	1.332E-10	1.721E-08	4.539E-10

(Appendix E.1. Cont.Included)

3.80	2.985E-10	5.727E-10	3.531E-12	2.546E-11	7.918E-11	3.026E-10	3.329E-10	0.000E+00	1.385E-10	1.704E-08	4.555E-10
3.85	2.963E-10	5.884E-10	3.391E-12	2.751E-11	7.396E-11	2.946E-10	3.210E-10	0.000E+00	1.447E-10	1.689E-08	4.582E-10
3.90	2.944E-10	6.063E-10	3.253E-12	2.973E-11	6.883E-11	2.870E-10	3.093E-10	0.000E+00	1.512E-10	1.674E-08	4.611E-10
Z	C6H5	C6H6	C8H2	C8H6	C10H2						
0.00	0.000E+00	5.903E-10	0.000E+00	0.000E+00	0.000E+00						
0.01	5.320E-13	6.021E-10	0.000E+00	5.751E-14	0.000E+00						
0.02	1.374E-12	6.131E-10	0.000E+00	1.381E-13	0.000E+00						
0.03	-3.100E-13	6.203E-10	-1.585E-18	7.570E-18	0.000E+00						
0.04	-7.124E-12	6.262E-10	5.145E-17	3.534E-13	0.000E+00						
0.05	-1.962E-11	6.323E-10	1.751E-16	-1.304E-12	2.058E-19						
0.06	-3.495E-11	6.385E-10	-2.997E-15	-2.807E-12	-2.255E-18						
0.07	-5.355E-11	6.455E-10	-2.746E-15	-5.005E-12	-3.866E-18						
0.08	-7.315E-11	6.535E-10	8.957E-15	-7.948E-12	-5.121E-18						
0.09	-9.075E-11	6.619E-10	2.900E-14	-1.164E-11	4.312E-17						
0.10	-1.034E-10	6.703E-10	3.629E-14	-1.605E-11	1.518E-16						
0.11	-1.087E-10	6.783E-10	-2.112E-15	-2.110E-11	-1.059E-15						
0.12	-1.044E-10	6.863E-10	-1.116E-13	-2.664E-11	-8.132E-16						
0.13	-9.001E-11	6.956E-10	-2.826E-13	-3.250E-11	3.859E-15						
0.14	-6.615E-11	7.055E-10	-4.441E-13	-3.843E-11	1.067E-14						
0.15	-3.488E-11	7.281E-10	-4.513E-13	-4.422E-11	1.038E-14						
0.16	8.045E-13	7.579E-10	-9.813E-14	-4.969E-11	-8.808E-15						
0.17	3.736E-11	8.010E-10	8.656E-13	-5.478E-11	-5.205E-14						
0.18	7.139E-11	8.600E-10	2.578E-12	-5.964E-11	-1.074E-13						
0.19	1.002E-10	9.362E-10	4.903E-12	-6.455E-11	-1.390E-13						
0.20	1.219E-10	1.030E-09	7.302E-12	-6.993E-11	-9.033E-14						
0.21	1.361E-10	1.141E-09	8.767E-12	-7.610E-11	1.018E-13						
0.22	1.433E-10	1.270E-09	7.836E-12	-8.311E-11	4.936E-13						
0.23	1.447E-10	1.416E-09	2.696E-12	-9.048E-11	1.070E-12						
0.24	1.421E-10	1.581E-09	-8.654E-12	-9.712E-11	1.694E-12						
0.25	1.372E-10	1.764E-09	-2.821E-11	-1.013E-10	2.091E-12						
0.26	1.315E-10	1.966E-09	-5.774E-11	-1.007E-10	1.876E-12						
0.27	1.260E-10	2.183E-09	-9.870E-11	-9.339E-11	6.115E-13						
0.28	1.212E-10	2.413E-09	-1.522E-10	-7.744E-11	-2.103E-12						
0.29	1.173E-10	2.650E-09	-2.188E-10	-5.207E-11	-6.550E-12						
0.30	1.141E-10	2.890E-09	-2.987E-10	-1.762E-11	-1.284E-11						
0.31	1.115E-10	3.127E-09	-3.914E-10	2.434E-11	-2.086E-11						
0.32	1.092E-10	3.359E-09	-4.950E-10	7.126E-11	-3.036E-11						
0.33	1.069E-10	3.586E-09	-6.067E-10	1.201E-10	-4.098E-11						
0.34	1.045E-10	3.808E-09	-7.220E-10	1.677E-10	-5.238E-11						
0.35	1.020E-10	4.026E-09	-8.355E-10	2.115E-10	-6.426E-11						
0.36	9.931E-11	4.237E-09	-9.413E-10	2.496E-10	-7.633E-11						
0.37	9.657E-11	4.435E-09	-1.034E-09	2.812E-10	-8.829E-11						
0.38	9.378E-11	4.611E-09	-1.111E-09	3.062E-10	-9.978E-11						
0.39	9.098E-11	4.750E-09	-1.173E-09	3.249E-10	-1.103E-10						
0.40	8.820E-11	4.839E-09	-1.225E-09	3.381E-10	-1.194E-10						
0.41	8.548E-11	4.865E-09	-1.275E-09	3.466E-10	-1.265E-10						
0.42	8.284E-11	4.822E-09	-1.336E-09	3.509E-10	-1.311E-10						
0.43	8.029E-11	4.709E-09	-1.419E-09	3.515E-10	-1.328E-10						
0.44	7.784E-11	4.533E-09	-1.534E-09	3.486E-10	-1.315E-10						
0.45	7.551E-11	4.306E-09	-1.683E-09	3.422E-10	-1.274E-10						
0.46	7.332E-11	4.043E-09	-1.861E-09	3.325E-10	-1.206E-10						

(Appendix E.1. Continued)

0.47 7.128E-11 3.759E-09 2.050E-09 3.196E-10 -1.114E-10
0.48 6.940E-11 3.466E-09 2.230E-09 3.037E-10 -1.001E-10
0.49 6.769E-11 3.172E-09 2.372E-09 2.854E-10 -8.708E-11
0.50 6.611E-11 2.881E-09 2.450E-09 2.654E-10 -7.251E-11
0.51 6.465E-11 2.597E-09 2.443E-09 2.445E-10 -5.671E-11
0.52 6.325E-11 2.320E-09 2.340E-09 2.236E-10 -3.995E-11
0.53 6.186E-11 2.054E-09 2.141E-09 2.035E-10 -2.253E-11
0.54 6.043E-11 1.802E-09 1.853E-09 1.850E-10 -4.761E-12
0.55 5.892E-11 1.569E-09 1.492E-09 1.685E-10 1.313E-11
0.56 5.733E-11 1.360E-09 1.075E-09 1.544E-10 3.100E-11
0.57 5.568E-11 1.180E-09 6.152E-10 1.425E-10 4.879E-11
0.58 5.401E-11 1.032E-09 1.217E-10 1.329E-10 6.657E-11
0.59 5.236E-11 9.128E-10 4.011E-10 1.251E-10 8.445E-11
0.60 5.078E-11 8.207E-10 9.515E-10 1.189E-10 1.026E-10
0.61 4.931E-11 7.502E-10 1.526E-09 1.138E-10 1.213E-10
0.62 4.795E-11 6.954E-10 2.119E-09 1.094E-10 1.406E-10
0.63 4.669E-11 6.510E-10 2.715E-09 1.055E-10 1.607E-10
0.64 4.551E-11 6.129E-10 3.295E-09 1.019E-10 1.818E-10
0.65 4.435E-11 5.786E-10 3.838E-09 9.819E-11 2.040E-10
0.66 4.319E-11 5.468E-10 4.323E-09 9.442E-11 2.272E-10
0.67 4.199E-11 5.176E-10 4.734E-09 9.052E-11 2.513E-10
0.68 4.074E-11 4.913E-10 5.065E-09 8.653E-11 2.762E-10
0.69 3.945E-11 4.683E-10 5.316E-09 8.255E-11 3.015E-10
0.70 3.815E-11 4.486E-10 5.497E-09 7.872E-11 3.271E-10
0.71 3.685E-11 4.321E-10 5.622E-09 7.517E-11 3.525E-10
0.72 3.560E-11 4.181E-10 5.705E-09 7.200E-11 3.778E-10
0.73 3.441E-11 4.062E-10 5.760E-09 6.928E-11 4.028E-10
0.74 3.329E-11 3.955E-10 5.794E-09 6.700E-11 4.276E-10
0.75 3.222E-11 3.856E-10 5.813E-09 6.512E-11 4.520E-10
0.76 3.118E-11 3.762E-10 5.821E-09 6.351E-11 4.759E-10
0.77 3.015E-11 3.670E-10 5.817E-09 6.205E-11 4.987E-10
0.78 2.911E-11 3.579E-10 5.804E-09 6.060E-11 5.198E-10
0.79 2.805E-11 3.485E-10 5.783E-09 5.904E-11 5.384E-10
0.80 2.695E-11 3.388E-10 5.756E-09 5.730E-11 5.538E-10
0.81 2.584E-11 3.294E-10 5.727E-09 5.538E-11 5.655E-10
0.82 2.473E-11 3.173E-10 5.698E-09 5.332E-11 5.734E-10
0.83 2.365E-11 3.053E-10 5.672E-09 5.121E-11 5.777E-10
0.84 2.262E-11 2.927E-10 5.647E-09 4.917E-11 5.790E-10
0.85 2.167E-11 2.797E-10 5.624E-09 4.726E-11 5.781E-10
0.86 2.078E-11 2.668E-10 5.602E-09 4.557E-11 5.760E-10
0.87 1.995E-11 2.546E-10 5.579E-09 4.408E-11 5.735E-10
0.88 1.919E-11 2.436E-10 5.555E-09 4.278E-11 5.711E-10
0.89 1.846E-11 2.340E-10 5.529E-09 4.162E-11 5.691E-10
0.90 1.777E-11 2.259E-10 5.502E-09 4.051E-11 5.679E-10
0.91 1.710E-11 2.195E-10 5.475E-09 3.943E-11 5.672E-10
0.92 1.644E-11 2.143E-10 5.447E-09 3.833E-11 5.671E-10
0.93 1.579E-11 2.101E-10 5.418E-09 3.721E-11 5.674E-10
0.94 1.514E-11 2.067E-10 5.388E-09 3.607E-11 5.680E-10
0.95 1.448E-11 2.036E-10 5.356E-09 3.495E-11 5.686E-10
0.96 1.380E-11 2.008E-10 5.321E-09 3.385E-11 5.692E-10
0.97 1.308E-11 1.981E-10 5.283E-09 3.279E-11 5.695E-10
0.98 1.231E-11 1.955E-10 5.241E-09 3.177E-11 5.693E-10
0.99 1.149E-11 1.929E-10 5.196E-09 3.079E-11 5.683E-10

(Appendix E.1. Continued)

1.00	1.059E-11	1.904E-10	5.150E-09	2.982E-11	5.662E-10
1.01	9.611E-12	1.881E-10	5.105E-09	2.888E-11	5.629E-10
1.02	8.535E-12	1.859E-10	5.062E-09	2.797E-11	5.584E-10
1.03	7.369E-12	1.839E-10	5.022E-09	2.708E-11	5.527E-10
1.04	6.137E-12	1.821E-10	4.987E-09	2.623E-11	5.460E-10
1.05	4.878E-12	1.804E-10	4.955E-09	2.543E-11	5.382E-10
1.06	3.650E-12	1.788E-10	4.924E-09	2.469E-11	5.296E-10
1.07	2.522E-12	1.771E-10	4.894E-09	2.401E-11	5.202E-10
1.08	1.561E-12	1.754E-10	4.860E-09	2.339E-11	5.099E-10
1.09	8.104E-13	1.735E-10	4.822E-09	2.282E-11	4.986E-10
1.10	2.859E-13	1.714E-10	4.776E-09	2.227E-11	4.864E-10
1.11	-2.889E-14	1.691E-10	4.720E-09	2.175E-11	4.730E-10
1.12	-1.682E-13	1.668E-10	4.654E-09	2.124E-11	4.586E-10
1.13	-1.884E-13	1.644E-10	4.577E-09	2.073E-11	4.433E-10
1.14	-1.464E-13	1.621E-10	4.489E-09	2.023E-11	4.272E-10
1.15	-8.613E-14	1.602E-10	4.393E-09	1.976E-11	4.111E-10
1.16	-1.840E-14	1.585E-10	4.293E-09	1.932E-11	3.952E-10
1.20	-4.343E-13	1.549E-10	3.969E-09	1.777E-11	3.647E-10
1.25	-4.426E-13	1.496E-10	3.634E-09	1.629E-11	3.186E-10
1.30	-2.072E-13	1.451E-10	3.349E-09	1.524E-11	2.833E-10
1.35	-2.058E-14	1.417E-10	3.118E-09	1.453E-11	2.576E-10
1.40	3.655E-14	1.391E-10	2.926E-09	1.405E-11	2.380E-10
1.45	1.731E-14	1.370E-10	2.751E-09	1.370E-11	2.211E-10
1.50	-3.126E-15	1.350E-10	2.578E-09	1.340E-11	2.050E-10
1.55	-1.418E-16	1.332E-10	2.405E-09	1.310E-11	1.891E-10
1.60	-2.488E-16	1.312E-10	2.239E-09	1.277E-11	1.735E-10
1.65	-2.617E-17	1.292E-10	2.087E-09	1.243E-11	1.585E-10
1.70	1.522E-17	1.269E-10	1.950E-09	1.208E-11	1.445E-10
1.75	3.369E-19	1.246E-10	1.826E-09	1.176E-11	1.321E-10
1.80	0.000E+00	1.225E-10	1.711E-09	1.151E-11	1.215E-10
1.85	0.000E+00	1.208E-10	1.603E-09	1.135E-11	1.125E-10
1.90	0.000E+00	1.198E-10	1.504E-09	1.130E-11	1.048E-10
1.95	0.000E+00	1.193E-10	1.418E-09	1.132E-11	9.786E-11
2.00	0.000E+00	1.193E-10	1.345E-09	1.139E-11	9.150E-11
2.05	0.000E+00	1.195E-10	1.283E-09	1.148E-11	8.548E-11
2.10	0.000E+00	1.198E-10	1.227E-09	1.158E-11	7.962E-11
2.15	0.000E+00	1.200E-10	1.174E-09	1.168E-11	7.369E-11
2.20	0.000E+00	1.205E-10	1.122E-09	1.178E-11	6.754E-11
2.25	0.000E+00	1.212E-10	1.072E-09	1.187E-11	6.119E-11
2.30	0.000E+00	1.224E-10	1.026E-09	1.196E-11	5.495E-11
2.35	0.000E+00	1.239E-10	9.836E-10	1.206E-11	4.918E-11
2.40	0.000E+00	1.255E-10	9.455E-10	1.218E-11	4.423E-11
2.45	0.000E+00	1.272E-10	9.105E-10	1.234E-11	4.020E-11
2.50	0.000E+00	1.288E-10	8.780E-10	1.257E-11	3.699E-11
2.55	0.000E+00	1.303E-10	8.478E-10	1.284E-11	3.436E-11
2.60	0.000E+00	1.321E-10	8.200E-10	1.316E-11	3.211E-11
2.65	0.000E+00	1.341E-10	7.938E-10	1.348E-11	3.005E-11
2.70	0.000E+00	1.366E-10	7.685E-10	1.379E-11	2.810E-11
2.75	0.000E+00	1.393E-10	7.432E-10	1.407E-11	2.618E-11
2.80	0.000E+00	1.422E-10	7.181E-10	1.432E-11	2.418E-11
2.85	0.000E+00	1.448E-10	6.937E-10	1.456E-11	2.199E-11
2.90	0.000E+00	1.470E-10	6.707E-10	1.483E-11	1.953E-11

(Appendix E.1. Continued)

2.95	0.000E+00	1.487E-10	6.495E-10	1.518E-11	1.688E-11
3.00	0.000E+00	1.503E-10	6.298E-10	1.560E-11	1.421E-11
3.05	0.000E+00	1.522E-10	6.112E-10	1.611E-11	1.184E-11
3.10	0.000E+00	1.547E-10	5.928E-10	1.665E-11	1.003E-11
3.15	0.000E+00	1.576E-10	5.739E-10	1.720E-11	8.946E-12
3.20	0.000E+00	1.606E-10	5.539E-10	1.774E-11	8.545E-12
3.25	0.000E+00	1.634E-10	5.327E-10	1.828E-11	8.657E-12
3.30	0.000E+00	1.657E-10	5.115E-10	1.881E-11	9.062E-12
3.35	0.000E+00	1.678E-10	4.917E-10	1.934E-11	9.586E-12
3.40	0.000E+00	1.703E-10	4.746E-10	1.988E-11	1.015E-11
3.45	0.000E+00	1.742E-10	4.605E-10	2.043E-11	1.075E-11
3.50	0.000E+00	1.806E-10	4.488E-10	2.098E-11	1.138E-11
3.55	0.000E+00	1.891E-10	4.385E-10	2.153E-11	1.205E-11
3.60	0.000E+00	1.959E-10	4.290E-10	2.209E-11	1.271E-11
3.65	0.000E+00	1.962E-10	4.205E-10	2.264E-11	1.330E-11
3.70	0.000E+00	1.850E-10	4.131E-10	2.318E-11	1.381E-11
3.75	0.000E+00	1.680E-10	4.077E-10	2.372E-11	1.429E-11
3.80	0.000E+00	1.508E-10	4.039E-10	2.428E-11	1.479E-11
3.85	0.000E+00	1.530E-10	4.019E-10	2.485E-11	1.546E-11
3.90	0.000E+00	1.620E-10	4.001E-10	2.544E-11	1.619E-11

Appendix E.2. Element and overall mass flux balances

Z	C flux	%Dev.	H flux	%Dev.	O flux	%Dev.	Total	%Dev.
0.000	0.35444	-6.06	0.02668	-15.73	0.58237	11.23	1.03714	3.71
0.010	0.35778	-5.18	0.02686	-15.17	0.57842	10.47	1.03763	3.76
0.020	0.36106	-4.31	0.02703	-14.63	0.57459	9.74	1.03817	3.82
0.030	0.36397	-3.54	0.02713	-14.31	0.57178	9.20	1.03918	3.92
0.040	0.36671	-2.81	0.02715	-14.25	0.56975	8.82	1.04056	4.06
0.050	0.36948	-2.08	0.02709	-14.42	0.56819	8.52	1.04218	4.22
0.060	0.37237	-1.31	0.02698	-14.77	0.56672	8.24	1.04383	4.38
0.070	0.37543	-0.50	0.02682	-15.30	0.56529	7.97	1.04548	4.55
0.080	0.37871	0.37	0.02661	-15.96	0.56361	7.64	1.04697	4.70
0.090	0.38214	1.28	0.02638	-16.68	0.56160	7.26	1.04820	4.82
0.100	0.38552	2.17	0.02614	-17.42	0.55935	6.83	1.04915	4.92
0.110	0.38858	2.99	0.02591	-18.17	0.55711	6.40	1.04988	4.99
0.120	0.39105	3.64	0.02568	-18.89	0.55521	6.04	1.05050	5.05
0.130	0.39266	4.07	0.02545	-19.63	0.55409	5.82	1.05116	5.12
0.140	0.39324	4.22	0.02520	-20.41	0.55410	5.83	1.05207	5.21
0.150	0.39279	4.10	0.02491	-21.32	0.55551	6.10	1.05338	5.34
0.160	0.39143	3.74	0.02456	-22.43	0.55839	6.65	1.05524	5.52
0.170	0.38946	3.22	0.02412	-23.82	0.56265	7.46	1.05769	5.77
0.180	0.38723	2.63	0.02358	-25.52	0.56801	8.48	1.06070	6.07
0.190	0.38507	2.05	0.02294	-27.53	0.57408	9.64	1.06418	6.42
0.200	0.38329	1.58	0.02222	-29.80	0.58046	10.86	1.06797	6.80
0.210	0.38202	1.25	0.02146	-32.21	0.58672	12.06	1.07185	7.18
0.220	0.38131	1.06	0.02071	-34.58	0.59255	13.17	1.07562	7.56
0.230	0.38107	0.99	0.02003	-36.74	0.59766	14.15	1.07909	7.91
0.240	0.38117	1.02	0.01947	-38.52	0.60188	14.95	1.08209	8.21
0.250	0.38191	1.10	0.01907	-39.75	0.60504	15.56	1.08450	8.45
0.260	0.38191	1.22	0.01889	-40.35	0.60699	15.93	1.08620	8.62
0.270	0.38247	1.36	0.01892	-40.24	0.60760	16.04	1.08711	8.71
0.280	0.38322	1.56	0.01918	-39.41	0.60670	15.87	1.08716	8.72
0.290	0.38424	1.83	0.01967	-37.88	0.60416	15.39	1.08625	8.63
0.300	0.38561	2.20	0.02036	-35.69	0.59992	14.58	1.08432	8.43
0.310	0.38733	2.65	0.02124	-32.91	0.59404	13.46	1.08131	8.13
0.320	0.38932	3.18	0.02227	-29.65	0.58676	12.06	1.07727	7.73
0.330	0.39142	3.74	0.02340	-26.08	0.57848	10.48	1.07231	7.23
0.340	0.39340	4.26	0.02456	-22.42	0.56978	8.82	1.06666	6.67
0.350	0.39504	4.70	0.02568	-18.89	0.56129	7.20	1.06062	6.06
0.360	0.39614	4.99	0.02668	-15.74	0.55359	5.73	1.05455	5.46
0.370	0.39663	5.12	0.02751	-13.12	0.54710	4.49	1.04876	4.88
0.380	0.39653	5.09	0.02814	-11.12	0.54199	3.51	1.04349	4.35
0.390	0.39597	4.94	0.02860	-9.67	0.53813	2.78	1.03884	3.88
0.400	0.39515	4.73	0.02892	-8.66	0.53517	2.21	1.03479	3.48
0.410	0.39431	4.50	0.02917	-7.87	0.53266	1.73	1.03124	3.12
0.420	0.39366	4.33	0.02940	-7.13	0.53013	1.25	1.02803	2.80
0.430	0.39333	4.24	0.02966	-6.33	0.52731	0.71	1.02505	2.51
0.440	0.39338	4.26	0.02994	-5.43	0.52412	-0.10	1.02225	2.22
0.450	0.39376	4.36	0.03023	-4.51	0.52072	-0.55	1.01964	1.96
0.460	0.39436	4.52	0.03049	-3.70	0.51740	-1.18	1.01731	1.73
0.470	0.39506	4.70	0.03067	-3.12	0.51449	-1.74	1.01533	1.53
0.480	0.39571	4.87	0.03076	-2.84	0.51224	-2.17	1.01376	1.38
0.490	0.39623	5.01	0.03076	-2.86	0.51074	-2.45	1.01257	1.26
0.500	0.39656	5.10	0.03067	-3.11	0.50992	-2.61	1.01172	1.17
0.510	0.39669	5.13	0.03056	-3.49	0.50961	-2.67	1.01108	1.11

(Appendix E.2. Continued)

0.5207	0.39666	2.5131	0.03044	-3.86	0.50957	-2.68	1.01058	1.06
0.530	0.39648	5.08	0.03034	-4.116	0.50965	-2.66	1.01013	1.01
0.540	0.39616	4.99	0.03028	-4.35	0.50976	-2.64	1.00973	0.97
0.550	0.39586	4.86	0.03026	-4.42	0.50993	-2.61	1.00937	0.94
0.560	0.39494	4.67	0.03027	-4.59	0.51024	-2.55	1.00905	0.91
0.570	0.39391	4.40	0.03031	-4.77	0.51077	-2.45	1.00877	0.88
0.580	0.39250	4.02	0.03039	-4.02	0.51157	-2.40	1.00844	0.84
0.590	0.39068	3.54	0.03052	-3.59	0.51261	-2.10	1.00799	0.80
0.600	0.38848	2.96	0.03074	-2.92	0.51378	-1.87	1.00732	0.73
0.610	0.38600	2.30	0.03108	-1.99	0.51495	-1.65	1.00639	0.64
0.620	0.38341	1.61	0.03140	-0.82	0.51598	-1.45	1.00571	0.52
0.630	0.38092	0.95	0.03181	0.88	0.51677	-1.20	1.00387	0.39
0.640	0.37874	0.38	0.03222	1.76	0.51731	-1.13	1.00253	0.25
0.650	0.37706	-0.07	0.03255	2.86	0.51765	-1.09	1.00138	0.14
0.660	0.37598	-0.36	0.03281	3.82	0.51787	-1.09	1.00057	0.06
0.670	0.37500	-0.48	0.03291	3.96	0.51809	-1.05	1.00020	0.02
0.680	0.37554	-0.47	0.03288	3.85	0.51839	-0.99	1.00029	0.03
0.690	0.37597	-0.36	0.03272	3.56	0.51881	-0.91	1.00076	0.08
0.700	0.37664	-0.18	0.03249	2.81	0.51935	-0.81	1.00150	0.15
0.710	0.37740	0.02	0.03220	1.92	0.51992	-0.70	1.00235	0.23
0.720	0.37845	0.22	0.03193	0.84	0.52044	-0.60	1.00316	0.32
0.730	0.37886	0.41	0.03168	0.08	0.52080	-0.53	1.00382	0.38
0.740	0.37882	0.58	0.03150	-0.52	0.52093	-0.51	1.00427	0.43
0.750	0.38015	0.75	0.03137	-0.93	0.52079	-0.54	1.00448	0.45
0.760	0.38078	0.92	0.03129	-1.18	0.52041	-0.61	1.00489	0.45
0.770	0.38140	1.08	0.03125	-1.50	0.51986	-0.71	1.00483	0.43
0.780	0.38200	1.24	0.03123	-1.35	0.51925	-0.80	1.00409	0.41
0.790	0.38256	1.39	0.03122	-1.39	0.51870	-0.89	1.00382	0.38
0.800	0.38303	1.51	0.03120	-1.44	0.51828	-1.01	1.00357	0.36
0.810	0.38337	1.60	0.03128	-1.52	0.51806	-1.06	1.00339	0.34
0.820	0.38358	1.66	0.03115	-1.52	0.51804	-1.06	1.00327	0.38
0.830	0.38363	1.67	0.03111	-1.73	0.51819	-1.09	1.00319	0.31
0.840	0.38352	1.64	0.03109	-1.81	0.51874	-0.93	1.00299	0.30
0.850	0.38325	1.57	0.03109	-1.81	0.51874	-0.93	1.00299	0.30
0.860	0.38285	1.47	0.03117	-1.55	0.51902	-0.87	1.00279	0.28
0.870	0.38252	1.42	0.03117	-1.55	0.51925	-0.87	1.00279	0.28
0.880	0.38289	1.16	0.03125	-1.58	0.51943	-0.79	1.00213	0.21
0.890	0.38101	0.98	0.03125	-0.49	0.51959	-0.76	1.00173	0.17
0.900	0.38034	0.80	0.03123	-0.71	0.51975	-0.73	1.00136	0.14
0.910	0.37974	0.64	0.03149	-0.52	0.51956	-0.69	1.00108	0.11
0.920	0.37906	0.52	0.03151	-0.47	0.52023	-0.63	1.00096	0.10
0.930	0.37806	0.46	0.03147	-0.60	0.52057	-0.58	1.00103	0.10
0.940	0.37730	0.53	0.03133	-0.91	0.52094	-0.51	1.00129	0.13
0.950	0.37695	0.54	0.03105	-1.33	0.52137	-0.45	1.00170	0.17
0.960	0.38032	0.60	0.03086	-2.53	0.52195	-0.31	1.00220	0.22
0.970	0.38094	0.66	0.03068	-3.08	0.52214	-0.28	1.00272	0.27
0.980	0.38151	0.91	0.03084	-3.04	0.52224	-0.26	1.00355	0.36
0.990	0.38151	1.11	0.03054	-3.54	0.52224	-0.26	1.00355	0.36

(Appendix E.2. Continued)

1.000	0.38195	1.23	0.03044	-3.87	0.52226	-0.25	1.00378	0.38
1.010	0.38223	1.30	0.03038	-4.05	0.52222	-0.26	1.00387	0.39
1.020	0.38235	1.33	0.03036	-4.11	0.52215	-0.27	1.00384	0.38
1.030	0.38232	1.32	0.03037	-4.09	0.52209	-0.29	1.00374	0.37
1.040	0.38220	1.29	0.03039	-4.03	0.52204	-0.30	1.00361	0.36
1.050	0.38205	1.25	0.03041	-3.96	0.52202	-0.30	1.00350	0.35
1.060	0.38191	1.22	0.03042	-3.93	0.52202	-0.30	1.00342	0.34
1.070	0.38181	1.19	0.03041	-3.93	0.52202	-0.30	1.00338	0.34
1.080	0.38176	1.18	0.03040	-3.97	0.52201	-0.30	1.00337	0.34
1.090	0.38174	1.17	0.03039	-4.02	0.52198	-0.31	1.00336	0.34
1.100	0.38174	1.17	0.03037	-4.08	0.52190	-0.32	1.00334	0.33
1.110	0.38176	1.18	0.03036	-4.12	0.52178	-0.35	1.00329	0.33
1.120	0.38177	1.18	0.03035	-4.15	0.52162	-0.38	1.00321	0.32
1.130	0.38178	1.18	0.03034	-4.16	0.52144	-0.41	1.00310	0.31
1.140	0.38180	1.19	0.03034	-4.18	0.52128	-0.44	1.00300	0.30
1.150	0.38180	1.19	0.03033	-4.19	0.52115	-0.47	1.00289	0.29
1.160	0.38176	1.18	0.03033	-4.19	0.52105	-0.48	1.00276	0.28
1.200	0.38116	1.09	0.03017	-4.71	0.52200	-0.30	1.00294	0.29
1.250	0.38079	0.92	0.02996	-5.04	0.52237	-0.23	1.00284	0.28
1.300	0.38033	0.80	0.02987	-5.38	0.52292	-0.13	1.00281	0.28
1.350	0.37972	0.64	0.02981	-5.67	0.52353	-0.01	1.00280	0.28
1.400	0.37896	0.43	0.02980	-5.84	0.52414	0.10	1.00275	0.27
1.450	0.37813	0.21	0.02980	-5.89	0.52470	0.21	1.00262	0.26
1.500	0.37739	0.02	0.02981	-5.86	0.52524	0.31	1.00243	0.24
1.550	0.37690	-0.11	0.02979	-5.85	0.52575	0.41	1.00226	0.23
1.600	0.37670	-0.16	0.02973	-5.91	0.52622	0.50	1.00219	0.22
1.700	0.37675	-0.15	0.02965	-6.09	0.52665	0.58	1.00223	0.22
1.750	0.37691	-0.11	0.02956	-6.35	0.52703	0.66	1.00238	0.24
1.800	0.37705	-0.07	0.02948	-6.64	0.52736	0.72	1.00256	0.26
1.850	0.37713	-0.05	0.02942	-6.89	0.52763	0.77	1.00272	0.27
1.900	0.37712	-0.05	0.02939	-7.08	0.52783	0.81	1.00282	0.28
1.950	0.37707	-0.07	0.02938	-7.19	0.52793	0.83	1.00273	0.27
2.000	0.37696	-0.09	0.02941	-7.11	0.52781	0.81	1.00251	0.25
2.050	0.37681	-0.14	0.02946	-6.94	0.52759	0.76	1.00218	0.22
2.100	0.37661	-0.19	0.02954	-6.71	0.52730	0.71	1.00176	0.18
2.150	0.37641	-0.24	0.02961	-6.48	0.52700	0.65	1.00133	0.13
2.200	0.37631	-0.27	0.02966	-6.33	0.52673	0.60	1.00100	0.10
2.250	0.37636	-0.25	0.02966	-6.31	0.52651	0.56	1.00084	0.08
2.300	0.37655	-0.20	0.02963	-6.40	0.52633	0.52	1.00084	0.08
2.350	0.37682	-0.13	0.02959	-6.54	0.52617	0.49	1.00094	0.09
2.400	0.37707	-0.07	0.02955	-6.67	0.52600	0.46	1.00102	0.10
2.450	0.37725	-0.02	0.02953	-6.72	0.52580	0.42	1.00103	0.10
2.500	0.37734	0.01	0.02954	-6.71	0.52557	0.38	1.00096	0.10
2.550	0.37739	0.02	0.02955	-6.66	0.52532	0.33	1.00083	0.08
2.600	0.37745	0.03	0.02957	-6.59	0.52508	0.28	1.00070	0.07
2.650	0.37751	0.05	0.02959	-6.55	0.52486	0.24	1.00060	0.06
2.700	0.37757	0.07	0.02960	-6.51	0.52469	0.21	1.00051	0.05
2.750	0.37758	0.07	0.02961	-6.47	0.52458	0.19	1.00042	0.04
2.800	0.37754	0.06	0.02963	-6.43	0.52451	0.18	1.00033	0.03
2.850	0.37746	0.04	0.02964	-6.39	0.52449	0.17	1.00023	0.02
2.900	0.37737	0.01	0.02965	-6.36	0.52451	0.18	1.00016	0.02
2.950	0.37730	-0.01	0.02965	-6.36	0.52456	0.19	1.00012	0.01

(Appendix E.2. Continued)

3.000	0.37724	-0.02	0.02964	-6.37	0.52462	0.20	1.00010	0.01
3.050	0.37718	-0.04	0.02964	-6.37	0.52467	0.21	1.00007	0.01
3.100	0.37711	-0.06	0.02966	-6.33	0.52468	0.21	0.99999	0.00
3.150	0.37702	-0.08	0.02968	-6.26	0.52467	0.21	0.99988	-0.01
3.200	0.37693	-0.10	0.02970	-6.20	0.52468	0.21	0.99977	-0.02
3.250	0.37683	-0.13	0.02971	-6.16	0.52472	0.22	0.99970	-0.03
3.300	0.37673	-0.16	0.02971	-6.14	0.52483	0.24	0.99967	-0.03
3.350	0.37661	-0.19	0.02972	-6.14	0.52497	0.26	0.99968	-0.03
3.400	0.37647	-0.22	0.02972	-6.13	0.52512	0.29	0.99968	-0.03
3.450	0.37633	-0.26	0.02973	-6.09	0.52522	0.31	0.99964	-0.04
3.500	0.37620	-0.30	0.02975	-6.03	0.52529	0.32	0.99957	-0.04
3.550	0.37609	-0.33	0.02977	-5.96	0.52533	0.33	0.99950	-0.05
3.600	0.37600	-0.35	0.02979	-5.91	0.52539	0.34	0.99945	-0.06
3.650	0.37589	-0.38	0.02980	-5.88	0.52549	0.36	0.99943	-0.06
3.700	0.37576	-0.41	0.02980	-5.87	0.52566	0.40	0.99946	-0.05
3.750	0.37562	-0.45	0.02981	-5.85	0.52584	0.43	0.99950	-0.05
3.800	0.37547	-0.49	0.02982	-5.82	0.52599	0.46	0.99952	-0.05
3.850	0.37539	-0.51	0.02983	-5.76	0.52601	0.46	0.99948	-0.05
3.900	0.37532	-0.53	0.02986	-5.70	0.52600	0.46	0.99942	-0.06

APPENDIX F.

Net molar reaction rates of species from flame data

Reaction rates were calculated from the smoothed flux curves of App. E using Eq. II.1. These are net reaction rates, and the data are best used in regions of the flame where curvature of the mole-fraction data is well-defined. Consequently, at the tails of the positive peaks (net formation) and negative peaks (net destruction) of reaction rate, values are not credible.

APPENDIX F. Net molar reaction rates of species from flame data

Z	AR	H	H2	CH3	CH4	OH	H2O	C2H2	C2H3	C2H4	CO
0.00	3.983E-06	-1.062E-05	-6.401E-07	-7.978E-07	-1.410E-07	-1.145E-07	-4.760E-06	2.724E-05	-4.279E-09	-8.028E-08	-4.471E-06
0.01	3.984E-06	-1.094E-05	-1.031E-06	-8.468E-07	-1.526E-07	-1.077E-07	-4.615E-06	2.744E-05	-4.491E-09	-7.547E-08	-5.512E-06
0.02	3.827E-06	-1.319E-05	-3.531E-06	-1.134E-06	-2.387E-07	-7.011E-08	-4.601E-06	2.875E-05	-5.276E-09	-4.242E-08	-1.203E-05
0.03	3.203E-06	-1.689E-06	-1.518E-06	-3.376E-07	-2.443E-08	-5.651E-06	3.077E-05	3.077E-05	-5.366E-09	6.874E-09	-2.063E-05
0.04	2.495E-06	-1.972E-05	-1.391E-05	-1.777E-06	-3.269E-07	-2.889E-09	-6.469E-06	3.240E-05	-4.637E-09	3.559E-08	-2.463E-05
0.05	1.776E-06	-2.185E-05	-1.941E-05	-1.957E-06	-2.167E-07	-4.784E-10	-6.816E-06	3.365E-05	-3.349E-09	4.691E-08	-2.481E-05
0.06	1.106E-06	-2.358E-05	-2.476E-05	-2.096E-06	-3.041E-08	-1.101E-08	-6.650E-06	3.447E-05	-1.720E-09	4.609E-08	-2.237E-05
0.07	5.977E-07	-2.463E-05	-2.926E-05	-2.172E-06	-2.419E-07	-3.746E-08	-5.705E-06	3.454E-05	-1.604E-10	2.899E-08	-1.673E-05
0.08	3.055E-07	-2.553E-05	-3.265E-05	-2.243E-06	5.612E-07	-6.995E-08	-4.000E-06	3.385E-05	1.991E-09	4.618E-09	-9.883E-06
0.09	2.602E-07	-2.658E-05	-3.444E-05	-2.312E-06	8.950E-07	-6.037E-07	-1.718E-06	3.222E-05	1.991E-09	4.618E-09	-9.883E-06
0.10	4.702E-07	-2.814E-05	-3.437E-05	-2.372E-06	1.208E-06	-1.338E-07	9.310E-07	2.953E-05	3.644E-09	-2.139E-08	-3.081E-06
0.11	9.170E-07	-3.052E-05	-3.234E-05	-2.402E-06	1.463E-06	-1.563E-07	6.697E-06	2.953E-05	4.958E-09	-4.261E-08	-2.348E-06
0.12	2.102E-06	-3.847E-05	-2.425E-05	-2.160E-06	1.694E-06	-1.774E-07	6.192E-06	2.090E-05	5.904E-09	-4.579E-08	4.999E-06
0.13	2.581E-06	-4.382E-05	-1.973E-05	-1.757E-06	1.653E-06	-1.834E-07	8.109E-06	1.524E-05	5.318E-09	-2.019E-08	1.921E-06
0.14	2.804E-06	-4.966E-05	-1.606E-05	-1.097E-06	1.518E-06	-1.935E-07	9.447E-06	9.014E-06	3.871E-09	2.386E-08	-2.994E-06
0.15	2.677E-06	-5.500E-05	-1.385E-05	-1.674E-07	1.312E-06	-2.121E-07	8.786E-06	2.557E-06	1.487E-09	8.352E-08	-8.231E-06
0.16	2.165E-06	-6.083E-05	-1.332E-05	9.964E-07	1.062E-06	-2.407E-07	7.441E-06	-3.794E-06	-1.831E-09	1.545E-07	-1.215E-05
0.17	1.307E-06	-6.521E-05	-1.418E-05	2.309E-06	7.973E-07	-2.772E-07	5.727E-06	-1.498E-05	-5.965E-08	2.327E-07	-1.343E-05
0.18	2.154E-07	-6.832E-05	-1.569E-05	3.644E-06	5.469E-07	-3.171E-07	4.032E-06	-1.934E-05	-1.065E-08	3.162E-07	-1.151E-05
0.20	9.447E-07	-6.991E-05	-1.691E-05	4.855E-06	3.354E-07	-3.556E-07	2.749E-06	-2.264E-05	-1.550E-08	4.072E-07	-6.702E-06
0.21	1.985E-06	-6.983E-05	-1.690E-05	5.804E-06	1.836E-07	-3.908E-07	2.179E-06	-2.477E-05	-2.011E-08	5.132E-07	-1.160E-07
0.22	-2.735E-06	-6.793E-05	-1.504E-05	6.386E-06	1.078E-07	-4.259E-07	2.454E-06	-2.565E-05	-2.780E-08	6.460E-07	6.641E-06
0.23	3.076E-06	-6.402E-05	-1.116E-05	6.550E-06	1.196E-07	-4.689E-07	3.500E-06	-2.527E-05	-3.127E-08	8.198E-07	1.194E-05
0.24	-2.968E-06	-5.788E-05	-5.600E-06	6.309E-06	2.244E-07	-5.304E-07	5.060E-06	-2.363E-05	-3.529E-08	1.047E-06	1.455E-05
0.25	-2.457E-06	-4.923E-05	5.747E-07	5.730E-06	4.202E-07	-6.177E-07	6.784E-06	-2.084E-05	-4.056E-08	1.333E-06	1.398E-05
0.26	1.664E-06	-3.788E-05	7.642E-06	4.923E-06	6.951E-07	-7.291E-07	8.358E-06	-1.706E-05	-4.742E-08	1.669E-06	1.051E-05
0.27	7.539E-07	-2.372E-05	1.363E-05	4.011E-06	1.026E-06	-8.486E-07	9.638E-06	-1.258E-05	-5.539E-08	2.031E-06	5.049E-06
0.28	9.485E-08	-6.883E-06	1.827E-05	3.110E-06	1.380E-06	-9.455E-07	1.072E-05	-7.815E-06	-6.289E-08	2.380E-06	-1.083E-06
0.29	7.287E-07	1.229E-05	2.116E-05	2.311E-06	1.714E-06	-9.778E-07	1.194E-05	-3.350E-06	-6.729E-08	2.828E-06	-9.951E-06
0.30	1.044E-06	3.321E-05	2.209E-05	1.195E-05	2.183E-06	-3.080E-07	1.647E-05	1.685E-06	-5.393E-08	2.639E-06	-7.271E-06
0.31	9.997E-07	5.509E-05	2.096E-05	1.995E-05	2.151E-06	-6.827E-07	2.026E-05	6.884E-07	-3.124E-08	2.265E-06	-6.199E-06
0.32	6.194E-07	7.699E-05	1.777E-05	8.890E-07	2.83E-06	-3.080E-07	1.647E-05	1.685E-06	-5.393E-08	2.639E-06	-7.271E-06
0.33	-2.016E-08	9.795E-05	1.267E-05	7.214E-07	2.068E-06	-3.080E-07	2.026E-05	6.884E-07	-3.124E-08	2.265E-06	-6.199E-06
0.34	-8.043E-07	1.170E-04	6.009E-06	6.608E-07	1.815E-06	8.183E-07	2.967E-05	-1.076E-05	4.501E-08	1.120E-06	2.611E-05
0.35	-1.592E-06	1.432E-04	-1.499E-06	6.776E-07	1.452E-06	1.458E-06	3.385E-05	-2.084E-05	9.126E-08	4.821E-07	4.366E-05
0.36	-2.272E-06	1.458E-04	-8.810E-06	7.474E-07	1.019E-06	2.051E-06	3.659E-05	-3.266E-05	1.353E-07	-1.032E-07	6.234E-05
0.37	-2.709E-06	1.542E-04	-1.467E-05	8.508E-07	5.661E-07	2.524E-06	3.731E-05	-4.473E-05	1.712E-07	-5.773E-07	8.023E-05
0.38	-2.839E-06	1.579E-04	-1.792E-05	9.717E-07	1.412E-07	2.826E-06	3.585E-05	-5.542E-05	1.943E-07	-9.074E-07	9.528E-05
0.39	-2.641E-06	1.570E-04	-1.782E-05	1.095E-06	-2.168E-07	2.933E-06	3.253E-05	-6.329E-05	2.026E-07	-1.090E-06	1.058E-04
0.40	-2.155E-06	1.516E-04	-1.439E-05	1.206E-06	-4.836E-07	2.852E-06	2.800E-05	-6.741E-05	1.967E-07	-1.090E-06	1.058E-04
0.41	-1.479E-06	1.426E-04	-8.477E-06	1.294E-06	6.517E-07	2.616E-06	2.311E-05	-6.756E-05	1.796E-07	-1.149E-06	1.08E-04
0.42	-7.463E-07	1.309E-04	-1.601E-06	1.351E-06	-6.517E-07	2.277E-06	1.862E-05	-6.428E-05	1.796E-07	-1.124E-06	1.02E-04
0.43	-1.046E-07	1.177E-04	4.468E-06	1.379E-06	-7.375E-07	1.888E-06	1.505E-05	-5.868E-05	1.561E-07	-1.060E-06	1.051E-04
0.44	3.231E-07	9.081E-05	8.260E-06	1.383E-06	-6.592E-07	1.499E-06	1.505E-05	-5.868E-05	1.310E-07	-9.987E-07	9.695E-05
0.45	4.656E-07	9.095E-06	1.383E-06	6.592E-07	-7.043E-07	1.145E-06	1.116E-05	-4.589E-05	1.082E-07	-9.632E-07	8.779E-05
0.46	3.209E-07	7.840E-05	7.329E-06	1.394E-06	-6.279E-07	8.460E-07	1.041E-05	-4.092E-05	9.026E-08	-9.606E-07	7.930E-05
0.47	-4.420E-08	6.669E-05	4.263E-06	1.394E-06	-6.284E-07	6.065E-07	1.004E-05	-3.767E-05	6.991E-08	-1.008E-06	6.819E-05
0.48	-5.132E-07	5.514E-05	1.405E-06	6.690E-07	-6.690E-07	4.179E-07	9.779E-06	-3.610E-05	6.516E-08	-1.018E-06	6.582E-05
0.49	-9.511E-07	4.307E-05	1.398E-06	7.492E-07	-7.492E-07	2.734E-07	9.541E-06	-3.586E-05	6.181E-08	-9.958E-07	6.491E-05
0.50	-1.240E-06	2.992E-05	4.435E-06	1.343E-06	-8.610E-07	1.545E-07	9.397E-06	-3.645E-05	5.854E-08	-9.375E-07	6.479E-05

(Appendix F. Continued)

0.51	-1.307E-06	1.554E-05	1.082E-05	1.210E-06	-9.926E-07	5.245E-08	9.546E-06	-3.744E-05	5.469E-08	-8.486E-07	6.488E-05
0.52	-1.139E-06	3.378E-07	1.960E-05	9.780E-07	-1.131E-06	-3.935E-08	1.024E-05	-3.851E-05	5.011E-08	-7.445E-07	6.476E-05
0.53	-1.830E-07	-1.477E-05	2.913E-05	6.453E-07	1.263E-06	-1.238E-07	1.174E-05	-3.946E-05	4.504E-08	-6.449E-07	6.417E-05
0.54	-3.244E-07	-2.856E-05	3.762E-05	2.340E-07	-1.379E-06	-2.012E-07	1.420E-05	-4.019E-05	3.978E-08	-5.683E-07	6.283E-05
0.55	-1.355E-07	-3.980E-05	4.370E-05	-2.122E-07	-1.469E-06	-2.708E-07	1.768E-05	-4.060E-05	3.452E-08	-5.273E-07	6.038E-05
0.56	5.066E-07	-4.756E-05	4.679E-05	-6.361E-07	-1.524E-06	-3.321E-07	2.206E-05	-4.057E-05	2.928E-08	-5.257E-07	5.642E-05
0.57	7.296E-07	-5.146E-05	4.714E-05	-9.804E-07	-1.535E-06	-3.856E-07	2.702E-05	-3.994E-05	2.391E-08	-5.586E-07	5.064E-05
0.58	7.845E-07	-5.173E-05	4.566E-05	-1.202E-06	-1.493E-06	-4.322E-07	3.207E-05	-3.860E-05	1.826E-08	-6.139E-07	4.300E-05
0.59	6.880E-07	-4.908E-05	4.345E-05	-1.282E-06	-1.399E-06	-4.731E-07	3.656E-05	-3.653E-05	1.221E-08	-6.764E-07	3.393E-05
0.60	4.814E-07	-4.453E-05	4.141E-05	-1.230E-06	-1.249E-06	-5.091E-07	3.976E-05	-3.386E-05	5.767E-09	-7.312E-07	2.455E-05
0.61	2.160E-07	-3.911E-05	3.995E-05	-1.079E-06	-1.056E-06	-5.094E-07	4.105E-05	-3.083E-05	9.472E-10	-7.674E-07	1.555E-05
0.62	-6.148E-08	-3.368E-05	3.889E-05	-8.772E-07	-8.369E-07	-5.618E-07	4.001E-05	-2.777E-05	7.724E-09	-7.792E-07	8.889E-06
0.63	-3.169E-07	-2.876E-05	3.767E-05	-6.751E-07	-6.150E-07	-5.731E-07	3.638E-05	-2.501E-05	-1.432E-08	-7.662E-07	5.432E-06
0.64	-5.312E-07	-2.457E-05	3.563E-05	-5.125E-07	-4.152E-07	-5.697E-07	3.106E-05	-2.278E-05	-2.048E-08	-7.319E-07	5.640E-06
0.65	-6.975E-07	-2.107E-05	3.229E-05	-4.116E-07	-2.590E-07	-5.489E-07	2.413E-05	-2.116E-05	-2.599E-08	-6.820E-07	9.214E-06
0.66	-8.155E-07	-1.818E-05	2.762E-05	-3.780E-07	-1.598E-07	-5.099E-07	1.667E-05	-2.007E-05	-3.067E-08	-6.220E-07	1.516E-05
0.67	-8.869E-07	-1.577E-05	2.202E-05	-3.889E-07	-1.212E-07	-4.542E-07	9.585E-06	-1.931E-05	-3.436E-08	-5.567E-07	2.206E-05
0.68	-9.130E-07	-1.384E-05	1.626E-05	-4.301E-07	-1.370E-07	-3.859E-07	3.613E-06	-1.861E-05	-3.703E-08	-4.892E-07	2.844E-05
0.69	-8.966E-07	-1.245E-05	1.121E-05	-4.746E-07	-1.932E-07	-2.368E-07	8.015E-07	-1.775E-05	-3.870E-08	-4.218E-07	3.314E-05
0.70	-8.441E-07	-1.167E-05	7.637E-06	-5.039E-07	-2.722E-07	-2.368E-07	3.579E-06	-1.656E-05	-3.953E-08	-3.564E-07	3.556E-05
0.71	-7.687E-07	-1.158E-05	5.997E-06	-5.094E-07	-3.561E-07	-1.693E-07	4.936E-06	-1.502E-05	-3.975E-08	-2.949E-07	3.570E-05
0.72	-6.897E-07	-1.214E-05	6.369E-06	-4.933E-07	-4.300E-07	-1.139E-07	5.369E-06	-1.321E-05	-3.962E-08	-2.396E-07	3.409E-05
0.73	-6.299E-07	-1.327E-05	8.476E-06	-4.661E-07	-4.835E-07	-7.408E-08	5.306E-06	-1.129E-05	-3.936E-08	-1.929E-07	3.152E-05
0.74	-6.093E-07	-1.484E-05	1.179E-05	-4.429E-07	-5.110E-07	-5.078E-08	5.179E-06	-9.459E-06	-3.912E-08	-1.564E-07	2.872E-05
0.75	-6.389E-07	-1.668E-05	1.565E-05	-4.380E-07	-5.112E-07	-4.320E-08	5.235E-06	-7.892E-06	-3.892E-08	-1.307E-07	2.631E-05
0.76	-7.171E-07	-1.866E-05	1.946E-05	-4.611E-07	-4.860E-07	-4.893E-08	5.545E-06	-6.718E-06	-3.865E-08	-1.155E-07	2.455E-05
0.77	-8.287E-07	-2.066E-05	2.272E-05	-5.134E-07	-4.398E-07	-6.455E-08	6.040E-06	-5.92E-06	-3.821E-08	-1.091E-07	2.345E-05
0.78	-9.486E-07	-2.255E-05	2.513E-05	-5.868E-07	-3.787E-07	-8.606E-08	6.586E-06	-5.702E-06	-3.745E-08	-1.093E-07	2.281E-05
0.79	-1.048E-06	-2.415E-05	2.662E-05	-6.50E-07	-3.097E-07	-1.094E-07	7.048E-06	-5.779E-06	-3.632E-08	-1.137E-07	2.235E-05
0.80	-1.102E-06	-2.526E-05	2.728E-05	-7.268E-07	-2.407E-07	-1.308E-07	7.345E-06	-6.123E-06	-3.480E-08	-1.202E-07	2.180E-05
0.81	-1.094E-06	-2.563E-05	2.734E-05	-7.513E-07	-1.794E-07	-1.473E-07	7.454E-06	-6.620E-06	-3.295E-08	-1.271E-07	2.098E-05
0.82	-1.019E-06	-2.506E-05	2.709E-05	-7.233E-07	-1.320E-07	-1.568E-07	7.401E-06	-7.166E-06	-3.081E-08	-1.372E-07	1.979E-05
0.83	-8.851E-07	-2.345E-05	2.678E-05	-6.377E-07	-1.032E-07	-1.529E-07	7.683E-06	-8.118E-06	-2.843E-08	-1.372E-07	1.824E-05
0.84	-7.061E-07	-2.087E-05	2.659E-05	-5.018E-07	-9.435E-08	-1.529E-07	6.964E-06	-8.118E-06	-2.586E-08	-1.387E-07	1.638E-05
0.85	-5.022E-07	-1.756E-05	2.652E-05	-3.344E-07	-1.040E-07	-1.415E-07	6.613E-06	-8.448E-06	-2.316E-08	-1.371E-07	1.436E-05
0.86	-2.948E-07	-1.390E-05	2.644E-05	-1.619E-07	-1.280E-07	-1.266E-07	6.161E-06	-8.667E-06	-2.045E-08	-1.323E-07	1.234E-05
0.87	-1.043E-07	-1.034E-05	2.605E-05	-1.219E-08	-1.598E-07	-1.108E-07	5.599E-06	-8.780E-06	-1.797E-08	-1.243E-07	1.056E-05
0.88	5.119E-08	-7.265E-06	2.505E-05	9.117E-08	-1.924E-07	-9.616E-08	4.944E-06	-8.789E-06	-1.596E-08	-1.137E-07	9.249E-06
0.89	1.567E-07	-4.929E-06	2.315E-05	1.338E-07	-2.192E-07	-8.450E-08	4.250E-06	-8.687E-06	-1.471E-08	-1.016E-07	8.601E-06
0.90	2.018E-07	-3.407E-06	2.021E-05	1.125E-07	-2.351E-07	-7.680E-08	3.605E-06	-8.460E-06	-1.440E-08	-8.891E-08	8.746E-06
0.91	1.816E-07	-2.603E-06	1.630E-05	3.439E-08	-2.375E-07	-7.360E-08	3.103E-06	-8.033E-06	-1.506E-08	-7.678E-08	9.699E-06
0.92	9.941E-08	-2.310E-06	1.173E-05	-8.624E-08	-2.264E-07	-7.364E-08	2.820E-06	-7.583E-06	-1.652E-08	-6.610E-08	1.134E-05
0.93	-3.285E-08	-2.282E-06	7.000E-06	-2.318E-07	-2.043E-07	-7.689E-08	-2.782E-06	-6.931E-06	-1.844E-08	-5.749E-08	1.343E-05
0.94	-1.945E-07	-2.213E-06	2.713E-06	-3.849E-07	-1.749E-07	-8.176E-08	2.950E-06	-6.250E-06	-2.037E-08	-5.122E-08	1.565E-05
0.95	-3.585E-07	-2.275E-06	-5.509E-07	-5.309E-07	-1.429E-07	-8.674E-08	3.230E-06	-5.557E-06	-2.190E-08	-4.727E-08	1.763E-05
0.96	-4.960E-07	-2.132E-06	-2.362E-06	-6.586E-07	-1.128E-07	-9.026E-08	3.501E-06	-4.964E-06	-2.275E-08	-4.538E-08	1.638E-05
0.97	-5.820E-07	-1.918E-06	-2.539E-06	-7.601E-07	-8.765E-08	-9.104E-08	3.654E-06	-4.545E-06	-2.281E-08	-4.510E-08	1.979E-05
0.98	-6.009E-07	-1.696E-06	-1.189E-06	-8.303E-07	-6.976E-08	-8.835E-08	3.627E-06	-4.381E-06	-2.219E-08	-4.587E-08	1.969E-05
0.99	-5.504E-07	-1.527E-06	1.316E-06	-8.668E-07	-5.913E-08	-8.222E-08	3.428E-06	-4.400E-06	-2.115E-08	-4.702E-08	1.888E-05
1.00	-4.417E-07	-1.445E-06	4.418E-06	-8.696E-07	-5.482E-08	-7.355E-08	3.128E-06	-4.611E-06	-2.000E-08	-4.786E-08	1.754E-05
1.01	-2.971E-07	-1.449E-06	7.502E-06	-8.415E-07	-5.492E-08	-6.391E-08	2.832E-06	-4.902E-06	-1.901E-08	-4.775E-08	1.597E-05
1.02	-1.432E-07	-1.509E-06	1.002E-05	-7.879E-07	-5.716E-08	-5.509E-08	2.644E-06	-5.156E-06	-1.831E-08	-4.620E-08	1.439E-05
1.03	-4.498E-09	-1.585E-06	1.159E-05	-7.157E-07	-5.946E-08	-4.857E-08	-2.617E-06	-5.265E-06	-1.792E-08	-4.297E-08	1.301E-05

(Appendix F. Cont. Innued)

1.04	1.024E-07	-1.637E-06	1.207E-05	-6.327E-07	-6.032E-08	-4.505E-08	-2.739E-06	-5.155E-06	-1.770E-08	-3.814E-08	1.188E-05
1.05	1.727E-07	-1.634E-06	1.152E-05	-5.463E-07	-5.908E-08	-4.419E-08	-2.932E-06	-4.795E-06	-1.751E-08	-3.212E-08	1.096E-05
1.06	2.124E-07	-1.564E-06	1.021E-05	-4.625E-07	-5.591E-08	-4.466E-08	-3.075E-06	-4.211E-06	-1.719E-08	-2.556E-08	1.013E-05
1.07	2.327E-07	-1.428E-06	8.479E-06	-3.868E-07	-5.165E-08	-4.480E-08	-3.064E-06	-3.473E-06	-1.669E-08	-1.932E-08	9.283E-06
1.08	2.452E-07	-1.242E-06	6.665E-06	-3.237E-07	-4.751E-08	-4.314E-08	-2.839E-06	-2.679E-06	-1.603E-08	-1.417E-08	8.362E-06
1.09	2.580E-07	-1.029E-06	5.056E-06	-2.766E-07	-4.480E-08	-3.882E-08	-2.408E-06	-1.931E-06	-1.527E-08	-1.073E-08	7.378E-06
1.10	2.697E-07	-8.150E-07	3.806E-06	-2.501E-07	-4.436E-08	-3.218E-08	-1.864E-06	-1.320E-06	-1.454E-08	-9.355E-09	6.472E-06
1.11	2.686E-07	-6.353E-07	2.991E-06	-2.485E-07	-4.679E-08	-2.496E-08	-1.357E-06	-9.167E-07	-1.378E-08	-9.996E-09	5.830E-06
1.12	2.504E-07	-5.096E-07	2.619E-06	-2.677E-07	-5.215E-08	-1.855E-08	-9.723E-07	-7.294E-07	-1.294E-08	-1.215E-08	5.496E-06
1.13	2.808E-07	-4.539E-07	2.650E-06	-3.043E-07	-6.018E-08	-1.460E-08	-7.900E-07	-7.464E-07	-1.188E-08	-1.520E-08	5.504E-06
1.14	1.319E-07	-4.800E-07	2.994E-06	-3.563E-07	-7.010E-08	-1.486E-08	-8.785E-07	-9.412E-07	-1.044E-08	-1.852E-08	5.900E-06
1.15	3.472E-08	-6.009E-07	3.855E-06	-4.018E-07	-8.285E-08	-1.974E-08	-1.113E-06	-1.255E-06	-8.044E-09	-2.091E-08	6.244E-06
1.16	6.540E-08	-7.757E-07	5.034E-06	-4.354E-07	-9.676E-08	-2.720E-08	-1.396E-06	-1.613E-06	-5.118E-09	-2.231E-08	6.438E-06
1.20	4.209E-08	-4.736E-07	3.234E-06	-3.138E-07	-4.707E-08	-2.364E-08	-1.761E-06	-1.620E-06	-8.385E-09	-1.359E-08	6.112E-06
1.25	7.189E-08	-5.369E-07	3.292E-06	-2.207E-07	-3.800E-08	-2.390E-08	-1.978E-06	-1.653E-06	-6.072E-09	-1.185E-08	5.505E-06
1.30	6.553E-08	-4.960E-07	3.519E-06	-1.417E-07	-3.384E-08	-2.513E-08	-2.143E-06	-1.806E-06	-4.433E-09	-1.028E-08	5.169E-06
1.35	2.261E-08	-4.031E-07	3.852E-06	-8.675E-08	-4.172E-08	-2.496E-08	-2.127E-06	-1.925E-06	-3.424E-09	-8.667E-09	4.793E-06
1.40	3.288E-08	-2.896E-07	4.151E-06	-5.887E-08	-6.275E-08	-2.260E-08	-1.923E-06	-1.945E-06	-2.815E-09	-7.407E-09	4.292E-06
1.45	6.748E-08	-1.726E-07	4.261E-06	-5.356E-08	-8.860E-08	-1.895E-08	-1.660E-06	-1.868E-06	-2.390E-09	-6.828E-09	3.817E-06
1.50	5.919E-08	-8.471E-08	4.105E-06	-6.085E-08	-1.054E-07	-1.570E-08	-1.506E-06	-1.719E-06	-2.042E-09	-6.811E-09	3.617E-06
1.55	9.513E-09	-6.401E-08	3.698E-06	-7.025E-08	-1.025E-07	-1.413E-08	-1.528E-06	-1.519E-06	-1.766E-09	-6.931E-09	3.686E-06
1.60	5.959E-08	-1.205E-07	3.109E-06	-7.544E-08	-7.864E-08	-1.429E-08	-1.650E-06	-1.282E-06	-1.605E-09	-6.774E-09	3.873E-06
1.65	1.189E-07	-2.203E-07	2.441E-06	-7.534E-08	-4.291E-08	-1.501E-08	-1.726E-06	-1.030E-06	-1.586E-09	-6.192E-09	3.943E-06
1.70	1.469E-07	-3.058E-07	1.820E-06	-7.152E-08	-8.254E-09	-1.488E-08	-1.655E-06	-7.951E-07	-1.682E-09	-5.335E-09	3.752E-06
1.75	1.382E-07	-3.315E-07	1.366E-06	-6.535E-08	1.558E-08	-1.326E-08	-1.451E-06	-6.084E-07	-1.808E-09	-4.506E-09	3.325E-06
1.80	1.040E-07	-2.911E-07	1.150E-06	-5.732E-08	2.578E-08	-1.072E-08	-1.211E-06	-4.822E-07	-1.860E-09	-3.963E-09	2.794E-06
1.85	6.301E-08	-2.132E-07	1.160E-06	-4.795E-08	2.551E-08	-8.498E-09	-1.027E-06	-4.058E-07	-1.770E-09	-3.779E-09	2.296E-06
1.90	3.095E-08	-1.366E-07	1.355E-06	-3.847E-08	2.051E-08	-8.722E-09	-9.201E-07	-3.567E-07	-1.549E-09	-3.849E-09	1.887E-06
1.95	1.356E-08	-8.538E-08	1.569E-06	-3.043E-08	1.562E-08	-8.745E-09	-8.535E-07	-3.184E-07	-1.281E-09	-3.983E-09	1.552E-06
2.00	7.521E-09	-6.123E-08	1.831E-06	-2.482E-08	1.310E-08	-1.105E-08	-7.872E-07	-2.897E-07	-1.080E-09	-4.015E-09	1.270E-06
2.05	6.320E-09	-5.278E-08	2.052E-06	-2.178E-08	1.264E-08	-1.357E-08	-7.300E-07	-2.788E-07	-1.016E-09	-3.874E-09	1.068E-06
2.10	5.403E-09	-4.931E-08	2.163E-06	-2.102E-08	1.267E-08	-1.515E-08	-7.338E-07	-2.874E-07	-1.081E-09	-3.597E-09	1.005E-06
2.15	3.223E-09	-4.665E-08	2.101E-06	-2.196E-08	1.198E-08	-1.507E-08	-8.431E-07	-3.025E-07	-1.193E-09	-3.294E-09	1.111E-06
2.20	6.454E-10	-4.495E-08	1.867E-06	-2.367E-08	1.071E-08	-1.338E-08	-1.043E-06	-3.023E-07	-1.252E-09	-3.076E-09	1.332E-06
2.25	6.781E-09	-4.436E-08	1.547E-06	-2.482E-08	9.901E-09	-1.091E-08	-1.255E-06	-2.734E-07	-1.191E-09	-2.983E-09	1.545E-06
2.30	1.521E-08	-4.357E-08	1.270E-06	-2.418E-08	1.038E-08	-8.792E-09	-1.381E-06	-2.221E-07	-1.013E-09	-2.962E-09	1.636E-06
2.35	2.436E-08	-4.107E-08	1.133E-06	-2.147E-08	1.188E-08	-7.759E-09	-1.368E-06	-1.699E-07	-7.760E-10	-2.912E-09	1.567E-06
2.40	3.159E-08	-3.586E-08	1.148E-06	-1.763E-08	1.342E-08	-7.714E-09	-1.242E-06	-1.375E-07	-5.662E-10	-2.763E-09	1.393E-06
2.45	3.487E-08	-2.747E-08	1.251E-06	-1.430E-08	1.434E-08	-7.955E-09	-1.083E-06	-1.313E-07	-4.577E-10	-2.526E-09	1.211E-06
2.50	3.385E-08	-1.641E-08	1.353E-06	-1.271E-08	1.488E-08	-7.825E-09	-9.649E-07	-1.428E-07	-6.444E-10	-2.280E-09	1.092E-06
2.55	2.940E-08	-5.134E-09	1.381E-06	-1.294E-08	1.575E-08	-7.246E-09	-9.048E-07	-1.576E-07	-6.255E-10	-2.112E-09	1.041E-06
2.60	2.263E-08	-2.329E-09	1.310E-06	-1.408E-08	1.720E-08	-6.682E-09	-8.590E-07	-1.651E-07	-8.123E-10	-2.056E-09	1.009E-06
2.65	1.451E-08	-2.772E-09	1.156E-06	-1.508E-08	1.886E-08	-6.674E-09	-7.688E-07	-1.618E-07	-9.616E-10	-2.077E-09	9.407E-07
2.70	6.219E-09	-3.346E-09	9.613E-07	-1.548E-08	2.007E-08	-7.386E-09	-6.123E-07	-1.502E-07	-1.019E-09	-2.090E-09	8.167E-07
2.75	6.888E-10	-1.149E-08	7.677E-07	-1.540E-08	2.046E-08	-8.536E-09	-4.214E-07	-1.361E-07	-9.918E-10	-2.015E-09	6.653E-07
2.80	4.888E-09	-1.602E-08	5.972E-07	-1.515E-08	1.806E-08	-9.662E-09	-2.541E-07	-1.259E-07	-9.416E-10	-1.832E-09	5.378E-07
2.85	6.689E-09	-1.415E-08	4.554E-07	-1.476E-08	1.989E-08	-1.039E-08	-1.523E-07	-1.248E-07	-9.391E-10	-1.593E-09	4.713E-07
2.90	7.166E-09	-7.661E-09	3.517E-07	-1.401E-08	1.504E-08	-1.190E-07	-1.331E-07	-1.331E-07	-1.013E-09	-1.391E-09	4.634E-07
2.95	8.256E-09	-1.340E-09	3.909E-07	-1.283E-08	1.122E-08	-1.004E-08	-1.280E-07	-1.456E-07	-1.128E-09	-1.297E-09	4.766E-07
3.00	1.105E-08	-2.189E-10	3.446E-07	-1.154E-08	7.864E-09	-8.982E-09	-1.482E-07	-1.542E-07	-1.208E-09	-1.301E-09	4.669E-07
3.05	1.525E-08	-4.648E-09	4.395E-07	-1.069E-08	6.342E-09	-1.611E-07	-1.533E-07	-1.533E-07	-1.181E-09	-1.325E-09	4.152E-07
3.10	1.935E-08	-1.401E-08	5.337E-07	-1.065E-08	7.152E-09	-6.383E-09	-1.621E-07	-1.447E-07	-1.023E-09	-1.284E-09	3.387E-07

(Appendix F. Cont Inued)

	HCO	H2CO	O2	H02	C3H2	C3H3	C3H4	HCCO	CH2CO	CO2	C4H2
3.15	-2.163E-08	-2.365E-08	5.624E-07	-1.123E-08	9.461E-09	-5.634E-09	-1.532E-07	-1.378E-07	-7.621E-10	-1.148E-09	2.752E-07
3.20	-2.111E-08	-2.930E-08	5.070E-07	-1.182E-08	1.166E-08	-5.491E-09	-1.369E-07	-1.437E-07	-4.703E-10	-9.649E-10	2.528E-07
3.25	-1.801E-08	-2.880E-08	4.109E-07	-1.184E-08	1.242E-08	-5.723E-09	-1.157E-07	-1.658E-07	-2.253E-10	-8.150E-10	2.685E-07
3.30	-1.370E-08	-2.303E-08	3.425E-07	-1.109E-08	1.149E-08	-5.942E-09	-9.368E-07	-1.945E-07	-7.866E-11	-7.560E-10	2.920E-07
3.35	-1.006E-08	-1.520E-08	3.392E-07	-9.876E-09	9.776E-09	-5.880E-09	-7.553E-08	-2.111E-07	-3.144E-11	-7.916E-10	2.902E-07
3.40	-8.622E-09	-8.843E-09	3.825E-07	-8.685E-09	8.777E-09	-5.536E-09	-6.522E-08	-2.013E-07	-3.282E-11	-8.797E-10	2.534E-07
3.45	-9.742E-09	-5.825E-09	4.219E-07	-7.897E-09	9.662E-09	-5.079E-09	-6.387E-08	-2.013E-07	-1.017E-11	-9.619E-10	2.003E-07
3.50	-1.231E-08	-5.663E-09	4.232E-07	-7.668E-09	1.239E-08	-4.664E-09	-6.924E-08	-1.305E-07	8.460E-11	-9.896E-10	1.664E-07
3.55	-1.426E-08	-6.318E-09	3.901E-07	-7.903E-09	1.541E-08	-4.307E-09	-7.555E-08	-1.177E-07	2.453E-10	-9.431E-10	1.751E-07
3.60	-1.356E-08	-5.798E-09	3.527E-07	-8.402E-09	1.637E-08	-3.940E-09	-7.574E-08	-1.429E-07	4.179E-10	-8.347E-10	2.270E-07
3.65	-9.784E-09	-3.129E-09	3.276E-07	-8.741E-09	1.382E-08	-3.453E-09	-6.397E-08	-1.822E-07	5.466E-10	-7.034E-10	2.810E-07
3.70	-4.165E-09	-1.115E-09	3.134E-07	-8.664E-09	8.364E-09	-2.847E-09	-4.128E-08	-2.064E-07	6.099E-10	-5.881E-10	3.018E-07
3.75	4.913E-10	6.087E-09	2.795E-07	-7.18E-09	2.574E-09	-2.076E-09	-1.220E-08	-1.605E-07	6.300E-10	-5.200E-10	2.312E-07
3.80	2.740E-09	1.037E-08	2.270E-07	-6.252E-09	-1.352E-09	-1.310E-09	-1.370E-08	-6.205E-08	6.341E-10	-4.973E-10	9.858E-08
3.85	1.687E-09	1.218E-08	1.753E-07	-5.013E-09	-1.334E-09	-8.499E-10	-2.370E-08	3.577E-08	6.444E-10	-5.064E-10	-2.346E-08
3.90	1.170E-09	1.227E-08	1.634E-07	-4.744E-09	-9.291E-10	-7.691E-10	-2.402E-08	5.481E-08	6.438E-10	-5.047E-10	-4.667E-08
0.00	5.176E-09	1.044E-07	-1.613E-05	4.759E-07	-5.151E-10	2.105E-09	-1.521E-08	-1.160E-08	4.717E-08	-1.181E-06	1.101E-07
0.01	4.932E-09	1.044E-07	-1.558E-05	4.935E-07	-5.288E-10	5.071E-09	-2.000E-08	-1.303E-08	4.783E-08	-9.686E-07	1.158E-07
0.02	3.321E-09	1.041E-07	-1.081E-05	5.427E-07	-1.419E-09	8.443E-09	-4.788E-08	-1.991E-08	4.903E-08	2.293E-07	1.414E-07
0.03	6.640E-10	1.371E-07	-2.416E-06	5.172E-07	-4.335E-09	-2.074E-08	-8.790E-08	-2.612E-08	4.419E-08	1.607E-06	1.429E-07
0.04	-1.356E-09	1.807E-07	2.977E-06	4.549E-07	-7.492E-09	-6.491E-08	-1.135E-07	-2.797E-08	3.647E-08	1.910E-06	9.609E-08
0.05	-2.814E-09	2.346E-07	5.643E-06	3.797E-07	-1.069E-08	-1.157E-07	-1.258E-07	-2.695E-08	2.769E-08	1.239E-06	6.348E-09
0.06	3.848E-09	2.929E-07	6.445E-06	3.032E-07	-1.383E-08	-1.674E-07	-1.054E-07	-2.421E-08	1.939E-08	1.743E-07	-1.182E-07
0.07	-4.193E-09	3.496E-07	4.631E-06	2.383E-07	-1.653E-08	-2.131E-07	-1.264E-07	-1.964E-08	1.325E-08	-2.455E-06	-2.781E-07
0.08	-4.125E-09	3.972E-07	1.676E-06	1.978E-07	-1.875E-08	-2.468E-07	-7.132E-08	-1.492E-08	1.113E-08	-5.195E-06	-4.602E-07
0.09	3.762E-09	4.295E-07	-1.319E-06	1.770E-07	-2.045E-08	-2.672E-07	-1.918E-08	-1.041E-08	1.133E-08	-8.062E-06	-6.538E-07
0.10	-3.257E-09	4.414E-07	-3.258E-06	1.712E-07	-2.165E-08	-2.740E-07	-4.938E-08	-6.568E-09	1.401E-08	-8.062E-06	-6.538E-07
0.11	-2.741E-09	4.293E-07	-3.233E-06	1.753E-07	-2.231E-08	-2.684E-07	-4.938E-08	-6.568E-09	2.665E-08	-1.064E-05	-8.448E-07
0.12	-2.331E-09	3.940E-07	-6.363E-07	1.639E-07	-2.258E-08	-2.398E-07	-1.324E-07	-3.778E-09	3.745E-08	-1.246E-05	-1.017E-06
0.13	-1.998E-09	3.386E-07	4.267E-06	1.639E-07	-2.258E-08	-2.398E-07	-1.324E-07	-3.778E-09	5.741E-08	-1.310E-05	-1.154E-06
0.14	-1.584E-09	2.680E-07	1.062E-05	1.363E-07	-2.252E-08	-2.241E-07	-4.139E-07	-1.162E-09	8.110E-08	-1.232E-05	-1.243E-06
0.15	-9.080E-10	1.872E-07	1.713E-05	9.422E-08	-2.262E-08	-2.086E-07	-4.957E-07	-1.913E-09	1.324E-07	-6.432E-06	-1.248E-06
0.16	2.697E-10	1.007E-07	2.237E-05	4.268E-08	-2.326E-08	-1.918E-07	6.045E-07	-5.938E-09	1.562E-07	-1.805E-06	-1.166E-06
0.17	2.123E-09	1.200E-08	2.512E-05	-1.044E-08	-2.491E-08	-1.715E-07	6.045E-07	-5.938E-09	1.767E-07	3.377E-06	-1.041E-06
0.18	4.699E-09	-7.661E-08	2.470E-05	-5.804E-08	-2.811E-08	-1.473E-07	6.286E-07	-9.303E-09	1.927E-07	8.628E-06	-8.904E-07
0.19	7.898E-09	-1.631E-07	2.110E-05	-9.560E-08	-3.337E-08	-1.231E-07	6.372E-07	-1.338E-08	2.034E-07	1.352E-05	-7.334E-07
0.20	1.149E-08	-2.450E-07	1.491E-05	-1.215E-07	-4.110E-08	-1.069E-07	6.380E-07	-1.773E-08	2.080E-07	1.774E-05	-5.857E-07
0.21	1.520E-08	-3.197E-07	7.130E-06	-1.370E-07	-5.146E-08	-1.096E-07	6.401E-07	-2.162E-08	2.062E-07	2.112E-05	-4.561E-07
0.22	1.874E-08	-3.835E-07	1.084E-06	-1.448E-07	-6.430E-08	-1.405E-07	6.514E-07	-2.408E-08	2.062E-07	2.361E-05	-3.432E-07
0.23	2.194E-08	-4.332E-07	-8.754E-06	-1.480E-07	-7.906E-08	-2.016E-07	6.748E-07	-2.406E-08	1.838E-07	2.524E-05	-2.359E-07
0.24	2.468E-08	-4.663E-07	-1.528E-05	-1.483E-07	-9.479E-08	-2.830E-07	7.065E-07	-2.058E-08	1.639E-07	2.607E-05	-1.160E-07
0.25	2.696E-08	-4.821E-07	-2.053E-05	-1.466E-07	-1.102E-07	-3.604E-07	7.347E-07	-1.296E-08	1.393E-07	2.617E-05	-3.628E-08
0.26	2.877E-08	-4.815E-07	-2.484E-05	-1.424E-07	-1.235E-07	-3.984E-07	7.413E-07	-1.026E-09	1.108E-07	2.607E-05	-1.160E-07
0.27	3.009E-08	-4.668E-07	-2.880E-05	-1.351E-07	-1.330E-07	-3.581E-07	7.059E-07	-1.477E-08	7.916E-08	2.433E-05	4.863E-07
0.28	3.082E-08	-4.417E-07	-3.314E-05	-1.244E-07	-1.366E-07	-2.085E-07	6.111E-07	-3.328E-08	4.512E-08	2.247E-05	7.804E-07
0.29	3.087E-08	-4.099E-07	-3.844E-05	-1.111E-07	-1.325E-07	-6.201E-07	4.486E-07	-5.275E-08	9.236E-09	2.007E-05	1.098E-06
0.30	3.015E-08	-3.750E-07	-4.501E-05	-9.688E-08	-1.191E-07	4.376E-07	2.232E-07	-7.100E-08	-2.776E-08	1.723E-05	1.413E-06
0.31	2.872E-08	-3.399E-07	-5.277E-05	-8.401E-08	-9.511E-08	8.740E-07	-4.571E-08	-8.576E-08	-6.471E-08	1.410E-05	1.700E-06
0.32	2.675E-08	-3.069E-07	-6.127E-05	-7.453E-08	-6.041E-08	1.306E-06	-3.278E-07	-9.507E-08	9.984E-08	1.086E-05	1.938E-06
0.33	2.455E-08	-2.779E-07	-6.980E-05	-6.961E-08	-1.578E-08	1.662E-06	-5.857E-07	-9.763E-08	-1.308E-07	7.713E-06	2.120E-06
0.34	2.250E-08	-2.542E-07	-7.753E-05	-6.922E-08	3.672E-08	1.880E-06	-7.852E-07	-9.308E-08	-1.550E-07	4.878E-06	2.247E-06

(Appendix F. Continued)

0.35	2.092E-08	-2.366E-07	-8.376E-05	-7.212E-08	9.375E-08	1.924E-06	-9.016E-07	8.213E-08	-1.703E-07	2.563E-06	2.329E-06
0.36	1.999E-08	-2.252E-07	-8.804E-05	-7.632E-08	1.509E-07	1.793E-06	-9.259E-07	6.641E-08	-1.752E-07	9.587E-07	2.378E-06
0.37	1.972E-08	-2.193E-07	-9.029E-05	-7.970E-08	2.031E-07	1.519E-06	-8.654E-07	4.820E-08	-1.701E-07	2.045E-07	2.403E-06
0.38	1.991E-08	-2.171E-07	-9.077E-05	-8.060E-08	2.455E-07	1.158E-06	-7.422E-07	2.995E-08	-1.567E-07	3.583E-07	2.407E-06
0.39	2.024E-08	-2.163E-07	-8.996E-05	-7.821E-08	2.738E-07	7.756E-07	-5.865E-07	1.385E-08	-1.382E-07	1.364E-06	2.390E-06
0.40	2.036E-08	-2.143E-07	-8.834E-05	-7.266E-08	2.855E-07	4.319E-07	-4.299E-07	1.447E-09	-1.185E-07	3.037E-06	2.349E-06
0.41	1.999E-08	-2.088E-07	-8.625E-05	-6.490E-08	2.801E-07	1.676E-07	-2.982E-07	6.599E-09	-1.014E-07	5.075E-06	2.283E-06
0.42	1.896E-08	-1.986E-07	-8.379E-05	-5.631E-08	2.591E-07	7.202E-07	-2.076E-07	1.046E-08	-8.961E-08	7.099E-06	2.199E-06
0.43	1.725E-08	-1.834E-07	-8.081E-05	-4.846E-08	2.261E-07	7.955E-08	-1.625E-07	1.097E-08	-8.463E-08	8.730E-06	2.111E-06
0.44	1.498E-08	-1.645E-07	-7.702E-05	-4.282E-08	1.858E-07	9.117E-08	-1.574E-07	9.333E-09	-8.610E-08	9.662E-06	2.039E-06
0.45	1.233E-08	-1.440E-07	-7.221E-05	-4.064E-08	1.437E-07	-6.447E-08	-1.801E-07	6.774E-09	-9.235E-08	9.737E-06	2.000E-06
0.46	9.526E-09	-1.241E-07	-6.641E-05	-4.289E-08	1.045E-07	2.607E-08	-2.155E-07	4.288E-09	-1.009E-07	8.975E-06	2.007E-06
0.47	6.801E-09	-1.071E-07	-5.994E-05	-5.019E-08	7.202E-08	5.464E-09	-2.499E-07	2.491E-09	-1.090E-07	7.568E-06	2.061E-06
0.48	4.359E-09	-9.452E-08	-5.340E-05	-6.263E-08	4.829E-08	2.160E-08	-2.789E-07	1.510E-09	-1.144E-07	5.824E-06	2.154E-06
0.49	2.369E-09	-8.679E-08	-4.750E-05	-7.956E-08	3.379E-08	2.248E-08	-2.728E-07	1.592E-09	-1.144E-07	2.658E-06	2.269E-06
0.50	9.393E-10	-8.359E-08	-4.288E-05	-9.941E-08	2.747E-08	1.359E-08	-2.789E-07	1.510E-09	-1.144E-07	4.088E-06	2.154E-06
0.51	1.130E-10	-8.385E-08	-3.990E-05	-1.197E-07	2.733E-08	1.977E-09	-2.410E-07	2.559E-09	-1.130E-07	2.658E-06	2.383E-06
0.52	-1.485E-10	-8.607E-08	-3.855E-05	-1.372E-07	3.091E-08	-6.771E-09	-2.052E-07	3.109E-09	-9.785E-08	1.720E-06	2.476E-06
0.53	3.817E-11	-8.868E-08	-3.846E-05	-1.488E-07	3.588E-08	1.008E-08	-1.658E-07	3.443E-09	-8.881E-08	1.398E-06	2.535E-06
0.54	4.947E-10	-9.030E-08	-3.902E-05	-1.518E-07	4.044E-08	-8.527E-09	-1.285E-07	3.537E-09	-8.116E-08	1.794E-06	2.524E-06
0.55	1.016E-09	-8.991E-08	-3.954E-05	-1.448E-07	4.358E-08	-4.971E-09	-9.753E-08	3.459E-09	-7.626E-08	2.351E-06	2.459E-06
0.56	1.415E-09	-8.698E-08	-3.947E-05	-1.284E-07	4.509E-08	-3.140E-09	-7.515E-08	3.321E-09	-7.484E-08	2.947E-06	2.362E-06
0.57	1.567E-09	-8.152E-08	-3.852E-05	-1.046E-07	4.550E-08	-6.298E-09	-6.186E-08	3.238E-09	-7.688E-08	3.533E-06	2.241E-06
0.58	1.438E-09	-7.402E-08	-3.668E-05	-7.704E-08	4.571E-08	-1.631E-08	-5.651E-08	3.290E-09	-8.171E-08	4.129E-06	2.107E-06
0.59	1.090E-09	-6.533E-08	-3.421E-05	-4.950E-08	4.674E-08	-3.288E-08	-5.695E-08	3.513E-09	-8.612E-08	4.796E-06	1.969E-06
0.60	6.550E-10	-5.651E-08	-3.153E-05	-2.552E-08	4.934E-08	-5.578E-08	-6.077E-08	3.892E-09	-9.474E-08	5.593E-06	1.838E-06
0.61	2.950E-10	-4.853E-08	-2.906E-05	-7.449E-09	5.374E-08	-8.146E-08	-6.573E-08	4.368E-09	-1.002E-07	6.535E-06	1.723E-06
0.62	1.442E-10	-4.215E-08	-2.711E-05	-3.866E-09	5.952E-08	-1.077E-07	-7.029E-08	4.856E-09	-1.037E-07	7.563E-06	1.628E-06
0.63	2.625E-10	-3.764E-08	-2.579E-05	-9.017E-09	6.568E-08	-1.322E-07	-7.364E-08	5.262E-09	-1.046E-07	8.552E-06	1.550E-06
0.64	6.066E-10	-3.486E-08	-2.502E-05	-9.569E-09	7.079E-08	-1.536E-07	-7.566E-08	5.262E-09	-1.046E-07	9.332E-06	1.483E-06
0.65	1.031E-09	-3.325E-08	-2.454E-05	-7.462E-09	7.332E-08	-1.708E-07	-7.618E-08	5.518E-09	-9.950E-08	9.739E-06	1.410E-06
0.66	1.318E-09	-3.206E-08	-2.404E-05	-4.461E-09	7.201E-08	-1.836E-07	-7.577E-08	4.866E-09	-8.948E-08	9.079E-06	1.319E-06
0.67	1.234E-09	-3.062E-08	-2.324E-05	-1.798E-09	6.610E-08	-1.920E-07	-7.456E-08	4.300E-09	-8.443E-08	8.056E-06	1.195E-06
0.69	-6.909E-10	-2.562E-08	-2.035E-05	-7.100E-10	5.561E-08	-1.958E-07	-7.279E-08	4.300E-09	-8.443E-08	9.079E-06	1.195E-06
0.70	-2.557E-09	-2.234E-08	-1.846E-05	-7.894E-10	4.130E-08	-1.954E-07	-7.072E-08	3.702E-09	-7.996E-08	8.742E-06	8.440E-07
0.71	-4.813E-09	-1.922E-08	-1.657E-05	-5.378E-10	2.456E-08	-1.914E-07	-6.873E-08	3.179E-09	-7.616E-08	5.318E-06	6.331E-07
0.72	-7.167E-09	-1.685E-08	-1.495E-05	-2.345E-10	7.157E-09	-1.846E-07	-6.727E-08	2.822E-09	-7.288E-08	3.958E-06	4.207E-07
0.73	-9.294E-09	-1.569E-08	-1.372E-05	-2.172E-11	-9.142E-09	-1.767E-07	-6.673E-08	2.661E-09	-6.983E-08	2.784E-06	2.248E-07
0.74	-1.092E-08	-1.588E-08	-1.289E-05	-6.683E-11	-3.321E-08	-1.694E-07	-6.731E-08	2.757E-09	-6.670E-08	1.851E-06	5.967E-08
0.75	-1.187E-08	-1.723E-08	-1.235E-05	-6.641E-11	3.321E-08	-1.643E-07	-6.801E-08	3.001E-09	-6.324E-08	1.149E-06	6.751E-08
0.76	-1.213E-08	-1.930E-08	-1.188E-05	-3.177E-11	-4.374E-08	-1.619E-07	-7.067E-08	3.333E-09	-5.938E-08	6.251E-07	-1.566E-07
0.77	-1.184E-08	-2.151E-08	-1.128E-05	-2.708E-12	4.552E-08	-1.626E-07	-7.204E-08	3.659E-09	-5.517E-08	2.173E-07	-2.133E-07
0.78	-1.122E-08	-2.332E-08	-1.043E-05	-7.451E-12	-4.608E-08	-1.608E-07	-7.002E-08	4.000E-09	-4.508E-08	-1.220E-07	-2.461E-07
0.79	-1.053E-08	-2.433E-08	-9.298E-06	-4.806E-12	4.772E-08	-1.538E-07	-6.579E-08	3.953E-09	-4.650E-08	-4.090E-07	-2.636E-07
0.80	-9.998E-09	-2.435E-08	-7.952E-06	-3.404E-13	-4.978E-08	-1.538E-07	-5.967E-08	3.781E-09	-4.252E-08	-6.302E-07	-2.727E-07
0.81	-9.814E-09	-2.343E-08	-6.539E-06	7.332E-13	5.272E-08	-1.160E-07	-5.242E-08	3.529E-09	-3.906E-08	-7.553E-07	-2.776E-07
0.82	-9.814E-09	-2.174E-08	-5.216E-06	1.246E-14	5.604E-08	-8.656E-08	-4.500E-08	3.246E-09	-3.398E-08	-6.210E-07	-2.795E-07
0.83	-1.010E-08	-1.957E-08	-4.107E-06	5.822E-15	5.890E-08	-5.512E-08	-4.832E-08	2.974E-09	-3.231E-08	-6.210E-07	-2.751E-07
0.84	-1.047E-08	-1.719E-08	-3.278E-06	8.033E-16	6.042E-08	-2.770E-08	-3.300E-08	2.733E-09	-3.105E-08	-2.572E-08	-2.655E-07
0.85	-1.081E-08	-1.485E-08	-2.733E-06	2.436E-16	5.992E-08	-1.074E-08	-2.929E-08	2.530E-09	-3.006E-08	3.453E-07	-2.491E-07
0.86	-1.106E-08	-1.274E-08	-2.434E-06	7.735E-17	5.718E-08	-9.325E-09	-2.704E-08	2.355E-09	-2.917E-08	6.943E-07	-2.249E-07
0.87	-1.124E-08	-1.101E-08	-2.324E-06	1.104E-17	5.242E-08	-2.564E-08	-2.588E-08	2.195E-09	-2.829E-08	9.759E-07	-1.926E-07

(Appendix F. ContInued)

0.88	-1.142E-08	9.748E-09	-2.357E-06	-4.838E-17	-4.631E-08	-5.803E-08	-2.531E-08	-2.042E-09	-2.738E-08	1.160E-06	-1.530E-07
0.89	-1.173E-08	9.002E-09	-2.503E-06	0.000E+00	-3.973E-08	-1.011E-07	-2.490E-08	-1.896E-09	-2.650E-08	1.233E-06	-1.087E-07
0.90	-1.226E-08	8.759E-09	-2.755E-06	0.000E+00	-3.354E-08	-1.467E-07	-2.436E-08	-1.771E-09	-2.576E-08	1.196E-06	-6.441E-08
0.91	-1.302E-08	8.950E-09	-3.115E-06	0.000E+00	-2.839E-08	-1.863E-07	-2.359E-08	-1.687E-09	-2.532E-08	1.061E-06	-2.611E-08
0.92	-1.396E-08	9.450E-09	-3.586E-06	0.000E+00	-2.458E-08	-2.125E-07	-2.263E-08	-1.665E-09	-2.530E-08	8.509E-07	-5.686E-10
0.93	-1.492E-08	1.010E-08	-4.156E-06	0.000E+00	-2.209E-08	-2.211E-07	-2.160E-08	-1.722E-09	-2.578E-08	5.933E-07	-6.406E-09
0.94	-1.572E-08	1.072E-08	-4.797E-06	0.000E+00	-2.061E-08	-2.119E-07	-2.065E-08	-1.864E-09	-2.670E-08	3.211E-07	-8.513E-09
0.95	-1.615E-08	1.118E-08	-5.461E-06	0.000E+00	-1.901E-08	-1.884E-07	-1.991E-08	-2.083E-09	-2.793E-08	6.861E-08	-4.503E-08
0.96	-1.611E-08	1.136E-08	-6.086E-06	0.000E+00	-1.822E-08	-1.765E-07	-1.919E-08	-2.357E-09	-2.924E-08	-1.319E-07	-9.899E-08
0.97	-1.553E-08	1.123E-08	-6.608E-06	0.000E+00	-1.802E-08	-1.227E-07	-1.919E-08	-2.653E-09	-3.037E-08	-2.558E-07	-1.633E-07
0.98	-1.447E-08	1.080E-08	-6.966E-06	0.000E+00	-1.730E-08	-9.282E-08	-1.913E-08	-2.932E-09	-3.106E-08	-2.914E-07	-2.292E-07
0.99	-1.307E-08	1.012E-08	-7.118E-06	0.000E+00	-1.635E-08	-7.019E-08	-1.912E-08	-3.161E-09	-3.116E-08	-2.424E-07	-2.895E-07
1.00	-1.149E-08	9.247E-09	-7.045E-06	0.000E+00	-1.560E-08	-5.577E-08	-1.906E-08	-3.314E-09	-3.060E-08	-1.285E-07	-3.393E-07
1.01	-9.908E-09	8.258E-09	-6.758E-06	0.000E+00	-1.532E-08	-4.834E-08	-1.882E-08	-3.376E-09	-2.944E-08	1.890E-08	-3.777E-07
1.02	-8.456E-09	7.214E-09	-6.289E-06	0.000E+00	-1.570E-08	-4.538E-08	-1.835E-08	-3.351E-09	-2.780E-08	1.640E-07	-4.072E-07
1.03	-7.225E-09	6.178E-09	-5.692E-06	0.000E+00	-1.681E-08	-4.421E-08	-1.760E-08	-3.251E-09	-2.591E-08	2.748E-07	-4.324E-07
1.04	-6.248E-09	5.216E-09	-5.030E-06	0.000E+00	-1.858E-08	-4.276E-08	-1.660E-08	-3.097E-09	-2.398E-08	3.298E-07	-4.574E-07
1.05	-5.515E-09	4.399E-09	-4.367E-06	0.000E+00	-2.080E-08	-4.012E-08	-1.539E-08	-2.909E-09	-2.221E-08	3.225E-07	-4.848E-07
1.06	-4.985E-09	3.801E-09	-3.761E-06	0.000E+00	-2.318E-08	-3.654E-08	-1.403E-08	-2.703E-09	-2.076E-08	2.604E-07	-5.130E-07
1.07	-4.606E-09	3.488E-09	-3.258E-06	0.000E+00	-2.541E-08	-3.308E-08	-1.259E-08	-2.489E-09	-1.969E-08	1.592E-07	-5.376E-07
1.08	-4.325E-09	3.494E-09	-2.886E-06	0.000E+00	-2.722E-08	-3.102E-08	-1.115E-08	-2.271E-09	-1.897E-08	3.751E-08	-5.526E-07
1.09	-4.097E-09	3.810E-09	-2.650E-06	0.000E+00	-2.841E-08	-3.139E-08	-9.755E-09	-2.052E-09	-1.851E-08	-8.733E-08	-5.26E-07
1.10	-3.889E-09	4.397E-09	-2.548E-06	0.000E+00	-2.893E-08	-3.468E-08	-8.481E-09	-1.832E-09	-1.815E-08	-2.083E-07	-5.341E-07
1.11	-3.666E-09	5.140E-09	-2.541E-06	0.000E+00	-2.874E-08	-4.024E-08	-7.380E-09	-1.631E-09	-1.770E-08	-3.241E-07	-5.006E-07
1.12	-3.410E-09	5.897E-09	-2.576E-06	0.000E+00	-2.794E-08	-4.688E-08	-6.454E-09	-1.468E-09	-1.703E-08	-4.303E-07	-4.942E-07
1.13	-3.109E-09	6.531E-09	-2.602E-06	0.000E+00	-2.663E-08	-5.317E-08	-5.702E-09	-1.363E-09	-1.606E-08	-5.262E-07	-4.194E-07
1.14	-2.756E-09	6.931E-09	-2.573E-06	0.000E+00	-2.494E-08	-5.762E-08	-5.139E-09	-1.337E-09	-1.472E-08	-6.165E-07	-3.909E-07
1.15	-2.311E-09	6.829E-09	-2.365E-06	0.000E+00	-2.274E-08	-5.761E-08	-4.613E-09	-1.448E-09	-1.296E-08	-6.705E-07	-3.951E-07
1.16	-1.830E-09	6.358E-09	-2.036E-06	0.000E+00	-2.032E-08	-5.430E-08	-4.118E-09	-1.448E-09	-1.107E-08	-6.900E-07	-3.237E-07
1.20	-1.879E-09	6.414E-09	-1.313E-06	-6.551E-13	-1.375E-08	-3.067E-08	-3.513E-09	-1.988E-09	-1.434E-08	-6.014E-07	-3.911E-07
1.25	-1.252E-09	2.699E-09	-6.880E-07	3.510E-14	9.902E-09	-2.308E-08	-2.106E-09	-1.736E-09	-1.257E-08	-6.300E-07	-3.536E-07
1.35	-7.201E-10	1.712E-09	-3.035E-07	9.302E-15	-6.251E-09	-1.618E-08	-1.534E-09	-1.513E-09	-1.094E-08	-5.621E-07	-3.248E-07
1.40	-5.435E-10	1.462E-09	-2.948E-07	0.000E+00	-3.610E-09	-1.093E-08	-1.495E-09	-1.360E-09	-9.234E-09	-4.449E-07	-3.123E-07
1.50	-3.892E-10	1.299E-09	-2.899E-07	0.000E+00	-1.502E-09	-8.137E-09	-1.635E-09	-1.250E-09	-5.977E-09	-3.805E-07	-3.159E-07
1.60	-3.911E-10	7.650E-10	-2.160E-07	0.000E+00	-1.327E-09	-9.1301E-08	-1.294E-09	-9.969E-10	-3.600E-09	-4.873E-07	-3.027E-07
1.65	-3.925E-10	9.658E-10	-2.468E-07	0.000E+00	-1.294E-09	-1.123E-08	-1.548E-09	-1.199E-09	-4.843E-09	-3.019E-07	-3.143E-07
1.70	-2.971E-10	4.317E-10	-1.770E-07	0.000E+00	-1.353E-09	-1.141E-08	-1.196E-09	-9.363E-10	-3.217E-09	-5.667E-07	-2.537E-07
1.75	-2.393E-10	3.455E-10	-8.625E-08	0.000E+00	-1.342E-09	-8.949E-09	-1.101E-09	-9.620E-10	-2.881E-09	-5.968E-07	-2.261E-07
1.80	-2.030E-10	3.139E-10	-5.294E-08	0.000E+00	-1.240E-09	-5.401E-09	-9.029E-10	-1.145E-09	-2.588E-09	-5.770E-07	-2.019E-07
1.85	-1.904E-10	3.168E-10	-3.551E-08	0.000E+00	-1.195E-09	-5.118E-09	-8.389E-10	-1.166E-09	-2.152E-09	-4.622E-07	-1.620E-07
1.90	-1.913E-10	3.271E-10	-3.099E-08	0.000E+00	-1.167E-09	-5.396E-09	-8.169E-10	-1.089E-09	-1.964E-09	-4.063E-07	-1.435E-07
1.95	-1.946E-10	3.217E-10	-3.246E-08	0.000E+00	-1.149E-09	-5.588E-09	-8.257E-10	-9.306E-10	-1.761E-09	-3.665E-07	-1.268E-07
2.00	-1.936E-10	2.912E-10	-3.387E-08	0.000E+00	-1.129E-09	-5.262E-09	-8.437E-10	-7.370E-10	-1.549E-09	-3.459E-07	-1.138E-07
2.05	-1.961E-10	2.425E-10	-3.276E-08	0.000E+00	-1.102E-09	-4.397E-09	-8.551E-10	-5.555E-10	-1.363E-09	-3.411E-07	-1.049E-07
2.10	-1.996E-10	1.919E-10	-2.978E-08	0.000E+00	-1.065E-09	-3.295E-09	-8.559E-10	-4.187E-10	-1.239E-09	-3.424E-07	-9.891E-08
2.15	-2.063E-10	1.531E-10	-2.657E-08	0.000E+00	-1.019E-09	-2.312E-09	-8.475E-10	-3.398E-10	-1.187E-09	-3.365E-07	-9.372E-08
2.20	-2.119E-10	1.302E-10	-2.428E-08	0.000E+00	-9.687E-10	-1.654E-09	-8.244E-10	-3.127E-10	-1.179E-09	-3.136E-07	-8.893E-08
2.25	-2.107E-10	1.180E-10	-2.307E-08	0.000E+00	-9.206E-10	-1.331E-09	-7.704E-10	-3.187E-10	-1.167E-09	-2.746E-07	-8.590E-08
2.30	-1.992E-10	1.081E-10	-2.239E-08	0.000E+00	-8.828E-10	-1.257E-09	-6.677E-10	-3.383E-10	-1.111E-09	-2.320E-07	-8.616E-08
2.35	-1.786E-10	9.532E-11	-2.136E-08	0.000E+00	-8.603E-10	-1.340E-09	-5.140E-10	-3.613E-10	-1.003E-09	-2.026E-07	-8.926E-08

(Appendix F. Continued)

2.40	-1.531E-10	-7.968E-11	-1.927E-08	0.000E+00	-8.509E-10	-1.499E-09	-3.334E-10	-3.866E-10	-8.647E-10	-1.964E-07	-9.226E-08
2.45	-1.284E-10	-6.430E-11	-1.610E-08	0.000E+00	-8.481E-10	-1.640E-09	-1.686E-10	-4.130E-10	-7.304E-10	-2.108E-07	-9.136E-08
2.50	-1.093E-10	-5.205E-11	-1.256E-08	0.000E+00	-8.492E-10	-1.669E-09	-5.748E-11	-4.264E-10	-6.237E-10	-2.321E-07	-8.465E-08
2.55	-9.904E-11	-4.403E-11	-9.829E-09	0.000E+00	-8.587E-10	-1.542E-09	-9.103E-12	-4.040E-10	-5.499E-10	-2.445E-07	-7.353E-08
2.60	-9.889E-11	-4.007E-11	-8.790E-09	0.000E+00	-8.828E-10	-1.308E-09	4.785E-13	-3.322E-10	-5.027E-10	-2.396E-07	-6.174E-08
2.65	-1.072E-10	-3.950E-11	-9.520E-09	0.000E+00	-9.162E-10	-1.086E-09	9.6307E-12	-2.217E-10	-4.752E-10	-2.195E-07	-5.299E-08
2.70	-1.189E-10	-4.125E-11	-1.142E-08	0.000E+00	-9.386E-10	-9.729E-10	4.307E-11	-1.063E-10	-4.631E-10	-1.936E-07	-4.886E-08
2.75	-1.275E-10	-4.352E-11	-1.378E-08	0.000E+00	-9.255E-10	-9.797E-10	1.017E-10	-2.136E-11	-4.601E-10	-1.700E-07	-4.845E-08
2.80	-1.282E-10	-4.404E-11	-1.630E-08	0.000E+00	-8.681E-10	-1.024E-09	1.639E-10	-1.802E-11	-4.556E-10	-1.508E-07	-4.947E-08
2.85	-1.213E-10	-4.134E-11	-1.906E-08	0.000E+00	-7.842E-10	-1.001E-09	2.116E-10	-2.128E-11	-4.386E-10	-1.342E-07	-4.954E-08
2.90	-1.117E-10	-3.561E-11	-2.204E-08	0.000E+00	-7.086E-10	-8.770E-10	2.408E-10	-9.938E-12	-4.067E-10	-1.181E-07	-4.714E-08
2.95	-1.046E-10	-2.860E-11	-2.477E-08	0.000E+00	-6.712E-10	-7.044E-10	2.599E-10	-7.623E-13	-3.676E-10	-1.028E-07	-4.202E-08
3.00	-1.023E-10	-2.231E-11	-2.634E-08	0.000E+00	-6.786E-10	-5.698E-10	2.785E-10	-2.012E-12	-3.329E-10	-8.916E-08	-3.521E-08
3.05	-1.025E-10	-1.786E-11	-2.586E-08	0.000E+00	-6.786E-10	-5.698E-10	2.785E-10	-1.055E-12	-3.075E-10	-7.583E-08	-2.855E-08
3.10	-1.013E-10	-1.527E-11	-2.315E-08	0.000E+00	-7.380E-10	-4.754E-10	3.173E-10	-7.781E-14	-2.870E-10	-6.055E-08	-2.377E-08
3.15	-9.600E-11	-1.397E-11	-1.885E-08	0.000E+00	-7.355E-10	-4.247E-10	3.277E-10	-1.905E-13	-2.633E-10	-4.287E-08	-2.131E-08
3.20	-8.717E-11	-1.341E-11	-1.415E-08	0.000E+00	-7.017E-10	-3.771E-10	3.288E-10	-2.876E-14	-2.324E-10	-2.542E-08	-2.026E-08
3.25	-6.997E-11	-1.323E-11	-1.013E-08	0.000E+00	-6.549E-10	-4.090E-10	3.246E-10	-1.379E-15	-1.976E-10	-1.190E-08	-1.924E-08
3.30	-6.997E-11	-1.308E-11	-7.325E-09	0.000E+00	-6.201E-10	-5.441E-10	3.229E-10	-1.007E-16	-1.654E-10	-4.056E-09	-1.778E-08
3.35	-6.622E-11	-1.263E-11	-5.624E-09	0.000E+00	-6.114E-10	-6.685E-10	3.320E-10	-4.219E-17	-1.410E-10	-1.277E-09	-1.673E-08
3.40	-6.21E-11	-1.172E-11	-4.567E-09	0.000E+00	-6.249E-10	-6.048E-10	3.542E-10	-1.012E-17	-1.257E-10	-2.187E-09	-1.716E-08
3.45	-6.860E-11	-1.045E-11	-3.717E-09	0.000E+00	-6.434E-10	-2.913E-10	3.827E-10	0.000E+00	-1.179E-10	-5.671E-09	-1.899E-08
3.50	-7.174E-11	-9.150E-12	-2.891E-09	0.000E+00	-6.513E-10	-1.026E-10	4.055E-10	0.000E+00	-1.143E-10	-1.089E-08	-2.073E-08
3.55	-7.373E-11	-8.093E-12	-2.118E-09	0.000E+00	-6.445E-10	-2.986E-10	4.133E-10	0.000E+00	-1.131E-10	-1.616E-08	-2.105E-08
3.60	-7.291E-11	-7.375E-12	-1.493E-09	0.000E+00	-6.301E-10	-1.170E-10	4.102E-10	0.000E+00	-1.099E-10	-1.943E-08	-2.010E-08
3.65	-6.720E-11	-6.858E-12	-1.049E-09	0.000E+00	-6.156E-10	-3.065E-10	4.022E-10	0.000E+00	-1.023E-10	-1.895E-08	-2.003E-08
3.70	-5.688E-11	-6.397E-12	-7.473E-10	0.000E+00	-6.045E-10	-7.158E-10	3.952E-10	0.000E+00	-9.039E-11	-1.495E-08	-2.239E-08
3.75	-4.190E-11	-5.772E-12	-4.980E-10	0.000E+00	-6.045E-10	-7.158E-10	3.952E-10	0.000E+00	-7.439E-11	-8.419E-09	-2.803E-08
3.80	-2.671E-11	-5.071E-12	-2.911E-10	0.000E+00	-5.906E-10	-7.494E-10	3.742E-10	0.000E+00	-5.881E-11	-1.787E-09	-3.467E-08
3.85	-1.831E-11	-4.553E-12	-1.705E-10	0.000E+00	-5.556E-10	-4.200E-11	2.998E-10	0.000E+00	-5.050E-11	-1.632E-09	-3.826E-08
3.90	-1.709E-11	-4.418E-12	-1.506E-10	0.000E+00	-5.472E-10	-3.722E-11	2.876E-10	0.000E+00	-4.903E-11	-2.057E-09	-3.829E-08
Z	C4H3	C4H4	C4H5	C4H6	C5H2	C5H3	C5H4	C5H5	C5H6	C6H2	C6H4
0.00	-1.631E-09	4.264E-09	9.084E-10	4.480E-10	-2.510E-11	-3.718E-11	2.935E-10	1.718E-09	1.275E-09	-9.898E-11	-2.795E-10
0.01	-1.847E-09	3.748E-09	9.269E-10	6.376E-10	-2.968E-11	-4.120E-11	3.537E-10	1.681E-09	1.177E-09	-1.270E-10	-3.200E-10
0.02	-3.089E-09	1.100E-09	8.183E-10	1.296E-09	-6.094E-11	-5.120E-11	5.560E-10	1.416E-09	2.485E-10	-2.849E-10	-5.786E-10
0.03	-4.573E-09	-1.631E-09	-1.124E-10	8.344E-10	-1.066E-10	-8.107E-11	-3.148E-09	9.383E-10	-1.485E-09	5.051E-10	-9.939E-10
0.04	-5.252E-09	-2.986E-09	-1.316E-09	4.396E-10	-1.329E-10	-1.973E-10	-7.289E-09	5.612E-10	-2.660E-09	-7.782E-10	-1.346E-09
0.05	-5.322E-09	-3.647E-09	-2.533E-09	-1.988E-09	-1.416E-10	-3.801E-10	-1.220E-08	2.829E-10	-3.293E-09	-1.166E-09	-1.663E-09
0.06	-4.976E-09	4.193E-09	-3.540E-09	-3.243E-09	-1.395E-10	-5.435E-10	-1.743E-08	8.646E-11	-3.451E-09	-1.681E-09	-1.970E-09
0.07	-4.110E-09	4.699E-09	-4.068E-09	-3.747E-09	-1.239E-10	-6.348E-10	-2.242E-08	2.622E-11	-2.901E-09	-2.332E-09	-2.238E-09
0.08	-3.027E-09	5.928E-09	-3.886E-09	-2.795E-09	-1.070E-10	-5.543E-10	-2.661E-08	6.040E-11	-1.786E-09	-3.126E-09	-2.512E-09
0.09	-1.831E-09	8.053E-09	-2.889E-09	-2.126E-11	-9.957E-11	-2.238E-10	-2.949E-08	1.646E-10	-1.540E-10	-4.025E-09	-2.794E-09
0.10	-6.384E-10	1.108E-08	-1.075E-09	5.085E-09	-1.142E-10	-3.484E-10	-3.057E-08	3.020E-10	1.955E-09	-4.992E-09	-3.083E-09
0.11	-4.508E-10	-1.476E-08	-1.450E-09	1.238E-09	-1.625E-10	1.023E-09	-3.041E-08	4.304E-10	4.522E-09	-6.019E-09	-3.360E-09
0.12	1.379E-09	-1.842E-08	4.343E-09	2.147E-08	-2.513E-10	1.480E-09	-2.598E-08	4.984E-10	7.482E-09	-7.149E-09	-3.591E-09
0.13	2.155E-09	-2.107E-08	7.188E-08	3.149E-08	-3.781E-10	-1.241E-09	-2.049E-08	4.791E-10	1.083E-08	-8.516E-09	-3.721E-09
0.14	2.792E-09	-2.166E-08	9.566E-09	4.134E-08	-5.330E-10	-2.427E-10	-1.338E-08	3.676E-10	1.453E-08	-1.034E-08	-3.700E-09
0.15	3.308E-09	-1.925E-08	1.114E-08	4.976E-08	-7.010E-10	-3.433E-09	-5.341E-09	1.894E-10	1.853E-08	-1.289E-08	-3.509E-09
0.16	3.717E-09	-1.321E-08	1.173E-08	5.561E-08	-8.697E-10	-8.524E-09	-1.835E-09	-1.226E-12	2.269E-08	-1.637E-08	-3.181E-09
0.17	4.021E-09	-3.343E-09	1.134E-08	5.805E-08	-1.038E-09	-1.529E-08	1.039E-08	1.296E-10	2.685E-08	-2.087E-08	-2.826E-09
0.18	4.214E-09	1.000E-08	1.018E-08	5.670E-08	-1.223E-09	-2.302E-08	1.672E-08	-1.187E-10	3.082E-08	-2.630E-08	-2.630E-09
0.19	4.304E-09	2.603E-08	8.535E-09	5.169E-08	-1.463E-09	-3.059E-08	2.146E-08	9.348E-11	3.437E-08	-3.248E-08	-2.822E-09

(Appendix F. Continued)

0.20	4.319E-09	4.365E-08	6.754E-09	4.362E-08	-1.810E-09	-3.666E-08	2.459E-08	5.375E-10	3.731E-08	-3.932E-08	-3.616E-09
0.21	4.309E-09	6.164E-08	5.128E-09	3.343E-08	-2.317E-09	-3.997E-08	2.635E-08	1.203E-09	3.950E-08	-4.712E-08	-5.129E-09
0.22	4.342E-09	7.886E-08	3.849E-09	2.228E-08	-3.019E-09	-3.964E-08	2.74E-08	2.041E-09	4.078E-08	-5.686E-08	-7.306E-09
0.23	4.484E-09	9.441E-08	2.989E-09	1.131E-08	-3.913E-09	-3.541E-08	2.785E-08	2.967E-09	4.104E-08	-7.032E-08	-9.873E-09
0.24	4.783E-09	1.077E-07	2.515E-09	1.504E-09	-4.948E-09	-2.770E-08	2.875E-08	3.887E-09	4.014E-08	-8.991E-08	-1.235E-08
0.25	5.248E-09	1.185E-07	2.322E-09	-6.453E-09	-6.021E-09	-1.754E-08	3.033E-08	4.710E-09	1.181E-08	-1.181E-08	-1.411E-08
0.26	5.851E-09	1.266E-07	2.277E-09	-1.221E-08	-6.989E-09	-6.309E-09	3.271E-08	5.366E-09	3.437E-08	-1.566E-07	-1.452E-08
0.27	6.528E-09	1.322E-07	2.261E-09	-1.575E-08	-7.691E-09	-4.518E-09	3.574E-08	5.820E-09	2.931E-08	-2.054E-07	-1.312E-08
0.28	7.197E-09	1.352E-07	2.188E-09	-1.738E-08	-7.973E-08	-1.371E-08	4.207E-08	6.165E-09	1.525E-08	-3.211E-07	-4.503E-09
0.29	7.778E-09	1.355E-07	2.014E-09	-1.759E-08	-7.714E-09	-2.046E-08	4.307E-08	6.150E-09	1.525E-08	-3.211E-07	-4.503E-09
0.30	8.206E-09	1.326E-07	1.729E-09	-1.696E-08	-6.843E-09	-2.446E-08	4.437E-08	6.150E-09	1.525E-08	-3.211E-07	-4.503E-09
0.31	8.445E-09	1.265E-07	1.349E-09	-1.604E-08	-5.355E-09	-2.587E-08	4.558E-08	6.099E-09	1.824E-09	-4.164E-07	-8.814E-09
0.32	8.486E-09	1.170E-07	8.978E-09	-1.526E-08	-3.312E-09	-2.520E-08	4.558E-08	6.079E-09	1.017E-08	-4.369E-07	-1.519E-08
0.33	8.350E-09	1.043E-07	4.075E-07	-1.486E-08	-8.404E-10	-2.322E-08	4.451E-08	6.141E-09	-1.764E-08	-4.314E-07	-2.033E-08
0.34	8.077E-09	8.937E-08	-9.165E-11	-1.489E-08	1.880E-09	-2.076E-08	4.274E-08	6.313E-09	-2.380E-08	-3.985E-07	-2.381E-08
0.35	7.726E-09	7.354E-08	-5.686E-10	-1.522E-08	4.635E-09	-1.868E-08	4.073E-08	6.597E-09	-2.837E-08	-3.402E-07	-2.568E-08
0.36	7.363E-09	5.854E-08	-9.929E-10	-1.565E-08	7.193E-09	-1.777E-08	3.891E-08	6.968E-09	-3.126E-08	-2.617E-07	-2.644E-08
0.37	7.054E-09	4.605E-08	-1.337E-09	-1.598E-08	9.341E-09	-1.867E-08	3.754E-08	7.379E-09	-3.255E-08	-1.701E-07	-2.690E-08
0.38	6.848E-09	3.728E-08	-1.579E-09	-1.608E-08	1.091E-08	-2.180E-08	3.655E-08	7.768E-09	-3.241E-08	-7.260E-08	-2.799E-08
0.39	6.767E-09	3.251E-08	-1.710E-09	-1.598E-08	1.180E-08	-2.733E-08	3.601E-08	8.067E-09	-3.112E-08	-2.448E-08	-3.046E-08
0.40	6.790E-09	3.093E-08	-1.734E-09	-1.580E-08	1.200E-08	-3.461E-08	3.513E-08	8.213E-09	-2.893E-08	-1.163E-07	-3.468E-08
0.41	6.853E-09	3.071E-08	-1.671E-09	-1.573E-08	1.161E-08	-4.315E-08	3.405E-08	8.154E-09	-2.614E-08	-1.993E-07	-4.701E-08
0.42	6.857E-09	2.945E-08	-1.549E-09	-1.595E-08	1.076E-08	-5.172E-08	3.050E-08	7.855E-09	-2.301E-08	-2.706E-07	-4.701E-08
0.43	6.696E-09	2.479E-08	-1.406E-09	-1.656E-08	9.652E-09	-5.898E-08	2.588E-08	7.309E-09	-1.978E-08	-3.279E-07	-5.318E-08
0.44	6.280E-09	1.510E-08	-1.271E-09	-1.751E-08	8.489E-09	-6.365E-08	1.953E-08	6.531E-09	-1.670E-08	-3.690E-07	-5.759E-08
0.45	5.717E-09	3.020E-11	-1.167E-09	-1.862E-08	7.430E-09	-6.476E-08	1.173E-08	5.557E-09	-1.395E-08	-3.927E-07	-5.901E-08
0.46	4.598E-09	-1.936E-08	-1.103E-09	-1.962E-08	6.575E-09	-6.190E-08	3.003E-09	4.438E-09	-1.169E-08	-4.001E-07	-5.661E-08
0.47	3.457E-09	-4.080E-08	-1.074E-09	-2.012E-08	5.962E-09	-5.252E-08	-5.925E-08	3.233E-09	-9.999E-09	-3.951E-07	-5.019E-08
0.48	2.291E-09	-6.140E-08	-1.069E-09	-2.018E-08	5.571E-09	-4.28E-08	-1.428E-08	1.996E-09	-8.866E-09	-3.845E-07	-4.021E-08
0.49	1.250E-09	-7.837E-08	-1.072E-09	-1.941E-08	5.344E-09	-3.416E-08	-2.139E-08	1.686E-09	-8.210E-09	-3.773E-07	-2.771E-08
0.50	4.580E-10	-8.976E-08	-1.063E-09	-1.793E-08	5.215E-09	-2.231E-08	-2.676E-08	-4.187E-09	-7.895E-09	-3.827E-07	-1.412E-08
0.51	-1.903E-11	-9.485E-08	-1.072E-09	-1.589E-08	5.123E-09	-1.131E-08	-3.017E-08	-1.551E-09	-7.757E-09	-4.069E-07	-9.506E-10
0.52	-1.891E-10	-9.424E-08	-1.051E-09	-1.354E-08	5.028E-09	-2.126E-09	-3.165E-08	-2.621E-09	-7.648E-09	-4.514E-07	-1.045E-08
0.53	-1.251E-10	-8.952E-08	-1.041E-09	-1.111E-08	4.908E-09	-4.735E-09	-3.146E-08	-3.625E-09	-7.458E-09	-5.118E-07	-1.912E-08
0.54	5.902E-11	-8.274E-08	-1.044E-09	-8.810E-09	4.758E-09	-9.215E-09	-3.001E-08	-4.554E-09	-7.132E-09	-5.782E-07	-2.463E-08
0.55	2.405E-10	-7.582E-08	-1.066E-09	-6.793E-09	4.582E-09	-1.163E-08	-2.778E-08	-5.392E-09	-6.668E-09	-6.380E-07	-2.703E-08
0.56	3.190E-10	-7.004E-08	-1.107E-09	-5.120E-09	4.387E-09	-1.250E-08	-2.526E-08	-6.116E-09	-6.104E-09	-6.787E-07	-2.678E-08
0.57	2.380E-10	-6.587E-08	-1.160E-09	-3.793E-09	4.185E-09	-1.245E-08	-2.286E-08	-6.701E-09	-5.490E-09	-6.916E-07	-2.462E-08
0.58	-8.977E-12	-6.301E-08	-1.211E-09	-2.776E-09	3.985E-09	-1.201E-08	-2.089E-08	-7.122E-09	-4.877E-09	-6.740E-07	-2.134E-08
0.59	-3.856E-10	-6.072E-08	-1.249E-09	-2.013E-09	3.800E-09	-1.156E-08	-1.953E-08	-7.361E-09	-4.301E-09	-6.296E-07	-1.769E-08
0.60	-8.296E-10	-5.817E-08	-1.262E-09	-1.455E-09	3.644E-09	-1.133E-08	-1.881E-08	-7.409E-09	-3.776E-09	-5.675E-07	-1.423E-08
0.61	-1.273E-09	-5.475E-08	-1.247E-09	-1.065E-09	3.528E-09	-1.137E-08	-1.864E-08	-7.267E-09	-3.306E-09	-4.995E-07	-1.133E-08
0.62	-1.658E-09	-5.030E-08	-1.205E-09	-8.160E-10	3.456E-09	-1.159E-08	-1.883E-08	-6.945E-09	-2.883E-09	-4.369E-07	-9.144E-09
0.63	-1.951E-09	-4.503E-08	-1.145E-09	-6.905E-10	3.431E-09	-1.185E-08	-1.923E-08	-6.466E-09	-2.503E-09	-3.878E-07	-7.647E-09
0.64	-2.140E-09	-3.945E-08	-1.079E-09	-6.702E-10	3.447E-09	-1.201E-08	-1.923E-08	-5.857E-09	-2.164E-09	-3.555E-07	-6.724E-09
0.65	-2.232E-09	-3.411E-08	-1.017E-09	-7.327E-10	3.502E-09	-1.193E-08	-1.895E-08	-5.157E-09	-1.870E-09	-3.387E-07	-6.213E-09
0.66	-2.249E-09	-2.939E-08	-9.677E-10	-8.4999E-10	3.595E-09	-1.155E-08	-1.873E-08	-4.419E-09	-1.626E-09	-3.19E-07	-5.954E-09
0.67	-2.214E-09	-2.550E-08	-9.344E-10	-9.8999E-10	3.733E-09	-1.088E-08	-1.673E-08	-3.687E-09	-1.437E-09	-3.281E-07	-5.830E-09
0.68	-2.150E-09	-2.236E-08	-9.188E-10	-1.121E-09	3.926E-09	-9.985E-09	-1.483E-08	-3.024E-09	-1.286E-09	-3.202E-07	-5.772E-09
0.69	-2.076E-09	-1.980E-08	-9.208E-10	-1.259E-09	4.183E-09	-8.966E-09	-1.483E-08	-2.074E-09	-1.176E-09	-3.031E-07	-5.758E-09
0.70	-2.006E-09	-1.761E-08	-9.404E-10	-1.259E-09	4.498E-09	-8.020E-09	-1.030E-08	-2.074E-09	-1.091E-09	-2.746E-07	-5.793E-09
0.71	-1.954E-09	-1.568E-08	-9.787E-10	-1.240E-09	4.845E-09	-7.208E-09	-8.113E-09	-1.829E-09	-1.017E-09	-2.353E-07	-5.892E-09
0.72	-1.930E-09	-1.398E-08	-1.036E-09	-1.165E-09	5.173E-09	-6.631E-09	-6.236E-09	-1.732E-09	-9.441E-10	-1.887E-07	-6.056E-09

(Appendix F. Continued)

0.73 -1.947E-09 -1.258E-08 -1.113E-09 -1.047E-09 5.401E-09 -6.311E-09 -4.770E-09 -1.755E-09 -8.691E-10 1.396E-07 -6.270E-09
0.74 -2.011E-09 -1.156E-08 -1.204E-09 -9.042E-10 5.435E-09 -6.212E-09 -3.733E-09 -1.861E-09 -7.940E-10 9.331E-08 -6.495E-09
0.75 -2.123E-09 -1.096E-08 -1.300E-09 -7.557E-10 5.178E-09 -6.255E-09 -3.069E-09 -2.008E-09 -7.243E-10 5.420E-08 -6.690E-09
0.76 -2.277E-09 -1.071E-08 -1.386E-09 -6.177E-10 4.555E-09 -6.345E-09 -2.680E-09 -2.159E-09 -6.663E-10 2.497E-08 -6.818E-09
0.77 -2.455E-09 -1.068E-08 -1.448E-09 -5.008E-10 3.532E-09 -6.397E-09 -2.448E-09 -2.288E-09 -6.245E-10 6.284E-09 -6.867E-09
0.78 -2.631E-09 -1.066E-08 -1.472E-09 -4.093E-10 2.132E-09 -6.359E-09 -2.275E-09 -2.375E-09 -5.994E-10 3.061E-09 -6.851E-09
0.79 -2.777E-09 -1.049E-08 -1.452E-09 -3.426E-10 4.436E-10 -6.223E-09 -2.091E-09 -2.413E-09 -5.882E-10 5.515E-09 -6.808E-09
0.80 -2.865E-09 -1.008E-08 -1.389E-09 -2.968E-10 -1.389E-09 -6.021E-09 -1.870E-09 -2.397E-09 -5.849E-10 3.925E-09 -6.786E-09
0.81 -2.878E-09 -9.412E-09 -1.295E-09 -2.674E-10 3.185E-09 -5.803E-09 -1.618E-09 -2.330E-09 -5.832E-10 7.021E-10 -6.816E-09
0.82 -2.672E-09 8.583E-09 -1.189E-09 -2.506E-10 4.760E-09 -5.626E-09 -1.362E-09 -2.165E-09 -5.779E-10 2.729E-09 -6.902E-09
0.83 -2.482E-09 6.982E-09 -1.019E-09 -2.428E-10 -5.962E-09 -5.524E-09 -1.136E-09 -2.064E-09 -5.663E-10 6.075E-09 -7.010E-09
0.84 -2.267E-09 6.451E-09 -9.800E-10 -2.472E-10 -6.699E-09 -5.500E-09 -9.694E-10 -1.883E-09 -5.489E-10 9.878E-09 -7.070E-09
0.85 -2.052E-09 6.176E-09 9.749E-10 -2.535E-10 -6.959E-09 -5.526E-09 -8.752E-10 -1.689E-09 -5.286E-10 1.492E-08 -6.999E-09
0.86 -1.858E-09 6.140E-09 9.930E-10 -2.586E-10 -6.805E-09 -5.551E-09 -8.521E-10 -1.496E-09 -5.099E-10 2.154E-08 -6.727E-09
0.87 -1.695E-09 6.280E-09 -1.018E-09 -2.598E-10 -6.360E-09 -5.518E-09 -8.851E-10 -1.319E-09 -4.975E-10 2.921E-08 -6.216E-09
0.88 -1.565E-09 6.514E-09 -1.032E-09 -2.561E-10 -5.768E-09 -5.380E-09 -9.512E-10 -1.173E-09 -4.949E-10 3.633E-08 -5.484E-09
0.89 -1.464E-09 6.763E-09 -1.022E-09 -2.479E-10 -4.645E-09 -5.116E-09 -1.026E-09 -1.067E-09 -5.039E-10 4.062E-08 -4.601E-09
0.90 -1.382E-09 6.964E-09 -9.822E-10 -2.376E-10 -4.252E-09 -4.266E-09 -1.120E-09 -1.003E-09 -5.239E-10 3.970E-08 -3.674E-09
0.91 -1.311E-09 7.079E-09 -9.162E-10 -2.282E-10 -3.977E-09 -3.768E-09 -1.121E-09 -9.813E-10 -5.23E-10 3.181E-08 -2.826E-09
0.92 -1.243E-09 7.097E-09 -8.349E-10 -2.227E-10 -3.784E-09 -3.293E-09 -1.089E-09 -1.029E-09 -6.147E-10 1.652E-08 -2.161E-09
0.93 -1.174E-09 7.025E-09 -7.537E-10 -2.225E-10 -3.626E-09 -2.889E-09 -1.032E-09 -1.077E-09 -6.376E-10 5.075E-09 -1.745E-09
0.94 -1.101E-09 6.890E-09 -6.871E-10 -2.273E-10 -3.466E-09 -2.585E-09 -9.600E-10 -1.129E-09 -6.376E-10 3.041E-08 -1.589E-09
0.95 -1.023E-09 6.726E-09 -6.450E-10 -2.349E-10 -3.290E-09 -2.386E-09 -8.838E-10 -1.180E-09 -6.442E-10 5.604E-08 -1.656E-09
0.96 -9.422E-10 6.572E-09 -6.303E-10 -2.423E-10 -3.104E-09 -2.281E-09 -8.115E-10 -1.233E-09 -6.442E-10 7.847E-08 -1.869E-09
0.97 -8.598E-10 6.460E-09 -6.384E-10 -2.462E-10 -2.925E-09 -2.244E-09 -7.485E-10 -1.272E-09 -6.244E-10 9.491E-08 -2.141E-09
0.98 -7.800E-10 6.413E-09 -6.432E-09 -2.477E-10 -2.767E-09 -2.243E-09 -6.971E-10 -1.339E-09 -5.482E-10 1.039E-07 -2.390E-09
0.99 -7.084E-10 6.432E-09 -6.793E-10 -2.372E-10 -2.637E-09 -2.252E-09 -6.567E-10 -1.471E-09 -5.009E-10 1.057E-07 -2.560E-09
1.00 -6.508E-10 6.496E-09 -6.875E-10 -2.247E-10 -2.525E-09 -2.251E-09 -6.252E-10 -1.591E-09 -4.547E-10 9.471E-08 -2.599E-09
1.01 -6.122E-10 6.561E-09 -6.754E-10 -2.091E-10 -2.417E-09 -2.230E-09 -6.001E-10 -1.720E-09 -4.138E-10 8.712E-08 -2.504E-09
1.02 -5.942E-10 6.575E-09 -6.401E-10 -1.928E-10 -2.293E-09 -2.193E-09 -5.787E-10 -1.840E-09 -3.810E-10 8.130E-08 -2.381E-09
1.03 -5.952E-10 6.483E-09 -5.838E-10 -1.777E-10 -2.142E-09 -2.174E-09 -5.592E-10 -1.928E-09 -3.567E-10 7.867E-08 -2.263E-09
1.04 -5.291E-10 5.856E-09 -4.345E-10 -1.649E-10 -2.107E-09 -2.107E-09 -5.403E-10 -1.962E-09 -3.399E-10 7.967E-08 -2.172E-09
1.05 -6.482E-10 5.342E-09 -3.580E-10 -1.455E-10 -1.577E-09 -2.097E-09 -4.996E-10 -1.819E-09 -3.185E-10 8.389E-08 -2.117E-09
1.06 -6.634E-10 4.764E-09 -2.894E-10 -1.370E-10 -1.400E-09 -2.140E-09 -4.766E-10 -1.645E-09 -3.089E-10 9.035E-08 -2.091E-09
1.07 -6.874E-10 4.197E-09 -2.326E-10 -1.278E-10 -1.253E-09 -2.213E-09 -4.551E-10 -1.645E-09 -3.089E-10 9.788E-08 -2.080E-09
1.08 -6.870E-10 3.729E-09 -1.890E-10 -1.166E-10 -1.139E-09 -2.308E-09 -4.551E-10 -1.425E-09 -2.979E-10 1.053E-07 -2.070E-09
1.09 -7.070E-10 3.424E-09 -1.576E-10 -1.027E-10 -1.060E-09 -2.399E-09 -4.183E-10 -1.182E-09 -2.853E-10 1.120E-07 -2.044E-09
1.10 -7.338E-10 3.282E-09 -1.356E-10 -8.696E-11 -1.012E-09 -2.465E-09 -4.113E-10 -7.287E-10 -2.732E-10 1.169E-07 -1.995E-09
1.11 -7.666E-10 3.285E-09 -1.201E-10 -7.010E-11 -9.880E-10 -2.484E-09 -4.159E-10 -5.495E-10 -2.604E-10 1.197E-07 -1.925E-09
1.12 -8.047E-10 3.404E-09 -1.083E-10 -5.284E-11 -9.846E-10 -2.440E-09 -4.351E-10 -5.495E-10 -2.513E-10 1.199E-07 -1.841E-09
1.13 -8.220E-10 3.481E-09 -9.692E-11 -3.833E-11 -1.003E-09 -2.440E-09 -4.351E-10 -4.134E-10 -2.467E-10 1.176E-07 -1.751E-09
1.14 -8.194E-10 3.496E-09 -8.626E-11 -2.735E-11 -1.035E-09 -2.286E-09 -4.744E-10 -3.189E-10 -2.492E-10 1.111E-07 -1.679E-09
1.15 -5.863E-10 2.335E-09 -6.989E-11 -6.792E-11 -5.727E-10 -2.065E-09 -5.245E-10 -2.586E-10 -2.568E-10 1.020E-07 -1.630E-09
1.16 -5.863E-10 1.591E-09 -2.716E-11 -8.712E-11 -4.449E-10 -1.582E-09 -4.609E-10 -2.045E-10 -2.749E-10 8.628E-08 -1.586E-09
1.17 -5.219E-10 1.130E-09 -1.214E-11 -8.371E-11 -3.828E-10 -1.425E-09 -4.508E-10 -2.749E-10 -2.732E-10 7.261E-08 -1.586E-09
1.18 -4.603E-10 9.077E-10 -1.149E-11 -8.432E-11 -3.370E-10 -1.267E-09 -4.360E-10 -4.764E-12 -2.736E-10 5.928E-08 -1.394E-09
1.19 -4.162E-10 8.315E-10 -1.432E-11 -8.639E-11 -2.932E-10 -1.097E-09 -4.153E-10 -4.764E-12 -2.658E-10 4.904E-08 -1.394E-09
1.20 -3.869E-10 7.549E-10 -1.499E-11 -8.643E-11 -2.541E-10 -9.089E-10 -3.70E-10 -4.764E-12 -2.541E-10 4.291E-08 -1.151E-10
1.21 -3.594E-10 6.039E-10 -1.530E-11 -8.221E-11 -2.267E-10 -7.203E-10 -3.927E-10 -4.764E-12 -2.541E-10 4.049E-08 -1.151E-10
1.22 -3.238E-10 5.419E-10 -1.133E-11 -7.242E-11 -2.153E-10 -5.605E-10 -3.577E-10 -2.645E-12 -1.886E-10 4.047E-08 -1.889E-10
1.23 -2.798E-10 5.198E-10 -9.370E-12 -5.781E-11 -2.165E-10 -4.502E-10 -3.487E-10 -2.105E-13 -1.751E-10 4.128E-08 -1.675E-10
1.24 -2.798E-10 5.198E-10 -9.370E-12 -5.781E-11 -2.165E-10 -4.502E-10 -3.487E-10 -2.105E-13 -1.751E-10 4.128E-08 -1.675E-10

(Appendix F. Continued)

1.65	-2.361E-10	-3.845E-10	-8.478E-12	-4.134E-11	-2.205E-10	-3.879E-10	-3.444E-10	-6.268E-13	-1.599E-10	-4.108E-08	-1.408E-10
1.70	-2.031E-10	-2.808E-10	-8.457E-12	-2.684E-11	-2.173E-10	-3.551E-10	-3.413E-10	-4.251E-13	-1.407E-10	-3.968E-08	-1.282E-10
1.75	-1.867E-10	-2.192E-10	-8.748E-12	-1.709E-11	-2.033E-10	-3.326E-10	-3.358E-10	-2.663E-14	-1.186E-10	-3.786E-08	-1.184E-10
1.80	-1.850E-10	-2.1893E-10	-8.806E-12	-1.240E-11	-1.820E-10	-3.106E-10	-3.259E-10	7.149E-14	-9.701E-11	-3.583E-08	-1.104E-10
1.85	-1.898E-10	-1.716E-10	-8.442E-12	-1.077E-11	-1.603E-10	-2.893E-10	-3.115E-10	-1.845E-15	-7.930E-11	-3.339E-08	-1.035E-10
1.90	-1.912E-10	-1.526E-10	-7.811E-12	-9.406E-12	-1.434E-10	-2.753E-10	-2.948E-10	-1.356E-15	-6.741E-11	-3.019E-08	-9.788E-11
1.95	-1.830E-10	-1.296E-10	-7.209E-12	-6.638E-12	-1.325E-10	-2.758E-10	-2.866E-10	-8.774E-16	-6.196E-11	-2.610E-08	-9.375E-11
2.00	-1.661E-10	-1.077E-10	-6.790E-12	-2.702E-12	-1.262E-10	-2.938E-10	-2.655E-10	-1.432E-16	-6.242E-11	-2.153E-08	-9.044E-11
2.05	-1.465E-10	-9.229E-11	-6.490E-12	8.937E-13	-1.228E-10	-3.237E-10	-2.575E-10	4.311E-17	-6.669E-11	-1.728E-08	-8.696E-11
2.10	-1.299E-10	-8.481E-11	-6.161E-12	2.767E-12	-1.217E-10	-3.516E-10	-2.544E-10	0.000E+00	-7.074E-11	-1.411E-08	-8.289E-11
2.15	-1.180E-10	-7.368E-11	-5.736E-12	2.624E-12	-1.203E-10	-3.615E-10	-2.541E-10	0.000E+00	-6.972E-11	-1.235E-08	-7.851E-11
2.20	-1.080E-10	-7.999E-11	-5.260E-12	1.268E-12	-1.260E-10	-3.448E-10	-2.536E-10	0.000E+00	-6.037E-11	-1.176E-08	-7.403E-11
2.25	-9.696E-11	-7.663E-11	-4.809E-12	1.015E-13	-1.285E-10	-3.057E-10	-2.505E-10	0.000E+00	-4.306E-11	-1.177E-08	-6.956E-11
2.30	-8.524E-11	-7.444E-11	-4.430E-12	-6.034E-13	-1.278E-10	-2.585E-10	-2.443E-10	0.000E+00	-2.170E-11	-1.188E-08	-6.619E-11
2.35	-7.620E-11	-7.753E-11	-4.135E-12	2.144E-14	-1.224E-10	-2.184E-10	-2.363E-10	0.000E+00	-1.492E-12	-1.182E-08	-6.706E-11
2.40	-7.268E-11	-8.734E-11	-3.944E-12	1.515E-12	-1.131E-10	-1.935E-10	-2.280E-10	0.000E+00	1.376E-11	-1.159E-08	-7.568E-11
2.45	-7.378E-11	-9.976E-11	-3.890E-12	3.405E-12	-1.026E-10	-1.827E-10	-2.198E-10	0.000E+00	2.302E-11	-1.122E-08	-9.199E-11
2.50	-7.540E-11	-1.066E-10	-3.975E-12	5.300E-12	-9.428E-11	-1.795E-10	-2.118E-10	0.000E+00	2.760E-11	-1.073E-08	-1.093E-10
2.55	-7.386E-11	-1.006E-10	-4.147E-12	6.965E-12	-9.061E-11	-1.774E-10	-2.041E-10	0.000E+00	2.966E-11	-1.009E-08	-1.161E-10
2.60	-6.870E-11	-8.026E-11	-4.311E-12	8.220E-12	-9.180E-11	-1.736E-10	-1.972E-10	0.000E+00	3.085E-11	-9.341E-09	-1.038E-10
2.65	-6.234E-11	-5.009E-11	-4.375E-12	8.792E-12	-9.549E-11	-1.682E-10	-1.923E-10	0.000E+00	3.183E-11	-8.581E-09	-7.340E-11
2.70	-5.727E-11	-4.807E-11	-4.291E-12	8.404E-12	-9.819E-11	-1.629E-10	-1.895E-10	0.000E+00	3.256E-11	-7.910E-09	-3.603E-11
2.75	-5.390E-11	8.344E-12	-4.074E-12	7.107E-12	-9.754E-11	-1.595E-10	-1.884E-10	0.000E+00	3.296E-11	-7.353E-09	-5.678E-12
2.80	-5.115E-11	2.423E-11	-3.777E-12	5.539E-12	-9.366E-11	-1.586E-10	-1.882E-10	0.000E+00	3.318E-11	-6.844E-09	-9.997E-12
2.85	-4.837E-11	2.786E-11	-3.472E-12	4.709E-12	-8.871E-11	-1.598E-10	-1.883E-10	0.000E+00	3.346E-11	-6.291E-09	1.294E-11
2.90	-4.630E-11	2.106E-11	-3.218E-12	5.346E-12	-8.500E-11	-1.612E-10	-1.883E-10	0.000E+00	3.373E-11	-5.660E-09	1.054E-11
2.95	-4.602E-11	9.451E-12	-3.039E-12	7.320E-12	-8.337E-11	-1.606E-10	-1.880E-10	0.000E+00	3.356E-11	-5.005E-09	9.184E-12
3.00	-4.730E-11	8.367E-13	-2.937E-12	9.670E-12	-8.324E-11	-1.564E-10	-1.868E-10	0.000E+00	3.240E-11	-4.441E-09	1.080E-11
3.05	-4.843E-11	1.294E-12	-2.903E-12	1.121E-11	-8.366E-11	-1.491E-10	-1.847E-10	0.000E+00	3.008E-11	-4.050E-09	1.404E-11
3.10	-4.781E-11	1.142E-11	-2.923E-12	1.122E-11	-8.411E-11	-1.404E-10	-1.819E-10	0.000E+00	2.692E-11	-3.832E-09	1.733E-11
3.15	-4.557E-11	2.628E-11	-2.975E-12	9.664E-12	-8.440E-11	-1.319E-10	-1.788E-10	0.000E+00	2.390E-11	-3.709E-09	1.992E-11
3.20	-4.345E-11	3.984E-11	-3.015E-12	7.050E-12	-8.416E-11	-1.241E-10	-1.758E-10	0.000E+00	2.000E+00	-3.590E-09	2.135E-11
3.25	-4.304E-11	5.022E-11	-3.005E-12	4.245E-12	-8.291E-11	-1.176E-10	-1.729E-10	0.000E+00	2.416E-11	-3.438E-09	2.100E-11
3.30	-4.403E-11	6.085E-11	-2.941E-12	2.559E-12	-8.064E-11	-1.128E-10	-1.705E-10	0.000E+00	2.983E-11	-3.276E-09	2.186E-11
3.35	-4.446E-11	7.612E-11	-2.862E-12	2.538E-12	-7.795E-11	-1.104E-10	-1.693E-10	0.000E+00	3.871E-11	-3.145E-09	1.561E-11
3.40	-4.254E-11	9.478E-11	-2.814E-12	5.448E-12	-7.560E-11	-1.104E-10	-1.702E-10	0.000E+00	4.848E-11	-3.052E-09	1.408E-11
3.45	-3.839E-11	1.083E-10	-2.792E-12	1.069E-11	-7.376E-11	-1.114E-10	-1.724E-10	0.000E+00	5.642E-11	-2.965E-09	1.567E-11
3.50	-3.412E-11	1.044E-10	-2.737E-12	1.660E-11	-7.208E-11	-1.120E-10	-1.739E-10	0.000E+00	6.076E-11	-2.846E-09	1.955E-11
3.55	-3.195E-11	7.880E-11	-2.591E-12	2.102E-11	-7.017E-11	-1.117E-10	-1.724E-10	0.000E+00	6.149E-11	-2.683E-09	2.300E-11
3.60	-3.266E-11	3.759E-11	-2.351E-12	2.229E-11	-6.826E-11	-1.118E-10	-1.680E-10	0.000E+00	5.962E-11	-2.500E-09	2.309E-11
3.65	-3.447E-11	5.593E-12	-2.075E-12	2.088E-11	-6.652E-11	-1.121E-10	-1.614E-10	0.000E+00	5.735E-11	-2.316E-09	2.029E-11
3.70	-3.538E-11	3.441E-13	-1.835E-12	1.836E-11	-6.505E-11	-1.117E-10	-1.542E-10	0.000E+00	5.616E-11	-2.147E-09	1.683E-11
3.75	-3.268E-11	4.543E-11	-1.670E-12	1.802E-11	-6.287E-11	-1.062E-10	-1.459E-10	0.000E+00	5.888E-11	-1.964E-09	1.804E-11
3.80	-2.745E-11	1.220E-10	-1.575E-12	2.016E-11	-6.005E-11	-9.647E-11	-1.374E-10	0.000E+00	6.442E-11	-1.788E-09	2.369E-11
3.85	-2.261E-11	1.858E-10	-1.539E-12	2.364E-11	-5.728E-11	-8.625E-11	-1.308E-10	0.000E+00	6.980E-11	-1.669E-09	3.075E-11
3.90	-2.152E-11	1.957E-10	-1.519E-12	2.427E-11	-5.623E-11	-8.332E-11	-1.283E-10	0.000E+00	7.037E-11	-1.635E-09	3.201E-11
Z	C6H5	C6H6	C8H2	C8H6	C8H8	C10H2					
0.00	5.320E-11	1.186E-09	0.000E+00	5.751E-12	0.000E+00						
0.01	6.860E-11	1.141E-09	0.000E+00	6.895E-12	0.000E+00						
0.02	3.231E-12	9.086E-10	-5.332E-16	4.148E-12	0.000E+00						
0.03	-4.247E-10	6.778E-10	3.189E-14	-2.292E-11	1.417E-17						
0.04	-9.076E-10	5.972E-10	-1.438E-13	-6.515E-11	-4.774E-17						

(Appendix F. Continued)

0.05 -1.361E-09 6.058E-10 2.310E-15 -1.199E-10 -7.377E-16
0.06 -1.725E-09 6.511E-10 5.854E-13 -1.844E-10 7.361E-15
0.07 -1.896E-09 7.306E-10 1.352E-12 -2.555E-10 6.617E-16
0.08 -1.819E-09 7.782E-10 1.538E-12 -3.293E-10 -3.596E-14
0.09 -1.473E-09 7.855E-10 1.401E-14 -4.021E-10 -5.732E-14
0.10 -8.645E-10 7.651E-10 -4.090E-12 -4.690E-10 2.584E-14
0.11 -2.766E-11 7.559E-10 -1.045E-11 -5.238E-10 2.494E-13
0.12 9.282E-10 8.337E-10 -1.671E-11 -5.614E-10 4.840E-13
0.13 1.879E-09 1.092E-09 -1.761E-11 -5.777E-10 4.072E-13
0.14 2.696E-09 1.613E-09 -5.667E-12 -5.718E-10 -3.652E-13
0.15 3.268E-09 2.443E-09 2.620E-11 -5.479E-10 -1.985E-12
0.16 3.524E-09 3.583E-09 8.040E-11 -5.161E-10 -4.024E-12
0.17 3.447E-09 4.987E-09 1.501E-10 -4.915E-10 -5.286E-12
0.18 3.074E-09 6.572E-09 2.161E-10 -4.902E-10 -3.727E-12
0.19 2.484E-09 8.254E-09 2.466E-10 -5.233E-10 2.968E-12
0.20 1.781E-09 9.971E-09 2.006E-10 -5.891E-10 1.607E-11
0.21 1.072E-09 1.170E-08 3.448E-11 -6.676E-10 3.419E-11
0.22 4.456E-10 1.343E-08 -2.897E-10 -7.186E-10 5.215E-11
0.23 -3.843E-11 1.520E-08 -7.964E-10 -6.870E-10 6.091E-11
0.24 -3.573E-10 1.699E-08 -1.493E-09 -5.139E-10 4.911E-11
0.25 -5.203E-10 1.873E-08 -2.372E-09 -1.537E-10 5.839E-12
0.26 -5.597E-10 2.033E-08 -3.409E-09 4.104E-10 -7.595E-11
0.27 -5.183E-10 2.165E-08 -4.575E-09 1.155E-09 -1.966E-10
0.28 -4.386E-10 2.255E-08 -5.829E-09 2.015E-09 -3.484E-10
0.29 -3.542E-10 2.299E-08 -7.120E-09 2.892E-09 -5.175E-10
0.30 -2.861E-10 2.300E-08 -8.379E-09 3.676E-09 -6.866E-10
0.31 -2.430E-10 2.271E-08 -9.512E-09 4.266E-09 -8.401E-10
0.32 -2.241E-10 2.227E-08 -1.040E-08 4.592E-09 -9.670E-10
0.33 -2.232E-10 2.181E-08 -1.092E-08 4.628E-09 -1.062E-09
0.34 -2.325E-10 2.134E-08 -1.095E-08 4.395E-09 -1.125E-09
0.35 -2.452E-10 2.073E-08 -1.043E-08 3.950E-09 -1.158E-09
0.36 -2.566E-10 1.968E-08 -9.408E-09 3.370E-09 -1.160E-09
0.37 -2.641E-10 1.785E-08 -8.029E-09 2.735E-09 -1.129E-09
0.38 -2.673E-10 1.492E-08 -6.578E-09 2.111E-09 -1.057E-09
0.39 -2.664E-10 1.072E-08 -5.427E-09 1.541E-09 -9.377E-10
0.40 -2.624E-10 5.342E-09 -4.964E-09 1.040E-09 -7.684E-10
0.41 -2.560E-10 -8.777E-10 -5.491E-09 6.072E-10 -5.523E-10
0.42 -2.477E-10 -7.403E-09 -7.118E-09 2.261E-10 -2.995E-10
0.43 -2.380E-10 -1.362E-08 -9.682E-09 -1.222E-10 -2.605E-11
0.44 -2.267E-10 -1.897E-08 -1.273E-08 -4.532E-10 2.506E-10
0.45 -2.140E-10 -2.309E-08 -1.555E-08 -7.745E-10 5.149E-10
0.46 -1.998E-10 -2.586E-08 -1.733E-08 -1.084E-09 7.561E-10
0.47 -1.846E-10 -2.737E-08 -1.732E-08 -1.370E-09 9.691E-10
0.48 -1.692E-10 -2.791E-08 -1.498E-08 -1.618E-09 1.153E-09
0.49 -1.549E-10 -2.779E-08 -1.020E-08 -1.810E-09 1.308E-09
0.50 -1.431E-10 -2.729E-08 -3.288E-09 -1.930E-09 1.435E-09
0.51 -1.351E-10 -2.653E-08 5.080E-09 -1.969E-09 1.535E-09
0.52 -1.318E-10 -2.559E-08 1.400E-08 -1.928E-09 1.606E-09
0.53 -1.331E-10 -2.434E-08 2.258E-08 -1.814E-09 1.651E-09
0.54 -1.380E-10 -2.270E-08 3.011E-08 -1.644E-09 1.672E-09
0.55 -1.446E-10 -2.060E-08 3.626E-08 -1.439E-09 1.675E-09
0.56 -1.508E-10 -1.809E-08 4.104E-08 -1.220E-09 1.669E-09
0.57 -1.545E-10 -1.532E-08 4.475E-08 -1.007E-09 1.663E-09

(Appendix F. Cont-Inued)

0.58 -1.542E-10 -1.250E-08 4.778E-08 -8.146E-10 1.664E-09
0.59 -1.497E-10 -9.871E-09 5.042E-08 -6.533E-10 1.680E-09
0.60 -1.417E-10 -7.617E-09 5.272E-08 -5.274E-10 1.712E-09
0.61 -1.317E-10 -5.856E-09 5.446E-08 -4.369E-10 1.763E-09
0.62 -1.218E-10 -4.603E-09 5.519E-08 -3.788E-10 1.830E-09
0.63 -1.138E-10 -3.791E-09 5.443E-08 -3.482E-10 1.913E-09
0.64 -1.090E-10 -3.297E-09 5.184E-08 -3.386E-10 2.004E-09
0.65 -1.077E-10 -2.989E-09 4.738E-08 -3.426E-10 2.098E-09
0.66 -1.094E-10 -2.754E-09 4.133E-08 -3.528E-10 2.186E-09
0.67 -1.128E-10 -2.517E-09 3.428E-08 -3.622E-10 2.260E-09
0.68 -1.164E-10 -2.250E-09 2.696E-08 -3.650E-10 2.311E-09
0.69 -1.187E-10 -1.959E-09 2.011E-08 -3.574E-10 2.338E-09
0.70 -1.187E-10 -1.668E-09 1.424E-08 -3.379E-10 2.344E-09
0.71 -1.163E-10 -1.406E-09 9.630E-09 -3.075E-10 2.333E-09
0.72 -1.118E-10 -1.193E-09 6.259E-09 -2.696E-10 2.314E-09
0.73 -1.062E-10 -1.037E-09 3.910E-09 -2.290E-10 2.290E-09
0.74 -1.008E-10 -9.327E-10 2.272E-09 -1.909E-10 2.259E-09
0.75 -9.662E-11 -8.705E-10 1.049E-09 -1.604E-10 2.210E-09
0.76 -9.448E-11 -8.388E-10 3.784E-11 -1.409E-10 2.128E-09
0.77 -9.442E-11 -8.295E-10 -8.474E-10 -1.338E-10 1.994E-09
0.78 -9.598E-11 -8.393E-10 -1.598E-09 -1.378E-10 1.797E-09
0.79 -9.820E-11 -8.683E-10 -2.161E-09 -1.499E-10 1.537E-09
0.80 -9.996E-11 -9.161E-10 -2.494E-09 -1.652E-10 1.225E-09
0.81 -1.003E-10 -9.794E-10 -2.596E-09 -1.788E-10 8.868E-10
0.82 -9.860E-11 -1.049E-09 -2.521E-09 -1.866E-10 5.541E-10
0.83 -9.488E-11 -1.113E-09 -2.353E-09 -1.862E-10 2.592E-10
0.84 -8.957E-11 -1.154E-09 -2.184E-09 -1.774E-10 2.716E-11
0.85 -8.343E-11 -1.160E-09 -2.079E-09 -1.623E-10 -1.292E-10
0.86 -7.727E-11 -1.123E-09 -2.062E-09 -1.441E-10 -2.104E-10
0.87 -7.172E-11 -1.043E-09 -2.122E-09 -1.264E-10 -2.284E-10
0.88 -6.713E-11 -9.281E-10 -2.222E-09 -1.121E-10 -2.018E-10
0.89 -6.359E-11 -7.928E-10 -2.324E-09 -1.027E-10 -1.506E-10
0.90 -6.098E-11 -6.536E-10 -2.403E-09 -9.819E-11 -9.178E-11
0.91 -5.916E-11 -5.256E-10 -2.462E-09 -9.742E-11 -3.686E-11
0.92 -5.806E-11 -4.197E-10 -2.523E-09 -9.851E-11 7.841E-12
0.93 -5.771E-11 -3.410E-10 -2.620E-09 -9.972E-11 3.960E-11
0.94 -5.821E-11 -2.887E-10 -2.779E-09 -9.984E-11 5.707E-11
0.95 -5.965E-11 -2.582E-10 -3.009E-09 -9.847E-11 5.855E-11
0.96 -6.210E-11 -2.426E-10 -3.292E-09 -9.584E-11 4.153E-11
0.97 -6.565E-11 -2.349E-10 -3.587E-09 -9.260E-11 3.462E-12
0.98 -7.040E-11 -2.292E-10 -3.839E-09 -8.939E-11 5.685E-11
0.99 -7.640E-11 -2.219E-10 -3.991E-09 -8.660E-11 -1.378E-10
1.00 -8.357E-11 -2.114E-10 -4.005E-09 -8.425E-11 -2.348E-10
1.01 -9.150E-11 -1.977E-10 -3.872E-09 -8.204E-11 3.403E-10
1.02 -9.940E-11 -1.822E-10 -3.616E-09 -7.953E-11 -4.464E-10
1.03 -1.060E-10 -1.672E-10 -3.292E-09 -7.632E-11 -5.463E-10
1.04 -1.096E-10 -1.547E-10 -2.975E-09 -7.223E-11 -6.365E-10
1.05 -1.088E-10 -1.469E-10 -2.746E-09 -6.737E-11 -7.171E-10
1.06 -1.026E-10 -1.453E-10 -2.670E-09 -6.211E-11 -7.918E-10
1.07 -9.088E-11 -1.501E-10 -2.797E-09 -5.697E-11 -8.661E-10
1.08 -7.469E-11 -1.604E-10 -3.146E-09 -5.247E-11 -9.450E-10
1.09 -5.594E-11 -1.743E-10 -3.701E-09 -4.898E-11 -1.030E-09
1.10 -3.706E-11 -1.892E-10 -4.444E-09 -4.666E-11 -1.122E-09

(Appendix F , Continued)

1.11 -2.050E-11 -2.007E-10 -5.331E-09 -4.528E-11 -1.215E-09
1.12 -7.634E-12 -2.058E-10 -6.269E-09 -4.441E-11 -1.298E-09
1.13 8.098E-13 -2.018E-10 -7.179E-09 -4.354E-11 -1.362E-09
1.14 4.800E-12 -1.872E-10 -8.015E-09 -4.218E-11 -1.401E-09
1.15 5.398E-12 -1.563E-10 -8.560E-09 -3.923E-11 -1.391E-09
1.16 3.822E-12 -1.163E-10 -8.828E-09 -3.529E-11 -1.346E-09
1.20 -6.551E-12 -9.572E-11 -5.981E-09 -2.949E-11 -8.711E-10
1.25 2.564E-12 -8.356E-11 -5.335E-09 -2.131E-11 -7.004E-10
1.30 4.287E-12 -6.676E-11 -4.391E-09 -1.472E-11 -5.177E-10
1.35 2.374E-12 -5.053E-11 -3.552E-09 -9.856E-12 -3.783E-10
1.40 4.078E-13 -3.919E-11 -3.051E-09 -6.742E-12 -3.003E-10
1.45 -3.621E-13 -3.314E-11 -2.875E-09 -5.212E-12 -2.696E-10
1.50 -2.576E-13 -3.090E-11 -2.845E-09 -4.841E-12 -2.616E-10
1.55 -1.242E-14 -3.096E-11 -2.778E-09 -5.091E-12 -2.580E-10
1.60 3.865E-14 -3.259E-11 -2.597E-09 -5.488E-12 -2.501E-10
1.65 -2.819E-15 -3.501E-11 -2.341E-09 -5.685E-12 -2.349E-10
1.70 9.612E-16 -3.667E-11 -2.094E-09 -5.433E-12 -2.120E-10
1.75 -2.911E-16 -3.553E-11 -1.906E-09 -4.599E-12 -1.837E-10
1.80 -1.014E-16 -3.033E-11 -1.765E-09 -3.242E-12 -1.551E-10
1.85 1.946E-17 -2.158E-11 -1.621E-09 -1.649E-12 -1.309E-10
1.90 4.586E-19 -1.162E-11 -1.441E-09 -2.127E-13 -1.135E-10
1.95 0.000E+00 -3.323E-12 -1.231E-09 7.822E-13 -1.019E-10
2.00 0.000E+00 1.605E-12 -1.034E-09 1.298E-12 -9.439E-11
2.05 0.000E+00 3.432E-12 -8.931E-10 1.490E-12 -9.004E-11
2.10 0.000E+00 3.997E-12 -8.185E-10 1.535E-12 -8.900E-11
2.15 0.000E+00 5.439E-12 -7.863E-10 1.510E-12 -9.081E-11
2.20 0.000E+00 8.924E-12 -7.593E-10 1.423E-12 -9.337E-11
2.25 0.000E+00 1.410E-11 -7.138E-10 1.314E-12 -9.346E-11
2.30 0.000E+00 1.939E-11 -6.503E-10 1.302E-12 -8.852E-11
2.35 0.000E+00 2.299E-11 -5.838E-10 1.526E-12 -7.831E-11
2.40 0.000E+00 2.403E-11 -5.271E-10 2.045E-12 -6.497E-11
2.45 0.000E+00 2.317E-11 -4.820E-10 2.783E-12 -5.172E-11
2.50 0.000E+00 2.221E-11 -4.431E-10 3.567E-12 -4.111E-11
2.55 0.000E+00 2.299E-11 -4.070E-10 4.199E-12 -3.398E-11
2.60 0.000E+00 2.629E-11 -3.764E-10 4.516E-12 -2.976E-11
2.65 0.000E+00 3.131E-11 -3.563E-10 4.448E-12 -2.740E-11
2.70 0.000E+00 3.615E-11 -3.471E-10 4.054E-12 -2.631E-11
2.75 0.000E+00 3.858E-11 -3.427E-10 3.546E-12 -2.653E-11
2.80 0.000E+00 3.711E-11 -3.345E-10 3.234E-12 -2.827E-11
2.85 0.000E+00 3.200E-11 -3.178E-10 3.384E-12 -3.123E-11
2.90 0.000E+00 2.565E-11 -2.940E-10 4.064E-12 -3.418E-11
2.95 0.000E+00 2.164E-11 -2.689E-10 5.082E-12 -3.536E-11
3.00 0.000E+00 2.261E-11 -2.485E-10 6.091E-12 -3.320E-11
3.05 0.000E+00 2.812E-11 -2.375E-10 6.781E-12 -2.728E-11
3.10 0.000E+00 3.467E-11 -2.378E-10 7.038E-12 -1.865E-11
3.15 0.000E+00 3.806E-11 -2.475E-10 6.968E-12 -9.383E-12
3.20 0.000E+00 3.643E-11 -2.600E-10 6.775E-12 -1.614E-12
3.25 0.000E+00 3.127E-11 -2.652E-10 6.622E-12 3.475E-12
3.30 0.000E+00 2.627E-11 -2.545E-10 6.562E-12 5.969E-12
3.35 0.000E+00 2.675E-11 -2.267E-10 6.564E-12 6.828E-12
3.40 0.000E+00 3.858E-11 -1.895E-10 6.583E-12 7.121E-12
3.45 0.000E+00 6.474E-11 -1.547E-10 6.591E-12 7.447E-12
3.50 0.000E+00 9.232E-11 -1.300E-10 6.574E-12 7.782E-12

(Appendix F . Continued)

3.55	0.000E+00	9.538E-11	-1.155E-10	6.520E-12	7.813E-12
3.60	0.000E+00	3.906E-11	-1.050E-10	6.415E-12	7.256E-12
3.65	0.000E+00	-6.372E-11	-9.159E-11	6.295E-12	6.350E-12
3.70	0.000E+00	-1.751E-10	-7.352E-11	6.198E-12	5.504E-12
3.75	0.000E+00	-1.852E-10	-5.130E-11	6.216E-12	5.597E-12
3.80	0.000E+00	-9.038E-11	-3.079E-11	6.319E-12	6.539E-12
3.85	0.000E+00	6.177E-11	-2.076E-11	6.421E-12	7.773E-12
3.90	0.000E+00	9.820E-11	-1.936E-11	6.387E-12	7.985E-12

APPENDIX G.

Estimates of ionization potentials

Ionization potentials can be calculated using heats of formation for the neutrals and ions involved. Uncertainties in ΔH due to reference temperatures of 298 K instead of 0 K will amount to only a few kcal/mol, on the order of 0.1 eV or less, so the distinction is ignored for this calculation. The following estimates are used in data analysis and interpretation in Chapter IV.

C₃H

The ionization potential for C₃H can be estimated from heats of formation for C₃H⁺ and C₃H to be:

$$\begin{aligned}
 \text{IP}[\text{C}_3\text{H}^+; \text{C}_3\text{H}] &= \Delta H_f^\circ(\text{C}_3\text{H}^+) + \Delta H_f^\circ(\text{e}^-) - \Delta H_f^\circ(\text{C}_3\text{H}) \\
 &= 303 \pm 39 \quad [\Delta H_f^\circ, 0, \text{Field and Franklin, 1970}] \\
 &\quad + 0 \\
 &\quad - (162) \quad [\text{Est. } \Delta H_f^\circ, 298; \text{Cole, 1982}] \\
 &= 149 \pm 39 \text{ kcal/mol} \\
 &= 6.5 \pm 1.7 \text{ eV}
 \end{aligned}$$

C₃H₂

The ionization potential for C₃H₂ can be estimated from heats of formation for C₃H₂⁺ and C₃H₂ to be:

$$\begin{aligned}
 \text{IP}[\text{C}_3\text{H}_2^+; \text{C}_3\text{H}_2] &= \Delta H_f^\circ(\text{C}_3\text{H}_2^+) + \Delta H_f^\circ(\text{e}^-) - \Delta H_f^\circ(\text{C}_3\text{H}_2) \\
 &= 365 \quad [\Delta H_f^\circ, 0, \text{Field and Franklin, 1970}] \\
 &\quad + 0 \\
 &\quad - (127) \quad [\Delta H_f^\circ, 298; \text{Bittner, 1981}] \\
 &= 238 \text{ kcal/mol} \\
 &= 10.3 \text{ eV}
 \end{aligned}$$

HCCO

From Rosenstock et al. (1977), the appearance potential for HCCO⁺ from CH₂CO is 14.91 ± 0.3 eV or 344 ± 7 kcal/mol. Then from:

$$\begin{aligned} \text{AP}[\text{HCCO}^+; \text{CH}_2\text{CO}] &= \Delta H_{\text{rxn}} \\ &= \Delta H_f^\circ(\text{HCCO}^+) + \Delta H_f^\circ(\text{e}^-) + \Delta H_f^\circ(\text{H}) - \Delta H_f^\circ(\text{CH}_2\text{CO}) \end{aligned}$$

solve:

$$\begin{aligned} 344 \pm 7 \text{ kcal/mol} &= \Delta H_f^\circ(\text{HCCO}^+) \\ &+ 0 \quad \quad \quad [\text{Reference state}] \\ &+ 52.1 \quad \quad \quad [\Delta H_f^\circ, 298, \text{Stull et al., 1972}] \\ &- (-14.6) \quad \quad \quad [\Delta H_f^\circ, 298, \text{Reid et al., 1977}] \end{aligned}$$

to obtain:

$$\Delta H_f^\circ(\text{HCCO}^+) = 277 \pm 7 \text{ kcal/mol.}$$

Thus the ionization potential is:

$$\begin{aligned} \text{IP}[\text{HCCO}^+; \text{HCCO}] &= \Delta H_f^\circ(\text{HCCO}^+) + \Delta H_f^\circ(\text{e}^-) - \Delta H_f^\circ(\text{HCCO}) \\ &= 277 \pm 7 \\ &+ 0 \\ &- (42.4) \quad \quad \quad [\Delta H_f^\circ, 298, \text{Oakes et al., 1983}] \\ &= 235 \pm 7 \text{ kcal/mol} \\ &= 10.2 \pm 0.3 \text{ eV} \end{aligned}$$

C₄H

The ionization potential for C₄H can be estimated from heats of formation for C₄H⁺ and C₄H to be:

$$\begin{aligned} \text{IP}[\text{C}_4\text{H}^+; \text{C}_4\text{H}] &= \Delta H_f^\circ(\text{C}_4\text{H}^+) + \Delta H_f^\circ(\text{e}^-) - \Delta H_f^\circ(\text{C}_4\text{H}) \\ &= 316 \pm 22 \quad \quad \quad [\Delta H_f^\circ, 0, \text{Field and Franklin, 1970}] \\ &+ 0 \\ &- (199) \quad \quad \quad [\text{Est. } \Delta H_f^\circ, 298; \text{Cole, 1982}] \\ &= 117 \pm 22 \text{ kcal/mol} \\ &= 5.1 \pm 1.0 \text{ eV} \end{aligned}$$

C₄H₃

The ionization potential for C₄H₃ can be estimated from heats of formation for C₄H₃⁺ and C₄H₃. However, there are two isomers of C₄H₃ with radical sites at the primary vinylic carbon (HC≡C-CH=CH·, designated 1-C₄H₃) and at the secondary vinylic carbon (HC≡C-C·=CH₂ or 2-C₄H₃); the same must be true for C₄H₃⁺. The radical in 2-C₄H₃

is resonantly stabilized by the adjacent acetylenic pi system, while 1-C₄H₃ has no such stabilization; again, the same would be true for C₄H₃⁺.

Field and Franklin (1970) report an appearance potential of 12.59 eV for C₄H₃⁺ from vinylacetylene (CH₂=C-CH=CH₂) from which they calculate ΔH_f^o=307 kcal/mol for C₄H₃⁺. Stability arguments suggest that this structure is 2-C₄H₃⁺. They also report an appearance potential of 15.1±0.2 eV for C₄H₃⁺ from 2-butyne (CH₃-C≡C-CH₃) from which they calculate ΔH_f^o(C₄H₃⁺)=331 kcal/mol. The co-products H₂+H suggest that this structure might be 1-C₄H₃⁺.

Heats of formation for 1-C₄H₃ and 2-C₄H₃ can be estimated from the heat of formation of vinylacetylene, 68.2 kcal/mol (Stein and Fahr, 1985). From the bond dissociation energy D₂₉₈^o of vinylic H from C₂H₄ (110±2 kcal/mol, McMillen and Golden, 1982), ΔH_f^o,₂₉₈(1-C₄H₃)= 126 kcal/mol. For 2-C₄H₃, the resonance energy can be estimated from the difference between D₂₉₈^o(H-C₃H₅)=86.3±1.5 and D₂₉₈^o(H-nC₃H₇)=97.9±1 kcal/mol (McMillen and Golden, 1982) to be 11.6 kcal/mol. Thus, ΔH_f^o,₂₉₈(2-C₄H₃)≅114 kcal/mol.

The calculation of ionization potentials for C₄H₃ then is:

$$\begin{aligned} \text{IP}[1\text{-C}_4\text{H}_3^+; 1\text{-C}_4\text{H}_3] &= \Delta H_f^o(1\text{-C}_4\text{H}_3^+) + \Delta H_f^o(e^-) - \Delta H_f^o(1\text{-C}_4\text{H}_3) \\ &= 331 + 0 - 126 \\ &= 205 \text{ kcal/mol} \\ &= 8.9 \text{ eV} \end{aligned}$$

$$\begin{aligned} \text{IP}[2\text{-C}_4\text{H}_3^+; 2\text{-C}_4\text{H}_3] &= \Delta H_f^o(2\text{-C}_4\text{H}_3^+) + \Delta H_f^o(e^-) - \Delta H_f^o(2\text{-C}_4\text{H}_3) \\ &= 307 + 0 - 114 \\ &= 193 \text{ kcal/mol} \\ &= 8.4 \text{ eV} \end{aligned}$$

C₄H₅

Similarly to C₄H₃, there are two isomers of C₄H₅ - CH₂=CH-CH=CH·, designated 1-C₄H₅, and CH₂=CH-CH·=CH₂ or 2-C₄H₅. From Rosenstock et al. (1977), the appearance potential for C₄H₅⁺ (probably 2-C₄H₅⁺) from 1,3-butadiene has been measured as 11.39±0.05

eV and as 11.56 ± 0.04 eV. The heat of formation for $2\text{-C}_4\text{H}_5^+$ can then be calculated from

$$\begin{aligned} \text{AP}[2\text{-C}_4\text{H}_5^+; \text{C}_4\text{H}_6] &= \Delta H_{rxn} \\ &= \Delta H_f^\circ(2\text{-C}_4\text{H}_5^+) + \Delta H_f^\circ(e^-) + \Delta H_f^\circ(\text{H}) - \Delta H_f^\circ(\text{C}_4\text{H}_6) \end{aligned}$$

and solving:

$$\begin{aligned} 11.48 \pm 0.15 \text{ eV} &= 265 \pm 4 \text{ kcal/mol} \\ &= \Delta H_f^\circ(2\text{-C}_4\text{H}_5^+) \\ &\quad + 0 \quad \quad \quad [\text{Reference state}] \\ &\quad + 52.1 \quad \quad \quad [\Delta H_f^\circ, 298, \text{Stull et al., 1972}] \\ &\quad - (26.33) \quad \quad \quad [\Delta H_f^\circ, 298, \text{Reid et al., 1977}] \end{aligned}$$

to obtain:

$$\Delta H_f^\circ(2\text{-C}_4\text{H}_5^+) = 239 \pm 4 \text{ kcal/mol.}$$

Field and Franklin (1970) also derived $\Delta H_f^\circ = 236$ kcal/mol for $2\text{-C}_4\text{H}_3^+$ from appearance potentials from 1,3-butadiene.

The heat of formation of $2\text{-C}_4\text{H}_5$ can be estimated as 72.3 kcal/mol from group additivity (Benson, 1976) by using the structure $\text{CH}_2=\text{C}=\text{CH}-\text{CH}_2$ or 73 kcal/mol from $\Delta H_f^\circ, 298(\text{butadiene}) = 26.75$, $D_{298}^\circ(\text{H}-\text{C}_2\text{H}_3) = 110 \pm 2$, and the resonance energy above of 11.6 kcal/mol.

The calculation of the ionization potential for $2\text{-C}_4\text{H}_5$ then is:

$$\begin{aligned} \text{IP}[2\text{-C}_4\text{H}_5^+; 2\text{-C}_4\text{H}_5] &= \Delta H_f^\circ(2\text{-C}_4\text{H}_5^+) + \Delta H_f^\circ(e^-) - \Delta H_f^\circ(2\text{-C}_4\text{H}_5) \\ &= 239 + 0 - 72.3 \\ &= 167 \text{ kcal/mol} \\ &= 7.2 \text{ eV.} \end{aligned}$$

The heat of formation of $1\text{-C}_4\text{H}_5$ can be estimated as 84 kcal/mol from 1,3-butadiene (26.33 kcal/mol, Reid et al., 1977) and the bond dissociation energy of 110 ± 2 kcal/mol for $\text{H}-\text{CH}=\text{CH}_2$ (McMillen and Golden, 1982). By analogy with C_4H_3 , the ionization potential for $1\text{-C}_4\text{H}_5$ would be approximately 7.7 eV.

APPENDIX H.

Summary of data from GC/MS analysis of sample V3650,
tabulated by elution time (spectrum number)

Spectrum number	Corrected signal (1000's)	Approximate mole fraction ($\cdot 10^6$ or ppm)	Molecular weight ^a	Identity ^b ; Other remarks
6	196	40	76	
10	44.6	8	68	
12	33.5	6	78	
15	6.8	1.3	78	
32	3804	700	74	C ₆ H ₂ - Hexatriyne
44	119	20	78	C ₆ H ₆ - Benzene
59	2.3	0.4	78	
72	17	0.007	92	
94	3.5	0.001	92	
106	17.8	0.007	92	
111	12.5	0.005	94	
120	8.4	0.003	90	
124	13.5	0.006	92	
128	14.2	0.006	88	
130	13.5	2	90	
137	4.4	0.002	92	
141	33.5	6	76	
154	961	0.4	92	C ₇ H ₈ - Toluene
161	315	0.13	90	
165	241	0.10	90	
169	7.0	0.003	92	
178	32.9	0.014	90	
185	3.7	0.001	90	
189	10.3	0.004	90	
202/3	4.4	0.002	90	
210	28.0	0.012	88	
211	20.	0.009	102	
213	19.	0.008	92	
217	116.	0.05	90	
226	40.	0.016	90	
236	12.	0.005	92	
240	57.	0.02	88	
244	38.	0.016	90	
248	64.	0.03	90	
251	9.	0.004	92	
259	38.	0.016	90	
260	19.	0.008	92/104	
261	19.	0.008	92	
268	60.	0.03	102	
269	33.	0.014	90	
278	24.	0.011	102	
281	9.	0.004	102	
283	2.	0.0009	102	
290	9.	0.004	102	

291	13.	0.006	104	
293	9.	0.004	104	
296	173.	0.08	104	
298	775.	0.3	106	C_8H_{10} : Ethylbenzene ^c
300	29.	0.013	104	
303	57.	0.03	104	
305	265.	0.11	88	
309	98.	0.04	106	m- and/or p-Xylene ^c
310	95.	0.04	100	
313	64.	0.03	104	
318	4747.	2	102	Phenylacetylene ^c
324	44.	0.02	104	
325	118.	0.05	104	
330	138.	0.06	90	
334	29.	0.013	102	
337	885.	0.4	104	C_8H_8 - Styrene ^c
340	52.	0.02	106	o-Xylene ^c
342	34.	0.015	104	
346	74.	0.03	102	
349	110.	0.05	106	
355	997.	0.4	88	
360	30.	0.013	102	
363	10.	0.004	104	
366	12.	0.005	106	
368	36.	0.016	108	
371	165.	0.07	100	
375	9.	0.004	104	
378	16.	0.007	106	
381	226.	0.1	100	
383	9.	0.004	102	
386	48.	0.02	104	
393	17.	0.007	104	
398	26.	0.010	116	
402	23.	0.010	106	
404	43.	0.02	102	
408	13.	0.005	104	
415	72.	0.03	102	
421	22.	0.009	120	
422	100.	0.04	106	C_7H_6O - Benzaldehyde ^c
426	21.	0.009	104	
430	706.	0.3	100	
431	1731.	18	98	C_8H_2 (polyacetylene)
436	1812.	0.8	94	C_6H_6O - Phenol ^c
443	240.	0.09	116	
449	114.	0.04	116	
452	108.	0.05	102	
454	114.	0.04	116	
457	42.	0.016	120	
460	28.	0.011	118	
463	122.	0.04	128	
467	7.	0.003	118	
470	8.	0.004	104	
477	20.	0.008	116	
481	14.	0.005	118	

485	20.	0.008	120	
488	11.	0.004	120	
490	17.	0.007	118	
492	16.	0.006	130	
494	31.	0.011	130	
496	27.	0.009	126	
499	53.	0.02	116	
505	20.	0.008	118	
507	19.	0.007	116	
511	217.	0.08	114	
512	185.	0.08	108	C ₇ H ₈ O - Benzyl alcohol ^c
515	3179.	1.2	116	C ₉ H ₈ - Indene ^c
521	361.	0.13	136	
525	183.	0.07	116	
530	83.	0.04	108	C ₇ H ₈ O - o-Cresol ^c
533	282.	0.1	126	Diethynylbenzene ^c
536	106.	0.04	126	Diethynylbenzene ^c
537/8	135.	0.05	130	
539	67.	0.02	130	
543	106.	0.04	114	
546	32.	0.011	130	
551	106.	0.04	130	
553	130.	0.05	126	Diethynylbenzene ^c
556	34.	0.012	128	
559	50.	0.018	128	
564	159.	0.06	130	
566	175.	0.06	130	
568	51.	0.018	128	
572	24.	0.008	130	
574	18.	0.006	132	
581	56.	0.02	114	
585	50.	0.02	114	
588/9	30.	0.012	116	
590	22.	0.008	130	
593	14.	0.004	150	
598	117.	0.04	130	
601	14.	0.005	128	
611	117.	0.04	130	
615	468.	0.16	130	
617	50.	0.018	128	
620	76.	0.03	130	
623	139.	0.05	128	
628	574.	0.2	126	Butadiynylbenzene ^c
631	32.	0.011	130	
635/6	52.	0.018	132	
637	30.	0.011	134	
639	39.	0.014	132	
643	41.	0.014	128	
647	124.	0.05	112	
650	2078.	0.7	128	Naphthalene ^c
656	30.	0.01	144	
659	32.	0.010	142	
668	34.	0.011	-NMI ^{-d}	

687	55.	0.018	140	
690	77.	0.02	-NMI-	
695	84.	0.03	144	
700	76.	0.02	144	
704	36.	0.012	144	
711	124.	0.04	140	
714	65.	0.02	140	
719	60.	0.019	140	
722	104.	0.03	142	
728	70.	0.02	142	
734	75.	0.02	154	
741	251.	0.08	142	2-methylnaphthalene ^c
753	21.	0.006	156	
756	204.	0.07	142	1-methylnaphthalene ^c
774	22.	0.006	156	
778	253.	0.07	-NMI-	
780	42.	0.012	150	
784	69.	0.02	154	
789	302.	0.09	-NMI-	
795	23.	0.007	156	
800	19.	0.006	156	
802	33.	0.01	154	
805	35.	0.010	154	
811	33.	0.01	152	
824	240.	0.07	152	
831/2	32.	0.009	154	
843	30.	0.009	156	
848	61.	0.02	-NMI-	
854	396.	0.1	180	
860	22.	0.006	156	
864	1363.	0.4	152	Acenaphthylene ^c
869	33.	0.01	150	
875	29.	0.008	156	
879	879.	0.3	-NMI-	
888	61.	0.018	154	
890	54.	0.016	-NMI-	
902	220.	0.06	-NMI-	
914/5	160.	0.04	180	
928	50.	0.012	180	
937	355.	0.09	178	
938	860.	0.2	-NMI-	
942	35.	0.009	166	
952	40.	0.011	166	
954	134.	0.04	166	
961	60.	0.015	180	

^aMolecular weight based on apparent molecular ion in mass spectrum.

^bIdentification by mass spectrum unless otherwise indicated.

^cIdentification by GC relative elution time to standards.

^dNMI = No molecular ion identified.

^eProbably mass 154 or 156, but all ions above 115 are less than 10% of the maximum ion signal within the spectrum.

APPENDIX I.

Summary of data from GC/MS analysis of sample V3650,
tabulated by molecular weight

Spectrum number	Corrected signal (1000's)	Approximate mole fraction ($\cdot 10^6$ or ppm)	Molecular weight ^a	Identity ^b ; Other remarks
10	44.6	8	68	
32	3804	700	74	C ₆ H ₂ - Hexatriyne
6	196	40	76	
141	33.5	6	76	
12	33.5	6	78	
15	6.8	1.3	78	
44	119	20	78	C ₆ H ₆ - Benzene
59	2.3	0.4	78	
128	14.2	0.006	88	
210	28.0	0.012	88	
240	57.	0.02	88	
305	265.	0.11	88	
355	997.	0.4	88	
120	8.4	0.003	90	
130	13.5	2	90	
161	315	0.13	90	
165	241	0.10	90	
178	32.9	0.014	90	
185	3.7	0.001	90	
189	10.3	0.004	90	
202/3	4.4	0.002	90	
217	116.	0.05	90	
226	40.	0.016	90	
244	38.	0.016	90	
248	64.	0.03	90	
259	38.	0.016	90	
269	33.	0.014	90	
330	138.	0.06	90	
72	17	0.007	92	
94	3.5	0.001	92	
106	17.8	0.007	92	
124	13.5	0.006	92	
137	4.4	0.002	92	
154	961	0.4	92	C ₇ H ₈ - Toluene
169	7.0	0.003	92	
213	19.	0.008	92	
236	12.	0.005	92	
251	9.	0.004	92	
260 ^f	10.	0.004	92	
261	19.	0.008	92	
111	12.5	0.005	94	
436	1812.	0.8	94	C ₆ H ₆ O - Phenol ^c
431	1731.	18	98	C ₈ H ₂ (polyacetylene)
310	95.	0.04	100	
371	165.	0.07	100	

381	226.	0.1	100	
430	706.	0.3	100	
211	20.	0.009	102	
268	60.	0.03	102	
278	24.	0.011	102	
281	9.	0.004	102	
283	2.	0.0009	102	
290	9.	0.004	102	
318	4747.	2	102	Phenylacetylene ^c
334	29.	0.013	102	
346	74.	0.03	102	
360	30.	0.013	102	
383	9.	0.004	102	
404	43.	0.02	102	
415	72.	0.03	102	
452	108.	0.05	102	
260 ^f	10.	0.004	104	
291	13.	0.006	104	
293	9.	0.004	104	
296	173.	0.08	104	
300	29.	0.013	104	
303	57.	0.03	104	
313	64.	0.03	104	
324	44.	0.02	104	
325	118.	0.05	104	
337	885.	0.4	104	C ₈ H ₈ - Styrene ^c
342	34.	0.015	104	
363	10.	0.004	104	
375	9.	0.004	104	
386	48.	0.02	104	
393	17.	0.007	104	
408	13.	0.005	104	
426	21.	0.009	104	
470	8.	0.004	104	
298	775.	0.3	106	C ₈ H ₁₀ : Ethylbenzene ^c
309	98.	0.04	106	m- and/or p-Xylene ^c
340	52.	0.02	106	o-Xylene ^c
349	110.	0.05	106	
366	12.	0.005	106	
378	16.	0.007	106	
402	23.	0.010	106	
422	100.	0.04	106	C ₇ H ₆ O - Benzaldehyde ^c
368	36.	0.016	108	
512	185.	0.08	108	C ₇ H ₈ O - Benzyl alcohol ^c
530	83.	0.04	108	C ₇ H ₈ O - o-Cresol ^c
647	124.	0.05	112	
511	217.	0.08	114	
543	106.	0.04	114	
581	56.	0.02	114	
585	50.	0.02	114	
398	26.	0.010	116	
443	240.	0.09	116	
449	114.	0.04	116	

454	114.	0.04	116	
477	20.	0.008	116	
499	53.	0.02	116	
507	19.	0.007	116	
515	3179.	1.2	116	C ₉ H ₈ - Indene ^c
525	183.	0.07	116	
588/9	30.	0.012	116	
460	28.	0.011	118	
467	7.	0.003	118	
481	14.	0.005	118	
490	17.	0.007	118	
505	20.	0.008	118	
421	22.	0.009	120	
457	42.	0.016	120	
485	20.	0.008	120	
488	11.	0.004	120	
496	27.	0.009	126	
533	282.	0.1	126	Diethynylbenzene ^c
536	106.	0.04	126	Diethynylbenzene ^c
553	130.	0.05	126	Diethynylbenzene ^c
628	574.	0.2	126	Butadiynylbenzene ^c
463	122.	0.04	128	
556	34.	0.012	128	
559	50.	0.018	128	
568	51.	0.018	128	
601	14.	0.005	128	
617	50.	0.018	128	
623	139.	0.05	128	
643	41.	0.014	128	
650	2078.	0.7	128	Naphthalene ^c
492	16.	0.006	130	
494	31.	0.011	130	
537/8	135.	0.05	130	
539	67.	0.02	130	
546	32.	0.011	130	
551	106.	0.04	130	
564	159.	0.06	130	
566	175.	0.06	130	
572	24.	0.008	130	
590	22.	0.008	130	
598	117.	0.04	130	
611	117.	0.04	130	
615	468.	0.16	130	
620	76.	0.03	130	
631	32.	0.011	130	
574	18.	0.006	132	
635/6	52.	0.018	132	
639	39.	0.014	132	
637	30.	0.011	134	
521	361.	0.13	136	
687	55.	0.018	140	
711	124.	0.04	140	
714	65.	0.02	140	
719	60.	0.019	140	

659	32.	0.010	142	
722	104.	0.03	142	
728	70.	0.02	142	
741	251.	0.08	142	2-methylnaphthalene ^c
756	204.	0.07	142	1-methylnaphthalene ^c
656	30.	0.01	144	
695	84.	0.03	144	
700	76.	0.02	144	
704	36.	0.012	144	
593	14.	0.004	150	
780	42.	0.012	150	
869	33.	0.01	150	
811	33.	0.01	152	
824	240.	0.07	152	
864	1363.	0.4	152	Acenaphthylene ^c
734	75.	0.02	154	
784	69.	0.02	154	
802	33.	0.01	154	
805	35.	0.010	154	
831/2	32.	0.009	154	
888	61.	0.018	154	
753	21.	0.006	156	
774	22.	0.006	156	
795	23.	0.007	156	
800	19.	0.006	156	
843	30.	0.009	156	
860	22.	0.006	156	
875	29.	0.008	156	
942	35.	0.009	166	
952	40.	0.011	166	
954	134.	0.04	166	
937	355.	0.09	178	
854	396.	0.1	180	
914/5	160.	0.04	180	
928	50.	0.012	180	
961	60.	0.015	180	
668	34.	0.011	-NMI- ^d	
690	77.	0.02	-NMI-	
778	253.	0.07	-NMI- ^e	
789	302.	0.09	-NMI-	
848	61.	0.02	-NMI-	
879	879.	0.3	-NMI-	
890	54.	0.016	-NMI-	
902	220.	0.06	-NMI-	
938	860.	0.2	-NMI-	

^aMolecular weight based on apparent molecular ion in mass spectrum.

^bIdentification by mass spectrum unless otherwise indicated.

^cIdentification by GC relative elution time to standards.

^dNMI = No molecular ion identified.

^eProbably mass 154 or 156, but all ions above 115 are less than 10% of the maximum ion signal within the spectrum.

^fApproximately 50% mass 92 and 50% mass 104.

APPENDIX J.

Reaction mechanisms tested in Chapter V.

Mechanisms MMSK, WB, WD, WZ, and WZ' are tabulated as Appendices J.1 to J.5 in a modified CHEMKIN input format, and the complete solutions for these mechanisms are included as Appendices J.6 to J.10.

In the mechanism descriptions, ELEMENTS and SPECIES are listed in the same way as normal for CHEMKIN. For REACTIONS, the format (and CHEMKIN subroutines) were modified to accept $\log_{10} A'$ instead of A' as the term for calculating rate constants [$A' \cdot T^b \exp(-E/RT)$]. The reason for this change is that fits to very non-Arrhenius rate constants can have A' values that are larger than the real numbers that a VAX 11/780 can use (approximately 10^{38}). For examples, see Table VII.8.

For the reader unfamiliar with the CHEMKIN input form for reactions, a reaction that is included only in its forward direction is designated by a hyphen (i.e., $A+B \rightarrow C+D$ is $A+B - C+D$), while a reaction whose reverse rate constant is to be included and calculated from microscopic reversibility is designated by = (i.e., $A+B \rightleftharpoons C+D$ is $A+B = C+D$).

Solutions are shown as tabulations of mole fraction vs. distance from the burner for all species.

Appendix J.1. Reaction Mechanism Tested As MMSK

ELEMENTS

H O C AR

END

SPECIES

AR

```

H          H2
CH         CH2      CH3
O          OH       H2O
C2H        C2H2     C2H3
CO         HCO      CH2O   CH3O
O2         HO2     H2O2
C3H2       C3H3     C3H4
HCCO       CH2CO    C2H2OH CO2
C4H2       C4H3     C4H2OH
    
```

END

REACTIONS

```

C2H2 + O          = CH2 + CO          (M#1)  1.0342423E+1  1.0  2583.
C2H2 + O          = HCCO + H         (M#2)  4.5514500E+0  2.7  1391.
C2H2OH + H        = CH2CO + H2       (M#3)  1.3301030E+1  0.   4000.
C2H2OH + O        = CH2CO + OH       (M#4)  1.3301030E+0  0.   4000.
C2H2OH + OH       = CH2CO + H2O      (M#5)  1.3000000E+0  0.   2000.
C2H2OH + O2       = CH2CO + HO2      (M#6)  1.2301030E+1  0.  10000.
C2H2OH           = CH2CO + H         (M#7*)  1.7871573E+1  -.944 28260.
C2H2 + OH         = C2H2OH          (M#8*)  1.4006466E+1  -.944  493.
C2H2 + OH         = CH2CO + H         (M#9)  1.1505150E+1  0.   200.
C2H + H2          = C2H2 + H         (M#10) 6.6117233E+0  2.39  864.
C2H2 + H          = C2H3            (M#11*) 1.8116940E+1 -2.24 2831.
C2H3 + H          = C2H2 + H2       (M#12) 1.2778151E+1  0.   0.
C2H3 + O2         = C2H2 + HO2      (M#13) 1.3198657E+1  0.  10000.
C2H3 + O          = CH2CO + H         (M#14) 1.3518514E+1  0.   0.
C2H3 + OH         = C2H2 + H2O      (M#15) 1.2698970E+1  0.   0.
CH2CO + OH        = CH2O + HCO       (M#16) 1.3447158E+1  0.   0.
CH2O + OH         = HCO + H2O        (M#17) 1.2876795E+1  0.   167.
CH2O + H          = HCO + H2         (M#18) 1.4519828E+1  0.  10500.
CH2O + M          = HCO + H + M       (M#19) 1.6519828E+1  0.  81000.
CH2O + O          = HCO + OH         (M#20) 1.3257679E+1  0.   3082.
HCO + OH          = CO + H2O         (M#21) 1.2698970E+1  0.   0.
HCO + M           = H + CO + M        (M#22) 1.4204120E+1  0.  14700.
HCO + H           = CO + H2          (M#23) 1.3602060E+1  0.   0.
HCO + O           = CO + OH          (M#24) 1.3000000E+1  0.   0.
HCO + O2          = CO + HO2         (M#25) 1.2477121E+1  0.   0.
CH2 + O2          = CO2 + H2         (M#26) 1.1838849E+1  0.   500.
CH2 + O2          = CO2 + H + H      (M#27) 1.2201397E+1  0.  1000.
CH2 + O2          = CO + H2O         (M#28) 1.0271842E+1  0. -1000.
CH2 + O2          = CO + OH + H      (M#29) 1.0936514E+1  0. -500.
CH2 + O2          = HCO + OH         (M#30) 1.0635484E+1  0. -500.
CO + O + M        = CO2 + M          (M#31) 1.3505150E+1  0. -4200.
CO + OH           = CO2 + H          (M#32) 7.1789769E+0  1.3 -758.
CO + O2           = CO2 + O          (M#33) 1.3204120E+1  0. 41000.
C2H2 + OH         = C2H + H2O       (M#34) 1.2778151E+1  0.  7000.
C2H2 + O          = C2H + OH         (M#35) 1.5499687E+1 -0.6 15000.
    
```

C2H	+	O2	-	HCCO	+	O	(M#36)	1.3698970E+1	0.	1500.
C2H2	+	C2H2	-	C4H3	+	H	(M#37)	1.2301030E+1	0.	45900.
C4H3	+	M	-	C4H2	+	H + M	(M#38)	1.6000000E+1	0.	59700.
C2H2	+	C2H	-	C4H2	+	H	(M#39)	1.3477121E+1	0.	0.
CH2	+	O	-	CH	+	OH	(M#40)	1.1301030E+1	0.68	25000.
CH2	+	O	-	CO	+	H + H	(M#41)	1.3892095E+1	0.	0.
CH2	+	C2H2	-	C3H3	+	H	(M#42)	1.2000000E+1	0.	0.
CH2	+	H	-	CH	+	H2	(M#43)	1.1399674E+1	0.67	25700.
CH2	+	OH	-	CH	+	H2O	(M#44)	1.1399674E+1	0.67	25700.
CH	+	O2	-	HCO	+	O	(M#45)	1.3000000E+1	0.	0.
CH3	+	O2	-	CH3O	+	O	(M#46)	1.2845098E+1	0.	25652.
CH3	+	O2	-	CH2O	+	OH	(M#47)	1.3716003E+1	0.	34574.
CH3O	+	M	-	CH2O	+	H + M	(M#48)	1.4301030E+1	0.	20000.
CH3O	+	H	-	CH2O	+	H2	(M#49)	1.3301030E+1	0.	0.
CH3O	+	OH	-	CH2O	+	H2O	(M#50)	1.3000000E+1	0.	0.
CH3O	+	O	-	CH2O	+	OH	(M#51)	1.3000000E+1	0.	0.
CH3O	+	O2	-	CH2O	+	HO2	(M#52)	1.0799341E+1	0.	2600.
CH3	+	O	-	CH2O	+	H	(M#53)	1.3832509E+1	0.	0.
CH3	+	OH	-	CH2O	+	H2	(M#54)	1.2875061E+1	0.	0.
C2H2	+	O2	-	HCCO	+	OH	(M#55)	8.3010300E+0	1.5	30100.
CH2CO	+	M	-	CH2	+	CO + M	(M#56)	1.6301030E+1	0.	60000.
C2H2	+	M	-	C2H	+	H + M	(M#57)	1.6623249E+1	0.	107000.
CH2CO	+	H	-	HCCO	+	H2	(M#58)	1.3875061E+1	0.	8000.
CH2CO	+	OH	-	HCCO	+	H2O	(M#59)	1.2875061E+1	0.	3000.
CH2CO	+	O	-	HCCO	+	OH	(M#60)	1.3698970E+1	0.	8000.
CH2CO	+	H	-	CO	+	CH3	(M#61)	1.3053078E+1	0.	3428.
CH2CO	+	O	-	CO	+	CH2O	(M#62)	1.3301030E+1	0.	0.
HCCO	+	OH	-	CO	+	H + HCO	(M#63)	1.3000000E+1	0.	0.
HCCO	+	H	-	CO	+	CH2	(M#64)	1.3698970E+1	0.	0.
HCCO	+	O2	-	CO	+	CO + OH	(M#65)	1.2164353E+1	0.	2500.
HCCO	+	O	-	CO	+	CO + H	(M#66)	1.3531479E+1	0.	2000.
C2H	+	O	-	CO	+	CH	(M#67)	1.3698970E+1	0.	0.
C2H	+	OH	-	HCCO	+	H	(M#68)	1.3301030E+1	0.	0.
C2H	+	C2H3	-	C2H2	+	C2H2	(M#69)	1.3477121E+1	0.	0.
CH2	+	CH2	-	C2H2	+	H2	(M#70)	1.3602060E+1	0.	0.
CH2	+	HCCO	-	C2H3	+	CO	(M#71)	1.3477121E+1	0.	0.
CH2	+	HCCO	-	CH2O	+	C2H	(M#72)	1.3000000E+1	0.	2000.
HCCO	+	HCCO	-	C2H2	+	CO + CO	(M#73)	1.3000000E+1	0.	0.
CH2	+	C2H3	-	CH3	+	C2H2	(M#74)	1.3477121E+1	0.	0.
C4H2	+	OH	-	C3H2	+	HCO	(M#75)	1.3477121E+1	0.	0.
C4H2	+	O	-	C3H2	+	CO	(M#76)	1.2079181E+1	0.	0.
C4H2	+	OH	-	C4H2OH			(M#77*)	1.4966142E+1	-.983	155.
C4H2OH	+	H	-	C4H2	+	H2O	(M#78)	1.3477121E+1	0.	0.
C2H2OH	+	H	-	C2H2	+	H2O	(M#79)	1.3477121E+1	0.	0.
C3H3	+	H	-	C3H4			(M#80*)	1.5270912E+1	-.984	157.
CO	+	HO2	-	CO2	+	OH	(M#81)	1.3763428E+1	0.	22934.
H2	+	O2	-	OH	+	OH	(M#82)	1.3230449E+1	0.	47780.
OH	+	H2	-	H2O	+	H	(M#83)	9.0681859E+0	1.3	3626.
H	+	O2	-	OH	+	O	(M#84)	1.6710117E+1	-0.816	16507.
O	+	H2	-	OH	+	H	(M#85)	1.0255273E+1	1.0	8826.
H	+	O2 + M	-	HO2	+	M	(M#86)	1.8322219E+1	-1.0	0.
H2O/21./ CO2/5.0/ CO/2./ H2/3.3/ O2/.00001/ AR/1.0/										
H	+	O2 + O2	-	HO2	+	O2	(M#87)	1.9826075E+1	-1.42	0.
OH	+	HO2	-	H2O	+	O2	(M#89)	1.3698970E+1	0.	1000.

H	+	HO2		-	OH	+	OH	(M#90)	1.4397940E+1	0.	1900.
O	+	HO2		-	O2	+	OH	(M#91)	1.3681241E+1	0.	1000.
OH	+	OH		-	H2O	+	O	(M#92)	8.7781513E+0	1.3	0.
H2	+	M		-	H	+	H + M	(M#93)	1.2348305E+1	0.5	92600.
		H2O/6./	H/2./		H2/3./		AR/1.0/				
O2	+	M		-	O	+	O + M	(M#94)	1.1267172E+1	0.5	95560.
H	+	OH	+ M	-	H2O	+	M	(M#95)	2.3875061E+1	-2.6	0.
		H2O/20./			AR/1.0/						
H	+	HO2		-	H2	+	O2	(M#96)	1.3397940E+1	0.	700.
HO2	+	HO2		-	H2O2	+	O2	(M#97)	1.2301030E+1	0.	0.
H2O2	+	M		-	OH	+	OH + M	(M#98)	1.7113943E+1	0.	45500.
H2O2	+	H		-	HO2	+	H2	(M#99)	1.2204120E+1	0.	3800.
H2O2	+	OH		-	H2O	+	HO2	(M#100)	1.3000000E+1	0.	1800.
END											

Appendix J.2. Reaction Mechanism Tested As WB

ELEMENTS									
H	O	C	AR						
END									
SPECIES									
AR									
H	H2								
CH	CH2	CH3	CH4						
O	OH	H2O							
C2H	C2H2	C2H3	C2H4	C2H5	C2H6				
CO	HCO	CH2O	CH3O	CH2OH	CH3OH				
O2	HO2	H2O2							
HCCO	CH2CO	CO2							
C4H	C4H2	C4H3	C4H6						
END									
REACTIONS									
H	+ O2		- OH	+ O	(WB #1)	14.27	0.	16790.	
OH	+ O		- H	+ O2	(WB #-1)	13.17	0.	680.	
O	+ H2		- OH	+ H	(WB #2)	10.26	1.	8900.	
OH	+ H		- O	+ H2	(WB #-2)	9.92	1.	6950.	
H2O	+ O		- OH	+ OH	(WB #3)	13.53	0.	18350.	
OH	+ OH		- O	+ H2O	(WB #-3)	12.50	0.	1100.	
H2O	+ H		- H2	+ OH	(WB #4)	13.98	0.	20300.	
H2	+ OH		- H2O	+ H	(WB #-4)	13.34	0.	5150.	
H2O2	+ OH		- H2O	+ HO2	(WB #5)	13.00	0.	1800.	
H2O	+ HO2		- H2O2	+ OH	(WB #-5)	13.45	0.	32790.	
H2O		+ M	- H	+ OH + M	(WB #6)	16.34	0.	105000.	
H	+ OH	+ M	- H2O	+ M	(WB #-6)	23.15	-2.	0.	
H	+ O2	+ M	- HO2	+ M	(WB #7)	15.22	0.	-1000.	
HO2		+ M	- H	+ O2 + M	(WB #-7)	15.36	0.	45900.	
HO2	+ O		- OH	+ O2	(WB #8)	13.70	0.	1000.	
O2	+ OH		- HO2	+ O	(WB #-8)	13.81	0.	56610.	
HO2	+ H		- OH	+ OH	(WB #9)	14.40	0.	1900.	
OH	+ OH		- HO2	+ H	(WB #-9)	13.08	0.	40100.	
HO2	+ H		- H2	+ O2	(WB #10)	13.40	0.	700.	
H2	+ O2		- HO2	+ H	(WB #-10)	13.74	0.	57800.	
HO2	+ OH		- H2O	+ O2	(WB #11)	13.70	0.	1000.	
H2O	+ O2		- HO2	+ OH	(WB #-11)	14.80	0.	73860.	
H2O2	+ O2		- HO2	+ HO2	(WB #12)	13.60	0.	42640.	
HO2	+ HO2		- H2O2	+ O2	(WB #-12)	13.00	0.	1000.	
H2O2		+ M	- OH	+ OH + M	(WB #13)	17.08	0.	45500.	
OH	+ OH	+ M	- H2O2	+ M	(WB #-13)	14.96	0.	-5070.	
H2O2	+ H		- H2	+ HO2	(WB #14)	12.23	0.	3750.	
H2	+ HO2		- H2O2	+ H	(WB #-14)	11.86	0.	18700.	
O	+ H	+ M	- OH	+ M	(WB #15)	16.00	0.	0.	
OH		+ M	- O	+ H + M	(WB #-15)	19.90	-1.	103720.	
O2		+ M	- O	+ O + M	(WB #16)	15.71	0.	115000.	
O	+ O	+ M	- O2	+ M	(WB #-16)	15.67	-0.28	0.	
H2		+ M	- H	+ H + M	(WB #17)	14.34	0.	96000.	
H	+ H	+ M	- H2	+ M	(WB #-17)	15.48	0.	0.	
CO	+ OH		- CO2	+ H	(WB #18)	7.11	1.3	-770.	
CO2	+ H		- CO	+ OH	(WB #-18)	9.15	1.3	21580.	

CO + HO2	- CO2 + OH	(WB #19)	14.18	0.	23650.
CO2 + OH	- CO + HO2	(WB #-19)	15.23	0.	85500.
CO + O + M	- CO2 + M	(WB #20)	15.77	0.	4100.
CO2 + M	- CO + O + M	(WB #-20)	21.74	-1.	131780.
CO2 + O	- CO + O2	(WB #21)	12.44	0.	43830.
CO + O2	- CO2 + O	(WB #-21)	11.50	0.	37600.
HCO + OH	- CO + H2O	(WB #22)	14.00	0.	0.
CO + H2O	- HCO + OH	(WB #-22)	15.45	0.	105150.
HCO + M	- H + CO + M	(WB #23)	14.16	0.	19000.
H + CO + M	- HCO + M	(WB #-23)	11.70	1.	1550.
HCO + H	- CO + H2	(WB #24)	14.30	0.	0.
CO + H2	- HCO + H	(WB #-24)	15.12	0.	90000.
HCO + O	- CO + OH	(WB #25)	14.00	0.	0.
CO + OH	- HCO + O	(WB #-25)	14.46	0.	87900.
HCO + HO2	- CH2O + O2	(WB #26)	14.00	0.	3000.
CH2O + O2	- HCO + HO2	(WB #-26)	15.56	0.	46040.
HCO + O2	- CO + HO2	(WB #27)	12.60	0.	7000.
CO + HO2	- HCO + O2	(WB #-27)	12.95	0.	39290.
CH2O + M	- HCO + H + M	(WB #28)	16.52	0.	81000.
HCO + H + M	- CH2O + M	(WB #-28)	11.15	1.	-11770.
CH2O + OH	- HCO + H2O	(WB #29)	12.88	0.	170.
H2O + HCO	- CH2O + OH	(WB #-29)	12.41	0.	29990.
CH2O + H	- HCO + H2	(WB #30)	14.52	0.	10500.
H2 + HCO	- CH2O + H	(WB #-30)	13.42	0.	25170.
CH2O + O	- HCO + OH	(WB #31)	13.70	0.	4600.
OH + HCO	- CH2O + O	(WB #-31)	12.24	0.	17170.
CH2O + HO2	- HCO + H2O2	(WB #32)	12.00	0.	8000.
HCO + H2O2	- CH2O + HO2	(WB #-32)	11.04	0.	659.
CH4 + M	- CH3 + H + M	(WB #33)	17.15	0.	88400.
CH3 + H + M	- CH4 + M	(WB #-33)	11.45	1.	-19520.
CH4 + H	- CH3 + H2	(WB #34)	14.10	0.	11900.
CH3 + H2	- CH4 + H	(WB #-34)	12.68	0.	11430.
CH4 + OH	- CH3 + H2O	(WB #35)	3.54	3.08	2000.
CH3 + H2O	- CH4 + OH	(WB #-35)	2.76	3.08	16680.
CH4 + O	- CH3 + OH	(WB #36)	13.20	0.	9200.
CH3 + OH	- CH4 + O	(WB #-36)	11.43	0.	6640.
CH4 + HO2	- CH3 + H2O2	(WB #37)	13.30	0.	18000.
CH3 + H2O2	- CH4 + HO2	(WB #-37)	12.02	0.	1450.
CH3 + HO2	- CH3O + OH	(WB #38)	13.51	0.	0.
CH3O + OH	- CH3 + HO2	(WB #-38)	10.00	0.	0.
CH3 + OH	- CH2O + H2	(WB #39)	12.60	0.	0.
CH2O + H2	- CH3 + OH	(WB #-39)	14.08	0.	71730.
CH3 + O	- CH2O + H	(WB #40)	14.11	0.	2000.
CH2O + H	- CH3 + O	(WB #-40)	15.23	0.	71630.
CH3 + O2	- CH3O + O	(WB #41)	13.38	0.	29000.
CH3O + O	- CH3 + O2	(WB #-41)	14.48	0.	730.
CH3 + CH2O	- CH4 + HCO	(WB #42)	10.00	0.5	6000.
CH4 + HCO	- CH3 + CH2O	(WB #-42)	10.32	0.5	21140.
CH3 + HCO	- CH4 + CO	(WB #43)	11.48	0.5	0.
CH4 + CO	- CH3 + HCO	(WB #-43)	13.71	0.5	90470.
CH3 + HO2	- CH4 + O2	(WB #44)	12.00	0.	400.
CH4 + O2	- CH3 + HO2	(WB #-44)	13.88	0.	58590.
CH3O + M	- CH2O + H + M	(WB #45)	13.70	0.	21000.
CH2O + H + M	- CH3O + M	(WB #-45)	9.00	1.	-2560.

CH30 + O2	-	CH20 + HO2	(WB #46)	12.00	0.	6000.	
CH20 + HO2	-	CH30 + O2	(WB #-46)	11.11	0.	32170.	
C2H6	-	CH3 + CH3	(WB #47)	19.35	-1.	88310.	
CH3 + CH3	-	C2H6	(WB #-47)	12.95	0.	0.	
C2H6 + CH3	-	C2H5 + CH4	(WB #48)	-0.26	4.	8280.	
C2H5 + CH4	-	C2H6 + CH3	(WB #-48)	10.48	0.	12500.	
C2H6 + H	-	C2H5 + H2	(WB #49)	2.73	3.5	5200.	
C2H5 + H2	-	C2H6 + H	(WB #-49)	2.99	3.5	27320.	
C2H6 + OH	-	C2H5 + H2O	(WB #50)	13.05	0.	2450.	
C2H5 + H2O	-	C2H6 + OH	(WB #-50)	13.30	0.	24570.	
C2H6 + O	-	C2H5 + OH	(WB #51)	13.40	0.	6360.	
C2H5 + OH	-	C2H6 + O	(WB #-51)	12.66	0.	11230.	
C2H5	+ M	C2H4 + H	+ M	(WB #52)	15.30	0.	30000.
C2H4 + H	+ M	C2H5	+ M	(WB #-52)	10.62	0.	-11030.
C2H5 + O2	-	C2H4 + HO2	(WB #53)	12.00	0.	5000.	
C2H4 + HO2	-	C2H5 + O2	(WB #-53)	11.12	0.	13700.	
C2H4 + C2H4	-	C2H5 + C2H3	(WB #54)	14.70	0.	64700.	
C2H5 + C2H3	-	C2H4 + C2H4	(WB #-54)	14.17	0.	-2610.	
C2H4	+ M	C2H2 + H2	+ M	(WB #55)	16.97	0.	77200.
C2H2 + H2	+ M	C2H4	+ M	(WB #-55)	12.66	1.	36520.
C2H4	+ M	C2H3 + H	+ M	(WB #56)	18.80	0.	108720.
C2H3 + H	+ M	C2H4	+ M	(WB #-56)	17.30	0.	0.
C2H4 + O	-	CH3 + HCO	(WB #57)	12.52	0.	1130.	
CH3 + HCO	-	C2H4 + O	(WB #-57)	11.20	0.	31180.	
C2H4 + O	-	CH20 + CH2	(WB #58)	13.40	0.	5000.	
CH20 + CH2	-	C2H4 + O	(WB #-58)	12.48	0.	15680.	
C2H4 + H	-	C2H3 + H2	(WB #59)	7.18	2.	6000.	
C2H3 + H2	-	C2H4 + H	(WB #-59)	6.24	2.	5110.	
C2H4 + OH	-	C2H3 + H2O	(WB #60)	12.68	0.	1230.	
C2H3 + H2O	-	C2H4 + OH	(WB #-60)	12.08	0.	14000.	
C2H4 + OH	-	CH3 + CH2O	(WB #61)	12.30	0.	960.	
CH3 + CH2O	-	C2H4 + O	(WB #-61)	11.78	0.	16480.	
C2H3	+ M	C2H2 + H	+ M	(WB #62)	14.90	0.	31500.
C2H2 + H	+ M	C2H3	+ M	(WB #-62)	11.09	1.	-10360.
C2H3 + O2	-	C2H2 + HO2	(WB #63)	12.00	0.	10000.	
C2H2 + HO2	-	C2H3 + O2	(WB #-63)	12.00	0.	17870.	
C2H2	+ M	C2H + H	+ M	(WB #64)	14.00	0.	114000.
C2H + H	+ M	C2H2	+ M	(WB #-64)	9.04	1	770.
C2H2 + O2	-	HCO + HCO	(WB #65)	12.60	0.	28000.	
HCO + HCO	-	C2H2 + O2	(WB #-65)	11.00	0.	63650.	
C2H2 + H	-	C2H + H2	(WB #66)	14.30	0.	19000.	
C2H + H2	-	C2H2 + H	(WB #-66)	13.62	0.	13210.	
C2H2 + OH	-	C2H + H2O	(WB #67)	12.78	0.	7000.	
C2H + H2O	-	C2H2 + OH	(WB #-67)	12.73	0.	16360.	
C2H2 + OH	-	CH2CO + H	(WB #68)	11.51	0.	200.	
CH2CO + H	-	C2H2 + OH	(WB #-68)	12.50	0.	20870.	
C2H2 + O	-	C2H + OH	(WB #69)	15.51	-0.6	17000.	
C2H + OH	-	C2H2 + O	(WB #-69)	14.47	-0.6	910.	
C2H2 + O	-	CH2 + CO	(WB #70)	13.83	0.	4000.	
CH2 + CO	-	C2H2 + O	(WB #-70)	13.10	0.	54670.	
C2H + O2	-	HCO + CO	(WB #71)	13.00	0.	7000.	
HCO + CO	-	C2H + O2	(WB #-71)	12.93	0.	138400.	
C2H + O	-	CO + CH	(WB #72)	13.70	0.	0.	
CO + CH	-	C2H + O	(WB #-72)	13.50	0.	59430.	

CH2 + O2		- HCO + OH	(WB #73)	14.00	0.	3700.
HCO + OH		- CH2 + O2	(WB #-73)	13.61	0.	76580.
CH2 + O		- CH + OH	(WB #74)	11.28	0.68	25000.
CH + OH		- CH2 + O	(WB #-74)	10.77	0.68	25930.
CH2 + H		- CH + H2	(WB #75)	11.43	0.67	25700.
CH + H2		- CH2 + H	(WB #-75)	11.28	0.67	28720.
CH2 + OH		- CH + H2O	(WB #76)	11.43	0.67	25700.
CH + H2O		- CH2 + OH	(WB #-76)	11.91	0.67	43880.
CH + O2		- CO + OH	(WB #77)	11.13	0.67	25700.
CO + OH		- CH + O2	(WB #-77)	11.71	0.67	185600.
CH + O2		- HCO + O	(WB #78)	13.00	0.	0.
HCO + O		- CH + O2	(WB #-78)	13.13	0.	71950.
CH3OH	+ M	- CH3 + OH + M	(WB #79)	18.48	0.	80000.
CH3 + OH	+ M	- CH3OH + M	(WB #-79)	13.16	1.	-10980.
CH3OH + OH		- CH2OH + H2O	(WB #80)	12.60	0.	2000.
CH2OH + H2O		- CH3OH + OH	(WB #-80)	7.27	1.66	25310.
CH3OH + O		- CH2OH + OH	(WB #81)	12.23	0.	2290.
CH2OH + OH		- CH3OH + O	(WB #-81)	5.90	1.66	8350.
CH3OH + H		- CH2OH + H2	(WB #82)	13.48	0.	7000.
CH2OH + H2		- CH3OH + H	(WB #-82)	7.51	1.66	15160.
CH3OH + H		- CH3 + H2O	(WB #83)	12.72	0.	5340.
CH3 + H2O		- CH3OH + H	(WB #-83)	12.32	0.	36950.
CH3OH + CH3		- CH2OH + CH4	(WB #84)	11.26	0.	9800.
CH2OH + CH4		- CH3OH + CH3	(WB #-84)	6.70	1.66	18430.
CH3OH + HO2		- CH2OH + H2O2	(WB #85)	12.80	0.	19360.
CH2OH + H2O2		- CH3OH + HO2	(WB #-85)	7.00	1.66	11440.
CH2OH	+ M	- CH2O + H + M	(WB #86)	13.40	0.	29000.
CH2O + H	+ M	- CH2OH + M	(WB #-86)	16.69	-0.66	7580.
CH2OH + O2		- CH2O + HO2	(WB #87)	12.00	0.	6000.
CH2O + HO2		- CH2OH + O2	(WB #-87)	17.94	-1.66	28320.
C2H3 + C2H4		- C4H6 + H	(WB #88)	12.00	0.	7300.
C4H6 + H		- C2H3 + C2H4	(WB #-88)	13.00	0.	4700.
C2H2 + C2H2		- C4H3 + H	(WB #89)	13.00	0.	45000.
C4H3 + H		- C2H2 + C2H2	(WB #-89)	13.18	0.	0.
C4H3	+ M	- C4H2 + H + M	(WB #90)	16.00	0.	60000.
C4H2 + H	+ M	- C4H3 + M	(WB #-90)	11.92	1.	2540.
C2H + C2H2		- C4H2 + H	(WB #91)	13.60	0.	0.
C4H2 + H		- C2H + C2H2	(WB #-91)	14.65	0.	550.
C4H2	+ M	- C4H + H + M	(WB #92)	17.54	0.	80000.
C4H + H	+ M	- C4H2 + M	(WB #-92)	12.30	1.	-16400.
C2H3 + H		- C2H2 + H2	(WB #93)	13.30	0.	2500.
C2H2 + H2		- C2H3 + H	(WB #-93)	13.12	0.	68080.
C2H2 + O		- HCCO + H	(WB #94)	4.55	2.7	1390.
HCCO + H		- C2H2 + O	(WB #-94)	2.70	2.7	12790.
CH2CO + H		- CH3 + CO	(WB #95)	13.04	0.	3400.
CH3 + CO		- CH2CO + H	(WB #-95)	12.38	0.	40200.
CH2CO + O		- HCO + HCO	(WB #96)	13.00	0.	2400.
HCO + HCO		- CH2CO + O	(WB #-96)	11.54	0.	33500.
CH2CO + OH		- CH2O + HCO	(WB #97)	13.45	0.	0.
CH2O + HCO		- CH2CO + OH	(WB #-97)	13.44	0.	18500.
CH2CO	+ M	- CH2 + CO + M	(WB #98)	16.30	0.	60000.
CH2 + CO	+ M	- CH2CO + M	(WB #-98)	10.66	0.	0.
CH2CO + O		- HCCO + OH	(WB #99)	13.00	0.	0.
HCCO + OH		- CH2CO + O	(WB #-99)	10.16	0.	0.

CH2CO + OH	- HCCO + H2O	(WB #100)	13.00	0.	0.
HCCO + H2O	- CH2CO + OH	(WB #-100)	11.15	0.	7990.
CH2CO + H	- HCCO + H2	(WB #101)	13.00	0.	0.
HCCO + H2	- CH2CO + H	(WB #-101)	10.51	0.	0.
HCCO + OH	- HCO + HCO	(WB #102)	13.00	0.	0.
HCO + HCO	- HCCO + OH	(WB #-102)	13.68	0.	40360.
HCCO + H	- CH2 + CO	(WB #103)	13.70	0.	0.
CH2 + CO	- HCCO + H	(WB #-103)	13.82	0.	39260.
HCCO + O	- HCO + CO	(WB #104)	13.53	0.	2000.
HCO + CO	- HCCO + C	(WB #-104)	13.92	0.	128260.

END

A'S ENTERED AS LOG10(A) FROM WESTBROOK, COMB.SCI.&TECH., 34, 201-225(1983).

Appendix J.3. Reaction Mechanism Tested As WD

ELEMENTS

H O C AR

END

SPECIES

AR

```

H      H2
CH     CH2     CH3     CH4
O      OH      H2O
C2H    C2H2    C2H3    C2H4    C2H5    C2H6
CO     HCO     CH2O    CH3O    CH2OH    CH3OH
O2     HO2     H2O2
C3H2   C3H4   C3H5   C3H6
HCCO   CH2CO  CH3CO  C2H2OH CH3CHO  CO2
C4H2   C4H3   C4H6
  
```

END

REACTIONS

H	+ O2		= OH	+ O	(WD #1)	16.71	-0.816	16510.
O	+ H2		= OH	+ H	(WD #2)	10.26	1.0	8900.
H2	+ OH		= H2O	+ H	(WD #3)	13.34	0.	5150.
H2O	+ O		= 2OH		(WD #4)	13.83	0.	18360.
2H		+ M	= H2		(WD #5)	15.48	0.	0.
2O		+ M	= O2		(WD #6)	13.28	0.	-1790.
O	+ H	+ M	= OH		(WD #7)	16.00	0.	0.
H	+ OH	+ M	= H2O		(WD #8)	23.15	-2.0	0.
H	+ O2	+ M	= HO2		(WD #9)	15.18	0.	-1000.
HO2	+ H		= H2	+ O2	(WD #10)	13.40	0.	700.
HO2	+ H		= 2OH		(WD #11)	14.40	0.	1900.
HO2	+ H		= H2O	+ O	(WD #12)	13.70	0.	1000.
HO2	+ OH		= H2O	+ O2	(WD #13)	13.70	0.	1000.
HO2	+ O		= O2	+ OH	(WD #14)	13.70	0.	1000.
2HO2			= H2O2	+ O2	(WD #15)	13.00	0.	1000.
H2O2	+ OH		= H2O	+ HO2	(WD #16)	13.00	0.	1800.
H2O2	+ H		= H2O	+ OH	(WD #17)	14.50	0.	8940.
H2O2	+ H		= H2	+ HO2	(WD #18)	12.23	0.	3750.
H2O2		+ M	= 2OH		(WD #19)	17.08	0.	45500.
O	+ OH	+ M	= HO2		(WD #20)	17.00	0.	0.
H2	+ O2		= 2OH		(WD #21)	12.40	0.	38950.
CO	+ O	+ M	= CO2		(WD #26)	15.77	0.	4100.
CO	+ O2		= CO2	+ O	(WD #27)	12.40	0.	47690.
CO	+ OH		= CO2	+ H	(WD #28)	7.18	1.3	-770.
CO	+ HO2		= CO2	+ OH	(WD #29)	13.76	0.	22930.
CH2O		+ M	= HCO	+ H	(WD #30)	16.52	0.	81000.
CH2O	+ OH		= HCO	+ H2O	(WD #31)	12.88	0.	170.
CH2O	+ H		= HCO	+ H2	(WD #32)	14.52	0.	10500.
CH2O	+ O		= HCO	+ OH	(WD #33)	13.70	0.	4600.
CH2O	+ HO2		= HCO	+ H2O2	(WD #34)	12.00	0.	8000.
HCO		+ M	= H	+ CO	(WD #35)	14.16	0.	19000.
HCO	+ O2		= CO	+ HO2	(WD #36)	12.52	0.	7000.
HCO	+ OH		= CO	+ H2O	(WD #37)	14.00	0.	0.
HCO	+ H		= CO	+ H2	(WD #38)	14.30	0.	0.
HCO	+ O		= CO	+ OH	(WD #39)	14.00	0.	0.

CH ⁴		+ M	- CH ₃ + H	+ M	(WD #40)	17.30	0.	88000.
CH ₄ + O ₂			- CH ₃ + HO ₂		(WD #41)	13.90	0.	56000.
CH ₄ + H			- CH ₃ + H ₂		(WD #42)	4.350	3.0	8750.
CH ₄ + OH			- CH ₃ + H ₂ O		(WD #43)	3.540	3.08	2000.
CH ₄ + O			- CH ₃ + OH		(WD #44)	7.07	2.08	7630.
CH ₄ + HO ₂			- CH ₃ + H ₂ O ₂		(WD #45)	13.30	0.	18000.
CH ₃ + O ₂			- CH ₃ O + O		(WD #46)	13.38	0.	29000.
2CH ₃			- C ₂ H ₆		(WD #47)	13.00	0.	0.
2CH ₃			- C ₂ H ₅ + H		(WD #48)	14.90	0.	26520.
2CH ₃			- C ₂ H ₄ + H ₂		(WD #49)	16.00	0.	32000.
CH ₃ + O			- CH ₂ O + H		(WD #50)	14.11	0.	2000.
CH ₃ + OH			- CH ₂ O + H ₂		(WD #51)	12.60	0.	0.
CH ₃ + OH			- CH ₃ O + H		(WD #52)	16.30	0.	27410.
CH ₃ + CH ₂ O			- CH ₄ + HCO		(WD #53)	10.00	0.5	6000.
CH ₃ + HCO			- CH ₄ + CO		(WD #54)	11.48	0.5	0.
CH ₃ + HO ₂			- CH ₃ O + OH		(WD #55)	13.30	0.	0.
CH ₃		+ M	- CH ₂ + H	+ M	(WD #56)	16.29	0.	91600.
CH ₃ O		+ M	- CH ₂ O + H	+ M	(WD #57)	13.70	0.	21000.
CH ₃ O + O ₂			- CH ₂ O + HO ₂		(WD #58)	12.00	0.	6000.
CH ₃ O + H			- CH ₂ O + H ₂		(WD #59)	13.30	0.	0.
C ₂ H ₆ + O ₂			- C ₂ H ₅ + HO ₂		(WD #60)	13.00	0.	51000.
C ₂ H ₆ + CH ₃			- C ₂ H ₅ + CH ₄		(WD #61)	-0.26	4.0	8280.
C ₂ H ₆ + H			- C ₂ H ₅ + H ₂		(WD #62)	2.73	3.5	5200.
C ₂ H ₆ + O			- C ₂ H ₅ + OH		(WD #63)	13.40	0.	6360.
C ₂ H ₆ + OH			- C ₂ H ₅ + H ₂ O		(WD #64)	9.94	1.05	1810.
C ₂ H ₅		+ M	- C ₂ H ₄ + H	+ M	(WD #65)	15.30	0.	30000.
C ₂ H ₅ + O ₂			- C ₂ H ₄ + HO ₂		(WD #66)	12.00	0.	5000.
C ₂ H ₅ + O			- CH ₃ CHO + H		(WD #67)	13.70	0.	0.
C ₂ H ₅ + O			- CH ₂ O + CH ₃		(WD #68)	13.00	0.	0.
C ₃ H ₆			- C ₂ H ₃ + CH ₃		(WD #71)	15.80	0.	85800.
2C ₂ H ₃			- C ₄ H ₆		(WD #73)	12.95	0.	0.
C ₂ H ₄		+ M	- C ₂ H ₂ + H ₂	+ M	(WD #74)	16.97	0.	77200.
C ₂ H ₄		+ M	- C ₂ H ₃ + H	+ M	(WD #75)	18.80	0.	108720.
2C ₂ H ₄			- C ₂ H ₃ + C ₂ H ₅		(WD #76)	14.70	0.	64700.
C ₂ H ₃		+ M	- C ₂ H ₂ + H	+ M	(WD #77)	14.90	0.	31500.
C ₂ H ₃ + O ₂			- C ₂ H ₂ + HO ₂		(WD #78)	12.00	0.	10000.
C ₂ H ₄ + H			- C ₂ H ₃ + H ₂		(WD #79)	7.18	2.0	6000.
C ₂ H ₄ + OH			- C ₂ H ₃ + H ₂ O		(WD #80)	12.68	0.	1230.
C ₂ H ₄ + O			- CH ₃ + HCO		(WD #81)	12.52	0.	1130.
C ₂ H ₄ + O			- CH ₂ O + CH ₂		(WD #82)	13.40	0.	5000.
C ₂ H ₄ + OH			- CH ₃ + CH ₂ O		(WD #83)	12.30	0.	960.
C ₂ H ₃ + H			- C ₂ H ₂ + H ₂		(WD #84)	13.30	0.	2500.
C ₂ H ₃ + O			- CH ₂ CO + H		(WD #85)	13.52	0.	0.
C ₂ H ₃ + OH			- C ₂ H ₂ + H ₂ O		(WD #86)	12.70	0.	0.
C ₂ H ₃ + C ₂ H ₄			- C ₄ H ₆ + H		(WD #87)	12.00	0.	7300.
C ₂ H ₂		+ M	- C ₂ H + H	+ M	(WD #88)	16.62	0.	107000.
2C ₂ H ₂			- C ₄ H ₃ + H		(WD #89)	13.00	0.	45000.
C ₂ H ₂ + O ₂			- HCCO + OH		(WD #90)	12.70	0.	23500.
C ₂ H ₂ + O ₂			- HCO + HCO		(WD #91)	12.60	0.	28000.
C ₂ H ₂ + H			- C ₂ H + H ₂		(WD #92)	14.30	0.	19000.
C ₂ H ₂ + O			- C ₂ H + OH		(WD #93)	15.50	-0.6	15000.
C ₂ H ₂ + O			- CH ₂ + CO		(WD #94)	10.34	1.0	2580.
C ₂ H ₂ + O			- HCCO + H		(WD #95)	4.55	2.7	1390.
C ₂ H ₂ + OH			- CH ₂ CO + H		(WD #96)	11.51	0.	200.

C2H2 + OH	-	C2H + H2O	(WD #97)	12.80	0.	7000.
C2H2 + OH	-	CH3 + CO	(WD #98)	12.08	0.	500.
C2H2 + OH	-	C2H2OH	(WD #99)	11.83	0.	232.
C2H2OH + H	-	CH2CO + H2	(WD #100)	13.30	0.	4000.
C2H2OH + O	-	CH2CO + OH	(WD #101)	13.30	0.	4000.
C2H2OH + OH	-	CH2CO + H2O	(WD #102)	13.00	0.	2000.
C2H2OH + O2	-	CH2CO + HO2	(WD #103)	12.30	0.	10000.
C2H2OH	+ M	- CH2CO + H + M	(WD #104)	15.70	0.	28000.
C2H + C2H2	-	C4H2 + H	(WD #105)	13.60	0.	0.
C4H2 + OH	-	C3H2 + HCO	(WD #106)	12.81	0.	1000.
CH2CO	+ M	- CH2 + CO + M	(WD #107)	16.30	0.	60000.
CH2CO + OH	-	CH2O + HCO	(WD #108)	13.45	0.	0.
CH2CO + OH	-	HCCO + H2O	(WD #109)	13.00	0.	0.
CH2CO + O	-	HCCO + OH	(WD #110)	13.00	0.	0.
CH2CO + O	-	2HCO	(WD #111)	13.00	0.	2410.
CH2CO + H	-	HCCO + H2	(WD #112)	13.00	0.	0.
CH2CO + H	-	CH3 + CO	(WD #113)	13.04	0.	3400.
HCCO + O2	-	2CO + OH	(WD #114)	11.80	0.	2000.
HCCO + O	-	2CO + H	(WD #115)	12.08	0.	0.
HCCO + H	-	CH2 + CO	(WD #116)	12.70	0.	0.
HCCO + OH	-	HCO + H + CO	(WD #117)	12.30	0.	0.
HCCO + CH2	-	C2H3 + CO	(WD #118)	13.48	0.	0.
CH2 + O2	-	CO2 + H2	(WD #119)	12.21	0.	1000.
CH2 + O2	-	CO2 + 2H	(WD #120)	12.57	0.	1500.
CH2 + O2	-	CO + H2O	(WD #121)	11.00	0.	0.
CH2 + O2	-	CO + OH + H	(WD #122)	11.30	0.	0.
CH2 + O2	-	HCO + OH	(WD #123)	14.00	0.	3700.
CH2 + O	-	CH + OH	(WD #124)	11.30	0.68	25000.
CH2 + O	-	CO + 2H	(WD #125)	12.70	0.	0.
CH2 + O	-	CO + H2	(WD #126)	12.70	0.	0.
CH2 + OH	-	CH + H2O	(WD #127)	11.40	0.67	25700.
CH2 + H	-	CH + H2	(WD #128)	11.40	0.67	25700.
2CH2	-	C2H3 + H	(WD #129)	12.70	0.	0.
2CH2	-	C2H2 + H2	(WD #130)	13.50	0.	0.
CH2 + C2H3	-	CH3 + C2H2	(WD #131)	13.48	0.	0.
C2H + O2	-	HCCO + O	(WD #132)	12.52	0.	0.
C2H + O2	-	HCO + CO	(WD #133)	13.00	0.	7000.
C2H + O	-	CO + CH	(WD #134)	13.70	0.	0.
C2H + C2H3	-	2C2H2	(WD #135)	13.48	0.	0.
CH + O2	-	HCO + O	(WD #136)	13.00	0.	0.
CH + O2	-	CO + OH	(WD #137)	11.13	0.67	25700.
C4H3	+ M	- C4H2 + H + M	(WD #138)	16.00	0.	60000.
CH3OH	+ M	- CH3 + OH + M	(WD #141)	18.48	0.	80000.
CH3OH + O2	-	CH2OH + HO2	(WD #142)	10.60	0.	50910.
CH3OH + H	-	CH3 + H2O	(WD #143)	12.72	0.	5340.
CH3OH + H	-	CH2OH + H2	(WD #144)	13.48	0.	7000.
CH3OH + OH	-	CH2OH + H2O	(WD #145)	12.60	0.	2000.
CH3OH + O	-	CH2OH + OH	(WD #146)	12.23	0.	2290.
CH3OH + CH3	-	CH2OH + CH4	(WD #147)	11.26	0.	9800.
CH3OH + HO2	-	CH2OH + H2O2	(WD #148)	12.80	0.	19360.
CH2OH	+ M	- CH2O + H + M	(WD #149)	13.40	0.	29000.
CH2OH + O2	-	CH2O + HO2	(WD #150)	12.00	0.	6000.
CH2OH + H	-	CH2O + H2	(WD #151)	12.48	0.	0.
CH3CHO	-	CH3 + HCO	(WD #162)	15.85	0.	81760.

CH3CHO	- CH3CO + H	(WD #163)	14.70	0.	87860.
CH3CHO + O2	- CH3CO + HO2	(WD #164)	13.30	0.5	42200.
CH3CHO + H	- CH3CO + H2	(WD #165)	13.60	0.	4200.
CH3CHO + OH	- CH3CO + H2O	(WD #166)	13.00	0.	0.
CH3CHO + O	- CH3CO + OH	(WD #167)	12.70	0.	1790.
CH3CHO + CH3	- CH3CO + CH4	(WD #168)	12.23	0.	8430.
CH3CHO + HO2	- CH3CO + H2O2	(WD #169)	12.23	0.	10700.
CH3CO	- CH3 + CO	(WD #170)	13.48	0.	17240.
C3H6	- C3H5 + H	(WD #196)	13.00	0.	78000.
C3H6 + O	- CH2O + C2H4	(WD #197)	13.77	0.	5000.
C3H6 + O	- CH3 + CH3CO	(WD #198)	12.70	0.	600.
C3H6 + OH	- CH3 + CH3CHO	(WD #199)	12.85	0.	0.
C3H6 + O	- C2H5 + HCO	(WD #200)	12.55	0.	0.
C3H6 + OH	- C3H5 + H2O	(WD #201)	12.60	0.	0.
C3H6 + OH	- C2H5 + CH2O	(WD #202)	12.90	0.	0.
C3H6 + H	- C3H5 + H2	(WD #203)	12.70	0.	1500.
C3H6 + CH3	- C3H5 + CH4	(WD #204)	10.95	0.	8500.
C3H6 + C2H5	- C3H5 + C2H6	(WD #206)	11.00	0.	9200.
C3H5	- C3H4 + H	(WD #207)	13.60	0.	70000.
C3H5 + O2	- C3H4 + HO2	(WD #208)	11.78	0.	10000.
C3H5 + H	- C3H4 + H2	(WD #210)	13.00	0.	0.
C3H5 + CH3	- C3H4 + CH4	(WD #211)	12.00	0.	0.
C3H4 + O	- CH2O + C2H2	(WD #212)	12.00	0.	0.
C3H4 + OH	- CH2O + C2H3	(WD #213)	12.00	0.	0.
C3H4 + O	- HCO + C2H3	(WD #214)	12.00	0.	0.
C3H4 + OH	- HCO + C2H4	(WD #215)	12.00	0.	0.

END

FROM WESTBROOK AND DRYER, PROG. ENERGY COMB. SCI., 10, PP. 1-57 (1984)

Appendix J.4. Reaction Mechanism Tested As WZ

ELEMENTS

H O C AR

END

SPECIES

```

H          H2
CH         CH2      CH3      CH4
O          OH       H2O
C2H        C2H2     C2H3     C2H4     C2H5     C2H6
CO         HCO      CH2O
O2         HO2
C3H3       C3H4     AR
HCCO       CH2CO   CO2      CH3CHO
C4H        C4H2     C4H3     C2HCHCO
C6H2       C6H3     C4HCHCO
  
```

END

REACTIONS

```

H   + O2          - OH   + O          1.707918E1 -0.91 16490.
OH  + O           - H    + O2         1.325527E1  0.0   0.
O   + H2          - OH   + H          7.176091E0  2.0  7540.
OH  + H           - O    + H2         6.826075E0  2.0  5560.
OH  + H2          - H2O  + H          8.000000E0  1.6  3290.
H2O + H           - OH   + H2         8.662758E0  1.6 18540.
2OH          - H2O  + O          9.176091E0  1.14  0.
H2O + O          - 2OH          1.017609E1  1.14 17230.
2H          + M    - H2   + M          1.825527E1 -1.0   0.
H   AR/0.35/ CH4/6.5/ H2O/6.5/ CO2/1.5/ CO/0.75/ O2/0.4/
  + OH + M    - H2O  + M          2.234242E1 -2.   0.
H   AR/0.35/ CH4/6.5/ H2O/6.5/ CO2/1.5/ CO/0.75/ O2/0.4/
  + O2 + M    - HO2  + M          1.830103E1 -0.8   0.
H   AR/0.35/ CH4/6.5/ H2O/6.5/ CO2/1.5/ CO/0.75/ O2/0.4/
  + HO2          - 2OH          1.417609E1  0.0  1000.
H   + HO2          - H2   + O2         1.339794E1  0.0   690.
O   + HO2          - OH   + O2         1.330103E1  0.0   0.
OH  + HO2          - H2O  + O2         1.330103E1  0.0   0.
CO  + OH           - CO2  + H          6.643453E0  1.5  -740.
CO2 + H           - CO   + OH          1.420412E1  0.0 26250.
CH3 + H + M       - CH4  + M          2.929979E1 -5.417 26.
H   AR/0.35/ CH4/6.5/ H2O/6.5/ CO2/1.5/ CO/0.75/ O2/0.4/
CH4 + H           - CH3  + H2         4.342423E0  3.0  8740.
CH3 + H2          - CH4  + H          2.819544E0  3.0  7730.
CH4 + O           - CH3  + OH          7.079181E0  2.1  7610.
CH3 + OH          - CH4  + O          5.113943E0  2.1  4700.
CH4 + OH          - CH3  + H2O        6.204120E0  2.1  2460.
CH3 + H2O         - CH4  + OH          5.462398E0  2.1 16780.
CH3 + O           - CH2O  + H          1.384510E1  0.0   0.
CH2O + H          - HCO   + H2         1.339794E1  0.0  3990.
CH2O + O          - HCO   + OH          1.354407E1  0.0  3500.
CH2O + OH         - HCO   + H2O        1.347712E1  0.0  1200.
HCO + H           - CO    + H2         1.430103E1  0.0   0.
HCO + O           - CO    + OH          1.347712E1  0.0   0.
HCO + O           - CO2   + H          1.347712E1  0.0   0.
  
```

HCO + OH	- CO + H2O	1.369897E1	0.0	0.
HCO + O2	- CO + HO2	1.247712E1	0.0	0.
HCO + M	- H + CO + M	1.485126E1	0.0	16780.
AR/0.35/	CH4/6.5/ H2O/6.5/ CO2/1.5/	CO/0.75/	O2/0.4/	
CH2 + H	- CH + H2	1.360206E1	0.0	0.
CH2 + O	- CO + 2H	1.369897E1	0.0	0.
CH2 + O2	- CO2 + 2H	1.311394E1	0.0	1500.
CH2 + CH3	- C2H4 + H	1.360206E1	0.0	0.
CH + O	- CO + H	1.360206E1	0.0	0.
CH + O2	- CO + OH	1.330103E1	0.0	0.
2CH3 + M	- C2H6 + M	3.713672E1	-5.57	4860.
AR/0.35/	CH4/6.5/ H2O/6.5/ CO2/1.5/	CO/0.75/	O2/0.4/	
2CH3	- C2H5 + H	1.490309E1	0.0	26500.
2CH3	- C2H4 + H2	1.600000E1	0.0	32000.
C2H6 + H	- C2H5 + H2	2.732394E0	3.5	5200.
C2H6 + O	- C2H5 + OH	7.477121E0	2.0	5110.
C2H6 + OH	- C2H5 + H2O	6.799341E0	2.0	640.
C2H5 + H	- 2CH3	1.347712E1	0.0	0.
C2H5 + O	- CH3CHO + H	1.369897E1	0.0	0.
C2H5 + O2	- C2H4 + HO2	1.230103E1	0.0	5000.
C2H5	- C2H4 + H	3.432777E1	-7.147	44730.
C2H4 + H	- C2H5	3.398507E1	-7.133	6590.
C2H4 + O	- CH3 + HCO	9.204120E0	1.2	740.
C2H4 + OH	- C2H3 + H2O	1.384510E1	0.0	3000.
C2H4 + H	- C2H3 + H2	1.417609E1	0.0	10190.
C2H3 + H	- C2H2 + H2	1.330103E1	0.0	0.
C2H3 + O2	- C2H2 + HO2	1.200000E1	0.0	0.
C2H3	- C2H2 + H	2.798227E1	-4.84	41000.
C2H2 + H	- C2H3	2.641497E1	-4.81	5410.
C2H2 + O	- CH2 + CO	8.612784E0	1.5	1690.
C2H2 + OH	- CH2CO + H	3.966276E1	-8.75	13800.
CH3CHO + H	- CH3 + CO + H2	1.360206E1	0.0	4200.
CH3CHO + O	- CH3 + CO + OH	1.269897E1	0.0	1790.
CH3CHO + OH	- CH3 + CO + H2O	1.300000E1	0.0	0.
CH2CO + H	- CH3 + CO	1.284510E1	0.0	3000.
CH2CO + O	- 2HCO	1.330103E1	0.0	2290.
CH2CO + OH	- CH2O + HCO	1.300000E1	0.0	0.
CH2CO + M	- CH2 + CO + M	1.600000E1	0.0	59200.
AR/0.35/	CH4/6.5/ H2O/6.5/ CO2/1.5/	CO/0.75/	O2/0.4/	
C2H2 + O	- HCCO + H	1.463347E1	0.0	12100.
HCCO + H	- CH2 + CO	1.347712E1	0.0	0.
HCCO + O	- 2CO + H	1.207918E1	0.0	0.
C2H2 + H	- C2H + H2	1.417609E1	0.0	19000.
C2H2 + OH	- C2H + H2O	1.300000E1	0.0	7000.
C2H + O	- CO + CH	1.300000E1	0.0	0.
C2H + H2	- C2H2 + H	1.254407E1	0.0	2100.
C2H + O2	- CO + HCO	1.369897E1	0.0	1500.
CH2 + C2H2	- C3H3 + H	1.225527E1	0.0	0.
CH + C2H2	- C3H3	1.327875E1	0.0	0.
C3H3 + O	- CO + C2H3	1.357978E1	0.0	0.
C3H3 + H	- C3H4	1.343136E1	0.0	0.
C3H4 + H	- CH3 + C2H2	1.330103E1	0.0	2390.
C3H4 + OH	- HCO + C2H4	1.369897E1	0.0	1290.
C2H + C2H2	- C4H2 + H	1.354407E1	0.0	0.

C4H2 + H	- C2H + C2H2	1.472428E1	0.0	17470.
C4H2 + OH	- C2HCHCO + H	1.347712E1	0.0	0.
C2HCHCO + OH	- C2H2 + 2CO + H	1.400000E1	0.0	0.
C4H2 + H	- C4H3	1.281291E1	0.0	1000.
2C2H2	- C4H3 + H	1.330103E1	0.0	53910.
C4H3	- C4H2 + H	1.330103E1	0.0	52910.
C4H3 + H	- 2C2H2	1.360206E1	0.0	0.
C4H2 + H	- C4H + H2	1.400000E1	0.0	19980.
C4H + H2	- C4H2 + H	1.300000E1	0.0	3000.
C2H + C4H2	- C6H2 + H	1.354407E1	0.0	0.
C6H2 + H	- C2H + C4H2	1.400000E1	0.0	17780.
C4H + C2H2	- C6H2 + H	1.354407E1	0.0	0.
C6H2 + H	- C4H + C2H2	1.400000E1	0.0	15680.
C6H2 + H	= C6H3	1.281291E1	0.0	1000.
C6H2 + OH	- C4HCHCO + H	1.347712E1	0.0	0.
C4HCHCO + OH	- C4H2 + 2CO + H	1.400000E1	0.0	0.

END

REACTIONS TAKEN FROM WARNATZ, COMB.SCI.&TECH.,34,177-200(1983);

ONLY EXPLICIT REVERSE RATE CONSTANTS INCLUDED.

PRODUCTS FOR C4H2+OH AND C6H2+OH TAKEN FROM CS&T DESCRIPTION.

PRESSURE-DEPENDENT RATE CONSTANTS (CS&T SUPERSCRIPIT A) WRITTEN AS

EXPLICITLY PRESSURE-DEPENDENT REACTIONS USING KO'S FROM WARNATZ (1984).

Appendix J.5. Reaction Mechanism Tested As WZ (Reversible)

ELEMENTS

H O C AR

END

SPECIES

H H2
 CH CH2 CH3 CH4
 O OH H2O
 C2H C2H2 C2H3 C2H4 C2H5 C2H6
 CO HCO CH2O
 O2 HO2
 C3H3 C3H4 AR
 HCCO CH2CO CO2 CH3CHO
 C4H C4H2 C4H3 C2HCHCO
 C6H2 C6H3 C4HCHCO

END

REACTIONS

H	+ O2		- OH	+ O	1.707918E1	-0.91	16490.
OH	+ O		- H	+ O2	1.325527E1	0.0	0.
O	+ H2		- OH	+ H	7.176091E0	2.0	7540.
OH	+ H		- O	+ H2	6.826075E0	2.0	5560.
OH	+ H2		- H2O	+ H	8.000000E0	1.6	3290.
H2O	+ H		- OH	+ H2	8.662758E0	1.6	18540.
2OH			- H2O	+ O	9.176091E0	1.14	0.
H2O	+ O		- 2OH		1.017609E1	1.14	17230.
2H		+ M	= H2	+ M	1.825527E1	-1.0	0.
	AR/0.35/	CH4/6.5/	H2O/6.5/	CO2/1.5/	CO/0.75/	O2/0.4/	
H	+ OH	+ M	= H2O	+ M	2.234242E1	-2.	0.
	AR/0.35/	CH4/6.5/	H2O/6.5/	CO2/1.5/	CO/0.75/	O2/0.4/	
H	+ O2	+ M	= HO2	+ M	1.830103E1	-0.8	0.
	AR/0.35/	CH4/6.5/	H2O/6.5/	CO2/1.5/	CO/0.75/	O2/0.4/	
H	+ HO2		= 2OH		1.417609E1	0.0	1000.
H	+ HO2		= H2	+ O2	1.339794E1	0.0	690.
O	+ HO2		= OH	+ O2	1.330103E1	0.0	0.
OH	+ HO2		= H2O	+ O2	1.330103E1	0.0	0.
CO	+ OH		- CO2	+ H	6.643453E0	1.5	-740.
CO2	+ H		- CO	+ OH	1.420412E1	0.0	26250.
CH3	+ H	+ M	= CH4	+ M	2.929979E1	-5.417	26.
	AR/0.35/	CH4/6.5/	H2O/6.5/	CO2/1.5/	CO/0.75/	O2/0.4/	
CH4	+ H		- CH3	+ H2	4.342423E0	3.0	8740.
CH3	+ H2		- CH4	+ H	2.819544E0	3.0	7730.
CH4	+ O		- CH3	+ OH	7.079181E0	2.1	7610.
CH3	+ OH		- CH4	+ O	5.113943E0	2.1	4700.
CH4	+ OH		- CH3	+ H2O	6.204120E0	2.1	2460.
CH3	+ H2O		- CH4	+ OH	5.462398E0	2.1	16780.
CH3	+ O		= CH2O	+ H	1.384510E1	0.0	0.
CH2O	+ H		= HCO	+ H2	1.339794E1	0.0	3990.
CH2O	+ O		= HCO	+ OH	1.354407E1	0.0	3500.
CH2O	+ OH		= HCO	+ H2O	1.347712E1	0.0	1200.
HCO	+ H		= CO	+ H2	1.430103E1	0.0	0.
HCO	+ O		= CO	+ OH	1.347712E1	0.0	0.
HCO	+ O		= CO2	+ H	1.347712E1	0.0	0.

HCO + OH	- CO + H2O	1.369897E1	0.0	0.
HCO + O2	- CO + HO2	1.247712E1	0.0	0.
HCO + M	- H + CO + M	1.485126E1	0.0	16780.
AR/0.35/	CH4/6.5/ H2O/6.5/ CO2/1.5/	CO/0.75/	O2/0.4/	
CH2 + H	- CH + H2	1.360206E1	0.0	0.
CH2 + O	- CO + 2H	1.369897E1	0.0	0.
CH2 + O2	- CO2 + 2H	1.311394E1	0.0	1500.
CH2 + CH3	- C2H4 + H	1.360206E1	0.0	0.
CH + O	- CO + H	1.360206E1	0.0	0.
CH + O2	- CO + OH	1.330103E1	0.0	0.
2CH3 + M	- C2H6 + M	3.713672E1	-5.57	4860.
AR/0.35/	CH4/6.5/ H2O/6.5/ CO2/1.5/	CO/0.75/	O2/0.4/	
2CH3	- C2H5 + H	1.490309E1	0.0	26500.
2CH3	- C2H4 + H2	1.600000E1	0.0	32000.
C2H6 + H	- C2H5 + H2	2.732394E0	3.5	5200.
C2H6 + O	- C2H5 + OH	7.477121E0	2.0	5110.
C2H6 + OH	- C2H5 + H2O	6.799341E0	2.0	640.
C2H5 + H	- 2CH3	1.347712E1	0.0	0.
C2H5 + O	- CH3CHO + H	1.369897E1	0.0	0.
C2H5 + O2	- C2H4 + HO2	1.230103E1	0.0	5000.
C2H5	- C2H4 + H	3.432777E1	-7.147	44730.
C2H4 + H	- C2H5	3.398507E1	-7.133	6590.
C2H4 + O	- CH3 + HCO	9.204120E0	1.2	740.
C2H4 + OH	- C2H3 + H2O	1.384510E1	0.0	3000.
C2H4 + H	- C2H3 + H2	1.417609E1	0.0	10190.
C2H3 + H	- C2H2 + H2	1.330103E1	0.0	0.
C2H3 + O2	- C2H2 + HO2	1.200000E1	0.0	0.
C2H3	- C2H2 + H	2.798227E1	-4.84	41000.
C2H2 + H	- C2H3	2.641497E1	-4.81	5410.
C2H2 + O	- CH2 + CO	8.612784E0	1.5	1690.
C2H2 + OH	- CH2CO + H	3.966276E1	-8.75	13800.
CH3CHO + H	- CH3 + CO + H2	1.360206E1	0.0	4200.
CH3CHO + O	- CH3 + CO + OH	1.269897E1	0.0	1790.
CH3CHO + OH	- CH3 + CO + H2O	1.300000E1	0.0	0.
CH2CO + H	- CH3 + CO	1.284510E1	0.0	3000.
CH2CO + O	- 2HCO	1.330103E1	0.0	2290.
CH2CO + OH	- CH2O + HCO	1.300000E1	0.0	0.
CH2CO + M	- CH2 + CO + M	1.600000E1	0.0	59200.
AR/0.35/	CH4/6.5/ H2O/6.5/ CO2/1.5/	CO/0.75/	O2/0.4/	
C2H2 + O	- HCCO + H	1.463347E1	0.0	12100.
HCCO + H	- CH2 + CO	1.347712E1	0.0	0.
HCCO + O	- 2CO + H	1.207918E1	0.0	0.
C2H2 + H	- C2H + H2	1.417609E1	0.0	19000.
C2H2 + OH	- C2H + H2O	1.300000E1	0.0	7000.
C2H + O	- CO + CH	1.300000E1	0.0	0.
C2H + H2	- C2H2 + H	1.254407E1	0.0	2100.
C2H + O2	- CO + HCO	1.369897E1	0.0	1500.
CH2 + C2H2	- C3H3 + H	1.225527E1	0.0	0.
CH + C2H2	- C3H3	1.327875E1	0.0	0.
C3H3 + O	- CO + C2H3	1.357978E1	0.0	0.
C3H3 + H	- C3H4	1.343136E1	0.0	0.
C3H4 + H	- CH3 + C2H2	1.330103E1	0.0	2390.
C3H4 + OH	- HCO + C2H4	1.369897E1	0.0	1290.
C2H + C2H2	- C4H2 + H	1.354407E1	0.0	0.

C4H2 + H	- C2H + C2H2	1.472428E1	0.0	17470.
C4H2 + OH	- C2HCHCO + H	1.347712E1	0.0	0.
C2HCHCO + OH	- C2H2 + 2CO + H	1.400000E1	0.0	0.
C4H2 + H	- C4H3	1.281291E1	0.0	1000.
2C2H2	- C4H3 + H	1.330103E1	0.0	53910.
C4H3	- C4H2 + H	1.330103E1	0.0	52910.
C4H3 + H	- 2C2H2	1.360206E1	0.0	0.
C4H2 + H	- C4H + H2	1.400000E1	0.0	19980.
C4H + H2	- C4H2 + H	1.300000E1	0.0	3000.
C2H + C4H2	- C6H2 + H	1.354407E1	0.0	0.
C6H2 + H	- C2H + C4H2	1.400000E1	0.0	17780.
C4H + C2H2	- C6H2 + H	1.354407E1	0.0	0.
C6H2 + H	- C4H + C2H2	1.400000E1	0.0	15680.
C6H2 + H	= C6H3	1.281291E1	0.0	1000.
C6H2 + OH	- C4HCHCO + H	1.347712E1	0.0	0.
C4HCHCO + OH	- C4H2 + 2CO + H	1.400000E1	0.0	0.

END

NUMBERED REACTIONS TAKEN FROM WARNATZ, *COMB.SCI.&TECH.*, 34,177-200(1983);
 EXPLICIT REVERSE RATE CONSTANTS NOT INCLUDED; REVERSE RATE CONSTANTS
 CALCULATED FROM EQUILIBRIA BY MICROSCOPIC REVERSIBILITY.
 PRODUCTS FOR C4H2+OH AND C6H2+OH TAKEN FROM CS&T DESCRIPTION.
 PRESSURE-DEPENDENT RATE CONSTANTS (CS&T SUPERScript A) WRITTEN AS
 EXPLICITLY PRESSURE-DEPENDENT REACTIONS USING KO'S FROM WARNATZ(1984).

Appendix J.6. Solution for MMSK

X	T	V	RHO	AR	H	H2	CO	HCO	CH	CH2	CH3	O
1	0.0000	6.196E+02	1.454E-05	4.739E-02	3.638E-03	4.362E-02	1.365E-01	6.829E-06	9.248E-14	3.002E-06	1.382E-03	1.177E-06
2	0.0047	6.302E+02	1.425E-05	4.737E-02	3.678E-03	4.423E-02	1.394E-01	7.004E-06	9.362E-14	3.057E-06	1.408E-03	1.193E-06
3	0.0094	6.424E+02	1.397E-05	4.734E-02	3.729E-03	4.483E-02	1.422E-01	7.399E-06	1.539E-13	3.362E-06	1.433E-03	1.302E-06
4	0.0141	6.550E+02	1.370E-05	4.732E-02	3.790E-03	4.543E-02	1.451E-01	7.956E-06	3.039E-13	3.906E-06	1.457E-03	1.494E-06
5	0.0188	6.676E+02	1.343E-05	4.730E-02	3.861E-03	4.603E-02	1.480E-01	8.651E-06	6.205E-12	4.711E-06	1.481E-03	1.766E-06
6	0.0281	6.946E+02	1.290E-05	4.724E-02	4.033E-03	4.726E-02	1.537E-01	1.042E-05	2.211E-12	7.213E-06	1.525E-03	2.565E-06
7	0.0375	7.240E+02	1.236E-05	4.719E-02	4.243E-03	4.853E-02	1.570E-01	1.270E-05	5.329E-11	1.142E-05	1.566E-03	3.813E-06
8	0.0563	7.944E+02	1.124E-05	4.706E-02	4.766E-03	5.131E-02	1.621E-01	1.876E-05	2.300E-10	2.715E-05	1.633E-03	8.141E-06
9	0.0750	8.735E+02	1.020E-05	4.693E-02	5.419E-03	5.420E-02	1.679E-01	2.573E-05	3.994E-10	5.965E-05	1.680E-03	1.600E-05
10	0.1225	1.070E+03	8.280E-06	4.661E-02	7.311E-03	6.089E-02	1.740E-01	4.167E-05	4.167E-09	2.494E-04	1.710E-03	5.486E-05
11	0.1700	1.255E+03	7.025E-06	4.631E-02	9.238E-03	6.678E-02	1.821E-01	6.089E-05	2.903E-08	6.234E-04	1.628E-03	1.196E-04
12	0.2350	1.436E+03	6.108E-06	4.602E-02	1.137E-02	7.284E-02	1.906E-01	1.595E-07	1.595E-07	1.230E-03	1.431E-03	2.073E-04
13	0.3000	1.560E+03	5.598E-06	4.579E-02	1.282E-02	7.761E-02	1.991E-01	4.859E-07	4.859E-07	1.713E-03	1.241E-03	2.667E-04
14	0.5000	1.781E+03	4.844E-06	4.525E-02	1.432E-02	8.953E-02	2.079E-01	2.847E-06	2.847E-06	2.203E-03	8.676E-04	2.805E-04
15	0.7500	1.891E+03	4.508E-06	4.479E-02	1.553E-02	1.010E-01	2.180E-01	7.96E-06	7.96E-06	1.971E-03	7.034E-04	1.709E-04
16	1.0000	1.898E+03	4.464E-06	4.458E-02	1.48E-02	1.086E-01	2.230E-01	8.781E-06	8.781E-06	1.524E-03	6.615E-04	8.152E-05
17	1.5000	1.846E+03	4.577E-06	4.449E-02	7.470E-03	1.168E-01	2.230E-01	7.145E-06	7.145E-06	8.727E-04	6.889E-04	2.174E-05
18	1.9375	1.784E+03	4.740E-06	4.453E-02	4.953E-03	1.203E-01	2.230E-01	4.832E-06	4.832E-06	5.169E-04	7.283E-04	2.212E-06
19	2.3750	1.728E+03	4.899E-06	4.459E-02	3.246E-03	1.223E-01	2.230E-01	2.981E-06	2.981E-06	3.016E-04	7.666E-04	2.592E-06
20	3.2500	1.621E+03	5.238E-06	4.471E-02	1.272E-03	1.234E-01	2.230E-01	9.047E-07	9.047E-07	9.154E-05	8.310E-04	4.477E-07
21	5.0000	1.414E+03	6.033E-06	4.493E-02	1.135E-04	1.208E-01	2.208E-01	7.209E-08	7.209E-08	4.328E-06	8.906E-04	2.072E-08
22	10.0000	1.414E+03	6.033E-06	4.493E-02	1.135E-04	1.208E-01	2.208E-01	7.209E-08	7.209E-08	4.328E-06	8.906E-04	2.072E-08
1	0.0000	1.396E-04	6.460E-10	3.108E-01	2.062E-03	1.365E-01	1.365E-01	6.829E-06	9.248E-14	3.002E-06	1.382E-03	1.177E-06
2	0.0047	1.415E-04	6.619E-10	3.076E-01	2.114E-03	1.394E-01	1.394E-01	7.004E-06	9.362E-14	3.057E-06	1.408E-03	1.193E-06
3	0.0094	1.455E-04	1.083E-09	3.045E-01	2.151E-03	1.422E-01	1.422E-01	7.399E-06	1.539E-13	3.362E-06	1.433E-03	1.302E-06
4	0.0141	1.515E-04	1.773E-09	3.013E-01	2.175E-03	1.451E-01	1.451E-01	7.956E-06	3.039E-13	3.906E-06	1.457E-03	1.494E-06
5	0.0188	1.593E-04	2.859E-09	2.981E-01	2.187E-03	1.480E-01	1.480E-01	8.651E-06	6.205E-12	4.711E-06	1.481E-03	1.766E-06
6	0.0281	1.801E-04	7.347E-09	2.918E-01	2.179E-03	1.537E-01	1.537E-01	1.042E-05	2.211E-12	7.213E-06	1.525E-03	2.565E-06
7	0.0375	2.078E-04	1.825E-08	2.854E-01	2.136E-03	1.595E-01	1.595E-01	1.270E-05	5.329E-11	1.142E-05	1.566E-03	3.813E-06
8	0.0563	2.837E-04	9.444E-08	2.726E-01	1.968E-03	1.709E-01	1.709E-01	1.876E-05	2.300E-10	2.715E-05	1.633E-03	8.141E-06
9	0.0750	3.865E-04	3.113E-07	2.600E-01	1.740E-03	1.821E-01	1.821E-01	2.573E-05	3.994E-10	5.965E-05	1.680E-03	1.600E-05
10	0.1225	7.455E-04	1.741E-06	2.289E-01	1.061E-03	2.096E-01	2.096E-01	4.167E-05	4.167E-09	2.494E-04	1.710E-03	5.486E-05
11	0.1700	1.180E-03	4.926E-06	2.000E-01	4.736E-04	2.352E-01	2.352E-01	6.089E-05	2.903E-08	6.234E-04	1.628E-03	1.196E-04
12	0.2350	1.704E-03	1.169E-05	1.652E-01	1.310E-04	2.670E-01	2.670E-01	5.431E-05	1.595E-07	1.230E-03	1.431E-03	2.073E-04
13	0.3000	2.059E-03	1.943E-05	1.370E-01	1.131E-04	2.940E-01	2.940E-01	8.623E-05	4.859E-07	1.713E-03	1.241E-03	2.667E-04
14	0.5000	2.352E-03	3.484E-05	8.683E-02	6.876E-06	3.486E-01	3.486E-01	2.847E-06	2.847E-06	2.203E-03	8.676E-04	2.805E-04
15	0.7500	2.053E-03	3.467E-05	6.430E-02	2.310E-06	3.803E-01	3.803E-01	7.96E-06	7.96E-06	1.971E-03	7.034E-04	1.709E-04
16	1.0000	1.516E-03	2.511E-05	5.658E-02	1.346E-06	3.956E-01	3.956E-01	1.876E-05	2.300E-10	2.715E-05	1.633E-03	8.141E-06
17	1.5000	7.795E-04	1.179E-05	5.275E-02	8.987E-07	4.062E-01	4.062E-01	4.167E-05	4.167E-09	2.494E-04	1.710E-03	5.486E-05
18	1.9375	4.257E-04	5.744E-06	5.104E-02	7.851E-07	4.121E-01	4.121E-01	6.089E-05	2.903E-08	6.234E-04	1.628E-03	1.196E-04
19	2.3750	3.499E-04	2.842E-06	4.982E-02	6.944E-07	4.121E-01	4.121E-01	3.169E-06	3.169E-06	5.089E-05	7.835E-09	1.723E-03
20	3.2500	6.769E-05	6.510E-07	4.847E-02	5.602E-07	4.136E-01	4.136E-01	1.504E-06	1.504E-06	4.542E-05	4.598E-09	9.839E-04
21	5.0000	3.002E-06	1.720E-08	4.831E-02	2.975E-07	4.154E-01	4.154E-01	5.540E-09	5.540E-09	3.610E-05	2.006E-09	4.876E-04
22	10.0000	3.002E-06	1.720E-08	4.831E-02	2.975E-07	4.154E-01	4.154E-01	5.540E-09	5.540E-09	3.610E-05	2.006E-09	4.876E-04

(Appendix J.6. Continued)

X	H02	H202	C3H2	C3H3	C3H4	HCCO	CH2CO	C2H2OH	CO2	C4H2
1	0.0000	6.141E-05	1.524E-08	1.067E-03	1.198E-02	7.293E-06	1.272E-03	7.278E-06	4.118E-02	4.115E-03
2	0.0047	6.267E-05	1.566E-08	1.103E-03	1.237E-02	7.416E-06	1.310E-03	7.487E-06	4.228E-02	4.281E-03
3	0.0094	6.381E-05	2.221E-08	1.146E-03	1.277E-02	7.846E-06	1.345E-03	6.565E-06	4.339E-02	4.451E-03
4	0.0141	6.493E-05	3.124E-08	1.196E-03	1.317E-02	8.565E-06	1.376E-03	5.210E-06	4.451E-02	4.625E-03
5	0.0188	6.608E-05	4.339E-08	1.254E-03	1.357E-02	9.570E-06	1.403E-03	3.877E-06	4.564E-02	4.802E-03
6	0.0281	6.854E-05	6.392E-08	1.393E-03	1.435E-02	1.245E-05	1.445E-03	1.904E-06	4.792E-02	5.167E-03
7	0.0375	7.115E-05	8.792E-08	1.560E-03	1.513E-02	1.668E-05	1.473E-03	1.904E-06	5.023E-02	5.544E-03
8	0.0563	7.425E-05	1.178E-07	1.974E-03	1.663E-02	2.983E-05	1.490E-03	8.934E-07	5.486E-02	6.329E-03
9	0.0750	7.898E-05	1.344E-06	2.479E-03	1.806E-02	5.112E-05	1.490E-03	4.742E-08	5.946E-02	7.142E-03
10	0.1225	8.800E-05	2.753E-06	4.321E-05	2.411E-02	1.436E-04	1.300E-03	4.109E-09	7.093E-02	9.264E-03
11	0.1700	4.502E-05	4.926E-07	5.735E-03	2.411E-02	2.831E-04	1.091E-03	9.054E-10	8.158E-02	1.112E-02
12	0.2350	2.296E-05	7.188E-07	7.750E-03	2.710E-02	4.617E-04	8.428E-04	3.043E-10	9.439E-02	1.287E-02
13	0.3000	1.370E-05	1.344E-07	9.305E-03	2.910E-02	5.635E-04	6.622E-04	1.567E-10	1.047E-01	1.373E-02
14	0.5000	3.960E-06	2.382E-03	1.279E-02	2.858E-02	5.207E-04	3.842E-04	4.760E-11	1.227E-01	1.264E-02
15	0.7500	1.117E-06	7.182E-03	1.145E-02	2.028E-02	3.141E-04	2.542E-04	2.203E-11	1.310E-01	1.025E-02
16	1.0000	3.672E-07	1.145E-02	1.915E-02	1.559E-02	1.691E-04	1.953E-04	1.409E-11	1.345E-01	8.951E-03
17	1.5000	9.479E-08	1.522E-02	1.658E-02	1.459E-02	7.028E-05	1.529E-04	8.134E-12	1.371E-01	8.415E-03
18	1.9375	3.797E-08	5.213E-10	1.554E-02	1.638E-02	3.801E-05	1.326E-04	5.477E-12	1.386E-01	8.504E-03
19	2.3750	1.923E-08	2.568E-10	1.555E-02	1.846E-02	2.384E-05	1.204E-04	3.746E-12	1.398E-01	8.710E-03
20	3.2500	9.805E-09	6.632E-11	1.535E-02	2.211E-02	1.238E-05	1.093E-04	1.804E-12	1.412E-01	9.090E-03
21	5.0000	8.535E-09	2.038E-11	1.531E-02	2.461E-02	3.064E-06	1.144E-04	3.211E-13	1.423E-01	9.275E-03
22	10.0000	8.535E-09	2.038E-11	1.531E-02	2.461E-02	3.064E-06	1.144E-04	3.211E-13	1.423E-01	9.275E-03
X	C4H3	C4H2OH								
1	0.0000	5.015E-13	8.527E-06	1.524E-08	1.198E-02	7.293E-06	1.272E-03	7.278E-06	4.118E-02	4.115E-03
2	0.0047	5.218E-13	8.792E-06	1.566E-08	1.237E-02	7.416E-06	1.310E-03	7.487E-06	4.228E-02	4.281E-03
3	0.0094	6.882E-13	9.117E-06	2.221E-08	1.277E-02	7.846E-06	1.345E-03	6.565E-06	4.339E-02	4.451E-03
4	0.0141	9.288E-13	9.504E-06	3.124E-08	1.317E-02	8.565E-06	1.376E-03	5.210E-06	4.451E-02	4.625E-03
5	0.0188	1.250E-12	9.951E-06	4.339E-08	1.357E-02	9.570E-06	1.403E-03	3.877E-06	4.564E-02	4.802E-03
6	0.0281	2.255E-12	1.101E-05	6.392E-08	1.435E-02	1.245E-05	1.445E-03	1.904E-06	4.792E-02	5.167E-03
7	0.0375	4.133E-12	1.227E-05	8.792E-08	1.513E-02	1.668E-05	1.473E-03	1.904E-06	5.023E-02	5.544E-03
8	0.0563	1.396E-11	1.525E-05	1.178E-07	1.663E-02	2.983E-05	1.490E-03	4.742E-08	5.486E-02	6.329E-03
9	0.0750	4.461E-11	1.861E-05	1.344E-06	1.806E-02	5.112E-05	1.490E-03	4.742E-08	5.946E-02	7.142E-03
10	0.1225	3.888E-10	2.787E-05	4.321E-05	2.411E-02	1.436E-04	1.300E-03	4.109E-09	7.093E-02	9.264E-03
11	0.1700	2.217E-09	3.583E-05	5.735E-03	2.411E-02	2.831E-04	1.091E-03	9.054E-10	8.158E-02	1.112E-02
12	0.2350	1.024E-08	4.308E-05	7.188E-07	2.710E-02	4.617E-04	8.428E-04	3.043E-10	9.439E-02	1.287E-02
13	0.3000	2.385E-08	4.609E-05	1.344E-07	2.910E-02	5.207E-04	6.622E-04	1.567E-10	1.047E-01	1.373E-02
14	0.5000	6.804E-08	3.913E-05	2.382E-03	1.279E-02	5.635E-04	3.842E-04	4.760E-11	1.227E-01	1.264E-02
15	0.7500	9.363E-08	2.799E-05	7.182E-03	1.145E-02	3.141E-04	2.542E-04	2.203E-11	1.310E-01	1.025E-02
16	1.0000	9.039E-08	2.121E-05	1.145E-02	1.915E-02	1.691E-04	1.953E-04	1.409E-11	1.345E-01	8.951E-03
17	1.5000	8.004E-08	1.609E-05	1.522E-02	1.559E-02	7.028E-05	1.529E-04	8.134E-12	1.371E-01	8.415E-03
18	1.9375	6.768E-08	1.381E-05	1.554E-02	1.638E-02	3.801E-05	1.326E-04	5.477E-12	1.386E-01	8.504E-03
19	2.3750	6.048E-08	1.233E-05	1.555E-02	1.846E-02	2.384E-05	1.204E-04	3.746E-12	1.398E-01	8.710E-03
20	3.2500	5.077E-08	1.002E-05	1.535E-02	2.211E-02	1.238E-05	1.093E-04	1.804E-12	1.412E-01	9.090E-03
21	5.0000	4.640E-08	6.136E-06	1.531E-02	2.461E-02	3.064E-06	1.144E-04	3.211E-13	1.423E-01	9.275E-03
22	10.0000	4.640E-08	6.136E-06	1.531E-02	2.461E-02	3.064E-06	1.144E-04	3.211E-13	1.423E-01	9.275E-03

Appendix J.7. Solution for WB

X	T	V	RHO	AR	H	H2	CH	CH2	CH3	CH4
1	0.0000	1.205E+02	1.443E-05	4.614E-02	2.864E-04	3.694E-02	1.527E-11	1.586E-06	2.292E-05	3.401E-04
2	0.0094	1.255E+02	1.385E-05	4.605E-02	2.928E-04	3.798E-02	1.565E-11	1.645E-06	2.379E-05	3.530E-04
3	0.0187	1.307E+02	1.330E-05	4.596E-02	3.048E-04	3.904E-02	2.428E-11	1.657E-06	2.840E-05	3.621E-04
4	0.0281	1.363E+02	1.276E-05	4.587E-02	3.214E-04	4.013E-02	4.391E-11	1.689E-06	3.533E-05	3.689E-04
5	0.0375	1.423E+02	1.222E-05	4.578E-02	3.417E-04	4.128E-02	8.443E-11	1.750E-06	4.377E-05	3.740E-04
6	0.0563	1.568E+02	1.109E-05	4.559E-02	3.922E-04	4.382E-02	2.918E-10	1.962E-06	6.342E-05	3.811E-04
7	0.0750	1.732E+02	1.004E-05	4.540E-02	4.519E-04	4.651E-02	9.897E-10	2.372E-06	8.412E-05	3.863E-04
8	0.1225	2.143E+03	8.116E-06	4.495E-02	6.278E-04	5.295E-02	9.014E-09	4.799E-06	1.370E-04	3.962E-04
9	0.1700	2.536E+02	6.856E-06	4.456E-02	8.346E-04	5.880E-02	4.910E-08	1.026E-05	1.884E-04	4.041E-04
10	0.2350	2.934E+02	5.926E-06	4.412E-02	1.144E-03	6.498E-02	2.377E-07	2.250E-05	2.572E-04	4.132E-04
11	0.2675	3.082E+02	5.642E-06	4.394E-02	1.302E-03	6.747E-02	4.410E-07	3.013E-05	2.910E-04	4.174E-04
12	0.3000	3.219E+02	5.403E-06	4.377E-02	1.464E-03	6.978E-02	7.533E-07	3.886E-05	3.244E-04	4.214E-04
13	0.3500	3.402E+02	5.111E-06	4.352E-02	1.712E-03	7.300E-02	1.504E-06	5.404E-05	3.739E-04	4.276E-04
14	0.4000	3.555E+02	4.892E-06	4.331E-02	1.949E-03	7.581E-02	2.634E-06	7.039E-05	4.182E-04	4.344E-04
15	0.5000	3.763E+02	4.622E-06	4.294E-02	2.372E-03	8.029E-02	6.003E-06	1.033E-04	4.873E-04	4.516E-04
16	0.7500	4.071E+02	4.272E-06	4.231E-02	3.136E-03	8.836E-02	1.855E-05	1.765E-04	5.814E-04	5.194E-04
17	1.0000	4.122E+02	4.219E-06	4.202E-02	3.354E-03	9.338E-02	2.581E-05	2.102E-04	6.178E-04	6.230E-04
18	1.5000	4.025E+02	4.320E-06	4.185E-02	2.996E-03	9.998E-02	2.229E-05	2.103E-04	6.126E-04	6.438E-04
19	2.3750	3.767E+02	4.616E-06	4.185E-02	2.070E-03	1.062E-01	1.365E-05	2.345E-04	4.956E-04	1.103E-03
20	3.2500	3.530E+02	4.926E-06	4.188E-02	1.320E-03	1.091E-01	1.432E-05	5.850E-04	3.365E-04	1.230E-03
21	4.1250	3.303E+02	5.264E-06	4.193E-02	7.780E-04	1.100E-01	1.602E-05	1.057E-03	2.004E-04	1.275E-03
22	5.0000	3.070E+02	5.665E-06	4.201E-02	4.421E-04	1.092E-01	1.672E-05	1.357E-03	1.129E-04	1.286E-03
23	10.0000	3.070E+02	5.665E-06	4.201E-02	4.421E-04	1.092E-01	1.672E-05	1.357E-03	1.129E-04	1.286E-03

X	O	OH	H2O	C2H	C2H2	C2H3	C2H4	C2H5	C2H6	CO
1	0.0000	3.537E-05	7.121E-02	1.902E-05	3.565E-01	5.872E-04	2.887E-04	1.728E-09	1.202E-05	1.212E-01
2	0.0094	3.633E-05	7.364E-02	1.997E-05	3.524E-01	6.170E-04	3.036E-04	1.824E-09	1.269E-05	1.262E-01
3	0.0187	3.873E-05	7.607E-02	2.297E-05	3.484E-01	6.236E-04	3.182E-04	2.538E-09	1.338E-05	1.313E-01
4	0.0281	4.247E-05	7.849E-02	2.674E-05	3.443E-01	6.149E-04	3.324E-04	4.066E-09	1.406E-05	1.365E-01
5	0.0375	4.758E-05	8.089E-02	3.133E-05	3.401E-01	5.961E-04	3.460E-04	7.015E-09	1.474E-05	1.417E-01
6	0.0563	5.560E-05	8.560E-02	4.339E-05	3.318E-01	5.398E-04	3.712E-04	2.023E-08	1.606E-05	1.520E-01
7	0.0750	6.294E-05	9.017E-02	5.959E-05	3.235E-01	4.770E-04	3.926E-04	5.382E-08	1.726E-05	1.622E-01
8	0.1225	7.100E-05	1.012E-01	1.221E-04	3.027E-01	3.258E-04	4.286E-04	2.852E-07	1.958E-05	1.878E-01
9	0.1700	8.075E-05	1.117E-01	2.252E-04	2.823E-01	2.149E-04	4.361E-04	7.720E-07	2.041E-05	2.130E-01
10	0.2350	9.225E-05	1.253E-01	4.438E-04	2.555E-01	1.219E-04	4.090E-04	1.484E-06	1.901E-05	2.473E-01
11	0.2675	1.049E-04	1.318E-01	5.846E-04	2.428E-01	9.247E-05	3.867E-04	1.647E-06	1.716E-05	2.641E-01
12	0.3000	1.171E-04	1.380E-01	7.468E-04	2.305E-01	7.134E-05	3.607E-04	1.650E-06	1.459E-05	2.804E-01
13	0.3500	1.319E-04	1.469E-01	1.030E-03	2.127E-01	5.037E-05	3.170E-04	1.381E-06	9.818E-06	3.047E-01
14	0.4000	1.598E-04	1.551E-01	1.337E-03	1.964E-01	3.739E-05	2.739E-04	9.626E-07	5.686E-06	3.273E-01
15	0.5000	1.253E-03	1.690E-01	1.946E-01	1.688E-01	2.397E-05	1.970E-04	4.163E-07	2.113E-06	3.671E-01
16	0.7500	6.628E-05	1.896E-01	3.018E-03	1.263E-01	1.029E-05	8.427E-05	1.335E-07	6.825E-07	4.318E-01
17	1.0000	8.335E-05	1.976E-01	3.269E-03	1.068E-01	4.904E-06	3.853E-05	1.351E-07	7.004E-07	4.627E-01
18	1.5000	9.953E-06	1.974E-01	2.717E-03	9.649E-02	2.634E-06	2.097E-05	6.708E-07	4.168E-06	4.809E-01
19	2.3750	1.243E-06	1.913E-01	1.641E-03	9.491E-02	3.549E-06	3.916E-05	2.441E-07	1.313E-06	4.786E-01
20	3.2500	1.544E-07	1.871E-01	9.312E-04	9.568E-02	5.175E-06	8.556E-05	1.193E-06	9.097E-06	4.809E-01
21	4.1250	2.767E-08	1.848E-01	4.930E-04	9.675E-02	6.000E-06	1.552E-04	1.522E-06	1.485E-05	4.797E-01
22	5.0000	5.770E-09	1.836E-01	2.526E-04	9.784E-02	5.680E-06	2.319E-04	1.628E-06	1.995E-05	4.800E-01
23	10.0000	5.770E-09	1.836E-01	2.526E-04	9.784E-02	5.680E-06	2.319E-04	1.628E-06	1.995E-05	4.800E-01

(Appendix J.7. Continued)

X	HCO	CH2O	CH3O	CH2OH	CH3OH	O2	HO2	H2O2	HCCO	CH2CO
1	0.0000	7.023E-05	6.009E-04	2.040E-07	4.442E-06	3.537E-01	4.736E-05	6.578E-06	2.073E-04	5.668E-04
2	0.0094	7.384E-05	6.319E-04	2.147E-07	4.677E-06	3.485E-01	4.932E-05	6.853E-06	2.144E-04	6.010E-04
3	0.0187	7.877E-05	6.625E-04	2.263E-07	4.874E-06	3.433E-01	5.195E-05	7.114E-06	2.232E-04	6.337E-04
4	0.0281	8.504E-05	6.944E-04	2.388E-07	5.041E-06	3.379E-01	5.523E-05	7.361E-06	2.339E-04	6.650E-04
5	0.0375	9.275E-05	7.216E-04	2.523E-07	5.180E-06	3.326E-01	5.915E-05	7.594E-06	2.463E-04	6.953E-04
6	0.0563	1.127E-04	7.770E-04	2.820E-07	5.383E-06	3.218E-01	6.874E-05	8.005E-06	2.759E-04	7.521E-04
7	0.0750	1.393E-04	8.281E-04	3.155E-07	5.514E-06	3.111E-01	8.028E-05	8.339E-06	3.117E-04	8.043E-04
8	0.1225	2.349E-04	9.382E-04	4.173E-07	5.645E-06	2.846E-01	1.149E-04	8.816E-06	4.285E-04	9.179E-04
9	0.1700	3.563E-04	1.018E-03	5.401E-07	5.655E-06	2.589E-01	1.453E-04	8.596E-06	5.802E-04	1.001E-03
10	0.2350	5.104E-04	1.078E-03	7.337E-07	5.597E-06	2.251E-01	1.630E-04	7.099E-06	8.194E-04	1.062E-03
11	0.2675	5.692E-04	1.086E-03	8.352E-07	5.575E-06	2.251E-01	1.630E-04	7.099E-06	8.194E-04	1.062E-03
12	0.3000	6.155E-04	1.080E-03	9.384E-07	5.511E-06	2.090E-01	1.614E-04	6.048E-06	9.334E-04	1.071E-03
13	0.3500	6.622E-04	1.047E-03	1.097E-06	5.430E-06	1.934E-01	1.546E-04	4.910E-06	1.039E-03	1.067E-03
14	0.4000	6.809E-04	9.909E-04	1.248E-06	5.342E-06	1.706E-01	1.373E-04	3.232E-06	1.177E-03	1.039E-03
15	0.5000	6.523E-04	8.398E-04	1.524E-06	5.152E-06	1.495E-01	1.167E-04	1.939E-06	1.273E-03	9.951E-04
16	0.7500	4.164E-04	4.542E-04	1.969E-06	4.591E-06	1.128E-01	7.632E-05	6.062E-07	1.326E-03	8.783E-04
17	1.0000	2.099E-04	2.369E-04	1.969E-06	4.129E-06	5.263E-02	2.013E-05	6.824E-08	9.667E-04	5.907E-04
18	1.5000	5.831E-05	9.260E-05	2.144E-06	3.544E-06	2.334E-02	4.471E-06	1.221E-08	5.233E-04	4.023E-04
19	2.3750	1.273E-05	3.155E-05	2.033E-07	3.544E-06	6.075E-03	3.862E-07	1.400E-09	1.631E-04	2.410E-04
20	3.2500	3.791E-06	2.178E-09	1.575E-06	2.859E-06	9.011E-05	2.153E-08	2.070E-10	4.832E-05	1.537E-04
21	4.1250	9.090E-07	1.045E-10	7.166E-07	1.728E-06	4.435E-06	5.147E-11	3.052E-11	2.597E-05	1.139E-04
22	5.0000	3.322E-07	1.011E-05	4.805E-07	1.371E-06	9.849E-08	1.540E-12	1.650E-11	1.298E-05	6.811E-05
23	10.0000	3.322E-07	1.011E-05	4.805E-07	1.371E-06	9.849E-08	1.540E-12	1.650E-11	1.298E-05	6.811E-05

X	CO2	C4H	C4H2	C4H3	C4H6
1	0.0000	8.168E-03	3.037E-03	6.230E-07	4.174E-07
2	0.0094	8.602E-03	3.283E-03	6.736E-07	4.517E-07
3	0.0187	9.043E-03	3.536E-03	7.353E-07	4.858E-07
4	0.0281	9.491E-03	3.798E-03	8.085E-07	5.193E-07
5	0.0375	9.944E-03	4.068E-03	8.937E-07	5.517E-07
6	0.0563	1.086E-02	4.627E-03	1.100E-06	6.118E-07
7	0.0750	1.178E-02	5.207E-03	1.358E-06	6.632E-07
8	0.1225	1.413E-02	6.764E-03	2.254E-06	7.504E-07
9	0.1700	1.651E-02	8.393E-03	3.606E-06	7.793E-07
10	0.2350	1.989E-02	1.058E-02	6.352E-06	7.550E-07
11	0.2675	2.160E-02	1.154E-02	8.023E-06	7.299E-07
12	0.3000	2.334E-02	1.237E-02	9.841E-06	6.991E-07
13	0.3500	2.601E-02	1.337E-02	1.274E-05	6.453E-07
14	0.4000	2.866E-02	1.402E-02	1.538E-05	5.898E-07
15	0.5000	3.377E-02	1.437E-02	1.900E-05	4.828E-07
16	0.7500	4.466E-02	1.255E-02	1.958E-05	2.772E-07
17	1.0000	5.236E-02	1.075E-02	1.536E-05	1.553E-07
18	1.5000	6.132E-02	8.025E-04	1.009E-05	5.889E-08
19	2.3750	6.911E-02	7.874E-03	6.112E-06	1.993E-08
20	3.2500	7.325E-02	7.138E-04	4.104E-06	1.948E-08
21	4.1250	7.548E-02	6.559E-03	2.807E-06	4.287E-08
22	5.0000	7.679E-02	6.037E-03	1.745E-06	8.247E-08
23	10.0000	7.679E-02	6.037E-03	1.745E-06	8.247E-08

Appendix J.8. Solution for WD

X	T	V	RIIO	AR	H	H2	CH	CH2	CH3	CH4
1	0.0000	1.208E+02	1.439E-05	4.616E-02	5.295E-04	4.055E-02	-4.274E-13	1.667E-07	5.387E-05	4.644E-03
2	0.0006	1.195E+02	1.435E-05	4.615E-02	5.303E-04	4.062E-02	-4.281E-13	1.671E-07	5.400E-05	4.655E-03
3	0.0012	1.215E+02	1.432E-05	4.615E-02	5.311E-04	4.069E-02	-4.284E-13	1.676E-07	5.430E-05	4.666E-03
4	0.0018	1.218E+02	1.428E-05	4.614E-02	5.319E-04	4.076E-02	-4.284E-13	1.683E-07	5.476E-05	4.677E-03
5	0.0023	1.221E+02	1.424E-05	4.614E-02	5.327E-04	4.083E-02	-4.281E-13	1.691E-07	5.537E-05	4.687E-03
6	0.0035	1.227E+02	1.417E-05	4.612E-02	5.346E-04	4.098E-02	-4.265E-13	1.710E-07	5.705E-05	4.708E-03
7	0.0047	1.230E+02	1.410E-05	4.611E-02	5.365E-04	4.112E-02	-4.236E-13	1.733E-07	5.931E-05	4.728E-03
8	0.0070	1.246E+02	1.396E-05	4.609E-02	5.408E-04	4.140E-02	-4.143E-13	1.788E-07	6.546E-05	4.766E-03
9	0.0094	1.258E+02	1.382E-05	4.607E-02	5.455E-04	4.169E-02	-4.002E-13	1.854E-07	7.365E-05	4.802E-03
10	0.0141	1.284E+02	1.354E-05	4.603E-02	5.566E-04	4.227E-02	-3.590E-13	2.014E-07	9.588E-05	4.865E-03
11	0.0188	1.310E+02	1.327E-05	4.598E-02	5.694E-04	4.285E-02	-3.029E-13	2.210E-07	1.254E-04	4.927E-03
12	0.0281	1.366E+02	1.273E-05	4.590E-02	6.007E-04	4.404E-02	-1.544E-13	2.728E-07	2.055E-04	5.022E-03
13	0.0375	1.427E+02	1.219E-05	4.581E-02	6.389E-04	4.530E-02	-1.809E-14	3.478E-07	3.100E-04	5.090E-03
14	0.0563	1.572E+02	1.106E-05	4.562E-02	7.346E-04	4.809E-02	4.168E-12	5.948E-07	5.747E-04	5.090E-03
15	0.0750	1.736E+02	1.002E-05	4.543E-02	8.449E-04	5.104E-02	2.955E-12	1.052E-06	8.713E-04	5.159E-03
16	0.1225	1.070E+03	8.093E-06	4.499E-02	1.149E-03	5.811E-02	5.648E-11	3.549E-06	1.666E-03	5.158E-03
17	0.1700	1.255E+03	6.837E-06	4.461E-02	1.478E-03	6.454E-02	5.416E-10	8.561E-06	2.506E-03	5.128E-03
18	0.2350	1.436E+03	5.392E-06	4.389E-02	2.488E-03	7.689E-02	1.171E-08	1.811E-05	3.728E-03	5.120E-03
19	0.3000	1.560E+03	3.235E+02	4.367E-02	2.938E-03	8.064E-02	2.369E-08	2.974E-05	5.130E-03	5.164E-03
20	0.3500	1.638E+03	3.407E+02	4.348E-02	3.390E-03	8.402E-02	4.083E-08	5.011E-05	6.217E-03	5.203E-03
21	0.4000	1.701E+03	3.558E+02	4.333E-02	3.797E-03	8.688E-02	6.129E-08	6.127E-05	7.168E-03	5.210E-03
22	0.4500	1.741E+03	3.658E+02	4.319E-02	4.160E-03	8.971E-02	8.600E-08	7.146E-05	8.02E-03	5.160E-03
23	0.5000	1.824E+03	3.865E+02	4.304E-02	4.528E-03	9.303E-02	1.203E-07	8.319E-05	8.802E-03	5.075E-03
24	0.5625	1.874E+03	4.299E+02	4.279E-02	4.962E-03	9.870E-02	1.809E-07	1.003E-04	9.602E-03	4.975E-03
25	0.6250	1.858E+03	3.952E+02	4.269E-02	5.055E-03	1.011E-01	2.018E-07	1.056E-04	1.029E-03	4.337E-03
26	0.6875	1.878E+03	4.007E+02	4.262E-02	5.055E-03	1.175E-01	1.475E-07	1.074E-04	1.324E-03	4.354E-03
27	0.7500	1.891E+03	4.045E+02	4.242E-02	4.854E-03	1.085E-01	2.209E-07	1.056E-04	1.629E-03	4.337E-03
28	1.0000	1.898E+03	4.088E+02	4.242E-02	4.854E-03	1.085E-01	2.209E-07	1.056E-04	1.629E-03	4.337E-03
29	1.5000	1.846E+03	3.998E+02	4.220E-02	3.626E-03	1.175E-01	1.475E-07	7.914E-05	3.324E-03	4.354E-03
30	2.3750	1.728E+03	3.747E+02	4.214E-02	1.936E-03	1.240E-01	1.561E-08	3.653E-05	2.214E-03	5.691E-03
31	3.2500	1.621E+03	4.952E+02	4.218E-02	9.757E-04	1.263E-01	1.098E-08	1.525E-05	1.346E-03	6.889E-03
32	5.0000	1.414E+03	3.051E+02	4.236E-02	2.052E-04	1.246E-01	3.750E-10	1.940E-06	3.207E-04	7.708E-03
33	10.0000	1.414E+03	3.051E+02	4.236E-02	2.052E-04	1.246E-01	3.750E-10	1.940E-06	3.207E-04	7.708E-03

X	O	OH	H2O	C2H	C2H2	C2H3	C2H4	C2H5	C2H6	CO
1	0.0000	3.803E-07	6.729E-02	4.561E-11	3.466E-01	1.746E-07	6.655E-04	4.471E-05	1.693E-03	1.272E-01
2	0.0006	3.809E-07	6.744E-02	4.575E-11	3.463E-01	1.752E-07	6.676E-04	4.486E-05	1.699E-03	1.275E-01
3	0.0012	3.818E-07	6.758E-02	4.749E-11	3.460E-01	1.758E-07	6.698E-04	4.502E-05	1.705E-03	1.278E-01
4	0.0018	3.828E-07	6.772E-02	4.941E-11	3.457E-01	1.764E-07	6.719E-04	4.518E-05	1.711E-03	1.282E-01
5	0.0023	3.840E-07	6.787E-02	5.142E-11	3.454E-01	1.769E-07	6.741E-04	4.535E-05	1.717E-03	1.285E-01
6	0.0035	3.870E-07	6.816E-02	5.571E-11	3.449E-01	1.772E-07	6.783E-04	4.568E-05	1.729E-03	1.292E-01
7	0.0047	3.907E-07	6.844E-02	6.038E-11	3.443E-01	1.766E-07	6.826E-04	4.602E-05	1.741E-03	1.298E-01
8	0.0070	4.003E-07	6.902E-02	7.099E-11	3.432E-01	1.725E-07	6.912E-04	4.674E-05	1.765E-03	1.312E-01
9	0.0094	4.125E-07	6.959E-02	8.355E-11	3.421E-01	1.658E-07	6.997E-04	4.749E-05	1.789E-03	1.325E-01
10	0.0141	4.450E-07	7.074E-02	1.170E-10	3.398E-01	1.486E-07	7.167E-04	4.910E-05	1.838E-03	1.352E-01
11	0.0188	4.894E-07	7.189E-02	1.643E-10	3.375E-01	1.320E-07	7.336E-04	5.086E-05	1.888E-03	1.379E-01
12	0.0281	6.112E-07	7.417E-02	3.328E-10	3.329E-01	1.090E-07	7.674E-04	5.477E-05	1.988E-03	1.433E-01
13	0.0375	7.986E-07	7.644E-02	6.963E-10	3.282E-01	9.897E-08	8.008E-04	5.917E-05	2.090E-03	1.487E-01
14	0.0563	1.441E-06	3.683E-05	3.268E-09	3.189E-01	1.092E-07	8.660E-04	6.920E-05	2.294E-03	1.594E-01
15	0.0750	2.630E-06	6.270E-05	1.367E-08	3.095E-01	1.619E-07	9.286E-04	8.015E-05	2.489E-03	1.700E-01
16	0.1225	8.655E-06	1.536E-04	1.788E-07	2.862E-01	6.804E-07	1.077E-03	1.069E-04	2.912E-03	1.963E-01

(Appendix J.B. Continued)

17	0.1700	1.922E-05	3.034E-04	9.871E-07	2.637E-01	2.610E-06	1.216E-03	1.188E-04	3.125E-03	2.214E-01
18	0.2350	3.603E-05	5.447E-04	3.516E-06	2.347E-01	9.044E-06	1.410E-03	1.131E-04	3.014E-03	2.544E-01
19	0.3000	5.296E-05	7.706E-04	7.136E-06	2.079E-01	2.804E-05	1.623E-03	8.927E-05	2.342E-03	2.853E-01
20	0.3500	6.585E-05	9.261E-04	1.050E-05	1.892E-01	6.534E-05	1.797E-03	6.337E-05	1.568E-03	3.071E-01
21	0.4000	7.738E-05	1.053E-03	1.385E-05	1.723E-01	1.257E-04	1.965E-03	3.989E-05	8.833E-04	3.272E-01
22	0.4500	8.580E-05	1.139E-03	1.617E-05	1.573E-01	1.824E-04	2.105E-03	2.533E-05	4.965E-04	3.455E-01
23	0.5000	9.225E-05	1.199E-03	1.841E-05	1.440E-01	2.378E-04	2.209E-03	1.646E-05	2.730E-04	3.619E-01
24	0.5625	9.663E-05	1.236E-03	2.055E-05	1.298E-01	2.810E-04	2.277E-03	1.055E-05	1.371E-04	3.798E-01
25	0.6250	9.678E-05	1.233E-03	1.685E-05	1.179E-01	2.948E-04	2.279E-03	7.576E-06	7.728E-05	3.951E-01
26	0.6875	9.303E-05	1.195E-03	2.168E-05	1.081E-01	2.902E-04	2.232E-03	5.998E-06	5.214E-05	4.081E-01
27	0.7500	8.694E-05	1.136E-03	2.097E-05	1.000E-01	2.794E-04	2.159E-03	4.994E-06	3.886E-05	4.192E-01
28	1.0000	5.591E-05	8.344E-04	1.571E-05	8.106E-02	2.134E-04	1.773E-03	3.202E-06	2.296E-05	4.466E-01
29	1.5000	1.941E-05	4.161E-04	7.539E-06	6.792E-02	1.198E-04	1.353E-03	2.317E-06	2.402E-05	4.670E-01
30	2.3750	4.016E-06	1.400E-04	2.139E-06	6.174E-02	5.329E-05	1.124E-03	2.501E-06	5.452E-05	4.761E-01
31	3.2500	9.932E-07	4.921E-05	5.936E-02	5.936E-02	2.404E-05	1.026E-03	3.098E-06	1.071E-04	4.792E-01
32	5.0000	1.014E-07	5.259E-06	1.753E-01	5.820E-02	3.922E-06	1.006E-03	3.750E-06	2.406E-04	4.819E-01
33	10.0000	1.014E-07	5.259E-06	1.753E-01	5.820E-02	3.922E-06	1.006E-03	3.750E-06	2.406E-04	4.819E-01
X										
HCO										
1	0.0000	7.415E-06	7.883E-04	1.163E-06	1.790E-06	2.102E-05	3.490E-01	2.304E-07	5.234E-10	2.548E-04
2	0.0006	7.439E-06	7.908E-04	1.167E-06	1.796E-06	2.108E-05	3.487E-01	2.310E-07	5.252E-10	2.558E-04
3	0.0012	7.465E-06	7.934E-04	1.171E-06	1.802E-06	2.115E-05	3.484E-01	2.316E-07	5.433E-10	2.569E-04
4	0.0018	7.495E-06	7.959E-04	1.174E-06	1.808E-06	2.122E-05	3.480E-01	2.322E-07	5.675E-10	2.580E-04
5	0.0023	7.527E-06	7.985E-04	1.178E-06	1.815E-06	2.129E-05	3.477E-01	2.328E-07	5.945E-10	2.591E-04
6	0.0035	7.600E-06	8.036E-04	1.186E-06	1.827E-06	2.143E-05	3.470E-01	2.340E-07	6.537E-10	2.612E-04
7	0.0047	7.683E-06	8.087E-04	1.194E-06	1.840E-06	2.156E-05	3.463E-01	2.351E-07	7.188E-10	2.634E-04
8	0.0070	7.884E-06	8.189E-04	1.220E-06	1.868E-06	2.183E-05	3.450E-01	2.374E-07	8.676E-10	2.677E-04
9	0.0094	8.127E-06	8.292E-04	1.261E-06	1.907E-06	2.210E-05	3.436E-01	2.396E-07	1.045E-09	2.721E-04
10	0.0141	8.740E-06	8.498E-04	1.261E-06	1.960E-06	2.263E-05	3.409E-01	2.439E-07	1.521E-09	2.810E-04
11	0.0188	9.524E-06	8.706E-04	1.298E-06	2.027E-06	2.314E-05	3.381E-01	2.480E-07	2.201E-09	2.900E-04
12	0.0281	1.162E-05	9.122E-04	1.376E-06	2.167E-06	2.412E-05	3.326E-01	2.480E-07	2.201E-09	2.900E-04
13	0.0375	1.449E-05	9.540E-04	1.462E-06	2.291E-06	2.501E-05	3.271E-01	2.556E-07	4.659E-09	3.085E-04
14	0.0563	2.279E-05	1.037E-03	1.557E-06	2.427E-06	2.775E-05	3.159E-01	2.628E-07	1.021E-08	3.275E-04
15	0.0750	3.511E-05	1.118E-03	1.880E-06	2.315E-06	3.048E-05	3.048E-01	2.760E-07	5.318E-08	3.664E-04
16	0.1225	8.413E-05	1.315E-03	2.557E-06	2.362E-06	3.488E-05	2.775E-01	2.888E-07	2.627E-07	4.066E-04
17	0.1700	1.518E-04	1.494E-03	4.463E-06	2.802E-05	4.820E-05	2.513E-01	3.608E-05	3.664E-07	5.133E-04
18	0.2350	2.358E-04	1.708E-03	7.335E-06	2.682E-05	6.82E-05	2.178E-01	4.020E-05	2.381E-05	6.258E-04
19	0.3000	2.938E-04	1.864E-03	5.550E-06	2.521E-05	9.170E-05	1.870E-01	3.656E-05	2.270E-04	7.921E-04
20	0.3500	3.210E-04	1.926E-03	6.286E-06	2.374E-05	1.653E-05	1.754E-01	3.154E-05	2.270E-04	9.725E-04
21	0.4000	3.295E-04	1.932E-03	6.895E-06	2.211E-05	1.455E-05	1.754E-01	2.706E-04	3.706E-04	1.113E-03
22	0.4500	3.231E-04	1.884E-03	7.351E-06	2.037E-05	1.278E-05	1.621E-05	2.144E-07	5.456E-04	1.243E-03
23	0.5000	3.116E-04	1.791E-03	7.640E-06	1.856E-05	1.119E-05	1.515E-05	8.264E-08	7.408E-04	1.349E-03
24	0.5625	2.914E-04	1.636E-03	7.713E-06	1.633E-05	9.452E-05	1.365E-05	5.612E-08	9.540E-04	1.429E-03
25	0.6250	2.666E-04	1.467E-03	7.713E-06	1.428E-05	7.980E-05	1.058E-05	2.332E-08	1.232E-03	1.494E-03
26	0.6875	2.392E-04	1.302E-03	7.505E-06	1.248E-05	6.739E-05	8.123E-06	1.590E-08	1.505E-03	1.532E-03
27	0.7500	2.121E-04	1.150E-03	7.207E-06	1.092E-05	5.695E-05	6.213E-06	1.119E-08	1.755E-03	1.554E-03
28	1.0000	1.250E-04	7.055E-04	5.581E-06	7.001E-06	3.120E-06	5.595E-07	4.003E-09	1.978E-03	1.568E-03
29	1.5000	4.826E-05	3.363E-04	3.396E-06	4.169E-06	1.268E-02	2.342E-06	1.90E-09	2.574E-03	1.581E-03
30	2.3750	1.382E-05	1.586E-04	1.866E-06	2.726E-06	4.963E-03	1.309E-07	4.689E-10	2.498E-03	1.771E-03
31	3.2500	4.433E-06	9.493E-05	1.099E-06	1.947E-06	2.631E-03	5.256E-08	3.185E-10	2.018E-03	1.929E-03
32	5.0000	3.328E-07	6.150E-05	4.464E-07	1.121E-06	1.688E-03	4.617E-08	8.582E-10	1.430E-03	2.107E-03
33	10.0000	3.328E-07	6.150E-05	4.464E-07	1.121E-06	1.688E-03	4.617E-08	8.582E-10	1.430E-03	2.107E-03
C3H2										
1	0.0000	7.415E-06	7.883E-04	1.163E-06	1.790E-06	2.102E-05	3.490E-01	2.304E-07	5.234E-10	2.548E-04
2	0.0006	7.439E-06	7.908E-04	1.167E-06	1.796E-06	2.108E-05	3.487E-01	2.310E-07	5.252E-10	2.558E-04
3	0.0012	7.465E-06	7.934E-04	1.171E-06	1.802E-06	2.115E-05	3.484E-01	2.316E-07	5.433E-10	2.569E-04
4	0.0018	7.495E-06	7.959E-04	1.174E-06	1.808E-06	2.122E-05	3.480E-01	2.322E-07	5.675E-10	2.580E-04
5	0.0023	7.527E-06	7.985E-04	1.178E-06	1.815E-06	2.129E-05	3.477E-01	2.328E-07	5.945E-10	2.591E-04
6	0.0035	7.600E-06	8.036E-04	1.186E-06	1.827E-06	2.143E-05	3.470E-01	2.340E-07	6.537E-10	2.612E-04
7	0.0047	7.683E-06	8.087E-04	1.194E-06	1.840E-06	2.156E-05	3.463E-01	2.351E-07	7.188E-10	2.634E-04
8	0.0070	7.884E-06	8.189E-04	1.220E-06	1.868E-06	2.183E-05	3.450E-01	2.374E-07	8.676E-10	2.677E-04
9	0.0094	8.127E-06	8.292E-04	1.261E-06	1.907E-06	2.210E-05	3.436E-01	2.396E-07	1.045E-09	2.721E-04
10	0.0141	8.740E-06	8.498E-04	1.261E-06	1.960E-06	2.263E-05	3.409E-01	2.439E-07	1.521E-09	2.810E-04
11	0.0188	9.524E-06	8.706E-04	1.298E-06	2.027E-06	2.314E-05	3.381E-01	2.480E-07	2.201E-09	2.900E-04
12	0.0281	1.162E-05	9.122E-04	1.376E-06	2.167E-06	2.412E-05	3.326E-01	2.480E-07	2.201E-09	2.900E-04
13	0.0375	1.449E-05	9.540E-04	1.462E-06	2.291E-06	2.501E-05	3.271E-01	2.556E-07	4.659E-09	3.085E-04
14	0.0563	2.279E-05	1.037E-03	1.557E-06	2.427E-06	2.775E-05	3.159E-01	2.628E-07	1.021E-08	3.275E-04
15	0.0750	3.511E-05	1.118E-03	1.880E-06	2.315E-06	3.048E-05	3.048E-01	2.760E-07	5.318E-08	3.664E-04
16	0.1225	8.413E-05	1.315E-03	2.557E-06	2.362E-06	3.488E-05	2.775E-01	2.888E-07	2.627E-07	4.066E-04
17	0.1700	1.518E-04	1.494E-03	4.463E-06	2.802E-05	4.820E-05	2.513E-01	3.608E-05	3.664E-07	5.133E-04
18	0.2350	2.358E-04	1.708E-03	7.335E-06	2.682E-05	6.82E-05	2.178E-01	4.020E-05	2.381E-05	6.258E-04
19	0.3000	2.938E-04	1.864E-03	5.550E-06	2.521E-05	9.170E-05	1.870E-01	3.656E-05	2.270E-04	7.921E-04
20	0.3500	3.210E-04	1.926E-03	6.286E-06	2.374E-05	1.653E-05	1.754E-01	3.154E-05	2.270E-04	9.725E-04
21	0.4000	3.295E-04	1.932E-03	6.895E-06	2.211E-05	1.455E-05	1.754E-01	2.706E-04	3.706E-04	1.113E-03
22	0.4500	3.231E-04	1.884E-03	7.351E-06	2.037E-05	1.278E-05	1.621E-05	2.144E-07	5.456E-04	1.243E-03
23	0.5000	3.116E-04	1.791E-03	7.640E-06	1.856E-05	1.119E-05	1.515E-05	8.264E-08	7.408E-04	1.349E-03
24	0.5625	2.914E-04	1.636E-03	7.713E-06	1.633E-05	9.452E-05	1.365E-05	5.612E-08	9.540E-04	1.429E-03
25	0.6250	2.666E-04	1.467E-03	7.713E-06	1.428E-05	7.980E-05	1.058E-05	2.332E-08	1.232E-03	1.494E-03
26	0.6875	2.392E-04	1.302E-03	7.505E-06	1.248E-05	6.739E-05	8.123E-06	1.590E-08	1.505E-03	1.532E-03
27	0.7500	2.121E-04	1.150E-03	7.207E-06	1.092E-05	5.695E-05	6.213E-06	1.119E-08	1.755E-03	1.554E-03
28	1.0000	1.250E-04	7.055E-04	5.581E-06	7.001E-06	3.120E-06	5.595E-07	4.003E-09	1.978E-03	1.568E-03
29	1.5000	4.826E-05	3.363E-04	3.396E-06	4.169E-06	1.268E-02	2.342E-06	1.90E-09	2.574E-03	1.581E-03
30	2.3750	1.382E-05	1.586E-04	1.866E-06	2.726E-06	4.963E-03	1.309E-07	4.689E-10	2.498E-03	1.771E-03
31	3.2500	4.433E-06	9.493E-05	1.099E-06	1.947E-06	2.631E-03	5.256E-08	3.185E-10	2.018E-03	1.929E-03
32	5.0000	3.328E-07	6.150E-05	4.464E-07	1.121E-06	1.688E-03	4.617E-08	8.582E-10	1.430E-03	2.107E-03
33	10.0000	3.328E-07	6.150E-05	4						

(Appendix J.8. Continued)

17	0.1700	4.099E-06
18	0.2350	5.729E-06
19	0.3000	7.987E-06
20	0.3500	1.033E-05
21	0.4000	1.324E-05
22	0.4500	1.645E-05
23	0.5000	1.947E-05
24	0.5625	2.214E-05
25	0.6250	2.303E-05
26	0.6875	2.253E-05
27	0.7500	2.127E-05
28	1.0000	1.408E-05
29	1.5000	8.321E-06
30	2.3750	5.595E-06
31	3.2500	3.916E-06
32	5.0000	2.502E-06
33	10.0000	2.502E-06

Appendix J.9. Solution for WZ

X	T	V	RHO	H	H2	CH	CH2	CH3	CH4	O
1	0.0000	1.274E+02	1.365E-05	2.870E-03	9.645E-02	2.206E-08	2.069E-06	4.469E-04	8.169E-04	4.539E-06
2	0.0094	6.424E+02	1.309E-05	2.933E-03	9.902E-02	2.259E-08	2.143E-06	4.633E-04	8.472E-04	4.657E-06
3	0.0187	6.676E+02	1.256E-05	3.032E-03	1.016E-01	2.772E-08	2.493E-06	4.945E-04	8.777E-04	5.035E-06
4	0.0281	6.946E+02	1.445E-02	3.166E-03	1.043E-01	3.12E-08	3.107E-06	5.386E-04	9.084E-04	5.687E-06
5	0.0375	7.240E+02	1.150E-05	3.311E-03	1.071E-01	5.302E-08	4.082E-06	5.945E-04	9.393E-04	6.728E-06
6	0.0563	7.944E+02	1.041E-05	3.747E-03	1.132E-01	1.174E-07	7.584E-06	7.370E-04	1.001E-03	1.045E-05
7	0.0750	8.735E+02	1.852E-02	4.241E-03	1.197E-01	2.690E-07	1.453E-05	9.096E-04	1.061E-03	1.739E-05
8	0.0938	9.739E+02	2.084E-02	4.920E-03	1.275E-01	6.903E-07	3.019E-05	1.153E-03	1.138E-03	3.112E-05
9	0.1225	1.070E+03	7.534E-06	5.618E-03	1.349E-01	1.540E-06	5.522E-05	1.403E-03	1.214E-03	4.957E-05
10	0.1463	1.165E+03	2.534E+02	6.317E-03	1.420E-01	3.019E-06	9.021E-05	1.643E-03	1.288E-03	7.158E-05
11	0.1700	1.255E+03	6.325E-06	6.989E-03	1.486E-01	5.255E-06	1.328E-04	1.860E-03	1.361E-03	9.463E-05
12	0.2025	1.364E+03	5.768E-06	7.843E-03	1.567E-01	9.568E-06	1.966E-04	2.116E-03	1.456E-03	1.238E-04
13	0.2350	1.436E+03	5.442E-06	8.552E-03	1.630E-01	1.491E-05	2.537E-04	2.327E-03	1.547E-03	1.443E-04
14	0.3000	1.560E+03	4.950E-06	9.717E-03	1.743E-01	2.859E-05	3.474E-04	2.630E-03	1.704E-03	1.705E-04
15	0.4000	1.701E+03	3.888E+02	4.473E-06	1.075E-02	1.885E-01	4.074E-04	2.870E-03	1.884E-03	1.737E-04
16	0.5000	1.781E+03	4.225E-06	1.109E-02	1.993E-01	6.784E-05	3.770E-04	2.936E-03	2.003E-03	1.480E-04
17	0.7500	1.891E+03	3.896E-06	1.065E-02	2.186E-01	6.829E-05	2.136E-04	2.609E-03	2.075E-03	7.857E-05
18	1.0000	1.898E+03	4.535E+02	3.835E-06	9.756E-03	2.302E-01	9.894E-05	2.188E-03	2.023E-03	3.653E-05
19	1.2500	1.879E+03	3.842E-06	8.873E-03	2.382E-01	2.460E-05	4.487E-05	1.802E-03	1.916E-03	1.703E-05
20	1.5000	1.846E+03	3.886E-06	8.053E-03	2.439E-01	1.193E-05	2.002E-05	1.802E-03	1.802E-03	7.896E-06
21	2.0000	1.728E+03	4.234E+02	4.107E-06	5.697E-03	2.545E-01	4.230E-06	8.901E-04	1.618E-03	1.629E-06
22	3.2500	1.621E+03	4.362E-06	3.726E-03	2.593E-01	3.902E-07	1.136E-06	5.474E-04	1.577E-03	3.827E-07
23	5.0000	1.414E+03	5.022E-06	9.878E-04	2.580E-01	1.023E-08	1.164E-07	1.609E-04	1.779E-03	2.224E-08
24	10.0000	1.414E+03	3.463E+02	9.878E-04	2.580E-01	1.023E-08	1.164E-07	1.609E-04	1.779E-03	2.224E-08
1	0.0000	6.526E-04	7.104E-07	3.113E-02	2.939E-04	4.313E-04	2.161E-05	9.344E-04	1.609E-01	7.184E-06
2	0.0094	8.751E-04	7.448E-07	3.058E-01	3.085E-04	4.529E-04	2.279E-05	9.856E-04	1.675E-01	7.542E-06
3	0.0187	8.688E-04	8.966E-07	3.002E-01	3.161E-04	4.758E-04	2.405E-05	1.024E-03	1.741E-01	8.321E-06
4	0.0281	8.402E-04	1.056E-06	2.945E-01	3.199E-04	4.998E-04	2.534E-05	1.050E-03	1.807E-01	9.125E-06
5	0.0375	7.963E-04	1.223E-06	2.888E-01	3.205E-04	5.247E-04	2.668E-05	1.066E-03	1.873E-01	9.891E-06
6	0.0563	6.822E-04	1.614E-06	2.771E-01	3.114E-04	5.759E-04	2.970E-05	1.063E-03	2.001E-01	1.136E-05
7	0.0750	5.731E-04	2.115E-06	2.654E-01	2.855E-04	6.270E-04	3.372E-05	1.023E-03	2.126E-01	1.293E-05
8	0.0938	4.737E-04	3.088E-06	2.508E-01	2.262E-04	6.909E-04	4.025E-05	9.325E-04	2.281E-01	1.539E-05
9	0.1225	4.293E-04	4.960E-06	2.365E-01	1.452E-04	7.532E-04	4.703E-05	8.147E-04	2.432E-01	1.904E-05
10	0.1463	4.329E-04	6.07E-06	2.225E-01	7.191E-05	8.128E-04	5.187E-05	6.849E-04	2.578E-01	2.410E-05
11	0.1700	4.674E-04	1.466E-05	2.088E-01	3.073E-05	8.684E-04	5.279E-05	5.766E-04	2.721E-01	2.974E-05
12	0.2025	5.333E-04	2.727E-05	1.909E-01	1.163E-05	9.337E-04	4.729E-05	4.036E-04	2.908E-01	3.659E-05
13	0.2350	5.832E-04	4.132E-05	1.743E-01	6.893E-06	9.807E-04	3.793E-05	2.850E-04	3.091E-01	4.064E-05
14	0.3000	6.40E-04	7.976E-05	1.443E-01	3.495E-06	1.009E-04	2.030E-05	1.364E-04	3.477E-01	4.385E-05
15	0.4000	6.522E-04	1.557E-04	1.082E-01	1.772E-06	9.308E-04	8.261E-06	4.908E-05	3.854E-01	4.017E-05
16	0.5000	5.904E-04	2.253E-04	8.309E-02	1.140E-06	8.066E-04	4.576E-06	4.908E-05	3.854E-01	4.017E-05
17	0.7500	4.416E-04	3.438E-04	5.177E-02	4.610E-07	4.926E-04	2.432E-06	8.950E-06	4.647E-01	3.197E-05
18	1.0000	3.098E-04	3.524E-04	3.829E-02	2.424E-07	2.903E-04	1.639E-06	6.145E-06	4.899E-01	1.560E-05
19	1.2500	2.254E-04	3.162E-04	3.179E-02	1.429E-07	1.743E-04	1.639E-06	4.931E-06	5.051E-01	2.880E-06
20	1.5000	1.675E-04	2.652E-04	2.821E-02	9.353E-08	1.071E-04	8.323E-07	4.300E-06	5.155E-01	1.140E-06
21	2.3750	7.257E-05	1.280E-04	2.448E-02	5.392E-08	4.101E-05	4.374E-07	4.035E-06	5.319E-01	1.665E-07
22	3.2500	3.132E-05	5.694E-05	2.334E-02	4.952E-08	2.223E-05	2.906E-07	4.348E-06	5.401E-01	3.015E-08
23	5.0000	3.620E-06	6.332E-06	2.462E-02	6.383E-08	1.370E-05	1.379E-07	5.584E-06	5.468E-01	2.805E-09
24	10.0000	3.620E-06	6.332E-06	2.462E-02	6.383E-08	1.370E-05	1.379E-07	5.584E-06	5.468E-01	2.805E-09

(Appendix J.9. Continued)

X	CH2O	O2	H2O	C3H3	C3H4	AR	HCCO	CH2CO	CO2	CH3CHO
1	0.0000	1.525E-04	2.852E-01	2.392E-05	1.533E-04	4.403E-02	1.231E-05	3.075E-04	2.962E-02	8.875E-07
2	0.0094	1.602E-04	2.777E-01	2.547E-05	1.633E-04	4.391E-02	1.473E-05	3.255E-04	3.116E-02	9.401E-07
3	0.0187	1.684E-04	2.703E-01	2.872E-05	1.784E-04	4.378E-02	1.238E-05	3.372E-04	3.269E-02	1.009E-06
4	0.0281	1.716E-04	2.630E-01	3.380E-05	1.987E-04	4.364E-02	1.735E-05	3.428E-04	3.420E-02	1.093E-06
5	0.0375	1.760E-04	2.557E-01	4.093E-05	2.244E-04	4.351E-02	2.175E-05	3.430E-04	3.569E-02	1.193E-06
6	0.0563	1.838E-04	2.413E-01	4.936E-05	2.504E-04	4.320E-02	3.531E-05	3.296E-04	3.857E-02	1.435E-06
7	0.0988	1.928E-04	2.273E-01	6.167E-05	2.904E-04	4.289E-02	5.712E-05	3.058E-04	4.132E-02	1.720E-06
8	0.1225	2.078E-04	2.102E-01	1.830E-04	3.723E-04	4.289E-02	8.998E-05	2.702E-04	4.466E-02	2.116E-06
9	0.1463	2.265E-04	1.940E-01	1.438E-04	4.921E-04	4.215E-02	1.587E-04	2.352E-04	4.785E-02	2.499E-06
10	0.1700	2.472E-04	1.785E-01	1.076E-04	6.197E-04	4.182E-02	2.346E-04	2.033E-04	5.083E-02	2.803E-06
11	0.1900	2.679E-04	1.638E-01	3.492E-04	7.456E-04	4.151E-02	3.203E-04	1.754E-04	5.359E-02	2.974E-06
12	0.2025	2.939E-04	1.452E-01	3.492E-04	8.632E-04	4.114E-02	4.386E-04	1.433E-04	5.699E-02	2.961E-06
13	0.2350	3.153E-04	1.285E-01	5.089E-04	1.005E-03	4.087E-02	5.351E-04	1.174E-04	6.000E-02	2.724E-06
14	0.3000	3.395E-04	1.1949E-01	5.089E-04	1.123E-03	4.038E-02	6.547E-04	7.941E-05	6.462E-02	1.897E-06
15	0.4000	3.311E-04	1.284E-01	5.949E-04	1.300E-03	3.978E-02	8.527E-04	4.494E-05	6.846E-02	9.061E-07
16	0.5000	2.914E-04	1.616E-01	6.066E-04	1.192E-03	3.934E-02	5.272E-04	2.565E-05	6.983E-02	4.156E-07
17	0.7500	1.585E-04	1.687E-02	5.364E-04	1.192E-03	3.856E-02	2.369E-04	8.858E-06	6.743E-02	1.078E-07
18	1.0000	7.642E-05	7.541E-07	3.093E-04	4.027E-04	3.812E-02	9.465E-05	3.493E-06	6.423E-02	3.362E-08
19	1.2500	3.525E-05	3.080E-03	1.575E-04	2.097E-04	3.782E-02	2.369E-05	1.598E-05	6.136E-02	1.167E-08
20	1.5000	1.544E-05	1.310E-03	1.649E-08	1.030E-04	3.761E-02	1.624E-05	8.413E-07	5.905E-02	4.140E-09
21	2.3750	2.947E-06	2.784E-04	8.092E-06	2.426E-05	3.724E-02	3.197E-06	4.440E-07	5.481E-02	6.604E-10
22	3.2500	6.923E-07	8.022E-05	8.859E-10	7.160E-06	3.712E-02	8.477E-07	3.676E-07	5.304E-02	1.592E-10
23	5.0000	8.770E-08	3.323E-05	4.029E-07	1.534E-06	3.730E-02	1.188E-07	3.428E-07	5.300E-02	2.379E-11
24	10.0000	8.770E-08	3.323E-05	4.029E-07	1.534E-06	3.730E-02	1.188E-07	3.428E-07	5.300E-02	2.379E-11
1	0.0000	3.765E-12	3.594E-04	1.355E-04	1.657E-05	1.761E-05	9.107E-06	9.107E-06	9.107E-06	9.107E-06
2	0.0094	4.060E-12	3.877E-04	1.441E-04	1.797E-05	1.911E-05	9.708E-06	9.708E-06	9.708E-06	9.708E-06
3	0.0187	8.208E-12	4.304E-04	1.584E-04	2.130E-05	2.020E-05	1.121E-05	1.121E-05	1.121E-05	1.121E-05
4	0.0281	1.761E-11	4.869E-04	1.782E-04	2.675E-05	2.082E-05	1.363E-05	1.363E-05	1.363E-05	1.363E-05
5	0.0375	3.963E-11	5.566E-04	2.031E-04	3.458E-05	2.084E-05	1.699E-05	1.699E-05	1.699E-05	1.699E-05
6	0.0563	2.057E-10	7.336E-04	2.672E-04	5.806E-05	1.873E-05	2.638E-05	2.638E-05	2.638E-05	2.638E-05
7	0.0750	9.744E-10	9.595E-04	3.475E-04	9.312E-05	1.329E-05	3.898E-05	3.898E-05	3.898E-05	3.898E-05
8	0.0988	5.050E-09	1.320E-03	4.684E-04	1.513E-04	1.329E-05	5.863E-05	5.863E-05	5.863E-05	5.863E-05
9	0.1225	1.928E-08	1.776E-03	6.065E-04	2.189E-04	1.474E-06	8.154E-05	8.154E-05	8.154E-05	8.154E-05
10	0.1463	6.069E-08	2.338E-03	7.582E-04	2.981E-04	1.474E-06	1.074E-04	1.074E-04	1.074E-04	1.074E-04
11	0.1700	1.600E-07	3.008E-03	9.204E-04	3.917E-04	2.692E-07	1.361E-04	1.361E-04	1.361E-04	1.361E-04
12	0.2025	4.675E-07	4.074E-03	1.154E-03	5.448E-04	1.376E-07	1.801E-04	1.801E-04	1.801E-04	1.801E-04
13	0.2350	1.003E-06	5.186E-03	1.803E-04	7.294E-04	1.052E-07	2.302E-04	2.302E-04	2.302E-04	2.302E-04
14	0.3000	3.255E-06	7.207E-03	8.109E-05	1.393E-03	7.347E-08	3.471E-04	3.471E-04	3.471E-04	3.471E-04
15	0.4000	1.037E-05	9.000E-03	2.721E-05	2.340E-03	7.347E-08	5.513E-04	5.513E-04	5.513E-04	5.513E-04
16	0.5000	1.985E-05	9.581E-03	1.444E-05	2.595E-03	5.442E-08	7.457E-04	7.457E-04	7.457E-04	7.457E-04
17	0.7500	4.023E-05	8.844E-03	5.169E-06	2.581E-03	4.901E-08	1.088E-03	1.088E-03	1.088E-03	1.088E-03
18	1.0000	4.457E-05	7.858E-03	3.985E-06	2.393E-03	3.667E-08	1.235E-03	1.235E-03	1.235E-03	1.235E-03
19	1.2500	4.044E-05	7.061E-03	3.795E-06	2.034E-03	3.634E-08	1.269E-03	1.269E-03	1.269E-03	1.269E-03
20	1.5000	3.362E-05	6.456E-03	4.090E-06	2.034E-03	3.713E-08	1.250E-03	1.250E-03	1.250E-03	1.250E-03
21	2.3750	1.535E-05	5.388E-03	6.737E-06	1.709E-03	4.134E-08	1.074E-03	1.074E-03	1.074E-03	1.074E-03
22	3.2500	6.615E-06	4.826E-03	1.132E-05	1.536E-03	4.603E-08	9.542E-04	9.542E-04	9.542E-04	9.542E-04
23	5.0000	7.470E-07	4.132E-03	1.404E-03	2.608E-03	5.239E-08	8.774E-04	8.774E-04	8.774E-04	8.774E-04
24	10.0000	7.470E-07	4.132E-03	1.404E-03	2.608E-03	5.239E-08	8.774E-04	8.774E-04	8.774E-04	8.774E-04

(Appendix J.10. Continued)

X	CH20	O2	H02	C3H3	C3H4	AR	HCCO	CH2CO	CO2	CH3CHO
1	0.0000	1.801E-04	2.821E-01	2.329E-05	1.342E-04	4.433E-02	9.430E-06	3.609E-04	3.648E-02	1.104E-06
2	0.0094	1.892E-04	2.744E-01	2.481E-05	1.429E-04	4.421E-02	9.741E-06	3.821E-04	3.838E-02	1.170E-06
3	0.0187	1.959E-04	2.668E-01	2.791E-05	1.571E-04	4.409E-02	1.117E-05	3.955E-04	4.027E-02	1.252E-06
4	0.0281	2.006E-04	2.593E-01	3.277E-05	1.770E-04	4.396E-02	1.377E-05	4.017E-04	4.214E-02	1.353E-06
5	0.0375	2.041E-04	2.519E-01	3.961E-05	2.026E-04	4.383E-02	1.768E-05	4.012E-04	4.398E-02	1.471E-06
6	0.0563	2.087E-04	2.371E-01	5.978E-05	2.704E-04	4.353E-02	2.998E-05	3.837E-04	4.754E-02	1.755E-06
7	0.0750	2.143E-04	2.228E-01	9.010E-05	3.569E-04	4.323E-02	5.037E-05	3.537E-04	5.094E-02	2.090E-06
8	0.0988	2.258E-04	2.054E-01	1.429E-04	4.860E-04	4.285E-02	9.064E-05	3.094E-04	5.508E-02	2.551E-06
9	0.1225	2.420E-04	1.889E-01	2.090E-04	6.258E-04	4.251E-02	1.495E-04	2.664E-04	5.903E-02	2.985E-06
10	0.1463	2.607E-04	1.731E-01	2.831E-04	7.648E-04	4.217E-02	2.256E-04	2.276E-04	6.275E-02	3.308E-06
11	0.1700	2.796E-04	1.583E-01	3.582E-04	8.952E-04	4.187E-02	3.125E-04	1.939E-04	6.620E-02	3.456E-06
12	0.2025	3.026E-04	1.395E-01	4.530E-04	1.052E-03	4.150E-02	4.333E-04	1.557E-04	7.050E-02	3.976E-06
13	0.2350	3.200E-04	1.227E-01	5.310E-04	1.183E-03	4.123E-02	5.319E-04	1.253E-04	7.436E-02	2.976E-06
14	0.3000	3.347E-04	9.405E-02	6.414E-04	1.351E-03	4.074E-02	6.588E-04	8.161E-05	8.046E-02	1.897E-06
15	0.5000	2.501E-04	4.159E-02	8.878E-04	1.866E-03	3.967E-02	5.848E-04	2.908E-05	8.768E-02	3.878E-07
16	0.7500	1.258E-04	1.640E-02	1.190E-03	6.834E-04	3.886E-02	2.836E-04	1.075E-05	8.705E-02	7.530E-08
17	1.0000	6.096E-05	7.088E-03	1.847E-07	8.863E-04	3.840E-02	1.307E-04	5.214E-06	8.443E-02	2.087E-08
18	1.2500	3.037E-05	3.288E-03	7.079E-08	2.900E-04	3.809E-02	6.267E-05	3.207E-06	8.178E-02	7.640E-09
19	1.5000	1.527E-05	1.519E-03	2.815E-08	1.869E-04	3.788E-02	3.073E-05	2.304E-06	7.959E-02	3.212E-09
20	2.3750	3.699E-06	3.639E-04	5.239E-09	6.570E-05	3.752E-02	7.157E-06	1.550E-06	7.581E-02	7.158E-10
21	3.2500	1.050E-06	1.136E-04	7.410E-09	2.784E-05	3.739E-02	2.104E-06	1.310E-06	7.460E-02	2.303E-10
22	5.0000	1.445E-07	4.400E-05	9.790E-10	1.145E-05	3.757E-02	2.766E-07	1.296E-06	7.566E-02	4.496E-11
23	10.0000	1.445E-07	4.400E-05	9.790E-10	1.145E-05	3.757E-02	2.766E-07	1.296E-06	7.566E-02	4.496E-11

X	C4H	C4H2	C4H3	C2CHCHO	C6H2	C6H3	CAHCHCO
1	0.0000	1.529E-12	1.594E-04	6.365E-05	4.538E-06	6.593E-06	2.509E-06
2	0.0094	1.649E-12	1.720E-04	6.770E-05	4.924E-06	7.154E-06	2.675E-06
3	0.0187	3.454E-12	1.964E-04	7.607E-05	5.992E-06	7.587E-06	3.173E-06
4	0.0281	7.753E-12	2.319E-04	8.864E-05	7.833E-06	7.863E-06	4.018E-06
5	0.0375	1.835E-11	2.784E-04	1.053E-04	1.053E-05	7.934E-06	5.231E-06
6	0.0563	1.041E-10	4.030E-04	1.499E-04	1.915E-05	7.294E-06	8.768E-06
7	0.0750	5.306E-10	5.677E-04	2.078E-04	3.264E-05	5.336E-06	1.374E-05
8	0.0988	2.951E-09	8.345E-04	2.972E-04	5.618E-05	2.110E-06	2.180E-05
9	0.1225	1.191E-08	1.174E-03	4.016E-04	8.482E-05	6.720E-07	3.149E-05
10	0.1463	3.915E-08	1.593E-03	5.180E-04	1.196E-04	2.616E-07	4.266E-05
11	0.1700	1.063E-07	2.093E-03	6.438E-04	1.616E-04	1.322E-07	5.529E-05
12	0.2025	3.181E-07	2.884E-03	8.266E-04	2.314E-04	6.942E-08	7.492E-05
13	0.2350	6.838E-07	3.699E-03	1.432E-04	3.152E-04	5.389E-08	9.733E-05
14	0.3000	2.161E-06	5.154E-05	1.52E-05	5.181E-04	3.786E-08	1.490E-04
15	0.5000	1.092E-05	6.487E-03	1.816E-03	1.191E-03	2.432E-08	3.263E-04
16	0.7500	1.860E-05	5.918E-03	1.756E-03	1.532E-03	1.686E-08	4.329E-04
17	1.0000	1.794E-05	5.220E-03	1.590E-03	1.550E-03	1.476E-08	4.530E-04
18	1.2500	1.497E-05	4.699E-03	1.444E-03	1.476E-03	1.366E-08	4.395E-04
19	1.5000	1.184E-05	4.306E-03	1.327E-03	1.371E-03	1.334E-08	4.164E-04
20	2.3750	5.242E-06	3.554E-03	1.098E-03	1.097E-03	1.430E-08	3.95E-04
21	3.2500	2.225E-06	3.077E-03	7.994E-06	9.075E-04	1.561E-08	2.848E-04
22	5.0000	2.428E-07	2.208E-03	2.115E-05	6.511E-04	1.779E-08	2.206E-04
23	10.0000	2.428E-07	2.208E-03	2.115E-05	6.511E-04	1.779E-08	2.206E-04

APPENDIX K.

Summary of thermochemical properties

These parameters are calculated from the seven-constant NASA-form fit to thermodynamic data as used by CHEMKIN. The basic data sources were Kee et al. (1984), Burcat (1984), group additivity calculations, and corrections to the above, generally based on recently reported experimental values of $\Delta H_f^\circ(298)$. Groups were taken from Benson (1977), supplemented by:

- Groups of Stein and Fahr (1985) for various C_t and C_d contributions;
- $C_d \cdot$, a vinylic group based on C_2H_3 properties including $\Delta H_f^\circ(298)=70.4$ kcal/mol for C_2H_3 (McMillen and Golden, 1982);
- $C_t \cdot$, an ethnyl group based on C_2H properties including $\Delta H_f^\circ(298)=135$ kcal/mol for C_2H_3 (McMillen and Golden, 1982; Wodtke and Lee, 1985);
- $C_d=O$, a group derived from ketene properties; and
- Ring corrections for cyclohexadienes, which are not shown in Table A.1 of Benson (1977) but which should be approximately $S=20$, $C_p = -3, -2, -1, -0.8, -0.1, 0$.

In the mechanism calculations (Ch. V, App. J), the Sandia data base was used, supplemented by these other sources. Where conflicting data are reported, both are noted, with an asterisk if one can be recommended as better.

Species	Ref.	$\Delta H_f^{\circ, 298}$ kcal/mol	S_{298}°	$C_p^{\circ}(T)$, cal/mol·K									
				298	400	500	600	800	1000	1500	2000		
Ar	Burcat(L), S	0.0	36.98	4.97	4.97	4.97	4.97	4.97	4.97	4.97	4.97	4.97	4.97
CH	Burcat(T), S	142.0	43.72	6.97	6.98	7.03	7.12	7.40	7.78	8.72	8.72	8.72	9.36
HCO	Burcat(J), S	10.4	53.67	8.26	8.74	9.26	9.79	10.75	11.49	12.55	12.55	13.15	13.15
CHO ⁺	Burcat(J)	199.1	48.60	8.61	9.38	10.00	10.50	11.32	12.01	13.14	13.14	13.80	13.80
CH ₂	S (J 12/72)	92.4	46.33	8.27	8.64	9.00	9.37	10.14	10.89	12.23	12.23	13.00	13.00
¹ CH ₂ [¹ A ₁]	PRW (J, G)	100.1	45.18	8.04	8.30	8.60	8.93	9.64	10.37	11.69	11.69	12.48	12.48
³ CH ₂ [³ B ₁]	PRW (J, T)	91.1	46.32	8.27	8.62	8.96	9.29	9.95	10.58	11.82	11.82	12.56	12.56
CH ₂ O	Burcat(J), S	-27.7	52.26	8.44	9.41	10.46	11.51	13.39	14.82	16.96	16.96	18.14	18.14
HOCO	PRW (G)	-50.0	61.05	10.44	11.86	13.01	13.95	15.35	16.31	17.79	17.79	18.54	18.54
CH ₂ OO	PRW (P)	50.9	64.30	12.67	14.73	16.38	17.73	19.71	21.02	23.00	23.00	24.17	24.17
HCOOH	Burcat(L)	-90.5	59.48	10.91	13.04	14.96	16.68	19.45	21.37	23.47	23.47	24.45	24.45
CH ₃	Burcat(T)	35.1	46.38	9.25	10.05	10.81	11.54	12.89	14.09	16.21	16.21	17.56	17.56
	S (J 6/69)	34.8	46.38	9.25	10.05	10.81	11.54	12.89	14.09	16.21	16.21	17.56	17.56
CH ₃ O	Burcat(U)	3.9	54.61	9.05	10.79	12.43	13.98	16.63	18.60	21.51	21.51	23.26	23.26
	S (no ref.)	3.5	54.37	10.91	12.44	13.81	15.02	16.91	18.21	19.22	19.22	19.59	19.59
CH ₂ OH	Burcat(U)	-4.0	57.89	10.79	12.18	13.47	14.66	16.67	18.23	20.73	20.73	22.36	22.36
	S (no ref.)	-14.0	54.37	10.91	12.44	13.81	15.02	16.91	18.21	19.22	19.22	19.59	19.59
CH ₃ OO	Burcat(L)	6.7	62.77	13.03	15.60	17.80	19.67	22.50	24.55	27.49	27.49	29.25	29.25
CH ₄	Burcat(J), S	-17.9	44.50	8.47	9.74	11.07	12.44	15.05	17.16	20.52	20.52	22.60	22.60
CH ₃ OH	Burcat(T)	-48.1	57.28	10.48	12.41	14.26	16.01	19.08	21.40	25.02	25.02	27.25	27.25
	S (no ref.)	-47.9	57.43	11.32	13.03	14.70	16.35	19.28	20.95	21.20	21.20	21.15	21.15
CO	Burcat(J), S	-26.4	47.21	6.96	7.01	7.12	7.27	7.62	7.93	8.41	8.41	8.67	8.67
CO ₂	Burcat(J), S	-94.1	51.08	8.88	9.87	10.67	11.32	12.29	12.98	13.93	13.93	14.45	14.45
C ₂	Burcat(J), S	200.2	47.64	10.32	9.46	8.91	8.60	8.50	8.60	8.93	8.93	9.25	9.25
C ₂ H	PRW (J, W)	135.0	49.56	8.87	9.65	10.24	10.72	11.52	12.21	13.29	13.29	14.13	14.13
HCCO (ketyl)	Bu(T)/PRW	42.4	58.94	10.83	11.68	12.43	13.09	14.22	15.24	16.98	16.98	18.07	18.07
C ₂ H ₂	S (no ref.)	32.0	62.73	14.91	17.00	18.64	19.88	21.47	22.52	24.25	24.25	25.49	25.49
C ₂ H ₂	Burcat(J), S	54.2	48.01	10.56	12.04	13.12	13.97	15.25	16.34	18.30	18.30	19.57	19.57
CH ₂ CO (ketene)	Burcat(T)	-12.4	57.80	12.40	14.18	15.67	16.91	18.80	20.25	22.44	22.44	23.78	23.78
	S (no ref.)	-8.6	57.36	12.29	14.07	15.56	16.82	18.76	20.12	22.46	22.46	26.14	26.14
C ₂ H ₂ O	S (no ref.)	4.0	56.25	12.92	15.15	16.95	18.38	20.27	21.63	23.83	23.83	25.57	25.57
C ₂ H ₂ O ₂	S (no ref.)	-8.0	64.05	15.83	18.43	20.43	22.01	24.26	25.82	28.39	28.39	30.01	30.01
C ₂ H ₂ OH	PRW	32.9	65.80	13.08	14.73	16.25	17.68	20.25	22.42	26.17	26.17	27.50	27.50
C ₂ H ₃	PRW ΔH ; J	70.4	54.47	10.91	12.44	13.82	15.07	17.19	18.83	21.33	21.33	23.16	23.16

Species	Ref.	$\Delta H_f^{\circ, 298}$ kcal/mol	S_{298}°	$C_p^{\circ}(T)$, cal/mol·K							
				298	400	500	600	800	1000	1500	2000
CH ₃ CO	Burcat(T), S	-5.4	63.75	12.38	14.44	16.33	18.06	20.94	23.07	26.19	28.07
CH ₂ CHO	Burcat(T)	6.0	64.01	13.14	15.15	16.96	18.60	21.30	23.35	26.35	28.16
C ₂ H ₄	Burcat(T), S	12.5	52.39	10.23	12.69	14.90	16.86	20.05	22.44	26.11	28.35
C ₂ H ₄ O	Burcat(J)	-12.6	58.04	11.43	14.96	18.01	20.62	24.61	27.48	31.61	34.09
CH ₃ CHO	Burcat(T), S	-39.5	63.06	13.20	15.87	18.31	20.52	24.17	26.89	30.88	33.27
CH ₃ COOH	Burcat(L)	-103.3	67.73	15.17	19.03	22.43	25.38	30.01	33.28	37.37	39.55
C ₂ H ₅	*Bu(R)/Tsang	28.2	60.14	11.11	13.67	16.09	18.37	22.31	25.29	29.84	32.59
	S (no ref.)	26.3	54.55	12.36	14.66	17.01	19.24	22.95	25.78	30.53	33.27
CH ₃ CH ₂ O	Burcat(T)	-4.0	64.17	13.53	16.70	19.54	22.06	26.15	29.20	33.77	36.55
CH ₂ CH ₂ OH	Burcat(T)	-5.0	66.25	14.52	17.77	20.49	22.74	26.03	28.41	32.01	34.23
CH ₂ CHOH	Burcat(T)	-5.0	67.11	14.91	18.01	20.78	23.22	27.15	30.07	34.57	37.34
CH ₃ OCH ₂	Burcat(T)	-2.0	67.36	15.51	18.30	20.87	23.24	27.24	30.28	34.85	37.61
C ₂ H ₆	Burcat(T)	-20.0	54.73	12.52	15.69	18.62	21.30	25.83	29.30	34.62	37.92
	S (L 5/72)	-20.2	54.86	12.56	15.70	18.64	21.34	25.84	29.33	34.91	40.14
C ₂ H ₅ OH	Burcat(U)	-56.1	67.53	15.63	19.41	22.75	25.68	30.36	33.85	39.15	42.66
CH ₃ OCH ₃	Burcat(T)	-44.0	63.98	15.73	19.12	22.26	25.16	30.09	33.81	39.38	42.73
CCO	Bu(J)/PRW	89.0	55.68	10.30	11.08	11.72	12.25	13.06	13.66	14.63	15.18
C ₃	Burcat(J), S	196.0	56.68	9.00	8.99	9.17	9.47	10.16	10.71	11.62	12.22
C ₃ H	Burcat(T)	128.4	62.08	11.08	11.62	12.26	12.99	14.54	15.84	17.84	19.05
C ₃ H ₂	Burcat(U)	106.5	56.23	13.17	15.25	16.95	18.32	20.26	21.63	24.13	25.75
	*PRW(Bittner)	127.0	56.26	12.92	15.14	16.94	18.37	20.25	21.59	23.85	25.59
C ₃ H ₃	Burcat(U)	76.5	59.91	13.96	16.35	18.33	19.96	22.36	24.23	27.26	29.00
	*PRW(Bittner)	81.4	59.92	14.01	16.32	18.29	19.94	22.40	24.25	27.23	28.88
C ₃ H ₄ (unspecified)	S (no ref.)	45.8	59.31	14.67	17.35	19.73	21.79	24.96	27.31	31.63	34.13
CH ₃ C≡CH	Burcat(U)	44.3	59.32	14.54	17.29	19.70	21.79	25.13	27.70	31.64	34.04
CH ₂ =C=CH ₂	Burcat(U)	45.9	59.54	14.10	17.17	19.78	22.00	25.40	27.96	31.82	34.17
c-C ₃ H ₄	Burcat(T)	66.2	58.20	12.67	16.22	19.20	21.69	25.34	27.98	31.87	34.22
2-C ₃ H ₅ (allyl)	Bu(U)/PRW	39.1	61.46	14.07	18.37	22.03	25.09	29.62	32.77	37.22	39.87
1-C ₃ H ₅ (propene)	PRW	62.6	65.17	15.12	18.26	21.00	23.43	27.47	30.56	35.48	38.00
C ₃ H ₆ (propene)	Burcat(T)	4.9	61.52	15.39	19.27	22.73	25.81	30.79	34.53	40.14	43.55
n-C ₃ H ₇	Bu(T)/Tsang	24.0	64.14	18.02	22.27	25.99	29.23	34.38	38.30	44.31	47.99
i-C ₃ H ₇	Bu(T)/Tsang	22.3	60.11	17.93	22.25	26.03	29.31	34.49	38.42	44.41	48.07
C ₃ H ₈ (propane)	Burcat(L)	-24.8	64.58	17.58	22.49	26.87	30.75	37.01	41.74	48.84	53.15
C ₃ O ₂	S (J 6/68)	-22.4	65.97	16.04	17.88	19.32	20.46	22.14	23.34	24.93	25.76

Species	Ref.	$\Delta H_f^{\circ}, 298$ kcal/mol	S_{298}°	$C_p^{\circ}(T)$, cal/mol·K							
				298	400	500	600	800	1000	1500	2000
C ₄	S (no ref.)	232.0	54.58	11.77	13.63	15.07	16.16	17.50	18.39	19.55	20.18
C ₄ H	Burcat(T)	155.1	60.90	14.08	15.37	16.56	17.67	19.59	21.15	23.44	24.82
	*PRW	185.9	61.33	14.50	17.60	19.93	21.69	24.07	25.71	28.00	29.34
C ₄ H ₂	PRW	105.1	59.78	17.59	20.13	21.90	23.19	25.05	26.60	29.08	30.45
HC≡C-CH=C=O	PRW	45.8	68.63	20.97	25.71	29.67	33.14	39.30	45.14	59.75	74.36
C ₄ H ₂ OH	PRW	87.0	42.42	22.51	24.96	27.09	28.96	32.00	34.26	37.54	39.46
C ₄ H ₃ (unspecified)	S (no ref.)	109.0	65.41	16.98	20.00	22.29	24.13	26.99	29.12	32.51	34.49
1-C ₄ H ₃	PRW	126.1	66.47	17.24	20.09	22.42	24.35	27.23	29.21	32.65	34.41
C ₄ H ₄ (vinylacetylene)	PRW	68.2	65.13	17.51	21.23	24.17	26.58	30.30	33.10	37.55	39.71
C ₄ H ₅ (3-butyne)	PRW	85.6	70.68	19.39	23.28	26.52	29.26	33.53	36.66	42.64	46.15
1-C ₄ H ₅ (≡≡≡)	PRW	84.2	68.71	18.63	23.26	26.77	29.52	33.58	36.57	41.40	44.09
2-C ₄ H ₅ (≡≡≡)	PRW	72.2	69.93	18.50	22.91	26.47	29.41	33.97	37.40	42.49	44.62
1-C ₄ H ₆ (1-butyne)	PRW	39.6	69.57	19.55	23.93	27.65	30.88	36.06	40.03	47.07	51.66
2-C ₄ H ₆ (2-butyne)	Burcat(T)	35.0	68.18	18.73	22.74	26.39	29.69	35.17	39.31	45.46	49.16
1,3-C ₄ H ₆ (butadiene)	PRW (API)	26.3	66.62	19.01	24.30	28.47	31.84	36.87	40.51	46.32	49.88
1-C ₄ H ₇	PRW	57.8	74.97	20.25	25.12	29.29	32.92	38.74	43.07	49.83	52.99
3-C ₄ H ₇	PRW	45.9	74.69	20.42	25.52	29.84	33.55	39.39	43.67	50.29	53.38
n-C ₄ H ₆	Burcat(T)	-0.1	73.57	20.40	25.92	30.79	35.05	41.83	46.85	55.10	58.89
i-C ₄ H ₆	Burcat(T)	-4.1	70.88	21.03	26.09	30.66	34.78	41.53	46.60	54.46	58.45
trans-C ₄ H ₆	Burcat(T)	-2.6	71.86	19.39	24.77	29.62	33.96	41.01	46.23	54.79	58.70
cis-C ₄ H ₆	Burcat(T)	-1.8	70.69	20.37	25.46	30.10	34.30	41.23	46.40	54.88	58.77
n-C ₄ H ₉	PRW	15.7	76.39	23.03	29.06	34.16	38.57	45.63	50.95	59.22	63.07
t-C ₄ H ₉	Burcat(T)	10.5	76.29	19.05	24.68	29.92	34.76	42.91	48.92	57.69	62.94
n-C ₄ H ₁₀	Burcat(L)	-30.1	74.27	23.43	29.78	35.44	40.43	48.43	54.39	63.24	68.59
i-C ₄ H ₁₀	Burcat(L)	-32.2	70.59	23.10	29.77	35.61	40.70	48.71	54.61	63.35	68.64
C ₅	S (J 12/69)	234.0	57.82	14.65	17.13	18.97	20.35	22.23	23.49	25.05	25.85
C ₅ H	Burcat(T)	186.0	62.22	15.57	18.48	20.68	22.32	24.32	25.85	28.11	29.45
C ₅ H ₂	Burcat(T)	165.3	63.70	19.83	23.27	25.98	28.08	30.85	32.81	35.40	36.89
C ₅ H ₃	Burcat(T)	135.4	70.54	20.99	24.29	27.01	29.23	32.48	34.91	38.46	40.59
c-C ₅ H ₆	Burcat(T)	32.0	64.46	16.54	23.12	28.70	33.39	40.32	45.10	51.83	55.83
2,4-pentadienyl (≡≡≡≡)	PRW	51.6	74.63	23.48	30.10	35.24	39.36	45.52	50.07	56.99	59.71
C ₆ H	Burcat(U)	213.2	74.12	22.08	25.22	27.67	29.53	31.81	33.27	35.88	37.36
	S (no ref.)	233.2	74.22	21.61	25.01	27.64	29.59	31.84	33.20	35.59	37.07

Species	Ref.	$\Delta H_f^{\circ, 298}$ kcal/mol	S_{298}°	$C_p^{\circ}(T)$, cal/mol·K							
				298	400	500	600	800	1000	1500	2000
C_6H_2	Burcat(U)	169.7	70.94	24.56	27.76	30.26	32.19	34.76	36.82	39.90	41.80
	*PRW	155.9	71.51	23.75	26.70	29.33	31.69	35.61	37.91	40.90	42.42
C_4HCHCO	PRW	96.8	80.38	26.03	32.85	38.31	42.84	50.06	56.10	71.35	86.60
C_6H_3	Burcat(U)	158.5	76.32	24.20	28.01	31.14	33.69	37.35	40.05	43.92	46.25
	*PRW	175.7	77.96	21.86	27.62	31.81	34.86	38.67	40.86	44.84	46.26
1,3- <i>k</i> - C_6H_4 (= \equiv)	PRW	119.4	76.88	24.59	29.33	32.98	35.89	40.28	43.56	48.71	51.15
1,5- <i>k</i> - C_6H_4 (= \equiv)	PRW	123.8	75.71	24.74	29.70	33.41	36.29	40.54	43.76	48.75	51.15
$C-C_6H_4$ - Benzynes	PRW	112.5	67.49	17.95	23.66	28.34	32.22	37.99	41.81	47.82	50.43
5- <i>k</i> - C_6H_5 (= \equiv)	PRW	139.6	79.24	26.15	31.53	35.84	39.32	44.24	47.36	52.87	55.57
1,5- <i>k</i> - C_6H_5 (= \equiv)	PRW	129.7	79.43	26.36	31.67	35.83	39.18	44.22	48.15	55.51	59.53
Phenyl ($C-C_6H_5$)	Burcat(L)	78.5	68.92	18.87	25.45	30.97	35.53	42.10	46.59	52.77	56.43
1- <i>k</i> - C_6H_6 (= \equiv)	PRW	81.7	80.64	26.43	32.80	37.67	41.51	47.16	51.23	57.76	60.89
1,5- <i>k</i> - C_6H_6 (= \equiv)	PRW	99.5	82.72	26.77	32.08	36.51	40.26	46.09	50.55	59.00	63.29
3- <i>k</i> - C_6H_6 (= \equiv)	PRW	82.5	83.25	24.51	30.33	35.19	39.31	45.64	50.05	57.10	60.53
Benzene	Burcat(L)	19.8	64.31	19.63	26.92	33.04	38.10	45.40	50.42	57.42	61.59
C_6H_5O (phenoxy)	Burcat(L)	11.4	73.57	22.57	29.77	35.74	40.61	47.50	52.17	58.53	62.29
C_6H_5OH (phenol)	Burcat(L)	-23.0	75.33	24.79	32.39	38.63	43.69	50.74	55.57	62.38	66.47
1,3,5- C_6H_7 (= \equiv)	PRW	97.5	82.10	27.71	34.70	40.17	44.52	50.73	54.94	61.82	65.28
$C-C_6H_7$	PRW (Tsang)	50.0	72.01	20.79	28.44	35.12	40.55	48.71	54.41	61.59	64.98
1,3,5- C_6H_8 (= \equiv)	PRW	39.7	82.94	28.13	35.67	41.79	46.79	54.07	58.82	66.77	70.65
1,2,5- C_6H_8 (= \equiv)	PRW	59.6	87.35	27.05	33.99	39.68	44.46	51.93	57.50	65.65	68.64
1,3-cyclohexadiene	PRW	26.0	67.59	24.44	33.55	40.55	46.08	54.15	60.00	68.09	70.87
1,4-cyclohexadiene	PRW	26.3	71.61	22.96	31.89	38.87	44.47	52.86	58.90	67.30	69.85
2,4- <i>k</i> - C_6H_9 (= \equiv)	PRW	43.8	83.11	28.91	36.80	43.16	48.41	56.44	62.26	71.15	74.87
2,5- <i>k</i> - C_6H_9 (= \equiv)	PRW	50.9	90.75	27.55	35.40	41.76	47.04	55.26	61.43	70.45	74.25
3,5- <i>k</i> - C_6H_9 (= \equiv)	PRW	59.5	90.21	29.29	36.94	43.26	48.52	56.42	61.91	70.42	73.89
2- $C-C_6H_9$	PRW	29.4	71.74	24.61	33.86	41.51	47.90	57.51	64.15	73.60	76.86
3- $C-C_6H_9$	PRW	41.6	77.19	24.81	33.77	41.20	47.41	56.80	63.34	72.69	75.86
1,3- <i>k</i> - C_6H_{10} (= \equiv)	PRW	13.5	87.74	29.34	37.71	44.49	50.12	58.80	65.14	74.88	78.70
1,4- <i>k</i> - C_6H_{10} (= \equiv)	PRW	56.5	80.67	27.90	36.96	44.50	50.85	60.52	67.32	77.17	80.67
1,5- <i>k</i> - C_6H_{10} (= \equiv)	PRW	20.2	90.75	28.66	36.55	43.18	48.84	57.78	64.38	74.23	78.36
$C-C_6H_{10}$ (cyclohexane)	Burcat(U)	-1.0	74.77	25.39	34.15	41.90	48.69	59.30	66.67	76.71	83.15
Benzyl ($C-C_7H_7$)	Burcat(T)	47.8	75.58	25.29	33.51	40.39	46.08	54.31	60.03	68.00	72.74
Toluene	Burcat(T)	12.0	76.46	24.72	33.31	40.62	46.79	55.96	62.36	71.38	76.75

Species	Ref.	$\Delta H_f^{\circ},_{298}$ kcal/mol	S_{298}°	$C_p^{\circ}(T)$, cal/mol·K							
				298	400	500	600	800	1000	1500	2000
C ₆ H	Burcat (U)	288.9	78.41	27.05	31.60	35.16	37.85	41.16	43.23	46.76	48.75
C ₆ H ₂	Burcat (U)	226.3	75.96	29.41	34.44	38.33	41.24	44.72	46.91	51.01	53.40
	*PRW	207.0	83.20	30.21	34.13	37.61	40.74	45.89	48.86	52.54	54.91
Phenylacetylene (C ₈ H ₆)	PRW	73.8	76.26	27.68	35.92	42.61	48.08	55.98	60.97	69.10	72.83
4-C ₆ H ₇ -C ₂ H	PRW	81.7	62.21	34.24	42.86	49.91	55.72	64.24	69.96	78.62	81.92
3-C ₆ H ₉ -C ₂ H ₃	PRW	17.5	91.73	33.05	45.01	54.91	63.21	75.72	84.40	97.02	101.49
p-Xylene	Burcat (L)	4.3	84.16	30.05	39.95	48.54	55.93	67.31	75.55	84.83	88.40
Naphthalene (C ₁₀ H ₈)	Burcat	36.0	79.64	31.63	42.97	52.41	60.17	71.21	78.68	88.86	94.88
e ⁻	Burcat (L)	0.0	4.99	4.97	4.97	4.97	4.97	4.97	4.97	4.97	4.97
H	Burcat (J), S	52.1	27.39	4.97	4.97	4.97	4.97	4.97	4.97	4.97	4.97
HO ₂	Burcat (J), S	0.5	54.73	8.34	8.92	9.48	9.98	10.78	11.38	12.46	13.23
H ₂	Burcat (J), S	0.0	31.21	6.91	6.96	6.99	7.02	7.08	7.22	7.73	8.18
H ₂ O	Burcat (J), S	-57.8	45.11	8.03	8.19	8.42	8.68	9.26	9.86	11.26	12.22
H ₂ O ₂	Burcat (L), S	-32.5	55.66	10.40	11.45	12.35	13.11	14.29	15.21	16.85	17.88
O	Burcat (J), S	59.6	38.47	5.24	5.14	5.08	5.05	5.02	5.00	4.98	4.98
OH	Burcat (J), S	9.3	43.88	7.17	7.09	7.06	7.06	7.15	7.33	7.87	8.28
O ₂	Burcat (J), S	0.0	49.01	7.02	7.20	7.43	7.67	8.06	8.33	8.73	9.04

- Burcat (J) - Burcat (1984) citing JANAF tables.
 Burcat (L) - Burcat (1984) citing NASA Lewis tables.
 Burcat (T) - Burcat (1984) citing Technion reports.
 Burcat (R) - Burcat (1984) citing Gurvitch TSIV tables.
 Burcat (U) - Burcat (1984) citing LSU calculations.
 Bu()/Tsang - Burcat () with corrected $\Delta H_f^{\circ}(298)$ from Tsang (1985).
 PRW (API) - 1,3-butadiene based on API-44 properties (Rossini, 1953).
 PRW (J,G) - ¹CH₂ from JANAF frequencies, $\Delta E_{S-T}=9$ kcal/mol.
 PRW (J,T) - ³CH₂ from JANAF frequencies, $\Delta H_f^{\circ}(298)$ from Böhland and Temps (1984).
 PRW (J,W) - C₂H from JANAF and $\Delta H_f^{\circ}(298)$ inferred from Wodtke and Lee (1985).
 PRW(Bittner) - ΔH from Bittner (1981).
 PRW(Tsang) - ΔH from Tsang (1986).
 PRW - Group additivity estimates.
 S - Sandia thermodynamic data base (Kee et al., 1984).

APPENDIX L.

QRRK computer programs and sample inputs.

The following programs are written in Microsoft BASIC © for the IBM PC ©, requiring the capability of screen graphics output and needing an Intel 8087 © arithmetic coprocessor for reasonable speed.

The programs can describe chemically activated bimolecular reactions (Appendix L.1) and thermally activated unimolecular reactions (Appendix L.3) having up to three decomposition channels and one isomerization channel:

- The first decomposition channel can have two secondary decompositions, each involving loss of an atom;
- The second channel allows for secondary decomposition into two polyatomic fragments, assuming that the energy released in the primary decomposition ($A^* \rightarrow B^*+C^*$) is apportioned according to the vibrational energies of the ground-state products (B and C);
- The third decomposition channel can have up to three further decompositions, all forming an atom and a polyatomic; for example, $CH_3+OH \rightarrow CH_3OH^* \rightarrow CH_3O^*+H$, $CH_3O^* \rightarrow CH_2O^*+H$, $CH_2O^* \rightarrow HCO^*+H$, and $HCO^* \rightarrow H+CO$; and
- The isomerization channel includes reversibility of the isomerization, two decomposition channels of atom loss, and a secondary decomposition for one of the isomerization/decomposition steps.

Input parameters may be entered interactively or by file (for example, Appendices L.2 and L.3).

The one feature that is not apparent from the other documentation or from the listing is that fall-off curves can be generated at a temperature T for pressures P_1 to P_2 . The temperature and pressure inputs necessary for this calculation are $T, T, 0$ and $P_1, P_2, PFAC$, where $PFAC$ is the multiplicative factor used to increment between P_1 and P_2 (e.g., 9.999 for factor-of-ten spacing).

Appendix L.1. BASIC Program For Bimolecular QRRK

```

1000 REM Bimolecular QRRK program - P.R.Westmoreland,Dept.Chem.Eng.,MIT,1985
1010 REM Developed in collaboration with A.M. Dean, ER&E, Annandale, NJ
1020 REM Lines 1240-4020: Input conditions (By file:      1430-2240
1030 REM                               T,P, re-start: 2250-2380
1040 REM                               Manual:      2400-3900)
1050 REM                               [Save conditions to disk 4030-4480]
1060 REM Lines 4500-4550: Compute quantum size, convert barriers.
1070 REM Lines 4560-5010: Iterate on T - Calc coll'n eff. & freq., kINF, kABS
1080 REM Lines 5020-5340: Calc chem-activation energy distribution.
1090 REM Lines 5350-7030: Calc k's by sum of k(E) over energy
1100 REM                               [Detailed output at T: 7040-7200;
1110 REM                               Save for summary:7210-7330]
1120 REM Lines 7390-7640 Summary output
1130 REM Lines 7650-8350 Graph/fit rate constants
1140 REM Subroutines: Collision efficiency 8390; Third-body parameters 8420;
1150 REM Formats 8530; Plotting 9350; Keyboard response 10060, 10250
1160 REM Calc k(DEAC)= $\beta$ *kCOLL*[M] 10140; Calc k(E) for a channel 10190
1170 DEFINT I-N '***** Set up the program
1180 DIM F(99),X(2,26),Y(25,26),KFORM$(25),XX(26),YY(26),ZZ(26),LN!(200)
1190 DIM YT(25),PRED(26),PRD1(26),ENTRY$(18),RXN$(25),YLBL(5)
1200 DIM XPLT(26),YPLT(26),IXPL(26),IYPLT(26),YPLT(26)
1210 GOSUB 8530 '**(Set up formats)
1220 KEY OFF: SCREEN 0: COLOR 0,6,2: CLS
1230 DEF FNALOG10(X)=LOG(X)/ELOG10
1240 ELOG10=LOG(10): E38=9.999999E+37: ELOG9=LOG(9.9999): K$=NADA$
1250 FIRST=1: EMINUS15=1E-15: ICLS=1: PTEST=0: IPLTP=0: UFLOWFAC=50: R=1.987165
1260 FOR I=1 TO 200: LN!(I)=LOG(I): NEXT '***Begin input:
1270 PRINT"New case - Will any results be saved to disk? Quit? (Y/N/Q,def=N) ";
1280 GOSUB 10260 '***Std. to read Y/N (keyboard)
1290 IF K$="Y" OR K$="y" THEN PRINT Y$: ISTO=1 ELSE GOTO 1340
1300 LINE INPUT " Then enter file name: ";FILE2$
1310 IF ICLS THEN OPEN FILE2$ FOR APPEND AS #2:FOLD$=FILE2$:ICLS=0:GOTO 1370
1320 IF ICLS OR FILE2$=FOLD$ THEN GOTO 1370
1330 CLOSE #2: OPEN FILE2$ FOR APPEND AS #2: FOLD$=FILE2$: ICLS=0: GOTO 1370
1340 IF K$="N" OR K$="n" THEN PRINT N$: ISTO=0 ELSE GOTO 1360
1350 IF ICLS THEN GOTO 1370 ELSE CLOSE #2: ICLS=1: GOTO 1370
1360 IF K$="Q" OR K$="q" THEN PRINT "Quit": END ELSE PRINT "?": GOTO 1270
1370 IFILE=0
1380 PRINT"File or Manual input, or Quit (F/M/Q,def=M)? ";; GOSUB 10260
1390 IF K$="Q" OR K$="q" THEN PRINT "Quit": END
1400 IF K$="F" OR K$="f" THEN PRINT"File": GOTO 1430
1410 PRINT"Manual": GOTO 2250
1420 REM ***** File input *****
1430 LINE INPUT " Enter file name: ";FILE1$
1440 OPEN FILE1$ FOR INPUT AS #1: LINE INPUT #1,L$:RP$=MID$(L$,19):R$=RP$+" - "
1450 FOR LL=1 TO 18: LINE INPUT #1,L$: RXN$(LL)=MID$(L$,43): NEXT
1460 LINE INPUT #1,L$: RXN$(25)=MID$(L$,43): LINE INPUT #1,L$
1470 LINE INPUT #1,L$: A1=VAL(MID$(L$,28,10))
1480 EN= VAL(MID$(L$,42,6)): EACT= VAL(MID$(L$,55,6))
1490 LINE INPUT #1,L$: FREQ=VAL(MID$(L$,23,6)): NS= VAL(MID$(L$,44,5))
1500 LINE INPUT #1,L$: XM1=VAL(MID$(L$,14,6))

```

```

1510 SIGMA1=VAL(MID$(L$,34,6)): EK1=VAL(MID$(L$,64,7))
1520 LINE INPUT #1,L$:IDCOLL$=MID$(L$,10): LINE INPUT #1,L$
1530 IF IDCOLL$="NEW" OR IDCOLL$="new" THEN GOTO 1590
1540 XMT=VAL(MID$(L$,5,7)): SIGT=VAL(MID$(L$,16,6))
1550 EKT=VAL(MID$(L$,28,7)): ECOLLT=VAL(MID$(L$,45,6))
1560 IF XMT=0 OR SIGT=0 OR EKT=0 OR ECOLLT=0 THEN GOTO 1580
1570 XM2=XMT: SIGMA2=SIGT: EK2=EKT: ECOLL=ECOLLT: GOTO 1610
1580 GOSUB 8430: IF IFLAG THEN 1590 ELSE 1610
1590 IFLAG=0: INPUT "Enter name of bath-gas molecule: ",TIDCOLL$
1600 IF LEN(TIDCOLL$)>1 THEN IDCOLL$=TIDCOLL$
1610 LINE INPUT #1,L$: AINF1=VAL(MID$(L$,38,11)): EM1=VAL(MID$(L$,50,7))
1620 LINE INPUT #1,L$
1630 LINE INPUT #1,L$: AINF2A=VAL(MID$(L$,38,11)): E2A=VAL(MID$(L$,50,7))
1640 LINE INPUT #1,L$: FREQSA=VAL(MID$(L$,16,4)) 'Secondary dec 2a
1650 NSA=VAL(MID$(L$,23,4)): DH2A=VAL(MID$(L$,53,6))
1660 LINE INPUT #1,L$: XMSA=VAL(MID$(L$,14,6))
1670 SIGMASA=VAL(MID$(L$,34,6)): EKSA=VAL(MID$(L$,64,7))
1680 LINE INPUT #1,L$: AINF2ADA=VAL(MID$(L$,38,11)): E2ADA=VAL(MID$(L$,50,7))
1690 LINE INPUT #1,L$: AINF2ADB=VAL(MID$(L$,38,11)): E2ADB=VAL(MID$(L$,50,7))
1700 LINE INPUT #1,L$: IF FREQSA=0 THEN FREQSA=FREQ
1710 LINE INPUT #1,L$: AINF2B=VAL(MID$(L$,38,11)): E2B=VAL(MID$(L$,50,7))
1720 LINE INPUT #1,L$: FREQSB1=VAL(MID$(L$,16,4)): NSB1=VAL(MID$(L$,23,4)) '2b1
1730 LINE INPUT #1,L$: XMSB1=VAL(MID$(L$,14,6))
1740 SIGMASB1=VAL(MID$(L$,34,6)): EKSB1=VAL(MID$(L$,64,7))
1750 LINE INPUT #1,L$: AINF2B1D=VAL(MID$(L$,38,11)): E2B1D=VAL(MID$(L$,50,7))
1760 LINE INPUT #1,L$: FREQSB2=VAL(MID$(L$,16,4)) 'Secondary dec 2b2
1770 NSB2=VAL(MID$(L$,23,4)): DH2B12=VAL(MID$(L$,53,6)) 'DH(prods vs adduct)
1780 LINE INPUT #1,L$: XMSB2=VAL(MID$(L$,14,6))
1790 SIGMASB2=VAL(MID$(L$,34,6)): EKSB2=VAL(MID$(L$,64,7))
1800 LINE INPUT #1,L$: AINF2B2D=VAL(MID$(L$,38,11)): E2B2D=VAL(MID$(L$,50,7))
1810 LINE INPUT #1,L$: FRQSB2D=VAL(MID$(L$,16,4)) 'Tert dec 2b2
1820 NSB2D=VAL(MID$(L$,23,4)): DH2B2D=VAL(MID$(L$,53,6)) 'DH(prod2D vs prod12)
1830 LINE INPUT #1,L$: XMSB2D=VAL(MID$(L$,14,6))
1840 SIGSB2D=VAL(MID$(L$,34,6)): EKSB2D=VAL(MID$(L$,64,7))
1850 LINE INPUT #1,L$: AINF2B2DD=VAL(MID$(L$,38,11)): E2B2DD=VAL(MID$(L$,50,7))
1860 IF FREQSB1=0 THEN FREQSB1=FREQ
1870 IF FREQSB2=0 THEN FREQSB2=FREQ
1880 IF FRQSB2D=0 THEN FRQSB2D=FREQ
1890 LINE INPUT #1,L$
1900 LINE INPUT #1,L$: AINF2C=VAL(MID$(L$,38,11)): E2C=VAL(MID$(L$,50,7))
1910 LINE INPUT #1,L$: FREQSC=VAL(MID$(L$,16,4)) 'Secondary decomp 2c
1920 NSC=VAL(MID$(L$,23,4)): DH2C=VAL(MID$(L$,53,6))
1930 LINE INPUT #1,L$: XMSC=VAL(MID$(L$,14,6))
1940 SIGMASC=VAL(MID$(L$,34,6)): EKSC=VAL(MID$(L$,64,7))
1950 LINE INPUT #1,L$: AINF2CD=VAL(MID$(L$,38,11)): E2CD=VAL(MID$(L$,50,7))
1960 LINE INPUT #1,L$: FRQSCD=VAL(MID$(L$,16,4)) 'Tertiary decompn 2c
1970 NSCD=VAL(MID$(L$,23,4)): DH2CD=VAL(MID$(L$,53,6)) 'H2CD-H2C
1980 LINE INPUT #1,L$: XMSCD=VAL(MID$(L$,14,6))
1990 SIGSCD=VAL(MID$(L$,34,6)): EKSCD=VAL(MID$(L$,64,7))
2000 LINE INPUT #1,L$: AINF2CDD=VAL(MID$(L$,38,11)): E2CDD=VAL(MID$(L$,50,7))
2010 LINE INPUT #1,L$: FRQSCDD=VAL(MID$(L$,16,4)) '4th-order decompn 2c
2020 NSCDD=VAL(MID$(L$,23,4)): DH2CDD=VAL(MID$(L$,53,6)) 'H2CDD-H2CD
2030 LINE INPUT #1,L$: XMSCDD=VAL(MID$(L$,14,6))
2040 SIGSCDD=VAL(MID$(L$,34,6)): EKSCDD=VAL(MID$(L$,64,7))

```



```

2050 LINE INPUT #1,L$: AINF2CDDD=VAL(MID$(L$,38,11)):E2CDDD=VAL(MID$(L$,50,7))
2060 IF FREQSC=0 THEN FREQSC=FREQ
2070 IF FRQSCD=0 THEN FRQSCD=FREQ
2080 IF FRQSCDD=0 THEN FRQSCDD=FREQ
2090 LINE INPUT #1,L$
2100 LINE INPUT #1,L$: AINF3=VAL(MID$(L$,38,11)): E3=VAL(MID$(L$,50,7))
2110 LINE INPUT #1,L$: AINFM3=VAL(MID$(L$,38,11)): EM3=VAL(MID$(L$,50,7))
2120 LINE INPUT #1,L$: DELISO= VAL(MID$(L$,23,7)) 'DELISO,FREQI
2130 FREQI=VAL(MID$(L$,45,6)):IF FREQI=0 THEN FREQI=FREQ
2140 LINE INPUT #1,L$
2150 LINE INPUT #1,L$: AINF4A=VAL(MID$(L$,38,11)): E4A=VAL(MID$(L$,50,7))
2160 LINE INPUT #1,L$: FREQIA=VAL(MID$(L$,16,4)) 'Secondary decomp 4a
2170 NSIA=VAL(MID$(L$,23,4)): DHIA=VAL(MID$(L$,53,6))
2180 LINE INPUT #1,L$: XMIA=VAL(MID$(L$,14,6))
2190 SIGMAIA=VAL(MID$(L$,34,6)): EKIA=VAL(MID$(L$,64,7))
2200 LINE INPUT #1,L$: AINF4AD=VAL(MID$(L$,38,11)): E4AD=VAL(MID$(L$,50,7))
2210 LINE INPUT #1,L$: IF FREQIA=0 THEN FREQIA=FREQ
2220 LINE INPUT #1,L$: AINF4B=VAL(MID$(L$,38,11)): E4B=VAL(MID$(L$,50,7))
2230 LINE INPUT #1,L$: LINE INPUT #1,L$: A1A=VAL(MID$(L$,24,10))
2240 ENA=VAL(MID$(L$,38,6)): EACTA=VAL(MID$(L$,51,6)): CLOSE #1: IFLAG=1
2250 PRINT: IF FIRST THEN GOTO 2300 '*****T,P*****
2260 PRINT USING TPFORS$;TLOW,THIGH,TSTEP,PLOW,PHIGH
2270 PRINT TOKFORM$;: GOSUB 10260
2280 IF K$="Y" OR K$="y" THEN PRINT Y$: GOTO 2330
2290 IF K$="Q" OR K$="q" THEN PRINT "Quit": END ELSE PRINT N$
2300 INPUT "Enter Tmin, Tmax, Tstep (K): ",TLOW,THIGH,TSTEP
2310 INPUT "Enter Pmin, Pmax, P factor (atm): ",PLOW,PHIGH,PFAC
2320 IF PFAC=1 THEN PFAC=0
2330 T=TLOW: P=PLOW: IF IFLAG=0 THEN GOTO 2360
2340 GOSUB 8430
2350 IFLAG=0: GOTO 3910
2360 IF FIRST THEN GOTO 2420
2370 PRINT "Other parameters unchanged (Y/N)? ";: GOSUB 10260
2380 IF K$="Y" OR K$="y" THEN PRINT Y$: GOTO 3910 ELSE PRINT N$
2390 REM***** Manual input *****
2400 PRINT "Reactants: "+RP$;: GOSUB 10250
2410 IF K$="Y" OR K$="y" THEN PRINT Y$: GOTO 2430 ELSE PRINT N$
2420 PRINT "Reactants: ";: LINE INPUT RP$
2430 R$=RP$+" - ": IF FIRST THEN GOTO 2540
2440 PRINT ASTFORM$+R$+RXN$(1)
2450 PRINT DECFORM$+R$+RXN$(2): PRINT DDFRM$+R$+RXN$(3): PRINT DDFRM$+R$+RXN$(4)
2460 PRINT DECFORM$+R$+RXN$(5): PRINT DDFRM$+R$+RXN$(6): PRINT DDFRM$+R$+RXN$(7)
2470 PRINT DDFRM$+R$+RXN$(8): PRINT TERTFRM$+R$+RXN$(9)
2480 PRINT TERTFRM$+R$+RXN$(10): PRINT DECFORM$+R$+RXN$(11)
2490 PRINT DDFRM$+R$+RXN$(12): PRINT TERTFRM$+R$+RXN$(13)
2500 PRINT QUARFRM$+R$+RXN$(14): PRINT ISOFORM$+R$+RXN$(15)
2510 PRINT IDECFORM$+R$+RXN$(16): PRINT DDFRM$+R$+RXN$(17)
2520 PRINT IDECFORM$+R$+RXN$(18): PRINT ABSFORM$+R$+RXN$(25): GOSUB 10250
2530 IF K$="Y" OR K$="y" THEN PRINT Y$: GOTO 2590 ELSE PRINT N$
2540 FOR LL=1 TO 18: PRINT ENTRY$(LL);
2550 LINE INPUT TEMP$: IF TEMP$<RXN$(LL) AND LEN(TEMP$)>1 THEN RXN$(LL)=TEMP$
2560 NEXT
2570 LINE INPUT "Enter abstraction products: ";TEMP$
2580 IF TEMP$<RXN$(25) AND LEN(TEMP$)>1 THEN RXN$(25)=TEMP$

```

```

2590 IF FIRST THEN GOTO 2620          '**kINF add'n parameters**
2600 PRINT USING KINFM$; A1,EN,EACT: GOSUB 10250
2610 IF K$="Y" OR K$="y" THEN PRINT Y$: GOTO 2630 ELSE PRINT N$
2620 INPUT "Enter hi-P A, b, and E for add'n/rec'n (mol,cc,kcal): ",A1,EN,EACT
2630 IF FIRST THEN GOTO 2660          '**Freq/S
2640 PRINT USING FFORM$;FREQ,NS: GOSUB 10250
2650 IF K$="Y" OR K$="y" THEN PRINT Y$: GOTO 2670 ELSE PRINT N$
2660 INPUT "Enter freq (1/cm) and # oscillators for adduct: ",FREQ,NS
2670 IF FIRST THEN GOTO 2700          '**Adduct props
2680 PRINT USING SPFORM$;X1,SIGMA1,EK1: GOSUB 10250
2690 IF K$="Y" OR K$="y" THEN PRINT Y$: GOTO 2710 ELSE PRINT N$
2700 PRINT ESPFORM$;: INPUT " ",X1,SIGMA1,EK1
2710 IF FIRST THEN GOTO 2750          '**Bath-gas properties
2720 PRINT USING IDFORM$;IDCOLL$: PRINT USING COLLFORM$;X2,SIGMA2,EK2,ECOLL
2730 GOSUB 10250
2740 IF K$="Y" OR K$="y" THEN PRINT Y$: GOTO 2820 ELSE PRINT N$
2750 INPUT "Choose bath gas (NEW for new properties): ",IDCOLL$
2760 IF IDCOLL$="NEW" OR IDCOLL$="new" THEN GOTO 2790
2770 GOSUB 8430: IF IFLAG=1 THEN GOTO 2720
2780 GOTO 2820
2790 INPUT "Enter name of bath-gas molecule: ",IDCOLL$
2800 PRINT " Enter MW, "+CHR$(229)+", "+CHR$(238)+"/K, coll'n energy (cal):";
2810 INPUT " ",X2,SIGMA2,EK2,ECOLL
2820 IF IFLAG THEN IFLAG=0
2830 IF FIRST THEN GOTO 2860          '**A(-1),Barrier(-1)
2840 PRINT USING AM1FORM$;AINFM1,EM1: GOSUB 10250
2850 IF K$="Y" OR K$="y" THEN PRINT Y$: GOTO 2870 ELSE PRINT N$
2860 INPUT "Enter A & barrier for dissoc'n of adduct to reactants: ",AINFM1,EM1
2870 PRINT: PRINT DECFORM$+R$+RXN$(2) '**(a) A to prods; E between**
2880 IF FIRST THEN GOTO 2910
2890 PRINT USING A2FORM$;AINF2A,E2A: GOSUB 10250
2900 IF K$="Y" OR K$="y" THEN PRINT Y$: GOTO 2920 ELSE PRINT N$
2910 INPUT "Enter A and barrier for decomposition: ", AINF2A,E2A
2920 PRINT DDFRM$+R$+RXN$(3):PRINT DDFRM$+R$+RXN$(4) '**Secondary decomp a-a,b
2930 FQ=FREQSA:NSQ=NSA:DHS=DH2A: XMS=XMSA:SIGMAS=SIGMASA:EKS=EKSA: GOSUB 10060
2940 FREQSA=FQ: NSA=NSQ: DH2A=DHS: XMSA=XMS: SIGMASA=SIGMAS: EKSA=EKS
2950 IF FIRST THEN GOTO 2980          '**A&E, ch. a-a
2960 PRINT USING ADFORM$;AINF2ADA,E2ADA: GOSUB 10250
2970 IF K$="Y" OR K$="y" THEN PRINT Y$: GOTO 2990 ELSE PRINT N$
2980 INPUT "Enter A and barrier for secondary decomp (a-a): ", AINF2ADA,E2ADA
2990 IF FIRST THEN GOTO 3020          '**A&E, ch. a-b
3000 PRINT USING ADFORM$;AINF2ADB,E2ADB: GOSUB 10250
3010 IF K$="Y" OR K$="y" THEN PRINT Y$: GOTO 3030 ELSE PRINT N$
3020 INPUT "Enter A and barrier for secondary decomp (a-b): ", AINF2ADB,E2ADB
3030 PRINT: PRINT DECFORM$+R$+RXN$(5) '**A to prods b; E between**
3040 IF FIRST THEN GOTO 3070
3050 PRINT USING A2FORM$;AINF2B,E2B: GOSUB 10250
3060 IF K$="Y" OR K$="y" THEN PRINT Y$: GOTO 3080. ELSE PRINT N$
3070 INPUT "Enter A and barrier for decomposition: ", AINF2B,E2B
3080 PRINT " Sec decomp of 1st decmp prod:"+R$+RXN$(6):FQ=FREQSB1 '*Sec dec, b1
3090 NSQ=NSB1:DHS=DH2B12: XMS=XMSB1:SIGMAS=SIGMASB1:EKS=EKSB1: GOSUB 10060
3100 FREQSB1=FQ:NSB1=NSQ:DH2B12=DHS:XMSB1=XMS:SIGMASB1=SIGMAS:EKSB1=EKS
3110 IF FIRST THEN GOTO 3140
3120 PRINT USING ADFORM$;AINF2B1D,E2B1D: GOSUB 10250

```

```

3130 IF K$="Y" OR K$="y" THEN PRINT Y$: GOTO 3150 ELSE PRINT N$
3140 INPUT "Enter A and barrier for secondary decompn: ",AINF2B1D,E2B1D
3150 PRINT " Sec decomp of 2nd decmp prod:"+R$+RXN$(7):FQ=FREQSB2 '*Sec dec, b2
3160 NSQ=NSB2:DHS=DH2B12: XMS=XMSB2:SIGMAS=SIGMASB2:EKS=EKSB2: GOSUB 10060
3170 FREQSB2=FQ:NSB2=NSQ:DH2B12=DHS:XMSB2=XMS:SIGMASB2=SIGMAS:EKSB2=EKS
3180 IF FIRST THEN GOTO 3210
3190 PRINT USING ADFORM$;AINF2B2D,E2B2D: GOSUB 10250
3200 IF K$="Y" OR K$="y" THEN PRINT Y$: GOTO 3220 ELSE PRINT N$
3210 INPUT "Enter A and barrier for secondary decompn: ",AINF2B2D,E2B2D
3220 PRINT " Tert decomp of 2nd decmp prod:"+R$+RXN$(9):FQ=FRQSB2D'Tert dec,b2D
3230 NSQ=NSB2D:DHS=DH2B2D: XMS=XMSB2D:SIGMAS=SIGSB2D:EKS=EKSB2D:GOSUB 10060
3240 FRQSB2D=FQ:NSB2D=NSQ:DH2B2D=DHS:XMSB2D=XMS:SIGSB2D=SIGMAS:EKSB2D=EKS
3250 IF FIRST THEN GOTO 3280
3260 PRINT USING ATFORM$;AINF2B2DD,E2B2DD: GOSUB 10250
3270 IF K$="Y" OR K$="y" THEN PRINT Y$: GOTO 3290 ELSE PRINT N$
3280 INPUT "Enter A and barrier for tertiary decompn: ",AINF2B2DD,E2B2DD
3290 PRINT: PRINT DECFORM$+R$+RXN$(11) '**A to prods c; E between**
3300 IF FIRST THEN GOTO 3330
3310 PRINT USING A2FORM$;AINF2C,E2C: GOSUB 10250
3320 IF K$="Y" OR K$="y" THEN PRINT Y$: GOTO 3340 ELSE PRINT N$
3330 INPUT "Enter A and barrier for decomposition: ", AINF2C,E2C
3340 PRINT DDFRM$+R$+RXN$(12) '**Secondary dec, c
3350 FQ=FREQSC:NSQ=NSC:DHS=DH2C: XMS=XMSC:SIGMAS=SIGMASC:EKS=EKSC: GOSUB 10060
3360 FREQSC=FQ: NSC=NSQ: DH2C=DHS: XMSC=XMS: SIGMASC=SIGMAS: EKSC=EKS
3370 IF FIRST THEN GOTO 3400
3380 PRINT USING ADFORM$;AINF2CD,E2CD: GOSUB 10250
3390 IF K$="Y" OR K$="y" THEN PRINT Y$: GOTO 3410 ELSE PRINT N$
3400 INPUT "Enter A and barrier for secondary decompn: ", AINF2CD,E2CD
3410 PRINT TERTFRM$+R$+RXN$(13) '**Tertiary dec, c
3420 FQ=FRQSCD:NSQ=NSCD:DHS=DH2CD: XMS=XMSCD:SIGMAS=SIGSCD:EKS=EKSCD:GOSUB 10060
3430 FRQSCD=FQ: NSCD=NSQ: DH2CD=DHS: XMSCD=XMS: SIGSCD=SIGMAS: EKSCD=EKS
3440 IF FIRST THEN GOTO 3470
3450 PRINT USING ATFORM$;AINF2CDD,E2CDD: GOSUB 10250
3460 IF K$="Y" OR K$="y" THEN PRINT Y$: GOTO 3480 ELSE PRINT N$
3470 INPUT "Enter A and barrier for tertiary decomposition: ", AINF2CDD,E2CDD
3480 PRINT QUARFRM$+R$+RXN$(14): FQ=FRQSCDD '**4th-order dec, c
3490 NSQ=NSCDD:DHS=DH2CDD: XMS=XMSCDD:SIGMAS=SIGSCDD:EKS=EKSCDD:GOSUB 10060
3500 FRQSCDD=FQ:NSCDD=NSQ:DH2CDD=DHS: XMSCDD=XMS:SIGSCDD=SIGMAS:EKSCDD=EKS
3510 IF FIRST THEN GOTO 3540
3520 PRINT USING AQFORM$;AINF2CDDD,E2CDDD: GOSUB 10250
3530 IF K$="Y" OR K$="y" THEN PRINT Y$: GOTO 3550 ELSE PRINT N$
3540 INPUT"Enter A and barrier for 4th-order decomposition: ", AINF2CDDD,E2CDDD
3550 PRINT: PRINT ISOFORM$+R$+RXN$(15)
3560 IF FIRST THEN GOTO 3590 '**A&E to isomer
3570 PRINT USING A3FORM$;AINF3,E3: GOSUB 10250
3580 IF K$="Y" OR K$="y" THEN PRINT Y$: GOTO 3600 ELSE PRINT N$
3590 INPUT"Enter A and barrier for isomeriz'n of adduct: ",AINF3,E3
3600 IF FIRST THEN GOTO 3630 '**A&E from isomer to adduct
3610 PRINT USING AM3FORM$;AINFM3,EM3: GOSUB 10250
3620 IF K$="Y" OR K$="y" THEN PRINT Y$: GOTO 3640 ELSE PRINT N$
3630 INPUT"Enter A and barrier for re-isom'n to adduct: ",AINFM3,EM3
3640 IF FIRST THEN GOTO 3670 '**H(isomer)-H(adduct); freq
3650 PRINT USING DELFORM$;DELISO,FREQI: GOSUB 10250
3660 IF K$="Y" OR K$="y" THEN PRINT Y$: GOTO 3690 ELSE PRINT N$

```

```

3670 INPUT"Enter E(isomer)-E(adduct) and mean freq of isomer: ", DELISO,FREI
3680 IF FREI=0 THEN FREI=FREQ
3690 PRINT IDECFORM$+R$+RXN$(16)
3700 IF FIRST THEN GOTO 3730 '**A&E for isomer dec, a
3710 PRINT USING A4FORM$;AINF4A,E4A: GOSUB 10250
3720 IF K$="Y" OR K$="y" THEN PRINT Y$: GOTO 3740 ELSE PRINT N$
3730 INPUT"Enter A & barrier for decomp'n of isomer to products:",AINF4A,E4A
3740 PRINT DDFRM$+R$+RXN$(17) '**Secondary dec
3750 FQ=FREQIA:NSQ=NSIA:DHS=DHIA: XMS=XMIA:SIGMAI=SIGMAIA:EKS=EKIA: GOSUB 10060
3760 FREQIA=FQ: NSIA=NSQ: DHIA=DHS: XMIA=XMS: SIGMAIA=SIGMAS: EKIA=EKS
3770 IF FIRST THEN GOTO 3800
3780 PRINT USING ADFORM$;AINF4AD,E4AD: GOSUB 10250
3790 IF K$="Y" OR K$="y" THEN PRINT Y$: GOTO 3810 ELSE PRINT N$
3800 INPUT "Enter A and barrier for secondary decomposition: ",AINF4AD,E4AD
3810 PRINT IDECFORM$+R$+RXN$(18)
3820 IF FIRST THEN GOTO 3850 '**A&E for isomer dec, b
3830 PRINT USING A4FORM$;AINF4B,E4B: GOSUB 10250
3840 IF K$="Y" OR K$="y" THEN PRINT Y$: GOTO 3860 ELSE PRINT N$
3850 INPUT"Enter A & barrier for decomp'n of isomer to products:",AINF4B,E4B
3860 PRINT: PRINT ABSFORM$+R$+RXN$(25) '*kABS parameters
3870 IF FIRST THEN GOTO 3900
3880 PRINT USING RABFORM$;A1A,ENA,EACTA: GOSUB 10250
3890 IF K$="Y" OR K$="y" THEN PRINT Y$: GOTO 3910 ELSE PRINT N$
3900 INPUT"Enter A, b, and E for abstraction rate constant: ",A1A,ENA,EACTA
3910 PRINT "Detailed output or Summary (D/S)? "; '**Now what?
3920 GOSUB 10260
3930 IF K$="D" OR K$="d" THEN PRINT "Detailed output.": IOUT=0: GOTO 3960
3940 IF K$="S" OR K$="s" THEN PRINT "Summary only.": IOUT=1: GOTO 3960
3950 PRINT "?";: GOTO 3920
3960 IF IFLAG THEN GOSUB 8430
3970 FIRST=0: IF ISTO THEN PRINT "Save to disk, just ";
3980 PRINT "Compute, or Re-enter data (S/C/R)? ";: GOSUB 10260
3990 IF (K$="S" OR K$="s") AND ISTO=1 THEN PRINT "Save": IFILE=1: GOTO 4030
4000 IF K$="C" OR K$="c" THEN PRINT "Begin...": GOTO 4490
4010 IF K$="R" OR K$="r" THEN PRINT "Re-enter ...": GOTO 2260
4020 PRINT "?": GOTO 3970
4030 PRINT #2,"Reaction set for: "+RP$ '**Write to disk
4040 PRINT #2,ASTFORM$+RXN$(1): PRINT #2,DECFORM$+RXN$(2)
4050 PRINT #2,DDFRM$+RXN$(3):PRINT #2,DDFRM$+RXN$(4):PRINT #2,DECFORM$+RXN$(5)
4060 PRINT #2,DDFRM$+RXN$(6):PRINT #2,DDFRM$+RXN$(7):PRINT #2,DDFRM$+RXN$(8)
4070 PRINT #2,TERTFRM$+RXN$(9): PRINT #2,TERTFRM$+RXN$(10)
4080 PRINT #2,DECFORM$+RXN$(11): PRINT #2,DDFRM$+RXN$(12)
4090 PRINT #2,TERTFRM$+RXN$(13): PRINT #2,QUARFRM$+RXN$(14)
4100 PRINT #2,ISOFORM$+RXN$(15): PRINT #2,IDECFORM$+RXN$(16)
4110 PRINT #2,DDFRM$+RXN$(17): PRINT #2,IDECFORM$+RXN$(18)
4120 PRINT #2,ABSFORM$+RXN$(25): PRINT #2,NADA$
4130 PRINT #2,USING KINFM$;A1,EN,EACT: PRINT #2,USING FFORM$;FREQ,NS
4140 PRINT #2,USING SPFORM$;XM1,SIGMA1,EK1: PRINT #2,USING IDFORM$;IDCOLL$
4150 PRINT #2,USING COLLFORM$;XM2,SIGMA2,EK2,ECOLL
4160 PRINT #2,USING AM1FORM$;AINFM1,EM1
4170 PRINT #2," "+DECFORM$+R$+RXN$(2): PRINT #2,USING A2FORM$;AINF2A,E2A
4180 PRINT #2,USING FSFORM$;FREQSA,NSA,DH2A
4190 PRINT #2,USING SPSFORM$;XMSA,SIGMASA,EKSA
4200 PRINT #2,USING ADFORM$;AINF2ADA,E2ADA

```

```

4210 PRINT #2,USING ADFORM$;AINF2ADB,E2ADB
4220 PRINT #2," "+DECFORM$+R$+RXN$(5): PRINT #2,USING A2FORM$;AINF2B,E2B
4230 PRINT #2,USING FSFORM$;FREQSB1,NSB1,DH2B12
4240 PRINT #2,USING SPSFORM$;XMSB1,SIGMASB1,EKSB1
4250 PRINT #2,USING ADFORM$;AINF2B1D,E2B1D
4260 PRINT #2,USING FSFORM$;FREQSB2,NSB2,DH2B12
4270 PRINT #2,USING SPSFORM$;XMSB2,SIGMASB2,EKSB2
4280 PRINT #2,USING ADFORM$;AINF2B2D,E2B2D
4290 PRINT #2,USING FSFORM$;FRQSB2D,NSB2D,DH2B2D
4300 PRINT #2,USING SPSFORM$;XMSB2D,SIGSB2D,EKSB2D
4310 PRINT #2,USING ATFORM$;AINF2B2DD,E2B2DD
4320 PRINT #2," "+DECFORM$+R$+RXN$(11)
4330 PKINT #2,USING A2FORM$;AINF2C,E2C: PRINT #2,USING FSFORM$;FREQSC,NSC,DH2C
4340 PRINT #2,USING SPSFORM$;XMSC,SIGMASC,EKSC
4350 PRINT #2,USING ADFORM$;AINF2CD,E2CD
4360 PRINT #2,USING FSFORM$;FRQSCD,NSCD,DH2CD
4370 PRINT #2,USING SPSFORM$;XMSCD,SIGSCD,EKSCD
4380 PRINT #2,USING ATFORM$;AINF2CDD,E2CDD
4390 PRINT #2,USING FSFORM$;FRQSCDD,NSCDD,DH2CDD
4400 PRINT #2,USING SPSFORM$;XMSCDD,SIGSCDD,EKSCDD
4410 PRINT #2,USING AQFORM$;AINF2CDDD,E2CDDD:PRINT #2," "+ISOFORM$+R$+RXN$(15)
4420 PRINT #2,USING A3FORM$;AINF3,E3: PRINT #2,USING AM3FORM$;AINFM3,EM3
4430 PRINT #2,USING DELFORM$;DELISO,FREI:PRINT #2," "+IDECFORM$+R$+RXN$(16)
4440 PRINT #2,USING A4FORM$;AINF4A,E4A: PRINT #2,USING FSFORM$;FREQIA,NSIA,DHIA
4450 PRINT #2,USING SPSFORM$;XMIA,SIGMAIA,EKIA
4460 PRINT #2,USING ADFORM$;AINF4AD,E4AD: PRINT #2," "+IDECFORM$+R$+RXN$(18)
4470 PRINT #2,USING A4FORM$;AINF4B,E4B
4480 PRINT #2," "+ABSFORM$+R$+RXN$(25):PRINT #2,USING RABSFORM$;A1A,ENA,EACTA
4490 GOSUB 9280 'More formats; then convert E's into quanta:
4500 HC=.002859: QUANTUM=HC*FREQ: QM1=EM1/QUANTUM
4510 MM1=INT(EM1/QUANTUM+.5):M2A=INT(E2A/QUANTUM+.5):M2B=INT(E2B/QUANTUM+.5)
4520 M2C=INT(E2C/QUANTUM+.5): M3=INT(E3/QUANTUM+.5)
4530 QUANTUMA=HC*FREQA: QUANTUMB1=HC*FREQSB1: QUANTUMB2=HC*FREQSB2
4540 QUANTUMB2D=HC*FRQSB2D: QUANTUMC=HC*FREQSC: QUANTUMCD=HC*FRQSCD
4550 QCDD=HC*FRQSCDD: QUANTUMI=HC*FREI: QUANTUMIA=HC*FREQIA
4560 GOSUB 8390 '**Start for T; Get coll'n efficiency (beta or lambda)
4570 IF IOUT THEN GOTO 4580 ELSE PRINT: IF IFILE THEN PRINT #2," "
4580 RK1LOG=LOG(A1) +EN*LOG(T) -EACT*1000/(R*T)
4590 IF A1A THEN RABSLOG=LOG(A1A)+ENA*LOG(T)-EACTA*1000/(R*T) ELSE RABSLOG=-90
4600 IF ABS(RK1LOG)<85 THEN GOTO 4650
4610 RK1LOG10=RK1LOG/ELOG10
4620 PRINT USING "Log10(k&) at #####. K = ###.##; Next T:";CHR$(236),T,RK1LOG10
4630 IF IFILE THEN PRINT #2, USING "Log10(k&) at #####. K = ###.##; Next T:";
CHR$(236),T,RK1LOG10
4640 GOTO 7350
4650 ISTEP=ISTEP+1: SSIG=SIGMA1: EEK=EK1: XXM=XM1: GOSUB 10140
4660 DEACT=DEAC: IF XMSA=0 THEN DEACT2A=0: GOTO 4690
4670 SSIG=SIGMASA: EEK=EKSA: XXM=XMSA: GOSUB 10140
4680 DEACT2A=DEAC
4690 IF AINF2B1D=0 THEN DEACT2B1=0: GOTO 4720
4700 SSIG=SIGMASB1: EEK=EKSB1: XXM=XMSB1: GOSUB 10140
4710 DEACT2B1=DEAC
4720 IF AINF2B2D=0 THEN DEACT2B2=0: GOTO 4750
4730 SSIG=SIGMASB2: EEK=EKSB2: XXM=XMSB2: GOSUB 10140

```

```

4740 DEACT2B2=DEAC
4750 IF XMSB2D=0 THEN DEACT2B2D=0: GOTO 4780
4760 SSIG=SIGSB2D: EEK=EKSB2D: XXM=XMSB2D: GOSUB 10140
4770 DEACT2B2D=DEAC
4780 IF XMSC=0 THEN DEACT2C=0: GOTO 4810
4790 SSIG=SIGMASC: EEK=EKSC: XXM=XMSC: GOSUB 10140
4800 DEACT2C=DEAC
4810 IF XMSCD=0 THEN DEACT2CD=0: GOTO 4840
4820 SSIG=SIGSCD: EEK=EKSCD: XXM=XMSCD: GOSUB 10140
4830 DEACT2CD=DEAC
4840 IF XMSCDD=0 THEN DEACT2CDD=0: GOTO 4870
4850 SSIG=SIGSCDD: EEK=EKSCDD: XXM=XMSCDD: GOSUB 10140
4860 DEACT2CDD=DEAC
4870 IF XMIA=0 THEN DEACTIA=0: GOTO 4900
4880 SSIG=SIGMAIA: EEK=EKIA: XXM=XMIA: GOSUB 10140
4890 DEACTIA=DEAC
4900 IP=IP+1: IF IOUT THEN GOTO 5020
4910 PRINT USING PFORM$;T,P
4920 IF ABS(RABSLOG)<85 THEN PRINT USING HPKFORM$+KABSFORM$;EXP(RK1LOG),
      EXP(RABSLOG): GOTO 4950
4930 IF RABSLOG=-90 THEN PRINT USING HPKFORM$;EXP(RK1LOG): GOTO 4950
4940 PRINT USING HPKFORM$+"log10(kABS)= +###.##";EXP(RK1LOG),RABSLOG/ELOG10
4950 PRINT USING DKFORM$;IDCOLL$,DEACT,XLAM
4960 IF IFILE=0 THEN GOTO 5020
4970 PRINT #2," ": PRINT #2,USING PFORM$;P,T
4980 IF ABS(RABSLOG)<85 THEN PRINT #2, USING HPKFORM$+KABSFORM$;EXP(RK1LOG),
      EXP(RABSLOG): GOTO 5010
4990 IF RABSLOG=-90 THEN PRINT #2, USING HPKFORM$;EXP(RK1LOG): GOTO 5010
5000 PRINT #2, USING HPKFORM$+"log10(kABS)= +###.##";EXP(RK1LOG),RABSLOG/ELOG10
5010 PRINT #2, USING DKFORM$;IDCOLL$,DEACT,XLAM
5020 IF (TLOW+TSTEP)>THIGH AND P>PLOW THEN GOTO 5350 'If fall-off, bypass F(N)
5030 DOLD=0: NMAX=MM1+20: A=EXP(-1.439*FREQ/T) 'Distrib fcn:
5040 REM D=(A**N)*FAC(N-MM1+NS-1)/FAC(N-MM1) ...
5050 FOR N=MM1 TO NMAX
5060 PROD=0!: ISTART=N-MM1+1: IEND=N-MM1+NS-1
5070 FOR I=ISTART TO IEND: PROD=PROD+LN!(I): NEXT
5080 LND!= LOG(A)*N +PROD +UFLOWFAC
5090 IF LND!>88 THEN GOSUB 8370
5100 IF LND!<-88.7 THEN GOSUB 8380
5110 D=EXP(LND!): IF N>MM1 AND D<1E-18*DOLD THEN NMAX=N-1:DTOT=DOLD: GOTO 5290
5120 DOLD=DOLD+D
5130 IF DOLD>1E+30 THEN GOSUB 8370
5140 NEXT N
5150 N=MM1+21 '**Now converged?
5160 PROD=0!: ISTART=N-MM1+1: IEND=N-MM1+NS-1
5170 FOR I=ISTART TO IEND: PROD=PROD+LN!(I): NEXT
5180 LND!= LOG(A)*N +PROD +UFLOWFAC
5190 IF LND!>88 THEN GOSUB 8370
5200 IF LND!<-88.7 THEN GOSUB 8380
5210 DR=DOLD+EXP(LND!): IF DR>1E+30 THEN GOSUB 8370
5220 IF DR/DOLD <1.0001 THEN GOTO 5240
5230 DOLD=DR: N=N+1: GOTO 5160
5240 DTOT=DR
5250 REM: Distribution F(N)=(A**N)* FAC(N-MM1+NS-1)/FAC(N-MM1) /DTOT ...

```

```

5260 NMAX=N: IF NMAX<100 THEN GOTO 5290
5270 PRINT QXS$: IF IFILE THEN PRINT #2,QXS$
5280 NMAX=99
5290 FOR N=MM1 TO NMAX
5300 PROD=0!: ISTART=N-MM1+1: IEND=N-MM1+NS-1
5310 FOR I=ISTART TO IEND: PROD=PROD+LN!(I): NEXT
5320 F(N)= LOG(A)*N +PROD -LOG(DTOT) +UFLOWFAC
5330 IF F(N)<-85 THEN F(N)=1E-37 ELSE F(N)=EXP(F(N))
5340 NEXT '*Finished calculating distribution fcn
5350 IDIST=0: TOTK0=0: TOTAS=0: TOTADAS=0:TOTADADA=0:TOTADADB=0
5360 TOTADBS=0: TOTADB1D2S=0: TOTADB1S2D=0: TOTADB1D2D=0: TOTADB1S2DD=0
5370 TOTADB1D2DD=0: TOTADCS=0:TOTADCDS=0:TOTADCDDS=0:TOTADCDDD=0
5380 TOTIS=0: TOTIDAS=0:TOTIDAD=0: TOTIDE=0
5390 IF IOUT THEN GOTO 5410
5400 PRINT HEADING$: IF IFILE THEN PRINT #2, HEADING$
5410 FOR N=MM1 TO NMAX
5420 NSUB=N:MSUB=MM1:NSSUB=NS:ASUB=AINFML: GOSUB 10200 '**Calc k(E),M1 by QRRK
5430 RKML=KSUB!: RK2A=0: RK2ADA=0: RK2ADB=0: RK2B=0
5440 FS=0: F1D2S=0: F1S2D=0: F1D2D=0: RK2B2DD=0: RK2C=0: RK2CD=0: RK2CDD=0
5450 IF M2A=0 OR N<M2A THEN GOTO 5560 '**Calc k(E),2A
5460 NSUB=N: MSUB=M2A: NSSUB=NS: ASUB=AINF2A: GOSUB 10200
5470 RK2A=KSUB! '*Secdry dec? Dissipate energy (N-M2A)
5480 IF AINF2ADA=0 AND AINFADB=0 THEN GOTO 5560
5490 QS= (N*QUANTUM - DH2A)/QUANTUMA: N2=INT(QS +.5): IF QS<0 THEN 5560
5500 MSUB=INT(E2ADA/QUANTUMA+.5):NSUB=N2:NSSUB=NSA:ASUB=AINF2ADA '**k(E),a-a
5510 IF AINF2ADA=0 OR N2<MSUB THEN GOTO 5530 ELSE GOSUB 10200
5520 RK2ADA=KSUB!
5530 MSUB=INT(E2ADB/QUANTUMA+.5):NSUB=N2:NSSUB=NSA:ASUB=AINF2ADB '**k(E),a-b
5540 IF AINF2ADB=0 OR N2<MSUB THEN GOTO 5560 ELSE GOSUB 10200
5550 RK2ADB=KSUB!
5560 IF M2B=0 OR N<M2B THEN GOTO 5930 '**Calc k(E),2b
5570 NSUB=N: MSUB=M2B: NSSUB=NS: ASUB=AINF2B: GOSUB 10200
5580 RK2B=KSUB! '*Sec dec? Dissipate energy (N-M2B):
5590 F1S=1: F2S=1: IF AINF2B1D=0 AND AINF2B2D=0 THEN GOTO 5840
5600 EXS=N*QUANTUM-DH2B12: IF EXS<0 THEN 5840
5610 IF AINF2B1D>0 AND AINF2B2D>0 THEN GOTO 5640
5620 IF AINF2B1D>0 THEN EB1=EXS: EB2=0: GOTO 5760 'So AINF2b2D=0
5630 EB1=0: EB2=EXS: GOTO 5800 'THEN AINF2b1D=0, AINF2b2D<0
5640 EQ1=FREQSB1/NSB1 *EXP(1.439*FREQSB1/T-1) '*Each can decompose
5650 EQ2=FREQSB2/NSB2 *EXP(1.439*FREQSB2/T-1)
5660 EB1=EXS/(1+ EQ1/EQ2): EB2=EXS/(1+ EQ2/EQ1)
5670 QS= EB1/QUANTUMB1: N2=INT(QS +.5): MSUB=INT(E2B1D/QUANTUMB1 +.5)
5680 NSUB=N2: NSSUB=NSB1: ASUB=AINF2B1D '**Calc f(b1S)
5690 IF AINF2B1D=0 OR N2<MSUB THEN F1S=1: GOTO 5710 ELSE GOSUB 10200
5700 F1S=DEACT2B1/(DEACT2B1+KSUB!)
5710 QS= EB2/QUANTUMB2: N2=INT(QS +.5): MSUB=INT(E2B2D/QUANTUMB2 +.5)
5720 NSUB=N2: NSSUB=NSB2: ASUB=AINF2B2D '**Calc f(b2S)
5730 IF AINF2B2D=0 OR N2<MSUB THEN F2S=1: GOTO 5750 ELSE GOSUB 10200
5740 F2S=DEACT2B2/(DEACT2B2+KSUB!)
5750 GOTO 5840
5760 QS= EB1/QUANTUMB1: N2=INT(QS +.5): MSUB=INT(E2B1D/QUANTUMB1 +.5)
5770 NSUB=N2: NSSUB=NSB1: ASUB=AINF2B1D '**Calc k(E),b1D
5780 IF AINF2B1D=0 OR N2<MSUB THEN F1S=0: GOTO 5840 ELSE GOSUB 10200
5790 F1S=DEACT2B1/(DEACT2B1+KSUB!): GOTO 5840

```

```

5800 QS= EB2/QUANTUMB2: N2=INT(QS +.5): MSUB=INT(E2B2D/QUANTUMB2 +.5)
5810 NSUB=N2: NSSUB=NSB2: ASUB=AINF2B2D '**Calc f(b2S)
5820 IF AINF2B2D=0 OR N2<MSUB THEN F2S=0: GOTO 5840 ELSE GOSUB 10200
5830 F2S=DEACT2B2/(DEACT2B2+KSUB!)
5840 IF F1S<F2S THEN FS=F1S:F1D2S=F2S-F1S:F1S2D=0:F1D2D=1-F1S-F1D2S: GOTO 5860
5850 FS=F2S: F1S2D=F1S-F2S: F1D2S=0: F1D2D=1-F2S-F1S2D
5860 IF AINF2B2DD=0 THEN GOTO 5930 '**Tertiary decomp of prod 2?
5870 QS=(EB2-DH2B12-DH2B2D)/QUANTUMB2D: N2=INT(QS +.5)
5880 IF QS<0 THEN GOTO 5930
5890 MSUB=INT(E2B2DD/QUANTUMB2D +.5)
5900 NSUB=N2: NSSUB=NSB2D: ASUB=AINF2B2DD '**Calc k(E),b2DD
5910 IF N2<MSUB THEN GOTO 5930 ELSE GOSUB 10200
5920 RK2B2DD=KSUB!
5930 IF M2C=0 OR N<M2C THEN GOTO 6130 '**Calc k(E),2c
5940 NSUB=N: MSUB=M2C: NSSUB=NS: ASUB=AINF2C: GOSUB 10200
5950 RK2C=KSUB! '*Secondry dec? Dissipate energy (N-M2C)
5960 IF AINF2CD=0 THEN GOTO 6130
5970 QS=(N*QUANTUM - DH2C)/QUANTUMC: N2=INT(QS +.5): IF QS<0 THEN 6010
5980 MSUB=INT(E2CD/QUANTUMC+.5): NSUB=N2: NSSUB=NSC: ASUB=AINF2CD '**k(E),cD
5990 IF N2<MSUB THEN GOTO 6130 ELSE GOSUB 10200
6000 RK2CD=KSUB! '*TERTIARY dec? Dissipate energy (N-E2CD)
6010 IF AINF2CDD=0 THEN GOTO 6130
6020 QS=(N*QUANTUM-DH2C-DH2CD)/QUANTUMCD: N2=INT(QS +.5): IF QS<0 THEN 6130
6030 MSUB=INT(E2CDD/QUANTUMCD +.5)
6040 NSUB=N2: NSSUB=NSCD: ASUB=AINF2CDD '**Calc k(E),cDD
6050 IF N2<MSUB THEN GOTO 6130 ELSE GOSUB 10200
6060 RK2CDD=KSUB! '*4TH-ORDER dec? Dissipate energy (N-E2CDD)
6070 IF AINF2CDDD=0 THEN GOTO 6130
6080 QS=(N*QUANTUM-DH2C-DH2CD-DH2CDD)/QCDD: N2=INT(QS +.5): IF QS<0 THEN 6130
6090 MSUB=INT(E2CDDD/QCDD +.5)
6100 NSUB=N2: NSSUB=NSCDD: ASUB=AINF2CDDD '**Calc k(E),cDDD
6110 IF N2<MSUB THEN GOTO 6130 ELSE GOSUB 10200
6120 RK2CDDD=KSUB!
6130 RK3=0: RKM3=0: RK4A=0: RK4AD=0: RK4B=0 '* Isomerizations
6140 IF M3=0 OR N<M3 THEN GOTO 6350 '**Calc k(E),M3
6150 NSUB=N: MSUB=M3: NSSUB=NS: ASUB=AINF3: GOSUB 10200
6160 RK3=KSUB! 'Next calc Isom* rate constants - need N relative to Isom
6170 IF AINFM3=0 THEN GOTO 6350 '**Calc k(E),MM3
6180 MM3=INT(EM3/QUANTUMI +.5)
6190 M4A=INT(E4A/QUANTUMI +.5): M4B=INT(E4B/QUANTUMI +.5)
6200 NNEW=(N*QUANTUM-DELISO)/QUANTUMI: IF NNEW<MM3 THEN GOTO 6350
6210 NSUB=NNEW: MSUB=MM3: NSSUB=NS: ASUB=AINFM3: GOSUB 10200
6220 RKM3=KSUB!
6230 IF AINF4A=0 OR NNEW<M4A THEN GOTO 6320 '**Calc k(E),4A
6240 NSUB=NNEW: MSUB=M4A: NSSUB=NS: ASUB=AINF4A: GOSUB 10200
6250 RK4A=KSUB! '*Secondry dec? Dissipate energy (NNEW-M4A)
6260 IF AINF4AD=0 THEN GOTO 6320
6270 QS=(NNEW*QUANTUMI -DH1A)/QUANTUMIA: N2=INT(QS +.5): IF QS<0 THEN 6320
6280 MSUB=INT(E4AD/QUANTUMIA +.5)
6290 NSUB=N2: NSSUB=NSIA: ASUB=AINF4AD '**Calc k(E),4AD
6300 IF N2<MSUB THEN GOTO 6320 ELSE GOSUB 10200
6310 RK4AD=KSUB!
6320 IF AINF4B=0 OR NNEW<M4B THEN GOTO 6350 '**Calc k(E),4B
6330 NSUB=NNEW: MSUB=M4B: NSSUB=NS: ASUB=AINF4B: GOSUB 10200

```



```

6340  RK4B=KSUB!
6350  DENOMISO=DEACT+RKM3+RK4A+RK4B
6360  DENOM=LOG(DEACT +RKM1 +RK2A+RK2B+RK2C +RK3 -RK3*RKM3/DENOMISO )
6370  RADA=0:RADAS=0:RADADA=0:RADADB=0: RIS=0:RIDAS=0:RIDAD=0:RIDB=0
6380  RADBS=0:RADB1D2S=0:RADB1S2D=0:RADB1D2D=0:RADB1S2DD=0:RADB1D2DD=0
6390  RADC=0: RADCS=0:RADCD=0: RADCDS=0:RADCDD=0: RADCDDS=0:RADCDDD=0
6400  RAS=EXP( LOG(F(N)) +RK1LOG +LOG(DEACT) -DENOM)
6410  DENISO=RKM3+RK4A+RK4B '*k0 contribution
6420  IF DENISO=0 THEN TERMISO=0 ELSE TERMISO=RK3*RKM3/DENISO
6430  DENISOM=LOG(RKM1 +RK2A+RK2B+RK2C +RK3 -TERMISO)
6440  RK0=EXP( LOG(F(N)) +RK1LOG +LOG(XLAM*KCOLL!) -DENISOM)
6450  IF RK2A=0 THEN GOTO 6500
6460  RADA=EXP( LOG(F(N)) +RK1LOG +LOG(RK2A) -DENOM)
6470  IF RK2ADA=0 AND RK2ADB=0 THEN RADAS=RADA: GOTO 6500
6480  DENOMA=DEACT2A+RK2ADA+RK2ADB: RADAS=RADA*DEACT2A/DENOMA
6490  RADADA=RADA*RK2ADA/DENOMA: RADADB=RADA*RK2ADB/DENOMA
6500  IF RK2B=0 THEN GOTO 6590
6510  RADBS=EXP( LOG(F(N)) +RK1LOG +LOG(RK2B) -DENOM): RADB1S2D=RADBS*F1S2D
6520  RADB1D2S=RADBS*F1D2S: RADB1D2D=RADBS*F1D2D: RADBS=RADBS*FS
6530  IF F1S2D=0 THEN GOTO 6560
6540  DB2D=DEACT2B2D+RK2B2DD
6550  RADB1S2DD=RADB1S2D*RK2B2DD/DB2D: RADB1S2D=RADB1S2D*DEACT2B2D/DB2D
6560  IF F1D2D=0 THEN GOTO 6590
6570  DB2D=DEACT2B2D+RK2B2DD
6580  RADB1D2DD=RADB1D2D*RK2B2DD/DB2D: RADB1D2D=RADB1D2D*DEACT2B2D/DB2D
6590  IF RK2C=0 THEN GOTO 6690
6600  RADC=EXP( LOG(F(N)) +RK1LOG +LOG(RK2C) -DENOM)
6610  IF RK2CD=0 THEN RADCS=RADC: GOTO 6690
6620  DENOMC=DEACT2C+RK2CD: RADCS=RADC*DEACT2C/DENOMC: RADCD=RADC*RK2CD/DENOMC
6630  IF RK2CDD=0 OR RADCD=0 THEN RADCDS=RACD: GOTO 6690
6640  DENOMCD=DEACT2CD+RK2CDD
6650  RADCDS=RACD*DEACT2CD/DENOMCD: RADCDD=RACD*RK2CDD/DENOMCD
6660  IF RK2CDDD=0 OR RADCDD=0 THEN RADCDDS=RACDD: GOTO 6690
6670  DENOMCDD=DEACT2CDD+RK2CDDD
6680  RADCDDS=RACDD*DEACT2CDD/DENOMCDD: RADCDDD=RACDD*RK2CDDD/DENOMCDD
6690  IF RK3=0 THEN GOTO 6770
6700  RIS=EXP( LOG(F(N))+RK1LOG-DENOM +LOG(DEACT*RK3/DENOMISO) )
6710  IF RK4A=0 THEN GOTO 6750
6720  RIDAS=EXP( LOG(F(N))+RK1LOG-DENOM +LOG(RK4A*RK3/DENOMISO) )
6730  IF RK4AD=0 THEN GOTO 6750
6740  DNMIA=DEACTIA+RK4AD:RIDAD=RIDAS*RK4AD/DNMIA:RIDAS=RIDAS*DEACTIA/DNMIA
6750  IF RK4B=0 THEN GOTO 6770
6760  RIDB=EXP( LOG(F(N))+RK1LOG-DENOM +LOG(RK4B*RK3/DENOMISO) )
6770  TOTAS=TOTAS+RAS: TOTKO=TOTKO+RK0: TOTADAS=TOTADAS+RADAS
6780  TOTADADA=TOTADADA+RADADA: TOTADADB=TOTADADB+RADADB
6790  TOTADBS=TOTADBS+RADBS: TOTADB1S2D=TOTADB1S2D+RADB1S2D
6800  TOTADB1D2S=TOTADB1D2S+RADB1D2S: TOTADB1D2D=TOTADB1D2D+RADB1D2D
6810  TOTADB1S2DD=TOTADB1S2DD+RADB1S2DD: TOTADB1D2DD=TOTADB1D2DD+RADB1D2DD
6820  TOTADCS=TOTADCS+RADCS: TOTADCDS=TOTADCDS+RADCDS
6830  TOTADCDDS=TOTADCDDS+RADCDDS: TOTADCDDD=TOTADCDDD+RADCDDD
6840  TOTIS=TOTIS+RIS: TOTIDAS=TOTIDAS+RIDAS: TOTIDAD=TOTIDAD+RIDAD
6850  TOTIDB=TOTIDB+RIDB: INDX=N-MM1: IF IOUT THEN GOTO 7010
6860  IF RKM1=0 THEN P1=0 ELSE P1=FNALOG10(RKM1)
6870  IF RK2A=0 THEN P2=0 ELSE P2=FNALOG10(RK2A)

```

```

6880 IF RK2ADA=0 THEN P3=0 ELSE P3=FNALOG10(RK2ADA)
6890 IF RK2ADB=0 THEN P4=0 ELSE P4=FNALOG10(RK2ADB)
6900 IF RK2C=0 THEN P5=0 ELSE P5=FNALOG10(RK2C)
6910 IF RK2CD=0 THEN P6=0 ELSE P6=FNALOG10(RK2CD)
6920 IF RK2CDD=0 THEN P7=0 ELSE P7=FNALOG10(RK2CDD)
6930 IF RK2CDDD=0 THEN P8=0 ELSE P8=FNALOG10(RK2CDDD)
6940 IF RK3=0 THEN P9=0 ELSE P9=FNALOG10(RK3)
6950 IF RKM3=0 THEN P10=0 ELSE P10=FNALOG10(RKM3)
6960 IF RK4A=0 THEN P11=0 ELSE P11=FNALOG10(RK4A)
6970 IF RK4AD=0 THEN P12=0 ELSE P12=FNALOG10(RK4AD)
6980 IF RK4B=0 THEN P13=0 ELSE P13=FNALOG10(RK4B)
6990 PRINT USING TBLE$;INDX,F(N),P1,P2,P3,P4,P5,P6,P7,P8,P9,P10,P11,P12,P13
7000 IF IFILE THEN PRINT #2,USING TBLE$;INDX,F(N),P1,P2,P3,P4,P5,P6,P7,P8,P9,
P10,P11,P12,P13
7010 IF F(N)>.001 THEN IDIST=1: GOTO 7030
7020 IF IDIST AND F(N)<1E-10 THEN GOTO 7040 '**Jump out?
7030 NEXT N
7040 IF IOUT THEN GOTO 7210
7050 RATIOA=EXP( LOG(TOTAS)-RK1LOG )
7060 PRINT USING KASFORM$; TOTAS,RATIOA,TOTKO
7070 PRINT USING KADAFORM$;TOTADAS,TOTADADA,TOTADADB
7080 PRINT USING KADBFORM$;TOTADBS,TOTADB1D2S,TOTADB1S2D
7090 PRINT USING KADBFM$;TOTAD1D2D,TOTADB1S2DD,TOTADB1D2DD
7100 PRINT USING KADCFORM$;TOTADCS,TOTADCDS,TOTADCDDS
7110 PRINT USING KISFORM$; TOTADCDDD,TOTIS
7120 PRINT USING KIDAFORM$;TOTIDAS,TOTIDAD,TOTIDB
7130 IF IFILE=0 THEN GOTO 7210
7140 PRINT #2,USING KASFORM$; TOTAS,RATIOA,TOTKO
7150 PRINT #2,USING KADAFORM$;TOTADAS,TOTADADA,TOTADADB
7160 PRINT #2,USING KADBFORM$;TOTADBS,TOTADB1D2S,TOTADB1S2D
7170 PRINT #2,USING KADBFM$;TOTAD1D2D,TOTADB1S2DD,TOTADB1D2DD
7180 PRINT #2,USING KADCFORM$;TOTADCS,TOTADCDS,TOTADCDDS
7190 PRINT #2,USING KISFORM$; TOTADCDDD,TOTIS
7200 PRINT #2,USING KIDAFORM$;TOTIDAS,TOTIDAD,TOTIDB
7210 ICOUNT=ICOUNT+1: X(1,ICOUNT)=1!/T: X(2,ICOUNT)=P '**Store results
7220 Y(1,ICOUNT)=TOTAS: Y(2,ICOUNT)=TOTADAS: Y(3,ICOUNT)=TOTADADA
7230 Y(4,ICOUNT)=TOTADADB: Y(5,ICOUNT)=TOTADBS: Y(6,ICOUNT)=TOTADB1D2S
7240 Y(7,ICOUNT)=TOTADB1S2D: Y(8,ICOUNT)=TOTADB1D2D: Y(9,ICOUNT)=TOTADB1S2DD
7250 Y(10,ICOUNT)=TOTADB1D2DD:Y(11,ICOUNT)=TOTADCS: Y(12,ICOUNT)=TOTADCDS
7260 Y(13,ICOUNT)=TOTADCDDS: Y(14,ICOUNT)=TOTADCDDD: Y(15,ICOUNT)=TOTIS
7270 Y(16,ICOUNT)=TOTIDAS: Y(17,ICOUNT)=TOTIDAD: Y(18,ICOUNT)=TOTIDBS
7280 Y(19,ICOUNT)=TOTAS*82.1*T/P: Y(20,ICOUNT)=TOTKO: Y(21,ICOUNT)=0
7290 FOR KT=1 TO 18: Y(21,ICOUNT)=Y(21,ICOUNT)+Y(KT,ICOUNT): NEXT
7300 Y(24,ICOUNT)=EXP(RK1LOG): Y(22,ICOUNT)=TOTAS/Y(24,ICOUNT)
7310 IF RABSLOG>-85 THEN Y(25,ICOUNT)=EXP(RABSLOG) ELSE Y(25,ICOUNT)=0!
7320 Y(21,ICOUNT)=Y(21,ICOUNT)+Y(25,ICOUNT)
7330 Y(23,ICOUNT)= (1+ LOG( TOTKO*P/(82.05*T*EXP(RK1LOG)) )^2)
7340 Y(23,ICOUNT)= (TOTAS*( 82.05*T/(TOTKO*P) +1/EXP(RK1LOG) ))^Y(23,ICOUNT)
7350 T=T+TSTEP
7360 IF T<THIGH AND TSTEP<0 THEN GOTO 4560
7370 IF P*PFAC<-PHIGH AND TSTEP=0 THEN P=P*PFAC: GOTO 4560
7380 IF IFILE=0 THEN GOTO 7520 '**Summary output
7390 PRINT #2,NADA$: PRINT #2, USING U1$;RP$,IDCOLL$,RXN$(1),RXN$(25)
7400 PRINT #2, USING U2$;RXN$(2),RXN$(3),RXN$(4)

```

```

7410 PRINT #2, USING U3$;RXN$(5),RXN$(6),RXN$(7)
7420 PRINT #2, USING U4$;RXN$(8),RXN$(9),RXN$(10)
7430 PRINT #2, USING U5$;RXN$(11),RXN$(12),RXN$(13),RXN$(14)
7440 PRINT #2, USING U6$;RXN$(15),RXN$(16),RXN$(17),RXN$(18): PRINT #2, THDFORM$
7450 FOR II=1 TO ICOUNT
7460   FOR KT=1 TO 21
7470     IF Y(KT,II) THEN YT(KT)=FNALOG10(Y(KT,II)) ELSE YT(KT)=0
7480     NEXT
7490   IF Y(25,II) THEN YT(25)=FNALOG10(Y(25,II)) ELSE YT(25)=0
7500   PRINT #2,USING TBLFORM$;1!/X(1,II),X(2,II),YT(1),YT(2),YT(3),YT(4),YT(5),
     YT(11),YT(15),YT(16),YT(18),YT(25),YT(21),Y(22,II)
7510   NEXT
7520 PRINT NADA$: PRINT USING U1$;RP$,IDCOLL$,RXN$(1),RXN$(25)
7530 PRINT USING U2$;RXN$(2),RXN$(3),RXN$(4)
7540 PRINT USING U3$;RXN$(5),RXN$(6),RXN$(7)
7550 PRINT USING U4$;RXN$(8),RXN$(9),RXN$(10)
7560 PRINT USING U5$;RXN$(11),RXN$(12),RXN$(13),RXN$(14)
7570 PRINT USING U6$;RXN$(15),RXN$(16),RXN$(17),RXN$(18): PRINT THDFORM$
7580 FOR II=1 TO ICOUNT
7590   FOR KT=1 TO 21
7600     IF Y(KT,II) THEN YT(KT)=FNALOG10(Y(KT,II)) ELSE YT(KT)=0
7610     NEXT
7620   IF Y(25,II) THEN YT(25)=FNALOG10(Y(25,II)) ELSE YT(25)=0
7630   PRINT USING TBLFORM$;1!/X(1,II),X(2,II),YT(1),YT(2),YT(3),YT(4),YT(5),
     YT(11),YT(15),YT(16),YT(18),YT(25),YT(21),Y(22,II)
7640   NEXT
7650 PRINT" kAS[1],kADa[2],kADaDa[3],kADaDb[4],kADb[5],kADb1D2S[6],kADb1S2D[7],
     kADb1D2D[8], "
7660 PRINT" kADb1S2DD[9],kADb1D2DD[10],kADc[11],kADcD[12],kADcDD[13],
     kADcDDD[14], kIS[15], "
7670 INPUT" kIDa[16],kIDaD[17],kIDb[18],k/[M][19],k0[20],kTOT[21],k/kINF[22],
     Sumry[26]";IFIT
7680 IF IFIT>25 THEN GOTO 7520
7690 N1=1: N=ICOUNT: IF IFIT<=0 THEN GOTO 7740 'ELSE new case
7700   IF PLOW=PHIGH OR PFAC=0 THEN ICOUNT=0: GOTO 1270
7710   IF P*PFAC>PHIGH THEN ICOUNT=0: GOTO 1270
7720   P=P*PFAC: IF THIGH<TLOW+TSTEP OR TSTEP=0 THEN T=TLOW: GOTO 4560 'Fall-off
7730   ICOUNT=0: T=TLOW: GOTO 4560
7740 IF N>3 THEN GOTO 7770
7750 PRINT:PRINT "Fewer points than 4 - too few to be fitted.": GOSUB 9990
7760 GOTO 7650
7770 IF X(2,1)<X(2,N) THEN IPLTP=1: GOTO 7820
7780 IF TSTEP<=0 AND THIGH=>(TLOW+TSTEP) THEN GOTO 7820
7790 GOSUB 9990
7800 PRINT "Strike any key to plot.": GOSUB 10260
7810 GOTO 7650
7820 FOR I=1 TO N: XX(I)=LOG(1/X(1,I)): YY(I)=X(1,I)
7830 IF IPLTP THEN YY(I)=FNALOG10(X(2,I))
7840 IF Y(IFIT,I)=0 THEN N1=N1+1 ELSE ZZ(I)=LOG(Y(IFIT,I))
7850 NEXT
7860 IF (N1+3)>N THEN GOTO 7750
7870 IF IPLTP OR IFIT>20 THEN GOSUB 9990 ELSE GOTO 7900
7880 PRINT "Strike any key to plot.": GOSUB 10260
7890 GOTO 8310

```

```

7900 PRINT: PRINT USING HEADERFORM$;KFORM$(IFIT),P
7910 IF IFILE THEN PRINT #2,"": PRINT #2,USING HEADERFORM$;KFORM$(IFIT),P
7920 NDIF=N-N1+1: SX2=0: SX=0: SY2=0: SY=0: SKY=0: SYZ=0: SZ=0: SXZ=0: SZ2=0
7930 FOR I=N1 TO N
7940 SX2=SX2+XX(I)*XX(I): SX =SX +XX(I): SY2=SY2+YY(I)*YY(I)
7950 SY =SY +YY(I): SKY=SKY+XX(I)*YY(I): SYZ=SYZ+YY(I)*ZZ(I)
7960 SZ =SZ +ZZ(I): SXZ=SXZ+XX(I)*ZZ(I): SZ2=SZ2+ZZ(I)*ZZ(I): NEXT
7970 AA=(NDIF*SX2-SX*SX)*(NDIF*SYZ-SY*SZ):BB=(NDIF*SKY-SX*SY)*(NDIF*SXZ-SX*SZ)
7980 C=(AA-BB)/((NDIF*SX2-SX*SX)*(NDIF*SY2-SY*SY)-(NDIF*SKY-SX*SY)^2)
7990 B=(NDIF*SXZ-SX*SZ) -C*(NDIF*SKY-SX*SY) /(NDIF*SX2-SX*SX)
8000 A=(SZ-C*SY-B*SX)/NDIF
8010 R2=(A*SZ +B*SXZ +C*SYZ -SZ*SZ/NDIF) /(SZ2-SZ*SZ/NDIF)
8020 C1=(SYZ-SY*SZ/NDIF) /(SY2-SY*SY/NDIF): Q1=(SZ - C1*SY)/NDIF
8030 PRINT PHEADFORM$: IF IFILE THEN PRINT #2,PHEADFORM$
8040 FOR I=N1 TO N: T=1/YY(I): K!=EXP(ZZ(I))
8050 PRED(I)=A+B*XX(I)+C*YY(I): PRD1(I)=Q1+C1*YY(I)
8060 IF PRED(I)<87 THEN KPRED!=EXP(PRED(I)) ELSE KPRED!=E38
8070 IF PRD1(I)<87 THEN KPRD1!=EXP(PRD1(I)) ELSE KPRD1!=E38
8080 IF PRED(I)<(ELOG9+ZZ(I)) THEN PD=(KPRED!-K!)/K!*100! ELSE PD=999.99
8090 IF PRD1(I)<(ELOG9+ZZ(I)) THEN PD1=(KPRD1!-K!)/K!*100! ELSE PD1=999.99
8100 PRINT USING ZFORM$;T,K!,KPRED!,PD,KPRD1!,PD1
8110 IF IFILE THEN PRINT #2, USING ZFORM$;T,K!,KPRED!,PD,KPRD1!,PD1
8120 NEXT
8130 PRINT USING" Z= "+V$+" _ + "+V$+"*X _ + "+V$+"*Y; R^2=+#.#####";A,B,C,R2
8140 IF A>88 THEN PRINT USING" k= 10_^(+##.###)*T_^( "+V$+
")*exp(_ - #####.###/RT)";A/ELOG10,B,-C*R/1000: GOTO 8160
8150 PRINT USING" k= "+V$+" *T_^( "+V$+)*exp(_ - #####.###/RT)";EXP(A),B,-C*R/1000
8160 IF Q1<88 THEN GOTO 8190
8170 PRINT USING" or k= 10_^(+##.###)*exp(_ - #####.###/RT)";Q1/ELOG10,-C1*R/1000
8180 GOTO 8200
8190 PRINT USING" or k= "+V$+" *exp(_ - #####.###/RT)";EXP(Q1),-C1*R/1000
8200 IF IFILE=0 THEN GOTO 8280
8210 PRINT #2, USING" Z= "+V$+" _ + "+V$+"*X _ + "+V$+"*Y; R^2=+#.#####";A,B,C,R2
8220 IF A>88 THEN PRINT #2, USING" k= 10_^(+##.###)*T_^( "+V$+
")*exp(_ - #####.###/RT)";A/ELOG10,B,-C*R/1000: GOTO 8240
8230 PRINT #2, USING" k= "+V$+" *T_^( "+V$+)*exp(_ - #####.###/RT)";
EXP(A),B,-C*R/1000
8240 IF Q1<88 THEN GOTO 8270
8250 PRINT #2, USING" or k= 10_^(+##.###)*exp(_ - #####.###/RT)";
Q1/ELOG10,-C1*R/1000
8260 GOTO 8280
8270 PRINT #2, USING" or k= "+V$+" *exp(_ - #####.###/RT)";EXP(Q1),-C1*R/1000
8280 PRINT "Plot results (Y/N)? [Then type X to leave plot.] ";: GOSUB 10260
8290 IF K$="Y" OR K$="y" THEN PRINT Y$: GOTO 8310
8300 IF K$="N" OR K$="n" THEN PRINT N$: GOTO 8350 ELSE GOTO 8280
8310 GOSUB 9350
8320 GOSUB 10260
8330 IF K$="X" OR K$="x" THEN GOTO 8340 ELSE GOTO 8320
8340 IPLTP=0: SCREEN 0: COLOR 0,6,2: CLS
8350 GOTO 7650
8360 REM***** End of main program ***** Begin subroutines *****
8370 UFLOWFAC=UFLOWFAC-10!: RETURN 5020
8380 UFLOWFAC=UFLOWFAC+10!: RETURN 5020
8390 EKT=ECOLL/(1.15*R*T): XLAM0=.1 'Newton's method sol'n for coll'n efficy.

```

```

8400 XLAM=XLAM0 - (XLAM0-EKT*(1-SQR(XLAM0)))/(1+.5*EKT/SQR(XLAM0))
8410 IF ABS(XLAM-XLAM0)<.0005 THEN RETURN ELSE XLAM0=XLAM: GOTO 8400
8420 REM*****Given a third-body gas's name, use these input parameters:
8430 IF IDCOLL$="Ar" THEN XM2=39.944: SIGMA2=3.33: EK2=136.5:ECOLL=740: RETURN
8440 IF IDCOLL$="He" THEN XM2=4.0026: SIGMA2=2.576: EK2=10.2: ECOLL=470: RETURN
8450 IF IDCOLL$="H2" THEN XM2=2.0014: SIGMA2=2.92: EK2=38!: ECOLL=610: RETURN
8460 IF IDCOLL$="N2" THEN XM2=28.01: SIGMA2=3.621: EK2=97.53:ECOLL=980: RETURN
8470 IF IDCOLL$="CO" THEN XM2=28.01: SIGMA2=3.65: EK2=98.1: ECOLL=1200:RETURN
8480 IF IDCOLL$="O2" THEN XM2=32!: SIGMA2=3.458: EK2=107.4:ECOLL=1100:RETURN
8490 IF IDCOLL$="CO2" THEN XM2=44.01: SIGMA2=3.763: EK2=244!: ECOLL=2400:RETURN
8500 IF IDCOLL$="CH4" THEN XM2=16.01: SIGMA2=3.746: EK2=141.4:ECOLL=2300:RETURN
8510 IF IDCOLL$="C2H6" THEN XM2=30.01:SIGMA2=4.302: EK2=252.3:ECOLL=4100:RETURN
8520 PRINT "Third-body data required...": IFLAG=1: RETURN
8530 NADA$="": OKFORM$=" Ok? (Y/N, def=N) ": Y$="Yes": N$="No" 'Text formats
8540 TPFORM$="T-####.# to ####.# by ####.# K, P-####.### to ####.### atm"
8550 V$="+#.#^####": TOKFORM$=" Use or Quit (Y/N/Q,def=N)? "
8560 QXS$="Quantum number greater than 99; use 99 ..."
8570 ASTFORM$= " (AS) Add'n/stabil'n reaction product: "
8580 DECFORM$= " (AD) Add'n/decomp'n to new products: "
8590 DDFRM$= " (ADD) Secndry decomp'n to new products: "
8600 TERTFRM$= " (ADDD) Tertiary decomp to new products: "
8610 QUARFRM$= " (ADDDD) 4th-ordr decmp to new products: "
8620 ISOFORM$= " (IS) Isomeriz'n/stabil'n product: "
8630 IDECFORM$=" (ID) Isomeriz'n/dissoc'n rxn products: "
8640 ABSFORM$= " (ABS) Abstraction reaction products: "
8650 ENTRY$(1) ="Enter addition product: "
8660 ENTRY$(2) ="Enter decomp'n products (a): "
8670 ENTRY$(3) =" Enter secndry decomp'n aa: "
8680 ENTRY$(4) =" Enter secndry decomp'n ab: "
8690 ENTRY$(5) ="Enter decomp'n products (b): "
8700 ENTRY$(6) =" Enter sec decmp of prod b1: "
8710 ENTRY$(7) =" Enter sec decmp of prod b2: "
8720 ENTRY$(8) =" Enter sec decmp of b1 & b2: "
8730 ENTRY$(9) =" Enter b1 & tert dcmp of b2: "
8740 ENTRY$(10) =" Enter complete dcmp, b1&b2: "
8750 ENTRY$(11) ="Enter decomp'n products (c): "
8760 ENTRY$(12) =" Enter secondary decomp'n: "
8770 ENTRY$(13) =" Enter tertiary decomp'n: "
8780 ENTRY$(14) =" Enter 4th-order decomp'n: "
8790 ENTRY$(15) ="Enter isom/stabil'n product: ": ENTRY$(17)=ENTRY$(12)
8800 ENTRY$(16) ="Enter isom/decomp prods (a): "
8810 ENTRY$(18) ="Enter isom/decomp prods (b): "
8820 KINFM$="High-pressure k(addition)= "+V$+" *T^#### *EXP(-####.##/RT)"
8830 FFORM$= "Mean freq of adduct= #####. wavenumbers,S=##### oscillators"
8840 FSFORM$="Product*: Freq=#####;S=#### oscillators,E(vs adduct)=###.## kcal"
8850 SPFORM$= "Complex: MW= ###.##, Diameter("+CHR$(229)+
")=##.### angstroms, Well ("+CHR$(238)+"/K)=####.##"
8860 SPSFORM$="Prodct*: MW= ###.##, Diameter("+CHR$(229)+
")=##.### angstroms, Well ("+CHR$(238)+"/K)=####.##"
8870 ESPFORM$= "Enter MW (amu), "+CHR$(229)+" (angstroms), and "+CHR$(238)+
" (K) for "
8880 ESPFORM$=ESPFORM$+"prodct*": ESPFORM$=ESPFORM$+"complex:"
8890 IDFORM$="Bath gas &": AE$=" "+V$+"",#####.##"
8900 COLLFORM$=" MW= ###.##, "+CHR$(229)+"=##.###, "+CHR$(238)

```

```

8910 COLFORM$=COLFORM$+"/K-####.##, E(coll)=####."
8920 AMLFORM$="A and barrier: dissoc'n to reactnts "+AE$
8930 A2FORM$="A and barrier for decomp'n of adduct"+AE$
8940 ADFORM$="A and barrier for secondary decomp'n "+AE$
8950 ATFORM$="A and barrier for tertiary decomp'n "+AE$
8960 AQFORM$="A and barrier for 4th-ordr decomp'n "+AE$
8970 A3FORM$="A and barrier for isomer'n of adduct"+AE$
8980 AM3FORM$="A and barrier for reverse isomeriz'n"+AE$
8990 DELFORM$="E(isomer)-E(adduct) = ####.##, Isomer freq= ####. wavenumbers"
9000 A4FORM$="A and barrier for decomp'n of isomer= +#.###^,####.##"
9010 RABFORM$="Abstr'n rate constant= +#.###^ *T_### *EXP(-###.##/RT)"
9020 HEADERFORM$="&; P = +#.###^ atm"
9030 PFORM$=" T= ####.## K P=+#.###^ atm"
9040 HPKFORM$=" k(add'n,hi-P limit)= +#.###^"
9050 KABSFORM$=" k(abstr'n)= "+V$
9060 DKFORM$=" kDEACT*{&}= "+V$+ " Beta=#.####"
9070 TBLES$="### +#.##^ ##.# ##.# ##.# ##.# ##.# ##.# ##.# ##.# ##.# "
9080 TBLES$= TBLES$+ "##.# ##.# ##.# ##.#"
9090 HEADING$=" Dist'n Log:k(-A) Da Daa Dab Dc DcD DcDD DcDDD I "
9100 HEADING$=HEADING$+ "-I IDa IDaa IDb"
9110 TBLFORM$="#####. +#.##^ ##.# ##.# ##.# ##.# ##.# ##.# ##.# ##.# "
9120 TBLFORM$=TBLFORM$+"##.# ##.# +#.##^"
9130 THDFORM$=" T(K) P(atm) AS ADa ADaDa ADaDb ADb ADc IS IDa IDb "
9140 THDFORM$=THDFORM$+ "ABS ktot k(AS)/k"+CHR$(236)
9150 KASFORM$=" kAS= "+V$+ " kAS/kINF= "+V$+ " kO= "+V$
9160 KADAFORM$=" kADaS= "+V$+ " kADaDa= "+V$+ " kADaDb = "+V$
9170 KADBFORM$=" kADbS= "+V$+ " kADb1D2S= "+V$+ " kADb1S2D= "+V$
9180 KADBFM$=" kADb1D2D= "+V$+ " kADb1S2DD= "+V$+ " kADb1D2DD= "+V$
9190 KADCFORM$=" kADcS= "+V$+ " kADcD= "+V$+ " kADcDD= "+V$
9200 KISFORM$=" kADcDDD= "+V$+ " kIS= "+V$
9210 KIDAFORM$=" kIDaS= "+V$+ " kIDaD= "+V$+ " kIDb= "+V$
9220 U1$="Reactants:&; M=&; AS:& ABS:&": U2$="ADa:& ADaDa:& ADaDb:&"
9230 U3$="ADb:& ADb1D2S:& ADb1S2D:&": U4$="ADb1D2D:& ADb1S2DD:& ADb1D2DD:&"
9240 U5$="ADc:& ADcD:& ADcDD:& ADcDDD:&": U6$="IS:& IDa:& IDaD:& IDb:&"
9250 PHEADFORM$=" T k Predict'n & Diff. Predict'n & Diff."
9260 ZFORM$="#####. "+V$+ " "+V$+ " +###.## "+V$+ " +###.##"
9270 YFORM$="+###.##": RETURN
9280 KFM$="Fit for ": RR$=R$+RXN$(1) '**Subroutine to set up titles
9290 RXN$(19)="kAS/[M] of "+RR$: RXN$(20)="kO (" +IDCOLL$+" ) of "+RR$
9300 RXN$(21)="overall rxn of "+RP$: RXN$(22)="k/kINF of "+RR$
9310 RXN$(23)="Troee Fc for "+RR$: RXN$(24)="kINF of "+RR$
9320 FOR KF=1 TO 18: KFORM$(KF)=KFM$+R$+RXN$(KF): NEXT
9330 FOR KF=19 TO 24: KFORM$(KF)=KFM$+RXN$(KF): NEXT
9340 KFORM$(25)= KFM$+R$+RXN$(25): RETURN
9350 IF IPLTP THEN GOTO 9420 '*****Plotting subroutine*****
9360 XMIN=0: TEST=1/TLOW: JXFORM$="#.###" 'Plot log k vs 1000/T
9370 IF TEST<=6.000001E-04 THEN XMAX=6.000001E-04: XMIN=.0002: GOTO 9480
9380 IF TEST<=.0008 THEN XMAX=.0008: GOTO 9480
9390 IF TEST<=.0012 THEN XMAX=.0012: GOTO 9480
9400 IF TEST<=.002 THEN XMAX=.002: GOTO 9480
9410 IF TEST<=.004 THEN XMAX=.004: GOTO 9480 ELSE XMAX=8.000001E-03: GOTO 9480
9420 JXFORM$="###.##": XMIN=INT(FNLOG10(PLOW)) 'Plot fall-off curve
9430 XMAX=INT(FNLOG10(PHIGH)+.5): DEL=XMAX-XMIN: XMEAN=.5*(XMIN+XMAX)
9440 IF DEL<=2.1 THEN XMIN=XMEAN-1: XMAX=XMEAN+1: GOTO 9480

```

```

9450 IF DEL<=-4.1 THEN XMIN=XMEAN-2: XMAX=XMEAN+2: GOTO 9480
9460 IF DEL<8.100001 THEN XMIN=XMEAN-4: XMAX=XMEAN+4: GOTO 9480
9470 XMIN=XMEAN-8: XMAX=XMEAN+8
9480 YMIN=E38: YMAX=-E38
9490 FOR I=N1 TO N
9500 IF ZZ(I)>YMAX THEN YMAX=ZZ(I)
9510 IF ZZ(I)<YMIN THEN YMIN=ZZ(I)
9520 NEXT
9530 YMIN=INT(YMIN/LOG(10)): YMAX=INT(YMAX/LOG(10)+1): DEL=YMAX-YMIN
9540 IF DEL<=-1.1 THEN YMIN=YMAX-1: GOTO 9590
9550 IF DEL<=-2.1 THEN YMIN=YMAX-2: GOTO 9590
9560 IF DEL<=-4.1 THEN YMIN=YMAX-4: GOTO 9590
9570 IF DEL<=-8.100001 THEN YMIN=YMAX-8: GOTO 9590
9580 YMIN=YMAX-16
9590 YMIN=YMIN*ELOG10: YMAX=YMAX*ELOG10: NPLT=0 '**Select points:
9600 FOR J=N1 TO N: NPLT=NPLT+1: XPLT(NPLT)=YY(J): YPLT(NPLT)=ZZ(J): NEXT
9610 FOR J=1 TO NPLT: IXPL(J)=639*(XPLT(J)-XMIN)/(XMAX-XMIN)
9620 IYPLT(J)=199-199*(YPLT(J)-YMIN)/(YMAX-YMIN): NEXT
9630 IYZERO=199+199*YMIN/(YMAX-YMIN)
9640 SCREEN 2:CLS:DX=(XMAX-XMIN)/640!:DY=(YMAX-YMIN)/200!
9650 LINE (0,0)-(0,199): LINE -(639,199): LINE -(639,0): LINE -(0,0)
9660 FOR J=10 TO 30 STEP 10: JVERT=16!*J-1 '**Label X-axis
9670 FOR JJ=10 TO 195 STEP 4: PSET (JVERT,JJ): NEXT
9680 JX=J/5*10-1: XES=DX*16!*J+XMIN
9690 IF IPLTP THEN GOTO 9700 ELSE XES=XES*1000
9700 LOCATE 1,JX: PRINT USING JXFORM$;XES;: NEXT
9710 DELY=(YMAX-YMIN)/4!: YLBL(1)=YMIN '**Label Y-axis
9720 FOR J=49 TO 149 STEP 50
9730 FOR JJ=7 TO 631 STEP 8: PSET (JJ,J): NEXT
9740 NEXT
9750 FOR J=2 TO 5: YLBL(J)=YLBL(J-1)+DY*50!: NEXT
9760 FOR J=1 TO 5: YLBL(J)=YLBL(J)/LOG(10): NEXT
9770 FOR J=1 TO 5: IF J<5 THEN LOCATE 1+(J-1)*6,1 ELSE LOCATE 24,1
9780 PRINT USING YFORM$;YLBL(6-J);: LOCATE 1,1: NEXT
9790 FOR J=1 TO NPLT
9800 IF YPLT(J)<YMIN THEN YPLOT(J)=199
9810 IF YPLT(J)>YMAX THEN YPLOT(J)=0
9820 YPLOT(J)=IYPLT(J): NEXT
9830 FOR J=1 TO NPLT '**Plot points
9840 LINE (IXPL(J)-6,YPLOT(J)-3)-(IXPL(J)-6,YPLOT(J)+3)
9850 LINE -(IXPL(J)+6,YPLOT(J)+3): LINE -(IXPL(J)+6,YPLOT(J)-3)
9860 LINE -(IXPL(J)-6,YPLOT(J)-3): PSET (IXPL(J),YPLOT(J)): NEXT J
9870 IF IPLTP THEN LOCATE 17,48: PRINT "log k vs log P (atm) for";: GOTO 9890
9880 LOCATE 17,48: PRINT"Log of k vs 1000/T for"; '**Label graph
9890 LOCATE 18,48: IF IFIT>18 THEN PRINT RXN$(IFIT); ELSE PRINT R$+RXN$(IFIT);
9900 IF IPLTP OR IFIT>21 THEN GOTO 9980
9910 IXPLT1=639*(YY(N1)-XMIN)/(XMAX-XMIN)
9920 KP=199-199*(PRED(N1)-YMIN)/(YMAX-YMIN): PSET (IXPLT1,KP)
9930 FOR I=N1 TO N: IXPLTT=639*(YY(I)-XMIN)/(XMAX-XMIN)
9940 KP=199-199*(PRED(I)-YMIN)/(YMAX-YMIN): LINE -(IXPLTT,KP): NEXT
9950 KP=199-199*(PRD1(N1)-YMIN)/(YMAX-YMIN): PSET (IXPLTT,KP)
9960 FOR I=N1 TO N: IXPLTT=639*(YY(I)-XMIN)/(XMAX-XMIN)
9970 KP=199-199*(PRD1(I)-YMIN)/(YMAX-YMIN): LINE -(IXPLTT,KP): NEXT
9980 RETURN

```

```

9990 PRINT KFORM$(IFIT): PRINT PHEADFORM$
10000 IF IFILE THEN PRINT #2,NADA$: PRINT #2,KFORM$(IFIT):PRINT #2,PHEADFORM$
10010 FOR I=1 TO N
10020 PRINT USING ZFORM$;1/X(1,I),Y(IFIT,I),0,0,0,0
10030 IF IFILE THEN PRINT #2,USING ZFORM$;1/X(1,I),Y(IFIT,I),0,0,0,0
10040 NEXT
10050 RETURN
10060 IF FIRST THEN GOTO 10100 'Subroutine to get freq,S,etc.
10070 PRINT USING FSFORM$;FQ,NSQ,DHS
10080 PRINT USING SPSFORM$;XMS,SIGMAS,EKS: GOSUB 10250
10090 IF K$="Y" OR K$="y" THEN PRINT Y$: GOTO 10130 ELSE PRINT N$
10100 INPUT"Enter freq, S, & E (vs previous level) for PRODS*: ",FQ,NSQ,DHS
10110 INPUT"Also MW, sigma, epsilon/K: ",XMS,SIGMAS,EKS
10120 IF FQ=0 THEN FQ=FREQ
10130 RETURN
10140 SIG=.5*(SSIG+SIGMA2)*1E-08: EK=SQR(EK*EK2) '*Collisional k (Forst, pl85)
10150 REDUCM=XM*XM2/(XM+XM2): F1=8!*8.314E+07*T/(3.14*REDUCM)
10160 KCOLL!=2.708* (EK/T)^.333 *6.02E+23*3.14*SIG*SIG*SQR(F1)
10170 DEAC=XLAM* KCOLL! *P/(82.1*T)
10180 RETURN
10190 REM *****Subr to calc. k(E)= (Ainf) *N!*(N+S-1)!/ (N-M)!*(N-M+S-1)!
10200 PROD1=0!: ISTART=NSUB-MSUB+1: IEND=NSUB '--- Calc. N!/(N-M)!
10210 FOR I=ISTART TO IEND: PROD1=PROD1+LN!(I): NEXT
10220 PROD2=0!: ISTART=NSUB-MSUB+NSSUB: IEND=NSUB+NSSUB-1 '(N-M+S-1)!/(N+S-1)!
10230 FOR I=ISTART TO IEND: PROD2=PROD2+LN!(I): NEXT
10240 KSUB!= EXP( LOG(ASUB)+PROD1-PROD2 ): RETURN
10250 PRINT OKFORM$; '*Subr for responses
10260 K$=NADA$
10270 K$=INKEY$: IF LEN(K$) THEN RETURN ELSE GOTO 10270

```


Appendix L.2. Example of Input Form for Bimolecular ORR

Reaction set for: 1-C4H5 + C2H2

(AS) Add'n/stabil'n reaction product: L-C6H7
 (AD) Add'n/decomp'n to new products: H + L-C6H6
 (ADD) Secndry decomp'n to new products:
 (ADD) Secndry decomp'n to new products:
 (AD) Add'n/decomp'n to new products:
 (ADD) Secndry decomp'n to new products:
 (ADD) Secndry decomp'n to new products:
 (ADD) Secndry decomp'n to new products:
 (ADDD) Tertiary decomp to new products:
 (ADDD) Tertiary decomp to new products:
 (AD) Add'n/decomp'n to new products:
 (ADD) Secndry decomp'n to new products:
 (ADDD) Tertiary decomp to new products:
 (ADDDD) 4th-ordr decmp to new products:
 (IS) Isomeriz'n/stabil'n product: c-C6H7
 (ID) Isomeriz'n/dissoc'n rxn products: H+Benzene
 (ADD) Secndry decomp'n to new products:
 (ID) Isomeriz'n/dissoc'n rxn products:
 (ABS) Abstraction reaction products:

High-pressure $k(\text{addition}) = +2.800\text{E}+02 *T^{\wedge} 2.900 *EXP(- 1.40/RT)$
 Mean freq of adduct= 1050. wavenumbers, S= 33 oscillators
 Complex: MW= 79.00, Diameter(σ)= 5.950 angstroms, Well (ϵ/K)= 400.00
 Bath gas Ar

MW= 39.94, σ = 3.330, ϵ/K = 136.50, E(coll)= 740.
 A and barrier: dissoc'n to reactnts = +4.000E+13, 43.60
 (AD) Add'n/decomp'n to new products: 1-C4H5 + C2H2 - H + L-C6H6
 A and barrier for decomp'n of adduct= +2.000E+13, 40.50
 Product*: Freq=1000;S= 0 oscillators,E(vs adduct)= 0.00 kcal
 Prodct*: MW= 0.00, Diameter(σ)= 0.000 angstroms, Well (ϵ/K)= 0.00
 A and barrier for secundry decomp'n = +0.000E+00, 0.00
 A and barrier for secundry decomp'n = +0.000E+00, 0.00
 (AD) Add'n/decomp'n to new products: **** -
 A and barrier for decomp'n of adduct= +0.000E+00, 0.00
 Product*: Freq=1000;S= 0 oscillators,E(vs adduct)= 0.00 kcal
 Prodct*: MW= 0.00, Diameter(σ)= 0.000 angstroms, Well (ϵ/K)= 0.00
 A and barrier for secundry decomp'n = +0.000E+00, 0.00
 Product*: Freq=1000;S= 0 oscillators,E(vs adduct)= 0.00 kcal
 Prodct*: MW= 0.00, Diameter(σ)= 0.000 angstroms, Well (ϵ/K)= 0.00
 A and barrier for secundry decomp'n = +0.000E+00, 0.00
 Product*: Freq=1000;S= 0 oscillators,E(vs adduct)= 0.00 kcal
 Prodct*: MW= 0.00, Diameter(σ)= 0.000 angstroms, Well (ϵ/K)= 0.00
 A and barrier for tertiary decomp'n = +0.000E+00, 0.00
 (AD) Add'n/decomp'n to new products: **** -
 A and barrier for decomp'n of adduct= +0.000E+00, 0.00
 Product*: Freq=1000;S= 0 oscillators,E(vs adduct)= 0.00 kcal
 Prodct*: MW= 0.00, Diameter(σ)= 0.000 angstroms, Well (ϵ/K)= 0.00
 A and barrier for secundry decomp'n = +0.000E+00, 0.00
 Product*: Freq=1000;S= 0 oscillators,E(vs adduct)= 0.00 kcal
 Prodct*: MW= 0.00, Diameter(σ)= 0.000 angstroms, Well (ϵ/K)= 0.00
 A and barrier for tertiary decomp'n = +0.000E+00, 0.00

Product*: Freq=1000;S= 0 oscillators,E(vs adduct)= 0.00 kcal
 Prodct*: MW= 0.00, Diameter(σ)= 0.000 angstroms, Well (ϵ/K)= 0.00
 A and barrier for 4th-ordr decomp'n = +0.000E+00, 0.00
 (IS) Isomeriz'n/stabil'n product: 1-C4H5 + C2H2 - c-C6H7
 A and barrier for isomer'n of adduct= +3.000E+10, 10.00
 A and barrier for reverse isomeriz'n= +2.000E+13, 59.40
 E(isomer)-E(adduct) = -49.40, Isomer freq= 1050. wavenumbers
 (ID) Isomeriz'n/dissoc'n rxn products: 1-C4H5 + C2H2 - H + Benzene
 A and barrier for decomp'n of isomer= +4.000E+13, 29.60
 Product*: Freq=1000;S= 0 oscillators,E(vs adduct)= 0.00 kcal
 Prodct*: MW= 0.00, Diameter(σ)= 0.000 angstroms, Well (ϵ/K)= 0.00
 A and barrier for seondry decomp'n = +0.000E+00, 0.00
 (ID) Isomeriz'n/dissoc'n rxn products: **** -
 A and barrier for decomp'n of isomer= +0.000E+00, 0.00
 (ABS) Abstraction reaction products: **** -
 Abstr'n rate constant= +0.000E+00 *T^ 0.000 *EXP(- 0.00/RT)

Appendix L.3. BASIC Program For Unimolecular QRRK

```
1000 REM Unimolecular QRRK calculation program - P.R. Westmoreland,
1010 REM                                     Dept. Chem. Eng.,MIT, May 1986
1020 REM Program locations:
1030 REM 1220-1380 Set-up
1040 REM           File input           1440-2210
1050 REM           Manual input         2360-3700
1060 REM           T,P,modify data     2220-2350
1070 REM 3710-3820 Begin calc
1080 REM           [Save parameters 3830-4260]
1090 REM 4270-4380 Calc quanta, get collision efficiency
1100 REM 4390-4710 Calc for T; first get k(DEAC)
1110 REM 4790-6210 Calc thermal E-distribn, k's as sum over E
1120 REM 6220-6500 Detailed output, save k's for summary
1130 REM 6440-6880 Print summary
1140 REM 6890-7650 Fit (7210), plot (7590,8450), or convert k to k/kinf, k/[M]
1150 REM Subroutines: Coll effcy 7670; Third-body props 7700; Formats 7810;
1160 REM Keyboard response 8960,9370; kDEAC 9260; k(E) 9310
1170 REM Convert to kUNI/kINF 9420, to kBI-k/[M] 9600, back to kUNI 9780
1180 DEFINT I-N
1190 DIM F(99),X(2,26),Y(21,26),KFORM$(21),XX(26),YY(26),ZZ(26),LN!(200)
1200 DIM YT(21),PRED(26),PRD1(26),ENTRY$(18),RXN$(21),YLBL(5)
1210 DIM XPLT(26),YPLT(26),IXPL(26),IYPLT(26),YPLOT(26)
1220 GOSUB 7810 'Formats
1230 KEY OFF: SCREEN 0: COLOR 0,6,2: CLS
1240 PRINT "Unimolecular QRRK calculation:"
1250 DEF FNALOG10(X)=LOG(X)/ELOG10
1260 ELOG10=LOG(10): E38=9.999999E+37: ELOG9=LOG(9.9999): K$=NADA$
1270 FIRST=1: EMINUS15=1E-15: ICLS=1: PTEST=0: IPLTP=0: R=1.987165
1280 FOR I=1 TO 200: LN!(I)=LOG(I): NEXT
1290 PRINT"New case - Will any results be saved to disk? Quit? (Y/N/Q,def=N) ";
1300 GOSUB 9380
1310 IF K$="Y" OR K$="y" THEN PRINT Y$: ISTO=1 ELSE GOTO 1360
1320 LINE INPUT " Then enter file name: ";FILE2$
1330 IF ICLS THEN OPEN FILE2$ FOR APPEND AS #2:FOLD$=FILE2$:ICLS=0:GOTO 1390
1340 IF ICLS OR FILE2$=FOLD$ THEN GOTO 1390
1350 CLOSE #2: OPEN FILE2$ FOR APPEND AS #2: FOLD$=FILE2$: ICLS=0: GOTO 1390
1360 IF K$="N" OR K$="n" THEN PRINT N$: ISTO=0 ELSE GOTO 1380
1370 IF ICLS THEN GOTO 1390 ELSE CLOSE #2: ICLS=1: GOTO 1390
1380 IF K$="Q" OR K$="q" THEN PRINT "Quit": END ELSE PRINT "?": GOTO 1290
1390 IFILE=0
1400 PRINT"File or Manual input, or Quit (F/M/Q,def=M)? ";: GOSUB 9380
1410 IF K$="Q" OR K$="q" THEN PRINT "Quit": END
1420 IF K$="F" OR K$="f" THEN PRINT"File": GOTO 1440
1430 PRINT"Manual": GOTO 2220
1440 LINE INPUT " Enter file name: ";FILE1$ '### Input from file ###
1450 OPEN FILE1$ FOR INPUT AS #1: LINE INPUT #1,L$:RP$=MID$(L$,19):R$=RP$+" - "
1460 FOR LL=2 TO 18: LINE INPUT #1,L$: RXN$(LL)=MID$(L$,43): NEXT
1470 LINE INPUT #1,L$
1480 LINE INPUT #1,L$: FREQ=VAL(MID$(L$,23,6)): NS= VAL(MID$(L$,44,5))
1490 LINE INPUT #1,L$: XML=VAL(MID$(L$,14,6))
1500 SIGMA1=VAL(MID$(L$,34,6)): EK1=VAL(MID$(L$,64,7))
```

```

1510 LINE INPUT #1,L$:IDCOLL$=MID$(L$,10): LINE INPUT #1,L$
1520 IF IDCOLL$="NEW" OR IDCOLL$="new" THEN GOTO 1580
1530 XMT=VAL(MID$(L$,5,7)): SIGT=VAL(MID$(L$,16,6))
1540 EKT=VAL(MID$(L$,28,7)): ECOLLT=VAL(MID$(L$,45,6))
1550 IF XMT=0 OR SIGT=0 OR EKT=0 OR ECOLLT=0 THEN GOTO 1570
1560 XM2=XMT: SIGMA2=SIGT: EK2=EKT: ECOLL=ECOLLT: GOTO 1600
1570 GOSUB 7710: IF IFLAG THEN 1580 ELSE 1600
1580 IFLAG=0: INPUT "Enter name of bath-gas molecule: ",TIDCOLL$
1590 IF LEN(TIDCOLL$)>1 THEN IDCOLL$=TIDCOLL$
1600 LINE INPUT #1,L$
1610 LINE INPUT #1,L$: AINF2A=VAL(MID$(L$,38,11)): E2A=VAL(MID$(L$,50,7))
1620 LINE INPUT #1,L$: FREQSA=VAL(MID$(L$,16,4)) 'Secondary dec 2a
1630 NSA=VAL(MID$(L$,23,4)): DH2A=VAL(MID$(L$,53,6))
1640 LINE INPUT #1,L$: XMSA=VAL(MID$(L$,14,6))
1650 SIGMASA=VAL(MID$(L$,34,6)): EKSA=VAL(MID$(L$,64,7))
1660 LINE INPUT #1,L$: AINF2ADA=VAL(MID$(L$,38,11)): E2ADA=VAL(MID$(L$,50,7))
1670 LINE INPUT #1,L$: AINF2ADB=VAL(MID$(L$,38,11)): E2ADB=VAL(MID$(L$,50,7))
1680 LINE INPUT #1,L$: IF FREQSA=0 THEN FREQSA=FREQ
1690 LINE INPUT #1,L$: AINF2B=VAL(MID$(L$,38,11)): E2B=VAL(MID$(L$,50,7))
1700 LINE INPUT #1,L$: FREQSB1=VAL(MID$(L$,16,4)): NSB1=VAL(MID$(L$,23,4))'2b1
1710 LINE INPUT #1,L$: XMSB1=VAL(MID$(L$,14,6))
1720 SIGMASB1=VAL(MID$(L$,34,6)): EKSB1=VAL(MID$(L$,64,7))
1730 LINE INPUT #1,L$: AINF2B1D=VAL(MID$(L$,38,11)): E2B1D=VAL(MID$(L$,50,7))
1740 LINE INPUT #1,L$: FREQSB2=VAL(MID$(L$,16,4)) 'Secondary dec 2b2
1750 NSB2=VAL(MID$(L$,23,4)): DH2B12=VAL(MID$(L$,53,6)) 'DH(prods vs adduct)
1760 LINE INPUT #1,L$: XMSB2=VAL(MID$(L$,14,6))
1770 SIGMASB2=VAL(MID$(L$,34,6)): EKSB2=VAL(MID$(L$,64,7))
1780 LINE INPUT #1,L$: AINF2B2D=VAL(MID$(L$,38,11)): E2B2D=VAL(MID$(L$,50,7))
1790 LINE INPUT #1,L$: FRQSB2D=VAL(MID$(L$,16,4)) 'Tert dec 2b2
1800 NSB2D=VAL(MID$(L$,23,4)): DH2B2D=VAL(MID$(L$,53,6)) 'DH(prod2D vs prod12)
1810 LINE INPUT #1,L$: XMSB2D=VAL(MID$(L$,14,6))
1820 SIGSB2D=VAL(MID$(L$,34,6)): EKSB2D=VAL(MID$(L$,64,7))
1830 LINE INPUT #1,L$: AINF2B2DD=VAL(MID$(L$,38,11)): E2B2DD=VAL(MID$(L$,50,7))
1840 IF FREQSB1=0 THEN FREQSB1=FREQ
1850 IF FREQSB2=0 THEN FREQSB2=FREQ
1860 IF FRQSB2D=0 THEN FRQSB2D=FREQ
1870 LINE INPUT #1,L$
1880 LINE INPUT #1,L$: AINF2C=VAL(MID$(L$,38,11)): E2C=VAL(MID$(L$,50,7))
1890 LINE INPUT #1,L$: FREQSC=VAL(MID$(L$,16,4)) 'Secondary decomp 2c
1900 NSC=VAL(MID$(L$,23,4)): DH2C=VAL(MID$(L$,53,6))
1910 LINE INPUT #1,L$: XMSC=VAL(MID$(L$,14,6))
1920 SIGMASC=VAL(MID$(L$,34,6)): EKSC=VAL(MID$(L$,64,7))
1930 LINE INPUT #1,L$: AINF2CD=VAL(MID$(L$,38,11)): E2CD=VAL(MID$(L$,50,7))
1940 LINE INPUT #1,L$: FRQSCD=VAL(MID$(L$,16,4)) 'Tertiary decompn 2c
1950 NSCD=VAL(MID$(L$,23,4)): DH2CD=VAL(MID$(L$,53,6)) 'H2CD-H2C
1960 LINE INPUT #1,L$: XMSCD=VAL(MID$(L$,14,6))
1970 SIGSCD=VAL(MID$(L$,34,6)): EKSCD=VAL(MID$(L$,64,7))
1980 LINE INPUT #1,L$: AINF2CDD=VAL(MID$(L$,38,11)): E2CDD=VAL(MID$(L$,50,7))
1990 LINE INPUT #1,L$: FRQSCDD=VAL(MID$(L$,16,4)) '4th-order decompn 2c
2000 NSCDD=VAL(MID$(L$,23,4)): DH2CDD=VAL(MID$(L$,53,6)) 'H2CDD-H2CD
2010 LINE INPUT #1,L$: XMSCDD=VAL(MID$(L$,14,6))
2020 SIGSCDD=VAL(MID$(L$,34,6)): EKSCDD=VAL(MID$(L$,64,7))
2030 LINE INPUT #1,L$: AINF2CDDD=VAL(MID$(L$,38,11)): E2CDDD=VAL(MID$(L$,50,7))
2040 IF FREQSC=0 THEN FREQSC=FREQ

```

```

2050 IF FRQSCD=0 THEN FRQSCD=FREQ
2060 IF FRQSCDD=0 THEN FRQSCDD=FREQ
2070 LINE INPUT #1,L$
2080 LINE INPUT #1,L$: AINF3=VAL(MID$(L$,38,11)): E3=VAL(MID$(L$,50,7))
2090 LINE INPUT #1,L$: AINFM3=VAL(MID$(L$,38,11)): EM3=VAL(MID$(L$,50,7))
2100 LINE INPUT #1,L$: DELISO= VAL(MID$(L$,23,7)) 'DELISO,FREQI
2110 FREQI=VAL(MID$(L$,45,6)):IF FREQI=0 THEN FREQI=FREQ
2120 LINE INPUT #1,L$
2130 LINE INPUT #1,L$: AINF4A=VAL(MID$(L$,38,11)): E4A=VAL(MID$(L$,50,7))
2140 LINE INPUT #1,L$: FREQIA=VAL(MID$(L$,16,4)) 'Secondary decomp 4a
2150 NSIA=VAL(MID$(L$,23,4)): DHIA=VAL(MID$(L$,53,6))
2160 LINE INPUT #1,L$: XMIA=VAL(MID$(L$,14,6))
2170 SIGMAIA=VAL(MID$(L$,34,6)): EKIA=VAL(MID$(L$,64,7))
2180 LINE INPUT #1,L$: AINF4AD=VAL(MID$(L$,38,11)): E4AD=VAL(MID$(L$,50,7))
2190 LINE INPUT #1,L$: IF FREQIA=0 THEN FREQIA=FREQ
2200 LINE INPUT #1,L$: AINF4B=VAL(MID$(L$,38,11)): E4B=VAL(MID$(L$,50,7))
2210 CLOSE #1: IFLAG=1
2220 PRINT: IF FIRST THEN GOTO 2270 '*****T,P*****
2230 PRINT USING TPFORMS;TLOW,THIGH,TSTEP,PLOW,PHIGH
2240 PRINT TOKFORMS;: GOSUB 9380
2250 IF K$="Y" OR K$="y" THEN PRINT Y$: GOTO 2300
2260 IF K$="Q" OR K$="q" THEN PRINT "Quit": END ELSE PRINT N$
2270 INPUT "Enter Tmin, Tmax, Tstep (K): ",TLOW,THIGH,TSTEP
2280 INPUT "Enter Pmin, Pmax, P factor (atm): ",PLOW,PHIGH,PFAC
2290 IF PFAC=1 THEN PFAC=0
2300 T=TLOW: P=PLOW: IF IFLAG=0 THEN GOTO 2330
2310 GOSUB 7710
2320 IFLAG=0: GOTO 3710
2330 IF FIRST THEN GOTO 2380
2340 PRINT "Other parameters unchanged (Y/N)? ";: GOSUB 9380
2350 IF K$="Y" OR K$="y" THEN PRINT Y$: GOTO 3710 ELSE PRINT N$
2360 PRINT "Reactant: "+RP$;: GOSUB 9370 '***Manual input:
2370 IF K$="Y" OR K$="y" THEN PRINT Y$: GOTO 2390 ELSE PRINT N$
2380 PRINT "Reactant: ";: LINE INPUT RP$
2390 R$=RP$+" - ": IF FIRST THEN GOTO 2490
2400 PRINT DECFORM$+R$+RXN$(2): PRINT DDFRM$+R$+RXN$(3):PRINT DDFRM$+R$+RXN$(4)
2410 PRINT DECFORM$+R$+RXN$(5): PRINT DDFRM$+R$+RXN$(6):PRINT DDFRM$+R$+RXN$(7)
2420 PRINT DDFRM$+R$+RXN$(8): PRINT TERTFRM$+R$+RXN$(9)
2430 PRINT TERTFRM$+R$+RXN$(10): PRINT DECFORM$+R$+RXN$(11)
2440 PRINT DDFRM$+R$+RXN$(12): PRINT TERTFRM$+R$+RXN$(13)
2450 PRINT QUARFRM$+R$+RXN$(14): PRINT ISOFORM$+R$+RXN$(15)
2460 PRINT IDECFORM$+R$+RXN$(16): PRINT DDFRM$+R$+RXN$(17)
2470 PRINT IDECFORM$+R$+RXN$(18): GOSUB 9370
2480 IF K$="Y" OR K$="y" THEN PRINT Y$: GOTO 2520 ELSE PRINT N$
2490 FOR LL=2 TO 18: PRINT ENTRY$(LL);
2500 LINE INPUT TEMP$: IF TEMP$<>RXN$(LL) AND LEN(TEMP$)>1 THEN RXN$(LL)=TEMP$
2510 NEXT
2520 IF FIRST THEN GOTO 2550 '**Freq/S
2530 PRINT USING FFORMS;FREQ,NS: GOSUB 9370
2540 IF K$="Y" OR K$="y" THEN PRINT Y$: GOTO 2560 ELSE PRINT N$
2550 INPUT "Enter freq (1/cm) and # oscillators for reactant: ",FREQ,NS
2560 IF FIRST THEN GOTO 2590 '**Reactant props
2570 PRINT USING SPFORMS;X1,SIGMA1,EK1: GOSUB 9370
2580 IF K$="Y" OR K$="y" THEN PRINT Y$: GOTO 2600 ELSE PRINT N$

```

```

2590 PRINT ESPFORM$;: INPUT " ",XM1,SIGMA1,EK1
2600 IF FIRST THEN GOTO 2640 '**Bath-gas properties
2610 PRINT USING IDFORM$;IDCOLL$: PRINT USING COLLFORM$;XM2,SIGMA2,EK2,ECOLL
2620 GOSUB 9370
2630 IF K$="Y" OR K$="y" THEN PRINT Y$: GOTO 2710 ELSE PRINT N$
2640 INPUT "Choose bath gas (NEW for new properties): ",IDCOLL$
2650 IF IDCOLL$="NEW" OR IDCOLL$="new" THEN GOTO 2680
2660 GOSUB 7710: IF IFLAG=1 THEN GOTO 2610
2670 GOTO 2710
2680 INPUT "Enter name of bath-gas molecule: ",IDCOLL$
2690 PRINT " Enter MW, "+CHR$(229)+", "+CHR$(238)+"/K, coll'n energy (cal):";
2700 INPUT " ",XM2,SIGMA2,EK2,ECOLL
2710 IF IFLAG THEN IFLAG=0
2720 PRINT: PRINT DECFORM$+R$+RXN$(2) '**(a) A to prods; E between**
2730 IF FIRST THEN GOTO 2760
2740 PRINT USING A2FORM$;AINF2A,E2A: GOSUB 9370
2750 IF K$="Y" OR K$="y" THEN PRINT Y$: GOTO 2770 ELSE PRINT N$
2760 INPUT "Enter A and barrier for decomposition: ", AINF2A,E2A
2770 PRINT DDFRM$+R$+RXN$(3):PRINT DDFRM$+R$+RXN$(4) '**Secondary decomp a-a,b
2780 FQ=FREQSA:NSQ=NSA:DHS=DH2A: XMS=XMSA:SIGMAS=SIGMASA:EKS=EKSA: GOSUB 9180
2790 FREQSA=FQ:NSA=NSQ:DH2A=DHS:XMSA=XMS:SIGMASA=SIGMAS:EKSA=EKS
2800 IF FIRST THEN GOTO 2830 '**A&E, ch. a-a
2810 PRINT USING ADFORM$;AINF2ADA,E2ADA: GOSUB 9370
2820 IF K$="Y" OR K$="y" THEN PRINT Y$: GOTO 2840 ELSE PRINT N$
2830 INPUT "Enter A and barrier for secondary decomp (a-a): ", AINF2ADA,E2ADA
2840 IF FIRST THEN GOTO 2870 '**A&E, ch. a-b
2850 PRINT USING ADFORM$;AINF2ADB,E2ADB: GOSUB 9370
2860 IF K$="Y" OR K$="y" THEN PRINT Y$: GOTO 2880 ELSE PRINT N$
2870 INPUT "Enter A and barrier for secondary decomp (a-b): ", AINF2ADB,E2ADB
2880 PRINT: PRINT DECFORM$+R$+RXN$(5) '**A to prods b; E between**
2890 IF FIRST THEN GOTO 2920
2900 PRINT USING A2FORM$;AINF2B,E2B: GOSUB 9370
2910 IF K$="Y" OR K$="y" THEN PRINT Y$: GOTO 2930 ELSE PRINT N$
2920 INPUT "Enter A and barrier for decomposition: ", AINF2B,E2B
2930 PRINT " Sec decomp of 1st decmp prod:"+R$+RXN$(6):FQ=FREQSB1 '*Sec dec, b1
2940 NSQ=NSB1:DHS=DH2B12: XMS=XMSB1:SIGMAS=SIGMASB1:EKS=EKSB1: GOSUB 9180
2950 FREQSB1=FQ:NSB1=NSQ:DH2B12=DHS:XMSB1=XMS:SIGMASB1=SIGMAS:EKSB1=EKS
2960 IF FIRST THEN GOTO 2990
2970 PRINT USING ADFORM$;AINF2B1D,E2B1D: GOSUB 9370
2980 IF K$="Y" OR K$="y" THEN PRINT Y$: GOTO 3000 ELSE PRINT N$
2990 INPUT "Enter A and barrier for secondary decompn: ",AINF2B1D,E2B1D
3000 PRINT " Sec decomp of 2nd decmp prod:"+R$+RXN$(7):FQ=FREQSB2 '*Sec dec, b2
3010 NSQ=NSB2:DHS=DH2B12: XMS=XMSB2:SIGMAS=SIGMASB2:EKS=EKSB2: GOSUB 9180
3020 FREQSB2=FQ:NSB2=NSQ:DH2B12=DHS:XMSB2=XMS:SIGMASB2=SIGMAS:EKSB2=EKS
3030 IF FIRST THEN GOTO 3060
3040 PRINT USING ADFORM$;AINF2B2D,E2B2D: GOSUB 9370
3050 IF K$="Y" OR K$="y" THEN PRINT Y$: GOTO 3070 ELSE PRINT N$
3060 INPUT "Enter A and barrier for secondary decompn: ",AINF2B2D,E2B2D
3070 PRINT " Tert decomp of 2nd decmp prod:"+R$+RXN$(9):FQ=FRQSB2D'Tert dec,b2D
3080 NSQ=NSB2D:DHS=DH2B2D: XMS=XMSB2D:SIGMAS=SIGSB2D:EKS=EKSB2D:GOSUB 9180
3090 FRQSB2D=FQ:NSB2D=NSQ:DH2B2D=DHS:XMSB2D=XMS:SIGSB2D=SIGMAS:EKSB2D=EKS
3100 IF FIRST THEN GOTO 3130
3110 PRINT USING ATFORM$;AINF2B2DD,E2B2DD: GOSUB 9370
3120 IF K$="Y" OR K$="y" THEN PRINT Y$: GOTO 3140 ELSE PRINT N$

```

```

3130 INPUT "Enter A and barrier for tertiary decompn: ",AINF2B2DD,E2B2DD
3140 PRINT: PRINT DECFORM$+R$+RXN$(11) '**A to prods c; E between**
3150 IF FIRST THEN GOTO 3180
3160 PRINT USING A2FORM$;AINF2C,E2C: GOSUB 9370
3170 IF K$="Y" OR K$="y" THEN PRINT Y$: GOTO 3190 ELSE PRINT N$
3180 INPUT "Enter A and barrier for decomposition: ", AINF2C,E2C
3190 PRINT DDFRM$+R$+RXN$(12) '**Secondary dec, c
3200 FQ=FREQSC:NSQ=NSC:DHS=DH2C: XMS=XMSC:SIGMAS=SIGMASC:EKS=EKSC: GOSUB 9180
3210 FREQSC=FQ: NSC=NSQ: DH2C=DHS: XMSC=XMS: SIGMASC=SIGMAS: EKSC=EKS
3220 IF FIRST THEN GOTO 3250
3230 PRINT USING ADFORM$;AINF2CD,E2CD: GOSUB 9370
3240 IF K$="Y" OR K$="y" THEN PRINT Y$: GOTO 3260 ELSE PRINT N$
3250 INPUT "Enter A and barrier for secondary decompn: ", AINF2CD,E2CD
3260 PRINT TERTFRM$+R$+RXN$(13) '**Tertiary dec, c
3270 FQ=FRQSCD:NSQ=NSCD:DHS=DH2CD:XMS=XMSCD:SIGMAS=SIGSCD:EKS=EKSCD:GOSUB 9180
3280 FRQSCD=FQ: NSCD=NSQ: DH2CD=DHS: XMSCD=XMS: SIGSCD=SIGMAS: EKSCD=EKS
3290 IF FIRST THEN GOTO 3320
3300 PRINT USING ATFORM$;AINF2CDD,E2CDD: GOSUB 9370
3310 IF K$="Y" OR K$="y" THEN PRINT Y$: GOTO 3330 ELSE PRINT N$
3320 INPUT "Enter A and barrier for tertiary decomposition: ", AINF2CDD,E2CDD
3330 PRINT QUARFRM$+R$+RXN$(14): FQ=FRQSCDD '**4th-order dec, c
3340 NSQ=NSCDD:DHS=DH2CDD:XMS=XMSCDD:SIGMAS=SIGSCDD:EKS=EKSCDD:GOSUB 9180
3350 FRQSCDD=FQ: NSCDD=NSQ: DH2CDD=DHS: XMSCDD=XMS: SIGSCDD=SIGMAS: EKSCDD=EKS
3360 IF FIRST THEN GOTO 3390
3370 PRINT USING AQFORM$;AINF2CDDD,E2CDDD: GOSUB 9370
3380 IF K$="Y" OR K$="y" THEN PRINT Y$: GOTO 3400 ELSE PRINT N$
3390 INPUT"Enter A and barrier for 4th-order decomposition: ", AINF2CDDD,E2CDDD
3400 PRINT: PRINT ISOFORM$+R$+RXN$(15)
3410 IF FIRST THEN GOTO 3440 '**A&E to isomer
3420 PRINT USING A3FORM$;AINF3,E3: GOSUB 9370
3430 IF K$="Y" OR K$="y" THEN PRINT Y$: GOTO 3450 ELSE PRINT N$
3440 INPUT"Enter A and barrier for isomeriz'n of adduct: ",AINF3,E3
3450 IF FIRST THEN GOTO 3480 '**A&E from isomer to adduct
3460 PRINT USING AM3FORM$;AINFM3,EM3: GOSUB 9370
3470 IF K$="Y" OR K$="y" THEN PRINT Y$: GOTO 3490 ELSE PRINT N$
3480 INPUT"Enter A and barrier for re-isom'n to adduct: ",AINFM3,EM3
3490 IF FIRST THEN GOTO 3520 '**H(isomer)-H(adduct); freq
3500 PRINT USING DELFORM$;DELISO,FREQI: GOSUB 9370
3510 IF K$="Y" OR K$="y" THEN PRINT Y$: GOTO 3540 ELSE PRINT N$
3520 INPUT"Enter E(isomer)-E(adduct) and mean freq of isomer: ", DELISO,FREQI
3530 IF FREQI=0 THEN FREQI=FREQ
3540 PRINT IDECFORM$+R$+RXN$(16)
3550 IF FIRST THEN GOTO 3580 '**A&E for isomer dec, a
3560 PRINT USING A4FORM$;AINF4A,E4A: GOSUB 9370
3570 IF K$="Y" OR K$="y" THEN PRINT Y$: GOTO 3590 ELSE PRINT N$
3580 INPUT"Enter A & barrier for decomp'n of isomer to products:",AINF4A,E4A
3590 PRINT DDFRM$+R$+RXN$(17) '**Secondary dec
3600 FQ=FREQIA:NSQ=NSIA:DHS=DHIA: XMS=XMIA:SIGMAS=SIGMAIA:EKS=EKIA: GOSUB 9180
3610 FREQIA=FQ: NSIA=NSQ: DHIA=DHS: XMIA=XMS: SIGMAIA=SIGMAS: EKIA=EKS
3620 IF FIRST THEN GOTO 3650
3630 PRINT USING ADFORM$;AINF4AD,E4AD: GOSUB 9370
3640 IF K$="Y" OR K$="y" THEN PRINT Y$: GOTO 3660 ELSE PRINT N$
3650 INPUT "Enter A and barrier for secondary decomposition: ",AINF4AD,E4AD
3660 PRINT IDECFORM$+R$+RXN$(18)

```

```

3670 IF FIRST THEN GOTO 3700 '**A&E for isomer dec, b
3680 PRINT USING A4FORM$;AINF4B,E4B: GOSUB 9370
3690 IF K$="Y" OR K$="y" THEN PRINT Y$: GOTO 3710 ELSE PRINT N$
3700 INPUT"Enter A & barrier for decomp'n of isomer to products:",AINF4B,E4B
3710 PRINT "Detailed output or Summary (D/S)? "; '**Now what?
3720 GOSUB 9380
3730 IF K$="D" OR K$="d" THEN PRINT "Detailed output.": IOUT=0: GOTO 3760
3740 IF K$="S" OR K$="s" THEN PRINT "Summary only.": IOUT=1: GOTO 3760
3750 PRINT "?";: GOTO 3720
3760 IF IFLAG THEN GOSUB 7710
3770 FIRST=0: IF ISTO THEN PRINT "Save to disk, just ";
3780 PRINT "Compute, or Re-enter data (S/C/R)? ";: GOSUB 9380
3790 IF (K$="S" OR K$="s") AND ISTO=1 THEN PRINT "Save": IFILE=1: GOTO 3830
3800 IF K$="C" OR K$="c" THEN PRINT "Begin...": GOTO 4270
3810 IF K$="R" OR K$="r" THEN PRINT "Re-enter ...": GOTO 2230
3820 PRINT "?": GOTO 3770
3830 PRINT #2,"Reaction set for: "+RP$ '**Write to disk
3840 PRINT #2,DECFORM$+RXN$(2)
3850 PRINT #2,DDFRM$+RXN$(3):PRINT #2,DDFRM$+RXN$(4):PRINT #2,DECFORM$+RXN$(5)
3860 PRINT #2,DDFRM$+RXN$(6):PRINT #2,DDFRM$+RXN$(7):PRINT #2,DDFRM$+RXN$(8)
3870 PRINT #2,TERTFRM$+RXN$(9): PRINT #2,TERTFRM$+RXN$(10)
3880 PRINT #2,DECFORM$+RXN$(11): PRINT #2,DDFRM$+RXN$(12)
3890 PRINT #2,TERTFRM$+RXN$(13): PRINT #2,QUARFRM$+RXN$(14)
3900 PRINT #2,ISOFORM$+RXN$(15): PRINT #2,IDECFORM$+RXN$(16)
3910 PRINT #2,DDFRM$+RXN$(17): PRINT #2,IDECFORM$+RXN$(18)
3920 PRINT #2,NADA$
3930 PRINT #2,USING FFORM$;FREQ,NS
3940 PRINT #2,USING SPFORM$;XM1,SIGMA1,EK1: PRINT #2,USING IDFORM$;IDCOLL$
3950 PRINT #2,USING COLLFORM$;XM2,SIGMA2,EK2,ECOLL
3960 PRINT #2," "+DECFORM$+R$+RXN$(2): PRINT #2,USING A2FORM$;AINF2A,E2A
3970 PRINT #2,USING FSFORM$;FREQSA,NSA,DH2A
3980 PRINT #2,USING SPSFORM$;XMSA,SIGMASA,EKSA
3990 PRINT #2,USING ADFORM$;AINF2ADA,E2ADA
4000 PRINT #2,USING ADFORM$;AINF2ADB,E2ADB
4010 PRINT #2," "+DECFORM$+R$+RXN$(5): PRINT #2,USING A2FORM$;AINF2B,E2B
4020 PRINT #2,USING FSFORM$;FREQSB1,NSB1,DH2B12
4030 PRINT #2,USING SPSFORM$;XMSB1,SIGMASB1,EKSB1
4040 PRINT #2,USING ADFORM$;AINF2B1D,E2B1D
4050 PRINT #2,USING FSFORM$;FREQSB2,NSB2,DH2B12
4060 PRINT #2,USING SPSFORM$;XMSB2,SIGMASB2,EKSB2
4070 PRINT #2,USING ADFORM$;AINF2B2D,E2B2D
4080 PRINT #2,USING FSFORM$;FRQSB2D,NSB2D,DH2B2D
4090 PRINT #2,USING SPSFORM$;XMSB2D,SIGSB2D,EKSB2D
4100 PRINT #2,USING ATFORM$;AINF2B2DD,E2B2DD
4110 PRINT #2," "+DECFORM$+R$+RXN$(11)
4120 PRINT #2,USING A2FORM$;AINF2C,E2C: PRINT #2,USING FSFORM$;FREQSC,NSC,DH2C
4130 PRINT #2,USING SPSFORM$;XMSC,SIGMASC,EKSC
4140 PRINT #2,USING ADFORM$;AINF2CD,E2CD
4150 PRINT #2,USING FSFORM$;FRQSCD,NSCD,DH2CD
4160 PRINT #2,USING SPSFORM$;XMSCD,SIGSCD,EKSCD
4170 PRINT #2,USING ATFORM$;AINF2CDD,E2CDD
4180 PRINT #2,USING FSFORM$;FRQCDD,NSCDD,DH2CDD
4190 PRINT #2,USING SPSFORM$;XMSCDD,SIGSCDD,EKSCDD
4200 PRINT #2,USING AQFORM$;AINF2CDDD,E2CDDD:PRINT #2," "+ISOFORM$+R$+RXN$(15)

```



```

4210 PRINT #2,USING A3FORM$;AINF3,E3: PRINT #2,USING AM3FORM$;AINFM3,EM3
4220 PRINT #2,USING DELFORM$;DELISO,FREQI:PRINT #2," "+IDECFORM$+R$+RXN$(16)
4230 PRINT #2,USING A4FORM$;AINF4A,E4A: PRINT #2,USING FSFORM$;FREQIA,NSIA,DHIA
4240 PRINT #2,USING SPSFORM$;XMLA,SIGMAIA,EKIA
4250 PRINT #2,USING ADFORM$;AINF4AD,E4AD: PRINT #2," "+IDECFORM$+R$+RXN$(18)
4260 PRINT #2,USING A4FORM$;AINF4B,E4B
4270 GOSUB 8410 'More formats; then convert E's into quanta:
4280 HC=.002859: QUANTUM=HC*FREQ
4290 MINM=1023
4300 M2A=INT(E2A/QUANTUM+.5): IF M2A>0 AND M2A<MINM THEN MINM=M2A
4310 M2B=INT(E2B/QUANTUM+.5): IF M2B>0 AND M2B<MINM THEN MINM=M2B
4320 M2C=INT(E2C/QUANTUM+.5): IF M2C>0 AND M2C<MINM THEN MINM=M2C
4330 M3 =INT(E3 /QUANTUM+.5): IF M3 >0 AND M3 <MINM THEN MINM=M3
4340 QUANTUMA=HC*FREQSA: QUANTUMB1=HC*FREQSB1: QUANTUMB2=HC*FREQSB2
4350 QUANTUMB2D=HC*FRQSB2D: QUANTUMC=HC*FREQSC: QUANTUMCD=HC*FRQSCD
4360 QCDD=HC*FRQSCDD: QUANTUMI=HC*FREQI: QUANTUMIA=HC*FREQIA
4370 SMIFAC=0!
4380 FOR I=1 TO NS-1: SMIFAC=SMIFAC+LN!(I): NEXT
4390 GOSUB 7670 '**Start for T; Get coll'n efficiency
4400 IF IOUT THEN GOTO 4410 ELSE PRINT: IF IFILE THEN PRINT #2," "
4410 ISTEP=ISTEP+1: SSIG=SIGMA1: EEK=EK1: XXM=XM1: GOSUB 9260
4420 DEACT=DEAC: IF XMSA=0 THEN DEACT2A=0: GOTO 4450
4430 SSIG=SIGMASA: EEK=EKSA: XXM=XMSA: GOSUB 9260
4440 DEACT2A=DEAC
4450 IF AINF2B1D=0 THEN DEACT2B1=0: GOTO 4480
4460 SSIG=SIGMASB1: EEK=EKSB1: XXM=XMSB1: GOSUB 9260
4470 DEACT2B1=DEAC
4480 IF AINF2B2D=0 THEN DEACT2B2=0: GOTO 4510
4490 SSIG=SIGMASB2: EEK=EKSB2: XXM=XMSB2: GOSUB 9260
4500 DEACT2B2=DEAC
4510 IF XMSB2D=0 THEN DEACT2B2D=0: GOTO 4540
4520 SSIG=SIGSB2D: EEK=EKSB2D: XXM=XMSB2D: GOSUB 9260
4530 DEACT2B2D=DEAC
4540 IF XMSC=0 THEN DEACT2C=0: GOTO 4570
4550 SSIG=SIGMASC: EEK=EKSC: XXM=XMSC: GOSUB 9260
4560 DEACT2C=DEAC
4570 IF XMSCD=0 THEN DEACT2CD=0: GOTO 4600
4580 SSIG=SIGSCD: EEK=EKSCD: XXM=XMSCD: GOSUB 9260
4590 DEACT2CD=DEAC
4600 IF XMSCDD=0 THEN DEACT2CDD=0: GOTO 4630
4610 SSIG=SIGSCDD: EEK=EKSCDD: XXM=XMSCDD: GOSUB 9260
4620 DEACT2CDD=DEAC
4630 IF XMIA=0 THEN DEACTIA=0: GOTO 4660
4640 SSIG=SIGMAIA: EEK=EKIA: XXM=XMIA: GOSUB 9260
4650 DEACTIA=DEAC
4660 IP=IP+1: IF IOUT THEN GOTO 4720
4670 PRINT USING PFORM$;T,P
4680 PRINT USING DKFORM$;IDCOLL$,DEACT,XLAM
4690 IF IFILE=0 THEN GOTO 4720
4700 PRINT #2," ": PRINT #2,USING PFORM$;P,T
4710 PRINT #2, USING DKFORM$;IDCOLL$,DEACT,XLAM
4720 NMAX=MINM+99: A=EXP(-1.439*FREQ/T)
4730 TOTADAS=0:TOTADADA=0:TOTADADB=0
4740 TOTADBS=0: TOTADB1D2S=0: TOTADB1S2D=0: TOTADB1D2D=0: TOTADB1S2DD=0

```

```

4750 TOTADB1D2DD=0: TOTADCS=0:TOTADCDS=0:TOTADCDD=0:TOTADCDDD=0
4760 TOTIS=0: TOTIDAS=0:TOTIDAD=0: TOTIDBS=0
4770 IF IOUT THEN GOTO 4790
4780 PRINT HEADING$: IF IFILE THEN PRINT #2, HEADING$
4790 FOR N=MINM TO NMAX
4800 PROD=0!: ISTART=N+1: IEND=N+NS-1      'Thermal dist'n function
4810   FOR I=ISTART TO IEND: PROD=PROD+LN!(I): NEXT
4820   WN= LOG(A)*N +LOG(1-A)*NS +PROD -SM1FAC
4830   IF WN<-85 THEN GOTO 6370
4840 RK2A=0: RK2ADA=0: RK2ADB=0: RK2B=0
4850 FS=0: F1D2S=0: F1S2D=0: F1D2D=0: RK2B2DD=0: RK2C=0: RK2CD=0: RK2CDD=0
4860 IF M2A=0 OR N<M2A THEN GOTO 4970      '**Calc k(E),2A
4870   NSUB=N: MSUB=M2A: NSSUB=NS: ASUB=AINF2A: GOSUB 9320
4880   RK2A=KSUB! '*Secdry dec? Dissipate energy (N-M2A)
4890   IF AINF2ADA=0 AND AINFADB=0 THEN GOTO 4970
4900   QS= (N*QUANTUM - DH2A)/QUANTUMA: N2=INT(QS +.5): IF QS<0 THEN 4970
4910   MSUB=INT(E2ADA/QUANTUMA+.5): NSUB=N2:NSSUB=NSA:ASUB=AINF2ADA '**k(E),a-a
4920   IF AINF2ADA=0 OR N2<MSUB THEN GOTO 4940 ELSE GOSUB 9320
4930   RK2ADA=KSUB!
4940   MSUB=INT(E2ADB/QUANTUMA+.5): NSUB=N2:NSSUB=NSA:ASUB=AINF2ADB '**k(E),a-b
4950   IF AINF2ADB=0 OR N2<MSUB THEN GOTO 4970 ELSE GOSUB 9320
4960   RK2ADB=KSUB!
4970 IF M2B=0 OR N<M2B THEN GOTO 5340      '**Calc k(E),2b
4980   NSUB=N: MSUB=M2B: NSSUB=NS: ASUB=AINF2B: GOSUB 9320
4990   RK2B=KSUB! '*Sec dec? Dissipate energy (N-M2B):
5000   F1S=1: F2S=1: IF AINF2B1D=0 AND AINF2B2D=0 THEN GOTO 5250
5010   EXS=N*QUANTUM-DH2B12: IF EXS<0 THEN 5250
5020   IF AINF2B1D>0 AND AINF2B2D>0 THEN GOTO 5050
5030   IF AINF2B1D>0 THEN EB1=EXS: EB2=0: GOTO 5170 'So AINF2b2D=0
5040   EB1=0: EB2=EXS: GOTO 5210 'THEN AINF2b1D=0, AINF2b2D<0
5050   EQ1=FREQSB1/NSB1 *EXP(1.439*FREQSB1/T-1) '*Each can decompose
5060   EQ2=FREQSB2/NSB2 *EXP(1.439*FREQSB2/T-1)
5070   EB1=EXS/(1+ EQ1/EQ2): EB2=EXS/(1+ EQ2/EQ1)
5080   QS= EB1/QUANTUMB1: N2=INT(QS +.5): MSUB=INT(E2B1D/QUANTUMB1 +.5)
5090   NSUB=N2: NSSUB=NSB1: ASUB=AINF2B1D '**Calc f(b1S)
5100   IF AINF2B1D=0 OR N2<MSUB THEN F1S=1: GOTO 5120 ELSE GOSUB 9320
5110   F1S=DEACT2B1/(DEACT2B1+KSUB!)
5120   QS= EB2/QUANTUMB2: N2=INT(QS +.5): MSUB=INT(E2B2D/QUANTUMB2 +.5)
5130   NSUB=N2: NSSUB=NSB2: ASUB=AINF2B2D '**Calc f(b2S)
5140   IF AINF2B2D=0 OR N2<MSUB THEN F2S=1: GOTO 5160 ELSE GOSUB 9320
5150   F2S=DEACT2B2/(DEACT2B2+KSUB!)
5160   GOTO 5250
5170   QS= EB1/QUANTUMB1: N2=INT(QS +.5): MSUB=INT(E2B1D/QUANTUMB1 +.5)
5180   NSUB=N2: NSSUB=NSB1: ASUB=AINF2B1D '**Calc k(E),b1D
5190   IF AINF2B1D=0 OR N2<MSUB THEN F1S=0: GOTO 5250 ELSE GOSUB 9320
5200   F1S=DEACT2B1/(DEACT2B1+KSUB!): GOTO 5250
5210   QS= EB2/QUANTUMB2: N2=INT(QS +.5): MSUB=INT(E2B2D/QUANTUMB2 +.5)
5220   NSUB=N2: NSSUB=NSB2: ASUB=AINF2B2D '**Calc f(b2S)
5230   IF AINF2B2D=0 OR N2<MSUB THEN F2S=0: GOTO 5250 ELSE GOSUB 9320
5240   F2S=DEACT2B2/(DEACT2B2+KSUB!)
5250 IF F1S<F2S THEN FS=F1S:F1D2S=F2S-F1S:F1S2D=0:F1D2D=1-F1S-F1D2S: GOTO 5270
5260   FS=F2S: F1S2D=F1S-F2S: F1D2S=0: F1D2D=1-F2S-F1S2D
5270   IF AINF2B2DD=0 THEN GOTO 5340 '**Tertiary decomp of prod 2?
5280   QS=(EB2-DH2B12-DH2B2D)/QUANTUMB2D: N2=INT(QS +.5)

```

```

5290 IF QS<0 THEN GOTO 5340
5300 MSUB=INT(E2B2DD/QUANTUMB2D+.5)
5310 NSUB=N2: NSSUB=NSB2D: ASUB=AINF2B2DD '**Calc k(E),b2DD
5320 IF N2<MSUB THEN GOTO 5340 ELSE GOSUB 9320
5330 RK2B2DD=KSUB!
5340 IF M2C=0 OR N<M2C THEN GOTO 5540 '**Calc k(E),2c
5350 NSUB=N: MSUB=M2C: NSSUB=NS: ASUB=AINF2C: GOSUB 9320
5360 RK2C=KSUB! '*Secondry dec? Dissipate energy (N-M2C)
5370 IF AINF2CD=0 THEN GOTO 5540
5380 QS=(N*QUANTUM - DH2C)/QUANTUMC: N2=INT(QS+.5): IF QS<0 THEN 5420
5390 MSUB=INT(E2CD/QUANTUMC+.5): NSUB=N2: NSSUB=NSC: ASUB=AINF2CD '**k(E),cD
5400 IF N2<MSUB THEN GOTO 5540 ELSE GOSUB 9320
5410 RK2CD=KSUB! '*TERTIARY dec? Dissipate energy (N-E2CD)
5420 IF AINF2CDD=0 THEN GOTO 5540
5430 QS=(N*QUANTUM-DH2C-DH2CD)/QUANTUMCD: N2=INT(QS+.5): IF QS<0 THEN 5540
5440 MSUB=INT(E2CDD/QUANTUMCD+.5)
5450 NSUB=N2: NSSUB=NSCD: ASUB=AINF2CDD '**Calc k(E),cDD
5460 IF N2<MSUB THEN GOTO 5540 ELSE GOSUB 9320
5470 RK2CDD=KSUB! '*4TH-ORDER dec? Dissipate energy (N-E2CDD)
5480 IF AINF2CDDD=0 THEN GOTO 5540
5490 QS=(N*QUANTUM-DH2C-DH2CD-DH2CDD)/QCDD: N2=INT(QS+.5): IF QS<0 THEN 5540
5500 MSUB=INT(E2CDDD/QCDD+.5)
5510 NSUB=N2: NSSUB=NSCDD: ASUB=AINF2CDDD '**Calc k(E),cDDD
5520 IF N2<MSUB THEN GOTO 5540 ELSE GOSUB 9320
5530 RK2CDDD=KSUB!
5540 RK3=0: RKM3=0: RK4A=0: RK4AD=0: RK4B=0 '* Isomerizations
5550 IF M3=0 OR N<M3 THEN GOTO 5760 '***Calc k(E),M3
5560 NSUB=N: MSUB=M3: NSSUB=NS: ASUB=AINF3: GOSUB 9320
5570 RK3=KSUB! 'Next calc Isom* rate constants - need N relative to Isom
5580 IF AINF3=0 THEN GOTO 5760 '**Calc k(E),MM3
5590 MM3=INT(EM3/QUANTUMI+.5)
5600 M4A=INT(E4A/QUANTUMI+.5): M4B=INT(E4B/QUANTUMI+.5)
5610 NNEW=(N*QUANTUM-DELISO)/QUANTUMI: IF NNEW<MM3 THEN GOTO 5760
5620 NSUB=NNEW: MSUB=MM3: NSSUB=NS: ASUB=AINFM3: GOSUB 9320
5630 RKM3=KSUB!
5640 IF AINF4A=0 OR NNEW<M4A THEN GOTO 5730 '**Calc k(E),4A
5650 NSUB=NNEW: MSUB=M4A: NSSUB=NS: ASUB=AINF4A: GOSUB 9320
5660 RK4A=KSUB! '*Secondry dec? Dissipate energy (NNEW-M4A)
5670 IF AINF4AD=0 THEN GOTO 5730
5680 QS=(NNEW*QUANTUMI -DHIA)/QUANTUMIA: N2=INT(QS+.5): IF QS<0 THEN 5730
5690 MSUB=INT(E4AD/QUANTUMIA+.5)
5700 NSUB=N2: NSSUB=NSIA: ASUB=AINF4AD '**Calc k(E),4AD
5710 IF N2<MSUB THEN GOTO 5730 ELSE GOSUB 9320
5720 RK4AD=KSUB!
5730 IF AINF4B=0 OR NNEW<M4B THEN GOTO 5760 '**Calc k(E),4B
5740 NSUB=NNEW: MSUB=M4B: NSSUB=NS: ASUB=AINF4B: GOSUB 9320
5750 RK4B=KSUB!
5760 DENOMISO=DEACT+RKM3+RK4A+RK4B
5770 DENOM=LOG(DEACT +RK2A+RK2B+RK2C +RK3 -RK3*RKM3/DENOMISO )
5780 RADA=0: RADAS=0: RADADA=0: RADADB=0: RIS=0: RIDAS=0: RIDAD=0: RIDB=0
5790 RADBS=0: RADB1D2S=0: RADB1S2D=0: RADB1D2D=0: RADB1S2DD=0: RADB1D2DD=0
5800 RADC=0: RADCS=0: RADCD=0: RADCDS=0: RADCCD=0: RADCDDS=0: RADCCDD=0
5810 IF RK2A=0 THEN GOTO 5860
5820 RADA=EXP( WN +LOG(DEACT) +LOG(RK2A) -DENOM)

```

```

5830 IF RK2ADA=0 AND RK2ADB=0 THEN RADAS=RADA: GOTO 5860
5840 DENOMA=DEACT2A+RK2ADA+RK2ADB: RADAS=RADA*DEACT2A/DENOMA
5850 RADADA=RADA*RK2ADA/DENOMA: RADADB=RADA*RK2ADB/DENOMA
5860 IF RK2B=0 THEN GOTO 5960
5870 RADBS=EXP( WN +LOG(DEACT) +LOG(RK2B) -DENOM)
5880 RADBS1S2D=RADBS*F1S2D
5890 RADBS1D2S=RADBS*F1D2S: RADBS1D2D=RADBS*F1D2D: RADBS=RADBS*FS
5900 IF F1S2D=0 THEN GOTO 5930
5910 DB2D=DEACT2B2D+RK2B2DD
5920 RADBS1S2DD=RADBS1S2D*RK2B2DD/DB2D: RADBS1S2D=RADBS1S2D*DEACT2B2D/DB2D
5930 IF F1D2D=0 THEN GOTO 5960
5940 DB2D=DEACT2B2D+RK2B2DD
5950 RADBS1D2DD=RADBS1D2D*RK2B2DD/DB2D: RADBS1D2D=RADBS1D2D*DEACT2B2D/DB2D
5960 IF RK2C=0 THEN GOTO 6060
5970 RADCS=EXP( WN +LOG(DEACT) +LOG(RK2C) -DENOM)
5980 IF RK2CD=0 THEN RADCS=RADC: GOTO 6060
5990 DENOMC=DEACT2C+RK2CD: RADCS=RADC*DEACT2C/DENOMC: RADCD=RADC*RK2CD/DENOMC
6000 IF RK2CDD=0 OR RADCD=0 THEN RADCS=RADC: GOTO 6060
6010 DENOMCD=DEACT2CD+RK2CDD
6020 RADCS=RADC*DEACT2CD/DENOMCD: RADCDD=RADC*RK2CDD/DENOMCD
6030 IF RK2CDD=0 OR RADCDD=0 THEN RADCS=RADC: GOTO 6060
6040 DENOMCDD=DEACT2CDD+RK2CDD
6050 RADCS=RADC*DEACT2CDD/DENOMCDD: RADCDD=RADC*RK2CDD/DENOMCDD
6060 IF RK3=0 THEN GOTO 6140
6070 RIS=EXP( WN +LOG(DEACT) -DENOM +LOG(DEACT*RK3/DENOMISO) )
6080 IF RK4A=0 THEN GOTO 6120
6090 RIDAS=EXP( WN +LOG(RK3) -DENOM +LOG(RK4A*RK3/DENOMISO) )
6100 IF RK4AD=0 THEN GOTO 6120
6110 DNMI A=DEACTIA+RK4AD: RIDA D=RIDAS*RK4AD/DNMI A: RIDAS=RIDAS*DEACTIA/DNMI A
6120 IF RK4B=0 THEN GOTO 6140
6130 RIDB=EXP( WN +LOG(RK3) -DENOM +LOG(RK4B*RK3/DENOMISO) )
6140 TOTADAS=TOTADAS+RADAS: TOTADADA=TOTADADA+RADADA: TOTADADB=TOTADADB+RADADB
6150 TOTADBS=TOTADBS+RADBS: TOTADBS1S2D=TOTADBS1S2D+RADBS1S2D
6160 TOTADBS1D2S=TOTADBS1D2S+RADBS1D2S: TOTADBS1D2D=TOTADBS1D2D+RADBS1D2D
6170 TOTADBS1S2DD=TOTADBS1S2DD+RADBS1S2DD: TOTADBS1D2DD=TOTADBS1D2DD+RADBS1D2DD
6180 TOTADCS=TOTADCS+RADCS: TOTADCS D=TOTADCS D+RADCS D
6190 TOTADCS D D=TOTADCS D D+RADCS D D: TOTADCS D D D=TOTADCS D D D+RADCS D D D
6200 TOTIS=TOTIS+RIS: TOTIDAS=TOTIDAS+RIDAS: TOTIDAD=TOTIDAD+RIDAD
6210 TOTIDBS=TOTIDBS+RIDB: INDX=N-MINM: IF IOUT THEN GOTO 6360
6220 IF RK2A=0 THEN P2=0 ELSE P2=FNALOG10(RK2A)
6230 IF RK2ADA=0 THEN P3=0 ELSE P3=FNALOG10(RK2ADA)
6240 IF RK2ADB=0 THEN P4=0 ELSE P4=FNALOG10(RK2ADB)
6250 IF RK2C=0 THEN P5=0 ELSE P5=FNALOG10(RK2C)
6260 IF RK2CD=0 THEN P6=0 ELSE P6=FNALOG10(RK2CD)
6270 IF RK2CDD=0 THEN P7=0 ELSE P7=FNALOG10(RK2CDD)
6280 IF RK2CDD D=0 THEN P8=0 ELSE P8=FNALOG10(RK2CDD D)
6290 IF RK3=0 THEN P9=0 ELSE P9=FNALOG10(RK3)
6300 IF RKM3=0 THEN P10=0 ELSE P10=FNALOG10(RKM3)
6310 IF RK4A=0 THEN P11=0 ELSE P11=FNALOG10(RK4A)
6320 IF RK4AD=0 THEN P12=0 ELSE P12=FNALOG10(RK4AD)
6330 IF RK4B=0 THEN P13=0 ELSE P13=FNALOG10(RK4B)
6340 PRINT USING TBLES;INDX,EXP(WN),P2,P3,P4,P5,P6,P7,P8,P9,P10,P11,P12,P13
6350 IF IFILE THEN PRINT #2,USING TBLES;INDX,EXP(WN),P2,P3,P4,P5,P6,P7,P8,P9,
P10,P11,P12,P13

```

```

6360 NEXT N
6370 IF IOUT THEN GOTO 6510
6380 PRINT USING KADAFORM$;TOTADAS,TOTADADA,TOTADADB
6390 PRINT USING KADBFORM$;TOTADBS,TOTADB1D2S,TOTADB1S2D
6400 PRINT USING KADBFM$;TOTAD1D2D,TOTADB1S2DD,TOTADB1D2DD
6410 PRINT USING KADCFORM$;TOTADCS,TOTADCDS,TOTADCDDS
6420 PRINT USING KISFORM$;TOTADCDDD,TOTIS
6430 PRINT USING KIDAFORM$;TOTIDAS,TOTIDAD,TOTIDBS
6440 IF IFILE=0 THEN GOTO 6510
6450 PRINT #2,USING KADAFORM$;TOTADAS,TOTADADA,TOTADADB
6460 PRINT #2,USING KADBFORM$;TOTADBS,TOTADB1D2S,TOTADB1S2D
6470 PRINT #2,USING KADBFM$;TOTAD1D2D,TOTADB1S2DD,TOTADB1D2DD
6480 PRINT #2,USING KADCFORM$;TOTADCS,TOTADCDS,TOTADCDDS
6490 PRINT #2,USING KISFORM$;TOTADCDDD,TOTIS
6500 PRINT #2,USING KIDAFORM$;TOTIDAS,TOTIDAD,TOTIDBS
6510 ICOUNT=ICOUNT+1: X(1,ICOUNT)=1!/T: X(2,ICOUNT)=P '**Store results
6520 Y(1,ICOUNT)=0!: Y(2,ICOUNT)=TOTADAS: Y(3,ICOUNT)=TOTADADA
6530 Y(4,ICOUNT)=TOTADADB: Y(5,ICOUNT)=TOTADBS: Y(6,ICOUNT)=TOTADB1D2S
6540 Y(7,ICOUNT)=TOTADB1S2D: Y(8,ICOUNT)=TOTADB1D2D: Y(9,ICOUNT)=TOTADB1S2DD
6550 Y(10,ICOUNT)=TOTADB1D2DD:Y(11,ICOUNT)=TOTADCS: Y(12,ICOUNT)=TOTADCDS
6560 Y(13,ICOUNT)=TOTADCDDS: Y(14,ICOUNT)=TOTADCDDD: Y(15,ICOUNT)=TOTIS
6570 Y(16,ICOUNT)=TOTIDAS: Y(17,ICOUNT)=TOTIDAD: Y(18,ICOUNT)=TOTIDBS
6580 Y(19,ICOUNT)=0!
6590 FOR KT=2 TO 18: Y(19,ICOUNT)=Y(19,ICOUNT)+Y(KT,ICOUNT): NEXT
6600 T=T+TSTEP
6610 IF T<THIGH AND TSTEP<0 THEN GOTO 4390
6620 IF P*PFAC<=PHIGH AND TSTEP=0 THEN P=P*PFAC: GOTO 4390
6630 IFLOP=1
6640 IF IFILE=0 THEN GOTO 6770
6650 PRINT #2,NADA$: PRINT #2, USING U1$;RP$,IDCOLL$
6660 PRINT #2, USING U2$;RXN$(2),RXN$(3),RXN$(4)
6670 PRINT #2, USING U3$;RXN$(5),RXN$(6),RXN$(7)
6680 PRINT #2, USING U4$;RXN$(8),RXN$(9),RXN$(10)
6690 PRINT #2, USING U5$;RXN$(11),RXN$(12),RXN$(13),RXN$(14)
6700 PRINT #2, USING U6$;RXN$(15),RXN$(16),RXN$(17),RXN$(18): PRINT #2,THDFORM$
6710 FOR II=1 TO ICOUNT
6720 FOR KT=2 TO 19
6730 IF Y(KT,II) THEN YT(KT)=FNLG10(Y(KT,II)) ELSE YT(KT)=0
6740 NEXT
6750 PRINT #2,USINGTBLFORM$;1!/X(1,II),X(2,II),YT(2),YT(3),YT(4),YT(5),YT(11),
YT(12),YT(13),YT(15),YT(16),YT(17),YT(18),YT(19)
6760 NEXT
6770 PRINT NADA$: PRINT USING U1$;RP$,IDCOLL$
6780 PRINT USING U2$;RXN$(2),RXN$(3),RXN$(4)
6790 PRINT USING U3$;RXN$(5),RXN$(6),RXN$(7)
6800 PRINT USING U4$;RXN$(8),RXN$(9),RXN$(10)
6810 PRINT USING U5$;RXN$(11),RXN$(12),RXN$(13),RXN$(14)
6820 PRINT USING U6$;RXN$(15),RXN$(16),RXN$(17),RXN$(18): PRINT THDFORM$
6830 FOR II=1 TO ICOUNT
6840 FOR KT=2 TO 19
6850 IF Y(KT,II) THEN YT(KT)=FNLG10(Y(KT,II)) ELSE YT(KT)=0
6860 NEXT
6870 PRINT USING TBLFORM$;1!/X(1,II),X(2,II),YT(2),YT(3),YT(4),YT(5),YT(11),
YT(12),YT(13),YT(15),YT(16),YT(17),YT(18),YT(19)

```

```

6880 NEXT
6890 IF IFLOP=1 THEN PRINT"Conv kUNI to k/kINF[1]? ";
6900 IF IFLOP=-1 THEN PRINT"Conv k/kINF to k/[M][1]? ";
6910 IF IFLOP=2 THEN PRINT"Conv k/[M] to kUNI [1]? ";
6920 PRINT"kDa[2],kDaDa[3],kDaDb[4], kDb[5],kDb1D2S[6],kDb1S2D[7],",
6930 PRINT" kDb1D2D[8],kDb1S2DD[9],kDb1D2DD[10], kDc[11],kDcD[12],kDcDD[13],",
6940 INPUT" kDcDDD[14],kIS[15],kIDa[16],kIDaD[17],kIDb[18],kTOT[19], Sumry[20]";
IFIT
6950 IF IFIT>19 THEN GOTO 6770
6960 IF IFIT<1 THEN GOTO 6990
6970 GOSUB 9400
6980 GOTO 6770
6990 N1=1: N=ICOUNT: IF IFIT<0 THEN GOTO 7050 'ELSE new case
7000 IF IFLOP=-1 OR IFLOP=2 THEN GOSUB 9400
7010 IF PLOW=PHIGH OR PFAC=0 THEN ICOUNT=0: GOTO 1290
7020 IF P*PFAC>PHIGH THEN ICOUNT=0: GOTO 1290
7030 P=P*PFAC: IF THIGH<TLOW+TSTEP OR TSTEP=0 THEN T=TLOW: GOTO 4390 'Fall-off
7040 ICOUNT=0: T=TLOW: GOTO 4390
7050 IF N>3 THEN GOTO 7080
7060 PRINT:PRINT "Fewer points than 4 - too few to be fitted.": GOSUB 9110
7070 GOTO 6890
7080 IF X(2,1)<X(2,N) THEN IPLTP=1: GOTO 7130
7090 IF TSTEP<0 AND THIGH=>(TLOW+TSTEP) THEN GOTO 7130
7100 GOSUB 9110
7110 PRINT "Strike any key to plot.": GOSUB 9380
7120 GOTO 6890
7130 FOR I=1 TO N: XX(I)=LOG(1/X(1,I)): YY(I)=X(1,I)
7140 IF IPLTP THEN YY(I)=FNALOG10(X(2,I))
7150 IF Y(IFIT,I)=0 THEN N1=N1+1 ELSE ZZ(I)=LOG(Y(IFIT,I))
7160 NEXT
7170 IF (N1+3)>N THEN GOTO 7060
7180 IF IPLTP OR IFIT>18 THEN GOSUB 9110 ELSE GOTO 7210
7190 PRINT "Strike any key to plot.": GOSUB 9380
7200 GOTO 7620
7210 PRINT: PRINT USING HEADERFORM$;KFORM$(IFIT),P
7220 IF IFILE THEN PRINT #2,"": PRINT #2,USING HEADERFORM$;KFORM$(IFIT),P
7230 NDIF=N-N1+1: SX2=0: SX=0: SY2=0: SY=0: SXY=0: SYZ=0: SZ=0: SXZ=0: SZ2=0
7240 FOR I=N1 TO N
7250 SX2=SX2+XX(I)*XX(I): SX =SX +XX(I): SY2=SY2+YY(I)*YY(I)
7260 SY =SY +YY(I): SXY=SXY+XX(I)*YY(I): SYZ=SYZ+YY(I)*ZZ(I)
7270 SZ =SZ +ZZ(I): SXZ=SXZ+XX(I)*ZZ(I): SZ2=SZ2+ZZ(I)*ZZ(I): NEXT
7280 AA=(NDIF*SX2-SX*SX)*(NDIF*SYZ-SY*SZ): BB=(NDIF*SXY-SX*SY)*(NDIF*SXZ-SX*SZ)
7290 C=(AA-BB)/((NDIF*SX2-SX*SX)*(NDIF*SY2-SY*SY)-(NDIF*SXY-SX*SY)^2)
7300 B=(NDIF*SXZ-SX*SZ) -C*(NDIF*SXY-SX*SY) /(NDIF*SX2-SX*SX)
7310 A=(SZ-C*SY-B*SX)/NDIF
7320 R2=(A*SZ +B*SXZ +C*SYZ -SZ*SZ/NDIF) /(SZ2-SZ*SZ/NDIF)
7330 C1=(SYZ-SY*SZ/NDIF) /(SY2-SY*SY/NDIF): Q1=(SZ - C1*SY)/NDIF
7340 PRINT PHEADFORM$: IF IFILE THEN PRINT #2,PHEADFORM$
7350 FOR I=N1 TO N: T=1/YY(I): K!=-EXP(ZZ(I))
7360 PRED(I)=A+B*XX(I)+C*YY(I): PRD1(I)=Q1+C1*YY(I)
7370 IF PRED(I)<87 THEN KPRED!=-EXP(PRED(I)) ELSE KPRED!=-E38
7380 IF PRD1(I)<87 THEN KPRD1!=-EXP(PRD1(I)) ELSE KPRD1!=-E38
7390 IF PRED(I)<(ELOG9+ZZ(I)) THEN PD=(KPRED!-K!)/K!*100! ELSE PD=999.99
7400 IF PRD1(I)<(ELOG9+ZZ(I)) THEN PD1=(KPRD1!-K!)/K!*100! ELSE PD1=999.99

```

```

7410 PRINT USING ZFORM$;T,K!,KPRED!,PD,KPRD1!,PD1
7420 IF IFILE THEN PRINT #2, USING ZFORM$;T,K!,KPRED!,PD,KPRD1!,PD1
7430 NEXT
7440 PRINT USING" Z= "+V$+" _+ "+V$+"*X _+ "+V$+"*Y; R^2=+#.#####";A,B,C,R2
7450 IF A>88 THEN PRINT USING" k= 10_^(+##.###)*T_^( "+V$+
    ")*exp(_- #####.###/RT)";A/ELOG10,B,-C*R/1000: GOTO 7470
7460 PRINT USING" k= "+V$+" *T_^( "+V$+)*exp(_- ###.###/RT)";EXP(A),B,-C*R/1000
7470 IF Q1<88 THEN GOTO 7500
7480 PRINT USING" or k= 10_^(+##.###)*exp(_- ###.###/RT)";Q1/ELOG10,-C1*R/1000
7490 GOTO 7510
7500 PRINT USING" or k= "+V$+" *exp(_- #####.###/RT)";EXP(Q1),-C1*R/1000
7510 IF IFILE=0 THEN GOTO 7590
7520 PRINT #2, USING" Z= "+V$+" _+ "+V$+"*X _+ "+V$+"*Y; R^2=+#.#####";A,B,C,R2
7530 IF A>88 THEN PRINT #2, USING" k= 10_^(+##.###)*T_^( "+V$+
    ")*exp(_- #####.###/RT)";A/ELOG10,B,-C*R/1000: GOTO 7550
7540 PRINT #2, USING" k= "+V$+" *T_^( "+V$+)*exp(_- #####.###/RT)";
    EXP(A),B,-C*R/1000
7550 IF Q1<88 THEN GOTO 7580
7560 PRINT #2, USING" or k= 10_^(+##.###)*exp(_- ###.###/RT)";
    Q1/ELOG10, -C1*R/1000
7570 GOTO 7590
7580 PRINT #2, USING" or k= "+V$+" *exp(_- #####.###/RT)";EXP(Q1),-C1*R/1000
7590 PRINT "Plot results (Y/N)? [Then type X to leave plot.] ";: GOSUB 9380
7600 IF K$="Y" OR K$="y" THEN PRINT Y$: GOTO 7620
7610 IF K$="N" OR K$="n" THEN PRINT N$: GOTO 7660 ELSE GOTO 7590
7620 GOSUB 8450
7630 GOSUB 9380
7640 IF K$="X" OR K$="x" THEN GOTO 7650 ELSE GOTO 7630
7650 IPLTP=0: SCREEN 0: COLOR 0,6,2: CLS
7660 GOTO 6890
7670 EKT=ECOLL/(1.15*R*T): XLAM0=.1 'Newton's method sol'n for beta
7680 XLAM=XLAM0 - (XLAM0-EKT*(1-SQR(XLAM0)))/(1+.5*EKT/SQR(XLAM0))
7690 IF ABS(XLAM-XLAM0)<.0005 THEN RETURN ELSE XLAM0=XLAM: GOTO 7680
7700 REM*****Given a third-body gas's name, use these input parameters:
7710 IF IDCOLL$="Ar" THEN XM2=39.944: SIGMA2=3.33: EK2=136.5: ECOLL=740: RETURN
7720 IF IDCOLL$="He" THEN XM2=4.0026: SIGMA2=2.576: EK2=10.2: ECOLL=470: RETURN
7730 IF IDCOLL$="H2" THEN XM2=2.0014: SIGMA2=2.92: EK2=38!: ECOLL=610: RETURN
7740 IF IDCOLL$="N2" THEN XM2=28.01: SIGMA2=3.621: EK2=97.53: ECOLL=980: RETURN
7750 IF IDCOLL$="CO" THEN XM2=28.01: SIGMA2=3.65: EK2=98.1: ECOLL=1200: RETURN
7760 IF IDCOLL$="O2" THEN XM2=32!: SIGMA2=3.458: EK2=107.4: ECOLL=1100: RETURN
7770 IF IDCOLL$="CO2" THEN XM2=44.01: SIGMA2=3.763: EK2=244!: ECOLL=2400: RETURN
7780 IF IDCOLL$="CH4" THEN XM2=16.01: SIGMA2=3.746: EK2=141.4: ECOLL=2300: RETURN
7790 IF IDCOLL$="C2H6" THEN XM2=30.01: SIGMA2=4.302: EK2=252.3: ECOLL=4100: RETURN
7800 PRINT "Third-body data required...": IFLAG=1: RETURN
7810 NADA$="": OKFORM$=" Ok? (Y/N, def=N) ": Y$="Yes": N$="No" 'Text formats
7820 TPFORM$="T-#####.# to #####.# by ###.# K, P-###.### to ###.### atm"
7830 V$="+#.###^^^": TOKFORM$=" Use or Quit (Y/N/Q,def=N)? "
7840 DECFORM$= " (D) Decomposition to products: "
7850 DDFRMS$= " (DD) Secndry decomp'n to new products: "
7860 TERTFRMS$= " (DDD) Tertiary decomp to new products: "
7870 QUARFRMS$= " (DDDD) 4th-ordr decmp to new products: "
7880 ISOFORM$= " (IS) Isomeriz'n/stabil'n product: "
7890 IDECFORM$= " (ID) Isomeriz'n/dissoc'n rxn products: "
7900 ENTRY$(2) ="Enter decomp'n products (a): "

```

7910 ENTRY\$(3) =" Enter secndry decomp'n aa: "
7920 ENTRY\$(4) =" Enter secndry decomp'n ab: "
7930 ENTRY\$(5) ="Enter decomp'n products (b): "
7940 ENTRY\$(6) =" Enter sec decomp of prod b1: "
7950 ENTRY\$(7) =" Enter sec decomp of prod b2: "
7960 ENTRY\$(8) =" Enter sec decomp of b1 & b2: "
7970 ENTRY\$(9) =" Enter b1 & tert dcmp of b2: "
7980 ENTRY\$(10) =" Enter complete dcmp, b1&b2: "
7990 ENTRY\$(11) ="Enter decomp'n products (c): "
8000 ENTRY\$(12) =" Enter secondary decomp'n: "
8010 ENTRY\$(13) =" Enter tertiary decomp'n: "
8020 ENTRY\$(14) =" Enter 4th-order decomp'n: "
8030 ENTRY\$(15) ="Enter isom/stabil'n product: ": ENTRY\$(17)-ENTRY\$(12)
8040 ENTRY\$(16) ="Enter isom/decomp prods (a): "
8050 ENTRY\$(18) ="Enter isom/decomp prods (b): "
8060 FFORM\$= "Mean freq of reactt= #####. wavenumbers,S=##### oscillators"
8070 FSFORM\$="Product*: Freq=#####;S=##### oscillators,E(vs adduct)=###.## kcal"
8080 SPFORM\$= "Complex: MW= ###.##, Diameter("+CHR\$(229)+")=##.### angstroms,"+
" Well ("+CHR\$(238)+")/K=#####.##"
8090 SPSFORM\$="Prodct*: MW= ###.##, Diameter("+CHR\$(229)+")=##.### angstroms,"+
" Well ("+CHR\$(238)+")/K=#####.##"
8100 ESPFORM\$= "Enter MW (amu), "+CHR\$(229)+ " (angstroms), and "+CHR\$(238)+
" (K) for "
8110 ESPSFORM\$=ESPFORM\$+"prodct*": ESPFORM\$=ESPFORM\$+"complex:"
8120 IDFORM\$="Bath gas &": AES\$=" "+V\$+",#####.##"
8130 COLLFORM\$=" MW= ###.##, "+CHR\$(229)+ "=##.###, "+CHR\$(238)+"/K=#####.##,"+
" E(coll)=#####."
8140 A2FORM\$="A and barrier for decomp'n "+AES\$
8150 ADFORM\$="A and barrier for secondary decomp'n "+AES\$
8160 ATFORM\$="A and barrier for tertiary decomp'n "+AES\$
8170 AQFORM\$="A and barrier for 4th-ordr decomp'n "+AES\$
8180 A3FORM\$="A and barrier for isomer'n "+AES\$
8190 AM3FORM\$="A and barrier for reverse isomeriz'n"+AES\$
8200 DELFORM\$="E(isomer)-E(adduct) = #####.##, Isomer freq= #####. wavenumbers"
8210 A4FORM\$="A and barrier for decomp'n of isomer= +#.###^^^^,#####.##"
8220 HEADERFORM\$="&; P = +#.###^^^^ atm"
8230 PFORM\$=" T= #####.## K P=+#.###^^^^ atm"
8240 DKFORM\$=" kDEACT*{&}= "+V\$+" Beta=#.#####"
8250 TBLES\$="## +#.###^^^^ +##.# +##.# +##.# +##.# ##.# ##.# ##.# +##.#"+
" +##.# +##.# ##.# ##.#"
8260 HEADING\$=" Dist'n Log:Da Daa Dab Db Dc DcD DcDD I "+
" -I IDa IDaa IDb"
8270 TBLFORM\$="#####. +#.###^^^^ ##.# ##.# ##.# ##.# ##.# ##.# ##.# ##.# ##.#"+
" ##.# ##.# +#.###^^^^"
8280 THDFORM\$=" T(K) P(atm) Da DaDa DaDb Db Dc DcD DcDD IS IDa"+
" IDaD IDb ktot"
8290 KADAFORM\$=" kDaS= "+V\$+" kDaDa= "+V\$+" kDaDb = "+V\$
8300 KADBFORM\$=" kDbS= "+V\$+" kDb1D2S= "+V\$+" kDb1S2D= "+V\$
8310 KADBFM\$=" kDb1D2D="+V\$+" kDb1S2DD="+V\$+" kDb1D2DD="+V\$
8320 KADCFORM\$=" kDcS= "+V\$+" kDcD= "+V\$+" kDcDD= "+V\$
8330 KISFORM\$=" kDcDDD= "+V\$+" kIS= "+V\$
8340 KIDAFORM\$=" kIDaS= "+V\$+" kIDaD= "+V\$+" kIDb= "+V\$
8350 U1\$="Reactant:&; M-&"; U2\$="Da:& DaDa:& DaDb:&"
8360 U3\$="Db:& Db1D2S:& Db1S2D:&"; U4\$="Db1D2D:& Db1S2DD:& Db1D2DD:&"


```

8370 U5$="Dc:& DcD:& DcDD:& DcDDD:&": U6$="IS:& IDa:& IDaD:& IDb:&"
8380 PHEADFORM$=" T k Predict'n & Diff. Predict'n & Diff."
8390 ZFORM$="#####. "+V$+" "+V$+" +####.## "+V$+" +####.##"
8400 YFORM$="+###.##": RETURN
8410 KFM$="Fit for ": RR$=R$+RXN$(1) '**Subroutine to set up titles
8420 RXN$(19)="overall rxn of "+RP$
8430 FOR KF=1 TO 18: KFORM$(KF)=KFM$+R$+RXN$(KF): NEXT
8440 KFORM$(19)=KFM$+RXN$(19): RETURN
8450 IF IPLTP THEN GOTO 8520 '*****Flotting subroutine*****
8460 XMIN=0: TEST=1/TLOW: JXFORM$="#.##" 'Plot log k vs 1000/T
8470 IF TEST<=-6.000001E-04 THEN XMAX=-6.000001E-04: XMIN=.0002: GOTO 8580
8480 IF TEST<=-.0008 THEN XMAX=.0008: GOTO 8580
8490 IF TEST<=-.0012 THEN XMAX=.0012: GOTO 8580
8500 IF TEST<=-.002 THEN XMAX=.002: GOTO 8580
8510 IF TEST<=-.004 THEN XMAX=.004: GOTO 8580 ELSE XMAX=8.000001E-03: GOTO 8580
8520 JXFORM$="###.##": XMIN=INT(FNALOG10(PLOW)) 'Plot fall-off curve
8530 XMAX=INT(FNALOG10(PHIGH)+.5): DEL=XMAX-XMIN: XMEAN=.5*(XMIN+XMAX)
8540 IF DEL<=2.1 THEN XMIN=XMEAN-1: XMAX=XMEAN+1: GOTO 8580
8550 IF DEL<=4.1 THEN XMIN=XMEAN-2: XMAX=XMEAN+2: GOTO 8580
8560 IF DEL<8.100001 THEN XMIN=XMEAN-4: XMAX=XMEAN+4: GOTO 8580
8570 XMIN=XMEAN-8: XMAX=XMEAN+8
8580 YMIN=E38: YMAX=-E38
8590 FOR I=N1 TO N
8600 IF ZZ(I)>YMAX THEN YMAX=ZZ(I)
8610 IF ZZ(I)<YMIN THEN YMIN=ZZ(I)
8620 NEXT
8630 YMIN=INT(YMIN/LOG(10)): YMAX=INT(YMAX/LOG(10)+1): DEL=YMAX-YMIN
8640 IF DEL<=1.1 THEN YMIN=YMAX-1: GOTO 8690
8650 IF DEL<=2.1 THEN YMIN=YMAX-2: GOTO 8690
8660 IF DEL<=4.1 THEN YMIN=YMAX-4: GOTO 8690
8670 IF DEL<=8.100001 THEN YMIN=YMAX-8: GOTO 8690
8680 YMIN=YMAX-16
8690 YMIN=YMIN*ELOG10: YMAX=YMAX*ELOG10: NPLT=0 '**Select points:
8700 FOR J=N1 TO N: NPLT=NPLT+1: XPLT(NPLT)=YY(J): YPLT(NPLT)=ZZ(J): NEXT
8710 FOR J=1 TO NPLT: IXPL(J)=639*(XPLT(J)-XMIN)/(XMAX-XMIN)
8720 IYPLT(J)=199-199*(YPLT(J)-YMIN)/(YMAX-YMIN): NEXT
8730 IYZERO=199+199*YMIN/(YMAX-YMIN)
8740 SCREEN 2:CLS:DX=(XMAX-XMIN)/640!:DY=(YMAX-YMIN)/200!
8750 LINE (0,0)-(0,199): LINE -(639,199): LINE -(639,0): LINE -(0,0)
8760 FOR J=10 TO 30 STEP 10: JVERT=16!*J-1 '**Label X-axis
8770 FOR JJ=10 TO 195 STEP 4: PSET (JVERT,JJ): NEXT
8780 JX=J/5*10-1: XES=DX*16!*J+XMIN
8790 IF IPLTP THEN GOTO 8800 ELSE XES=XES*1000
8800 LOCATE 1,JX: PRINT USING JXFORM$;XES;: NEXT
8810 DELY=(YMAX-YMIN)/4!: YLBL(1)=YMIN '**Label Y-axis
8820 FOR J=49 TO 149 STEP 50
8830 FOR JJ=7 TO 631 STEP 8: PSET (JJ,J): NEXT
8840 NEXT
8850 FOR J=2 TO 5: YLBL(J)=YLBL(J-1)+DY*50!: NEXT
8860 FOR J=1 TO 5: YLBL(J)=YLBL(J)/LOG(10): NEXT
8870 FOR J=1 TO 5: IF J<5 THEN LOCATE 1+(J-1)*6,1 ELSE LOCATE 24,1
8880 PRINT USING YFORM$;YLBL(6-J);: LOCATE 1,1: NEXT
8890 FOR J=1 TO NPLT
8900 IF YPLT(J)<YMIN THEN YPLOT(J)=199

```

```

8910 IF YPLT(J)>YMAX THEN YPLOT(J)=0
8920 YPLOT(J)=IYPLT(J): NEXT
8930 FOR J=1 TO NPLT '**Plot points
8940 LINE (IXPL(J)-6,YPLOT(J)-3)-(IXPL(J)-6,YPLOT(J)+3)
8950 LINE -(IXPL(J)+6,YPLOT(J)+3): LINE -(IXPL(J)+6,YPLOT(J)-3)
8960 LINE -(IXPL(J)-6,YPLOT(J)-3): PSET (IXPL(J),YPLOT(J)): NEXT J
8970 IF IPLTP THEN LOCATE 17,48: PRINT "log k vs log P (atm) for";: GOTO 9010
8980 LOCATE 17,48: IF IFLOP=1 THEN PRINT"Log kUNI vs 1000/T for";: GOTO 9010
8990 IF IFLOP=-1 THEN PRINT"Log k/kINF vs 1000/T for";: GOTO 9010
9000 IF IFLOP= 2 THEN PRINT"Log k/[M] vs 1000/T for";
9010 LOCATE 18,48: IF IFIT>18 THEN PRINT RXN$(IFIT); ELSE PRINT R$+RXN$(IFIT);
9020 IF IPLTP OR IFIT>21 THEN GOTO 9100
9030 IXPLT1=639*(YY(N1)-XMIN)/(XMAX-XMIN)
9040 KP=199 -199*(PRED(N1)-YMIN)/(YMAX-YMIN): PSET (IXPLT1,KP)
9050 FOR I=N1 TO N: IXPLTT=639*(YY(I)-XMIN)/(XMAX-XMIN)
9060 KP=199-199*(PRED(I)-YMIN)/(YMAX-YMIN): LINE -(IXPLTT,KP): NEXT
9070 KP=199 -199*(PRD1(N1)-YMIN)/(YMAX-YMIN): PSET (IXPLT1,KP)
9080 FOR I=N1 TO N: IXPLTT=639*(YY(I)-XMIN)/(XMAX-XMIN)
9090 KP=199-199*(PRD1(I)-YMIN)/(YMAX-YMIN): LINE -(IXPLTT,KP): NEXT
9100 RETURN
9110 PRINT KFORM$(IFIT): PRINT PHEADFORM$
9120 IF IFILE THEN PRINT #2,NADA$: PRINT #2,KFORM$(IFIT):PRINT #2,PHEADFORM$
9130 FOR I=1 TO N
9140 PRINT USING ZFORM$;1/X(1,I),Y(IFIT,I),0,0,0,0
9150 IF IFILE THEN PRINT #2,USING ZFORM$;1/X(1,I),Y(IFIT,I),0,0,0,0
9160 NEXT
9170 RETURN
9180 IF FIRST THEN GOTO 9220 'Subroutine to get freq,S,etc.
9190 PRINT USING FSFORM$;FQ,NSQ,DHS
9200 PRINT USING SPSFORM$;XMS,SIGMAS,EKS: GOSUB 9370
9210 IF K$="Y" OR K$="y" THEN PRINT Y$: GOTO 9250 ELSE PRINT N$
9220 INPUT"Enter freq, S, & E (vs previous level) for PRODS*: ",FQ,NSQ,DHS
9230 INPUT"Also MW, sigma, epsilon/K: ",XMS,SIGMAS,EKS
9240 IF FQ=0 THEN FQ=FREQ
9250 RETURN
9260 SIG=.5*(SSIG+SIGMA2)*1E-08: EK=SQR(EEK*EK2) '*Collisional k (Forst, p185)
9270 REDUCM=XXM*XM2/(XXM+XM2): F1=8!*8.314E+07*T/(3.14*REDUCM)
9280 KCOLL!=2.708* (EK/T)^.333 *6.02E+23*3.14*SIG*SIG*SQR(F1)
9290 DEAC=XLAM* KCOLL! *P/(82.1*T)
9300 RETURN
9310 REM *****Subr to calc. k(E)= (Ainf) *N!(N+S-1)!/ (N-M)!*(N-M+S-1)!
9320 PROD1=0!: ISTART=NSUB-MSUB+1: IEND=NSUB ' -- Calc. N!/(N-M)!
9330 FOR I=ISTART TO IEND: PROD1=PROD1+LN!(I): NEXT
9340 PROD2=0!: ISTART=NSUB-MSUB+NSSUB: IEND=NSUB+NSSUB-1 '(N-M+S-1)!/(N+S-1)!
9350 FOR I=ISTART TO IEND: PROD2=PROD2+LN!(I): NEXT
9360 KSUB!= EXP( LOG(ASUB)+PROD1-PROD2 ): RETURN
9370 PRINT OKFORM$; '*Subr for responses
9380 K$=NADA$
9390 K$=INKEY$: IF LEN(K$) THEN RETURN ELSE GOTO 9390
9400 IF IFLOP<0 THEN IFLOP=1:GOTO 9600 '*Conversions of k(UNI) to k/kINF to kBI
9410 IF IFLOP=2 THEN GOTO 9780
9420 IFLOP=-1 'Convert to kUNI/kINF [from kUNI]
9430 FOR I=1 TO ICOUNT
9440 IF AINF2A=0 THEN RKLOG2A=-85: GOTO 9470

```

```

9450  RKLOG2A=LOG(AINF2A)-E2A*1000*X(1,I)/R
9460  IF RKLOG2A<-85 THEN RKLOG2A=-85
9470  IF AINF2B=0 THEN RKLOG2B=-85: GOTO 9500
9480  RKLOG2B=LOG(AINF2B) - E2B*1000*X(1,I)/R
9490  IF RKLOG2B<-85 THEN RKLOG2B=-85
9500  IF AINF2C=0 THEN RKLOG2C=-85: GOTO 9530
9510  RKLOG2C=LOG(AINF2C) - E2C*1000*X(1,I)/R
9520  IF RKLOG2C<-85 THEN RKLOG2C=-85
9530  IF AINF3 =0 THEN RKLOG3 --85: GOTO 9560
9540  RKLOG3 =LOG(AINF3 ) - E3 *1000*X(1,I)/R
9550  IF RKLOG3 <-85 THEN RKLOG3 --85
9560  TOTKINF=EXP(RKLOG2A)+EXP(RKLOG2B)+EXP(RKLOG2C)+EXP(RKLOG3)
9570  FOR KT=2 TO 19: Y(KT,I)=Y(KT,I)/TOTKINF: NEXT
9580  NEXT
9590  GOTO 9820
9600  IFLOP=2          'Convert to kBI=kUNI/[M]  { (kUNI/kINF *kINF) /[M] }
9610  FOR I=1 TO ICOUNT
9620  IF AINF2A=0 THEN RKLOG2A=-85: GOTO 9650
9630  RKLOG2A=LOG(AINF2A)-E2A*1000*X(1,I)/R
9640  IF RKLOG2A<-85 THEN RKLOG2A=-85
9650  IF AINF2B=0 THEN RKLOG2B=-85: GOTO 9680
9660  RKLOG2B=LOG(AINF2B) - E2B*1000*X(1,I)/R
9670  IF RKLOG2B<-85 THEN RKLOG2B=-85
9680  IF AINF2C=0 THEN RKLOG2C=-85: GOTO 9710
9690  RKLOG2C=LOG(AINF2C) - E2C*1000*X(1,I)/R
9700  IF RKLOG2C<-85 THEN RKLOG2C=-85
9710  IF AINF3 =0 THEN RKLOG3 --85: GOTO 9740
9720  RKLOG3 =LOG(AINF3 ) - E3 *1000*X(1,I)/R
9730  IF RKLOG3 <-85 THEN RKLOG3 --85
9740  TOTKINF=EXP(RKLOG2A)+EXP(RKLOG2B)+EXP(RKLOG2C)+EXP(RKLOG3)
9750  FOR KT=2 TO 19: Y(KT,I)=(Y(KT,I)*TOTKINF) /(X(2,I)*X(1,I)*.01219): NEXT
9760  NEXT
9770  GOTO 9820
9780  IFLOP=1          'Convert to kUNI { kBI*[M] - kUNI/[M] *[M] }
9790  FOR I=1 TO ICOUNT
9800  FOR KT=2 TO 19: Y(KT,I)=Y(KT,I)*X(2,I)*X(1,I)*.01219: NEXT
9810  NEXT
9820  RETURN

```

Appendix L.4. Example of Input Form for Unimolecular QRRK

Reaction set for: Phenyl

(D) Decomposition to products: H+Benzyne
(DD) Secndry decomp'n to new products:
(DD) Secndry decomp'n to new products:
(D) Decomposition to products:
(DD) Secndry decomp'n to new products:
(DD) Secndry decomp'n to new products:
(DD) Secndry decomp'n to new products:
(DDD) Tertiary decomp to new products:
(DDD) Tertiary decomp to new products:
(D) Decomposition to products:
(DD) Secndry decomp'n to new products:
(DDD) Tertiary decomp to new products:
(DDDD) 4th-ordr decmp to new products:
(IS) Isomeriz'n/stabil'n product: L-C6H5
(ID) Isomeriz'n/dissoc'n rxn products: 1-C4H3 + C2H2
(DD) Secndry decomp'n to new products:
(ID) Isomeriz'n/dissoc'n rxn products: H + L-C6H4

Mean freq of reactt= 1180. wavenumbers,S= 27 oscillators
Complex: MW= 77.00, Diameter(σ)= 5.950 angstroms, Well (ϵ/K)= 400.00
Bath gas Ar

MW= 39.94, σ = 3.330, ϵ/K = 136.50, E(coll)= 740.

(AD) Add'n/decomp'n to new products: Phenyl - Benzyne+H
A and barrier for decomp'n of adduct= +4.900E+13, 87.50
Product*: Freq=1000;S= 0 oscillators,E(vs adduct)= 0.00 kcal
Prodct*: MW= 0.00, Diameter(σ)= 0.000 angstroms, Well (ϵ/K)= 0.00
A and barrier for secondary decomp'n = +0.000E+00, 0.00
A and barrier for secondary decomp'n = +0.000E+00, 0.00
(AD) Add'n/decomp'n to new products: **** -
A and barrier for decomp'n of adduct= +0.000E+00, 0.00
Product*: Freq=1000;S= 0 oscillators,E(vs adduct)= 0.00 kcal
Prodct*: MW= 0.00, Diameter(σ)= 0.000 angstroms, Well (ϵ/K)= 0.00
A and barrier for secondary decomp'n = +0.000E+00, 0.00
Product*: Freq=1000;S= 0 oscillators,E(vs adduct)= 0.00 kcal
Prodct*: MW= 0.00, Diameter(σ)= 0.000 angstroms, Well (ϵ/K)= 0.00
A and barrier for secondary decomp'n = +0.000E+00, 0.00
Product*: Freq=1000;S= 0 oscillators,E(vs adduct)= 0.00 kcal
Prodct*: MW= 0.00, Diameter(σ)= 0.000 angstroms, Well (ϵ/K)= 0.00
A and barrier for tertiary decomp'n = +0.000E+00, 0.00
(AD) Add'n/decomp'n to new products: **** -
A and barrier for decomp'n of adduct= +0.000E+00, 0.00
Product*: Freq=1000;S= 0 oscillators,E(vs adduct)= 0.00 kcal
Prodct*: MW= 0.00, Diameter(σ)= 0.000 angstroms, Well (ϵ/K)= 0.00
A and barrier for secondary decomp'n = +0.000E+00, 0.00
Product*: Freq=1000;S= 0 oscillators,E(vs adduct)= 0.00 kcal
Prodct*: MW= 0.00, Diameter(σ)= 0.000 angstroms, Well (ϵ/K)= 0.00
A and barrier for tertiary decomp'n = +0.000E+00, 0.00
Product*: Freq=1000;S= 0 oscillators,E(vs adduct)= 0.00 kcal
Prodct*: MW= 0.00, Diameter(σ)= 0.000 angstroms, Well (ϵ/K)= 0.00
A and barrier for 4th-ordr decomp'n = +0.000E+00, 0.00

(IS) Isomeriz'n/stabil'n product: C-C6H5 - L-C6H5
 A and barrier for isomer'n of adduct= +1.200E+14, 70.90
 A and barrier for reverse isomeriz'n= +4.000E+10, 7.00
 E(isomer)-E(adduct) = 63.90, Isomer freq= 990. wavenumbers
 (ID) Isomeriz'n/dissoc'n rxn products: C-C6H5 - 1-C4H3 + C2H2
 A and barrier for decomp'n of isomer= +5.500E+14, 45.80
 Product*: Freq=1000;S= 0 oscillators,E(vs adduct)= 0.00 kcal
 Product*: MW= 0.00, Diameter(σ)= 0.000 angstroms, Well (ϵ /K)= 0.00
 A and barrier for secondary decomp'n = +0.000E+00, 0.00
 (ID) Isomeriz'n/dissoc'n rxn products: C-C6H7 - H + L-C6H4
 A and barrier for decomp'n of isomer= +8.000E+12, 36.70

APPENDIX M.

Selection of $\langle \Delta E_{c011} \rangle$ from data compilations (kJ/g-mol)

	<u>He</u>	<u>Ar</u>	<u>H₂</u>	<u>N₂</u>	<u>O₂</u>	<u>CO</u>	<u>CH₄</u>	<u>CO₂</u>	<u>C₂H₆</u>	<u>C₃H₈</u>	<u>C₄H₁₀</u>	<u>C₅H₁₂</u>
-From Troe, 1979-												
I+NO ₂ →												
INO ₂ ,												
300 K	1.2	3.3	0.8	4.1	6	8	3.7	-	-	>8	-	-
CH ₃ NC→												
CH ₃ NC,												
554 K	2.1	2.8	2.1	4.6	-	5.5	11	9	-	>20	-	-
C ₂ H ₅ NC→												
C ₂ H ₅ NC,												
504 K	2.5	5.0	2.4	6.1	-	-	≤16	16	-	>20	-	-
Azulene→												
Toluene,												
300 K	1.7	3.8	2.9	3.1	4.6	5.2	9.0	9.9	-	17	-	-
CH ₃ +CF ₃												
→ CH ₃ CF ₃ ,												
300 K	2.6	1.9	4.5	4.5	-	-	10	6.5	-	-	-	-
- From Gardiner and Troe, 1984-												
C ₇ H ₈												
isom.,												
300 K	1.8	3.7	2.6	2.9	4.4	-	8.8	10	17	18	30	18
CINO												
decomp.,												
1000K	2.0	1.2	-	2.0	-	-	-	2.6	-	-	-	-
NO ₂												
decomp.,												
1800K	11	3.0	-	5.5	3.6	-	-	17	-	-	-	-
Mean,												
kJ/mol	2.0	3.1	2.6	4.1	4.6	5.0	9.7	9.8	17	18.5	30	18
cal/mol	470	740	610	980	1110	1200	2320	2350	4100	4180	7200	4300
	(a)						(b)			(c)		

(a) Did not include 11 kJ/mol.

(b) Did not include 3.7 or ≤16 kJ/mol.

(c) Did not include >8, >20, >20 kJ/mol.

APPENDIX N.

Estimation of rate constants for recombination of radicals

Benson (1983) has developed a "restricted free rotor" equation to correlate and predict the recombination rate constants k_{rec} for hydrocarbon radicals, based on a loose transition state and the resulting cross-section for effective collisions. The analysis is extended here to H, O, OH, $^3\text{CH}_2$, and other radicals of interest in combustion.

N.1. Benson's formulation

In essence, the general rate-constant equation for combination of radicals i and j was expressed by Benson as a collision-frequency rate constant Z_r corrected for electronic spin degeneracies g_i and steric restrictions:

$$k_{rec} = Z_r \cdot g_e \cdot \beta_i \beta_j \quad [\text{N.1}]$$

where g_e is the ratio of transition state to reactant spin degeneracies, $g^*/g_i g_j$,
 β_i is the "active" fraction of the surface area of the sphere having diameter $\langle b^* \rangle$, and
 $\langle b^* \rangle$ is the collision diameter required for combination.
 Thus, β_i is the fraction of the surface area of species i that is occupied by unpaired electrons.

Benson worked out an equation for Z_r that properly averages velocities over a Boltzmann distribution, but the published form (Eq. 11 in Benson, 1983) contains several typographical errors. Corrected, it becomes:

$$\langle Z_r \rangle = \frac{2.25}{(\mu/2)^{1/2}} (v_0)^{1/3} (RT)^{1/6} (1.019) \cdot \frac{\pi r_0^2 N}{\sigma} \quad [\text{N.2}]$$

where μ is $M_i M_j / (M_i + M_j)$, the reduced molecular weight of the two radicals,

V_0 is the potential energy of the bond that will be formed,
 $(D^\circ + \epsilon_z^{AB} - \epsilon_z^A - \epsilon_z^B)$,

D° is the bond dissociation energy,

ϵ_z is the zero-point vibrational energy, $0.5\sum(h\nu_k)$ with the
sum over $k=1$ to s vibrational frequencies of the species,

r_0 is the normal bond length,

N_{Av} is Avogadro's number, and

σ is a symmetry factor such that $\sigma=2$ for identical radicals
or $\sigma=1$ for different radicals.

At 300 K, with V_0 (D° , ϵ_z) in kcal/mol and r_0 in Å, Eq. N.2 becomes:

$$\langle Z_r \rangle_{300} = 1.151 \cdot 10^{14} \frac{V_0^{1/3} r_0^2}{\sigma \mu^{1/2}} \quad [N.3]$$

where $\langle Z_r \rangle$ is in $\text{cm}^3 \text{mol}^{-1} \text{s}^{-1}$, V_0 is in kcal/mol, and r_0 is in Å.

Benson considered only recombination of simple (doublet)
radicals to form stable (singlet) species, so his ratio of spin
degeneracies g_e was always $1/(2 \cdot 2)$ or $1/4$.

The active-surface fractions β_i were analyzed in two ways.
First, Eq. N.1 was used to obtain $\beta_1 \beta_2$ by dividing measured rate
constants by $Z_r g_e$, a method which gives β_{12} if the recombining
radicals are the same. Second, β_i was estimated geometrically by
calculating $\langle b^* \rangle$ from

$$\frac{\langle b^* \rangle}{r_0} = 1.52 \left(\frac{V_0}{RT} \right)^{1/6} \quad [N.4]$$

and estimating the fraction of sphere surface area that is obstructed
by atoms or groups, which is the inactive surface area. Benson
showed good agreement between the two estimates.

N.2. Estimation of β_i for the present calculations

The first method (inference from data) would appear to be the
most reliable for obtaining values useful in making predictions. To
do this, sufficient data on high-pressure-limit recombination rate

constants $k_{rec, \infty}$ are necessary. As implied in Ch. VI.4 and illustrated in Ch. VII, low-pressure-limit rate constants for exothermic, chemically activated decompositions can be equal to $k_{rec, \infty}$. These two sources of data are used here to estimate β_i for various radicals of interest.

H. - A zero-th order case is H atom, which has a single unpaired electron ($g_H=1$) in an s-orbital, so $\beta(H)=1$.

CH₃. - Methyl may be analyzed from k_{∞} for $CH_3+CH_3 \rightarrow C_2H_6$, as Benson did, or from k_{∞} for $H+CH_3$.

CH₃ recombination was recently studied at elevated pressures by Hippler et al. (1985), giving $k_{\infty}(298\text{ K})=3.4_3 \cdot 10^{13} \text{ cm}^3\text{mol}^{-1}\text{s}^{-1}$. Use of high pressures makes this measurement particularly reliable, and it is in excellent agreement with previous measurements (see the recent review by Warnatz, 1984).

The barrier may be calculated as:

$$\begin{aligned} \Delta H_{iBS}^{\ddagger}(0\text{ K}) &= 87.7 \text{ kcal/mol} \\ + \epsilon_z(C_2H_6) &= 42.6 &= 0.5 \cdot (0.0026865) \cdot (2954 + 1388 + 995 \\ & & + 2896 + 1379 + 2 \cdot 2969 + 2 \cdot 1468 + \\ & & 2 \cdot 1190 + 2 \cdot 2985 + 2 \cdot 1469 + 2 \cdot 822 \\ & & [\text{Burcat, 1984}] + 320 \text{ cm}^{-1} [\text{internal} \\ & & \text{rotation at 300 K, Benson, 1976}]) \\ - 2 \cdot \epsilon_z(CH_3) &= 2 \cdot 17.1 &\text{from } 3002, 580, 2 \cdot 3184, 2 \cdot 1383 \text{ cm}^{-1} \\ & & (\text{Burcat, 1984}) \end{aligned}$$

$$V_0 = 96.1 \text{ kcal/mol}$$

and by using $r_0=1.54 \text{ \AA}$ (Benson, 1976), $\mu=15^2/(15+15)$, and $g_e=1/2 \cdot 2$, the rest of the calculation gives:

$$\begin{aligned} \langle Z_r \rangle &= 2.28 \cdot 10^{14} \text{ cm}^3\text{mol}^{-1}\text{s}^{-1} \\ \beta(CH_3)^2 &= k_{\infty} / (\langle Z_r \rangle \cdot g_e) = 3.4 \cdot 10^{13} / (2.28 \cdot 10^{14} / 4) = 0.60 \\ \beta(CH_3) &= 0.77 . \end{aligned}$$

Benson obtained a lower $\beta(CH_3)$ of 0.55 by geometric analogies. For the experimental inference, he reported $\beta(CH_3)^2=0.42$, which gives $\beta(CH_3)=0.65$. The reason that this is lower than the present calculations is that Benson chose to use a larger k_{∞} ($2.4 \cdot 10^{13}$).

The other estimate of $\beta(\text{CH}_3)$ comes from k_{∞} of $\text{H}+\text{CH}_3 \rightarrow \text{CH}_4$, which has been reported as $1.2 \cdot 10^{14}$ at 298 K (Sworsky et al., 1980). Using $r_0=1.091$ Å (Stull et al., 1971), $\mu=1.15/(1+15)$, and $g_e=1/2 \cdot 2$, calculation of the various parameters gives:

$$\begin{array}{ll} \Delta H_{\text{fiss}}^{\circ}(0 \text{ K}) = 103.2 \text{ kcal/mol} & \text{(Stull et al., 1971)} \\ + \epsilon_z(\text{CH}_4) = 25.5 & \text{from 2917, 2.1534, 3.3019, and} \\ & \text{3.1306 (Stull et al., 1971)} \\ - \epsilon_z(\text{CH}_3) = 17.1 & \text{from above} \\ - \epsilon_z(\text{H}) = 0 & \end{array}$$

$$\begin{array}{ll} V_0 = 111.6 \text{ kcal/mol} \\ \langle Z_r \rangle = 6.80 \cdot 10^{14} \text{ cm}^3 \text{ mol}^{-1} \text{ s}^{-1} \\ \beta(\text{H})\beta(\text{CH}_3) = k_{\infty}/(\langle Z_r \rangle \cdot g_e) = 1.2 \cdot 10^{14}/(6.80 \cdot 10^{14}/4) = 0.71 \\ \beta(\text{CH}_3) = 0.71 \end{array}$$

The two values are in good agreement with each other and give a mean value of $\beta(\text{CH}_3)=0.74 \pm 5\%$.

OH. - The best data from which to analyze $\beta(\text{OH})$ are the $\text{CH}_3\text{OH} \rightarrow \text{CH}_3+\text{OH}$ data of Spindler and Wagner (1982). They inferred $k_{\infty}=9.4 \cdot 10^{15} \exp(-89.9/\text{RT})$ for dissociation from 1600-2100 K. In that range, the equilibrium constant for dissociation is $205 \cdot \exp(-90.0/\text{RT})$ (K_c), yielding $k_{\infty}(\text{CH}_3+\text{OH} \rightarrow \text{CH}_3\text{OH})=4.6 \cdot 10^{13} \text{ cm}^3 \text{ mol}^{-1} \text{ s}^{-1}$ by microscopic reversibility. Then:

$$\begin{array}{ll} \Delta H_{\text{fiss}}^{\circ}(0 \text{ K}) = 90.2 \text{ kcal/mol} & \text{(from data base of Burcat, 1984)} \\ + \epsilon_z(\text{CH}_3\text{OH}) = 29.3 & \text{from 3681, 3000, 2844, 1477,} \\ & \text{1455, 1345, 1060, 1033, 2960,} \\ & \text{1477, 1165, 298 (Burcat, 1984)} \\ - \epsilon_z(\text{CH}_3) = 17.1 & \text{from above} \\ - \epsilon_z(\text{OH}) = 5.0 & 3735 \text{ cm}^{-1} \text{ (Chase et al., 1974)} \end{array}$$

$$\begin{array}{ll} V_0 = 97.4 \text{ kcal/mol} \\ r_0 = 1.43 \text{ Å (Benson, 1976); } g_e=1/2 \cdot 2=1/4 \\ \langle Z_r \rangle = 3.84 \cdot 10^{14} \text{ cm}^3 \text{ mol}^{-1} \text{ s}^{-1} \\ \beta(\text{CH}_3)\beta(\text{OH}) = k_{\infty}/(\langle Z_r \rangle \cdot g_e) = 4.6 \cdot 10^{13}/(3.84 \cdot 10^{14}/4) = 0.48 \\ \beta(\text{OH}) = 0.64 \end{array}$$

O-atom (³P). - Rate constants for the chemically activated addition/decomposition reactions of O-atom with OH and CH_3 correspond to 53% and 100% of the k_{∞} for simple addition, according to QRRK

calculations (Ch. VII). These rate constants then lead to estimates of $\beta(0)$.

For $O+OH \rightarrow (HO_2)^* \rightarrow H+O_2$, previous reviews and measurements gave $k_{298}=2.3, 2.6, 1.7, \text{ and } 2.3 \cdot 10^{13} \text{ cm}^3\text{mol}^{-1}\text{s}^{-1}$ (Warnatz, 1984) with a recommended value of $1.8 \cdot 10^{13}$. Recent measurements by Cobos et al. (1985a) gave the very similar value of $1.7 \cdot 10^{13} \text{ cm}^3\text{mol}^{-1}\text{s}^{-1}$. Using the QRRK result, these values imply $k_{\infty}(O+OH \rightarrow HO_2)=3.4 \cdot 10^{13}$. The calculation of $\beta(0)$ from this rate constant may be summarized as follows:

$$\begin{array}{ll}
 \Delta H_{\text{diss}}^{\circ}(0 \text{ K}) = 65.2 \text{ kcal/mol} & \text{from Stull et al., 1971, except} \\
 & \text{for } \Delta H_{298}^{\circ}(HO_2)=2.5 \text{ kcal/mol} \\
 + \epsilon_z(HO_2) = 7.9 & \text{from Howard (1976)} \\
 - \epsilon_z(O) = 0.0 & \text{from 1389, 1101, 3414 (Stull et} \\
 - \epsilon_z(OH) = 5.0 & \text{al., 1971)} \\
 \hline
 V_0 = 68.1 \text{ kcal/mol} & \\
 r_0 = 1.30 \text{ \AA} & \text{(Stull et al., 1971); } g_e=2/3 \cdot 2=1/3 \\
 \langle Z_r \rangle = 2.77 \cdot 10^{14} \text{ cm}^3\text{mol}^{-1}\text{s}^{-1} & \\
 \beta(O)\beta(OH) = k_{\infty}/(\langle Z_r \rangle \cdot g_e) = 3.4 \cdot 10^{13}/(2.77 \cdot 10^{14}/3) = 0.37 & \\
 \beta(O) = 0.58 . &
 \end{array}$$

Alternatively, $O+CH_3 \rightarrow (CH_3-O\cdot)^* \rightarrow H+H_2CO$ should proceed at 298 K at k_{∞} for $O+CH_3 \rightarrow CH_3-O\cdot$. Unfortunately, there is appreciable scatter in reported measurements - 4.8, 6.0, 8.3, $11 \cdot 10^{13} \text{ cm}^3\text{mol}^{-1}\text{s}^{-1}$ at 298 K (Warnatz, 1984), with a mean of $7.6 \cdot 10^{13} \text{ cm}^3\text{mol}^{-1}\text{s}^{-1}$. Warnatz chose to recommend $7.0 \cdot 10^{13}$ over the full range of 300-2500 K. This rate constant also provides an estimate of $\beta(0)$:

$$\begin{array}{ll}
 \Delta H_{\text{diss}}^{\circ}(0 \text{ K}) = 88.7 \text{ kcal/mol} & \text{from data base of Burcat (1984)} \\
 + \epsilon_z(CH_3O) = 22.1 & \text{from 3000, 2844, 1477, 1455,} \\
 & \text{1060, 1033, 2960, 1477, 1165} \\
 & \text{(Burcat, 1984)} \\
 - \epsilon_z(CH_3) = 17.1 & \text{from above} \\
 - \epsilon_z(O) = 0.0 & \\
 \hline
 V_0 = 93.7 \text{ kcal/mol} & \\
 r_0 = 1.43 \text{ \AA} & \text{(for C-O bond, Benson, 1976); } g_e=2/2 \cdot 3=1/3 \\
 \langle Z_r \rangle = 3.84 \cdot 10^{14} \text{ cm}^3\text{mol}^{-1}\text{s}^{-1} &
 \end{array}$$

$$\beta(\text{CH}_3)\beta(0) = k_{\infty}/(\langle Z_r \rangle \cdot g_e) = 7.6 \cdot 10^{13} / (3.84 \cdot 10^{14} / 3) = 0.59$$

$$\beta(0) = 0.80 \quad (0.50 \text{ to } "1.15").$$

This second value of $\beta(0)$ is higher than the other by 40%. The calculation from O+OH is based on a more certain rate constant, but $\beta(\text{OH})$ is also needed, and it has an unknown amount of uncertainty. The range of rate constants for CH_3+O gives a range of $\beta(0)$ from 0.51 to 1.16 [sic], but $\beta(\text{CH}_3)$ seems to be correct within 5%. Geometric arguments would favor a number somewhat higher than $\beta(\text{OH})=0.65$, as O-atom has nearly the same geometry but an unpaired electron in place of the H in OH.

A mean of the two values, 0.69, then can be used with an uncertainty of 20% or less. It is worthwhile to note that with the O+OH calculation, $\beta(0)=0.69$ would imply $\beta(\text{OH})=0.54$, suggesting that its uncertainty is 10-20%.

$^3\text{CH}_2$. - There are three reactions for estimating $\beta(^3\text{CH}_2)$, all relying on $k_{\infty}(\text{addition/stabilization})=k(\text{addition/decomposition})$ in a low-pressure limit. These are $^3\text{CH}_2$ combinations with CH_3 , O, and itself.

In the first case, $^3\text{CH}_2+\text{CH}_3$ forms $\text{H}+\text{C}_2\text{H}_4$. As shown in Ch. VII, the reaction is initially a combination to make excited ethyl radical, C_2H_5^* , which then undergoes chemically activated decomposition. Warnatz (1984) chose $k=4 \cdot 10^{13}$ for the reaction from measurements of 3 to $6 \cdot 10^{13}$. Calculations for the combination step give:

$\Delta H_{\text{diss}}^{\circ}(0 \text{ K}) = 98.2 \text{ kcal/mol}$	calculated from Burcat (1984),
	$\Delta H_{\text{f}, 298}^{\circ}(^3\text{CH}_2)=91.1 \pm 0.7 \text{ kcal/mol}$
	(Böhland and Temps, 1984)
$+ \epsilon_z(\text{C}_2\text{H}_5) = 35.3$	from 2925, 3·3000, 2950, 3·1050,
	1400, 3·1450, 800, 1250, 1300
	(Burcat, 1984) and 200 for the
	internal rotation, calculated
	from moments of inertia and the
	torsion barrier (after Benson,
	1976)
$- \epsilon_z(^3\text{CH}_2) = 9.6$	from 2954, 1056, 3123 (Chase et
	al., 1975)
$- \epsilon_z(\text{CH}_3) = 17.1$	from above
<hr style="width: 50%; margin-left: 0;"/>	
$V_C = 106.8 \text{ kcal/mol}$	
$r_O = 1.54 \text{ \AA}$ (for C-C bond, Benson, 1976);	$g_e=2/3 \cdot 2=1/3$

$$\langle Z_T \rangle = 4.81 \cdot 10^{14} \text{ cm}^3 \text{ mol}^{-1} \text{ s}^{-1}$$

$$\beta(^3\text{CH}_2)\beta(\text{CH}_3) = k_\infty / (\langle Z_T \rangle \cdot g_e) = 4 \cdot 10^{13} / (4.81 \cdot 10^{14} / 3) = 0.25$$

$$\beta(^3\text{CH}_2) = 0.34 \quad (0.25-0.51 \text{ from various } k_\infty \text{ measurements}).$$

For $^3\text{CH}_2+\text{O}$, Warnatz (1984) reviewed the rate constants of 5 to $8 \cdot 10^{13}$ for formation of the products $\text{CO}+2\text{H}$, selecting $5 \cdot 10^{13}$. More recently, Böhlend, Temps, and Wagner (1984) have measured the rate constant for $^3\text{CH}_2+\text{O}$ as $(8.1 \pm 3.0) \cdot 10^{13}$. This reaction is analyzed in Ch. VII as formation of $(\cdot\text{CH}_2-\text{O}\cdot)^*$, rapidly forming $\text{H}_2\text{C}=\text{O}^*$, decomposing to $\text{H}+\text{HCO}^*$ and then to $2\text{H}+\text{CO}$.

To analyze the combination rate constant, $\Delta H_{\text{diss}}^\ddagger(0 \text{ K})$ and the frequencies for $\cdot\text{CH}_2-\text{O}\cdot$ first must be estimated. The heat of dissociation is estimated using the pi-bond energy $E_{\pi}^\circ(\text{H}_2\text{C}=\text{O})$ at 0 K following Benson's analysis (Benson, 1976) of $E_{\pi}^\circ(\text{H}_2\text{C}=\text{CH}_2)$:

$$\begin{aligned} E_{\pi,0}^\circ(\text{H}_2\text{C}=\text{O}) &= \Delta\text{H}(\text{H}) + \Delta\text{H}(\text{CH}_2\text{OH}) - \Delta\text{H}(\text{CH}_3\text{OH}) \\ &\quad - [\Delta\text{H}(\text{H}) + \Delta\text{H}(\text{H}_2\text{CO}) - \Delta\text{H}(\text{CH}_2\text{OH})] \\ &= 2 \cdot \Delta\text{H}(\text{CH}_2\text{OH}) - \Delta\text{H}(\text{CH}_3\text{OH}) - \Delta\text{H}(\text{H}_2\text{CO}) \\ &= 2(-4.0-2.6) - (-48.1-2.3) - (-27.7-2.3) \\ &= 67.2 \text{ kcal/mol} \end{aligned}$$

$$\begin{aligned} \text{or} &= \Delta\text{H}(\text{H}) + \Delta\text{H}(\text{CH}_3\text{O}) - \Delta\text{H}(\text{CH}_3\text{OH}) \\ &\quad - [\Delta\text{H}(\text{H}) + \Delta\text{H}(\text{H}_2\text{CO}) - \Delta\text{H}(\text{CH}_3\text{O})] \\ &= 2 \cdot \Delta\text{H}(\text{CH}_3\text{O}) - \Delta\text{H}(\text{CH}_3\text{OH}) - \Delta\text{H}(\text{H}_2\text{CO}) \\ &= 2(-4.0-2.6) - (-48.1-2.3) - (-27.7-2.3) \\ &= 84.2 \text{ kcal/mol} \end{aligned}$$

$$\begin{aligned} \Delta H_{\text{diss}}^\ddagger &= \Delta H^\circ(\text{H}_2\text{CO} \rightarrow ^3\text{CH}_2+\text{O}) - E_{\pi}^\circ(\text{H}_2\text{CO}) \\ &= [(91.1-2.3) + (59.6-1.7) - (-27.7-2.3)] - (67.2+84.2)/2 \\ &= 101.0 \text{ kcal/mol} \end{aligned}$$

and the six frequencies may be estimated by the frequency-assignment methods of Benson (1976) to be:

2 C-H stretches at 3100 cm^{-1}
 1 C-O stretch at 1100 cm^{-1}
 1 H-C-H scissors at 1450 cm^{-1}
 2 H-C-O bends at 1140 cm^{-1} .

Then, estimation of $\beta(^3\text{CH}_2)$ proceeds as before:

$$\begin{aligned}
\Delta H_{\text{iss}}^{\circ}(0 \text{ K}) &= 101.0 \text{ kcal/mol} \\
+ \epsilon_z(\cdot\text{CH}_2\text{-O}\cdot) &= 14.8 \\
- \epsilon_z(^3\text{CH}_2) &= 9.6 \\
- \epsilon_z(\text{O}) &= 0.0
\end{aligned}$$

$$V_0 = 106.2 \text{ kcal/mol}$$

$$r_0 = 1.43 \text{ \AA} \quad (\text{for C-O bond, Benson, 1976}); \quad g_e = 3/3 \cdot 3 = 1/3$$

$$\langle Z_r \rangle = 4.08 \cdot 10^{14} \text{ cm}^3 \text{ mol}^{-1} \text{ s}^{-1}$$

$$\beta(^3\text{CH}_2)\beta(\text{O}) = k_{\infty} / (\langle Z_r \rangle \cdot g_e) = 5 \cdot 10^{13} / (4.08 \cdot 10^{14} / 3) = 0.37$$

$$\beta(^3\text{CH}_2) = 0.54 \quad (0.81 \text{ from measurements by Böhland et al.}).$$

The third combination reaction that gives an estimate of $\beta(^3\text{CH}_2)$ is the recombination of $^3\text{CH}_2$ itself. Experimentally there is some uncertainty as to the rate constant, given as $3.2 \cdot 10^{13}$ by Braun et al. (1970), and more questions about the products. Calculations in Ch. VII indicate that the products $\text{C}_2\text{H}_2 + 2\text{H}$ are expected, with a rate constant at 298 K that is the same as k_{∞} for recombination.

As in the case of $^3\text{CH}_2 + \text{O}$, analysis of $\beta(^3\text{CH}_2)$ requires estimation of $\Delta H_{\text{iss}}^{\circ}(0 \text{ K})$ and the frequencies for $\cdot\text{CH}_2\text{-CH}_2\cdot$. The pi-bond energy $E_{\pi}^{\circ}(\text{H}_2\text{C}=\text{CH}_2)$ and $\Delta H_{\text{iss}}^{\circ}(0 \text{ K})$ are calculated as follows:

$$\begin{aligned}
E_{\pi,0}^{\circ}(\text{H}_2\text{C}=\text{CH}_2) &= \Delta H(\text{H}) + \Delta H(\text{C}_2\text{H}_5) - \Delta H(\text{C}_2\text{H}_6) \\
&\quad - [\Delta H(\text{H}) + \Delta H(\text{C}_2\text{H}_4) - \Delta H(\text{C}_2\text{H}_5)] \\
&= 2 \cdot \Delta H(\text{C}_2\text{H}_5) - \Delta H(\text{C}_2\text{H}_6) - \Delta H(\text{C}_2\text{H}_4) \\
&= 2(25.6 - 2.2) - (-20.0 - 2.3) - (12.5 - 1.9) \\
&= 58.5 \text{ kcal/mol}
\end{aligned}$$

$$\begin{aligned}
\Delta H_{\text{iss}}^{\circ}(0 \text{ K}) &= \Delta H^{\circ}(\text{C}_2\text{H}_4 \rightarrow ^3\text{CH}_2 + ^3\text{CH}_2) - E_{\pi}^{\circ}(\text{C}_2\text{H}_4) \\
&= [2 \cdot (91.1 - 2.3) - (12.5 - 1.9)] - 58.5 \\
&= 108.5 \text{ kcal/mol}
\end{aligned}$$

and the 12 frequencies may be estimated to be:

4 C-H stretches	at 3100 cm^{-1}
1 C-C stretch	at 1000 cm^{-1}
2 H-C-H scissors	at 1450 cm^{-1}
4 H-C-C bends	at 1150 cm^{-1}
1 free rotor	at <100 cm^{-1} .

Then $\beta(^3\text{CH}_2)$ may be estimated as:

$$\Delta H_{\text{iss}}^{\circ}(0 \text{ K}) = 108.5 \text{ kcal/mol}$$

$$\begin{aligned}
 + \epsilon_2 (\cdot\text{CH}_2\text{-CH}_2\cdot) &= 28.2 \\
 - 2 \cdot \epsilon_2 ({}^3\text{CH}_2) &= 2 \cdot 9.6
 \end{aligned}$$

$$\begin{aligned}
 V_0 &= 117.5 \text{ kcal/mol} \\
 r_0 &= 1.54 \text{ \AA} \quad (\text{for C-C bond, Benson, 1976}); \quad g_e = 3/3 \cdot 3 = 1/3 \\
 \langle Z_r \rangle &= 2.53 \cdot 10^{14} \text{ cm}^3 \text{ mol}^{-1} \text{ s}^{-1} \quad [\sigma = 2] \\
 \beta({}^3\text{CH}_2)^2 &= k_{\infty} / (\langle Z_r \rangle \cdot g_e) = 3.2 \cdot 10^{13} / (2.53 \cdot 10^{14} / 3) = 0.38 \\
 \beta({}^3\text{CH}_2) &= 0.62 .
 \end{aligned}$$

In summary, estimates from the three reactions for $\beta({}^3\text{CH}_2)$ are 0.34 (0.25-0.51), 0.54 (or up to 0.81), and 0.62. These are in reasonable agreement, but the range of uncertainty for the first (${}^3\text{CH}_2 + \text{CH}_3$) and the agreement of the other two suggests that the best value is $\beta({}^3\text{CH}_2) = 0.58$, the mean of the second two estimates, with an uncertainty that appears to be well within 50% and probably within 25%. It is appropriate to note that $\beta(0)$, which is isoelectronic with ${}^3\text{CH}_2$, was estimated to be 0.69 (to within 20%). Also, the selected value of $\beta({}^3\text{CH}_2)$ gives an improved estimate of $k({}^3\text{CH}_2 + \text{CH}_3) = 6.9 \cdot 10^{13} \text{ cm}^3 \text{ mol}^{-1} \text{ s}^{-1}$ at 298 K.

CH(${}^2\Delta$). - The steric factor for CH can be estimated from the rate constant for $\text{CH} + \text{O} \rightarrow \text{H} + \text{CO}$. That reaction is shown in Ch. VII to be chemically activated addition/decomposition of excited formyl radical, and its rate constant should equal k_{∞} for the combination $\text{CH}({}^2\Delta) + \text{O}({}^3\text{P})$. The initial combination would form a doublet carbene species, $:\text{CH}-\text{O}\cdot$, which should undergo rapid, barrierless transitions to $\cdot\text{CH}-\text{O}\cdot$ and then to $\cdot\text{HC}=\text{O}$.

The review of Warnatz (1984) includes measurements of 2 to $5.7 \cdot 10^{13} \text{ cm}^3 \text{ mol}^{-1} \text{ s}^{-1}$. He selected $4.0 \cdot 10^{13} \text{ cm}^3 \text{ mol}^{-1} \text{ s}^{-1}$ as the best value.

The heat of dissociation for $:\text{CH}-\text{O}\cdot$ may be estimated by assuming the energy difference from $\cdot\text{CH}-\text{O}\cdot$ is 9.0 kcal/mol, the same as the singlet-triplet gap between $:\text{CH}_2$ (${}^1\text{CH}_2$) and $\cdot\text{CH}_2\cdot$ (${}^3\text{CH}_2$) (Goddard, 1985). The heat of formation of $\cdot\text{CH}-\text{O}\cdot$ would be higher than that of $\cdot\text{HC}=\text{O}$ approximately by the pi-bond energy $E_{\pi^{\circ}}(\text{H}_2\text{C}=\text{O})$, 75.7 kcal/mol. Then from $\Delta H_0(\cdot\text{HCO} \rightarrow \text{CH} + \text{O}) = 189.8 \text{ kcal/mol}$, $\Delta H_{\text{fiss},0}^{\circ}(:\text{CH}-\text{O}\cdot \rightarrow \text{CH} + \text{O}) = 189.8 - 9.0 - 75.7 = 105.1 \text{ kcal/mol}$.

The three frequencies of $\cdot\text{CH-O}\cdot$ may be estimated by the frequency-assignment methods of Benson (1976) to be 3100, 1100, and 1140 (C-H stretch, C-O stretch, and H-C-O bend).

Finally, estimation of $\beta(\text{CH})$ is as before:

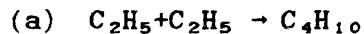
$$\begin{aligned}
 \Delta H_{\text{fiss}}^{\ddagger}(0 \text{ K}) &= 105.1 \text{ kcal/mol} \\
 + \epsilon_z(\cdot\text{CH-O}\cdot) &= 7.2 \\
 - \epsilon_z(\text{CH}) &= 3.8 \quad \text{from } \omega=2861 \text{ cm}^{-1} \text{ (Stull et al., 1971)} \\
 - \epsilon_z(\text{O}) &= 0.0 \\
 \hline
 V_0 &= 108.5 \text{ kcal/mol} \\
 r_0 &= 1.43 \text{ \AA} \quad (\text{for C-O bond, Benson, 1976}); \quad g_e=2/2 \cdot 3=1/3 \\
 \langle Z_T \rangle &= 4.19 \cdot 10^{14} \text{ cm}^3 \text{ mol}^{-1} \text{ s}^{-1} \\
 \beta(\text{CH})\beta(\text{O}) &= k_{\infty}/(\langle Z_T \rangle \cdot g_e) = 4.0 \cdot 10^{13}/(4.19 \cdot 10^{14}/3) = 0.29 \\
 \beta(\text{CH}) &= 0.42 \pm 50\% \quad (0.21-0.59) .
 \end{aligned}$$

C₂H₅. - Two reactions of C₂H₅ may be used to obtain estimates of $\beta(\text{C}_2\text{H}_5)$ with rather different results. These are the simple combinations $\text{C}_2\text{H}_5 + \text{C}_2\text{H}_5 \rightarrow \text{C}_4\text{H}_{10}$ and $\text{C}_2\text{H}_5 + \text{CH}_3 \rightarrow \text{C}_3\text{H}_8$. For the rate constants, Warnatz (1984) selected $1.0 \cdot 10^{13}$ (300-1200 K; from $8.4 \cdot 10^{12}$ to $1.6 \cdot 10^{13}$) and $7.0 \cdot 10^{12}$ (2.5 to $7.5 \cdot 10^{12}$), respectively.

For these two reactions, frequencies of the n-alkanes C₄H₁₀ and C₃H₈ must be estimated to obtain zero-point energies:

	$\omega(\text{cm}^{-1})$	Degeneracy	
		C ₄ H ₁₀	C ₃ H ₈
C-H stretches	3100	10	8
C-C stretches	1000	3	2
C-C-C bends	420	2	1
CH ₃ groups:			
H-C-H scissors	1450	6	6
H-C-C rock/wag/twists	1150	4	4
CH ₂ groups:			
H-C-H scissors	1450	2	1
H-C-C wag	1150	2	1
H-C-C twist	1150	2	1
H-C-C rock	700	2	1
Ethyl-ethyl rotation	250	1	-
Methyl-propyl rotation	230	2	-
Methyl-ethyl rotation	250	-	1

Calculations then may then be summarized for the two cases:



$$\begin{aligned} \Delta H_{\text{dis}}^{\circ}(0 \text{ K}) &= 80.7 \text{ kcal/mol} \\ + \epsilon_z(C_4H_{10}) &= 77.3 \\ - 2 \cdot \epsilon_z(C_2H_5) &= -2 \cdot 35.3 \end{aligned}$$

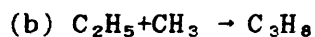
$$V_0 = 87.4 \text{ kcal/mol}$$

$$r_0 = 1.54 \text{ \AA} \quad (\text{for C-C bond, Benson, 1976}); \quad g_e = 1/2 \cdot 2 = 1/4$$

$$\langle Z_r \rangle = 1.59 \cdot 10^{14} \text{ cm}^3 \text{ mol}^{-1} \text{ s}^{-1} \quad [\sigma = 2]$$

$$\beta(C_2H_5)^2 = k_{\infty} / (\langle Z_r \rangle \cdot g_e) = 1.0 \cdot 10^{13} / (1.59 \cdot 10^{14} / 4) = 0.25$$

$$\beta(C_2H_5) = 0.50 \quad (0.46 - 0.63) .$$



$$\begin{aligned} \Delta H_{\text{dis}}^{\circ}(0 \text{ K}) &= 83.8 \text{ kcal/mol} \\ + \epsilon_z(C_3H_8) &= 61.1 \\ - \epsilon_z(C_2H_5) &= 35.3 \\ - \epsilon_z(CH_3) &= 17.1 \end{aligned}$$

$$V_0 = 92.5 \text{ kcal/mol}$$

$$r_0 = 1.54 \text{ \AA} \quad (\text{for C-C bond, Benson, 1976}); \quad g_e = 1/2 \cdot 2 = 1/4$$

$$\langle Z_r \rangle = 3.93 \cdot 10^{14} \text{ cm}^3 \text{ mol}^{-1} \text{ s}^{-1}$$

$$\beta(C_2H_5)\beta(CH_3) = k_{\infty} / (\langle Z_r \rangle \cdot g_e) = 7.0 \cdot 10^{12} (3.93 \cdot 10^{14} / 4) = 0.071$$

$$\beta(C_2H_5) = 0.096 \quad (0.034 \text{ to } 0.099) .$$

These estimates are quite different, 0.50 vs. 0.096, but it is not clear whether the source of the problem is in the data or in Benson's model. If anything, $C_2H_5 + CH_3 \rightarrow C_3H_8$ ought to be faster than $C_2H_5 + C_2H_5 \rightarrow C_4H_{10}$ because $\beta(CH_3)$ ought to be greater than $\beta(C_2H_5)$ on conceptual grounds. The data for the reactions appear to indicate the reverse. The most reliable rate constant here is the first, so 0.50 is selected, recognizing its uncertainty.

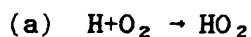
C_2H_3 . - Recombination rate constants for C_2H_3 are in some dispute, so the other data source that might lead to $\beta(C_2H_3)$ is the reaction $C_2H_3 + O \rightarrow \text{products}$. Warnatz (1984) chooses $3 \cdot 10^{13}$ from rate constants of 2 to $3.3 \cdot 10^{13} \text{ cm}^3 \text{ mol}^{-1} \text{ s}^{-1}$. If the product channel(s) are addition/decomposition in the low-pressure limit, a likely possibility, then this rate constant could be used.

Estimation of β proceeds as above:

$\Delta H_{\text{diss}}^{\circ}(0 \text{ K}) = 122.8 \text{ kcal/mol}$	calculated from Burcat (1984), recognizing the initial adduct to be $\cdot\text{CH}_2\text{-CH=O}$
$+ \epsilon_z(\text{C}_2\text{H}_3\text{O}) = 24.2$	from 3005, 2822, 1743, 1441, 1400, 1352, 1113, 509, 2967, 867, 763 (Burcat, 1984) and internal rotation of <100
$- \epsilon_z(\text{C}_2\text{H}_3) = 22.6$	from 3311, 3295, 3178, 1774, 1357, 1176, 1174, 791, 773 (Harding et al., 1982)
$- \epsilon_z(\text{O}) = 0.0$	
<hr/>	
$V_0 = 124.4 \text{ kcal/mol}$	
$r_0 = (1.54+1.43)/2 = 1.49 \text{ \AA}$	$g_e = 2/2 \cdot 3 = 1/3$
$\langle Z_r \rangle = 4.00 \cdot 10^{14} \text{ cm}^3 \text{ mol}^{-1} \text{ s}^{-1}$	
$\beta(\text{C}_2\text{H}_3)\beta(\text{O}) = k_{\infty}/(\langle Z_r \rangle \cdot g_e) = 3 \cdot 10^{13}/(4.00 \cdot 10^{14}/3) = 0.23$	
$\beta(\text{C}_2\text{H}_3) = 0.33$	(uncertainty 50%)

O₂. - O₂ is not a radical, but it is a triplet species because two of its π molecular orbitals are each half-cancelled by antibonding electrons. It is reasonable, then, to examine whether Benson's recombination model fits radical-O₂ reactions. The best-characterized rate constants for testing are k_{∞} 's for $\text{H}+\text{O}_2 \rightarrow \text{HO}_2$ and $\text{CH}_3+\text{O}_2 \rightarrow \text{CH}_3\text{OO}\cdot$. Cobos et al. have recently measured $k_{\infty}(\text{H}+\text{O}_2 \rightarrow \text{HO}_2) = 4.52 \cdot 10^{13}$ (1985a) and $k_{\infty}(\text{CH}_3+\text{O}_2 \rightarrow \text{CH}_3\text{OO}\cdot) = 1.32 \cdot 10^{12}$ (1985c) at 298 K.

$\beta(\text{O}_2)$ can be estimated as before:



$\Delta H_{\text{diss}}^{\circ}(0 \text{ K}) = 48.3$	from Burcat, 1984
$+ \epsilon_z(\text{HO}_2) = 7.9$	from above
$- \epsilon_z(\text{H}) = 0.0$	
$- \epsilon_z(\text{O}_2) = 2.1$	from $\omega = 1580 \text{ cm}^{-1}$ (Stull et al., 1971)
<hr/>	
$V_0 = 54.1 \text{ kcal/mol}$	
$r_0 = 0.958 \text{ \AA}$	(Stull et al., 1971); $g_e = 2/2 \cdot 3 = 1/3$
$\langle Z_r \rangle = 4.06 \cdot 10^{14} \text{ cm}^3 \text{ mol}^{-1} \text{ s}^{-1}$	
$\beta(\text{H})\beta(\text{O}_2) = k_{\infty}/(\langle Z_r \rangle \cdot g_e) = 4.52 \cdot 10^{13}/(4.06 \cdot 10^{14}/3) = 0.33$	
$\beta(\text{O}_2) = 0.33$.

$$\begin{aligned}
 & \text{(b) } \text{CH}_3 + \text{O}_2 \rightarrow \text{CH}_3\text{OO}\cdot \\
 \Delta H_{155}^\ddagger (0 \text{ K}) &= 26.5 && \text{from Burcat (1984)} \\
 + \epsilon_z(\text{CH}_3\text{OO}\cdot) &= 23.6 && \text{from } 3 \cdot 2930, 2 \cdot 1400, 1350, 1100, 960, \\
 & && 2 \cdot 900, 450, 300 \text{ (Burcat, 1984)} \\
 - \epsilon_z(\text{CH}_3) &= 17.1 \\
 - \epsilon_z(\text{O}_2) &= 2.1 \\
 \hline
 V_0 &= 30.9 \text{ kcal/mol} \\
 r_0 &= 1.43 \text{ \AA} \text{ (for C-O bond, Benson, 1976); } g_e = 2/2 \cdot 3 = 1/3 \\
 \langle Z_r \rangle &= 2.31 \cdot 10^{14} \text{ cm}^3 \text{ mol}^{-1} \text{ s}^{-1} \\
 \beta(\text{CH}_3)\beta(\text{O}_2) &= k_\infty / (\langle Z_r \rangle \cdot g_e) = 1.32 \cdot 10^{12} / (2.31 \cdot 10^{14} / 3) = 0.017 \\
 \beta(\text{O}_2) &= 0.023 \text{ .}
 \end{aligned}$$

Geometric arguments would favor a steric factor similar to that of C_2H_3 (0.33), favoring the first estimate and ruling out the second. However, in molecular-orbital theory, the "unpaired" electrons are not free, but rather they are the remains of two π bonding orbitals that are offset in part by two half-filled anti-bonding π^* orbitals. It is reasonable to suspect that O_2 would have barrierless, combination-type reactions with radicals but might not be described very well by Benson's model. If O_2 combinations with alkyl radicals are to be estimated, then, the factor of $\beta(\text{O}_2)=0.023$ would be most appropriate.

Summary of β estimates. - Steric factors may be estimated for CH_2OH and CH_3O by analogy with isoelectronic C_2H_5 and for HC=O by analogy with isoelectronic C_2H_3 . The above results may then be summarized for hydrocarbons and oxygenates as:

0.74 \pm 5%	$\beta(\text{CH}_3)$;	0.64 \pm 15%	$\beta(\text{OH})$
0.58 \pm 25%	$\beta(^3\text{CH}_2)$;	0.69 \pm 20%	$\beta(^3\text{O})$
0.37 \pm 50%	$\beta(\text{CH})$;		
0.5 \pm 80%	$\beta(\text{C}_2\text{H}_5)$;	0.5 \pm 80%	$\beta(\text{CH}_2\text{OH})$ by analogy
		0.5 \pm 80%	$\beta(\text{CH}_3\text{O})$ by analogy
0.33 \pm 50%	$\beta(\text{C}_2\text{H}_3)$;	0.33 \pm 50%	$\beta(\text{HC=O})$ by analogy
		0.023	" $\beta(\text{O}_2)$ " for alkyl radicals (see above)

N.3. Estimates of rate constants for Ch. VII

Using these steric factors, values of $k_{\infty, 298}$ can be estimated with some assurance for reactions examined in Ch. VII. Calculations are shown here in the order used in Ch. VII.

CH(²Δ)+³CH₂ via C₂H₃*. - Calculations are similar to those above for CH+³O in that a doublet species :CH-CH₂· is formed by simple radical combination. Like :CH-O·, this electronically excited species should rapidly convert by barrierless transitions, forming vibrationally excited ·CH·-CH₂· and ·HC=CH₂.

The heat of dissociation for :CH-CH₂· may be estimated by assuming that (1) the energy difference from ·CH·-CH₂· is the same as the singlet-triplet gap between ¹CH₂ and ³CH₂ and (2) that the heat of formation of ·CH·-CH₂· would be higher than that of ·HC=CH₂ by the pi-bond energy E_π^o(H₂C=CH₂).

:CH-O· would have nine frequencies, which may be estimated by the frequency-assignment methods of Benson (1976) to be

3 C-H stretches at 3100 cm⁻¹
 1 C-C stretch at 1000 cm⁻¹
 1 H-C-H scissors at 1450 cm⁻¹
 3 H-C-C bends at 1150 cm⁻¹
 1 free rotor at <100 cm⁻¹.

Estimation of the rate constant then follows a similar form to that used for estimating steric factors:

$$\begin{aligned} \Delta H_{i55}^{\ddagger}(0 \text{ K}) &= \Delta H^{\circ}(\text{C}_2\text{H}_3 \rightarrow \text{CH} + {}^3\text{CH}_2) - E_{\pi}^{\circ}(\text{C}_2\text{H}_4) + E_{\text{S-T}} \\ &= (162.9 - 1.9) - 58.5 + 9.0 \\ &= 111 \text{ kcal/mol} \\ + \epsilon_z(\text{:CH-CH}_2\text{·}) &= 20.6 \\ - \epsilon_z(\text{CH}) &= 3.8 \quad \text{from } \omega=2861 \text{ cm}^{-1} \text{ (Stull et al., 1971)} \\ - \epsilon_z({}^3\text{CH}_2) &= 9.6 \end{aligned}$$

$$V_0 = 118 \text{ kcal/mol}$$

$$r_0 = 1.54 \text{ \AA} \text{ (for C-C bond); } \langle Z_r \rangle = 5.16 \cdot 10^{14} \text{ cm}^3 \text{mol}^{-1} \text{s}^{-1}$$

$$\beta(\text{CH})=0.42 \text{ (50%); } \beta({}^3\text{CH}_2)=0.58 \text{ (25%); } g_e=2/2 \cdot 3=1/3$$

$$\therefore k_{\infty} = \beta(\text{CH}) \cdot \beta({}^3\text{CH}_2) \cdot g_e \cdot \langle Z_r \rangle = 4 \cdot 10^{13} \text{ cm}^3 \text{mol}^{-1} \text{s}^{-1}$$

H+C₂H → C₂H₂. - No steric factor for C₂H was determined, but it may be estimated from geometric considerations to be $\geq \beta(\text{C}_2\text{H}_3)=0.37$. For these purposes, choosing $\beta(\text{C}_2\text{H})=0.5$ is reasonable.

Estimation of k_{∞} is then straightforward:

$$\begin{aligned}
\Delta H_{155}^{\ddagger}(0 \text{ K}) &= 132 \pm 2 && \text{(Wodtke and Lee, 1985)} \\
+ \epsilon_z(\text{HC}\equiv\text{CH}) &= 15.2 && \text{from 3374, 1974, 3282, } 2 \cdot 612, 2 \cdot 729 \\
&&& \text{cm}^{-1} \text{ (Stull et al., 1971)} \\
- \epsilon_z(\text{C}_2\text{H}) &= 7.8 && \text{from 1920, 1640, 3220 cm}^{-1} \text{ (Stull et} \\
&&& \text{al., 1971)} \\
- \epsilon_z(\text{H}) &= 0
\end{aligned}$$

$$\begin{aligned}
V_0 &= 139 \text{ kcal/mol} \\
r_0 &= 1.10 \text{ \AA} \text{ (for C-H bond); } \langle Z_r \rangle = 7.35 \cdot 10^{14} \text{ cm}^3 \text{mol}^{-1} \text{s}^{-1} \\
\beta(\text{C}_2\text{H}) &= 0.5 \text{ (50%); } \beta(\text{H}) = 1; g_e = 1/2 \cdot 2 = 1/4 \\
\therefore k_{\infty} &= \beta(\text{C}_2\text{H}) \cdot \beta(\text{H}) \cdot g_e \cdot \langle Z_r \rangle = 9 \cdot 10^{13} \text{ cm}^3 \text{mol}^{-1} \text{s}^{-1}
\end{aligned}$$

H+C₂H₃ → C₂H₄. - Using the steric factor for C₂H₃ from above (from C₂H₃+O → products, β=0.33), k_∞ is estimated to be:

$$\begin{aligned}
\Delta H_{155}^{\ddagger}(0 \text{ K}) &= 107.9 && \text{using } \Delta H_{298}^{\ddagger} = 70.4 \text{ kcal/mol (McMillen} \\
&&& \text{and Golden, 1982)} \\
+ \epsilon_z(\text{H}_2\text{C}=\text{CH}_2) &= 29.0 && \text{from 3026, 3103, 3106, 1623, 1222, 826,} \\
&&& \text{1342, 949, 2989, 1023, 943, 1444 cm}^{-1} \\
&&& \text{(Stull et al., 1971)} \\
- \epsilon_z(\text{C}_2\text{H}_3) &= 22.6 && \text{from above} \\
- \epsilon_z(\text{H}) &= 0
\end{aligned}$$

$$\begin{aligned}
V_0 &= 114.3 \text{ kcal/mol} \\
r_0 &= 1.10 \text{ \AA} \text{ (for C-H bond); } \langle Z_r \rangle = 6.88 \cdot 10^{14} \text{ cm}^3 \text{mol}^{-1} \text{s}^{-1} \\
\beta(\text{C}_2\text{H}_3) &= 0.33 \text{ (50%); } \beta(\text{H}) = 1; g_e = 1/2 \cdot 2 = 1/4 \\
\therefore k_{\infty} &= \beta(\text{C}_2\text{H}_3) \cdot \beta(\text{H}) \cdot g_e \cdot \langle Z_r \rangle = 5.7 \cdot 10^{13} \text{ cm}^3 \text{mol}^{-1} \text{s}^{-1}
\end{aligned}$$

Note that the analyses of Ch. VII.5 indicate that measurements of the rate constant for H+C₂H₃ → H₂+C₂H₂ reach values close to k_∞(H+C₂H₃ → C₂H₄). The Warnatz (1984) recommendation of 3·10¹³ would imply β(C₂H₃)=0.17, which is half that inferred from C₂H₃+O.

³CH₂+CH₃ → C₂H₅*. - A rate constant of 4·10¹³ cm³mol⁻¹s⁻¹ was selected by Warnatz (1984) from three measurements (2, 3, and 6·10¹³) of "CH₂" + CH₃ → C₂H₅. This was used above as one of three reactions to estimate β(³CH₂), but it gave a number sufficiently lower than the other two (0.34 vs. 0.54 and 0.62) that only the latter two were used to generate β=0.58. Using this β, the rate constant would be estimated to be 6.9·10¹³ cm³mol⁻¹s⁻¹.

H+C₂H₅ → C₂H₆. - There is some uncertainty in β(C₂H₅)=0.50, but it can be used to estimate k_∞ for the present reaction:

$$\begin{array}{rcl}
 \Delta H_{155}^{\circ}(0 \text{ K}) & = & 96.3 \text{ kcal/mol} \\
 + \epsilon_z(\text{C}_2\text{H}_6) & = & 42.6 \\
 - \epsilon_z(\text{C}_2\text{H}_5) & = & 35.3 \\
 - \epsilon_z(\text{H}) & = & 0.0
 \end{array}$$

$$V_0 = 103.6 \text{ kcal/mol}$$

$$r_0 = 1.10 \text{ \AA} \text{ (for C-H bond, Benson, 1976); } g_e = 1/2 \cdot 2 = 1/4$$

$$\langle Z_r \rangle = 6.65 \cdot 10^{14} \text{ cm}^3 \text{mol}^{-1} \text{s}^{-1}$$

$$\beta(\text{C}_2\text{H}_5) = 0.5 \text{ (80%); } \beta(\text{H}) = 1; g_e = 1/2 \cdot 2 = 1/4$$

$$\therefore k_{\infty} = \beta(\text{C}_2\text{H}_5) \cdot \beta(\text{H}) \cdot g_e \cdot \langle Z_r \rangle = 8 \cdot 10^{13} \text{ cm}^3 \text{mol}^{-1} \text{s}^{-1}$$

APPENDIX O.

Calculation of rate constants by thermochemical kinetics

Several rate constants had to be estimated for the calculations of Ch. VII using Benson's methods of thermochemical kinetics. As described by Benson (1976), these methods use correlated and estimated thermodynamic properties of the transition state along with transition-state theory to estimate rate constants.

0.1. Rate constant for $C_2H_3 \rightarrow (\cdot HC=CH---H)^\ddagger [\rightarrow C_2H_2+H]$

This calculation, summarized in Table O.1, gives $k_{300} = 5.4 \cdot 10^{13} \exp(-37.4/RT) \text{ s}^{-1}$, $k_{300-1500} = 3.0 \cdot 10^6 T^{2.5} \exp(-36.5/RT)$, and $k_{1300} = 2.2 \cdot 10^{15} \exp(-43.0/RT)$. By microscopic reversibility, $A_{300}(H+C_2H_2 \rightarrow C_2H_3) = 1.0 \cdot 10^{13}$ (E_{300} was used to calculate the energies above). Note that rate constants from such calculations are k_{∞} .

Chapter VII.4 shows how this non-Arrhenius behavior in the high-pressure limit rationalizes some of the data. However, it also limits the utility of QRRK to ranges over which Arrhenius behavior is reasonably well maintained.

0.2. Rate constant for $C_2H_4 \rightarrow (4\text{-centered})^\ddagger [\rightarrow C_2H_2+H_2]$

Benson and Haugen (1966) proposed a transition state and an estimation method that described activation energies of 4-centered molecular eliminations from alkene species. Elimination of hydrogen halides and molecular halogens were the principal experimental tests, but application to simple alkenes like C_2H_4 was suggested.

The activation energy for $H_2+C_2H_2 \rightarrow \ddagger$ was calculated by Benson and Haugen to be 40.0 kcal/mol (298 K). Using $K_{c,298}(C_2H_4 \rightarrow H_2+C_2H_2) = 11.0 \exp(-41.1/RT)$ at 298 K, the activation energy for decomposition was calculated to be 81.1 kcal/mol.

Benson and Haugen did not estimate A-factors, but their method estimates the dimensions of the transition state, which is all that is needed to make the estimate by normal thermochemical kinetics. The ring-like C_2H_4 "species" would lie in a plane with C/C bond distance reduced from 1.34 (C=C) to 1.25 Å (C-C), C-H 1.09 Å increased to 2.09 Å (C-H), and H-H at 1.14 Å (0.4 Å greater than H-H of

Table O.1. Calculation of Arrhenius constants for the reaction $C_2H_2 \rightarrow (\cdot CH=CH\text{---}H)^\ddagger \rightarrow HC\equiv CH+H$.

Mode ^a	$C_2H_3 \rightarrow \ddagger$	ΔS^\ddagger	ΔC_p^\ddagger					
			300	300	500	800	1000	1500
Translation	(unchanged)	0	0	0	0	0	0	0
Rotation (I_m^3)	664 → 1025	0.43	0	0	0	0	0	0
Symmetry, spin	1,2 → 1,2	0	0	0	0	0	0	0
C-H _a stretch	3178 → - ^b	0	1.99	1.97	1.77	1.55	1.02	
C-H _b stretch	3311 → 3314	0	0	0	0	0	0	
C-H _c stretch	3295 → 3375	0	0	0	-0.02	-0.03	-0.03	
C-C stretch	1774 → 1894	0	-0.01	-0.06	-0.09	-0.08	-0.05	
H _a -C-H _b bend	1357 → 843	0.1	0.46	0.61	1.04	0.30	0.15	
H-C=C-H _c bends	1174 678	0.3	0.65	0.63	0.37	0.26	0.13	
	1176 966	0.1	0.20	0.26	0.17	0.12	0.06	
	791 422	0.7	0.75	0.45	0.21	0.13	0.07	
	773 470	0.6	0.62	0.37	0.18	0.12	0.06	
			2.3	4.20	4.23	3.63	2.37	1.41

$\langle \Delta C_p^\ddagger \rangle$ (Weighted average over temperature)

2.97

$E_{act,300}(C_2H_2+H \rightarrow C_2H_3) = 2.7$ kcal/mol (Ellul et al., 1981, Sugawara et al., 1981).

$\Delta H_{300}^\ddagger(C_2H_3 \rightarrow C_2H_2+H) = 35.3$ kcal/mol (using 70.4 kcal/mol C_2H_3)

$\therefore E_{act,300}(C_2H_3 \rightarrow C_2H_2+H) = 38.0$ kcal/mol;

$\Delta H_{300}^\ddagger = E_{act,300} - RT = 37.4$ kcal/mol

Then $k_{300} = A \cdot \exp(-E_{act}/RT)$

$$= \left(\frac{eK T}{h} \exp\left(\frac{\Delta S^\ddagger}{R}\right) \right) \exp\left(-\frac{(\Delta H^\ddagger + RT)}{RT}\right)$$

$$= 5.4 \cdot 10^{13} \exp(-37.4/RT)$$

For $k_{300-1500} = A' T^b \exp(-E'/RT)$:

$$A' = \frac{K}{h} (300)^{-\langle \Delta C_p^\ddagger \rangle / R} \exp\left(\frac{\Delta S_{300}^\ddagger - \langle \Delta C_p^\ddagger \rangle}{R}\right) = 3.0 \cdot 10^6 \text{ s}^{-1}$$

$$b = (\langle \Delta C_p^\ddagger \rangle + R) / R = 2.5$$

$$E' = \Delta H_{300}^\ddagger - \langle \Delta C_p^\ddagger \rangle \cdot (300 \text{ K}) = 36.5 \text{ kcal/mol}$$

^a Frequencies and moments of inertia taken from GVB-POL-CI potential-energy surface calculations of Harding et al. (1982). Hydrogen positions: H_a is the leaving atom, H_b is the adjacent H on the same carbon as H_a, and H_c is the (cis-) H on the other carbon atom.

^b Reaction coordinate.

0.742 Å). It will be assumed that the remaining hydrogens have the geometries and frequencies of acetylenic hydrogens (Stull et al., 1971). Then S_{298}^\ddagger of the transition state may be estimated from moments of inertia, symmetry, and frequencies to be:

$$\begin{aligned}
 I_m &= 14.34 \text{ amu} \cdot \text{Å}^2, \quad \sigma = 2 \\
 \text{Stretches: } & 2 \text{ C}^\ddagger\text{-H (3300); in the ring, C}\equiv\text{C (1810), C}\cdot\text{H} \\
 & \text{(reaction coordinate), C}\cdot\text{H (2200), H}\cdot\text{H (70\% of H}_2\text{ stretch} \\
 & \text{at 4405, so 3100)} \\
 \text{CCH bends: } & 2 \text{ (H-C}\equiv\text{C)}_{t,w} \text{ (1150), } 2 \text{ (H-C}\equiv\text{C)}_r \text{ (700)} \\
 \text{Ring bends: } & 2 \text{ (H}\cdot\text{C}\equiv\text{C)}_{op} \text{ (470) = 70\% of mean value of} \\
 & \text{(H-C=C-H) } \textit{trans} \text{ bend (612) and } \textit{cis} \text{ bend (729)} \\
 \therefore S_{298}^\ddagger &= 56.09 \text{ cal/mol} \cdot \text{K (calculated)}
 \end{aligned}$$

From $S_{298}^\ddagger(\text{C}_2\text{H}_4) = 52.396 \text{ cal/mol} \cdot \text{K}$ (Stull et al., 1971), $\Delta S^\ddagger = 3.69 \text{ cal/mol} \cdot \text{K}$, and A_∞ is predicted to be $1.08 \cdot 10^{14} \text{ s}^{-1}$.

0.3. Rate constants for cyclization

1-C₆H₅ → Phenyl. - A-factors were calculated by estimating the entropy of the transition state from the entropy of phenyl:

		<u>ΔS^\ddagger, cal/mol · K</u>	
<u>Phenyl:</u>	<u>‡:</u>	<u>298</u>	<u>1500</u>
Symmetry $\sigma=2$	$\sigma=1$	+1.38	+1.38
C-C stretch, 1000 cm ⁻¹	C·C stretch (Rxn. coordinate)	-0.09	-2.1
C=C stretch, 1650	C≡C stretch, 1840	-0.003	-0.2
2 C=C-C bends, 420	2 C≡C·C bends, 290	+1.1	+1.5
		<hr/>	<hr/>
		+2.4	+0.6
	+ ΔS^\ddagger (cyc)	-10.3	-15.7
		<hr/>	<hr/>
	ΔS^\ddagger (‡)	-7.9	-15.1
	$\therefore \log A_\infty =$	11.51	10.63

1-C₆H₇ → Cyclohexadienyl. - A-factors were calculated by estimating the entropy of the transition state from the entropy of cyclohexadienyl:

<u>Cyclohexadienyl</u>	<u>‡:</u>	<u>ΔS°, cal/mol·K</u>
		1500
Symmetry $\sigma=2$	$\sigma=1$	+1.4
C-C stretch, 1000 cm^{-1}	C-C stretch (Rxn. coordinate)	-2.1
C-C stretch, 1000	C=C stretch, 1300	-0.5
2 C-C-C bends, 420	2 C=C-C bends, 250	+1.5

		+0.3
	$+\Delta S^\circ$ (cyc)	-12.6

	ΔS° (‡)	-12.3
	$\therefore \log A_\infty =$	11.23

LIST OF SYMBOLS

A	= Arrhenius pre-exponential factor
A	= area-expansion ratio, a function of z (Ch. II)
A'	= fitting factor in Eq. VI.2
A_{∞}	= A in the high-pressure limit
b	= exponent of temperature in Eq. VI.2
c	= velocity of light
C_p	= specific heat
d	= thermocouple diameter
$D_{i,mix}$	= molecular diffusivity of species i in the mixture
E	= energy content (variable) of adduct A
E_{act}	= Arrhenius activation energy
$E_{act,\infty}$	= E_{act} in the high-pressure limit
E_0	= energy barrier to unimolecular reaction
E_{-1}	= barrier for dissociation of A to reactants
E_2	= barrier for dissociation of A to new products
E'	= fitting parameter in Eq. VI.2
$f(E,T)$	= energy distribution function for chemical activation
$F(E)$	= energy dependence factor of the density of states
F_1	= net molar flux of i
h	= Planck's constant (Ch. VI, VII)
h	= heat transfer coefficient
H	= enthalpy
I	= AC heating current through thermocouple (variable)
k	= thermal conductivity (Ch. III)
$k_{a/s}$	= apparent rate constant for addition with stabilization
$k_{a/d}$	= apparent rate constant for addition with chemically activated decomposition of the excited adduct to new products
k_{bi}	= observed bimolecular rate constant
k_{de-exc}	= rate constant for collisional stabilization = βZ
k_{exc}	= rate constant for collisional excitation
k_{rxn}	= rate constant for unimolecular reaction of A^*
k_{uni}	= observed unimolecular rate constant
k_0	= rate constant in the low-pressure limit
$k_{1,\infty}$	= rate constant for addition in the high-pressure limit
$k_{-1}(E)$	= rate constant for dissociation of $A^*(E)$ to reactants
$k_2(E)$	= rate constant for dissociation of $A^*(E)$ to products
k_{∞}	= rate constant in the high-pressure limit
$K(E,T)$	= thermal energy distribution function
K_c	= equilibrium constant, concentration standard state
K_i	= net molar rate of formation of species i
L	= basis length in Eq. III.1
m	= quantized energy barrier to unimolecular reaction
n	= quantized energy variable ($=E/h\langle\nu\rangle$)
n_{atoms}	= number of atoms in a molecule
Nu	= Nusselt number, hd/k
P	= pressure
Pr	= Prandtl number, $C_p\mu/k$
R	= gas constant
Re	= Reynolds number, $\rho vd/\mu$
s	= number of vibrational degrees of freedom in species A
S	= entropy
S	= flow cross-section (Ch. II)

T	= absolute temperature
T _{Tc}	= absolute temperature of the thermocouple
T _{film}	= (T _{Tc} +T _{flame})/2
v	= mass-average convection velocity
V _i	= diffusion velocity of <i>i</i>
x _i	= mole fraction of <i>i</i>
z	= distance from the burner
Z	= collision frequency at unit concentration
Z _{LJ}	= Lennard-Jones Z

Greek Letters

α	= $\exp(-h\langle\nu\rangle/kT)$
β	= collision efficiency for energy removal
$\langle\Delta E_{coll}\rangle$	= average energy transferred per collision
ϵ	= Lennard-Jones interaction energy (Ch. VI, VII)
ϵ	= thermocouple surface emissivity (Ch. III)
K	= Boltzmann constant; also transmission coefficient
ν	= frequency (s ⁻¹)
$\langle\nu\rangle$	= geometric-mean frequency of A
μ	= viscosity
ρ	= mass density
ρ_e	= electrical resistivity per unit length
ρ_m	= molar density
σ	= Lennard-Jones collision diameter (Ch. VI, VII)
σ	= Stefan-Boltzmann constant (Ch. III)
$\langle\omega\rangle$	= geometric-mean frequency of A (cm ⁻¹ ; $\nu=\omega\cdot c$)

LITERATURE CITED

- Ashford, M. N. R., M. A. Fullstone, G. Hancock, and G. W. Ketley, Chem. Phys., 55, 245 (1981).
- Badger, G. M., R. G. Buttery, R. W. L. Kimber, et al., J. Chem. Soc. (London), 2449 (1958).
- Baulch, D. L., D. D. Drysdale, J. Duxbury, and S. J. Grant, Evaluated Kinetic Data for High Temperature Reactions, Vol. 3, Butterworths, London, 1976.
- Bauer, S. H., Eleventh Symposium (International) on Combustion, The Combustion Institute, Pittsburgh, 105, 1967.
- Benson, S. W., Thermochemical Kinetics, 2nd Ed., Wiley, 1976.
- Benson, S. W., Can. J. Chem., 61, 881 (1983).
- Benson, S. W., and G. R. Haugen, J. Am. Chem. Soc., 87, 18 (1965).
- Benson, S. W., and G. R. Haugen, J. Phys. Chem., 70, 3336 (1966).
- Benson, S. W., and G. R. Haugen, J. Phys. Chem., 71, 4404 (1967).
- Benson, S. W., and M. Weissr poster session PS58, Twentieth Symposium (International) on Combustion, University of Michigan, Ann Arbor, August 12-17, 1984.
- Berman, M. R., and M. C. Lin, J. Chem. Phys., 81, 5743 (1984).
- Biordi, J. C., C. P. Lazzara, and J. F. Papp, Fourteenth Symposium (International) on Combustion, The Combustion Institute, Pittsburgh, 367, 1973.
- Biordi, J. C., C. P. Lazzara, and J. F. Papp, Combustion and Flame, 21, 371 (1974).
- Biordi, J. C., C. P. Lazzara, and J. F. Papp, Fifteenth Symposium (International) on Combustion, The Combustion Institute, Pittsburgh, 917, 1975a.
- Biordi, J. C., C. P. Lazzara, and J. F. Papp, in Halogenated Fire Suppressants (R. G. Gann, ed.), ACS Symposium Series No. 16, 256 (1975b).
- Bird, R. B., W. E. Stewart, and E. N. Lightfoot, Transport Phenomena, Wiley, New York, 1960.
- Bittner, J. D., A Molecular-Beam Mass Spectrometer Study of Fuel-Rich and Sooting Benzene-Oxygen Flames, Sc. D. thesis, Department of Chemical Engineering, Massachusetts Institute of Technology, 1981.

- Bittner, J. D., and J. B. Howard, Eighteenth Symposium (International) on Combustion, The Combustion Institute, Pittsburgh, 1105, 1981.
- Blauwens, J., B. Smets, and J. Peeters, Sixteenth Symposium (International) on Combustion, The Combustion Institute, Pittsburgh, 1055, 1977.
- Bockhorn, H., F. Fetting, and H. W. Wenz, Ber. Bunsenges. Phys. Chem., 87, 1067 (1983).
- Bonne, U., K. H. Homann, and H. Gg. Wagner, Tenth Symposium (International) on Combustion, The Combustion Institute, Pittsburgh, 503, 1965.
- Böhland, T., and F. Temps, Ber. Bunsenges. Phys. Chem., 88, 459 (1984).
- Böhland, T., F. Temps, and H. Gg. Wagner, Ber. Bunsenges. Phys. Chem., 88, 455 (1984a).
- Böhland, T., F. Temps, and H. Gg. Wagner, Ber. Bunsenges. Phys. Chem., 88, 1222 (1984b).
- Böhland, T., S. Dóbe, F. Temps, and H. Gg. Wagner, "Kinetics of the Reactions between $\text{CH}_2(\text{X } ^3\text{B}_1)$ -Radicals and Saturated Hydrocarbons in the Temperature Range $296 \leq T \leq 705 \text{ K}$," Ber. Bunsenges. Phys. Chem. (in press).
- Botha, J. P., and D. B. Spalding, Proc. Royal Soc., A225, 71 (1954).
- Braun, W., A. M. Bass, and M. Pilling, J. Chem. Phys., 52, 5131 (1970).
- Burcat, A., Appendix C, "Table of Coefficient Sets for NASA Polynomials," in Combustion Chemistry, (W. C. Gardiner, Jr., ed.), Springer-Verlag, New York, 1984.
- Calcote, H. F., personal communication to J. B. Howard (1984).
- Cattolica, R. J., S. Yoon, and E. L. Knuth, Comb. Sci. Tech., 28, 225 (1982).
- Chase, M. W., et al., "JANAF Thermochemical Tables, 1974 Supplement," J. Phys. Chem. Ref. Data, 3, 311, 1974.
- Chase, M. W., et al., "JANAF Thermochemical Tables, 1975 Supplement," J. Phys. Chem. Ref. Data, 4, 1, 1975.
- Cobos, C. J., H. Hippler, and J. Troe, J. Phys. Chem., 89, 342 (1985a).
- Cobos, C. J., H. Hippler, and J. Troe, J. Phys. Chem., 89, 1778 (1985b).

Cobos, C. J., H. Hippler, K. Luther, A. R. Ravishankara, and J. Troe, J. Phys. Chem., **89**, 4332 (1985c).

Cohen, N., Nineteenth Symposium (International) on Combustion, The Combustion Institute, Pittsburgh, 31, 1982.

Cole, J. A., A Molecular-Beam Mass-Spectrometric Study of Stoichiometric and Fuel-Rich 1,3-Butadiene Flames, M. S. thesis, Department of Chemical Engineering, Massachusetts Institute of Technology, 1982.

Cole, J. A., J. D. Bittner, J. B. Howard, and J. P. Longwell, Combustion and Flame, **56**, 51 (1984).

Colket, M., "Pyrolysis of Vinylacetylene," paper 53; 1985 Fall Technical Meeting, Eastern Section of the Combustion Institute, November 4-6, 1985, Philadelphia (1985).

Colket, M., "Pyrolysis of C_6H_6 ," ACS Division of Fuel Chemistry, New York City, April 13-16, 1986 (1986).

Dean, A. M., J. Phys. Chem., **89**, 4600 (1985).

Delfau, J.-L., and Ch. Vovelle, Combustion Sci. Tech., **41**, 1 (1984a).

Delfau, J.-L., and Ch. Vovelle, personal communication, 1984b.

Delfau, J.-L., and Ch. Vovelle, J. Chimie Physique, **82**, 747 (1985).

Dobé, S., T. Böhland, F. Temps, and H. Gg. Wagner, Ber. Bunsenges. Phys. Chem., **89**, 432 (1985).

Egerton, A., and S. K. Thabat, Proc. Royal Soc., **A211**, 445 (1952).

Ellul, R., P. Potzinger, B. Reimann, and P. Carillieri, Ber. Bunsenges. Phys. Chem., **85**, 407 (1981).

Eltenton, G. C., J. Chem. Phys., **10**, 403 (1942).

Eltenton, G. C., J. Chem. Phys., **15**, 455 (1947).

Faist, S. M., Analysis of Stable Species in a Benzene-Oxygen-Argon Laminar Premixed Flame by Chemical and Spectroscopic Techniques: Applications to Soot Formation and Combustion Chamber Deposits, M. S. thesis, M.I.T., 1979.

Fairbanks, D., and C. R. Wilke, Ind. and Eng. Chem., **42**, 471 (1950).

Field, F. H., and J. L. Franklin, Electron Impact Phenomena and the Properties of Gaseous Ions, New York: Academic Press, 1970.

Foner, S. N., and R. L. Hudson, J. Chem. Phys., **21**, 1374 (1953).

Forst, W., Theory of Unimolecular Reactions, Academic Press, New York, 1973.

- Frank, P., K. A. Bhaskaran, and Th. Just, "High Temperature Reactions of Triplet Methylene and Ketene with Radicals," J. Phys. Chem. (in press).
- Frank, P., K. A. Bhaskaran, and Th. Just, "Acetylene oxidation: The reaction $C_2H_2 + O$ at high temperatures," to be presented at the Twenty-first Symposium (International) on Combustion, Munich, August 3-8, 1986.
- Frank, P., and Th. Just, Ber. Bunsenges. Phys. Chem., **89**, 181 (1985).
- Frenklach, M., D. W. Clary, W. C. Gardiner, Jr., and S. E. Stein, Twentieth Symposium (International) on Combustion, The Combustion Institute, Pittsburgh, 887, 1984.
- Frenklach, M., D. W. Clary, W. C. Gardiner, Jr., and S. E. Stein, "Shock-Tube Pyrolysis of Acetylene: Sensitivity Analysis of the Reaction Mechanism for Soot Formation," Proceedings of the Fifteenth International Symposium on Shock Waves and Shock Tubes (1985; in press).
- Fristrom, R. M., and A. A. Westenberg, Flame Structure, McGraw-Hill, New York, 73 (1965).
- Fujii, N., and T. Asaba, Fourteenth Symposium (International) on Combustion, The Combustion Institute, Pittsburgh, 433, 1973.
- Gardiner, W. C., Jr., and J. Troe, "Rate Coefficients of Thermal Dissociation, Isomerization, and Recombination Reactions," in Combustion Chemistry, (W. C. Gardiner, Jr., ed.), Springer-Verlag, New York, 1984.
- Gay, I. D., R. D. Kern, G. B. Kistiakowsky, and H. Niki, J. Chem. Phys., **45**, 2371 (1966).
- Glassman, I., "Phenomenological Models of Soot Processes in Combustion Systems," Dept. of Mech. and Aerospace Engineering, Princeton University, Report 1450 (1979).
- Glänzer, K., and J. Troe (1977), cited by Warnatz (1984).
- Goddard, W. A., Science, **227**, 917 (1985).
- Golden, D. M., J. Phys. Chem., **83**, 108 (1979).
- Golden, D. M., N. Gac, and S. W. Benson, J. Am. Chem. Soc., **91**, 2136 (1969).
- Hague, E. N., and R. V. Wheeler, J. Chem. Soc. (London), 378 (1929).
- Harding, L., J. Phys. Chem., **85**, 10 (1981).

- Harding, L. B., A. F. Wagner, et al., J. Phys. Chem., 86, 4312 (1982).
- Harvey, R., and A. Maccoll, Seventeenth Symposium (International) on Combustion, The Combustion Institute, Pittsburgh, 857, 1979.
- Hase, W. L., and H. B. Schlegel, J. Phys. Chem., 86, 3901 (1982).
- Hippler, H., K. Luther, A. R. Ravishankara, and J. Troe, Z. Phys. Chem. N. F., 142, 1 (1984).
- Homann, K. H., personal communication, August 1984; confirmed that the source of "C₂H" in Bonne, Homann, and Wagner (1965) was [C₂H⁺; C₂H₂].
- Homann, K. H., M. Mochizuki, and H. Gg. Wagner, Z. Phys. Chem. N. F., 37, 299 (1963).
- Homann, K. H., and H. Gg. Wagner, Ber. Bunsenges. Phys. Chem., 69, 20 (1965).
- Howard, C. J., J. Am. Chem. Soc., 102, 6937 (1980).
- Hoyermann, K., private communication (1981) cited by J. Warnatz (1984).
- Hoyermann, K., N. S. Loftfield, R. Sievert, and H. Gg. Wagner, Eighteenth Symposium (International) on Combustion, The Combustion Institute, Pittsburgh, 831, 1981.
- Just, Th., P. Roth, and R. Damm, Sixteenth Symposium (International) on Combustion, The Combustion Institute, Pittsburgh, 961, 1977.
- Kaskan, W. E., Sixth Symposium (International) on Combustion, The Combustion Institute, Pittsburgh, 134, 1957.
- Kassel, L. S., J. Phys. Chem., 32, 225 (1928a).
- Kassel, L. S., J. Phys. Chem., 32, 1065 (1928b).
- Kee, R. J., J. A. Miller, and T. H. Jefferson, CHEMKIN: A General-Purpose, Problem-Independent, Transportable, Fortran Chemical Kinetics Code Package, SAND80-8003, 1980.
- Kee, R. J., J. Warnatz, and J. A. Miller, A Fortran Computer Code Package for the Evaluation of Gas-phase Viscosities, Conductivities, and Diffusion Coefficients, SAND83-8209, 1983.
- Kee, R. J., et al., CHEMKIN data base of thermodynamics, Sandia National Laboratories, Livermore, California, 1984.
- Keil, D. G., K. P. Lynch, J. A. Cowfer, and J. V. Michael, Int. J. Chem. Kin., 8, 825 (1976).

- Kent, J. H., Combustion and Flame, 14, 279 (1970).
- Kerr, J. A., and S. J. Moss (eds.), Handbook of Bimolecular and Termolecular Gas Reactions, CRC Press, 1981.
- Kerr, J. A., and M. J. Parsonage, Evaluated Kinetic Data on Gas Phase Addition Reactions: Reactions of Atoms and Radicals with Alkenes, Alkynes, and Aromatic Compounds, CRC Press, Cleveland, 1972.
- Kiefer, J. H., L. J. Mizerka, M. R. Patel, and H. C. Wei, J. Phys. Chem., 89, 2013 (1985).
- Kinney, R. E., and D. J. Crowley, Ind. Eng. Chem., 46, 258 (1954).
- Kramer, M. A., H. Rabitz, J. M. Calo, and R. J. Kee, Int. J. Chem. Kinetics, 16, 559 (1984).
- Kramers, H., Physica, 12, 61 (1946).
- Lazzara, C. P., J. C. Biordi, and J. F. Papp, Combustion and Flame, 21, 371 (1973).
- Laidler, K. J., Chemical Kinetics, 2nd Ed., McGraw-Hill, 1965.
- Langford, A. O., H. Petek, and C. B. Moore, J. Chem. Phys., 78, 6650 (1983).
- Laufer, A., Reviews of Chemical Intermediates, 4, 225 (1981).
- Laufer, A., and A. M. Bass, J. Phys. Chem., 78, 1635 (1974).
- Laufer, A. H., and R. Lechleider, J. Phys. Chem., 88, 66 (1984).
- Lee, Y. T., "Recent Investigations on the Heat of Formation of the C₂H Radical," Division of Physical Chemistry, 190th ACS National Meeting, Chicago, September 8-13, 1985.
- Levin, R.D., and S.G. Lias, Ionization Potential and Appearance Potential Measurements, 1971-1981, NSRDS-NBS 71, U.S. Department of Commerce, 1982.
- Levy, J. M., B. R. Taylor, J. P. Longwell, and A. F. Sarofim, Nineteenth Symposium (International) on Combustion, The Combustion Institute, Pittsburgh, 167, 1983.
- Lewis, R. S., and R. T. Watson, J. Phys. Chem., 84, 3495 (1980).
- Lin, M. C., and M. H. Back, Can. J. Chem., 44, 2357 (1966).
- Löhr, R., and P. Roth, Ber. Bunsenges. Phys. Chem., 85, 153 (1981).
- Loucks, L. F., and K. J. Laidler, Can. J. Chem., 45, 2795 (1967).

- Mahnen, G., doctoral thesis, Universite Catholique de Louvain, Belgium, 1973.
- McMillen, D. F., and D. M. Golden, Ann. Rev. Phys. Chem., 33, 493 (1982).
- Michaud, P., J. L. Delfau, and A. Barassin, Eighteenth Symposium (International) on Combustion, The Combustion Institute, Pittsburgh, 443, 1981.
- Miller, J. A., R. E. Mitchell, M. D. Smooke, and R. J. Kee, Nineteenth Symposium (International) on Combustion, The Combustion Institute, Pittsburgh, 181, 1983.
- Milne, T. A., and F. T. Greene, Tenth Symposium (International) on Combustion, The Combustion Institute, Pittsburgh, 153, 1965.
- Mozurkewich, M., J. J. Lamb, and S. W. Benson, J. Phys. Chem., 88, 6435 (1984).
- Neoh, K. G., Soot Burnout in Flames, Sc. D. thesis, Department of Chemical Engineering, Massachusetts Institute of Technology, 1980.
- Nicovich, J. M., and A. R. Ravishankara, J. Phys. Chem., 88, 2534 (1984).
- Oakes, J.M., M. E. Jones, V. M. Bierbaum, and G. B. Ellison, J. Phys. Chem., 87, 4810 (1983).
- Olson, D. B., and H. F. Calcote, Eighteenth Symposium (International) on Combustion, The Combustion Institute, Pittsburgh, 453, 1981.
- Olson, D. B., and W. C. Gardiner, Combustion and Flame, 32, 151 (1978).
- Olsson, J. O., L. S. Karlsson, and L. L. Anderson, J. Phys. Chem., 90, 1458 (1986).
- Park, J.-Y., M. Heaven, and D. Gutman, Chem. Phys. Letters, 104, 469 (1984).
- Powling, J. A., Fuel, 28, 25 (1949).
- Payne, W. A., and L. J. Stief, J. Chem. Phys., 64, 1150 (1976).
- Peeters, J., and G. Mahnen, Fourteenth Symposium (International) on Combustion, The Combustion Institute, Pittsburgh, 133, 1973a.
- Peeters, J., and G. Mahnen, First European Symposium on Combustion, Sheffield, England, 245, 1973b.
- Peeters, J., and C. Vinckier, Fifteenth Symposium (International) on Combustion, The Combustion Institute, Pittsburgh, 969, 1975.

- Peterson, R. C., and N. M. Laurendeau, Combustion and Flame, **60**, 279 (1985).
- Prado, G., P. R. Westmoreland, et al., "Formation of Polycyclic Aromatic Hydrocarbons in Premixed Flames. Chemical Analysis and Mutagenicity," in Analytical Chemistry and Biological Fate (M. Cooke and A. J. Dennis, eds.), Battelle Memorial Institute, Columbus, Ohio, p. 189, 1981.
- Rao, V. S., and G. B. Skinner, J. Phys. Chem., **88**, 5990 (1984).
- Reid, R. C., J. M. Prausnitz and T. K. Sherwood, The Properties of Gases and Liquids, 3rd Ed., McGraw-Hill, New York, 1977.
- Rice, O. K., and H. C. Ramsperger, J. Am. Chem. Soc., **49**, 1617 (1927).
- Robinson, P. J., and K. A. Holbrook, Unimolecular Reactions, Wiley-Interscience, London, 1972.
- Rosenstock, H. M., et al., J. Phys. Chem. Ref. Data, **6**, Supplement No. 1, 1977.
- Rossini, F. D., et al., Selected Values of Physical and Thermodynamic Properties of Hydrocarbons and Related Compounds, Carnegie Press, Pittsburgh, 1953.
- Russell, R. L., and F. S. Rowland, J. Phys. Chem., **83**, 2073 (1979).
- Safieh, H. Y., J. Vandooren, and P. J. Van Tiggelen, Nineteenth Symposium (International) on Combustion, The Combustion Institute, Pittsburgh, 117, 1982.
- Sakai, T., D. Nohara, and K. Kunugi, in Industrial and Laboratory Pyrolyses, ACS Symposium Series, **32**, 152 (1976).
- Sakai, T., K. Soma, et al., "A Kinetic Study on the Formation of Aromatics During Pyrolysis of Petroleum Hydrocarbons," in Refining Petroleum for Chemicals, ACS Advances in Chemistry Series, **97**, 68 (1970).
- Savitsky, A., and M. J. E. Golay, Analytical Chem., **36**, 1627 (1964); but see also Steinier et al. (1972).
- Seery, D. J., and M. F. Zabielski, Eighteenth Symposium (International) on Combustion, The Combustion Institute, Pittsburgh, 397, 1981.
- Sharma, R. B., N. M. Semo, and W. S. Koski, Int. J. Chem. Kin., **17**, 831 (1985).
- Skinner, G. B., R. C. Sweet, and S. K. Davis, J. Phys. Chem., **75**, 1 (1971).
- Slagle, I., Q. Feng, and D. Gutman, J. Phys. Chem., **88**, 3648 (1984).

- Slagle, I. R., J.-Y. Park, M. C. Heaven, and D. Gutman, J. Am. Chem. Soc., 106, 4356 (1984).
- Smith, G. P., P. W. Fairchild, and D. R. Crosley, J. Chem. Phys., 81, 2667 (1984).
- Smith, O. I., S.-N. Wang, S. Tseregounis, and C. K. Westbrook, Comb. Sci. Tech., 30, 241 (1983).
- Smooke, M. D., J. Comp. Phys., 48, 72 (1982).
- Spindler, K. G., and H. Gg. Wagner, Ber. Bunsenges. Phys. Chem., 86, 119 (1982).
- Stehling, F. C., J. D. Frazee, and R. C. Anderson, Sixth Symposium (International) on Combustion, The Combustion Institute, Pittsburgh, 247, 1956.
- Stein, S. E., and A. Fahr, J. Phys. Chem., 89, 3714 (1985).
- Steinier, J., Y. Termonia, and J. Deltour, Analytical Chem., 44, 1906 (1972).
- Stepowski, D., D. Puechberty, and M. J. Cottureau, Eighteenth Symposium (International) on Combustion, The Combustion Institute, Pittsburgh, 1569, 1981.
- Stull, D. R., H. Prophet et al., JANAF Thermochemical Tables, 2nd Ed., Nat. Bur. Standards, Washington, DC, NSRDS-NBS 37, 1971.
- Sworsky, T. J., C. J. Hochanadel, and P. J. Ogren, J. Phys. Chem., 84, 129 (1980).
- Sugawara, K., K. Okazaki, and S. Sato, Bull. Chem. Soc. Japan, 54, 2872 (1981).
- Tanzawa, T., and W. C. Gardiner, Jr., Combustion and Flame, 39, 241 (1980).
- Taylor, B. R., Reactions of Fixed Nitrogen Species in Fuel-Rich Flames, Sc. D. thesis, Department of Chemical Engineering, Massachusetts Institute of Technology, 1984.
- Throssell, J., Int. J. Chem. Kinetics, 4, 273 (1972).
- Troe, J., Fifteenth Symposium (International) on Combustion, The Combustion Institute, Pittsburgh, 667, 1974.
- Troe, J., J. Chem. Phys., 66, 4745 and 4758 (1977).
- Troe, J., J. Phys. Chem., 83, 114 (1979).
- Troe, J., J. Chem. Phys., 75, 226 (1981).

Tsang, W., and R. F. Hampson, "Chemical Kinetic Data Base for Methane Combustion," Chemical Kinetics Division, Center for Chemical Physics, National Bureau of Standards, Washington DC, 1985.

Tsang, W., J. Chem. Phys., 42, 1805 (1965).

Tsang, W., J. Am. Chem. Soc., 107, 2872 (1985).

Tsang, W., J. Phys. Chem., 90, 1152 (1986).

Tseregounis, S. I., and O. I. Smith, Twentieth Symposium (International) on Combustion, The Combustion Institute, Pittsburgh, 761, 1984.

Uchiyama, M., T. Tomioka, and A. Amano, J. Phys. Chem., 68, 1878 (1964).

Van den Bergh, H. E., and A. B. Callear, Trans. Faraday Soc., 66, 2681 (1970).

Vandooren, J., Contribution a l'étude des deflagrations. Flammes acetylene-oxygene et hydrogene - oxyde nitreux, Ph. D. thesis, Université Catholique de Louvain, Belgium, 1976.

Vandooren, J., L. Oldenhove de Guertechin, and P. J. Van Tiggelen, Combustion and Flame, 64, 127 (1986).

Vandooren, J., J. Peeters, and P. J. Van Tiggelen, Fifteenth Symposium (International) on Combustion, The Combustion Institute, Pittsburgh, 745, 1975.

Vandooren, J., and P. J. Van Tiggelen, Sixteenth Symposium (International) on Combustion, The Combustion Institute, Pittsburgh, 1133, 1977.

Vandooren, J., and P. J. Van Tiggelen, Eighteenth Symposium (International) on Combustion, The Combustion Institute, Pittsburgh, 473, 1981.

Vinckier, C., M. Schaekers, and J. Peeters, J. Phys. Chem., 89, 508 (1985).

Volpi, G. G., and F. Zocchi, J. Chem. Phys., 44, 4010 (1966).

Warnatz, J., Eighteenth Symposium (International) on Combustion, The Combustion Institute, Pittsburgh, 369, 1981.

Warnatz, J., Combustion Sci. Tech., 34, 177 (1983); typographical corrections to Table IV are $A_{42}=8.0 \cdot 10^{14}$, $A_{49}=2.0 \cdot 10^{12}$.

Warnatz, J., H. Bockhorn, A. Möser, and H. W. Wenz, Nineteenth Symposium (International) on Combustion, The Combustion Institute, Pittsburgh, 197, 1983.

Warnatz, J., "Rate Coefficients in the C/H/O System," in Combustion Chemistry, (W. C. Gardiner, Jr., ed.), Springer-Verlag, New York, 1984.

Wheeler, R. V., and W. L. Wood, J. Chem. Soc. (London), 1819 (1930).

Weissman, M., and S. W. Benson, Int. J. Chem. Kin., 16, 307 (1984).

Weissman, M., and S. W. Benson, "The Mechanism of Soot Formation in Methane System," Division of Industrial and Engineering Chemistry, 190th ACS National Meeting, Chicago, September 10-14, 1985.

Wenz, H. W., Untersuchungen zur Bildung von Höhermolekularen Kohlenwasserstoffen in Brennerstabilisierten Flammen Unterschiedlicher Brennstoffe und Gemischzusammensetzungen, Dissertation, Technische Hochschule Darmstadt, 1983.

Wersborg, B., Physical Mechanisms of Carbon Formation in Flames, Sc. D. thesis, M.I.T., 1972.

Westbrook, C. K., Combustion Sci. Tech., 34, 201 (1983).

Westbrook, C. K., F. L. Dryer, and K. P. Schug, Nineteenth Symposium (International) on Combustion, The Combustion Institute, Pittsburgh, 153, 1983.

Westbrook, C. K., and F. L. Dryer, Prog. Energy Combustion Sci., 10, 1 (1984).

Westmoreland, P. R., J. B. Howard, J. P. Longwell, and A. M. Dean, "Prediction of Rate Constants for Combustion and Pyrolysis Reactions by Bimolecular QRRK," AIChE J. (in press).

Wodtke, A. M., and Y. T. Lee, J. Phys. Chem., 89, 4722 (1985).

Zellner, R., "Bimolecular Reaction Rate Coefficients," in Combustion Chemistry, (W. C. Gardiner, Jr., ed.), Springer-Verlag, New York, 1984.

BIOGRAPHICAL NOTE

Mr. Westmoreland is a native of Asheboro, North Carolina, born to Ray H. and Jewell R. Westmoreland on March 20, 1951. He attended public schools in Asheboro and in Statesville, graduating from high school in 1969 as salutatorian. Entering with a National Merit Scholarship, he earned a B.S.Ch.E. degree from North Carolina State University in 1973. While there, he was chosen to the Engineering Honors program and served two terms as representative to the Engineers' Council from chemical engineering.

In 1974 Mr. Westmoreland earned an M.S.Ch.E. degree in chemical engineering from Louisiana State University in 1974. His thesis was entitled "Desulfurization of Gasified Coal: Evaluation of Candidate High-Temperature Sulfur Acceptors" and involved screening of metal oxides for sulfur capture by thermodynamics (free-energy minimization) and kinetics (thermogravimetric analysis).

From 1974 to 1979 Mr. Westmoreland was a research engineer in the Coal Research Program at Oak Ridge (TN) National Laboratory. In the first years he was a member of research teams on coal hydrocarbonization (lab-scale and pilot plant), solid-liquid separations, and environmental and process monitoring. Subsequently, he was principal investigator on coal research projects involving pyrolysis of large coal blocks, physical properties of coal and char, fluidization, and supercritical extraction. He also was a consultant (technical advisor) to four groups from the MIT School of Chemical Engineering Practice.

While in Oak Ridge, Mr. Westmoreland was active in the American Institute of Chemical Engineers. He served the Knoxville-Oak Ridge Section as public-relations chairman and as secretary, and for 1976 he was awarded the Public Relations Award of the national AIChE.

He entered MIT in September 1979. In the summer of 1980 he was an Instructor in the Unit Operations Laboratory at Virginia Tech, and in 1984 he helped organize 10.731, Seminar on Combustion Chemistry. At Oak Ridge and MIT, he has been author of 16 published articles and 10 other papers.

Mr. Westmoreland married Kathleen J. Beach in August 1979. She then completed research for a master's degree at Virginia Tech during 1979-1980 while Mr. Westmoreland was in his first year at MIT, a method of beginning married life that neither recommends. She is a chemical engineer by background (B.S. Tennessee Tech '78, M.S. Virginia Tech '80) and now a medical student (U. Mass. class of 1989). They are happy parents of a personality-filled one-year-old named Nathaniel (Nate) P. Beach-Westmoreland.

Mr. Westmoreland will join the faculty of the Department of Chemical Engineering, University of Massachusetts at Amherst, in September 1986.